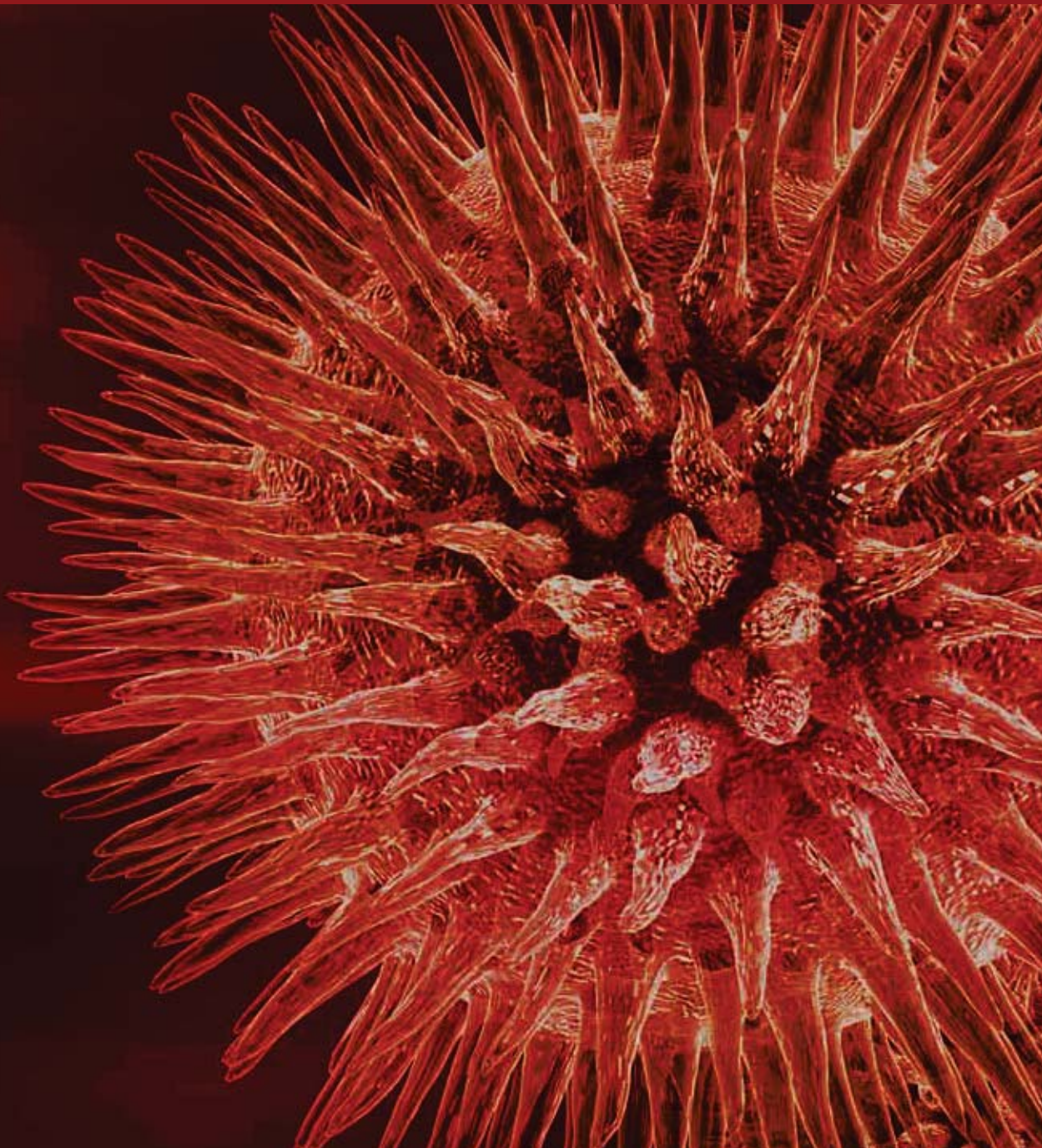


Advances in Muscle Physiology and Pathophysiology

Guest Editors: Aikaterini Kontrogianni-Konstantopoulos,
Guy Benian, and Henk Granzier





**Advances in Muscle Physiology
and Pathophysiology**

Journal of Biomedicine and Biotechnology

**Advances in Muscle Physiology
and Pathophysiology**

Guest Editors: Aikaterini Kontrogianni-Konstantopoulos, Guy Benian, and Henk Granzier



Copyright © 2010 Hindawi Publishing Corporation. All rights reserved.

This is a special issue published in volume 2010 of “Journal of Biomedicine and Biotechnology.” All articles are open access articles distributed under the Creative Commons Attribution License, which permits unrestricted use, distribution, and reproduction in any medium, provided the original work is properly cited.

Editorial Board

The editorial board of the journal is organized into sections that correspond to the subject areas covered by the journal.

Agricultural Biotechnology

Guihua H. Bai, USA
Christopher P. Chanway, Canada
Ravindra N. Chibbar, Canada
Ian Godwin, Australia

Hari B. Krishnan, USA
Carol A. Mallory-Smith, USA
Dennis P. Murr, Canada
Rodomiro Ortiz, Mexico

Badal Chandra Saha, USA
Mariam B. Sticklen, USA
Chiu-Chung Young, Taiwan

Animal Biotechnology

Ernest S. Chang, USA
Hans H. Cheng, USA
Bhanu P. Chowdhary, USA
Noelle E. Cockett, USA
Peter Dovc, Slovenia
Scott C. Fahrenkrug, USA
Dorian J. Garrick, USA
Thomas A. Hoagland, USA

Tosso Leeb, Switzerland
James D. Murray, USA
Anita M. Oberbauer, USA
Jorge A. Piedrahita, USA
Daniel Pomp, USA
Kent M. Reed, USA
Lawrence Reynolds, USA
Sheila M. Schmutz, Canada

Lawrence B. Schook, USA
Mari A. Smits, The Netherlands
Leon Spicer, USA
John P. Versteegen, USA
Matthew B. Wheeler, USA
Kenneth L. White, USA

Biochemistry

Robert Blumenthal, USA
David R. Brown, UK
Saulius Butenas, USA
Vittorio Calabrese, Italy
Francis J. Castellino, USA
Roberta Chiaraluce, Italy
David M. Clarke, Canada
Francesca Cutruzzola, Italy
Paul W. Doetsch, USA
Hicham Fenniri, Canada

Nick V. Grishin, USA
J. Guy Guillemette, Canada
Yusuf A. Hannun, USA
Paul W. Huber, USA
Chen-Hsiung Hung, Taiwan
Michael Kalafatis, USA
Bruce E. Kemp, Australia
Phillip E. Klebba, USA
Wen-Hwa Lee, USA
Richard D. Ludescher, USA

George Makhatadze, USA
Leonid Medved, USA
Susan A. Rotenberg, USA
Jason Shearer, USA
Mark Smith, USA
Andrei Surguchov, USA
John B. Vincent, USA
Yujun George Zheng, USA

Bioinformatics

Tatsuya Akutsu, Japan
Miguel A. Andrade, Germany
Mark Borodovsky, USA
Rita Casadio, Italy
Artem Cherkasov, Canada
David Wolfe Corne, UK
Sorin Draghici, USA

Stavros J. Hamodrakas, Greece
Paul Harrison, Canada
George Karypis, USA
J. A. Leunissen, The Netherlands
Guohui Lin, Canada
Satoru Miyano, Japan
Zoran Obradovic, USA

Florencio Pazos, Spain
Zhirong Sun, China
Ying Xu, USA
Alexander Zelikovsky, USA
Albert Zomaya, Australia

Biophysics

Miguel Castanho, Portugal
P. Bryant Chase, USA
Kuo-Chen Chou, USA
Rizwan Khan, India

Ali A. Khraibi, Saudi Arabia
Rumiana Koynova, USA
Serdar Kuyucak, Australia
Jianjie Ma, USA

S. B. Petersen, Denmark
Peter Schuck, USA
Claudio M. Soares, Portugal

Cell Biology

Ricardo Benavente, Germany
Omar Benzakour, France
Sanford I. Bernstein, USA
Phillip I. Bird, Australia
Eric Bouhassira, USA
Mohamed Boutjdir, USA
Chung-Liang Chien, Taiwan
Richard Gomer, USA
Paul J. Higgins, USA
Pavel Hozak, Czech Republic

Xudong Huang, USA
Anton M. Jetten, USA
Seamus J. Martin, Ireland
Manuela Martins-Green, USA
Shoichiro Ono, USA
George Perry, USA
Mauro Piacentini, Italy
George E. Plopper, USA
Lawrence Rothblum, USA
Ulrich Scheer, Germany

Michael Sheetz, USA
G. S. Stein, USA
Richard Tucker, USA
Thomas van Groen, USA
Andre Van Wijnen, USA
Steve Winder, UK
Chuan Yue Wu, USA
Bin-Xian Zhang, USA

Genetics

Adewale Adeyinka, USA
Claude Bagnis, France
James Birchler, USA
Susan Blanton, USA
Barry J. Byrne, USA
R. Chakraborty, USA
Domenico Coviello, Italy
Sarah H. Elsea, USA
Celina Janion, Poland
J. Spencer Johnston, USA

M. Ilyas Kamboh, USA
Feige Kaplan, Canada
Manfred Kayser, The Netherlands
Brynn Levy, USA
Xiao Jiang Li, USA
Thomas Liehr, Germany
James M. Mason, USA
Mohammed Rachidi, France
Raj S. Ramesar, South Africa
Elliot D. Rosen, USA

Dharambir K. Sanghera, USA
Michael Schmid, Germany
Markus Schuelke, Germany
Wolfgang A. Schulz, Germany
Jorge Sequeiros, Portugal
Mouldy Sioud, Norway
Meena Upadhyaya, UK
Rongjia Zhou, China

Genomics

Vladimir Bajic, Saudi Arabia
Margit Burmeister, USA
Settara Chandrasekharappa, USA
Yataro Daigo, Japan
J. Spencer Johnston, USA
Vladimir Larionov, USA

Hans R. Lehrach, Germany
Thomas Lufkin, Singapore
Joakim Lundeberg, Sweden
John L. McGregor, France
John V. Moran, USA
Henry T. Nguyen, USA

Yasushi Okazaki, Japan
Gopi K. Podila, USA
Mariano Rocchi, Italy
Paul B. Samollow, USA
Momiao Xiong, USA

Immunology

Hassan Alizadeh, USA
Peter Bretscher, Canada
Robert E. Cone, USA
Terry L. Delovitch, Canada
Anthony L. DeVico, USA
Nick Di Girolamo, Australia
Don Mark Estes, USA
Soldano Ferrone, USA
Jeffrey A. Frelinger, USA
John Gordon, UK
John Robert Gordon, Canada

James D. Gorham, USA
Silvia Gregori, Italy
Thomas Griffith, USA
Young S. Hahn, USA
Dorothy E. Lewis, USA
Bradley W. McIntyre, USA
R. Lee Mosley, USA
Marija Mostarica-Stojković, Serbia
Hans Konrad Muller, Australia
Ali Ouaiissi, France
Kanury V. S. Rao, India

Yair Reisner, Israel
Harry W. Schroeder, USA
Wilhelm Schwaeble, UK
Nilabh Shastri, USA
Yufang Shi, China
Piet Stinissen, Belgium
Hannes Stockinger, Austria
J. W. Tervaert, The Netherlands
Graham R. Wallace, UK

Microbial Biotechnology

Jozef Anné, Belgium
Yoav Bashan, Mexico
Marco Bazzicalupo, Italy
Nico Boon, Belgium
Luca Simone Cocolin, Italy

Peter Coloe, Australia
Daniele Daffonchio, Italy
Han de Winde, The Netherlands
Yanhe Ma, China
Bernd Rehm, New Zealand

Angela Sessitsch, Austria
Effie Tsakalidou, Greece
Juergen Wiegel, USA

Microbiology

David Beighton, UK
Steven R. Blanke, USA
Stanley Brul, The Netherlands
Isaac K. O. Cann, USA
John E. Degener, The Netherlands
Peter Dimroth, Switzerland
Stephen K. Farrand, USA

Alain Filloux, UK
Gad Frankel, UK
Roy Gross, Germany
Hans-Peter Klenk, Germany
Tanya Parish, UK
Gopi K. Podila, USA
Frederick D. Quinn, USA

Didier Raoult, France
Isabel Sá-Correia, Portugal
Pamela L. C. Small, USA
Lori Snyder, UK
Michael Thomm, Germany
Henny van der Mei, The Netherlands
Schwan William, USA

Molecular Biology

Rudi Beyaert, Belgium
Michael Bustin, USA
Douglas Cyr, USA
Kostas Iatrou, Greece
Lokesh Joshi, Ireland
David W. Litchfield, Canada

Noel F. Lowndes, Ireland
Wuyuan Lu, USA
Patrick Matthias, Switzerland
John L. McGregor, France
Sherry Mowbray, Sweden
Elena Orlova, UK

Yeon-Kyun Shin, USA
William S. Trimble, Canada
Lisa Wiesmuller, Germany
Masamitsu Yamaguchi, Japan

Oncology

Colin Cooper, UK	Steve B. Jiang, USA	Peter J. Oefner, Germany
F. M. J. Debruyne, The Netherlands	Daehee Kang, South Korea	Allal Ouhtit, USA
Nathan Ames Ellis, USA	Abdul R. Khokhar, USA	Frank Pajonk, USA
Dominic Fan, USA	Rakesh Kumar, USA	Waldemar Priebe, USA
Gary E. Gallick, USA	Macus Tien Kuo, USA	Fernando Carlos Schmitt, Portugal
Daila S. Gridley, USA	Eric W Lam, UK	Sonshin Takao, Japan
Xin-yuan Guan, Hong Kong	Sue-Hwa Lin, USA	Ana M. Tari, USA
Anne Hamburger, USA	Kapil Mehta, USA	Henk G. Van Der Poel, The Netherlands
Manoor Prakash Hande, Singapore	Orhan Nalcioğlu, USA	Haodong Xu, USA
Beric Henderson, Australia	Vincent C. O. Njar, USA	David J. Yang, USA

Pharmacology

Abdel A. Abdel-Rahman, USA	Ayman El-Kadi, Canada	Kennerly S. Patrick, USA
Mostafa Z. Badr, USA	Jeffrey Hughes, USA	Vickram Ramkumar, USA
Stelvio M. Bandiera, Canada	Kazim Husain, USA	Michael J. Spinella, USA
Ronald E. Baynes, USA	Farhad Kamali, UK	Quadiri Timour, France
R. Keith Campbell, USA	Michael Kassiou, Australia	Todd W. Vanderah, USA
Hak-Kim Chan, Australia	Joseph J. McArdle, USA	Val J. Watts, USA
Michael D. Coleman, UK	Mark McKeage, New Zealand	David J. Waxman, USA
Jacques Descotes, France	Daniel T. Monaghan, USA	
Dobromir Dobrev, Germany	T. Narahashi, USA	

Plant Biotechnology

Prem L. Bhalla, Australia	Liwen Jiang, Hong Kong	Ralf Reski, Germany
Jose Botella, Australia	Pulugurtha B. Kirti, India	Sudhir Kumar Sopory, India
Elvira Gonzalez De Mejia, USA	Yong Pyo Lim, South Korea	Neal Stewart, USA
H. M. Häggman, Finland	Gopi K. Podila, USA	

Toxicology

Michael Aschner, USA	Youmin James Kang, USA	Kenneth Turteltaub, USA
Michael L. Cunningham, USA	M. Firoze Khan, USA	Brad Upham, USA
Laurence D. Fechter, USA	Pascal Kintz, France	
Hartmut Jaeschke, USA	Ronald Tjeerdema, USA	

Virology

Nafees Ahmad, USA
Edouard Cantin, USA
Ellen Collisson, USA
Kevin M. Coombs, Canada
Norbert K. Herzog, USA
Tom Hobman, Canada
Shahid Jameel, India

Fred Kibenge, Canada
Fenyong Liu, USA
Éric Rassart, Canada
Gerald G. Schumann, Germany
Young-Chul Sung, South Korea
Gregory Tannock, Australia

Ralf Wagner, Germany
Jianguo Wu, China
Decheng Yang, Canada
Jiing-Kuan Yee, USA
Xueping Zhou, China
Wen-Quan Zou, USA

Contents

Advances in Muscle Physiology and Pathophysiology, Aikaterini Kontrogianni-Konstantopoulos, Guy Benian, and Henk Granzier
Volume 2010, Article ID 780417, 1 page

Assembly and Dynamics of Myofibrils, Joseph W. Sanger, Jushuo Wang, Yingli Fan, Jennifer White, and Jean M. Sanger
Volume 2010, Article ID 858606, 8 pages

Sarcomere Control Mechanisms and the Dynamics of the Cardiac Cycle, R. John Solaro
Volume 2010, Article ID 105648, 8 pages

Ordered Assembly of the Adhesive and Electrochemical Connections within Newly Formed Intercalated Disks in Primary Cultures of Adult Rat Cardiomyocytes, Sarah B. Geisler, Kathleen J. Green, Lori L. Isom, Sasha Meshinchi, Jeffrey R. Martens, Mario Delmar, and Mark W. Russell
Volume 2010, Article ID 624719, 14 pages

Molecular Structure of Sarcomere-to-Membrane Attachment at M-Lines in *C. elegans* Muscle, Hiroshi Qadota and Guy M. Benian
Volume 2010, Article ID 864749, 9 pages

Physiologic Basis and Pathophysiologic Implications of the Diastolic Properties of the Cardiac Muscle, João Ferreira-Martins and Adelino F. Leite-Moreira
Volume 2010, Article ID 807084, 12 pages

Force Transmission between Synergistic Skeletal Muscles through Connective Tissue Linkages, Huub Maas and Thomas G. Sandercock
Volume 2010, Article ID 575672, 9 pages

What We Know and Do Not Know about Sex and Cardiac Disease, John P. Konhilas
Volume 2010, Article ID 562051, 11 pages

Identification of Candidate Genes Potentially Relevant to Chamber-Specific Remodeling in Postnatal Ventricular Myocardium, Mario Torrado, Raquel Iglesias, Beatriz Nespereira, and Alexander T. Mikhailov
Volume 2010, Article ID 603159, 10 pages

Comparative Biomechanics of Thick Filaments and Thin Filaments with Functional Consequences for Muscle Contraction, Mark S. Miller, Bertrand C. W. Tanner, Lori R. Nyland, and Jim O. Vigoreaux
Volume 2010, Article ID 473423, 14 pages

Contractile Properties of Esophageal Striated Muscle: Comparison with Cardiac and Skeletal Muscles in Rats, Takahiko Shiina, Takeshi Shima, Kazuaki Masuda, Haruko Hirayama, Momoe Iwami, Tadashi Takewaki, Hirofumi Kuramoto, and Yasutake Shimizu
Volume 2010, Article ID 459789, 7 pages

Characteristics of Tetanic Force Produced by the Sternomastoid Muscle of the Rat, Stanislaw Sobotka and Liancai Mu
Volume 2010, Article ID 194984, 11 pages

Efficient Isolation of Cardiac Stem Cells from Brown Adipose, Zhiqiang Liu, Haibin Wang, Ye Zhang, Jin Zhou, Qiuxia Lin, Yanmeng Wang, Cuimi Duan, Kuiwu Wu, and Changyong Wang
Volume 2010, Article ID 104296, 9 pages

Pre-mRNA Processing Is Partially Impaired in Satellite Cell Nuclei from Aged Muscles, Manuela Malatesta, Federica Perdoni, Sylviane Muller, Carlo Pellicciari, and Carlo Zancanaro
Volume 2010, Article ID 410405, 9 pages

Mechanism of Catch Force: Tethering of Thick and Thin Filaments by Twitchin, Thomas M. Butler and Marion J. Siegman
Volume 2010, Article ID 725207, 20 pages

Titin Diversity—Alternative Splicing Gone Wild, Wei Guo, Sheila J. Bharmal, Karla Esbona, and Marion L. Greaser
Volume 2010, Article ID 753675, 8 pages

Roles of Titin in the Structure and Elasticity of the Sarcomere, Larissa Tskhovrebova and John Trinick
Volume 2010, Article ID 612482, 7 pages

Dynamic Strength of Titin's Z-Disk End, Veronika Kollár, Dávid Szatmári, László Grama, and Miklós S. Z. Kellermayer
Volume 2010, Article ID 838530, 8 pages

Titin-Isoform Dependence of Titin-Actin Interaction and Its Regulation by S100A1/Ca²⁺ in Skinned Myocardium, Hideto Fukushima, Charles S. Chung, and Henk Granzier
Volume 2010, Article ID 727239, 9 pages

S100A1: A Regulator of Striated Muscle Sarcoplasmic Reticulum Ca²⁺ Handling, Sarcomeric, and Mitochondrial Function, Mirko Völkers, David Rohde, Chelain Goodman, and Patrick Most
Volume 2010, Article ID 178614, 10 pages

Myosin Binding Protein-C Slow: An Intricate Subfamily of Proteins, Maegen A. Ackermann and Aikaterini Kontrogianni-Konstantopoulos
Volume 2010, Article ID 652065, 10 pages

Functional Differences between the N-Terminal Domains of Mouse and Human Myosin Binding Protein-C, Justin F. Shaffer, Peony Wong, Kristina L. Bezold, and Samantha P. Harris
Volume 2010, Article ID 789798, 9 pages

New Insights into the Structural Roles of Nebulin in Skeletal Muscle, Coen A. C. Ottenheijm and Henk Granzier
Volume 2010, Article ID 968139, 6 pages

Isolation of Nebulin from Rabbit Skeletal Muscle and Its Interaction with Actin, Ryo Chitose, Atsushi Watanabe, Masato Asano, Akira Hanashima, Kouhei Sasano, Yulong Bao, Koscak Maruyama, and Sumiko Kimura
Volume 2010, Article ID 108495, 8 pages

Contents

Cardiac Troponin Mutations and Restrictive Cardiomyopathy, Michelle S. Parvatiyar, Jose Renato Pinto, David Dweck, and James D. Potter
Volume 2010, Article ID 350706, 9 pages

The Functional Role of Calcineurin in Hypertrophy, Regeneration, and Disorders of Skeletal Muscle, Kunihiro Sakuma and Akihiko Yamaguchi
Volume 2010, Article ID 721219, 8 pages

Modulation of Muscle Atrophy, Fatigue and MLC Phosphorylation by MuRF1 as Indicated by Hindlimb Suspension Studies on MuRF1-KO Mice, Siegfried Labeit, Christine H. Kohl, Christian C. Witt, Dittmar Labeit, Jeong Jung, and Henk Granzier
Volume 2010, Article ID 693741, 9 pages

Aquaporin Expression in Normal and Pathological Skeletal Muscles: A Brief Review with Focus on AQP4, Yoshihiro Wakayama
Volume 2010, Article ID 731569, 9 pages

Epo Is Relevant Neither for Microvascular Formation Nor for the New Formation and Maintenance of Mice Skeletal Muscle Fibres in Both Normoxia and Hypoxia, Luciana Hagström, Onnik Agbulut, Raja El-Hasnaoui-Saadani, Dominique Marchant, Fabrice Favret, Jean-Paul Richalet, Michle Beaudry, and Thierry Launay
Volume 2010, Article ID 137817, 13 pages

The Masticatory Contractile Load Induced Expression and Activation of Akt1/PKB α in Muscle Fibers at the Myotendinous Junction within Muscle-Tendon-Bone Unit, Yüksel Korkmaz, Franz J. Klinz, Mehrnoush Moghbeli, Klaus Addicks, Wolfgang H.-M. Raab, and Wilhelm Bloch
Volume 2010, Article ID 163203, 8 pages

Skeletal Dysplasias Associated with Mild Myopathy—A Clinical and Molecular Review, Katarzyna A. Piróg and Michael D. Briggs
Volume 2010, Article ID 686457, 13 pages

Impaired Skeletal Muscle Repair after Ischemia-Reperfusion Injury in Mice, A. Vignaud, C. Hourde, F. Medja, O. Agbulut, G. Butler-Browne, and A. Ferry
Volume 2010, Article ID 724914, 10 pages

Temporal Adaptive Changes in Contractility and Fatigability of Diaphragm Muscles from Streptozotocin-Diabetic Rats, Marco Brotto, Leticia Brotto, J.-P. Jin, Thomas M. Nosek, and Andrea Romani
Volume 2010, Article ID 931903, 8 pages

Proteomic Profiling of the Dystrophin-Deficient MDX Heart Reveals Drastically Altered Levels of Key Metabolic and Contractile Proteins, Caroline Lewis, Harald Jockusch, and Kay Ohlendieck
Volume 2010, Article ID 648501, 20 pages

Mechanical and Electrophysiological Properties of the Sarcolemma of Muscle Fibers in Two Murine Models of Muscle Dystrophy: Col6a1^{-/-} and Mdx, M. Canato, M. Dal Maschio, F. Sbrana, R. Raiteri, C. Reggiani, S. Vassanelli, and A. Megighian
Volume 2010, Article ID 981945, 13 pages

There Goes the Neighborhood: Pathological Alterations in T-Tubule Morphology and Consequences for Cardiomyocyte Ca²⁺ Handling, William E. Louch, Ole M. Sejersted, and Fredrik Swift
Volume 2010, Article ID 503906, 17 pages

Mitochondrial Translation and Beyond: Processes Implicated in Combined Oxidative Phosphorylation Deficiencies, Paulien Smits, Jan Smeitink, and Lambert van den Heuvel
Volume 2010, Article ID 737385, 24 pages

The Role of Exercise-Induced Myokines in Muscle Homeostasis and the Defense against Chronic Diseases, Claus Brandt and Bente K. Pedersen
Volume 2010, Article ID 520258, 6 pages

Skeletal Muscle Insulin Resistance in Endocrine Disease, Melpomeni Peppas, Chrysi Koliaki, Panagiotis Nikolopoulos, and Sotirios A. Raptis
Volume 2010, Article ID 527850, 13 pages

Pathogenesis of Insulin Resistance in Skeletal Muscle, Muhammad A. Abdul-Ghani and Ralph A. DeFronzo
Volume 2010, Article ID 476279, 19 pages

Inborn Errors of Energy Metabolism Associated with Myopathies, Anibh M. Das, Ulrike Steuerwald, and Sabine Illsinger
Volume 2010, Article ID 340849, 19 pages

Extracorporeal Immunoglobulin Elimination for the Treatment of Severe Myasthenia Gravis, M. Blaha, J. Pit'ha, V. Blaha, M. Lanska, J. Maly, S. Filip, and H. Langrova
Volume 2010, Article ID 419520, 6 pages

Combining Microdialysis and Near-Infrared Spectroscopy for Studying Effects of Low-Load Repetitive Work on the Intramuscular Chemistry in Trapezius Myalgia, Gerd M. Flodgren, Albert G. Crenshaw, Fredrik Hellström, and Martin Fahlström
Volume 2010, Article ID 513803, 9 pages

Editorial

Advances in Muscle Physiology and Pathophysiology

Aikaterini Kontrogianni-Konstantopoulos,¹ Guy Benian,² and Henk Granzier³

¹ Department of Biochemistry and Molecular Biology, Baltimore School of Medicine, University of Maryland, Baltimore, MD 20742, USA

² Departments of Pathology and Cell Biology, Emory University, Atlanta, GA 30322, USA

³ Department of Physiology and Molecular and Cellular Biology, University of Arizona, Tucson 85721, AZ, USA

Correspondence should be addressed to Aikaterini Kontrogianni-Konstantopoulos, akons001@umaryland.edu

Received 6 June 2010; Accepted 6 June 2010

Copyright © 2010 Aikaterini Kontrogianni-Konstantopoulos et al. This is an open access article distributed under the Creative Commons Attribution License, which permits unrestricted use, distribution, and reproduction in any medium, provided the original work is properly cited.

During the recent years, unprecedented amounts of new knowledge have seen the light, revealing *key factors* that modulate the essential processes of the structure and function of muscle. The assembly of the sarcomeric and extrasarcomeric cytoskeleton, the formation of internal membrane systems and their contribution to the regulation of Ca²⁺ homeostasis, the molecular dissection of specialized sarcolemmal microdomains, and the anchoring of the intracellular cytoskeletal network with the extracellular matrix are only some of the themes where rapid progress has been made. Advanced genetic, molecular, cellular, biochemical, genomic, and proteomic approaches, using diverse animal models, have unraveled the intricate details of these complex pathways both during health and disease and highlighted new questions and challenges. The breadth of new information has been overwhelming yet exciting, emphasizing once again the absolute need for development of sophisticated, multidisciplinary, and integrated approaches to study the roles of *subproteomes* rather than individual proteins during development and in adulthood, under normal and stress conditions.

In this volume, we invited authors who study muscle structure and function from *different perspectives and angles* to contribute original and review articles. A wide array of topics is discussed in this special issue, including the regulated assembly of myofibrils, the biomechanical and biophysical properties of sarcomeric contraction, the dynamic tethering of thin and thick filaments and the unique, compensatory, or even redundant roles of their accessory proteins, the giant sarcomeric proteins, and their roles as molecular blueprints and sensors, the sarcolemma

and its role in the mechanical and electrochemical coupling of neighboring cells, the tripartite regulation of Ca²⁺ cycling orchestrated by the activities of the t-tubules, sarcoplasmic reticulum, and mitochondria, the roles of exercise, fatigue and injury in muscle contraction, and the isolation and use of muscle stem cells. Importantly, many of these processes are altered, compromised, or dysregulated in different forms of skeletal and cardiac myopathies and dystrophies. Some of these are discussed as well.

The editors of this special issue are indebted to all the authors who provided either original data or a comprehensive review of the previous and recent literature, making this special issue appealing to a diverse audience of muscle researchers. Our goal was to touch on different aspects of muscle physiology and pathophysiology at the molecular, cellular, organ, and organismal level. We are delighted to see the outcome of our call in the form of this special volume, and we hope that it will provide a wealthy source of knowledge and information and further stimulate muscle research at all different fronts.

Aikaterini Kontrogianni-Konstantopoulos
Guy Benian
Henk Granzier

Review Article

Assembly and Dynamics of Myofibrils

Joseph W. Sanger, Jushuo Wang, Yingli Fan, Jennifer White, and Jean M. Sanger

Department of Cell and Developmental Biology, SUNY Upstate Medical University, Syracuse, NY 13210, USA

Correspondence should be addressed to Joseph W. Sanger, sangerjo@upstate.edu

Received 31 December 2009; Accepted 15 March 2010

Academic Editor: Aikaterini Kontrogianni-Konstantopoulos

Copyright © 2010 Joseph W. Sanger et al. This is an open access article distributed under the Creative Commons Attribution License, which permits unrestricted use, distribution, and reproduction in any medium, provided the original work is properly cited.

We review some of the problems in determining how myofibrils may be assembled and just as importantly how this contractile structure may be renewed by sarcomeric proteins moving between the sarcomere and the cytoplasm. We also address in this personal review the recent evidence that indicates that the assembly and dynamics of myofibrils are conserved whether the cells are analyzed *in situ* or in tissue culture conditions. We suggest that myofibrillogenesis is a fundamentally conserved process, comparable to protein synthesis, mitosis, or cytokinesis, whether examined *in situ* or *in vitro*.

1. Introduction

Myofibrils of striated muscle are characterized by groups of proteins arranged in contractile units, or sarcomeres, that consist of distinct subunits that extend in a repeating pattern along the length of the muscle cell. Although sarcomeres of cross-striated muscle vary among species in length and in some protein constituents, all have a similar subunit arrangement of three major components: thin filaments, thick filaments, and Z-bands that each forms from multiple interactions among the proteins that produce and control contraction (Figure 1). Vertebrate skeletal and cardiac sarcomeres at rest length are 2.5 microns in length whereas the sarcomeres of cross-striated muscles in the invertebrate world vary widely from one micron in a jellyfish [1] to 25 microns in the pharynx of a syllid worm [2]. A-band lengths of thick filaments and thin filament lengths vary in concert with sarcomere size: the shortest at 0.6 microns and 0.5 microns, respectively, in jellyfish, the longest at 20 microns and 12 microns, respectively, in the syllid worm, and 1.6 microns and 1.0 micron in vertebrate skeletal muscle [3]. In vertebrate ventricular muscles, the thin filament lengths are variable up to one micron [4].

Despite all that is known about the binding of myofibrillar proteins, one with one another in biochemical assays, much is unknown about the multiplicity of interactions that support myofibril formation and stability in the live

cell. The importance of myofibrillar protein interactions in cardiac health has been reinforced by the realization that mutated sarcomeric proteins are involved in a growing number of cardiomyopathies [9, 10]. Interactions of the major proteins responsible for force production in the thin and thick filament subunits have been described in detail [11]. Proteins of the Z-band, a region of the sarcomere where novel proteins and novel interactions of known proteins are still being discovered [12, 13], present a particularly challenging network of potential multiple interactions, many of which have been determined by biochemical methods not by methods inside the living cell (Figure 2). The Z-band functions as a scaffold that links the sarcomeric contractile units in series by anchoring the thin and titin filaments of adjacent sarcomeres. Z-bands also anchor the ends of myofibrils in specialized junctions, termed intercalated discs in cardiac muscle cells, and they link sarcomeres laterally to the cell membrane through costameric proteins [14, 15]. The multifunctional nature of the Z-band is reflected in the variety of proteins that colocalize in this structure: channels, signaling molecules, enzymes, cytoskeletal filament complex that interacts with the cell membrane, and sarcomeric filaments essential for contraction (Figure 2) [11, 16, 17]. Two of the most surprising recent reports on new Z-band proteins concern (a) heat shock proteins in zebrafish skeletal muscles (reviewed in [12]) and (b) the protein, CLOCK, which is involved in circadian regulation in neonatal rat cardiomyocytes (reviewed in [13]).

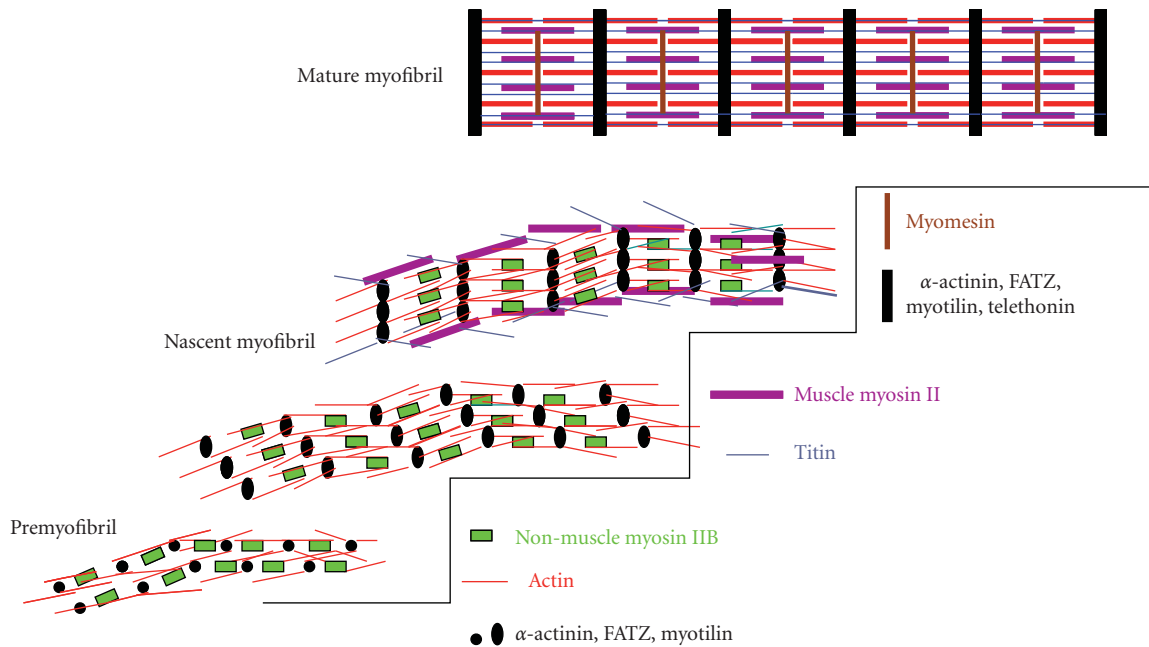


FIGURE 1: Premyofibril model of myofibrillogenesis. Assembly begins at the edges of muscle cells with premyofibrils composed of minisarcmeres (bounded by alpha-actinin containing z-bodies) with muscle actin and actin-binding proteins and the nonmuscle isoform of myosin II. Muscle myosin and titin are added and z-bodies align in register to form nascent myofibrils with beaded Z-bands. As mature myofibrils form, the beaded Z-bands gradually become linear, nonmuscle myosin is lost, and myosin-binding proteins (C-protein and myomesin) are incorporated into aligned A-bands [5–8]. Diagram modified from Stout et al. [8].

2. Formation of Myofibrils

As the list of myofibril proteins and their binding reactions grows, the assembly pathways that the interacting protein complexes follow to form myofibrils have increasing import for understanding the problems of aberrant formation and maintenance of myofibrils containing mutated sarcomeric proteins [9, 10, 16, 18]. In the early 1900s, Heidenhain [19] examined fixed muscles in the light microscope and noted nonstriated fibers near the cell membrane of developing trout skeletal muscles before striated structures that we now know were Z-bands and A-bands were detected. Electron micrographs of forming chick muscle showed nonstriated fibers near the cell membrane, as well, before banded myofibrils appeared (see review by Sanger et al. [6]). Growth in A-band length to mature size was also observed with electron microscopy of embryonic fly muscle fixed at daily intervals. The first fibers observed were nonstriated with dense bodies but lacking thick filaments, succeeded by fibers with Z-bands and short A-bands and later by fibers with A-bands of mature muscle length [20]. Striated sarcomeres in forming mite muscle that were analyzed with polarized light in the live animal increased over a 30-hour period from 2.2 microns to 4 microns in length, accompanied by an increase in A-band length from 1.4 microns to 3 micron [21].

The advent of probes for fluorescent detection of proteins inside cells allowed fibers in nonmuscle cells and embryonic muscle cells to be characterized. In nonmuscle cells many stress fibers, previously described as unstriated in [22, 23] were shown to be composed of repeating concentrations of

alpha-actinin and nonmuscle myosin II distributed in alternating bands along overlapping actin filaments [24–28]. In a short presentation, a three-page report, published in a book describing the proceedings of short talks honoring the late John Marshall, Kulikowski and Manasek [29], described how embryonic chick cultured cardiomyocytes appeared when stained with muscle-specific myosin II antibodies after different periods of time in culture. They noted the appearance of nonstriated continuous myosin fibers in the cardiomyocytes in early days of culture. These fibers were described as having “...a stress fiberlike morphology...” In older cultures, the authors recorded typical myofibrils with A-Bands. They concluded that myofibrils could “...reassemble via the stress fiberlike intermediates in cultured cardiac myocytes.”

A nonmuscle isoform of myosin II was first shown to be present in skeletal muscle cells near the membrane in fibers distinct from the mature myofibrils [30]. These fibers were later termed “stress-fiber-like” by Dlugosz et al. [31]. Three isoforms of nonmuscle myosin II have since been detected in fibers in vertebrate striated muscle cells [32–34]. Subsequent studies have differed over the role that these “stress-fiber-like” fibers might play in myofibrillogenesis. They were suggested by the Holtzer lab to function as templates along which muscle proteins assemble and form cross-striated myofibrils [31]. The templates were thought to then disassemble with the subunits reassembling in another region of the cell to restart the templating process. Thus, one stress fiber-like structure was proposed to serve as the template for each new myofibril myofibril.

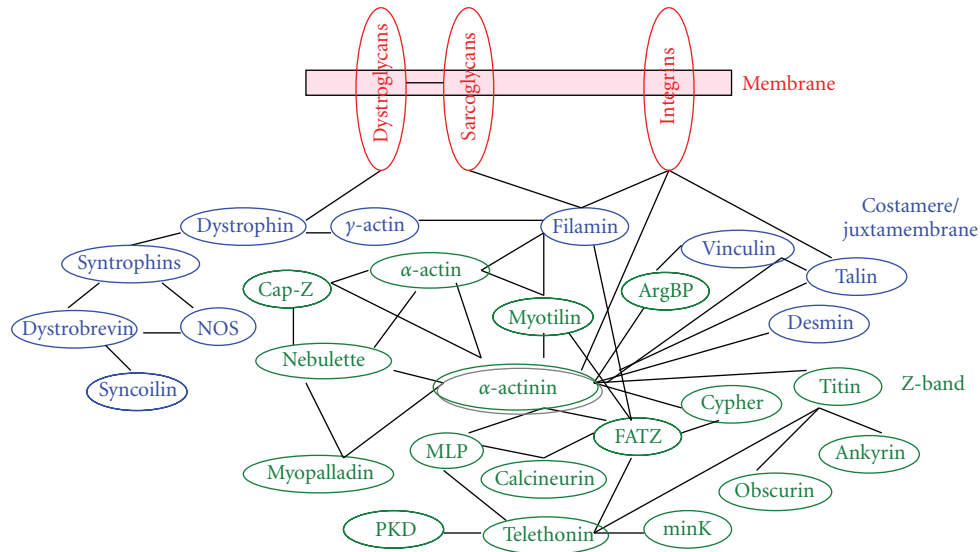


FIGURE 2: Diagram of some proteins reported to be in the Z-bands of mature myofibrils. The Z-bands of the mature myofibrils are attached via costameric proteins to the membrane of the muscle cells.

The fibers, that were nonstriated when F-actin were stained with phalloidin, were revealed to be formed of minisarcmeres when fluorescent alpha-actinin was injected into live cells or perfused into permeabilized muscle cells [35–37]. Small puncta of alpha-actinin were spaced at intervals varying from 0.3 to 1.5 microns. In live cells injected with fluorescent alpha-actinin, the distance between puncta increased with time [37], as a later study confirmed in embryonic heart cells transfected with GFP-alpha-actinin in which small puncta of alpha-actinin aligned laterally and Z-bands appeared beaded before appearing as a smooth band [38]. Bands of nonmuscle myosin II were detected alternating with the sarcomeric alpha-actinin densities (z-bodies) in these fibers [39]. Identical minisarcmeric patterns of alternating z-bodies (sarcomeric alpha-actinin) and bands of nonmuscle myosin II were also discovered in precardiac chick mesoderm explants [5] and in stained intact hearts in early chick embryos [40]. Thus there were no differences between cultured or intact hearts in the detection of a pathway for myofibrillogenesis (Figure 1). We suggest that myofibrillogenesis is a fundamentally conserved process, comparable to protein synthesis, mitosis, or cytokinesis, whether examined *in situ* or *in vitro*.

Nonmuscle myosin II light chains that were fluorescently labeled and injected into cultured cells from avian embryonic muscle also were localized in small periodically spaced bands along the thinnest actin fibers near the cell membrane [27]. In addition, the light chains also localized in A-bands in the myofibrils in the embryonic cells and in an unstriated pattern along the length of other actin fibers [27]. The unstriated pattern represents the nascent myofibrils (Figure 1). The unstriated pattern results from the overlapping thick filaments in the nascent myofibrils [5–7]. In dividing avian cardiomyocytes, Conrad et al. [41] discovered that nonmuscle myosin II, but not muscle myosin

II, was present in the cleavage furrows. The nonmuscle myosin II in avian cardiomyocytes is now known to be the II B isoform [39, 42]. The antibody to II A does not react with embryonic chick cardiomyocytes [39], and early reports revealed that fibers with minisarcmeric bands of nonmuscle myosin were not present in avian cardiomyocytes [43, 44]) resulted because antibodies to II A were used. The small diameter and unstriated appearance of the fibers with phalloidin staining fibers resembles those of stress fibers, thus the term stress fiber-like structures [31]. However, we now know that most of the proteins in these fibers are muscle-specific proteins, for example, alpha-actinin, actin, tropomyosin, and so forth [7, 39, 45, 46]. They are also less sensitive than stress fibers to a number of different inhibitors (gelsolin [47], DNase1, Vitamin-D binding protein [48], and latrunculin-A [49]). J. M. Sanger and J. W. Sanger [50] demonstrated that cleavage furrows contained oppositely polarized actin filaments interdigitating with nonmuscle II-like filaments in minisarcmeric patterns similar to those in the stress fibers of interphase cells.

We have proposed that the fibers with minisarcmeric bands of nonmuscle myosin II in muscle cells are premyofibrils, the precursors of myofibrils (see [7, 39]; Figure 1). We consider the small puncta of alpha-actinin z-bodies, precursors of Z-bands. Patterns of myosin II localization in embryonic chick cardiomyocytes fixed at different times after spreading and reformation of myofibrils in culture points to three types of fibers (Figure 1). *Premyofibrils* consist of thin filaments with periodic mini-A-Bands spaced between the puncta of alpha-actinin (z-bodies). *Nascent myofibrils* possess two types of myosin II staining: small periodic mini-A-Bands of nonmuscle myosin IIB and unbanded staining of muscle-specific myosin II. *Mature myofibrils* stain for only one type of myosin II, that is, the muscle-specific myosin IIs in A-bands. Thus, the original unbanded

staining of fibers with phalloidin, which Dlugosz et al. [31] originally termed stress fiber-like fibers, represents both pre- and nascent myofibrils. Subsequent observations of forming muscle in fixed embryonic avian myocytes by the Holtzer group led them to propose an additional model in which myofibril assembly occurred through independent assembly of thick filaments and Z-bands linked to their associated thin filaments (I-Z-I brushes) [43, 44]. Titin was proposed to associate with the I-Z-I brushes, capture the muscle myosin II filaments and align them into A-bands, and join the A-bands and I-Z-I brushes into sarcomere units without involvement of stress fiber-like structures. However, it is now known that the precursors of the Z-bands (z-bodies) and associated actin are not scattered in the cell but are aligned by the minisarcomeric arrangement of nonmuscle myosin IIs, that is, premyofibrils (Figure 1; [7, 39, 51]). The minisarcomeric arrangements of cleavage furrows, stress fibers, and premyofibrils would appear to have evolved very early [27, 28, 50, 52, 53]. Live cell imaging has allowed us to follow myofibrillogenesis from the deposition of premyofibrils to nascent myofibrils to mature myofibrils in cultured cardiomyocytes, skeletal muscle cells and in living zebrafish [37, 38, 49, 53–56]. Live cell imaging of muscle cells transfected with truncated Z-band regions of titin demonstrated the importance of titin to myofibrillogenesis [57, 58]. We were able to use exposure of early myoblasts to different concentrations of ethyl methanesulfonate to arrest myofibrillogenesis at the premyofibril or nascent myofibril stage [55]. Removal of this inhibitor led to the resumption of the assembly process that resulted in mature myofibrils (Figure 1). The role of nonmuscle myosin II appears to be essential for the alignment of the thin filaments in the premyofibrils and nascent myofibrils [5, 6, 49]. Disruption of the formation of nonmuscle myosin II filaments with an inhibitor of the phosphorylation of the myosin light chains that are essential for the assembly of the filaments, leads to the loss of the premyofibrils and an unorganized array of myosin thick filaments [5]. Removal of the ML-7 inhibitor led to the reformation of premyofibrils and nascent myofibrils and the assembly of ordered arrays of thick filaments in the A-bands in the mature myofibrils [5].

How the overlapping thick filaments composed of muscle myosin II hexamers in the nascent myofibrils become aligned into A-bands of mature myofibrils is not clear. Titin, M-band proteins, and other proteins like obscurin have been proposed to play roles in this process [59–62]. There are myofibrils that lack M-bands and yet their A-Bands are fully aligned. Lange et al. [63] have recently reported that A-Bands and myofibrils are formed normally in obscuring knockout mice. They did find that the longitudinal arrays of the sarcoplasmic reticulum (SR) were changed, supporting a role for coupling the SR to the myofibril.

The premyofibril model (Figure 1) has not been accepted universally because it appears discordant with several published papers (see review by Sanger et al. [7]). In particular one of two reports from the Adelstein lab revealed that mice null for nonmuscle myosin IIB [64], if they survived to birth, had abnormal hearts and brains and died on the day of birth. Nevertheless, the abnormal hearts did contain normal

myofibrils suggesting that nonmuscle myosin IIB was not necessary for the formation of all myofibrils. Western gel studies in the few surviving animals, however, indicated that in half the surviving neonates, the myosin IIA isoform was upregulated, and thus the IIA isoform may have taken the place of the IIB isoform. Embryonic skeletal muscle cells have both isoforms of nonmuscle myosin IIA and IIB. Thus, the skeletal muscle cells were normal in these IIB knockouts, presumably due to the IIA being present. A recent paper by Lu et al. [34] reports that both isoforms of nonmuscle myosin IIs, A and B, are present in the early mouse hearts. In another paper the Adelstein group has reported that nonmuscle myosin II is a Z-band protein in both cardiac (IIB) and skeletal (A and B) muscle cells [65]. They also reported in the same paper that the IIB isoform was localized in the intercalated discs of fixed and stained cardiac muscle cells. Since these two studies from the Adelstein labs were published, a third isoform of nonmuscle myosin IIC has been discovered [32, 33]. This isoform is also present in the heart, skeletal muscles, and several organs. The role of nonmuscle myosin IIC in myofibrillogenesis has still to be explored. Our use of antibodies directed against nonmuscle II A or B in cardiac and skeletal muscle cells has never detected these antigens in either Z-bands or intercalated discs [5, 39, 40, 56]. Our preliminary results show that cardiac and skeletal muscle cells cotransfected with Cerulean Fluorescent Protein (CeFP) and one of the three isoforms of nonmuscle myosin IIs (Green Fluorescent Protein (GFP)-nonmuscle myosin II A or B or C), contradicting the results of Takeda et al. [65] paper. GFP-nonmuscle myosin IIs were not localized in the Z-bands of either type of muscle cells or in the intercalated discs of cardiac muscle cells. The three nonmuscle myosin II isoforms were localized in areas of the cells in linear arrays, in alternating arrays with z-bodies containing CeFP-alpha-actinin, that is, premyofibrils.

There are two other papers that have been cited as inconsistent with the premyofibril model of myofibrillogenesis. Ehler et al. [59] and Rudy et al. [66] reported their inability to detect the presence of premyofibrils or nascent myofibrils in either intact fixed embryonic avian hearts or precardiac mesoderm explants. However, improved fixation and immunofluorescent techniques lead to the detection of nonmuscle myosin II B in organized arrays in both types of preparations [5, 40] that were identical to the premyofibrils and nascent myofibrils originally reported in cultured embryonic cardiomyocytes [39]. Furthermore, Du et al. [5] were able to reversibly inhibit the assembly of mature myofibrils by the application of ML-7, an inhibitor of myosin light chain kinase, an enzyme that is responsible for the phosphorylation of the nonmuscle light chains, and a prerequisite for the ability of nonmuscle myosin IIs to form filaments. Removal of this inhibitor led to the reformation of the premyofibrils with their arrays of mini-A-bands of nonmuscle myosin II B and the resumption of myofibrillogenesis leading to the formation of mature myofibrils. All of these results support a common model for myofibrillogenesis in cardiomyocytes, whether in intact hearts, precardiac mesoderm explants, or in tissue culture as diagramed in Figure 1. The filaments of nonmuscle myosin

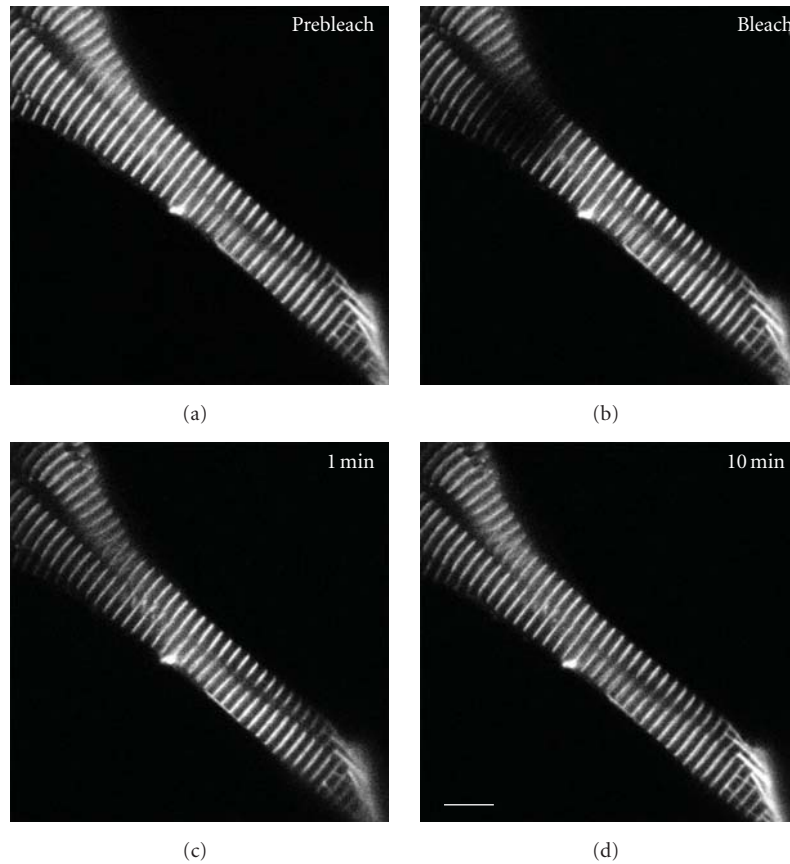


FIGURE 3: FRAP of YFP-myotilin in the Z-bands of mature myofibrils in two different muscle cells in a living zebrafish (three days old), prebleach, bleach, and 1 and 10 minutes after photobleaching. The recovery is almost complete by the end of the ten-minute period. Scale = 10 microns.

IIs may link the actin filaments attached to the z-bodies to form organized linear arrays we have termed premyofibrils [7, 39], the first step that leads to the formation of mature myofibrils (Figure 1).

3. Optical Techniques to Explore Myofibrillogenesis

Fluorescence microscopy of fluorescently tagged sarcomeric proteins (dye or GFP labels) has permitted myofibril assembly to be detected in living cardiac and skeletal muscle cells [37, 38, 49]. The technique of Fluorescence Recovery After Photobleaching (FRAP) has shown that superimposition on the addition of newly synthesized proteins to z-body and Z-band complexes is an active exchange between molecules in a cytoplasmic pool and the same species of molecule residing in z-bodies and Z-bands [46, 56, 67–69]. In general, the extent and half time of the exchange of fluorescent molecules analyzed with FRAP techniques are a function of the binding interaction of the protein in the cellular complex where it is concentrated, with shorter recovery times suggesting lower affinity [70]. Wang et al. [46] demonstrated that seven different Z-band proteins exchanged independently of each other

and that the exchange was independent of protein synthesis and molecular weight. Furthermore, the dynamics of the same proteins in z-bodies of premyofibrils were decreased in the Z-bands of the mature myofibrils. The decrease was suggested to be due to the incorporation of additional proteins into the forming of Z-band (Figure 1; [46]). These observations were extended to skeletal muscle cells in living zebrafish [56] where five different Z-bands were followed (actin, alpha-actinin, FATZ, myotilin, and telethonin). Their order of exchange was similar to the exchange of the same proteins in cultured quail skeletal muscle cells indicating that the behavior in culture conditions was comparable to that in cells in the live animal. Figures 3 and 4 are examples of this exchange process in the skeletal muscle cells along the flank of zebrafish using YFP-myotilin. The premyofibril model with its postulated three steps for the formation of myofibrils suggests mechanisms for the repositioning of molecules as premyofibrils are transformed into mature myofibrils over a period of several hours [7, 38]. The exchange of molecules into and out of the forming myofibrils would permit this transformation (Figure 1).

Although fluorescence microscopy is widely used for examining colocalization of proteins in cells, the resolution limit of visible light microscopy is on the order of 200 nm,

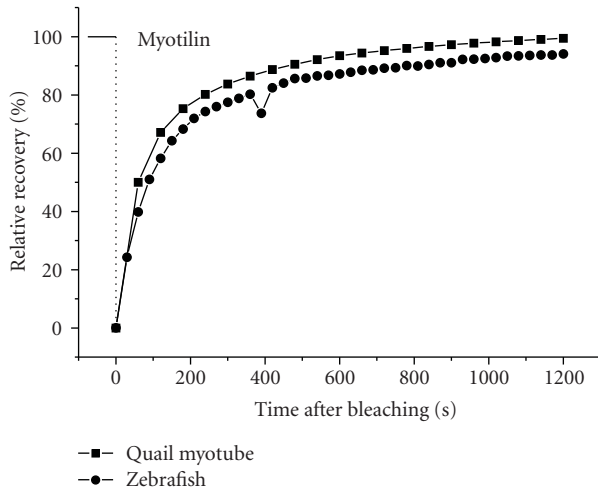


FIGURE 4: Comparison of the dynamics of YFP-myotilin after photobleaching in the Z-bands of mature myofibrils in skeletal muscle cells in tissue culture versus skeletal muscle cells along the flank of an embryonic zebrafish. Note the similarity of the recoveries of the same Z-band protein in the two different animals under two different conditions.

a distance much larger than the length scale of interprotein bonds. In the recent years, the technique of Fluorescence Resonance Energy Transfer (FRET) imaging has emerged as a way to improve upon the resolution of conventional light microscopy [10, 71]. FRET has been referred to as a “spectroscopic ruler” because it is possible, through application of the appropriate theory, to infer the distance between donor and acceptor from the resulting FRET signals in fixed and in living cells. Typically, measurable FRET signals result only when donor and acceptor are within ~ 10 nm of each other. As fluorescence imaging technology has advanced, there has been growing interest in using FRET to map inter- and intramolecular interactions in cells. Stout et al. [8] used FRET techniques on living skeletal muscle cells to demonstrate that there are rearrangements of alpha-actinin and FATZ molecules as z-bodies fuse and realign to form Z-bands. These FRET results supported the interpretations of FRAP experiments during myofibrillogenesis [46] and the premyofibril model (Figure 1). The current development of microscopes that break the diffraction limit of light [72] should reveal further insights into the disposition of protein networks in myofibrils and the changes they undergo in the processes of assembly and disassembly.

In summary, our goal is to understand how myofibrils are assembled, remodeled, and maintained (Figures 1 and 3). We are using wild type and mutated sarcomeric proteins to investigate the assembly (confocal and deconvolution microscopes), dynamics and remodeling (FRAP), and interactions (FRET) of the proteins in myofibrils in the living state. Standard biochemical binding assays will be used to support newly revealed FRET relationships detected in living muscle cells. We will also be able to test the idea that myofibrillogenesis shares both the same pathway and molecular sarcomeric interactions, whether the assembly

takes place in tissue culture or in a living animal like the zebrafish. In other words, we suggest that myofibrillogenesis is a fundamentally conserved process, comparable to protein synthesis, mitosis, or cytokinesis, whether examined *in situ* or *in vitro*.

Acknowledgment

This work was supported by NIH grants to Jean M. Sanger and Joseph W. Sanger.

References

- [1] D. M. Chapman, C. F. A. Pantin, and E. A. Robson, “Muscle in coelenterates,” *Revue Canadienne de Biologie*, vol. 21, pp. 267–278, 1962.
- [2] J. del Castillo, M. Anderson, and D. S. Smith, “Proventriculus of a marine annelid: muscle preparation with the longest recorded sarcomere,” *Proceedings of the National Academy of Sciences of the United States of America*, vol. 69, no. 7, pp. 1669–1672, 1972.
- [3] H. E. Huxley, “Electron microscope studies on the structure of natural and synthetic protein filaments from striated muscle,” *Journal of Molecular Biology*, vol. 7, pp. 281–308, 1963.
- [4] T. F. Robertson and S. Winegrad, “Variation of thin filament length in heart muscle,” *Nature*, vol. 267, pp. 74–75, 1977.
- [5] A. Du, J. M. Sanger, K. K. Linask, and J. W. Sanger, “Myofibrillogenesis in the first cardiomyocytes formed from isolated quail precardiac mesoderm,” *Developmental Biology*, vol. 257, no. 2, pp. 382–394, 2003.
- [6] J. W. Sanger, J. M. Sanger, and C. Franzini-Armstrong, “Assembly of the skeletal muscle cell,” in *Myology*, A. G. Engel and C. Franzini-Armstrong, Eds., pp. 45–65, McGraw-Hill, New York, NY, USA, 3rd edition, 2004.
- [7] J. W. Sanger, S. Kang, C. C. Siebrands, et al., “How to build a myofibril,” *Journal of Muscle Research and Cell Motility*, vol. 26, no. 6–8, pp. 343–354, 2005.
- [8] A. L. Stout, J. Wang, J. M. Sanger, and J. W. Sanger, “Tracking changes in Z-band organization during myofibrillogenesis with FRET imaging,” *Cell Motility and the Cytoskeleton*, vol. 65, no. 5, pp. 353–367, 2008.
- [9] S. Morimoto, “Sarcomeric proteins and inherited cardiomyocytes,” *Cardiovascular Research*, vol. 77, pp. 659–666, 2008.
- [10] D. W. Piston and G.-J. Kremers, “Fluorescent protein FRET: the good, the bad and the ugly,” *Trends in Biochemical Sciences*, vol. 32, no. 9, pp. 407–414, 2007.
- [11] K. A. Clark, A. S. McElhinny, M. C. Beckerle, and C. C. Gregorio, “Striated muscle cytoarchitecture: an intricate web of form and function,” *Annual Review of Cell and Developmental Biology*, vol. 18, pp. 637–706, 2002.
- [12] J. M. Sanger and J. W. Sanger, “The dynamic Z bands of striated muscle cells,” *Science Signaling*, vol. 1, no. 32, article pe37, 2008.
- [13] S. Y. Boateng and P. H. Goldspink, “Assembly and maintenance of the sarcomere night and day,” *Cardiovascular Research*, vol. 77, no. 4, pp. 667–675, 2008.
- [14] B. A. Danowski, K. Imanaka-Yoshida, J. M. Sanger, and J. W. Sanger, “Costameres are sites of force transmission to the substratum in adult rat cardiomyocytes,” *Journal of Cell Biology*, vol. 118, no. 6, pp. 1411–1420, 1992.

- [15] J. M. Ervasti, "Costameres: the Achilles' heel of Herculean muscle," *Journal of Biological Chemistry*, vol. 278, no. 16, pp. 13591–13594, 2003.
- [16] D. Frank, C. Kuhn, H. A. Katus, and N. Frey, "The sarcomeric Z-disc: a nodal point in signaling and disease," *Journal of Molecular Medicine*, vol. 84, pp. 446–468, 2006.
- [17] S. Lange, E. Ehler, and M. Gautel, "From A to Z and back? Multicompartment proteins in the sarcomere," *Trends in Cell Biology*, vol. 16, no. 1, pp. 11–18, 2006.
- [18] A. G. Engel and B. Q. Banker, "Ultrastructural changes in diseased muscle," in *Myology*, A. G. Engel and C. Franzini-Armstrong, Eds., pp. 749–887, McGraw-Hill, New York, NY, USA, 3rd edition, 2004.
- [19] M. Heidenhain, "Über die Entstehung der quergestreiften Muskelsubstanz bei der Forelle," *Archiv Mikroskopische Anatomie EntwMech*, vol. 83, pp. 427–522, 1913.
- [20] J. Auber, "La myofibrillogenese du muscle stile. I. Insectes," *Journal of Microscopy*, vol. 8, pp. 197–232, 1969.
- [21] J. Aronson, "Sarcomere size in developing muscles of a tarsonemid mite," *The Journal of Biophysical and Biochemical Cytology*, vol. 11, pp. 147–156, 1961.
- [22] E. Lazarides and K. Weber, "Actin antibody: the specific visualization of actin filaments in nonmuscle cells," *Proceedings of the National Academy of Sciences of the United States of America*, vol. 71, pp. 2268–2271, 1974.
- [23] J. W. Sanger, "Changing patterns of actin localization during cell division," *Proceedings of the National Academy of Sciences of the United States of America*, vol. 72, no. 5, pp. 1913–1916, 1975.
- [24] E. Lazarides and K. Burridge, "Alpha-actinin: immunofluorescent localization of a muscle structural protein in non-muscle cells," *Cell*, vol. 6, pp. 289–299, 1975.
- [25] K. Weber and U. Groeschel-Stewart, "Antibody to myosin: the specific visualization of myosin containing filaments in nonmuscle cells," *Proceedings of the National Academy of Sciences of the United States of America*, vol. 71, no. 11, pp. 4561–4564, 1974.
- [26] J. W. Sanger, J. M. Sanger, and B. M. Jockusch, "Differences in the stress fibers between fibroblasts and epithelial cells," *Journal of Cell Biology*, vol. 96, no. 4, pp. 961–969, 1983.
- [27] B. Mittal, J. M. Sanger, and J. W. Sanger, "Visualization of myosin in living cells," *Journal of Cell Biology*, vol. 105, no. 4, pp. 1753–1760, 1987.
- [28] B. Mittal, J. M. Sanger, and J. W. Sanger, "Binding and distribution of fluorescently labeled filamin in permeabilized and living cells," *Cell Motility and the Cytoskeleton*, vol. 8, no. 4, pp. 345–359, 1987.
- [29] R. R. Kulikowski and F. J. Manasek, "Myosin localization in cultured embryonic cardiac myocytes," in *Motility in Cell Function*, F. A. Pepe, J. W. Sanger, and V. T. Nachmias, Eds., pp. 433–435, Academic Press, New York, NY, USA, 1979.
- [30] J. R. Fallon and V. T. Nachmias, "Localization of cytoplasmic and skeletal myosins in developing muscle cells by double-label immunofluorescence," *Journal of Cell Biology*, vol. 87, no. 1, pp. 237–247, 1980.
- [31] A. A. Dlugosz, P. B. Antin, V. T. Nachmias, and H. Holtzer, "The relationship between stress fiber-like structures and nascent myofibrils in cultured cardiac myocytes," *Journal of Cell Biology*, vol. 99, no. 6, pp. 2268–2278, 1984.
- [32] A. Leal, S. Endeled, C. Stengel, et al., "A novel myosin heavy chain gene in human chromosome 19q13.3," *Gene*, vol. 312, no. 1–2, pp. 165–171, 2003.
- [33] E. Golomb, X. Ma, S. S. Jana, et al., "Identification and characterization of nonmuscle myosin II-C, a new member of the myosin II family," *Journal of Biological Chemistry*, vol. 279, no. 4, pp. 2800–2808, 2004.
- [34] W. Lu, S. H. Seeholzer, M. Han, et al., "Cellular nonmuscle myosins NMHC-IIA and NMHC-IIB and vertebrate heart looping," *Developmental Dynamics*, vol. 237, no. 12, pp. 3577–3590, 2008.
- [35] J. W. Sanger, B. Mittal, and J. M. Sanger, "Formation of myofibrils in spreading chick cardiac myocytes," *Cell Motility*, vol. 4, no. 6, pp. 405–416, 1984.
- [36] J. W. Sanger, B. Mittal, and J. M. Sanger, "Analysis of myofibrillar structure and assembly using fluorescently labeled contractile proteins," *Journal of Cell Biology*, vol. 98, no. 3, pp. 825–833, 1984.
- [37] J. M. Sanger, B. Mittal, M. B. Pochapin, and J. W. Sanger, "Myofibrillogenesis in living cells microinjected with fluorescently labeled alpha-actinin," *Journal of Cell Biology*, vol. 102, no. 6, pp. 2053–2066, 1986.
- [38] G. A. Dabiri, K. K. Turnacioglu, J. M. Sanger, and J. W. Sanger, "Myofibrillogenesis visualized in living embryonic cardiomyocytes," *Proceedings of the National Academy of Sciences of the United States of America*, vol. 94, no. 17, pp. 9493–9498, 1997.
- [39] D. Rhee, J. M. Sanger, and J. W. Sanger, "The premyofibril: evidence for its role in myofibrillogenesis," *Cell Motility and the Cytoskeleton*, vol. 28, no. 1, pp. 1–24, 1994.
- [40] A. Du, J. M. Sanger, and J. W. Sanger, "Cardiac myofibrillogenesis inside intact embryonic hearts," *Developmental Biology*, vol. 318, no. 2, pp. 236–246, 2008.
- [41] A. H. Conrad, W. A. Clark, and G. W. Conrad, "Subcellular compartmentalization of myosin isoforms in embryonic chick heart ventricle myocytes during cytokinesis," *Cell Motility and the Cytoskeleton*, vol. 19, no. 3, pp. 189–206, 1991.
- [42] A. H. Conrad, T. Jaffredo, and G. W. Conrad, "Differential localization of cytoplasmic myosin II isoforms a and B in avian interphase and dividing embryonic and immortalized cardiomyocytes and other cell types in vitro," *Cell Motility and the Cytoskeleton*, vol. 31, no. 2, pp. 93–112, 1995.
- [43] M.-H. Lu, C. DiLullo, T. Schultheiss, et al., "The vinculin/sarcomeric- α -actinin/ α -actin nexus in cultured cardiac myocytes," *Journal of Cell Biology*, vol. 117, no. 5, pp. 1007–1022, 1992.
- [44] H. Holtzer, T. Hijikata, Z. X. Lin, et al., "Independent assembly of 1.6 μ m long bipolar MHC filaments and I-Z-I bodies," *Cell Structure and Function*, vol. 22, no. 1, pp. 83–93, 1997.
- [45] S. M. Wang, M. L. Greaser, E. Schultz, J. C. Bulinski, J. J. Lin, and J. L. Lessard, "Studies on cardiac myofibrillogenesis with antibodies to titin, actin, tropomyosin, and myosin," *The Journal of Cell Biology*, vol. 107, pp. 1075–1083, 1988.
- [46] J. Wang, N. Shaner, B. Mittal, et al., "Dynamics of Z-band based proteins in developing skeletal muscle cells," *Cell Motility and the Cytoskeleton*, vol. 61, no. 1, pp. 34–48, 2005.
- [47] J. M. Sanger, B. Mittal, A. Wegner, B. M. Jockusch, and J. W. Sanger, "Differential response of stress fibers and myofibrils to gelsolin," *European Journal of Cell Biology*, vol. 43, no. 3, pp. 421–428, 1987.
- [48] J. M. Sanger, G. Dabiri, B. Mittal, M. A. Kowalski, J. G. Haddad, and J. W. Sanger, "Disruption of microfilament organization in living non-muscle cells by microinjection of vitamin-D binding protein or DNaseI," *Proceedings of the*

- National Academy of Sciences of the United States of America*, vol. 87, pp. 5474–5478, 1990.
- [49] J. Wang, J. M. Sanger, and J. W. Sanger, “Differential effects of Latrunculin-A on myofibrils in cultures of skeletal muscle cells: insights into mechanisms of myofibrillogenesis,” *Cell Motility and the Cytoskeleton*, vol. 62, no. 1, pp. 35–47, 2005.
- [50] J. M. Sanger and J. W. Sanger, “Banding and polarity of actin filaments in interphase and cleaving cells,” *Journal of Cell Biology*, vol. 86, no. 2, pp. 568–575, 1980.
- [51] S. M. LoRusso, D. Rhee, J. M. Sanger, and J. W. Sanger, “Premyofibrils in spreading adult cardiomyocytes in tissue culture: evidence for reexpression of the embryonic program for myofibrillogenesis in adult cells,” *Cell Motility and the Cytoskeleton*, vol. 37, no. 3, pp. 183–198, 1997.
- [52] J. M. Sanger, J. S. Dome, and J. W. Sanger, “Unusual cleavage furrows in vertebrate tissue culture cells: insights into the mechanisms of cytokinesis,” *Cell Motility and the Cytoskeleton*, vol. 39, no. 2, pp. 95–106, 1998.
- [53] J. M. Sanger and J. W. Sanger, “Assembly of cytoskeletal proteins into cleavage furrows of tissue culture cells,” *Microscopy Research and Technique*, vol. 49, no. 2, pp. 190–201, 2000.
- [54] J. W. Sanger and J. M. Sanger, “Green fluorescent proteins improve myofibril research,” *Biophotonics International*, vol. 8, no. 3, pp. 44–46, 2001.
- [55] M. L. Golson, J. M. Sanger, and J. W. Sanger, “Inhibitors arrest myofibrillogenesis in skeletal muscle cells at early stages of assembly,” *Cell Motility and the Cytoskeleton*, vol. 59, no. 1, pp. 1–16, 2004.
- [56] J. W. Sanger, J. Wang, B. Holloway, A. Du, and J. M. Sanger, “Myofibrillogenesis in skeletal muscle cells in zebrafish,” *Cell Motility and the Cytoskeleton*, vol. 66, no. 8, pp. 556–566, 2009.
- [57] K. K. Turnacioglu, B. Mittal, G. A. Dabiri, J. M. Sanger, and J. W. Sanger, “Zeugmatin is part of the Z-band targeting region of titin,” *Cell Structure and Function*, vol. 22, no. 1, pp. 73–82, 1997.
- [58] K. K. Turnacioglu, B. Mittal, G. A. Dabiri, J. M. Sanger, and J. W. Sanger, “An N-terminal fragment of titin coupled to green fluorescent protein localizes to the Z-bands in living muscle cells: overexpression leads to myofibril disassembly,” *Molecular Biology of the Cell*, vol. 8, no. 4, pp. 705–717, 1997.
- [59] E. Ehler, B. M. Rothen, S. P. Hämmerle, M. Komiyama, and J.-C. Perriard, “Myofibrillogenesis in the developing chicken heart: assembly of Z-disk, M-line and the thick filaments,” *Journal of Cell Science*, vol. 112, no. 10, pp. 1529–1539, 1999.
- [60] P. F. M. Van der Ven, J. W. Bartsch, M. Gautel, H. Jockusch, and D. O. Fürst, “A functional knock-out of titin results in defective myofibril assembly,” *Journal of Cell Science*, vol. 113, no. 8, pp. 1405–1414, 2000.
- [61] M. Gotthardt, R. E. Hammer, N. Hübner, et al., “Conditional expression of mutant M-line titins results in cardiomyopathy with altered sarcomere structure,” *Journal of Biological Chemistry*, vol. 278, no. 8, pp. 6059–6065, 2003.
- [62] A. Kontogianni-Konstantopoulos, D. H. Catino, J. C. Strong, and R. J. Bloch, “De novo myofibrillogenesis in C2C12 cells: evidence for the independent assembly of M bands and Z disks,” *American Journal of Physiology*, vol. 290, no. 2, pp. C626–C637, 2006.
- [63] S. Lange, K. Ouyang, G. Meyer, et al., “Obscurin determines the architecture of the longitudinal sarcoplasmic reticulum,” *Journal of Cell Science*, vol. 122, no. 15, pp. 2640–2650, 2009.
- [64] A. N. Tullio, D. Accili, V. J. Ferrans, et al., “Nonmuscle myosin II-B is required for normal development of the mouse heart,” *Proceedings of the National Academy of Sciences of the United States of America*, vol. 94, no. 23, pp. 12407–12412, 1997.
- [65] K. Takeda, Z.-X. Yu, S. Qian, T. K. Chin, R. S. Adelstein, and V. J. Ferrans, “Nonmuscle myosin II localizes to the Z-lines and intercalated discs of cardiac muscle and to the Z-lines of skeletal muscle,” *Cell Motility and the Cytoskeleton*, vol. 46, no. 1, pp. 59–68, 2000.
- [66] D. E. Rudy, T. A. Yatskievych, P. B. Antin, and C. C. Gregorio, “Assembly of thick, thin, and titin filaments in chick precordial explants,” *Developmental Dynamics*, vol. 221, no. 1, pp. 61–71, 2001.
- [67] N. M. McKenna, J. B. Meigs, and Y.-L. Wang, “Exchangeability of alpha-actinin in living cardiac fibroblasts and muscle cells,” *Journal of Cell Biology*, vol. 101, no. 6, pp. 2223–2232, 1985.
- [68] J. Wang, J. M. Sanger, S. Kang, et al., “Ectopic expression and dynamics of TPM1 α and TPM1 κ in myofibrils of avian myotubes,” *Cell Motility and the Cytoskeleton*, vol. 64, no. 10, pp. 767–776, 2007.
- [69] J. Wang, H. Thurston, E. Essandoh, et al., “Tropomyosin expression and dynamics in developing avian embryonic muscles,” *Cell Motility and the Cytoskeleton*, vol. 65, no. 5, pp. 379–392, 2008.
- [70] M. Vink, M. Simonetta, P. Transidico, et al., “In vitro FRAP identifies the minimal requirements for Mad2 kinetochore dynamics,” *Current Biology*, vol. 16, no. 8, pp. 755–766, 2006.
- [71] L. Stryer, “Fluorescence energy transfer as a spectroscopic ruler,” *Annual Review of Biochemistry*, vol. 47, pp. 819–846, 1978.
- [72] K. R. Chi, “Microscopy: ever-increasing resolution,” *Nature*, vol. 462, no. 7273, pp. 675–678, 2009.

Review Article

Sarcomere Control Mechanisms and the Dynamics of the Cardiac Cycle

R. John Solaro

Department of Physiology and Biophysics, Center for Cardiovascular Research, College of Medicine, University of Illinois at Chicago, 835 S. Wolcott Ave, Chicago, IL 60612, USA

Correspondence should be addressed to R. John Solaro, solarorj@uic.edu

Received 11 December 2009; Accepted 1 March 2010

Academic Editor: Aikaterini Kontrogianni-Konstantopoulos

Copyright © 2010 R. John Solaro. This is an open access article distributed under the Creative Commons Attribution License, which permits unrestricted use, distribution, and reproduction in any medium, provided the original work is properly cited.

This review focuses on recent developments in the molecular mechanisms by which Ca activates cardiac sarcomeres and how these mechanisms play out in the cardiac cycle. I emphasize the role of mechanisms intrinsic to the sarcomeres as significant determinants of systolic elastance and ventricular stiffening during ejection. Data are presented supporting the idea that processes intrinsic to the thin filaments may promote cooperative activation of the sarcomeres and be an important factor in maintaining and modifying systolic elastance. Application of these ideas to translational medicine and rationale drug design forms an important rationale for detailed understanding of these processes.

1. Introduction

One of the significant challenges to investigations of control mechanisms in cardiac contraction and relaxation is the understanding of the relation between the molecular and cellular biology of working ventricular myocytes and the dynamics of the heart beat. There is wide acceptance that the transition from diastole to systole requires electrochemical coupling involving a membrane controlled release of Ca^{2+} into the sarcoplasmic space [1]. The rise in intracellular Ca^{2+} induces chemomechanical coupling in which Ca-binding to cardiac troponin C (cTnC) triggers a series of protein-protein interactions releasing the thin filaments from inhibition and promoting a force generating interaction between myosin cross-bridges and actin. The rise in intracellular Ca is transient as highly effective processes actively transport the Ca^{2+} back into cellular storage depots within the sarcoplasmic reticulum or back to the extra-cellular space. Thus, chemomechanical uncoupling has generally been considered to occur by a fall in intracellular Ca^{2+} , release of Ca^{2+} from cTnC, waning of the actin-cross-bridge reaction, and a return of the myocytes to their diastolic state. In relating these molecular and cellular processes to the heart beat, there has been much focus on the idea that the

dynamics are determined largely by the amounts and rates of movements of Ca^{2+} to and from the sarcomeres. A natural and understandable extension of this idea is that variations in the amounts of Ca^{2+} released to the sarcomeres largely determine contractility.

However, this perspective ignores the significant role of processes intrinsic to the sarcomeric proteins as determinants of the dynamics of the heart beat and as a controlled variable determining contractility. Early studies demonstrated that switches in isoform population of the myosin heavy chain have significant effects on dynamics of the heart beat independent of altered Ca^{2+} fluxes. More recent studies have demonstrated that isoform switches, posttranslational modifications, and mutations in sarcomeric proteins may also affect cardiac dynamics apart from membrane controlled alterations in cellular Ca^{2+} fluxes [2, 3]. It is also significant that the emphasis on Ca^{2+} as the main determinant of altered contractility is based largely on studies with unloaded cardiac myocytes in which intracellular Ca-transients and shortening are determined. The critical question, however, is how do these molecular events relate in time to the heart beat in which pressure first develops with no change in volume then pressure is sustained while ejection is ongoing and volume is decreasing, and finally pressure falls

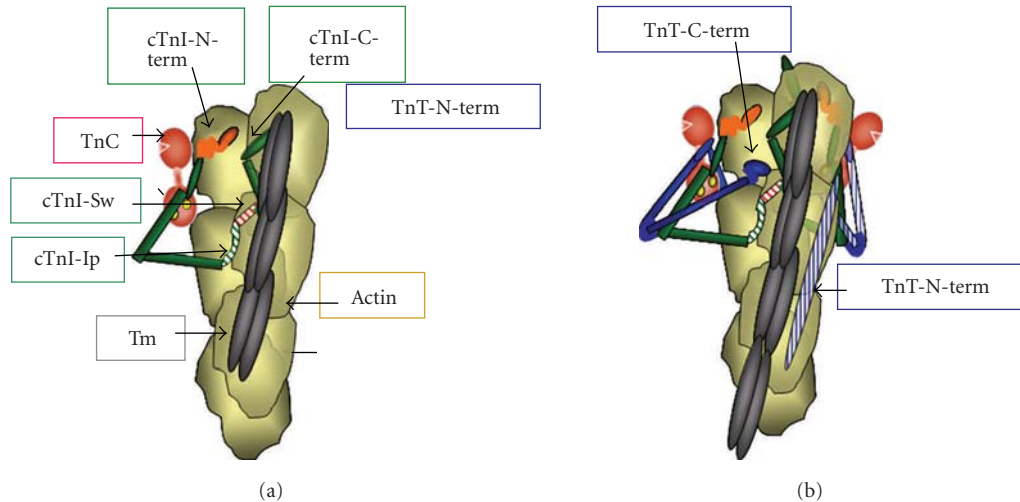


FIGURE 1: Structure of a patch of cardiac thin filament demonstrating the position of troponin components with tropomyosin (Tm) in the “off” state. (a) Thin filament containing, only troponin I (cTnI) and troponin C (cTnC). cTnC is shown as a dumbbell shaped protein with the N-lobe containing a single regulatory Ca-binding site. cTnI is shown tethered to actin on an actin strand by an inhibitory peptide (Ip) and a second actin binding region flanking a switch peptide (Sw), which interacts with cTnC upon Ca-activation. The distal C-terminal end of cTnI drapes across azimuthal actins and may interact with Tm. cTnI has a unique stretch of N-terminal amino acids, which contain phosphorylation sites at S23, S24. The N-peptide interacts with the N-lobe of cTnC, but is released upon phosphorylation and may react with the Sw or Ip of cTnI. (b) Thin filament contains the complete Tn complex. Note that the Ip of cTnI binds to one actin strand, whereas the N-terminal tail of troponin T (cTnT) interacts with Tm on the adjacent actin strand. The consequence is that Tm is wedged and held in a blocking position.

with no change in volume. What we need to know is how do the Ca^{2+} transients change in an ejecting beat, where is the Ca^{2+} bound during this time, and how does free and bound Ca^{2+} change with physiological, pathophysiological, and pharmacological manipulations of cardiac function. We need to fully integrate processes upstream and downstream to Ca-binding to cTnC and to know their relative significance in these manipulations.

In the present review, I focus on the molecular and cellular events in the ventricular heart beat that occur after Ca^{2+} binds to cTnC and induce conformational changes in the thin and the state of the thin and thick filaments after Ca^{2+} is released from cTnC. I discuss a current view of the molecular interactions among sarcomeric proteins responsible for the transition from diastole to systole and potential mechanisms by which activation of the actin-cross reaction may be sustained by cooperative processes in sarcomeric activation. I also present recent developments supporting the hypothesis that sarcomeric proteins are effective targets for inotropic agents useful in cardiac disorders including heart failure.

2. Promotion of the Actin-Cross-Bridge Reaction by On-Off Control of the Troponin Ca-Switch

Ca-binding to cTnC engages a remarkable and complex set of protein-protein interactions that result in the release of the thin filament from an inhibited state and in a force generating interaction between the myosin cross-bridge and

actin. These interactions provide many potential control points for regulation of the sensitivity and steepness of the response to Ca^{2+} , as well as force, ATPase rate, and cross-bridge kinetics at a given level of bound Ca^{2+} . Recent studies [4–7] continue to illuminate these interactions and provide new perspectives.

Figure 1 illustrates a portion of a structural unit of the thin filament (7 actins in 1:1:1:1 complex with tropomyosin (Tm), troponin C (cTnC), troponin I (cTnI), and troponin T (cTnT)). Figure 1 includes a current perception of these interactions based on evidence from the core crystal structure of cardiac troponin (Tn) [8], from elucidation of the structures by NMR [9], from biochemical investigations of protein-protein interactions [10–12], and from reconstructions and single particle analysis from electron micrographs of reconstituted myofilament preparations [5]. To clarify the relatively recent updates and new concepts in the structure functions relations, Figure 1 (a) shows only the cTnI and cTnC (with Ca^{2+} -bound to two C-terminal lobe structural sites) components binding to an actin-tropomyosin strand in the thin filament. Figure 1 (b) adds cTnT and illustrates new data demonstrating that the N-terminal tail of cTnT binds to an actin strand opposite to that to which cTnI-cTnC binds. Figure 1(a) depicts cTnI and cTnC in the thin filament based on the core crystal structure of cTn. The crystal structure did not resolve significant regions including an inhibitory peptide (Ip), which tethers cTnI to actin, and the unique N-terminal peptide (~30 amino acids). The structure of these regions is based on biochemical evidence including determination of protein-protein interactions, fluorescence energy transfer, and NMR solution structure determination

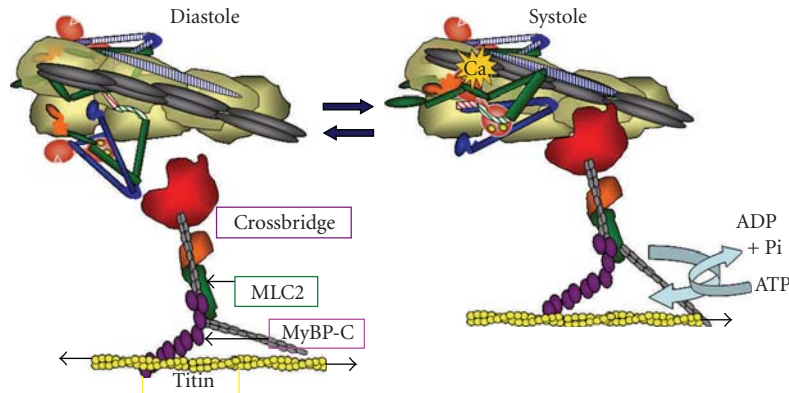


FIGURE 2: Alterations in thin filament structure and promotion of the actin-cross-bridge reaction induced by Ca^{2+} -binding to cTnC. The left panel shows the diastolic state as in Figures 1 and 2. The right panel shows the systolic state and illustrates the release of cTnI from actin and binding of the switch peptide to cTnC most likely at a hydrophobic patch induced by Ca^{2+} -binding to the N-lobe of cTnC. cTnI from the Tn complex on the adjacent actin strand is shown with stripes. Activation is associated with release of Tm from an immobilized state by protein signaling to cTnT and possible release of Tm from an interaction with the C-terminal end of cTnI. See text for further description.

(reviewed in [10]). Figure 1(a) illustrates an off state with binding of cTnI to actin via two regions, a highly basic inhibitory peptide (Ip) and a second actin binding region. Importantly these regions flank a “switch peptide.” New data provide evidence for a role of the cTnI C-terminal mobile domain in the off state. This C-terminal domain has been demonstrated to bind to azimuthally localized actins with the far cTnI C-terminus lying across Tm [4]. Direct biochemical evidence for an interaction between this region of TnI and Tm has been reported by Mudalige et al. [13], who employed photochemical cross-linking studies with Tm labeled at positions 146 or 174. Their data indicate a cross-linking of Tm-146 with fast skeletal TnI (fsTnI) peptide 157-163 (DVGDWWRK), which corresponds to a nearly identical C-terminal peptide in the cTnI (EVGDWWRK). Importantly this study also demonstrated that the cross-linking between Tm and fsTnI occurred only under low Ca^{2+} conditions, whereas cross-linking of Tm-174 to TnT was not Ca^{2+} -dependent. This interaction may be critical to control of thin filament activation state and provides a mechanism for earlier observations indicating a significant role for the far C-terminal peptide of cTnI [14, 15] in thin filament activation. Figure 1(b) illustrates the position of cTnT in the thin filament complex with the C-terminal regions interacting together with the near N-terminal region of cTnI and the C-terminal lobe of cTnC. cTnT is the main anchor site of the Tn complex to Tm. Sites of interaction occur between N-terminal regions of cTnT and Tm-175-190 and Tm-258-284 [10, 11, 16]. Figure 1(b) shows a new concept of the interaction of cTnT with the thin filament based on predictions reported by Galinska-Rakoczy et al. [4]. This study predicted that the N-terminal extension of cTnT binds to the strand of actins opposite to that binding the main core Tn complex. Thus, as described [4] and illustrated in Figures 1 and 2, Tm is wedged in the blocking position between the cTnI mobile domain on one side and the troponin core domain and TnT on the

other. Thus the off state of the thin filament involves an immobilized Tm blocking the actin cross-bridge reaction. Immobilization of Tm involves anchoring of cTnI to actin as well as interactions between the N-terminal tail of TnT with Tm and possibly the C-terminal mobile domain of cTnI with Tm.

Figure 2 shows the transition in myofilament state with Ca^{2+} binding to cTnC. With its release into the intracellular space, Ca^{2+} binds to cTnC at a single site in the N-lobe and promotes the “on” state by inducing the generation of a hydrophobic patch, which draws the cTnI switch peptide to cTnC. This critical event in the on-off switching mechanisms releases the thin filament from inhibition by movements of the Ip and second actin binding site of cTnI from actin. The Ca^{2+} -binding signal also induces a release of TnT from its interaction from Tm. These Ca^{2+} -induced alterations in thin filament protein-protein interactions result in transition of Tm from a relatively immobilized state to a mobile state permitting the reaction of cross-bridges with actin. The propensity of interaction of the cross-bridges with actin is also governed by the relative radial position of the cross-bridge with respect to the thick filament proper. As discussed below there is compelling evidence that regulatory mechanisms control this radial movement of cross-bridges. These regulatory mechanisms involve thick filament associated proteins, myosin light chain 2 (MLC2) [17], myosin binding protein C (MyBPC) [18], and titin [19].

3. Modulation of the Troponin Ca^{2+} Switch

To illustrate modulation of the Ca^{2+} switch I discuss phosphorylation of cTnI. A major region of phosphorylation is the cTnI-N-terminal peptide, which is unique to the cardiac isoform. I have reviewed the multiple kinases controlling sarcomeric protein phosphorylation elsewhere

[12]. Figure 1(a) indicates an interaction of the N-terminus of cTnI, which contains 2 prominent phosphorylation sites, which are substrates for PKA, PKG, PKD, and PKC- δ [12]. As discussed below this interaction is an important determinant of the affinity the cTnC N-lobe for Ca^{2+} . Figure 1 also shows interactions of the unique N-terminal peptide of cTnI with the N-lobe of cTnC. This interaction is strong when the N-peptide is not phosphorylated at Ser 23, Ser 24, but with phosphorylation at these sites the N-peptide is released from cTnC [20]. The release of the peptide induces a significant depression in Ca-affinity of cTnC [21] and appears to promote an increase in kinetics of the actin-cross bridge reaction [22, 23]. These effects together with adrenergic control of Ca fluxes are important aspects of the tuning of the contraction relaxation cycle of the heart to alterations in heart rate. On the basis of NMR determination of the solution structure on the N-peptide of cTnI, we hypothesized that this peptide, which has negatively charged residues, might interact with the positively charged regions of the cTnI Ip [9, 24]. We tested this possibility employing a hetero-bifunctional cross linker linked to a Cys residue engineered into position 5 of cTnI normally containing Ser 5 and into position 19 normally containing an Iso residue [24]. Our data demonstrated an intermolecular interaction with positions Met-47 and Met-80 of cTnC and an intramolecular interaction between the N-peptide of cTnI and cTnI at Met-154 (I19C mutant) and Met-155 (S5C mutant). Met 154 and Met 155 are residues located in the cTnI switch peptide, and thus we hypothesized that this interaction may be a critical regulatory device and dependent on the charge state of the cTnI N-peptide. The hypothesis needs to be further tested by experiments employing other probes of conformation changes such as fluorescence resonance energy transfer and electron spin resonance. Other prominent and unique sites of phosphorylation of cTnI are Thr 144 in the Ip and Ser 43, Ser 45 in a near N-terminal region of cTnI, which interacts with the C-lobe of cTnC and C-terminal regions of cTnT [10, 12]. Phosphorylation of Thr 144 has been demonstrated to either enhance Ca^{2+} sensitivity or have little effect, whereas phosphorylation of Ser 43/Ser 45 has been reported to depress maximum tension and Ca^{2+} sensitivity of skinned fiber preparations. Phosphorylation of these sites has also been reported to slow down velocity of thin filament sliding in the motility assay, whereas phosphorylation of cTnI Ser 23/Ser 24 enhances sliding velocity [10].

4. The Time Course of Systolic Elastance and Rates of Isovolumic Relaxation Reflect Mechanisms at the Level of Sarcomeric Proteins

Relating the molecular mechanisms summarized in Figures 1 and 2 to the cardiac cycle especially in large animals remains a significant challenge, which is critical in translational studies. Figure 3 illustrates the cardiac cycle simply by the time course of the change in left ventricular pressure during an ejecting beat in basal conditions in a dog heart. The time course

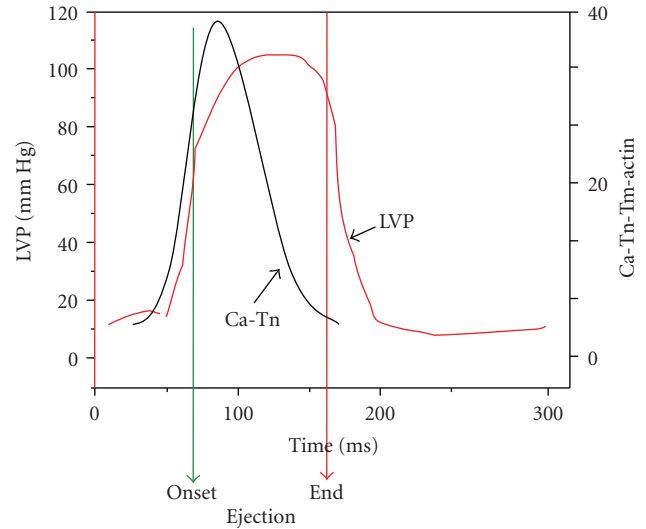


FIGURE 3: Relation between left ventricular pressure changes during the cardiac cycle and Ca^{2+} -binding to cTnC in the myofilament lattice. The onset and end of ejection are indicated. Note that pressure (systolic stiffening or elastance) is maintained despite the fall in bound Ca^{2+} . The Ca^{2+} binding kinetics are based on computations described Burkhoff and colleagues [25, 26]. See text for further discussion.

of the beat serves to constrain theories relating the cellular and molecular mechanisms of contraction and relaxation. Studies employing hearts loaded with Ca-sensitive dyes such as Rhod 2 and use of fiber optic directed excitation, and emission measurements have been carried out to determine the time course of cellular Ca^{2+} transients in a heartbeat [27, 28]. However, these studies have employed isovolumic rodent hearts. It is not clear therefore how the time course of the Ca^{2+} transient relates to the time course of systolic elastance in a beating ventricle. Even so, studies of Ca^{2+} transients and isometric force generation reveal that the duration of the Ca^{2+} transient is faster than the duration of force development [25, 29]. The critical dynamic is the time course of Ca^{2+} -binding to cTnC during a beat of the heart. Unfortunately, we do not have measurements of the amounts of Ca^{2+} bound to the myofilaments during the heart beat. Early and more recent studies have demonstrated that the only site capable of exchanging Ca^{2+} during the beat is the single regulatory binding site on the N-lobe of cTnC (Figure 2). As illustrated in Figure 3, indirect estimations [30] and computations [25, 26] based on rate constants of Ca^{2+} exchange with cTnC indicate that, as expected, the Ca-binding increases with the transition from diastole to systole, but these same computations also indicate that cTnC bound Ca may decrease significantly during maintenance of systolic elastance and ahead of isovolumic relaxation. The data illustrated in Figure 3 have important consequences with regard to our understanding of physiological control of ejection, its modification in cardiac disorders, and in approaches to alterations in sarcomeric function by drug targeting. Moreover if Ca^{2+} -binding and the Ca^{2+} -transient are essentially over at the end of ejection and closure

of the atrioventricular valves this means that isovolumic relaxation and re-establishment of the diastolic state depends on mechanisms intrinsic to the myofilaments. Hinken and Solaro [3] have previously discussed this disparity and potential mechanisms by which systolic elastance might be maintained in the face of a declining Ca^{2+} transient and cTnC bound Ca^{2+} . The mechanisms involve a cooperative activation of the thin filaments in which Ca^{2+} binding to a cTnC on the thin filament promotes activation of near neighbor units. However, recent evidence has provided highly relevant and new perspectives on the cooperative processes, and on the modifications in the myofilaments that may modulate elastance [4–7]. These control processes intrinsic to the myofilaments are also of significance in preload (sarcomere length) sensing and engagement of immediate responses in terms of the Frank-Starling relations. Intrinsic myofilament mechanisms also are important in sensing the load in a negative feedback mechanism related to the force-velocity relation and in power generation [31, 32], and also in the relaxation kinetics related to rates of cross-bridge detachment and intersarcomere dynamics (as described by Pogessi et al. [33]).

5. Thin and Thick Filament Mechanisms Related to Maintenance of Systolic Elastance

Cooperative activation of cardiac myofilaments has long been appreciated as a significance aspect of control of cardiac function including diastolic filling, the triggering and sustaining of developed pressure, and the dynamics of relaxation [10, 34]. Strong evidence for this cooperativity comes from measurements of the steady-state relation between free Ca^{2+} and force generation in detergent extracted single myocytes or bundles of myocytes. Despite control of activation by a single regulatory site on cTnC, the force- Ca^{2+} relations are steep and are commonly fit with Hill coefficients in the range of 3–5 [35]. Moreover as mentioned above in presteady state measurements of the relation between the duration force generation in fiber preparations, the dynamics of the Ca^{2+} transient show that the decline of the Ca^{2+} transient occurs well ahead of the Ca^{2+} -transient.

Interactions among proteins within a functional unit and among the functional units of the sarcomere form the basis of the most prominent theories for the mechanism of the steep dependence of force on Ca^{2+} . These interactions are illustrated in Figure 4. What promotes these interactions is under current debate. Detailed balance drives one of the theories in which the energies of interaction between cTnC and the actin-myosin interface flows in both directions. That is, the promotion of the actin-myosin interaction by Ca^{2+} signaling through cTnC in turn promotes Ca^{2+} binding to cTnC [10, 16, 34]. For example, in steady-state measurements of the Ca^{2+} -force relation in skinned fibers, as more force generating cross-bridges react with the thin filament with increases in Ca^{2+} , this theory predicts an increase in the affinity of cTnC also increases. Longitudinal spread of activation along the thin filament forms the basis for a second theory. The mechanism for

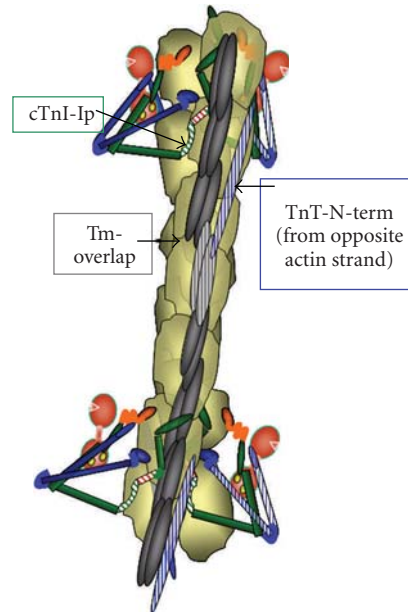


FIGURE 4: View of an extended region of a functional unit of the thin filament illustrating the position of the Tn complexes and the possible interactions among contiguous functional units. Cooperative spread of activation of one region of the thin filament may occur by actin-actin interactions or by spread via Tm overlap. Color coding of proteins as in Figure 2.

the longitudinal spread remains a matter of debate. There are data demonstrating that strongly bound (rigor) cross-bridges are able to move Tm away from the cross-bridge binding sites on actin and closer to the groove in the actin helix [5]. Contiguous Tms overlap forming a continuous molecular strand believed to sensitive to this cross-bridge induced movement of Tm (Figure 4). Thus, in this theory activation spreads to a near neighbor functional unit without the need for Ca^{2+} binding to the cTnC in that unit. One of the issues with the theories described above is that they are based on measurements of Ca^{2+} -binding and spread of activation in which nucleotide free (rigor) cross-bridges or cross-bridges modified with NEM are used as a surrogate for the strongly interacting and force generating cross-bridge. These cross-bridges strongly react with the thin filament but do not cycle and generate tension. Recent direct tests have failed to demonstrate that force generating, cycling cross-bridges promote molecular modifications in the thin filament in the same way as to rigor cross-bridges. One set of studies involved measurements of Ca^{2+} binding to the regulatory site of cTnC in reconstituted thin filaments alone or reacting with nucleotide-containing or nucleotide free cross-bridges in the form of myosin-S1[36]. The data are summarized in Table 1. A significant findings in these data are that Ca^{2+} binding to the single regulatory site is cooperative ($nH = 1.65$) in the presence and absence of nucleotide bound myosin S-1. Moreover, reaction of the thin filaments with nucleotide-free S-1 increased Ca^{2+} -affinity as predicted from previous studies, with a significant decrease in cooperativity ($nH = 0.85$). These data indicate that

TABLE 1: Strong binding rigor cross-bridges but no cycling cross-bridges affect Ca-binding to troponin C in reconstituted myofilament preparations. Data are from Davis et al. [36].

System	Kd nM	Hill n	Koff(/s)
Thin Filament	4810 \pm 300	1.65 \pm 0.04	105 + 1
Thin Filament + S1	777 \pm 30	0.81 \pm 0.02	13 \pm .1
Thin Filament + S1 + ATP	5040 \pm 400	1.65 \pm 0.08	110 \pm 1

cooperative activation of myofilaments relies on mechanisms intrinsic to the thin filaments. Studies probing thin filament activation by use of fluorescent probes at specific sites on cTnC support this concept [6, 7]. cTnC labeled with probes sensing the “on” state and incorporated into skinned fiber preparations, tracked the Ca²⁺-force relation and show a similar cooperative response. The relation between the “on” states of cTnC remained the same when the cross-bridge interactions were completely blocked with blebbistatin. Thus these results indicate that the promotion of near-neighbor interactions along the thin filament do not require force generating cross-bridges. These results alter thinking with regard to the relative roles of cycling and rigor cross-bridges. There may be some effects of cycling cross-bridges on cooperative activation of the thin that are more apparent in presteady state measurements, but evidence of the relative low numbers of interacting cross-bridges during contractions suggests that this would be a minor influence. On the other hand in conditions of compromised generation of ATP and the elaboration of nucleotide free cross-bridges, there would be an influence on activation. Thus, the current evidence does not dismiss effects of rigor cross-bridges on myofilament activation, but relegates this mechanism to a patho-physiological role as in ischemia and cardiomyopathies rather than in physiological control mechanisms.

6. Signaling to Cardiac Sarcomeres and Control of Cooperative Activation

Modifications in thin filament proteins appear to affect cooperative spread of activation induced by force generating and rigor cross-bridges. Cross-bridge dependent thin filament activation depends on the isoform population of TnI. In myofilaments regulated by slow skeletal TnI (ssTnI), the ability of rigor and NEM-modified cross-bridges to activate force generation in the absence of Ca²⁺ was less than in the case of myofilaments controlled by cTnI [37]. This difference was particularly evident at acidic pH and evidence was developed to implicate a role. His residue at position 34 in ssTnI. When His-34 was replaced by Ala, which is the residue at the homologous position (Ala-66) in cTnI, activation by rigor cross-bridges was similar to that of myofilaments controlled by cTnI. These findings led us to compare cross-bridge dependent activation in cardiac myofilaments controlled either by wild type cTnI or by cTnI-A66H. When pH was reduced from pH 7.0 to pH 6.5, there was enhanced cross-bridge-dependent activation

in cTnI myofilaments, but depressed activation in cTnI (A66H) myofilaments. These data may be of significance in our finding that compared to wild-type controls that adult hearts expressing ssTnI demonstrate protection against the stress of ischemia and reperfusion, where rigor cross-bridges are likely to be present [38]. In view of evidence that ischemia is associated with activation of protein kinase C (PKC), Engel et al. [39] also compared the ability of NEM-S1, a mimic of rigor cross-bridges to activate control cardiac myofilaments regulated by cTnI and myofilaments controlled by cTn complex containing either cTnI-(S43E/S45E) or cTnI-(T144E). These pseudo-phosphorylated sites are predominant PKC sites in Tn. Our data show that compared to controls, the myofilaments controlled by cTnI-(S43E/S45E) demonstrated a significant reduction in the ability of NEM-S1 to recruit cycling cross-bridges. Pseudo-phosphorylation of cTnI-(T144) had similar but less extensive effect. The functional significance of the modifications in Tn may be important in sparing energy consumption in ischemia.

Studies with transgenic models expressing cardiac specific and pseudo-phosphorylated mutants of cTnI (cTnI-S43E, S45E, T144E) also provide evidence of the significance of potential thin filament related cooperative mechanism [40]. In these studies extensive two-dimensional gel analysis demonstrated replacement of the endogenous cTnI with only 7.2 \pm 0.5% of the mutant. Even with this modest increase in PKC-dependent phosphorylation, data from studies with perfused hearts, and intact and skinned myocardial preparations showed an induction of highly significant depressions in pressure and force generation with no change in Ca²⁺ transients. There were also significant depressions in relaxation rates. Mathematical modeling revealed that these effects are likely to be induced by a simultaneous reduction in the rate of cross-bridge entry into the force generating state, and by an increase in Ca²⁺ -independent persistence of the myofilament active state. Whatever the case, these data indicate that the small number of modified TnI proteins in the hearts of the transgenic mice expressing the mutant protein must be able to influence their neighbors on the thin filament. Effects of the expression of the pseudo-phosphorylated cTnI on systolic elastance and isovolumic relaxation have not as yet been carried out.

Modifications in thick filament proteins especially MyBP-C and MLC2 appear especially important in affecting systolic elastance. In comparing various transgenic models Palmer et al. [41] reported that only the hearts of the cMyPP-C t/t mice demonstrated a significant change in stiffening during ejection. Whereas the controls reached 42% of maximum elastance at the onset of ejection, the t/t mutant hearts reached 77% of peak elastance. Moreover, elastance peaked earlier and was abbreviated in hearts of the cMyBP-C t/t mice compared to controls. Thus these data indicate that normal cardiac function and duration of systolic elastance rely on the integrity of MyBP-C. Scruggs et al. [17] have also generated evidence indicating the phosphorylation of MLC2 may be an important factor in determining the duration of systolic elastance. The states of both MyBP-C and MLC2 are likely to be important factors in determining radial disposition of the heads of myosin.

7. Sarcomeric Proteins as Targets for Inotropic Agents

Potential application to rational drug design is a significant aspect of the understanding of the relations between cellular and molecular mechanisms at the level of the sarcomeres. There has been a long standing effort to develop agents that directly modify the sarcomere response to Ca^{2+} with some success (see [42, 43] for reviews). Levosimendan and pimobendan are examples of such agents, which progressed into clinical use, and which are able to promote sarcomere responsiveness to Ca^{2+} and demonstrate some therapeutic benefits in acute and chronic heart failure. However, these agents have off target effects and there is a need for agents or approaches with more specific targeting to the sarcomeres [42]. For example, both Levosimendan and Pimobendan have been demonstrated to inhibit phosphor-diesterase III in addition to directly affecting Ca^{2+} -signaling to TnC. The identification of the molecular processes involved in maintenance of systolic elastance and as determinants of isovolumic relaxation provides clues as to the location of these targets. A recent apparent success in the search for sarcomere activators has been the identification of a compound developed by Cytokinetics, Inc (CK-1827452) directly reacting with myosin and prolonging systolic elastance (reviewed in [44]). Evidence for factors maintaining systolic elastance summarized is thus significant in translational medicine, as these results with CK indicate that modification of systolic elastance is a viable pharmacological target. Modification of Tn, MLC2, MyBP-C or titin by drugs may also be an important road to success, but has not been explicitly investigated.

Acknowledgments

I am grateful to many colleagues for valuable interactions. Support from NIH grants PO1 HL 62426, RO1 HL 22231, and RO1 HL 64035 provide the bulk of support for experiments from our laboratory.

References

- [1] D. M. Bers, "Calcium fluxes involved in control of cardiac myocyte contraction," *Circulation Research*, vol. 87, no. 4, pp. 275–281, 2000.
- [2] R. J. Solaro and P. P. de Tombe, "Review focus series: sarcomeric proteins as key elements in integrated control of cardiac function," *Cardiovascular Research*, vol. 77, no. 4, pp. 616–618, 2008.
- [3] A. C. Hinken and R. J. Solaro, "A dominant role of cardiac molecular motors in the intrinsic regulation of ventricular ejection and relaxation," *Physiology*, vol. 22, no. 2, pp. 73–80, 2007.
- [4] A. Galińska-Rakoczy, P. Engel, C. Xu, et al., "Structural basis for the regulation of muscle contraction by troponin and tropomyosin," *Journal of Molecular Biology*, vol. 379, no. 5, pp. 929–935, 2008.
- [5] W. Lehman, A. Galińska-Rakoczy, V. Hatch, L. S. Tobacman, and R. Craig, "Structural basis for the activation of muscle contraction by troponin and tropomyosin," *Journal of Molecular Biology*, vol. 388, no. 4, pp. 673–681, 2009.
- [6] R. J. Solaro, "Maintaining cooperation among cardiac myofilament proteins through thick and thin," *The Journal of Physiology*, vol. 587, no. 1, article 3, 2009.
- [7] Y.-B. Sun, F. Lou, and M. Irving, "Calcium- and myosin-dependent changes in troponin structure during activation of heart muscle," *The Journal of Physiology*, vol. 587, no. 1, pp. 155–163, 2009.
- [8] S. Takeda, A. Yamashita, K. Maeda, and Y. Maéda, "Structure of the core domain of human cardiac troponin in the Ca^{2+} -saturated form," *Nature*, vol. 424, no. 6944, pp. 35–41, 2003.
- [9] J. W. Howarth, J. Meller, R. J. Solaro, J. Trehwella, and P. R. Rosevear, "Phosphorylation-dependent conformational transition of the cardiac specific N-extension of troponin I in cardiac troponin," *Journal of Molecular Biology*, vol. 373, no. 3, pp. 706–722, 2007.
- [10] T. Kobayashi and R. J. Solaro, "Calcium, thin filaments, and the integrative biology of cardiac contractility," *Annual Review of Physiology*, vol. 67, pp. 39–67, 2005.
- [11] L. S. Tobacman, "Thin filament-mediated regulation of cardiac contraction," *Annual Review of Physiology*, vol. 58, pp. 447–481, 1996.
- [12] R. J. Solaro, "Multiplex kinase signaling modifies cardiac function at the level of sarcomeric proteins," *Journal of Biological Chemistry*, vol. 283, no. 40, pp. 26829–26833, 2008.
- [13] W. A. K. A. Mudalige, T. C. Tao, and S. S. Lehrer, " Ca^{2+} -dependent photocrosslinking of tropomyosin residue 146 to residues 157–163 in the C-terminal domain of troponin I in reconstituted skeletal muscle thin filaments," *Journal of Molecular Biology*, vol. 389, no. 3, pp. 575–583, 2009.
- [14] D. B. Foster, T. Noguchi, P. VanBuren, A. M. Murphy, and J. E. Van Eyk, "C-terminal truncation of cardiac troponin I causes divergent effects on ATPase and force: implications for the pathophysiology of myocardial stunning," *Circulation Research*, vol. 93, no. 10, pp. 917–924, 2003.
- [15] H. M. Rarick, X.-H. Tu, R. J. Solaro, and A. F. Martin, "The C terminus of cardiac troponin I is essential for full inhibitory activity and Ca^{2+} sensitivity of rat myofibrils," *Journal of Biological Chemistry*, vol. 272, no. 43, pp. 26887–26892, 1997.
- [16] L. S. Tobacman and D. Sawyer, "Calcium binds cooperatively to the regulatory sites of the cardiac thin filament," *Journal of Biological Chemistry*, vol. 265, no. 2, pp. 931–939, 1990.
- [17] S. B. Scruggs, A. C. Hinken, A. Thawornkaiwong, et al., "Ablation of ventricular myosin regulatory light chain phosphorylation in mice causes cardiac dysfunction in situ and affects neighboring myofilament protein phosphorylation," *Journal of Biological Chemistry*, vol. 284, no. 8, pp. 5097–5106, 2009.
- [18] S. Sadayappan, J. Gulick, H. Osinska, et al., "Cardiac myosin-binding protein-C phosphorylation and cardiac function," *Circulation Research*, vol. 97, no. 11, pp. 1156–1163, 2005.
- [19] N. Fukuda, H. L. Granzier, S. Ishiwata, and S. Kurihara, "Physiological functions of the giant elastic protein titin in mammalian striated muscle," *Journal of Physiological Sciences*, vol. 58, no. 3, pp. 151–159, 2008.
- [20] D. G. Ward, S. M. Brewer, M. J. Calvert, C. E. Gallon, Y. Gao, and I. P. Trayer, "Characterization of the interaction between the N-terminal extension of human cardiac troponin I and troponin C," *Biochemistry*, vol. 43, no. 13, pp. 4020–4027, 2004.

- [21] S. P. Robertson, J. D. Johnson, and M. J. Holroyde, "The effect of troponin I phosphorylation on the Ca^{2+} -binding properties of the Ca^{2+} -regulatory site of bovine cardiac troponin," *Journal of Biological Chemistry*, vol. 257, no. 1, pp. 260–263, 1982.
- [22] J. C. Kentish, D. T. McCloskey, J. Layland, et al., "Phosphorylation of troponin I by protein kinase A accelerates relaxation and crossbridge cycle kinetics in mouse ventricular muscle," *Circulation Research*, vol. 88, no. 10, pp. 1059–1065, 2001.
- [23] B. J. Biesiadecki, T. Kobayashi, J. S. Walker, R. J. Solaro, and P. P. de Tombe, "The troponin C G159D mutation blunts myofilament desensitization induced by troponin I Ser23/24 phosphorylation," *Circulation Research*, vol. 100, no. 10, pp. 1486–1493, 2007.
- [24] C. M. Warren, T. Kobayashi, and R. J. Solaro, "Sites of intra- and intermolecular cross-linking of the N-terminal extension of troponin I in human cardiac whole-troponin complex," *Journal of Biological Chemistry*, vol. 284, no. 21, pp. 14258–14266, 2009.
- [25] D. Burkhoff, "Explaining load dependence of ventricular contractile properties with a model of excitation-contraction coupling," *Journal of Molecular and Cellular Cardiology*, vol. 26, no. 8, pp. 959–978, 1994.
- [26] D. Baran, K. Ogino, R. Stennett, et al., "Interrelating of ventricular pressure and intracellular calcium in intact hearts," *American Journal of Physiology*, vol. 273, no. 3, part 2, pp. H1509–H1522, 1997.
- [27] C. A. Valverde, C. Mundiña-Weilenmann, M. Reyes, E. G. Kranias, A. L. Escobar, and A. Mattiazzi, "Phospholamban phosphorylation sites enhance the recovery of intracellular Ca^{2+} after perfusion arrest in isolated, perfused mouse heart," *Cardiovascular Research*, vol. 70, no. 2, pp. 335–345, 2006.
- [28] R. Mejía-Alvarez, C. Manno, C. A. Villalba-Galea, et al., "Pulsed local-field fluorescence microscopy: a new approach for measuring cellular signals in the beating heart," *Pflugers Archiv European Journal of Physiology*, vol. 445, no. 6, pp. 747–758, 2003.
- [29] P. H. Backx, W.-D. Gao, M. D. Azan-Backx, and E. Marban, "The relationship between contractile force and intracellular $[\text{Ca}^{2+}]$ in intact rat cardiac trabeculae," *Journal of General Physiology*, vol. 105, no. 1, pp. 1–19, 1995.
- [30] J. N. Peterson, W. C. Hunter, and M. R. Berman, "Estimated time course of Ca^{2+} bound to troponin C during relaxation in isolated cardiac muscle," *American Journal of Physiology*, vol. 260, no. 3, part 2, pp. H1013–H1024, 1991.
- [31] A. Landesberg, "End-systolic pressure-volume relationship and intracellular control of contraction," *American Journal of Physiology*, vol. 270, no. 1, part 2, pp. H338–H349, 1996.
- [32] K. S. McDonald and T. J. Herron, "It takes 'heart' to win: what makes the heart powerful?" *News in Physiological Sciences*, vol. 17, no. 5, pp. 185–190, 2002.
- [33] C. Poggesi, C. Tesi, and R. Stehle, "Sarcomeric determinants of striated muscle relaxation kinetics," *Pflugers Archiv European Journal of Physiology*, vol. 449, no. 6, pp. 505–517, 2005.
- [34] R. L. Moss, M. Razumova, and D. P. Fitzsimons, "Myosin crossbridge activation of cardiac thin filaments: implications for myocardial function in health and disease," *Circulation Research*, vol. 94, no. 10, pp. 1290–1300, 2004.
- [35] B. S. Pan and R. J. Solaro, "Calcium-binding properties of troponin C in detergent-skinned heart muscle fibers," *Journal of Biological Chemistry*, vol. 262, no. 16, pp. 7839–7849, 1987.
- [36] J. P. Davis, C. Norman, T. Kobayashi, R. J. Solaro, D. R. Swartz, and S. B. Tikunova, "Effects of thin and thick filament proteins on calcium binding and exchange with cardiac troponin C," *Biophysical Journal*, vol. 92, no. 9, pp. 3195–3206, 2007.
- [37] P. L. Engel, T. Kobayashi, B. Biesiadecki, et al., "Identification of a region of troponin I important in signaling cross-bridge-dependent activation of cardiac myofilaments," *Journal of Biological Chemistry*, vol. 282, no. 1, pp. 183–193, 2007.
- [38] G. M. Arteaga, C. M. Warren, S. Milutinovic, A. F. Martin, and R. J. Solaro, "Specific enhancement of sarcomeric response to Ca^{2+} protects murine myocardium against ischemia-reperfusion dysfunction," *American Journal of Physiology*, vol. 289, no. 5, pp. H2183–H2192, 2005.
- [39] P. L. Engel, A. Hinken, and R. J. Solaro, "Differential effects of phosphorylation of regions of troponin I in modifying cooperative activation of cardiac thin filaments," *Journal of Molecular and Cellular Cardiology*, vol. 47, no. 3, pp. 359–364, 2009.
- [40] J. A. Kirk, G. A. MacGowan, C. Evans, et al., "Left ventricular and myocardial function in mice expressing constitutively pseudophosphorylated cardiac troponin I," *Circulation Research*, vol. 105, no. 12, pp. 1232–1239, 2009.
- [41] B. M. Palmer, D. Georgakopoulos, P. M. Janssen, et al., "Role of cardiac myosin binding protein C in sustaining left ventricular systolic stiffening," *Circulation Research*, vol. 94, no. 9, pp. 1249–1255, 2004.
- [42] D. A. Kass and R. J. Solaro, "Mechanisms and use of calcium-sensitizing agents in the failing heart," *Circulation*, vol. 113, no. 2, pp. 305–315, 2006.
- [43] T. Sorsa, P. Pollesello, and R. J. Solaro, "The contractile apparatus as a target for drugs against heart failure: interaction of levosimendan, a calcium sensitizer, with cardiac troponin c," *Molecular and Cellular Biochemistry*, vol. 266, no. 1-2, pp. 87–107, 2004.
- [44] R. J. Solaro, "CK-1827452, a sarcomere-directed cardiac myosin activator for acute and chronic heart disease," *IDrugs*, vol. 12, no. 4, pp. 243–251, 2009.

Research Article

Ordered Assembly of the Adhesive and Electrochemical Connections within Newly Formed Intercalated Disks in Primary Cultures of Adult Rat Cardiomyocytes

Sarah B. Geisler,¹ Kathleen J. Green,² Lori L. Isom,^{3,4} Sasha Meshinchi,⁵ Jeffrey R. Martens,⁴ Mario Delmar,^{3,6} and Mark W. Russell¹

¹ Division of Pediatric Cardiology, Department of Pediatrics and Communicable Diseases, University of Michigan, 1150 West Medical Center Dr., Ann Arbor, MI 48109, USA

² Department of Pathology, Feinberg School of Medicine, Northwestern University, 303 E. Chicago Avenue, Chicago, IL 60611, USA

³ Department of Molecular and Integrative Physiology, University of Michigan, 1150 West Medical Center Dr., Ann Arbor, MI 48109, USA

⁴ Department of Pharmacology, University of Michigan, 1150 West Medical Center Dr., Ann Arbor, MI 48109, USA

⁵ Department of Cell and Developmental Biology, University of Michigan, 1150 West Medical Center Dr., Ann Arbor, MI 48109, USA

⁶ Department of Internal Medicine, University of Michigan, 1150 West Medical Center Dr., Ann Arbor, MI 48109, USA

Correspondence should be addressed to Mark W. Russell, mruess@med.umich.edu

Received 21 November 2009; Accepted 17 February 2010

Academic Editor: Guy M. Benian

Copyright © 2010 Sarah B. Geisler et al. This is an open access article distributed under the Creative Commons Attribution License, which permits unrestricted use, distribution, and reproduction in any medium, provided the original work is properly cited.

The intercalated disk (ID) is a complex structure that electromechanically couples adjoining cardiac myocytes into a functional syncytium. The integrity of the disk is essential for normal cardiac function, but how the diverse elements are assembled into a fully integrated structure is not well understood. In this study, we examined the assembly of new IDs in primary cultures of adult rat cardiac myocytes. From 2 to 5 days after dissociation, the cells flatten and spread, establishing new cell-cell contacts in a manner that recapitulates the *in vivo* processes that occur during heart development and myocardial remodeling. As cells make contact with their neighbors, transmembrane adhesion proteins localize along the line of apposition, concentrating at the sites of membrane attachment of the terminal sarcomeres. Cx43 gap junctions and ankyrin-G, an essential cytoskeletal component of voltage gated sodium channel complexes, were secondarily recruited to membrane domains involved in cell-cell contacts. The consistent order of the assembly process suggests that there are specific scaffolding requirements for integration of the mechanical and electrochemical elements of the disk. Defining the relationships that are the foundation of disk assembly has important implications for understanding the mechanical dysfunction and cardiac arrhythmias that accompany alterations of ID architecture.

1. Introduction

Cardiac myocytes are linked to each other along their axis of contraction by complex connections called intercalated disks (reviewed in [1]). The cardiac intercalated disk (ID) is composed of three types of cell-cell contacts: adherens junctions, gap junctions, and desmosomes. These connections serve as anchorage sites for the actin cytoskeleton, the intermediate filament network, microfilaments, microtubules, and the terminal ends of the myofibrils. They stabilize the cellular

cytoskeleton and electromechanically couple adjoining cardiac myocytes to form a functional syncytium. Alterations in the structure of the disk, either due to mutation of one of its components or aberrant remodeling during heart failure, can lead to progressive contractile dysfunction and cardiac arrhythmias [2].

ID remodeling may be an important ventricular adaptation to congestive heart failure. In response to dilated cardiomyopathy (DCM) and congestive failure, there is a marked upregulation of adherens junction constituents,

including N-cadherin, and β -catenin, and the plicate region of the intercalated disk becomes much more undulated [3]. Since the increased undulation will decrease the angle of incidence between the working myofibrils and their membrane anchorage sites, this will result in an improved force transmission and diminished shear stress at the intercalated disk. Therefore, structural adaptations within the intercalated disk, specifically within the adherens junctions, may in part compensate for the increased myocardial strain that accompanies congestive heart failure and DCM and may enable optimization of force transmission in this setting.

In contrast to the adhesive complex proteins of the intercalated disk, connexin43 (Cx43), a gap junction protein is not upregulated and, according to some reports, even downregulated in the setting of DCM [4]. Several studies have also shown significant redistribution of Cx43 in the setting of cardiomyopathies and heart failure [5]. This suggests that there are distinct regulatory pathways governing the expression of the mechanical and electrical elements of the ID, and that these pathways can be affected by disease. Additional studies have shown a close interaction between the mechanical and electrical components of the intercalated disk since loss of N-cadherin disrupts connexin localization and cardiac impulse propagation [6], and correct targeting of Cx43 to the ID depends on transport of the intact protein to cadherin-containing adherens junctions of the disk [7]. This suggests that the disruption of the mechanical components of the disk may lead to destabilization of the gap junctions and ventricular arrhythmias.

Perhaps the most direct evidence of the important relationship between the structural and electrophysiologic properties of the ID involves the clinical syndrome of Arrhythmogenic Right Ventricular Cardiomyopathy/Dysplasia (ARVC). ARVC is a heterogenous disorder characterized by severe ventricular arrhythmias and, commonly, fibro-fatty replacement of regions of the right and/or left ventricle (reviewed in [8]). It has been estimated that, although ARVC is a relatively rare condition, affecting approximately 1 in 5000 people in the U.S., it is responsible for approximately 10% of the cases of sudden death in individuals under the age of 35 [9–11]. To date, ten different genes have been determined to be responsible for causing ARVC, including desmocollin, desmoglein, desmoplakin, plakophilin-2 (PKP2), plakoglobin, desmin, ZASP, Transmembrane Protein 43 (TP43), and Transforming Growth Factor β 3 (TGF β 3). For many of these genes, mutations have only been identified in a few pedigrees worldwide [8] or lead to “atypical” forms of ARVC.

The great majority of ARVC cases with identified genetic mutations are linked to genes coding for proteins of the desmosome. Since none of these proteins directly participate in propagation of the cardiac impulse, alteration in the properties of the desmosome must have important secondary effects on the electrochemical connections within the ID including the gap junctions and/or the voltage-gated sodium channels (VGSC). Recent studies have supported this assertion, demonstrating that plakophilin-2 (PKP2), a part of the desmosomal complex, is involved in stabilization of gap junctions and VGSCs within the ID. Loss of PKP-2 was associated with redistribution of Cx43 gap junctions in cell

culture models and in patients with ARVC [12–14] and with decreased sodium current and lower conduction velocity in cultured cardiac myocytes [15]. Yet the relationships between the assembly and organization of the desmosomes and the recruitment and stabilization of the gap junctions and VGSCs have not been well characterized. In this study, we examined the assembly of IDs in remodeling adult rat cardiac myocytes in primary culture. The findings suggest progressive and coordinated maturation of the transmembrane adhesion complexes, intracellular cytoskeletal networks, and, ultimately, specialized sarcolemmal domains.

2. Materials and Methods

2.1. Cell Culture. Primary cultures of cardiac myocytes were isolated from adult female rats using enzymatic dissociation of myocardial tissue with trypsin and collagenase as previously described [16]. Cells were cultivated on coverslips in 199 medium as described [17].

2.2. Immunohistochemistry. Cells on coverslips were washed with PBS, fixed in methanol for two minutes, and rinsed with PBS. Coverslips were incubated in PBS+0.1%TX100+1 mg/ml BSA for 30 minutes, rinsed three times with PBS, and incubated with primary antibody diluted in PBS+BSA for 1.5 hours at room temperature. Following three PBS washes, coverslips were incubated with secondary antibodies. Cells were incubated with monoclonal and polyclonal antibodies together, followed by combined corresponding secondary antibodies. Controls for immunostaining were the omission of both primary antibodies and omission of both secondary antibodies. Sequential staining was performed when two monoclonal antibodies were used on one sample. After the first primary/secondary incubations, coverslips were incubated at 4°C overnight with goat antimouse IgG, then washed with PBS and incubated with Fab fragment of goat antimouse IgG. The second primary/secondary antibodies were then applied. Additional controls included reversing order of secondary antibodies and reversing order of primary incubations.

The following primary antibodies were used: 4B2 against Dsg [18], PKP2 (1:20, Biodesign International, Meridian Life Science, Saco, ME. K44262M), pan-cadherin (1.4 mg/ml, Sigma C3678), NW6 against desmoplakin (1:100), ankyrinG (10 μ g/mL, SCBT, SC28561), connexin43 (750 μ g/mL, Sigma C8093), plakoglobin (1:100, Sigma P8087), Na_v1.5 (40 μ g/mL, Alamone ASC-005). FITC conjugated goat-antimouse IgG, Texas Red conjugated goat-antimouse IgG, FITC conjugated goat anti-rabbit IgG, and Texas Red-conjugated goat antirabbit IgG were obtained from Jackson ImmunoResearch Laboratories Inc. (West Grove, PA). Coverslips were mounted on slides using the Prolong Gold antifade reagent with DAPI (Molecular Probes Inc., Eugene, OR). Immunostained samples were examined with an Olympus FV-500 Meta confocal microscope using a 60x objective.

2.3. Electron Microscopy. Cells were plated on laminin-coated coverslips as above. Five days post plating, the cells

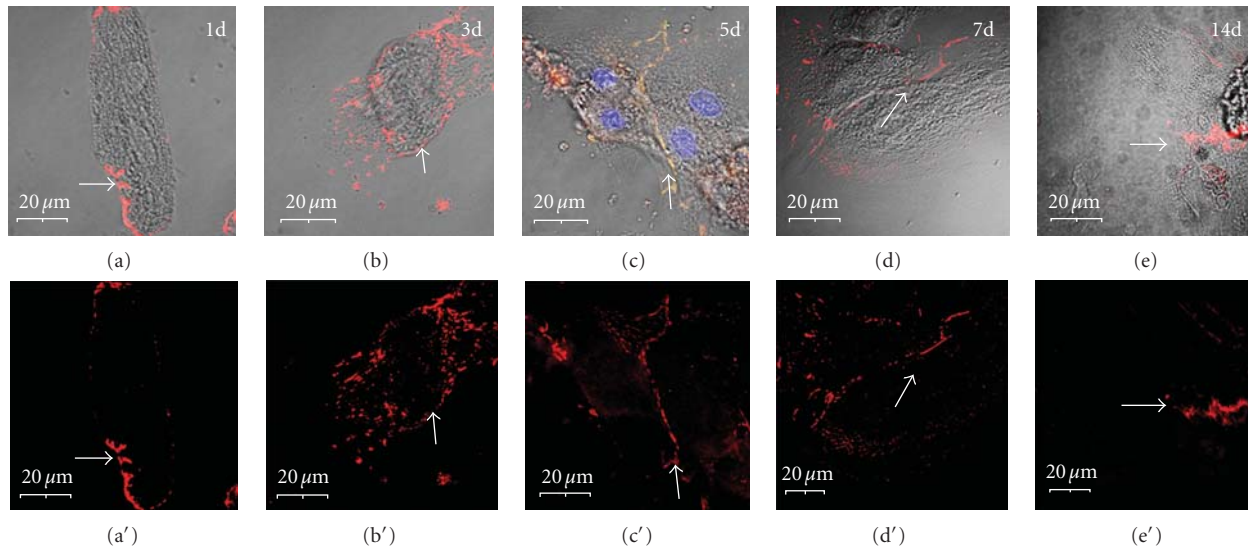


FIGURE 1: Reassembly of cell-cell contacts in remodeling adult rat cardiac myocytes in culture. (a, b) On days 1–3 post plating, the cell rounds up, the IDs disassemble, and cadherins redistribute along the periphery of the cell (arrow in b). (c, d) Between days 5–7, new cell-cell contacts form and cadherin localizes to specific domains along the line of apposition (arrows). (e) By 14 days post plating, the cell-cell contacts have remodeled to form more localized and mature structures (arrow). Scale bars are 20 μm .

were fixed overnight at 4°C in 2.5% glutaraldehyde and 2.0% paraformaldehyde and post fixed in 1% osmium tetroxide. After washing, they were stained with saturated uranyl acetate, and embedded in Epon 812. Ultra-thin sections were prepared and stained with saturated uranyl acetate and lead citrate. The sections were examined with a Philips CM100 transmission electron microscope, at an accelerating voltage of 60 kV.

3. Results

3.1. Time Course of ID Remodeling in Primary Culture. Adult rat cardiac myocytes grown in primary culture in the presence of serum disassemble their contractile structures and remodel their cellular cytoskeleton [19]. Over the course of 2–5 days, the cells extend processes, form new cell-matrix and cell-cell contacts, assemble new myofibrils, and resume spontaneous beating. During the remodeling process, the components of the ID are dismantled and subsequently reassembled at the new sites of cell-cell contact. To assess the time course of intercalated disk reassembly, primary cultures were immunolabeled with a pan-cadherin and PKP2 antibodies at timepoints from 1 to 14 days post plating (Figures 1 and 2). It was noted that, as a result of cell spreading and redistribution of adhesive junction components, new cell-cell contacts began to form as early as 3 days post plating along the boundaries between adjoining cells (Figure 2). Over the next 1–2 weeks in culture, the degree of myofibril alignment increased and the new IDs became focused at the polar ends of the myocyte along the new axis of contraction (see Figures 1(e) and 1(e')).

Based on these studies, the 5 day post-plating timepoint was selected for further analyses. This timepoint allowed the evaluation of the order of incorporation of cytoskeletal

elements into more complex and organized assemblies (Figure 3). At later timepoints, contractile activity and ongoing remodeling made it more difficult to differentiate assembling from disassembling structures.

3.2. Adhesive Junction and Armadillo Family Proteins Colocalize during the Early Phase of ID Assembly. To determine the scaffolding requirements for each element of the ID, their inclusion into new cell-cell contacts of varying complexity and maturity was examined at 5-days post plating. The order of incorporation was determined by pairwise comparison of double immunolabelings with an array of ID components. If two elements precisely colocalized in all cells sampled then they were scored as essentially concurrent in their incorporation into the new cell-cell contact. For some pairs, one of the two elements was never noted at cell contacts in the absence of the other; that element was determined to be recruited after the other to the new cell contacts. For some pairs, the localization patterns did not precisely overlap and either protein could localize to the new contact without the other. In those cases, the localization was determined to be simultaneous but not strictly interdependent.

Using this approach, the earliest components of the ID to localize to new cell-cell contacts were the transmembrane proteins, including N-cadherin and desmocollin, and the armadillo family proteins, including β -catenin (data not shown), plakoglobin (PG), and PKP2 (Figure 4). Of these, N-cadherin seemed to be required for adhesive contact formation as none of the other components were noted along the line of cell apposition in its absence. There was some variability in the ratio of PKP2 to desmocollin (Figures 4(d)–4(f)), indicating that there may be a nonstoichiometric relationship between the two, at least early in the assembly process or that PKP2 can localize to contacts that do not

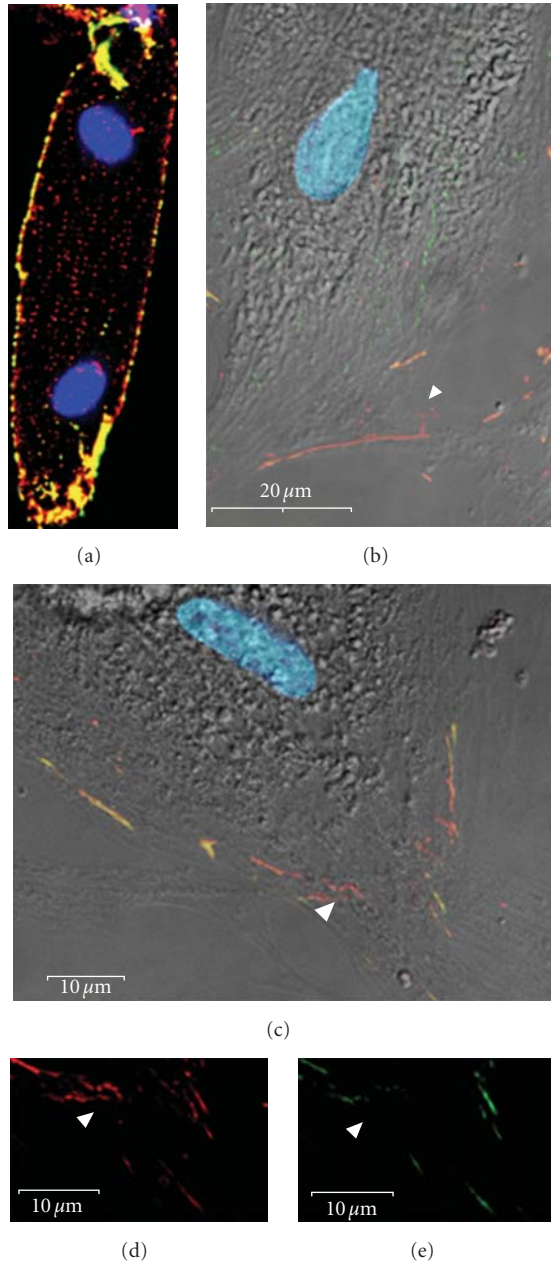


FIGURE 2: Early remodeling of the intercalated disks of isolated adult rat ventricular cardiomyocytes in primary culture. (a) One day post plating, PKP2 (green) and N-cadherin (red) relocalize from the intercalated disks to the lateral sarcolemma. (b)–(e) By day 3 post plating, very immature cell-cell contacts have begun to form between the spreading cardiomyocytes. N-cadherin (red) specifically localizes to these contact sites before PKP2 (green). Note that these new cell contacts predominantly contain either N-cadherin (arrowheads in (b)–(f)) or both N-cadherin and PKP2 ((b)–(f): yellow) but not PKP2 alone. Scale bars are 20 μm (b) and 10 μm (c)–(f).

contain desmocollin. However, the localization patterns were nearly identical, indicating simultaneous or virtually simultaneous incorporation of the cadherin-armadillo protein complexes of both desmosomal and adherens junctions

subtypes into the new cell adhesive domains. The most notable differences were in regions where N-cadherin was noted along projections within the cell extending from the site of cell-cell contact. These may represent filopodial-like cellular projections that, once the contact with the adjoining cell is established, recruit desmosomal components including PKP2 (Figures 4(a)–4(c)).

Localization of the desmosomal cadherins, PKP2 and PG to overlapping sarcolemmal domains closely followed N-cadherin incorporation. Variations in the relative abundance of the two within the adhesive contacts (Figure 5) suggests that, while PKP-2 and PG are localizing to the same sarcolemmal regions concurrently, the presence of one may not be required for the localization of the other and both may be dependent on the presence of other components, namely, the cadherins, for proper incorporation into the adhesion complex.

Insertion of the intermediate filaments into the desmosomal complex requires desmoplakin (DP), a plaque protein that binds to intermediate filaments and to desmosomal proteins such as PKP2, PG, desmocollin, and desmoglein. DP appeared to be recruited to the newly-formed cell contacts after the assembly of complexes of the cadherin and armadillo family of proteins. In addition, it appeared to be recruited to only a subset of the contact sites. In contrast to PKP2 which distributed along the entire adhesive contact, DP localization was more granular in appearance, indicating the assembly of desmosomal plaques (Figure 6).

3.3. Connexin43 Concentrates at New IDs after the Assembly of the Adhesive Junction-Armadillo Protein Complexes. Previous studies have demonstrated that gap junction formation is dependent on the prior assembly of adhesive contacts in multiple cell types including cardiac myocytes [20–22]. Disruption of either desmosomal or adherens junction complexes results in the loss of gap junctions from the intercalated disk and the development of malignant ventricular arrhythmias [23, 24]. Prior work by Kostin et al. [25] demonstrated that, in primary adult rat cardiac myocytes in primary culture, both adherens junctions (as determined by immunolocalization of N-cadherin and α - and β -catenin) and desmosomal contacts (as determined by desmoplakin and PG) were recruited to new cell-cell contacts prior to the formation of gap junctions. We similarly noted the recruitment of gap junctions selectively to membrane domains involved in adhesive contacts (Figure 7). Subsarcolemmal assembly of connexons preceded their insertion into adhesive domains (Figures 7(a), 7(b), and 7(d)).

3.4. Recruitment VGSCs to the Intercalated Disk. Previous studies examining the localization of VGSC signaling complexes to specific subcellular membrane domains have highlighted the role of ankyrins in the targeting and stabilization process. It has been demonstrated that $\text{Na}_v1.5$ physically interacts with ankyrin-G [26]. A mutation in *SCN5A*, the gene encoding $\text{Na}_v1.5$, that impairs its ability to bind ankyrin-G results in loss of the channel from the sarcolemma and causes Brugada Syndrome, an electrophysiologic defect of the heart associated with ventricular fibrillation and

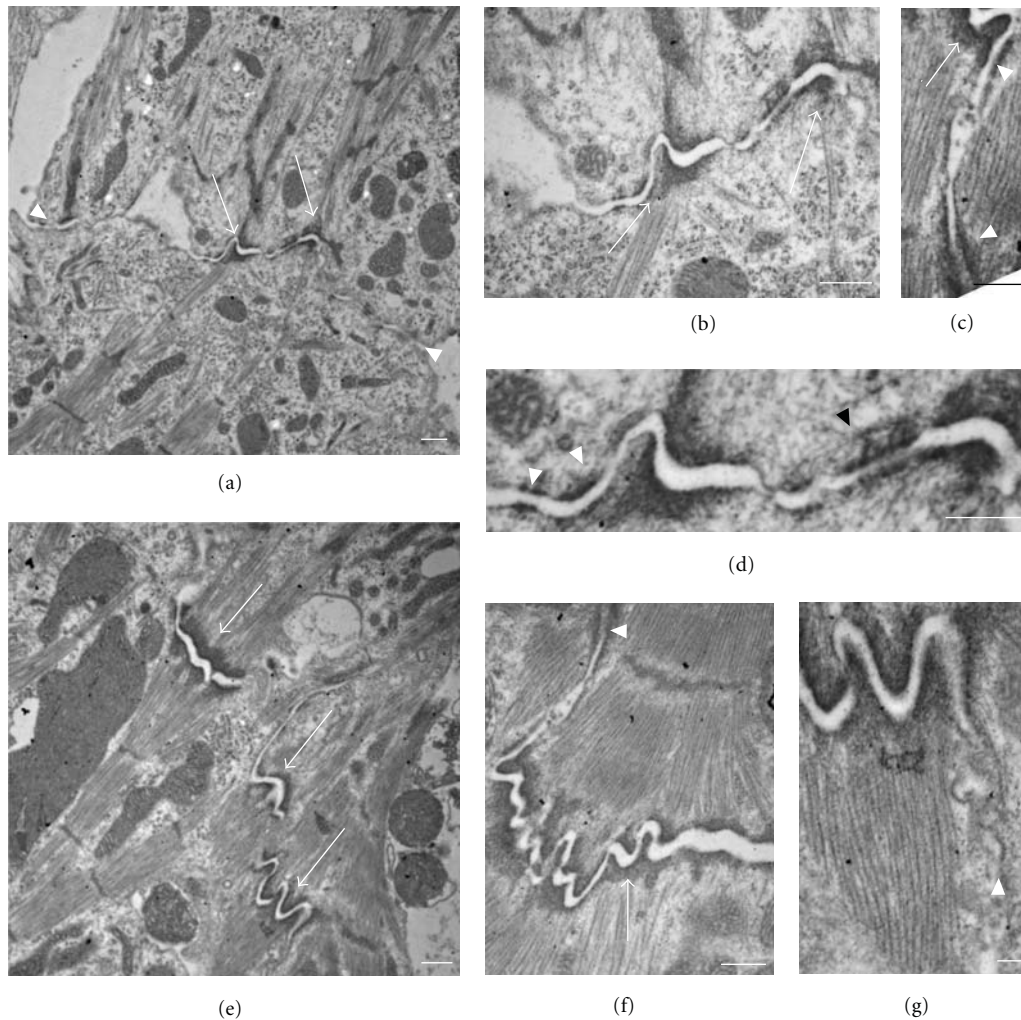


FIGURE 3: Ultrastructural analysis of new cardiomyocyte cell-cell contacts at 5-days post plating. At this timepoint, cell contacts form and develop rapidly, allowing the observation of both nascent (a, b, d) and more mature (c, e, f, g) contact sites. (a) Remodeling cardiomyocytes extend fingerlike projections (arrowheads) that interact with neighboring cells to form adhesive contacts (arrows) thereby electromechanically linking the two cells. (b, d) Higher magnifications of an adhesive domain indicated in (a) shows insertion of actin filaments into nascent adherens junctions (AJs) (arrows in (b)). Note the nascent (white arrowheads in (d)) and more mature (black arrowhead in (d)) desmosomal contacts in close proximity to the maturing AJ. (c) A mature adhesive domain again demonstrates desmosomal contacts (arrowheads) near a newly formed adherens junction (arrow). (e)–(g) More mature adhesive contacts demonstrate adherens junctions (arrows in (e)) at the insertion of the terminal actin filaments of newly formed myofibrils, along with closely associated desmosomal contacts (arrowhead in (f)) and gap junctions (arrowhead in (g)). Scale bars are 500 nm (a)–(f) and 100 nm (g).

sudden death [27]. Recent studies have further demonstrated an interaction between PKP2 and $\text{Na}_v1.5$, suggesting functional integration of the VGSC with other membrane proteins such as ankyrin and with desmosomal adhesive complexes [15].

Therefore, to determine the structural requirements for the recruitment of the VGSC to newly formed IDs, the pattern of localization of ankyrin-G, $\text{Na}_v1.5$, and the desmosomal protein PKP2 was examined at 5 and 13 days post plating. By 5 days post plating, ankyrin-G was specifically recruited to sarcolemmal domains involved in cell-cell contacts as determined by PKP2 colocalization (Figure 8). It appeared to arrive at the new ID significantly prior to the $\text{Na}_v1.5$ α subunit, consistent with ankyrin-G recruiting

VGSCs to the sarcolemma. Furthermore, it suggests that ankyrin-G is likewise dependent for its localization on targeting mechanisms that specifically direct it to sites of cell-cell contact.

The $\text{Na}_v1.5$ α subunit itself arrives at the newly formed ID much later than ankyrin-G. At the 5-day timepoint, when new cell-cell contacts are forming and ankyrin-G is beginning to co-localize to cell contact sites, immunostaining for $\text{Na}_v1.5$ demonstrates a more diffuse localization (Figures 9(a)–9(d)). The antibody detects epitopes closely associated with newly assembled myofibrils. Previous work has demonstrated that membrane domains are closely associated with these new myofibrils [28]. Whether or not this truly represents localization of $\text{Na}_v1.5$ to membrane structures

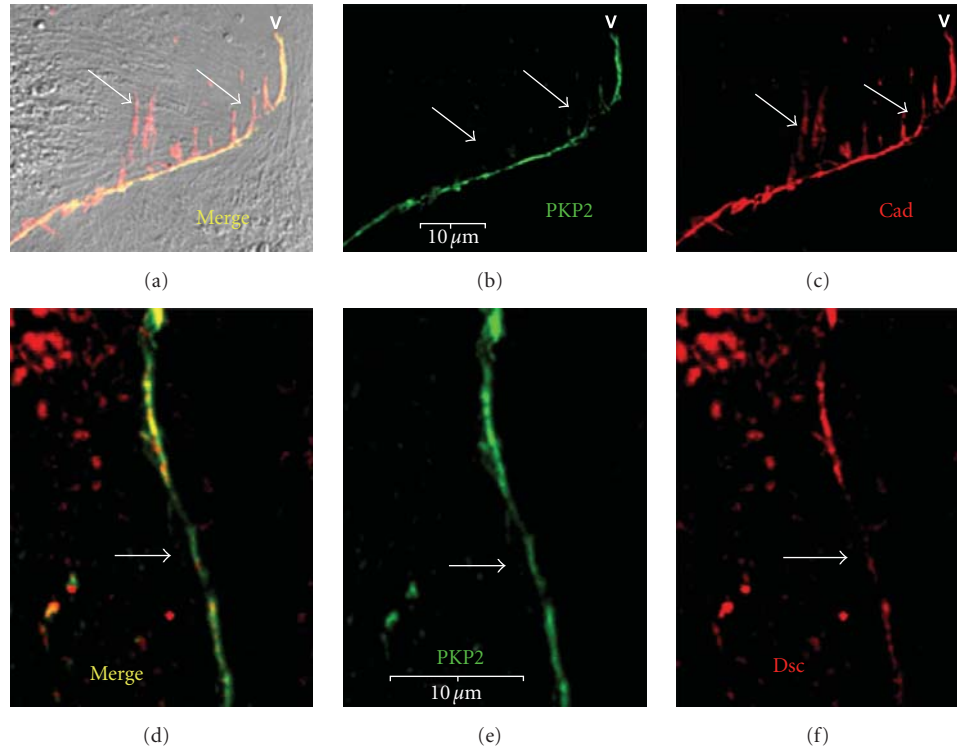


FIGURE 4: Co-localization of PKP2 with N-cadherin and desmocollin in newly formed cell-cell contacts. ARCs were immunolabeled with antibodies to PKP2 (green: a, b, d, e) and pan-cadherin (red: a, c) or desmocollin (red: d, f) on day 5 post plating. There is an extensive overlap in localization of PKP2 with both N-cadherin and desmocollin. Note that there was a localization of N-cadherin along the lateral aspects of cellular projections at the cell-contact sites (arrows in (a)–(c)). These may represent filopodial extensions that mature into cell-adhesion domains. There was also noted to be some regional variation in the relative amounts of PKP2 and desmocollin (arrows in (d)–(f)). Scale bars are 10 μm .

associated with the myofibril remains to be determined. That ankyrin-G co-localized with $\text{Na}_v1.5$ to these sites suggests that the immunostaining is specific and may represent a developmental intermediate as the membrane domains reorganize in the redifferentiation phase of remodeling. Later relocalization of $\text{Na}_v1.5$ to the ID was demonstrated by immunostaining at 13 days post plating (Figures 9(e)–9(g)).

4. Discussion

The de- and redifferentiation of adult rat ventricular myocytes in primary culture has long been used to examine the processes guiding the reorganization of cytoskeletal and contractile structures that occurs during cardiac development and during the cellular remodeling that accompanies adaptation to pathophysiologic conditions [19]. Perhaps no model system is more ideally suited for characterizing the stepwise assembly and functional integration of complex cardiomyocyte structures such as the intercalated disk and the cardiac myofibril.

Pioneering studies by the laboratories of Werner Franke [29, 30] and Jutta Schaper [25, 31] have used primary cultures of neonatal and adult rat cardiac myocytes to make important contributions to our understanding of ID assembly and organization. The findings presented here build on

this previous work by focusing on the ordered assembly of the desmosome and on the relationship between the desmosomal complex and the electrochemical connections within the disk (Figure 10).

4.1. Relationship of Desmosomes and Adherens Junctions. Traditionally, the intercalated disk was viewed as the sum of distinct intercellular contacts that could be readily categorized as desmosomes, adherens junctions, or gap junctions. More recent studies however have suggested that interrelationships of the desmosomes and the adherens junction components may be more extensive than previously recognized. There is now strong evidence that, in the mammalian heart, components of the desmosome and adherens junction routinely interact to form composite structures [32], leading to the coining of the term “area composita” to refer to domains within the plicate region of the ID disk in which there is an extensive intermingling of the two types of contacts. These cross-type connections would be predicted to form a strong network linking the actin filaments at the terminal ends of the myofibrils, with the cortical actin and intermediate filaments of the cellular cytoskeleton. The transmembrane portions of the connections would extend this network to the adjoining cells to form a “tissue-skeleton” for the heart, preserving ventricular architecture in the face of the hemodynamic demands.

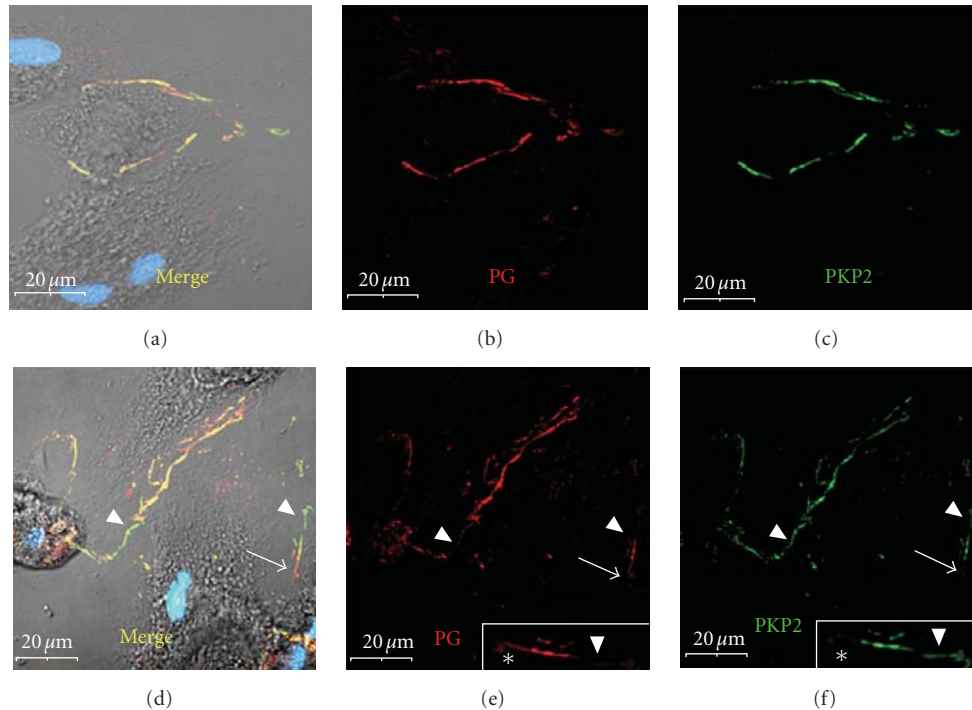


FIGURE 5: Localization of plakoglobin and plakophilin-2 in remodeling adult rat cardiac myocytes. ARCs were immunolabeled with antibodies to plakoglobin (PG) (red: a, b, d, e) and PKP2 (green: a, c, d, f) on day 5 post plating. Note the extensive co-localization of the two armadillo family proteins to new cell adhesion domains between contacting cells (a)–(c). There was some regional variation in the relative abundance of the two such that some newly-formed contacts contained predominately plakoglobin ((e): arrow; (e)-inset: asterisks) or PKP2 ((f) and (f)-inset: arrowheads). Scale bars are $20\ \mu\text{m}$ and the insets in (e) and (f) are a $2\times$ magnification of a region of cell-cell contact.

Despite the important relationship between the two cell adhesion systems, how these interconnections are established and maintained is still not well understood. Previous studies have demonstrated the dependence of desmosome formation on the prior assembly of adherens junctions, suggesting a hierarchy within the assembly process. Human keratinocytes treated with antibodies to E- and P-cadherin are unable to form adherens junctions and have a dramatically reduced number of desmosomes [33]. Overexpression of a dominant negative cadherin in keratinocytes likewise impaired desmosome formation [34]. The mediator of this interaction between the two transmembrane systems may be plakoglobin, which is capable of interacting with both desmosomal and classic cadherins.

Our studies would suggest that a similar hierarchy exists in cardiac myocytes. Yet the extensive overlap in the localization patterns for the cadherin and armadillo protein components of both the desmosomes and the adherens junctions suggests that these processes occur nearly simultaneously in the remodeling cardiac myocyte and supports the previous observation that there is intermingling of the two types of adhesive contacts early in ID assembly [25]. The extent to which these contacts are subsequently sorted into distinct contact types (desmosome versus adherens junction) has been debated, but studies by the Franke laboratory suggest that in mammals, as opposed to fish and amphibians

[35], these contacts will ultimately be intermingled within the area composita of the ID after birth [32].

4.2. Desmosomal Assembly in Newly Formed Cardiomyocyte Cell-Cell Contacts. The assembly of the elements of the intercalated disk would suggest that it progresses in a layered fashion, beginning with the organization of the transmembrane components and ultimately resulting in the remodeling of the cellular cytoskeleton. The “outside the cell” to “inside the cell” progressive organization of the intercalated disk is reminiscent of focal adhesion formation in that contact of the cell with extracellular environment (either the surrounding matrix in the case of the focal adhesion or the neighboring cells for the IDs) initiates organization of transmembrane molecules, followed by assembly of the submembrane complexes and integration with the cellular cytoskeleton. As with focal adhesions, dynamic cellular processes then promote “inside-out” remodeling of the transmembrane complexes leading to the clustering at specific contact sites, in this case, those that are localized to the termini of the cardiac myofibrils. Although there are two types of cell-cell contacts that form between neighboring cardiac myocytes, desmosomes and adherens junctions, the current study is in agreement with prior observations [25] that there may be a mixture of these two types of adhesive contacts. That PKP2, a desmosomal component, was noted to localize to

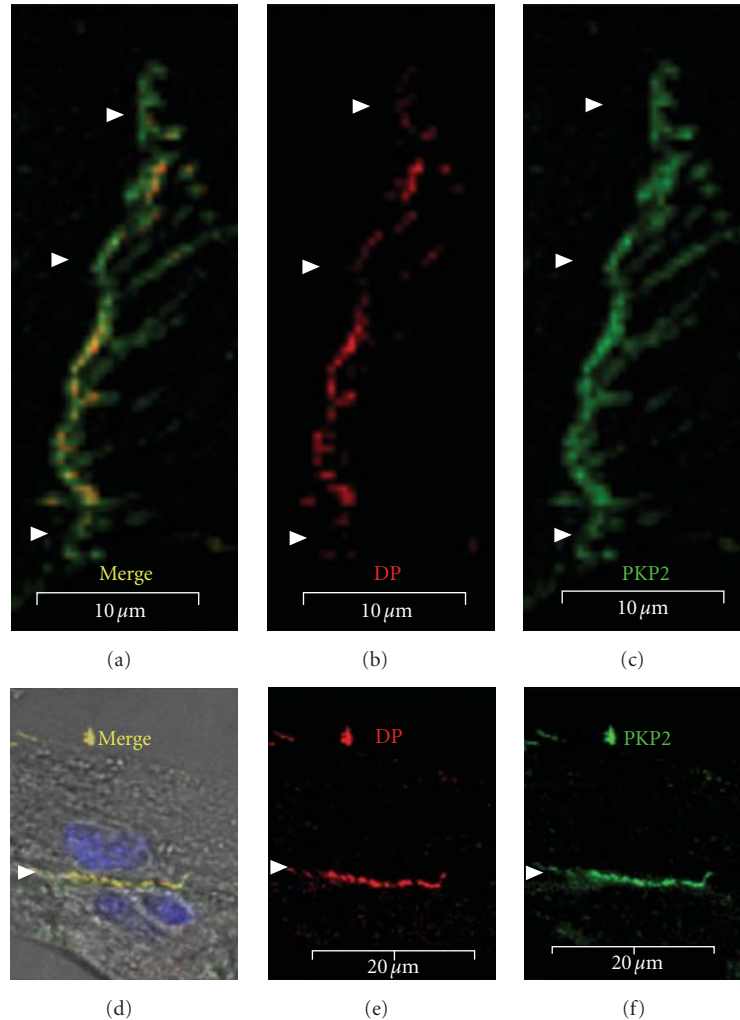


FIGURE 6: Localization of DP to a subset of adhesive sites. ARCs were immunolabeled with antibodies to desmoplakin (red: a, b) and PKP-2 (green: a, c) on days 5 (a)–(c) and 7 (d)–(f) post plating. The absence of DP from some of the adhesive domains ((a)–(c): arrowheads) suggests that its localization to the newly forming structures occurs after PKP2. DP and PKP2 do fully co-localize at more mature adhesive contacts ((d)–(f): arrowheads). Scale bars are 10 μm (a)–(c) and 20 μm (e, f).

contact sites lacking desmocollin, but never to domains lacking N-cadherin supports this assertion. Although direct interactions have not been described between PKP2 and classic cadherins, PG interacts with both classic cadherins and PKP2 and may promote localization of PKP2 to the contact site even in the absence of desmosomal cadherins. The ability of PG to bind to both classic and desmosomal cadherins and to interact with PKP2 may allow it to promote interactions of the two types of contacts both early in the formation of new intercalated disks as noted by Kostin et al. [25], and within the area composita later in the maturation of the disk [32].

The recruitment of PKP2 to the new intercalated disk may be required for the next phase of desmosomal assembly, namely, the linkage of the transmembrane complex with the intermediate filaments of the cellular cytoskeleton through the desmosomal plaque protein, desmoplakin. At the amino terminus of desmoplakin is a plakin domain that interacts

with desmocollin, desmoglein, PKP2, and PG [36–38]. The carboxy terminus has an intermediate filament binding domain that promotes interactions with desmin intermediate filaments, vimentin, and cytokeratins [39]. Therefore, desmoplakin is required for the docking and integration of the intermediate filament system with the desmosomal cadherins, either through direct physical interaction or as part of a complex through interaction with the armadillo proteins, PG and PKP2. Once established, this connection physically links the cellular cytoskeleton of one myocyte with the next through the transmembrane and intercellular connections of the desmosome. This linkage is critical for the integrity of the desmosome and for the stability of the cellular cytoskeleton. Prior studies have demonstrated that PKP2 scaffolds PKCα, which prepares desmoplakin for incorporation into the desmosome [22]. Therefore, it is not surprising that DP only localized to regions of cell contact that already had recruited PKP2. Whether or not DP would

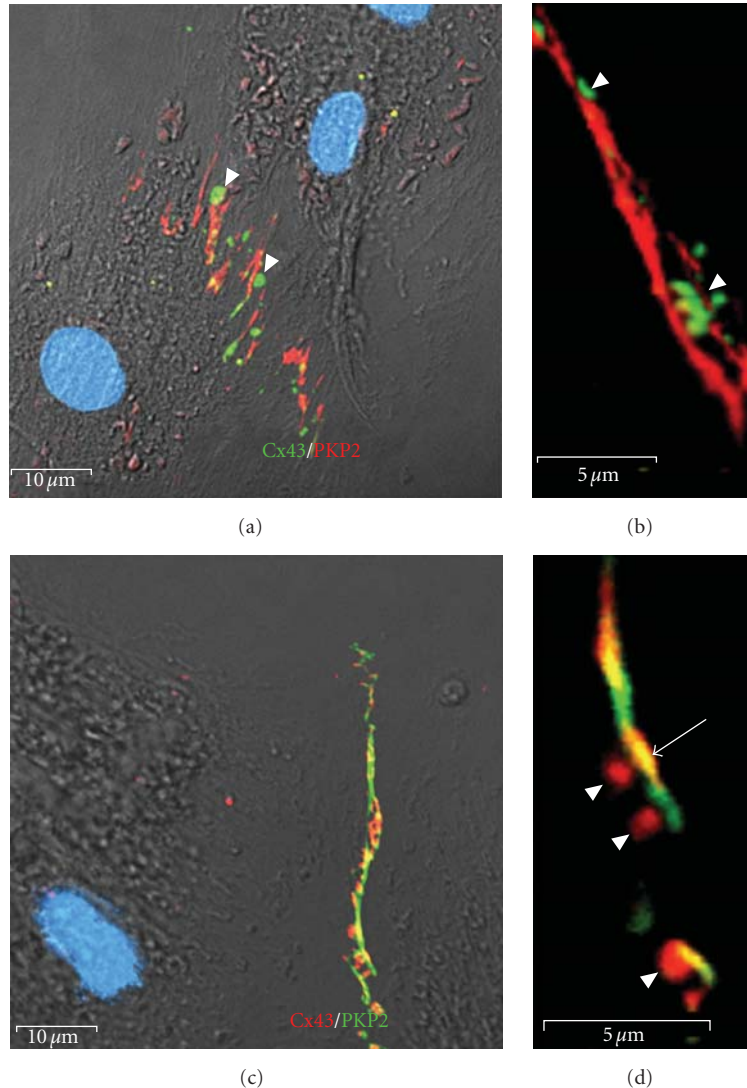


FIGURE 7: Connexin43 localization to cell-cell contact domains follows adhesion complex assembly. ARCs at 5 days post plating were immunolabeled for Cx43 (green: (a, b); red: (c, d)) and PKP2 (red: (a, b); green: (c, d)). Early in the assembly and organization of cell-cell contacts in ARCs in primary culture, adhesive sites do not contain appreciable amounts of Cx43 (green: (a, b); red: (c, d)). (a) Connexin43 localization to newly formed adhesive contacts as identified by PKP2 immunostaining. Note the subsarcolemmal accumulation of connexons at the apices of the interdigitized contacts (arrowheads). (b) High magnification image of newly formed contact with subsarcolemmal accumulation of connexons prior to insertion into the membrane. (c, d) Low and higher magnification images of subsarcolemmal accumulation of connexons (arrowheads) prior to their insertion into the membrane. Note the regions of overlap of PKP2 and Cx43 immunolabeling indicating areas of mature gap junctions within the adhesive domains (arrow). Also, note that the Cx43 inserts into the membrane preferentially at adhesive sites (a, d). Scale bars are 10 μm (a, c) and 5 μm (b, d).

have been able to localize to the ID in the absence of PKP2 or other elements of the adhesion complex was not examined in this study.

4.3. Relationship of Adhesive Contacts to Electrochemical Connections within the ID. As noted above, our findings regarding the assembly of gap junctions following the formation of adhesive contacts are consistent with the prior studies using this model system [25, 30–32]. This is true both for newly assembled contacts and for more mature intercalated disk-like structures. Connexin43 was recruited

to new cell contacts after formation of adhesive contacts. As those contacts remodeled and more mature intercalated disk-like structures were organized, connexin43 remained more diffusely localized around the cell periphery before relocating to the new ID.

The factors that recruit gap junctions to and stabilize them within the ID are of particular interest for understanding the genesis of ventricular arrhythmias. Redistribution of gap junctions from the intercalated disk to the lateral sarcolemma is a characteristic feature of a range of myocardial disorders including myocardial ischemia, myocardial

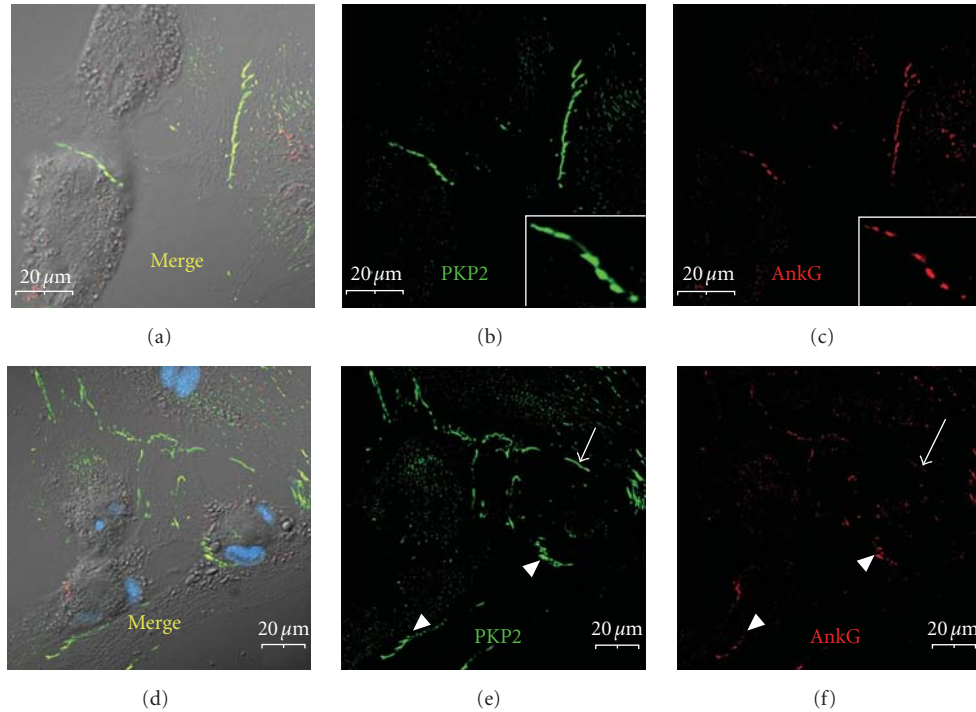


FIGURE 8: Ankyrin-G is selectively recruited to membrane domains involved in adhesive contacts. At 5 days post plating, ARCs were immunolabeled for PKP2 (green: a, b, d, e) and ankyrin-G (red: a, c, d, f). (a)–(c) Ankyrin-G localizes to mature cell adhesion domains where it co-localizes with PKP2 (see insets). (d)–(f) Ankyrin-G is far less abundant (arrowheads) or not yet detectable (arrow) in immature or newly-formed adhesive contacts. Scale bars are 20 μm with the insets being 2 \times magnifications of the larger image.

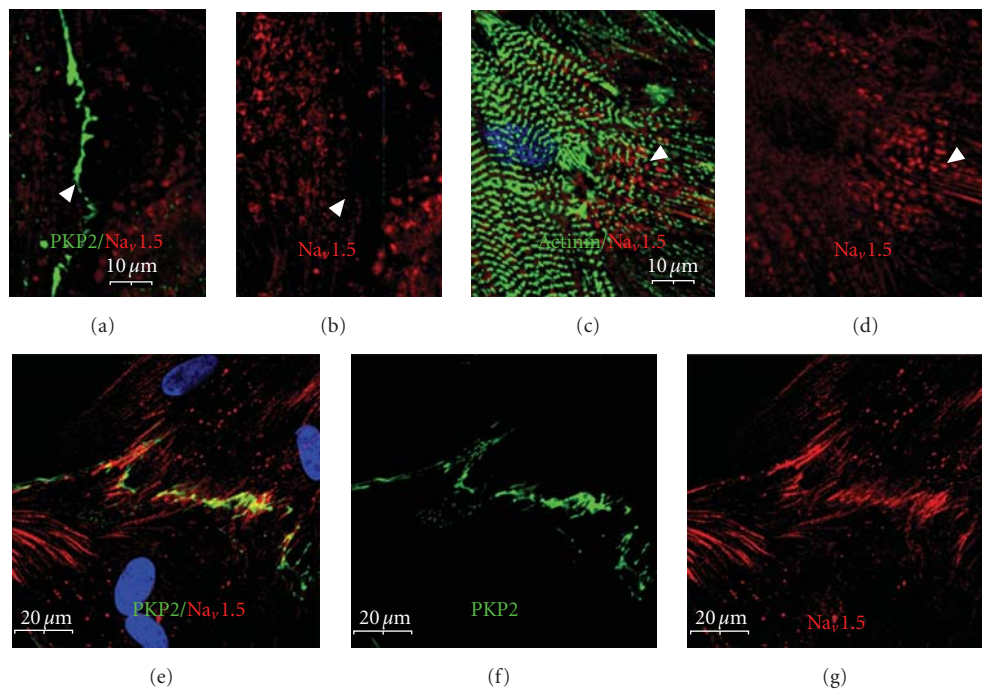


FIGURE 9: The α subunit of the voltage-gated sodium channel is incorporated significantly later into the newly-formed intercalated disks. ARCs at 5 (a)–(d) and 13 (e)–(g) days post plating were immunolabeled for Na_v1.5 (red: (a)–(e) and (g)) and PKP2 (green: a, e, f) or α -actinin (green: (c)). (a, b) At the 5-day timepoint, there is no detectable localization of Na_v1.5 even to mature cell adhesion sites (arrowhead). (c, d) Instead, Na_v1.5 appears to be more closely associated with assembling myofibrils (arrowhead). Note the linear arrays of Na_v1.5 immunolabeling between α -actinin-labeled myofibrils. (e)–(g) By 13 days post plating, the channel has localized to the new intercalated disk, significantly after the other components. Scale bars are 10 μm (a)–(d) and 20 μm (e)–(g).

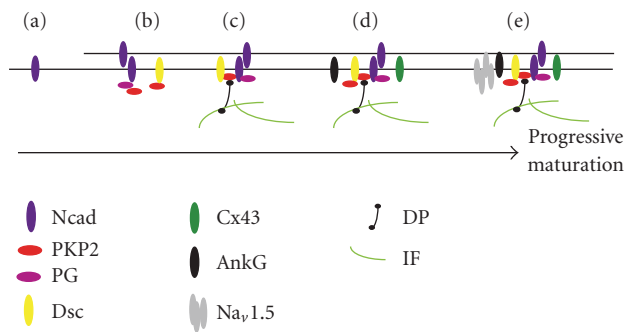


FIGURE 10: Progressive maturation of the intercalated disk (a)–(e). (a) As cardiomyocytes remodel, N-cadherin (Ncad) distributes diffusely around the cell periphery. (b) When cells contact adjoining cells, desmocollin (Dsc) proteins of the armadillo family including plakoglobin (PG) and plakophilin-2 (PKP2) co-localize with N-cadherin at the cell contact site. (c) The nascent adhesive contacts recruit desmoplakin (DP) and the associated intermediate filaments. (d) After assembly of the adhesive plaque, connexin-43 (Cx43) and ankyrin-G (AnkG), a component of the VGSC, selectively localize to the adhesive contact site. (e) The α subunit of the voltage-gated sodium channel Na is incorporated significantly later into the more mature intercalated disks where they associate with ankyrin-G. The assembly process begins with the clustering of transmembrane adhesive contacts, followed by the recruitment of the plaque proteins and reorganization of the subcortical cytoskeleton. The process culminates with the recruitment of gap junctions and components of the VGSC complex (AnkG and $\text{Na}_v1.5$) which are also assembled in a step-wise fashion.

hypertrophy, and hypertrophic and dilated (or congestive) cardiomyopathy [4, 5]. This process, termed lateralization of the gap junctions, appears to be dependent upon or at least associated with changes in the phosphorylation state of specific residues within the carboxy terminus of connexin43 [40]. While heart failure and ischemic cardiomyopathy is only associated with an overall reduction in gap junction content of approximately 50% [41], compared to the 80% reduction required to see abnormalities of conduction velocity in animal models [42], regional variation in gap junction content can result in some regions within the diseased ventricle with greater than 90% reduction [41]. Direct electrical measurements are still required to properly assess the impact of this redistribution in the context of action potential propagation. Yet, we speculate that the genesis of ventricular arrhythmias in this setting may be due to the overall reduction and redistribution of gap junctions from the ID and, even more importantly, to the heterogeneity of electrical coupling within afflicted regions, thus setting the stage for generation of reentrant arrhythmias. Therefore, defining the interactions that affect gap junction localization to and retention within the ID region will be important for identifying strategies to limit its redistribution and the resulting effects this has on impulse propagation and cell connectivity within the myocardium.

Like the gap junctions, the VGSC ion conducting pore also appears to be recruited to the ID significantly after

the formation of the adhesive complexes and is specifically localized to adhesion domains within the region of cell-cell contact. As noted previously [15], this suggests an interrelationship between the VGSC and the desmosome. How ID remodeling during pathophysiologic stress affects VGSCs has not been well studied. Given the array of cardiac dysrhythmias and conduction abnormalities that can occur with *SCN5A* mutations [43–45], it would be anticipated that a change in channel distribution or function within the ID might have a dramatic effect on the propensity for cardiac arrhythmias. As with the gap junctions, structural remodeling of the ID may result in redistribution of $\text{Na}_v1.5$ and reduction in conduction velocity. Regional variation in conduction velocity can, in turn, lead to abnormal impulse propagation that supports ventricular arrhythmias.

While previous studies have examined the relationship of desmosomal and gap junction assembly in redifferentiating cardiac myocytes as noted above, the localization of $\text{Na}_v1.5$ to the ID has not been well described. $\text{Na}_v1.5$ is responsible for impulse generation and propagation in the heart. The complex includes a pore-forming α subunit, and two different structural and regulatory β subunits. An essential component of the VGSC complex is ankyrin-G, a membrane protein that binds both $\text{Na}_v1.5$ and $\beta 1$ and localizes VGSCs to specific subcellular domains [46–48]. There are nine different VGSC α subunit genes [49], four of which are expressed in the ventricular myocyte, including the tetrodotoxin sensitive (TTX-S) channels, $\text{Na}_v1.1$, $\text{Na}_v1.3$, and $\text{Na}_v1.6$ and the tetrodotoxin-resistant (TTX-R) channel $\text{Na}_v1.5$ [50]. In heart, the TTX-S channels localize with ankyrin-B to the transverse T-tubule system while TTX-R $\text{Na}_v1.5$ interacts with ankyrin-G and is targeted to the intercalated disk and to the lateral sarcolemma [26]. The importance of $\text{Na}_v1.5$ to normal cardiac physiology is evident from the range of severe cardiovascular disorders associated with alterations in the function or integrity of the $\text{Na}_v1.5$ signaling complex as well as the severe phenotype of the *Scn5a* null mouse model [51]. Mutations in *SCN5A* have been described in patients with Long QT syndrome (LQT3) [43], Brugada Syndrome (BS) [44], Progressive Familial Heart Block (PFHB1A), and Dilated Cardiomyopathy with conduction disorder and arrhythmia (CMD1E) [52]. These disorders are associated with abnormal impulse propagation (PFHB1A and CMDE1) and/or severe ventricular arrhythmias and sudden death (LQT3, BS, and CMDE1). The finding of dilated cardiomyopathy in a subset of patients may be due to the adhesive properties of $\beta 1$ and/or $\beta 2$ subunits [53, 54] and is further evidence of the close relationship of the structural and electrochemical properties of the ID.

In this study, we noted that ankyrin-G was selectively recruited to cell-cell contact domains involved in adhesive interactions, suggesting that cell adhesion is required for localization of $\text{Na}_v1.5$ to the ID. This targeting concentrates the channel at specific sarcolemmal domains, most specifically those domains that are also involved in direct electrochemical communication between adjacent cells through co-localization with gap junctions.

5. Summary

The current study builds on prior work using the de- and redifferentiation model of cardiac myocyte remodeling to examine the ordered assembly and integration of the elements of the ID. The current study demonstrates that desmoplakin and ankyrin-G are specifically recruited to PKP-containing adhesion plaques in remodeling cardiac myocytes and that localization of ankyrin-G to new intercalated disks significantly precedes the recruitment of Na_v1.5, the alpha subunit of the VGSC. These new findings have important implications for the scaffolding of critical elements of the cellular cytoskeleton involved in the pathogenesis of disease processes including ARVD and Na_v1.5-dependent disorders (e.g., Long QT Syndrome type 3 and Brugada Syndrome). The observed hierarchy for the assembly of the mechanical and electrochemical components of the disk has important implications for determining the genesis of ventricular arrhythmias in these disorders. Through the identification of mechanisms of arrhythmia generation, it may be possible to develop novel treatment strategies to prevent serious ventricular arrhythmias and lower the risk for sudden cardiac death in patients with ischemic or genetic myocardial disease.

Acknowledgments

The authors would like to recognize Sarah Schumacher, Guadalupe Guerrero-Serna, Priscilla Sato, and Oksana Nekrasova for their technical advice and assistance. The work was supported by funds from the NIH [R01-HL075093 (MWR)], from the Stern Professorship (MWR) at the University of Michigan, from the Joseph L. Mayberry Endowment (KJG), and a grant from the LeDucq Foundation (MD, KJG).

References

- [1] M. S. Forbes and N. Sperelakis, "Intercalated discs of mammalian heart: a review of structure and function," *Tissue and Cell*, vol. 17, no. 5, pp. 605–648, 1985.
- [2] J.-C. Perriard, A. Hirschy, and E. Ehler, "Dilated cardiomyopathy: a disease of the intercalated disc?" *Trends in Cardiovascular Medicine*, vol. 13, no. 1, pp. 30–38, 2003.
- [3] E. Ehler, R. Horowitz, C. Zuppinger, et al., "Alterations at the intercalated disk associated with the absence of muscle LIM protein," *Journal of Cell Biology*, vol. 153, no. 4, pp. 763–772, 2001.
- [4] R. R. Kaprielian, M. Gunning, E. Dupont, et al., "Downregulation of immunodetectable connexin43 and decreased gap junction size in the pathogenesis of chronic hibernation in the human left ventricle," *Circulation*, vol. 97, no. 7, pp. 651–660, 1998.
- [5] J. H. Smith, C. R. Green, N. S. Peters, S. Rothery, and N. J. Severs, "Altered patterns of gap junction distribution in ischemic heart disease. An immunohistochemical study of human myocardium using laser scanning confocal microscopy," *American Journal of Pathology*, vol. 139, pp. 801–821, 1991.
- [6] J. Li, M. D. Levin, Y. Xiong, N. Petrenko, V. V. Patel, and G. L. Radice, "N-cadherin haploinsufficiency affects cardiac gap junctions and arrhythmic susceptibility," *Journal of Molecular and Cellular Cardiology*, vol. 44, no. 3, pp. 597–606, 2008.
- [7] R. M. Shaw, A. J. Fay, M. A. Puthenveedu, M. von Zastrow, Y.-N. Jan, and L. Y. Jan, "Microtubule plus-end-tracking proteins target gap junctions directly from the cell interior to adherens junctions," *Cell*, vol. 128, no. 3, pp. 547–560, 2007.
- [8] P. Muthappan and H. Calkins, "Arrhythmogenic right ventricular dysplasia," *Progress in Cardiovascular Diseases*, vol. 51, no. 1, pp. 31–43, 2008.
- [9] J.-S. Hulot, X. Jouven, J.-P. Empana, R. Frank, and G. Fontaine, "Natural history and risk stratification of arrhythmogenic right ventricular dysplasia/cardiomyopathy," *Circulation*, vol. 110, no. 14, pp. 1879–1884, 2004.
- [10] A. Tabib, R. Loire, L. Chalabreysse, et al., "Circumstances of death and gross and microscopic observations in a series of 200 cases of sudden death associated with arrhythmogenic right ventricular cardiomyopathy and/or dysplasia," *Circulation*, vol. 108, no. 24, pp. 3000–3005, 2003.
- [11] D. Dalal, K. Nasir, C. Bomma, et al., "Arrhythmogenic right ventricular dysplasia: a United States experience," *Circulation*, vol. 112, no. 25, pp. 3823–3832, 2005.
- [12] E. M. Oxford, H. Musa, K. Maass, W. Coombs, S. M. Taffet, and M. Delmar, "Connexin43 remodeling caused by inhibition of plakophilin-2 expression in cardiac cells," *Circulation Research*, vol. 101, no. 7, pp. 703–711, 2007.
- [13] R. Joshi-Mukherjee, W. Coombs, H. Musa, E. Oxford, S. Taffet, and M. Delmar, "Characterization of the molecular phenotype of two arrhythmogenic right ventricular cardiomyopathy (ARVC)-related plakophilin-2 (PKP2) mutations," *Heart Rhythm*, vol. 5, no. 12, pp. 1715–1723, 2008.
- [14] H. Tandri, A. Asimaki, D. Dalal, J. E. Saffitz, M. K. Halushka, and H. Calkins, "Gap junction remodeling in a case of arrhythmogenic right ventricular dysplasia due to plakophilin-2 mutation," *Journal of Cardiovascular Electrophysiology*, vol. 19, no. 11, pp. 1212–1214, 2008.
- [15] P. Y. Sato, H. Musa, W. Coombs, et al., "Loss of plakophilin-2 expression leads to decreased sodium current and slower conduction velocity in cultured cardiac myocytes," *Circulation Research*, vol. 105, no. 6, pp. 523–526, 2009.
- [16] M. V. Westfall, E. M. Rust, F. Albayya, and J. M. Metzger, "Adenovirus-mediated myofilament gene transfer into adult cardiac myocytes," *Methods in Cell Biology*, no. 52, pp. 307–322, 1997.
- [17] V. Person, S. Kostin, K. Suzuki, S. Labeit, and J. Schaper, "Antisense oligonucleotide experiments elucidate the essential role of titin in sarcomerogenesis in adult rat cardiomyocytes in long-term culture," *Journal of Cell Science*, vol. 113, no. 21, pp. 3851–3859, 2000.
- [18] S. Getsios, E. V. Amargo, R. L. Dusek, et al., "Coordinated expression of desmoglein 1 and desmocollin 1 regulates intercellular adhesion," *Differentiation*, vol. 72, no. 8, pp. 419–433, 2004.
- [19] R. L. Moses and W. C. Claycomb, "Disorganization and reestablishment of cardiac muscle cell ultrastructure in cultured adult rat ventricular muscle cells," *Journal of Ultrastructure Research*, vol. 81, no. 3, pp. 358–374, 1982.
- [20] A. P. Kowalczyk, E. A. Bornslaeger, J. E. Borgwardt, et al., "The amino-terminal domain of desmoplakin binds to plakoglobin and clusters desmosomal cadherin-plakoglobin complexes," *Journal of Cell Biology*, vol. 139, no. 3, pp. 773–784, 1997.
- [21] T. S. Stappenbeck and K. J. Green, "The desmoplakin carboxyl terminus coaligns with and specifically disrupts intermediate filament networks when expressed in cultured cells," *Journal of Cell Biology*, vol. 116, no. 5, pp. 1197–1209, 1992.

- [22] A. E. Bass-Zubek, R. P. Hobbs, E. V. Amargo, et al., "Plakophilin 2: a critical scaffold for PKC α that regulates intercellular junction assembly," *Journal of Cell Biology*, vol. 181, no. 4, pp. 605–613, 2008.
- [23] B. Gerull, A. Heuser, T. Wichter, et al., "Mutations in the desmosomal protein plakophilin-2 are common in arrhythmic right ventricular cardiomyopathy," *Nature Genetics*, vol. 36, no. 11, pp. 1162–1164, 2004.
- [24] B. D. Angst, L. U. R. Khan, N. J. Severs, et al., "Dissociated spatial patterning of gap junctions and cell adhesion junctions during postnatal differentiation of ventricular myocardium," *Circulation Research*, vol. 80, no. 1, pp. 88–94, 1997.
- [25] S. Kostin, S. Hein, E. P. Bauer, and J. Schaper, "Spatiotemporal development and distribution of intercellular junctions in adult rat cardiomyocytes in culture," *Circulation Research*, vol. 85, no. 2, pp. 154–167, 1999.
- [26] J. S. Lowe, O. Palygin, N. Bhasin, et al., "Voltage-gated Nav channel targeting in the heart requires an ankyrin-G-dependent cellular pathway," *Journal of Cell Biology*, vol. 180, no. 1, pp. 173–186, 2008.
- [27] P. J. Mohler, I. Rivolta, C. Napolitano, et al., "Na $_v$ 1.5 E1053K mutation causing Brugada syndrome blocks binding to ankyrin-G and expression of Na $_v$ 1.5 on the of cardiomyocytes," *Proceedings of the National Academy of Sciences of the United States of America*, vol. 101, no. 50, pp. 17533–17538, 2004.
- [28] A. B. Borisov, M. G. Martynova, and M. W. Russell, "Early incorporation of obscurin into nascent sarcomeres: implication for myofibril assembly during cardiac myogenesis," *Histochemistry and Cell Biology*, vol. 129, no. 4, pp. 463–478, 2008.
- [29] S. Pieperhoff, H. Schumacher, and W. W. Franke, "The area composita of adhering junctions connecting heart muscle cells of vertebrates. V. The importance of plakophilin-2 demonstrated by small interference RNA-mediated knockdown in cultured rat cardiomyocytes," *European Journal of Cell Biology*, vol. 87, no. 7, pp. 399–411, 2008.
- [30] W. W. Franke, H. Schumacher, C. M. Borrmann, et al., "The area composita of adhering junctions connecting heart muscle cells of vertebrates—III: assembly and disintegration of intercalated disks in rat cardiomyocytes growing in culture," *European Journal of Cell Biology*, vol. 86, no. 3, pp. 127–142, 2007.
- [31] S. Kostin and J. Schaper, "Tissue-specific patterns of gap junctions in adult rat atrial and ventricular cardiomyocytes in vivo and in vitro," *Circulation Research*, vol. 88, no. 9, pp. 933–939, 2001.
- [32] W. W. Franke, C. M. Borrmann, C. Grund, and S. Pieperhoff, "The area composita of adhering junctions connecting heart muscle cells of vertebrates. I. Molecular definition in intercalated disks of cardiomyocytes by immunoelectron microscopy of desmosomal proteins," *European Journal of Cell Biology*, vol. 85, no. 2, pp. 69–82, 2006.
- [33] J. E. Lewis, P. J. Jensen, and M. J. Wheelock, "Cadherin function is required for human keratinocytes to assemble desmosomes and stratify in response to calcium," *Journal of Investigative Dermatology*, vol. 102, no. 6, pp. 870–877, 1994.
- [34] M. Amagai, T. Fujimori, T. Masunaga, et al., "Delayed assembly of desmosomes in keratinocytes with disrupted classic-cadherin-mediated cell adhesion by a dominant negative mutant," *Journal of Investigative Dermatology*, vol. 104, no. 1, pp. 27–32, 1995.
- [35] S. Pieperhoff and W. W. Franke, "The area composita of adhering junctions connecting heart muscle cells of vertebrates. VI. Different precursor structures in non-mammalian species," *European Journal of Cell Biology*, vol. 87, no. 7, pp. 413–430, 2008.
- [36] J. K. Wahl, P. A. Sacco, T. M. McGranahan-Sadler, L. M. Sauppé, M. J. Wheelock, and K. R. Johnson, "Plakoglobin domains that define its association with the desmosomal cadherins and the classical cadherins: identification of unique and shared domains," *Journal of Cell Science*, vol. 109, no. 5, pp. 1143–1154, 1996.
- [37] L. L. Witcher, R. Collins, S. Puttagunta, et al., "Desmosomal cadherin binding domains of plakoglobin," *Journal of Biological Chemistry*, vol. 271, no. 18, pp. 10904–10909, 1996.
- [38] A. P. Kowalczyk, M. Hatzfeld, E. A. Bornslaeger, et al., "The head domain of plakophilin-1 binds to desmoplakin and enhances its recruitment to desmosomes. Implications for cutaneous disease," *Journal of Biological Chemistry*, vol. 274, no. 26, pp. 18145–18148, 1999.
- [39] E. A. Smith and E. Fuchs, "Defining the interactions between intermediate filaments and desmosomes," *Journal of Cell Biology*, vol. 141, no. 5, pp. 1229–1241, 1998.
- [40] P. D. Lampe, C. D. Copper, T. J. King, and J. M. Burt, "Analysis of Connexin43 phosphorylated at S325, S328 and S330 in normoxic and ischemic heart," *Journal of Cell Science*, vol. 119, no. 16, pp. 3435–3442, 2006.
- [41] E. Dupont, T. Matsushita, R. A. Kaba, et al., "Altered connexin expression in human congestive heart failure," *Journal of Molecular and Cellular Cardiology*, vol. 33, no. 2, pp. 359–371, 2001.
- [42] S. B. Danik, F. Liu, J. Zhang, et al., "Modulation of cardiac gap junction expression and arrhythmic susceptibility," *Circulation Research*, vol. 95, no. 10, pp. 1035–1041, 2004.
- [43] Q. Wang, J. Shen, I. Splawski, et al., "SCN5A mutations associated with an inherited cardiac arrhythmia, long QT syndrome," *Cell*, vol. 80, no. 5, pp. 805–811, 1995.
- [44] M. B. Rook, C. B. Alshinawi, W. A. Groenewegen, et al., "Human SCN5A gene mutations alter cardiac sodium channel kinetics and are associated with the Brugada syndrome," *Cardiovascular Research*, vol. 44, no. 3, pp. 507–517, 1999.
- [45] J.-J. Schott, C. Alshinawi, F. Kyndt, et al., "Cardiac conduction defects associate with mutations in SCN5A," *Nature Genetics*, vol. 23, no. 1, pp. 20–21, 1999.
- [46] S. M. Hashemi, T. J. Hund, and P. J. Mohler, "Cardiac ankyrins in health and disease," *Journal of Molecular and Cellular Cardiology*, vol. 47, no. 2, pp. 203–209, 2009.
- [47] D. P. McEwen and L. L. Isom, "Heterophilic interactions of sodium channel β 1 subunits with axonal and glial cell adhesion molecules," *Journal of Biological Chemistry*, vol. 279, no. 50, pp. 52744–52752, 2004.
- [48] J. D. Malhotra, M. C. Koopmann, K. A. Kazen-Gillespie, N. Fettman, M. Hortsch, and L. L. Isom, "Structural requirements for interaction of sodium channel β 1 subunits with ankyrin," *Journal of Biological Chemistry*, vol. 277, no. 29, pp. 26681–26688, 2002.
- [49] A. L. Goldin, R. L. Barchi, J. H. Caldwell, et al., "Nomenclature of voltage-gated sodium channels," *Neuron*, vol. 28, no. 2, pp. 365–368, 2000.
- [50] J. D. Malhotra, C. Chen, I. Rivolta, et al., "Characterization of sodium channel α - and β -subunits in rat and mouse cardiac myocytes," *Circulation*, vol. 103, no. 9, pp. 1303–1310, 2001.
- [51] G. A. Papadatos, P. M. R. Wallerstein, C. E. G. Head, et al., "Slowed conduction and ventricular tachycardia after targeted disruption of the cardiac sodium channel gene Scn5a," *Proceedings of the National Academy of Sciences of the United States of America*, vol. 99, no. 9, pp. 6210–6215, 2002.

- [52] W. P. McNair, L. Ku, M. R. G. Taylor, et al., “SCN5A mutation associated with dilated cardiomyopathy, conduction disorder, and arrhythmia,” *Circulation*, vol. 110, no. 15, pp. 2163–2167, 2004.
- [53] W. J. Brackenbury, M. B. A. Djamgoz, and L. L. Isom, “An emerging role for voltage-gated Na⁺ channels in cellular migration: regulation of central nervous system development and potentiation of invasive cancers,” *Neuroscientist*, vol. 14, no. 6, pp. 571–583, 2008.
- [54] W. J. Brackenbury and L. L. Isom, “Voltage-gated Na⁺ channels: potential for β subunits as therapeutic targets,” *Expert Opinion on Therapeutic Targets*, vol. 12, no. 9, pp. 1191–1203, 2008.

Review Article

Molecular Structure of Sarcomere-to-Membrane Attachment at M-Lines in *C. elegans* Muscle

Hiroshi Qadota and Guy M. Benian

Department of Pathology, Emory University, Atlanta, GA 30322, USA

Correspondence should be addressed to Guy M. Benian, pathgb@emory.edu

Received 8 December 2009; Accepted 30 January 2010

Academic Editor: Aikaterini Kontrogianni-Konstantopoulos

Copyright © 2010 H. Qadota and G. M. Benian. This is an open access article distributed under the Creative Commons Attribution License, which permits unrestricted use, distribution, and reproduction in any medium, provided the original work is properly cited.

C. elegans is an excellent model for studying nonmuscle cell focal adhesions and the analogous muscle cell attachment structures. In the major striated muscle of this nematode, all of the M-lines and the Z-disk analogs (dense bodies) are attached to the muscle cell membrane and underlying extracellular matrix. Accumulating at these sites are many proteins associated with integrin. We have found that nematode M-lines contain a set of protein complexes that link integrin-associated proteins to myosin thick filaments. We have also obtained evidence for intriguing additional functions for these muscle cell attachment proteins.

1. Structure of *C. elegans* Body Wall Muscle

Sarcomeres, highly ordered assemblages of several hundred proteins, perform the work of muscle contraction. Despite ever increasing knowledge of the components of sarcomeres and their functions, we still do not have a clear picture about how sarcomeres are assembled and maintained in the face of muscle contraction. A number of laboratories are studying the questions of sarcomere assembly and maintenance in the model genetic organism, *C. elegans*. In addition to being an excellent system to carry out mutational analysis in a whole organism, through both forward and reverse genetics, this nematode offers several advantages for studying muscle. These include its optical transparency, which allows evaluation of myofibrillar structure by polarized light, and localization of GFP-tagged proteins. In addition, its usual mode of self-fertilization allows propagation of muscle mutants that would be unable to mate. In the major striated muscle of *C. elegans* which is found in the body wall and used for locomotion (Figure 1), the myofibrils are restricted to a narrow $\sim 1.5 \mu\text{m}$ zone adjacent to the cell membrane along the outer side of the muscle cell [1–3]. The thin filaments are attached to the dense bodies (Z-disk analogs), and the thick filaments are organized around M-lines. Moreover, all the dense bodies and M-lines are anchored to the muscle cell membrane and extracellular matrix (ECM), which is

attached to the hypodermis and cuticle (see Figure 1). This allows the force of muscle contraction to be transmitted directly to the cuticle and allows movement of the whole animal. Thus, worm muscle M-lines and dense bodies serve the function of analogous structures in vertebrate muscle. But, in addition, because of their membrane anchorage and protein composition, they are also similar to focal adhesions of non-muscle cells and costameres of vertebrate muscle [4, 5].

2. Discovery of Muscle Attachment Components through Immunological and Genetic Approaches

First success in identifying muscle attachment components came from an immunological approach. Francis and Waterston [7, 8] used protein fractions enriched in nematode body wall muscle components to generate a battery of monoclonal antibodies and then determined their staining patterns in nematodes and their western blot reactivities. These monoclonal antibodies recognize several muscle or hypodermis attachment structures. Using two of these antibodies that localize to the base of dense bodies to screen an expression library, *C. elegans* vinculin, encoded by the *deb-1* gene, was identified [9]. After placing *deb-1* on the *C. elegans* genetic map, a genetic screen was conducted for loss of function

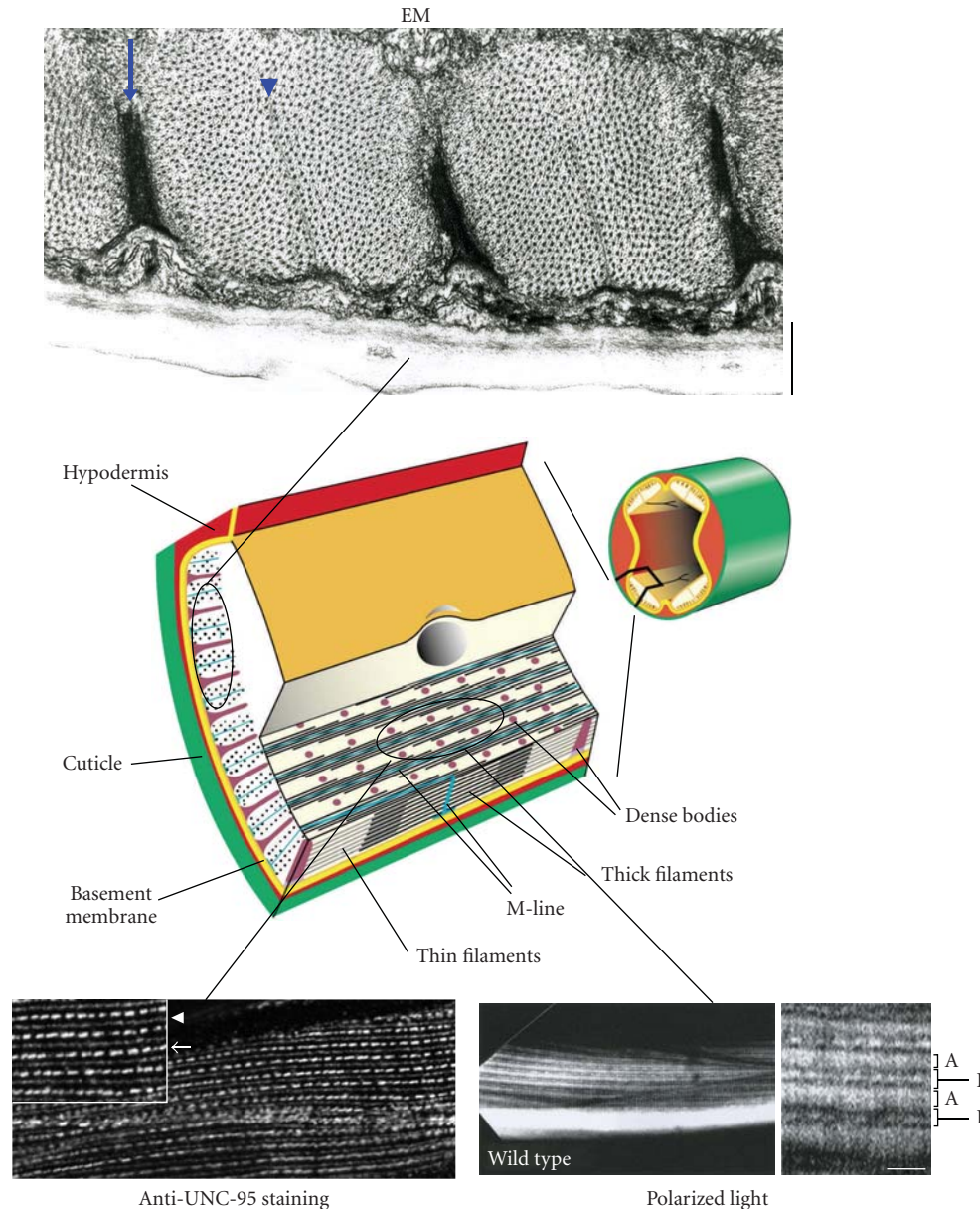


FIGURE 1: The body wall muscle of *C. elegans*. The color drawing on the right depicts a cross-section through an adult nematode emphasizing that the body wall muscle is organized into four quadrants. Each quadrant consists of interlocking pairs of mononuclear spindle-shaped cells (23 or 24 per quadrant). In the enlargement, notice that the myofilament lattice is restricted to one side of the cell, rather than filling the entire cross-sectional area as in a vertebrate striated muscle cell. Several planes of section are depicted; one of which emphasizes that fundamentally this is striated muscle with typical A-bands containing thick filaments organized around M-lines, and overlapping thin filaments attached to the Z-disk analogs called dense bodies. Note the plane parallel to the paper; this is the plane viewed when an animal, lying on a glass slide, is examined by light microscopy. At the bottom right is a typical image obtained with polarizing optics showing that bright A-bands alternate with dark I-bands; in the enlargement (right), the cross-sections of the dense bodies can be seen in the I-bands. At the bottom left is a typical image obtained by immunofluorescence microscopy using an antibody to UNC-95 [6] (enlargement is shown at the top left); notice that UNC-95 localizes to both rows of dense bodies (arrow) and M-lines (arrowhead). In the large drawing, the plane of section shown on the left side is a true cross-section through the nematode and through a body wall muscle cell; at the top of the figure is a typical transmission EM view of two sarcomeres; an arrow marks a dense body and an arrowhead marks an M-line. In the EM, at the bottom is located the thick cuticle and thin hypodermal cell and basement membrane; the cross-sections of thick filaments in the A-bands and the cross sections of the thin filaments in the I-bands (surrounding the dense bodies) can be seen. Notice that in the drawing and in the EM, all of the dense bodies and the M-lines are anchored to the muscle cell membrane. Indeed, the EM reveals that there is electron dense material at the base of each dense body and M-line that is likely to be responsible for this anchorage. This is in contrast to vertebrate striated muscle in which only the peripherally-located sarcomeres are anchored to the muscle cell membrane through costameres at the level of the Z-disks and possibly the M-lines.

mutations [10]. Two mutants in *deb-1* were shown to be embryonic lethal and displayed the same phenotype that was first identified for loss of function mutations in the *myo-3* gene [11]. *myo-3* encodes one of two myosin heavy chains, called MHC A, that is expressed in nematode body wall muscle and is localized to the middle of thick filaments [12]. Soon after the discovery of the *myo-3* phenotype, it was shown that strong loss of function alleles for the *unc-45* gene display a similar embryonic lethal phenotype [13]. (*unc-45* was later shown to encode a highly conserved myosin head chaperone [14, 15]). The phenotype of loss of function alleles consistent with a null state for *myo-3*, *unc-45*, and *deb-1* is “Pat”, which is an abbreviation for paralyzed and arrested at two-fold embryonic stage. During normal nematode embryonic development there are both an expansion of cell number and morphogenesis in which the initially football-shaped embryo elongates 4-fold, going through stages that are named according to length, 1.5-fold, 2-fold, and 3-fold, before hatching from the eggshell. Pat embryos do not move in the eggshell at the 1.5-fold stage and arrest development at the 2-fold stage. Other aspects of development continue and the embryo hatches as an abnormal L1 larva and dies. Encouraged by finding the Pat phenotype for *myo-3*, *deb-1*, and *unc-45*, Williams and Waterston [16] conducted a genome-wide screen and identified 13 additional genes with a Pat phenotype, and new alleles of *deb-1* and *myo-3*. From the precise characterization of the Pat mutant embryos, the Pat genes were classified into five classes. The other major phenotypic class of muscle affecting mutant genes is the “Unc” (uncoordinated) class, which result in slow moving or paralyzed adult worms [17, 18]. This class includes about 40 genes. However, the severity of the Pat phenotype suggests that genes of this class are crucial for the initial assembly of myofibrils. Interestingly, for a number of genes (*unc-45*, *unc-52*, *unc-97*, and *unc-112*), the phenotype of hypomorphic alleles is Unc, and the phenotype of alleles consistent with a null state is Pat. Later molecular cloning of the Pat genes revealed that classes I and II both have severe defects in myosin and actin organization, and encode many components of muscle attachment structures: *unc-52* encodes the ECM protein, perlecan [19], *pat-3* encodes β -integrin [20], *pat-2* encodes α -integrin (16; B. Williams, pers. commun.), *unc-112* encodes the nematode ortholog of mammalian Kindlin [21], *pat-4* encodes integrin-linked kinase, ILK [22], and *pat-6* encodes the nematode ortholog of mammalian actopaxin [23]. In addition to these cloned Pat genes, molecular analysis of *unc-97* revealed that *unc-97* encodes the *C. elegans* ortholog of mammalian PINCH [24], and the null state for *unc-97* is also Pat [25]. All of the abovementioned *pat* and *unc* gene products, except for *unc-45*, have been localized to both dense bodies and M-lines by GFP fusions (original papers cited above), and also in some cases by specific antibodies [6, 26]. Yeast two-hybrid assays using cloned fragments fused to yeast two-hybrid vectors and binding experiments using purified proteins have demonstrated that these class I and II Pat gene products interact with each other (see Figure 2). Based on what is known about its mammalian counterparts, it is likely that UNC-52 (perlecan) associates with PAT-2

(α -integrin) and PAT-3 (β -integrin) at the outside of muscle cells. Inside the muscle cell, it has been demonstrated that the cytoplasmic tail of the PAT-3 associates with a four-protein complex consisting of UNC-112 (Kindlin)/PAT-4 (ILK)/UNC-97 (PINCH)/PAT-6 (actopaxin) (22, 23, 25; H. Qadota, D. G. Moerman, G. M. Benian, submitted). As indicated in Figure 2, UNC-52 (perlecan), integrins (PAT-2/PAT-3), and the four-protein complex are found at the base of both M-lines and dense bodies. At the dense bodies, there are additional dense body-specific proteins such as DEB-1 (vinculin) [9], ATN-1 (α -actinin) [27], UIG-1 (Cdc42 GEF) [28], ALP-1 (ALP/Enigma) [29], DYC-1 [30], and ELP-1 (EMAP-like protein) [31]. The only known nematode M-line-specific protein is UNC-89 (obscurin) [32, 33]; as mentioned below, UNC-98 and UNC-96 are most prominent at M-lines. In this review, we will focus on the M-line and its molecular components. For the structure and molecular components of dense bodies see the recent review by Lecroisey et al. [34].

3. UNC-98, UNC-96, and UNC-95

Our interest in the molecular mechanisms by which sarcomeres are attached to the muscle cell membrane at the M-line began with our molecular cloning of two muscle Unc genes, *unc-98* and *unc-96*, that have similar mutant phenotypes. These two genes were first identified by Zengel and Epstein [18] from their genetic screen for mutants that are defective in muscle function and structure, which involved mutagenesis followed by enrichment for mutants with slow motility, and then examination of myofilament lattice structure by polarized light microscopy. *unc-98* and *unc-96* mutants are slower moving than wild type, and by polarized light microscopy display a moderately disorganized myofilament lattice and birefringent “needle-like” structures at the ends of their body wall muscle cells. These “needles” correspond to accumulations of proteins that contain paramyosin, but not actin, myosin, UNC-89, or α -actinin [35–37]. By electron microscopy, both *unc-98* and *unc-96* mutants display indistinct A and I bands, and short and irregularly shaped dense bodies, and short or even absent M-lines. *unc-98* encodes a 310 residue polypeptide containing 4 C2H2 Zn finger domains and several predicted nuclear localization and nuclear export signal sequences [35]. Antibodies to UNC-98 localize to M-lines. However, in transgenic animals, UNC-98::GFP localizes to M-lines, dense bodies, and muscle cell nuclei. In addition, *unc-98* mutant animals, when rescued with a wild-type copy of the gene, show localization of anti-UNC-98 antibodies to M-lines, dense bodies and nuclei. Our interpretation is that UNC-98 is mainly localized to M-lines, but also exists normally at low levels at dense bodies and nuclei, but below the level of detection by antibody staining. Deletion derivatives of UNC-98::GFP in transgenic worms demonstrates that the N-terminal 110 residues of UNC-98 are necessary and sufficient for nuclear localization, and that all four Zn fingers are sufficient for localization to M-lines and dense bodies. Using an UNC-98 bait to screen a collection of 2-hybrid clones representing 16 known M-line and dense body proteins, interaction with UNC-97 (PINCH)

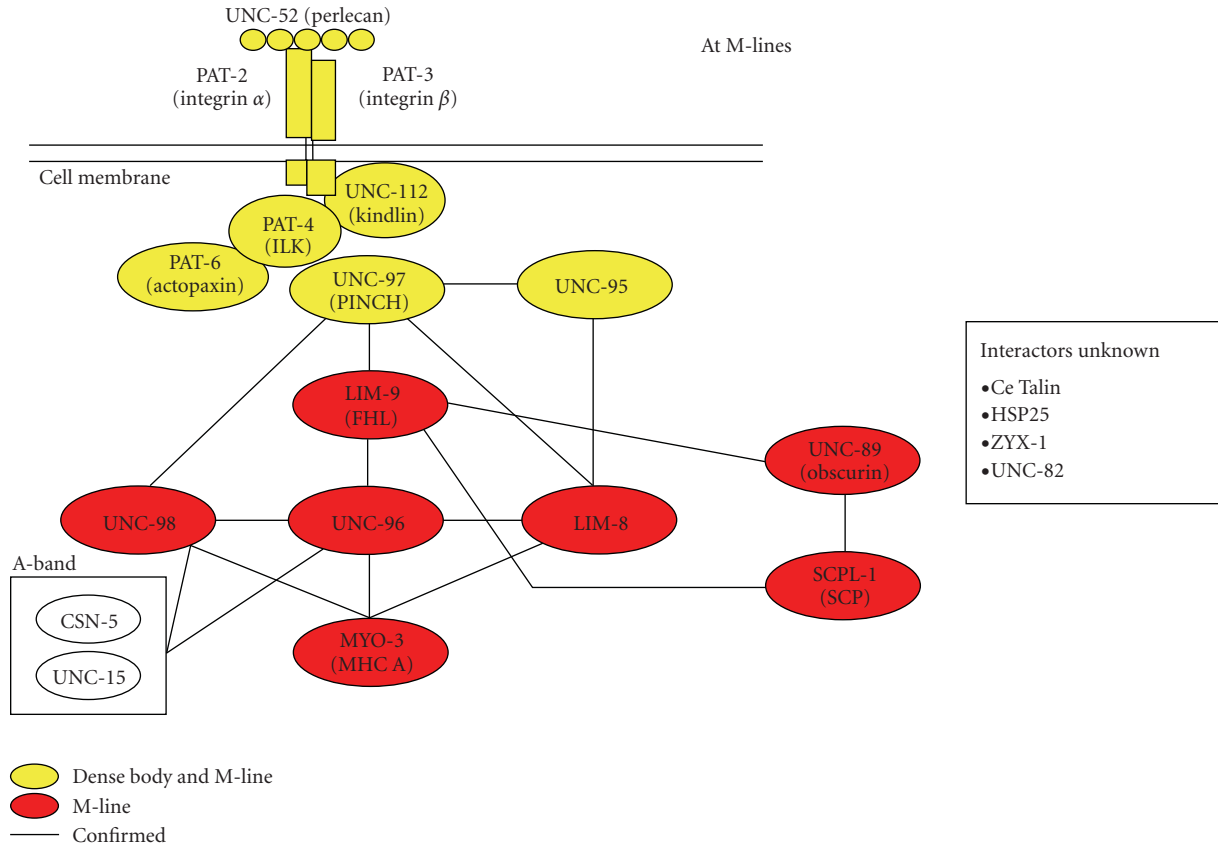


FIGURE 2: A protein interaction matrix for M-lines in *C. elegans* striated muscle. The myofilament lattice is located close to the surface and anchored by M-lines and dense bodies to the muscle cell membrane. At these attachment structures, UNC-52 (perlecan) is located in the ECM, and by homology is likely to interact with an integrin $\alpha\beta$ heterodimer (PAT-2 and PAT-3). Inside the muscle cell, the cytoplasmic tail of PAT-3 (β integrin) is associated with a complex of four conserved proteins [UNC-112 (Kindlin), PAT-4 (ILK), PAT-6 (actopaxin), UNC-97 (PINCH)]. UNC-95 is also found at both M-lines and dense bodies. At M-lines, specific proteins link UNC-97 (PINCH) to myosin heavy chains (MHC A). These are UNC-98, LIM-9 (FHL) and UNC-96, LIM-8, and UNC-95 and LIM-8. UNC-98, UNC-96 and LIM-8 have all been shown to interact with portions of the rod domain of MHC A. LIM-9 links to the giant protein UNC-89 (obscurin) and to the phosphatase SCPL-1 (SCP). Additionally, UNC-98 and UNC-96 interact with UNC-15 (paramyosin) and to CSN-5 (COP9 signalosome component), but these interactions occur outside the M-line. The box on the right indicates that there are four more proteins that have been reported to reside at the M-line (Ce Talin, HSP25, ZYX-1 (zyxin), and UNC-82 (ARK5/SNARK)), but these have not yet been connected with components of the interaction matrix. Lines indicate interactions that were identified by 2-hybrid screens and later shown to occur with purified proteins in vitro. All proteins indicated have been localized to M-lines by specific antibodies and/or GFP fusions. References for all the interactions have been cited in the text except for the LIM-8/UNC-95 interaction (A. Simionescu, H. Qadota, and G. Benian, unpub. data).

was revealed, thus showing a connection to the conserved four-protein complex associated with integrin. The UNC-98/UNC-97 interaction was confirmed by in vitro binding using purified proteins. Moreover, binding requires the first two LIM domains of the 5 LIM domain protein UNC-97, and all 4 C2H2 Zn fingers of UNC-98.

We later showed that *unc-96* encodes 408 and 418 residue polypeptides by alternative splicing, and these proteins lack recognizable domains [36]. Nonetheless, UNC-96 may consist of two domains separated by a flexible loop or linker [37]. Antibodies to UNC-96 localize the protein to muscle M-lines, although UNC-96::GFP localizes to both M-lines and dense bodies and not to nuclei [36]. A role for UNC-96 in embryonic muscle development is uncertain: although UNC-96 is detectable by the 1.5-fold stage, its

expression decreases with time and by the 3-fold stage is nearly undetectable. The strongest mutant allele of *unc-96*, *sf18*, is not Pat embryonic lethal, and yet is presumably a null mutant, as it is a nonsense mutation, and no protein can be detected by western blot. Intriguingly, either a decreased (by loss of function mutation) or an increased level (by a heat-shock promoter in adult muscle) of UNC-96 results in disorganization of thick filaments [6]. Thus, the level of UNC-96 must be precisely controlled in order to obtain proper organization of thick filaments. By both genetic and biochemical criteria, UNC-98 and UNC-96 interact with each other. Although *unc-98; unc-96* double mutants do not show an enhanced or suppressed phenotype, when either UNC-98 is overexpressed in an *unc-96* mutant background, or UNC-96 is overexpressed in an *unc-98* mutant background

there is enhancement; by polarized light microscopy, there is a greater degree of myofibril disorganization and larger and brighter needles. Moreover, protein accumulations at the ends of the muscle cells contain UNC-98 protein in *unc-96* mutants, and contain UNC-96 protein in *unc-98* mutants. UNC-96 was shown to interact with UNC-98 by both a yeast 2-hybrid assay and a far Western assay using purified proteins. This interaction requires the C-terminal half of UNC-96 and the C-terminal three C2H2 domain of UNC-98. Although obvious homologs of either UNC-98 or UNC-96 cannot be found in vertebrate proteomes, it is possible that structural or functional homologs do exist.

unc-95 was also first isolated from the genetic screen reported by Zengel and Epstein [18], and then molecularly cloned by Broday and colleagues [38]. *unc-95* mutants are slow moving and have disorganized muscle structure. Immunostaining with various antibodies shows that thick and thin filaments and dense bodies are disorganized [38]. Myofibrillar disorganization is also obvious by EM; moreover, dense bodies are short and irregular and M-lines are missing. *unc-95* encodes a 350-residue polypeptide with a single LIM domain near its C-terminus, and a region predicted to have coiled-coil structure and a predicted NLS sequence [38]. Although the UNC-95 LIM domain was reported to be most homologous to LIM domains in fly and vertebrate paxillin [38], more recently, a true ortholog of vertebrate paxillin has been found in *C. elegans*, PXL-1 (A. Warner and D. G. Moerman, pers. commun.). An UNC-95::GFP translational fusion localizes to M-lines, dense bodies, muscle cell-cell boundaries, and nuclei in adult body wall muscle [38]. UNC-95::GFP is clearly also expressed in embryonic muscle, and by the 3-fold stage is localized to muscle attachment sites and nuclei. Antibodies that we later developed to UNC-95 clearly label the M-lines, dense bodies, and cell-cell boundaries, but not nuclei in adult body wall muscle [6].

4. Multiple Protein Complexes Link Integrin to Myosin in Thick Filaments at Nematode M-Lines

During the past 7 years, we have discovered proteins that interact with UNC-97 (PINCH) at nematode M-lines. The first of these was the M-line protein UNC-98 [35], as mentioned above: the first two of the five total LIM domains of UNC-97 interact with the 4 C2H2 Zn fingers of UNC-98. In Miller et al. [26] we showed that the N-terminal 110 residues of UNC-98 interact with the C-terminal portion of a myosin heavy chain, MHC A, which resides in the middle of thick filaments in the proximity of M-lines. A combination of genetic, cell biologic and biochemical evidence supports a model in which UNC-98 links integrin-associated proteins to myosin in thick filaments at M-lines. Although vertebrate costameres are usually regarded to reside at the level of Z-disks, some components of focal adhesions, including α integrin, have also been found at M-lines [39]. Thus, our results for *C. elegans* muscle suggest the possibility of a similar mechanism of linkage between integrins and myosin

thick filaments at the M-lines of peripheral myofibrils of vertebrate muscle.

In Qadota et al. [6] we demonstrated additional mechanisms by which this linkage from muscle cell membrane to myosin occurs. To identify additional proteins that interact with UNC-97, we screened a collection of known and candidate components of M-lines and/or dense bodies, UNC-112 interactors, and UIG-1 interactors, by the 2-hybrid method. Three new UNC-97 (PINCH) interactors were identified: LIM-8, LIM-9, and UNC-95. It was shown that these proteins are involved in three additional mechanisms by which linkage from UNC-97 to myosin occurs: from UNC-97 through LIM-8 to myosin, or from UNC-97 through LIM-9/UNC-96 to myosin, or from UNC-97 through UNC-95/LIM-8 to myosin. LIM-8 is a novel LIM domain-containing protein. LIM-9 is the nematode homolog of mammalian FHL (four-and-a-half LIM domain protein). All three new UNC-97 interactors contain LIM domains that are required for binding. Among the three interactors, LIM-8 and LIM-9 also bind to UNC-96. UNC-96 and LIM-8 also bind to the C-terminal portion of MHC A (to a slightly different portion of MHC A that binds to UNC-98). All interactions were first identified by yeast 2-hybrid and then confirmed by in vitro binding assays using purified proteins. All three novel UNC-97 interactors are expressed in body wall muscle and by antibodies localize at least partially to M-lines. LIM-8 and LIM-9 localize also to I-bands, around and between dense bodies.

Like UNC-98 and UNC-96, UNC-89 (mammalian homolog is called "obscurin" [40–42]) is also an M-line protein in *C. elegans* muscle. UNC-89 is a giant (up to 900 kDa) multidomain protein consisting primarily of Ig domains, SH3, DH and PH domains, and two protein kinase domains. We have shown recently that a portion of UNC-89 (containing the kinase domains) interacts with a member of the UNC-98/UNC-96 complex, namely, LIM-9 (FHL) [43]. Moreover, LIM-9 also interacts with an additional M-line protein that was first identified as an UNC-89 interactor, namely, SCPL-1, a CTD-type protein phosphatase [44]. This class of phosphatases was known to be involved in the regulation of transcription either through dephosphorylation of the C-terminal domain (CTD) of the largest subunit of RNA polymerase II, or in dephosphorylating Smad transcription factors. However, our results implicate new functions for this class of protein phosphatases, namely, in the assembly or maintenance of the M-line, and/or giant kinase signaling. We can now incorporate the majority of the known *C. elegans* M-line proteins into an M-line protein interaction matrix; the interactions were first identified through 2-hybrid analysis and later confirmed by both in vitro binding using purified proteins and immunolocalization to M-lines (Figure 2).

5. Additional Functions for M-Line Attachment Proteins

In addition to a structural and signaling role for UNC-96 and UNC-98 at the M-line, we have shown that these proteins interact with paramyosin to promote paramyosin's

incorporation into thick filaments [36, 37]. Paramyosin is an invertebrate-specific protein that is primarily an α -helical coiled-coil rod and is ~40% identical in amino acid sequence to the rod domains of myosin heavy chains. In *C. elegans* body wall muscle, the myosins and a portion of paramyosin are organized around a tubular core consisting of paramyosin and filagenins in a specific geometry [45–47]. The birefringent needles in *unc-96* and *unc-98* mutants contain paramyosin located outside the thick filaments. By genetic and biochemical criteria, paramyosin interacts with UNC-98 and UNC-96. By both yeast 2-hybrid analysis and ELISAs using purified proteins, UNC-98 interacts with paramyosin residues 31–693, whereas UNC-96 interacts with a separate region of paramyosin, residues 699–798. Although UNC-98 and UNC-96 affect, at least partially, the localization of paramyosin (some in accumulations, some in its normal A-band location), they do not affect the total level of paramyosin: paramyosin levels do not change in either *unc-96* or *unc-98* loss of function mutants. Nevertheless, the state of paramyosin does affect the localization and total amount of UNC-98 and possibly UNC-96: UNC-98 and UNC-96 colocalize with paramyosin aggregates of *unc-15* missense mutants, and when paramyosin is undetectable (*unc-15* nonsense mutant), UNC-98 and UNC-96 are diffusely localized. Indeed, by quantitative immunoblot, the levels of UNC-98 follow the paramyosin state: when paramyosin is undetectable (in the *unc-15* nonsense mutant *e1214*), the level of UNC-98 is diminished, and in paramyosin missense mutants (*e1215* and *e73*, which form paramyosin aggregates), the level of UNC-98 is increased. The dependence of UNC-98, and possibly UNC-96, levels on the state of paramyosin might be due to a chaperone function for UNC-98 and UNC-96 to prevent aggregation of paramyosin. An additional piece of data supports the idea that UNC-96 could act as a chaperone for paramyosin: both *unc-96* mutant alleles are suppressed at lower temperature; that is, when grown at 15°C, rather than the usual 20°C, the paramyosin “needles” (containing aggregated paramyosin) are not seen. One *unc-96* mutant allele is a stop codon, the other is a splicing site mutation, types of mutations not usually associated with temperature sensitivity. Alternative possibilities are that (1) the formation of paramyosin paracrystals is temperature dependent, and thus reduced at cold temperatures, and/or (2) the competing formation of proper thick filaments is enhanced at lower temperatures. However, the temperature effect seems to be specific to *unc-96*: neither *unc-98* nor *unc-15* is suppressed at lower temperature [36]. Therefore, these alternative possibilities do not seem to be supported. Perhaps the lower temperature might even reduce the rate of thick filament assembly or turnover so that the UNC-96 chaperone is no longer required to prevent aggregation.

Most recently, we have demonstrated that both UNC-98 and UNC-96 interact with CSN-5 [48]. Interactions were identified by a yeast 2-hybrid screen and confirmed by biochemical methods. CSN-5 is a member of the highly conserved “COP9 signalosome complex” which has been found in multiple organisms to regulate protein stability, usually through SCF ubiquitin ligases [49, 50]. Anti-CSN-5 antibody colocalizes with paramyosin at A-bands in wild

type, and co-localizes with abnormal accumulations of paramyosin found in *unc-98*, *unc-96*, and *unc-15* mutants. Knockdown of *csn-5* results in an increase in the level of UNC-98 protein and a slight reduction in the level of UNC-96 protein, suggesting that normally CSN-5 promotes the degradation of UNC-98 and that CSN-5 stabilizes UNC-96. In *unc-15* and *unc-96* mutants, CSN-5 protein is reduced, implying the existence of feedback regulation from myofibril proteins to CSN-5 protein levels. This is the first report to implicate CSN-5 or the COP9 signalosome in myofibrillar organization or function. Nevertheless, the report is consistent with the growing recognition that the ubiquitin proteasome system is required for muscle protein turnover in vertebrate muscle, and mediated by the muscle-specific ubiquitin ligase Atrogin-1, and the MuRF family (Muscle-specific RING Finger proteins) [51, 52]. Indeed, for *C. elegans* muscle, the RING finger protein, RNF-5 is localized to dense bodies and regulates the levels of UNC-95 [38]: RNF-5 and UNC-95 interact by yeast 2-hybrid [53]; heat shock induced overexpression of RNF-5 results in a reduction in UNC-95::GFP, and this reduction depends on the presence of an active RING finger domain in RNF-5; in contrast, RNAi knockdown of *rnf-5* results in an increase in UNC-95::GFP [38].

6. Nuclear Function for Muscle Focal Adhesion Proteins?

In recent years, there has been growing recognition that in mammalian striated muscle, a number of Z-disk and M-line proteins translocate to the nucleus in response to mechanical stimuli or extracellular signals, and once inside the nucleus, influence gene transcription [54, 55]. A similar situation appears to exist for nematode muscle, but at this time, the mechanisms of nuclear translocation and the functional significance of M-line and dense body proteins in the nucleus are less understood than they are for mammalian muscle. But given the power of worm genetics and its advantages for imaging live muscle cells, this area holds much promise for future insights. Here is what we know for proteins that are at least partly localized to M-lines: In transgenic worms, translational GFP fusions of full-length UNC-97 [24], UNC-98 [35], UNC-95 [38], and ZYX-1 (zyxin) [30] show localization to M-lines, dense bodies, and nuclei. However, antibodies that we have developed to UNC-98 [35], to UNC-97 [26], and to UNC-95 [6], when used in immunofluorescent experiments, failed to localize to nuclei under normal conditions. There are no reports of antibodies having been generated or localized for ZYX-1. Nevertheless, anti-UNC-98 reacted to nuclei, when a nonstandard fixation method was used on wild-type nematodes, or when UNC-98 was overexpressed [35]. Additional support that endogenous UNC-98 and UNC-97 reside in nuclei was obtained during our purification of native thick filaments reported in Miller et al. [26]: nuclear-enriched fractions from wild-type worms contain western blot detectable UNC-98 and UNC-97. In the 2-hybrid system, when either UNC-98 [35] or UNC-97 (H. Qadota, K. Norman, and D. Moerman, unpub. data) is fused to the GAL4 DNA-binding domain, they can activate

transcription, suggesting that UNC-98 and UNC-97 may activate transcription *in vivo*. By testing deletion derivatives of UNC-98::GFP, we have shown that the N-terminal 110 residues of UNC-98 are sufficient for nuclear localization [35]. A similar approach by Norman et al. [25] indicates that LIM2 and LIM3 are required for nuclear localization of UNC-97 (PINCH).

In addition to nuclear localization of proteins that are localized to M-lines and dense bodies, nuclear localization has also been found for the dense-body-specific protein ALP-1 [29]. The *alp-1* gene encodes 4 different isoforms; one is ALP-like (ALP-1A), and three are Enigma-like (ALP-1B, -1C, -1D). Use of GFP translational fusions demonstrates a complex pattern of expression of these proteins in embryos and adults, and localization to muscle cell dense bodies, and nuclei of muscle and hypodermal (epithelial) cells. In fact, ALP-1 is one of the few muscle focal adhesion proteins showing strong localization to embryonic muscle (ALP-1A) and hypodermal cell (ALP-1B,C,D) nuclei.

7. Future Directions

Three additional proteins have been localized at both M-lines and dense bodies; these are ZYX-1 (zyxin) [30] (as noted above), HSP25 [56], and Ce Talin [57]. However, the mutant or RNAi phenotypes and molecular interactions of these proteins have not yet been reported. Although ZYX-1 has been demonstrated to interact with the dense-body-specific protein DYC-1 [30], its interactions with proteins at the M-line have not been determined. The most recently discovered M-line component is UNC-82, a 1600-residue polypeptide with a serine/threonine kinase domain (orthologous to human ARK5 or SNARK) near its N-terminus [58]. It is required for maintaining proper organization of thick filaments and the M-line during growth of muscle cells. It will be interesting to determine how UNC-82, HSP25, Ce Talin, and ZYX-1 fit into the growing M-line protein interaction matrix (Figure 2).

So far, there are no reports on the molecular cloning of one muscle Unc gene, *unc-100*, and 3 Pat genes (*pat-9*, *pat-11*, and *pat-12*). It will be interesting to learn the molecular nature of the encoded proteins for these genes, and whether the proteins are localized to M-line, dense bodies, or both. Additionally, we will also be able to determine with which existing proteins of the M-line and dense body interacting network these proteins interact. As mentioned above, we have found that two M-line proteins, LIM-9 and SCPL-1, interact with the C-terminal portion of the giant protein UNC-89 (obscurin). Efforts are underway to search for additional binding partners for this giant, and this is likely to identify new M-line proteins. Finally, it will be interesting to determine how many of the 108 new genes identified by Meissner et al. [59] encode proteins localized to M-lines and/or dense bodies. It will then be interesting to determine how they interact with previously described and new components of these structures, to obtain a more complete picture of sarcomere assembly.

Intragenic deletions (consistent with a null state) of the genes encoding many of the proteins that have been iden-

tified recently as components of M-lines and dense bodies have either weak defects or no obvious defects in myofibril assembly or motility (e.g., UIG-1, ATN-1, LIM-9, LIM-8, SCPL-1, ZYX-1). One explanation is that these proteins have noncrucial functions, or are redundant. Redundancy would be a reasonable explanation if such proteins were members of closely-related multigene families (e.g., the actin gene family). However, this does not appear to be the case. Another possibility is that our ability to discern a phenotype depends on the assay employed. Indeed, we can hypothesize that under the usual laboratory growth conditions and motility assays worm muscle operates far below its maximal capacity. Therefore, assays for motility usually employed may not be sufficient to reveal the requirement of many of these individual components. Perhaps more sophisticated assays, in which, for example, worms are required to “work harder” will reveal phenotypes. Indeed, we would expect that M-line and dense body components should function in the transmission of force from the thick and thin filaments through the muscle cell membrane, ECM, and ultimately to the cuticle.

Acknowledgment

The authors wish to thank support for their studies from Grants nos. AR052133 and AR051466 from the National Institutes of Health.

References

- [1] R. H. Waterston, “Muscle,” in *The Nematode Caenorhabditis Elegans*, W. B. Wood, Ed., pp. 281–335, Cold Spring Harbor Laboratory Press, Plainview, NY, USA, 1988.
- [2] D. G. Moerman and A. Fire, “Muscle structure, function and development,” in *C. Elegans II*, D. L. Riddle, T. Blumenthal, B. J. Meyer, and J. R. Priess, Eds., pp. 417–470, Cold Spring Harbor Laboratory Press, Plainview, NY, USA, 1997.
- [3] D. G. Moerman and B. D. Williams, “Sarcomere assembly in *C. elegans* muscle,” in *The C. Elegans Research community*, WormBook, 2006.
- [4] J. M. Ervasti, “Costameres: the Achilles’ heel of Herculean muscle,” *Journal of Biological Chemistry*, vol. 278, no. 16, pp. 13591–13594, 2003.
- [5] A. M. Samarel, “Costameres, focal adhesions, and cardiomyocyte mechanotransduction,” *American Journal of Physiology*, vol. 289, no. 6, pp. H2291–H2301, 2005.
- [6] H. Qadota, K. B. Mercer, R. K. Miller, K. Kaibuchi, and G. M. Benian, “Two LIM domain proteins and UNC-96 link UNC-97/PINCH to myosin thick filaments in *Caenorhabditis elegans* muscle,” *Molecular Biology of the Cell*, vol. 18, no. 11, pp. 4317–4326, 2007.
- [7] G. R. Francis and R. H. Waterston, “Muscle organization in *Caenorhabditis elegans*: localization of proteins implicated in thin filament attachment and I-band organization,” *Journal of Cell Biology*, vol. 101, no. 4, pp. 1532–1549, 1985.
- [8] G. R. Francis and R. H. Waterston, “Muscle cell attachment in *Caenorhabditis elegans*,” *Journal of Cell Biology*, vol. 114, no. 3, pp. 465–479, 1991.
- [9] R. J. Barstead and R. H. Waterston, “The basal component of the nematode dense-body is vinculin,” *Journal of Biological Chemistry*, vol. 264, no. 17, pp. 10177–10185, 1989.

- [10] R. J. Barstead and R. H. Waterston, "Vinculin is essential for muscle function in the nematode," *Journal of Cell Biology*, vol. 114, no. 4, pp. 715–724, 1991.
- [11] R. H. Waterston, "The minor myosin heavy chain, mhCA, of *Caenorhabditis elegans* is necessary for the initiation of thick filament assembly," *EMBO Journal*, vol. 8, no. 11, pp. 3429–3436, 1989.
- [12] D. M. Miller, I. Ortiz, G. C. Berliner, and H. F. Epstein, "Differential localization of two myosins within nematode thick filaments," *Cell*, vol. 34, no. 2, pp. 477–490, 1983.
- [13] L. Venolia and R. H. Waterston, "The unc-45 gene of *Caenorhabditis elegans* is an essential muscle-affecting gene with maternal expression," *Genetics*, vol. 126, no. 2, pp. 345–353, 1990.
- [14] J. M. Barral, C. C. Bauer, I. Ortiz, and H. F. Epstein, "Unc-45 mutations in *Caenorhabditis elegans* implicate a CRO1/She4p-like domain in myosin assembly," *Journal of Cell Biology*, vol. 143, no. 5, pp. 1215–1225, 1998.
- [15] J. M. Barral, A. H. Hutagalung, A. Brinker, F. U. Hartl, and H. F. Epstein, "Role of the myosin assembly protein UNC-45 as a molecular chaperone for myosin," *Science*, vol. 295, no. 5555, pp. 669–671, 2002.
- [16] B. D. Williams and R. H. Waterston, "Genes critical for muscle development and function in *Caenorhabditis elegans* identified through lethal mutations," *Journal of Cell Biology*, vol. 124, no. 4, pp. 475–490, 1994.
- [17] R. H. Waterston, J. N. Thomson, and S. Brenner, "Mutants with altered muscle structure in *Caenorhabditis elegans*," *Developmental Biology*, vol. 77, no. 2, pp. 271–302, 1980.
- [18] J. M. Zengel and H. F. Epstein, "Identification of genetic elements associated with muscle structure in the nematode *Caenorhabditis elegans*," *Cell Motility*, vol. 1, no. 1, pp. 73–97, 1980.
- [19] T. M. Rogalski, B. D. Williams, G. P. Mullen, and D. G. Moerman, "Products of the unc-52 gene in *Caenorhabditis elegans* are homologous to the core protein of the mammalian basement membrane heparan sulfate proteoglycan," *Genes and Development*, vol. 7, no. 8, pp. 1471–1484, 1993.
- [20] S. N. Gettner, C. Kenyon, and L. F. Reichardt, "Characterization of β pat-3 heterodimers, a family of essential integrin receptors in *C. elegans*," *Journal of Cell Biology*, vol. 129, no. 4, pp. 1127–1141, 1995.
- [21] T. M. Rogalski, G. P. Mullen, M. M. Gilbert, B. D. Williams, and D. G. Moerman, "The UNC-112 gene in *Caenorhabditis elegans* encodes a novel component of cell-matrix adhesion structures required for integrin localization in the muscle cell membrane," *Journal of Cell Biology*, vol. 150, no. 1, pp. 253–264, 2000.
- [22] A. C. Mackinnon, H. Qadota, K. R. Norman, D. G. Moerman, and B. D. Williams, "C. elegans PAT-4/ILK functions as an adaptor protein within integrin adhesion complexes," *Current Biology*, vol. 12, no. 10, pp. 787–797, 2002.
- [23] X. Lin, H. Qadota, D. G. Moerman, and B. D. Williams, "C. elegans PAT-6/actopaxin plays a critical role in the assembly of integrin adhesion complexes in vivo," *Current Biology*, vol. 13, no. 11, pp. 922–932, 2003.
- [24] O. Hobert, D. G. Moerman, K. A. Clark, M. C. Beckerle, and G. Ruvkun, "A conserved LIM protein that affects muscular adherens junction integrity and mechanosensory function in *Caenorhabditis elegans*," *Journal of Cell Biology*, vol. 144, no. 1, pp. 45–57, 1999.
- [25] K. R. Norman, S. Cordes, H. Qadota, P. Rahmani, and D. G. Moerman, "UNC-97/PINCH is involved in the assembly of integrin cell adhesion complexes in *Caenorhabditis elegans* body wall muscle," *Developmental Biology*, vol. 309, no. 1, pp. 45–55, 2007.
- [26] R. K. Miller, H. Qadota, M. L. Landsverk, K. B. Mercer, H. F. Epstein, and G. M. Benian, "UNC-98 links an integrin-associated complex to thick filaments in *Caenorhabditis elegans* muscle," *Journal of Cell Biology*, vol. 175, no. 6, pp. 853–859, 2006.
- [27] R. J. Barstead, L. Kleiman, and R. H. Waterston, "Cloning, sequencing, and mapping of an alpha-actinin gene from the nematode *Caenorhabditis elegans*," *Cell Motility and the Cytoskeleton*, vol. 20, no. 1, pp. 69–78, 1991.
- [28] T. Hikita, H. Qadota, D. Tsuboi, S. Taya, D. G. Moerman, and K. Kaibuchi, "Identification of a novel Cdc42 GEF that is localized to the PAT-3-mediated adhesive structure," *Biochemical and Biophysical Research Communications*, vol. 335, no. 1, pp. 139–145, 2005.
- [29] C. R. McKeown, H.-F. Han, and M. C. Beckerle, "Molecular characterization of the *Caenorhabditis elegans* ALP/Enigma gene *alp-1*," *Developmental Dynamics*, vol. 235, no. 2, pp. 530–538, 2006.
- [30] C. Lecroisey, E. Martin, M.-C. Mariol, et al., "DYC-1, a protein functionally linked to dystrophin in *Caenorhabditis elegans* is associated with the dense body, where it interacts with the muscle LIM domain protein ZYX-1," *Molecular Biology of the Cell*, vol. 19, no. 3, pp. 785–796, 2008.
- [31] J. L. Hueston and K. A. Suprenant, "Loss of dystrophin and the microtubule-binding protein ELP-1 causes progressive paralysis and death of adult *C. elegans*," *Developmental Dynamics*, vol. 238, no. 8, pp. 1878–1886, 2009.
- [32] G. M. Benian, T. L. Tinley, X. Tang, and M. Borodovsky, "The *Caenorhabditis elegans* gene *unc-89*, required for muscle M-line assembly, encodes a giant modular protein composed of Ig and signal transduction domains," *Journal of Cell Biology*, vol. 132, no. 5, pp. 835–848, 1996.
- [33] T. M. Small, K. M. Gernert, D. B. Flaherty, K. B. Mercer, M. Borodovsky, and G. M. Benian, "Three new isoforms of *Caenorhabditis elegans* UNC-89 containing MLCK-like protein kinase domains," *Journal of Molecular Biology*, vol. 342, no. 1, pp. 91–108, 2004.
- [34] C. Lecroisey, L. Segalat, and K. Gieseler, "The *C. elegans* dense body: anchoring and signaling structure of the muscle," *Journal of Muscle Research and Cell Motility*, vol. 28, no. 1, pp. 79–87, 2007.
- [35] K. B. Mercer, D. B. Flaherty, R. K. Miller, et al., "Caenorhabditis elegans UNC-98, a C2H2 Zn finger protein, is a novel partner of UNC-97/PINCH in muscle adhesion complexes," *Molecular Biology of the Cell*, vol. 14, no. 6, pp. 2492–2507, 2003.
- [36] K. B. Mercer, R. K. Miller, T. L. Tinley, S. Sheth, H. Qadota, and G. M. Benian, "Caenorhabditis elegans UNC-96 is a new component of M-lines that interacts with UNC-98 and paramyosin and is required in adult muscle for assembly and/or maintenance of thick filaments," *Molecular Biology of the Cell*, vol. 17, pp. 3832–3847, 2006.
- [37] R. K. Miller, H. Qadota, K. B. Mercer, K. M. Gernert, and G. M. Benian, "UNC-98 and UNC-96 interact with paramyosin to promote its incorporation into thick filaments of *Caenorhabditis elegans*," *Molecular Biology of the Cell*, vol. 19, no. 4, pp. 1529–1539, 2008.
- [38] L. Broday, I. Kolotuev, C. Didier, A. Bhoumik, B. Podbilewicz, and Z. Ronai, "The LIM domain protein UNC-95 is required for the assembly of muscle attachment structures and is regulated by the RING finger protein RNF-5 in *C. elegans*," *Journal of Cell Biology*, vol. 165, no. 6, pp. 857–867, 2004.

- [39] K. A. McDonald, M. Lakonishok, and A. F. Horwitz, " α_v and α_3 integrin subunits are associated with myofibrils during myofibrillogenesis," *Journal of Cell Science*, vol. 108, no. 7, pp. 2573–2581, 1995.
- [40] P. Young, E. Ehler, and M. Gautel, "Obscurin, a giant sarcomeric Rho guanine nucleotide exchange factor protein involved in sarcomere assembly," *Journal of Cell Biology*, vol. 154, no. 1, pp. 123–136, 2001.
- [41] M.-L. Bang, T. Centner, F. Fornoff, et al., "The complete gene sequence of titin, expression of an unusual approximately 700 kDa titin isoform, and its interaction with obscurin identify a novel Z-line to I-band linking system," *Circulation Research*, vol. 89, no. 11, pp. 1065–1072, 2001.
- [42] A. Fukuzawa, S. Idowu, and M. Gautel, "Complete human gene structure of obscurin: implications for isoform generation by differential splicing," *Journal of Muscle Research and Cell Motility*, vol. 26, no. 6–8, pp. 427–434, 2005.
- [43] G. Xiong, H. Qadota, K. B. Mercer, L. A. McGaha, A. F. Oberhauser, and G. M. Benian, "A LIM-9 (FHL) / SCPL-1 (SCP) complex interacts with the C-terminal protein kinase regions of UNC-89 (obscurin) in *Caenorhabditis elegans* muscle," *Journal of Molecular Biology*, vol. 386, pp. 976–988, 2009.
- [44] H. Qadota, L. A. McGaha, K. B. Mercer, T. J. Stark, T. M. Ferrara, and G. M. Benian, "A novel protein phosphatase is a binding partner for the protein kinase domains of UNC-89 (obscurin) in *Caenorhabditis elegans*," *Molecular Biology of the Cell*, vol. 19, no. 6, pp. 2424–2432, 2008.
- [45] P. R. Deitiker and H. F. Epstein, "Thick filament substructures in *C. elegans*: evidence for two populations of paramyosin," *The Journal of Cell Biology*, vol. 123, pp. 303–311, 1993.
- [46] H. F. Epstein, G. Y. Lu, P. R. Deitiker, I. Ortiz, and M. F. Schmid, "Preliminary three-dimensional model for nematode thick filament core," *Journal of Structural Biology*, vol. 115, no. 2, pp. 163–174, 1995.
- [47] S. A. Muller, M. Haner, I. Ortiz, U. Aebi, and H. F. Epstein, "Stem analysis of *Caenorhabditis elegans* muscle thick filaments: evidence for microdifferentiated substructures," *Journal of Molecular Biology*, vol. 305, no. 5, pp. 1035–1044, 2001.
- [48] R. K. Miller, H. Qadota, T. J. Stark, et al., "CSN-5, a component of the COP9 signalosome complex, regulates the levels of UNC-96 and UNC-98, two components of M-lines in *Caenorhabditis elegans* muscle," *Molecular Biology of the Cell*, vol. 20, no. 15, pp. 3608–3616, 2009.
- [49] G. A. Cope and R. J. Deshaies, "COP9 signalosome: a multi-functional regulator of SCF and other cullin-based ubiquitin ligases," *Cell*, vol. 114, no. 6, pp. 663–671, 2003.
- [50] C. Schwechheimer, "The COP9 signalosome (CSN): an evolutionary conserved proteolysis regulator in eukaryotic development," *Biochimica et Biophysica Acta*, vol. 1695, no. 1–3, pp. 45–54, 2004.
- [51] M. D. Gomes, S. H. Lecker, R. T. Jagoe, A. Navon, and A. L. Goldberg, "Atrogin-1, a muscle-specific F-box protein highly expressed during muscle atrophy," *Proceedings of the National Academy of Sciences of the United States of America*, vol. 98, no. 25, pp. 14440–14445, 2001.
- [52] S. C. Bodine, E. Latres, S. Baumhueter, et al., "Identification of ubiquitin ligases required for skeletal muscle atrophy," *Science*, vol. 294, no. 5547, pp. 1704–1708, 2001.
- [53] C. Didier, L. Broday, A. Bhoumik, et al., "RNF5, a RING finger protein that regulates cell motility by targeting paxillin ubiquitination and altered localization," *Molecular and Cellular Biology*, vol. 23, no. 15, pp. 5331–5345, 2003.
- [54] S. Lange, E. Ehler, and M. Gautel, "From A to Z and back? Multicompartments proteins in the sarcomere," *Trends in Cell Biology*, vol. 16, no. 1, pp. 11–18, 2006.
- [55] M. Gautel, "The sarcomere and the nucleus: functional links to hypertrophy, atrophy and sarcopenia," in *The Sarcomere and Skeletal Muscle Disease*, N. G. Laing, Ed., pp. 176–191, Landes Bioscience and Springer Science + Business Media, New York, NY, USA, 2008.
- [56] L. Ding and E. P. M. Candido, "HSP25, a small heat shock protein associated with dense bodies and M-lines of body wall muscle in *Caenorhabditis elegans*," *Journal of Biological Chemistry*, vol. 275, no. 13, pp. 9510–9517, 2000.
- [57] G. L. Moulder, M. M. Huang, R. H. Waterston, and R. J. Barstead, "Talin requires β -integrin, but not vinculin, for its assembly into focal adhesion-like structures in the nematode *Caenorhabditis elegans*," *Molecular Biology of the Cell*, vol. 7, no. 8, pp. 1181–1193, 1996.
- [58] P. E. Hoppe, J. Chau, K. A. Flanagan, A. R. Reedy, and L. A. Schriefer, "*Caenorhabditis elegans* unc-82 encodes a serine/threonine kinase important for myosin filament organization in muscle during growth," *Genetics*, vol. 184, no. 1, pp. 79–90, 2010.
- [59] B. Meissner, A. Warner, K. Wong, et al., "An integrated strategy to study muscle development and myofibril structure in *Caenorhabditis elegans*," *PLoS Genetics*, vol. 5, no. 6, Article ID e1000537, pp. 1–14, 2009.

Review Article

Physiologic Basis and Pathophysiologic Implications of the Diastolic Properties of the Cardiac Muscle

João Ferreira-Martins and Adelino F. Leite-Moreira

Department of Physiology, Faculty of Medicine, University of Porto, Alameda Prof. Hernâni Monteiro, 4200-319 Porto, Portugal

Correspondence should be addressed to Adelino F. Leite-Moreira, amoreira@med.up.pt

Received 1 November 2009; Revised 15 February 2010; Accepted 21 March 2010

Academic Editor: Henk L. M. Granzier

Copyright © 2010 J. Ferreira-Martins and A. F. Leite-Moreira. This is an open access article distributed under the Creative Commons Attribution License, which permits unrestricted use, distribution, and reproduction in any medium, provided the original work is properly cited.

Although systole was for long considered the core of cardiac function, hemodynamic performance is evenly dependent on appropriate systolic and diastolic functions. The recognition that isolated diastolic dysfunction is the major culprit for approximately fifty percent of all heart failure cases imposes a deeper understanding of its underlying mechanisms so that better diagnostic and therapeutic strategies can be designed. Risk factors leading to diastolic dysfunction affect myocardial relaxation and/or its material properties by disrupting the homeostasis of cardiomyocytes as well as their relation with surrounding matrix and vascular structures. As a consequence, slower ventricular relaxation and higher myocardial stiffness may result in higher ventricular filling pressures and in the risk of hemodynamic decompensation. Thus, determining the mechanisms of diastolic function and their implications in the pathophysiology of heart failure with normal ejection fraction has become a prominent field in basic and clinical research.

1. Introduction

From the earliest stages of an individual's life, the heart has the challenging mission to uninterruptedly transfer its kinetic energy to the blood. This task is accomplished by means of its intrinsic mechanical activity, which can be considered as being composed of two continuous and interdependent functions: *systole* and *diastole*. Being a living structure with biomechanical sensing features [1] the heart is a paradigmatic organ of continuous mechanical adaptation [2]. In this way, it is able to adapt its intrinsic mechanical properties when different loads and neurohumoral conditions are imposed so that new mechanical and biological steady states may be eventually achieved [1, 3, 4]. However, permanent pathologic stimuli make this equilibrium at best, short-termed, imposing an imbalance towards a progressive impairment of cardiac function and inexorably leading to a dysfunctional phenotype. This process consists of both intra- and extracellular remodeling, with deleterious consequences at structural, molecular, and functional levels.

Despite the knowledge that the heart spends almost two-thirds of its time in diastole (relaxing and filling), its

contractile activity was for a long time considered the core of its mechanical function and over which major concerns had been focused. Indeed, it was not until the nineteen eighties that the scientific community began to realize the clinical significance of diastolic dysfunction among patients with signs and symptoms of heart failure (HF) but in whom ejection fraction was rather preserved. The recognition of the latter condition as "heart failure with normal ejection fraction" (HFNEF) impelled major efforts in order to identify the pathophysiological mechanisms underlying this emerging concept. Female gender, older age, arterial hypertension, diabetes, obesity, and left ventricular (LV) hypertrophy are currently well-established risk factors [5–21], showing a strong association with impaired diastolic function with a concomitant normal or only mildly abnormal systolic function. However, and according to the Heart Failure and Echocardiography Associations of the European Society of Cardiology, these patients are only classified as having HFNEF if they develop signs or symptoms of HF along with the objective recognition of normal systolic LV function and of diastolic LV dysfunction [22]. Deserving special relief is the fact that the therapeutic management of HFNEF is still

relying on an empirical framework and is not translating into any survival improvement in this particular group of patients. However, it is currently not clear whether these neutral outcomes are due to specific mechanisms in the pathophysiology of HFNEF and/or to the nonadherence of clinical trials to the existing diagnostic guidelines of HFNEF. The latter has been recently shown to be responsible for a high variability among the recruited patients in HFNEF trials and therefore in their reported final results [23, 24]. Importantly, a deeper understanding of the mechanisms leading to the development of HFNEF as well as a systematic compliance of the clinical trials to the current guidelines is seriously warranted, setting the necessary conditions for an efficient cross-talk between clinical and basic research.

2. Risk Factors, Diastolic Function, and HFNEF

It has been documented that LV structure and function differ between HFNEF and HFREF [25], which may depend on the relative impact that associated clinical conditions have on the development of a particular cardiac phenotype or disease. Regarding HFNEF, female gender seems to be a major risk factor for its development [16–20], not only by being more frequently associated with other risk factors (e.g., arterial hypertension) but also by rendering the postmenopausal heart more susceptible to the remodeling features associated with slower relaxation and lower ventricular compliance. Even if the first studies indicating a higher risk in females [17, 26] have missed an objective evaluation of diastolic dysfunction among the diagnosed cases, the conclusion that such a trend may actually exist got early support from clinical cardiologists. Indeed, recent epidemiological data from the Framingham Heart Study [27] showed that within the HF population studied (median age of HF onset of 78 years old), individuals with HFNEF were more likely to be women (65% women versus 35% men), with an age-adjusted odds ratio of 2.55 when compared to men. Arterial hypertension or valvular heart disease also duplicated the risk of developing HFNEF and both risk factors were more frequent in women as well. Although this study showed that survival was similar between genders and independent from left ventricular ejection fraction (LVEF), results from the CHARM program [28] indicated that women had a better survival than men, even after adjustment for cause of heart failure, LVEF, and age.

All these cumulative epidemiological data supporting gender specificities in the risk of diastolic dysfunction and HFNEF impelled basic research to study the mechanisms underlying such differences, whose knowledge may contribute to design more specific therapeutic targets and guidelines for HF in general and HFNEF in particular. In this regard, 17β -estradiol is a distinctive feature between genders and has been shown to be an important modulator of myocardial relaxation and passive properties [16]. Considering cardiomyocyte Ca^{2+} -handling and relaxation, 17β -estradiol modulates the expression and activity of L-type Ca^{2+} channels [29], the phosphorylation levels of PLB [30], myofilaments Ca^{2+} sensitivity [31] and protects

single cardiomyocytes against Ca^{2+} loading induced by hypoxia [32]. Important mediators of 17β -estradiol within the cardiovascular system and with recognized benefits on diastolic function are nitric oxide (NO) and endogenous brain natriuretic peptide (BNP) whose levels are also higher in females than in males [16]. By promoting the actions of these neurohumoral agents, estrogens may increase the speed of relaxation and ventricular compliance, improving overall diastolic function. Beyond these acute and indirect effects, estrogens also modify myocardial material properties by reducing cardiac fibroblast proliferation, collagen turnover and pressure overload-induced cardiomyocyte hypertrophy [33, 34]. Therefore, it seems reasonable to speculate that the loss of these beneficial effects after menopause may render the female heart especially vulnerable to diastolic dysfunction. Of special remark, the absence of the long-term protective influences of estrogens confers a higher susceptibility of the female heart to the risk factors commonly leading to HFNEF, such as obesity, hypertension, and diabetes [35, 36]. Actually, comparing individuals from both genders with similar degrees of arterial hypertension or aortic stenosis, women develop more often concentric cardiac remodeling while males develop more often eccentric remodeling [35]. As concentric hypertrophy leads to increased wall thickness and possibly smaller chambers, the resulting ventricular geometry leads to earlier partial chamber filling, with increases in operating stiffness [16]. The synergic effects of obesity and hypertension to the development of left ventricular hypertrophy are much stronger in women than in men as is greater the effect of diabetes to the development of congestive HF in the female gender [37].

Independently or in association, all these risk factors may cause structural and functional changes at the organ, cellular and molecular levels of the heart, leading to a slower relaxation and/or increased chamber stiffness. A detailed discussion on these determinants of diastolic function follows.

3. Diastolic Properties of the Cardiac Muscle—A Composite Material

Cardiac muscle tissue is a composite material consisting of cardiomyocytes, fibroblasts, blood vessels, and extracellular matrix (ECM). Therefore, it is reasonable to postulate that changes in any of the elements within the myocardium may affect its material properties [38] and, consequently, its mechanical function. Both cellular and matrix structures contribute to myocardial physical properties, based on their intrinsic mechanical features, spatial and functional relations with the surrounding structures and tissue geometry, which finally ensues in the adult heart. Thus, when considering heart biomechanical properties, we have to conceptually integrate not only the single contribution of the various cardiac muscle tissue elements but also the complex interactions among them as well as their ability to modify their intrinsic mechanics under different pathophysiological conditions.

Considering the dynamic nature of diastole, it is not surprising that myocardial material properties are a central determinant of diastolic function and dysfunction. Generally

TABLE 1: Determinants of diastolic function and myocardial stiffness.

Determinants of diastolic function
Myocardial relaxation
Load
Inactivation (calcium homeostasis, myofilaments, energetics)
Nonuniformity
Passive properties of ventricular wall
Myocardial stiffness
Wall thickness
Chamber geometry
Other determinants
Structures surrounding the ventricle (pericardium, lungs, remaining, cardiac chambers)
Left atrium, pulmonary veins and mitral valve
Heart rate
Determinants of myocardial stiffness
Cardiomyocytes
Ca ²⁺ homeostasis
Diastolic calcium concentration: residual cross-bridges
Cytoskeleton
Microtubules (tubulin) and intermediate filaments (desmin): density and cellular stiffness
Myofilaments: actin and myosin (residual cross-bridges)
Titin: isoforms expression ratio; isoforms' phosphorylation status
Extracellular matrix
Collagen: content, type, alignment, spatial distribution, cross-linking
Proteoglycans: putative role in interstitial water flow and content within the myocardium
Elastin: putative decrease in elastin/collagen ratio with increased myocardial stiffness

defined as the ability of the ventricle to relax and fill [39], diastolic function depends on *active* myocardial relaxation and on *passive* properties. While relaxation is the process whereby the myocardium returns to an unstressed length and force, passive properties mostly influence the extent of muscle relength and end-diastolic pressure-volume relationship (EDPVR). Although *active* myocardial relaxation is responsible for its motion and blood flow, it is only through the perfect match of both active and passive properties that overall diastolic function is preserved. For conceptual purposes, myocardial *passive* properties are considered as such because they are assessed after complete muscle relaxation, that is, a mostly energy-consuming and, hence, *active* process. However, a growing body of evidence clearly shows that myocardial passive properties might as well be actively modulated and depend on cardiac high-energy phosphate metabolism.

The contribution of both active and passive properties to diastolic dysfunction and to the clinical syndrome of HFNEF will be discussed in the next sections.

3.1. Relaxation and Its Physiological Modulators. In the normal heart, myocardial relaxation comprises the major part of ventricular ejection, pressure fall and the initial part of rapid filling [39–42].

At the cellular level, the central players of the relaxation process are the cardiomyocytes, whose homeostatic balance

is a major determinant in the maintenance of an appropriate relaxation speed. In this way, any process interfering with cardiomyocyte physiology may delay relaxation long enough and significantly impair LV diastolic filling, especially at faster heart rates.

Conceptually, the determinants of ventricular relaxation (either by disturbing diastolic cardiomyocyte performance or by disrupting the synchrony of their actions) are load, inactivation, and nonuniformity (Table 1) [39].

3.1.1. Load. The effects of load depend on its type (preload versus afterload), magnitude, duration, and timing in the cardiac cycle at which it occurs [40]. For instance, severe or late systolic afterload elevations are particularly effective in delaying relaxation rate, even in healthy hearts [43].

In the clinical setting, marked arterial hypertension is a paradigmatic example of severe afterload imposition on the left ventricle and is a major risk factor for myocardial hypertrophy and failure. As relaxation in failing hearts is especially vulnerable to load, increases in afterload may significantly delay relaxation and result in pulmonary congestion in HF patients [44]. Taking into account that neurohumoral activation takes place both in HFNEF and HFREF, the failing heart in HFNEF is not only faced with a higher afterload (increased peripheral vascular resistance) but also with a higher preload (volume retention), further increasing the odds of hemodynamic decompensation [45].

Even if the underlying mechanisms are still unclear, changes in the activity of Ca^{2+} -handling proteins and myofilaments' sensitivity to this ion (e.g., troponin I) are the most likely effectors of the observed slower relaxation upon changes in load [46–49].

3.1.2. Inactivation. Deserving special relief, inactivation refers to the process underlying Ca^{2+} extrusion from the cytosol and cross-bridge detachment. As abovementioned, its importance stems from the fact that disturbances in this process may represent the ultimate effectors of several pathophysiological conditions leading to impaired relaxation, including load [49].

In the healthy human heart, the pathways involved in Ca^{2+} extrusion from the cytosol are the phospholamban-modulated uptake of this ion by the sarcoplasmic reticulum Ca^{2+} ATPase (SERCA2a, 70%), the $\text{Na}^+/\text{Ca}^{2+}$ -exchanger (28%), and, to a lesser extent, the Ca^{2+} -pump and the mitochondrial Ca^{2+} uniport (2%) [50]. Equally important is the phosphorylation state of the proteins that regulate SERCA2a activity, such as phospholamban (PLB), calmodulin, and calsequestrin. PLB stands as a classic example of a protein that interacts with and inhibits SERCA2a activity in a reversible manner. Although its relevance in cardiac physiology has been extensively studied over the last years, there is now an emerging field of interest focusing on the structurally-related protein sarcolipin (SLN). Most notably, this protein is absent in the ventricles but is significantly expressed in the atria, which may indicate the existence of chamber-specific mechanisms of SERCA2a function regulation. Nonetheless, overexpression of sarcolipin in mice ventricular myocytes was found to inhibit SERCA2a by direct binding or through stabilization of the interaction between SERCA2a and phospholamban [51, 52]. As a consequence, the affinity of SERCA2a for calcium was decreased, calcium transients amplitude was lower, and the time of calcium decay and relaxation was significantly extended [53, 54]. Despite the atrial-specific expression of SLN and the higher expression of PLB in the mouse ventricle, SLN expression may not be confined to the atria in other species [54] and possibly in pathological conditions, such as heart failure.

Besides the importance of the aforementioned mechanisms concerning the velocity and extent of Ca^{2+} reuptake into the SR, it has been proposed that diastolic Ca^{2+} leakage from the ryanodine receptor (associated with diminished FK 506-binding protein 12.6) may also increase diastolic Ca^{2+} levels and contribute to a higher thick-thin filament interaction and delayed relaxation [55]. Therefore, the functional integrity of the SR must translate not only in an effective reuptake but also a subsequent diastolic sequestration of Ca^{2+} .

As relaxation is an energy-consuming process, high-energy phosphate metabolism is a centerpiece in several steps involved in this phase of diastole, namely, in Ca^{2+} dissociation from troponin C, myosin-actin detachment, active sequestration of Ca^{2+} into the SR, and in several phosphorylation reactions of Ca^{2+} -handling proteins [46]. Indeed, any energetic imbalance leading to an abnormally high ADP

concentration or ADP/ATP ratio is associated with slower relaxation rates and increased diastolic stiffness [39]. Besides slower Ca^{2+} transients' decay, a higher sensitivity of the myofilament proteins to this ion might as well decrease the pace of myocardial relaxation. An important example is cardiac troponin-I (cTnI) which is less phosphorylated in HFREF and therefore shows a higher sensitivity to Ca^{2+} [56]. As a result, comparable increases in Ca^{2+} concentration may result in greater myofilaments' activation and enhanced myocardial contractility. However, as corroborated by the recent findings of Yasuda et al., the flip side of the coin may be a delay in myocardial relaxation and a consequent increase in diastolic stiffness. In the latter study, both in vitro and in vivo experiments designed to engineer sarcomeres with a PKA nonphosphorylatable TnI or a PKA phosphomimetic of cardiac TnI indicated an important role of cardiac TnI phosphorylation status in regulating cardiomyocyte relaxation velocity [57].

3.1.3. Nonuniformity. Nonuniformity represents asynchronous changes in ventricular shape during contraction and relaxation, being most frequent in the setting of coronary artery disease and intraventricular conduction disturbances. During isovolumic relaxation, it may be represented by reextension of one ventricular segment accompanied by post-systolic shortening of another, generating an asynchrony in ventricular relengthening and possibly in ventricular pressure fall. Consequently, this may further contribute to diastolic dysfunction [39].

Most, if not all, the risk factors pointed to be associated with HFNEF invariably lead to impaired relaxation, even if some may be especially involved in modifying the myocardial passive properties. However, unraveling the mechanisms through which a single risk factor induces diastolic dysfunction/HFNEF has been a challenging task due to the high prevalence of several comorbidities among HF patients. The latter condition promotes the interaction among the existent risk factors, which may significantly modify the phenotype of the disease, its clinical presentation, and prognosis.

3.2. Ventricular Passive Properties and Their Physiological Modulators. Although active properties of the myocardium are responsible for its motion and blood flow, overall diastolic function is stringently dependent on the maintenance of adequate passive properties as well. Indeed, current data strongly associates changes in myocardial material properties and various forms of heart disease. The passive properties of the ventricular wall depend on myocardial stiffness, wall thickness, and chamber geometry (Table 1) and are evaluated by observing the position and shape of the EDPVR [39]. This is an exponential curve which is derived by plotting the lower right corner of multiple pressure-volume (PV) loops at various preloads. Considering the three-parameter monoexponential formula ($P = P_0 + A * e^{kc * V}$), the EDPVR is dependent on *ventricular distensibility* (represented by changes in vertical position, i.e., in the value of the pressure intercept P_0), *ventricular size* (represented by changes in horizontal position, that is, in constant A), and *ventricular*

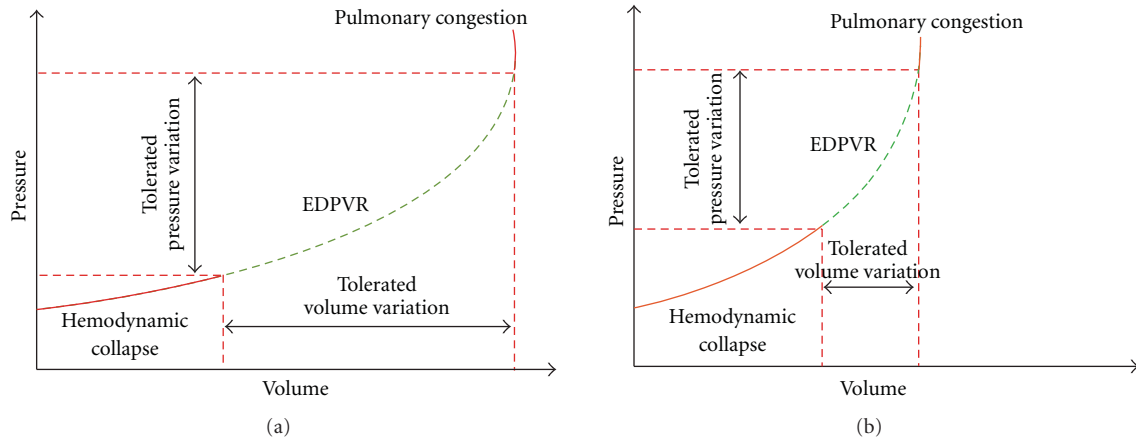


FIGURE 1: Schematic representation of the end-diastolic pressure-volume relationship (EDPVR) in the absence (a) or presence (b) of diastolic dysfunction. The dashed segment of the EDPVR represents the pressure-volume interval in which an individual remains hemodynamically stable. In (b), the steeper EDPVR narrows the ventricular pressure-volume interval and increases the individual's susceptibility to hemodynamic decompensation.

compliance (represented by changes in the slope of the curve, i.e., in the modulus of chamber stiffness, Kc).

Due to the concentric hypertrophy and stiffer myocardial wall commonly associated with HFNEF, the hallmarks of this condition are decreased distensibility, decreased compliance, and smaller cavity size. As a consequence, the ventricular wall displays stronger elastic forces resisting expansion during diastolic filling, which is translated into an upward and leftward shift of the EDPVR, that is, into a steeper relation. Indeed, changes in its slope deserve special emphasis as it reflects the patient's vulnerability to hemodynamic decompensation, regardless of the HF phenotype (HFNEF or HFREF) and ventricular cavity size [45].

As depicted in Figure 1, the slope of the curve at operating conditions is a valuable surrogate of these patients' clinical susceptibility: the steeper the curve, the smaller the volume variation capable of markedly increasing ventricular filling pressures and inducing pulmonary congestion.

However, we must bear in mind that the EDPVR is not solely dependent on intrinsic passive properties of the ventricular wall but also on extrinsic factors (e.g., pericardium, lungs) [39, 46] as well as conditions leading to incomplete myocardial relaxation, such as severe tachycardia in HF patients (Table 1). The latter situation is especially important because their hearts may exhibit a flat or even negative relaxation velocity-versus-heart rate relationship [58]. In this way, when heart rate increases, relaxation rate does not increase or even decreases, leading to a stiffer ventricle in late diastole and hence higher filling pressures.

3.2.1. Myocardial Stiffness. Considering the importance of myocardial material properties in determining ventricular compliance and clinical severity of HFNEF, their study became an attractive field in HF research. In further sections, there will be emphasized the relative contribution of cardiomyocytes and extracellular matrix to overall myocardial stiffness, both in physiological and pathological conditions (Table 1).

4. Cardiomyocytes and Myocardial Material Properties

Several studies have shown that changes in myocardial material properties can be caused by mechanisms intrinsic to the cardiomyocytes themselves [38, 59–68]. These include mechanisms that may alter (i) the relative content, (ii) the isoforms expression, (iii) posttranslational modifications and/or (iv) active interactions among the cytoskeletal structures of cardiac cells, thus affecting the overall resistance to changes in shape.

The cardiomyocyte cytoskeleton is composed of microtubules (tubulin), intermediate filaments (desmin), microfilaments (actin), and endosarcomeric proteins, of which titin has lately received particular attention.

4.1. Microtubules and Intermediate Filaments. At operating sarcomere lengths (1.9–2.2 μm), microtubules and intermediate filaments were found to contribute less than 10% to passive tension [67]. However, in the setting of right-ventricular pressure overload hypertrophy (RVPOH) and at physiological rates of muscle length variation, there is a higher resistance to changes in cardiomyocyte shape, a result that is significantly attenuated when microtubules are chemically or physically depolymerized. Thus, although microtubules may not significantly contribute to myocardial stiffness both in healthy states and in slowly stretched muscles, their increased density may play a role under pressure-overloaded conditions and at physiological rates of contraction and relaxation [60, 67]. In these conditions, microtubules are mainly responsible for an increase in cardiomyocyte resistance when rapidly stretched.

4.2. Myofilaments. Since the interaction between actin and myosin was shown to occur even at low diastolic calcium levels, it was hypothesized that the establishment of residual

diastolic cross-bridges might as well mediate myocardial passive stiffness [46]. As described for microtubules, Zile and colleagues also showed that, in pressure-overloaded conditions, there is a correlation between increased myocardial stiffness, higher intracellular calcium concentration, and increased number of cross-bridge interactions [38]. Therefore, changes in calcium transients or myofilament's calcium-sensitivity may increase myocardial stiffness [46, 69] even if these are most commonly regarded as determinants of myocardial relaxation rate. The latter findings mean that beyond the biophysical properties of structural cytoskeletal proteins, cardiomyocyte stiffness may also be under active control, thus evoking the concept of active muscle tone [46].

4.3. Titin. Over the last decade, the contribution of the endosarcomeric protein titin in the modulation of myocardial stiffness has been elucidated. However, its relevance in cardiac function goes beyond the scaffold and passive force generating properties, being an important regulator of systolic function [70, 71], a mechanotransducer in cardiomyocytes [72], and a central player in cardiac development, growth, and hypertrophy [73–75].

4.3.1. Titin Isoforms and Myocardial Stiffness. Titin spans the half-sarcomere from the Z-disk to M-line and its ability to generate passive tension is associated with extensible segments in the I-band of sarcomeres, comprised of serially linked but distinct domains: the proline-glutamate-valine-lysine (PEVK) element, immunoglobulin-(Ig)-like domains and the segment with unique aminoacid sequences called N2B, N2A, or N2BA (which contains both N2B and N2A) [46, 59, 61, 63, 76]. It is expressed in the heart as two different isoforms, the smaller and stiffer N2B, and the larger and more compliant N2BA. While the former expresses only the cardiac specific N2B domain, the latter expresses both N2B and N2A as well as additional PEVK and Ig domains. Upon application of a longitudinal force, stretch of cardiomyocytes within physiological sarcomere length ranges is accompanied by unfolding of the PEVK, Ig domains, and unique sequences N2A and/or N2B, resulting in the generation of passive force. Upon release, these spring elements tend to refold and achieve a state of lower contour length and higher entropy. Given the presence of additional segments in the N2BA titin isoform, it can accommodate longer variations in length for the same levels of passive force generated, being therefore more compliant than N2B isoform. However, because these isoforms are coexpressed in the same half sarcomere in a ratio that varies among species and in different locations within the heart, titin-based cardiomyocyte stiffness is usually anywhere in-between of that generated by N2B- or N2BA-purely expressing cells. Accordingly, the predominant expression of N2B in rodents [46, 69] accounts for a high cardiomyocyte stiffness, while the more abundant expression of N2BA in large mammals (pig, cow, human) accounts for a comparably lower passive stiffness. However, and regardless of the animal species, myocardial stiffness undergoes significant changes

during physiological and pathological conditions, which are partially accounted by shifts in titin isoforms expression ratio as well as titin posttranslational modifications. The earliest and probably the most robust shift occurs during the perinatal period. In the fetal myocardium of mice, rats, and pigs, titin is predominantly expressed as a compliant N2BA titin isoform (fetal cardiac titin), which is characterized by the presence of additional Ig and PEVK segments in its extensible region than the adult N2BA titin [77]. Around birth, this fetal isoform is downregulated and titin transcripts are translated into a shorter, less extensible N2BA protein, together with the onset N2B titin isoform expression. With a time course that varies among species, N2B becomes the predominant isoform in the adult heart, including humans. As a consequence, the highly compliant fetal myocardium becomes progressively stiffer and better adapted to higher ventricular end-diastolic pressures that accompany post-natal cardiac growth. Even in adulthood, titin isoforms expression ratio is highly dynamic and contributes to changes in myocardial stiffness upon pathological insults. However, the direction of isoform shift is not consistent among studies and the mechanisms that may lead to one type of switch over another in HF remain unclear [46, 59]. A plausible explanation for these discrepancies relies on the different experimental/clinical contexts where the shift in titin isoforms expression was studied, mostly likely on differences in the nature, severity, and duration of the disease. As depicted in Figure 2, the development of HF or HF-associated pathological conditions is accompanied by an increase in myocardial stiffness (Figure 2(a)), where remodeling of the ECM invariably leads to a higher collagen-based stiffness (Figure 2(b)). However, while in 2 canine models of pacing-induced dilated cardiomyopathy (DCM) [78, 79] the increase in myocardial stiffness with HF was accompanied by a higher expression of the stiff N2B titin isoform (Figure 2(c)), the opposite was observed in HF human hearts, either with normal [80] or reduced ejection fraction [81–83]. (Figure 2(d)). In these studies, the net increase in myocardial stiffness was accounted by a higher collagen-based stiffness and/or changes titin isoforms phosphorylation ratio. The observed increase in N2BA/N2B expression ratio has been rather interpreted as a compensatory mechanism in which the presence of more compliant titin isoforms counteracts the progressive increase in myocardial stiffness and diastolic dysfunction. Similar findings in titin isoforms shift have been recently reported in long-term hypothyroidism, a condition commonly associated with diastolic dysfunction [84]. Of note, Figure 2 does not take into consideration the relative proportions of N2B and N2BA titin isoforms but rather the main direction of their shift, as reported in several studies.

4.3.2. Titin Posttranslational Modifications and Myocardial Stiffness. Besides the molecular structure and relative expression ratio, posttranslational modifications of titin isoforms (through either phosphorylation or calcium binding effects) may significantly impact myocardial stiffness. N2B titin's segment was shown to be the target for protein kinase A

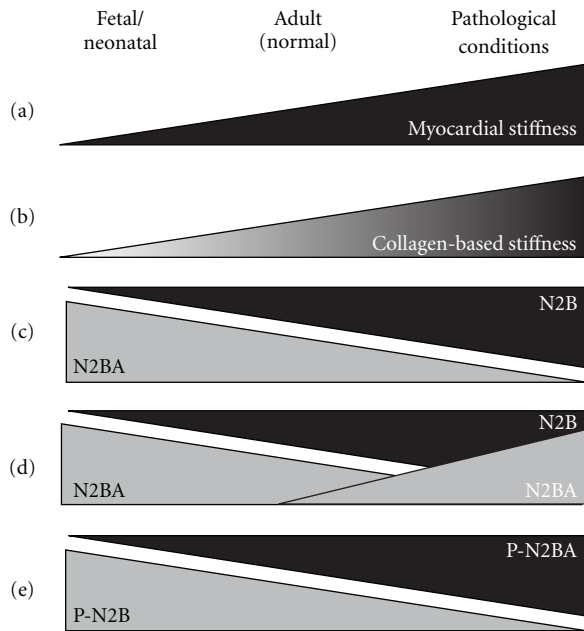


FIGURE 2: Progressive increase in myocardial (a) and collagen-based stiffness (b) during physiologic cardiac growth as well as HF or HF-associated pathological conditions. The increase in myocardial stiffness can be paralleled by a concordant increase in the expression of the stiff titin isoform N2B (c) or by a compensatory increase in the expression of the compliant titin isoform N2BA (d). Relative hypophosphorylation of the stiff N2B titin also accounts for an increase in myocardial stiffness in HF, especially in HFNEF (e) (P-N2B: phosphorylated N2B; P-N2BA: phosphorylated N2BA).

(PKA) and protein kinase G (PKG) phosphorylation [61, 76, 85–87], which possibly destabilizes its structure and induces an increase in N2B segment length, thus reducing cardiomyocyte passive tension. Because N2B element is included in all cardiac titin isoforms, its extension is predicted to reduce passive stiffness of both N2B and N2BA titins. However, the magnitude of the phosphorylation-induced decrease in passive stiffness is isoform dependent, because the shorter N2B titin makes its increase in length to have a greater impact on its fractional extension. Accordingly, a relative deficit in N2B titin phosphorylation status was found to significantly raise cardiomyocyte stiffness in failing human myocardium (Figure 2(e)), despite the compensatory increase in N2BA titin isoform expression and phosphorylation. Interestingly, patients with HFNEF had not only more N2B titin protein (i.e., stiffer) but also less phosphorylated N2B titin (i.e., stiffer) than HFREF patients, explaining both the significantly higher stiffness and the more pronounced decay in of passive tension upon to PKA-mediated phosphorylation [80].

Titin phosphorylation by PKA and PKG clearly supports the effects of β -adrenergic signaling and nitric oxide in reducing cardiomyocyte stiffness, respectively [86, 87]. However, the association between titin phosphorylation by Protein Kinase C (PKC) and the reported effects of several agonists of Gq protein-coupled receptors is not straightforward. As recently published, PKC phosphorylates titin's

PEVK segment and leads to an increase in cardiomyocyte stiffness [88, 89] suggesting that the adaptation of myocardial stiffness upon adrenergic stimulation may be finely regulated by a balance between alpha and beta adrenergic receptors' activation. However, acute activation of other Gq protein coupled receptors (AT1, ET_A, among others) has been associated with a decrease in myocardial stiffness, an effect that was blunted when PKC was specifically inhibited [90, 91]. Whether a broader effect of PKC on the phosphorylation status of cardiac myofilaments, the isoform of PKC or the simultaneous activation of other pathways may have accounted for these results warrants further assessment.

Besides titin extension, diastolic stiffness may be also produced by titin-calcium interactions in an isoform dependent manner. Calcium binding directly increases the passive stiffness of N2BA expressing myocardium by changes in its structure but has no effect on exclusively N2B expressing myocardium. In the latter case, calcium exerts an indirect effect by promoting titin-actin interactions, which may serve to retard thin filament sliding and contribute to myocyte passive stiffness [59].

5. ExtraCellular Matrix and Myocardial Material Properties

Besides cardiomyocytes, the ECM is another major determinant of the myocardial material properties [92]. Among the proteins within the ECM, fibrillar proteins such as collagen and elastin, proteoglycans, and the basement membrane proteins each may play a role in determining the constitutive properties of the myocardium [93, 94]. However, collagen molecules have been hypothesized to be the most important component within the ECM contributing to myocardial stiffness and HFNEF [46], as it is a relatively stiff material with high tensile strength. However, its influence on the stress-strain relation of the myocardium depends on many factors including its concentration, fibril and fiber diameter, degree of crosslinking, spatial alignment, and collagen types. In physiological conditions and at sarcomere lengths less than 2.2 μm , the combined passive fiber stiffness of the myocardium has been predominantly attributed to intracellular structures, notably titin. However, at longer sarcomere lengths, parallel collagen fibers bear an increasing fraction of the axial stress as collagen perimysial fibers untwist and straighten [94]. Interestingly enough, the increase in myocardial stiffness across different species and heart chambers is associated not only to a higher expression of the stiff N2B titin isoform but also by a parallel increase in collagen content, which suggests coordination between collagen synthesis and titin isoform expression. This might preserve the relative stiffness contributions of titin (lower sarcomere lengths) and collagen (higher sarcomere lengths) among species. However, this relationship may not be preserved in pathological states [46] such as arterial hypertension, diabetes [95, 96], or myocardial infarction [97, 98], because of their role in disrupting the balance between collagen biosynthesis, degradation, and posttranslational processing [46].

6. Neurohumoral Modulation of Myocardial Mechanical Properties

Besides mechanical inputs, growing evidence points to neurohumoral agents such as nitric oxide (NO) [99–101], angiotensin II [90, 102], endothelin-1 [91, 103, 104], urotensin-II [105, 106], and adrenomedullin [107] to acutely alter myocardial mechanical properties as well [108].

In isolated cardiomyocytes, NO was shown to shift the stress-strain relation down and to the right. Accordingly, intracoronary infusion of the exogenous NO donor, sodium nitroprusside, resulted in a similar displacement of the end-diastolic pressure-volume relation, both in normal and in hypertrophied human hearts as a result PKG-mediated phosphorylation of myofilaments [101]. In further experiments, substance P was shown to promote the release of endogenous NO, decreasing ventricular stiffness in patients with dilated cardiomyopathy [39, 102]. Although some previous reports [109] stated that higher coronary perfusion pressures might cause an upward displacement of EDPVR by increasing myocardial vascular engorgement, the latter results also suggest that a simultaneous increase in endothelial shear-stress may enhance the release of endogenous NO and attenuate the aforementioned effect. As titin is currently known to be a target of PKG phosphorylation, an increase in titin distensibility might have as well contributed to the observed effects [87].

Chronic activation of the renin-angiotensin system is also a well-recognized mechanism that leads to increased myocardial stiffness by promoting structural remodeling in both cardiomyocytes and ECM. However, acute activation of this system was shown to decrease myocardial and ventricular chamber stiffness in a time frame that was too short to alter the ECM [90]. Therefore, its effects on myocardial tissue must be caused by direct action on the cardiomyocytes to alter one or more determinants of its mechanical properties. Interestingly, a similar finding was also ascribed to endothelin-1 in isolated papillary muscles [91]. As angiotensin II and endothelin-1 exerted their effects through the activation of Gq Protein-Coupled Receptors which are established activators of PKC signaling, further studies are necessary to reconcile these observations with the recently described PKC-mediated increase in titin and cardiomyocyte stiffness.

7. Conclusion

The maintenance of normal diastolic performance is only possible through the appropriate expression of cellular and matrix phenotypes, which in turn are dependent on the perfect match between the myocardial inputs and its biological responses. Myocardial tissue is regarded as composite material whose properties depend on each of its specific constituent elements and the dynamic interplay between their structure and function. In addition, the biomechanical sensing features of the myocardium allow it to alter its structural and functional phenotypes when subjected to physiological inputs, thus achieving a new

biological equilibrium that preserves overall ventricular function. In pathological settings, however, such equilibrium can be easily disrupted, with both cardiomyocytes and ECM exhibiting changes that may impair ventricular relaxation and chamber stiffness. The growing knowledge about the causal mechanisms of abnormal myocardial properties will possibly allow us to diagnose earlier and choose the best therapeutic strategies in patients with HF in general and HFNEF in particular.

References

- [1] J. Lammerding, R. D. Kamm, and R. T. Lee, "Mechanotransduction in cardiac myocytes," *Annals of the New York Academy of Sciences*, vol. 1015, pp. 53–70, 2004.
- [2] M. A. Sussman, A. McCulloch, and T. K. Borg, "Dance band on the Titanic: biomechanical signaling in cardiac hypertrophy," *Circulation Research*, vol. 91, no. 10, pp. 888–898, 2002.
- [3] A. W. Orr, B. P. Helmke, B. R. Blackman, and M. A. Schwartz, "Mechanisms of mechanotransduction," *Developmental Cell*, vol. 10, no. 1, pp. 11–20, 2006.
- [4] B. Swynghedauw, "Phenotypic plasticity of adult myocardium: molecular mechanisms," *Journal of Experimental Biology*, vol. 209, no. 12, pp. 2320–2327, 2006.
- [5] D. D. Bonnema, C. S. Webb, W. R. Pennington, et al., "Effects of age on plasma matrix metalloproteinases (MMPs) and tissue inhibitor of metalloproteinases (TIMPs)," *Journal of Cardiac Failure*, vol. 13, no. 7, pp. 530–540, 2007.
- [6] B. P. Shapiro, C. S. P. Lam, J. B. Patel, et al., "Acute and chronic ventricular-arterial coupling in systole and diastole: insights from an elderly hypertensive model," *Hypertension*, vol. 50, no. 3, pp. 503–511, 2007.
- [7] H. Masugata, S. Senda, F. Goda, et al., "Left ventricular diastolic dysfunction in normotensive diabetic patients in various age strata," *Diabetes Research and Clinical Practice*, vol. 79, no. 1, pp. 91–96, 2008.
- [8] L. van Heerebeek, N. Hamdani, M. L. Handoko, et al., "Diastolic stiffness of the failing diabetic heart: importance of fibrosis, advanced glycation end products, and myocyte resting tension," *Circulation*, vol. 117, no. 1, pp. 43–51, 2008.
- [9] C. Y. Wong, T. O'Moore-Sullivan, R. Leano, N. Byrne, E. Beller, and T. H. Marwick, "Alterations of left ventricular myocardial characteristics associated with obesity," *Circulation*, vol. 110, no. 19, pp. 3081–3087, 2004.
- [10] B. D. Powell, M. M. Redfield, K. A. Bybee, W. K. Freeman, and C. S. Rihal, "Association of obesity with left ventricular remodeling and diastolic dysfunction in patients without coronary artery disease," *American Journal of Cardiology*, vol. 98, no. 1, pp. 116–120, 2006.
- [11] J. F. Carroll, R. L. Summers, D. J. Zielak, K. Cockrell, J.-P. Montani, and H. L. Mizelle, "Diastolic compliance is reduced in obese rabbits," *Hypertension*, vol. 33, no. 3, pp. 811–815, 1999.
- [12] J. M. McGavock, R. G. Victor, R. H. Unger, and L. S. Szczepaniak, "Adiposity of the heart, revisited," *Annals of Internal Medicine*, vol. 144, no. 7, pp. 517–524, 2006.
- [13] M. Pascual, D. A. Pascual, F. Soria, et al., "Effects of isolated obesity on systolic and diastolic left ventricular function," *Heart*, vol. 89, no. 10, pp. 1152–1156, 2003.

- [14] J. F. Carroll, D. S. Braden, K. Cockrell, and H. L. Mizelle, "Obese hypertensive rabbits develop concentric and eccentric hypertrophy and diastolic filling abnormalities," *American Journal of Hypertension*, vol. 10, no. 2, pp. 230–233, 1997.
- [15] L. R. Peterson, A. D. Waggoner, K. B. Schechtman, et al., "Alterations in left ventricular structure and function in young healthy obese women: assessment by echocardiography and tissue Doppler imaging," *Journal of the American College of Cardiology*, vol. 43, no. 8, pp. 1399–1404, 2004.
- [16] V. Regitz-Zagrosek, S. Brokat, and C. Tschope, "Role of gender in heart failure with normal left ventricular ejection fraction," *Progress in Cardiovascular Diseases*, vol. 49, no. 4, pp. 241–251, 2007.
- [17] F. A. Masoudi, E. P. Havranek, G. Smith, et al., "Gender, age, and heart failure with preserved left ventricular systolic function," *Journal of the American College of Cardiology*, vol. 41, no. 2, pp. 217–223, 2003.
- [18] P. R. Mitoff, A. Al-Hesayen, E. Azevedo, G. E. Newton, and S. Mak, "Sex differences in basal hemodynamics and left ventricular function in humans with and without heart failure," *American Heart Journal*, vol. 154, no. 3, pp. 575–580, 2007.
- [19] M. M. Redfield, S. J. Jacobsen, B. A. Borlaug, R. J. Rodeheffer, and D. A. Kass, "Age- and gender-related ventricular-vascular stiffening: a community-based study," *Circulation*, vol. 112, no. 15, pp. 2254–2262, 2005.
- [20] Y. Izumi, K. Matsumoto, Y. Ozawa, et al., "Effect of age at menopause on blood pressure in postmenopausal women," *American Journal of Hypertension*, vol. 20, no. 10, pp. 1045–1050, 2007.
- [21] C. S. P. Lam, V. L. Roger, R. J. Rodeheffer, et al., "Cardiac structure and ventricular-vascular function in persons with heart failure and preserved ejection fraction from Olmsted County, Minnesota," *Circulation*, vol. 115, no. 15, pp. 1982–1990, 2007.
- [22] W. J. Paulus, C. Tschöpe, J. E. Sanderson, et al., "How to diagnose diastolic heart failure: a consensus statement on the diagnosis of heart failure with normal left ventricular ejection fraction by the Heart Failure and Echocardiography Associations of the European Society of Cardiology," *European Heart Journal*, vol. 28, no. 20, pp. 2539–2550, 2007.
- [23] W. J. Paulus and J. J. M. van Ballegoij, "Treatment of heart failure with normal ejection fraction. An inconvenient truth!" *Journal of the American College of Cardiology*, vol. 55, no. 6, pp. 526–537, 2010.
- [24] S. S. Najjar, "Heart failure with preserved ejection fraction. Failure to preserve, failure of reserve, and failure on the compliance curve," *Journal of the American College of Cardiology*, vol. 54, no. 5, pp. 419–421, 2009.
- [25] L. van Heerebeek, A. Borbély, H. W. M. Niessen, et al., "Myocardial structure and function differ in systolic and diastolic heart failure," *Circulation*, vol. 113, no. 16, pp. 1966–1973, 2006.
- [26] M. Klapholz, M. Maurer, A. M. Lowe, et al., "Hospitalization for heart failure in the presence of a normal left ventricular ejection fraction: results of the New York heart failure registry," *Journal of the American College of Cardiology*, vol. 43, no. 8, pp. 1432–1438, 2004.
- [27] D. S. Lee, P. Gona, R. S. Vasan, et al., "Relation of disease pathogenesis and risk factors to heart failure with preserved or reduced ejection fraction: insights from the framingham heart study of the national heart, lung, and blood institute," *Circulation*, vol. 119, no. 24, pp. 3070–3077, 2009.
- [28] E. O'Meara, T. Clayton, M. B. McEntegart, et al., "Sex differences in clinical characteristics and prognosis in a broad spectrum of patients with heart failure—results of the Candesartan in Heart failure: assessment of reduction in mortality and morbidity (CHARM) program," *Circulation*, vol. 115, no. 24, pp. 3111–3120, 2007.
- [29] V. M. Vizgirda, G. M. Wahler, K. L. Sondgeroth, M. T. Ziolo, and D. W. Schwartz, "Mechanisms of sex differences in rat cardiac myocyte response to β -adrenergic stimulation," *American Journal of Physiology*, vol. 282, no. 1, pp. H256–H263, 2002.
- [30] R. Dash, K. F. Frank, A. N. Carr, C. S. Moravec, and E. G. Kranias, "Gender influences on sarcoplasmic reticulum Ca^{2+} -handling in failing human myocardium," *Journal of Molecular and Cellular Cardiology*, vol. 33, no. 7, pp. 1345–1353, 2001.
- [31] D. W. Schwartz, V. Vizgirda, R. J. Solaro, M. R. Piano, and C. Ryjewski, "Sexual dimorphism in rat left atrial function and response to adrenergic stimulation," *Molecular and Cellular Biochemistry*, vol. 200, no. 1-2, pp. 143–153, 1999.
- [32] S. Jovanović, A. Jovanović, W. K. Shen, and A. Terzic, "Low concentrations of 17β -estradiol protect single cardiac cells against metabolic stress-induced Ca^{2+} loading," *Journal of the American College of Cardiology*, vol. 36, no. 3, pp. 948–952, 2000.
- [33] M. van Eickels, C. Grohé, J. P. M. Cleutjens, B. J. Janssen, H. J. J. Wellens, and P. A. Doevendans, " 17β -estradiol attenuates the development of pressure-overload hypertrophy," *Circulation*, vol. 104, no. 12, pp. 1419–1423, 2001.
- [34] Y. Xu, I. A. Arenas, S. J. Armstrong, and S. T. Davidge, "Estrogen modulation of left ventricular remodeling in the aged heart," *Cardiovascular Research*, vol. 57, no. 2, pp. 388–394, 2003.
- [35] B. Kuch, M. Muscholl, A. Luchner, et al., "Gender specific differences in left ventricular adaptation to obesity and hypertension," *Journal of Human Hypertension*, vol. 12, no. 10, pp. 685–691, 1998.
- [36] V. Regitz-Zagrosek and E. Lehmkuhl, "Heart failure and its treatment in women: role of hypertension, diabetes, and estrogen," *Herz*, vol. 30, no. 5, pp. 356–367, 2005.
- [37] W. B. Kannel, M. Hjortland, and W. P. Castelli, "Role of diabetes in congestive heart failure: the Framingham study," *American Journal of Cardiology*, vol. 34, no. 1, pp. 29–34, 1974.
- [38] T. S. Harris, C. F. Baicu, C. H. Conrad, et al., "Constitutive properties of hypertrophied myocardium: cellular contribution to changes in myocardial stiffness," *American Journal of Physiology*, vol. 282, no. 6, pp. H2173–H2182, 2002.
- [39] A. F. Leite-Moreira, "Current perspectives in diastolic dysfunction and diastolic heart failure," *Heart*, vol. 92, no. 5, pp. 712–718, 2006.
- [40] T. C. Gillebert, A. F. Leite-Moreira, and S. G. De Hert, "Load dependent diastolic dysfunction in heart failure," *Heart Failure Reviews*, vol. 5, no. 4, pp. 345–355, 2000.
- [41] T. C. Gillebert, A. F. Leite-Moreira, and S. G. De Hert, "The hemodynamic manifestation of normal myocardial relaxation. A framework for experimental and clinical evaluation," *Acta Cardiologica*, vol. 52, no. 3, pp. 223–246, 1997.
- [42] T. C. Gillebert, A. F. Leite-Moreira, and S. G. De Hert, "Relaxation-systolic pressure relation: a load-independent assessment of left ventricular contractility," *Circulation*, vol. 95, no. 3, pp. 745–752, 1997.

- [43] A. F. Leite-Moreira and J. Correia-Pinto, "Load as an acute determinant of end-diastolic pressure-volume relation," *American Journal of Physiology*, vol. 280, no. 1, pp. H51–H59, 2001.
- [44] S. K. Gandhi, J. C. Powers, A.-M. Nomeir, et al., "The pathogenesis of acute pulmonary edema associated with hypertension," *The New England Journal of Medicine*, vol. 344, no. 1, pp. 17–22, 2001.
- [45] B. A. Borlaug and D. A. Kass, "Mechanisms of diastolic dysfunction in heart failure," *Trends in Cardiovascular Medicine*, vol. 16, no. 8, pp. 273–279, 2006.
- [46] D. A. Kass, J. G. F. Bronzwaer, and W. J. Paulus, "What mechanisms underlie diastolic dysfunction in heart failure?" *Circulation Research*, vol. 94, no. 12, pp. 1533–1542, 2004.
- [47] A. F. Leite-Moreira, J. Correia-Pinto, and T. C. Gillebert, "Load dependence of left ventricular contraction and relaxation. Effects of caffeine," *Basic Research in Cardiology*, vol. 94, no. 4, pp. 284–293, 1999.
- [48] S. F. J. Langer and H. D. Schmidt, "Different left ventricular relaxation parameters in isolated working rat and guinea pig hearts: influence of preload, afterload, temperature, and isoprenaline," *International Journal of Cardiac Imaging*, vol. 14, no. 4, pp. 229–240, 1998.
- [49] A. F. Leite-Moreira, J. Correia-Pinto, and T. C. Gillebert, "Afterload induced changes in myocardial relaxation: a mechanism for diastolic dysfunction," *Cardiovascular Research*, vol. 43, no. 2, pp. 344–353, 1999.
- [50] D. M. Bers, "Cardiac excitation-contraction coupling," *Nature*, vol. 415, no. 6868, pp. 198–205, 2002.
- [51] A. R. Tupling, M. Asahi, and D. H. MacLennan, "Sarcolipin overexpression in rat slow twitch muscle inhibits sarcoplasmic reticulum Ca^{2+} uptake and impairs contractile function," *Journal of Biological Chemistry*, vol. 277, no. 47, pp. 44740–44746, 2002.
- [52] M. Asahi, Y. Sugita, K. Kurzydowski, et al., "Sarcolipin regulates sarco(endo)plasmic reticulum Ca^{2+} -ATPase (SERCA) by binding to transmembrane helices alone or in association with phospholamban," *Proceedings of the National Academy of Sciences of the United States of America*, vol. 100, no. 9, pp. 5040–5045, 2003.
- [53] G. J. Babu, P. Bhupathy, N. N. Petrashevskaya, et al., "Targeted overexpression of sarcolipin in the mouse heart decreases sarcoplasmic reticulum calcium transport and cardiac contractility," *Journal of Biological Chemistry*, vol. 281, no. 7, pp. 3972–3979, 2006.
- [54] M. Asahi, K. Otsu, H. Nakayama, et al., "Cardiac-specific overexpression of sarcolipin inhibits sarco(endo)plasmic reticulum Ca^{2+} ATPase (SERCA2a) activity and impairs cardiac function in mice," *Proceedings of the National Academy of Sciences of the United States of America*, vol. 101, no. 25, pp. 9199–9204, 2004.
- [55] S. O. Marx, S. Reiken, Y. Hisamatsu, et al., "PKA phosphorylation dissociates FKBP12.6 from the calcium release channel (ryanodine receptor): defective regulation in failing hearts," *Cell*, vol. 101, no. 4, pp. 365–376, 2000.
- [56] J. van der Velden, Z. Papp, R. Zaremba, et al., "Increased Ca^{2+} -sensitivity of the contractile apparatus in end-stage human heart failure results from altered phosphorylation of contractile proteins," *Cardiovascular Research*, vol. 57, no. 1, pp. 37–47, 2003.
- [57] S.-I. Yasuda, P. Coutu, S. Sadayappan, J. Robbins, and J. M. Metzger, "Cardiac transgenic and gene transfer strategies converge to support an important role for troponin I in regulating relaxation in cardiac myocytes," *Circulation Research*, vol. 101, no. 4, pp. 377–386, 2007.
- [58] M. R. Zile and D. L. Brutsaert, "New concepts in diastolic dysfunction and diastolic heart failure: part II. Causal mechanisms and treatment," *Circulation*, vol. 105, no. 12, pp. 1503–1508, 2002.
- [59] M. M. LeWinter, Y. Wu, S. Labeit, and H. Granzier, "Cardiac titin: structure, functions and role in disease," *Clinica Chimica Acta*, vol. 375, no. 1-2, pp. 1–9, 2007.
- [60] H. Shintani and S. A. Glantz, "The left ventricular diastolic pressure-volume relation, relaxation and filling," in *Left Ventricular Diastolic Dysfunction and Heart Failure*, W. H. Gaash and M. M. LeWinter, Eds., pp. 3–24, Lea & Febiger, Philadelphia, Pa, USA, 1994.
- [61] H. L. Granzier and S. Labeit, "The giant protein titin: a major player in myocardial mechanics, signaling and disease," *Circulation Research*, vol. 94, no. 3, pp. 284–295, 2004.
- [62] A. J. Brady, "Length dependence of passive stiffness in single cardiac myocytes," *American Journal of Physiology*, vol. 260, no. 4, pp. H1062–H1071, 1991.
- [63] M. Helmes, C. C. Lim, R. Liao, A. Bharti, L. Cui, and D. B. Sawyer, "Titin determines the Frank-Starling relation in early diastole," *Journal of General Physiology*, vol. 121, no. 2, pp. 97–110, 2003.
- [64] K. Trombitas, A. Redkar, T. Centner, Y. Wu, S. Labeit, and H. Granzier, "Extensibility of isoforms of cardiac titin: variation in contour length of molecular subsegments provides a basis for cellular passive stiffness diversity," *Biophysical Journal*, vol. 79, no. 6, pp. 3226–3234, 2000.
- [65] S. Nishimura, S.-I. Yasuda, M. Katoh, et al., "Single cell mechanics of rat cardiomyocytes under isometric, unloaded, and physiologically loaded conditions," *American Journal of Physiology*, vol. 287, no. 1, pp. H196–H202, 2004.
- [66] A. Borbély, J. van der Velden, Z. Papp, et al., "Cardiomyocyte stiffness in diastolic heart failure," *Circulation*, vol. 111, no. 6, pp. 774–781, 2005.
- [67] H. L. Granzier and T. C. Irving, "Passive tension in cardiac muscle: contribution of collagen, titin, microtubules, and intermediate filaments," *Biophysical Journal*, vol. 68, no. 3, pp. 1027–1044, 1995.
- [68] M. R. Zile, K. Richardson, M. K. Cowles, et al., "Constitutive properties of adult mammalian cardiac muscle cells," *Circulation*, vol. 98, no. 6, pp. 567–579, 1998.
- [69] O. Cazorla, A. Freiburg, M. Helmes, et al., "Differential expression of cardiac titin isoforms and modulation of cellular stiffness," *Circulation Research*, vol. 86, no. 1, pp. 59–67, 2000.
- [70] O. Cazorla, Y. Wu, T. C. Irving, and H. Granzier, "Titin-based modulation of calcium sensitivity of active tension in mouse skinned cardiac myocytes," *Circulation Research*, vol. 88, no. 10, pp. 1028–1035, 2001.
- [71] N. Fukuda, Y. Wu, G. Farman, T. C. Irving, and H. Granzier, "Titin isoform variance and length dependence of activation in skinned bovine cardiac muscle," *Journal of Physiology*, vol. 553, no. 1, pp. 147–154, 2003.
- [72] M. Krüger and W. A. Linke, "Titin-based mechanical signalling in normal and failing myocardium," *Journal of Molecular and Cellular Cardiology*, vol. 46, no. 4, pp. 490–498, 2009.
- [73] P. F. M. van der Ven, J. W. Bartsch, M. Gautel, H. Jockusch, and D. O. Fürst, "A functional knock-out of titin results in defective myofibril assembly," *Journal of Cell Science*, vol. 113, no. 8, pp. 1405–1414, 2000.

- [74] H. L. Granzier, M. H. Radke, J. Peng, et al., "Truncation of titin's elastic PEVK region leads to cardiomyopathy with diastolic dysfunction," *Circulation Research*, vol. 105, no. 6, pp. 557–564, 2009.
- [75] M. H. Radke, J. Peng, Y. Wu, et al., "Targeted deletion of titin N2B region leads to diastolic dysfunction and cardiac atrophy," *Proceedings of the National Academy of Sciences of the United States of America*, vol. 104, no. 9, pp. 3444–3449, 2007.
- [76] N. Fukuda, Y. Wu, P. Nair, and H. L. Granzier, "Phosphorylation of titin modulates passive stiffness of cardiac muscle in a titin isoform-dependent manner," *Journal of General Physiology*, vol. 125, no. 3, pp. 257–271, 2005.
- [77] S. Lahmers, Y. Wu, D. R. Call, S. Labeit, and H. Granzier, "Developmental control of titin isoform expression and passive stiffness in fetal and neonatal myocardium," *Circulation Research*, vol. 94, no. 4, pp. 505–513, 2004.
- [78] Y. Wu, S. P. Bell, K. Trombitas, et al., "Changes in titin isoform expression in pacing-induced cardiac failure give rise to increased passive muscle stiffness," *Circulation*, vol. 106, no. 11, pp. 1384–1389, 2002.
- [79] W. A. Jaber, C. Maniu, J. Krysiak, et al., "Titin isoforms, extracellular matrix, and global chamber remodeling in experimental dilated cardiomyopathy: functional implications and mechanistic insight," *Circulation. Heart failure*, vol. 1, no. 3, pp. 192–199, 2008.
- [80] A. Borbély, I. Falcao-Pires, L. van Heerebeek, et al., "Hypophosphorylation of the Stiff N2B titin isoform raises cardiomyocyte resting tension in failing human myocardium," *Circulation Research*, vol. 104, no. 6, pp. 780–786, 2009.
- [81] I. Makarenko, C. A. Opitz, M. C. Leake, et al., "Passive stiffness changes caused by upregulation of compliant titin isoforms in human dilated cardiomyopathy hearts," *Circulation Research*, vol. 95, no. 7, pp. 708–716, 2004.
- [82] S. F. Nagueh, G. Shah, Y. Wu, et al., "Altered titin expression, myocardial stiffness, and left ventricular function in patients with dilated cardiomyopathy," *Circulation*, vol. 110, no. 2, pp. 155–162, 2004.
- [83] C. Neagoe, M. Kulke, F. del Monte, et al., "Titin isoform switch in ischemic human heart disease," *Circulation*, vol. 106, no. 11, pp. 1333–1341, 2002.
- [84] Y. Wu, J. Peng, K. B. Campbell, S. Labeit, and H. Granzier, "Hypothyroidism leads to increased collagen-based stiffness and re-expression of large cardiac titin isoforms with high compliance," *Journal of Molecular and Cellular Cardiology*, vol. 42, no. 1, pp. 186–195, 2007.
- [85] R. Yamasaki, Y. Wu, M. McNabb, M. Greaser, S. Labeit, and H. Granzier, "Protein kinase A phosphorylates titin's cardiac-specific N2B domain and reduces passive tension in rat cardiac myocytes," *Circulation Research*, vol. 90, no. 11, pp. 1181–1188, 2002.
- [86] M. Krüger and W. A. Linke, "Protein kinase-A phosphorylates titin in human heart muscle and reduces myofibrillar passive tension," *Journal of Muscle Research and Cell Motility*, vol. 27, no. 5–7, pp. 435–444, 2006.
- [87] M. Krüger, S. Kötter, A. Grützner, et al., "Protein kinase G modulates human myocardial passive stiffness by phosphorylation of the titin springs," *Circulation Research*, vol. 104, no. 1, pp. 87–94, 2009.
- [88] C. Hidalgo, B. Hudson, J. Bogomolovas, et al., "PKC phosphorylation of titin's PEVK element: a novel and conserved pathway for modulating myocardial stiffness," *Circulation Research*, vol. 105, no. 7, pp. 631–638, 2009.
- [89] B. D. Hudson, C. G. Hidalgo, M. Gotthardt, and H. L. Granzier, "Excision of titin's cardiac PEVK spring element abolishes PKC β -induced increases in myocardial stiffness," *Journal of Molecular and Cellular Cardiology*, vol. 48, no. 5, pp. 972–978, 2010.
- [90] A. F. Leite-Moreira, P. Castro-Chaves, P. Pimentel-Nunes, et al., "Angiotensin II acutely decreases myocardial stiffness: a novel AT1, PKC and Na⁺/H⁺ exchanger-mediated effect," *British Journal of Pharmacology*, vol. 147, no. 6, pp. 690–697, 2006.
- [91] A. F. Leite-Moreira, C. Bras-Silva, C. A. Pedrosa, and A. A. Rocha-Sousa, "ET-1 increases distensibility of acutely loaded myocardium: a novel ETA and Na⁺/H⁺ exchanger-mediated effect," *American Journal of Physiology*, vol. 284, no. 4, pp. H1332–H1339, 2003.
- [92] J. S. Janicki and B. B. Matsubara, "Myocardial collagen and left ventricular diastolic dysfunction," in *Left Ventricular Diastolic Dysfunction and Heart Failure*, W. H. Gaash and M. M. LeWinter, Eds., pp. 3–24, Lea & Febiger, Philadelphia, Pa, USA, 1994.
- [93] G. M. Fomovsky, S. Thomopoulos, and J. W. Holmes, "Contribution of extracellular matrix to the mechanical properties of the heart," *Journal of Molecular and Cellular Cardiology*, vol. 48, no. 3, pp. 490–496, 2010.
- [94] J. Asbun and F. J. Villarreal, "The pathogenesis of myocardial fibrosis in the setting of diabetic cardiomyopathy," *Journal of the American College of Cardiology*, vol. 47, no. 4, pp. 693–700, 2006.
- [95] M. R. Zile and D. L. Brutsaert, "New concepts in diastolic dysfunction and diastolic heart failure: part I: diagnosis, prognosis, and measurements of diastolic function," *Circulation*, vol. 105, no. 11, pp. 1387–1393, 2002.
- [96] W. C. Little, M. R. Zile, D. W. Kitzman, W. G. Hundley, T. X. O'Brien, and R. C. Degroof, "The effect of alagebrium chloride (ALT-711), a novel glucose cross-link breaker, in the treatment of elderly patients with diastolic heart failure," *Journal of Cardiac Failure*, vol. 11, no. 3, pp. 191–195, 2005.
- [97] Y. Sun and K. T. Weber, "Infarct scar: a dynamic tissue," *Cardiovascular Research*, vol. 46, no. 2, pp. 250–256, 2000.
- [98] J. W. Holmes, T. K. Borg, and J. W. Covell, "Structure and mechanics of healing myocardial infarcts," *Annual Review of Biomedical Engineering*, vol. 7, pp. 223–253, 2005.
- [99] W. J. Paulus, P. J. Vantrimpont, and A. M. Shah, "Acute effects of nitric oxide on left ventricular relaxation and diastolic distensibility in humans: assessment by bicoronary sodium nitroprusside infusion," *Circulation*, vol. 89, no. 5, pp. 2070–2078, 1994.
- [100] A. M. Shah, B. D. Prendergast, R. Grocott-Mason, M. J. Lewis, and W. J. Paulus, "The influence of endothelium-derived nitric oxide on myocardial contractile function," *International Journal of Cardiology*, vol. 50, no. 3, pp. 225–231, 1995.
- [101] W. J. Paulus, "Beneficial effects of nitric oxide on cardiac diastolic function: 'the flip side of the coin,'" *Heart Failure Reviews*, vol. 5, no. 4, pp. 337–344, 2000.
- [102] P. Castro-Chaves, R. Fontes-Carvalho, M. Pintalhão, P. Pimentel-Nunes, and A. F. Leite-Moreira, "Angiotensin II-induced increase in myocardial distensibility and its modulation by the endocardial endothelium in the rabbit heart," *Experimental Physiology*, vol. 94, no. 6, pp. 665–674, 2009.
- [103] C. Brás-Silva and A. F. Leite-Moreira, "Obligatory role of the endocardial endothelium in the increase of myocardial distensibility induced by endothelin-1," *Experimental Biology and Medicine*, vol. 231, no. 6, pp. 876–881, 2006.

- [104] C. Brás-Silva, D. Monteiro-Sousa, A. J. Duarte, et al., “Nitric oxide and prostaglandins—important players in endothelin-1 induced myocardial distensibility,” *Physiological Research*, vol. 57, no. 2, pp. 165–174, 2008.
- [105] A. P. Fontes-Sousa, C. Brás-Silva, A. L. Pires, D. Monteiro-Sousa, and A. F. Leite-Moreira, “Urotensin II acutely increases myocardial length and distensibility: potential implications for diastolic function and ventricular remodeling,” *Naunyn-Schmiedeberg’s Archives of Pharmacology*, vol. 376, no. 1-2, pp. 107–115, 2007.
- [106] A. P. Fontes-Sousa, A. L. Pires, V. F. Monteiro-Cardoso, and A. F. Leite-Moreira, “Urotensin II-induced increase in myocardial distensibility is modulated by angiotensin II and endothelin-1,” *Physiological Research*, vol. 58, no. 5, pp. 653–660, 2009.
- [107] A. P. Fontes-Sousa, A. L. Pires, C. S. Carneiro, C. Brás-Silva, and A. F. Leite-Moreira, “Effects of adrenomedullin on systolic and diastolic myocardial function,” *Peptides*, vol. 30, no. 4, pp. 796–802, 2009.
- [108] R. Ladeiras-Lopes, J. Ferreira-Martins, and A. F. Leite-Moreira, “Acute neurohumoral modulation of diastolic function,” *Peptides*, vol. 30, no. 2, pp. 419–425, 2009.
- [109] C. S. Apstein, “Influence of the coronary vasculature on left ventricular diastolic chamber stiffness: the erectile properties of the myocardium,” in *Left Ventricular Diastolic Dysfunction and Heart Failure*, W. H. Gaash and M. M. LeWinter, Eds., pp. 3–24, Lea & Febiger, Philadelphia, Pa, USA, 1994.

Review Article

Force Transmission between Synergistic Skeletal Muscles through Connective Tissue Linkages

Huub Maas¹ and Thomas G. Sandercock²

¹ Research Institute MOVE, Faculty of Human Movement Sciences, VU University, Van der Boerhorststraat 9, 1081 BT Amsterdam, The Netherlands

² Feinberg School of Medicine, Northwestern University, 303 East Chicago Avenue, Chicago, IL 60611, USA

Correspondence should be addressed to Huub Maas, h.maas@fbw.vu.nl

Received 30 November 2009; Accepted 1 February 2010

Academic Editor: Henk L. M. Granzier

Copyright © 2010 H. Maas and T. G. Sandercock. This is an open access article distributed under the Creative Commons Attribution License, which permits unrestricted use, distribution, and reproduction in any medium, provided the original work is properly cited.

The classic view of skeletal muscle is that force is generated within its muscle fibers and then directly transmitted in-series, usually via tendon, onto the skeleton. In contrast, recent results suggest that muscles are mechanically connected to surrounding structures and cannot be considered as independent actuators. This article will review experiments on mechanical interactions between muscles mediated by such epimuscular myofascial force transmission in physiological and pathological muscle conditions. In a reduced preparation, involving suprphysiological muscle conditions, it is shown that connective tissues surrounding muscles are capable of transmitting substantial force. In more physiologically relevant conditions of intact muscles, however, it appears that the role of this myofascial pathway is small. In addition, it is hypothesized that connective tissues can serve as a safety net for traumatic events in muscle or tendon. Future studies are needed to investigate the importance of intermuscular force transmission during movement in health and disease.

1. Introduction

When skeletal muscle fibers are excited, a cascade of events is triggered, which ultimately leads to forces exerted on the skeleton. Muscle forces are needed for movements, such as locomotion, and the maintenance of body balance. There are many structures involved at several levels organization: from actin, myosin, and titin of the sarcomeric cytoskeleton, desmin of the intermyofibrillar cytoskeleton, transsarcolemmal proteins such as dystrophin and integrin of the subsarcolemmal cytoskeleton, endo-, peri-, and epimysium, as well as tendon and aponeurosis at the muscle level to inter- and extramuscular connective tissues (e.g., the neurovascular tract, fascia) at the compartmental level. For understanding how forces are transmitted from sarcomere to the bony skeleton in normal and diseased muscle, it is necessary to investigate the role of each of these structural elements as well as their interaction. The present review focuses on the connective tissues that are found in the direct environment of skeletal muscles and their potential effects in muscle function during movement.

The most recognized pathway of force transmission from muscle fibers to bone is via the specialized myotendinous junction [1] and tendon, named myotendinous force transmission. Classical anatomy has defined each muscle as a separate entity with a unique function at the joint(s) it spans. Therefore, it has long been common to view muscles as mechanically independent actuators. This is readily apparent from biomechanical models of the musculoskeletal system in which muscles are connected to the skeleton at their origin and insertion [2, 3]. However, many scientists from the last century were aware of mechanical interactions between muscles (for a historical overview see [4]). For example, during measurements of soleus muscle forces in the cat, upon stimulation of the lateral gastrocnemius-soleus nerve branch Denny-Brown [5] noticed that “...it is found to be extremely difficult to avoid a slight early rise of tension, and fall in the plateau, due to the vibration or pull of gastrocnemius.” More recently, Nichols [6] stated “Mechanical artifacts due to direct mechanical action of the stretched muscle on those isometrically constrained were indicated by essentially instantaneous latencies or by effects

observed after pharmacological block of heterogenic reflexes.” Note that in these experiments the tendons are severed from their insertion site and individually connected to force transducers. This means that the mechanical linkage was provided by structures at the muscle belly boundary (i.e., the epimysium).

The purpose of this article is first to review the initial series of systematic experiments on mechanical interactions between synergistic muscles (i.e., neighboring muscles which produce the same movement at the joint) via connective tissue linkages (named epimuscular myofascial pathways) that revealed the presence and capacity of this phenomenon (mechanical interactions between antagonistic muscles have been reviewed elsewhere; see [7]); second, to discuss the current debate on the importance of epimuscular myofascial force transmission during normal movements; and third, to discuss the potential functions of inter- and extramuscular connective tissues for pathological muscle-tendon conditions.

2. Mechanical Interaction between Muscles through Connective Tissue Structures

2.1. Epimuscular Myofascial Pathways. Epimuscular myofascial force transmission is defined as transmission of muscle forces to the skeleton via pathways other than the muscular origin and insertion. A direct proof of epimuscular myofascial force transmission is a difference in force exerted at the origin (proximal) and insertion (distal) of a muscle. Another feature of this phenomenon is that length changes in one muscle can affect forces exerted at the tendons of muscles that are kept at a constant length.

Two epimuscular pathways are distinguished (Figure 1): (i) *intermuscular*, if force is transmitted between two neighboring muscles via the continuous connective tissue at their muscle belly interface, and (ii) *extramuscular*, if force is transmitted between the epimysium of a muscle and an adjacent nonmuscular structure. The direct intermuscular pathway is provided by an areolar connective tissue layer at the interface between muscle bellies (for images see [8]). Several structures provide an anatomical substrate for the extramuscular myofascial pathway: (i) the matrix supporting nerves and blood vessels, that is, the neurovascular tract (see [8, 9]) (Note that the neurovascular tract is continuous with the extensive intramuscular connective tissue network, which reinforces the nerves innervating muscle fibers and the blood vessels entering the muscle.), (ii) fascia layers forming the borders of synergistic muscle groups that are continuous with more superficial layers (e.g., subcutaneous connective tissue), and (iii) connective tissue around tendons (for images the reader is referred to previous publications, e.g., [10–13]).

Dissection of a limb shows a vast network of collagen-based structures linking muscles together. Clearly muscles are connected by fascial sheets, loose areolar tissue, vascular links, nerves, and supporting collagen. Sometimes muscle fibers originate from neighboring muscle (e.g., in the cat there are some LG fibers that seem to terminate in MG

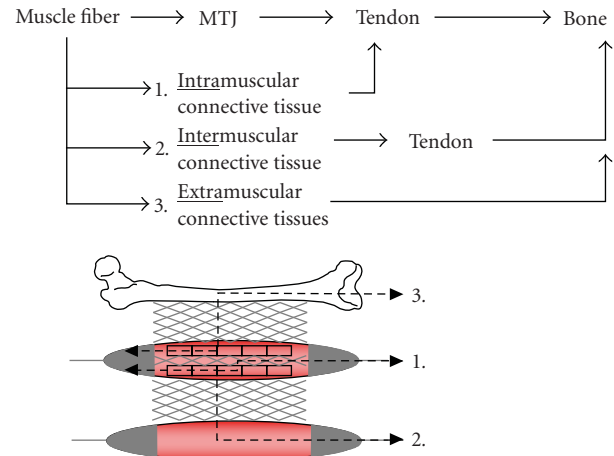


FIGURE 1: The different pathways via which force generated within muscle fibers can leave the muscle to be transmitted to the skeleton. Two epimuscular pathways are distinguished. (i) Intermuscular: force transmission between two neighboring muscles via the continuous connective tissue at their muscle belly interface. (ii) Extramuscular: force transmission between a muscle and adjacent nonmuscular structures. The term epimuscular myofascial force transmission is used to indicate transmission via inter- or extramuscular pathways.

muscle). Tendons appear to run together. Pushing or pulling on one muscle leads to movement of a neighbor. Thus, muscles are unquestionably linked. The question is how significant these links are to the normal function of muscle.

2.2. Mechanical Interactions between Muscles in the Anterior Crural Compartment. An in-depth analysis of transmission of extensor digitorum longus (EDL) muscle force in the rat, which is embedded within the anterior crural compartment together with extensor hallucis longus (EHL) and tibialis anterior (TA) muscles, has been performed. Because both the proximal and distal tendons of EDL can be attached to force transducers, EDL is a very suitable muscle for the assessment of epimuscular myofascial effects. Isometric forces were measured simultaneously at the proximal and distal tendons of EDL muscle as well as at the tied distal tendons of TA, and EHL muscles. These tendons can all be dissected with minimal disruption of the compartment, leaving epimuscular myofascial pathways mostly intact. By manipulating the position of the force transducers, the muscle-tendon complex length of one or all muscles as well as muscle relative position were changed.

Mechanical interactions between EDL and TA + EHL were found for various experimental conditions. Length changes of the TA + EHL complex affected the forces exerted at the proximal and distal tendons of EDL, which was kept at a constant length [9]. More specifically, lengthening TA + EHL distally increased proximal EDL force (by 37%), but decreased distal EDL force (by 39%). The mechanical interactions between synergistic muscles can be ascribed to changes in the position of one muscle relative to the other [15] and, consequently, changes in the configuration

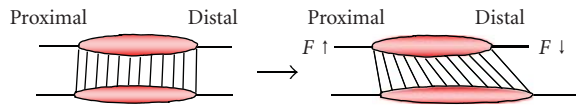


FIGURE 2: Schematic drawing to illustrate changes in the configuration of connective tissue between two muscles if one muscle is lengthened. Modified from Maas et al. [14].

(length and angle) of inter- and extramuscular connective tissues (Figure 2). It may appear obvious to explain these results by mechanical effects of intermuscular connective tissue. However, EDL, TA and EHL are also linked to each other via extramuscular structures. A clear example is the neurovascular tract that runs in between the muscles while giving off branches of nerves and blood vessels which enter the endo-perimysial network of the muscle [8, 9]. Therefore, we conducted a followup study to investigate the contribution of each pathway [16]. Equal experimental conditions were imposed before and after disruption of the connective tissue layer between EDL and TA + EHL, thereby eliminating force transmission via intermuscular myofascial pathways. This significantly decreased the effects of TA + EHL length on force exerted at the distal tendon of EDL. However, the interaction between TA + EHL and proximal EDL force did not change. Therefore, we concluded that mechanical interactions between synergistic muscles originate from both inter- and extramuscular connective tissues. Besides the above-described study [16], there is only one other study [10] that reports data indicating that the areolar connective tissues are stiff and strong enough to transmit force. Changes in the length-force characteristics were found following disruption of the intermuscular myofascial pathway [10].

In the above-described studies, relative displacements of muscle bellies were the result of length changes in a single muscle group. To distinguish between effects of muscle length and relative position, isolated effects of muscle relative position were studied [14]. The muscle-tendon complex length of EDL and TA + EHL was kept constant. The position of EDL muscle relative to its surroundings was changed by moving both the proximal and the distal tendons to an equal extent and in the same direction. Displacements of EDL in distal direction decreased force exerted at the distal tendons of TA + EHL. Simultaneously, distal EDL force increased and proximal EDL force decreased. Force changes in opposite direction were found if EDL muscle was repositioned more proximally. Each movement affected the proximo-distal force difference and, thus, the magnitude of net epimuscular myofascial force transmission. In addition, the sign of the force difference between proximal and distal EDL forces changed. Similar effects of muscle relative position were reported for slightly different experimental conditions [17]. Length-force characteristics of EDL muscle obtained by movements of the distal tendon were significantly different from its length-force characteristics if EDL muscle was lengthened by moving its proximal tendon.

In conclusion, the position of a muscle relative to surrounding tissues codetermines isometric muscle force.

Position effects can be explained by changes in the configuration of the tissues representing the epimuscular myofascial pathways (Figure 2). In general, the muscle end that is positioned farthest in a particular direction (e.g., distal) will draw force from neighboring muscles.

2.3. Do Mechanical Interactions between Muscles Occur In Vivo? The above in situ studies have shown the potential of force transmission between skeletal muscles via inter- and extramuscular connective tissues. The functional relevance of this phenomenon is dependent on the magnitude of the effects found in physiological muscle conditions. However, this mode of force transmission may be small in normal muscles during physiological conditions, because (1) the above studies all used tetanic stimulation. This rarely occurs during voluntary movement, so observations may be relevant only to lab conditions; (2) the muscle-tendon complex length of a single muscle was changed while the length of its synergists was kept constant, compared to simultaneous length changes in synergistic muscles during normal movements; (3) when individual muscles are stimulated alone and together, the force sums linearly which is surprising if the epimuscular pathway is used; and (4) a recent experiment studying force transmission between cat soleus (SO) and its synergistic muscles in an intact animal showed little epimuscular force transmission. Each of these points will be discussed below.

In the studies described up to this point, the effects of epimuscular pathways on muscular force transmission were tested predominantly during simultaneous maximal activation of both synergistic and antagonistic muscles. Coactivation of synergistic and antagonistic muscles has been observed in the awake, freely moving animal (e.g., [18]), but in most cases at submaximal levels of activation (e.g., [19]). Recently, using the in situ setup described above, substantial proximo-distal EDL force differences (up to 30% of maximal force at each frequency) as well as mechanical interactions with TA + EHL were found during nerve stimulation at submaximal frequencies (10–30 Hz) [20]. This suggests that also at firing frequencies encountered in vivo muscle forces can be transmitted via epimuscular myofascial pathways.

Another experimental condition of the studies described in Section 2.2 that was different from the conditions under which muscles function in vivo was changing the length of only one muscle. Due to differences in moment arms between synergists [21, 22], the change in length of one muscle can be different from that of its neighbor, but the relative movements imposed during lengthening a single muscle were beyond the physiological range. Recently, this issue was addressed by investigating proximal-distal force differences in EDL muscle while lengthening EDL, TA, and EHL simultaneously, as is the case during ankle movements [23]. Also in these experimental conditions, a large force difference (up to 30% of maximal force) was found. At submaximal stimulation frequencies, however, the difference (5%) and, hence, net epimuscular myofascial force transmission became small [23]. It should be noted that different myofascial pathways can be arranged in such a way that

they exert forces on a muscle in opposite direction (see [9, Figure 8]) and that the proximo-distal force difference is the net result of all myofascial loads [7]. A small difference can thus be explained by limited epimuscular myofascial force transmission or opposing myofascial loads of similar magnitude.

If force transmission through epimuscular pathways is substantial, then nonlinear summation of force is expected when different muscles are activated alone and together. Nonlinear force summation is defined as the difference between the force exerted when two muscle parts are excited simultaneously and the sum of the forces exerted when each muscle part is excited individually [24]. Force transmission between the medial gastrocnemius (MG) and lateral gastrocnemius/soleus muscles (LG/SO) was studied in the cat hindlimb [25, 26]. The muscles were activated by stimulation of the nerve branches to each of the muscle groups. LG and SO muscles were stimulated together because of the difficult surgery required to separate their nerves (see [27]). The cat hindlimb was left intact and the foot attached to a 6-degree-of-freedom (dof) load cell to measure force and torque. The femur was fixed to a rigid frame. MG was stimulated alone, LG/SO alone, and then both together. When both muscles were stimulated together, the resulting forces and torques (all 6 dof) were less than the sum of the individual forces. The peak error occurred during the onset of activation where force was about 9% less compared to the plateau where steady state force was about 2% less. There was no evidence that the direction of the forces changed during simultaneous activation of the muscles compared to activation of the muscles independently. These results suggest that when both muscle groups were activated together there was increased shortening of the muscle fibers, and hence less force due to a higher velocity of shortening during force onset. Thus, there is some interaction, either between the muscle bellies or between their tendons. However, the interaction was small, and during steady state, it was almost immeasurable. Similar experiments were performed on the vastus medialis and rectus femoris in cat. Both muscles are knee extensors. They share a border and a tendon and thus may be expected to show nonlinear summation. Nonlinear summation error was small in all 6 degrees of freedom. The average peak error was 8.4% and the mean average error during the contraction was 1.3% (unpublished observations). Note that these experiments do not preclude epimuscular force transmission, but rather suggest that in normal muscle it has little functional effect on the overall force delivered to the skeleton.

To tackle some of the concerns of previous studies, a new experimental approach was developed to measure directly the mechanical interactions between muscles in conditions that simulate those present during normal movements [28]. The latter was assured by testing the muscles in a nearly intact limb of the cat. The tendons were not cut, but left attached to their insertion sites. Length changes were obtained by movements of the joints and, thus, only physiological relative movements could be imposed. The mechanical interactions between the one-joint SO and its two-joint synergistic muscles were studied. The muscle bellies of LG and plantaris

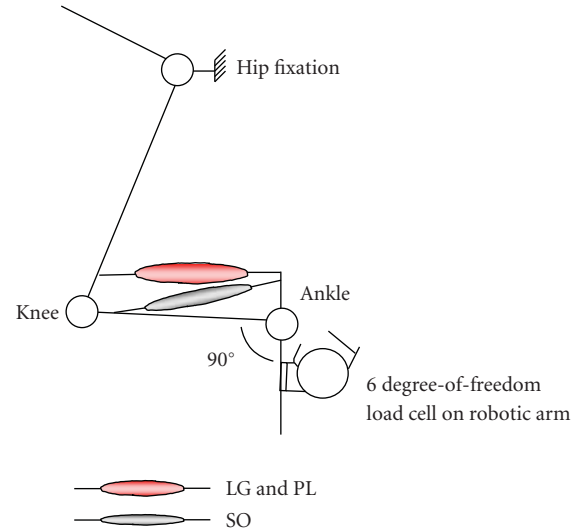


FIGURE 3: A schematic presentation of the cat hindlimb in the experimental setup used to investigate inter-synergist interactions [28].

(PL) muscles share an interface with SO [29]. Ankle moment exerted upon the isolated excitation of SO was measured at various knee angles while the ankle was kept at a constant position ($\sim 90^\circ$), using a 6-degree-of-freedom load cell coupled to a 6-degree-of-freedom robotic manipulator (Figure 3). Note that knee movements will only alter the length and relative position of the two-joint muscles, but not of SO. This involves the greatest relative displacements between these muscles *in vivo*. We hypothesized that force transmission from SO muscle fibers will be affected by length changes of its synergists through configuration changes of connective tissues between these muscles.

Changing the knee angle from 70° to 140° lengthened LG and PL profoundly (4.5–7.2 mm), as calculated using the geometric model presented by Goslow et al. [30]. In contrast to our expectations, active ankle moment generated by SO and the rate of muscle relaxation were not significantly affected by changes in knee angle. These results demonstrate that the presence of relative muscle movements does not necessarily mean force transmission between muscles. To further test the apparent independency of SO, an additional set of experiments was performed. With minimal disruption of the connective tissues at the muscle belly level, the distal tendon of SO was dissected free from the other tendons in the Achilles tendon complex, cut, and connected to a force transducer. As this eliminated force transmission to its insertion on the calcaneus, any ankle joint moment following SO excitation was attributed to force transmission via epimuscular myofascial pathways to the Achilles tendon. If the tendon of SO was placed at its original position, corresponding to the above reported ankle joint angle, the moment exerted at the ankle was close to zero while force exerted at the distal tendon of SO was near its optimal value. A substantial ankle moment was found only if SO was excited at positions distant from physiological. These results confirm

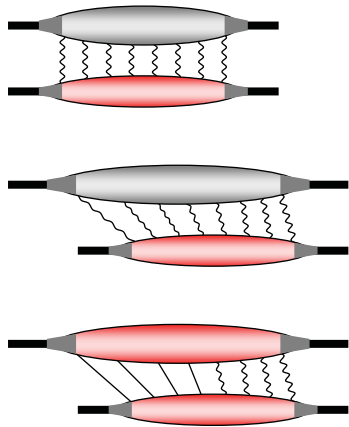


FIGURE 4: Drawings to illustrate length changes of connective tissue linkages between passive (grey) and active (red) synergistic muscles. Changing the length of one muscle results in reorientation as well as unfolding of those linkages. Unfolding is also seen with coactivation. Such straightening of macroscopic crimp in collagen fibrils is correlated to the toe region of the stress-strain curve [35]. Modified from Maas and Sandercock [28].

that for *in vivo* muscle lengths and relative positions force generated in SO muscle fibers is transmitted to its distal tendon.

The above-described nearly linear force summation between MG and LG/SO as well as between rectus femoris and vastus lateralis is in agreement with this finding. Others have found that human SO fascicle length was not affected by changes in knee angle, as measured in both passive and maximally active conditions of the ankle plantar flexors [31]. In contrast, recent imaging studies in humans suggest that mechanical connections between gastrocnemius and SO muscles are effective also within the *in vivo* length range. Isolated excitation of MG at a fixed angle of the ankle and knee joints elicited a decrease in fascicle length, not only in the excited muscle, but also in SO [32, 33]. However, MG activation did not cause displacements in flexor hallucis longus muscle [33], suggesting that not all muscles are equally connected. In addition, effects of knee movements on SO muscle have been reported [33, 34]. Note that the mechanical effects (e.g., ankle moment) of such displacements in SO were not measured.

How can the different results between the rat and cat studies be explained? We have hypothesized that the intermuscular linkages between SO and adjacent muscles within the intact cat may be slack or operate on the toe region of their lumped stress-strain curve (Figure 4, see also [28]). The steep portion of this curve and, hence, epimuscular force transmission will then be attained only with supraphysiological displacements. The stiffness of the intermuscular linkages may also be a local property, being more compliant in the proximal region of the cat ankle extensors. Note that Maas and Sandercock [28] lengthened the two-joint muscles by knee movements; thus, there was more movement proximally. Preliminary data suggest indeed that cat SO muscle is more rigidly connected to LG

distally than proximally (Sandercock and Maas, unpublished observations). Also in line with this hypothesis are the results of an earlier study in the rat in which lengthening a muscle distally resulted in substantial force changes exerted at the distal tendon of a neighboring muscle, while effects of proximal lengthening were not significant [17].

A major difference between the experiments on epimuscular myofascial force transmission in the rat (see above) and the cat [28] is the number of muscles that is activated simultaneously. In the rat studies all synergists and some antagonists were activated versus a single muscle in the cat. Coactivation leads to several changes within the muscle compartment that may affect the mechanical interaction between adjacent muscles. Muscle fibers contract and, hence, the muscle belly shortens and expands radially. The former will result in a small change of the muscle relative position, whereas the expansion will increase the lateral tension of the connective tissue network. In a recent study, we tested the hypothesis that the net effect of coactivation is an increase in the stiffness of the epimuscular pathways (Figure 4), which will facilitate force transmission between muscles. Effects of antagonist coactivation on mechanical interactions between synergistic muscles in the rat forelimb were assessed [36]. In contrast to the hypothesis, changes in force of the restrained muscle with length changes of its synergist were unaffected by antagonist coactivation. Testing intermuscular interaction with other combinations of active muscles (e.g., excluding the activity of some synergistic muscles) may be necessary to elucidate the effects of muscle coactivation on the magnitude of epimuscular myofascial force transmission.

Finally, it is also conceivable that the mechanical characteristics of the connective tissue system are different between muscle groups within an animal and across species. The muscle-connective tissue architecture and composition of each synergistic group is different. Therefore, generalizing the current results to the whole musculoskeletal system should be done with caution. Although mechanical interactions between synergistic muscles have been shown in many animals (e.g., mouse, rat, cat, locust, frog), differences in connective tissue mechanical properties or differences in animal size may affect the importance of such force transmission. In contrast to mammals, it has been reported that amphibians have a relatively poorly developed connective tissue network [37] and that insects contain very little connective tissue [38, 39]. Another aspect that should be taken into account is the scaling of muscle surface area (to the 2nd power) versus muscle volume (to the 3rd power). This means that, for example, mice have a relatively larger epimysial surface to volume ratio than humans. To date, whether these variations between species lead also to different mechanical interactions remains unclear.

The contradictory findings between the rat and cat studies are not fully understood and, thus, the responsible mechanisms requires further investigation. Specifically, future studies should continue to test if the magnitude of intermuscular force transmission is dependent on the number of muscles that is simultaneously activated. Is the extent of force transmission between muscles the same throughout the body? This is another question that needs to

be addressed. In conclusion, the importance of epimuscular myofascial pathways for muscle function during normal movements remains unclear.

2.4. Connective Tissue Function in Pathological Muscle-Tendon Conditions. Besides a potential role for normal muscle function, epimuscular myofascial pathways may be important in pathological conditions of the musculoskeletal system. Street observed [41], “After the distal tendon of a frog’s semitendinosus muscle is cut, pathological changes appear first in the distal part. We found that when part of a muscle was normal the muscle as a whole generally developed the normal amount of tension and we guessed that some cell component other than the myofibril arrays served as a tension bypass through or around the damaged areas (Ramsey and Street, unpublished).” In the same paper, Street suggested [41], “In injured whole muscle it is probable that the connective tissue sheath near damaged fibers can pick up and transfer active tension generated in normal areas and, at the same time, stabilize abnormal areas against length changes. This might promote healing.” This suggests the hypothesis that the connective tissue network may act also as a safety net for traumatic events in muscle or tendon. In other words, due to the presence of myofascial pathways, the acute effects of muscle or tendon trauma are limited and muscle function is preserved.

Injury within a muscle or tendon is a common occurrence, especially during sport activities (e.g., [42, 43]). Thus, it is essential that basic function is maintained while the injury is healed. In the same study by Maas and Sandercock [28] that showed little epimuscular force transmission in intact SO, they also showed that during complete tendon transection the SO can produce substantial force. The insertion of the SO on the calcaneus was completely severed, yet the SO produced an extensor moment at the ankle that was about 45% of normal. There was greater shortening, 17 mm compared to 1 mm, than before tendon transection. Yet function was partially maintained possibly allowing use during recovery.

The results of several previous studies support the idea that connective tissues within and surrounding muscles can limit injury and support repair. It has been reported that one of the four distal tendons of rat EDL (a multitendoned muscle, see [44]) can be cut or considerably shortened with minimal effects on force measured at the proximal tendon [45, 46]. This can only be explained by transmission of force from the tenotomized muscle fibers to the intact distal tendons via the endomysial-perimysial network. Similar phenomena have been reported following transection of the whole distal or proximal tendon. During some of the above-described rat experiments, the connection between tendon and force transducer was suddenly severed. Following such a release of the proximal EDL tendon, a substantial force was still found at the distal tendon [47]. The muscle fibers of EDL are thus prevented from shortening all the way, most likely by inter- and/or extramuscular connective tissues. In a different experiment, the connection of the TA + EHL tendon was released

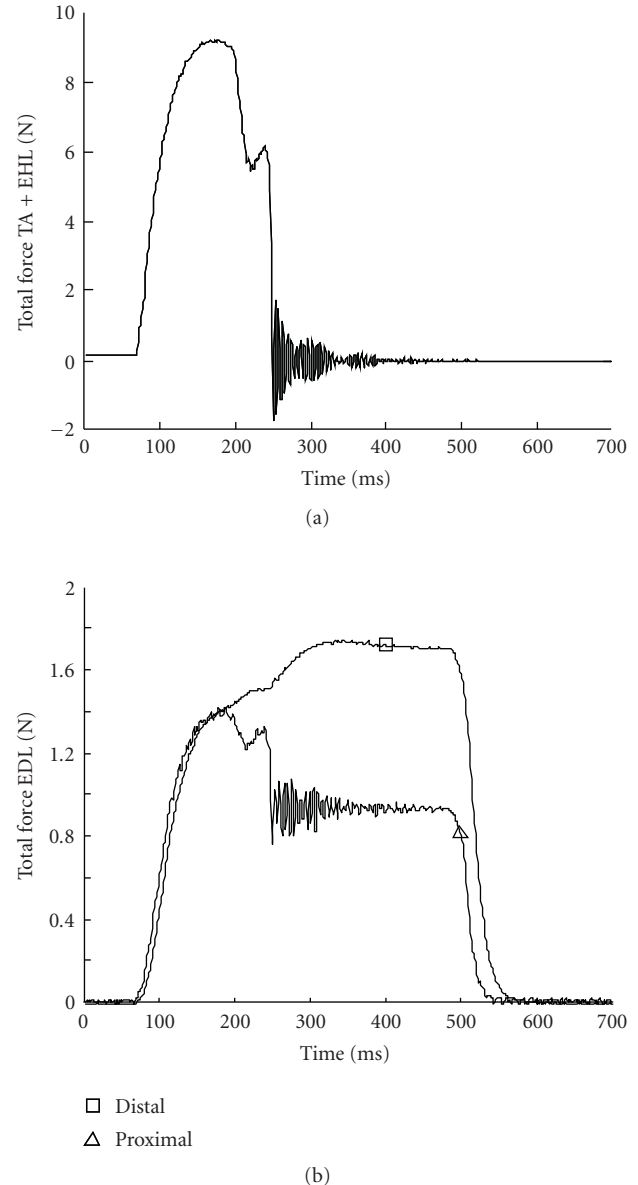


FIGURE 5: Waveforms of simultaneously measured force exerted at the distal tendon of TA + EHL (a) and forces exerted at the tendons of EDL muscle (b). During isometric contraction, the connection between TA + EHL and the force transducer was severed ($t \sim 200$ ms). TA + EHL force dropped to zero and at the same time proximal EDL force decreased and distal EDL force increased. These results have been presented in abstract form [40].

suddenly. Proximal TA + EHL force was not measured, but the changes in proximal and distal EDL forces clearly indicate mechanical interactions between these synergistic muscles (Figure 5).

In addition to the acute backup from connective tissues following muscle and tendon trauma, long-term adaptations also suggest that myofascial pathways serve temporarily as a safety net. It has been reported that the integrin-vinculin mediated connections between the subsarcolemmal

cytoskeleton and extracellular matrix are temporarily reinforced in ruptured muscle fibers [48, 49]. As a consequence, force generated within the sarcomeres of these damaged fibers will be transmitted via the endomysium. This will reduce the load on the injured site allowing repair with less chance of rerupture. In the case that not the muscle fibers but the tendon is fully or partially torn, connective tissue linkages with adjacent structures may in a similar fashion prevent further trauma and facilitate the recovery process. Such adhesions have been reported in chronically tenotomized muscle in the rat, cat, and rabbit [50–52], which ultimately results in reattachment of the tendon. Nonsurgical treatment (e.g., immobilization at low length) is also frequently applied following tendon ruptures in humans (e.g., [53]). Preserving and restoring function after injury clearly is important in wild animals and will be selected for. In contrast to humans, where the damage can be treated in a hospital, most animals must maintain some degree of function while the muscle-tendon injury heals.

Epimuscular myofascial transmission may also be important during reconstructive surgery. Several surgical interventions include manipulation of tendon, muscle, and/or the surrounding connective tissues (e.g., fasciotomy in compartment syndrome, tendon transfer in cerebral palsy). In tendon transfer surgery limb function is improved in a patient by cutting and reattaching a tendon to a new insertion point (e.g., [54]). Preliminary results suggest that scar tissue formation following an agonist-to-antagonist tendon transfer in the rat significantly affects transmission of forces from the transferred muscle [55]. Therefore, knowledge of the acute and long-term effects of disrupting connective tissues has important implications for surgical practice.

3. Conclusions

In the last decade, the potential of force transmission between skeletal muscles via inter- and extramuscular connective tissues has been demonstrated. Investigators have definitively shown that epimuscular pathways can transmit substantial force. More recent efforts have resulted in new insights regarding effects of epimuscular myofascial force transmission in more physiologically relevant muscle conditions (e.g., in vivo relative muscle movements). While not conclusive, these insights suggest that the role of this pathway may be small in normal undamaged muscles. Future studies should investigate force transmission during muscle activation patterns that resemble those of normal movements. In particular, effects of decreasing the number of muscles that are active simultaneously on the mechanical connectivity between muscles need to be investigated. Furthermore, the material properties of the connective tissue links need to be characterized. A full understanding requires knowing how the deformation of the border of a muscle affects the strain throughout the muscle. While the significance of epimuscular myofascial force transmission for muscle function in vivo remains unclear, potential functions for pathological muscle-tendon conditions (e.g., tendon rupture) have emerged.

Acknowledgments

The authors thank professor Peter Huijting and Guus Baan who coauthored the manuscripts that part of this work was based on. Huub Maas is currently supported by Marie Curie International Reintegration Grant no. MIRG-CT-2007-203846 within the 7th European Community Framework Programme. T. G. Sandercock is currently supported by NIH NS034382 and NS061208.

References

- [1] J. A. Trotter, A. Samora, and C. Wofsy, "A morphometric analysis of the muscle-tendon junction," *Anatomical Record*, vol. 213, no. 1, pp. 26–32, 1985.
- [2] J. L. McKay, T. J. Burkholder, and L. H. Ting, "Biomechanical capabilities influence postural control strategies in the cat hindlimb," *Journal of Biomechanics*, vol. 40, no. 10, pp. 2254–2260, 2007.
- [3] S. H. Yeo, M. C. Tresch, and D. K. Pai, "Optimal design of musculoskeletal models using force field data," in *Proceedings of the 30th Annual International Conference of the IEEE Engineering in Medicine and Biology Society (EMBS '08)*, pp. 3710–3714, Vancouver, Canada, August 2008.
- [4] P. A. Huijting, "Epimuscular myofascial force transmission: a historical review and implications for new research. International society of biomechanics Muybridge award lecture, Taipei, 2007," *Journal of Biomechanics*, vol. 42, no. 1, pp. 9–21, 2009.
- [5] D. E. Denny-Brown, "The histological features of striped muscle in relation to its functional activity," *Proceedings of the Royal Society of London. Series B*, vol. 104, pp. 371–411, 1929.
- [6] T. R. Nichols, "Receptor mechanisms underlying heterogenic reflexes among the triceps surae muscles of the cat," *Journal of Neurophysiology*, vol. 81, no. 2, pp. 467–478, 1999.
- [7] P. A. Huijting, "Epimuscular myofascial force transmission between antagonistic and synergistic muscles can explain movement limitation in spastic paresis," *Journal of Electromyography and Kinesiology*, vol. 17, no. 6, pp. 708–724, 2007.
- [8] P. A. Huijting, H. Maas, and G. C. Baan, "Compartmental fasciotomy and isolating a muscle from neighboring muscles interfere with myofascial force transmission within the rat anterior crural compartment," *Journal of Morphology*, vol. 256, no. 3, pp. 306–321, 2003.
- [9] H. Maas, G. C. Baan, and P. A. Huijting, "Intermuscular interaction via myofascial force transmission: effects of tibialis anterior and extensor hallucis longus length on force transmission from rat extensor digitorum longus muscle," *Journal of Biomechanics*, vol. 34, no. 7, pp. 927–940, 2001.
- [10] P. A. Huijting and G. C. Baan, "Myofascial force transmission causes interaction between adjacent muscles and connective tissue: effects of blunt dissection and compartmental fasciotomy on length force characteristics of rat extensor digitorum longus muscle," *Archives of Physiology and Biochemistry*, vol. 109, pp. 97–109, 2001.
- [11] J. M. Rijkelijhuizen, G. C. Baan, A. de Haan, C. J. de Ruyter, and P. A. Huijting, "Extramuscular myofascial force transmission for in situ rat medial gastrocnemius and plantaris muscles in progressive stages of dissection," *Journal of Experimental Biology*, vol. 208, no. 1, pp. 129–140, 2005.

- [12] C. A. Yucesoy and P. A. Huijting, "Substantial effects of epimuscular myofascial force transmission on muscular mechanics have major implications on spastic muscle and remedial surgery," *Journal of Electromyography and Kinesiology*, vol. 17, no. 6, pp. 664–679, 2007.
- [13] H. J. M. Meijer, J. M. Rijkelijhuizen, and P. A. Huijting, "Myofascial force transmission between antagonistic rat lower limb muscles: effects of single muscle or muscle group lengthening," *Journal of Electromyography and Kinesiology*, vol. 17, no. 6, pp. 698–707, 2007.
- [14] H. Maas, G. C. Baan, and P. A. Huijting, "Muscle force is determined also by muscle relative position: isolated effects," *Journal of Biomechanics*, vol. 37, no. 1, pp. 99–110, 2004.
- [15] H. Maas, C. A. Yucesoy, G. C. Baan, and P. A. Huijting, "Implications of muscle relative position as a co-determinant of isometric muscle force: a review and some experimental results," *Journal of Mechanics in Medicine and Biology*, vol. 3, pp. 145–168, 2003.
- [16] H. Maas, H. J. M. Meijer, and P. A. Huijting, "Intermuscular interaction between synergists in rat originates from both intermuscular and extramuscular myofascial force transmission," *Cells Tissues Organs*, vol. 181, no. 1, pp. 38–50, 2005.
- [17] P. A. Huijting and G. C. Baan, "Myofascial force transmission: muscle relative position and length determine agonist and synergist muscle force," *Journal of Applied Physiology*, vol. 94, no. 3, pp. 1092–1107, 2003.
- [18] B. I. Hyland and V. M. B. Jordan, "Muscle activity during forelimb reaching movements in rats," *Behavioural Brain Research*, vol. 85, no. 2, pp. 175–186, 1997.
- [19] R. Hennig and T. Lomo, "Firing patterns of motor units in normal rats," *Nature*, vol. 314, no. 6007, pp. 164–166, 1985.
- [20] H. J. M. Meijer, G. C. Baan, and P. A. Huijting, "Myofascial force transmission is increasingly important at lower forces: firing frequency-related length-force characteristics of rat extensor digitorum longus," *Acta Physiologica*, vol. 186, no. 3, pp. 185–195, 2006.
- [21] W. L. Johnson, D. L. Jindrich, R. R. Roy, and V. R. Edgerton, "A three-dimensional model of the rat hindlimb: musculoskeletal geometry and muscle moment arms," *Journal of Biomechanics*, vol. 41, no. 3, pp. 610–619, 2008.
- [22] T. J. Burkholder and T. R. Nichols, "Three-dimensional model of the feline hindlimb," *Journal of Morphology*, vol. 261, no. 1, pp. 118–129, 2004.
- [23] H. J. M. Meijer, J. M. Rijkelijhuizen, and P. A. Huijting, "Effects of firing frequency on length-dependent myofascial force transmission between antagonistic and synergistic muscle groups," *European Journal of Applied Physiology*, vol. 104, no. 3, pp. 501–513, 2008.
- [24] T. G. Sandercock, "Nonlinear summation of force in cat soleus muscle results primarily from stretch of the common-elastic elements," *Journal of Applied Physiology*, vol. 89, no. 6, pp. 2206–2214, 2000.
- [25] E. J. Perreault, C. J. Heckman, and T. G. Sandercock, "Three-dimensional moment and stiffness summation for muscles sharing a common tendon," in *Proceedings of the 2nd Joint Engineering in Medicine and Biology, the 24th Annual Conference and the Annual Meeting of the Biomedical Engineering Society (BMES/EMBS '02)*, vol. 3, pp. 2554–2555, Houston, Tex, USA, October 2002.
- [26] T. G. Sandercock and H. Maas, "Force summation between muscles: are muscles independent actuators?" *Medicine and Science in Sports and Exercise*, vol. 41, no. 1, pp. 184–190, 2009.
- [27] H. Maas, B. I. Prilutsky, T. R. Nichols, and R. J. Gregor, "The effects of self-reinnervation of cat medial and lateral gastrocnemius muscles on hindlimb kinematics in slope walking," *Experimental Brain Research*, vol. 181, no. 2, pp. 377–393, 2007.
- [28] H. Maas and T. G. Sandercock, "Are skeletal muscles independent actuators? Force transmission from soleus muscle in the cat," *Journal of Applied Physiology*, vol. 104, no. 6, pp. 1557–1567, 2008.
- [29] A. W. English and W. D. Letbetter, "Anatomy and innervation patterns of cat lateral gastrocnemius and plantaris muscles," *American Journal of Anatomy*, vol. 164, no. 1, pp. 67–77, 1982.
- [30] G. E. Goslow Jr., R. M. Reinking, and D. G. Stuart, "The cat step cycle: hind limb joint angles and muscle lengths during unrestrained locomotion," *Journal of Morphology*, vol. 141, no. 1, pp. 1–42, 1973.
- [31] Y. Kawakami, Y. Ichinose, and T. Fukunaga, "Architectural and functional features of human triceps surae muscles during contraction," *Journal of Applied Physiology*, vol. 85, no. 2, pp. 398–404, 1998.
- [32] T. Oda, H. Kanehisa, K. Chino, et al., "In vivo behavior of muscle fascicles and tendinous tissues of human gastrocnemius and soleus muscles during twitch contraction," *Journal of Electromyography and Kinesiology*, vol. 17, no. 5, pp. 587–595, 2007.
- [33] J. Bojsen-Moller, S. Schwartz, T. Finni, K. Kalliokoski, and S. P. Magnusson, "Lateral force transmission between lower leg muscles," in *Proceedings of the 14th Annual Congress of the European College of Sport Science*, Oslo, Norway, 2009.
- [34] A. Yaman, M. Ledesma-Carbayo, G. C. Baan, P. A. Huijting, C. A. Yucesoy, and C. Ozturk, "MRI assesment of passive muscular-mechanics in vivo using intensity based non-rigid B-spline registration: effects of epimuscular myofascial force transmission," in *Proceedings of the 17th International Society for Magnetic Resonance in Medicine Scientific Meeting & Exhibition*, Honolulu, Hawaii, USA, 2009.
- [35] J. Diamant, A. Keller, E. Baer, M. Litt, and R. G. Arridge, "Collagen; ultrastructure and its relation to mechanical properties as a function of ageing," *Proceedings of the Royal Society of London. Series B*, vol. 180, no. 60, pp. 293–315, 1972.
- [36] H. Maas and P. A. Huijting, "Synergistic and antagonistic interactions in the rat forelimb: acute effects of coactivation," *Journal of Applied Physiology*, vol. 107, no. 5, pp. 1453–1462, 2009.
- [37] R. L. Lieber, *Skeletal Muscle Structure, Function and Plasticity: The Physiological Basis of Rehabilitation*, Lippincott Williams and Wilkins, Baltimore, Md, USA, 2nd edition, 2002.
- [38] C. M. Pond, "The importance of connective tissue within and between muscles," *The Behavioral and Brain Sciences*, vol. 5, p. 562, 1982.
- [39] D. E. Ashurst, "The connective tissues of insects," *Annual Review of Entomology*, vol. 13, pp. 45–74, 1968.
- [40] H. Maas, G. C. Baan, and P. A. Huijting, "Force transmission via myofascial pathways between EDL muscle and other muscles of the rat anterior compartment," in *Proceedings of the International Society of Biomechanics 18th Congress*, Zürich, Switzerland, 2001, CD-ROM.
- [41] S. F. Street, "Lateral transmission of tension in frog myofibers: a myofibrillar network and transverse cytoskeletal connections are possible transmitters," *Journal of Cellular Physiology*, vol. 114, no. 3, pp. 346–364, 1983.

- [42] M. Paavola, P. Kannus, T. A. H. Jarvinen, K. Khan, L. Jozsa, and M. Jarvinen, "Current concepts review achilles tendinopathy," *Journal of Bone and Joint Surgery. American*, vol. 84, pp. 2062–2076, 2002.
- [43] D. T. Kirkendall and W. E. Garrett Jr., "Clinical perspectives regarding eccentric muscle injury," *Clinical Orthopaedics and Related Research*, no. 403, pp. S81–S89, 2002.
- [44] R. J. Balice-Gordon and W. J. Thompson, "The organization and development of compartmentalized innervation in rat extensor digitorum longus muscle," *Journal of Physiology*, vol. 398, pp. 211–231, 1988.
- [45] P. A. Huijting, G. C. Baan, and G. T. Rebel, "Non-myotendinous force transmission in rat extensor digitorum longus muscle," *Journal of Experimental Biology*, vol. 201, no. 5, pp. 682–691, 1998.
- [46] H. Maas, R. T. Jaspers, G. C. Baan, and P. A. Huijting, "Myofascial force transmission between a single muscle head and adjacent tissues: length effects of head III of rat EDL," *Journal of Applied Physiology*, vol. 95, no. 5, pp. 2004–2013, 2003.
- [47] P. A. Huijting, "Muscular force transmission: a unified, dual or multiple system? A review and some explorative experimental results," *Archives of Physiology and Biochemistry*, vol. 107, no. 4, pp. 292–311, 1999.
- [48] M. Kääriäinen, T. Järvinen, M. Järvinen, J. Rantanen, and H. Kalimo, "Relation between myofibers and connective tissue during muscle injury repair," *Scandinavian Journal of Medicine and Science in Sports*, vol. 10, no. 6, pp. 332–337, 2000.
- [49] M. Kääriäinen, J. Kääriäinen, T. L. N. Järvinen, et al., "Integrin and dystrophin associated adhesion protein complexes during regeneration of shearing-type muscle injury," *Neuromuscular Disorders*, vol. 10, no. 2, pp. 121–132, 2000.
- [50] J. Estavillo, H. Yellin, Y. Sasaki, and E. Eldred, "Observations on the expected decrease in proprioceptive discharge and purported advent of non proprioceptive activity from the chronically tenotomized muscle," *Brain Research*, vol. 63, pp. 75–91, 1973.
- [51] A. J. Buller and D. M. Lewis, "Some observations on the effects of tenotomy in the rabbit," *Journal of Physiology*, vol. 178, pp. 326–342, 1965.
- [52] P. G. Nelson, "Functional consequences of tenotomy in hind limb muscles of the cat," *Journal of Physiology*, vol. 201, no. 2, pp. 321–333, 1969.
- [53] J. Wong, V. Barrass, and N. Maffulli, "Quantitative review of operative and nonoperative management of Achilles tendon ruptures," *American Journal of Sports Medicine*, vol. 30, no. 4, pp. 565–575, 2002.
- [54] M. J. C. Smeulders and M. Kreulen, "Myofascial force transmission and tendon transfer for patients suffering from spastic paresis: a review and some new observations," *Journal of Electromyography and Kinesiology*, vol. 17, no. 6, pp. 644–656, 2007.
- [55] H. Maas and P. A. Huijting, "Muscular force transmission following tendon transfer," in *Fascia Research II*, P. A. Huijting, A. P. Hollander, T. W. Findley, and R. Schleip, Eds., p. 104, Elsevier, München, Germany, 2009.

Review Article

Myosin Binding Protein-C Slow: An Intricate Subfamily of Proteins

Maegen A. Ackermann and Aikaterini Kontrogianni-Konstantopoulos

Department of Biochemistry and Molecular Biology, School of Medicine, University of Maryland, Baltimore, MD 21201, USA

Correspondence should be addressed to Aikaterini Kontrogianni-Konstantopoulos, akons001@umaryland.edu

Received 7 December 2009; Accepted 1 February 2010

Academic Editor: Henk L. M. Granzier

Copyright © 2010 M. A. Ackermann and A. Kontrogianni-Konstantopoulos. This is an open access article distributed under the Creative Commons Attribution License, which permits unrestricted use, distribution, and reproduction in any medium, provided the original work is properly cited.

Myosin binding protein C (MyBP-C) consists of a family of thick filament associated proteins. Three isoforms of MyBP-C exist in striated muscles: cardiac, slow skeletal, and fast skeletal. To date, most studies have focused on the cardiac form, due to its direct involvement in the development of hypertrophic cardiomyopathy. Here we focus on the slow skeletal form, discuss past and current literature, and present evidence to support that: (i) MyBP-C slow comprises a subfamily of four proteins, resulting from complex alternative shuffling of the single MyBP-C slow gene, (ii) the four MyBP-C slow isoforms are expressed in variable amounts in different skeletal muscles, (iii) at least one MyBP-C slow isoform is preferentially found at the periphery of *M*-bands and (iv) the MyBP-C slow subfamily may play important roles in the assembly and stabilization of sarcomeric *M*- and *A*-bands and regulate the contractile properties of the actomyosin filaments.

1. Introduction

Myofibrils, the workhorses of skeletal muscle, consist of interdigitating thick and thin filaments, and their associated membrane systems [1]. Muscle contraction and relaxation is mediated by the sliding of thick myosin filaments past thin actin filaments, under the strict regulation of Ca^{2+} release and reuptake via the sarcoplasmic reticulum (SR) [2]. In addition to housing the basic thick and thin filaments, the sarcomere also contains several accessory proteins that are involved in the assembly, maintenance, and regulation of contractile activity [1]. Myosin Binding Protein-C (MyBP-C) comprises a family of accessory proteins that contributes to the assembly and stabilization of thick filaments, and regulates the formation of cross-bridges between myosin and actin by interacting directly with both filamentous systems (as reviewed in [3]).

MyBP-C was originally identified from mammalian skeletal muscle as an impurity of isolated myosin. Using SDS-polyacrylamide gel electrophoresis (SDS-PAGE), Star and Offer were the first to separate a number of unidentified myosin-associated proteins that were consistently found in preparations of purified myosin [4]. MyBP-C, originally

termed C-protein for its location on SDS-PAGE as band C, was further characterized as a myosin binding protein of ~140 kDa using a combination of biochemical methods, ranging from gel filtration, to ammonium sulfate fractionation and single molecule electron microscopy [4–6]. The location of MyBP-C at striped intervals within the C-zone of the A-band of skeletal muscle was first observed with X-ray diffraction and immunoelectron microscopy [7], further supporting its association with the thick myosin filaments. Subsequent studies revealed that MyBP-C is arranged along the length of the A-band in 7–9 transverse stripes that are ~43 nm apart, with ~2–4 molecules of MyBP-C associating with each myosin cross-bridge [8–11].

The family of MyBP-C contains three isoforms: cardiac, slow skeletal, and fast skeletal, which are encoded by separate genes; in humans, these map to chromosomes 11, 12, and 19, respectively [12, 13]. The different isoforms have been cloned and sequenced from various species, including human, chicken, rabbit and mouse, allowing a thorough comparison of their molecular composition and primary sequence [13–16]. An ~65% identity is shared among the individual isoforms across species, while an ~50% homology is shared among the human cardiac, slow and fast forms.

The core structure of MyBP-C is composed of seven immunoglobulin (Ig) domains and three fibronectin type III (Fn-III) repeats, numbered from the NH₂-terminus as C1–C10 [17]. The C1 domain is flanked by two unique motifs, one enriched in proline and alanine residues, termed proline/alanine rich motif and a conserved linker, referred to as MyBP-C motif. Notably, the cardiac isoform possesses three additional features, which are absent from the skeletal forms of the protein. These include an Ig domain at the extreme NH₂-terminus of the molecule, termed C0, a unique 9-residues long insertion within the MyBP-C motif containing phosphorylation sites necessary for the protein's regulatory role in contraction, and a 28-amino acids long loop in the middle of the C5 domain [12, 16].

In mammals, cardiac MyBP-C is expressed early in development, along with titin and myosin [18, 19]. The skeletal isoforms of MyBP-C, however, are detected later in development, after the expression of titin and myosin, with the expression of slow MyBP-C preceding that of fast [18, 20]. By contrast, in chicken skeletal muscles the slow and fast isoforms appear concurrently at the end of late embryogenesis [21]. As development proceeds, though, the amounts of the slow form diminish, while the expression of the fast form persists through adulthood [21]. The fast and slow skeletal isoforms have been shown to coexpress in the same muscle type and can even coexist in the same sarcomere; expression of the cardiac isoform, however, is restricted to the developing and mature heart [15, 18, 22–24]. Interestingly, a recent study demonstrated that the expression of MyBP-C slow is not restricted to skeletal muscle but is also evidenced in the right atrium and interatrial septum of adult mammalian cardiac muscle [25].

To date, much of our knowledge on the molecular properties and functional activities of MyBP-C originates from the numerous studies that focus on the cardiac isoform. The reader is referred to excellent reviews discussing the structure of cardiac MyBP-C, its key roles in maintaining the normal structure of thick filaments and regulating cross-bridge cycling, and its involvement in the development of hypertrophic cardiomyopathy [3, 26, 27]. Here, we will focus on the slow form(s) of MyBP-C found in skeletal muscles. We will review past and current literature, discuss its role in the organization and stabilization of thick filaments, and provide evidence that MyBP-C slow comprises a subfamily of four alternatively spliced proteins that are expressed in variable amounts in slow and fast twitch skeletal muscles.

2. Materials and Methods

2.1. Reverse Transcription-Polymerase Chain Reaction. Total RNA was isolated with Trizol reagent (Invitrogen, Carlsbad, CA) from P1 rat skeletal myotubes cultured for seven days and from adult rat extensor digitorum longus (EDL), flexor digitorum brevis (FDB), tibialis anterior (TA), gastrocnemius (gastroc), quadriceps (quad), and soleus muscles. Aliquots containing ~5 µg of RNA were reverse transcribed using the Superscript First Strand Synthesis System for RT-PCR (Invitrogen, Carlsbad, CA) following the

manufacturer's instructions. PCR amplification of MyBP-C slow transcripts was performed with primer sets that flanked each of the three insertions; for the NH₂-terminal insert: Forward-1 (F1): 5' CCAGAACCCACTAAGAAAG 3' and Reverse-1 (R1): 5' GATCCTCGAGGTGCACTT CAA-GATCAA 3', for the insert within Ig7: Forward-2 (F2): 5' GATCGAATTCAGCCC TCCTACTCTT 3' and Reverse-2 (R2): 5' GATCCTCGAGGGGCTCGCTGGCACCA 3' and for the COOH-terminal insert: Forward-3 (F3): 5' CACC-CATGTTTACTCAACCCT 3' and Reverse-3 (R-3) 5' GTGACAAATATACATTGAA 3'. To amplify the COOH-terminal insert from EDL and TA muscles, it was necessary to reamplify 0.5 µL of the original PCR for an additional 30 cycles for a total of 80 cycles. All other PCRs were carried out for 50 cycles. PCR products were analyzed by electrophoresis in 1% agarose gels and their authenticity was verified by sequence analysis.

2.2. Generation of Protein Lysates from P1 Myotubes and Adult Rat Muscle. Homogenates of P1 myotubes cultured for seven days as well as of EDL, FDB, TA, gastrocnemius, quadriceps and soleus muscles of adult Sprague-Dawley rats (Zivic-Miller Laboratories, Zelienople, PA) were prepared at RT with a Brinkman Polytron homogenizer at setting 3 (VWR, West Chester, PA) in 10 mM NaPO₄, pH 7.2, 2 mM EDTA, 10 mM NaN₃, 120 mM NaCl, 0.5% deoxycholate, 0.5% NP-40, supplemented with Complete protease inhibitors (Roche, Indianapolis, IN). Each sample (~60 µg) was solubilized in 4xNuPAGE reducing sample buffer (Invitrogen, Carlsbad, CA) at 90°C for 5 minutes, fractionated by 4–12% SDS-PAGE BisTris gel using MES running buffer (Invitrogen, Carlsbad, CA), transferred to nitrocellulose and probed with an antibody that recognizes the slow forms of MyBP-C (300 ng/mL, Abnova) or with an antibody that specifically recognizes the COOH-terminal insert [28]. After incubation with the appropriate secondary antibodies, immunoreactive bands were visualized with a chemiluminescence detection kit (Tropix, Bedford, MA).

2.3. Immuno-Electron Microscopy. Immuno-electron microscopy was performed as previously described with minor modifications [29, 30]. Briefly, adult mouse FDB skeletal muscle was fixed both *in situ*, via whole animal perfusion-fixation and *ex vivo* with 2% paraformaldehyde in PBS. Samples were snap-frozen in a slush of liquid N₂, cryosectioned (~20 µm thick), and incubated overnight at 4°C with the antibody that specifically recognizes the COOH-terminal insert of MyBP-C slow. Samples were incubated with secondary goat antirabbit IgG adsorbed on 1 nm gold particles (Nanoprobes Incorporated, Yaphank, NY) and subsequently with fluorescein-conjugated anti-goat IgG (Jackson ImmunoResearch Laboratories Inc., West Grove, PA). Samples were enhanced with silver (HiQ Silver Kit, Nanoprobes) for 5 minutes, fixed overnight at 4°C in 2% glutaraldehyde and 5 mg/mL tannic acid in 0.2 M cacodylate buffer and postfixed with 50 mM acetate buffer 1% osmium tetroxide. They were further stained *en bloc* for 2 hours with 1% uranyl acetate in 65% ethanol,

dehydrated, and embedded in araldite (Electron Microscopy Sciences, Fort Washington, PA). Ultrathin (60–90 nm) sections were prepared with an MT5000 ultramicrotome (LKB instruments Inc., Gaithersburg, MD), mounted on grids, labeled with 1% uranyl acetate followed by Reynolds lead citrate, and examined with a Philips-201 electron microscope.

3. Results and Discussion

3.1. MyBP-C Slow: A Subfamily of Proteins. To date, four different MyBP-C slow transcripts have been identified in human skeletal muscle referred to as variants 1–4 (Figure 1; accession numbers NM_002465, NM_206819, NM_206820, and NM_206821, respectively). The four variants differ from one another at three regions, due to alternative splicing events that result in inclusion of exons 3 and 4 in the proline/alanine-rich motif, exon 23 in the Ig7 domain and exon 31 at the extreme COOH-terminus (Figure 1(a)); these encode novel sequences of 25 (Figure 1(b)), 18 (Figure 1(c)), and 26 (Figure 1(d)) amino acids, respectively. Analysis of the primary sequence of the four MyBP-C slow variants indicated that variants 1 and 2 contain the NH₂-terminal insertion located in the proline/alanine rich motif, variant 3 carries the insertion within domain Ig7, while variant 4 also contains the unique COOH-terminal region (Figure 1(a)). Notably, variant 3 is the prototypical human isoform of MyBP-C slow that was characterized by Furst and colleagues in 1992 [14].

To study the relative expression of the four MyBP-C slow transcripts in different rat skeletal muscles, we used RT-PCR analysis to amplify the unique regions described above. To this end, we prepared cDNAs from a panel of adult and developing rat skeletal muscles that contained distinct compositions of slow and fast twitch skeletal myofibers. These included extensor digitorum longus (EDL; ~90:10, fast:slow; [31, 32]), flexor digitorum brevis (FDB; ~80:20, fast:slow; [33]), tibialis anterior (TA; ~70:30, fast:slow; [34]), gastrocnemius (gastroc; ~40:60, fast:slow; [35]), quadriceps (quad; ~60:40, fast:slow; [36]), soleus (20:80, fast:slow; [35]), and hindlimb skeletal myotubes of postnatal day 1 (P1) rat pups (Figure 2). Primer sets were designed to flank each of the three novel insertions (Figures 2(a)–2(c), cartoons in the upper left corner). Amplification of two PCR products with distinct sizes within each reaction indicated the presence of a mixed population of transcripts that contained (larger size product) and lacked (smaller size product) the respective insertion. On the contrary, amplification of one PCR product indicated the presence of a homogeneous population of transcripts that either included or excluded the corresponding insertion, depending on its size. Accordingly, PCR products that carry the NH₂-terminal, Ig7 and COOH-terminal inserts would be ~600, ~310, and ~350 nucleotides long, respectively, whereas PCR products that lack them would be ~530, ~260, and ~290 nucleotides long, respectively.

All skeletal muscles examined, independent of their fiber type composition, contained sufficient amounts of MyBP-C

slow transcripts to be amplified by conventional RT-PCR. Figure 2(a) shows the results following amplification of the NH₂-terminal insertion located within the proline/alanine rich motif. All muscle samples express MyBP-C slow transcripts that include the NH₂-terminal insert, albeit to varying degrees, as seen by the presence of an ~600 nts amplicon (Figure 2(a), upper band). This finding suggested that all muscles tested express variants 1 and/or 2, with EDL, TA, and soleus containing the highest amounts. Notably, all seven muscles also contain different amounts of transcripts that lack the NH₂-terminal insert, as shown by the presence of an ~530 nts product, indicating that they also express variants 3 and/or 4, with FDB showing the highest levels (Figure 2(a), lower band). Contrary to EDL, TA, soleus, and FDB that appear to preferentially contain MyBP-C slow variants that either include (EDL, TA and soleus) or exclude (FDB) the NH₂-terminal insert, gastroc, quad, and P1 myotubes show similar amounts of both amplification products, suggesting that transcripts possessing and lacking the NH₂-terminal insert may exist in similar levels within these muscles (Figure 2(a) lanes 4–5 and 7).

Next, we extended our analysis to the second novel insertion located within Ig7. As before, our primers set was designed to amplify MyBP-C slow variants that contained or skipped the Ig7 insert. Only soleus and P1 myotubes possess transcripts that include the unique insertion within Ig7, as indicated by the presence of an ~310 nts band (Figure 2(b), lanes 6 and 7, upper band), corresponding to variant 3. As expected, all skeletal muscles tested contained transcripts that lack the Ig7 insertion, as shown by the amplification of an ~260 nts product, representing variants 1, 2 and/or 4. Thus, variant 3 is restricted to soleus muscle and developing myotubes.

Last, we generated the appropriate primers to amplify the region flanking the COOH-terminal insert of MyBP-C slow. With the exception of quadriceps muscle, all other muscles tested, contained an amplification product of ~350 nucleotides, that includes the novel COOH-terminal insert detected only in variant 1, with soleus and FDB showing the highest amounts (Figure 2(c), lanes 6 and 2, upper band). A second amplification product of ~290 nucleotides was also detected in all seven muscles, which lacks the unique COOH-terminal insertion, present in variant 1, but includes the common COOH-terminal region shared by variants 2, 3, and 4 (Figure 2(c), lower band).

The RT-PCR data is summarized in Table 1. Taken together, our results suggest that: (i) mRNA encoding MyBP-C slow is present in all skeletal muscles examined, regardless of fiber type composition or age, and (ii) complex alternative shuffling of the single MyBP-C slow gene in the various muscles results in the differential expression of the four MyBP-C slow isoforms.

To correlate the mRNA expression of the transcripts that contain or lack the three novel insertions, as seen by the RT-PCR, to the expression of the proteins that they encode, we used western blot analysis. Homogenates from EDL, FDB, TA, gastroc, quad, soleus, and P1 skeletal myotubes were separated on 4–12% gradient gel, which our laboratory has previously shown to provide optimal

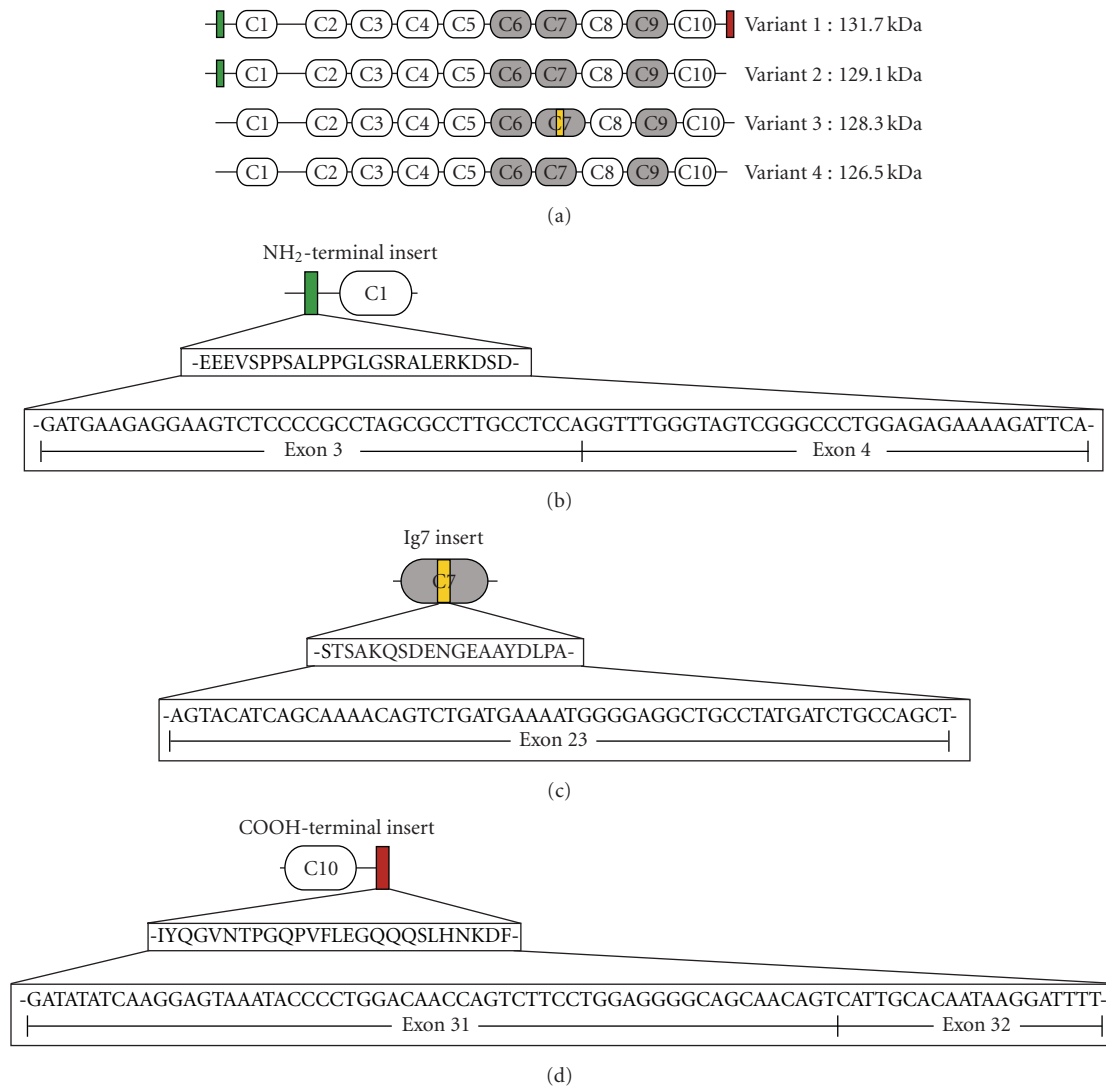


FIGURE 1: (a): Schematic representation of MyBP-C slow variants 1–4, showing their common structural motifs and novel insertions; white and grey ovals represent Ig and FN-III domains, respectively, while green, yellow, and red rectangles correspond to the NH₂-terminal, Ig7, and COOH-terminal inserts, respectively. The NH₂-terminal insert is present in variants 1 and 2, while the Ig7 and COOH-terminal inserts are present in variants 3 and 1, respectively. Variant 4 does not contain any of the three inserts. (b–d): Complex alternative splicing events result in the inclusion of exons 3 and 4, exon 23 and exon 31 that encode the NH₂-terminal (b), Ig7 (c), and COOH-terminal (d) novel insertions. The amino acid and nucleotide compositions of the three insertions are shown.

separation of the MyBP-C slow isoforms (see Section 2, and [28]). Homogenates were probed with a commercial antibody that recognizes a region within domain C5 common to all MyBP-C slow variants (Figure 3(a)). We were able to resolve at least 3 immunoreactive bands based on their distinct electrophoretic mobilities. The top band may represent variant 1 (~132 kDa, Figure 3(a), top panel, marked with a blue dot), the middle band may correspond to variants 2 and/or 3 (~129 and ~128 kDa, respectively, Figure 3(a), top panel, denoted with a red dot), and the bottom band may represent variant 4 (~126 kDa, Figure 3(a), top panel, marked with a green dot). The cartoon shown in the bottom panel of Figure 3(a) illustrates a representative image of several western blots, analyzed at

varying exposure times. The dotted lines indicate immunoreactive bands that only become evident after periods of long exposure.

Consistent with the RT-PCR data, our immunoblots also demonstrated the presence of at least one form of MyBP-C slow in each skeletal muscle tested. EDL and gastrocnemius possess three immunoreactive bands with the most prominent being the middle one (Figure 3(a), lanes 1 and 4). FDB also contains three distinct bands, however, the top and middle bands appear to be of similar intensities and occasionally appear as a broad, single band (Figure 3(a), lane 2). Similar to FDB, TA also shows two closely migrating bands, but lacks the bottom one (Figure 3(a) lane 3). Contrary to the rest of the muscles analyzed, quadriceps

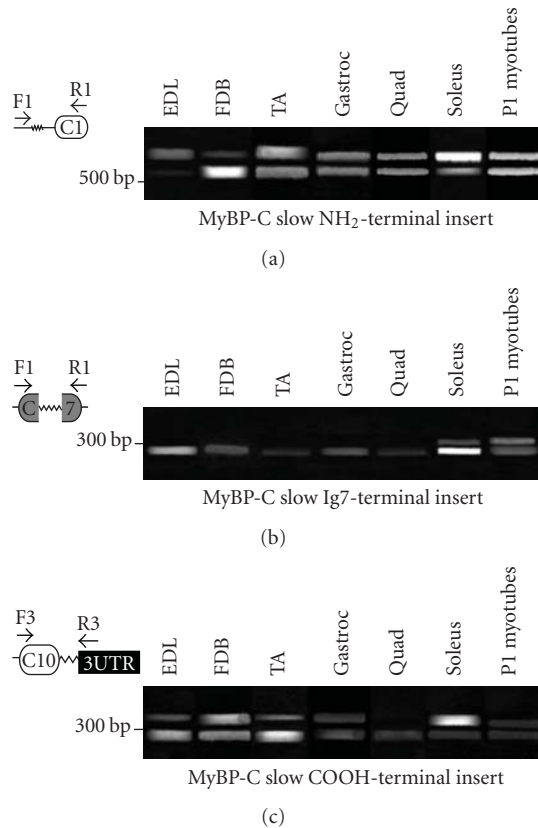


FIGURE 2: RT-PCR analysis using cDNA generated from developing and adult rat extensor digitorum longus (EDL), flexor digitorum brevis (FDB), tibialis anterior (TA), gastrocnemius (gastroc), quadriceps (quad) and soleus skeletal muscles and primer sets designed to flank the NH₂-terminal (a), Ig7 (b), and COOH-terminal (c) insertions. A schematic representation of the amplified region is shown in the upper left corner of each panel. White and grey ovals depict Ig and FN-III domains, respectively, while the 3' UTR is shown as a black line. The zig-zag lines denote the three novel insertions. In each amplification reaction, the top band corresponds to transcripts that include the insertion of interest, whereas the bottom band corresponds to transcripts that lack it. (a): All skeletal muscles tested contain a mixed population of MyBP-C slow variants that contain and lack the NH₂-terminal insertion, as indicated by the presence of two amplification products. (b): On the contrary, only soleus and developing myotubes express transcripts that include the Ig7 insertion. (c): With the exception of quadriceps muscle that only contains MyBP-C slow variants that lack the COOH-terminal insertion, all other muscles examined contain a mixed pool of transcripts that carry and lack the novel COOH-terminal insertion.

appears to contain only the middle band, although, the bottom one becomes evident after long exposure times (Figure 3(a) lane 5). Soleus expresses high amounts of the upper and lower bands, but moderate to low amounts of the middle one (Figure 3(a) lane 6). Finally, developing P1 skeletal myotubes show only one immunoreactive band with the same mobility as the top one, however, following longer exposure, the middle immunoreactive band is also apparent (Figure 3(a) lane 7).

TABLE 1: Tabulated summary of the RT-PCR data shown in Figure 2. The plus (+) and minus (–) signs denote the presence or absence of mRNAs encoding the three regions of interest, respectively; the relative abundance of the respective transcripts is illustrated by the number of plus signs.

Muscle Type	NH ₂ -insert	Ig7-insert	COOH-insert
Extensor Digitorum Longus	++	–	+
Flexor Digitorum Brevis	+	–	++
Tibialis Anterior	+++	–	+
Gastrocnemius	++	–	+
Quadriceps	++	–	–
Soleus	++++	+	+++
P1 Myotubes	+++	++	+

We also probed the same muscle homogenates with an antibody that is specific for the COOH-terminal insert and therefore only recognizes MyBP-C slow variant 1 (Figure 3(b)). With the exception of quadriceps, all of the other muscles were immunopositive for variant 1. This finding is in agreement with our immunoblot data shown in panel A, and the RT-PCR analysis shown in Figure 2(c), which revealed that quadriceps was the sole muscle to lack the top immunoreactive band (i.e., variant 1) and the COOH-terminal insert, respectively. Notably, MyBP-C slow variant 1 appears to be expressed more abundantly in soleus muscle and least prominently in developing myotubes, while the remaining muscles tested contained intermediate amounts. The slight differences in the sizes of the bands detected in the different muscles are likely due to posttranslational modifications, as it has previously been shown that MyBP-C slow is capable of phosphorylation [37, 38].

Taken together, our RT-PCR and immunoblotting data (summarized in Table 2) clearly indicate that all skeletal muscles tested, apart from quadriceps, express variant 1, albeit to different extents, with soleus and FDB containing the highest amounts. Variants 2 and 3 have complementary expression profiles, with variant 2 being preferentially expressed in muscles that have a higher composition of fast twitch fibers, such as EDL, FDB, TA, gastrocnemius and quadriceps, and variant 3 being selectively present in slow twitch muscles, like soleus, and developing myotubes. Finally, variant 4 is detected in all muscles examined, with the exception of TA and developing myotubes. It therefore appears that different forms of MyBP-C slow are present within the same muscle, independently of its fiber type composition, developmental stage, or age.

3.2. MyBP-C at the A-band. Early studies have confirmed the direct interaction between MyBP-C and myosin and identified the sites of binding on both proteins. The light meromyosin (LMM) region of the myosin rod, that forms the backbone of the thick filament, binds the COOH-terminal C10 region of all three MyBP-C isoforms [39–41]. Positively charged residues on the surface of the C10 domain mediate binding to LMM [42], however, the interaction is significantly strengthened by the presence of the C8

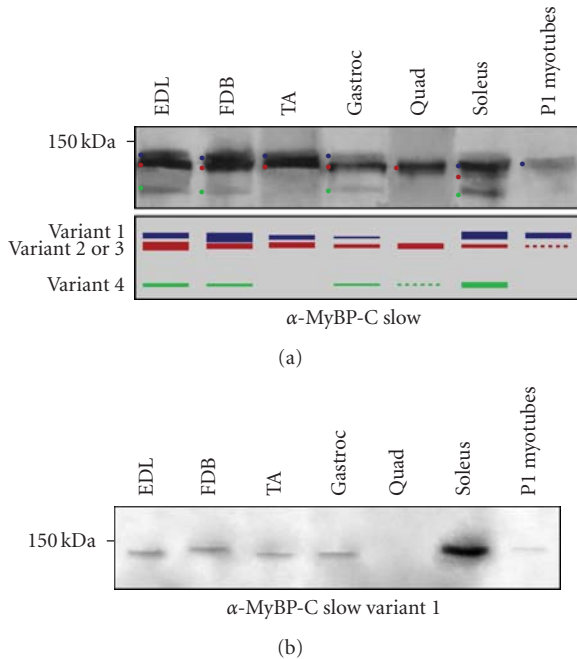


FIGURE 3: Western blot analysis of protein homogenates prepared from rat skeletal muscles and blotted with antibodies to the fifth Ig domain that recognize all MyBP-C slow variants (a) or to the novel COOH-terminal insertion that specifically recognizes variant 1 (b). (a) Top panel: With the exception of quadriceps, all other muscles express variant 1, represented by the upper most band, marked by a blue dot. All adult skeletal muscles tested, but not the developing myofibers, express variants 2 and/or 3, corresponding to the band with the intermediate mobility, and denoted with a red dot. As variants 2 and 3 have similar molecular weights (129 and 128 kDa, respectively), it is not feasible to separate them in the current gel system. Moreover, variant 4 is detected in homogenates prepared from EDL, FDB, gastrocnemius, and soleus, and is represented by the lower immunoreactive band, marked with a green dot. Bottom panel: A cartoon showing the presence of the different MyBP-C slow variants in developing and adult skeletal muscles. Dotted lines correspond to immunoreactive bands, which are evident only after long exposure times. (b) In agreement with the immunoblot shown in panel (a), antibodies specific for the novel COOH-terminal insert demonstrated that EDL, FDB, TA, gastrocnemius, soleus, and P1 skeletal myotubes express variant 1, with soleus containing the highest amounts.

and C9 regions. Another interaction between the MyBP-C motif, located at the NH₂-terminus of MyBP-C and subfragment 2 (S2) of myosin has been also identified, albeit of weaker affinity [43]. In addition to binding myosin, MyBP-C associates with actin, in a Ca²⁺ dependent manner, through its NH₂-terminal proline/alanine rich motif [44–46]. The ability of MyBP-C to directly interact with both myosin and actin facilitates its role as a regulator of cross-bridge formation during contraction. Interestingly, at low ionic strength MyBP-C inhibits actomyosin ATPase activity, while at higher ionic strength it acts as a mild activator [47, 48].

In addition to myosin, MyBP-C also associates with titin at the A-band [14, 49–51]. The COOH-terminal C8–C10

TABLE 2: MyBP-C slow variants 1–4 are present in varying amounts in different skeletal muscles. A plus (+) sign indicates the presence of the respective variant in a select muscle. The relative abundance of variants 1–4 in the skeletal muscles tested is illustrated by the number of plus signs.

Muscle Type	Variant 1	Variant 2	Variant 3	Variant 4
Extensor Digitorum Longus	++	+++	—	++
Flexor Digitorum Brevis	+++	++	—	++
Tibialis Anterior	++	++	—	—
Gastrocnemius	+	+	—	+
Quadriceps	—	++	—	—
Soleus	++++	—	+	+++
P1 Myotubes	++	—	+	—

domains of MyBP-C directly bind to the 11-domain super-repeat [Ig-(FN-III)₂-Ig-(FN-III)₃-Ig-(FN-III)₃] present in the C-zone portion of titin, and specifically the first Ig domain, although flanking motifs further strengthen the interaction [52, 53]. Notably, the arrangement of MyBP-C in 11 transverse stripes at regular intervals of ~43 nm corresponds to that of the 11-domain super-repeat of titin, to which MyBP-C binds. Consequently, It has been suggested that binding to titin's super-repeats specifies the subsarcomeric distribution of MyBP-C in the C-zone of the A-band [52].

Recent studies have proposed that MyBP-C forms a trimeric “collar” around each thick filament in which domains C5–C7 of one molecule overlap with domains C8–C10 of the neighboring molecule [54, 55]. In vitro binding studies using the respective peptides postulated that this arrangement might apply to the cardiac and fast skeletal isoforms, but not the slow isoform. Interestingly, for these studies Flashman and coworkers generated a recombinant protein that contained domains C8–C10, present in all four slow variants, followed by the novel COOH-terminal insertion, present only in variant 1. It is, therefore, possible that the presence of the COOH-terminal 26-amino acids may inhibit binding of the C8–C10 domains of variant 1 to the C5–C7 domains of the neighboring molecule of MyBP-slow. Indeed, this is consistent with our recent studies indicating that variant 1 is preferentially localized at the periphery of the M-band [28]. Conversely, an interaction between the respective motifs present in variants 2–4 is likely, as these contain a short COOH-terminus following domain C10 that, similar to the cardiac and fast isoforms, consists of four amino acids.

Through its interactions with myosin and titin, MyBP-C contributes to the stabilization and maintenance of the sarcomeric A-band. In vitro studies indicate that myosin filaments are capable of forming in the absence of MyBP-C, however, its addition results in increased filament length, and improved structure and uniformity across the filament [40, 56, 57]. Additionally, in vivo deletion of the myosin

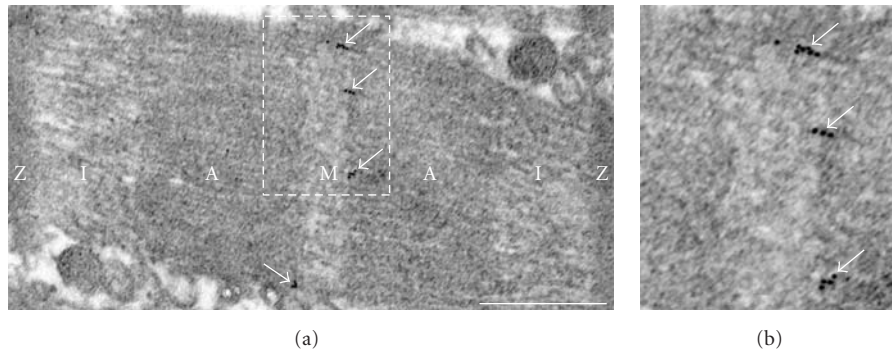


FIGURE 4: Ultrathin cryo-sections of adult mouse FDB skeletal muscle were labeled with antibodies specific for the COOH-terminal insertion present in MyBP-C slow variant 1. (a) Variant 1 was detected at the periphery of the *M*-band (arrows). The boxed area in (a) is blown up in (b) for ease of visualization of the immunolabeling. Scale bar corresponds to 0.5 μm .

and titin binding sites on MyBP-C results in disorganized *A*-bands [58, 59]. Consistent with this, the C8–C10 domains that harbor the binding sites for myosin and titin are deleted in patients suffering from familial hypertrophic cardiomyopathy [3, 60, 61]. Interestingly, though, normal *A*-bands are formed in animals deficient of cardiac MyBP-C [62, 63], suggesting the presence of a compensatory mechanism that maintains the myosin and titin filaments within the *A*-band of the sarcomere. Taken together, these studies suggest that MyBP-C, through its direct interaction with myosin and titin, and possibly its self-association, may stabilize the sarcomeric *A*-band.

In addition to maintaining the structure of thick filaments, MyBP-C may also play key roles in regulating contractile function by modulating the rate of cross-bridges formation. Consistent with this, in cardiomyocytes lacking MyBP-C, actomyosin filaments exhibited increased power output during contraction and faster rates of force development at half maximal Ca^{2+} activation [64]. Reintroduction of the NH_2 -terminal region of cardiac MyBP-C, containing the myosin S2 binding site (i.e., domains C1 and C2), enhanced Ca^{2+} sensitivity and restored the contractile properties of the null cardiomyocytes to normal levels [65], suggesting that cardiac MyBP-C contributes to the regulation of myofilament tension and their cycling rates.

Contrary to the cardiac isoform that has been directly implicated in the regulation of the contractile properties of cardiomyocytes (reviewed in [3]), studies focusing on the function of the skeletal forms of MyBP-C are limited. However, early studies have suggested that the role of MyBP-C in skeletal muscle likely parallels that of the cardiac isoform [66]. Consistent with this, the amounts of MyBP-C slow were recently found significantly increased in EDL muscles from a mouse model in which the kinase domain of titin was deleted [67]. Deficient EDL muscles exhibited reduced myofilament Ca^{2+} sensitivity and altered contractile properties, which were restored to normal levels upon extraction of MyBP-C slow. Contrary to the slow form of MyBP-C, the fast form was significantly downregulated in the same muscles, while the expression levels of other proteins of the *A*- and *M*-bands remained unaffected. It is, therefore, likely that the

kinase domain of titin affects the expression of genes involved in the regulation of myofilament Ca^{2+} sensitivity and force production. Experimental evidence has therefore started to emerge suggesting a key role for the skeletal forms of MyBP-C in modulating contractility, too.

3.3. Mybp-C Slow Variant 1 Selectively Concentrates at the *M*-Band. The presence of MyBP-C slow at the C-zones of the *A*-band has been studied extensively during the last three decades [3, 26, 68]. Recent studies from our laboratory, however, have provided evidence that at least one form of MyBP-C slow, specifically variant 1, has a unique topography in the muscle cell [28]. Detailed immunofluorescence studies combined with confocal microscopy demonstrated that MyBP-C slow variant 1 is selectively localized at the periphery of the *M*-band in adult rat soleus muscle [28]. The unique localization of MyBP-C slow variant 1 is further supported by our ultrastructural studies, shown in Figure 4. Immunolabeling of ultrathin cryosections prepared from adult mouse FDB muscle with antibodies to the unique COOH-terminus of variant 1 also demonstrated that it preferentially concentrates at the edges of the sarcomeric *M*-band (Figures 4(a)–4(b), arrowheads). Thus, it appears that the different MyBP-C slow isoforms have distinct distributions in skeletal myofibers, with variants 2–4 localizing at the *A*-band and variant 1 at the *M*-band.

At the *M*-band, MyBP-C slow variant 1 interacts with obscurin and four and a half lim protein 1 (FHL1) [28, 69]. The second Ig domain of obscurin and the last Ig domain of MyBP-C slow variant 1 are both necessary and sufficient to support their interaction, however, binding is enhanced significantly in the presence of the novel 26 amino acids at the COOH-terminus of variant 1. Overexpression of the second Ig domain of obscurin in primary cultures of skeletal myotubes inhibited the integration of MyBP-C slow variant 1 at the *M*-band and severely disrupted the formation of *M*- and *A*-bands. These findings suggested that variant 1 might contribute to the assembly and integrity of these structures via its interaction with obscurin and possibly other proteins. Similarly, McGrath et al. also demonstrated

that overexpression or downregulation of FHL1, which is localized at the A-I junction and the M-band, in adult mouse soleus muscle resulted in impaired thick filament assembly, which was accompanied by reduced sarcomeric incorporation of different forms of MyBP-C slow, including variant 1 [69].

3.4. MyBP-C Slow in Muscle Disease. Mutations within the cardiac isoform of MyBP-C cause familial hypertrophic cardiomyopathy (reviewed in [70, 71]). To date, there are no muscle diseases causally associated with mutations in the transcripts of the skeletal forms of MyBP-C. However, changes in the expression levels of the skeletal isoforms have been reported in hypertrophic and dystrophic skeletal muscles. The expression levels of MyBP-C slow were significantly increased in rat plantaris muscle induced to hypertrophy by surgical ablation of the neighboring soleus and gastrocnemius muscles, whereas the amounts of MyBP-C fast were dramatically decreased [72]. Likewise, the protein levels of MyBP-C slow were increased in both chicken and mouse dystrophic skeletal muscles [20, 24]. Further research is required in order to understand the molecular mechanisms that lead to the differential regulation of the skeletal forms of MyBP-C in these models, and their potentially unique roles in regulating the formation and activity of contractile structures.

4. Summary and Future Perspectives

MyBP-C slow comprises a subfamily of at least four isoforms that result from complex alternative splicing of the single MyBP-C slow gene. The presence of the four MyBP-C slow variants is not restricted to slow-twitch muscles, as select isoforms are abundantly expressed in fast-twitch muscles, too, where they may coexist with MyBP-C fast. More importantly, the four isoforms of MyBP-C slow may be coexpressed in the same muscle, fiber or sarcomere, where they may exhibit unique topographies concentrating either at A-bands (variants 2, 3, and 4) or M-bands (variant 1). Previous and current findings strongly favor a structural role for MyBP-C slow at the sarcomeric A- and M-bands, and point to a regulatory role on muscle contraction. Consequently, the detailed characterization of the biochemical and biophysical properties of the four MyBP-C slow variants, and the development of the appropriate molecular tools and animal models are imperative in order to study the cell biology and functional properties of this intricate subfamily of proteins.

Acknowledgments

The authors wish to thank S. Adediran and N. Perry for their technical assistance in the initial stages of this work. Our research has been supported by Grants to Aikaterini Kontrogianni-Konstantopoulos from the National Institutes of Health (R01 AR52768) and the Muscular Dystrophy Association (RG 4214) and to Maegen A. Ackermann from the National Institutes of Health (F32 AR058079).

References

- [1] K. A. Clark, A. S. McElhinny, M. C. Beckerle, and C. C. Gregorio, "Striated muscle cytoarchitecture: an intricate web of form and function," *Annual Review of Cell and Developmental Biology*, vol. 18, pp. 637–706, 2002.
- [2] C. Franzini-Armstrong, "Functional significance of membrane architecture in skeletal and cardiac muscle," *Society of General Physiologists series*, vol. 51, pp. 3–18, 1996.
- [3] C. E. Oakley, J. Chamoun, L. J. Brown, and B. D. Hambly, "Myosin binding protein-C: enigmatic regulator of cardiac contraction," *International Journal of Biochemistry and Cell Biology*, vol. 39, no. 12, pp. 2161–2166, 2007.
- [4] R. Starr and G. Offer, "Polypeptide chains of intermediate molecular weight in myosin preparations," *FEBS Letters*, vol. 15, no. 1, pp. 40–44, 1971.
- [5] H. C. Hartzell and W. S. Sale, "Structure of C protein purified from cardiac muscle," *Journal of Cell Biology*, vol. 100, no. 1, pp. 208–215, 1985.
- [6] G. Offer, C. Moos, and R. Starr, "A new protein of the thick filaments of vertebrate skeletal myofibrils. Extraction, purification and characterization," *Journal of Molecular Biology*, vol. 74, no. 4, pp. 653–662, 1973.
- [7] R. Craig and G. Offer, "The location of C protein in rabbit skeletal muscle," *Proceedings of the Royal Society of London. Series B*, vol. 192, no. 1109, pp. 451–461, 1976.
- [8] P. Bennett, R. Craig, R. Starr, and G. Offer, "The ultrastructural location of C-protein, X-protein and H-protein in rabbit muscle," *Journal of Muscle Research and Cell Motility*, vol. 7, no. 6, pp. 550–567, 1986.
- [9] F. A. Pepe, "Structure of muscle filaments from immunohistochemical and ultrastructural studies," *Journal of Histochemistry and Cytochemistry*, vol. 23, no. 7, pp. 543–562, 1975.
- [10] F. A. Pepe, F. T. Ashton, C. Street, and J. Weisel, "The myosin filament. X. Observation of nine subfilaments in transverse sections," *Tissue and Cell*, vol. 18, no. 4, pp. 499–508, 1986.
- [11] E. Rome, G. Offer, and F. A. Pepe, "X ray diffraction of muscle labelled with antibody to C protein," *Nature: New Biology*, vol. 244, no. 135, pp. 152–154, 1973.
- [12] M. Gautel, M. A. C. Morelli, M. Pfuhl, A. Motta, and A. Pastore, "A calmodulin-binding sequence in the C-terminus of human cardiac titin kinase," *European Journal of Biochemistry*, vol. 230, no. 2, pp. 752–759, 1995.
- [13] F. E. Weber, K. T. Vaughan, F. C. Reinach, and D. A. Fischman, "Complete sequence of human fast-type and slow-type muscle myosin-binding-protein C (MyBP-C). Differential expression, conserved domain structure and chromosome assignment," *European Journal of Biochemistry*, vol. 216, no. 2, pp. 661–669, 1993.
- [14] D. O. Fürst, U. Vinkemeier, and K. Weber, "Mammalian skeletal muscle C-protein: purification from bovine muscle, binding to titin and the characterization of a full-length human cDNA," *Journal of Cell Science*, vol. 102, no. 4, pp. 769–778, 1992.
- [15] F. C. Reinach, T. Masaki, and D. A. Fischman, "Characterization of the C-protein from posterior latissimus dorsi muscle of the adult chicken: heterogeneity within a single sarcomere," *Journal of Cell Biology*, vol. 96, no. 1, pp. 297–300, 1983.
- [16] M. Yasuda, S. Koshida, N. Sato, and T. Obinata, "Complete primary structure of chicken cardiac C-protein (MyBP-C) and its expression in developing striated muscles," *Journal of Molecular and Cellular Cardiology*, vol. 27, no. 10, pp. 2275–2286, 1995.

- [17] S. Einheber and D. A. Fischman, "Isolation and characterization of a cDNA clone encoding avian skeletal muscle C-protein: an intracellular member of the immunoglobulin superfamily," *Proceedings of the National Academy of Sciences of the United States of America*, vol. 87, no. 6, pp. 2157–2161, 1990.
- [18] M. Gautel, D. O. Fürst, A. Cocco, and S. Schiaffino, "Isoform transitions of the myosin binding protein C family in developing human and mouse muscles: lack of isoform transcomplementation in cardiac muscle," *Circulation Research*, vol. 82, no. 1, pp. 124–129, 1998.
- [19] M. Kawashima, S. Kitani, T. Tanaka, and T. Obinata, "The earliest form of C-protein expressed during striated muscle development is immunologically the same as cardiac-type C-protein," *Journal of Biochemistry*, vol. 99, no. 4, pp. 1037–1047, 1986.
- [20] M. Kurasawa, N. Sato, A. Matsuda, S. Koshida, T. Totsuka, and T. Obinata, "Differential expression of C-protein isoforms in developing and degenerating mouse striated muscles," *Muscle and Nerve*, vol. 22, no. 2, pp. 196–207, 1999.
- [21] T. Obinata, F. C. Reinach, D. M. Bader, T. Masaki, S. Kitani, and D. A. Fischman, "Immunohistochemical analysis of C-protein isoform transitions during the development of chicken skeletal muscle," *Developmental Biology*, vol. 101, no. 1, pp. 116–124, 1984.
- [22] F. Fougères, A.-L. Delezoide, M. Y. Fiszman, K. Schwartz, J. S. Beckmann, and L. Carrier, "Cardiac myosin binding protein C gene is specifically expressed in heart during murine and human development," *Circulation Research*, vol. 82, no. 1, pp. 130–133, 1998.
- [23] T. Obinata, S. Kitani, T. Masaki, and D. A. Fischman, "Coexistence of fast-type and slow-type C-proteins in neonatal chicken breast muscle," *Developmental Biology*, vol. 105, no. 1, pp. 253–256, 1984.
- [24] T. Obinata and K. Shinbo, "Slow-type C-protein in dystrophic chicken fast pectoralis muscle," *Muscle and Nerve*, vol. 10, no. 4, pp. 351–358, 1987.
- [25] G. K. Dhoot and S. V. Perry, "Expression of slow skeletal myosin binding C-protein in normal adult mammalian heart," *Journal of Muscle Research and Cell Motility*, vol. 26, no. 2, pp. 143–148, 2005.
- [26] L. Carrier, "Cardiac myosin-binding protein C in the heart," *Archives des Maladies du Cœur et des Vaisseaux*, vol. 100, no. 3, pp. 238–243, 2007.
- [27] P. P. de Tombe, "Myosin binding protein C in the heart," *Circulation Research*, vol. 98, no. 10, pp. 1234–1236, 2006.
- [28] M. A. Ackermann, L.-Y. R. Hu, A. L. Bowman, R. J. Bloch, and A. Kontogianni-Konstantopoulos, "Obscurin interacts with a novel isoform of MyBP-C slow at the periphery of the sarcomeric M-band and regulates thick filament assembly," *Molecular Biology of the Cell*, vol. 20, no. 12, pp. 2963–2978, 2009.
- [29] A. Kontogianni-Konstantopoulos and R. J. Bloch, "Obscurin: a multitasking muscle giant," *Journal of Muscle Research and Cell Motility*, vol. 26, no. 6-8, pp. 419–426, 2005.
- [30] S. V. Yap, E. Vafiadaki, J. Strong, and A. Kontogianni-Konstantopoulos, "HAX-1: a multifaceted antiapoptotic protein localizing in the mitochondria and the sarcoplasmic reticulum of striated muscle cells," *Journal of Molecular and Cellular Cardiology*. In press.
- [31] J. Lexell, J. C. Jarvis, J. Currie, D. Y. Downham, and S. Salmons, "Fibre type composition of rabbit tibialis anterior and extensor digitorum longus muscles," *Journal of Anatomy*, vol. 185, no. 1, pp. 95–101, 1994.
- [32] T. Soukup, G. Zacharova, and V. Smerdu, "Fibre type composition of soleus and extensor digitorum longus muscles in normal female inbred Lewis rats," *Acta Histochemica*, vol. 104, no. 4, pp. 399–405, 2002.
- [33] E. Gonzalez, M. L. Messi, Z. Zheng, and O. Delbono, "Insulin-like growth factor-1 prevents age-related decrease in specific force and intracellular Ca^{2+} in single intact muscle fibres from transgenic mice," *Journal of Physiology*, vol. 552, no. 3, pp. 833–844, 2003.
- [34] N. Hamalainen and D. Pette, "The histochemical profiles of fast fiber types IIB, IID, and IIA in skeletal muscles of mouse, rat, and rabbit," *Journal of Histochemistry and Cytochemistry*, vol. 41, no. 5, pp. 733–743, 1993.
- [35] P. D. Gollnick, B. Sjoedin, J. Karlsson, E. Jansson, and B. Saltin, "Human soleus muscle: a comparison of fiber composition and enzyme activities with other leg muscles," *Pflügers Archiv European Journal of Physiology*, vol. 348, no. 3, pp. 247–255, 1974.
- [36] A. R. Tupling, E. Bombardier, R. D. Stewart, C. Vigna, and A. E. Aquiri, "Muscle fiber type-specific response of Hsp70 expression in human quadriceps following acute isometric exercise," *Journal of Applied Physiology*, vol. 103, no. 6, pp. 2105–2111, 2007.
- [37] M. S. Lim and M. P. Walsh, "Phosphorylation of skeletal and cardiac muscle C-proteins by the catalytic subunit of cAMP-dependent protein kinase," *Biochemistry and Cell Biology*, vol. 64, no. 7, pp. 622–630, 1986.
- [38] I. M. Vikhliantsev and Z. A. Podlubnaia, "Phosphorylation of sarcomeric cytoskeletal proteins—an adaptive factor for inhibiting the contractile activity of muscle during hibernation," *Biofizika*, vol. 48, no. 3, pp. 499–504, 2003.
- [39] T. N. Alyoncheva, T. Mikawa, F. C. Reinach, and D. A. Fischman, "Isoform-specific interaction of the myosin-binding proteins (MyBPs) with skeletal and cardiac myosin is a property of the C-terminal immunoglobulin domain," *Journal of Biological Chemistry*, vol. 272, no. 33, pp. 20866–20872, 1997.
- [40] C. Moos, G. Offer, R. Starr, and P. Bennett, "Interaction of C protein with myosin, myosin rod and light meromyosin," *Journal of Molecular Biology*, vol. 97, no. 1, pp. 1–9, 1975.
- [41] T. Okagaki, F. E. Weber, D. A. Fischman, K. T. Vaughan, T. Mikawa, and F. C. Reinach, "The major myosin-binding domain of skeletal muscle MyBP-C (C protein) resides in the COOH-terminal, immunoglobulin C2 motif," *Journal of Cell Biology*, vol. 123, no. 3, pp. 619–626, 1993.
- [42] C. A. Miyamoto, D. A. Fischman, and F. C. Reinach, "The interface between MyBP-C and myosin: site-directed mutagenesis of the CX myosin-binding domain of MyBP-C," *Journal of Muscle Research and Cell Motility*, vol. 20, no. 7, pp. 703–715, 1999.
- [43] R. Starr and G. Offer, "The interaction of C-protein with heavy meromyosin and subfragment-2," *Biochemical Journal*, vol. 171, no. 3, pp. 813–816, 1978.
- [44] C. Moos, "Fluorescence microscope study of the binding of added C protein to skeletal muscle myofibrils," *Journal of Cell Biology*, vol. 90, no. 1, pp. 25–31, 1981.
- [45] C. Moos, C. M. Mason, and J. M. Besterman, "The binding of skeletal muscle C-protein to F-actin, and its relation to the interaction of actin with myosin subfragment-1," *Journal of Molecular Biology*, vol. 124, no. 5, pp. 571–586, 1978.
- [46] K. Yamamoto, "The binding of skeletal muscle C-protein to regulated actin," *FEBS Letters*, vol. 208, no. 1, pp. 123–127, 1986.

- [47] N. A. Freydina, Z. I. Vishnevskaya, S. N. Udaltsov, and Z. A. Podlubnaya, "Effect of C-protein and LC-light chains on actomyosin ATPase at various ionic strength and calcium levels," *Acta Biochimica et Biophysica Hungarica*, vol. 21, no. 3, pp. 247–256, 1986.
- [48] C. Moos and I. N. Feng, "Effect of C-protein on actomyosin ATPase," *Biochimica et Biophysica Acta*, vol. 632, no. 2, pp. 141–149, 1980.
- [49] J. F. Koretz, T. C. Irving, and K. Wang, "Filamentous aggregates of native titin and binding of C-protein and AMP-deaminase," *Archives of Biochemistry and Biophysics*, vol. 304, no. 2, pp. 305–309, 1993.
- [50] S. Labeit, M. Gautel, A. Lakey, and J. Trinick, "Towards a molecular understanding of titin," *The EMBO Journal*, vol. 11, no. 5, pp. 1711–1716, 1992.
- [51] A. Soteriou, M. Gamage, and J. Trinick, "A survey of interactions made by the giant protein titin," *Journal of Cell Science*, vol. 104, no. 1, pp. 119–123, 1993.
- [52] A. Freiburg and M. Gautel, "A molecular map of the interactions between titin and myosin-binding protein C: implications for sarcomeric assembly in familial hypertrophic cardiomyopathy," *European Journal of Biochemistry*, vol. 235, no. 1–2, pp. 317–323, 1996.
- [53] A. Kontrogianni-Konstantopoulos, M. A. Ackermann, A. L. Bowman, S. V. Yap, and R. J. Bloch, "Muscle giants: molecular scaffolds in sarcomerogenesis," *Physiological Reviews*, vol. 89, no. 4, pp. 1217–1267, 2009.
- [54] E. Flashman, L. Korkie, H. Watkins, C. Redwood, and J. C. Moolman-Smook, "Support for a trimeric collar of myosin binding protein C in cardiac and fast skeletal muscle, but not in slow skeletal muscle," *FEBS Letters*, vol. 582, no. 3, pp. 434–438, 2008.
- [55] B. Decker and M. S. Z. Kellermyer, "Periodically arranged interactions within the myosin filament backbone revealed by mechanical unzipping," *Journal of Molecular Biology*, vol. 377, no. 2, pp. 307–310, 2008.
- [56] J. S. Davis, "Interaction of C-protein with pH 8.0 synthetic thick filaments prepared from the myosin of vertebrate skeletal muscle," *Journal of Muscle Research and Cell Motility*, vol. 9, no. 2, pp. 174–183, 1988.
- [57] J. F. Koretz, "Effects of C-protein on synthetic myosin filament structure," *Biophysical Journal*, vol. 27, no. 3, pp. 433–446, 1979.
- [58] R. Gilbert, J. A. Cohen, S. Pardo, A. Basu, and D. A. Fischman, "Identification of the A-band localization domain of myosin binding proteins C and H (MyBP-C, MyBP-H) in skeletal muscle," *Journal of Cell Science*, vol. 112, no. 1, pp. 69–79, 1999.
- [59] R. Gilbert, M. G. Kelly, T. Mikawa, and D. A. Fischman, "The carboxyl terminus of myosin binding protein C (MyBP-C, C-protein) specifies incorporation into the A-band of striated muscle," *Journal of Cell Science*, vol. 109, no. 1, pp. 101–111, 1996.
- [60] G. Bonne, L. Carrier, J. Bercovici, et al., "Cardiac myosin binding protein-C gene splice acceptor site mutation is associated with familial hypertrophic cardiomyopathy," *Nature Genetics*, vol. 11, no. 4, pp. 438–440, 1995.
- [61] C. E. Oakley, B. D. Hambly, P. M. Curmi, and L. J. Brown, "Myosin binding protein C: structural abnormalities in familial hypertrophic cardiomyopathy," *Cell research*, vol. 14, no. 2, pp. 95–110, 2004.
- [62] L. Carrier, R. Knöll, N. Vignier, et al., "Asymmetric septal hypertrophy in heterozygous cMyBP-C null mice," *Cardiovascular Research*, vol. 63, no. 2, pp. 293–304, 2004.
- [63] S. P. Harris, C. R. Bartley, T. A. Hacker, et al., "Hypertrophic cardiomyopathy in cardiac myosin binding protein-C knockout mice," *Circulation Research*, vol. 90, no. 5, pp. 594–601, 2002.
- [64] F. S. Korte, K. S. McDonald, S. P. Harris, and R. L. Moss, "Loaded shortening, power output, and rate of force redevelopment are increased with knockout of cardiac myosin binding protein-C," *Circulation Research*, vol. 93, no. 8, pp. 752–758, 2003.
- [65] S. P. Harris, E. Rostkova, M. Gautel, and R. L. Moss, "Binding of myosin binding protein-C to myosin subfragment S2 affects contractility independent of a tether mechanism," *Circulation Research*, vol. 95, no. 9, pp. 930–936, 2004.
- [66] P. A. Hofmann, M. L. Greaser, and R. L. Moss, "C-protein limits shortening velocity of rabbit skeletal muscle fibres at low levels of Ca^{2+} activation," *Journal of Physiology*, vol. 439, pp. 701–715, 1991.
- [67] C. A. C. Ottenheijm, C. Hidalgo, K. Rost, M. Gotthardt, and H. Granzier, "Altered contractility of skeletal muscle in mice deficient in titin's M-band region," *Journal of Molecular Biology*, vol. 393, no. 1, pp. 10–26, 2009.
- [68] S. Winegrad, "Cardiac myosin binding protein C," *Circulation Research*, vol. 84, no. 10, pp. 1117–1126, 1999.
- [69] M. J. McGrath, D. L. Cottle, M.-A. Nguyen, et al., "Four and a half LIM protein 1 binds myosin-binding protein C and regulates myosin filament formation and sarcomere assembly," *Journal of Biological Chemistry*, vol. 281, no. 11, pp. 7666–7683, 2006.
- [70] E. Flashman, C. Redwood, J. Moolman-Smook, and H. Watkins, "Cardiac myosin binding protein C: its role in physiology and disease," *Circulation Research*, vol. 94, no. 10, pp. 1279–1289, 2004.
- [71] D. Sanoudou, E. Vafiadaki, D. A. Arvanitis, E. Kranias, and A. Kontrogianni-Konstantopoulos, "Array lessons from the heart: focus on the genome and transcriptome of cardiomyopathies," *Physiological Genomics*, vol. 21, pp. 131–143, 2005.
- [72] K. M. McCormick, K. M. Baldwin, and F. Schachat, "Coordinate changes in C protein and myosin expression during skeletal muscle hypertrophy," *American Journal of Physiology*, vol. 267, no. 2, pp. C443–C449, 1994.

Research Article

Identification of Candidate Genes Potentially Relevant to Chamber-Specific Remodeling in Postnatal Ventricular Myocardium

Mario Torrado, Raquel Iglesias, Beatriz Nespereira, and Alexander T. Mikhailov

Developmental Biology Unit, Institute of Health Sciences, University of La Coruña, Campus de Oza, As Xubias Street s/n, 15006 La Coruña, Spain

Correspondence should be addressed to Alexander T. Mikhailov, margot@udc.es

Received 8 October 2009; Accepted 7 January 2010

Academic Editor: Aikaterini Kontrogianni-Konstantopoulos

Copyright © 2010 Mario Torrado et al. This is an open access article distributed under the Creative Commons Attribution License, which permits unrestricted use, distribution, and reproduction in any medium, provided the original work is properly cited.

Molecular predisposition of postnatal ventricular myocardium to chamber-dependent (concentric or eccentric) remodeling remains largely elusive. To this end, we compared gene expression in the left (LV) versus right ventricle (RV) in newborn piglets, using a differential display reverse transcription-PCR (DDRT-PCR) technique. Out of more than 5600 DDRT-PCR bands, a total of 153 bands were identified as being differentially displayed. Of these, 96 bands were enriched in the LV, whereas the remaining 57 bands were predominant in the RV. The transcripts, displaying over twofold LV-RV expression differences, were sequenced and identified by BLAST comparison to known mRNA sequences. Among the genes, whose expression was not previously recognized as being chamber-dependent, we identified a small cohort of key regulators of muscle cell growth/proliferation (MAP3K7IP2, MSTN, PHB2, APOBEC3F) and gene expression (PTPLAD1, JMJD1C, CEP290), which may be relevant to the chamber-dependent predisposition of ventricular myocardium to respond differentially to pressure (LV) and volume (RV) overloads after birth. In addition, our data demonstrate chamber-dependent alterations in expression of as yet uncharacterized novel genes, which may also be suitable candidates for association studies in animal models of LV/RV hypertrophy.

1. Introduction

Ventricular (or cardiac) remodeling is commonly defined as a physiological or pathological process that can occur under various conditions of pressure/volume overload. A common feature of ventricular remodeling is hypertrophy of the cardiomyocytes. The type of cardiac workload determines the pattern of ventricular hypertrophy: volume overload induces eccentric, while pressure overload induces concentric remodeling. Under various pathological conditions, compensatory concentric hypertrophy can lead to eccentric hypertrophy, dilatory ventricular remodelling, and heart failure (reviewed in [1, 2]). The molecular signature of concentric versus eccentric hypertrophy, although poorly defined as yet, is nevertheless of critical relevance in cardiac basic and clinical research [3–8].

The early neonatal heart is a conventional model for the study of distinct patterns of ventricular hypertrophy (i.e., concentric versus eccentric). At birth, cardiomyocytes

begin to enlarge in response to the demands of physiological workload, as opposed to processes driven predominantly by developmental mechanisms. Particularly, the left ventricle (LV) is exposed to a higher-pressure overload in comparison to the right ventricle (RV), which is exposed to a relatively higher-volume overload. As a result, the LV undergoes rapid concentric hypertrophy, while the RV undergoes eccentric hypertrophy associated with dilatory RV-chamber remodeling. Our previous data revealed differences in the expression of cardiac ankyrin repeat domain 1 factor (ANKRD1/CARP) between the LV and RV before the appearance of morphologically identifiable signs of LV-concentric or RV-eccentric hypertrophy in newborn piglets [9]. Other research reported certain LV/RV-specific metabolic differences in normal and ischemic newborn piglet heart [7]. We interpreted these results as reflecting a certain type of molecular predisposition of newborn ventricular myocardium to LV-concentric and RV-eccentric remodeling during postnatal development.

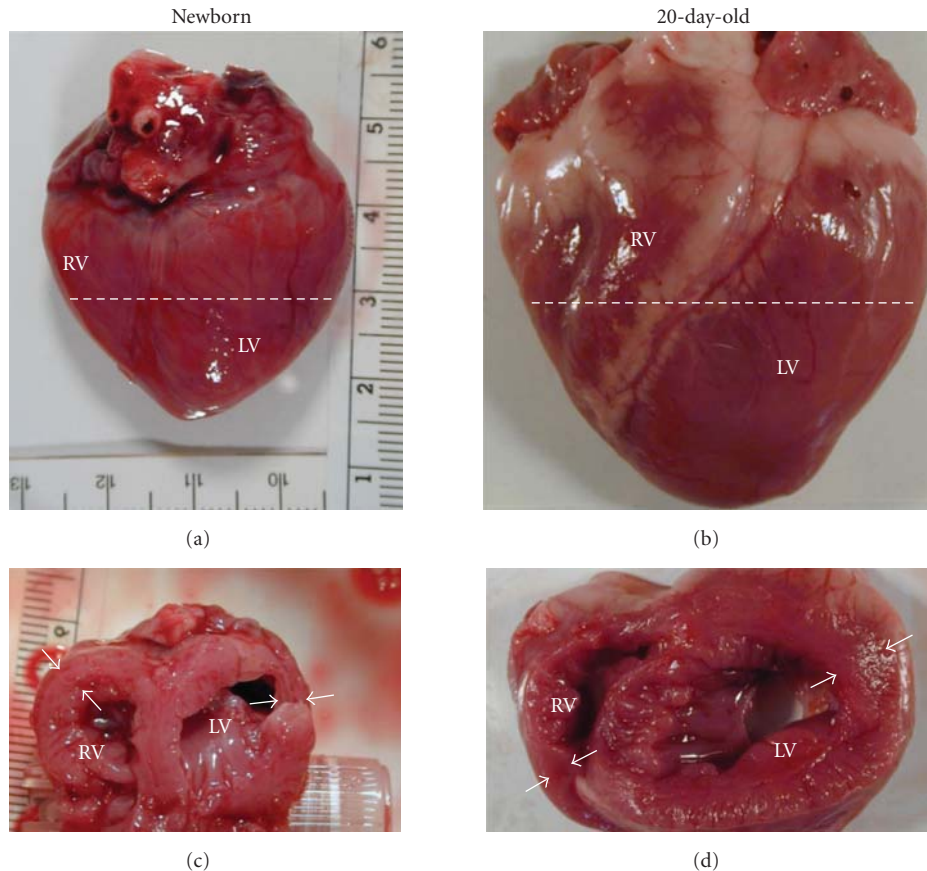


FIGURE 1: Heart dimensions (a and b) and left/right ventricular cross-sections (c and d) of newborn and 20-day-old piglets. LV/RV—left/right ventricle. (a), (b) Levels of cross sections are shown by dotted lines. (c), (d) Boundaries of the LV/RV free wall are marked by white arrows.

In the present study, we focused on large-scale transcriptomic analysis to compare differences in gene expression levels in the LV versus RV in newborn piglets. Given that commercially available DNA microarray platforms suitable for performing transcriptional profiling in pig are still poorly developed, we conducted comparative LV versus RV gene expression profiling in newborn piglets using mRNA differential display (DDRT-PCR). In addition, unlike microarray-based platforms, DDRT-PCR can be used to detect expression changes in both known and novel transcripts including alternate splice variants [10]. This approach allowed us (1) to perform an unbiased assessment of genes which expression is predominantly associated with piglet LV or RV myocardium and (2) to distil a large body of expression data into a discrete set of candidate genes for which regulation was not previously recognized as being chamber-dependent. Further studies on these differentially regulated genes will likely lead to the identification of additional novel gene families and pathways involved in the chamber-dependent response of ventricular myocardium to a variety of physiological and pathological stimuli.

2. Materials and Methods

2.1. Animals and Tissue Sampling. Animals were treated and cared for in accordance with the European commission

directive 86/609/EEC on the protection of animals used for experimental and other scientific purposes, and all animal protocols were approved by the ethical research committee of Galicia (Spain). Newborn (10–12 hours after birth) Large White piglets were obtained from a local commercial breeder (La Coruña, Galicia) and maintained in an automatic nursery system (Nütinger System). The newborn and 20-day-old animals were anaesthetized, the thoracic cavity was opened through a median sternotomy, and the entire heart was rapidly removed, weighed, and photographed while still beating. Then the isolated heart was placed on an ice-cold petri dish, partially sectioned at the midpoint of the LV length and photographs of the open ventricular chambers were taken (Figure 1). Immediately after this step, the LV and RV free walls were dissected, flash frozen in liquid nitrogen, and stored at -80°C until study.

2.2. RNA Isolation. Deep-frozen tissue samples (100–150 mg), encompassing the full thickness of the free wall of the LV and RV ventricle, were directly disrupted in RLT buffer (Qiagen) using a high-speed rotor-stator homogenizer (Ultra-Turrax T8, Germany), digested with Proteinase K (Qiagen), loaded onto a RNeasy Midi column (Qiagen), subjected to on-column digestion of DNA with RNase-free DNase (Qiagen) and the analysis proceeded in accordance

with the manufacturer's recommendations. Resulting RNA preparations were ethanol-precipitated, resolved in RNase-free water, and kept at -80°C . RNA yield and purity was determined spectrophotometrically at 260–280 nm and RNA integrity was verified by running samples on 1.5% agarose gels and staining with ethidium bromide.

2.3. Differential Display mRNA Analysis. The reverse transcription-PCR differential display (DDRT-PCR) analysis was performed as described [11] with minor modifications [12]. To yield starting material for the DDRT-PCR, total RNA preparations independently isolated from the LV and RV of three newborn piglets were, respectively, pooled at equal ratios, and $4\ \mu\text{g}$ of RNA was reverse transcribed using the SuperScript III (Invitrogen) and T7-oligo-dT primer. Pooled first-strand cDNAs were amplified side-by-side by PCR using 230 different primer combinations (10 two-base-anchored oligo-dT and 23 arbitrary primers purified by HPLC, Table 1).

Nontemplate (NT) and non-RT RNA (N-RT) template reactions were used as negative controls. In each DDRT-PCR set-up, reactions were performed at least in duplicate to test whether differences in LV/RV gene expression are likely to be real. PCR was performed, using the AmpliTaq DNA polymerase (Invitrogen), under the following conditions: initial denaturation (94°C , 2 minutes), stage I (5 cycles, each of which included: 94°C , 30 seconds; 40°C , 1 minute; 72°C , 1 minute), stage II (25 cycles, each on which included: 94°C , 30 seconds; 50°C , 1 minute; 72°C , 1 minute), and final extension (72°C , 10 minutes), sample store at 6°C . PCR-amplified products were subjected to fractionation on 8% polyacrylamide gels (PAAG) (Mini-Protean-III, Bio-Rad) and fluorescently stained by SYBR Green I (Sigma). Image acquisition and intensity of bands were estimated by densitometry (VersaDoc 1000) and Quantity One software (Bio-Rad). Differentially regulated amplification products were defined as those bands that were similarly displayed at least in two experimental replicates. Using a sharp, sterile razor blade, a rectangular piece of gel corresponding to an individual band of interest on the PAAG was excised and electroeluted (D-tube Electroelution Kit, Novagen). After a short centrifugation, the eluate was transferred to a clean tube. The extracted DNA was used directly as the template for PCR with T7 and M13 reamplification primers (see Table 1). Cycling conditions were as described for DDRT-PCR except stage I at 45°C and stage II (20 cycles) at 55°C . After reamplification, each PCR reaction was electrophoresed through a 1.5% agarose gel with ethidium bromide to assure that the correct sized fragment was amplified. Reamplified cDNA fragments were eluted (QIAquick Gel Extraction Kit, Qiagen), cloned into pCRII-TOPO vector (Invitrogen), and sequenced by (Secugen), (Madrid, Spain). The nucleotide sequences obtained were compared with known sequences by searching the GenBank database with BLAST algorithms.

2.4. Quantitative RT-PCR. Differential gene expression was further confirmed by real-time quantitative PCR (qRT-PCR) as described [13] using Bio-Rad IQ5 instrument and Bio-Rad

TABLE 1: Primers used in differential display RT-PCR analysis.

T7-Oligo(dT)	
	ACGACTCACTATAGGGCTTTTTTTTTTTTTT
two-base anchored oligo-dT antisense primers*	
H01	ACGACTCACTATAGGGCTTTTTTTTTTTTGA
H02	ACGACTCACTATAGGGCTTTTTTTTTTTTGC
H03	ACGACTCACTATAGGGCTTTTTTTTTTTTGG
H04	ACGACTCACTATAGGGCTTTTTTTTTTTTGT
H05	ACGACTCACTATAGGGCTTTTTTTTTTTTCA
H06	ACGACTCACTATAGGGCTTTTTTTTTTTTCC
H07	ACGACTCACTATAGGGCTTTTTTTTTTTTCG
H08	ACGACTCACTATAGGGCTTTTTTTTTTTTAA
H09	ACGACTCACTATAGGGCTTTTTTTTTTTTAC
H10	ACGACTCACTATAGGGCTTTTTTTTTTTTAT
10-mer arbitrary sense primers**	
A01	ACAATTTACACAGGACGACTCCAAG
A02	ACAATTTACACAGGAGCTAGCATGG
A03	ACAATTTACACAGGAGACCATTGCA
A04	ACAATTTACACAGGAGCTAGCAGAC
A05	ACAATTTACACAGGAATGGTCGTCT
A06	ACAATTTACACAGGATAACAACGAGG
A07	ACAATTTACACAGGATGGATTGGTC
A08	ACAATTTACACAGGATGGTAAAGGG
A09	ACAATTTACACAGGATAAGCCTAGC
A10	ACAATTTACACAGGAGATCTCAGAC
A11	ACAATTTACACAGGAACGCTAGTGT
A12	ACAATTTACACAGGAGGTTACTAAGG
A13	ACAATTTACACAGGAGTTGCACCAT
A14	ACAATTTACACAGGATCCATGACTC
A15	ACAATTTACACAGGACTTTCTACCC
A16	ACAATTTACACAGGATCGGTCATAG
A17	ACAATTTACACAGGACTGCTAGGTA
A18	ACAATTTACACAGGATGATGCTACC
A19	ACAATTTACACAGGATTTGGCTCC
A20	ACAATTTACACAGGATCGATACAGG
A21	ACAATTTACACAGGACAGGCAGCAG
A23	ACAATTTACACAGGATATGGCGCCG
A24	ACAATTTACACAGGAGCTGAACCGG
primers for reamplification of DD bands	
T7	GTAATACGACTCACTATAGGGC
M13rev-48p	AGCGGATAACAATTTACACAGGA

* Each anchor primer has T7 sequence (bold) on the 5' end.

** Each arbitrary primer has M13 sequence (bold) on the 5' end.

SYBR Green Mix [14, 15]. Whenever possible, the primer pairs were designed to be located in different exons of a given sequence. Individual heart-matched LV/RV cDNAs isolated from three newborn and three 20-day-old piglets were used as templates. Each primer pair used yielded a single peak of dissociation on the melting curve and a single band with expected size on PAAG [12]. A negative NT and N-RT controls were included in each reaction set. Detection of ribosomal protein L19 (RPL19) mRNA was used to normalize the expression of target mRNAs. The efficiency of

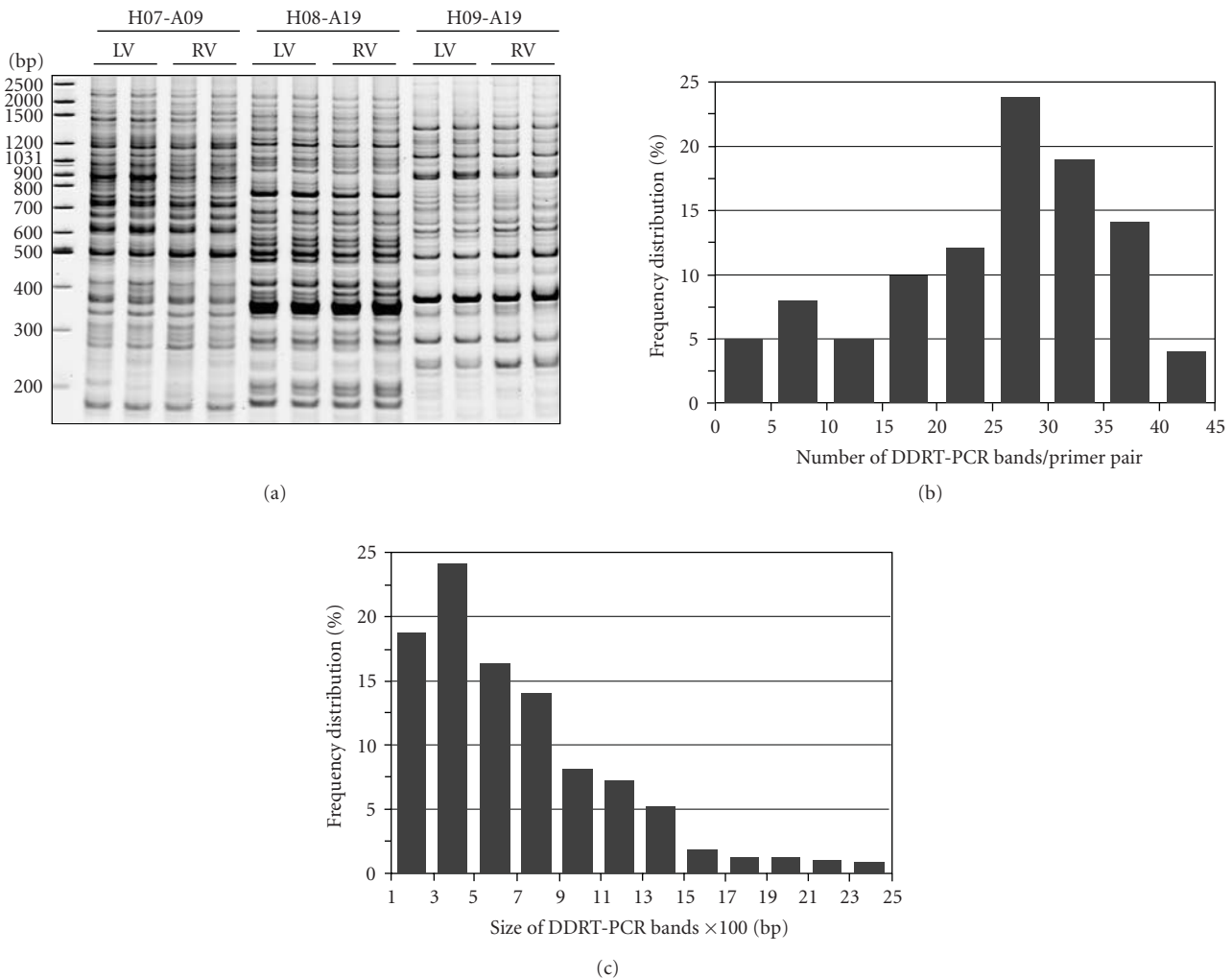


FIGURE 2: Differential display (DDRT-PCR) analysis of gene expression in left/right ventricles (LV/RV) of newborn piglets. (a) Representative gel images of DDRT-PCR bands amplified with three distinct sets of primer combinations (H07-A09, H08-A19, and H09-A19), showing highly reproducible band patterns in each replicate. Nondenaturing 8% PAAG poststained with SYBR Green I. 200–2500 bp—DNA size standards (GeneRuler DNA ladder mix, Fermentas). (b and c) Number and size distribution frequencies of bands generated by DDRT-PCR.

target and reference amplification was tested and found to be approximately equal. Results were defined as the target genes expression normalized against *rpl19* gene expression in both ventricles. Fold changes were calculated using the C_T method. Primer sequences and additional details on qRT-PCR are available upon request.

2.5. Data Analysis. Values were expressed as means \pm SEM. mRNA expression was quantified using the comparative threshold cycle method. Statistical analyses were performed with the SPSS 13 software. A P value $< .05$ was considered to be statistically significant.

3. Results

3.1. DDRT-PCR Analysis Allows Reliable Transcriptomic Profiling of Ventricular Myocardium in Newborn Piglets. For mammalian cells, it was calculated that 20 arbitrary in conjunction with 12 anchored primers would statistically amplify all mRNA sequences [16]. We used 23 arbitrary and

10 two-base-oligo(dT) anchored primers (Table 1), resulting in 230 display primer combinations. A total of about 5,600 distinct cDNA fragments corresponding to genes expressed in piglet LV/RV myocardium were detected. A representative example of DDRT-PCR banding patterns is illustrated in Figure 2(a).

The average number of bands generated by one primer pair was 26, the minimum was 0, and the maximum was 44. About 70% of the primer pairs produced 20–40 bands (Figure 2(b)). Size distribution analysis of cDNA bands generated by DDRT-PCR revealed a minor fraction of short-sized (100–300 nt) bands, while the fragments with a size from 300 to 1,000 nt, which is a preferable choice for cloning and sequencing, made up about 60% of all detected bands (Figure 2(c)).

Taken together, the results indicated that under our experimental conditions, transcript-banding patterns generated by DDRT-PCR could be sufficient for comparative expression analysis of the LV versus RV myocardium of newborn piglets.

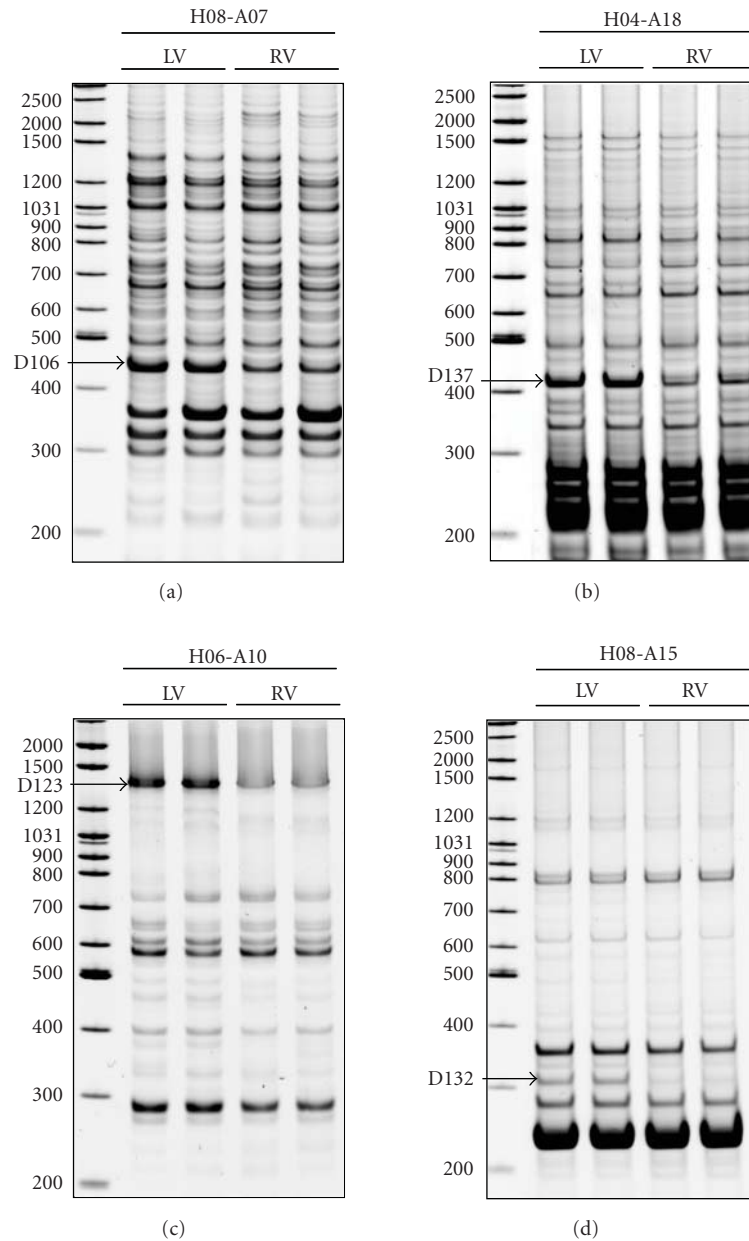


FIGURE 3: Examples of the bands, displaying over twofold LV versus RV expression differences in newborn piglets. The primer pairs used for DDRT-PCR amplifications are shown. Nondenaturing 8% PAAG poststained with SYBR Green I. LV/RV: left/right ventricle. 200–2500 bp: DNA size standards (GeneRuler DNA ladder mix, Fermentas). Arrows: the bands (D106, D137, D123, and D132), which correspond to the transcripts differentially displayed between LV and RV. For further details see Table 2.

3.2. DDRT-PCR Profiling Identifies Differentially Expressed Genes in the LV versus RV Myocardium of Newborn Piglets. Direct side-by-side comparison of the mRNAs between the LV and RV of the newborn piglet heart revealed that the majority of profiled genes (97%) were similarly expressed in both ventricles. Out of more than 5,600 DDRT-PCR bands amplified by the primer combinations used, a total of 153 bands, ranging in size from 300 to 1,000 nt, were identified as being qualitatively differentially displayed. Of these, 96 transcripts were enriched in the LV, whereas the remaining 57 were predominant in the RV.

Figure 3 illustrates the relative differential expression of a representative set of bands in the LV as compared to the RV myocardium. Once differentially displayed PCR products were detected, the fragments which displayed over twofold LV-RV expression differences (40 bands) were recovered from gels, reamplified, cloned, and sequenced. The differential expression of these genes was further confirmed using qRT-PCR analysis. In this manner, over 80% (32 bands) of the selected bands were confirmed to be differentially expressed in the two ventricular chambers of newborn piglets (Table 2).

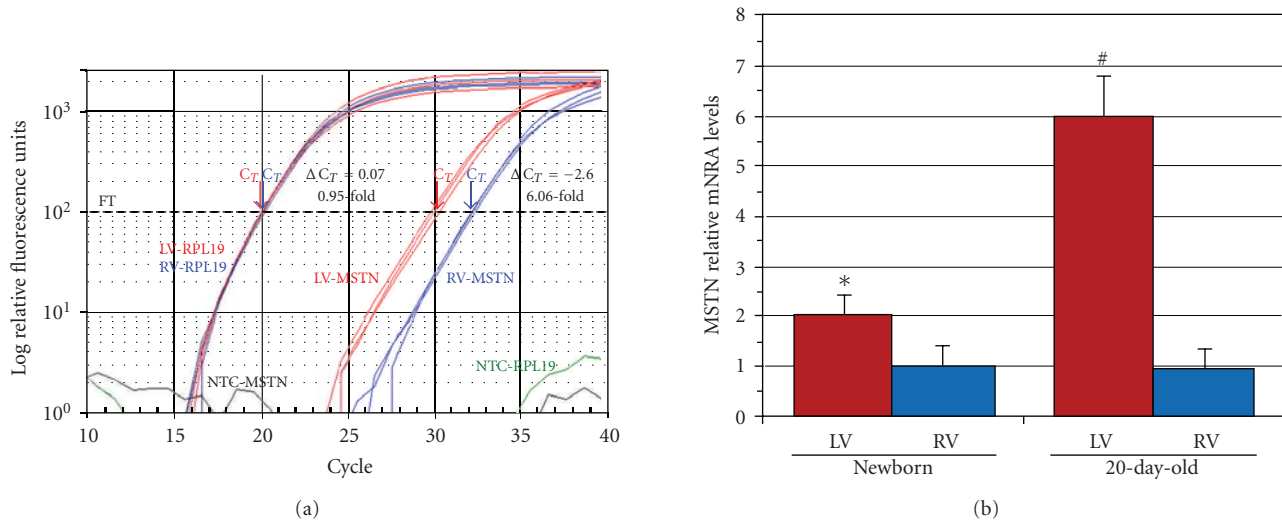


FIGURE 4: Estimation of myostatin (MSTN) mRNA levels in the LV and RV of newborn and 20-day-old piglets. (a) Representative qPCR amplification plot of MSTN mRNA levels in the LV (red) and RV (blue) of three 20-day-old piglet hearts. Internal RPL19 reference levels in the LV (red) and RV (blue) are shown. Arrows: threshold cycle (C_T). FT: fluorescent threshold. ΔC_T : differences in threshold cycles for target and reference. NTC: nontemplate controls. B: MSTN mRNA levels in the LV versus RV ventricle of newborn and 20-day-old piglets. * $P < .05$, newborn piglets ($n = 3$). # $P < .05$, 20-day-old piglets ($n = 3$).

The BLAST searches for sequence similarity revealed that 6 of the 32 cloned cDNA fragments with confirmed differential expression are potentially novel transcripts with no significant match in the current databases, suggesting that they may either encode as yet uncharacterized proteins or correspond to unknown regions of identified genes (untranslated, nonconserved regions). The remaining 26 cDNA sequences were identified by BLAST sequence comparisons as genes related to modulation of gene expression (PTPLAD1, PHB2, CEP290, JMJD1C), regulation of cell growth and differentiation (MSTN, MAP3K71P2, APOBEC3E, PHB2), biomechanical stress sensing and myofibrillar assembly (TTN, ANKRD1), muscle contraction (TNNT2, ACTC1), extracellular matrix remodeling (ADAMTS3, COL1A2), calcium control (SLC8A1), and energy metabolism (ATP5C1, ND6).

Table 2 provides details of the extent of relative LV/RV upregulation (fold change) as well as the known function(s) of identified genes. Among the differentially expressed genes, only a small portion displayed over 4-fold expression differences between LV and RV (PTPLAD1, TPM2, ACTC1, ANKRD1, ANKRD1-I8, PDE3A, D162, TNMD, D170). In this sense, chamber-dependent regulation of expression of these known and novel transcripts may be primarily associated with different patterns of postnatal ventricular remodeling.

MSTN (myostatin) characterized by LV-predominant expression in newborn myocardium also stood out as an interesting candidate, given its roles in cell growth and proliferation. Recently, it has been demonstrated that MSTN is a potent repressor of cardiac muscle cell proliferation and growth, and that in vivo loss of MSTN induces eccentric hypertrophy associated with enhanced responsiveness of ventricular myocytes to beta-adrenergic stimulation [17, 18]. We, therefore, examined this gene expression in both

ventricles at advanced stages of postnatal development when morphological differences between concentric (LV) and eccentric (RV) remodeling become evident, that is in 20-day-old piglets (see Figure 1(d)). The LV/RV MSTN mRNA ratio found in newborn piglets (i.e., 2 : 1) was significantly amplified in 20-day-old animals (i.e., 6 : 1) due to MSTN upregulation in the LV of the latter age group, while the gene's expression levels in the RV were similar in two groups studied (Figure 4). The results indicate that in neonatal piglets a process of RV-eccentric remodeling is associated with the same relative low MSTN level as was found in the RV at birth.

Collectively, the comparison of gene expression between the LV and RV shortly after birth, when LV/RV loading conditions are dramatically changed as compared to the late-fetal period, demonstrates that such analysis provides clues for identifying hallmark genes whose expression is regulated in a chamber-dependent manner at the earliest stages of postnatal LV-concentric and RV-eccentric remodeling.

4. Discussion

The DDRT-PCR technique, which was first developed in 1992 [19], is still the method of choice for an unbiased comparison of mRNA expression patterns between samples that are very similar and often results in identification of nonabundant, rare, or novel transcripts [10, 20, 21].

Using a nonradioactive DDRT-PCR technique, we identified the transcripts that reproducibly showed different expression levels between LV and RV in newborn piglets. These differences do not correlate with either cardiomyocyte cell volume [22] or ventricular wall thickness ([9]; see also Figure 1(b), this work), which are practically equal in both piglet ventricles during or shortly after birth. Thus, in

TABLE 2: Analysis of the transcripts identified by DDRT-PCR as upregulated in the LV/RV of newborn piglets.

Band number	Enriched in	Size, Bp	Primer Pair	Fold change*	Gene symbol	GenBank Acc. N°	Base pair match	Species	Gene identification	
									Function	Species
D005	LV	250	H01-A05	2.1 ± 0.3	<i>TTN</i>	AJ560658	98%	<i>S. Scrofa</i>	—	myofibrillar stretch-sensor system,
D015	LV	500	H03-A04	1.7 ± 0.2	<i>MAP3K7IP2</i>	NM_015093	94%	<i>H. sapiens</i>	—	proliferation and anti-apoptotic signalling
D024	LV	275	H04-A01	1.5 ± 0.2	<i>TNNT2</i>	AY277394	71%	<i>H. sapiens</i>	—	regulation of muscle contraction
D034	LV	450	H06-A03	2.1 ± 0.3	<i>ATP5C1</i>	NM_005174	86%	<i>H. sapiens</i>	—	ATP synthesis
D036	LV	400	H06-A04	4.2 ± 0.3	<i>ANKRD1-i8</i>	FJ475066	100%	<i>S. scrofa</i>	—	ANKRD1 splice isoform
D046	LV	400	H08-A01	2.0 ± 0.3	<i>ADAMTS3</i>	BC132735	88%	<i>H. sapiens</i>	—	extracellular matrix degrading enzyme
D106	LV	450	H08-A07	2.2 ± 0.4	<i>Unknown</i>	—	—	—	—	—
D123	LV	1400	H06-A10	4.2 ± 0.2	<i>PTPLAD1</i>	NM_001103316	90%	<i>B. taurus</i>	—	modulation of gene expression
D128A	LV	900	H05-A14	2.3 ± 0.2	<i>SLC8A1</i>	NM_001112802	87%	<i>H. sapiens</i>	—	calcium level control
D128B	LV	900	H05-A14	3.2 ± 0.5	<i>CTSH</i>	EU532429	79%	<i>S. scrofa</i>	—	degradation of proteins in lysosomes
D130	LV	800	H06-A14	4.2 ± 0.4	<i>PDE3A</i>	XM_520783	77%	<i>P. troglodytes</i>	—	hydrolysis of cyclic nucleotides
D132	LV	310	H08-A15	5.6 ± 0.4	<i>TPM2</i>	NG_011620	80%	<i>H. sapiens</i>	—	regulation of muscle contraction
D133	LV	350	H10-A13	2.1 ± 0.4	<i>SERPINB9</i>	NM_004155	73%	<i>H. sapiens</i>	—	inactivation of serine proteinases
D134	LV	200	H08-A18	2.6 ± 0.4	<i>ND6</i>	AY063320	96%	<i>H. sapiens</i>	—	ATP production
D137	LV	415	H04-A18	2.6 ± 0.4	<i>MSTN</i>	AY208121	95%	<i>S. scrofa</i>	—	negative regulator of muscle growth
D144	LV	180	H03-A18	4.0 ± 0.2	<i>ACTC1</i>	FM212567	83%	<i>S. scrofa</i>	—	contractile apparatus assembling
D147	LV	500	H02-A07	3.7 ± 0.3	<i>INHBA</i>	NM_214028	86%	<i>S. scrofa</i>	—	myocardial remodelling and tissue repair
D151A	LV	435	H05-A07	2.1 ± 0.3	<i>Unknown</i>	—	—	—	—	—
D151B	LV	435	H05-A07	1.6 ± 0.2	<i>COL1A2</i>	NG_007405	77%	<i>H. sapiens</i>	—	formation of fibrillar collagen
D153	LV	300	H05-A02	1.6 ± 0.3	<i>PHB2</i>	NM_001046198	80%	<i>B. taurus</i>	—	transcriptional repression regulation
D155	LV	930	H10-A23	9.2 ± 0.3	<i>ANKRD1</i>	NM_213922	100%	<i>S. scrofa</i>	—	myofibrillar stretch-sensor system
D162	LV	930	H05-A23	4.1 ± 0.5	<i>Unknown</i>	—	—	—	—	—
D165	LV	1000	H03-A24	2.1 ± 0.4	<i>Unknown</i>	—	—	—	—	—
D170	LV	360	H06-A21	10.8 ± 0.7	<i>NPPB</i>	NM_213846	100%	<i>S. scrofa</i>	—	new NPPB putative splice isoform**
D006	RV	600	H01-A05	2.5 ± 0.4	<i>Unknown</i>	—	—	—	—	—
D42B	RV	600	H07-A01	3.1 ± 0.2	<i>CEP290</i>	NM_025114	89%	<i>H. sapiens</i>	—	transcription activation (via ATF-4 factor)
D050	RV	450	H08-A04	2.0 ± 0.5	<i>SPTBN1</i>	AB371586	92%	<i>H. sapiens</i>	—	determination of cell shape
D051	RV	400	H08-A05	1.9 ± 0.2	<i>SLC41A1</i>	NM_173854	78%	<i>H. sapiens</i>	—	magnesium transporter
D103	RV	350	H06-A12	5.5 ± 0.2	<i>TNMD</i>	XM_001088536	69%	<i>M. mulatta</i>	—	angiogenesis inhibitor
D104	RV	900	H06-A07	2.1 ± 0.3	<i>APOBEC3F</i>	FJ042939	83%	<i>S. scrofa</i>	—	growth and cell cycle control
D145	RV	375	H08-A19	3.3 ± 0.4	<i>Unknown</i>	—	—	—	—	—
D146	RV	850	H05-A13	1.9 ± 0.2	<i>JMJD1C</i>	NM_032776	91%	<i>H. sapiens</i>	—	hormone-dependent transcriptional activation

* Fold change determined by qPCR. ** The D170 band sequence exhibits homology with exon 1 and 3 sequences of the pig *nppb* gene.

ACTC1: actin, alpha, cardiac muscle 1; *ADAMTS3*: ADAM metalloproteinase with thrombospondin type 1 motif 3; *ANKRD1*: ankyrin repeat domain 1 (cardiac muscle); *ANKRD1-i8*: *ANKRD1* retaining intron 8; *APOBEC3F*: apolipoprotein B mRNA editing enzyme, catalytic polypeptide-like 3F; *ATP5C1*: ATP synthase, mitochondrial F1 complex, gamma polypeptide 1; *CEP290*: centrosomal protein 290 kDa; *COL1A2*: collagen, type I, alpha 2; *CTSH*: cathepsin H; *INHBA*: inhibin, beta A; *JMJD1C*: jumonji domain containing 1C; *MAP3K7IP2*: mitogen-activated protein kinase kinase 7 interacting protein 2; *MSTN*: myostatin; *ND6*: mitochondrially encoded NADH dehydrogenase 6; *NPPB*: natriuretic peptide precursor B; *PDE3A*: phosphodiesterase 3A, cGMP-inhibited; *PHB2*: prohibitin 2; *PTPLAD1*: protein tyrosine phosphatase-like A domain containing 1; *SERPINB9*: serpin peptidase inhibitor, clade B (ovalbumin), member 9; *SLC41A1*: solute carrier family 41, member 1; *SLC8A1*: solute carrier family 8 (sodium/calcium exchanger), member 1; *SPTBN1*: spectrin, beta, non-erythrocytic 1; *TNMD*: tenomodulin; *TNNT2*: tropomyosin 2 (beta); *TTN*: titin.

this system a molecular prepattern precedes the appearance of morphologically identifiable signs of LV-concentric and RV-eccentric hypertrophy. We suggest that the observed differences in gene expression are intrinsic to the distinct molecular makeup of the LV versus RV rather than to their hyperplastic/hypertrophic growth status, which is similar in both ventricles at birth. Further, the content of certain well-known markers of cardiomyocyte hypertrophy (beta-myosin heavy chain and myosin light chain 2 ventricular) was found to be similar in both the LV and RV of newborn piglets [9]. Moreover, expression levels of the transcriptional cofactor, myocardin, which induces cardiomyocyte hypertrophy [23, 24], are equal in both ventricles of these animals [25]. Therefore, it seems reasonable to interpret the differences in gene expression detected in our present work as indicative of an L–R molecular predisposition of the newborn myocardium to respond to dramatic changes of the hemodynamic loads shortly after birth when the LV is exposed to a higher-pressure load (concentric hypertrophy promoting condition) in comparison to the RV, which is exposed to a higher-volume load (eccentric hypertrophy promoting condition).

The vast majority of the transcripts differentially expressed in the LV and RV of newborn piglets correspond to genes which were not previously known to be asymmetrically expressed in the LV versus RV myocardium, excepting those coding for beta-spectrin [4], ANKRD1 [9], BNP [6, 9], calcium ATPase, matrix metalloproteinases, type 1 procollagens, and troponins [3]. In addition, other reports demonstrated that transcripts for proteins such as fibronectin, alpha-myosin heavy chain and transforming growth factor [26], and cytochrome c oxidase and heart isoforms of uncoupling proteins [27] are asymmetrically enriched in the LV versus RV mammalian myocardium.

Regulatory mechanisms resulting in LV/RV transcriptional differences in the newborn and early neonatal heart are largely unknown, but of special interest, because the functionally different roles of the two ventricles become apparent after birth. Our study characterizes the transcription status of the LV and RV at birth rather than the establishment of LV/RV transcription differences in the course of development [28]. In embryonic and fetal heart, expression of a number of transcription factors, including Hand1, Hand2, and Tbx5, shows LV/RV differences [29, 30]. We found [9] that Hand1 and Hand2 are equally expressed in both the LV and RV of newborn piglets, suggesting that these factors are not involved in maintaining L/R ventricular transcriptional differences after birth.

In this work, among the genes whose expression levels differentiate between the LV and RV, there is a small cohort of genes which could be involved in concentric versus eccentric hypertrophy signalling (see Table 2). In this regard, several key regulators of muscle cell growth and proliferation (MAP3K7IP2, MSTN, PHB2, APOBEC3F) and gene expression (PTPLAD1, JMJD1C, CEP290) are differentially expressed between LV and RV piglet myocardium that may be relevant to intrinsic differences [31] that can regulate the chamber-dependent response of ventricular myocardium to workload. Interestingly, transition from “early” to “late” hypertension-induced hypertrophy in young adult rats is

associated with predominant changes in expression of cell growth/proliferation and signal transduction factors [32].

Sequence analysis of the 32 cDNAs chosen based on differential LV/RV screening revealed a number of sequences, which may correspond to either previously uncharacterized genes or yet unidentified splice variants of the known cardioexpressed genes. In this sense, identification of the D36 fragment sequence (see Table 2) as being completely identical to that located within intron 8 of the pig *ankrd1* gene led us to isolate and characterize three novel alternatively spliced *ankrd1* variants which are predominantly expressed in the LV of neonatal and adult pig and human hearts and markedly upregulated in the ventricular myocardium at experimental heart failure [12]. Similarly, the D170 fragment (see Table 2), exhibiting homology with exon 1 and 3 sequences of the pig *nppb* gene, may represent a new form of alternative splicing of this cardioprotective factor.

Various cardiac disease states can result in an imbalance of chamber-associated expression patterns in ventricular myocardium. In the rat infarct model, a shift in chamber-dependent gene expression towards relative downregulation of gene expression in the RV as compared to the LV has been reported [3]. In the porcine model of cardiotoxic cardiomyopathy we have demonstrated that the normal asymmetric LV/RV pattern of ANKRD1 mRNA and protein distribution was completely abolished at end-stage heart failure; improvement of cardiac performance resulted in the restoration of this gene’s LV/RV asymmetric expression [9]. In the pig model of volume overload (eccentric hypertrophy promoting condition), angiotensinogen and prepro-endothelin expression levels were significantly upregulated in the RV while remaining unchanged in the LV [31]. In the mouse model of RV pressure-overload hypertrophy, over 10 transcripts showed significant upregulation in the afterload stressed RV, but not in the afterload stressed LV, including three genes from the Wnt signaling pathway, and genes involved in apoptosis [33]. In young rats, chronic hypoxia resulted in a shift from an LV- to an RV-predominant pattern in cytochrome c oxidase expression [27].

In sum, although not all of the identified genes with differential LV/RV expression have a clearly defined cardiac-related function(s) at this time, the results of our work do advance the understanding of the complex mechanisms that could be involved in concentric versus eccentric remodeling of ventricular myocardium under normal conditions. More broadly, the identification of specific expression signatures of concentric versus eccentric hypertrophy may be useful in the elucidation of molecular pathways involved not only in physiological but also in pathological myocardial remodelling and heart failure.

5. Conclusions

Using an unbiased DDRT-PCR analysis, we were able to identify a set of genes with divergent LV versus RV expression. To our knowledge, this is the first study to account for large-scale gene expression profiling in early neonatal myocardium in mammals which revealed a certain molecular predisposition of the LV and RV, respectively, to concentric

or eccentric hypertrophic remodeling. The reliability of these findings is supported by confirmation of the results by qRT-PCR and recognition of a fraction of the differentially expressed genes as known genes involved in pathological ventricular remodeling and heart failure. In addition, our data demonstrate chamber-dependent alterations in the expression of as yet uncharacterised novel genes that may be associated with different patterns of ventricular hypertrophic remodeling and can be used to study a board range of heart disease phenotypes.

Acknowledgments

HPLC-purified primers for DDRT-PCR were a generous gift from Dr. Max Rothschild (Iowa State University, USA). This work was partially supported by Grants (SAF2004-01462 and SAF2008-00337) from the Spanish Ministry of Science and Innovation and by a Grant (08CSA008161PR) from the Autonomic Government of Galicia.

References

- [1] J. Heineke and J. D. Molkentin, "Regulation of cardiac hypertrophy by intracellular signalling pathways," *Nature Reviews Molecular Cell Biology*, vol. 7, no. 8, pp. 589–600, 2006.
- [2] D. Hilfiker-Kleiner, U. Landmesser, and H. Drexler, "Molecular mechanisms in heart failure. Focus on cardiac hypertrophy, inflammation, angiogenesis, and apoptosis," *Journal of the American College of Cardiology*, vol. 48, no. 9, pp. A56–A66, 2006.
- [3] S. S. Chugh, S. Whitesel, M. Turner, C. T. Roberts Jr., and S. R. Nagalla, "Genetic basis for chamber-specific ventricular phenotypes in the rat infarct model," *Cardiovascular Research*, vol. 57, no. 2, pp. 477–485, 2003.
- [4] R. Tabibiazar, R. A. Wagner, A. Liao, and T. Quertermous, "Transcriptional profiling of the heart reveals chamber-specific gene expression patterns," *Circulation Research*, vol. 93, no. 12, pp. 1193–1201, 2003.
- [5] K. Lemmens, V. F. M. Segers, M. Demolder, M. Michiels, P. Van Cauwelaert, and G. W. De Keulenaer, "Endogenous inhibitors of hypertrophy in concentric versus eccentric hypertrophy," *European Journal of Heart Failure*, vol. 9, no. 4, pp. 352–356, 2007.
- [6] B. D. Kaufman, M. Desai, S. Reddy, et al., "Genomic profiling of left and right ventricular hypertrophy in congenital heart disease," *Journal of Cardiac Failure*, vol. 14, no. 9, pp. 760–767, 2008.
- [7] D. Quaglietta, M. P. Belanger, and C. Wittnich, "Ventricle-specific metabolic differences in the newborn piglet myocardium in vivo and during arrested global ischemia," *Pediatric Research*, vol. 63, no. 1, pp. 15–19, 2008.
- [8] S. Champetier, A. Bojmehrani, J. Beaudoin, et al., "Gene profiling of left ventricle eccentric hypertrophy in aortic regurgitation in rats: rationale for targeting the β -adrenergic and renin-angiotensin systems," *American Journal of Physiology—Heart and Circulatory Physiology*, vol. 296, no. 3, pp. H669–H677, 2009.
- [9] M. Torrado, E. Lopez, A. Centeno, A. Castro-Beiras, and A. T. Mikhailov, "Left-right asymmetric ventricular expression of CARP in the piglet heart: regional response to experimental heart failure," *European Journal of Heart Failure*, vol. 6, no. 2, pp. 161–172, 2004.
- [10] M. Steinau and M. S. Rajeevan, "RNA profiling in peripheral blood cells by fluorescent differential display PCR," *Methods in Molecular Biology*, vol. 496, pp. 211–222, 2009.
- [11] K. Kokame, H. Kato, and T. Miyata, "Nonradioactive differential display cloning of genes induced by homocysteine in vascular endothelial cells," *Methods*, vol. 16, no. 4, pp. 434–443, 1998.
- [12] M. Torrado, R. Iglesias, B. Nespereira, A. Centeno, E. Lopez, and A. T. Mikhailov, "Intron retention generates ANKRD1 splice variants that are co-regulated with the main transcript in normal and failing myocardium," *Gene*, vol. 440, no. 1–2, pp. 28–41, 2009.
- [13] M. S. Rajeevan, D. G. Ranamukhaarachchi, S. D. Vernon, and E. R. Unger, "Use of real-time quantitative PCR to validate the results of cDNA array and differential display PCR technologies," *Methods*, vol. 25, no. 4, pp. 443–451, 2001.
- [14] M. Torrado, B. Nespereira, Y. Bouzamayor, A. Centeno, E. Lopez, and A. T. Mikhailov, "Differential atrial versus ventricular ANKRD1 gene expression is oppositely regulated at diastolic heart failure," *FEBS Letters*, vol. 580, no. 17, pp. 4182–4187, 2006.
- [15] M. Torrado, A. Centeno, E. López, and A. T. Mikhailov, "In vivo forced expression of myocardin in ventricular myocardium transiently impairs systolic performance in early neonatal pig heart," *International Journal of Developmental Biology*, vol. 53, no. 8–10, pp. 1457–1467, 2009.
- [16] S. Yang and P. Liang, "Global analysis of gene expression by differential display: a mathematical model," *Methods in Molecular Biology*, vol. 317, pp. 3–21, 2006.
- [17] B. D. Rodgers, J. P. Interlichia, D. K. Garikipati, et al., "Myostatin represses physiological hypertrophy of the heart and excitation-contraction coupling," *The Journal of Physiology*, vol. 587, pp. 4873–4886, 2009.
- [18] T. E. Callis, K. Pandya, H. Y. Seok, et al., "MicroRNA-208a is a regulator of cardiac hypertrophy and conduction in mice," *Journal of Clinical Investigation*, vol. 119, no. 9, pp. 2772–2786, 2009.
- [19] P. Liang and A. B. Pardee, "Differential display of eukaryotic messenger RNA by means of the polymerase chain reaction," *Science*, vol. 257, no. 5072, pp. 967–971, 1992.
- [20] M. M. Shen, "Identification of differentially expressed genes in mouse development using differential display and in situ hybridization," *Methods*, vol. 24, no. 1, pp. 15–27, 2001.
- [21] D. Tesfaye, S. Ponsuksili, K. Wimmers, M. Gilles, and K. Schellander, "Identification and quantification of differentially expressed transcripts in in vitro-produced bovine preimplantation stage embryos," *Molecular Reproduction and Development*, vol. 66, no. 2, pp. 105–114, 2003.
- [22] C. T. Beinlich, C. J. Rissinger, and H. E. Morgan, "Mechanisms of rapid growth in the neonatal pig heart," *Journal of Molecular and Cellular Cardiology*, vol. 27, no. 1, pp. 273–281, 1995.
- [23] C. Badorff, F. H. Seeger, A. M. Zeiher, and S. Dimmeler, "Glycogen synthase kinase β inhibits myocardin-dependent transcription and hypertrophy induction through site-specific phosphorylation," *Circulation Research*, vol. 97, no. 7, pp. 645–654, 2005.
- [24] W. Xing, T.-C. Zhang, D. Cao, et al., "Myocardin induces cardiomyocyte hypertrophy," *Circulation Research*, vol. 98, no. 8, pp. 1089–1097, 2006.
- [25] M. Torrado, E. Lopez, A. Centeno, et al., "Myocardin mRNA is augmented in the failing myocardium: expression profiling in the porcine model and human dilated cardiomyopathy," *Journal of Molecular Medicine*, vol. 81, no. 9, pp. 566–577, 2003.

- [26] M. O. Boluyt, L. O'Neill, A. L. Meredith, et al., "Alterations in cardiac gene expression during the transition from stable hypertrophy to heart failure: marked upregulation of genes encoding extracellular matrix components," *Circulation Research*, vol. 75, no. 1, pp. 23–32, 1994.
- [27] M. Zungu, M. E. Young, W. C. Stanley, and M. F. Essop, "Expression of mitochondrial regulatory genes parallels respiratory capacity and contractile function in a rat model of hypoxia-induced right ventricular hypertrophy," *Molecular and Cellular Biochemistry*, vol. 318, no. 1-2, pp. 175–181, 2008.
- [28] R. G. Kelly, M. Lemonnier, S. Zaffran, A. Munk, and M. E. Buckingham, "Cell history determines the maintenance of transcriptional differences between left and right ventricular cardiomyocytes in the developing mouse heart," *Journal of Cell Science*, vol. 116, no. 24, pp. 5005–5013, 2003.
- [29] B. G. Bruneau, Z.-Z. Bao, D. Fatkin, et al., "Cardiomyopathy in *Irx4*-deficient mice is preceded by abnormal ventricular gene expression," *Molecular and Cellular Biology*, vol. 21, no. 5, pp. 1730–1736, 2001.
- [30] H. Akazawa and I. Komuro, "Roles of cardiac transcription factors in cardiac hypertrophy," *Circulation Research*, vol. 92, no. 10, pp. 1079–1088, 2003.
- [31] P. A. Modesti, S. Vanni, I. Bertolozzi, et al., "Different growth factor activation in the right and left ventricles in experimental volume overload," *Hypertension*, vol. 43, no. 1, pp. 101–108, 2004.
- [32] J. Gallego-Delgado, S. B. Connolly, A. Lazaro, et al., "Transcriptome of hypertension-induced left ventricular hypertrophy and its regression by antihypertensive therapies," *Hypertension Research*, vol. 32, no. 5, pp. 347–357, 2009.
- [33] T. Urashima, M. Zhao, R. Wagner, et al., "Molecular and physiological characterization of RV remodeling in a murine model of pulmonary stenosis," *American Journal of Physiology—Heart and Circulatory Physiology*, vol. 295, no. 3, pp. H1351–H1368, 2008.

Review Article

Comparative Biomechanics of Thick Filaments and Thin Filaments with Functional Consequences for Muscle Contraction

Mark S. Miller,¹ Bertrand C. W. Tanner,¹ Lori R. Nyland,¹ and Jim O. Vigoreaux^{1,2}

¹Department of Molecular Physiology & Biophysics, University of Vermont, Burlington, VT 05405, USA

²Department of Biology, University of Vermont, Burlington, VT 05405, USA

Correspondence should be addressed to Jim O. Vigoreaux, jvigorea@uvm.edu

Received 29 January 2010; Accepted 26 March 2010

Academic Editor: Guy M. Benian

Copyright © 2010 Mark S. Miller et al. This is an open access article distributed under the Creative Commons Attribution License, which permits unrestricted use, distribution, and reproduction in any medium, provided the original work is properly cited.

The scaffold of striated muscle is predominantly comprised of myosin and actin polymers known as thick filaments and thin filaments, respectively. The roles these filaments play in muscle contraction are well known, but the extent to which variations in filament mechanical properties influence muscle function is not fully understood. Here we review information on the material properties of thick filaments, thin filaments, and their primary constituents; we also discuss ways in which mechanical properties of filaments impact muscle performance.

1. Introduction

Muscle is a remarkable and intriguing tissue that performs a broad range of specialized functions. While the mention of muscle may elicit images of physical strength, a quick sampling of the animal world reveals that muscle has extraordinary functional diversity and has evolved to provide power for lifting, speed for rapid locomotion, endurance for sustained activity, ultrafast vibrations for sound production, and braking action for stopping movement. This diversity relies upon muscle's active and passive viscoelastic properties providing a range of mechanical versatility in response to loads or forces that vary with time. Muscle is also a highly structured biological material, where proteins are organized into ordered filament arrays that combine to form successively higher ordered, repeated structures (sarcomeres, myofibrils, fibers, and fascicles). Research into muscle function occurs at nearly all levels of its hierarchical organization: single molecule, cell, whole organ, and organism (Figure 1). Pioneering studies on the mechanism of muscle contraction were conducted primarily at the level of the intact muscle, fiber, and to a lesser extent myofibrils (for review, see [1]). Over the past two decades, research on cellular mechanics, *in vitro* systems, and single molecules has been the dominant theme. Studies at the intermediate levels of filaments and myofibrils have been less common. Knowledge of the

biomechanical properties of filaments is important because they reveal how molecular properties scale up and how bulk properties of muscle fibers are dictated by nanoscale phenomena. Because muscle contraction is not simply the sum of individual motor molecules, understanding the properties at each organizational level is important to fully appreciate the behavior of this complex system.

Structural information has been extremely valuable for interpreting mechanical data. Titin, the large sarcomeric protein that extends from the Z-band to the M-line, provides a case in point, where knowledge of its molecular organization and domain structure expedited understanding of its role as a molecular spring (for review, see [26]). The advent of high-resolution structures of native thin filaments and thick filaments (e.g., see [27, 28]) provides an ideal opportunity to examine their mechanical properties and elucidate the molecular basis of their passive and active behavior. Here we will review what is known about the biomechanics of thick filaments, thin filaments, and their constituents, while providing a comparison of shared and unique properties among muscle types.

1.1. Functional Models and the Influence of Filament Compliance. Early models of muscle contraction described the mechanism of filament sliding using rigid thin filament and

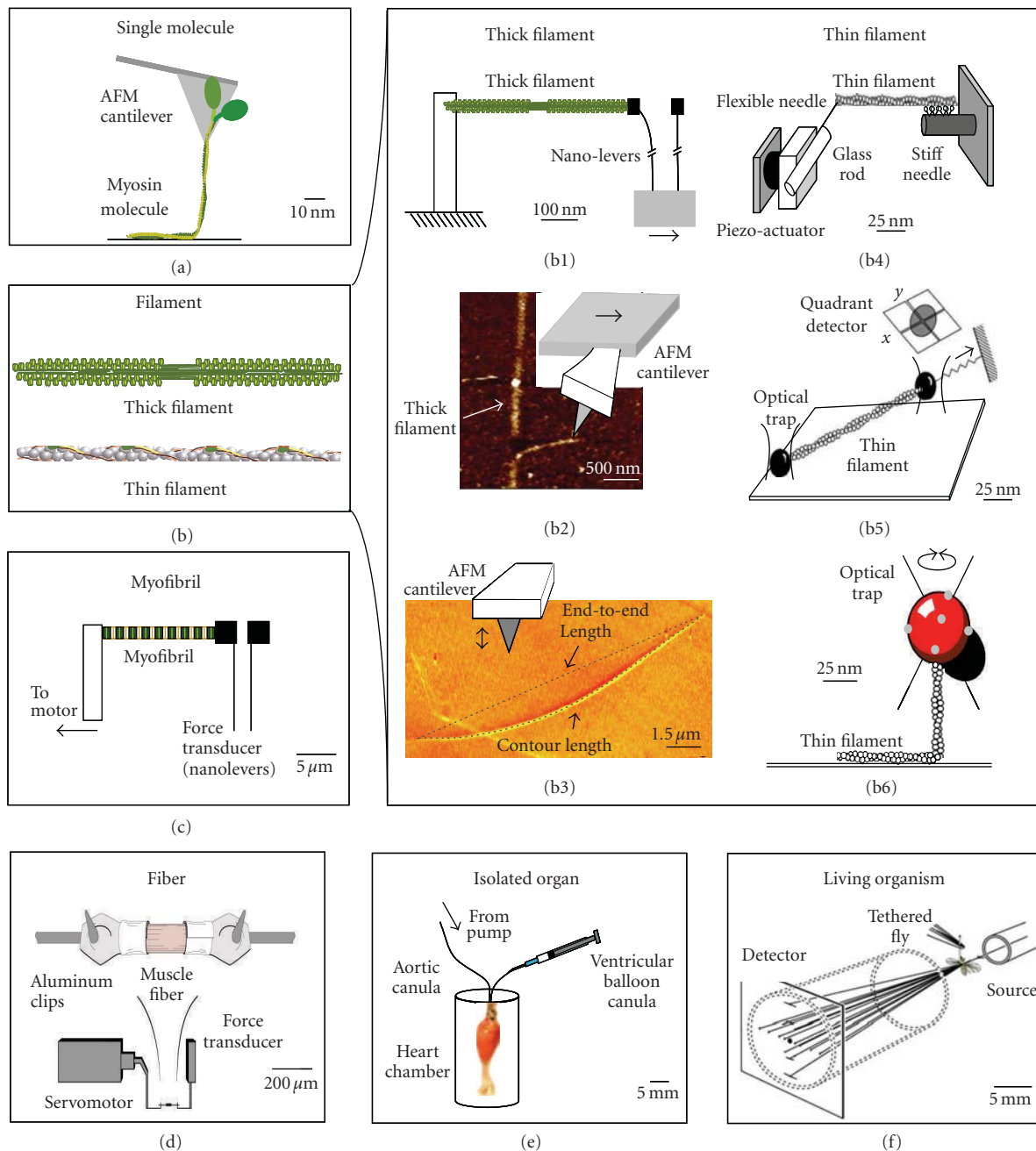


FIGURE 1: Some approaches used to measure the biomechanical properties of muscle, from single molecules to a living organism. Scale bars are approximate and are based on the size of the preparations, not the equipment. (a) Measurement of axial forces produced when pulling individual myosin molecules [2, 3] (figure adapted from [3]). (b) The biomechanical characteristics of thick filaments and thin filaments have been measured with a variety of techniques. (b1) Measurement of elastic properties of thick filaments with cantilevers [4, 5] (figure adapted from [5]). Thin filament elastic properties also have been measured in this way [6]. (b2) Shearing and bending of thick filaments with an AFM probe [7] (figure modified from [7]). (b3) Young's modulus and persistence length of thick filaments calculated from AFM images [8, 9] (figure modified from [9]). The persistence length of thin filaments has also been measured by monitoring their thermal fluctuations in shape [10–12]. (b4) Axial stiffness of thin filaments measured with a glass microneedle [13] (figure adapted from [13]). (b5) Flexural rigidity of thin filaments measured in an optical trap [14] (figure modified from [14]). (b6) Torsional rigidity of thin filaments [15, 16] (figure adapted from [16]). (c) Axial passive stiffness of myofibrils measured with cantilever force transducers [17–19] (adapted from [17]). (d) Elastic and viscous properties of skinned muscle fibers [20–22]. (e) Elastance of the heart [23, 24]. The scale bar here reflects a mouse heart. (f) X-ray diffraction of live *Drosophila* flight muscles [25].

thick filament backbones, attributing force production and the elastic response of muscle to actin-myosin cross-bridges [29]. Over the past two decades, a number of studies demonstrated that a considerable portion of sarcomere compliance resides in non-cross-bridge structures, revealed by low angle X-ray diffraction measurements of individual fibers [30, 31] and intact tissue within the organism (Figure 1(f)) [25]. Some estimate that approximately half of the sarcomere compliance resides in the thin filaments [13, 32, 33] and a smaller (20–30%), but significant, amount resides in the thick filaments [31]. Other studies suggest that the filament contribution to sarcomere elasticity may be much less (1–20%) [34, 35]. Nonetheless, these measurements of filament extensibility describe a fundamentally different mechanical system than one with rigid thick filaments and thin filaments, providing an opportunity for investigating the consequently altered mechanisms underlying force production within a lattice of compliant thick filaments and thin filaments.

Recent studies measuring thick filament and thin filament flexibility bestow a striking and fascinating level of complexity at the molecular and cellular level, as hundreds to millions of cross-bridges coordinate to produce force and shortening during muscle contraction. Much of this complexity builds on the behavior outlined by mathematical models of muscle contraction, implementing the well-accepted idea about cross-bridge elasticity being related to cycling kinetics [29, 36–38], although the earliest mathematical models assumed rigid (inextensible) filaments. Extending these ideas about strain-, load-, or position-dependent cross-bridge cycling to the level of filament behavior begins to illustrate that filament extensibility during force development may affect the relative position of actins and myosins along the filaments and the manner by which force is transmitted throughout the filament lattice [39–45].

Even though cross-bridges within a particular muscle likely follow similar chemomechanical processes (or a similar set of rules), filament compliance implies that cross-bridges may not behave identically along the length of a thick filament. As a simple example, consider a compliant thick filament with multiple myosins attached and producing force isometrically (i.e., in the absence of filament sliding) with a compliant thin filament. As these myosins produce greater and greater levels of force, the myosins and myosin binding sites along the actin filament will realign, changing their positions because the thick filaments and thin filaments are stretching in opposite directions towards the Z-band and M-line, respectively [41, 43]. Now imagine a similar situation where the filaments are rigid, resulting in no realignment of myosin and myosin binding sites along the thin filament and no dynamic redistribution of forces along the filament. In contrast, filament compliance permits realignment of actin filaments and myosin heads, along with a dynamic redistribution of forces as cross-bridges cycle. Filament compliance, therefore, alters behavior between cross-bridges because the forces generated by one cross-bridge affect the position and force experienced by its neighboring cross-bridges. This compliance provides a mechanism of cross-bridge recruitment that enhances force production and coordination of cross-bridge turnover [44], which can lead to an increase in

force production compared to a system of rigid filaments. The mechanisms underlying force production become even more intriguing when one envisions the molecular behavior associated with shortening and lengthening transients during normal contraction in the heart, skeletal, or insect flight muscles. For instance, coordinated mechanical and X-ray measurements using intact fibers show that muscle stiffness increases with a 2–6 nm stretch during tetanic contraction, which may be attributed to the attachment of additional myosin cross-bridge heads [46].

The elastic properties of filaments potentially influence how a striated muscle responds to stretch. Stretching of skeletal muscle results in a decrease in myosin ATPase and a braking action that is largely attributed to the attachment of the second myosin head of a dimer, which implies the attached motor acts as a strain sensor that detects the external stretch and recruits the attachment of its partner [46]. Recruitment of the second motor suggests a mechanical coupling between the two heads and/or a possible role for the rod in modulating motor activity, which may depend upon different mechanical properties of the filaments or regions of myosin [2, 47]. Conversely, stretching an insect flight muscle (and to some extent, cardiac muscle) leads to an increase in myosin ATPase activity and a delayed rise in tension [48]. Recent models suggest that activation by stretch (and high calcium) may be the result of breaking ATPase inhibiting interhead interactions [49]. The distinct response of the motors to stretch in skeletal versus insect flight muscle may result from differences in how they perceive tension, or the extent to which the filaments are strained and transmit tension to the heads. Regardless of the mechanism, differences in the mechanical behavior of thick filaments and thin filaments in different muscle types may modulate their distinct responses.

While the consequences of filament compliance on cross-bridge behavior have been largely illustrated through computational studies [40–45, 50], these studies illustrate the complex protein dynamics that likely exist for a myriad of cellular processes coordinating piconewton forces and nanometer motions among multiple proteins. These models have scaled up from a population of myosins along a single thick filament and thin filament pair [41, 43], to multiple filaments [42, 44, 50], and to a recent study probing the coordinated behavior of multiple sarcomeres [51]. In summary, these models indicate that filament compliance can lead to greater recruitment of force-bearing cross-bridges, and that the level of force produced by the muscle depends upon the relative stiffnesses of thick filaments, thin filaments, and cross-bridges. Filament compliance may also affect the overall rate of force development by modulating the force transmitted from cross-bridges into the myofilament lattice, where a more compliant lattice leads to decreased rates of force development [39, 43], in agreement with recent experimental results [52]. These models increasingly demonstrate that muscle is a classic example of a complex system stemming from coordinated behavior of cross-bridges, filaments, and sarcomeres to produce a complicated response from a set of rules [44, 51]. Advancements in computational resources, rapid data acquisition, and massive data storage increase the

feasibility of novel and important experiments probing and illustrating the molecular mechanisms responsible for this complicated behavior underlying muscle contraction.

2. Filament Biomechanics

2.1. Thick Filaments. Unlike thin filaments, the structure and molecular composition of thick filaments is quite diverse, especially among nonvertebrate species. In this group, thick filaments can have a hollow or solid core, single or multiple myosin isoforms, a low-to-high content of the core protein paramyosin [53], and distinct myosin associated proteins uniquely coupled with specific muscle types (for reviews, see [54–56]). Differences in molecular composition dictate structure and mechanical behavior but little is known about these differences throughout the nonvertebrate species and the extent to which they influence the contractile properties of muscle. Accumulating evidence indicates thick filaments change length under physiological forces (e.g., [25]) and these changes influence contractile properties. In addition, the potential for non-myosin thick filament proteins to influence motor behavior may be greater than previously anticipated, meaning functional alterations to muscle contraction may be accomplished through alterations of non-myosin proteins that can greatly increase the rate and range of adaptability in muscle.

The major component of most, but not all, thick filaments is myosin II, a dimeric protein characterized by two globular (motor) domains and an alpha-helical coiled-coil tail, or rod domain. Atomic force microscopy (AFM) studies on single myosin (Figure 1(a)) showed that the tail region is elastic [3]. The coiled-coil of rabbit skeletal muscle myosin undergoes a large structural transition at forces between 20 and 25 pN where short coiled-coil segments extend to about two and a half times their original length [3]. These force values are more consistent with estimates for actomyosin rigor bonds (10–30 pN) [57–60]. However, nucleotide state and loading rate also affect actomyosin bond strength, and some actomyosin-ADP bonds appear to rupture at forces higher than those of rigor bonds [60]. These single molecule measurements reveal some very complicated and interesting mechanochemical behavior that is fundamental to lengthening and shortening kinetics during muscle contraction, where estimated strengths of an actomyosin rigor bond may not set an upper limit on possible load borne by an actomyosin bond.

The structural transition of the coiled-coil is reversible up to ~30 pN on a timescale of less than one second and the refolding of the coiled-coil dissipates no energy [3], that is, the complete mechanical energy absorbed in the stretching cycle is given back during relaxation. The length extension is very close to the expected length difference between a folded coiled-coil and a completely unfolded polypeptide. These results suggest that myosin may be able to unfold and refold within the timescale and force regime of a contracting muscle. The force data was fit to a two-state model of coiled-coil elasticity in which unfolding occurs initially within short segments of the coiled-coil. Thus, local differences in

amino acid sequence that influence the strength of the intra- and inter-chain interactions determine the rate and energy of unfolding and refolding. This raises the possibility that differences in rod sequences among myosins from different muscle types may be functionally significant in defining rod elasticity. This also may explain why several rod binding proteins (e.g., M-line myomesin [61], A-band titin [62], A-band flightin [63], and C-zone myosin binding protein C (MyBP-C) [64]) only bind to specific sequences within the light meromyosin (LMM) region despite the high structural homogeneity of the LMM coiled-coil.

Additional observations about the elasticity of the myosin coiled-coil have come from AFM spectra using single rabbit skeletal muscle myosin and several of its proteolytic subfragments (single-headed myosin, myosin rod, S2, and LMM) [2]. All these molecules exhibited a similar force spectra consisting of a rise phase at low (<15 pN) forces, an intermediate (~15–100 pN) plateau phase, and a final exponential phase (>100 pN). The length of the rise phase was shortest in the LMM fragment suggesting that S2, and specifically the hinge connecting S2 and the LMM, is primarily responsible for increasing the length of the rise phase. The results from this study suggest a reversible, force-induced unfolding and extension of the S2 hinge could occur during muscle contraction [2]. It is unclear, however, the extent to which amino acid sequence variation in the S2 hinge region may be exploited to modulate muscle properties. In *Drosophila*, part of the S2 hinge is encoded by two alternative exons, one expressed in slow (embryonic) muscle and the other expressed in fast (adult jump and flight) muscle. Studies have tested whether the expression of the slow muscle S2 hinge in an otherwise fast muscle myosin affected myofibril [17] and fiber [20] properties. Expression of the slow muscle S2 hinge produced several structural changes, including an increased myosin rod length, A-band length, and sarcomere length [65]. Despite these structural changes, myofibril (Figure 1(c)) and fiber (Figure 1(d)) mechanics showed that passive properties (tension as well as elastic and viscous modulus) were not affected even though the embryonic S2 hinge was predicted to have a higher propensity to form a coiled-coil than the adult S2 hinge. Myosin kinetics under active conditions were altered by changing the S2 hinge and were consistent with this region increasing the length of the myosin rod [20]. These structural and functional changes were manifested at the whole fly level as a decreased wing-beat frequency and flight performance [20, 65], providing an example as to how changes at the molecule level can affect performance and function at the whole organism level. Notably, the observed structural changes indicate that the myosin rod plays an important role in thick filament organization during myofibrillogenesis.

Force-extension studies, similar to the AFM work described above, have been conducted with reconstituted myosin filaments (from rabbit psoas muscle) [4] and non-vertebrate (mussel and crab) native filaments [5] using nanofabricated cantilevers (Figure 1(b1)). Force elongation curves for the skeletal myosin filaments showed that stiffness increased with load and the filaments were more compliant

at low forces. Under load conditions of approximately 100 pN the filaments exhibit an elastic response. Imposed loads between ~240 and 440 pN resulted in strains of ~1.1 to 1.5%. These results are consistent with changes in spacing of the 14.3 nm reflection (i.e., the longitudinal distance between myosin heads) previously reported from real time X-ray diffraction data of actively contracting frog skeletal muscle [30]. In contrast, native thick filaments isolated from blue mussels (*Mytilus edulis*) and horseshoe crabs (*Limulus polyphemus*) are substantially more flexible. Blue mussel thick filaments (length: 10 to 50 μm) were elastic up to stretches of ~23% of the filament length but did not break until stretched 2-3 times the filament length. The much shorter horseshoe crab thick filaments (length: 4 to 5 μm) were elastic up to stretches of ~66% of the filament length but did not break until stretched 5-6 times the filament length [5]. These large elastic deformations were repeatable, although a significant amount of hysteresis was evident in both filament types. The elastic behavior is produced at low (~1 to 10 nN) forces that are within the estimated physiological range of tension produced by the thick filaments. As suggested by the single myosin molecule studies, the extensibility of the thick filament at low forces is likely to arise from stretching and uncoiling of segments of the rod domain. In addition, shearing between myosin rods is likely to contribute to filament elasticity [7].

While the degree to which thick filaments deform during contraction is difficult to quantify, there is evidence suggesting *Limulus* thick filaments undergo large changes in length during contraction [66]. Using *Mytilus* thick filaments, length changes were found to occur in steps of 2.7 nm and integer multiples during lengthening and shortening [67]. The stepwise length change was predicted to occur from the charge distribution along the myosin rod and to contribute to sarcomere length changes and force generation in contracting muscle (see [67] for discussion). Lastly, the yield strength (i.e., the force required to break the filament) of *Mytilus* thick filaments was not much higher than the estimated physiological force suggesting that the force range experienced by these filaments *in vivo* is rather narrow. Interestingly, the yield strength of *Drosophila* flight muscle thick filaments (~8–17 nN), measured by stretching filaments with an AFM tip [7] (Figure 1(b2)), is comparable to that of horseshoe crab (~7 nN) and mussel (~18 nN), suggesting that regardless of their molecular composition, the upper limit yield strength of thick filaments may not exceed 20 nN. In summary, the piconewton forces produced by multiple actomyosin interactions per thick filament produce the requisite forces to produce nanometer deformations of thick filaments, but are likely much too small to compromise the structural integrity of native filaments. These studies provide evidence that thick filament extensibility is part of muscle contraction across a wide range of species.

The greater extensibility of the blue mussel and horseshoe crab thick filaments mentioned above may result from their high content of paramyosin (and high paramyosin to myosin ratio) when compared to thick filaments from vertebrate muscle (which lack paramyosin) or *Drosophila* indirect flight muscle (IFM; which have very low amounts

of paramyosin) [68]. Paramyosin is an α -helical coiled-coil protein, similar to the myosin rod, that forms a core onto which the myosin molecules pack to form the thick filament [68]. The ability for paramyosin to directly influence filament compliance is supported by the finding that disrupting phosphorylation sites in *Drosophila* paramyosin reduced IFM myofibril passive elastic modulus by 15% [17], consistent with a previous study that found similar reductions in passive, active, and rigor fiber stiffness [21]. This relatively large reduction was unexpected given that the major contributor to passive stiffness is the connecting filaments [69], in light of the assumption that thick filaments are more than 15 times stiffer than connecting filaments [17]. One possibility is that paramyosin serves as, or is part of, an anchoring site for connecting filaments on thick filaments. It is interesting to note that thick filaments from non-vertebrate muscles exhibit a wide range of lengths and widths and that the paramyosin to myosin ratio tends to increase proportionally with filament length [53]. The large extensibility of the long (>4 μm) non-vertebrate filaments is also consistent with the suggestion that paramyosin directly influences filament stiffness.

Other notable non-myosin thick filament proteins implicated in filament stiffness include MyBP-C in cardiac thick filaments and flightin in IFM thick filaments. MyBP-C, a modular protein consisting of immunoglobulin-like C2-type domains and fibronectin type-III domains, is found in the nine distal stripes of the C-zone region of the cardiac A band [70]. Early studies demonstrated that MyBP-C considerably stiffened the filament's calculated persistence length (an index of flexural rigidity) from electron micrographs of reconstituted filaments in the presence and absence of MyBP-C [71]. The mechanical contribution of these proteins to native thick filament properties has become possible with the availability and viability of mutant flies and transgenic mice, such as the cMyBP-C^{ut} mice that fail to express cardiac MyBP-C [72]. Using images obtained by AFM, Nyland et al. calculated the persistence length of native cardiac thick filaments with and without MyBP-C [8] (Table 1 and Figure 1(b3)). Aside from a small but significantly shorter length ($1.48 \pm 0.02 \mu\text{m}$ t/t versus $1.56 \pm 0.02 \mu\text{m}$ +/+), thick filaments lacking MyBP-C exhibited an ~40% reduction in specific persistence length and Young's (elastic) modulus. Furthermore, they showed that filaments lacking MyBP-C had a greater bending propensity throughout the C zone suggesting that MyBP-C is directly involved in stiffening the filament. The increased compliance of thick filaments lacking MyBP-C may explain why skinned papillary muscle from t/t mice showed a 50% reduction in the stiffness of rigor-bridge-attached thick filaments [73] and why hearts from t/t mice exhibited an abbreviated and reduced systolic elastance (Figure 1(e)) [23]. Altogether, these results illustrate the important role of MyBP-C in modulating cardiac output and provide a plausible mechanism for understanding how some MyBP-C mutations may lead to cardiomyopathies.

Drosophila IFM thick filaments have flightin, a protein that is distributed throughout most of the overlap region of the A band [74]. Similar to mice lacking MyBP-C, thick filaments from mutant flies unable to express flightin in

TABLE 1: Mechanical properties of thick filaments and thin filaments.

Filament	Measurement	Method	Muscle Source	Stiffness (pN/nm)	Young's Modulus (GPa)	Persistence Length (μm)
Thick ^(a)	Longitudinal stiffness	X-ray diffraction	Frog skeletal	252	1.9 [30]	642
Thick ^(a)	Flexural rigidity	AFM	Mouse cardiac	165	0.8	639 [8]
Thick ^(a)	Flexural rigidity	AFM	Fruit fly IFM	442	3.0	1742 [9]
Actin ^(b)	Flexural rigidity	thermal fluctuations	Rabbit skeletal	19	0.8	9 [10]
Actin* ^(b)	Flexural rigidity	thermal fluctuations	Rabbit skeletal	37	1.5	18 [10, 12]
Actin* ^(b)	Longitudinal stiffness	microneedle	Rabbit skeletal	44 [13]	1.8	21
Actin* + Tm ^(c)	Longitudinal stiffness	microneedle	Rabbit skeletal	65 [13]	1.3	63
Actin + Tm + Cad ^(c)	Flexural rigidity	thermal fluctuations	Rabbit skeletal + turkey gizzard	21	0.4	20 [10]
Thin ^(c)	Fiber longitudinal stiffness	X-ray diffraction	Frog skeletal	125	2.5 [30]	121
Thin ^(c)	Fiber longitudinal stiffness	mechanics	Rabbit skeletal	46–68 [32]	0.9–1.4	44–66

Measured values are listed in bold, along with the referenced study. Stiffness values represent the spring constant for a filament length (L) of $1000 \mu\text{m}$. To compare between measurements, the calculations for stiffness (k), Young's modulus (E), and persistence length (L_p) required an estimate of filament geometry listed in the footnotes. Otherwise, $E = kL/A_c$, where A_c is cross-sectional area [13] and $L_p = EI/k_B T$, where I is the second moment of inertia, k_B is the Boltzman constant, and temperature (T) was 300 K [129].

^(a)Calculations assumed a solid, cylindrical filament backbone of radius 6.5 nm for skeletal thick filaments [30] and 8 nm [130] for cardiac thick filaments. For insect flight muscle filaments, calculations assumed a hollow cylinder with an outer radius of 7.5 nm and an inner radius of 3 nm [131].

^(b)Calculations for undecorated actin filaments assumed a solid, cylindrical filament backbone of radius 2.8 nm [13]. * In the presence of phalloidin.

^(c)Calculations for thin filaments and decorated actin filaments assumed a solid, cylindrical filament backbone of radius 4 nm [30].

Abbreviations: Tm: Tropomyosin; Cad: Caldesmon; Thin: Native thin filament; Thick: Native thick filament; AFM: Atomic force microscope; IFM: Indirect flight muscles.

their IFM (fln^0) were significantly more compliant and had larger bend angles than their wild-type counterparts [9]. Calculations of persistence length from AFM images between fln^0 and wild-type filaments from the same age flies revealed that flightin increases total thick filament bending stiffness by ~ 30 – 45% , similar to the MyBP-C contribution to cardiac thick filaments [9]. These results are consistent with a model in which flightin (and similarly, MyBP-C) provide lateral reinforcement to the thick filaments via their interaction with a common LMM site [63, 64]. The existence of connections between myosin rods in *Drosophila* IFM filaments was further suggested by the shear modulus obtained from bending the filaments with the tip of an AFM cantilever [7]. The values ranged from 3 MPa, a value similar to that obtained for purely coiled-coil filaments [75], to ~ 13 MPa. The higher values are thought to arise from the presence of proteins that cross link neighboring coiled-coils. Flightin, along with another A band protein myofilin [76] could fulfill the cross-linking role in *Drosophila* flight muscles, helping to provide the high stiffness typical of insect flight muscle. The high stiffness of insect flight muscles facilitates stretch activation and the fast oscillatory contraction necessary to beat their wings up to several hundred times per second [48].

The effect of flightin on thick filament mechanics is also clearly manifested at the level of the cell. A comparison of the mechanical properties of skinned flight muscle fibers from fln^0 and wild-type IFM revealed that passive and dynamic stiffness are reduced by more than 50% in fln^0 fibers [22]. This large increase in sarcomere compliance resulted in fibers

that absorbed, rather than produced, work. Deficits in whole body locomotion were also evident as flies carrying the flightin mutation were unable to beat their wings and therefore flightless [74]. These studies point to an important role for flightin in reinforcing the structural integrity of the thick filaments and enhancing the production or transmission of force from the cross-bridge to the thorax to elevate flight performance. These studies demonstrate that although thick filament compliance can increase force generation compared to rigid filaments, too much compliance greatly reduces fiber performance and negatively impacts the ability of the animal to move.

Comparing thick filament persistence length between fiber types and species provides an opportunity to examine how the mechanical properties of thick filaments relate to the mechanical performance of the muscle or organ. Persistence length is a commonly used index of the flexibility of a polymer that conveys valuable information about a polymer's mechanical properties. Given that there are different methods of obtaining persistence length, one must keep in mind that differences in values may be the result of variations in assumptions or experimental procedures. Thus, a direct comparison of absolute values obtained by different investigators using various techniques could be misleading and should, at best, be considered as a general approximation. The persistence length values for cardiac thick filaments and IFM thick filaments reported in Table 1 were obtained using a similar AFM approach [8, 9], thus a direct comparison is more meaningful in this

case despite some differences in experimental conditions. The comparison indicates that IFM filaments were almost three times as stiff as cardiac filaments, in proportion to the elastic moduli differences found at the myofibrillar level [18]. The difference in persistence length is quite remarkable especially when one considers the hollow core of the insect flight muscle filaments. While the structure of the insect filaments is not yet known in detail, their extraordinary high stiffness suggests the existence of structures that enhance the rigidity of the myosin rods or that form an inner rigid core. A rigid core consisting of paramyosin filaments held together by cross-linking proteins has been suggested for nematode (*C. elegans*) body wall thick filaments [71]. However, the persistence length calculated for nematode filaments from electron micrographs is only ~15% of that calculated for IFM filaments by AFM. In that same study, persistence length calculated for rabbit psoas muscle thick filaments is approximately 25-fold less than that calculated for frog skeletal muscle from fiber X-ray diffraction studies (Table 1). This difference may arise from the use of a methodological approach that relied only on measured contour and end-to-end length of the filament [71], rather than the most common and statistically robust approach of measuring filament segments of increasing length [8, 9, 77]. Clearly, an understanding of the experimental techniques and procedures is required to facilitate comparisons within and across different studies. The estimates listed in Table 1 summarize measurements performed under similar conditions wherever possible, and the versatility of persistence length for comparing relative flexibilities of biological polymers and nonbiological materials is demonstrated in Table 2. Interestingly, the bending stiffness of thick filaments is quite large, especially the insect IFM filaments, which are near the range of nanotubes and microtubules (Table 2).

2.2. Thin Filaments. Early studies by Oosawa and colleagues revealed that actin filaments are compliant *in vitro* as well as in the myofibril, prompting speculation that changes in thin filament length may contribute to muscle contraction [78, 79]. More recent studies using X-ray diffraction of frog sartorius and semitendinosus muscles estimate that ~40–50% of the sarcomere compliance of actively contracting muscle originates from the thin filaments [30, 31]. Measurements of mechanical compliance in rabbit psoas are consistent with these X-ray studies, showing that thin filaments contribute ~44% to sarcomere compliance under active conditions [32]. However, one study with carbodiimide-cross-linked rabbit fibers found virtually no compliance in the actin filaments, with all the compliance in the myosin motor domain [34]. Mechanical experiments in frog tibialis anterior muscle suggest a smaller thin filament contribution to the total sarcomere compliance (~20–29%) [35, 80], an estimate that could be significantly higher if thin filament compliance were nonlinear [35] (thus, more consistent with the values from X-ray studies). Thin filament extensibility was determined to be ~50% of the sarcomere compliance in active muscle using single actin filaments reconstituted from rabbit psoas tissue [13]. Overall, these studies suggest that the thin filament

TABLE 2: Range of persistence length for biological polymers and nanotubes.

Material	Persistence Length (μm)	Comments and References
Silk	0.0004	Recombinant spider dragline silk nanofibers [132]
Titin	0.0007–0.04	For intact (rabbit skeletal) protein, individual domains, and elastic and inelastic regions [133–135]
Hyaluronan	0.0045	Articular cartilage [136]
Collagen	0.0112–0.057	Types I, II, III [136, 137]
Projectin	0.030	Lethocerus flight muscle [138]
Mucins	0.036	Human ocular [139]
Kettin	0.045	Recombinant fragments [138]
DNA	0.053	<3000 bp [140]
Intermediate filaments	1	<i>In vitro</i> polymerized human vimentin [77]
Cofilactin	2.2	<i>In vitro</i> polymerized [92]
Actin	9.0–17.7	<i>In vitro</i> polymerized with or without phalloidin [10, 12, 92, 141]
Nanotubes	17–32	Single walled carbon nanotubes [142]
Flagellar filaments	2.4–41.1	From bacteria [129]
Thin filaments	44–121	See Table 1
Thick filaments	27–1742	From various species and muscle types [8, 9, 71]
Microtubules	110–5200	<i>In vitro</i> polymerized with taxol or paclitaxel [12, 141, 143]

contributes ~20–50% to the total sarcomere compliance, indicating that the extension of actin plays a significant role in muscle contraction.

The mechanical properties of reconstituted actin polymers, with and without regulatory proteins, have been studied extensively using a variety of methods. Investigating the mechanical effects of adding different regulatory proteins to bare actin provides insight into the function and performance of the native thin filament. The two primary sources of actin were rabbit [10, 11, 13] and chicken skeletal muscle [11], with the actin binding proteins being derived from rabbit skeletal muscle [10, 13], turkey gizzards (smooth muscle) [10], or other sources [11]. Since actin and regulatory proteins are highly conserved, species differences are seldom considered important even though mutations of single amino acids can considerably affect contractility. Persistence length measurements of fluorescent rhodamine-actin filaments indicate that flexural rigidity increases with the addition of tropomyosin alone [10, 11, 13] and tropomyosin-troponin with or without Ca^{2+} [10] (Table 1). Isoform specific effects that have been noted in that smooth muscle tropomyosin had a lesser effect on persistence length than skeletal muscle tropomyosin [10, 11]. The flexural rigidity of actin with tropomyosin-troponin decreased with

the addition of Ca^{2+} , remaining above that of actin alone, and suggests that thin filaments become more flexible upon activation [10]. The increased compliance may allow for better alignment of actin with the myosin heads, providing more binding sites for myosin compared to a rigid thin filament. Flexural rigidity of fluorescent rhodamine-actin filaments increases with the addition of phalloidin [10, 11], a peptide commonly used to stabilize actin filaments, and could therefore significantly affect experimental results when this peptide is present. Notably, studies where phalloidin was added to the actin filaments still indicate significant actin filament compliance using a glass microneedle (Figure 1(b4)) with rabbit actin [13], the optical trap (Figure 1(b5)) with chicken pectoralis [14], and microfabricated cantilevers [6]. Other factors were found not to dramatically affect the longitudinal flexibility of filamentous actin including the presence of metal ions Mg^{2+} or Ca^{2+} , ionic strength ranging from 5 to 100 mM, or whether the filaments were assembled from ADP or ATP monomers [10]. While not explored, post-translational modification of tropomyosin and other actin-binding proteins may play a role in modulating thin filament mechanical properties.

The torsional rigidity of actin with phalloidin (Figure 1(b6)) was found to be three times higher for bound Ca^{2+} compared with bound Mg^{2+} while the flexural rigidity remained unchanged [15]. This raises the possibility that these cations, as well as myosin binding, may influence thin filament properties, potentially promoting more effective muscle contraction by modulating the torsional rigidity of the filaments [81]. Other studies show actin filaments with phalloidin to be more flexible and less durable in torsion, compared to bending or stretching [16, 82]. Thus, changes in the twist of the actin helix resulting from the attachment of cross-bridges may propagate considerable distances along the filament, contributing to a suite of cooperative mechanisms that coordinate or amplify active force generation [83–86].

Phosphorylation may also play an important role in regulating actin filament stiffness. An actin-binding C terminal fragment of caldesmon, a protein that regulates smooth muscle contraction through its binding to actin, myosin and tropomyosin [87], increases persistence length in a phosphorylation-dependent manner [11]. Phosphorylation of tropomyosin at Ser 283 (the second-to-last residue at the C-terminus) has been shown to increase the strength of the tropomyosin head-to-tail interaction and the tropomyosin-troponin T interaction, and may also modulate tropomyosin's affinity for actin [88, 89]. Other studies have shown that tropomyosin phosphorylation is essential for long range cooperative activation along the thin filament [90]. Whether this phosphorylation effect is achieved through changes in thin filament mechanical properties remains to be established.

In contrast to most actin binding proteins that increase filament radius and mass, cofilin, a protein known to sever actin filaments, decreases actin filament torsional [91] and flexural rigidity [92], reflected as a fivefold decrease in persistence length. Cofilin reduces stiffness by changing the filament elasticity and geometry, hypothetically through a

reorganization of the actin subdomain 2 [92]. Similarly, formins, a family of proteins that are associated with the polymerization of actin, decrease the flexural rigidity of actin filaments, suggesting these proteins regulate actin filament conformation and may affect the ability of actin binding proteins to attach [93]. While these actin binding proteins do not participate in muscle contraction, understanding their effects increases our knowledge of thin filament mechanics and may lead to important discoveries surrounding myofibrillogenesis and/or repair mechanisms.

2.3. Other Sarcomeric Structures. The extent to which thin filament and thick filament compliance contributes to active force production *in vivo* is likely determined by the nature of their connections to, and the properties of, other sarcomeric structures, namely Z-bands, M-bands and filaments of nebulin (a large modular actin binding protein with multiple functions [94]), titin, and related proteins (e.g., the connecting filament proteins kettin and projectin that in insect flight muscle connect the thick filaments to the Z-line [95]). Many studies have examined the mechanical behavior of several of these individual components (for reviews, see [96–98]) but a limited number of studies have explored whether there is a correlation between fiber type and expression of specific isoform sets among these different elastic structures (e.g., [99]). Despite these efforts, we lack a general understanding of how individual component properties are related to those of other sarcomeric components or how, for example, the expression of titin length isoforms in a particular fiber type is tuned mechanically to the molecular composition of the thick filament and its mechanical capabilities. These relationships may play a significant role in the developing heart and diseased heart, where shifts in titin isoforms are correlated with changes in cardiac output [100–102]. Similarly, the relation between connecting filament (kettin and projectin) isoforms and thick filament composition in insect flight muscle is likely to be significant given the large contribution of the connecting filaments to active properties in this muscle type [69, 103].

2.4. Open Questions, Interpretations, and Future Studies. Recent studies suggest that the functional unit of contraction is the half-sarcomere [104]. As we inch closer towards elucidating the complete catalogue of proteins that constitute this elaborate structure and a better understanding of their mechanical properties, a clearer picture of the mechanism of muscle contraction will benefit from merging information from bottom-up approaches such as those described here, and the more classical top-down (fiber and muscle mechanical/structural) approaches. The functional significance of filament compliance and its role in the evolutionary divergence of striated muscle remain open questions. As reviewed here, it is becoming increasingly clear that from a mechanical perspective, all thin filaments and thick filaments are not created equal and that large differences exist among thick filaments from different muscle types. We envision multiple possibilities, not mutually exclusive, for

how filament compliance could come into play in defining the functional properties of muscle.

(i) Filament strain and stiffness influence the placement of myosin heads along the thin filament with implications for cooperative activation, regulatory mechanisms, and overall force production. A compliant filament (both longitudinal and torsional) may expand the axial range for myosin motors to find target zones along actin, increasing the probability of cross-bridge binding. These processes may be modulated by the number of actins exposed along the thin filament, following Ca^{2+} activation of the troponin/tropomyosin complex, differentially affecting contractile dynamics on a twitch-to-twitch or beat-to-beat basis depending upon muscle type [105–107]. While stretch activation is present in all muscles (where force transiently increases to a greater level following a stretch), it affects most strongly impact oscillatory muscle systems that are constantly undergoing length changes, such as in insect flight muscle or cardiac muscle. Although not completely understood, these cooperative mechanisms involving the spatial and mechanical properties of the filaments and cross-bridges may fundamentally underlie the Frank-Starling relationship in the heart [108].

(ii) Thick filament stiffness and/or strain influence the orientation and kinetic properties of the motor domain. Significant myosin loss has been found with aging [109], cancer [110], heart failure [111–113], chronic obstructive pulmonary disease [114], acute quadriplegia [115], and severe spinal injury [116]. The myofibrillar protein loss appears to be specific for myosin as several studies have shown no alterations in other proteins, such as actin. This loss of myosin may increase thick filament strain through a reduction of thick filament stiffness and/or decrease thin filament and thick filament strain since the number of heads available for binding are reduced. The modulation of thick filament and thin filament strain could lead to alterations in myosin kinetics, as suggested by recent work in heart failure patients [112]. Although not directly measured, orientation changes in the myosin head relative to actin via thick filament strain have been suggested by experiments in insects to explain changes in passive and active fiber properties due to sarcomere lengthening [103] and aging [117]. Thus, altering thick filament stiffness may be a means of regulating fiber contractile properties; whether this result is a consequence of aging and/or disease or is an adaptation to these specific conditions is still unknown.

(iii) Filament stiffness defines muscle's ability to recycle energy, for example, in the form of elastic recoil in oscillatory systems such as the vertebrate heart and the insect flight muscle. Flying insects rely on elastic recoil to lower the energetic cost of flight [118]. The extent to which an insect relies on muscle to store elastic energy for inertial work depends on its size, wing beat frequency and mode of operation (i.e., synchronous versus asynchronous) [119]. Varying the stiffness of the thoracic musculature, via the stiffness of its underlying filaments, may be one way mother nature adjusts to the challenge of energetically expensive locomotive activities.

(iv) Filament stiffness influences muscle performance by defining the effective transmission of actomyosin forces to

end-connecting structures. Increasing evidence points to the Z-band (and to a lesser extent the M-line) as the nexus of signaling pathways that define the muscle's short- and long-term response to physiological demand [120–122]. Sensitive stress or strain sensors reside in the Z-band, particularly in cardiac muscle, where they integrate and coordinate the responses to internal and external mechanical signals. Mutations and genetic polymorphisms in several Z-band associated proteins have been implicated in adaptive and maladaptive remodeling via complex, mechanically activated cell signaling events whose details are just beginning to be elucidated [120]. More studies are needed to identify how differences in the mechanical properties of thin filaments and thick filaments are interpreted by the elaborate sensing and signaling complexes that reside in the Z-bands and M-lines.

(v) Filament stiffness and the corresponding strains induced during muscle contraction promote sarcomeric stability and influence muscle's ability to sustain external forces or repetitive cycles of high force. An extreme example is seen in *Drosophila* IFM where the absence of flightin leads to decreased thick filament stiffness and stability and complete loss of muscle's ability to sustain force [9, 74, 123]. Another example in skeletal muscles is that fast contracting fibers are more easily damaged with large external forces [124] and have increased sarcomere disarray and greater force reduction after multiple contractions, especially near physiological temperatures [125], compared to slow oxidative fibers. These skeletal muscle fiber type differences in stability may be due to different loads being transmitted to the thick filaments during high force or repetitive loading given that skeletal muscles express different proteins in the M-line [126] and Z-band [97, 120], as well as different isoforms of titin [99] based upon the type of myosin heavy chain (MHC) expressed (e.g., MHC I or slow contracting versus MHC IIA or fast contracting). In addition, thick filament stiffness may be altered with fiber type due to different intramolecular interactions between myosin rods because of their varying amino acid sequences [127]. In summary, the thick filaments from different fiber types may vary in their stiffness and the forces experienced during loading, altering their stability and susceptibility to damage.

(vi) The mechanical properties of the filaments may influence how they align during myofibrillogenesis, and whether the resulting structure is a simple lattice or a superlattice [128].

This list of possibilities is by no means exhaustive and many important questions remain to be answered. As we learn more about the molecular composition and structure of filaments from different muscle types and apply some of the aforementioned techniques to elucidate their material properties and those of their underlying components, we will improve our understanding of the microscopic principles that quantitatively and qualitatively define the salient features of muscle and gain an appreciation for the remarkable versatility of this most amazing *machina carnis*. This, in turn, will contribute to our knowledge of the evolution of muscle, its capacity for adaptation, and susceptibility to disease, and open doors for using muscle filaments as a paradigm for biologically inspired materials.

Acknowledgments

M. S. Miller, B. C. W. Tanner, and L. R. Nyland contributed equally to this paper. The authors thank members of the Vigoreaux laboratory for helpful comments. They acknowledge the following support: NSF IOS-0718417 to J. O. Vigoreaux, NIH K01 Mentored Research Grant to M. S. Miller (AG-031303), and NSF Postdoctoral Fellowship in Biology to B. C. W. Tanner (DBI-0905830). The content is solely the responsibility of the authors and does not necessarily represent the official view of the National Institute on Aging, National Institutes of Health, or National Science Foundation.

References

- [1] H. E. Huxley, "Fifty years of muscle and the sliding filament hypothesis," *European Journal of Biochemistry*, vol. 271, no. 8, pp. 1403–1415, 2004.
- [2] D. D. Root, V. K. Yadavalli, J. G. Forbes, and K. Wang, "Coiled-coil nanomechanics and uncoiling and unfolding of the superhelix and α -helices of myosin," *Biophysical Journal*, vol. 90, no. 8, pp. 2852–2866, 2006.
- [3] I. Schwaiger, C. Sattler, D. R. Hostetter, and M. Rief, "The myosin coiled-coil is a truly elastic protein structure," *Nature Materials*, vol. 1, no. 4, pp. 232–235, 2002.
- [4] D. Dunaway, M. Fauver, and G. Pollack, "Direct measurement of single synthetic vertebrate thick filament elasticity using nanofabricated cantilevers," *Biophysical Journal*, vol. 82, no. 6, pp. 3128–3133, 2002.
- [5] T. Neumann, M. Fauver, and G. H. Pollack, "Elastic properties of isolated thick filaments measured by nanofabricated cantilevers," *Biophysical Journal*, vol. 75, no. 2, pp. 938–947, 1998.
- [6] X. Liu and G. H. Pollack, "Mechanics of F-actin characterized with microfabricated cantilevers," *Biophysical Journal*, vol. 83, no. 5, pp. 2705–2715, 2002.
- [7] L. Kreplak, L. R. Nyland, J. L. Contompasis, and J. O. Vigoreaux, "Nanomechanics of native thick filaments from indirect flight muscles," *Journal of Molecular Biology*, vol. 386, no. 5, pp. 1403–1410, 2009.
- [8] L. R. Nyland, B. M. Palmer, Z. Chen, et al., "Cardiac myosin binding protein-C is essential for thick-filament stability and flexural rigidity," *Biophysical Journal*, vol. 96, no. 8, pp. 3273–3280, 2009.
- [9] J. L. Contompasis, L. R. Nyland, D. W. Maughan, and J. O. Vigoreaux, "Flightin is necessary for length determination, structural integrity, and large bending stiffness of insect flight muscle thick filaments," *Journal of Molecular Biology*, vol. 395, no. 2, pp. 340–348, 2010.
- [10] H. Isambert, P. Venier, A. C. Maggs, et al., "Flexibility of actin filaments derived from thermal fluctuations. Effect of bound nucleotide, phalloidin, and muscle regulatory proteins," *Journal of Biological Chemistry*, vol. 270, no. 19, pp. 11437–11444, 1995.
- [11] M. J. Greenberg, C.-L. Wang, W. Lehman, and J. R. Moore, "Modulation of actin mechanics by caldesmon and tropomyosin," *Cell Motility and the Cytoskeleton*, vol. 65, no. 2, pp. 156–164, 2008.
- [12] F. Gittes, B. Mickey, J. Nettleton, and J. Howard, "Flexural rigidity of microtubules and actin filaments measured from thermal fluctuations in shape," *Journal of Cell Biology*, vol. 120, no. 4, pp. 923–934, 1993.
- [13] H. Kojima, A. Ishijima, and T. Yanagida, "Direct measurement of stiffness of single actin filaments with and without tropomyosin by in vitro nanomanipulation," *Proceedings of the National Academy of Sciences of the United States of America*, vol. 91, no. 26, pp. 12962–12966, 1994.
- [14] D. E. Dupuis, W. H. Guilford, J. Wu, and D. M. Warshaw, "Actin filament mechanics in the laser trap," *Journal of Muscle Research and Cell Motility*, vol. 18, no. 1, pp. 17–30, 1997.
- [15] R. Yasuda, H. Miyata, and K. Kinoshita Jr., "Direct measurement of the torsional rigidity of single actin filaments," *Journal of Molecular Biology*, vol. 263, no. 2, pp. 227–236, 1996.
- [16] Y. Tsuda, H. Yasutake, A. Ishiura, and T. Yanagida, "Torsional rigidity of single actin filaments and actin-actin bond breaking force under torsion measured directly by in vitro micromanipulation," *Proceedings of the National Academy of Sciences of the United States of America*, vol. 93, no. 23, pp. 12937–12942, 1996.
- [17] Y. Hao, M. S. Miller, D. M. Swank, et al., "Passive stiffness in *Drosophila* indirect flight muscle reduced by disrupting paramyosin phosphorylation, but not by embryonic myosin S2 hinge substitution," *Biophysical Journal*, vol. 91, no. 12, pp. 4500–4506, 2006.
- [18] M. Kulke, C. Neagoe, B. Kolmerer, et al., "Kettin, a major source of myofibrillar stiffness in *Drosophila* indirect flight muscle," *Journal of Cell Biology*, vol. 154, no. 5, pp. 1045–1057, 2001.
- [19] V. Joumaa, D. E. Rassier, T. R. Leonard, and W. Herzog, "Passive force enhancement in single myofibrils," *Pflügers Archiv European Journal of Physiology*, vol. 455, no. 2, pp. 367–371, 2007.
- [20] M. S. Miller, C. M. Dambacher, A. F. Knowles, et al., "Alternative S2 hinge regions of the myosin rod affect myofibrillar structure and myosin kinetics," *Biophysical Journal*, vol. 96, no. 10, pp. 4132–4143, 2009.
- [21] H. Liu, M. S. Miller, D. M. Swank, W. A. Kronert, D. W. Maughan, and S. I. Bernstein, "Paramyosin phosphorylation site disruption affects indirect flight muscle stiffness and power generation in *Drosophila melanogaster*," *Proceedings of the National Academy of Sciences of the United States of America*, vol. 102, no. 30, pp. 10522–10527, 2005.
- [22] J. A. Henkin, D. W. Maughan, and J. O. Vigoreaux, "Mutations that affect flightin expression in *Drosophila* alter the viscoelastic properties of flight muscle fibers," *American Journal of Physiology*, vol. 286, pp. C65–C72, 2004.
- [23] B. M. Palmer, D. Georgakopoulos, P. M. Janssen, et al., "Role of cardiac myosin binding protein C in sustaining left ventricular systolic stiffening," *Circulation Research*, vol. 94, no. 9, pp. 1249–1255, 2004.
- [24] Y. Araki, A. Usui, O. Kawaguchi, et al., "Pressure-volume relationship in isolated working heart with crystalloid perfusate in swine and imaging the valve motion," *European Journal of Cardio-Thoracic Surgery*, vol. 28, no. 3, pp. 435–442, 2005.
- [25] M. Dickinson, G. Farman, M. Frye, et al., "Molecular dynamics of cyclically contracting insect flight muscle in vivo," *Nature*, vol. 433, no. 7023, pp. 330–334, 2005.
- [26] H. Granzier and S. Labeit, "Structure-function relations of the giant elastic protein titin in striated and smooth muscle cells," *Muscle and Nerve*, vol. 36, no. 6, pp. 740–755, 2007.
- [27] A. Pirani, M. V. Vinogradova, P. M. Curmi, et al., "An atomic model of the thin filament in the relaxed and Ca^{2+} -activated

- states,” *Journal of Molecular Biology*, vol. 357, no. 3, pp. 707–717, 2006.
- [28] M. E. Zoghbi, J. L. Woodhead, R. L. Moss, and R. Craig, “Three-dimensional structure of vertebrate cardiac muscle myosin filaments,” *Proceedings of the National Academy of Sciences of the United States of America*, vol. 105, no. 7, pp. 2386–2390, 2008.
- [29] A. F. Huxley, “Muscle structure and theories of contraction,” *Progress in Biophysics and Biophysical Chemistry*, vol. 7, pp. 255–318, 1957.
- [30] H. E. Huxley, A. Stewart, H. Sosa, and T. Irving, “X-ray diffraction measurements of the extensibility of actin and myosin filaments in contracting muscle,” *Biophysical Journal*, vol. 67, no. 6, pp. 2411–2421, 1994.
- [31] K. Wakabayashi, Y. Sugimoto, H. Tanaka, Y. Ueno, Y. Takezawa, and Y. Amemiya, “X-ray diffraction evidence for the extensibility of actin and myosin filaments during muscle contraction,” *Biophysical Journal*, vol. 67, no. 6, pp. 2422–2435, 1994.
- [32] H. Higuchi, T. Yanagida, and Y. E. Goldman, “Compliance of thin filaments in skinned fibers of rabbit skeletal muscle,” *Biophysical Journal*, vol. 69, no. 3, pp. 1000–1010, 1995.
- [33] Y. E. Goldman and A. F. Huxley, “Actin compliance: are you pulling my chain?” *Biophysical Journal*, vol. 67, no. 6, pp. 2131–2133, 1994.
- [34] K. Tawada and M. Kimura, “Stiffness of carbodiimide-crosslinked glycerinated muscle fibres in rigor and relaxing solutions at high salt concentrations,” *Journal of Muscle Research and Cell Motility*, vol. 7, no. 4, pp. 339–350, 1986.
- [35] M. A. Bagni, G. Cecchi, B. Colombini, and F. Colomo, “Sarcomere tension-stiffness relation during the tetanus rise in single frog muscle fibres,” *Journal of Muscle Research and Cell Motility*, vol. 20, no. 5–6, pp. 469–476, 1999.
- [36] A. F. Huxley and R. M. Simmons, “Proposed mechanism of force generation in striated muscle,” *Nature*, vol. 233, no. 5321, pp. 533–538, 1971.
- [37] E. Eisenberg, T. L. Hill, and Y. Chen, “Cross-bridge model of muscle contraction. Quantitative analysis,” *Biophysical Journal*, vol. 29, no. 2, pp. 195–227, 1980.
- [38] E. Pate and R. Cooke, “A model of crossbridge action: the effects of ATP, ADP and Pi,” *Journal of Muscle Research and Cell Motility*, vol. 10, no. 3, pp. 181–196, 1989.
- [39] Y. Luo, R. Cooke, and E. Pate, “A model of stress relaxation in cross-bridge systems: effect of a series elastic element,” *American Journal of Physiology*, vol. 265, no. 1, part 1, pp. C279–C288, 1993.
- [40] S. M. Mijailovich, J. J. Fredberg, and J. P. Butler, “On the theory of muscle contraction: filament extensibility and the development of isometric force and stiffness,” *Biophysical Journal*, vol. 71, no. 3, pp. 1475–1484, 1996.
- [41] T. L. Daniel, A. C. Trimble, and P. B. Chase, “Compliant realignment of binding sites in muscle: transient behavior and mechanical tuning,” *Biophysical Journal*, vol. 74, no. 4, pp. 1611–1621, 1998.
- [42] P. B. Chase, J. M. Macpherson, and T. L. Daniel, “A spatially explicit nanomechanical model of the half-sarcomere: myofilament compliance affects Ca^{2+} -activation,” *Annals of Biomedical Engineering*, vol. 32, no. 11, pp. 1559–1568, 2004.
- [43] K. S. Campbell, “Filament compliance effects can explain tension overshoots during force development,” *Biophysical Journal*, vol. 91, no. 11, pp. 4102–4109, 2006.
- [44] B. C. Tanner, T. L. Daniel, and M. Regnier, “Sarcomere lattice geometry influences cooperative myosin binding in muscle,” *PLoS Computational Biology*, vol. 3, no. 7, article e115, 2007.
- [45] A. Vilfan, E. Frey, and F. Schwabl, “Elastically coupled molecular motors,” *European Physical Journal B*, vol. 3, no. 4, pp. 535–546, 1998.
- [46] E. Brunello, M. Reconditi, R. Elangovan, et al., “Skeletal muscle resists stretch by rapid binding of the second motor domain of myosin to actin,” *Proceedings of the National Academy of Sciences of the United States of America*, vol. 104, no. 50, pp. 20114–20119, 2007.
- [47] D. A. Smith and S. M. Mijailovich, “Toward a unified theory of muscle contraction. II: predictions with the mean-field approximation,” *Annals of Biomedical Engineering*, vol. 36, no. 8, pp. 1353–1371, 2008.
- [48] J. W. Pringle, “Stretch activation of muscle: function and mechanism,” *Proceedings of the Royal Society B*, vol. 201, no. 1143, pp. 107–130, 1978.
- [49] H. A. Al-Khayat, L. Hudson, M. K. Reedy, T. C. Irving, and J. M. Squire, “Myosin head configuration in relaxed insect flight muscle: X-ray modeled resting cross-bridges in a pre-powerstroke state are poised for actin binding,” *Biophysical Journal*, vol. 85, no. 2, pp. 1063–1079, 2003.
- [50] B. C. Tanner, M. Regnier, and T. L. Daniel, “A spatially explicit model of muscle contraction explains a relationship between activation phase, power and ATP utilization in insect flight,” *Journal of Experimental Biology*, vol. 211, no. 2, pp. 180–186, 2008.
- [51] K. S. Campbell, “Interactions between connected half-sarcomeres produce emergent mechanical behavior in a mathematical model of muscle,” *PLoS Computational Biology*, vol. 5, no. 11, Article ID e1000560, 2009.
- [52] M. Linari, G. Piazzesi, and V. Lombardi, “The effect of myofilament compliance on kinetics of force generation by myosin motors in muscle,” *Biophysical Journal*, vol. 96, no. 2, pp. 583–592, 2009.
- [53] R. J. Levine, M. Elfvin, M. M. Dewey, and B. Walcott, “Paramyosin in invertebrate muscles. II. Content in relation to structure and function,” *Journal of Cell Biology*, vol. 71, no. 1, pp. 273–279, 1976.
- [54] R. Craig and J. L. Woodhead, “Structure and function of myosin filaments,” *Current Opinion in Structural Biology*, vol. 16, no. 2, pp. 204–212, 2006.
- [55] S. L. Hooper, K. H. Hobbs, and J. B. Thuma, “Invertebrate muscles: thin and thick filament structure; molecular basis of contraction and its regulation, catch and asynchronous muscle,” *Progress in Neurobiology*, vol. 86, no. 2, pp. 72–127, 2008.
- [56] J. M. Squire, *Muscle: Design, Diversity, and Disease*, Benjamin/Cummings, Menlo Park, Calif, USA, 1986.
- [57] T. Nishizaka, H. Miyata, H. Yoshikawa, S. Ishiwata, and K. Kinoshita Jr., “Unbinding force of a single motor molecule of muscle measured using optical tweezers,” *Nature*, vol. 377, no. 6546, pp. 251–254, 1995.
- [58] T. Nishizaka, R. Seo, H. Tadokuma, K. Kinoshita Jr., and S. Ishiwata, “Characterization of single actomyosin rigor bonds: load dependence of lifetime and mechanical properties,” *Biophysical Journal*, vol. 79, no. 2, pp. 962–974, 2000.
- [59] H. Nakajima, Y. Kunioka, K. Nakano, K. Shimizu, M. Seto, and T. Ando, “Scanning force microscopy of the interaction events between a single molecule of heavy meromyosin and actin,” *Biochemical and Biophysical Research Communications*, vol. 234, no. 1, pp. 178–182, 1997.
- [60] B. Guo and W. H. Guilford, “Mechanics of actomyosin bonds in different nucleotide states are tuned to muscle contraction,” *Proceedings of the National Academy of Sciences*

- of the United States of America, vol. 103, no. 26, pp. 9844–9849, 2006.
- [61] W. M. Obermann, M. Gautel, K. Weber, and D. O. Fürst, “Molecular structure of the sarcomeric M band: mapping of titin and myosin binding domains in myomesin and the identification of a potential regulatory phosphorylation site in myomesin,” *EMBO Journal*, vol. 16, no. 2, pp. 211–220, 1997.
- [62] A. Houmeida, J. Holt, L. Tskhovrebova, and J. Trinick, “Studies of the interaction between titin and myosin,” *Journal of Cell Biology*, vol. 131, no. 6, part 1, pp. 1471–1481, 1995.
- [63] G. Ayer and J. O. Vigoreaux, “Flightin is a myosin rod binding protein,” *Cell Biochemistry and Biophysics*, vol. 38, no. 1, pp. 41–54, 2003.
- [64] E. Flashman, H. Watkins, and C. Redwood, “Localization of the binding site of the C-terminal domain of cardiac myosin-binding protein-C on the myosin rod,” *Biochemical Journal*, vol. 401, no. 1, pp. 97–102, 2007.
- [65] J. A. Suggs, A. Cammarato, W. A. Kronert, et al., “Alternative S2 hinge regions of the myosin rod differentially affect muscle function, myofibril dimensions and myosin tail length,” *Journal of Molecular Biology*, vol. 367, no. 5, pp. 1312–1329, 2007.
- [66] M. M. Dewey, B. Walcott, D. E. Colflesh, H. Terry, and R. J. Levine, “Changes in thick filament length in *Limulus* striated muscle,” *Journal of Cell Biology*, vol. 75, no. 2, part 1, pp. 366–380, 1977.
- [67] E. M. Nagornyyak, F. A. Blyakhman, and G. H. Pollack, “Step-wise length changes in single invertebrate thick filaments,” *Biophysical Journal*, vol. 89, no. 5, pp. 3269–3276, 2005.
- [68] M. Cervera, J. J. Arredondo, and R. M. Ferreres, “Paramyosin and miniparamyosin,” in *Nature’s Versatile Engine: Insect Flight Muscle Inside and Out*, J. O. Vigoreaux, Ed., pp. 76–85, Springer, New York, NY, USA, 2006.
- [69] D. C. White, “The elasticity of relaxed insect fibrillar flight muscle,” *Journal of Physiology*, vol. 343, pp. 31–57, 1983.
- [70] P. K. Luther, P. M. Bennett, C. Knupp, et al., “Understanding the organisation and role of myosin binding protein C in normal striated muscle by comparison with MyBP-C knockout cardiac muscle,” *Journal of Molecular Biology*, vol. 384, no. 1, pp. 60–72, 2008.
- [71] M. F. Schmid and H. F. Epstein, “Muscle thick filaments are rigid coupled tubules, not flexible ropes,” *Cell Motility and the Cytoskeleton*, vol. 41, no. 3, pp. 195–201, 1998.
- [72] B. K. McConnell, K. A. Jones, D. Fatkin, et al., “Dilated cardiomyopathy in homozygous myosin-binding protein-C mutant mice,” *Journal of Clinical Investigation*, vol. 104, no. 9, pp. 1235–1244, 1999.
- [73] B. M. Palmer, B. K. McConnell, G. H. Li, et al., “Reduced cross-bridge dependent stiffness of skinned myocardium from mice lacking cardiac myosin binding protein-C,” *Molecular and Cellular Biochemistry*, vol. 263, no. 1–2, pp. 73–80, 2004.
- [74] M. C. Reedy, B. Bullard, and J. O. Vigoreaux, “Flightin is essential for thick filament assembly and sarcomere stability in *Drosophila* flight muscles,” *Journal of Cell Biology*, vol. 151, no. 7, pp. 1483–1499, 2000.
- [75] C. Guzmán, S. Jeney, L. Kreplak, et al., “Exploring the mechanical properties of single vimentin intermediate filaments by atomic force microscopy,” *Journal of Molecular Biology*, vol. 360, no. 3, pp. 623–630, 2006.
- [76] F. Qiu, S. Brendel, P. M. Cunha, et al., “Myofilin, a protein in the thick filaments of insect muscle,” *Journal of Cell Science*, vol. 118, no. 7, pp. 1527–1536, 2005.
- [77] N. Mücke, L. Kreplak, R. Kirmse, et al., “Assessing the flexibility of intermediate filaments by atomic force microscopy,” *Journal of Molecular Biology*, vol. 335, no. 5, pp. 1241–1250, 2004.
- [78] F. Oosawa, “Actin actin bond strength and the conformational change of F-actin,” *Biorheology*, vol. 14, no. 1, pp. 11–19, 1977.
- [79] F. Oosawa, Y. Maeda, S. Fujime, S. Ishiwata, T. Yanagida, and M. Taniguchi, “Dynamic characteristics of F-actin and thin filaments in vivo and in vitro,” *Journal of Mechanochemistry & Cell Motility*, vol. 4, no. 1, pp. 63–78, 1977.
- [80] M. Linari, I. Dobbie, M. Reconditi, et al., “The stiffness of skeletal muscle in isometric contraction and rigor: the fraction of myosin heads bound to actin,” *Biophysical Journal*, vol. 74, no. 5, pp. 2459–2473, 1998.
- [81] C. A. Rebello and R. D. Ludescher, “Differential dynamic behavior of actin filaments containing tightly-bound Ca^{2+} or Mg^{2+} in the presence of myosin heads actively hydrolyzing ATP,” *Biochemistry*, vol. 38, no. 40, pp. 13288–13295, 1999.
- [82] H. Yoshimura, T. Nishio, K. Mihashi, K. Kinoshita Jr., and A. Ikegami, “Torsional motion of eosin-labeled F-actin as detected in the time-resolved anisotropy decay of the probe in the sub-millisecond time range,” *Journal of Molecular Biology*, vol. 179, no. 3, pp. 453–467, 1984.
- [83] T. Nishizaka, T. Yagi, Y. Tanaka, and S. Ishiwata, “Right-handed rotation of an actin filament in an in vitro motile system,” *Nature*, vol. 361, no. 6409, pp. 269–271, 1993.
- [84] C. E. Schutt and U. Lindberg, “Actin as the generator of tension during muscle contraction,” *Proceedings of the National Academy of Sciences of the United States of America*, vol. 89, no. 1, pp. 319–323, 1992.
- [85] R. Jarosch, “Large-scale models reveal the two-component mechanics of striated muscle,” *International Journal of Molecular Sciences*, vol. 9, no. 12, pp. 2658–2723, 2008.
- [86] E. Prochniewicz, Q. Zhang, P. A. Janmey, and D. D. Thomas, “Cooperativity in F-actin: binding of gelsolin at the barbed end affects structure and dynamics of the whole filament,” *Journal of Molecular Biology*, vol. 260, no. 5, pp. 756–766, 1996.
- [87] C. L. Wang, “Caldesmon and the regulation of cytoskeletal functions,” *Advances in Experimental Medicine and Biology*, vol. 644, pp. 250–272, 2008.
- [88] D. H. Heeley, M. H. Watson, A. S. Mak, P. Dubord, and L. B. Smillie, “Effect of phosphorylation on the interaction and functional properties of rabbit striated muscle α -tropomyosin,” *Journal of Biological Chemistry*, vol. 264, no. 5, pp. 2424–2430, 1989.
- [89] K.-I. Sano, K. Maeda, T. Oda, and Y. Maéda, “The effect of single residue substitutions of serine-283 on the strength of head-to-tail interaction and actin binding properties of rabbit skeletal muscle α -tropomyosin,” *Journal of Biochemistry*, vol. 127, no. 6, pp. 1095–1102, 2000.
- [90] V. S. Rao, E. N. Marongelli, and W. H. Guilford, “Phosphorylation of tropomyosin extends cooperative binding of myosin beyond a single regulatory unit,” *Cell Motility and the Cytoskeleton*, vol. 66, no. 1, pp. 10–23, 2009.
- [91] E. Prochniewicz, N. Janson, D. D. Thomas, and E. M. De La Cruz, “Cofilin increases the torsional flexibility and dynamics of actin filaments,” *Journal of Molecular Biology*, vol. 353, no. 5, pp. 990–1000, 2005.
- [92] B. R. McCullough, L. Blanchoin, J.-L. Martiel, and E. M. De La Cruz, “Cofilin increases the bending flexibility of actin filaments: implications for severing and cell mechanics,”

- Journal of Molecular Biology*, vol. 381, no. 3, pp. 550–558, 2008.
- [93] B. Bugyi, G. Papp, G. Hild, et al., “Formins regulate actin filament flexibility through long range allosteric interactions,” *Journal of Biological Chemistry*, vol. 281, no. 16, pp. 10727–10736, 2006.
- [94] A. S. McElhinny, S. T. Kazmierski, S. Labeit, and C. C. Gregorio, “Nebulin: the nebulous, multifunctional giant of striated muscle,” *Trends in Cardiovascular Medicine*, vol. 13, no. 5, pp. 195–201, 2003.
- [95] B. Bullard, C. Burkart, S. Labeit, and K. Leonard, “The function of elastic proteins in the oscillatory contraction of insect flight muscle,” *Journal of Muscle Research and Cell Motility*, vol. 26, no. 6–8, pp. 479–485, 2005.
- [96] I. Agarkova and J.-C. Perriard, “The M-band: an elastic web that crosslinks thick filaments in the center of the sarcomere,” *Trends in Cell Biology*, vol. 15, no. 9, pp. 477–485, 2005.
- [97] J. O. Vigoreaux, “The muscle Z band: lessons in stress management,” *Journal of Muscle Research and Cell Motility*, vol. 15, no. 3, pp. 237–255, 1994.
- [98] A. A. Shabarchin and A. K. Tsaturyan, “Proposed role of the M-band in sarcomere mechanics and mechano-sensing: a model study,” *Biomechanics and Modeling in Mechanobiology*, vol. 9, no. 2, pp. 163–175, 2009.
- [99] L. G. Prado, I. Makarenko, C. Andresen, M. Krüger, C. A. Opitz, and W. A. Linke, “Isoform diversity of giant proteins in relation to passive and active contractile properties of rabbit skeletal muscles,” *Journal of General Physiology*, vol. 126, no. 5, pp. 461–480, 2005.
- [100] N. Fukuda, T. Terui, S. Ishiwata, and S. Kurihara, “Titin-based regulations of diastolic and systolic functions of mammalian cardiac muscle,” *Journal of Molecular and Cellular Cardiology*, vol. 48, no. 5, pp. 876–881, 2010.
- [101] M. Krüger and W. A. Linke, “Titin-based mechanical signalling in normal and failing myocardium,” *Journal of Molecular and Cellular Cardiology*, vol. 46, no. 4, pp. 490–498, 2009.
- [102] C. Neagoe, M. Kulke, F. Del Monte, et al., “Titin isoform switch in ischemic human heart disease,” *Circulation*, vol. 106, no. 11, pp. 1333–1341, 2002.
- [103] H. L. Granzier and K. Wang, “Interplay between passive tension and strong and weak binding cross-bridges in insect indirect flight muscle: a functional dissection by gelsolin-mediated thin filament removal,” *Journal of General Physiology*, vol. 101, no. 2, pp. 235–270, 1993.
- [104] I. A. Telley, J. Denoth, E. Stüssi, G. Pfitzer, and R. Stehle, “Half-sarcomere dynamics in myofibrils during activation and relaxation studied by tracking fluorescent markers,” *Biophysical Journal*, vol. 90, no. 2, pp. 514–530, 2006.
- [105] M. A. Geeves and S. S. Lehrer, “Dynamics of the muscle thin filament regulatory switch: the size of the cooperative unit,” *Biophysical Journal*, vol. 67, no. 1, pp. 273–282, 1994.
- [106] M. Regnier, A. J. Rivera, C.-K. Wang, M. A. Bates, P. B. Chase, and A. M. Gordon, “Thin filament near-neighbour regulatory unit interactions affect rabbit skeletal muscle steady-state force- Ca^{2+} relations,” *Journal of Physiology*, vol. 540, no. 2, pp. 485–497, 2002.
- [107] T. E. Gillis, D. A. Martyn, A. J. Rivera, and M. Regnier, “Investigation of thin filament near-neighbour regulatory unit interactions during force development in skinned cardiac and skeletal muscle,” *Journal of Physiology*, vol. 580, no. 2, pp. 561–576, 2007.
- [108] F. Fuchs and D. A. Martyn, “Length-dependent Ca^{2+} activation in cardiac muscle: some remaining questions,” *Journal of Muscle Research and Cell Motility*, vol. 26, no. 4–5, pp. 199–212, 2005.
- [109] G. D’Antona, M. A. Pellegrino, R. Adami, et al., “The effect of ageing and immobilization on structure and function of human skeletal muscle fibres,” *Journal of Physiology*, vol. 552, no. 2, pp. 499–511, 2003.
- [110] S. Acharyya, K. J. Ladner, L. L. Nelsen, et al., “Cancer cachexia is regulated by selective targeting of skeletal muscle gene products,” *Journal of Clinical Investigation*, vol. 114, no. 3, pp. 370–378, 2004.
- [111] M. J. Toth, D. E. Matthews, P. A. Ades, et al., “Skeletal muscle myofibrillar protein metabolism in heart failure: relationship to immune activation and functional capacity,” *American Journal of Physiology*, vol. 288, no. 4, pp. E685–E692, 2005.
- [112] M. S. Miller, P. Vanburen, M. M. Lewinter, et al., “Mechanisms underlying skeletal muscle weakness in human heart failure: alterations in single fiber myosin protein content and function,” *Circulation*, vol. 2, no. 6, pp. 700–706, 2009.
- [113] H. W. Van Hees, H. F. Van Der Heijden, C. A. Ottenheijm, et al., “Diaphragm single-fiber weakness and loss of myosin in congestive heart failure rats,” *American Journal of Physiology*, vol. 293, no. 1, pp. H819–H828, 2007.
- [114] C. A. Ottenheijm, L. M. Heunks, T. Hafmans, et al., “Titin and diaphragm dysfunction in chronic obstructive pulmonary disease,” *American Journal of Respiratory and Critical Care Medicine*, vol. 173, no. 5, pp. 527–534, 2006.
- [115] L. Larsson, X. Li, L. Edstrom, et al., “Acute quadriplegia and loss of muscle myosin in patients treated with nondepolarizing neuromuscular blocking agents and corticosteroids: mechanisms at the cellular and molecular levels,” *Critical Care Medicine*, vol. 28, no. 1, pp. 34–45, 2000.
- [116] F. Haddad, R. R. Roy, H. Zhong, V. R. Edgerton, and K. M. Baldwin, “Atrophy responses to muscle inactivity. I. Cellular markers of protein deficits,” *Journal of Applied Physiology*, vol. 95, no. 2, pp. 781–790, 2003.
- [117] M. S. Miller, P. Lekkas, J. M. Braddock, et al., “Aging enhances indirect flight muscle fiber performance yet decreases flight ability in *Drosophila*,” *Biophysical Journal*, vol. 95, no. 5, pp. 2391–2401, 2008.
- [118] M. H. Dickinson and J. R. Lighton, “Muscle efficiency and elastic storage in the flight motor of *Drosophila*,” *Science*, vol. 268, no. 5207, pp. 87–90, 1995.
- [119] C. P. Ellington, “The aerodynamics of hovering insect flight. VI. Lift and power requirements,” *Philosophical Transactions of the Royal Society of London Series B*, vol. 305, no. 1122, pp. 145–181, 1984.
- [120] D. Frank, C. Kuhn, H. A. Katus, and N. Frey, “The sarcomeric Z-disc: a nodal point in signalling and disease,” *Journal of Molecular Medicine*, vol. 84, no. 6, pp. 446–468, 2006.
- [121] N. D. Epstein and J. S. Davis, “Sensing stretch is fundamental,” *Cell*, vol. 112, no. 2, pp. 147–150, 2003.
- [122] M. Hoshijima, “Mechanical stress-strain sensors embedded in cardiac cytoskeleton: Z disk, titin, and associated structures,” *American Journal of Physiology*, vol. 290, no. 4, pp. H1313–H1325, 2006.
- [123] U. Nongthomba, M. Cummins, S. Clark, J. O. Vigoreaux, and J. C. Sparrow, “Suppression of muscle hypercontraction by mutations in the myosin heavy chain gene of *Drosophila melanogaster*,” *Genetics*, vol. 164, no. 1, pp. 209–222, 2003.
- [124] K. Vijayan, J. L. Thompson, K. M. Norenberg, R. H. Fitts, and D. A. Riley, “Fiber-type susceptibility to eccentric contraction-induced damage of hindlimb-unloaded rat AL muscles,” *Journal of Applied Physiology*, vol. 90, no. 3, pp. 770–776, 2001.

- [125] E. P. Debold, J. Romatowski, and R. H. Fitts, "The depressive effect of Pi on the force-pCa relationship in skinned single muscle fibers is temperature dependent," *American Journal of Physiology*, vol. 290, no. 4, pp. C1041–C1050, 2006.
- [126] S. Lange, I. Agarkova, J.-C. Perriard, and E. Ehler, "The sarcomeric M-band during development and in disease," *Journal of Muscle Research and Cell Motility*, vol. 26, no. 6–8, pp. 375–379, 2005.
- [127] A. Weiss, S. Schiaffino, and L. A. Leinwand, "Comparative sequence analysis of the complete human sarcomeric myosin heavy chain family: implications for functional diversity," *Journal of Molecular Biology*, vol. 290, no. 1, pp. 61–75, 1999.
- [128] J. M. Squire, T. Bekyarova, G. Farman, et al., "The myosin filament superlattice in the flight muscles of flies: a-band lattice optimisation for stretch-activation?" *Journal of Molecular Biology*, vol. 361, no. 5, pp. 823–838, 2006.
- [129] S. Trachtenberg and I. Hammel, "The rigidity of bacterial flagellar filaments and its relation to filament polymorphism," *Journal of Structural Biology*, vol. 109, no. 1, pp. 18–27, 1992.
- [130] R. W. Kensler, "The mammalian cardiac muscle thick filament: backbone contributions to meridional reflections," *Journal of Structural Biology*, vol. 149, no. 3, pp. 313–324, 2005.
- [131] M. D. Goode, "Ultrastructure and contractile properties of isolated myofibrils and myofilaments from drosophila flight muscle," *Transactions of the American Microscopical Society*, vol. 91, no. 2, pp. 182–194, 1972.
- [132] E. Oroudjev, J. Soares, S. Arcidiacono, J. B. Thompson, S. A. Fossey, and H. G. Hansma, "Segmented nanofibers of spider dragline silk: atomic force microscopy and single-molecule force spectroscopy," *Proceedings of the National Academy of Sciences of the United States of America*, vol. 99, supplement 2, pp. 6460–6465, 2002.
- [133] E. Di Cola, T. A. Waigh, J. Trinick, et al., "Persistence length of titin from rabbit skeletal muscles measured with scattering and microrheology techniques," *Biophysical Journal*, vol. 88, no. 6, pp. 4095–4106, 2005.
- [134] M. S. Z. Kellermayer, C. Bustamante, and H. L. Granzier, "Mechanics and structure of titin oligomers explored with atomic force microscopy," *Biochimica et Biophysica Acta*, vol. 1604, no. 2, pp. 105–114, 2003.
- [135] A. Nagy, L. Grama, T. Huber, et al., "Hierarchical extensibility in the PEVK domain of skeletal-muscle titin," *Biophysical Journal*, vol. 89, no. 1, pp. 329–336, 2005.
- [136] Z.-P. Luo, Y.-L. Sun, T. Fujii, and K.-N. An, "Single molecule mechanical properties of type II collagen and hyaluronan measured by optical tweezers," *Biorheology*, vol. 41, no. 3-4, pp. 247–254, 2004.
- [137] Y.-L. Sun, Z.-P. Luo, A. Fertala, and K.-N. An, "Stretching type II collagen with optical tweezers," *Journal of Biomechanics*, vol. 37, no. 11, pp. 1665–1669, 2004.
- [138] B. Bullard, T. Garcia, V. Benes, M. C. Leake, W. A. Linke, and A. F. Oberhauser, "The molecular elasticity of the insect flight muscle proteins projectin and kettin," *Proceedings of the National Academy of Sciences of the United States of America*, vol. 103, no. 12, pp. 4451–4456, 2006.
- [139] A. N. Round, M. Berry, T. J. McMaster, et al., "Heterogeneity and persistence length in human ocular mucins," *Biophysical Journal*, vol. 83, no. 3, pp. 1661–1670, 2002.
- [140] C. Rivetti, M. Guthold, and C. Bustamante, "Scanning force microscopy of DNA deposited onto mica: equilibration versus kinetic trapping studied by statistical polymer chain analysis," *Journal of Molecular Biology*, vol. 264, no. 5, pp. 919–932, 1996.
- [141] C. P. Brangwynne, G. H. Koenderink, E. Barry, Z. Dogic, F. C. MacKintosh, and D. A. Weitz, "Bending dynamics of fluctuating biopolymers probed by automated high-resolution filament tracking," *Biophysical Journal*, vol. 93, no. 1, pp. 346–359, 2007.
- [142] R. Duggal and M. Pasquali, "Dynamics of individual single-walled carbon nanotubes in water by real-time visualization," *Physical Review Letters*, vol. 96, no. 24, Article ID 246104, 2006.
- [143] F. Pampaloni, G. Lattanzi, A. Jonáš, T. Surrey, E. Frey, and E.-L. Florin, "Thermal fluctuations of grafted microtubules provide evidence of a length-dependent persistence length," *Proceedings of the National Academy of Sciences of the United States of America*, vol. 103, no. 27, pp. 10248–10253, 2006.

Research Article

Contractile Properties of Esophageal Striated Muscle: Comparison with Cardiac and Skeletal Muscles in Rats

Takahiko Shiina,¹ Takeshi Shima,¹ Kazuaki Masuda,¹ Haruko Hirayama,¹ Momoe Iwami,¹ Tadashi Takewaki,¹ Hirofumi Kuramoto,² and Yasutake Shimizu¹

¹Laboratory of Physiology, Department of Basic Veterinary Science, The United Graduate School of Veterinary Sciences, Gifu University, 1-1 Yanagido, Gifu 501-1193, Japan

²Department of Applied Biology, Kyoto Institute of Technology, Matsugasaki, Sakyo, Kyoto 606-8585, Japan

Correspondence should be addressed to Yasutake Shimizu, yshimizu@gifu-u.ac.jp

Received 30 October 2009; Accepted 1 February 2010

Academic Editor: Henk L. M. Granzier

Copyright © 2010 Takahiko Shiina et al. This is an open access article distributed under the Creative Commons Attribution License, which permits unrestricted use, distribution, and reproduction in any medium, provided the original work is properly cited.

The external muscle layer of the mammalian esophagus consists of striated muscles. We investigated the contractile properties of esophageal striated muscle by comparison with those of skeletal and cardiac muscles. Electrical field stimulation with single pulses evoked twitch-like contractile responses in esophageal muscle, similar to those in skeletal muscle in duration and similar to those in cardiac muscle in amplitude. The contractions of esophageal muscle were not affected by an inhibitor of gap junctions. Contractile responses induced by high potassium or caffeine in esophageal muscle were analogous to those in skeletal muscle. High-frequency stimulation induced a transient summation of contractions followed by sustained contractions with amplitudes similar to those of twitch-like contractions, although a large summation was observed in skeletal muscle. The results demonstrate that esophageal muscle has properties similar but not identical to those of skeletal muscle and that some specific properties may be beneficial for esophageal peristalsis.

1. Introduction

The external muscle layer of the mammalian esophagus consists of striated muscle fibers, which extend from the pharyngoesophageal junction to the thoracic or abdominal portion [1–3]. This is in contrast to the tunica muscularis of the stomach, small intestine, and large intestine which are constituted entirely of smooth muscle. In humans and cats, the upper and lower portions of the esophagus are composed of striated and smooth muscle fibers, respectively, with mixed composition of these fibers in the middle portion. In dogs, ruminants, and rodents including mice, rats, and hamsters, the muscle layer of the esophagus consists largely of striated muscle fibers. These striated muscle fibers were hitherto considered as “classical” skeletal muscle fibers, innervated exclusively by excitatory vagal efferents that arise from motor neurons originating in the nucleus ambiguus and terminate on motor endplates [4–6].

The major function of the esophagus is propulsion of swallowed food into the stomach by peristalsis [7]. To accomplish effective peristalsis, contraction of each muscle needs to be well coordinated [8, 9]. The peristaltic motility of small and large intestines is mainly regulated by the intrinsic nervous system, which consists of intrinsic sensory neurons, interneurons, and motor neurons that project into the smooth muscle layers [8, 10–12]. In contrast, it has been shown that peristalsis in the esophageal “skeletal” muscle is controlled by the swallowing center in the medulla oblongata through a mediation of extrinsic vagus nerves [7, 13–16]. However, recent studies have revealed that intrinsic neurons also play roles in regulating the motility of the esophageal striated muscle. Morphological studies have shown that esophageal striated muscle receives dual innervation from both vagal motor fibers originating in the brainstem and varicose intrinsic nerve fibers originating in the myenteric plexus, which is called “enteric coinnervation” of esophageal motor endplates [3, 17]. We have also provided evidence that

a local neural reflex pathway in the esophagus, consisting of primary afferent neurons and myenteric neurons, can modulate motility of the striated muscle portion of the esophagus [18–21]. Thus, both extrinsic and intrinsic neural regulations would be important in coordinating the peristaltic motility of the esophagus.

In addition to the neural mechanisms, contractile properties of smooth muscles are beneficial in coordinating motility of small and large intestines. For instance, relatively long duration time of each contraction enables summation of contractions, which in turn results in effective compression of the intraluminal space [22–24]. Furthermore, coupling of neighboring cells by gap junctions would be essential to adjust the timing of muscle contractions [9]. On the other hand, skeletal muscle fibers are insulated from each other [25] and thus may be unfavorable for coordinated motility. To compensate the disadvantages of striated muscle, cardiac muscle possesses several specific properties including expression of gap junctions [26]. We speculated that the striated muscle of the esophagus also has specific properties to establish coordinated peristaltic motility.

Hence, the aim of the present study was to clarify the contractile properties of esophageal muscle with focus on the similarities to cardiac muscle. For this purpose, we compared the mechanical responses of isolated preparations from the esophagus, soleus muscle, and heart in rats.

2. Materials and Methods

2.1. Animals. Male Wistar rats (*Rattus norvegicus*, 12 weeks of age and weighing 200–400 g) were used for the experiments. They were maintained in plastic cages at $22 \pm 2^\circ\text{C}$ with a 12:12 h light-dark cycle (light on 07:00–19:00 h) and given free access to laboratory chow and water. The experiments were approved by the Animal Care and Use Committee of Gifu University.

2.2. Solutions and Drugs. During experiments, tissues were maintained in Krebs' solution consisting of (mM): NaCl 118.4, KCl 4.7, CaCl_2 2.5, MgSO_4 1.2, KH_2PO_4 1.2, NaHCO_3 25, and glucose 11.7. High potassium Krebs' solution consisting of NaCl 4.7, KCl 118.4, CaCl_2 2.5, MgSO_4 1.2, KH_2PO_4 1.2, NaHCO_3 25, and glucose 11.7 was used for inducing high potassium contracture. Tetrodotoxin was used as a blocker of voltage-dependent sodium channels on striated muscle cells. Halothane was used as an inhibitor of gap junctions [27]. Caffeine was used as a releaser of calcium from intracellular stores. Tetrodotoxin, halothane, and caffeine were obtained from Sigma-Aldrich (St. Louis, MO, USA). Tetrodotoxin was initially dissolved in citrate buffer and then dissolved in Krebs' solution to the desired concentration. Halothane was directly dissolved in Krebs' solution in an organ bath. Caffeine was initially dissolved in Krebs' solution to the desired concentration and then Krebs' solution was exchanged for caffeine-containing Krebs' solution in an organ bath.

2.3. Tissue Preparations. Rats were anesthetized with diethyl ether and were exsanguinated via the axillary arteries. The abdominal and thoracic cavities were opened, and the stomach, esophagus up to the larynx, heart, and lungs were removed and immediately placed in a dish containing precooled aerated Krebs' solution. A 5 mm long segment of the middle part of the thoracic esophagus was carefully dissected out for mechanical recording. The heart was also dissected out and retrogradely perfused through the aorta with Krebs' solution for washing out intracardiac blood. The right ventricle was longitudinally cut into strips of 1 cm in length, 2 mm in width, and 1 mm in thickness. For estimating mechanical activity of the representative skeletal muscle, hind limbs were exposed and the soleus was excised from both legs. The soleus muscle was also cut into strips of the same size as that of heart muscle strips. For connecting the heart and soleus muscle strips to the isometric tension transducer, a silk-snare was placed at an end of each strip.

2.4. Recordings of Mechanical Activity. The whole segment of each muscle preparation was transferred to a 3 mL thermostatically controlled (35°C) organ bath containing Krebs' solution bubbled with 95% O_2 + 5% CO_2 gas mixture, maintained at pH 7.4. For recording contractile responses of the esophageal segments, two L-shaped stainless-steel pins were introduced into the esophageal lumen; one pin was fixed to the bottom of the organ bath and the other was connected to the bar of the isometric force transducer (T7-30-240; Orientec, Tokyo, Japan). For recording contractile responses of the muscle strips isolated from the heart and the soleus muscle, one end was fixed to an L-shaped hook at the bath side and the other end was connected to an isometric tension transducer via a placed silk-snare. The contractile responses were recorded isometrically on PowerLab system (ADInstruments, Bella Vista NSW, Australia) through an AC amplifier (AS1202, NEC, Tokyo, Japan). An initial resting tension of 1 g was applied to each preparation, which was subsequently allowed to equilibrate for at least 30 minutes.

2.5. Electrical Field Stimulation. For inducing muscle contractile response, electrical field stimulation (EFS) was applied through a pair of platinum electrodes placed on either sides of each preparation. EFS was applied using an electronic stimulator (model SEN-3201, Nihon Kohden, Tokyo, Japan) connected to the electrodes. For EFS with single pulses, square-wave pulses of supramaximal intensity (80 V) and 10 ms in duration were applied at intervals of 2 minutes. For repeated multipulse EFS, square-wave pulses of supramaximal intensity (80 V) and 10 ms in duration were applied at frequency of 20 Hz for 1 s.

2.6. Data Processing and Statistical Analysis. Data are presented as means \pm standard deviation (S.D). Isometric contractile responses were given as g contraction/ mm^3 tissue volume. n indicates the number of separate preparations. The significance of differences between mean values was determined by one-way analysis of variance followed by

Tukey-Kramer's test. A P -value less than .05 denotes the presence of a statistically significant difference.

3. Results

3.1. EFS-Induced Contractile Responses of Esophageal, Skeletal, and Cardiac Muscles. To clarify the contractile properties, the mechanical responses to EFS were recorded in esophageal, skeletal, and cardiac muscle preparations. Spontaneous contractions occurred without electrical stimulations in some preparations of cardiac muscle but not in preparations of esophageal and skeletal muscles (data not shown). EFS with single pulses (voltage: 80 V, duration: 10 ms) evoked twitch-like contractions in all types of muscle preparations (Figure 1(a)). The contractile responses were abolished by tetrodotoxin ($1 \mu\text{M}$) in esophageal and skeletal muscles, whereas the blocker failed to affect the contractions in cardiac muscle (data not shown). The amplitude of the twitch-like contraction of esophageal muscle was larger than that of skeletal muscle and was comparable to that of cardiac muscle (Figure 1(a)). The duration of the twitch-like contraction of esophageal muscle was comparable to that of skeletal muscle but shorter than that of cardiac muscle (Figure 1(b)).

3.2. Characterization of Summation of Contraction in Esophageal, Skeletal, and Cardiac Muscles. To determine whether esophageal muscle shows summation of contractions, repeated EFS (80 V-10 ms, 20 Hz for 1 s) was applied to the preparations. Skeletal muscle and cardiac muscle preparations were also used to obtain positive and negative controls of summation, respectively. Repeated multipulse EFS evoked summation of contraction in skeletal muscle, resulting in tetanic contractions (Figure 2(b)). In contrast, cardiac muscle did not show summation of contraction (Figure 2(c)). Esophageal muscle preparation responded to all 20 individual stimulations and summated transiently in response to the initial several stimulations (Figure 2(a)). However, the response observed in esophageal muscle was different from that in skeletal muscle. Maximal amplitude of tetanic contractions was 2-3 times larger than that of twitch-like responses induced by single-pulse EFS in skeletal muscle (Figure 2(b)). Esophageal muscle reached a peak of tetanic contractions after 3-4 pulses, the amplitude of which was about 1.5 times larger than that of twitch-like responses (Figure 2(a)). Then an amplitude similar to that of the twitch-like contraction was sustained until the end of the stimulations (Figure 2(a)).

3.3. Effects of an Inhibitor of Gap Junctions on EFS-Induced Contractions in Esophageal and Cardiac Muscles. To clarify the involvement of gap junctions in the contractile responses, we examined the effects of an inhibitor of gap junctions, halothane, on the EFS-induced contractions in esophageal and cardiac muscles. Application of halothane (50 mM) inhibited the contractions in cardiac muscle (Figure 3(b)). In

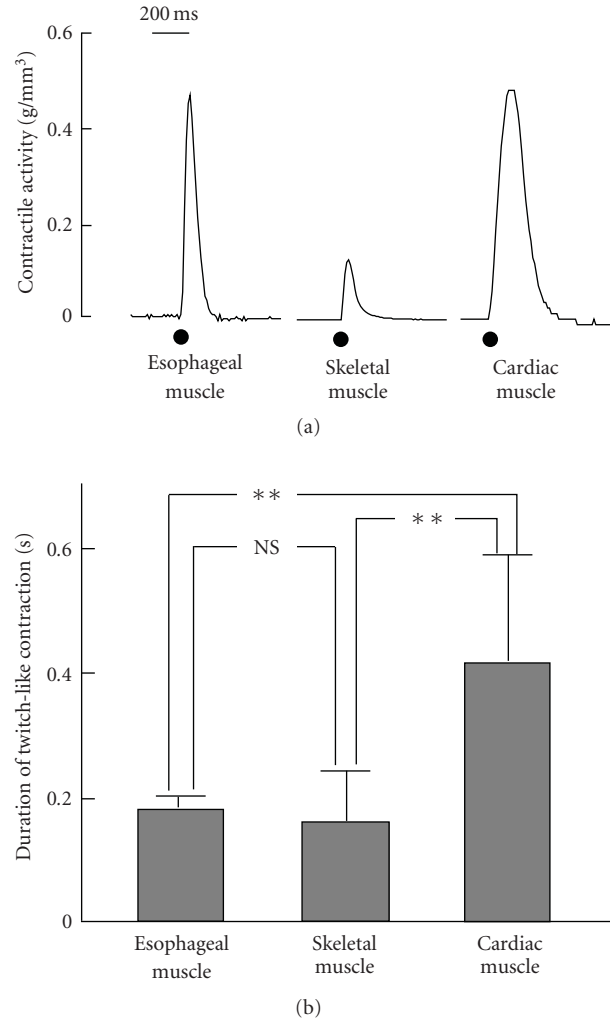


FIGURE 1: Single-pulse electrical stimulation-induced twitch-like contractions of esophageal, skeletal, and cardiac muscles in rats. (a) Representative traces of the contractile responses to electrical field stimulations (EFS) in esophageal, skeletal, and cardiac muscle preparations are shown. EFS was applied by using single pulses (voltage: 80 V, duration: 10 ms). Closed circles indicate the points of EFS. (b) Summary graphs of the duration of the EFS-evoked twitch-like contractions in esophageal ($n = 16$), skeletal ($n = 6$), and cardiac ($n = 5$) muscle preparations. Each bar represents the mean \pm S.D. ** shows significant difference ($P < .01$). NS shows no significant difference.

contrast, esophageal muscle contractions were not affected by halothane (Figure 3(a)).

3.4. Contractile Responses Induced by High Potassium Stimulation in Esophageal, Skeletal, and Cardiac Muscles. We then compared the effects of high potassium stimulation on the contractile responses in the three muscles. Application of high potassium (118.4 mM) in the organ bath evoked phasic contractions in esophageal and skeletal muscles (Figure 4(a)). In contrast, cardiac muscle showed long-lasting contractions, which were sustained at least for 2 minutes.

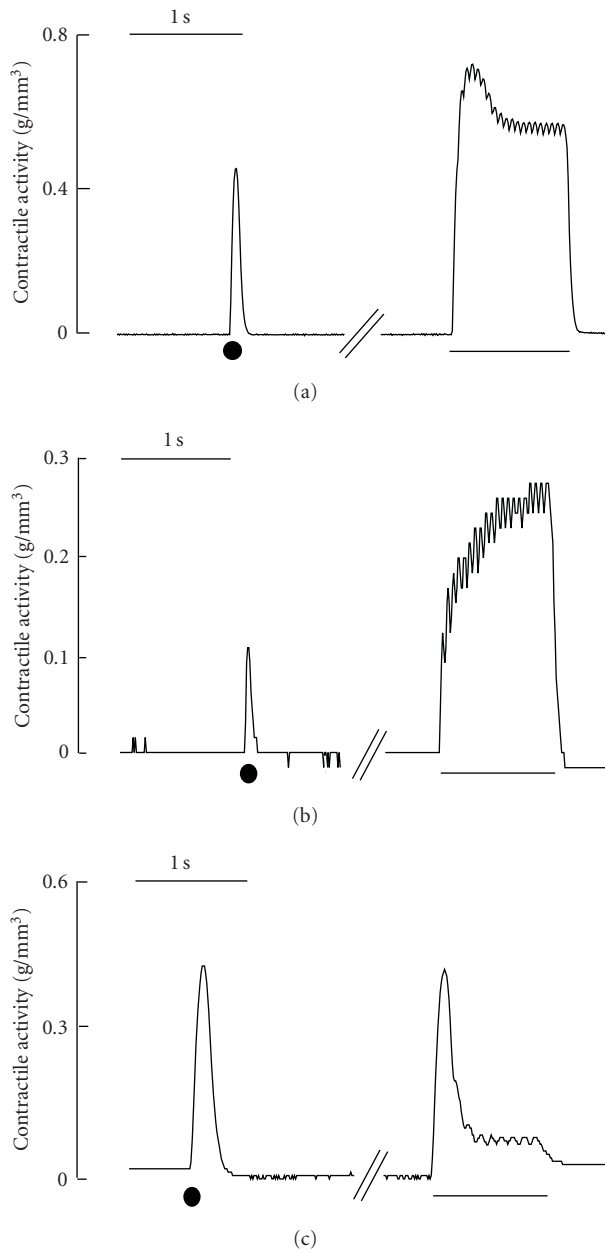


FIGURE 2: Multipulse electrical stimulation-induced contractile responses of esophageal, skeletal, and cardiac muscles. Representative traces of the contractile responses to single and multipulse repeated EFS in esophageal (a), skeletal (b), and cardiac (c) muscle preparations are shown. Similar results were reproducibly obtained in five independent experiments. EFS was applied by using single or repeated pulses (80 V-10 ms, 20 Hz for 1 s). Closed circles and underbars indicate the points of single EFS and the location of multiple EFS, respectively.

3.5. Contractile Responses Induced by Caffeine in Esophageal, Skeletal, and Cardiac Muscles. Exogenous application of caffeine (20 mM), a releaser of calcium from intracellular stores, caused two-phase contractions in esophageal and skeletal muscles (Figure 4(b)). First-phase contraction occurred just after application of caffeine and sustained the tension for

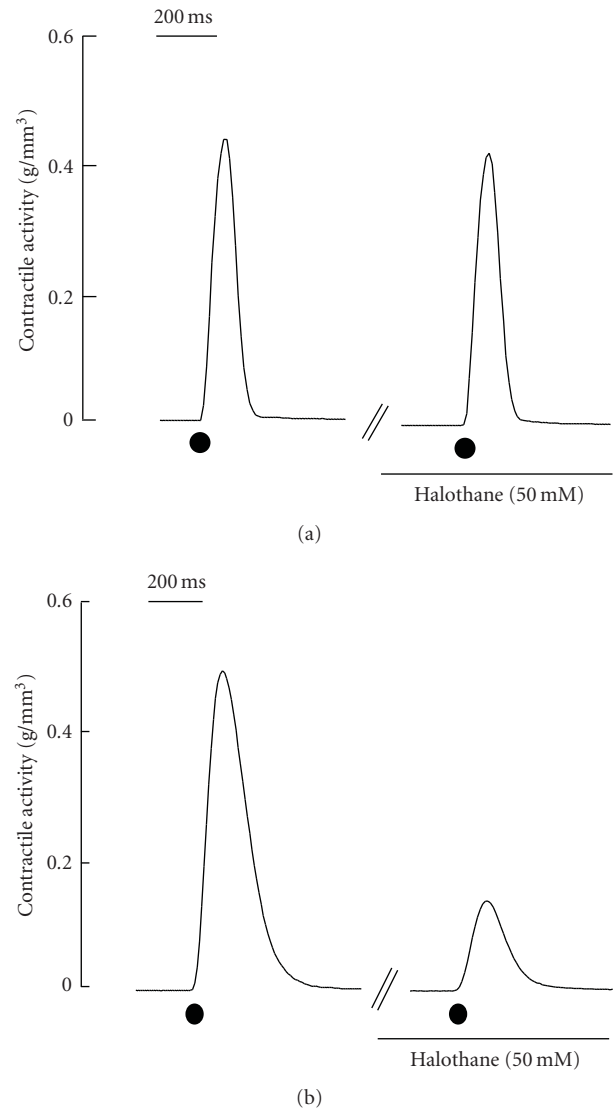


FIGURE 3: Effects of halothane on the contractile responses in esophageal and cardiac muscles. Single-pulse EFS was applied in the absence and presence of halothane (50 mM), an inhibitor of gap junctions, and the contractile responses were recorded. Representative traces of esophageal (a) and cardiac (b) muscle preparations are shown. Similar results were reproducibly obtained in four independent experiments.

about 5 minutes. After the first contraction, the tension was increased again, inducing the second-phase contraction (Figure 4(b)). On the other hand, cardiac muscle showed a small sustained contraction.

4. Discussion

In the present study, we investigated the contractile properties of esophageal striated muscle by comparison with those of other types of striated muscle, that is, skeletal and cardiac muscles. The major findings are (1) EFS with single pulses evoked twitch-like contractile responses in esophageal muscle, similar to those in skeletal muscle in duration and

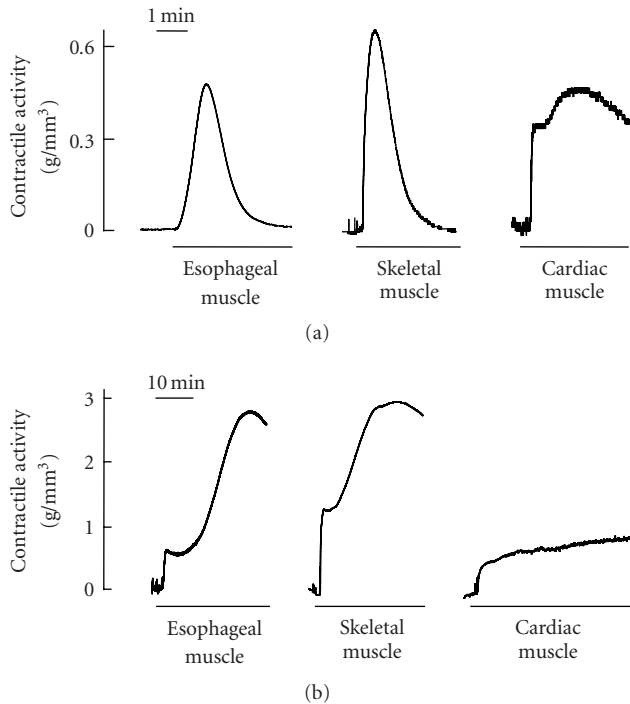


FIGURE 4: Contractile responses induced by high potassium or caffeine in esophageal, skeletal, and cardiac muscles. Muscle preparations were stimulated with high potassium (a) or caffeine (b). Representative traces of the contractile responses in esophageal, skeletal and cardiac preparations are shown. Similar results were reproducibly obtained in five independent experiments. Underbars indicate the application of high potassium (118.4 mM) and caffeine (20 mM).

similar to those in cardiac muscle in amplitude, (2) EFS with a high frequency induced a transient summation of contractions followed by a sustained contraction with an amplitude comparable to that of twitch-like contraction induced by the single-pulse EFS, (3) an inhibitor of gap junctions did not affect the esophageal contractions, and (4) both high potassium stimulation and application of caffeine induced contractions of esophageal muscle in a manner analogous to that of skeletal muscle. These findings suggest that contractile properties of esophageal striated muscle are not identical to those of skeletal muscle. The specific characteristics revealed in the present study might be associated with effective peristalsis in the striated muscle portion of the esophagus.

It has generally been accepted that striated muscle fibers in the esophagus are a type of “skeletal” muscle [3, 5, 6]. In agreement with this, esophageal striated muscle showed properties similar to those of skeletal muscle (soleus muscle) in terms of duration of twitch-like contraction, sensitivity to tetrodotoxin, and responses to high potassium or caffeine. It was of interest to determine whether esophageal striated muscle has the ability to contract spontaneously, but it never showed contractile activity unless appropriate stimulus was applied. This is also in line with the general concept that esophageal muscle fibers are skeletal muscles. However,

summation of the contractions during tetanic stimulation was not obvious in the esophageal muscle, although large summation of contractions is one of the important characteristics of skeletal muscles. Moreover, large amplitude of twitch-like contraction in the esophageal muscle after application of a single-pulse stimulus is analogous to that in cardiac, but not skeletal, muscle. It is therefore thought that esophageal striated muscle is similar but not identical to skeletal muscle.

Low amplitude in twitch-like contraction is a potential basis for large summation of contractions in skeletal muscle since it provides a wide margin to summate sequential contractions. It is thus reasonable to expect that the modest summation of contractions in the esophageal muscle may be related, at least in part, to the large amplitude of contraction in response to single-pulse stimulation. In the case of cardiac muscle, the large amplitude of twitch-like contraction can contribute to generation of sufficient ventricular pressure during isovolumic contraction and to effective reduction of ventricular end-systolic volume [28–30]. The absence of summation is also essential to ensure diastolic intervals for ventricular filling [30]. Considering that properties of cardiac muscle are adequately utilized to accomplish effective pumping out of blood in the heart, the properties of esophageal muscle would be suitable for the esophageal peristalsis. In contrast to small and large intestines, where intraluminal contents are usually chyme, the esophagus needs to propel solid foods rapidly. For this purpose, rapid and large contraction of the esophageal muscle in response to neural messages may be convenient. Furthermore, esophageal function is specialized for propulsion, but not agitation or retention [7, 16]. It is therefore most probable that keeping the maximal contraction at a particular portion of the esophagus is dispensable but that dilation of muscle after propelling the intraluminal contents is required to receive additional foods or to prevent stagnation. Accordingly, it seems likely that only a transient summation of contractions, which is one of the specific properties of esophageal muscle, is suitable for the function of the esophagus.

In the cardiac muscle preparation, EFS applied at 20 Hz caused one complete twitch-like contraction followed by small rise in tension. It is well established that the lack of summation in cardiac muscle depends on a long-lasting refractory period of the action potential, which results in substantial overlapping between the refractory period and duration of contraction [30]. However, the refractory period of esophageal muscle would not overlap with its contraction. This is based on the fact that esophageal muscle contractions induced by high-frequency stimulation were maintained after the transient summation, with the amplitudes being comparable to those of twitch-like contractions. Taking into consideration the fact that strength of striated muscle contraction is correlated with intracellular calcium concentration [31], it can be postulated that esophageal muscle has the ability to keep calcium level at a constant level during repeated stimulation. Since caffeine, a calcium releaser from the intracellular calcium store, caused similar tetanic contractions in esophageal and skeletal muscles, it is

possible that calcium uptake into the store is unique in the esophageal striated muscle.

Electrical coupling of cardiac muscle cells through gap junctions is essential for coordinated contraction [32, 33]. In the present study, we tried to elucidate the possible involvement of gap junctions in coordination of the contractions of esophageal striated muscles. An inhibitor of gap junctions, halothane, failed to affect EFS-induced contractile responses in esophageal muscle, whereas the inhibitor blocked those in cardiac muscle. Gap junctional protein connexin 43, which is a major connexin expressed in cardiac muscles [32], was not detected in esophageal muscles in our immunohistochemical analysis (unpublished observation). At present, the most probable conclusion is that esophageal muscles do not couple to each other through gap junction channels. However, gap junction channels are formed by a family of more than 20 connexin proteins [34, 35], and halothane might not inhibit all of the gap junction proteins. Hence, there remains the possibility that the halothane-insensitive channels are operated in the esophageal muscles.

5. Conclusion

We characterized the contractile properties of esophageal muscle in comparison with those of skeletal and cardiac muscles in rats. The results demonstrate that esophageal muscle has properties that are similar but not identical to those of skeletal muscle. It is thought that some specific properties of esophageal muscle may be beneficial for peristaltic motility in the esophagus.

Acknowledgment

This work was supported in part by Grants-In-Aid for Scientific Research from the Ministry of Education, Culture, Sports, Science, and Technology of Japan.

References

- [1] N. Izumi, H. Matsuyama, Y. Yamamoto, et al., "Morphological and morphometrical characteristics of the esophageal intrinsic nervous system in the golden hamster," *European Journal of Morphology*, vol. 40, no. 3, pp. 137–144, 2002.
- [2] T. Shiina, Y. Shimizu, N. Izumi, et al., "A comparative histological study on the distribution of striated and smooth muscles and glands in the esophagus of wild birds and mammals," *Journal of Veterinary Medical Science*, vol. 67, no. 1, pp. 115–117, 2005.
- [3] J. Wörl and W. L. Neuhuber, "Enteric co-innervation of motor endplates in the esophagus: state of the art ten years after," *Histochemistry and Cell Biology*, vol. 123, no. 2, pp. 117–130, 2005.
- [4] D. Bieger and D. A. Hopkins, "Viscerotopic representation of the upper alimentary tract in the medulla oblongata in the rat: the nucleus ambiguus," *Journal of Comparative Neurology*, vol. 262, no. 4, pp. 546–562, 1987.
- [5] E. T. Cunningham Jr. and P. E. Sawchenko, "Central neural control of esophageal motility: a review," *Dysphagia*, vol. 5, no. 1, pp. 35–51, 1990.
- [6] W. L. Neuhuber, M. Kressel, A. Stark, and H.-R. Berthoud, "Vagal efferent and afferent innervation of the rat esophagus as demonstrated by anterograde DiI and DiA tracing: focus on myenteric ganglia," *Journal of the Autonomic Nervous System*, vol. 70, no. 1-2, pp. 92–102, 1998.
- [7] R. K. Goyal and A. Chaudhury, "Physiology of normal esophageal motility," *Journal of Clinical Gastroenterology*, vol. 42, no. 5, pp. 610–619, 2008.
- [8] C. Olsson and S. Holmgren, "The control of gut motility," *Comparative Biochemistry and Physiology A*, vol. 128, no. 3, pp. 481–503, 2001.
- [9] G. M. Makhlof and K. S. Murthy, "Smooth muscle and the gut," in *Textbook of Gastroenterology*, T. Yamada, Ed., pp. 103–132, Blackwell, Oxford, UK, 5th edition, 2009.
- [10] W. A. A. Kunze and J. B. Furness, "The enteric nervous system and regulation of intestinal motility," *Annual Review of Physiology*, vol. 61, pp. 117–142, 1999.
- [11] M. B. Hansen, "Neurohumoral control of gastrointestinal motility," *Physiological Research*, vol. 52, no. 1, pp. 1–30, 2003.
- [12] J. B. Furness, *The Enteric Nervous System*, Blackwell, Malden, Mass, USA, 2006.
- [13] A. K. Mukhopadhyay and N. W. Weisbrodt, "Neural organization of esophageal peristalsis: role of vagus nerve," *Gastroenterology*, vol. 68, no. 3, pp. 444–447, 1975.
- [14] H. Park and J. L. Conklin, "Neuromuscular control of esophageal peristalsis," *Current Gastroenterology Reports*, vol. 1, no. 3, pp. 186–197, 1999.
- [15] A. Jean, "Brain stem control of swallowing: neuronal network and cellular mechanisms," *Physiological Reviews*, vol. 81, no. 2, pp. 929–969, 2001.
- [16] R. E. Clouse and N. E. Diamant, "Motor function of the esophagus," in *Physiology of the Gastrointestinal Tract*, L. R. Johnson, Ed., pp. 913–926, Elsevier Academic, Burlington, Mass, USA, 4th edition, 2006.
- [17] W. L. Neuhuber, M. Raab, J. Wörl, and H. R. Berthoud, "Innervation of the mammalian esophagus," *Advances in Anatomy, Embryology, and Cell Biology*, vol. 185, pp. 1–73, 2006.
- [18] N. Izumi, H. Matsuyama, M. Ko, Y. Shimizu, and T. Takewaki, "Role of intrinsic nitrergic neurones on vagally mediated striated muscle contractions in the hamster oesophagus," *Journal of Physiology*, vol. 551, no. 1, pp. 287–294, 2003.
- [19] T. Shiina, Y. Shimizu, A. Boudaka, J. Wörl, and T. Takewaki, "Tachykinins are involved in local reflex modulation of vagally mediated striated muscle contractions in the rat esophagus via tachykinin NK1 receptors," *Neuroscience*, vol. 139, no. 2, pp. 495–503, 2006.
- [20] A. Boudaka, J. Wörl, T. Shiina, et al., "Involvement of TRPV1-dependent and -independent components in the regulation of vagally induced contractions in the mouse esophagus," *European Journal of Pharmacology*, vol. 556, no. 1–3, pp. 157–165, 2007.
- [21] A. Boudaka, J. Wörl, T. Shiina, Y. Shimizu, T. Takewaki, and W. L. Neuhuber, "Galanin modulates vagally induced contractions in the mouse oesophagus," *Neurogastroenterology and Motility*, vol. 21, no. 2, pp. 180–188, 2009.
- [22] E. E. Daniel and S. Sarna, "The generation and conduction of activity in smooth muscle," *Annual Review of Pharmacology and Toxicology*, vol. 18, pp. 145–166, 1978.
- [23] E. Chow and J. D. Huizinga, "Myogenic electrical control activity in longitudinal muscle of human and dog colon," *Journal of Physiology*, vol. 392, pp. 21–34, 1987.

- [24] M. J. Berridge, "Smooth muscle cell calcium activation mechanisms," *Journal of Physiology*, vol. 586, no. 21, pp. 5047–5061, 2008.
- [25] W. F. Ganong, *Review of Medical Physiology*, McGraw-Hill, New York, NY, USA, 22nd edition, 2005.
- [26] T. Desplantez, E. Dupont, N. J. Severs, and R. Weingart, "Gap junction channels and cardiac impulse propagation," *Journal of Membrane Biology*, vol. 218, no. 1–3, pp. 13–28, 2007.
- [27] A. Rodriguez-Sinovas, D. Garcia-Dorado, M. Ruiz-Meana, and J. Soler-Soler, "Enhanced effect of gap junction uncouplers on macroscopic electrical properties of reperfused myocardium," *Journal of Physiology*, vol. 559, no. 1, pp. 245–257, 2004.
- [28] M. I. Noble, "The contribution of blood momentum to left ventricular ejection in the dog," *Circulation Research*, vol. 23, no. 5, pp. 663–670, 1968.
- [29] J. S. Rankin, P. A. McHale, and C. E. Arentzen, "The three dimensional dynamic geometry of the left ventricle in the conscious dog," *Circulation Research*, vol. 39, no. 3, pp. 304–313, 1976.
- [30] J. R. Levick, *An Introduction to Cardiovascular Physiology*, Butterworth-Heinemann, Oxford, UK, 2nd edition, 1995.
- [31] S. Buvinic, G. Almarza, M. Bustamante, et al., "ATP released by electrical stimuli elicits calcium transients and gene expression in skeletal muscle," *Journal of Biological Chemistry*, vol. 284, no. 50, pp. 34490–34505, 2009.
- [32] E. C. Beyer, L. M. Davis, J. E. Saffitz, and R. D. Veenstra, "Cardiac intercellular communication: consequences of connexin distribution and diversity," *Brazilian Journal of Medical and Biological Research*, vol. 28, no. 4, pp. 415–425, 1995.
- [33] G. Mese, G. Richard, and T. W. White, "Gap junctions: basic structure and function," *Journal of Investigative Dermatology*, vol. 127, no. 11, pp. 2516–2524, 2007.
- [34] K. Willecke, J. Eiberger, J. Degen, et al., "Structural and functional diversity of connexin genes in the mouse and human genome," *Biological Chemistry*, vol. 383, no. 5, pp. 725–737, 2002.
- [35] H. S. Duffy, A. G. Fort, and D. C. Spray, "Cardiac connexins: genes to nexus," *Advances in Cardiology*, vol. 42, pp. 1–17, 2006.

Research Article

Characteristics of Tetanic Force Produced by the Sternomastoid Muscle of the Rat

Stanislaw Sobotka^{1,2} and Liancai Mu¹

¹Department of Research, Upper Airway Research Laboratory, Hackensack University Medical Center, Hackensack, NJ 07601, USA

²Department of Neurosurgery, Mount Sinai School of Medicine, NY 10029, USA

Correspondence should be addressed to Stanislaw Sobotka, ssobotka@humed.com

Received 2 November 2009; Revised 9 February 2010; Accepted 4 March 2010

Academic Editor: Henk L. M. Granzier

Copyright © 2010 S. Sobotka and L. Mu. This is an open access article distributed under the Creative Commons Attribution License, which permits unrestricted use, distribution, and reproduction in any medium, provided the original work is properly cited.

The sternomastoid (SM) muscle plays an important role in supporting breathing. It also has unique anatomical advantages that allow its wide use in head and neck tissue reconstruction and muscle reinnervation. However, little is known about its contractile properties. The experiments were run on rats and designed to determine in vivo the relationship between muscle force (active muscle contraction to electrical stimulation) with passive tension (passive force changing muscle length) and two parameters (intensity and frequency) of electrical stimulation. The threshold current for initiating noticeable muscle contraction was 0.03 mA. Maximal muscle force (0.94 N) was produced by using moderate muscle length/tension (28 mm/0.08 N), 0.2 mA stimulation current, and 150 Hz stimulation frequency. These data are important not only to better understand the contractile properties of the rat SM muscle, but also to provide normative values which are critical to reliably assess the extent of functional recovery following muscle reinnervation.

1. Introduction

The sternocleidomastoid (SCM) muscle lies on the lateral side of the neck. Anatomically, it is composed of two bellies, a medially and superficially localized sternomastoid (SM), and a laterally and deeply positioned cleidomastoid (CM). Functionally, the SCM participates in head movements and respiration [1]. In respiration, it serves as an “accessory” inspiratory muscle in the neck. Activation of the SCM causes cranial displacement of the sternum and ribcage during conscious inspiratory efforts [2–4]. In general, the SCM is not active during resting breathing, but contracts during strong respiratory efforts [5]. Previous studies demonstrated that the SCM plays a particularly important role in patients with obstructive lung disease, where its increased activity even at rest improves oxygen delivery to the lungs [2].

As the SM belly is located more superficially in the neck and has a relatively larger muscle mass when compared with the CM belly, it has been widely used as a muscle or myocutaneous flap for reconstruction of oral cavity and

facial defects [6, 7]. In addition, the SM muscle [8] and cervical strap muscles [9, 10] have been commonly used in laryngeal and facial reinnervation.

We have a longstanding interest in the development of novel surgical techniques to effectively reinnervate paralyzed muscles as the presently used reinnervation methods result in poor outcomes (for review see [11, 12]). Although the nerve-muscle pedicle (NMP) technique has been commonly employed to treat laryngeal and facial paralysis in animal experiments and clinical practice, controversy exists concerning the optimal results and success rate of the functional recovery [13–16]. In our on-going reinnervation studies, the SM muscle has been chosen as a studied muscle in a rat model because this muscle has anatomical advantages over other neck muscles. Specifically, the SM muscle and its innervating nerve can be easily accessed and manipulated. In addition, we have established a large database regarding the patterns of nerve supply, motor endplate morphology, and muscle fiber-type distribution of the SM muscle in the rat (unpublished data) which is critical for designing new reinnervation procedures.

A number of morphological and physiological approaches have been used to assess the success of axonal regeneration and the extent of functional recovery of a reinnervated muscle after a given reinnervation procedure. Electromyography (EMG) [17, 18] and muscle force measurement [19–22] are often used to assess functional recovery after muscle reinnervation. The amplitude and frequency of the recorded EMG bursts are indicative of the quantity of the activating motor units involved in a given motor task. However, the maximum force provides a better overall estimate of the mechanics of a whole muscle, and the muscle force measurements are usually used to evaluate quantitatively the mechanical function and contractile properties of a reinnervated muscle.

Although some researchers investigated *in vivo* SM muscle force in rabbits [23], the force characteristics of the SM muscle in rats have never been determined. Measuring the force of isometric tetanic muscle contraction can be an invaluable tool to evaluate muscle strength after nerve injury and subsequent repair [21, 24]. Intraspecimen comparison seems to be a practical method for evaluating the recovery of maximum force. It has been recognized that opposite muscles have the same strength in healthy animals [25]. However, after unilateral injury, the left-right muscle balance is not present any more. The healthy muscle is overstrained, as it is now responsible for the constant support of functions previously maintained by muscles from both sides. It leads to changes in the anatomical and physiological characteristics of the neuromuscular system at the noninjured side. Therefore, interspecimen normative data are needed for a nonbiased evaluation of the degree of recovery in a reinnervated muscle.

The present study is focused on determining the muscle force characteristics of the SM muscle in healthy rats. These results would provide normative data which could be useful for understanding the physiological role of the SM muscle and for evaluating the extent of functional recovery after reinnervation of a paralyzed SM muscle. We would also like to establish the optimal stimulation parameters which could be used to produce the strongest isometric force by this muscle.

2. Materials and Methods

2.1. Animals. Twelve adult (3.5 months old) Sprague-Dawley male rats (Charles River Laboratories, MA), weighing 350–450 grams, were used in this study. Previous studies [26] showed that there is no gender difference in rat upper airway muscle force and other muscle contractile properties. The animals were provided with *ad libitum* access to food and water and housed in standard cages in a 22°C environment with a 12:12-h light-dark cycle. All experimental procedures were reviewed and approved by the Institutional Animal Care and Use Committee prior to the onset of experiments. The experiments were performed in accordance with the *Guide for Care and Use of Laboratory Animals* published by the US National Institutes of Health (NIH Publication no. 85-23, revised 1996). All efforts were made to minimize the number of animals and their suffering in the experiments.

2.2. Surgical Procedures. All rats underwent open neck surgery under an Olympus SZX12 Stereo zoom surgical microscope (Olympus America Inc., Center Valley, PA) to expose the right SM muscle through a midline skin incision from the hyoid bone to the sternum. Animals were anesthetized with an initial intraperitoneal injection of ketamine (80 mg/kg body wt) and xylazine (5 mg/kg body wt); supplementary doses were administered as needed to maintain an adequate state of anesthesia. The rat was placed on a heating pad (homeothermic blanket system, Stoelting, Wood Dale, IL) to maintain its temperature at 35°C.

2.3. Muscle Preparation. Our studies have demonstrated that the rat SM is supplied by a branch derived from the spinal accessory nerve and has a single motor endplate band at the midpoint of the muscle (data not shown). The right SM muscle and its innervating nerve were isolated from surrounding tissues and prepared for nerve stimulation and force measurement. First of all, the rostral tendon of the SM was identified, transected, and attached with a 2-0 suture to a servomotor lever arm (Model 305B Dual-Mode Lever Arm System, Aurora Scientific Inc., Aurora, Ontario, Canada, see Figure 1). The adjustable arm of the servomotor was used to alter muscle length and to provide a measure of muscle force. Then, the SM nerve was placed on a bipolar stimulating electrode constructed from two hooked silver wires separated by 4 mm (Figure 1) attached to a high precision micromanipulator (Narishige Scientific Instruments, Tokyo, Japan).

2.4. Nerve Stimulation and Muscle Force Measurement. Isometric contraction of the SM muscle was obtained with two 200 ms trains of biphasic rectangular pulses (0.2 msec duration) separated by a 20-second break. A break of at least 1 minute was used before trying subsequent pairs of trains. The maximum value of muscle force during each 200 ms contraction was identified. The maximal force during the first and second stimulation trains was averaged. Initial passive tension before stimulation was subtracted from this value. This difference between output force and preload force represents the muscle force measurement. Typically, current was set to 0.1 mA and frequency of stimulation to 200 Hz. The force generated by the contraction of the SM muscle was transduced with the servomotor of a 305B lever system and displayed on a computer screen. At the moment of force measurements, the lever arm was stationary.

To prevent cooling and drying, the SM muscle and nerve were regularly bathed with warm mineral oil throughout the testing. Although changes in muscle temperatures above 25°C significantly influence twitch force, they only have a small influence on tetanic force [27, 28]. To reduce the variability of collected force data, the temperature of the SM muscle was monitored regularly and maintained between 35–36°C.

During force measurement, several parameters influencing force production were examined to establish the optimal settings for obtaining maximum muscle force as described below.

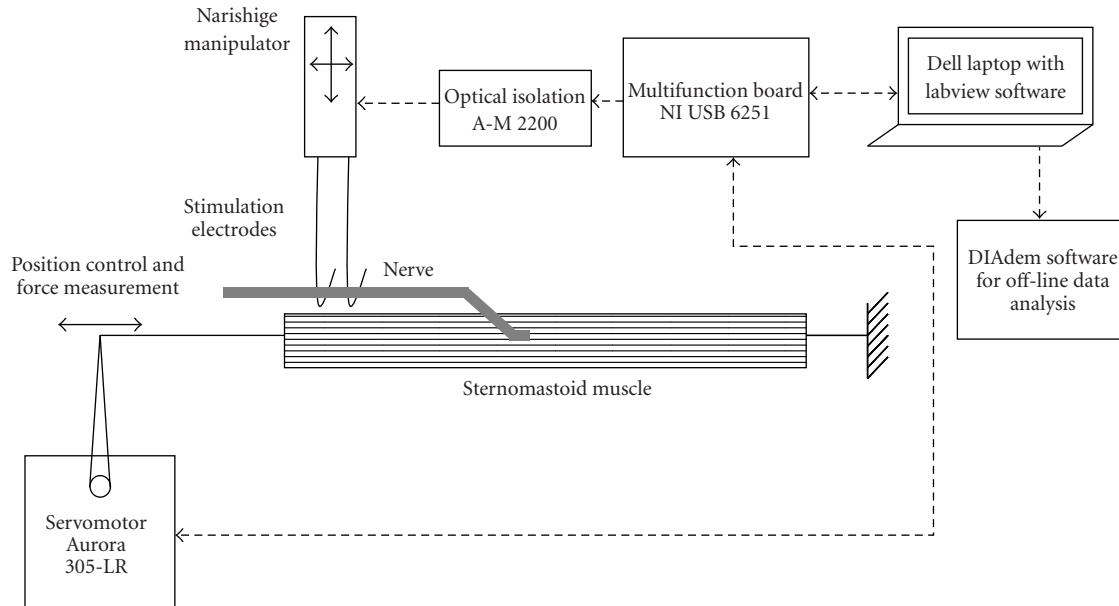


FIGURE 1: A diagram of the data acquisition system, which provides electrical stimulation and records muscle force. Note that a dell laptop with user written software in Labview 8.2 is used to control the experiment. The SM muscle is detached from its rostral tendon and attached to the lever of servomotor, which controls muscle stretch and measures muscle force. Electrical stimulation with parameters controlled by LabView software (National Instruments) is generated by the Multifunctional board 6251 (National Instruments) and delivered to the SM nerve. Data are analyzed off line with DIAdem 11.0 software (National Instruments).

2.4.1. Muscle Length/Tension. As maximal muscle force can be generated at optimal muscle length, we examined the length-force relationship. Muscle length was controlled by gradually stretching the SM muscle using the lever arm to pull the muscle with different tensions (very low tension—0.04 N, low tension—0.06 N, medium tension—0.08 N, high tension—0.1 N, and very high tension—0.24 N). Finally, the length of the muscle (in millimeters) was measured at different levels of passive tension (0.04–0.24 N). These passive tension values were chosen based on our preliminary studies. The optimal tension that generates the highest muscle force was determined by our preliminary work and confirmed in the experimental group presented in this paper. The muscle force at a given muscle length was measured in response to electrical stimulation with a train of pulses of 0.1 mA current, at a frequency of 200 pulses per second.

2.4.2. Stimulation Intensity. The SM muscle was stretched with the medium tension of 0.08 N at which the highest muscle force was consistently produced. Then, the muscle force was measured as a function of stimulation current. The intensity of stimulation current was increased starting from 0.01 mA through the level where the muscle force reached a plateau (about 0.1 mA) and continued at the supramaximal level until 0.5 mA.

2.4.3. Stimulation Frequency. To analyze the other parameters responsible for maximum force generation, a force-frequency curve was built. Two trains of stimuli (200 msec duration each, with a rest period of 20 seconds between contractions) with incrementally increasing frequencies were

delivered. The stimulation frequency was increased gradually from 5 Hz (when only one pulse during the 200 ms stimulation period was given and could be used to evaluate twitch muscle force), through frequencies for which the muscle force reached a plateau (about 100 Hz) and continued to increase until 500 Hz.

2.5. Muscle Weight. Following the completion of isometric force testing, the rat was euthanized with an overdose of anesthetic. The entire SM muscle was removed and weighed (in grams).

2.6. Data Acquisition System. The experiment was controlled by an Acquisition System built from a multifunction I/O National Instruments Acquisition Board (NI USB 6251, 16 bit 1.25 Ms/s, National Instruments, Austin, TX) connected to a DELL laptop with a custom written program using labVIEW 8.2 software (National Instruments, see Figure 1). The system produced two output signals with all parameters set by the user through virtual control knobs created by the LabView program. One output provided stimulation pulses, which after isolation from the ground through an optical isolation unit (Analog Stimulus Isolator Model 2200, A-M Systems, Inc, Carlsborg, WA) were used for the current controlled nerve stimulation. The other output provided a position signal, which was used by the servomotor of the 305B Dual-Mode Lever System to control muscle length. The Acquisition System was also used to collect a muscle force signal from the 305B Dual-Mode Lever System. Collected data were analyzed offline with DIAdem 11.0 software (National Instruments).

2.7. Statistical Analysis. Experimental variables included three independent variables (initial passive tension before stimulation, current and frequency of stimulation) and one dependent variable: muscle force generated during stimulation. Minimal stimulation current (when the stimulation train was set at 200 Hz), minimal stimulation frequency (when stimulation pulses were set at 0.1 mA), and optimal length of the muscle (when stimulation parameters were set at 0.1 mA and 200 Hz), which were able to produce maximal tetanic muscle contraction, were described by the means and standard deviations. The *t*-test for pairs was used to determine the statistical significance of difference between data points. The significance level was set at $P < .05$.

3. Results

SM muscle force was defined as the difference between maximal muscle contraction observed during electrical stimulation (with 200 ms train of pulses) and the initial tension of the muscle just before stimulation. Our goal was to establish optimal muscle length and characteristics of muscle force generated by electrical stimulation, which could be used in our further studies as a reference (muscle force generated by the muscle with an intact nerve) to evaluate the level of muscle force recovery after reinnervation. Therefore, we evaluated how muscle force depends on initial passive tension and how it changes with intensity and frequency of nerve stimulation.

3.1. Optimal Muscle Length/Tension for Maximal Muscle Force. Muscle force is a function of muscle length produced by an initial stretch of the muscle before electrical stimulation. The muscle was stretched with the following tensions before stimulation: very loose (0.04 N), loose (0.06 N), moderate (0.08 N), tense (0.1 N), and very tense (0.24 N). We used 0.1 mA pulses at 200 Hz. The averaged data from the whole group of rats illustrating the decrease of muscle force at different passive tensions is shown in Figure 2. The typical length-force “inverted U” relationship was found as described by others [29, 30].

The muscle force was found to be the highest (mean = 0.94 N), when the muscle was initially stretched at a moderate tension (set at 0.08 N). Decreasing initial tension to “loose” (set at 0.06 N) decreased muscle force by 12% (0.82 N—statistically significant decrease $P < .01$, $t = 3.2$, two-tailed *t*-test for pairs, $df = 11$), whereas increasing initial tension to “tense” (set at 0.1 N) reduced muscle force by 6% (0.88 N—not statistically significant decrease, $P > .05$, $t = 0.5$, $df = 11$).

3.2. Muscle Force Evoked by Different Intensity of Stimulation. To examine the relationship between muscle force and stimulation current, we varied the current from 0 to 0.5 mA at 200 Hz trains of pulses when the muscle was stretched with moderate tension of 0.08 N, which produced optimal muscle length. Figure 3 shows the time course of muscle force responses to different stimulation currents in a representative rat. The difference between the maximal force produced by

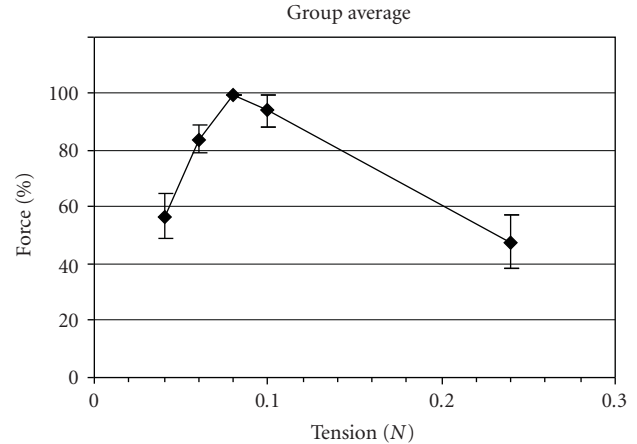


FIGURE 2: Muscle force as a function of passive tension before stimulation. This force-tension curve was normalized by maximal force to illustrate the rate of decline of force at different passive tensions (set up just before electrical stimulation). The nerve was stimulated with 0.1 mA pulses at 200 Hz. The group average is shown. Vertical bars represent standard error of the mean. Nerve stimulation at moderate tension of the muscle (0.08 N) yielded maximal muscle force (0.94 N). The data presented in this and all following figures were collected, when the nerve was stimulated with a 200 ms train of biphasic pulses of 0.2 ms width.

the SM muscle during nerve stimulation and the passive tension before stimulation was used to generate the current-force curve. The relationship between the density of force produced by the SM muscle (normalized by its cross-section area) and stimulation current in the group average is shown in Figure 4. In most of our animals, 0.03 mA was the threshold current, which produced noticeable muscle contraction. Contraction force gradually increased with an increase of stimulation current until reaching the level of maximal muscle force at a stimulation current between 0.1 mA and 0.2 mA. In most of our animals, increasing stimulation current from 0.1 mA to 0.2 mA still produced an increase in muscle force (in average 11% increase—statistically significant increase $P < .05$, $t = 2.3$, two-tailed *t*-test for pairs, $df = 11$). Further increases of stimulation current did not increase muscle force.

3.3. Muscle Force as a Function of Stimulation Frequency. We also analyzed how muscle force changes with regard to the frequency of stimulation pulses (from 0 to 500 Hz). We used a 200 ms train of 0.1 mA pulses. The muscle was stretched with a moderate tension (0.08 N). Figure 5 illustrates in a representative rat the muscle force in response to 6 different frequencies of stimulation (maximal values of force for each frequency were measured to create a frequency-force curve). Stimulation pulses below 25 Hz produced individual twitches of the muscle in response to each pulse separately, with a small summation of responses observed already at 25 Hz. The frequency-density relationship of muscle force (normalized by cross-section area of the muscle) in the group data is shown in Figure 6. Muscle force increased with stimulation frequency, starting at 25 Hz (with almost a full tetanic fusion

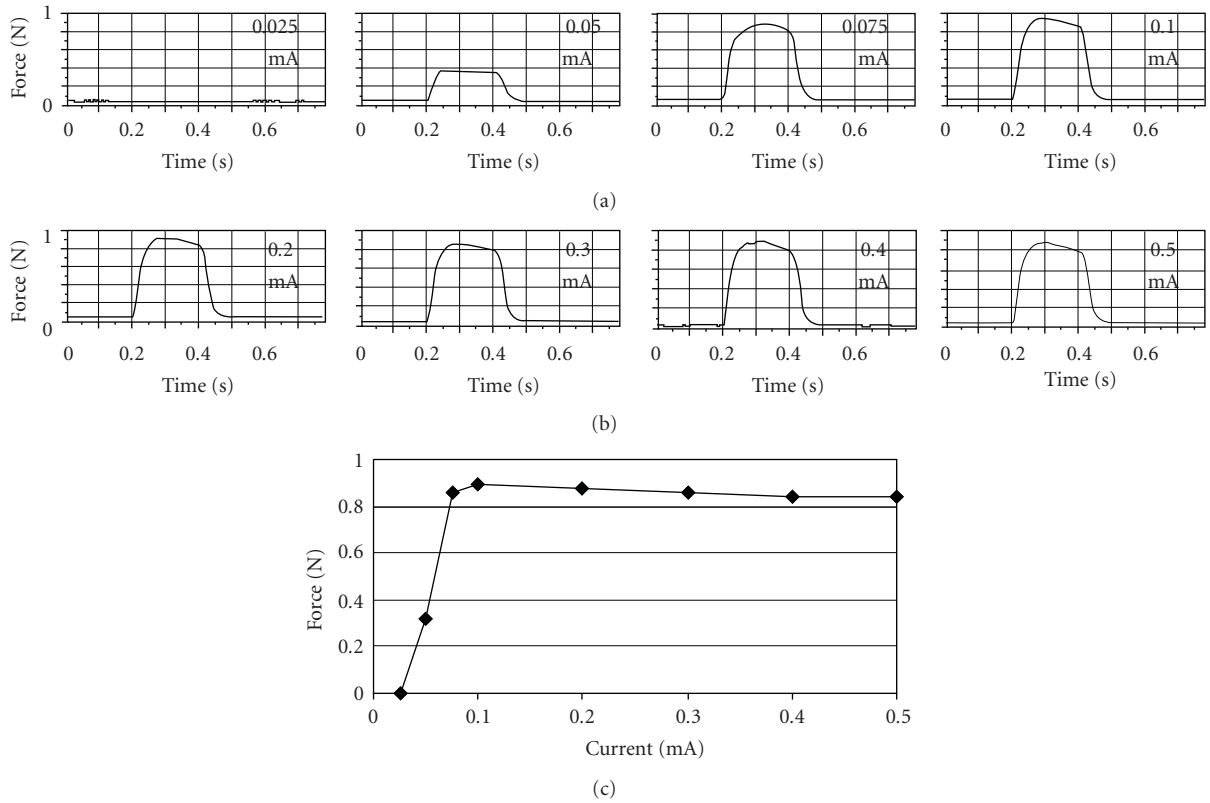


FIGURE 3: Force measurements from a representative rat, showing the stimulation intensity-force relationship. (a and b) show the time course of muscle force produced by electrical stimulation of the SM nerve at eight different intensities. Note that stimulation at 0.1 mA resulted in maximal muscle contraction. (c) illustrates the outcome from these 8 measurements—the relationship between muscle force and stimulation intensity.

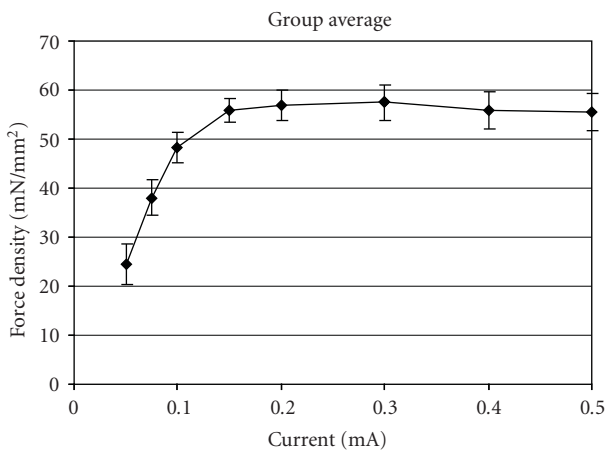


FIGURE 4: Muscle force as a function of stimulation current. This group average shows the density of force produced by the SM muscle and normalized by its cross-section area at different stimulation currents. Vertical bars represent the standard error of the mean. The passive tension was at a moderate level (0.08 N). The nerve was stimulated at 200 Hz.

of force at 50 Hz) and reached maximal value at 150 Hz. Further increases of stimulation frequency (above 300 Hz)

produced a small but consistent decrease of muscle force. The muscle force generated by the stimulation train of 500 Hz (the highest frequency used in this study) was 21% smaller than that generated by the stimulation of 150 Hz. The difference was statistically significant ($P < .01$, $t = 3.5$, two-tailed t -test for pairs, $df = 11$). A similar shape of the frequency-force relationship was seen for different stimulation currents (see Figure 7).

3.4. Muscle Length and Weight. Immediately after the experimental session, the length of the SM muscle was measured at different stretching forces, and then the muscle was removed and weighed. The average length was 25.7 mm (range 24–27 mm) at very loose tension (0.04 N), 26.8 mm at loose tension (0.06 N), 27.7 mm at moderate tension (0.08 N), 28.6 mm at tense (0.1 N), and 31.4 mm at very tense (0.24 N). The average muscle weight was 0.50 g (range 0.47–0.53 g).

4. Discussion

This study investigated the muscle force features of the SM muscle in a rat model. We determined the correlations of muscle force (active muscle contraction to electrical stimulation) with passive tension (passive force changing muscle length) and two parameters of electrical stimulation,

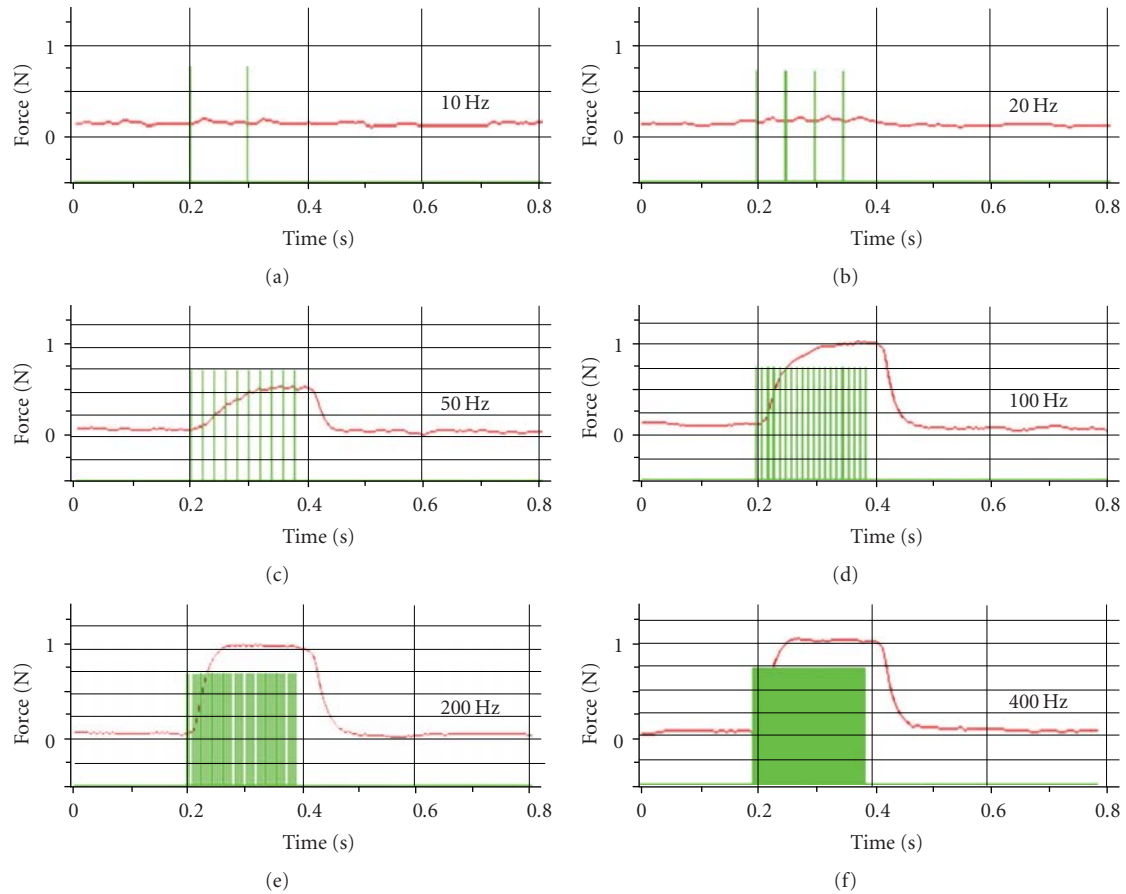


FIGURE 5: Illustration of muscle force measurement as a function of stimulation frequency in a representative rat. Individual muscle contractions to stimulation pulses at different frequencies are shown in red. Single stimulation pulses are indicated by green vertical lines. The muscle responded with single twitches until 25 Hz. At 50 Hz the muscle contractions were fused. With an increasing frequency of stimulation, the muscle responded with increased force, which reached a plateau at about 150 Hz.

intensity and frequency. There are several key findings of this study. First of all, moderate muscle length/tension (28 mm/0.08 N) produced maximal muscle force (0.94 N). Second, 0.03 mA was the threshold current for initiating noticeable muscle contraction. Third, 0.2 mA was the stimulation current which produced the maximal force in the SM. Finally, the stimulation frequency that produced maximal muscle force was about 150 Hz. Taken together, in the normal rat, maximal force in the SM can be produced with moderate passive tension, 0.2 mA current, and 150 Hz frequency. These findings are important not only for better understanding the contractile properties of the rat SM muscle, but also for providing normative values which would be useful for reliably evaluating the extent of functional recovery induced by muscle reinnervation.

4.1. Passive Tension-Muscle Force Relationship. Muscle length is an important variable affecting active muscle force generated in response to electrical stimulation. However, establishing the optimal length of the muscle, which could produce maximal muscle force, requires lengthy investigation at many different lengths each time a new muscle is studied.

The present study shows the highest SM muscle force when the muscle is stretched with a tension of 0.08 N before stimulation (8.5% of maximal isometric tetanic force). Data from this study showed the typical “U shape” relationship between length and force in the SM muscle. Our results are consistent with the general characteristics obtained in muscle force measurements where other muscles were studied in the rat and other species [23, 25]. Optimal muscle length also varies with stimulation frequency. A higher optimal muscle length was found for lower stimulation frequencies as described [29, 31]. A straightforward and efficient method to stretch a muscle to optimal length, which would result in optimal active muscle force, is to apply a passive force to the muscle with the previously established tension. Therefore, we analyzed the relationship between passive tension stretching a muscle and active force generated by the muscle in response to electrical stimulation.

Previous studies showed a very wide range of optimal passive tensions in different muscles and species which allow muscles to be stretched to optimal length and contract with maximal force. Celichowski et al. [32] stretched the rat’s medial gastrocnemius muscle up to a passive tension

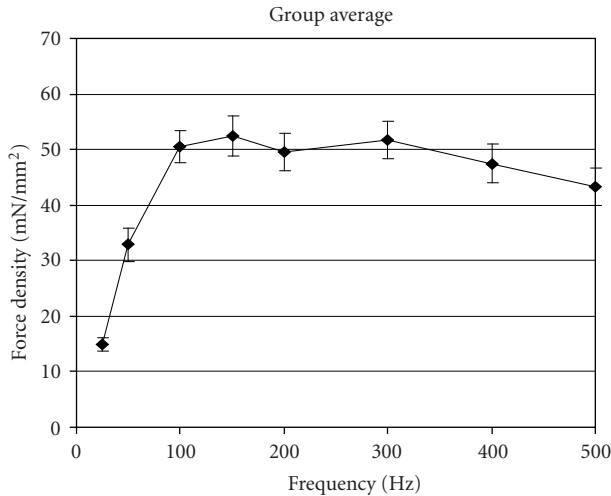


FIGURE 6: Muscle force as a function of stimulation frequency. The group data shows the relationship between muscle force density (normalized to cross-section area) and stimulation frequency. Vertical bars represent standard error of the mean. The passive tension was at a moderate level (0.08 N). The nerve stimulation current was 0.1 mA.

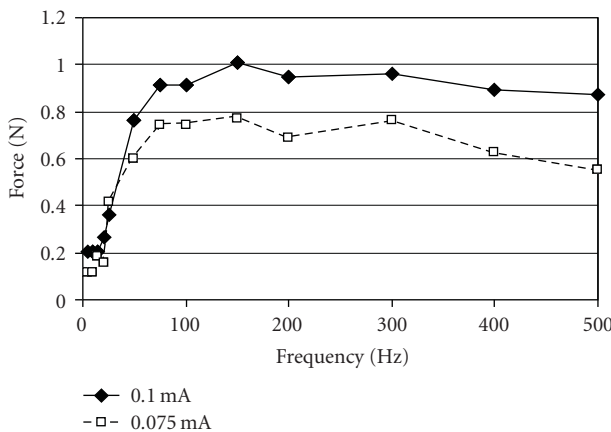


FIGURE 7: A representative example in an individual rat to show the relation between muscle force and stimulation frequency at two levels of stimulation current. The passive tension was at a moderate level (0.08 N). The nerve stimulation current was 0.1 mA (continuous line) or 0.075 mA (dashed line). Muscle force is higher for a bigger current but otherwise both curves share similar characteristics with a slight decline of force for the highest frequency of stimulation.

of 100 mN to get muscle contraction with maximal force. Johns et al. [33] studied the length-tension relationships in the thyroarytenoid and digastric muscles of the cat. They showed that the thyroarytenoid muscle requires 0.14 N of passive tension (39% of maximal isometric tetanic force) to stretch the muscle to optimum length (L_0), whereas the digastric muscle requires a much smaller 0.028 N of passive tension (9% of maximal isometric tetanic force). The authors claimed that a large passive tension of the thyroarytenoid muscle is needed to allow a modulation of tension in the

vocal cord during phonation. The underlining mechanism can be also related to a considerable amount of connective tissue in parallel with the muscle fibers. Krier et al. [34] found substantial passive tension in the striated muscle of the external anal sphincter when the muscle was stretched to optimal muscle length (12% of active isometric tetanus tension). The authors hypothesized that the substantial passive tension of this muscle provides a sphincteric contractile tone and plays a role in the maintenance of fecal continence. Floyd and Morrison [35] studied cat and sheep esophageal striated muscle strips. They found that the passive tension at the optimal length is equal to 10% of the active isometric contraction. Kim et al. [36] studied the canine diaphragm. The optimal muscle length (for maximal force) was 125% of the muscle length at which passive tension was noticed for the first time. At the optimal length, resting tension was 12% of active muscle force. The authors speculated that their diaphragm's length-tension curve may represent an evolutionary adaptation to the volume and pressure requirements of mammalian respiration. The position of the length-passive tension curve with respect to the length-active tension curve might also depend on the amount of elastic material in the muscle [37]. Therefore, the removal of a substantial amount of connective tissue from a muscle for testing the muscle outside a body may also lead to different length-passive tension curve (as compared to testing the same muscle in vivo). Farkas and Rochester [38] showed that the canine SM and other inspiratory muscles do not share common length-tension properties or resting lengths. The muscles modify different resting lengths with lung volume and body position. These changes in muscle lengths influence muscle force generating capacity.

Large muscle stretching during measurement could have a detrimental impact on subsequent measurements due to stretch-induced damage. Davis et al. [39] reported length-tension data from the rabbit tibialis anterior. They used excessive tensions and showed that passive muscle force grows with an increase of muscle length until reaching almost (92%) of maximal active muscle force (12 N) and then starts to decrease. The authors speculated that the decrease in passive muscle force is "presumably due to injury of passive muscle structures such as the surrounding connective tissue or intracellular parallel structures". In our study, maximal passive tension was only 0.24 N, about 25% of maximal active force generated by the SM muscle (0.94 N), which is considerably less than 92% of the passive tension limit beyond which Davis et al. observed decline in passive force. A tension of 0.24 N when recalculated per the relatively large muscle cross-sectional area of our SM muscle (17.5 mm²) produced quite a limited density of force 13.7 mN/mm² which should not produce excessive or damaging tension on muscle fibers.

Normalized force by cross-section area in our rat SM muscle was 54 mN/mm² (940 mN/17.5 mm²), which is lower than that obtained from the rabbit sternocleidomastoid muscle as reported by Falkenberg et al. [23]. In the rabbit maximal tetanic force of sternocleidomastoid muscle (during stimulation with 1s train of 0.3 ms pulses at 100 Hz) was about 4.5 N whereas a cross-section area of the muscle

was 39 mm², which results in a muscle force density of 115 mN/mm².

4.2. Stimulation Intensity-Force Relationship. Our results showed that SM muscle force in the rat grows with stimulation current until about 0.1-0.2 mA when it reaches a plateau. The threshold of stimulation current, which can generate muscle contraction with noticeable force, is about 0.03 mA. Muscle force characteristics were repeatable across different animals and therefore can be used as a normal control reference in reinnervation studies.

In many previous muscle force studies, due to the simplicity of the stimulator's circuitry and the necessity for safety during nerve stimulation (limited maximal amplitude of stimulation), the nerves were stimulated with rectangular pulses with regulated voltage. For example, Yoshimura et al. [21, 24] stimulated the peroneal nerve with bipolar silver electrodes and recorded muscle force from the extensor digitorum longus in the rat. The authors used a 250 ms train of 0.2 ms pulses with a regulated voltage between 2 and 6 V. Cheng et al. [40] used a 30 V train of 0.2 ms pulses at 100 Hz to stimulate the femoral nerve and record force from the rectus femoris muscle in rabbits. The amplitude of stimulation pulses, which produced maximal active muscle force, was influenced by electrode placement on the nerve and varied radically across the different muscles and species used in those studies.

Stimulation with regulated current provides more reproducible results than stimulation with regulated voltage. Regardless of electrode impedance, a reproducible electric field can be created within stimulated tissue [41]. Therefore, we used stimulation with regulated current in the present study. Roszek et al. [29] stimulated the ischiadic nerve with bipolar silver electrodes and recorded force from the medial gastrocnemius muscle in a rat. They used 200 ms trains of 0.1 ms pulses of 3 mA current at different frequencies. Gradation in stimulation frequency from 15 to 100 Hz produced gradation in muscle force. Frieswijk et al. [42] searched for the threshold current for a single 0.1 ms pulse (monopolar stimulation of peroneal nerve with NiCr wire), which can generate a minimal muscle twitch response in the extensor digitorum longus in the rat. They found that the threshold current can be as low as 0.0026 mA.

On the basis of the discussed results, we selected the optimal circumstances (initial passive tension and electrical stimulation parameters) for the rat SM muscle to contract with maximal force. This maximal muscle force will be used as a target level in our further study of muscle force recovery in a denervated SM muscle where different reinnervation techniques will be compared.

4.3. Stimulation Frequency-Force Relationship. Our experiments demonstrated that SM muscle force grows with the frequency of pulses until about 100–200 Hz when it reaches a plateau. A further increase of stimulation frequency produces a slight decrease of muscle force. The muscle force fusion frequency is higher than 50 Hz. The relatively high frequency of tetanic fusion might result from muscle fiber

type composition. The SM muscle is a fast muscle with over 80% of type II fibers (in rats Luff [43] in rabbits and primates McLoon [44] as well as our unpublished data in rats). Our results from the rat SM muscle are in agreement with those from other muscles or species used in previous studies. For instance, Devrome and MacIntosh [45] analyzed the force-frequency relationship for a rat gastrocnemius muscle with sciatic nerve stimulation using a 100 ms train of 0.05 ms pulses at a frequency up to 200 Hz. They found the shape of the muscle force curve, which is similar to that observed in the present study with the highest muscle force at 200 Hz. Interestingly, for this frequency of stimulation (200 Hz) muscle force was also significantly less sensitive to repetitive fatiguing contractions than for a lower frequency of stimulation (<100 Hz). This finding would indicate that the stimulation train of 200 Hz might be preferable to use (generating stronger and less variable contractions than stimulation at 100 Hz) in our further study evaluating the level of tetanic force recovery in a reinnervated muscle. Roszek et al. [29] showed an interaction between the frequency of gastrocnemius stimulation and the length-force characteristics (shifting optimal muscle length to longer values with low frequency of stimulation (<50 Hz)). However, with a higher frequency of stimulation this shift of optimal length was minimal. Therefore, 200 Hz would be preferable over lower frequencies of stimulation to eliminate this confounding variable.

The results of Roszek et al. point out that the commonly used procedure of establishing optimal muscle length only once at the beginning of the study with a particular frequency of stimulation might not be appropriate when the muscle force is later analyzed at different frequencies. Repetitive testing to reveal the force-length relationship at all studied frequencies seems to be more appropriate. However, the analysis of Roszek et al. also showed that the optimal muscle length changes significantly with the frequency of stimulation only when the stimulation frequency is very low—below 40 Hz. There was no significant difference in optimal muscle length between stimulation at 50 Hz and 100 Hz. Stimulation frequencies below 40 Hz were not the focus of the present study, because one of our main goals was to establish optimal stimulation parameters which would generate a frequency fused contraction of maximal force in the SM muscle. Our investigations showed that muscle contraction to a train of stimulation pulses starts to be fused at about 50 Hz (see Figure 5). At this frequency muscle force reaches only about 60% of maximal force reached at 100–200 Hz (see Figures 6 and 7). Our study was focused at higher frequencies of stimulation where the change in optimal muscle length for maximal muscle force was not significant.

Brooks et al. [46] compared the force-frequency relationships between slow soleus and fast extensor digitorum longus (EDL) muscles in mice. Isometric force grew faster and reached a plateau at about 110 Hz for the soleus muscle (with a possible slight decline at 250 Hz), but was still growing with the frequency set at 350 Hz in the case of the EDL muscle. These observations once again indicate that maximal muscle force is produced with a high frequency

of stimulation and that the optimal frequency reflects the proportion of fast to slow fibers. Marsh et al. [47] studied the force-frequency relationship in the rat tibialis anterior with stimulation of the peroneal nerve with a 250 ms train of pulses of different frequencies (50–300 Hz). The authors found a similar relationship between force and frequency as observed in the present study (with decreased force at higher frequencies). The stimulation frequency, which generated maximum muscle force, decreased slightly in older animals. The strongest muscle contraction was produced at 200 Hz in young rats (3 months old) and at 150 Hz in older rats (1.5–2.5 years old). Older (as well as injured) rats also showed “tetanic fade” (rapid decrease of muscle contraction despite continued stimulation) at a higher frequency of stimulation. The tetanic fade was particularly pronounced at the highest frequency (300 Hz) used by the authors. Therefore, in our further study on muscle reinnervation, the 200 Hz would be a preferable stimulation frequency over 300 Hz to achieve maximal muscle force and to reduce the influence of tetanic fade as confounding factor.

Falkenberg et al. [23] examined twitch and tetanic force generation in the sternocleidomastoid muscle in rabbits (by stimulation of the spinoaccessory nerve). The muscle was stimulated with a 1 s train of 0.3 ms pulses with a growing frequency until 100 Hz. Muscle force was the largest for 100 Hz but the force might be still larger if the authors would have used a higher stimulation frequency. The single twitch muscle force was $0.44 \text{ N} \pm 0.06$ and tetanic muscle force was about $10\times$ larger for stimulation with a 100 Hz train of pulses. The present study showed a similar relationship between tetanic and twitch force in the rat. Interestingly, Falkenberg et al. [23] also noticed that muscle force induced by direct muscle stimulation is similar to that induced by nerve stimulation. These findings are consistent with our results obtained from the rat SM muscle.

To produce tetanic contraction, we used a 200 ms train of biphasic pulses of 0.2 ms width, typically at 200 Hz. Different frequencies of stimulation were used only when the influence of frequency of stimulation on muscle force was directly studied. This 200 ms time ensured that muscle force reached a plateau (see Figures 3 and 5). A similar duration (250–300 ms) of the train of pulses (with pulse width 0.5 ms at 100 Hz) was used by Cairns and Dulhunty [48] for the fast twitch SM muscle. The authors used a much longer—1 s train of pulses to ensure a force plateau in the slow twitch soleus fibers.

Shin et al. [25] looked for the optimal stimulation parameters to produce maximal muscle force in the rat tibialis anterior. The authors showed a large standard deviation (35–50%) of these parameters, not only between rats but also within each rat. Our data confirm this large variability of optimal stimulation parameters in the SM muscle.

Integrated EMG activity is sometimes used as a nondirect method of muscle force evaluation during muscle contraction. However, gross movement of the EMG electrode caused by SM muscle contractions during obstructive breathing (as well as during electrical stimulation) might be the source of unpredictable electrical artifacts causing a lack of good correlation between integrated EMG and muscle

contractions [2]. Therefore, direct measurement of muscle force with a force transducer is an irreplaceable method to accurately measure muscle function.

5. Conclusions

Optimization of the variables affecting the isometric tetanic force of the rat SM muscle resulted in a choice of the following stimulation parameters to produce maximal tetanic force: 0.08 N (moderate) passive tension before stimulation, 0.2 mA stimulation current (with biphasic 0.2 ms width pulse), and 150 Hz stimulation frequency.

Grants

This research was supported by NIH Grant 5R01DC008599 from the National Institute on Deafness and Other Communication Disorders (to Liancai Mu).

Acknowledgment

The authors are grateful to Drs. Hungxi Su and Xiaolin Zhang for their excellent technical assistance during the surgical operations and data collection.

References

- [1] D. Costa, M. Vitti, D. T. Oliveira, and R. P. Costa, “Participation of the sternocleidomastoid muscle on deep inspiration in man. An electromyographic study,” *Electromyography and Clinical Neurophysiology*, vol. 34, no. 5, pp. 315–320, 1994.
- [2] A. J. Raper, W. T. Thompson Jr., W. Shapiro, and J. L. Patterson, “Scalene and sternomastoid muscle function,” *Journal of Applied Physiology*, vol. 21, no. 2, pp. 497–502, 1966.
- [3] A. Legrand, E. Schneider, P.-A. Geveno, and A. De Troyer, “Respiratory effects of the scalene and sternomastoid muscles in humans,” *Journal of Applied Physiology*, vol. 94, no. 4, pp. 1467–1472, 2003.
- [4] A. L. Hudson, S. C. Gandevia, and J. E. Butler, “The effect of lung volume on the co-ordinated recruitment of scalene and sternomastoid muscles in humans,” *Journal of Physiology*, vol. 584, no. 1, pp. 261–270, 2007.
- [5] A. De Troyer, P. A. Kirkwood, and T. A. Wilson, “Respiratory action of the intercostal muscles,” *Physiological Reviews*, vol. 85, no. 2, pp. 717–756, 2005.
- [6] J. Hamilton, S. Avitia, and R. F. Osborne, “Designing a bipediced sternocleidomastoid muscle flap for parotidectomy contour deformities,” *Ear, Nose and Throat Journal*, vol. 85, no. 1, pp. 20–21, 2006.
- [7] V. Kumar, U. Gaud, M. Shukla, and M. Pandey, “Sternocleidomastoid island flap preserving the branch from superior thyroid artery for the reconstruction following resection of oral cancer,” *European Journal of Surgical Oncology*, vol. 35, no. 9, pp. 1011–1015, 2009.
- [8] L. Kaser and M. Muntener, “Delayed muscle fiber transformation after foreign-reinnervation of excessive muscle tissue,” *The Anatomical Record*, vol. 223, no. 3, pp. 347–355, 1989.
- [9] H. M. Tucker, “Reinnervation of the unilaterally paralyzed larynx,” *Annals of Otolaryngology, Rhinology and Laryngology*, vol. 86, no. 6, pp. 789–794, 1977.

- [10] D. Meikle, R. E. Trachy, and C. W. Cummings, "Reinnervation of skeletal muscle: a comparison of nerve implantation with neuromuscular pedicle transfer in an animal model," *Annals of Otolaryngology, Rhinology and Laryngology*, vol. 96, no. 2, pp. 152–157, 1987.
- [11] S. K. Lee and S. W. Wolfe, "Peripheral nerve injury and repair," *The Journal of the American Academy of Orthopaedic Surgeons*, vol. 8, no. 4, pp. 243–252, 2000.
- [12] B. J. F. Wong and R. L. Crumley, "Nerve wound healing: an overview," *Otolaryngologic Clinics of North America*, vol. 28, no. 5, pp. 881–895, 1995.
- [13] H. M. Tucker, "Human laryngeal reinnervation," *Laryngoscope*, vol. 86, no. 6, pp. 769–779, 1976.
- [14] H. M. Tucker, "Reinnervation of the paralyzed larynx: a review," *Head and Neck Surgery*, vol. 1, no. 3, pp. 235–242, 1979.
- [15] R. L. Crumley, "Experiments in laryngeal reinnervation," *Laryngoscope*, vol. 92, pp. 1–27, 1982.
- [16] G. S. Goding, C. W. Cummings, and D. A. Bright, "Extension of neuromuscular pedicles and direct nerve implants in the rabbit," *Archives of Otolaryngology—Head and Neck Surgery*, vol. 115, no. 2, pp. 217–223, 1989.
- [17] N. D. Hogikyan, M. M. Johns, P. R. Kileny, M. Urbanek, W. R. Carroll, and W. M. Kuzon Jr., "Motion-specific laryngeal reinnervation using muscle-nerve-muscle neurotization," *Annals of Otolaryngology and Laryngology*, vol. 110, no. 9, pp. 801–810, 2001.
- [18] M. J. Bolesta, W. E. Garrett, B. M. Ribbeck, R. R. Glisson, A. V. Seaber, and J. L. Goldner, "Immediate and delayed neurotization in a rabbit model: a functional, histologic, and biochemical comparison," *Journal of Hand Surgery*, vol. 13, no. 3, pp. 352–357, 1988.
- [19] L. K. Kalliainen, P. S. Cederna, and W. M. Kuzon Jr., "Mechanical function of muscle reinnervated by end-to-side neurotization," *Plastic and Reconstructive Surgery*, vol. 103, no. 7, pp. 1919–1927, 1999.
- [20] P. S. Cederna, M. K. H. Youssef, H. Asato, M. G. Urbanek, and W. M. Kuzon Jr., "Skeletal muscle reinnervation by reduced axonal numbers results in whole muscle force deficits," *Plastic and Reconstructive Surgery*, vol. 105, no. 6, pp. 2003–2009, 2000.
- [21] K. Yoshimura, H. Asato, S. S. Jejurikar, P. S. Cederna, M. G. Urbanek, and W. M. Kuzon Jr., "The effect of two episodes of denervation and reinnervation on skeletal muscle contractile function," *Plastic and Reconstructive Surgery*, vol. 109, no. 1, pp. 212–219, 2002.
- [22] M. G. Urbanek, D. E. Ganz, M. A. Aydin, J. H. van der Meulen, and W. M. Kuzon Jr., "Muscle-nerve-muscle neurotization for the reinnervation of denervated somatic muscle," *Neurological Research*, vol. 26, no. 4, pp. 388–394, 2004.
- [23] J. H. Falkenberg, P. A. Iazzo, and L. K. McLoon, "Muscle strength following direct injection of doxorubicin into rabbit sternocleidomastoid muscle in situ," *Muscle and Nerve*, vol. 25, no. 5, pp. 735–741, 2002.
- [24] K. Yoshimura, H. Asato, P. S. Cederna, M. G. Urbanek, and W. M. Kuzon Jr., "The effect of reinnervation on force production and power output in skeletal muscle," *Journal of Surgical Research*, vol. 81, no. 2, pp. 201–208, 1999.
- [25] R. H. Shin, T. Vathana, G. A. Giessler, P. F. Friedrich, A. T. Bishop, and A. Y. Shin, "Isometric tetanic force measurement method of the tibialis anterior in the rat," *Microsurgery*, vol. 28, no. 6, pp. 452–457, 2008.
- [26] D. Cantillon and A. Bradford, "Effects of age and gender on rat upper airway muscle contractile properties," *Journals of Gerontology Series A*, vol. 55, no. 8, pp. B396–B400, 2000.
- [27] J. Lannergren and H. Westerblad, "The temperature dependence of isometric contractions of single, intact fibres dissected from a mouse foot muscle," *Journal of Physiology*, vol. 390, pp. 285–293, 1987.
- [28] Y. Ishii, T. Watari, and T. Tsuchiya, "Enhancement of twitch force by stretch in a nerve-skeletal muscle preparation of the frog *Rana porosa brevipoda* and the effects of temperature on it," *Journal of Experimental Biology*, vol. 207, no. 26, pp. 4505–4513, 2004.
- [29] B. Roszek, G. C. Baan, and P. A. Huijings, "Decreasing stimulation frequency-dependent length-force characteristics of rat muscle," *Journal of Applied Physiology*, vol. 77, no. 5, pp. 2115–2124, 1994.
- [30] D. E. Rassier, B. R. MacIntosh, and W. Herzog, "Length dependence of active force production in skeletal muscle," *Journal of Applied Physiology*, vol. 86, no. 5, pp. 1445–1457, 1999.
- [31] P. M. Rack and D. R. Westbury, "The effects of length and stimulus rate on tension in the isometric cat soleus muscle," *Journal of Physiology*, vol. 204, no. 2, pp. 443–460, 1969.
- [32] J. Celichowski, K. Grottel, and E. Bichler, "Differences in the profile of unfused tetani of fast motor units with respect to their resistance to fatigue in the rat medial gastrocnemius muscle," *Journal of Muscle Research and Cell Motility*, vol. 20, no. 7, pp. 681–685, 1999.
- [33] M. M. Johns, M. Urbanek, D. B. Chepeha, W. M. Kuzon Jr., and N. D. Hogikyan, "Length-tension relationship of the feline thyroarytenoid muscle," *Journal of Voice*, vol. 18, no. 3, pp. 285–291, 2004.
- [34] J. Krier, R. A. Meyer, and W. H. Percy, "Length-tension relationship of striated muscle of cat external anal sphincter," *American Journal of Physiology*, vol. 256, no. 4, pp. 773–778, 1989.
- [35] K. Floyd and J. F. B. Morrison, "The mechanical properties of oesophageal striated muscle in the cat and sheep," *Journal of Physiology*, vol. 248, no. 3, pp. 717–724, 1975.
- [36] M. J. Kim, W. S. Druz, and J. Danon, "Mechanics of the canine diaphragm," *Journal of Applied Physiology*, vol. 41, no. 3, pp. 369–382, 1976.
- [37] K. K. McCully and J. A. Faulkner, "Length-tension relationship of mammalian diaphragm muscles," *Journal of Applied Physiology*, vol. 54, pp. 1681–1686, 1983.
- [38] G. A. Farkas and D. F. Rochester, "Contractile characteristics and operating lengths of canine neck inspiratory muscles," *Journal of Applied Physiology*, vol. 61, no. 1, pp. 220–226, 1986.
- [39] J. Davis, K. R. Kaufman, and R. L. Lieber, "Correlation between active and passive isometric force and intramuscular pressure in the isolated rabbit tibialis anterior muscle," *Journal of Biomechanics*, vol. 36, no. 4, pp. 505–512, 2003.
- [40] N. Cheng, L. Xuexiang, and A. Huang, "Experimental comparison of muscle contractility after three methods of reinnervation," *Annals of Plastic Surgery*, vol. 33, no. 2, pp. 166–170, 1994.
- [41] J. P. Reilly, *Applied Bioelectricity: From Electrical Stimulation to Electropathology*, Springer, New York, NY, USA, 1998.
- [42] T. A. Frieswijk, J. P. A. Smit, W. L. C. Rutten, and H. B. K. Boom, "Force—current relationships in intraneural stimulation: role of extraneural medium and motor fibre clustering," *Medical and Biological Engineering and Computing*, vol. 36, pp. 422–430, 1998.

- [43] A. R. Luff, "Dynamic properties of fiber bundles from the rat sternomastoid muscle," *Experimental Neurology*, vol. 89, no. 3, pp. 491–502, 1985.
- [44] L. K. McLoon, "Muscle fiber type compartmentalization and expression of an immature myosin isoform in the sternocleidomastoid muscle of rabbits and primates," *Journal of the Neurological Sciences*, vol. 156, no. 1, pp. 3–11, 1998.
- [45] A. N. Devrome and B. R. MacIntosh, "The biphasic force-velocity relationship in whole rat skeletal muscle in situ," *Journal of Applied Physiology*, vol. 102, no. 6, pp. 2294–2300, 2007.
- [46] S. V. Brooks, J. A. Faulkner, and D. A. McCubbrey, "Power outputs of slow and fast skeletal muscles of mice," *Journal of Applied Physiology*, vol. 68, no. 3, pp. 1282–1285, 1990.
- [47] D. R. Marsh, L. R. Hinds, W. S. Lester, B. E. Reinking, and F. W. Booth, "The force-frequency relationship is altered in regenerating and senescent rat skeletal muscle," *Muscle and Nerve*, vol. 21, no. 10, pp. 1265–1274, 1998.
- [48] S. P. Cairns and A. F. Dulhunty, "The effects of beta-adrenoreceptor activation on contraction in isolated fast- and slow-twitch skeletal muscle fibers of the rat," *British Journal of Pharmacology*, vol. 110, pp. 1133–1141, 1993.

Research Article

Efficient Isolation of Cardiac Stem Cells from Brown Adipose

Zhiqiang Liu, Haibin Wang, Ye Zhang, Jin Zhou, Qiuxia Lin, Yanmeng Wang, Cuimi Duan, Kuiwu Wu, and Changyong Wang

Department of Tissue Engineering, Institute of Basic Medical Sciences and Tissue Engineering Research Center, Academy of Military Medical Sciences, Beijing 100850, China

Correspondence should be addressed to Kuiwu Wu, ammswu@sina.com and Changyong Wang, wcy2000.te@yahoo.com

Received 30 October 2009; Revised 5 February 2010; Accepted 10 February 2010

Academic Editor: Aikaterini Kontrogianni-Konstantopoulos

Copyright © 2010 Zhiqiang Liu et al. This is an open access article distributed under the Creative Commons Attribution License, which permits unrestricted use, distribution, and reproduction in any medium, provided the original work is properly cited.

Cardiac stem cells represent a logical cell type to exploit in cardiac regeneration. The efficient harvest of cardiac stem cells from a suitable source would turn promising in cardiac stem cell therapy. Brown adipose was recently found to be a new source of cardiac stem cells, instrumental to myocardial regeneration. Unfortunately, an efficient method for the cell isolation is unavailable so far. In our study we have developed a new method for the efficient isolation of cardiac stem cells from brown adipose by combining different enzymes. Results showed that the total cell yield dramatically increased (more than 10 times, $P < .01$) compared with that by previous method. The content of CD133-positive cells (reported to differentiate into cardiomyocytes with a high frequency) was much higher than that in the previous report (22.43% versus 3.5%). Moreover, the isolated cells could be efficiently differentiated into functional cardiomyocytes in optimized conditions. Thus, the new method we established would be of great use in further exploring cardiac stem cell therapy.

1. Introduction

Despite the notion that adult hearts are terminally differentiated organs without self-renewal potential undermined by the discovery of resident cardiac stem/progenitor cells, the endogenous regenerative mechanisms are too limited to sufficiently compensate for the cardiomyocytes loss occurring in pathological state (e.g., myocardial infarction) [1–3]. This led to numerous investigations to identify a putative source of new cardiomyocytes to ameliorate the injured myocardium and improve the cardiac function. Stem cells, capable of differentiating into other cell types, that is, functional cardiomyocytes, have intrigued intensive studies. So far various stem cell sources have been explored for myocardial regeneration, including embryonic stem, skeletal myoblasts, bone marrow mesenchymal stem cells [4–7]. Data demonstrated functional improvement of the infarcted heart by transplanting these cells. However, the cells also have shortfalls, for example, the potential of tumorigenicity with embryonic stem cells, arrhythmogenicity with skeletal myoblasts, and the controversial transdifferentiation of bone marrow-derived stem cells [8]. These problems underscore

the need to search for new sources of adult stem cells to generate cardiomyocytes against the failing myocardium.

The identification and isolation of cardiac stem cells (CSCs) reignited the excitement in this field [3, 9, 10]. Different from other adult stem cells, cardiac stem cells represent a logical source to exploit in myocardial regeneration because of their likelihood to be intrinsically programmed to generate cardiac tissues *in vitro* and increase its viability *in vivo*. Therefore, the cardiac stem cell therapy may pioneer an innovative approach to treat heart diseases [11]. However, technical difficulties exist in collecting the cells at present. The number of cells upon harvest is too low [12, 13]. Therefore, it would be appealing to search for an alternative source of cardiac stem cells.

Adipose tissues are abundant in mammals. Once successfully explored, the tissue source would have far-reaching effects in regenerative medicine [14, 15]. Therefore, adipose-derived cells were also extensively investigated as candidates for the myocardial regeneration by many groups [16, 17]. Planat-Bénard et al. first reported the spontaneous differentiation of murine adipose-derived cells into cardiomyocytes in 2004 [1]. In spite of its rather low rate (0.02% to 0.07%),

the cardiomyogenic differentiation suggested that adipose tissue may provide a new source for cardiac progenitor/stem cells. The subsequent studies by Yamada et al. further demonstrated that the cardiac differentiation was far more efficient in brown adipose-derived cells ($\geq 20\%$) than that described by Planat-Bénard [1, 12]. They have proved brown adipose to be an abundant source of cardiac stem cells.

The discovery of the cardiac stem cells in brown adipose opened a new channel to provide cardiomyocytes for myocardial regeneration. However, the previous methods [1, 12] for cell isolation are ineffective. In the present study, we developed a new method to isolate brown adipose-derived cardiac stem cells with great efficiency by combining collagenase IV and dispase II, with trypsin. The optimized isolation and differentiation of obtained cells were detailed. Moreover, the cardiomyogenic efficiency of isolated cells with this new method was also evaluated.

2. Materials and Methods

2.1. Animals and Tissue Samples. All animals were purchased from the Experimental Animal Center, Academy of Military Medical Science (Beijing, China). The Institutional Animal Care and Use Committee (IACUC) of the Chinese Academy of Military Medical Science, Beijing, China, approved all experiments in this study. To obtain tissue samples, animals were killed by intraperitoneally injecting with overdose sodium pentobarbital. The brown adipose tissue was derived from interscapular of neonatal SD rats (Postnatal 7–14 days). Every effort was made to minimize animal suffering and the number of animals used.

2.2. Cell Isolation from Rat Brown Adipose. Isolated brown adipose tissues were washed extensively with sterile phosphate-buffered saline (PBS) to remove contaminating debris and red blood cells. Then it was minced with scissors and digested with 0.1% collagenase IV (m/v, Sigma), 0.1% dispase II (m/v, Roche Diagnostics, Mannheim, Germany) and 0.05% trypsin (m/v, Sigma) in serum-free medium. The digestion was performed at 37°C for 30–60 minutes with gentle agitation. Then, the enzymes were inactivated with an equal volume of α -MEM/10% fetal bovine serum (FBS, Gibco) and the samples were filtered through a 75- μ m mesh filter to remove debris. The cellular pellets were resuspended in α -MEM/10% fetal bovine serum (FBS); red cell lysis buffer was added. After a 5-minute lysis period, cells were centrifuged and resuspended. Nucleated cells were counted for cell yield. Then cells were plated onto conventional culture plates and cultured under 37°C, 5% CO₂ conditions. For cell viability determination, a portion of cells were stained with propidium iodide (PI) and analyzed by flow cytometry.

2.3. Flow Cytometry Analysis. For flow cytometry, the newly isolated stromal cells from brown adipose were lysed by red cell lysis buffer as described above. Then, cells were harvested for flow cytometry analysis as previously described [18]. Briefly, cells were fixed for 30 minutes in

ice-cold 2% paraformaldehyde. The fixed cells were washed in flow cytometry buffer (FBS, Biologend, 420201) and incubated for 30 minutes in FBS containing the following antibodies: fluorescein isothiocyanate-conjugated antiCD90 (Biologend, 202503), phycoerythrin-conjugated antiCD29 (Biologend, 102221), FITC-conjugated antiCD45 (Biologend, 202205), FITC-conjugated CD34 (Santa Cruze, sc-7324), as well as CD133 (Santa Cruze, sc-32596). For unlabelled primary antibodies, FITC-conjugated secondary antibodies were added. All analyses were performed using a BD flow cytometer (BD Bioscience, San Jose, CA).

2.4. Differentiating CSCs into Cardiomyocytes. CSCs from brown adipose have the potential to spontaneously differentiate into functional cardiomyocytes as previously reported [12]. To determine the optimal seeding density for cardiomyocytes differentiation, primary stromal cells were seeded onto culture plates at different densities, ranging from 2.5×10^3 to 8×10^4 cells/cm². The cells were incubated in 37°C, 5% CO₂ for culture and differentiation. The medium was changed every 2 days. Cells of different seeding densities were observed every day under an inverted phase-contrast microscope (IX70 inverted system microscopy, Olympus Optical, Melville, NY). Number as well as morphology of developing clones was recorded.

2.5. Immunohistochemistry. To investigate the expression of cardiac specific antigens in the CSC-derived cardiomyocytes, immunohistochemical analyses on slides with elongated clusters of cells [19]. Briefly, isolated cells from brown adipose were seeded on slides. The cells were cultured and differentiated for 3–4 w as described above. Then, differentiated cells grown in slides were washed and fixed with 4% paraformaldehyde in 0.1 M phosphate buffer (pH 7.4). After permeabilization with 0.1% Triton X-100, the cells were incubated with the primary antibody against cTnT (diluted 1:200, Sigma) and α -sarcomeric actinin (diluted 1:200; Sigma) overnight at 4°C. FITC-labeled goat antimouse IgG was used as the secondary antibody. The cells were incubated with Hoechst33258 for genomic DNA staining and observed under a fluorescent microscope (Olympus Optical, Melville, NY).

2.6. Pharmacological Studies. Differentiated cells with a regular contractile activity were selected. The basal beating rate was recorded before and after the replacement of culture medium by the fresh α MEM medium (Gibco) containing 10% of fetal bovine serum. Chronotropic responses were then assessed in α MEM/10%FBS by extra-cellular recording of the beating rate in the presence of the appropriate drugs. Dose-response experiments were performed with 0.25 to 5×10^{-6} μ mol/L isoproterenol and 5 to 10×10^{-6} μ mol/L diltiazem. Antagonist was added after the maximal dose of agonist. The values were represented as mean \pm SD.

2.7. RNA Extraction and RT-PCR Analysis. For RNA extraction, elongated clusters of cells were dissected under an inverted phase-contrast microscope as previous report [20].

TABLE 1: Correlation between digest time and cell yield when different enzymes were used for brown adipose digest.

Time	Enzyme*	Digest time—Cell yield		
		Cell yield [§]	Cell viability	Viable cell yield [§]
30 minutes	D/IV/T	8.49 ± 0.57	93.47 ± 1.18%	7.94 ± 0.58
	IV/T	2.74 ± 0.39	93.79 ± 1.22%	2.57 ± 0.39
	IV	1.47 ± 0.19	94.66 ± 0.99%	1.39 ± 0.18
	I	0.18 ± 0.02	93.95 ± 1.05%	0.17 ± 0.02
	D	0.78 ± 0.07	94.96 ± 0.88%	0.74 ± 0.07
45 minutes	D/IV/T	11.65 ± 1.07	90.72 ± 1.38%	10.56 ± 0.98 [#]
	IV/T	4.26 ± 0.56	91.87 ± 1.34%	3.92 ± 0.54
	IV	1.82 ± 0.20	92.87 ± 1.69%	1.69 ± 0.20
	I	0.23 ± 0.04	91.96 ± 0.77%	0.22 ± 0.04
	D	0.87 ± 0.06	93.18 ± 1.36%	0.81 ± 0.07
60 minutes	D/IV/T	11.72 ± 0.86	86.88 ± 1.50%	10.19 ± 0.91
	IV/T	4.66 ± 0.33	90.86 ± 1.45%	4.23 ± 0.31 [#]
	IV	1.96 ± 0.15	91.17 ± 1.55%	1.79 ± 0.14 [#]
	I	0.28 ± 0.04	90.10 ± 1.14%	0.26 ± 0.04 [#]
	D	1.02 ± 0.13	91.14 ± 1.57%	0.93 ± 0.12 [#]

Nucleated cell yields of cell viability were compared among different enzymes and different digest time. Data are presented as mean ± standard deviation of $n=6$ for each group.

*D Dispase II; IV: collagenase IV; T: trypsin; I: collagenase I;

[#]Optimal cell yield for the enzyme.

[§] 10^6 cells/g tissue.

Total RNA was extracted with RNAPrep pure Cell/Bacteria Kit (TIANGEN) according to manufacturer's instruction. Reverse transcription were performed using standard procedures to synthesize first-strand cDNA. The gene-specific primers for cTnI (5'-CTCGGAGTATCAGGAAGAGCACA; 3'-TAAACTTGCCACGCAGGTCATAG, 216bp), GATA4 (5'-CTGTTCATCTCACTATGGGCA; 3'-CCAAGTCCGAGCAGGAATT, 257 bp), Nkx2.5 (5'-CAGTGGAGCTGGACAAAGCC; 3'-TAGCGACGGTCTGGAACCA, 216 bp), MEF2C (5'-AGCAAGAATACGATGCCATC; 3'-GAAGGGGTGGTGGTACGGTC, 347 bp), β -Actin (5'-AGAGGGAAATCGTGCGTGAC; 3'-AGGAGCCAGGCAGTAATC, 353 bp) were used in the following PCR amplification. Each cycle consisted of denaturation at 94°C for 30 seconds, and annealing/extension at 72°C for 45 seconds.

2.8. Statistical Analysis. The data are reported as means ± SD. Multiple related samples were compared using the Friedman test, results of which were complemented with posthoc pairwise analysis by Wilcoxon signed-rank test. Statistical analyses was performed with SPSS 11.0 (SPSS, Inc., Chicago, IL). Significance was accepted at $P < .05$.

3. Results

3.1. Optimized Isolation and High Cell Yield. To optimize isolating conditions for cell yield as high as possible, tissue digest was performed in 37°C, 5% CO₂ incubator. The correlation between digesting time and cell yield was investigated, so did cell viability. Comparisons have been made

TABLE 2: Phenotypic characterization of rat brown adipose-derived cells ($n = 6$).

Surface marker	Positive cells (%)
CD90	54.82 ± 3.50
CD133	22.43 ± 2.13
CD29	18.23 ± 1.97
CD29/CD133	8.22 ± 1.11
CD45	2.09 ± 0.72
CD34	0.12 ± 0.05

against the established method to isolate brown adipose-derived cardiac progenitor/stem cells with Dispase II and the classic one for stromal cell isolation from adipose tissue with collagenase I. In addition, other collagenases beside collagenase I were also tried. Collagenase IV was found more efficient than collagenase I for rat adipose digest (Table 1, Figure 1(a)). Thus, collagenase IV was selected for the enzyme combination in the experiment ensued. Data show that cell yield was up to $7.94 \pm 0.58 \times 10^6$ /g tissue when digesting for 30 minutes using the combined enzymes consisting of 0.1% collagenase IV, 0.1% dispase II and 0.05% trypsin. With the prolonged digest, both cell yield and cell death rate were increased (Table 1). When digesting time was prolonged to 60 minutes, cell yield did not significantly increase compared with that of 45 minutes, but cell death rate was significantly increased (up to 13.12%, Figure 1(b)). The highest viable cell yield was obtained at the digesting time of 45 minutes (more than 107 cells/g tissue), while cell viability was maintained up to ~91%. The data show that cell yield was dramatically enhanced compared with previously described method (Figure 1(a), $P < .01$) by combining collagenase IV, dispase II and trypsin for brown adipose tissue digest.

3.2. High Cardiomyogenic Potential of Isolated Cells and Cardiac Differentiation. To understand the characteristics of stromal cells isolated from rat brown adipose, we analyzed several surface markers with fluorescence-activated cell sorting (FACS) analyses (Figure 2, Table 2). The expression of CD29, CD90 (suggested to be one of MSC markers), is $18.23 \pm 1.97\%$ and $54.82 \pm 3.50\%$, respectively [21]. Most of the cells were negative for CD45, a hematopoietic and leukocyte marker. They also expressed negative for CD34, a myeloid progenitor cell antigen present in endothelial cells and some fibroblasts too [22]. In addition, the percentage of CD133-positive cells was up to ~22.43%. Such cells were confirmed by the previous report [23] to differentiate into cardiomyocytes with a high incidence. The percentage is significantly higher than the previous report [12, 23] (which only obtained 3.5% CD133-positive cells in total brown adipose-derived cells). Among the CD133 positive cells, about $8.22 \pm 1.11\%$ cells simultaneously express CD29.

After seeding on culture plates at different densities, cells adhered and proliferated, while cardiac stem cells began to differentiate with prolonged culture. As shown in Figure 3, around 6 days of culture, emergence of various

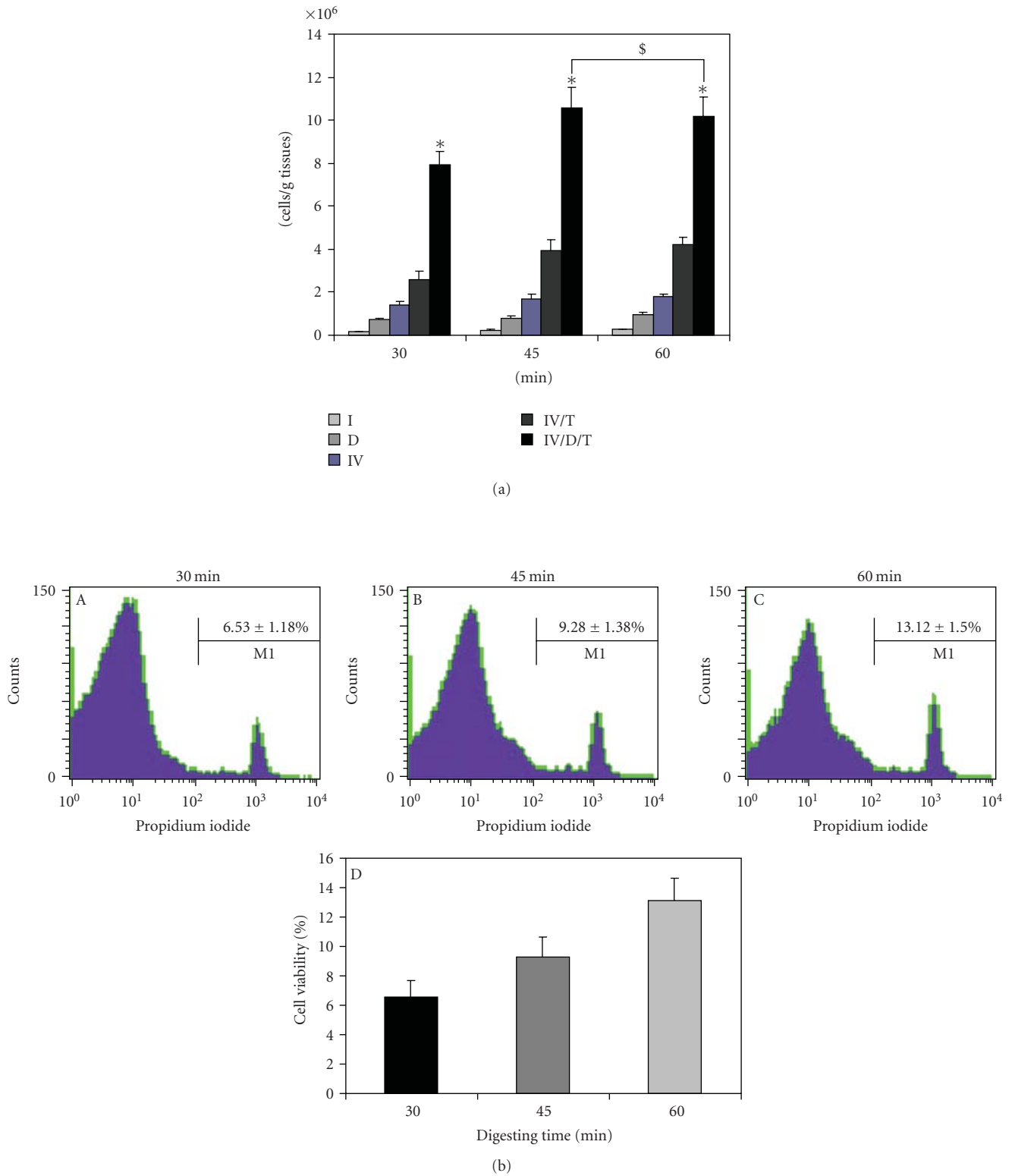


FIGURE 1: (a) Comparisons between different methods in nucleated cell yield within one hour's digest ($n = 6$ for each group). \$: no significant difference, $P > .05$; *: $P < .01$ compared with all other groups in the same digest time. (b) Representative images of cell viability analysis. Newly isolated cells from rat brown adipose were stained with Propidium iodide and then analyzed using flow cytometry. A: Cell viability after 30 minutes digestion with collagenase IV, dispase II, and trypsin; B: cell viability after 45 minutes digestion with collagenase IV, dispase II, and trypsin; C: cell viability after 60 minutes digestion with collagenase IV, dispase II, and trypsin; D: Comparison of cell viabilities after digesting for different time with collagenase IV, dispase II, and trypsin, ($n = 6$ for each group).

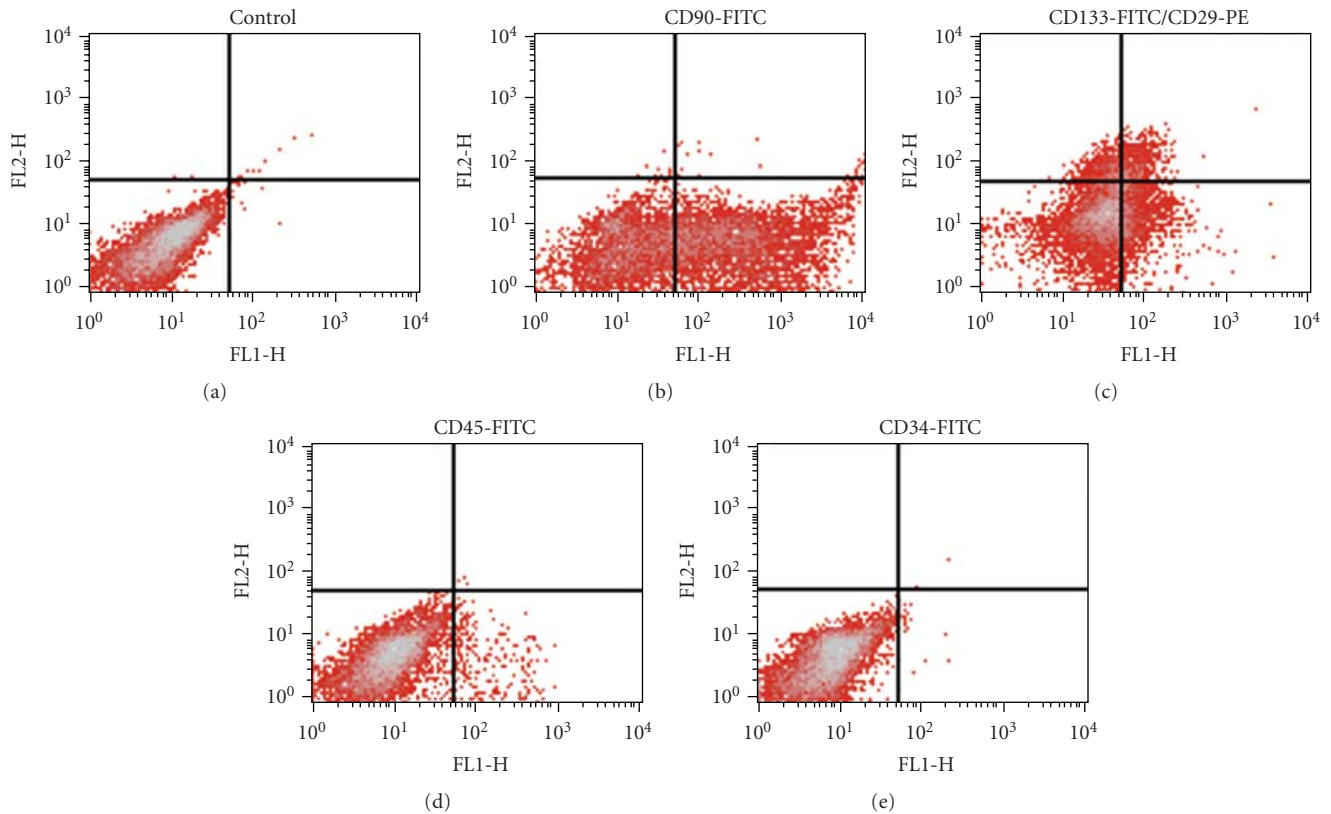


FIGURE 2: Representative images of flow cytometry analyses for rat brown adipose-derived cells. Brown adipose-derived cells are partly positive for CD-29, CD90, and CD133, while negative for CD45 and CD34. (a) Control; (b) Flow cytometry analysis for surface marker CD90; (c) Flow cytometry analysis for surface marker CD29 and CD133; (d) Flow cytometry analysis for surface marker CD45; (e) Flow cytometry analysis for surface marker CD34.

cell morphologies were identified, that is, fibroblast-like appearance, clusters of preadipocytes/adipocytes, and clones of rounded cells together with small tube cells. At 1 week, elongated cells appeared and started a contractile activity independently. Following this, increasingly more elongated morphology and contractile cells appeared with the time (Figure 3). In 3 to 4 weeks, groups of contractile cells could be seen in nearly any field under an inverted phase-contrast microscope. In the whole process, differentiation proceeded spontaneously, using no inductor. However, the percentage of beating cells counted at 3-4 weeks varied among the seeding densities of isolated cells (details below).

3.3. CSC-Derived Cardiomyocytes Demonstrate Characteristic Similar to Functional Cardiomyocytes

3.3.1. Expression of Cardiac Markers. In order to define the phenotype of differentiated cells, immunofluorescent staining of cardiac-specific antigens was performed on the slides with elongated clusters of cells. In addition, the expression of cardiac genes was analyzed by RT-PCR. As expected, a specific positive staining was obtained with antibodies against the sarcomeric α -actinin (Figure 4(a) A–C) and cardiac troponin T (Figure 4(a) E–G); even the transverse striation can be clearly observed (Figure 4(a) D, H). Some

elongated cells that do not contract under conditions could also be stained by cTnT/ α -actinin. In contrast, antibodies against the skeletal muscle protein MyoD (data not show) did not stain the elongated cells. The expressions of cTnI, GATA4, Nkx2.5, MEF2C were also verified (Figure 4(b)). These data strongly argued for the cardiomyocyte nature of the contracting cells.

3.3.2. Reaction with Pharmacologic Reagents. To test the functionality of CSC-derived cardiomyocytes, pharmacological studies were performed at 28 days after differentiation of brown adipose-derived CSCs. Several pharmacologic agents known to influence the heart rate were added and the chronotropic responses of contracting cells to these agents were examined. As expected for differentiated cardiomyocytes, the β -agonist isoproterenol induced a dose-dependent increase of the spontaneous contraction rate measured as beatings per minute (Figure 5). Diltiazem, a nonselective β -adrenergic antagonist, reversed the isoproterenol-induced acceleration (Figure 5). These chronotropic responses definitively demonstrated that these cells responded like functional cardiomyocytes. Note that there was a great heterogeneity in the sensitivity to these heart pharmacologic agents among different cardiomyocytes. For instance, some cardiomyocytes that did not contract

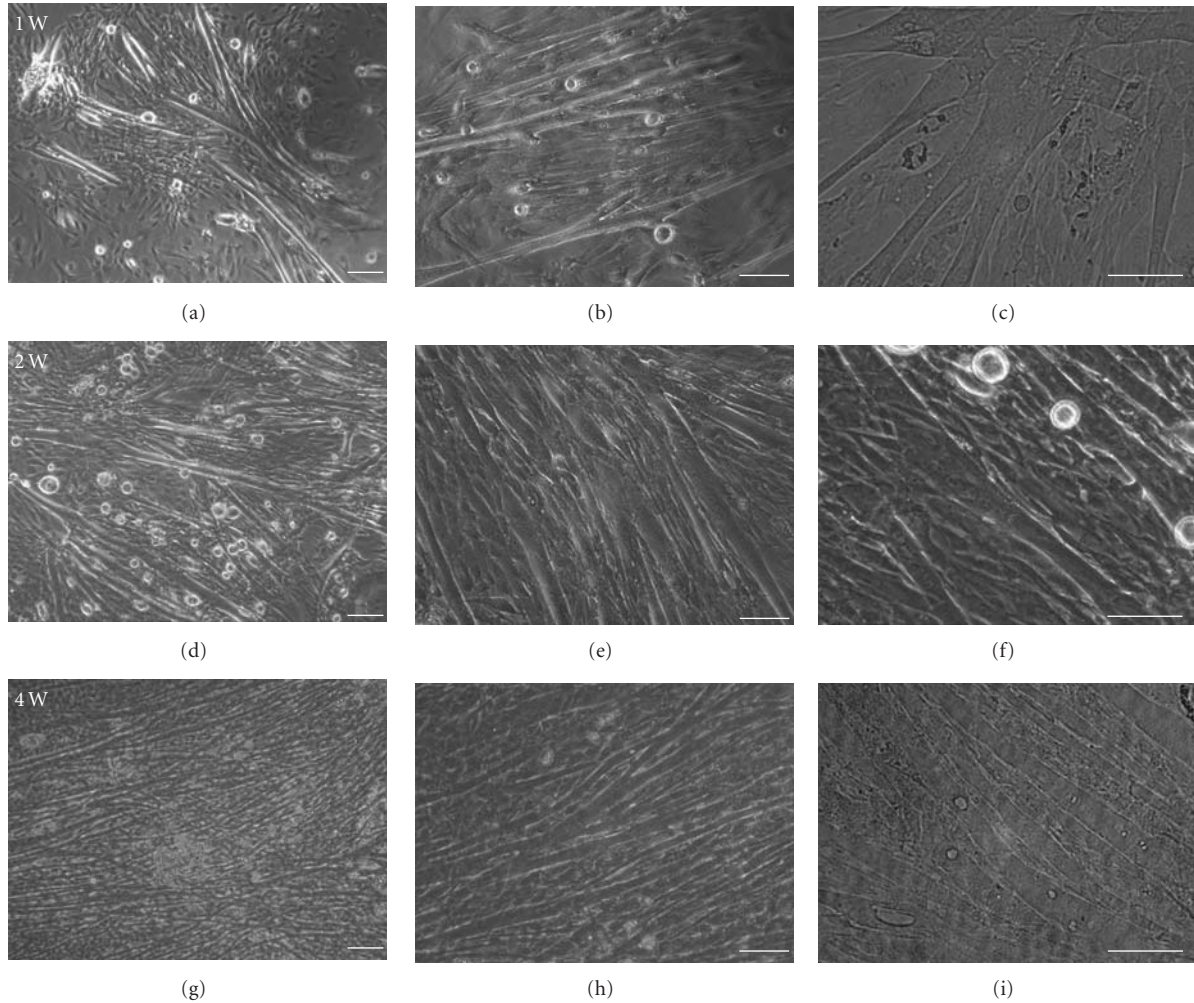


FIGURE 3: Culture and differentiation of brown adipose-derived cardiac stem cells. Phase-contrast microscopy of differentiated cardiomyocytes-like cells at days 7, 14, and 28. Isolated primary cells were plated into culture dishes (2.5×10^4 cells/cm²) and observed every day under an inverted phase-contrast microscope at (a)–(c) 1 weeks after spontaneous differentiation, (d)–(f) 2 weeks after spontaneous differentiation, (g)–(i) 4 weeks after spontaneous differentiation. Differentiated cells gradually increased in size with time due to cell proliferation. Early differentiated cells were rare in plates (day 7), then elongated cells appeared (day 14 and 28) more and more, and they could spontaneously beat like functional cardiomyocytes (bar = 100 μ m).

TABLE 3: Comparison of differentiated cTnT+ cardiomyocytes (%) from brown adipose-derived cells at different seeding densities.

Cell density	$5 \times 10^4/\text{cm}^2$	$2.5 \times 10^4/\text{cm}^2$	$1 \times 10^4/\text{cm}^2$	$5 \times 10^3/\text{cm}^2$	$2.5 \times 10^3/\text{cm}^2$	$1 \times 10^3/\text{cm}^2$
Combination*	24.78 ± 2.4	$29.93 \pm 3.2^\#$	25.41 ± 2.23	21.43 ± 1.62	16.7 ± 1.41	5.3 ± 0.6
Dispase II*	11.64 ± 1.98	15.43 ± 2.76	12.35 ± 2.21	9.64 ± 2.55	5.7 ± 1.24	2.41 ± 0.91

*Combination: cells isolated by combination of collagenase IV, dispase II, and trypsin; Dispase II: cells isolated by dispase II alone.

[#]The optimal seeding density for brown adipose-derived cardiac stem cells differentiation into cardiomyocytes ($P < .01, n = 6$).

under control conditions started to beat under β -adrenergic stimulation (data not shown). However, when cells were responsive, similar pattern toward the drugs was also observed.

3.4. Optimal Seeding Density for Cardiac Stem Cell Differentiation. The primary seeding density of brown adipose-derived cells influences the differentiation efficiency of cardiac stem cells into cardiomyocytes, as was demonstrated

in the previous report [12]. So correlation between seeding density of primary cells and percentage of differentiated cardiomyocytes was investigated to achieve the optimal cardiac differentiation. As shown in Table 3, the appearance of cTnT⁺ CM cells varies from $\sim 5.3 \pm 0.6\%$ to $\sim 29.93 \pm 3.2\%$ with the primary seeding densities increasing from $1 \times 10^3/\text{cm}^2$ – $5 \times 10^4/\text{cm}^2$. These data showed that cells we isolated from brown adipose by using this new method have even higher cardiomyogenic potential than that previously

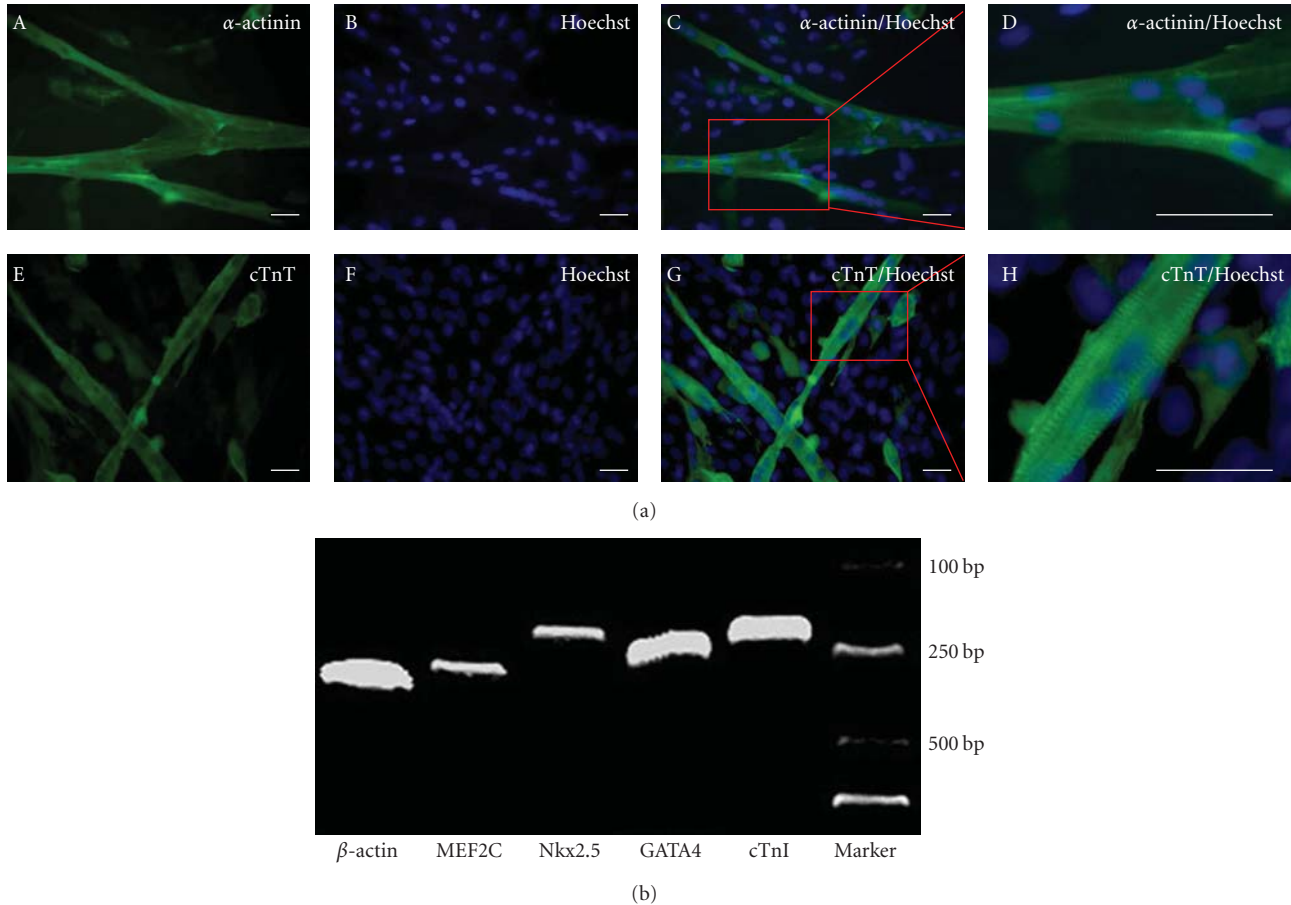


FIGURE 4: (a) *Immunostaining of differentiated cells for cardiac-specific antibodies.* Differentiated cardiomyocytes-like cells were specifically stained with anti- α -sarcomeric actinin A–D, and anticardiac troponin A–I antibodies; the transverse striation can be clearly observed under high magnification microscopy (D and I, 4 magnifications of red frame in C and G, resp.). Furthermore, no specific staining was obtained with the antiMyoD (data not shown) (Bar = 50 μ m). (b) *Expression of cardiac-specific genes in the differentiated cells analyzed by RT-PCR.*

reported [12]. Note that no sorting procedure was performed in our study (also different from the previous report) [12].

4. Discussion

Heart disease is the leading cause of death in the industrial world. The stem cell therapy seems to be a promising treatment for injured myocardium. To reach this goal, it is desirable to find a good source of stem cells that can be used to obtain new myocardium on time [21]. Several cell types, for example, ESC, BMMSC, skeletal myoblasts, have been considered candidates for myocardial regeneration. However, each of them has shortfalls in clinical applications [4–8]. The best candidates seem to be cardiac “progenitor” and/or “stem” cells [21]. Currently the cardiac stem cell transplantation for regenerating infarcted myocardium has invited a great deal of interest. Many laboratories have attempted to isolate potential cardiac stem cells from several tissues [22]. In this study, we firstly combined collagenase and dispase II with trypsin for brown adipose digestion to isolate cardiac stem cells. Our main findings are the following: (1) We established a new method to efficiently

isolate cells from rat brown adipose with a high content of CSCs, and total cell yield increased up to more than 10^7 /gram tissue. (2) We corroborated brown adipose to be an abundant source of cardiac stem cells, useful for in vitro studies of cardiomyocytes differentiation/(patho) physiology and in vivo studies of cardiac stem cell therapy.

We demonstrated that a single collagenase or dispase II was insufficient for brown adipose digestion, leading to relative lower cell yield (Figure 1(a)). However, when collagenase was combined with dispase II supplemented by trypsin, cell yield dramatically increased by manifolds (Figure 1(a)). Efficient tissue digestion was also observed. In our experiment, tissue blocks also left undigested when collagenase or dispase II was applied alone, albeit digesting time extended to more than 2 hours (data not shown). In contrast, tissue blocks could be hardly found in 30 minutes digestion by combining three enzymes, indicating optimally sufficient tissue digestion.

Several years ago, a single protease was demonstrated to have limitations in digesting capacity when applied to digest adipose tissues. Different protease activity was necessary for optimal tissue digest efficacy and cell yield [19, 24–26].

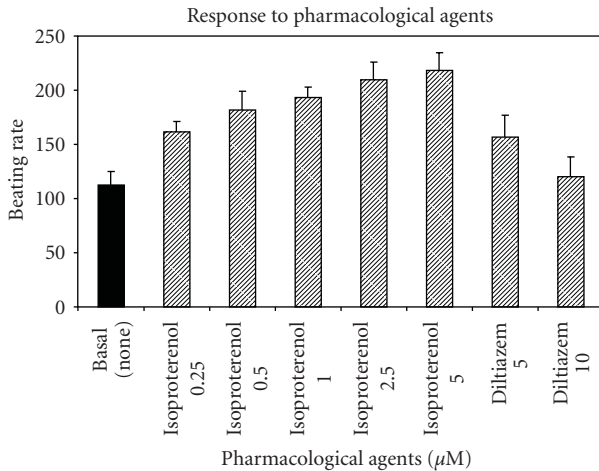


FIGURE 5: Chronotropic response of contracting cells to adrenergic and diltiazem stimulation. Isolated cells were plated into 6-well plate for 28 days. Basal beating rate was recorded. Contracting rate was measured by the treatment with the β -adrenergic agonist isoproterenol and antagonist diltiazem. Results represent the mean of 6 to 10 separate experiments.

However, the challenge is to balance the combination of enzymes and digesting time for the desired cell yield and function [27]. Additionally, it has been shown that parameters (e.g., digest time and enzyme activity) applied in the isolating procedure of primary cells have a significant effect on cell yield, viability, and phenotype. Therefore, isolating conditions were optimized. Isolated cells were also evaluated for cardiomyogenic potential in our study. The tissue was digested in 37°C, pH7.2–7.4, favorable for enzyme activities. A magnetic stirrer was used to facilitate tissue digestion. Under these conditions, optimal digesting time was determined to be 45 minutes (to balance the total cell yield and viability). When differentiating obtained cells into cardiomyocytes, the isolated cells by this new method were of high cardiomyogenic potential compared with what was previously described [12]. Thus, this new method is proved efficient in total cell yield from brown adipose with high cardiomyogenic potential. It is noteworthy that the method is also suitable for multipotent stem cell isolation from rat white adipose tissues (data not shown).

In consistency with the previous reports [12, 23], we failed to get purified cardiac stem cells from brown adipose-derived cell population. Thus a valid procedure for their expansion in undifferentiated states was not established. To further their applications in cell therapies, a technique for rapid purification as well as a method of clinical grade expansion for the cardiac stem cells is needed.

5. Conclusion

In this study, we have found an optimal combination of digest enzymes consisting of 0.1% collagenase IV, 0.1% dispase II, and 0.05% trypsin for efficient isolation of cardiac stem cells from brown adipose tissues. The procedure was

optimized for maximum viable cell yield (up to 10^7 /cells from 1 gram tissue sample). Furthermore, the obtained cells could be effectively differentiated into functional cardiomyocytes. Therefore, we established a novel and efficient method for cardiac stem cell isolation from brown adipose. It will pave the way for cardiac stem cell therapy as well as in basic research.

Acknowledgment

This work was supported by the National High Technology Research and Development Program of China (no. 2006AA02A105), the Nature Science Foundation of China (no. 30530220), Beijing Nature science Foundation of China (no. 7062053). The authors thank C. Chen for technical assistance in histological preparation and staining Z. Liu, H. Wang, Y. Zhang, and J. Zhou contributed equally to this work.

References

- [1] V. Planat-Bénard, C. Menard, M. André, et al., “Spontaneous cardiomyocyte differentiation from adipose tissue stroma cells,” *Circulation Research*, vol. 94, no. 2, pp. 223–229, 2004.
- [2] W. H. Zimmermann, I. Melnychenko, G. Wasmeier, et al., “Engineered heart tissue grafts improve systolic and diastolic function in infarcted rat hearts,” *Nature Medicine*, vol. 12, no. 4, pp. 452–458, 2006.
- [3] A. P. Beltrami, L. Barlucchi, D. Torella, et al., “Adult cardiac stem cells are multipotent and support myocardial regeneration,” *Cell*, vol. 114, no. 6, pp. 763–776, 2003.
- [4] T. Kofidis, D. R. Lebl, E. C. Martinez, G. Hoyt, M. Tanaka, and R. C. Robbins, “Novel injectable bioartificial tissue facilitates targeted, less invasive, large-scale tissue restoration on the beating heart after myocardial injury,” *Circulation*, vol. 112, no. 9, supplement, pp. I.173–I.177, 2005.
- [5] K. L. Christman, A. J. Vardanian, Q. Fang, R. E. Sievers, H. H. Fok, and R. J. Lee, “Injectable fibrin scaffold improves cell transplant survival, reduces infarct expansion, and induces neovasculature formation in ischemic myocardium,” *Journal of the American College of Cardiology*, vol. 44, no. 3, pp. 654–660, 2004.
- [6] A. A. Mangi, N. Noiseux, D. Kong, et al., “Mesenchymal stem cells modified with Akt prevent remodeling and restore performance of infarcted hearts,” *Nature Medicine*, vol. 9, no. 9, pp. 1195–1201, 2003.
- [7] R. Passier, L. W. van Laake, and C. L. Mummery, “Stem-cell-based therapy and lessons from the heart,” *Nature*, vol. 453, no. 7193, pp. 322–329, 2008.
- [8] Z. Li, A. Lee, M. Huang, et al., “Imaging survival and function of transplanted cardiac resident stem cells,” *Journal of the American College of Cardiology*, vol. 53, no. 14, pp. 1229–1240, 2009.
- [9] A. G. Latronico, M. Coletta, E. Vivarelli, et al., “Isolation and expansion of adult cardiac stem cells from human and murine heart,” *Circulation Research*, vol. 95, no. 9, pp. 911–921, 2004.
- [10] A. Linke, P. Müller, D. Nurzynska, et al., “Stem cells in the dog heart are self-renewing, clonogenic, and multipotent and regenerate infarcted myocardium, improving cardiac function,” *Proceedings of the National Academy of Sciences of the United States of America*, vol. 102, no. 25, pp. 8966–8971, 2005.

- [11] L. Barile, I. Chimenti, R. Gaetani, et al., "Cardiac stem cells: isolation, expansion and experimental use for myocardial regeneration," *Nature Clinical Practice Cardiovascular Medicine*, vol. 4, no. 1, pp. S9–S14, 2007.
- [12] Y. Yamada, X.-D. Wang, S.-I. Yokoyama, N. Fukuda, and N. Takakura, "Cardiac progenitor cells in brown adipose tissue repaired damaged myocardium," *Biochemical and Biophysical Research Communications*, vol. 342, no. 2, pp. 662–670, 2006.
- [13] A. M. Smits, P. van Vliet, C. H. Metz, et al., "Human cardiomyocyte progenitor cells differentiate into functional mature cardiomyocytes: an in vitro model for studying human cardiac physiology and pathophysiology," *Nature Protocols*, vol. 4, no. 2, pp. 232–243, 2009.
- [14] G. Löffler and H. Hauner, "Adipose tissue development: the role of precursor cells and adipogenic factors. Part II: the regulation of the adipogenic conversion by hormones and serum factors," *Klinische Wochenschrift*, vol. 65, no. 17, pp. 812–817, 1987.
- [15] J. M. Gimble, A. J. Katz, and B. A. Bunnell, "Adipose-derived stem cells for regenerative medicine," *Circulation Research*, vol. 100, no. 9, pp. 1249–1260, 2007.
- [16] Y. Miyahara, N. Nagaya, K. Masaharu, et al., "Monolayered mesenchymal stem cells repair scarred myocardium after myocardial infarction," *Nature Medicine*, vol. 12, no. 4, pp. 459–465, 2006.
- [17] M. Mazo, V. Planat-Bénard, G. Abizanda, et al., "Transplantation of adipose derived stromal cells is associated with functional improvement in a rat model of chronic myocardial infarction," *European Journal of Heart Failure*, vol. 10, no. 5, pp. 454–462, 2008.
- [18] P. A. Zuk, M. Zhu, P. Ashjian, et al., "Human adipose tissue is a source of multipotent stem cells," *Molecular Biology of the Cell*, vol. 13, no. 12, pp. 4279–4295, 2002.
- [19] S. Lü, S. Liu, W. He, et al., "Bioreactor cultivation enhances NTEB formation and differentiation of NTES cells into cardiomyocytes," *Cloning and Stem Cells*, vol. 10, no. 3, pp. 363–370, 2008.
- [20] B. Léobon, J. Roncalli, C. Joffre, et al., "Adipose-derived cardiomyogenic cells: in vitro expansion and functional improvement in a mouse model of myocardial infarction," *Cardiovascular Research*, vol. 83, no. 4, pp. 757–767, 2009.
- [21] V. Di Felice, A. De Luca, M. L. Colorito, et al., "Cardiac stem cell research: an elephant in the room?" *Anatomical Record*, vol. 292, no. 3, pp. 449–454, 2009.
- [22] J. Pouly, P. Bruneval, C. Mandet, et al., "Cardiac stem cells in the real world," *Journal of Thoracic and Cardiovascular Surgery*, vol. 135, no. 3, pp. 673–678, 2008.
- [23] Y. Yamada, S.-I. Yokoyama, X.-D. Wang, N. Fukuda, and N. Takakura, "Cardiac stem cells in brown adipose tissue express CD133 and induce bone marrow nonhematopoietic cells to differentiate into cardiomyocytes," *Stem Cells*, vol. 25, no. 5, pp. 1326–1333, 2007.
- [24] P. Georges, R. P. Muirhead, L. Williams, et al., "Comparison of size, viability, and function of fetal pig islet-like cell clusters after digestion using collagenase or liberase," *Cell Transplantation*, vol. 11, no. 6, pp. 539–545, 2002.
- [25] H. Wang, C. A. Van Blitterswijk, M. Bertrand-De Haas, A. H. Schuurman, and E. N. Lamme, "Improved enzymatic isolation of fibroblasts for the creation of autologous skin substitutes," *In Vitro Cellular and Developmental Biology—Animal*, vol. 40, no. 8–9, pp. 268–277, 2004.
- [26] D. M. Hayman, T. J. Blumberg, C. C. Scott, and K. A. Athanasiou, "The effects of isolation on chondrocyte gene expression," *Tissue Engineering*, vol. 12, no. 9, pp. 2573–2581, 2006.
- [27] L. Pilgaard, P. Lund, J. G. Rasmussen, T. Fink, and V. Zachar, "Comparative analysis of highly defined proteases for the isolation of adipose tissue-derived stem cells," *Regenerative Medicine*, vol. 3, no. 5, pp. 705–715, 2008.

Research Article

Pre-mRNA Processing Is Partially Impaired in Satellite Cell Nuclei from Aged Muscles

Manuela Malatesta,¹ Federica Perdoni,² Sylviane Muller,³ Carlo Pellicciari,² and Carlo Zancanaro¹

¹*Dipartimento di Scienze Morfologico-Biomediche, Sezione di Anatomia e Istologia, University of Verona, Strada Le Grazie 8, 37134 Verona, Italy*

²*Laboratorio di Biologia Cellulare, Dipartimento di Biologia Animale, University of Pavia, Via Ferrata 9a, 27100 Pavia, Italy*

³*CNRS, Institut de Biologie Moléculaire et Cellulaire, Immunologie et Chimie Thérapeutiques, 15 rue R. Descartes, 67084 Strasbourg Cedex, France*

Correspondence should be addressed to Manuela Malatesta, manuela.malatesta@univr.it

Received 30 October 2009; Accepted 3 February 2010

Academic Editor: Guy M. Benian

Copyright © 2010 Manuela Malatesta et al. This is an open access article distributed under the Creative Commons Attribution License, which permits unrestricted use, distribution, and reproduction in any medium, provided the original work is properly cited.

Satellite cells are responsible for the capacity of mature mammalian skeletal muscles to repair and maintain mass. During aging, skeletal muscle mass as well as the muscle strength and endurance progressively decrease, leading to a condition termed sarcopenia. The causes of sarcopenia are manifold and remain to be completely elucidated. One of them could be the remarkable decline in the efficiency of muscle regeneration; this has been associated with decreasing amounts of satellite cells, but also to alterations in their activation, proliferation, and/or differentiation. In this study, we investigated the satellite cell nuclei of biceps and quadriceps muscles from adult and old rats; morphometry and immunocytochemistry at light and electron microscopy have been combined to assess the organization of the nuclear RNP structural constituents involved in different steps of mRNA formation. We demonstrated that in satellite cells the RNA pathways undergo alterations during aging, possibly hampering their responsiveness to muscle damage.

1. Introduction

The capacity of mature mammalian skeletal muscles to repair and maintain mass is due to the presence of undifferentiated mononuclear myogenic precursor cells, that is, the satellite cells, located at the periphery of myofiber, between the sarcolemma and the surrounding basal lamina. Satellite cells remain quiescent until appropriate stimuli (e.g., muscle injury) trigger their re-entry into the cell cycle; they then undergo activation and proliferation, and the daughter cells fuse to form muscle fibers which increase muscle mass. The availability and responsiveness of satellite cells are therefore necessary for efficient muscle regeneration.

During aging, a progressive loss of skeletal muscle mass and a parallel decrease in muscle strength and endurance take place. This condition, termed sarcopenia, has important health-care and socioeconomic implications for humans,

since it contributes to frailty, functional loss, dependence, disability, high health care costs, and premature death (the recent review in [1]).

The mechanisms leading to sarcopenia are probably manifold and they still remain to be completely elucidated (review in [2, 3]). One of the possible causes could be the remarkable decline in the efficiency of muscle regeneration; this has been associated with decreasing amounts of satellite cells (e.g., [4–8]), possibly due to apoptotic cell death [9, 10], although this is controversial [11–13]. It has also been suggested that activation, proliferation, and/or differentiation of satellite cells and their progeny may be altered in sarcopenia [14, 15].

It is known that aging involves alterations in the pathways of gene expression, which are not necessarily associated with mutations but can imply impairments in pre-mRNA transcription and/or splicing (review in [16]). In particular, it has

been shown that aging affects intranuclear RNA pathways by altering the organization, composition, and location of the ribonucleoprotein-(RNP-) containing structures [17–21]. These structures are part of the transcription and splicing machinery: perichromatin fibrils (PFs) are the morphological equivalent of hnRNA transcription and cotranscriptional splicing, perichromatin granules (PG), which form by PF coiling, are involved in the storage and the nucleus-to-cytoplasm transport of mRNA, while interchromatin granules (IG) represent the storage, assembly, and recycling site for snRNP and non-snRNP splicing factors [22–24].

In a recent study [25], we have analyzed the fine structure of myonuclei as well as the distribution and amount of RNA processing factors in myofibers of biceps brachii and quadriceps femoris from adult and old rats. We thus showed that in myonuclei of aged fibers a decrease in the transcription, processing, and transport rate of pre-mRNA takes place. Both muscles contain a high proportion (about 90%) of type II fibers and are therefore largely affected by sarcopenia [26–28].

In the present study, we focused our attention on satellite cells of those same muscles. To determine whether the RNA pathways also undergo alterations in the satellite cells of aging muscles, we combined morphometry and immunocytochemistry at light and electron microscopy and investigated the distribution and content of nuclear RNP structural constituents involved in different steps of mRNA formation.

2. Materials and Methods

2.1. Animals. Two adult (9 months of age) and two old (28 months of age) male Wistar rats were used. All animals were bred under controlled environmental conditions with a 12-hour light/dark cycle and fed ad libitum with a standard commercial chow. The experimental protocols comply with the guidelines of the Italian Ministry of Health as well as with internationally recognized guidelines.

The rats were deeply anesthetized with pentobarbital (50 mg/Kg i.p.) and then perfused via the ascending aorta with a brief prewash of 0.09% NaCl solution followed by 300 mL of a fixative solution containing 4% (v/v) paraformaldehyde in 0.1 M phosphate buffer, pH 7.4 at 4°C. Biceps brachii and quadriceps femoris muscles were quickly removed and placed in the same fixation solution for 2 hours at 4°C.

2.2. Light Microscopy. After fixation, muscle samples were dehydrated with ethanol and embedded in paraffin wax. Seven- μm -thick muscle samples were cross-sectioned then submitted to immunohistochemical procedures for identification of satellite cells by using a mouse monoclonal antibody directed against the membrane-bound neural cell adhesion molecule (N-CAM/CD56/Leu-19), which has been demonstrated on satellite cells in normal adult skeletal muscle and represents an established marker [29] (BD Biosciences, San Jose, CA). The primary antibody was then revealed with an Alexa 488 conjugated antibody against mouse IgG (Molecular Probes, Invitrogen, Milan, Italy). The

sections were finally counterstained for DNA with 0.1 $\mu\text{g}/\text{mL}$ Hoechst 33258 to label the cell nuclei and to detect the occurrence of apoptosis based on chromatin morphology. Observations were made with an Olympus BX51 microscope equipped with a 100 W mercury lamp under the following conditions: 330- to 385-nm excitation filter (excf), 400-nm dichroic mirror (dm), and 420-nm barrier filter (bf), for Hoechst 33258; 450- to 480-nm excf, 500-nm dm, and 515 nm bf for Alexa 488. Micrographs were recorded with an Olympus Camedia C-5050 digital camera and stored on a PC by the Olympus software for processing and printing. Morphometrical evaluations were performed by using the software Image J (NIH, USA).

To estimate the possible decrease in the amount of satellite cells in the muscles, the number of satellite cells was determined over areas of cross-sectioned muscles containing only myofibers and endomysium; using a 40 \times objective lens, a total of 880,000 μm^2 were considered per each muscle, and the density of satellite cells was expressed as satellite cells/1000 μm^2 of muscle area. The percentage of apoptotic nuclei was evaluated in the counted satellite cells.

The percentage of apoptotic nuclei was also evaluated on myofibers, on a total of 25 microscope fields, using an $\times 20$ objective lens (at least 2000 myonuclei per muscle sample were counted).

2.3. Transmission Electron Microscopy. After fixation, muscle samples were washed in Sørensen buffer and subsequently in phosphate buffered saline (PBS), kept in 0.5 M NH_4Cl in PBS for 45 minutes to block free aldehydes, dehydrated with ethanol, and embedded in LR White resin polymerized under U.V. light. This fixation procedure is optimal to allow antigen detection at electron microscopy, although the ultrastructural morphology of especially the cellular membranes cannot be perfectly preserved.

Ultrathin sections were collected on Formvar-carbon coated nickel grids and used for morphometrical and immunocytochemical analyses.

Morphometrical evaluations ($\times 11,000$) were made on twelve satellite cell nuclei per muscle by using a computerized image analysis system (AnalySIS Image processing, Soft Imaging System GmbH, Muenster, Germany). The following parameters were considered: area of nuclei and nucleoli, percentage of nuclear area occupied by condensed chromatin and PG density ($\text{PG}/\mu\text{m}^2$ of interchromatin space, i.e., the nucleoplasmic region devoid of condensed chromatin), area of the fibrillar centers, and percentage of the nucleolar area occupied by the dense fibrillar component and by the granular component.

To investigate the fine distribution of some RNA transcription and processing factors, thin muscle sections were treated with one of the following probes: mouse monoclonal antibodies directed against the activated, phosphorylated form of RNA polymerase II (Research Diagnostic Inc., Flanders, NJ) or against the snRNP (small nuclear RNP) Sm core proteins (Abcam, Cambridge, MA); rabbit polyclonal antibodies were used against DNA/RNA hybrid molecules [30] specifically occurring in the transcription sites [25, 31], and the cleavage stimulation factors CstF [32]. Sections were

floated for 3 minutes on normal goat serum (NGS) diluted 1 : 100 in PBS and then incubated overnight at 4°C with the primary antibodies diluted with PBS containing 0.1% (w/v) bovine serum albumin (Fluka, Buchs, Switzerland) and 0.05% (v/v) Tween 20. After rinsing, sections were floated on NGS, and then allowed to react for 20 minutes at room temperature with the secondary 12 nm or 18 nm-gold-conjugated antibody (Jackson ImmunoResearch Laboratories Inc., West Grove, PA) diluted 1 : 10 in PBS. Finally, the sections were rinsed and air-dried. As controls, some grids were incubated without the primary antibody and then processed as described above.

To reduce chromatin contrast and selectively reveal nuclear RNP constituents, the sections were bleached by the EDTA method [33], observed in a Philips Morgagni TEM operating at 80 kV, and equipped with a Megaview II camera for digital image acquisition.

Quantitative assessment of the immunolabeling was carried out by estimating the gold grain density over selected cellular compartments on sections treated in the same run. The surface area of the interchromatin space and IG was measured on fifteen satellite cell nuclei (x22,000) from each muscle by using a computerized image analysis system (AnalySIS Image processing). For background evaluation samples treated in the absence of primary antibody were considered. The gold grains over each selected compartment were counted, and the labeling density was expressed as the number of gold grains/ μm^2 .

2.4. Statistics. For each analyzed variable, the Kolmogorov-Smirnov two-sample test was performed in order to verify the hypothesis of identical distribution among animals of each experimental group (i.e., adult and old rats). The data were then pooled according to the experimental groups and the means \pm standard error of the mean (SE) values were calculated. Statistical comparisons were performed by the Mann Whitney *U*-test (significance was set at $P \leq 0.05$).

3. Results

As previously reported [25], a dramatic mass reduction was observed in both the biceps and quadriceps muscles of old rats in comparison to adult animals.

3.1. Light Microscopy. Satellite cells were specifically labeled by the anti-N-CAM antibody (Figure 1(a)); their density (number of satellite cells/1000 μm^2 of muscle area) was significantly higher in adult than in old rats, in both the biceps and quadriceps muscle. Morphologically recognizable apoptotic nuclei in satellite cells of both muscles from adult rats were quite scarce; in muscles of old animals the percentage of apoptotic nuclei increased although not significantly (Figure 1(b)). It is, however, worth underlying that the absolute number of satellite apoptotic cells counted was very low, in both animal groups. Morphologically recognizable apoptotic nuclei in the myofibres were quite scarce and their percentage was similar in adult and old animals in both biceps ($0.16 \pm 0.06\%$ versus 0.22 ± 0.09 , resp.) and quadriceps ($0.15 \pm 0.06\%$ versus 0.18 ± 0.07 , resp.) muscles.

3.2. Transmission Electron Microscopy. In spite of the nonoptimal ultrastructural preservation due to the fixation procedure necessary for immunocytochemistry, in all the muscle samples satellite cells were morphologically recognizable as small cells with scanty cytoplasm and located between the sarcolemma and the surrounding basal lamina of the muscle fibers (Figure 2(a)). Satellite cell nuclei generally were ovoid in shape with finely irregular border and contained abundant condensed chromatin distributed both at the nuclear and nucleolar periphery, and one roundish compact nucleolus with prominent granular component, scarce dense fibrillar component, and rare small fibrillar centers (Figure 2(b)). In the nucleoplasm, all the usual RNP structural constituents involved in pre-mRNA transcription and processing were evident; few PF and PG were mainly distributed at the periphery of the condensed chromatin and small IG clusters occurred in the interchromatin space. In satellite cell nuclei of old muscles, PF sometimes occurred as clusters (Figures 2(d) and 2(h)). At electron microscopy, the satellite cell nuclei were structurally similar in adult and old rats, and morphological evidence of apoptosis was never found in any of the muscle samples examined.

In both biceps and quadriceps muscles, we did not observe significant differences between the satellite cells from adult and old rats as for the nuclear or nucleolar area, the percentage of condensed chromatin, the PG density, and the percentage of the dense fibrillar and the granular components of nucleoli (Figure 3). The area of the rare fibrillar centers observed ranged from 0.001 to 0.003 μm^2 , without difference between muscles or age groups.

The immunocytochemical labeling for polymerase II, the DNA/RNA hybrid molecules, snRNPs, and the cleavage factor CstF were similar in the nucleoplasm of satellite cells from adult and old rats. In both animal groups, polymerase II and DNA/RNA hybrid molecules were exclusively associated with PF (Figures 2(c) and 2(d); snRNPs were restricted to PF and IG (Figures 2(e) and 2(f)); CstF was located essentially on PF and on RNP tails rising from PG (Figures 2(g) and 2(h)).

The quantitative evaluation of the immunolabeling (Figure 4) revealed similar densities of polymerase II and DNA/RNA hybrid molecules in both biceps and quadriceps muscles of adult and old rats; conversely, snRNPs and CstF were more abundant in the interchromatin space of old rats compared to adult rats. In addition, snRNPs were found to be more abundant in the IG of old rats (biceps brachii: 16.12 ± 2.86 gold grains/ μm^2 in adult versus 33.76 ± 5.25 in old rats, $P = 0.047$; quadriceps femoris: 15.56 ± 3.88 gold grains/ μm^2 in adult versus 34.97 ± 5.94 in old rats, $P = 0.042$); conversely, in all the samples the labeling for polymerase II, the DNA/RNA hybrid molecules and CstF were almost absent on IG (Figures 2(c), 2(d), 2(g), and 2(h)). Background values were negligible in all immunolabeling experiments (not shown).

4. Discussion

The biceps brachii and the quadriceps femoris of the old rats were severely affected by sarcopenia, as demonstrated by the remarkable muscle mass reduction and the drastic decrease

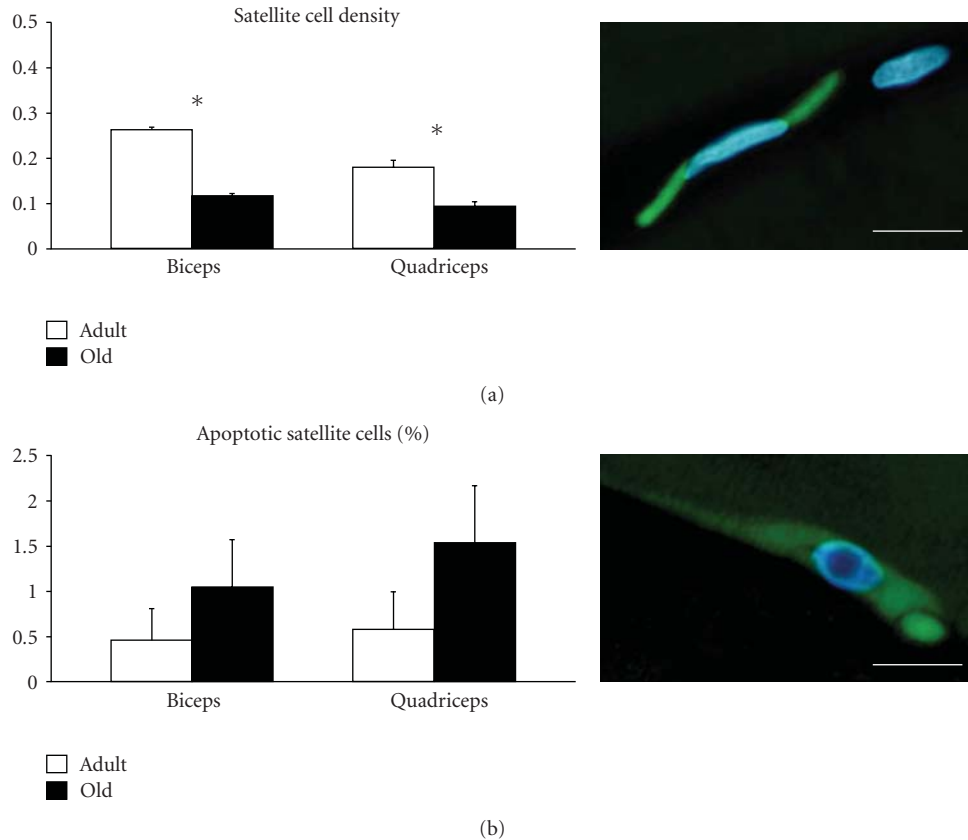


FIGURE 1: (a) Satellite cell density (number of satellite cells/1000 μm^2 of muscle) in the biceps and quadriceps muscles of adult and old rats (mean \pm SE). Asterisks show significantly different values ($P < 0.001$ for both muscles). The inset shows a satellite cell labeled with the anti-N-CAM antibody (green fluorescence); DNA was stained with Hoechst 33258. Bar: 10 μm . (b) Percentage of apoptotic satellite cells in the biceps and quadriceps muscles of adult and old rats (mean \pm SE). The values were not significantly different ($P = 0.136$ for biceps and $P = 0.157$ for quadriceps). The inset shows an apoptotic satellite cell (green fluorescence); DNA was stained with Hoechst 33258, note the margined chromatin. Bar: 10 μm .

in the size of type II myofiber [25]. The density of satellite cells was also significantly decreased in old rats compared to adult rats, consistent with the impaired regenerative capacity of muscles in sarcopenia. A smaller amount of satellite cells has already been reported in different aging muscles (e.g., [4–8]), although some authors did not observe these quantitative changes [11–13]. This discrepancy could be due to the differences in muscle, myofiber, and atrophy types that were investigated (for a recent review, see [34]); in particular, it has been reported that satellite cell content is specifically reduced in type II skeletal muscle fibers in the elderly [8], thus making muscles, which are mainly composed of this fiber type (like the biceps brachii and the quadriceps femoris), especially prone to satellite cell loss.

The scarce presence of morphologically recognizable apoptotic nuclei in satellite cells (at both light and electron microscopy) suggests that cell death via apoptosis might rarely occur in aging skeletal muscles. However, it should be also considered that our data have been collected in old animals where the sarcopenic process had already come to an advanced stage; this implies that a substantial role of apoptosis in earlier phases cannot be excluded. In any case,

in both muscles of old rats the percentage of apoptotic satellite cell nuclei was increased (though not significantly); whereas apoptotic nuclei were rare in myofibers, without differences between adult and old animals [25, 35]; these findings support the hypothesis that the apoptotic signals in old muscles may mostly originate from satellite cells [36].

The satellite cells bordering the myofibers of old muscles are morphologically similar to those found in adult muscles; in particular, the structural features of their nuclei are typical of quiescent cells. They contain abundant clumps of condensed chromatin, few PF and PG [22], compact nucleoli with abundant granular components, and scarce dense fibrillar components [37], which are all markers of low nuclear activity. Accordingly, the quantitative evaluation of the fine structural features of satellite cell nuclei gave similar values in adult and old rats; however, the in situ analysis of pre-mRNA processing factors revealed significant differences in the amount and intranuclear distribution of snRNPs and CstF. In detail, the snRNPs (involved in the cotranscriptional splicing of pre-mRNA [38]) were found to increase in satellite cell nuclei of old muscles; however, analysis of their intranuclear distribution reveals that snRNPs accumulate in

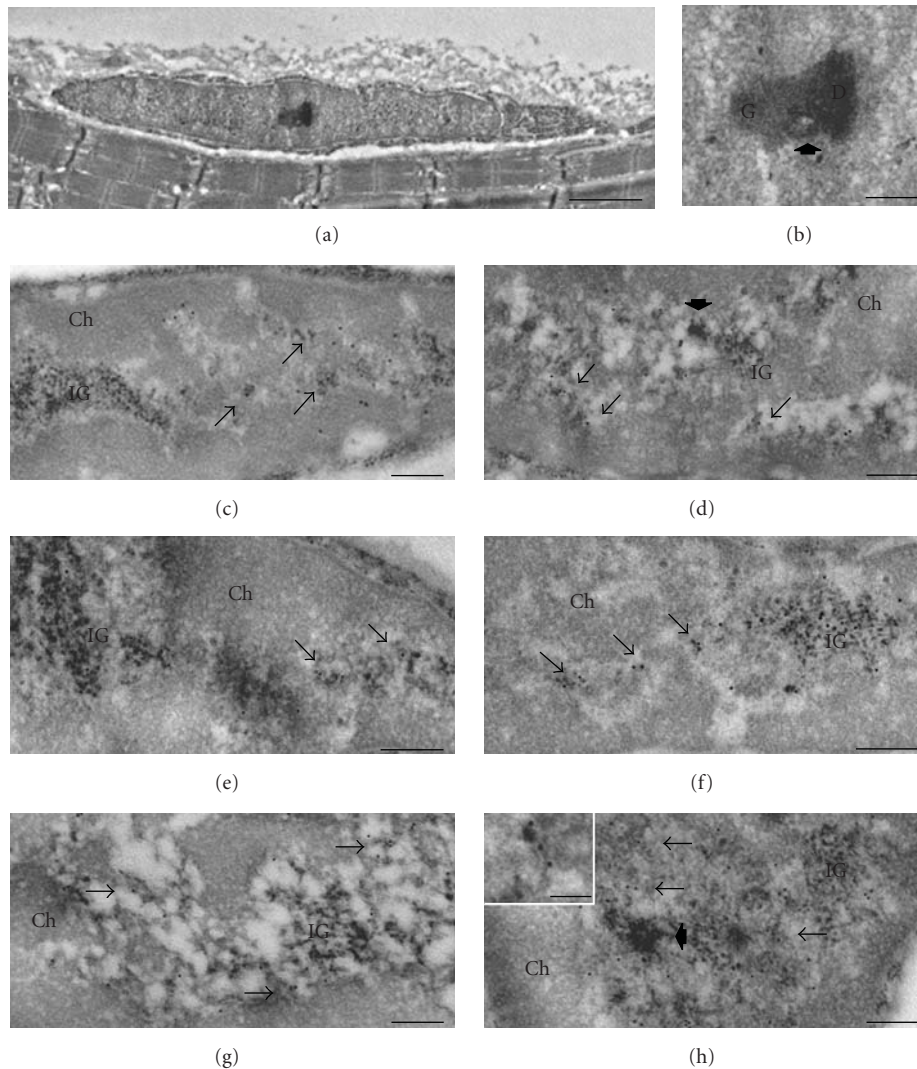


FIGURE 2: Transmission electron micrographs. (a) Satellite cell bordering a myofiber. (b) Detail showing the nucleolus mostly composed of granular component (G); whereas the dense fibrillar component (D) is less abundant, note the small fibrillar center (arrowhead). Satellite cell nuclei from adult (c, e and g) and old (d, f and h) rats. (c and d) Quadriceps muscles, anti-polymerase II (12 nm), and anti-DNA/RNA hybrid (18 nm) antibodies: both antibody probes specifically label perichromatin fibrils (arrows). Note the clustered perichromatin fibrils in (d) (arrowhead). The interchromatin granules (IG) are unlabeled. (e, f) Biceps muscles, anti-snRNP antibody: perichromatin fibrils (arrows) and interchromatin granules (IG) are labeled. (g, h) Quadriceps muscles, anti-CstF antibody: gold grains specifically label perichromatin fibrils (arrows) and RNP tails rising from perichromatin granules (inset). Note the cluster of perichromatin fibrils in (h) (arrowhead). Interchromatin granules (IGs) are unlabeled. Ch: condensed chromatin. Bars: (a) 1 μ m; (b–h) 250 nm; inset 100 nm.

the IG, known to represent the site of storage, transit and recycling of many nuclear factors [24, 39], but not on PF, which represent the in situ form of nascent transcripts, as well as of their splicing and 3' end processing (reviews in [22, 23]). Therefore, the increase in snRNPs is not associated with an increase in the transcriptional rate, according to the results obtained for polymerase II and the DNA/RNA hybrid molecules. A similar accumulation of nuclear factors in IG has been previously described in hepatocytes and neurons of old rodents [19–21], suggesting that the RNA pathways impairment may represent a common event during aging, independently on the cell type. The cleavage factor CstF also increases in satellite cell nuclei of old muscles in

comparison to the adult ones; however, this factor was always and exclusively located on PF. A similar accumulation of CstF has been previously observed in myonuclei of old muscles [25] as well as in aging hepatocyte nuclei [21]. Consistent with the data on snRNPs, the accumulation of CstF suggests that the processing and/or the intranuclear transport of transcripts are impaired. The presence of clustered PF as well as the increase in PG density observed in satellite cell nuclei of old muscles (although below the level of statistical significance) supports the hypothesis of altered pre-mRNA cotranscriptional activities and reduced cytoplasmic export. In fact, PF (which represent sensitive markers for the pre-mRNA processing impairment [23]) have been already

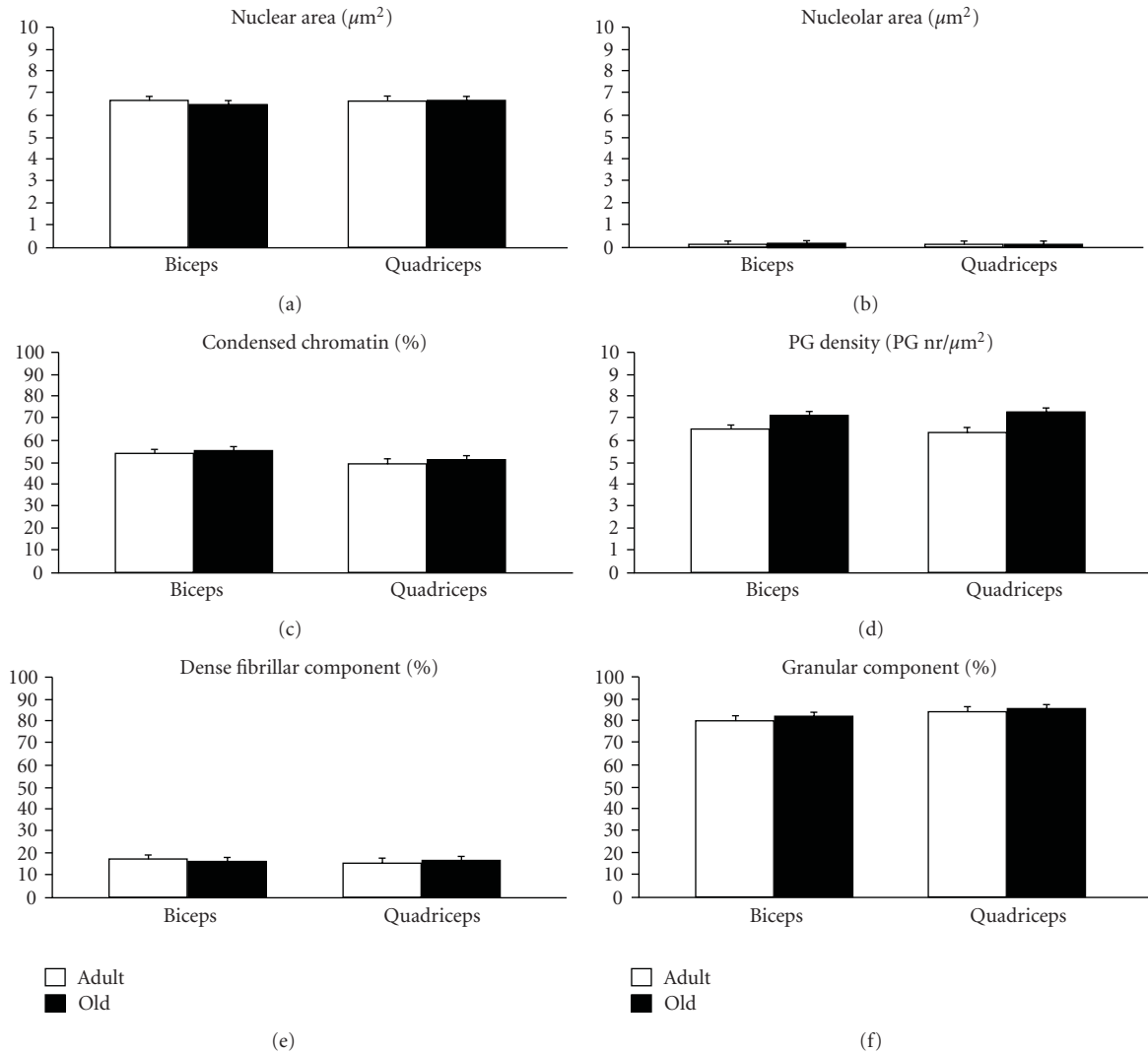


FIGURE 3: Morphometrical parameters measured on electron micrographs of satellite cell nuclei from the biceps and quadriceps muscles of adult and old rats (mean \pm SE). No significant difference was found between the two ages.

observed to accumulate in aging hepatocytes [17, 21]; moreover, PG (which represent storage and/or transport sites for spliced (pre-)mRNA [22]) generally increase in number as a consequence of altered pre-mRNA processing as well as of impaired intranuclear or nucleus-to-cytoplasm transport of mRNAs (e.g., [40, 41]). Consistent with this hypothesis, a decrease in the nucleus-to-cytoplasm transport factors [42] has been reported during aging, when the degradation systems also undergo alterations [43] leading to the accumulation of cross-linked, insoluble, and often oxidized proteins, which may damage the intracellular transport mechanisms [44, 45]. Accordingly, several proteins have been found to accumulate in satellite cell nuclei of old skeletal muscles [46]. In this view, the intranuclear accumulation of some nuclear factors in aging cell nuclei could be also related to the reduced efficacy of their degradation machinery. It is worth noting that the abnormal accumulation of reactive oxygen species in skeletal myofibers and satellite cells [47, 48] as well

as dysfunctions in the proteolytic and autophagic pathways [49, 50] is thought to be involved in sarcopenia.

Interestingly, when the results obtained for satellite cells are compared to those recently reported for myonuclei of the same muscles [25], it appears that satellite cell nuclei are less affected by aging: myonuclei show alterations in their fine structural and molecular features indicating that the entire mRNA production chain, from the synthesis to the cytoplasmic export, becomes less efficient; whereas in satellite cell nuclei the pre-mRNA processing/transport only is affected. This could be due to the relatively low nuclear activity of satellite cells, compared to myonuclei, which could in turn results in the slowing down of the progressive age-related deterioration of the whole cell function, including the RNA production [43]. The changes in the mRNA production machinery revealed in this study, however, suggest that satellite cell nuclei of aged individuals might be less responsive to the activating stimuli that those in adults,

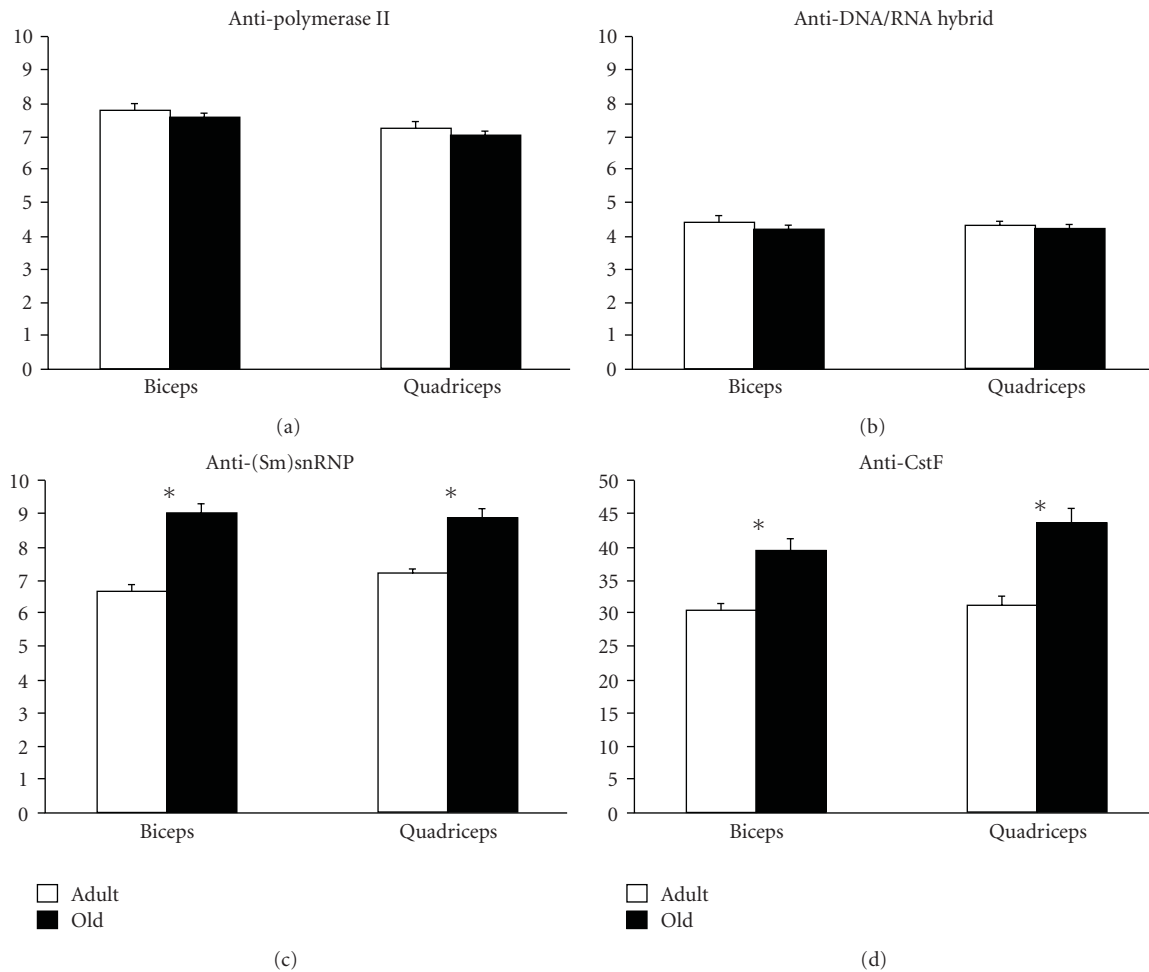


FIGURE 4: Quantitative immunoelectron microscopy of satellite cell nuclei of biceps and quadriceps muscles from adult and old rats; labeling density (gold grains/ μm^2) of some RNA processing factors in the interchromatin space (mean \pm SE). Asterisks show significantly different values.

thus compromising the regenerative capacity of old skeletal muscles.

5. Conclusions

There is growing evidence in the literature that aging affects cell nuclear function by impairing the transcriptional/cotranscriptional mechanisms in a wide variety of cell types in different organs, including muscles; this leads to a number of metabolic consequences, which finally result in the impairment of the specific physiological role(s) of each cell type. Recently, it has been demonstrated that defects in the RNA pathways are paralleled by altered intranuclear distribution of pre-mRNAs processing factors in some diseases characterized by muscle atrophy/dystrophy [51–53]. It is likely that the age-related nuclear dysfunctions of satellite cells could hamper their capability to become activated and to proliferate in response to muscle damage.

Thus nuclear dysfunction of both muscle fibers and satellite cells seems to play a pivotal role in the sarcopenia of aged individuals, and this should be taken into account

in the perspective to prevent and treat this ever-increasing health-risk factor.

Acknowledgment

F. Perdoni is a Ph.D. student in receipt of a fellowship from the Dottorato di Ricerca in Biologia Cellulare (University of Pavia).

References

- [1] T. Lang, T. Streeper, P. Cawthon, K. Baldwin, D. R. Taaffe, and T. B. Harris, "Sarcopenia: etiology, clinical consequences, intervention, and assessment," *Osteoporosis International*, pp. 1–17, 2009.
- [2] J. G. Ryall, J. D. Schertzer, and G. S. Lynch, "Cellular and molecular mechanisms underlying age-related skeletal muscle wasting and weakness," *Biogerontology*, vol. 9, no. 4, pp. 213–228, 2008.
- [3] L. V. Thompson, "Age-related muscle dysfunction," *Experimental Gerontology*, vol. 44, no. 1-2, pp. 106–111, 2009.

- [4] M. C. Gibson and E. Schultz, "Age-related differences in absolute numbers of skeletal muscle satellite cells," *Muscle & Nerve*, vol. 6, no. 8, pp. 574–580, 1983.
- [5] V. Renault, E. Rolland, L. E. Thornell, V. Mouly, and G. Butler-Browne, "Distribution of satellite cells in the human vastus lateralis muscle during aging," *Experimental Gerontology*, vol. 37, no. 12, pp. 1513–1514, 2002.
- [6] F. Kadi, N. Charifi, C. Denis, and J. Lexell, "Satellite cells and myonuclei in young and elderly women and men," *Muscle & Nerve*, vol. 29, no. 1, pp. 120–127, 2004.
- [7] A. S. Brack, H. Bildsoe, and S. M. Hughes, "Evidence that satellite cell decrement contributes to preferential decline in nuclear number from large fibres during murine age-related muscle atrophy," *Journal of Cell Science*, vol. 118, no. 20, pp. 4813–4821, 2005.
- [8] L. B. Verdijk, R. Koopman, G. Schaart, K. Meijer, H. H. C. M. Savelberg, and L. J. C. van Loon, "Satellite cell content is specifically reduced in type II skeletal muscle fibers in the elderly," *American Journal of Physiology*, vol. 292, no. 1, pp. E151–E157, 2007.
- [9] S. S. Jejurikar, E. A. Henkelman, P. S. Cederna, C. L. Marcelo, M. G. Urbanchek, and W. M. Kuzon Jr., "Aging increases the susceptibility of skeletal muscle derived satellite cells to apoptosis," *Experimental Gerontology*, vol. 41, no. 9, pp. 828–836, 2006.
- [10] S. E. Alway and P. M. Siu, "Nuclear apoptosis contributes to sarcopenia," *Exercise and Sport Sciences Reviews*, vol. 36, no. 2, pp. 51–57, 2008.
- [11] S. M. Roth, G. F. Martel, F. M. Ivey, et al., "Skeletal muscle satellite cell populations in healthy young and older men and women," *Anatomical Record*, vol. 260, no. 4, pp. 351–358, 2000.
- [12] R. Schafer, M. Zweyer, U. Knauf, R. R. Mundegar, and A. Wernig, "The ontogeny of soleus muscles in mdx and wild type mice," *Neuromuscular Disorders*, vol. 15, no. 1, pp. 57–64, 2005.
- [13] N. E. Brooks, M. D. Schuenke, and R. S. Hikida, "No change in skeletal muscle satellite cells in young and aging rat soleus muscle," *The Journal of Physiological Sciences*, vol. 59, no. 6, pp. 465–471, 2009.
- [14] E. Schultz and B. H. Lipton, "Skeletal muscle satellite cells: changes in proliferation potential as a function of age," *Mechanisms of Ageing and Development*, vol. 20, no. 4, pp. 377–383, 1982.
- [15] S. Machida and M. Narusawa, "The roles of satellite cells and hematopoietic stem cells in impaired regeneration of skeletal muscle in old rats," *Annals of the New York Academy of Sciences*, vol. 1067, no. 1, pp. 349–353, 2006.
- [16] E. Meshorer and H. Soreq, "Pre-mRNA splicing modulations in senescence," *Ageing Cell*, vol. 1, no. 1, pp. 10–16, 2002.
- [17] M. Malatesta, C. Bertoni-Freddari, P. Fattoretti, C. Caporali, S. Fakan, and G. Gazzanelli, "Altered RNA structural constituents in aging and vitamin E deficiency," *Mechanisms of Ageing and Development*, vol. 124, no. 2, pp. 175–181, 2003.
- [18] M. Malatesta, C. Bertoni-Freddari, P. Fattoretti, B. Baldelli, S. Fakan, and G. Gazzanelli, "Aging and vitamin E deficiency are responsible for altered RNA pathways," *Annals of the New York Academy of Sciences*, vol. 1019, pp. 379–382, 2004.
- [19] M. Malatesta, B. Baldelli, S. Battistelli, P. Fattoretti, and C. Bertoni-Freddari, "Aging affects the distribution of the circadian CLOCK protein in rat hepatocytes," *Microscopy Research and Technique*, vol. 68, no. 1, pp. 45–50, 2005.
- [20] M. Malatesta, P. Fattoretti, B. Baldelli, S. Battistelli, M. Baliaetti, and C. Bertoni-Freddari, "Effects of ageing on the fine distribution of the circadian CLOCK protein in reticular formation neurons," *Histochemistry and Cell Biology*, vol. 127, no. 6, pp. 641–647, 2007.
- [21] M. Malatesta, M. Biggiogera, B. Cisterna, M. Baliaetti, C. Bertoni-Freddari, and P. Fattoretti, "Perichromatin fibrils accumulation in hepatocyte nuclei reveals alterations of pre-mRNA processing during ageing," *DNA and Cell Biology*, vol. 29, no. 2, pp. 49–57, 2010.
- [22] S. Fakan, "Ultrastructural cytochemical analyses of nuclear functional architecture," *European Journal of Histochemistry*, vol. 48, no. 1, pp. 5–14, 2004.
- [23] M. Biggiogera, B. Cisterna, A. Spedito, L. Vecchio, and M. Malatesta, "Perichromatin fibrils as early markers of transcriptional alterations," *Differentiation*, vol. 76, no. 1, pp. 57–65, 2008.
- [24] D. Bogolyubov, I. Stepanova, and V. Parfenov, "Universal nuclear domains of somatic and germ cells: some lessons from oocyte interchromatin granule cluster and Cajal body structure and molecular composition," *BioEssays*, vol. 31, no. 4, pp. 400–409, 2009.
- [25] M. Malatesta, F. Perdoni, S. Muller, C. Zancanaro, and C. Pellicciari, "Nuclei of aged myofibres undergo structural and functional changes suggesting impairment in RNA processing," *European Journal of Histochemistry*, vol. 53, no. 2, pp. 97–106, 2009.
- [26] L. Larsson, B. Sjodin, and J. Karlsson, "Histochemical and biochemical changes in human skeletal muscle with age in sedentary males, age 22–65 yrs," *Acta Physiologica Scandinavica*, vol. 103, no. 1, pp. 31–39, 1978.
- [27] J. Lexell, "Human aging, muscle mass, and fiber type composition," *The Journals of Gerontology. Series A*, vol. 50, pp. 11–16, 1995.
- [28] C. D. Shorey, L. A. Manning, and A. V. Everitt, "Morphometrical analysis of skeletal muscle fibre ageing and the effect of hypophysectomy and food restriction in the rat," *Gerontology*, vol. 34, no. 3, pp. 97–109, 1988.
- [29] J. Covault, J. P. Merlie, C. Goridis, and J. R. Sanes, "Molecular forms of N-CAM and its RNA in developing and denervated skeletal muscle," *The Journal of Cell Biology*, vol. 102, no. 3, pp. 731–739, 1986.
- [30] P. S. Testillano, E. Gorab, and M. C. Risueno, "A new approach to map transcription sites at the ultrastructural level," *Journal of Histochemistry and Cytochemistry*, vol. 42, no. 1, pp. 1–10, 1994.
- [31] M. Malatesta, F. Perdoni, S. Battistelli, S. Muller, and C. Zancanaro, "The cell nuclei of skeletal muscle cells are transcriptionally active in hibernating edible dormice," *BMC Cell Biology*, vol. 10, article 19, 2009.
- [32] K. L. Veraldi, G. K. Arhin, K. Martincic, L.-H. Chung-Ganster, J. Wilusz, and C. Milcarek, "hnRNP F influences binding of a 64-kilodalton subunit of cleavage stimulation factor to mRNA precursors in mouse B cells," *Molecular and Cellular Biology*, vol. 21, no. 4, pp. 1228–1238, 2001.
- [33] W. Bernhard, "A new staining procedure for electron microscopical cytology," *Journal of Ultrastructure Research*, vol. 27, no. 3–4, pp. 250–265, 1969.
- [34] N. E. Brooks, M. D. Schuenke, and R. S. Hikida, "Ageing influences myonuclear domain size differently in fast and slow skeletal muscle of rats," *Acta Physiologica*, vol. 197, no. 1, pp. 55–63, 2009.

- [35] C. Zancanaro, R. Mariotti, F. Perdoni, E. Nicolato, and M. Malatesta, "Physical training is associated with changes in nuclear magnetic resonance and morphometrical parameters of the skeletal muscle in senescent mice," *European Journal of Histochemistry*, vol. 51, no. 4, pp. 305–309, 2007.
- [36] K. Gundersen and J. C. Bruusgaard, "Nuclear domains during muscle atrophy: nuclei lost or paradigm lost?" *Journal of Physiology*, vol. 586, no. 11, pp. 2675–2681, 2008.
- [37] H. G. Schwarzacher and F. Wachtler, "The nucleolus," *Anatomy and Embryology*, vol. 188, no. 6, pp. 515–536, 1993.
- [38] R. Lührmann, B. Kastner, and M. Bach, "Structure of spliceosomal snRNPs and their role in pre-mRNA splicing," *Biochimica et Biophysica Acta*, vol. 1087, no. 3, pp. 265–292, 1990.
- [39] E. Puvion and F. Puvion-Dutilleul, "Ultrastructure of the nucleus in relation to transcription and splicing: roles of perichromatin fibrils and interchromatin granules," *Experimental Cell Research*, vol. 229, no. 2, pp. 217–225, 1996.
- [40] F. Puvion-Dutilleul and E. Puvion, "Relationship between chromatin and perichromatin granules in cadmium-treated isolated hepatocytes," *Journal of Ultrastructure Research*, vol. 74, no. 3, pp. 341–350, 1981.
- [41] C. Zancanaro, M. Malatesta, P. Vogel, F. Osculati, and S. Fakan, "Ultrastructural and morphometrical analyses of the brown adipocyte nucleus in a hibernating dormouse," *Biology of the Cell*, vol. 79, no. 1, pp. 55–61, 1993.
- [42] G. Pujol, H. Soderqvist, and A. Radu, "Age-associated reduction of nuclear protein import in human fibroblasts," *Biochemical and Biophysical Research Communications*, vol. 294, no. 2, pp. 354–358, 2002.
- [43] C. W. Jameson, "Towards a unified and interdisciplinary model of ageing," *Medical Hypotheses*, vol. 63, no. 1, pp. 83–86, 2004.
- [44] A. Hallen, "Accumulation of insoluble protein and aging," *Biogerontology*, vol. 3, no. 5, pp. 307–315, 2002.
- [45] J. H. Kim, H. E. Choy, K. H. Nam, and S. C. Park, "Transglutaminase-mediated crosslinking of specific core histone subunits and cellular senescence," *Annals of the New York Academy of Sciences*, vol. 928, pp. 65–70, 2001.
- [46] S. Machida and F. W. Booth, "Increased nuclear proteins in muscle satellite cells in aged animals as compared to young growing animals," *Experimental Gerontology*, vol. 39, no. 10, pp. 1521–1525, 2004.
- [47] S. Fulle, F. Protasi, G. Di Tano, et al., "The contribution of reactive oxygen species to sarcopenia and muscle ageing," *Experimental Gerontology*, vol. 39, no. 1, pp. 17–24, 2004.
- [48] S. Fulle, S. Di Donna, C. Puglielli, et al., "Age-dependent imbalance of the antioxidative system in human satellite cells," *Experimental Gerontology*, vol. 40, no. 3, pp. 189–197, 2005.
- [49] D. Attaix, L. Mosoni, D. Dardevet, L. Combaret, P. P. Mirand, and J. Grizard, "Altered responses in skeletal muscle protein turnover during aging in anabolic and catabolic periods," *The International Journal of Biochemistry & Cell Biology*, vol. 37, no. 10, pp. 1962–1973, 2005.
- [50] L. Combaret, D. Dardevet, D. Béchet, D. Taillandier, L. Mosoni, and D. Attaix, "Skeletal muscle proteolysis in aging," *Current Opinion in Clinical Nutrition and Metabolic Care*, vol. 12, no. 1, pp. 37–41, 2009.
- [51] R. Cardani, E. Mancinelli, G. Rotondo, V. Sansone, and G. Meola, "Muscleblind-like protein 1 nuclear sequestration is a molecular pathology marker of DM1 and DM2," *European Journal of Histochemistry*, vol. 50, no. 3, pp. 177–182, 2006.
- [52] T. M. Wheeler and C. A. Thornton, "Myotonic dystrophy: RNA-mediated muscle disease," *Current Opinion in Neurology*, vol. 20, no. 5, pp. 572–576, 2007.
- [53] F. Perdoni, M. Malatesta, R. Cardani, et al., "RNA/MBNL1-containing foci in myoblast nuclei from patients affected by myotonic dystrophy type 2: an immunocytochemical study," *European Journal of Histochemistry*, vol. 53, no. 3, pp. 151–158, 2009.

Review Article

Mechanism of Catch Force: Tethering of Thick and Thin Filaments by Twitchin

Thomas M. Butler and Marion J. Siegman

Department of Molecular Physiology and Biophysics, Jefferson Medical College, Thomas Jefferson University, Philadelphia, PA 19107, USA

Correspondence should be addressed to Marion J. Siegman, marion.siegman@jefferson.edu

Received 20 January 2010; Accepted 10 March 2010

Academic Editor: Henk L. M. Granzier

Copyright © 2010 T. M. Butler and M. J. Siegman. This is an open access article distributed under the Creative Commons Attribution License, which permits unrestricted use, distribution, and reproduction in any medium, provided the original work is properly cited.

Catch is a mechanical state occurring in some invertebrate smooth muscles characterized by high force maintenance and resistance to stretch during extremely slow relaxation. During catch, intracellular calcium is near basal concentration and myosin crossbridge cycling rate is extremely slow. Catch force is relaxed by a protein kinase A-mediated phosphorylation of sites near the N- and C- termini of the myosin-binding protein C (~526 kDa). Some catch force maintenance can also occur together with cycling myosin crossbridges at submaximal calcium concentrations, but not when the muscle is maximally activated. Additionally, the link responsible for catch can adjust during shortening of submaximally activated muscles and maintain catch force at the new shorter length. Twitchin binds to both thick and thin filaments, and the thin filament binding shown by both the N- and C-terminal portions of twitchin is decreased by phosphorylation of the sites that regulate catch. The data suggest that the twitchin molecule itself is the catch force-bearing tether between thick and thin filaments. We present a model for the regulation of catch in which the twitchin tether can be displaced from thin filaments by both (a) the phosphorylation of twitchin and (b) the attachment of high force myosin crossbridges.

1. Introduction

The hallmark of the contractile process in smooth muscle is its ability to maintain force with a very high economy, that is, a low expenditure of energy, through the slow cycling of force-bearing crossbridges. In certain invertebrate smooth muscles, such as adductors, force can be maintained for many hours. This force, familiar to those who have attempted to open the shells of oysters, scallops, clams, and mussels, as well as the contraction of the anterior byssus retractor muscle (ABRM) of the edible mussel *Mytilus edulis*, reflects an unusual contractile state called “catch.” Functionally, the catch state is an adaptation that allows the muscle to resist stretch; this is important in the scallop, for example, in controlling gape (openness of its shell) and for the mussel in holding its byssus threads, which anchor it to rocks and other substrates, tautly. The term “catch” was coined nearly one hundred years ago by von Uexküll to describe the state of prolonged tonic force maintenance on the

assumption that the muscle is “caught” in the shortened state by a ratchet mechanism [1]. In molluscan smooth muscle, calcium activates contraction by direct binding to myosin [2]. Upon cholinergic nerve stimulation of the intact ABRM, intracellular calcium rises rapidly and then decays to near-resting concentrations [3] (Figure 1(b)). It is at these low calcium concentrations that the catch state ensues, and (in the absence of stimulation) force declines very slowly, over a period of minutes, or even hours. Catch is characterized by an extremely slow relaxation of force and a very high resistance to extension in the face of a very low expenditure of energy [4, 5]. Stimulation of serotonergic nerves “releases” catch, that is, causes rapid relaxation, which is mediated by the resultant increase in cAMP and activation of protein kinase A [6, 7]. The simultaneous stimulation of excitatory and inhibitory nerves leads to a phasic contraction (Figure 1(a)), reflecting the overriding influence of some cAMP-dependent process, leading to decreased force production. The question of how cAMP

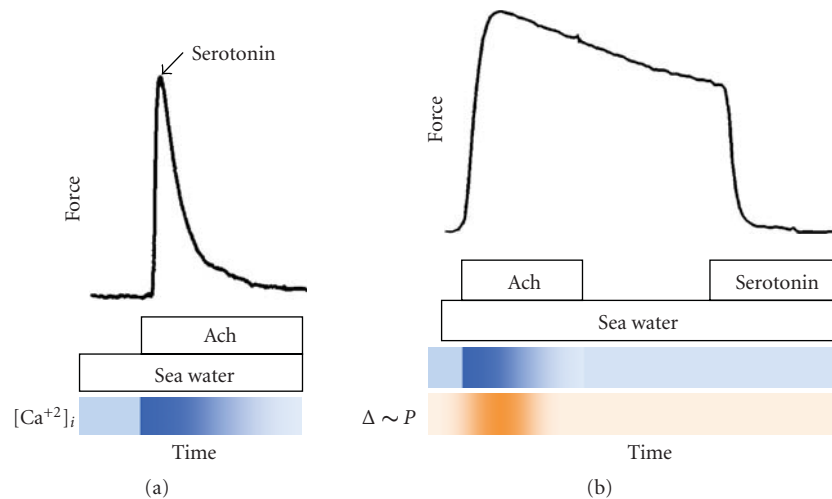


FIGURE 1: Contractile responses of intact anterior byssus retractor muscle of *Mytilus edulis*. Muscles were bathed in artificial seawater (ASW) and then treated as shown. (a) Phasic contraction. Muscle was activated with acetylcholine ($50 \mu\text{M}$) and at peak force serotonin ($10 \mu\text{M}$) was added. (b) Activation, catch, and release of catch in intact muscle. Muscle was activated with acetylcholine ($50 \mu\text{M}$) for 1.5 minutes which was washed out with ASW for 1.5 minutes. The condition of high-force maintenance is catch. Catch force was rapidly released upon addition of $10 \mu\text{M}$ serotonin. Lower panel (orange) shows the time course of high-energy phosphate usage during activation and catch [8]. Lower panels (blue) show the time course of the accompanying changes in intracellular Ca^{++} during phasic and catch contractions based on the work of Ishii et al. [3].

leads to abrupt relaxation was of interest to us because it might provide a handle on how highly economical force (latch, catch) was maintained and eventually released during relaxation in mammalian as well as invertebrate smooth muscles.

2. Theories on the Mechanism of Catch

Two main theories have been put forward for the catch mechanism (reviewed by Ruegg [9]). The “linkage hypothesis”, proposed by Lowy et al. [10], suggests that the links between actin and myosin filaments (myosin crossbridges) cycle rapidly during the early, phasic portion of contraction, but are either locked in the attached state or detach very slowly during the catch phase. This stands in contrast to the “paramyosin hypothesis,” proposed earlier by Ruegg [11], which assumes the operation of two functionally distinct linkage systems for contraction and catch. In this model, myosin crossbridges link with actin, but catch linkages may involve paramyosin-paramyosin interactions among neighboring thick filaments.

Catch muscles of molluscs contain actin filaments that are generally similar to those in other invertebrate muscles as well as vertebrate muscles (see extensive review in [12]). However, the thick filaments are very large, with diameters of 40–90 nm and lengths up to $50 \mu\text{m}$ [10]. The thick filaments are comprised of paramyosin, which forms a large diameter core, and a monolayer of myosin which covers the surface [13]. Paramyosin serves as a scaffold for myosin; it is bipolar and myosin that attaches to it in a helical antipolar manner [14]. The paramyosin content of the filaments varies, being

largest in muscles generating high forces. Thick filaments in invertebrate muscles generating high forces also typically have the largest diameters and longest lengths [15]. Force produced by the intact ABRM is about $10\text{--}14 \text{ kg}\cdot\text{wt}/\text{cm}^2$, in contrast to vertebrate skeletal muscle, where the force is $\sim 2.3 \text{ kg}\cdot\text{wt}/\text{cm}^2$ [10, 16]. Thick filaments from catch muscles also contain the protein catchin (myorod), which is an alternative product of the myosin heavy chain gene that has a unique N-terminal sequence of 156 residues and the C-terminal 830 residues of the myosin heavy chain [17, 18]. The function of catchin is not known. In *in vitro* motility studies catchin was not essential for demonstration of the catch state [19]. Although there is some ultrastructural evidence for aggregation of thick filaments in catch [20], other studies showed the same filament distribution during phasic and catch contractions of ABRM and provided compelling evidence that filament aggregation may be a fixation artifact [21]. In more recent studies by Takahashi et al. [22] no thick filament aggregation was observed in the cross-section of the fibers quickly frozen in the relaxed, actively contracting and in the catch state. The thick filaments were occasionally interconnected with each other either directly or by distinct projections in all the three states studied, but to the greatest extent in the catch state, leading the authors to suggest that thick filament interconnections are responsible for the catch state. However, it is difficult to envision how links among thick filaments alone would maintain catch force. It is interesting that *in vitro* the actin-activated myosin ATPase activity of catch muscle can be inhibited by disorderly aggregated “amorphous” paramyosin [23], but not by the orderly aggregated paramyosin core of thick filaments [24]. Ruegg [25] speculated that such a phase change within

paramyosin filaments may be induced by phosphorylation of paramyosin by a cAMP-dependent protein kinase [26, 27]. This could influence the interaction of paramyosin-myosin and/or paramyosin-paramyosin, actomyosin ATPase and possibly crossbridge movement, and thereby enhance catch [13]. The precise role of paramyosin in the contractile process of intact muscle remains an enigma.

There is evidence from other early studies that address the issues of relative crossbridge cycling rates during phasic and catch contractions, and the basis of the high resistance to stretch during catch. Sinusoidal vibrations of appropriate frequency and amplitude have been found to reduce force production during phasic contractions of vertebrate vascular smooth muscle as well as ABRM, with complete recovery of active force after cessation of vibration. However, during catch in ABRM, force fails to recover following the vibration-induced inhibition. The vibrations presumably act by increasing the rate of detachment of crossbridges [28, 29] and, if so, this would suggest that once detached, the crossbridges in catch do not reattach, or when reattached, do not generate force. On the other hand, Kobayashi et al. [30] found that sinusoidal vibrations reduced force but not stiffness during catch and argued that catch force may not simply be maintained by “locked-on” actin-myosin cross-links, as originally proposed by Lowy and Millman [31]. Along these lines, in a rather limited study, a higher stiffness to tension ratio was observed during catch than in active contraction [32]. Taken together with the observation of an exceptionally high, serotonin-sensitive resistance to stretch during catch, it is conceivable that some additional filament interactions occur during catch. During catch, the muscle shows an extremely high resistance to stretch (up to 100 kg/cm²) but does not redevelop force following a quick release; upon return to the initial length, the prerelease force is restored [16, 31, 33]. Catch stiffness is similar to rigor of skeletal muscle, but unlike rigor, is not due to the depletion of ATP from the muscle and is reversible [5, 34]. This is in contrast to the phasic portion of the contraction, in which the muscle resists stretch and redevelops force following a quick release of 5%–10% of the muscle length [16, 31]. When catch is released, the resistance to stretch decreases, with no compromise of the phasic contractile response [35].

3. Catch and the Economy of Force Maintenance

Although initiated and controlled by neural activity, the cellular basis of phasic and tonic behavior in invertebrate smooth muscles, like mammalian muscles, resides in the contractile machinery itself. An important property that these smooth muscles share is the ability to regulate the energy cost of force production and force maintenance. The ability to maintain high force with low-energy usage was first noted from measurements of heat production during the contraction of the pharynx muscle of the edible snail (*Helix pomatia*) by Bozler in 1930 [36]. Later measurements of oxygen consumption during contraction of the ABRM of *Mytilus edulis* showed that the energy usage for maintaining a given force during catch is about one-tenth of that required

during the preceding period of contraction [4, 5]. Due to their ability to maintain force with little energy usage (actomyosin ATPase activity), vertebrate and invertebrate smooth muscles are considered to be very “economical”. The marked change in economy was traced to an ability to regulate the rate at which crossbridges cycle during the course of a contraction, such that crossbridge cycling rate was high during force development and very slow during force maintenance [16, 37–39]. Early evidence of a slow-cycling rate and a catch-like state during force maintenance (based on the absence of force recovery following a quick release) in rabbit main pulmonary artery was reported in a discussion of catch by the Somlyos [40]. The condition of highly economical force maintenance in invertebrate smooth muscle later served as the model for what is known as the “latch” state of mammalian smooth muscle [39], primarily because of similarities in mechanical behavior (slow velocity of shortening) of the two muscle groups. At that time there was no information on the regulation of catch.

4. Studies on Permeabilized Muscles

Phasic and catch contractions have been studied in muscles from ABRM that have been permeabilized by treatment with detergents or by glycerol extraction. Such preparations provide the investigator the advantages of control of the milieu of a structured contractile system and, as such, a model system that is useful for the study of the regulation of catch. The addition of calcium (10 μ M) fully activates contraction by binding to myosin [41], and its removal establishes the catch state [42]. Catch can be released by the addition of cyclic AMP or by addition of the catalytic subunit of the cyclic AMP-dependent kinase [32, 43–46], which has no effect on force development. Guth and colleagues [47] measured the ATPase activity of permeabilized ABRM of *Mytilus edulis* and found that following a calcium-induced contraction lowering the calcium concentration rapidly reduced the ATPase activity to resting levels at a time when catch force had declined by only 30%–50% of maximum. Treatment with cAMP released catch force with no effect on ATPase activity. In a parallel experiment on the guinea pig taenia coli, the changes in force and corresponding ATPase activity during the application and subsequent removal of calcium were qualitatively similar to those of the ABRM, including a period of slow relaxation, during which Pi rather than cAMP was used to release the latch state and accelerate relaxation (similar responses, although probably based on very different mechanisms). The taenia coli, like the ABRM, shows no recovery of force following a quick release in length during the period of slow relaxation [48]. Thus, the permeabilized muscles faithfully follow the behavior of intact catch and mammalian smooth muscles, and the two muscle groups are strikingly similar in their contractile behavior.

The role of cAMP with the activation of the cAMP-dependent kinase in the release of catch is certain [32, 43, 46, 49]. Paramyosin, myosin rod, and myosin light chains have been shown to be substrates for phosphorylation. Watabe et al. [50] noted that in myofibrils isolated from the

white adductor (catch) muscle of *Mercenaria*, thiophosphorylation of paramyosin, through the action of an endogenous kinase resulted in an inhibition of ATPase activity. One of the regulatory light chains of myosin of scallop adductor muscle has been shown to be phosphorylated by a calcium- and calmodulin-independent cAMP-dependent protein kinase [51, 52]. The kinase also phosphorylated myosin heavy chains and paramyosin [53]. Phosphorylatable serine residues close to the C-terminus on the rod portion of myosin have been identified, and this favors folding (6 S–10 S transition) of the myosin molecule [46, 54, 55].

Castellani and Cohen showed that phosphatase inhibition with NaF, or the use of a nonhydrolysable substrate such as ATP- γ -S prevents catch, but not the initial force development [46]. This suggests that calcium and phosphorylation of specific proteins (either kinases or contractile proteins) have separate roles in the regulation of contraction and catch, but these have not yet been defined. They also showed that prolonged treatment of the muscle with detergent during permeabilization leads to the loss of catch force maintenance which can be restored by the addition of calcineurin, a calcium-calmodulin-regulated type 2B phosphatase [56]. Further, trifluoroperazine, a calmodulin inhibitor, reversibly accelerates the loss of catch force. Taken together, the results point to a calcium-regulated phosphatase, possibly activated during the onset of contraction, which is essential for the maintenance of catch force [56]. These two studies provided the first link between the phosphorylation of some substrate to release catch, and the calcium-dependent dephosphorylation of that substrate during the transition to catch following activation. It is not known, however, whether more than one kinase operates and how this relates to the phosphatases that have been implicated, nor is there information on the dephosphorylation reactions. Traditional studies measuring ^{32}P incorporation into various proteins from γ - ^{32}P -ATP were not successful at identifying the proteins whose change in state of phosphorylation mediate entry into and/or exit from catch [57].

5. Phosphorylation of a High Molecular Weight Protein Regulates Catch

In order to identify the target(s) of A kinase-mediated phosphorylation, we set out to determine the proteins that undergo a change in phosphorylation on a time course that corresponds to the release of catch in permeabilized ABRM [58]. To do this, we took advantage of technology involving flash photolysis of caged compounds. Specifically, permeabilized muscles were put into catch in the presence of ATP and caged ^{33}P -ATP. cAMP was then added and the muscles were immediately subjected to a UV flash that caused photolysis of the caged ATP and a step increase in the ^{33}P content of ATP. The muscles were frozen at different times after the flash. Figure 2 shows that there was a large incorporation of ^{33}P into a high-molecular-weight protein (about 600 kDa) during the time that the catch force underwent relaxation. Surprisingly, this could also be shown in muscles that were not subjected to flash photolysis and

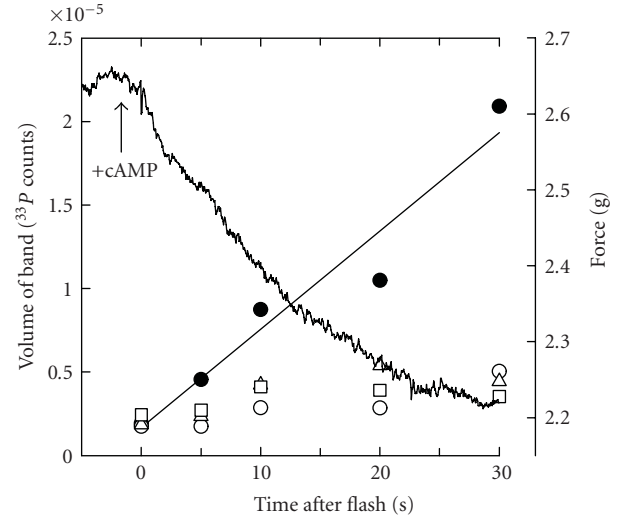


FIGURE 2: Time course of release of catch force and corresponding incorporation of ^{33}P into proteins of permeabilized ABRM following cAMP treatment and photolysis of caged ^{33}P -ATP. Muscles were frozen at times indicated after photolysis. Labeled proteins are shown by the following symbols: \square , ~ 45 kDa; \circ , ~ 100 kDa; Δ , ~ 200 kDa; \bullet , high-molecular-weight protein. $T = 20$ C. Reproduced from [58] with permission.

were, rather, simply incubated in ^{32}P -ATP before addition of cAMP. A phosphorimage of a gel-containing proteins from muscles incubated in ^{32}P -ATP and frozen under different mechanical conditions is shown in Figure 3. The only protein showing an increased degree of phosphorylation with the addition of cAMP was the high-molecular-weight protein. The only other obvious change in ^{32}P incorporation in the different conditions was an increase in phosphorylation in the myosin light chain region of the gel with an increase in calcium concentration (compare lanes A and B). Importantly, this did not increase further with cAMP treatment, and the amount of ^{32}P incorporated was only about 13% of that in the high molecular weight protein. We also found that (1) inhibition of the cAMP-dependent protein kinase, which prevented the cAMP-induced increase in phosphorylation of the protein, also inhibited the cAMP-dependent release of catch; (2) cAMP dependent thiophosphorylation of the protein prevents catch; (3) in intact muscle the phosphorylation of the protein is low when the muscle is activated by acetylcholine, but increases significantly when catch is released with serotonin treatment.

6. The High Molecular Weight Protein Whose Phosphorylation State Regulates Catch is Twitchin

The molecular weight of the catch-regulating protein was similar to that of the minititin, twitchin. Twitchin is a member of a family of giant protein kinases, which also includes projectin and titin, having molecular masses from 700 to >3000 kDa. Twitchin is a protein that is encoded by the gene *unc-22* in *C. elegans*, and gained its name

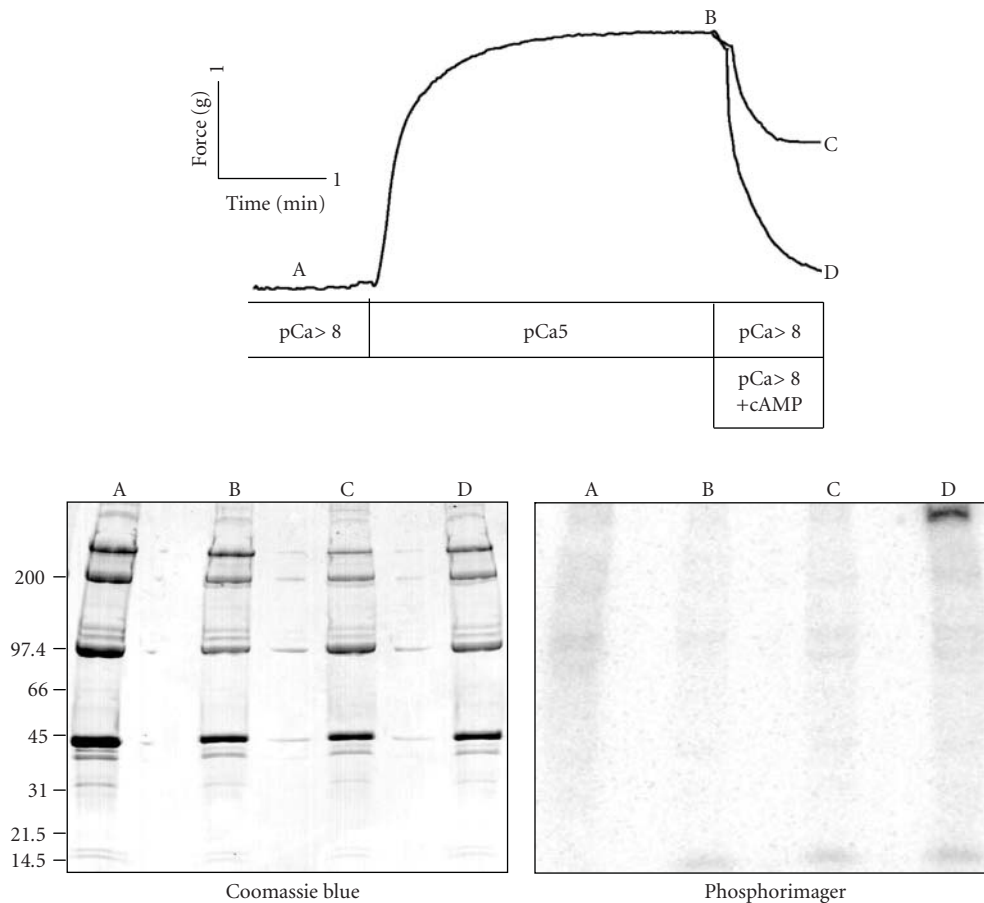


FIGURE 3: Protein phosphorylation under different mechanical conditions in permeabilized ABRM. Muscles were incubated with ^{32}P -ATP starting in an initial relaxing solution and then either frozen (a) after 4 min in relaxing solution, (b) after 1 minute in relaxing solution and 3 minutes in activation solution (pCa5), (c) treatment as in (b), plus 1 minute in relaxing solution (catch), and (d) after treatment as in (b), plus 1 min in relaxing solution containing cAMP (release of catch). Shown are a Coomassie Blue-stained 4%–15% acrylamide gradient gel and corresponding phosphorimager autoradiogram. $T = 20$ C. Reproduced from [58] with permission.

because animals lacking *unc-22* showed a nearly constant twitching rather than prolonged undulating contractions of the body muscles [59]. Numerous immunolocalization studies have shown that twitchin is associated with the A band of nematode striated muscle [60], molluscan fast striated muscle, and thick filaments of molluscan smooth (noncatch) and catch muscles [61]. Along these lines, in the noncatch accessory radula closer muscle of *Aplysia*, a correlation between the cAMP-dependent phosphorylation of twitchin and the rate of relaxation was found [62].

The above findings prompted the use of a procedure designed for twitchin to isolate and purify the high-molecular-weight protein from *Mytilus* ABRM. The mobility in gels of the protein isolated in this manner was identical to the catch-regulating protein, and it was phosphorylated by the catalytic subunit of protein kinase A. Primers designed from an N-terminal amino acid sequence of a peptide from the catch-regulating protein and from the sequence of *Aplysia* twitchin were used to obtain a derived amino acid sequence for a partial cDNA of the isolated protein. The *Mytilus* protein was 58% and 77% identical to *C. elegans* and

Aplysia twitchin, respectively. An affinity-purified polyclonal antibody made against a peptide in the derived sequence bound to the catch-relaxing protein. Based on these findings, we concluded that the catch-relaxing protein is the *Mytilus* isoform of the minititin twitchin [63].

7. Primary Structure and Domain Organization of *Mytilus* Twitchin

The amino acid sequence derived from the full length cDNA for twitchin from *Mytilus* ABRM showed a molecule with a molecular weight of about 526 kDa containing 24 Ig and 15 fibronectin motifs in addition to a single kinase domain [64]. The motif arrangement is shown in Figure 4. A comparison of minititins from *Drosophila*, crayfish, *C. elegans*, mosquito and *Mytilus* shows that all of the known minititins have an N-terminal region consisting of 9 to 12 Ig-like domains. This is followed by a core region containing a variable number of (Fn)₂Ig repeats. There are 14 such repeats in *Drosophila* projectin and only two in *Mytilus* twitchin. The

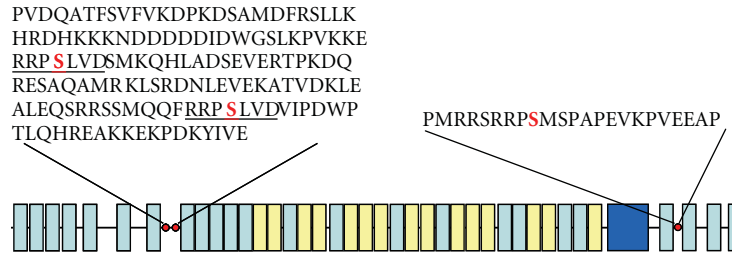


FIGURE 4: The domain structure of *Mytilus* twitchin. Green, immunoglobulin-like motifs; yellow, fibronectin type III motifs; purple, kinase domain; and red circles, phosphorylation sites. The underlined sequences near the N-terminus share 7 identical amino acids and contain the DX and D1 phosphorylation sites (S). The D2 phosphorylation site (S) is near the N-terminus.

variable number of these structures appears to be the main determinant of the difference in size of the proteins varying from about 530,000 in *Mytilus* to 1,000,000 in *Drosophila*. It is not known for what function, if any, the length of the molecule is optimized. The exact number of (Fn)₂Ig domains does not appear to be critical, since in *C. elegans* up to 6 of these domains can be deleted without the animal taking on the twitching phenotype associated with loss of twitchin function [65, 66]. The next region of the molecule containing the domains (Fn)₃Ig(Fn)₂Ig(Fn)₃(Ig)₂(Fn)₂(Ig)₂FnKinase is identical in all of the munititins. Lastly, there are either 4 or 5 Ig domains at the C-terminus of the molecule following the kinase domain.

There is considerable variability in the extent to which munititins contain PEVK regions so named for a high incidence of proline (P), glutamic acid (E), valine (V), and lysine (K) residues. *Mytilus* twitchin includes a 79-residue sequence between Ig domains 6 and 7 (from the N terminus) in which more than 60% of the residues are P, E, V, or K [64]. The short length of this segment may not be sufficient to contribute much elasticity to the protein. There is also a short PEVK sequence in mosquito projectin [66]. *Drosophila* projectin contains a PEVK region (between Ig domains 8 and 9) and there appears to be alternative splicing in this region resulting in a host of isoforms of projectin. The PEVK region varies from 100 to 624 amino acids in these different isoforms [67]. The similarity of this region to the PEVK region in titin has led to the expectation that this portion of projectin would, like titin, contribute to the passive elastic properties of the muscle. The same region of crayfish projectin contains a series of twelve 19-amino acid repeats, and each repeat contains a high proportion of glutamic acid, lysine, and valine. Although this region does not show much homology with the PEVK region from *Drosophila* projectin, it does contribute to the elastic properties of crayfish projectin [68]. Twitchin from *C. elegans* lacks a PEVK domain as such, but has short regions rich in proline, glutamic/aspartic acid, and serine in the inter Ig domains on each side of the third Ig domain from the N-terminus [67, 69].

Mytilus twitchin also contains a DFRXXL motif in the N-terminal portion of the molecule, as do all munititins. The presence of this motif is interesting because studies by Stull and collaborators suggest that it is this motif that is responsible for binding of smooth and nonmuscle myosin light chain kinase (MLCK) to actin [70–75]. The short form

of MLCK has its actin-binding site in the N-terminal 142 residues and included in this segment are three DFRXXL motifs that are necessary and sufficient for actin binding. Structural studies show that this N-terminal portion of the short MLCK binds to F-actin at a specific site that is different from, and thus should not interfere with, other actin-binding proteins such as myosin, tropomyosin, caldesmon, and calponin [75]. The presence of the DFRXXL motif in the N-terminal region of all munititins suggests that this portion of the molecules would show a tendency to bind to actin. All of the PEVK-like domains noted above for the munititins are in the inter-Ig domain just N-terminal to the domain containing the DFRXXL motif. Fragments of the PEVK domain of titin from both cardiac and skeletal muscle have been shown to interact with actin and to slow actin sliding over myosin in *in vitro* motility assays [76]. If the PEVK-like domains bind actin, then the close proximity of the PEVK-like domains and the DFRXXL motif might be additive in their effect on the actin-binding properties of the munititins.

8. Protein Kinase A Phosphorylation Sites in *Mytilus* Twitchin

When twitchin isolated from *Mytilus* is treated with the catalytic subunit of PKA, the stoichiometry of phosphorylation is about 3 mole phosphate per mole of twitchin. Two phosphorylated peptides have been isolated from tryptic digests of twitchin, and have been identified as D1 and D2. The D2 phosphorylated peptide is located in the linker region between the two Ig domains that are C-terminal to the kinase domain. The D1 sequence is located in the linker region between Ig domains 7 and 8 [64] in the N-terminal portion of the molecule. A third phosphorylated peptide was not successfully sequenced. It was noted, however, that there is a potential phosphorylation site that shares a seven-residue sequence with the D1 site and was located in the same inter-Ig domain as D1. This site was named DX [64]. We have since performed mass spectrometry experiments that show the DX site is phosphorylated when cAMP is added to permeabilized muscles. The mass of the DX peptide in Lys C digests of twitchin is 1317.5 + H. In digests of twitchin from muscles in catch, a peptide with this mass was identified, but it was not present in digests of twitchin from muscles

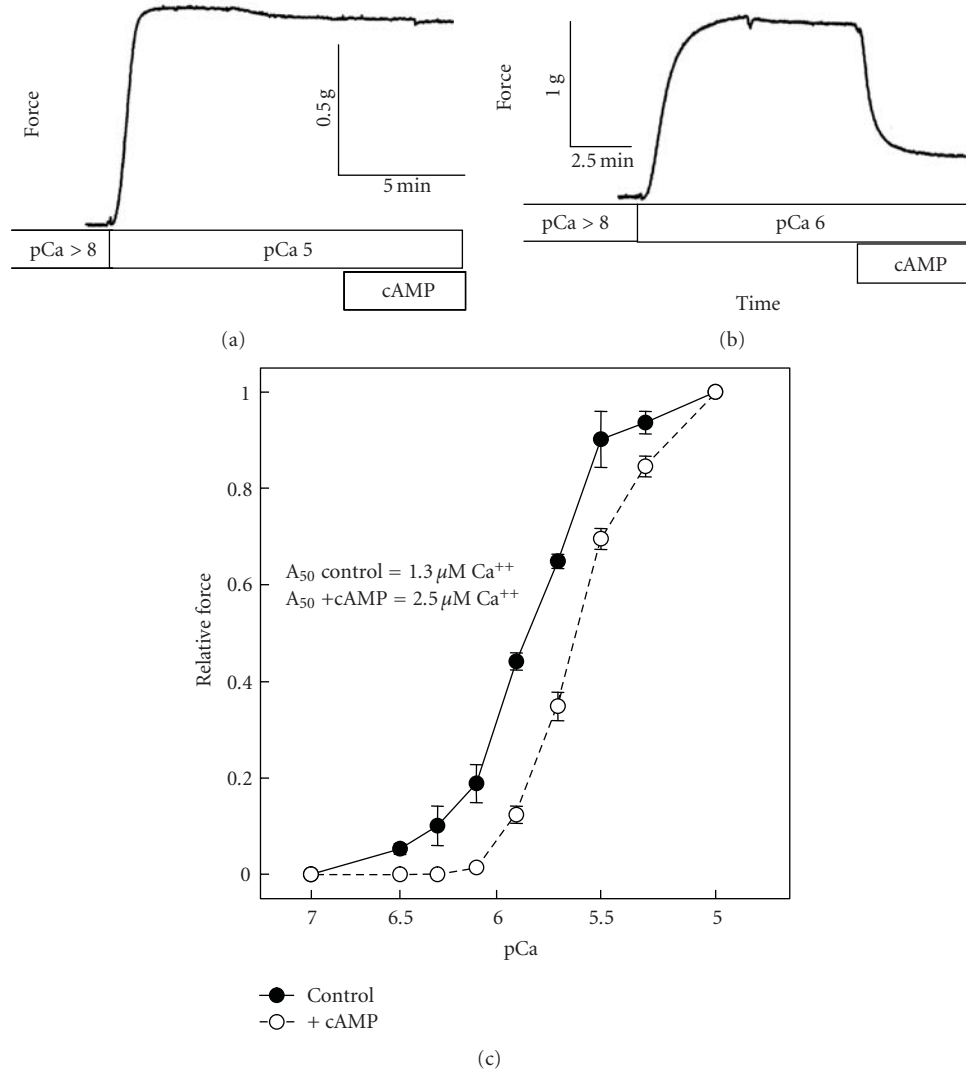


FIGURE 5: The effect of cAMP on the mechanical responses of permeabilized ABRM following activation at high (pCa 5) (a) and intermediate (pCa 6) (b) concentrations of calcium, and the effect of cAMP on the relationship between isometric force and $[\text{Ca}^{2+}]$ in permeabilized ABRM (c). In (a) and (b), permeabilized muscles were incubated in relaxing solution, followed by activation with calcium for 10 minutes prior to addition of cAMP ($100 \mu\text{M}$) for 6 minutes. In (c), muscles were treated in a cumulative manner with increasing concentrations of calcium. After a series of steady-state force measurements at a number of incrementing $[\text{Ca}^{2+}]$ were completed, a transition was made to calcium solutions containing cAMP. Force responses were normalized to the maximum force at pCa 5 + cAMP. $T = 20 \text{ C}$. Reproduced from [63] with permission.

that were subjected to cAMP treatment. Treatment of these digests with Lambda phosphatase caused a reappearance of the 1317.5 + H peptide. These experiments suggest that in addition to phosphorylating the D1 and D2 sites, the DX site in twitchin is also phosphorylated by PKA when cAMP is added to permeabilized muscles and catch force is relaxed.

9. Relationships Among Twitchin D1 and D2 Site Phosphorylation and Relaxation of Catch Force

Phosphorylation-sensitive antibodies were used to determine how the phosphorylation state of the D1 and D2 sites

of twitchin varied under different mechanical conditions [64]. In intact muscles in catch the D2 site was less than 10% phosphorylated while the D1 site was about 40% phosphorylated. Addition of serotonin to the muscle relaxed catch force and caused maximum phosphorylation of both sites. The increase in phosphorylation is reversed when the muscle is subsequently put into the catch state. These results are consistent with the idea that phosphorylation of both sites causes relaxation of catch force and that maintenance of catch force requires full dephosphorylation of the D2 site and dephosphorylation of the D1 site in at least half of the twitchin molecules. D1 site phosphorylations from 0 to 50% appear to have little effect on catch force whereas higher values are associated with relaxation of catch. On the other

hand, phosphorylation levels in the D2 site exceeding 15% were associated with relaxation. Interestingly, for both intact and permeabilized muscles, phosphorylation of D2 to more than 15% only occurred when D1 phosphorylation was 50% or greater. Therefore, relaxation of catch only occurs when both the D1 and D2 sites are phosphorylated, and the D1 site is more readily phosphorylated than the D2 site. The maintenance of catch force when up to 50% of twitchin molecules have the D1 site phosphorylated shows that phosphorylation of this site alone does not cause detachment of the catch link. On the other hand, full relaxation of catch force occurs only when the D1 site is fully phosphorylated. Phosphorylation of this site is therefore necessary, but not sufficient to detach the catch link.

Twitchin isoforms have been identified in muscles from *Mytilus galloprovincialis* [77]. All of the isoforms contain the kinase domain and the D2 phosphorylation site, but they show different sequences in the linker region containing the DX and D1 phosphorylation sites resulting from alternative splicing. In some isoforms a 63 amino acid sequence containing the D1 phosphorylation site is deleted. These isoforms are present only in muscles that do not exhibit catch. In other words, the D1 phosphorylation site is always found in catch muscle twitchin. These data led the authors to conclude that the D1 site of twitchin is “essential to the mechanism of catch” [77].

10. Catch Force is Present in Submaximally Activated Muscles

Phosphorylation of twitchin has no effect on force at calcium concentrations required for maximum force production, but decreases force at calcium concentrations that yield submaximum force production [63]. This observation can be summarized as a twitchin-phosphorylation-dependent shift in the force-calcium relationship as shown in Figure 5. At intermediate calcium concentrations, phosphorylation of twitchin causes a decrease in force with little or no associated change in ATPase activity [8]. The “extra” force that is maintained when twitchin is unphosphorylated does not require an “extra” ATPase activity which makes it very unlikely that the extra force is due to normal ATP-driven myosin crossbridge cycling. Rather, the extra force has a very high economy (i.e., very low energy demand) as does catch force maintenance. This suggests that the mechanism that gives rise to catch force maintenance can operate to some extent together with that of cycling myosin crossbridges.

11. The Structure Responsible for Catch Force Can Adjust During Shortening if the Muscle Is Activated

One of the hallmarks of the catch state is the absence of force redevelopment following a quick release in length. This has been interpreted to mean that the catch force—maintaining structures do not cycle and redevelop force when muscle length is decreased. The observation that catch force exists during activation at intermediate calcium concentrations

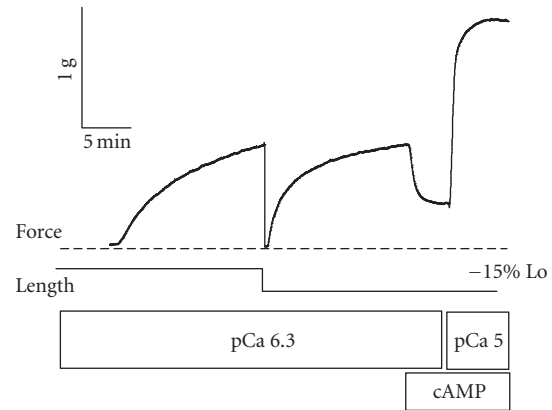


FIGURE 6: Effect of muscle shortening and force redevelopment on cAMP-dependent force production at pCa 6.3 in permeabilized ABRM. After activation in pCa 6.3 for ~15 minutes, the muscle was subjected to a quick release of 15% Lo. Force quickly fell to zero and then redeveloped. 100 μ M cAMP was then added to the bathing medium, and force decreased. The muscle was then maximally activated in pCa5 in the presence of cAMP. $T = 20$ C. Reproduced from [8] with permission.

raised the question as to whether the structures responsible for catch force can cycle when the muscle is activated. If the structures adjust during muscle shortening, then catch force could be redeveloped and subsequently maintained at a new shorter muscle length. This was tested in a muscle activated at submaximal calcium (pCa 6.3) and then subjected to various quick releases in the range 10%–30% Lo. The large releases that caused force to decrease to zero would be expected to cause a buckling or detachment of all of the force-maintaining structures. Force redeveloped following the release, and, as shown in Figure 6, addition of cAMP and phosphorylation of twitchin still resulted in a decrease in force [8]. This means that some of the redeveloped force was due to structures that are dependent on twitchin phosphorylation. That is, the catch force-maintaining structures present following activation can detach upon shortening and subsequently reattach to maintain newly developed force at the shorter muscle length. Even though the structures responsible for catch force do not require an energy input for force maintenance, they do appear to readjust (cycle) when an activated muscle is allowed to shorten. The fact that redevelopment of catch force following a quick release only occurs in activated muscles suggests that cycling myosin crossbridges may be required for catch force-maintaining structures to readjust and contribute to the redeveloped force.

12. In Activated Muscles, the Presence of Catch Does Not Affect the Kinetics of Crossbridge Cycling under Isometric Conditions, but Does Alter the Kinetics During Shortening

The rate of myosin crossbridge cycling was measured as the single turnover of myosin-bound ADP. The basic premise of

the method is that most myosin has ADP bound at any given time, and that the time course of release of the bound ADP and replacement with new ADP subsequent to ATP binding and splitting gives an accurate measure of kinetics of myosin crossbridge turnover. This method was used to test whether twitchin phosphorylation in activated muscles changed the *kinetics* of myosin cycling. Under isometric conditions, there is no effect of twitchin phosphorylation on the rate of myosin crossbridge turnover at a calcium concentration that gives submaximal force output, even though force output decreased as a result of the phosphorylation [78]. This supports the view that removal of catch links has no effect on myosin crossbridge turnover under isometric conditions at intermediate calcium concentrations.

In the 1920s, Fenn described experiments that showed that muscles that shortened and performed external work liberated a higher total energy than muscles kept under isometric conditions [79]. This observation means that the rates of the energy producing reactions in muscle change as a function of the mechanical conditions. Many years later, Huxley formulated a model of muscle contraction in which the rate constants for the attachment and/or detachment of myosin and actin depend on the amount of strain on the myosin crossbridge [80]. More recent experiments suggest that the rate constant for ADP release from actin-attached myosin is one of the main strain-dependent steps in the myosin crossbridge cycle [81]. High force conditions (associated with isometric conditions) would tend to minimize the movement of the myosin crossbridge and keep ADP release slow, whereas low-force conditions following a decrease in muscle length would lower the strain on the crossbridge and increase both the rate of ADP release as well as the overall rate of myosin crossbridge cycling.

The strain dependence of myosin crossbridge turnover in catch muscle was determined by comparing myosin-bound ADP turnover under isometric and shortening conditions [78]. When a muscle is maintaining catch force at very low (basal) calcium concentrations, no strain dependence following a quick release was detectable. On the other hand, at calcium concentrations that result in near-maximal activation (no catch component of force output), there is an approximately three-fold increase in the rate constant for myosin-bound ADP turnover when the crossbridge is unstrained by a quick release compared to isometric conditions. The use of similar methods showed about a five-fold increase in myosin-bound ADP turnover following a quick release in mammalian smooth muscle [82]. In addition, Khromov et al. [83], using different methods, found about a two-fold increase in the rate constant for ADP release from myosin with a decrease in strain in mammalian smooth muscle. So, the fully activated catch muscle shows a similar increase in myosin crossbridge turnover as do other smooth muscles.

Surprisingly, at intermediate calcium concentrations where the muscle is only partially activated, there was no significant increase in the rate of turnover of myosin following a quick release when twitchin was unphosphorylated. In contrast, when twitchin is phosphorylated and the catch component of force output is thereby removed, there is

an increase in myosin turnover associated with shortening. Clearly, the presence of the catch force-maintaining structure alters the response of myosin to a decrease in muscle length. It is possible that the catch link prevents the immediate motion of the myosin head following the quick release. This could occur if the link tightly connects thick and thin filaments and prevents or slows the relative motion of the filaments following release. A slowing in the relative motion of the filaments by such a linkage would delay much of the expected increased turnover of myosin-bound ADP following a quick release. Since the single turnover protocol only measures the kinetics of the first turnover of each myosin-bound ADP, the ADP turnover on myosin for the first crossbridges that cycle following a quick release would be similar to isometric conditions, whereas the crossbridges that cycle later could have a higher rate reflecting the progressive detachment of the catch link as the shortening progresses.

13. Is Catch Force Maintenance Due to the Unique Kinetics of Myosin Crossbridges or is it Due to the Presence of Some Other Protein Linking Thick and Thin Filaments When Myosin Crossbridges Detach?

Several studies have attempted to determine which of the two prevailing theories of catch, described above, was correct. The fact that catch force-maintaining structures appear able to slowly detach and reattach during and following muscle shortening (as does myosin) led us to initially favor the view that myosin-actin linkages are responsible for the maintenance of catch force [8, 84]. However, as discussed below, the preponderance of current evidence favors the idea that there is a link between thick and thin filaments other than the myosin crossbridge that mediates catch. Some of the unique mechanical aspects of catch that support this view are summarized in the following findings.

13.1. Catch Force Remains Following Detachment of Myosin Rigor Crossbridges by Addition of MgATP. The relationship between the catch link and myosin crossbridge detachment from actin was studied by determining how rigor force relaxes following addition of MgATP [84]. Addition of MgATP to permeabilized muscles in high-force rigor in the absence of calcium resulted in a rapid loss of a small component of force followed by a very slow rate of relaxation that is characteristic of catch (Figure 7). Subsequent addition of cAMP causes a relaxation of the remaining force. If twitchin is thiophosphorylated before the addition of ATP, no catch component remains. These results show that catch force persists following detachment of rigor myosin crossbridges as long as twitchin is unphosphorylated. A similar dependence of force relaxation from rigor on twitchin phosphorylation is seen with AMP-PNP and ATP γ S (nonhydrolysable analogs of ATP). This suggests that the catch force persistence is not due to crossbridges that detach and then go through cooperative reattachment to actin [85] since there would be no hydrolysis of nucleotide to ADP that necessary as

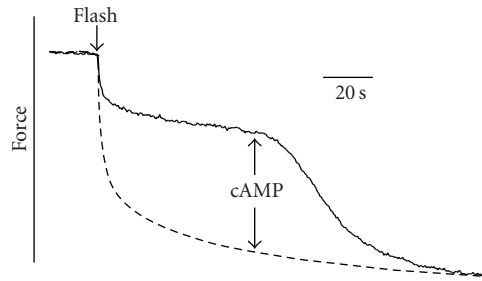


FIGURE 7: Force responses following release of ATP from caged ATP in permeabilized ABRM. Muscles were put into high-force rigor by activation in pCa5 and then transferred to a pCa5-rigor solution containing apyrase (0.2 mg/mL). Calcium was then lowered to pCa > 8. Caged ATP (4 mM) was added 4 min before the flash and the muscle was transferred to a solution containing 1 mM MgATP ~4 s following the flash. cAMP was added at the time shown. *Solid line*, twitchin not phosphorylated; *dashed lines*, twitchin thiophosphorylated. $T = 20$ C. Reproduced from [84] with permission.

a prelude to attachment. Under rigor conditions, where there is little if any ADP bound to myosin, the burst of ADP formation following addition of ATP (measured from ^3H -ADP formation following photolysis of caged ^3H -ATP) equals the myosin head concentration and is not dependent on the state of twitchin phosphorylation. This means that all of the myosin binds ATP and that catch force is not due to rigor crossbridges that persist following addition of ATP. It also argues against the possibility that there is a significant fraction of myosin having ADP bound in the rigor muscle that could possibly be responsible for continued force maintenance after addition of ATP. These results strongly suggest that if catch force is maintained by myosin crossbridges, then ATP binding to the rigor catch crossbridge does not lead to detachment of the catch crossbridge even though ATP is rapidly hydrolyzed. The experiments also show that if myosin crossbridges are responsible for catch force maintenance, then they have ADP bound. Of course, such experiments are also consistent with a mechanism in which catch force is maintained by an independent link between thick and thin filaments that is not mediated by the myosin crossbridge.

13.2. Relaxation of Catch Force by Phosphorylation of Twitchin Is Not Associated with a Measurable Turnover of Myosin-Bound ADP. If myosin crossbridges with ADP bound interact with actin to maintain catch force, then relaxation of catch force by twitchin phosphorylation should bring the crossbridge back to the resting state by completion of the myosin crossbridge cycle. This would involve the release of ADP followed by ATP binding, crossbridge detachment, and subsequent ATP splitting with ADP and Pi remaining bound to the myosin. The results of single turnover experiments showed that a major fraction of myosin does not turnover ADP during the detachment of catch force-maintaining links [78]. It is therefore unlikely that relaxation of catch involves the detachment of myosin from actin through

steps normally occurring during completion of the myosin crossbridge cycle. Although such experiments do not rule out the involvement of an actin-myosin crossbridge attachment in catch force maintenance, they make it less likely since detachment of myosin from actin during relaxation of catch would have to be different from that exhibited by every other myosin II studied.

14. Is the Catch Force-Maintaining Structure a Myosin Crossbridge Whose Detachment Is Prevented by Unbinding of Calcium?

A scheme that would include myosin in catch force maintenance is based on a modification of the original “latchbridge” model for the regulation of force output in mammalian smooth muscle [86]. In this model, phosphorylation of the regulatory light chain of myosin results in myosin crossbridge cycling with force development and maintenance. Subsequent dephosphorylation of the myosin light chain while myosin is attached to actin and generating high force results in a large decrease in the rate constant for detachment of the unphosphorylated crossbridge. In this way, high force would be maintained by the dephosphorylated myosin crossbridge with little associated myosin ATPase activity, and with little myosin light chain phosphorylation. It is now known that there are other mechanisms that play a role in the maintenance of force by myosin with unphosphorylated light chains. These include cooperative activation of unphosphorylated crossbridges by phosphorylated crossbridges [85, 87–91] and possibly tight binding of ADP to myosin giving rise to a slow detachment rate from actin associated with accumulation of ADP [92]. Even with these other mechanisms the idea that dephosphorylation of attached myosin leads to slowed detachment from thin filaments and results in force maintenance is an attractive mechanism.

Application of the latch model to catch muscle requires two major modifications. Since invertebrate catch smooth muscle is regulated directly by calcium binding, the binding of calcium to and release from myosin would replace the phosphorylation and dephosphorylation of the myosin light chain. The other modification is that the detachment rate constant of the catch crossbridge would presumably be regulated by the state of phosphorylation of twitchin. In such a myosin crossbridge model of catch, calcium binding to myosin initiates myosin interaction with actin, and the myosin crossbridge would go through normal cycles involving attachment to actin, development of force, and subsequent detachment. But unbinding of calcium while the myosin is in the actin-attached high force state would lead to a catch crossbridge whose detachment rate constant would be very slow. Phosphorylation of twitchin would increase the detachment rate constant for the calcium free-catch crossbridge, and relax catch force. Myosin could also detach from actin by rebinding calcium and re-entering the normal crossbridge cycle. Such a general model of catch involving the myosin crossbridge could account for many of the mechanical responses in intact [93] and permeabilized catch muscle [8].

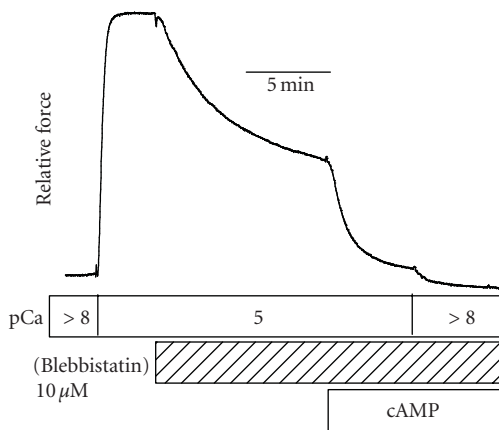


FIGURE 8: Effect of blebbistatin on force output and on the sensitivity of force to twitchin phosphorylation in permeabilized ABRM. Note that the addition of cAMP after blebbistatin treatment decreased force in pCa5 to nearly that present in relaxing solution (pCa > 8). $T = 20\text{ C}$. Reproduced from [98] with permission.

15. How Is Catch Force Modified by Agents that Inhibit the Transition from Low Force to High Force in Myosin?

The amount of catch force that exists under different mechanical conditions in permeabilized muscles can be quantified by determination of the amount of force that is relaxed upon the addition of cAMP and associated phosphorylation of twitchin. This allows the assessment of how catch force depends on factors that modify myosin interaction with actin and provides a powerful tool in probing the mechanism responsible for catch force maintenance. Such experiments provide a direct means of determining whether the catch force-maintaining structure is a myosin crossbridge that is attached to actin, whose detachment is prevented by the unbinding of calcium from myosin.

Blebbistatin inhibits the actin-activated ATPase activity of myosin II [94, 95] by preventing phosphate release from the myosin head, and thus trapping myosin in the ADP and phosphate-bound state with low actin affinity [96]. Blebbistatin acts by binding to the 50 kDa cleft of myosin near the γ -phosphate-binding site [97], thereby keeping the myosin crossbridge in the weak actin-binding state. Blebbistatin is an effective inhibitor of myosin in catch muscle since it totally inhibits the increase in ATPase activity when calcium is increased from pCa > 8 to pCa 5 [98]. The effect of blebbistatin on force output in catch muscle at pCa 5 is shown in Figure 8. Under these conditions, blebbistatin causes a partial relaxation of force that can be fully relaxed by the addition of cAMP. As expected, the cAMP results in phosphorylation of twitchin. This twitchin phosphorylation-dependent decrease in force was unexpected because previous experiments at high calcium had shown that there is no such effect in the absence of blebbistatin. Since the residual force during treatment with blebbistatin is not associated with a measurable myosin ATPase activity and is relaxed by twitchin phosphorylation, it

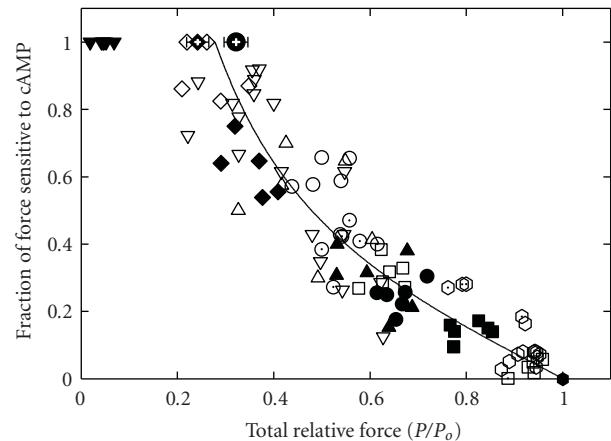


FIGURE 9: Relationship between the fractional decrease in force caused by phosphorylation of twitchin and the total force (P/P_0) before twitchin phosphorylation in permeabilized ABRM. Data for individual muscles are shown as the following: pCa 4.5, + P_i (\square); pCa 5, control (\bullet), P_i 5 mM (\circ), P_i 25 mM (\odot), blebbistatin 1.25–25 μM (∇); pCa 5.7, control (\blacksquare), P_i 5 mM (\square); pCa 6, control (\blacklozenge), P_i 5 mM (\circ), BDM 10 mM (\triangle), TFP 200 μM (\odot); pCa 6.3 (\blacklozenge), P_i 5 mM (\square); pCa 7, (\blacktriangledown). Mean \pm SE ($N = 16$) for catch force remaining 10 minutes (\bullet), 20 minutes (\blacklozenge) after switch from pCa 6 to pCa > 8. The line is a least squares quadratic fit to the data. $T = 20\text{ C}$. Reproduced from [98] with permission.

is catch force. Therefore, catch force can be maintained under high calcium conditions in the presence of blebbistatin. *Such results are not consistent with the idea that catch force is maintained by a high force actin-attached myosin crossbridge whose detachment is prevented by the unbinding of calcium from myosin.* Calcium is still present under these conditions and calcium-bound high force myosin would be expected to have a high rate of detachment from actin. This detachment, in addition to the blebbistatin-mediated inhibition of the transition of the myosin crossbridges into the high-force state would result in all of the myosin being in the weakly bound low-force state and, thereby, unable to maintain catch force in this model.

Other inhibitors of the low-to-high force transition of the myosin crossbridge including inorganic phosphate, butanedione monoxime, and trifluoperazine caused a decrease in total force and an increase in the catch force, measured as relaxation on addition of cAMP and phosphorylation of twitchin [98]. A decrease in force for any reason (other than twitchin phosphorylation) may be inherently associated with an increase in catch force. It may be that the total force itself determines the amount of catch force present, rather than other factors such as calcium concentration. For example, the amount of catch force may be the same at a force of 50% P_0 whether that force was generated in a muscle activated with submaximal calcium concentrations or in a muscle that is maximally activated in high calcium in the presence of an inhibitor of the low-to-high force transition of myosin. Figure 9 shows the relationship between the fraction of force that is catch and the total force output of the muscle. At high forces there is little catch force, and at low forces the

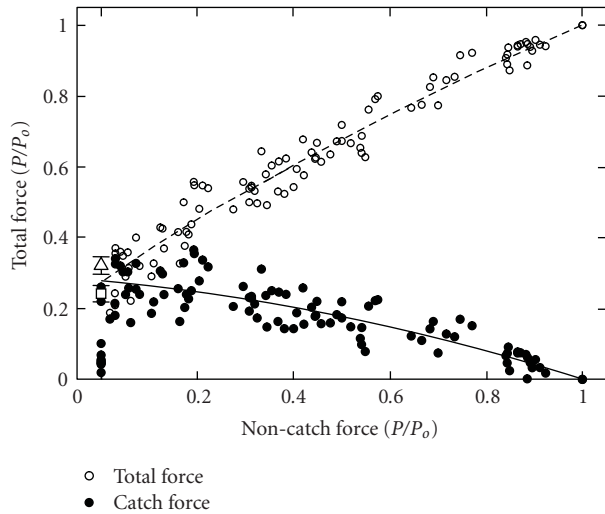


FIGURE 10: Dependence of total force and catch force on noncatch force under various conditions in permeabilized ABRM. The data are derived from the same experiments shown in Figure 9. Noncatch force is that remaining after addition of cAMP, while catch force (●, solid line) is the change in force resulting from addition of cAMP. Total force (○, dashed line) is the force before cAMP addition. Also shown are the mean \pm SE for catch force remaining 10 minutes (Δ) and 20 minutes (\square) after switch from pCa 6 to pCa $>$ 8. The lines are least squares quadratic fits to the data. Reproduced from [98] with permission.

fraction of total force that is catch increases. At a given total force, the amount of catch force is not affected by the calcium concentration or presence of the above inhibitors.

Total force output can be apportioned into catch force and noncatch force which is presumably due to cycling myosin crossbridges using the data shown in Figure 9. Since twitchin phosphorylation does not change the muscle ATPase activity or the turnover of myosin-bound ADP, crossbridge cycling and its associated noncatch force are not modified by twitchin phosphorylation. Figure 10 shows the dependence of total and catch force on noncatch force. When the force output from myosin crossbridge cycling is high, catch force is low. As the force from myosin crossbridge cycling decreases, catch force increases almost linearly to about 30% of total force.

16. Is the Catch Structure a Molecule Other than Myosin That Can Bind Both Thick and Thin Filaments and Which Can Be Displaced from the Thin Filament by High-Force Myosin Binding to Actin?

The data suggest that myosin in the high-force state is associated with detachment of catch links whereas myosin in the low-force state promotes formation of catch links. It is possible that myosin interacts with the catch link in such a way that when myosin is attached to actin in the high force state it displaces the catch link from actin, preventing any catch force maintenance. When myosin detaches from

actin and enters the low force state, the catch link has access to actin-binding sites and the force-maintaining catch link can reform. Phosphorylation of twitchin will also detach the catch link regardless of the state of activation of the muscle. The binding of the catch link to the thin filament may be regulated by structural changes in the thin filament caused by interactions of the myosin crossbridges.

A mechanism that includes a myosin crossbridge-mediated control of the binding of an independent catch link to the thin filament could be the basis of several of the mechanical and biophysical results obtained. Some examples are the following. (1) *Catch force maintenance with no associated ATPase and no effect of twitchin phosphorylation on myosin crossbridge kinetics under isometric conditions.* The catch link itself has no ATPase activity and any force that is maintained results from myosin crossbridge cycling or resistance to lengthening of the muscle. Also, the detachment of the catch link would not be expected to affect myosin crossbridge turnover so there would be no change in myosin ATPase or myosin-bound ADP turnover under isometric conditions as a result of twitchin phosphorylation. (2) *Catch force inhibits the strain-dependent increase in myosin-bound ADP turnover during shortening at intermediate calcium concentrations, but not under maximally activated conditions.* The catch linkage which provides a connection between thick and thin filaments would be expected to partially interfere with the relative motion of the filaments following release of the muscle. This would slow the initial cycling of myosin. Detachment of the linkage by either myosin binding as described above or by the relative translation of filaments resulting from some myosin cycles would subsequently allow robust shortening of the muscle. There would be no such interference with relative translation of the filaments when the muscle is fully activated since no catch link is present before the shortening. The expected increase in rate constant for single turnover of myosin-bound ADP occurs under this condition. (3) *Catch force maintenance coexists with myosin crossbridge cycling.* Catch force maintenance would be present under all conditions except when the maximum number of myosin crossbridges is attached to actin. When a myosin crossbridge detaches from actin, the catch linkage forms between thick and thin filaments. If the linkage forms after the crossbridge detaches from the thin filament, then the linkage cannot maintain the force generated from that crossbridge. But the catch link would maintain some of the force from myosin crossbridges that are attached when the catch linkage forms, but which detach during the time that the catch link is still attached. In this way there is, on average, an extra force output resulting from such catch linkages. In effect, the catch linkage extends the duty cycle of myosin crossbridges that are generating force when the linkage is formed and which detach before the catch link. (4) *Redevelopment of catch force maintenance following muscle shortening at intermediate calcium concentrations.* The catch link would cycle during shortening because myosin would still interact with actin and displace the link which would re-form when the myosin crossbridge detaches. Both catch and noncatch force would redevelop at the new muscle length. (5) *Catch force remains following detachment of rigor*

myosin crossbridges by addition of MgATP. If myosin in the high-force actin-attached state displaces the catch link from the thin filament, then one would expect that when the muscle is in high-force rigor, catch links would be detached. But when the rigor myosin crossbridges bind ATP and detach from actin, the catch link would bind to the thin filament. Since not all myosin crossbridges would detach at the same instant, some catch linkages could form before all rigor myosin crossbridges detach. In this case, these linkages would maintain some of the force from such late detaching crossbridges even after they have bound ATP and detached. There would, therefore, be catch force maintenance when ATP is added to a muscle in high-force rigor.

17. The Twitchin Molecule is a Likely Candidate for the Catch Link Between Thick and Thin Filaments

Since the phosphorylation state of twitchin controls catch force maintenance it is an obvious candidate for the catch link. *In vitro* motility studies on isolated proteins including thick filaments formed from only purified myosin, F-actin and twitchin have shown mechanical results consistent with the catch state [19]. When added to permeabilized human skeletal muscle fibers, twitchin isolated from molluscan catch muscle causes a “catch-like stiffness” which decreases when twitchin is phosphorylated [99]. This strongly suggests that twitchin is sufficient to mediate catch behavior between thick and thin filaments.

Muscles that do not exhibit catch may also contain twitchin, but their twitchin content is considerably less than that of catch muscles. For example, there is 3-fold less twitchin per myosin heavy chain in the scallop obliquely striated adductor muscle than in the smooth adductor muscle that shows catch. The twitchin from noncatch muscles also shows the ability to confer catch-like properties on isolated proteins [100]. This suggests that the twitchin-mediated interaction between thick and thin filaments may occur in other than catch muscle and that such interactions may modulate relaxation rate [100]. The amount of twitchin, and perhaps the specific isoform present (see [77]) may determine the extent to which classical catch properties are exhibited by a particular type of muscle.

18. Biochemical Evidence that Twitchin is the Catch Link

18.1. Twitchin Binds to the Thick Filament. In molluscan catch muscle, an antibody against twitchin binds along the entire length of isolated thick filaments as well as thick filaments in tissues as observed in immunoelectron microscopy [61]. This is also shown in greater structural detail in Figure 11, in which the kinase domain of twitchin was immunogold labeled in isolated thick filaments from the ABRM of *Mytilus edulis* (Siegman and Butler, unpublished). Comparison of the Coomassie Blue staining of twitchin and myosin heavy chain in gels containing whole protein extracts from intact ABRM of *Mytilus edulis* show that twitchin is



FIGURE 11: Thick filament from ABRM with immunogold labeling of the kinase domain of twitchin. Gold particles are 10 nm in diameter. Filaments were stained with 2% uranyl acetate. Striated appearance of filaments has a ~14 nm repeat and there is about 200 nm between clusters of gold particles.

9% of myosin heavy chain. Given the difference in molecular weights, there is one twitchin for every 14-double-headed myosins [58]. A similar ratio of twitchin to myosin heavy chain was found in whole muscle samples as in isolated thick filaments (Butler and Siegman, unpublished observations). These data show that most of the twitchin is bound to the thick filament tightly enough to remain attached during the thick filament isolation procedure [101]. *In vitro* binding of twitchin has been shown to myosin, paramyosin, and catchin, all of which are components of the thick filaments [102]. Although twitchin binds to both the rod and heavy meromyosin portions of myosin, binding to the latter was stronger. Phosphorylation of twitchin only slightly decreased the extent of twitchin binding to myosin [102].

18.2. Twitchin Binds to the Thin Filament. Turbidity, viscosity and cosedimentation experiments show that twitchin interacts with F-actin [103]. The interaction was not dependent on calcium concentration, but was highly regulated by the phosphorylation state of twitchin. Twitchin that was treated with the catalytic subunit of protein kinase A did not interact with actin. It is interesting that under some conditions, twitchin appeared to crosslink thin filaments such that co-sedimentation of twitchin and F-actin mixtures occurred at centrifugal forces at which the individual proteins do not pellet. This suggests that there are at least two actin-binding regions in the molecule.

18.3. The C-Terminal Portion of Twitchin Containing the D2 Phosphorylation Site and Adjacent Ig Domains Forms a Trimeric Complex with Myosin and Actin. The D2 regulatory phosphorylation site in the C-terminal portion of twitchin is located in a linker region between the Ig domains that are immediately adjacent to the kinase domain. A recombinant protein containing these Ig domains and the linker region (IGD2IG) has been shown to bind to F-actin, myosin, and paramyosin [104]. Thiophosphorylation of the D2 site (which mimics phosphorylation) causes a decrease in binding of IGD2IG to all of these proteins. Co-sedimentation of a trimeric complex of F-actin, myosin, and IGD2IG occurred only when IGD2IG was unphosphorylated. The IGD2IG-binding site on actin was identified by making enzymatic digests of actin and determining which of the peptides bound to the unphosphorylated twitchin fragment. Only one peptide with a sequence of LVCDNGS bound to IGD2IG [104]. This sequence is located near the

sequence of actin that interacts with the loop 2 region of myosin, and a synthetic peptide containing the sequence was found to compete with actin for binding of IGD2IG. Thiophosphorylation of the D2 site prevents the binding of the actin peptide [104]. Additional studies have shown that a peptide derived from the myosin loop 2 sequence (CAQNKEAETTGTHKKRKSSA) binds to IGD2IG and also interferes with formation of the trimeric complex among F-actin, myosin, and IGD2IG [105]. These results suggest IGD2IG links myosin and actin by binding to the loop 2 portion of myosin and to the region of actin where the loop 2 region of myosin binds [105]. Taken together, these results support the idea that the D2 region of twitchin is part of the mechanical link tethering thick and thin filaments and is at least partially responsible for catch force maintenance. The fact that the IGD2IG binds to the loop 2 region of myosin and its corresponding binding site on actin suggests that the binding of myosin to actin during crossbridge cycling might prevent IGD2IG binding and remove the twitchin-mediated tether between thick and thin filaments. This possibility is supported by the finding that addition of calcium and resulting myosin crossbridge cycling decreased the co-sedimentation of the trimeric complex of myosin, actin, and IGD2IG [105].

18.4. The N-Terminal Portion of Twitchin Containing the DX and D1 Phosphorylation Sites Binds Both Thick and Thin Filaments. The DX and D1 regulatory phosphorylation sites are located in the linker region between the 7th and 8th IG domains from the N-terminus of twitchin. This linker region also contains a DFRXXL actin-binding motif. Our experiments involving a recombinant protein containing this linker region and adjacent IG domains (IGDXD1IG) show phosphorylation-dependent co-sedimentation of the protein with both native thick and thin filaments from the ABRM of *Mytilus edulis*. Similar phosphorylation-dependent co-sedimentation with thick and thin filaments occurs with a recombinant protein (DXD1) consisting of only the linker region containing the two phosphorylation sites. The binding of DXD1 to native thin filaments shows a K_d of approximately $16 \mu\text{M}$ and a maximum binding of 1 mole per mole of actin. Phosphorylation of DXD1 increases the K_d by about 6-fold if it is assumed that maximum binding is 1 mole per mole of actin. Unphosphorylated IGDXD1IG shows somewhat tighter binding to actin ($K_d < 5 \mu\text{M}$). Both of these unphosphorylated proteins increase force output in permeabilized ABRM under conditions of submaximal activation, and this effect is not present when the proteins are phosphorylated. This suggests that both IGDXD1IG and DXD1 are sufficient for tethering thick and thin filaments and for adding a catch force component to total force output from the muscle.

There appear to be at least two thin filament interaction sites in the DXD1 linker region. Both a 52-residue peptide surrounding the DX site (which also contains the DFRXXL actin-binding motif) and a 47-residue peptide surrounding the D1 site show co-sedimentation with native thin filaments. Addition of these peptides to permeabilized muscles causes

an increased rate of relaxation of catch force. This result is consistent with these peptides displacing native twitchin from actin during catch and confirms the central role that the DXD1 region plays in the mechanism of catch. Interestingly, in muscles in which twitchin has been thiophosphorylated and all force is due to cycling myosin crossbridges, the unphosphorylated DX peptide inhibits force output. When the DX peptide is phosphorylated, the extent of inhibition is decreased. These findings suggest that the unphosphorylated DX region of twitchin can interact with actin to either interfere with myosin binding to actin or to prevent the transition of myosin crossbridge from the low-force to high-force state. The inhibition of force by the DX peptide suggests that this region of twitchin may compete with myosin for binding to actin and, as such, may be responsible for the proposed displacement of twitchin from actin and associated loss in catch force when myosin crossbridges interact with actin.

19. A Belt and Suspenders Model of Catch

The data are consistent with twitchin being a tether between thick and thin filaments that is responsible for catch force maintenance. Both the N- and C-terminal portions of twitchin contain phosphorylation sites that regulate catch, and both of these regions have properties consistent with twitchin being an independent tether between thick and thin filaments. A cartoon of two such tethers in a twitchin molecule is shown in Figure 12. The redundancy provided by *two* force-bearing tethers in each twitchin molecule would provide an especially secure “belt and suspenders” connection between thick and thin filaments and would promote long-term force maintenance and resistance to stretch during catch.

A model for catch that is a modification of one we described earlier [98] is shown in Figure 13. The myosin-twitchin-actin interactions described apply independently to both the N- and C-terminal regions of twitchin as shown in the “belt and suspenders” cartoon. In the relaxed state, (a) the myosin crossbridge is in the low-force state and detached from the thin filament. The DX, D1, and D2 regulatory sites in twitchin are phosphorylated, and twitchin is detached from the thin filament. When the muscle is activated there is an increase in $[\text{Ca}^{+2}]$ and the crossbridge binds to the thin filament in the low-force state (b). Twitchin is displaced from the thin filament as a result of crossbridge binding to the thin filament. Twitchin is also dephosphorylated by activation of the phosphatase calcineurin. The crossbridge then makes the transition to the high-force state (c) resulting in force generation. Twitchin is still detached from the thin filament because of the myosin interaction with the thin filament. When the calcium concentration decreases, myosin detaches from the thin filament and the unphosphorylated twitchin is attached to both the thick and thin filaments (d). This is the catch state. The asynchronous activity of crossbridge cycling allows some crossbridges to detach from actin with formation of the trimeric catch complex while some other crossbridges are still attached and maintaining

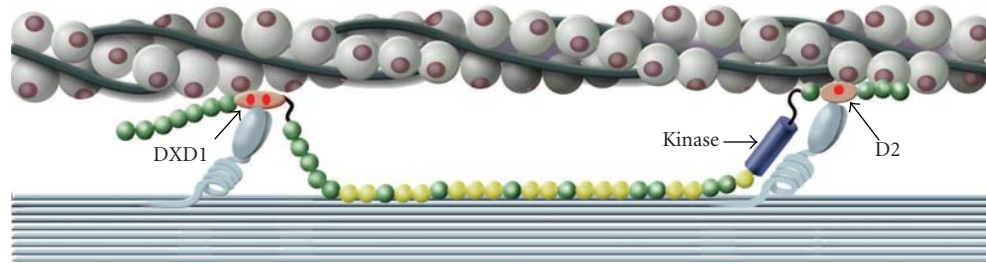


FIGURE 12: A belt and suspenders model of twitchin interaction with the thick and thin filaments in catch. The redundancy provided by two force-bearing tethers in each twitchin molecule is shown. The N- and C-terminal portions of twitchin that contain regulatory phosphorylation sites are shown to be independent tethers. The N-terminal tether shows the region surrounding the DX and D1 phosphorylation sites interacting with the thin filament, and the C-terminal tether shows the region surrounding the D2 phosphorylation site interacting with the thin filament. The evidence for the DXD1 region binding to the thin filament comes from this work and the evidence for D2 and adjacent Ig domains comes from [104, 105].

force. The tether formed when the first crossbridges detach will then maintain some of the force of those crossbridges that detach later. In this way force maintenance results from catch linkages when the calcium concentration is decreased. The catch linkage essentially extends the duty cycle of myosin crossbridges that are generating force when the linkage is formed and which detach while the catch link is maintained. Phosphorylation of the regulatory sites in twitchin at resting $[Ca^{+2}]$ results in detachment of the tether from the thin filament (and possibly the thick filament), relaxation of catch force, and the loss of the tether-mediated resistance to stretch (Figure 13(a)).

20. Similarities between Twitchin and Myosin Binding Protein-C (MyBP-C)

We have previously noted that there are similarities in the domain organization of twitchin around the D1 phosphorylation site with that of cardiac MyBP-C [64]. Although MyBP-C has obviously been known to bind to myosin, there is recent evidence that several regions near the N-terminus of cardiac MyBP-C bind to filamentous actin [106]. One of the actin binding regions includes the cardiac specific regulatory region between domains C1 and C2, and phosphorylation of MyBP-C at the cardiac specific sites reduces the interaction with actin [106]. This same region includes a DFRXXL-like actin binding motif (DLRGML) that is similar to that present in twitchin. When unphosphorylated, this regulatory region of cardiac MyBP-C binds to the myosin S2 region [107], but not when phosphorylated [108]. The similarities in actin and myosin binding properties of the DXD1 region of twitchin and the N-terminal portion of MyBP-C as well as their phosphorylation dependence suggest that they may share similar functions. The idea that MyBP-C may be a phosphorylation-dependent tether between thick and thin filaments may seem unusual, given that cardiac muscle goes through rapid and frequent contraction and relaxation cycles. However, if the tethering of the thick and thin filaments via MyBP-C is prevented by myosin crossbridge interaction with the thin filament as suggested for twitchin, then the main effect of such a MyBP-C tether may be to

act as a regulated viscous element during relaxation when crossbridge interaction with actin wanes. For example, the rate of relaxation of force seems to be modulated by the phosphorylation of twitchin in *Aplysia* [62], and the same may be the case for MyBP-C in the heart. Of course, the multiple thick and thin filament tethers present in twitchin from catch muscle would be expected to give a much tighter connection between the contractile filaments and provide a much more prolonged force maintenance following inactivation of catch muscle than would a MyBP-C tether in cardiac muscle.

21. Summary

- (1) Catch is a mechanical state occurring in certain invertebrate smooth muscles initiated by cholinergic nerve stimulation, and characterized by high-force maintenance and resistance to stretch during extremely slow relaxation. Catch occurs following a transient increase in intracellular calcium and its return to near-basal concentrations. During catch, crossbridge cycling rate is extremely slow as is the rate of ATP utilization.
- (2) The release of catch, or rapid relaxation, occurs *in vivo* upon stimulation of serotonergic nerves, which cause an increase in cAMP and activation of protein kinase A. The primary target of protein kinase A activation is the phosphorylation of the minititin, twitchin. Subsequent activation of the muscle causes an increase in the activity of a calcium-dependent phosphatase, presumably calcineurin, which dephosphorylates twitchin and allows catch force maintenance when intracellular calcium decreases. The simultaneous stimulation of cholinergic and serotonergic nerves results in a phasic contraction.
- (3) Twitchin from *Mytilus* ABRM is a ~526 kDa protein that is associated with the A band of nematode striated and molluscan smooth muscles, specifically with the thick filament. It bears similarity to minititins from other invertebrates with variations in the number of specific domains.

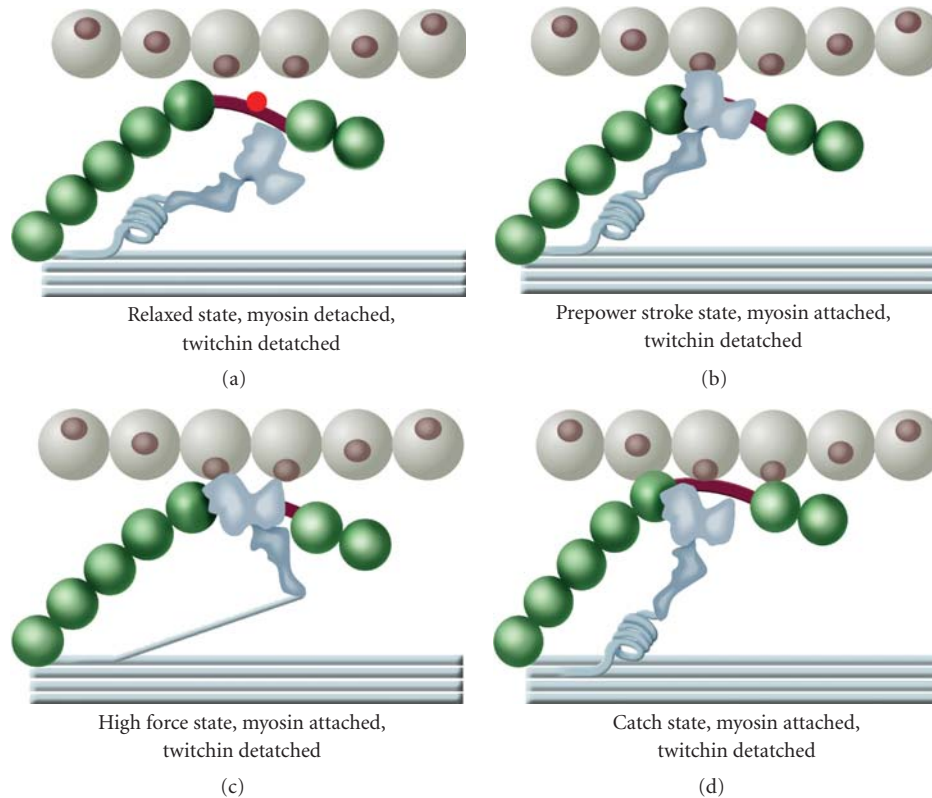


FIGURE 13: A model showing twitchin interaction with thick and thin filaments during the myosin crossbridge cycle. (a) The relaxed state. The myosin crossbridge is in the low-force state and detached from the thin filament. The regulatory sites in twitchin are phosphorylated, and twitchin is detached from the thin filament. (b) The prepower stroke state. The myosin crossbridge has been activated by an increase in $[Ca^{+2}]$ and the crossbridge binds to the thin filament. Twitchin has been displaced from the thin filament as a result of crossbridge binding to the thin filament. Twitchin is also dephosphorylated by activation of the phosphatase calcineurin. (c) The high-force state. Myosin has gone through the power stroke resulting in force generation. Twitchin is detached from the thin filament by myosin interaction with the thin filament. (d) The catch state. Myosin is in the low-force state and detached from the thin filament. Unphosphorylated twitchin is attached to both the thick and thin filaments. Phosphorylation of twitchin would result in detachment of twitchin from the thin filament and lead to the relaxed state (a). The myosin-twitchin-thin filament interactions described apply independently to both the N- and C-terminal regions of twitchin as shown in the “belt and suspenders” cartoon in Figure 12.

- (4) Protein kinase A phosphorylates twitchin to the extent of 3 mole phosphate per mole of twitchin. The sites of phosphorylation, D1 and DX, near the N-terminus, and D2, near the C-terminus have been identified.
- (5) Catch occurs in submaximally activated permeabilized ABRM, but not in muscles that are maximally activated with high calcium. On phosphorylation of twitchin, force declines at all submaximal calcium concentrations, with no associated change in ATPase activity. Therefore, catch force maintenance can occur together with cycling myosin crossbridges at submaximal calcium concentrations. Additionally, the catch link can adjust during shortening of submaximally activated muscles and maintain force at the new shorter muscle length.
- (6) The twitchin molecule is the catch link that tethers thick and thin filaments. Twitchin binds to both thick and thin filaments, but binding to the latter

is phosphorylation dependent. Both the N- and C-terminal portions of twitchin contain phosphorylation sites that regulate catch, and both of these regions have properties consistent with twitchin being an independent tether between thick and thin filaments.

- (7) A model for the mechanism of regulation of catch via a twitchin tether is based on both (a) the phosphorylation state of twitchin and (b) the attachment of myosin crossbridges to actin. When the catch muscle is stimulated, the increase in intracellular calcium is sufficient to maximally activate crossbridges and twitchin is dephosphorylated; the binding of myosin crossbridges to actin displaces twitchin from the thin filament and myosin cyclically interacts with actin with force development and shortening. As the intracellular calcium concentration wanes and catch ensues, the myosin crossbridges detach from actin and the trimeric complex between myosin, twitchin, and actin tethers the thick and thin filaments. The

muscle relaxes from catch when twitchin is phosphorylated, and the twitchin tether detaches from the thin filament.

- (8) The catch state of invertebrate smooth muscle bears many similarities to the tonic force-maintaining state of vertebrate smooth muscles, but represents the extreme condition in terms of economy, largely through the use of an accessory protein (twitchin) to maintain force for extended periods of time. The operation of a similar mechanism in vertebrate smooth muscle remains to be determined, and the challenge for the future will be to identify the counterpart of twitchin and its regulation.

Acknowledgments

The authors' research has been supported by AR042758-14 from the NIH to MJS and to TMB. They thank Susan Mooers and Srinivasa Narayan for their extraordinary dedication and technical expertise. They acknowledge their colleagues Drs. Betty M. Twarog and Carolyn Cohen, whose research inspired their interest in catch.

References

- [1] J. von Uexkull, "Studien uber den tonus VI. Die pilgermuschel," *Zeitschrift für Biologie*, vol. 58, pp. 305–322, 1919.
- [2] V. N. Kalabokis, E. O'Neill-Hennessey, and A. G. Szent-Gyorgyi, "Regulatory domains of myosins: influence of heavy chain on Ca²⁺-binding," *Journal of Muscle Research and Cell Motility*, vol. 15, no. 5, pp. 547–553, 1994.
- [3] N. Ishii, A. W. M. Simpson, and C. C. Ashley, "Free calcium at rest during "catch" in single smooth muscle cells," *Science*, vol. 243, no. 4896, pp. 1367–1368, 1989.
- [4] F. Baguet and J. M. Gillis, "Energy cost of tonic contraction in lamellibranch catch muscle," *The Journal of Physiology*, vol. 198, pp. 127–143, 1968.
- [5] K. M. Nauss and R. E. Davies, "Changes in inorganic phosphate & arginine during the development, maintenance and loss of tension in the anterior byssus retractor muscle of *Mytilus edulis*," *Biochemische Zeitschrift*, vol. 345, pp. 173–187, 1966.
- [6] R. A. Cole and B. M. Twarog, "Relaxation of catch in a molluscan smooth muscle. I. Effects of drugs which act on the adenyl cyclase system," *Comparative Biochemistry and Physiology*, vol. 43, no. 2, pp. 321–330, 1972.
- [7] R. K. Achazi, B. Doelling, and R. Haakshorst, "5 Ht induced relaxation & cyclic AMP in a molluscan smooth muscle," *Pflugers Archiv*, vol. 349, no. 1, pp. 19–27, 1974.
- [8] T. M. Butler, S. U. Mooers, C. Li, S. Narayan, and M. J. Siegman, "Regulation of catch muscle by twitchin phosphorylation: effects on force, ATPase, and shortening," *Biophysical Journal*, vol. 75, no. 4, pp. 1904–1914, 1998.
- [9] J. C. Ruegg, "Smooth muscle tone," *Physiological Reviews*, vol. 51, no. 1, pp. 201–248, 1971.
- [10] J. Lowy, B. M. Millman, and J. Hanson, "Structure and function in smooth tonic muscles of lammelibranch molluscs," *Proceedings of the Royal Society of London. Series B*, vol. 160, pp. 525–536, 1964.
- [11] J. C. Ruegg, "On the tropomyosin-paramyosin system in relation to the viscous tone of lammelibranch "catch" muscle," *Proceedings of the Royal Society of London. Series B*, vol. 154, pp. 224–249, 1961.
- [12] S. L. Hooper, K. H. Hobbs, and J. B. Thuma, "Invertebrate muscles: thin and thick filament structure; molecular basis of contraction and its regulation, catch and asynchronous muscle," *Progress in Neurobiology*, vol. 86, no. 2, pp. 72–127, 2008.
- [13] C. Cohen, "Matching molecules in the catch mechanism," *Proceedings of the National Academy of Sciences of the United States of America*, vol. 79, no. 10, pp. 3176–3178, 1982.
- [14] N. Pante, "Paramyosin polarity in the thick filament of molluscan smooth muscles," *Journal of Structural Biology*, vol. 113, no. 2, pp. 148–163, 1994.
- [15] R. J. C. Levine, M. Elfvin, M. M. Dewey, and B. Walcott, "Paramyosin in invertebrate muscles. II. Content in relation to structure and function," *Journal of Cell Biology*, vol. 71, no. 1, pp. 273–279, 1976.
- [16] B. R. Jewell, "The nature of the phasic and the tonic responses of the anterior byssal retractor muscle of *Mytilus*," *The Journal of Physiology*, vol. 149, pp. 154–177, 1959.
- [17] N. S. Shelud'ko, K. F. Tuturova, T. V. Permyakova, S. V. Plotnikov, and A. A. Orlova, "A novel thick filament protein in smooth muscles of bivalve molluscs," *Comparative Biochemistry and Physiology B*, vol. 122, no. 3, pp. 277–285, 1999.
- [18] A. Yamada, M. Yoshio, K. Oiwa, and L. Nyitray, "Catchin, a novel protein in molluscan catch muscles, is produced by alternative splicing from the myosin heavy chain gene," *Journal of Molecular Biology*, vol. 295, no. 2, pp. 169–178, 2000.
- [19] A. Yamada, M. Yoshio, H. Kojima, and K. Oiwa, "An in vitro assay reveals essential protein components for the "catch" state of invertebrate smooth muscle," *Proceedings of the National Academy of Sciences of the United States of America*, vol. 98, no. 12, pp. 6635–6640, 2001.
- [20] R. Hauck and R. K. Achazi, "The ultrastructure of a molluscan catch muscle during a contraction catch relaxation cycle," *European Journal of Cell Biology*, vol. 45, pp. 30–35, 1987.
- [21] P. M. Bennett and A. Elliott, "The "catch" mechanism in molluscan muscle: an electron microscopy study of freeze-substituted anterior byssus retractor muscle of *Mytilus edulis*," *Journal of Muscle Research and Cell Motility*, vol. 10, no. 4, pp. 297–311, 1989.
- [22] I. Takahashi, M. Shimada, T. Akimoto, T. Kishi, and H. Sugi, "Electron microscopic evidence for the thick filament interconnections associated with the catch state in the anterior byssal retractor muscle of *Mytilus edulis*," *Comparative Biochemistry and Physiology A*, vol. 134, no. 1, pp. 115–120, 2003.
- [23] A. G. Szent-Gyorgyi, C. Cohen, and J. Kendrick-Jones, "Paramyosin and the filaments of molluscan "catch" muscles. II. Native filaments: Isolation and characterization," *Journal of Molecular Biology*, vol. 56, no. 2, pp. 239–248, 1971.
- [24] H. F. Epstein, B. J. Aronow, and H. E. Harris, "Myosin paramyosin cofilaments: enzymatic interaction with F-actin," *Proceedings of the National Academy of Sciences of the United States of America*, vol. 73, no. 9, pp. 3015–3019, 1976.
- [25] J. C. Ruegg, "Myosin-linked regulation of molluscan muscle," in *Calcium in Muscle Contraction*, Springer, New York, NY, USA, 2nd edition, 1992.

- [26] R. K. Achazi, "Phosphorylation of molluscan paramyosin," *Pflugers Archiv European*, vol. 379, no. 2, pp. 197–201, 1979.
- [27] R. K. Achazi, "The catch muscle," in *Basic Biology of Muscle: A Comparative Approach*, pp. 291–308, Plenum, New York, NY, USA, 1982.
- [28] B. Ljung and P. Hallgren, "On the mechanism of inhibitory action of vibratins as studied in a molluscan catch muscle and in vertebrate vascular smooth muscle," *Acta Physiologica Scandinavica*, vol. 95, no. 4, pp. 424–430, 1975.
- [29] B. Ljung and R. Sivertsson, "Vibration induced inhibition of vascular smooth muscle contraction," *Blood Vessels*, vol. 12, no. 1, pp. 38–52, 1975.
- [30] T. Kobayashi, C. Ichikawa, and H. Sugi, "Differential effects of sinusoidal vibrations on tension and stiffness in *Mytilus* smooth muscle during catch state," *Japanese Journal of Physiology*, vol. 35, no. 4, pp. 689–692, 1985.
- [31] J. Lowy and B. M. Millman, "The contractile mechanism of the anterior byssus retractor of *Mytilus edulis*," *Proceedings of the Royal Society of London. Series B*, vol. 246, pp. 105–148, 1963.
- [32] G. Pfitzer and J. C. Ruegg, "Molluscan catch muscle: regulation and mechanics in living and skinned anterior byssus retractor muscle of *Mytilus edulis*," *Journal of Comparative Physiology*, vol. 147, no. 1, pp. 137–142, 1982.
- [33] W. H. Johnson and B. M. Twarog, "The basis for prolonged contractions in molluscan muscles," *The Journal of General Physiology*, vol. 43, pp. 941–960, 1960.
- [34] M. J. Kushmerick and R. E. Davies, "The chemical energetics of muscle contraction. II. The chemistry, efficiency and power of maximally working sartorius muscles," *Proceedings of the Royal Society of London. Series B*, vol. 174, no. 36, pp. 315–353, 1969.
- [35] B. M. Twarog, "The regulation of catch in molluscan muscle," *Journal of General Physiology*, vol. 50, no. 6, pp. 157–169, 1967.
- [36] E. Bozler, "The heat production of smooth muscle," *The Journal of Physiology*, vol. 69, pp. 442–462, 1930.
- [37] T. Tameyasu and H. Sugi, "The series elastic component and the force-velocity relation in the anterior byssal retractor muscle of *Mytilus edulis* during active and catch contractions," *Journal of Experimental Biology*, vol. 64, no. 2, pp. 497–510, 1976.
- [38] M. J. Siegman, T. M. Butler, S. U. Mooers, and R. E. Davies, "Chemical energetics of force development, force maintenance, and relaxation in mammalian smooth muscle," *Journal of General Physiology*, vol. 76, no. 5, pp. 609–629, 1980.
- [39] P. F. Dillon, M. O. Aksoy, S. P. Driska, and R. A. Murphy, "Myosin phosphorylation and crossbridge cycle in arterial smooth muscle," *Science*, vol. 211, pp. 495–497, 1981.
- [40] A. P. Somlyo and A. V. Somlyo, "Discussion," *The Journal of General Physiology*, vol. 50, pp. 168–169, 1967.
- [41] J. Kendrick-Jones, W. Lehman, and A. G. Szent-Györgyi, "Regulation in molluscan muscles," *Journal of Molecular Biology*, vol. 54, no. 2, pp. 313–326, 1970.
- [42] F. Baguet, "The catch-state in glycerol extracted fibres from a lamellibranch smooth muscle," *European Journal of Physiology*, vol. 340, no. 1, pp. 19–34, 1973.
- [43] G. Marchand Dumont and F. Baguet, "The control mechanism of relaxation in molluscan catch muscle (ABRM)," *Pflugers Archiv*, vol. 354, no. 1, pp. 87–100, 1975.
- [44] F. Cornelius, "The regulation of tension in a chemically skinned molluscan smooth muscle. Effect of Mg^{2+} on the Ca^{2+} -activated tension generation," *Journal of General Physiology*, vol. 75, no. 6, pp. 709–725, 1980.
- [45] F. Cornelius, "Tonic contraction and the control of relaxation in a chemically skinned molluscan smooth muscle," *Journal of General Physiology*, vol. 79, no. 5, pp. 821–834, 1982.
- [46] L. Castellani and C. Cohen, "Myosin rod phosphorylation and the catch state of molluscan-muscles," *Science*, vol. 235, no. 4786, pp. 334–337, 1987.
- [47] K. Guth, M. Gagelmann, and J. C. Ruegg, "Skinned smooth muscle: time course of force and ATPase activity during contraction cycle," *Experientia*, vol. 40, no. 2, pp. 174–176, 1984.
- [48] M. Schneider, M. Sparrow, and J. C. Rueegg, "Inorganic phosphate promotes relaxation of chemically skinned smooth muscle of guinea-pig *Taenia coli*," *Experientia*, vol. 37, no. 9, pp. 980–982, 1981.
- [49] S. Watabe and D. J. Hartshorne, "Paramyosin and the catch mechanism," *Comparative Biochemistry and Physiology*, vol. 96, no. 4, pp. 639–646, 1990.
- [50] S. Watabe, T. Tsuchiya, and D. J. Hartshorne, "Phosphorylation of paramyosin," *Comparative Biochemistry and Physiology B*, vol. 94, no. 4, pp. 813–821, 1989.
- [51] H. Sohma, M. Yazawa, and F. Morita, "Phosphorylation of regulatory light chain a (RLC-a) in smooth muscle myosin of scallop, *Patinopecten yessoensis*," *Journal of Biochemistry*, vol. 98, no. 2, pp. 569–572, 1985.
- [52] H. Sohma and F. Morita, "Purification of a protein kinase phosphorylating myosin regulatory light chain-a (RLC-a) from smooth muscle of scallop, *Patinopecten yessoensis*," *Journal of Biochemistry*, vol. 100, no. 5, pp. 1155–1163, 1986.
- [53] H. Sohma, H. Sasada, K. Inoue, and F. Morita, "Regulatory light chain-a myosin kinase (aMK) catalyzes phosphorylation of smooth muscle myosin heavy chains of scallop, *Patinopecten yessoensis*," *Journal of Biochemistry*, vol. 104, no. 6, pp. 889–893, 1988.
- [54] L. Castellani and C. Cohen, "Rod phosphorylation favors folding in a catch muscle myosin," *Proceedings of the National Academy of Sciences of the United States of America*, vol. 84, no. 12, pp. 4058–4062, 1987.
- [55] L. Castellani, B. W. Elliott Jr., and C. Cohen, "Phosphorylatable serine residues are located in a non-helical tailpiece of a catch muscle myosin," *Journal of Muscle Research and Cell Motility*, vol. 9, no. 6, pp. 533–540, 1988.
- [56] L. Castellani and C. Cohen, "A calcineurin-like phosphatase is required for catch contraction," *FEBS Letters*, vol. 309, no. 3, pp. 321–326, 1992.
- [57] R. Hauck and R. K. Achazi, "In situ phosphorylation of contractile proteins of a molluscan (*Mytilus edulis*) catch muscle in different functional states," *Comparative Biochemistry and Physiology B*, vol. 100, no. 2, pp. 237–242, 1991.
- [58] M. J. Siegman, S. U. Mooers, C. Li, et al., "Phosphorylation of a high molecular weight (approximately 600 kDa) protein regulates catch in invertebrate smooth muscle," *Journal of Muscle Research and Cell Motility*, vol. 18, no. 6, pp. 655–670, 1997.
- [59] R. H. Waterston, J. N. Thomson, and S. Brenner, "Mutants with altered muscle structure in *Caenorhabditis elegans*," *Developmental Biology*, vol. 77, no. 2, pp. 271–302, 1980.
- [60] D. G. Moerman, G. M. Benian, R. J. Barstead, L. A. Schriefer, and R. H. Waterston, "Identification and intracellular localization of the unc-22 gene product of *Caenorhabditis elegans*," *Genes & Development*, vol. 2, no. 1, pp. 93–105, 1988.

- [61] P. Vibert, S. M. Edelstein, L. Castellani, and B. W. Elliott Jr., "Mini-titins in striated and smooth molluscan muscles: structure, location and immunological crossreactivity," *Journal of Muscle Research and Cell Motility*, vol. 14, no. 6, pp. 598–607, 1993.
- [62] W. C. Probst, E. C. Cropper, J. Heierhorst, et al., "cAMP-dependent phosphorylation of *Aplysia* twitchin may mediate modulation of muscle contractions by neuropeptide cotransmitters," *Proceedings of the National Academy of Sciences of the United States of America*, vol. 91, no. 18, pp. 8487–8491, 1994.
- [63] M. J. Siegman, D. Funabara, S. Kinoshita, S. Watabe, D. J. Hartshorne, and T. M. Butler, "Phosphorylation of a twitchin-related protein controls catch and calcium sensitivity of force production in invertebrate smooth muscle," *Proceedings of the National Academy of Sciences of the United States of America*, vol. 95, no. 9, pp. 5383–5388, 1998.
- [64] D. Funabara, S. Watabe, S. U. Mooers, et al., "Twitchin from molluscan catch muscle. Primary structure and relationship between site-specific phosphorylation and mechanical function," *Journal of Biological Chemistry*, vol. 278, no. 31, pp. 29308–29316, 2003.
- [65] J. E. Kiff, D. G. Moerman, L. A. Schriefer, and R. H. Waterston, "Transposon-induced deletions in *unc-22* of *C. elegans* associated with almost normal gene activity," *Nature*, vol. 331, no. 6157, pp. 631–633, 1988.
- [66] B. Bullard, W. A. Linke, and K. Leonard, "Varieties of elastic protein in invertebrate muscles," *Journal of Muscle Research and Cell Motility*, vol. 23, no. 5-6, pp. 435–447, 2002.
- [67] R. Southgate and A. Ayme-Southgate, "Alternative splicing of an amino-terminal PEVK-like region generates multiple isoforms of *Drosophila* projectin," *Journal of Molecular Biology*, vol. 313, no. 5, pp. 1035–1043, 2001.
- [68] T. Oshino, J. Shimamura, A. Fukuzawa, K. Maruyama, and S. Kimura, "The entire cDNA sequences of projectin isoforms of crayfish claw closer and flexor muscles and their localization," *Journal of Muscle Research and Cell Motility*, vol. 24, no. 7, pp. 431–438, 2003.
- [69] G. M. Benian, S. W. L'Hernault, and M. E. Morris, "Additional sequence complexity in the muscle gene, *unc-22*, and its encoded protein, twitchin, of *Caenorhabditis elegans*," *Genetics*, vol. 134, no. 4, pp. 1097–1104, 1993.
- [70] P.-J. Lin, K. Luby-Phelps, and J. T. Stull, "Properties of filament-bound myosin light chain kinase," *Journal of Biological Chemistry*, vol. 274, no. 9, pp. 5987–5994, 1999.
- [71] L. Smith, M. Parizi-Robinson, M.-S. Zhu, et al., "Properties of long myosin light chain kinase binding to F-actin in vitro and in vivo," *Journal of Biological Chemistry*, vol. 277, no. 38, pp. 35597–35604, 2002.
- [72] P.-J. Lin, K. Luby-Phelps, and J. T. Stull, "Binding of myosin light chain kinase to cellular actin-myosin filaments," *Journal of Biological Chemistry*, vol. 272, no. 11, pp. 7412–7420, 1997.
- [73] L. Smith, X. Su, P.-J. Lin, G. Zhi, and J. T. Stull, "Identification of a novel actin binding motif in smooth muscle myosin light chain kinase," *Journal of Biological Chemistry*, vol. 274, no. 41, pp. 29433–29438, 1999.
- [74] L. Smith and J. T. Stull, "Myosin light chain kinase binding to actin filaments," *FEBS Letters*, vol. 480, no. 2-3, pp. 298–300, 2000.
- [75] V. Hatch, G. Zhi, L. Smith, J. T. Stull, R. Craig, and W. Lehman, "Myosin light chain kinase binding to a unique site on F-actin revealed by three-dimensional image reconstruction," *Journal of Cell Biology*, vol. 154, no. 3, pp. 611–617, 2001.
- [76] W. A. Linke, M. Kulke, H. Li, et al., "PEVK domain of titin: an entropic spring with actin-binding properties," *Journal of Structural Biology*, vol. 137, no. 1-2, pp. 194–205, 2002.
- [77] M. Kusaka, D. Ikeda, D. Funabara, D. J. Hartshorne, and S. Watabe, "The occurrence of tissue-specific twitchin isoforms in the mussel *Mytilus galloprovincialis*," *Fisheries Science*, vol. 74, no. 3, pp. 677–686, 2008.
- [78] A. S. Franke, S. U. Mooers, S. R. Narayan, M. J. Siegman, and T. M. Butler, "Myosin cross-bridge kinetics and the mechanism of catch," *Biophysical Journal*, vol. 93, no. 2, pp. 554–565, 2007.
- [79] W. O. Fenn, "A quantitative comparison between the energy liberated and the work performed by the isolated sartorius muscle of the frog," *The Journal of Physiology*, vol. 58, pp. 175–203, 1923.
- [80] A. F. Huxley, "Muscle structure and theories of contraction," *Progress in Biophysics and Biophysical Chemistry*, vol. 7, pp. 255–318, 1957.
- [81] M. Nyitrai and M. A. Geeves, "Adenosine diphosphate and strain sensitivity in myosin motors," *Philosophical Transactions of the Royal Society B*, vol. 359, no. 1452, pp. 1867–1877, 2004.
- [82] T. M. Butler, S. R. Narayan, S. U. Mooers, and M. J. Siegman, "Strain dependence of crossbridge kinetics in smooth muscle," *Biophysical Journal*, vol. 68, p. A169, 1995.
- [83] A. S. Khromov, M. R. Webb, M. A. Ferenczi, D. R. Trentham, A. P. Somlyo, and A. V. Somlyo, "Myosin regulatory light chain phosphorylation and strain modulate adenosine diphosphate release from smooth muscle myosin," *Biophysical Journal*, vol. 86, no. 4, pp. 2318–2328, 2004.
- [84] T. M. Butler, S. R. Narayan, S. U. Mooers, D. J. Hartshorne, and M. J. Siegman, "The myosin cross-bridge cycle and its control by twitchin phosphorylation in catch muscle," *Biophysical Journal*, vol. 80, no. 1, pp. 415–426, 2001.
- [85] A. V. Somlyo, Y. E. Goldman, T. Fujimori, M. Bond, D. R. Trentham, and A. P. Somlyo, "Cross-bridge kinetics, cooperativity, and negatively strained cross-bridges in vertebrate smooth muscle. A laser-flash photolysis study," *Journal of General Physiology*, vol. 91, no. 2, pp. 165–192, 1988.
- [86] C.-M. Hai and R. A. Murphy, "Cross-bridge phosphorylation and regulation of latch state in smooth muscle," *American Journal of Physiology*, vol. 254, no. 1, pp. C99–C106, 1988.
- [87] T. B. Vyas, S. U. Mooers, S. R. Narayan, J. C. Witherell, M. J. Siegman, and T. M. Butler, "Cooperative activation of myosin by light chain phosphorylation in permeabilized smooth muscle," *American Journal of Physiology*, vol. 263, no. 1, pp. C210–C219, 1992.
- [88] T. B. Vyas, S. U. Mooers, S. R. Narayan, M. J. Siegman, and T. M. Butler, "Cross-bridge cycling at rest and during activation: turnover of myosin-bound ADP in permeabilized smooth muscle," *Journal of Biological Chemistry*, vol. 269, no. 10, pp. 7316–7322, 1994.
- [89] C. M. Rembold, R. L. Wardle, C. J. Wingard, T. W. Batts, E. F. Etter, and R. A. Murphy, "Cooperative attachment of cross bridges predicts regulation of smooth muscle force by myosin phosphorylation," *American Journal of Physiology—Cell Physiology*, vol. 287, no. 3, pp. C594–C602, 2004.
- [90] P. A. Ellison, J. R. Sellers, and C. R. Cremona, "Kinetics of smooth muscle heavy meromyosin with one thiophosphorylated head," *Journal of Biological Chemistry*, vol. 275, no. 20, pp. 15142–15151, 2000.
- [91] H. Tanaka, K. Homma, H. D. White, T. Yanagida, and M. Ikebe, "Smooth muscle myosin phosphorylated at single

- head shows sustained mechanical activity," *Journal of Biological Chemistry*, vol. 283, no. 23, pp. 15611–15618, 2008.
- [92] A. Khromov, A. V. Somlyo, D. R. Trentham, B. Zimmermann, and A. P. Somlyo, "The role of MgADP in force maintenance by dephosphorylated cross-bridges in smooth muscle: a flash photolysis study," *Biophysical Journal*, vol. 69, no. 6, pp. 2611–2622, 1995.
- [93] S.-N. Yu, P. E. Crago, and H. J. Chiel, "A nonisometric kinetic model for smooth muscle," *American Journal of Physiology*, vol. 272, no. 3, pp. C1025–C1039, 1997.
- [94] A. F. Straight, A. Cheung, J. Limouze, et al., "Dissecting temporal and spatial control of cytokinesis with a myosin II inhibitor," *Science*, vol. 299, no. 5613, pp. 1743–1747, 2003.
- [95] J. Limouze, A. F. Straight, T. Mitchison, and J. R. Sellers, "Specificity of blebbistatin, inhibitor of myosin II," *Journal of Muscle Research and Cell Motility*, vol. 25, no. 4-5, pp. 337–341, 2004.
- [96] M. Kovacs, J. Toth, C. Hetenyi, A. Malnasi-Csizmadia, and J. R. Sella, "Mechanism of blebbistatin inhibition of myosin II," *Journal of Biological Chemistry*, vol. 279, no. 34, pp. 35557–35563, 2004.
- [97] J. S. Allingham, R. Smith, and I. Rayment, "The structural basis of blebbistatin inhibition and specificity for myosin II," *Nature Structural and Molecular Biology*, vol. 12, no. 4, pp. 378–379, 2005.
- [98] T. M. Butler, S. U. Mooers, and M. J. Siegman, "Catch force links and the low to high force transition of myosin," *Biophysical Journal*, vol. 90, no. 9, pp. 3193–3202, 2006.
- [99] S. V. Avrova, N. S. Shelud'ko, Y. S. Borovikov, and S. Galler, "Twitchin of mollusc smooth muscles can induce "catch"-like properties in human skeletal muscle: support for the assumption that the "catch" state involves twitchin linkages between myofilaments," *Journal of Comparative Physiology B*, vol. 179, no. 8, pp. 945–950, 2009.
- [100] Y. Tsutsui, M. Yoshio, K. Oiwa, and A. Yamada, "Striated muscle twitchin of bivalves has "catchability", the ability to bind thick filaments tightly to thin filaments, representing the catch state," *Journal of Molecular Biology*, vol. 365, no. 2, pp. 325–332, 2007.
- [101] A. Yamada, N. Ishii, T. Shimmen, and K. Takahashi, "Mg-ATPase activity and motility of native thick filaments isolated from the anterior byssus retractor muscle of *Mytilus edulis*," *Journal of Muscle Research and Cell Motility*, vol. 10, no. 2, pp. 124–134, 1989.
- [102] N. S. Shelud'ko, O. S. Matusovsky, T. V. Permyakova, and G. G. Matusovskaya, "Twitchin-actin linkage hypothesis" for the catch mechanism in molluscan muscles: evidence that twitchin interacts with myosin, myosin rod, and paramyosin core and affects properties of actomyosin," *Archives of Biochemistry and Biophysics*, vol. 466, pp. 125–135, 2007.
- [103] N. S. Shelud'ko, G. G. Matusovskaya, T. V. Permyakova, and O. S. Matusovsky, "Twitchin, a thick-filament protein from molluscan catch muscle, interacts with F-actin in a phosphorylation-dependent way," *Archives of Biochemistry and Biophysics*, vol. 432, no. 2, pp. 269–277, 2004.
- [104] D. Funabara, C. Hamamoto, K. Yamamoto, et al., "Unphosphorylated twitchin forms a complex with actin and myosin that may contribute to tension maintenance in catch," *Journal of Experimental Biology*, vol. 210, no. 24, pp. 4399–4410, 2007.
- [105] D. Funabara, R. Osawa, M. Ueda, S. Kanoh, D. J. Hartshorne, and S. Watabe, "Myosin loop 2 is involved in the formation of a trimeric complex of twitchin, actin, and myosin," *Journal of Biological Chemistry*, vol. 284, no. 27, pp. 18015–18020, 2009.
- [106] J. F. Shaffer, R. W. Kensler, and S. P. Harris, "The myosin-binding protein C motif binds to F-actin in a phosphorylation-sensitive manner," *Journal of Biological Chemistry*, vol. 284, no. 18, pp. 12318–12327, 2009.
- [107] M. Gruen and M. Gautel, "Mutations in β -myosin S2 that cause familial hypertrophic cardiomyopathy (FHC) abolish the interaction with the regulatory domain of myosin-binding protein-C," *Journal of Molecular Biology*, vol. 286, no. 3, pp. 933–949, 1999.
- [108] M. Gruen, H. Prinz, and M. Gautel, "cAPK-phosphorylation controls the interaction of the regulatory domain of cardiac myosin binding protein C with myosin-S2 in an on-off fashion," *FEBS Letters*, vol. 453, no. 3, pp. 254–259, 1999.

Review Article

Titin Diversity—Alternative Splicing Gone Wild

Wei Guo, Sheila J. Bharmal, Karla Esbona, and Marion L. Greaser

Muscle Biology Laboratory, University of Wisconsin-Madison, Madison, WI 53706, USA

Correspondence should be addressed to Marion L. Greaser, mgreaser@ansci.wisc.edu

Received 1 December 2009; Accepted 13 January 2010

Academic Editor: Henk L. M. Granzier

Copyright © 2010 Wei Guo et al. This is an open access article distributed under the Creative Commons Attribution License, which permits unrestricted use, distribution, and reproduction in any medium, provided the original work is properly cited.

Titin is an extremely large protein found in highest concentrations in heart and skeletal muscle. The single mammalian gene is expressed in multiple isoforms as a result of alternative splicing. Although titin isoform expression is controlled developmentally and in a tissue specific manner, the vast number of potential splicing pathways far exceeds those described in any other alternatively spliced gene. Over 1 million human splice pathways for a single individual can be potentially derived from the PEVK region alone. A new splicing pattern for the human cardiac N2BA isoform type has been found in which the PEVK region includes only the N2B type exons. The alterations in splicing and titin isoform expression in human heart disease provide impetus for future detailed study of the splicing mechanisms for this giant protein.

1. Introduction

Titin is the third most abundant protein (after myosin and actin) in vertebrate striated muscle, with an average adult human containing ~0.5 kg [1]. This extremely large protein [2], which is also known as connectin [3], spans each half sarcomere from the Z-line to the M-line or center of the sarcomere [4, 5] (Figure 1). The C-terminal A-band segment of titin is attached to the thick filament via multiple binding sites for myosin and C-protein [6] and two C-terminal titin regions from adjacent half-sarcomeres overlap in the M-line region of the sarcomere [7]. Similarly titin's N-terminal segment is anchored in the Z-disk and overlaps another titin N-terminus from the adjacent sarcomere [8]. Titin thus constitutes a continuous filament system along the myofibril. Titin is believed to function as a template in sarcomere assembly and for maintenance of sarcomere integrity [9, 10] (Figure 1). These concepts have been confirmed by recent work showing that titin loss in long-term disuse of skeletal muscle results in the disorganization of the ordered sarcomeric structure [11, 12]. Each end of the thick filament is linked to the nearest Z-disk by titin. This provides axial continuity for the production of resting tension and maintains the thick filament in the center of sarcomere during generation of active force [13]. Titin's several extensible elements establish titin as a critical, multi-functional sarcomeric component. These extensible elements

are composed of (1) Tandem Ig segments (consisting of serially linked immunoglobulin-like domains), (2) the PEVK region (so called for its high content of proline (P), glutamate (E), valine (V), and lysine (K) residues), and (3) the cardiac-specific N2B unique sequence (N2B-U_s) (Figure 1). In slack sarcomeres the tandem Ig and PEVK segments are collapsed. Upon initial stretch, the collapsed tandem Ig segments are straightened while their individual Ig domains remained folded. With further stretch the PEVK region extends [14, 15]. Modeling tandem Ig and PEVK segments as entropic springs with different bending rigidities indicated that in the physiological SL range (a) the Ig-like domains of the tandem Ig segments remain folded and (b) the PEVK segment behaves as a permanently unfolded polypeptide [16–19]. The cardiac-specific N2B unique sequence (N2B-U_s) forms a third spring element in cardiac titin and provides extensibility at the upper range of physiological sarcomere lengths in the heart [17, 20–23].

The original description of titin isoforms suggested that the N2B unique sequence occurred in cardiac muscle and a different unique region called N2A was found only in skeletal muscles. Names of the full isoforms in these tissues were then N2B and N2A, respectively [5]. It was later found that the myocardium expresses two major classes of titin isoforms: a smaller N2B and a larger N2BA that contained both the N2B and N2A unique sequences [24, 25] (Figure 2). All these known titin isoforms contain PEVK and tandem Ig segments

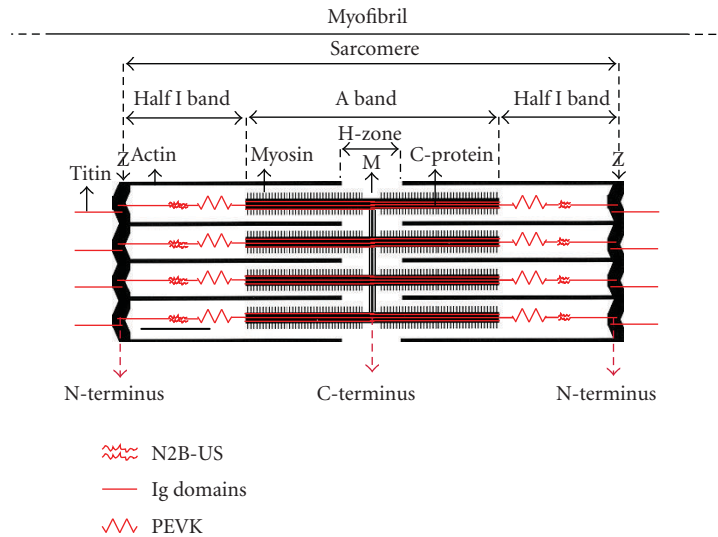


FIGURE 1: Titin location and arrangement in the cardiac sarcomere.

[5, 25, 26]. The N2B isoform has fewer Ig domains and a short PEVK region; the N2A class of isoforms contains more Ig domains and a somewhat longer PEVK region. Nearly all Z-disk and A-band/M-band titin domains are constitutively expressed in titin isoforms of human cardiac muscle. The main titin differential splicing occurs in the middle Ig and PEVK domains of the I-band-titin segment [24, 27].

The current review will discuss the isoforms of titin and the alternative splicing patterns that lead to the different forms. A number of excellent reviews should be consulted for further details on the structure and function of titin [6, 19, 28–33].

2. Electrophoresis Detection of Titin

Titin is the biggest protein in the human body, and there are a number of size variants. The earliest reports indicated that there were two electrophoretic bands: a larger T1 (which was the full length version) and T2 (a proteolytic fragment extending from the PEVK region through the carboxyl terminal M line end) [2]. Because of titin's extremely large size, migration is minimal in typical SDS polyacrylamide gels, and it has been difficult to develop a reliable and quantitative gel procedure. An earlier study used 3.3–12% gradient polyacrylamide gels to detect and quantify titin and nebulin from short segments of single muscle fibers [34]. This system separated titin T1 (intact titin, Mr ~3300kDa) and T2 (breakdown product of titin, Mr ~2000kDa). Another group employed 2% polyacrylamide slab gels strengthened with agarose to resolve two T1 bands plus the T2 [35]. More recently 2–9.5% acrylamide gradient gels have been used to separate the large titin isoforms and fragments [25]. These gels showed that the T1 mobility varied greatly between muscle sources, reflecting the difference in molecular mass of the 3.7-MDa soleus titin and the 2.97-MDa rat cardiac titin isoform. The two major T1 bands were ascribed to the titin isoforms N2B and N2BA in cardiac muscle.

However, the gels mentioned above are physically difficult to work with, are more complex to pour, and often undergo distortion or tearing during fixing and staining. It is also very difficult to transfer large proteins out of acrylamide gels for Western blotting. More recently our group has developed a different more reliable and reproducible system called vertical SDS-agarose gel electrophoresis (VAGE) [36]. This method employs Sea Kem Gold agarose and allows high-resolution separation of titin isoforms. In addition the blot transfer efficiency was almost 100% [36]. This system can also be easily adapted for the characterization of other very large proteins from a variety of sources.

The SDS agarose system resolves at least four classes of N2BA titin isoforms. Two rat embryonic/neonatal forms (N2BA-N1; N2BA-N2) with apparent sizes of approximately 3710 and 3590kDa, respectively, are found during late embryonic and immediately after birth [37]. These are gradually replaced by two adult forms (N2BA-A1; N2BA-A2) with sizes of 3390 and 3220. It has been postulated that these shorter versions are due to deletion of large numbers of exons from the exon 50 to 71 and 50 to 90 middle Ig regions (see below) [37].

3. Titin Tissue and Species cDNA Sequence Comparisons

Early cDNA sequencing of titin from human cardiac and soleus indicated that both isoforms were derived from a single gene and obtained by alternative splicing [5, 24]. The single titin gene contained 363 exons [27]. The complete cDNA and genomic sequence determination of human cardiac titin have provided a template for later study of titin splicing variants.

3.1. M Line Region. Kolmerer and coworkers [39] searched for alternatively expressed exons in the M-line region of titin and found that six exons (called Mex1 to 6) coded for the

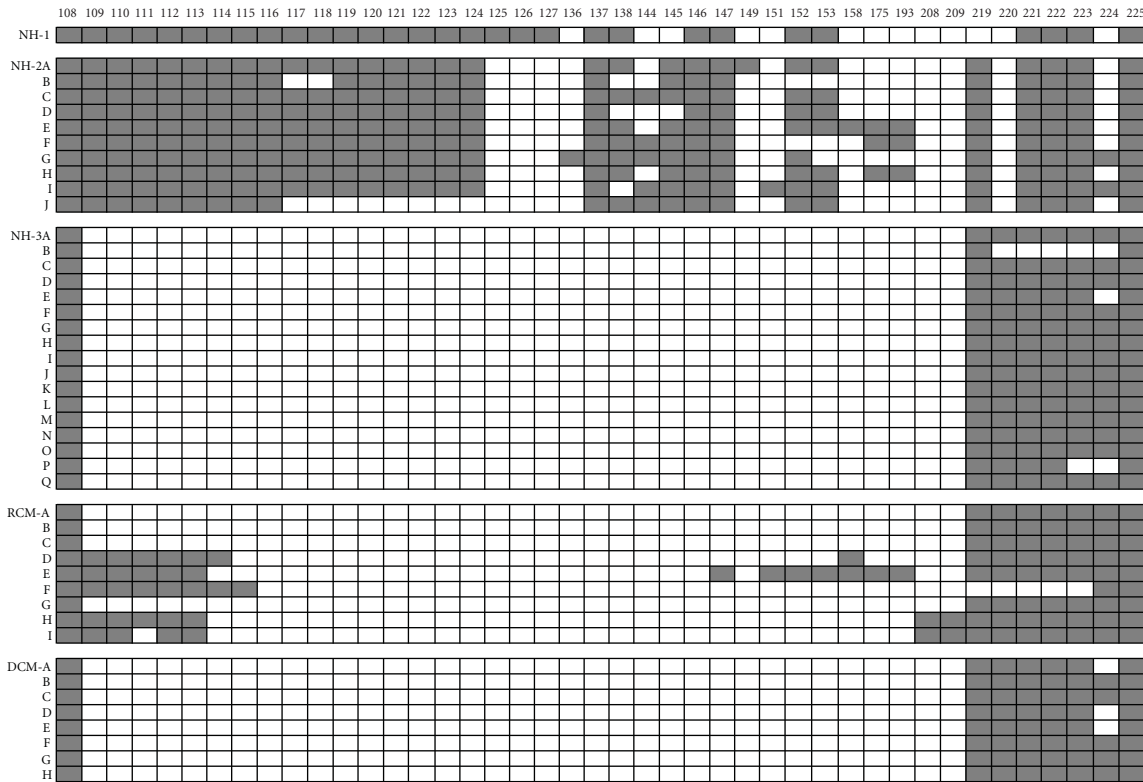


FIGURE 3: Exon inclusion in clones from the human titin PEVK region. Data from left ventricle samples of five different individuals—three normal (NH-1, NH-2, NH-3), one restrictive cardiomyopathy (RCM), and one dilated cardiomyopathy (DCM). Exon number is listed across the top. Filled boxes denote exon inclusion. Letter designations in each block refer to separate clones from each individual. Clones were obtained by PCR amplification after RT-PCR using primers from exons 108 and 225. Full details on the methods have been published [38]. Data from sample NH-1 is from [38] and for NH-2 clones from [37].

ventricle short PEVK peptide contains a deletion of 53 amino acid residues from the amino terminal end of the N2B PEVK region (corresponding to exons 219 and 220). The absence of exon 224 also occurs in some clones from human heart (see Figure 3 and discussion below).

Variable numbers of titin exons between 50 and 219, including the N2A unique region, are expressed in cardiac and skeletal muscle. This splicing pattern gives rise to the N2A protein isoforms in skeletal muscle and the N2BA isoforms in cardiac muscle [24, 27]. N2BA isoforms (containing both N2A and N2B unique elements) have multiple splicing pathways in the I27 to I68 segment (Figure 2). Splice pathways have been identified between I27 (exon 50) and exons 51, 70, 71, 75, 77, 80, and 90 [24, 38]. The expression of more middle Ig domains in fetal rat ventricle is consistent with the larger size of fetal titin N2BA isoforms observed by electrophoresis [37].

The N2B unique exon 49 is excluded in skeletal muscles by splicing together I15 to I27, and only human soleus muscle expresses consecutive exons between 50 and 102 (I27 to I79). Rabbit psoas muscle skips I30 to I47 (Figure 2). Altogether, skeletal titin transcripts always include the N2A segment and exclude the N2B exon; cardiac titins always include the N2B exon [24].

The N2BA PEVK region has an exceptionally varied pattern of splicing (Figure 3). Initial studies with dog cardiac muscle resulted in six clones (A46 A-F) [38], all from the same PCR amplification, having different exon patterns and PEVK lengths (703, 788, 894, 900, 703, and 819 amino acids respectively). Subsequent work with the human PEVK revealed that 10 different clones from a single individual had 10 different patterns of splicing [26]. In addition a completely new pattern of N2BA splicing has been recently obtained in which exon 108, found only in N2BA isoforms, was directly linked to the constitutively expressed PEVK cluster in the 219 to 225 exon region (Figure 3). This so-called “short PEVK N2BA” class of isoforms has been observed in clones from both healthy and diseased hearts. Such a pattern would result in titin molecules with apparently less potential PEVK extension during stretch and thus leads to a stiffer sarcomere. It is not clear whether such message types are expressed into protein and whether there are a significant proportion of such messages transcribed to affect the passive tension. However, if an increased proportion of these splicing products occurred with aging, for example, it might partially explain the increased cardiac stiffness that often occurs during the later period of life.

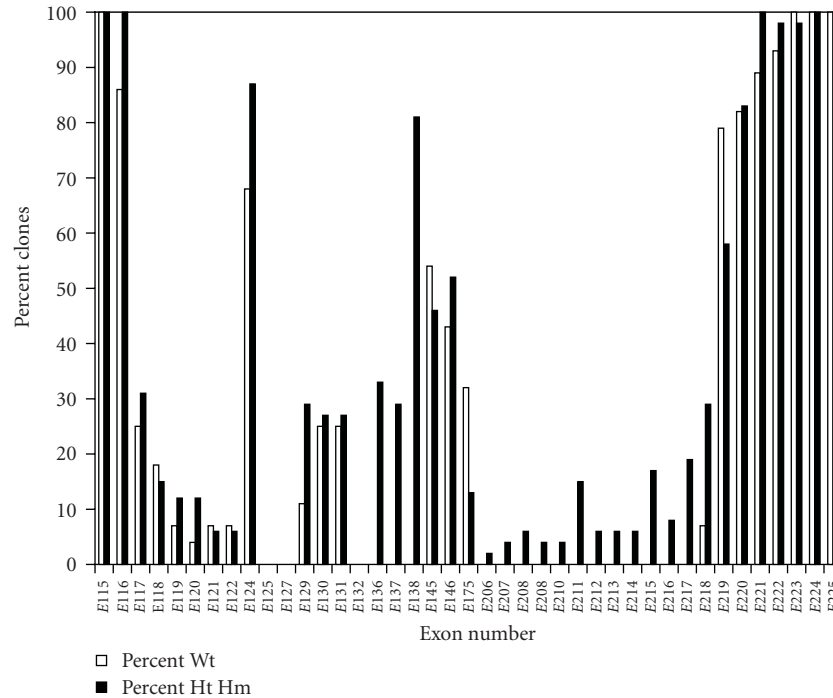


FIGURE 4: Exon inclusion in clones from rat left ventricle of wild type and mutant rats. The percent of clones that contain the exons shown is plotted versus exon position. Only exons 115, 224, and 225 were found in all wild type and mutant clones (heterozygote [Ht] and homozygote [Hm]). Data was pooled from four different ages [47].

A mutant rat model has been recently described that results in significant alterations in titin isoform expression [26, 47]. Homozygous mutants express a giant titin with apparent size on SDS agarose gels of about 3.9 MDa. This is larger than the size of titin from human soleus (3.7 MDa). Since the soleus sequence includes all the middle Ig domains and virtually all the Ig domains from the rest of the gene, it was initially assumed that the mutant rat heart must then express the full PEVK exon cohort plus the N2B unique region. Sequences obtained from PCR clones bridging the exon 108 to 225 region were not much larger than those from wild type [47]. Comparisons of exon expression between wild type and mutants showed some differences, primarily in the exon region between 175 and 219 typically associated with fetal exons (Figure 2) [26, 48]. Thus it appears that more than one mechanism must be involved in titin splicing. The lack of additional PEVK exons in the mutants exacerbates the mass calculation. The inclusion of the N2B unique region would add some mass, but the possible inclusion of exon 48 would add 243 kDa. This idea remains to be verified.

The number of potential PEVK splice variants is huge. Among the ten clones from the normal human 2 in Figure 3 human clones listed, there are 20 exons that are not present in all clones. If all these splicing events were independent, this means that there are 2^{20} combinations, a total of 1,048,576 possible pathways. This far exceeds the approximately 38,016 potential splice variants identified previously with the Dscam (Down syndrome cell adhesion molecule) gene [49, 50]. If all the clones in this table from 5 different individuals are

included, then there are 38 differential exons and the number of potential clones exceeds 274 billion.

Microarrays have also been used to compare tissue sources for exon expression [48, 51]. Fetal titins express more middle Ig domains and additional PEVK exons. These results are consistent with the cloning and sequencing results [37]. The identification of exon 156 as skeletal muscle specific [48] is also consistent with the absence of this exon from every human (Figure 4) and rat cardiac clone we have sequenced [47]. Microarrays give more global information since all messages from a sample are included. Their disadvantages include the fact that almost no splicing information can be obtained and the results include pooled data from all titins in the sample, including the Novex isoforms. Additionally the duplication of three segments of the titin gene in the region of the PEVK [27] means that some microarray probes are identical. The cloning approach yields actual splice patterns. The major disadvantages include the fact that only possible splice patterns are sampled and that identified clones may not adequately represent, either quantitatively or qualitatively, the actual tissue patterns. However, the cloning approach has verified that titin splicing is highly diverse, and this complicates interpretation of mechanical experiments.

4. The Ratio of Titin Isoforms and Heart Disease

Titin isoform splicing not only generates diversity of titin isoforms in skeletal muscle [52], but also results in changes of

the ratio of titin isoforms (N2BA/N2B) during heart development. Before birth, mammalian heart mainly expresses more compliant N2BA isoforms. During perinatal heart development the larger N2BA isoform is gradually replaced by a smaller isoform N2B, and the N2B isoform becomes the predominant titin isoform in the adult left ventricles (LV) of smaller mammalian species [37, 53, 54]. The N2BA titin isoform prevails over N2B in the adult hearts of larger mammals, including humans [25, 55]. Recent studies have shown that the ratio of titin isoforms is altered in some heart diseases. A canine tachycardia-induced model of dilated cardiomyopathy (DCM) used to understand titin response to a chronic mechanical challenge of the heart indicated that two weeks of pacing gives rise to an exaggerated transmural titin isoform ratio gradient [56] and four weeks of pacing results in a decrease of the N2BA/N2B titin ratio, accompanied by an increase in titin-based passive tension [57]. Another study of spontaneously hypertensive rat model (SHR) also showed a reduced ratio of N2BA/N2B titin in response to pressure overload, consistent with elevated passive tension of heart [58]. More recent analyses showed that the left ventricle biopsies from patients with diastolic heart failure (HF) had a reduced N2BA/N2B titin [59]. Chronically ischemic LVs of coronary-artery-disease (CAD) patients with congestive heart failure (HF) had nearly 50% N2BA titin (compared to N2BA+N2B) while approximate 30% N2BA was found in the LVs of control donor patients [60]. Analysis of explanted nonischemic human DCM hearts again demonstrated increased proportions of N2BA/N2B [61, 62]. These results are similar to the recently described rat model with lower ejection fraction (unpublished data) which expresses the N2BA isoform almost exclusively [26, 47]. Long-term hypothyroidism (which results in diastolic dysfunction) changed the titin isoform ratios as well. Propylthiouracil (PTU) treatment in rats induced the expression of additional cardiac PEVK and I domain exons similar to those in the large titin isoform of the fetal heart. Consequently, titin-based passive and restoring forces were found to be significantly reduced in cardiac muscle of PTU-treated rats [63, 64]. The mechanisms controlling titin splicing remain unknown, but the ability to manipulate the splicing of this protein has great potential for affecting human health.

Acknowledgment

This work was supported by the University of Wisconsin-Madison College of Agricultural and Life Sciences and a grant from the National Institutes of Health (HL77196).

References

- [1] S. Labeit, B. Kolmerer, and W. A. Linke, "The giant protein titin: emerging roles in physiology and pathophysiology," *Circulation Research*, vol. 80, no. 2, pp. 290–294, 1997.
- [2] K. Wang, J. McClure, and A. Tu, "Titin: major myofibrillar components of striated muscle," *Proceedings of the National Academy of Sciences of the United States of America*, vol. 76, no. 8, pp. 3698–3702, 1979.

- [3] K. Maruyama, "Connectin, an elastic protein from myofibrils," *Journal of Biochemistry*, vol. 80, no. 2, pp. 405–407, 1976.
- [4] D. O. Furst, M. Osborn, R. Nave, and K. Weber, "The organization of titin filaments in the half-sarcomere revealed by monoclonal antibodies in immunoelectron microscopy: a map of ten nonrepetitive epitopes starting at the Z-line extends close to the M line," *Journal of Cell Biology*, vol. 106, no. 5, pp. 1563–1572, 1988.
- [5] S. Labeit and B. Kolmerer, "Titins: giant proteins in charge of muscle ultrastructure and elasticity," *Science*, vol. 270, no. 5234, pp. 293–296, 1995.
- [6] J. Trinick and L. Tskhovrebova, "Titin: a molecular control freak," *Trends in Cell Biology*, vol. 9, no. 10, pp. 377–380, 1999.
- [7] W. M. J. Obermann, M. Gautel, F. Steiner, P. F. M. van der Ven, K. Weber, and D. O. Furst, "The structure of the sarcomeric M band: localization of defined domains of myomesin, M-protein, and the 250-kD carboxy-terminal region of titin by immunoelectron microscopy," *Journal of Cell Biology*, vol. 134, no. 6, pp. 1441–1453, 1996.
- [8] C. C. Gregorio, K. Trombitás, T. Centner, et al., "The NH2 terminus of titin spans the Z-disc: its interaction with a novel 19-kD ligand (T-cap) is required for sarcomeric integrity," *Journal of Cell Biology*, vol. 143, no. 4, pp. 1013–1027, 1998.
- [9] L. Tskhovrebova and J. Trinick, "Titin: properties and family relationships," *Nature Reviews Molecular Cell Biology*, vol. 4, no. 9, pp. 679–689, 2003.
- [10] H. L. Granzier and S. Labeit, "The giant protein titin: a major player in myocardial mechanics, signaling, and disease," *Circulation Research*, vol. 94, no. 3, pp. 284–295, 2004.
- [11] J. Udaka, S. Ohmori, T. Terui, et al., "Disuse-induced preferential loss of the giant protein titin depresses muscle performance via abnormal sarcomeric organization," *Journal of General Physiology*, vol. 131, no. 1, pp. 33–41, 2008.
- [12] N. Fukuda, H. L. Granzier, S. Ishiwata, and S. Kurihara, "Physiological functions of the giant elastic protein titin in mammalian striated muscle," *Journal of Physiological Sciences*, vol. 58, no. 3, pp. 151–159, 2008.
- [13] R. Horowitz, E. S. Kempner, M. E. Bisher, and R. J. Podolsky, "A physiological role for titin and nebulin in skeletal muscle," *Nature*, vol. 322, no. 6084, pp. 160–164, 1986.
- [14] W. A. Linke, M. Ivemeyer, N. Olivieri, B. Kolmerer, J. C. Ruegg, and S. Labeit, "Towards a molecular understanding of the elasticity of titin," *Journal of Molecular Biology*, vol. 261, no. 1, pp. 62–71, 1996.
- [15] K. Trombitás, M. Greaser, S. Labeit, et al., "Titin extensibility in situ: entropic elasticity of permanently folded and permanently unfolded molecular segments," *Journal of Cell Biology*, vol. 140, no. 4, pp. 853–859, 1998.
- [16] M. S. Z. Kellermayer, S. B. Smith, H. L. Granzier, and C. Bustamante, "Folding-unfolding transitions in single titin molecules characterized with laser tweezers," *Science*, vol. 276, no. 5315, pp. 1112–1116, 1997.
- [17] K. Watanabe, P. Nair, D. Labeit, et al., "Molecular mechanics of cardiac titin's PEVK and N2B spring elements," *Journal of Biological Chemistry*, vol. 277, no. 13, pp. 11549–11558, 2002.
- [18] H. Li, W. A. Linke, A. F. Oberhauser, et al., "Reverse engineering of the giant muscle protein titin," *Nature*, vol. 418, no. 6901, pp. 998–1002, 2002.
- [19] H. Granzier and S. Labeit, "Cardiac titin: an adjustable multi-functional spring," *Journal of Physiology*, vol. 541, no. 2, pp. 335–342, 2002.
- [20] M. Helmes, K. Trombitás, T. Centner, et al., "Mechanically driven contour-length adjustment in rat cardiac titin's unique

- N2B sequence: titin is an adjustable spring,” *Circulation Research*, vol. 84, no. 11, pp. 1339–1352, 1999.
- [21] W. A. Linke, D. E. Rudy, T. Centner, et al., “I-band titin in cardiac muscle is a three-element molecular spring and is critical for maintaining thin filament structure,” *Journal of Cell Biology*, vol. 146, no. 3, pp. 631–644, 1999.
 - [22] K. Trombitas, A. Freiburg, T. Centner, S. Labeit, and H. Granzier, “Molecular dissection of N2B cardiac titin’s extensibility,” *Biophysical Journal*, vol. 77, no. 6, pp. 3189–3196, 1999.
 - [23] K. Trombitas, A. Redkar, T. Centner, Y. Wu, S. Labeit, and H. Granzier, “Extensibility of isoforms of cardiac titin: variation in contour length of molecular subsegments provides a basis for cellular passive stiffness diversity,” *Biophysical Journal*, vol. 79, no. 6, pp. 3226–3234, 2000.
 - [24] A. Freiburg, K. Trombitas, W. Hell, et al., “Series of exon-skipping events in the elastic spring region of titin as the structural basis for myofibrillar elastic diversity,” *Circulation Research*, vol. 86, no. 11, pp. 1114–1121, 2000.
 - [25] O. Cazorla, A. Freiburg, M. Helmes, et al., “Differential expression of cardiac titin isoforms and modulation of cellular stiffness,” *Circulation Research*, vol. 86, no. 1, pp. 59–67, 2000.
 - [26] M. L. Greaser, P. R. Krzesinski, C. M. Warren, B. Kirkpatrick, K. S. Campbell, and R. L. Moss, “Developmental changes in rat cardiac titin/connectin: transitions in normal animals and in mutants with a delayed pattern of isoform transition,” *Journal of Muscle Research and Cell Motility*, vol. 26, no. 6–8, pp. 325–332, 2005.
 - [27] M.-L. Bang, T. Centner, F. Fornoff, et al., “The complete gene sequence of titin, expression of an unusual \approx 700-kDa titin isoform, and its interaction with obscurin identify a novel Z-line to I-band linking system,” *Circulation Research*, vol. 89, no. 11, pp. 1065–1072, 2001.
 - [28] K. Wang, “Titin/connectin and nebulin: giant protein rulers of muscle structure and function,” *Advances in Biophysics*, vol. 33, pp. 123–134, 1996.
 - [29] K. Maruyama, “Connectin/titin, giant elastic protein of muscle,” *FASEB Journal*, vol. 11, no. 5, pp. 341–345, 1997.
 - [30] C. C. Gregorio, H. Granzier, H. Sorimachi, and S. Labeit, “Muscle assembly: a titanic achievement?” *Current Opinion in Cell Biology*, vol. 11, no. 1, pp. 18–25, 1999.
 - [31] M. M. LeWinter, Y. Wu, S. Labeit, and H. Granzier, “Cardiac titin: structure, functions and role in disease,” *Clinica Chimica Acta*, vol. 375, no. 1-2, pp. 1–9, 2007.
 - [32] W. A. Linke, “Sense and stretchability: the role of titin and titin-associated proteins in myocardial stress-sensing and mechanical dysfunction,” *Cardiovascular Research*, vol. 77, no. 4, pp. 637–648, 2008.
 - [33] M. Krüger and W. A. Linke, “Titin-based mechanical signalling in normal and failing myocardium,” *Journal of Molecular and Cellular Cardiology*, vol. 46, no. 4, pp. 490–498, 2009.
 - [34] H. L. M. Granzier and K. Wang, “Gel electrophoresis of giant proteins: solubilization and silver-staining of titin and nebulin from single muscle fiber segments,” *Electrophoresis*, vol. 14, no. 1-2, pp. 56–64, 1993.
 - [35] R. Tatsumi and A. Hattori, “Detection of giant myofibrillar proteins connectin and nebulin by electrophoresis in 2% polyacrylamide slab gels strengthened with agarose,” *Analytical Biochemistry*, vol. 224, no. 1, pp. 28–31, 1995.
 - [36] C. M. Warren, P. R. Krzesinski, and M. L. Greaser, “Vertical agarose gel electrophoresis and electroblotting of high-molecular-weight proteins,” *Electrophoresis*, vol. 24, no. 11, pp. 1695–1702, 2003.
 - [37] C. M. Warren, P. R. Krzesinski, K. S. Campbell, R. L. Moss, and M. L. Greaser, “Titin isoform changes in rat myocardium during development,” *Mechanisms of Development*, vol. 121, no. 11, pp. 1301–1312, 2004.
 - [38] M. L. Greaser, M. Berri, C. M. Warren, and P. E. Mozdziak, “Species variations in cDNA sequence and exon splicing patterns in the extensible I-band region of cardiac titin: relation to passive tension,” *Journal of Muscle Research and Cell Motility*, vol. 23, no. 5-6, pp. 473–482, 2002.
 - [39] B. Kolmerer, N. Olivieri, C. C. Witt, B. G. Herrmann, and S. Labeit, “Genomic organization of M line titin and its tissue-specific expression in two distinct isoforms,” *Journal of Molecular Biology*, vol. 256, no. 3, pp. 556–563, 1996.
 - [40] M. Sjöström and J. M. Squire, “Fine structure of the A band in cryo sections. The structure of the A band of human skeletal muscle fibres from ultra thin cryo sections negatively stained,” *Journal of Molecular Biology*, vol. 109, no. 1, pp. 49–68, 1977.
 - [41] A.-C. Edman, J. Lexell, M. Sjöström, and J. M. Squire, “Structural diversity in muscle fibres of chicken breast,” *Cell and Tissue Research*, vol. 251, no. 2, pp. 281–289, 1988.
 - [42] Z. A. Podlubnaya, M. D. Shpagina, and V. V. Lednev, “Manifestation of the stripes of minor proteins location in A-bands of rabbit cardiac myofibrils,” *Journal of Molecular Biology*, vol. 210, no. 3, pp. 655–658, 1989.
 - [43] E. Carlsson and L.-E. Thornell, “Diversification of the myofibrillar M-band in rat skeletal muscle during postnatal development,” *Cell and Tissue Research*, vol. 248, no. 1, pp. 169–180, 1987.
 - [44] H. T. Pask, K. L. Jones, P. K. Luther, and J. M. Squire, “M-band structure, M-bridge interactions and contraction speed in vertebrate cardiac muscles,” *Journal of Muscle Research and Cell Motility*, vol. 15, no. 6, pp. 633–645, 1994.
 - [45] M. Gautel, D. Goulding, B. Bullard, K. Weber, and D. O. Fürst, “The central Z-disk region of titin is assembled from a novel repeat in variable copy numbers,” *Journal of Cell Science*, vol. 109, no. 11, pp. 2747–2754, 1996.
 - [46] H. Sorimachi, S. Ishiura, and K. Suzuki, “Structure and physiological function of calpains,” *Biochemical Journal*, vol. 328, part 3, pp. 721–732, 1997.
 - [47] M. L. Greaser, C. M. Warren, K. Esbona, et al., “Mutation that dramatically alters rat titin isoform expression and cardiomyocyte passive tension,” *Journal of Molecular and Cellular Cardiology*, vol. 44, no. 6, pp. 983–991, 2008.
 - [48] S. Lahmers, Y. Wu, D. R. Call, S. Labeit, and H. Granzier, “Developmental control of titin isoform expression and passive stiffness in fetal and neonatal myocardium,” *Circulation Research*, vol. 94, no. 4, pp. 505–513, 2004.
 - [49] D. Schmucker, J. C. Clemens, H. Shu, et al., “Drosophila Dscam is an axon guidance receptor exhibiting extraordinary molecular diversity,” *Cell*, vol. 101, no. 6, pp. 671–684, 2000.
 - [50] C. Lee, N. Kim, M. Meenakshi Roy, and B. R. Graveley, “Massive expansions of Dscam splicing diversity via staggered homologous recombination during arthropod evolution,” *RNA*, vol. 16, no. 1, pp. 91–105, 2010.
 - [51] S. Labeit, S. Lahmers, C. Burkart, et al., “Expression of distinct classes of titin isoforms in striated and smooth muscles by alternative splicing, and their conserved interaction with filamins,” *Journal of Molecular Biology*, vol. 362, no. 4, pp. 664–681, 2006.
 - [52] L. G. Prado, I. Makarenko, C. Andresen, M. Krüger, C. A. Opitz, and W. A. Linke, “Isoform diversity of giant proteins in relation to passive and active contractile properties of rabbit skeletal muscles,” *Journal of General Physiology*, vol. 126, no. 5, pp. 461–480, 2005.
 - [53] C. A. Opitz, M. C. Leake, I. Makarenko, V. Benes, and W. A. Linke, “Developmentally regulated switching of titin size

- alters myofibrillar stiffness in the perinatal heart,” *Circulation Research*, vol. 94, no. 7, pp. 967–975, 2004.
- [54] C. A. Opitz and W. A. Linke, “Plasticity of cardiac titin/connectin in heart development,” *Journal of Muscle Research and Cell Motility*, vol. 26, no. 6–8, pp. 333–342, 2005.
- [55] C. Neagoe, C. A. Opitz, I. Makarenko, and W. A. Linke, “Gigantic variety: expression patterns of titin isoforms in striated muscles and consequences for myofibrillar passive stiffness,” *Journal of Muscle Research and Cell Motility*, vol. 24, no. 2-3, pp. 175–189, 2003.
- [56] S. P. Bell, L. Nyland, M. D. Tischler, M. McNabb, H. Granzier, and M. M. LeWinter, “Alterations in the determinants of diastolic suction during pacing tachycardia,” *Circulation Research*, vol. 87, no. 3, pp. 235–240, 2000.
- [57] Y. Wu, S. P. Bell, K. Trombitas, et al., “Changes in titin isoform expression in pacing-induced cardiac failure give rise to increased passive muscle stiffness,” *Circulation*, vol. 106, no. 11, pp. 1384–1389, 2002.
- [58] C. M. Warren, M. C. Jordan, K. P. Roos, P. R. Krzesinski, and M. L. Greaser, “Titin isoform expression in normal and hypertensive myocardium,” *Cardiovascular Research*, vol. 59, no. 1, pp. 86–94, 2003.
- [59] L. Van Heerebeek, A. Borbely, H. W. M. Niessen, et al., “Myocardial structure and function differ in systolic and diastolic heart failure,” *Circulation*, vol. 113, no. 16, pp. 1966–1973, 2006.
- [60] C. Neagoe, M. Kulke, F. Del Monte, et al., “Titin isoform switch in ischemic human heart disease,” *Circulation*, vol. 106, no. 11, pp. 1333–1341, 2002.
- [61] I. Makarenko, C. A. Opitz, M. C. Leake, et al., “Passive stiffness changes caused by upregulation of compliant titin isoforms in human dilated cardiomyopathy hearts,” *Circulation Research*, vol. 95, no. 7, pp. 708–716, 2004.
- [62] S. F. Nagueh, G. Shah, Y. Wu, et al., “Altered titin expression, myocardial stiffness, and left ventricular function in patients with dilated cardiomyopathy,” *Circulation*, vol. 110, no. 2, pp. 155–162, 2004.
- [63] Y. Wu, J. Peng, K. B. Campbell, S. Labeit, and H. Granzier, “Hypothyroidism leads to increased collagen-based stiffness and re-expression of large cardiac titin isoforms with high compliance,” *Journal of Molecular and Cellular Cardiology*, vol. 42, no. 1, pp. 186–195, 2007.
- [64] N. Fukuda, T. Terui, S. Ishiwata, and S. Kurihara, “Titin-based regulations of diastolic and systolic functions of mammalian cardiac muscle,” *Journal of Molecular and Cellular Cardiology*. In press.

Review Article

Roles of Titin in the Structure and Elasticity of the Sarcomere

Larissa Tskhovrebova and John Trinick

Institute for Molecular and Cellular Biology and Astbury Centre for Structural Molecular Biology, University of Leeds, Leeds LS2 9JT, UK

Correspondence should be addressed to John Trinick, j.trinick@leeds.ac.uk

Received 16 February 2010; Accepted 13 May 2010

Academic Editor: Aikaterini Kontrogianni-Konstantopoulos

Copyright © 2010 L. Tskhovrebova and J. Trinick. This is an open access article distributed under the Creative Commons Attribution License, which permits unrestricted use, distribution, and reproduction in any medium, provided the original work is properly cited.

The giant protein titin is thought to play major roles in the assembly and function of muscle sarcomeres. Structural details, such as widths of Z- and M-lines and periodicities in the thick filaments, correlate with the substructure in the respective regions of the titin molecule. Sarcomere rest length, its operating range of lengths, and passive elastic properties are also directly controlled by the properties of titin. Here we review some recent titin data and discuss its implications for sarcomere architecture and elasticity.

1. Introduction

The complex but extremely ordered structure of the sarcomere is the elemental force-producing machinery of striated muscles. Recent studies of sarcomere assembly [1, 2], protein turnover [1, 3], and signalling cascades [4, 5] provide new insights into the spectrum of intermolecular interactions that support sarcomere structure and function. There is increasing evidence that many of sarcomere properties involve the giant protein titin [2, 6–10].

The titin molecule is more than one micrometer long and *in situ* spans half the sarcomere, with the N-terminus in the Z-line and the C-terminus in the M-line (Figure 1(a)) [11–13]. Different isoforms (MW ~ 3.0–3.7 MDa [14]) vary in the size and structure of the elastic I-band part of the molecule, which connects the end of the thick filament to the Z-line, as well as in the Z- and M-line regions. The size and structure of the thick filament part of titin is conserved, which is consistent with the conserved structure of thick filaments in vertebrates. Sequence shows that titin consists mainly of about 300 domains similar to immunoglobulins (Ig, I-set) and fibronectins (Fn, type-3). The elastic I-band part consists mainly of Ig domains arranged in tandem. Near the N2-line in the I-band, this arrangement is interrupted by unique sequences that bridge the “proximal” and “distal” (to the Z-line) tandem-Ig segments. In contrast, the thick filament part of titin is formed by both Ig and Fn3 domains.

Purified titin molecules visualized by metal shadowing appear in electron micrographs as strings about one micrometer in length and four nanometers in diameter [15–18]. In negatively stained samples, a distinct “beads-on-the-string” appearance can be seen [15], showing the chain of Ig and Fn3-like domains [19, 20].

2. Titin Structure—Conformational Periodicity in the Thick Filament Region

Sequence shows that the titin Ig and Fn3 domains are arranged in long-range patterns or super-repeats. Two types of super-repeats are found in the constitutively expressed thick filament region [19–21]: seven consecutive copies of the seven-domain or small superrepeat occupy the N-terminal part of this region; these are followed by eleven copies of the eleven-domain large superrepeat. In the I-band region, only the differentially expressed Ig-segments have super-repeats: in human soleus isoform, the N-terminal three copies of a six-domain superrepeat are followed by three copies of a ten-domain superrepeat [22, 23]. In both A- and I-band regions, the super-repeats show increased sequence conservation between domains at comparable positions in the super-repeats.

The two super-repeats of Ig and Fn3 domains in A-band titin (Figure 1(b)) closely reflect the underlying periodic

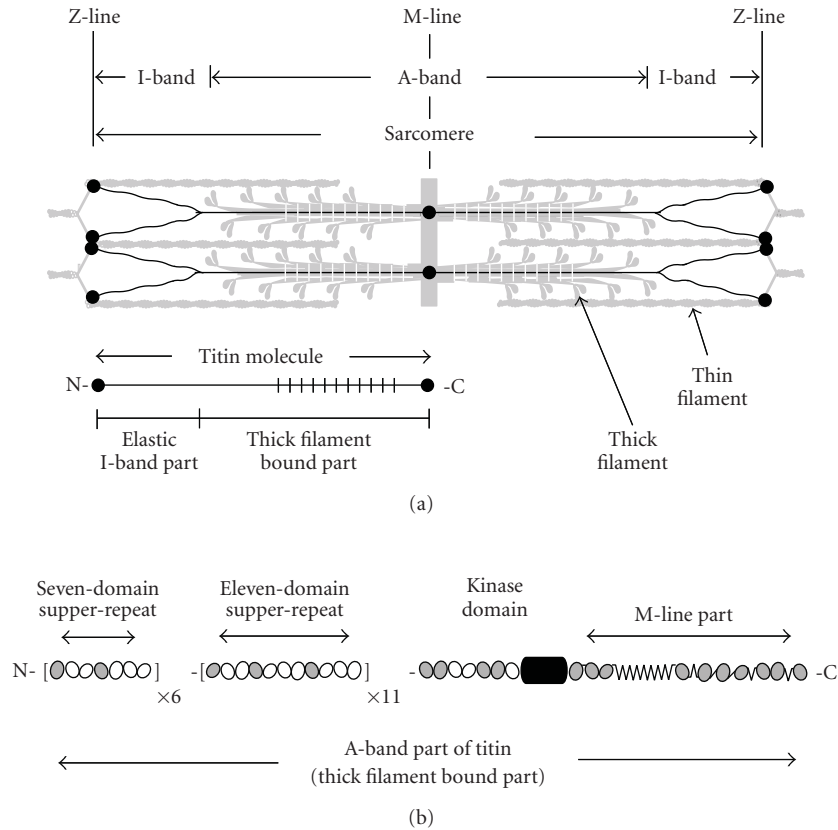


FIGURE 1: Schematic representation of titin layout in the sarcomere (a) and of the domain periodicity in the thick filament bound part (b). Striated zones in the sarcomere and the titin molecule (a) show the location of the large superrepeat.

structure of the thick filament. The size of the large superrepeat (~ 45 nm) is same as the myosin and C-protein periodicities of the filament, while the number of the large super-repeats (eleven) is the same as the number of binding sites for C-protein and related molecules. A single Ig domain in each large superrepeat binds C-protein and this defines the ~ 43 nm interval of C-protein localization in the C-zone [24]. Interactions between titin and myosin are probably grouped in three clusters of Fn3 domains, defining a period of ~ 15 nm in titin-myosin interactions [19].

Atomic structures of recombinant titin fragments, supported by homology modelling [25, 26], indicate that the Ig and Fn3 domains are unlikely to be similarly oriented along a titin molecule but bend and twist relative to each other. The likelihood of periodic interactions with other thick filament proteins requires titin domains spaced by 43 nm to be in the same orientation. This indicates that in the A-band the orientation of Ig and Fn3 domains in the super-repeats is periodically repeated.

There are only two main possibilities for such periodic architecture: either planar and zigzag-like or three-dimensional and helical. Homology modelling [26, 27] and crystallography studies [28, 29] show that small, two- or three-domain recombinant fragments have rather flat conformations, in which the long axes of the molecules

bend in a single plane. However, longer segments may well have a tendency to bend three-dimensionally, as suggested by modelling of the periodic differentially expressed I-band Ig-segment [30]. The latter shape is supported by electron microscopy of purified titin also suggesting helicity [31]. A tendency of the relaxed titin molecule to adopt a helical conformation is likely to be controlled by a preferred inter-domain orientation [25, 30, 32] and may reflect a long-distance directional regularity in the bending and twisting angles. The existing atomic structures of titin fragments appear to be consistent with this possibility [30], although the number of these is still too small to discern a long-distance pattern.

Another important question concerning titin interactions with other thick filament proteins is the significance of the fact that super-repeats in the A-band titin, although very similar, are not identical. Average sequence identity, even for domains at comparable positions, is below 40% [27], and only about 60% of their surface is conserved [33]. It is unclear at present how these small differences affect periodic interactions of titin with C-protein and myosin, both of which provide identical sites for interaction with super-repeats. It may be noted, however, that if there are dissimilar titin-myosin and titin-C-protein interactions in different super-repeats, this would agree with predictions

of nonequivalency of the ~ 43 nm repeats in thick filament structure suggested by X-ray diffraction studies of muscle [34].

3. Titin Flexibility—Persistence Length of the Elastic I-Band Region

Providing elasticity to sarcomeres is one of the major functions of titin [35–39]. This role derives from the ability of titin to increase the length under applied force and then to shorten to the original length when the force is removed. The mechanism of extensibility is known to be multiphase: overall shape changes that occur under small applied forces are followed at higher forces by hierarchical unfolding of the polypeptide [40–43]. While the physiological relevance of relatively large sarcomere lengths that lead to titin unfolding can be disputed, there is no doubt that conformational changes must occur in the molecule during both passive extension and active contraction of muscle. However, the exact pattern of these changes remains unknown. It is generally thought that they are entropic in nature and occur according to rod-coil transitions seen in individual titin molecules *in vitro* (e.g., [31]). However, the likely bundled state of titin molecules in the sarcomere is not usually taken into account [44–48]. In the following, we present some estimates related to titin flexibility *in vitro* and *in situ*.

Electron and atomic force microscopy (AFM) of purified titin molecules illustrate a tendency to coil up in the absence of applied extensional force (Figure 2(a)) [15, 16, 31, 49] or to straighten when a small pulling force is applied [17, 18, 31, 38, 50]. The persistence length (L_p) of monomeric titin is estimated to be 9–19 nm [31, 49, 51, 52]. A somewhat smaller range of values, 2–10 nm, was suggested by AFM and optical tweezer mechanical experiments on single molecules [43, 53–55], and a tendency of the protein to unfolding was discussed [53, 55].

The estimates of L_p are likely to mainly reflect average flexibility of the Ig/Fn3 parts of the molecule, since the unique sequences and other structures are a small proportion of the molecule. In a multidomain protein, overall bending flexibility mainly derives from the mobility at the inter-domain interfaces. Taking average interdomain distance s to be about 4.0 nm [27] and the average persistence length L_p to be about 13.5 nm, the average inter-domain angle can be approximately estimated from the relationship $\langle \theta^2(s) \rangle = 2s/L_p$ [56], from which a $\langle \theta \rangle$ value of $\sim 44^\circ$ can be obtained. This value (i.e., $180^\circ - 44^\circ = 136^\circ$) is close to the average inter-domain angle in the NMR and crystal structures of titin fragments, $\sim 140^\circ$ [25, 26, 28–30, 32, 57, 58]. This suggests that the inter-domain angles and shapes of titin constructs reflect the equilibrium-relaxed conformation of the native titin molecule. In this conformation, the inter-domain angles and twists are likely to be different from those *in situ*, at least in the case of A-band titin, which is extended and stressed by the interactions with myosin and C-protein in the thick filament backbone.

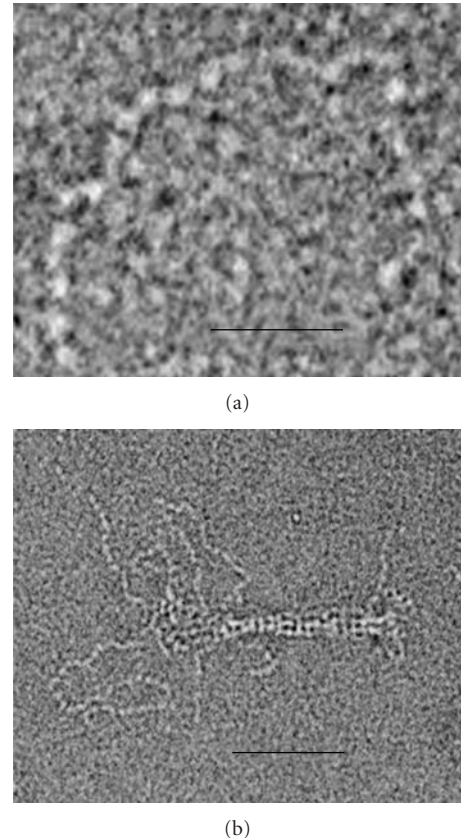


FIGURE 2: Electron micrographs of negatively stained titin, illustrating domain substructure and flexibility (a), and the effect of bundling on the apparent stiffness of the molecule (b). (a) Note that each of the flexibility “waves” seen in the titin contour contains about 4 domains. This number is comparable with the number of domains (3–4) expected for segments of about the persistence length of the protein. (b) This micrograph shows partially dissolved titin “end-filament”. The “wavy” contours of the molecules in the unbundled region contrast with their relatively straight shapes in the bundled part. Magnification: bar (a) 20 nm; (b) 50 nm.

Only slightly higher L_p values (15–40 nm) were estimated for individual titin molecules from mechanical experiments on muscle fibres [41] and myofibrils [59]. The difference between the *in vitro* and *in situ* results is smaller than might be expected since, in the sarcomere, the extensible I-band parts of titin are known to be bundled [44–48]. Inspection of the bundled and unbundled parts of I-band titin seen in electron microscope images (Figure 2(b)) clearly illustrates different bending properties. As was estimated earlier for an analogous case [60], the persistence length of a bundle scales with the square of the number of subfilaments in the bundle, that is, $L_p \sim N^2$. In the case of titin, this means that a bundle of six molecules will make L_p at least 500 nm, that is, 36 times larger than L_p for a single molecule, taken as 13.5 nm. Even for smaller bundles, composed of only two–three molecules, the expected L_p value is in the region of ~ 55 –120 nm.

The two L_p values, 55–120 nm and 500 nm, reflect the expected stiffness of the two Ig-tandem segments of I-band

titin that are separated by the unique N2-PEVK region: the proximal N-terminal segment, attached to the Z-line, and the bundled distal C-terminal segment, attached to the tip of the thick filament, known as the end-filament [44–48]. The fact that the L_p values from mechanical experiments on muscle fibres and myofibrils closely correspond to the *in vitro* L_p value of the monomeric molecule is unlikely to correctly reflect titin's state and flexibility *in situ*. Alternatively, this may indicate dissociation of end-filaments during experiments, possibly due to their fragility, or may reflect the specificity of conformational changes *in situ*, related, for instance, to helicity (see above) and/or the confined environment in the sarcomere.

4. Adaptation of Titin Organization in the Sarcomere to the Symmetry Mismatch between Z- and M-Lines

How the arrangement of titin in the sarcomere accommodates the different symmetries of thick and thin filament lattices, and of the M- and Z-line regions, is a major unresolved problem in sarcomere structure. The number of six molecules bound to each half of thick filament [39, 47] correlates well with the threefold rotational symmetry of the filament [61], its three-stranded substructure [44, 62, 63], and with the hexagonal lattice of the M-line region [61, 64]. However, titin extension through the I-band, and especially its interaction with thin filaments near and within Z-line region, suggests a rearrangement to fit to the twofold rotational symmetry of thin filaments and the tetragonal lattice of the Z-line. The question is thus how titin molecules rearrange in the I-band.

One of the factors that may affect this rearrangement is self-association (see also above). Titin self-association in the I-band is suggested by electron microscope studies of muscle and separate thick filaments, which show the ~100 nm stalk-like structures called end-filaments, referred to above, projecting from the ends of thick filaments [44–46]. It is also supported by *in vitro* observations of self-association of the titin segment from this region [48]. This includes the entire distal (with respect to the Z-line) tandem-Ig segment of I-band titin, from the thick filament tip up to the PEVK-N2 region. At this point the bundle is likely to branch, although not necessarily into single molecules.

The relatively high negative charge on the PEVK (N2B) region(s) of titin would favour branching of the end-filaments, unless the charge is neutralised by interactions either with cations (e.g., Ca^{++} ions [65, 66]) or with other cytoplasmic components. It should also be noted that the N2-PEVK-region is the site where thin filaments appear to rearrange from hexagonal to tetragonal packing, which then becomes especially ordered near and within the Z-line [67]. However, structural studies have so far failed to provide an unambiguous answer for the number of the branched subfilaments. Three alternatives end-filament branching schemes are possible: (1) into two subfilaments, each containing three titin molecules; (2) into three subfilaments with two titin

molecules in each; and (3) into six subfilaments, each a single titin molecule. In the first case, such a division would give 1:1 ratio of titin to thin filaments, which would imply interaction of each thin filament with a single bundle of three titin molecules near and within the Z-line region. This would satisfy tetragonal Z-line symmetry; however, there would be no agreement with the twofold symmetry of thin filament. Splitting the end-filament into a larger number of subfilaments would not satisfy either the Z-line or thin filament symmetries.

Thus, some asymmetry has to be assumed to exist in the titin arrangement and interactions in either the I-band or within the Z-line. A possible arrangement of titin in the Z-line has been discussed [47]. This scheme suggests splitting of end-filament into six individual titin molecules with only four of these molecules interacting side-by-side with two thin filaments of the same sarcomere and extending throughout the Z-line. The remaining two titins would attach to the tips of two incoming thin filaments of the adjacent sarcomere. This arrangement gives a 2:1 ratio of side-by-side interactions between titin molecules and thin filaments and is in agreement with both thin filament and Z-line symmetries. It would also provide the required mechanical balance in Z-line region and appears to be in a good agreement with structural data [68].

Another possibility relates to involvement of small titin isoforms, for example, Novex-3, which are present in skeletal and cardiac muscles in varying amounts in parallel with the main full-length isoforms, but which span only half the I-band, between the Z-line and N2-line [14, 69]. This location potentially helps to resolve the problem of correlation of the number of titin molecules with the thin filaments and Z-line symmetries. However, the low amount of Novex-3 expressed by muscles [14] is apparently not compatible with this role of the protein. Also, involvement of additional isoforms would not eliminate the asymmetry in titin interactions in the I-band but will only shift the site of asymmetry from the Z-line to the N2-line region of sarcomere where the different titin isoforms meet.

5. Concluding Remarks

Although an enormous amount has been learnt about the properties of the titin molecule, both *in vitro* and *in situ*, integrating this information to give a comprehensive picture is not straightforward. This is mainly because in no part of the sarcomere—A- or I-band, Z- or M-line—is the disposition of the components known in molecular detail. Much therefore remains to be learnt about sarcomere structure and titin layout and function, and how these are compromised in disease.

Acknowledgment

The authors thank the British Heart Foundation for supporting this work (PG/06/006/20236).

References

- [1] S. Y. Boateng and P. H. Goldspink, "Assembly and maintenance of the sarcomere night and day," *Cardiovascular Research*, vol. 77, no. 4, pp. 667–675, 2008.
- [2] E. Ehler and M. Gautel, "The sarcomere and sarcomerogenesis," *Advances in Experimental Medicine and Biology*, vol. 642, pp. 1–14, 2008.
- [3] M. S. Willis, J. C. Schisler, A. L. Portbury, and C. Patterson, "Build it up-tear it down: protein quality control in the cardiac sarcomere," *Cardiovascular Research*, vol. 81, no. 3, pp. 439–448, 2009.
- [4] W. G. Pyle and R. J. Solaro, "At the crossroads of myocardial signaling: the role of Z-discs in intracellular signaling and cardiac function," *Circulation Research*, vol. 94, no. 3, pp. 296–305, 2004.
- [5] R. J. Solaro and P. P. De Tombe, "Review focus series: sarcomeric proteins as key elements in integrated control of cardiac function," *Cardiovascular Research*, vol. 77, no. 4, pp. 616–618, 2008.
- [6] L. Tskhovrebova and J. Trinick, "Titin: properties and family relationships," *Nature Reviews Molecular Cell Biology*, vol. 4, no. 9, pp. 679–689, 2003.
- [7] H. Granzier and S. Labeit, "Structure-function relations of the giant elastic protein titin in striated and smooth muscle cells," *Muscle and Nerve*, vol. 36, no. 6, pp. 740–755, 2007.
- [8] W. A. Linke, "Sense and stretchability: the role of titin and titin-associated proteins in myocardial stress-sensing and mechanical dysfunction," *Cardiovascular Research*, vol. 77, no. 4, pp. 637–648, 2008.
- [9] M. L. Greaser, "Stressing the giant: a new approach to understanding dilated cardiomyopathy," *Journal of Molecular and Cellular Cardiology*, vol. 47, no. 3, pp. 347–349, 2009.
- [10] A. Kontogianni-Konstantopoulos, M. A. Ackermann, A. L. Bowman, S. V. Yap, and R. J. Bloch, "Muscle giants: molecular scaffolds in sarcomerogenesis," *Physiological Reviews*, vol. 89, no. 4, pp. 1217–1267, 2009.
- [11] K. Maruyama, T. Yoshioka, and H. Higuchi, "Connectin filaments link thick filaments and Z lines in frog skeletal muscle as revealed by immunoelectron microscopy," *Journal of Cell Biology*, vol. 101, no. 6, pp. 2167–2172, 1985.
- [12] D. O. Furst, M. Osborn, R. Nave, and K. Weber, "The organization of titin filaments in the half-sarcomere revealed by monoclonal antibodies in immunoelectron microscopy: a map of ten nonrepetitive epitopes starting at the Z line extends close to the M line," *Journal of Cell Biology*, vol. 106, no. 5, pp. 1563–1572, 1988.
- [13] D. O. Furst, R. Nave, M. Osborn, and K. Weber, "Repetitive titin epitopes with a 42 nm spacing coincide in relative position with known A band striations also identified by major myosin-associated proteins. An immunoelectron-microscopical study on myofibrils," *Journal of cell science*, vol. 94, pp. 119–125, 1989.
- [14] M.-L. Bang, T. Centner, F. Fornoff et al., "The complete gene sequence of titin, expression of an unusual \approx 700-kDa titin isoform, and its interaction with obscurin identify a novel Z-line to I-band linking system," *Circulation Research*, vol. 89, no. 11, pp. 1065–1072, 2001.
- [15] J. Trinick, P. Knight, and A. Whiting, "Purification and properties of native titin," *Journal of Molecular Biology*, vol. 180, no. 2, pp. 331–356, 1984.
- [16] K. Wang, R. Ramirez-Mitchell, and D. Palter, "Titin is an extraordinarily long, flexible, and slender myofibrillar protein," *Proceedings of the National Academy of Sciences of the United States of America*, vol. 81, no. 12, pp. 3685–3689, 1984.
- [17] R. Nave, D. O. Furst, and K. Weber, "Visualization of the polarity of isolated titin molecules: a single globular head on a long thin rod as the M band anchoring domain?" *Journal of Cell Biology*, vol. 109, no. 5, pp. 2177–2187, 1989.
- [18] M. Sonoda, S. Kimura, H. Moriya, Y. Shimada, and K. Maruyama, "Molecular shape of α -Connectin, an elastic filamentous protein of skeletal muscle," *Proceedings of the Japan Academy. Series B*, vol. 66, no. 10, pp. 213–216, 1990.
- [19] S. Labeit, M. Gautel, A. Lakey, and J. Trinick, "Towards a molecular understanding of titin," *EMBO Journal*, vol. 11, no. 5, pp. 1711–1716, 1992.
- [20] S. Labeit and B. Kolmerer, "Titins: giant proteins in charge of muscle ultrastructure and elasticity," *Science*, vol. 270, no. 5234, pp. 293–296, 1995.
- [21] S. Labeit, D. P. Barlow, M. Gautel et al., "A regular pattern of two types of 100-residue motif in the sequence of titin," *Nature*, vol. 345, no. 6272, pp. 273–276, 1990.
- [22] M. Gautel, "The super-repeats of titin/connectin and their interactions: glimpses at sarcomeric assembly," *Advances in Biophysics*, vol. 33, pp. 27–37, 1996.
- [23] C. C. Witt, N. Olivieri, T. Centner et al., "A survey of the primary structure and the interspecies conservation of I-band titin's elastic elements in vertebrates," *Journal of Structural Biology*, vol. 122, no. 1-2, pp. 206–215, 1998.
- [24] A. Freiburg and M. Gautel, "A molecular map of the interactions between titin and myosin-binding protein C. Implications for sarcomeric assembly in familial hypertrophic cardiomyopathy," *European Journal of Biochemistry*, vol. 235, no. 1-2, pp. 317–323, 1996.
- [25] S. Improta, J. K. Krueger, M. Gautel et al., "The assembly of immunoglobulin-like modules in titin: implications for muscle elasticity," *Journal of Molecular Biology*, vol. 284, no. 3, pp. 761–777, 1998.
- [26] C. Muhle-Goll, A. Pastore, and M. Nilges, "The three-dimensional structure of a type I module from titin: a prototype of intracellular fibronectin type III domains," *Structure*, vol. 6, no. 10, pp. 1291–1302, 1998.
- [27] P. Amodeo, F. Fraternali, A. M. Lesk, and A. Pastore, "Modularity and homology: modelling of the titin type I modules and their interfaces," *Journal of Molecular Biology*, vol. 311, no. 2, pp. 283–296, 2001.
- [28] M. Mrosek, D. Labeit, S. Witt et al., "Molecular determinants for the recruitment of the ubiquitin-ligase MuRF-1 onto M-line titin," *FASEB Journal*, vol. 21, no. 7, pp. 1383–1392, 2007.
- [29] S. Müller, S. Lange, M. Gautel, and M. Wilmanns, "Rigid conformation of an immunoglobulin domain tandem repeat in the A-band of the elastic muscle protein titin," *Journal of Molecular Biology*, vol. 371, no. 2, pp. 469–480, 2007.
- [30] E. Von Castellmur, M. Marino, D. I. Svergun et al., "A regular pattern of Ig super-motifs defines segmental flexibility as the elastic mechanism of the titin chain," *Proceedings of the National Academy of Sciences of the United States of America*, vol. 105, no. 4, pp. 1186–1191, 2008.
- [31] L. Tskhovrebova and J. Trinick, "Flexibility and extensibility in the titin molecule: analysis of electron microscope data," *Journal of Molecular Biology*, vol. 310, no. 4, pp. 755–771, 2001.
- [32] M. Marino, P. Zou, D. Svergun et al., "The Ig Doublet Z1Z2: a model system for the hybrid analysis of conformational dynamics in Ig tandems from titin," *Structure*, vol. 14, no. 9, pp. 1437–1447, 2006.

- [33] C. Muhle-Goll, M. Habeck, O. Cazorla, M. Nilges, S. Labeit, and H. Granzier, "Structural and functional studies of titin's fn3 modules reveal conserved surface patterns and binding to myosin S1—a possible role in the Frank-Starling mechanism of the heart," *Journal of Molecular Biology*, vol. 313, no. 2, pp. 431–447, 2001.
- [34] J. M. Squire, M. Roessle, and C. Knupp, "New X-ray diffraction observations on vertebrate muscle: organisation of C-protein (MyBP-C) and troponin and evidence for unknown structures in the vertebrate A-band," *Journal of Molecular Biology*, vol. 343, no. 5, pp. 1345–1363, 2004.
- [35] K. Maruyama, T. Yoshioka, and H. Higuchi, "Connectin filaments link thick filaments and Z lines in frog skeletal muscle as revealed by immunoelectron microscopy," *Journal of Cell Biology*, vol. 101, no. 6, pp. 2167–2172, 1985.
- [36] K. Wang, "Sarcomere-associated cytoskeletal lattices in striated muscle. Review and hypothesis," *Cell and Muscle Motility*, vol. 6, pp. 315–369, 1985.
- [37] R. Horowitz and R. J. Podolsky, "The positional stability of thick filaments in activated skeletal muscle depends on sarcomere length: evidence for the role of titin filaments," *Journal of Cell Biology*, vol. 105, no. 5, pp. 2217–2223, 1987.
- [38] A. Soteriou, A. Clarke, S. Martin, and J. Trinick, "Titin folding energy and elasticity," *Proceedings of the Royal Society B*, vol. 254, no. 1340, pp. 83–86, 1993.
- [39] H. L. Granzier and T. C. Irving, "Passive tension in cardiac muscle: contribution of collagen, titin, microtubules, and intermediate filaments," *Biophysical Journal*, vol. 68, no. 3, pp. 1027–1044, 1995.
- [40] M. Gautel and D. Goulding, "A molecular map of titin/connectin elasticity reveals two different mechanisms acting in series," *FEBS Letters*, vol. 385, no. 1-2, pp. 11–14, 1996.
- [41] K. Trombitás, M. Greaser, S. Labeit et al., "Titin extensibility in situ: entropic elasticity of permanently folded and permanently unfolded molecular segments," *Journal of Cell Biology*, vol. 140, no. 4, pp. 853–859, 1998.
- [42] K. Trombitás, A. Redkar, T. Centner, Y. Wu, S. Labeit, and H. Granzier, "Extensibility of isoforms of cardiac titin: variation in contour length of molecular subsegments provides a basis for cellular passive stiffness diversity," *Biophysical Journal*, vol. 79, no. 6, pp. 3226–3234, 2000.
- [43] H. Li, W. A. Linke, A. F. Oberhauser et al., "Reverse engineering of the giant muscle protein titin," *Nature*, vol. 418, no. 6901, pp. 998–1002, 2002.
- [44] J. A. Trinick, "End filaments: a new structural element of vertebrate skeletal muscle thick filaments," *Journal of Molecular Biology*, vol. 151, no. 2, pp. 309–314, 1981.
- [45] T. Funatsu, E. Kono, H. Higuchi et al., "Elastic filaments in situ in cardiac muscle: deep-etch replica analysis in combination with selective removal of actin and myosin filaments," *Journal of Cell Biology*, vol. 120, no. 3, pp. 711–724, 1993.
- [46] P. M. Bennett, T. E. Hodkin, and C. Hawkins, "Evidence that the tandem ig domains near the end of the muscle thick filament form an inelastic part of the I-band titin," *Journal of Structural Biology*, vol. 120, no. 1, pp. 93–104, 1997.
- [47] A. D. Liversage, D. Holmes, P. J. Knight, L. Tskhovrebova, and J. Trinick, "Titin and the sarcomere symmetry paradox," *Journal of Molecular Biology*, vol. 305, no. 3, pp. 401–409, 2001.
- [48] A. Houmeida, A. Baron, J. Keen et al., "Evidence for the oligomeric state of 'elastic' titin in muscle sarcomeres," *Journal of Molecular Biology*, vol. 384, no. 2, pp. 299–312, 2008.
- [49] M. S. Z. Kellermayer, C. Bustamante, and H. L. Granzier, "Mechanics and structure of titin oligomers explored with atomic force microscopy," *Biochimica et Biophysica Acta*, vol. 1604, no. 2, pp. 105–114, 2003.
- [50] L. Tskhovrebova and J. Trinick, "Direct visualization of extensibility in isolated titin molecules," *Journal of Molecular Biology*, vol. 265, no. 2, pp. 100–106, 1997.
- [51] H. Higuchi, Y. Nakauchi, K. Maruyama, and S. Fujime, "Characterization of β -connectin (titin 2) from striated muscle by dynamic light scattering," *Biophysical Journal*, vol. 65, no. 5, pp. 1906–1915, 1993.
- [52] E. Di Cola, T. A. Waigh, J. Trinick et al., "Persistence length of titin from rabbit skeletal muscles measured with scattering and microrheology techniques," *Biophysical Journal*, vol. 88, no. 6, pp. 4095–4106, 2005.
- [53] M. S. Z. Kellermayer, S. B. Smith, H. L. Granzier, and C. Bustamante, "Folding-unfolding transitions in single titin molecules characterized with laser tweezers," *Science*, vol. 276, no. 5315, pp. 1112–1116, 1997.
- [54] M. Rief, M. Gautel, F. Oesterhel, J. M. Fernandez, and H. E. Gaub, "Reversible unfolding of individual titin immunoglobulin domains by AFM," *Science*, vol. 276, no. 5315, pp. 1109–1112, 1997.
- [55] L. Tskhovrebova, J. Trinick, J. A. Sleep, and R. M. Simmons, "Elasticity and unfolding of single molecules of the giant muscle protein titin," *Nature*, vol. 387, no. 6630, pp. 308–312, 1997.
- [56] A. Yu. Grosberg and A. R. Khokhlov, *Statistical Physics of Macromolecules*, AIP Press, New York, NY, USA, 2004.
- [57] M. Marino, D. I. Svergun, L. Kreplak et al., "Poly-Ig tandems from I-band titin share extended domain arrangements irrespective of the distinct features of their modular constituents," *Journal of Muscle Research and Cell Motility*, vol. 26, no. 6–8, pp. 355–365, 2005.
- [58] P. Zou, N. Pinotsis, S. Lange et al., "Palindromic assembly of the giant muscle protein titin in the sarcomeric Z-disk," *Nature*, vol. 439, no. 7073, pp. 229–233, 2006.
- [59] W. A. Linke, M. R. Stockmeier, M. Ivemeyer, H. Hosser, and P. Mundel, "Characterizing titin's I-band Ig domain region as an entropic spring," *Journal of Cell Science*, vol. 111, no. 11, pp. 1567–1574, 1998.
- [60] J. C. Wang, M. S. Turner, G. Agarwal et al., "Micromechanics of isolated sickle cell hemoglobin fibers: bending moduli and persistence lengths," *Journal of Molecular Biology*, vol. 315, no. 4, pp. 601–612, 2002.
- [61] P. K. Luther, P. M. G. Munro, and J. M. Squire, "Three-dimensional structure of the vertebrate muscle A-band. III. M-region structure and myosin filament symmetry," *Journal of Molecular Biology*, vol. 151, no. 4, pp. 703–730, 1981.
- [62] M. C. Maw and A. J. Rowe, "Fraying of a-filaments into three subfilaments," *Nature*, vol. 286, no. 5771, pp. 412–414, 1980.
- [63] R. W. Kensler and M. Stewart, "Frog skeletal muscle thick filaments are three-stranded," *Journal of Cell Biology*, vol. 96, no. 6, pp. 1797–1802, 1983.
- [64] G. G. Knappeis and F. Carlsen, "The ultrastructure of the M line in skeletal muscle," *Journal of Cell Biology*, vol. 38, no. 1, pp. 202–211, 1968.
- [65] R. Tatsumi, K. Maeda, A. Hattori, and K. Takahashi, "Calcium binding to an elastic portion of connectin/titin filaments," *Journal of Muscle Research and Cell Motility*, vol. 22, no. 2, pp. 149–162, 2001.

- [66] D. Labeit, K. Watanabe, C. Witt et al., “Calcium-dependent molecular spring elements in the giant protein titin,” *Proceedings of the National Academy of Sciences of the United States of America*, vol. 100, no. 23, pp. 13716–13721, 2003.
- [67] L. Traeger, J. M. Mackenzie Jr., H. F. Epstein, and M. A. Goldstein, “Transition in the thin-filament arrangement in rat skeletal muscle,” *Journal of Muscle Research and Cell Motility*, vol. 4, no. 3, pp. 353–366, 1983.
- [68] C. Knupp, P. K. Luther, and J. M. Squire, “Titin organisation and the 3D architecture of the vertebrate-striated muscle I-band,” *Journal of Molecular Biology*, vol. 322, no. 4, pp. 731–739, 2002.
- [69] H. Granzier, M. Radke, J. Royal et al., “Functional genomics of chicken, mouse, and human titin supports splice diversity as an important mechanism for regulating biomechanics of striated muscle,” *American Journal of Physiology*, vol. 293, no. 2, pp. R557–R567, 2007.

Research Article

Dynamic Strength of Titin's Z-Disk End

Veronika Kollár,¹ Dávid Szatmári,¹ László Grama,¹ and Miklós S. Z. Kellermayer²

¹Department of Biophysics, Faculty of Medicine, University of Pécs, Szigeti ut 12., Pécs 7624, Hungary

²Department of Biophysics and Radiation Biology, Faculty of Medicine, Semmelweis University, Tűzoltó u. 37-47., Budapest 1094, Hungary

Correspondence should be addressed to Miklós S. Z. Kellermayer, miklos.kellermayer@eok.sote.hu

Received 7 December 2009; Accepted 11 February 2010

Academic Editor: Henk L. M. Granzier

Copyright © 2010 Veronika Kollár et al. This is an open access article distributed under the Creative Commons Attribution License, which permits unrestricted use, distribution, and reproduction in any medium, provided the original work is properly cited.

Titin is a giant filamentous protein traversing the half sarcomere of striated muscle with putative functions as diverse as providing structural template, generating elastic response, and sensing and relaying mechanical information. The Z-disk region of titin, which corresponds to the N-terminal end of the molecule, has been thought to be a hot spot for mechanosensing while also serving as anchorage for its sarcomeric attachment. Understanding the mechanics of titin's Z-disk region, particularly under the effect of binding proteins, is of great interest. Here we briefly review recent findings on the structure, molecular associations, and mechanics of titin's Z-disk region. In addition, we report experimental results on the dynamic strength of titin's Z1Z2 domains measured by nanomechanical manipulation of the chemical dimer of a recombinant protein fragment.

1. Introduction

The giant muscle protein titin (also known as connectin) is the third most abundant protein in muscle after actin and myosin, and forms a third myofilament system in skeletal as well as in cardiac muscle [1–3]. Individual titin molecules span half of the sarcomere and run between the Z-disk and the M-line. The main function of titin is to provide a passive mechanical tension in muscle, generating the force responsible for restoring the resting length of the sarcomere [4–7]. In fulfilling its role as a molecular spring it is of great importance that the N- and C-termini of the molecule be firmly anchored in the Z-disk and the M-line, respectively.

1.1. Titin in the Z-Disk. Immunoelectron microscopic studies revealed that an approximately 800-residue-long segment at titin's N-terminus is localized within the Z-disk [8]. This region of titin includes the first four immunoglobulin-type domains (Z1 to Z4) and a series of 45-residue repeats, called Z-repeats [9], situated between Z2 and Z3 [10]. While domains Z1 to Z4 are present in all titin isoforms, the number of Z-repeats (up to 7) varies due to extensive differential splicing (Figure 1(a)).

Titin interacts with α -actinin via the Z-repeats [11]. The binding more readily detected is found between 7th Z-repeat (Zr7) and the C-lobe of the C-terminal calmodulin-like domain of α -actinin. This interaction is similar to that of troponin I to troponin C and of peptide C20W to calmodulin [12]. However, it has been shown that the central Z-repeats are also able to interact with the C-terminal domain of α -actinin, and another interaction may occur via a single binding site between titin and the two central spectrin-like repeats of the outermost pair of alpha-actinin molecules [13]. These interactions also enable titin, α -actinin and actin to form a ternary complex and contribute to the formation of a stable network structure within the Z-disk.

The thickness and structural properties of Z-disks are largely variable, which was proposed to serve the adaptation of the Z-disk structure to the level of mechanical strain [14]. The observation that the number of Z-repeats in titin varies between species and between muscle types led to the hypothesis that it is the differential expression of titin that accounts for the different thickness and protein composition of Z-disks [9]. However, a direct correlation between the characteristics of Z-disks and the expression of different titin isoforms has not been established.

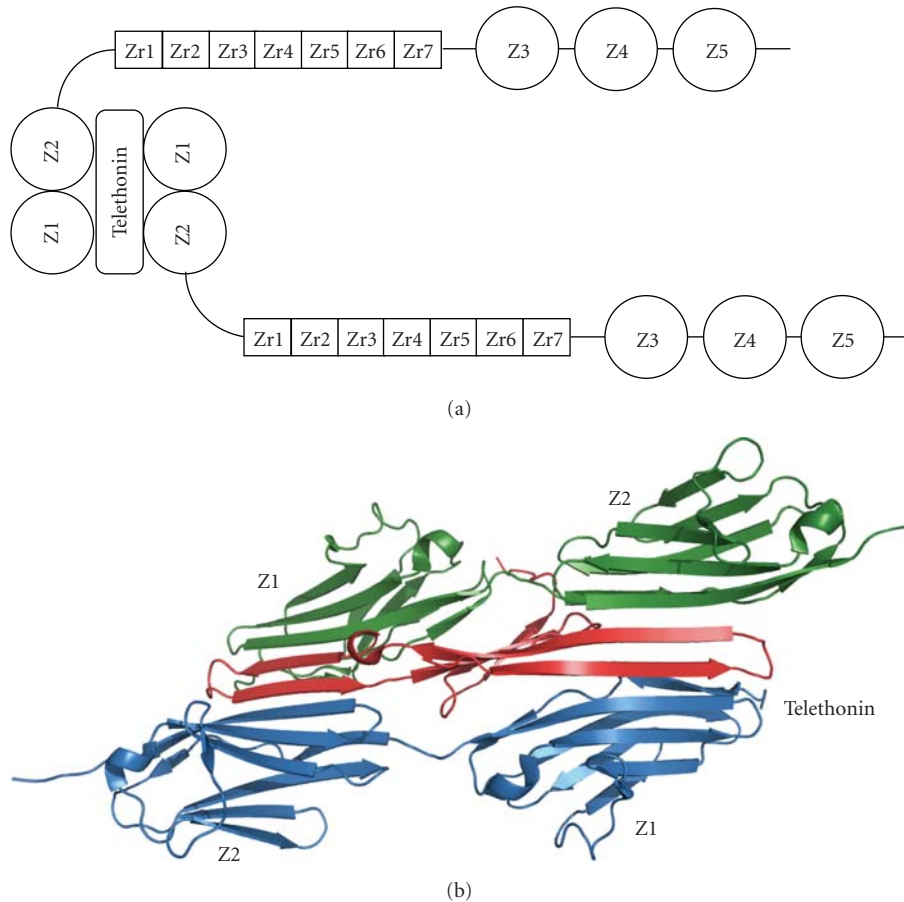


FIGURE 1: (a) Schematic diagram of the structure of the Z-disk region of titin. (b) Structural model of the Z1Z2-telethonin complex.

1.2. Mechanosensing in the Z-Disk. The Z-disk acts as a link that mechanically integrates contractile and elastic elements, hence it plays a key role in the transmission of active and passive forces. In the last decade, however, new functions of the Z-disk emerged beyond the simple role of a mechanical force transmitter [15, 16]. As new proteins of the Z-disk were discovered, it became obvious that many of these new components take part in important signaling pathways, many of them having a possible role in stretch sensing.

Stretch is a major factor that is able to induce changes in the morphology and function of muscle. The steps between the onset of mechanical stress and the development of morphological and functional changes include the propagation of the mechanical force to a stress sensor, sensation of stretch, and conversion of the mechanical signal to a biochemical one, finally resulting in alterations of gene expression. This process involves a multitude of molecular players [17].

Titin has been one of the major candidates for the role of the stretch sensor in muscle. Since titin molecules extend in concert with the sarcomere itself, they are well positioned for monitoring the sarcomere's contractile status and possibly transmitting the corresponding mechanical signals. Transduction of the mechanical signal most likely occurs through the interaction of titin with its associated proteins. Different regions ("hot spots") along titin molecules (Z-disk, I-band,

A-band and M-line titin) all participate in a relatively large number of interactions with more than 20 partners known so far [17]. It has been proposed that different regions may sense different parameters: protein complexes in the Z-disk may act as stress sensors that detect and respond to both passive force generated by the titin filaments and active force generated during contraction via the thin filaments, whereas the extensible, I-band region of titin can function as a strain sensor, responding to passive tension alone [18].

1.3. Telethonin Interaction with Z-Disk Titin. One of the most important interactions responsible for anchoring titin in the Z-disk is binding of the titin N-terminus to the Z-disk protein telethonin. Telethonin was identified as a 19 kDa muscle protein present in heart and skeletal muscle. Its transcript is amongst the most abundant in skeletal muscle [19]. Independently, it was discovered as an interacting partner of the titin N-terminus, an interaction that is required for the structural integrity of sarcomere, and the protein was named titin-cap or T-cap [20]. Since its discovery it has been revealed that mutations in the telethonin gene cause limb-girdle muscular dystrophy type 2G, a relatively mild form of autosomal recessive limb-girdle muscular dystrophies [21]. Telethonin has been suggested to be involved in stress sensing, through its interaction with muscle LIM protein

(MLP) [22]. MLP deficient mice have been shown to develop widened and disorganized Z-disks, while the W4R MLP mutation has been shown to lead to a loss of interaction with telethonin, telethonin mislocalization [22], and has been associated with hypertrophic cardiomyopathy (HCM) [23, 24].

Telethonin interacts with the two N-terminal immunoglobulin-like domains of titin (Z1 and Z2), and it colocalizes with the N-terminal part of titin in cultured human skeletal muscle cells [25]. Interestingly, longer titin constructs, including the serine-proline-rich linker region, and the Z3 domain, failed to bind telethonin in yeast two-hybrid assays.

In recent years, the structure of the Z1Z2 doublet and its interaction with telethonin have been subject of numerous investigations. Conformational dynamics studies showed that Z1Z2 preferentially adopts a semiextended conformation with restricted dynamics and a moderately rigid linker that might facilitate the recruitment of its binding partner, telethonin [26]. The term “tertiary structure elasticity” has been introduced for Z1Z2, referring to elasticity resulting from bending and twisting of the domains at intermediate forces, in addition to the entropic elasticity that dominates at low forces and secondary-structure elasticity (unravelling of the domains) that dominates at high forces [27]. X-ray scattering studies on the solution structure of the Z1Z2-telethonin complex indicated a 1:2 association in an antiparallel manner, with telethonin as the central linker [28]. Hence, telethonin was not a simple cap, but rather a possible cross-linker between two titin filaments. The major breakthrough in deciphering the interaction and the building of the complex was solving the structure of the complex by X-ray crystallography (Figure 1(b)) and confirming the antiparallel, palindromic arrangement of the two titin filaments [29]. It is interesting to note that telethonin alone has no stable structure in solution, and it acquires its conformation only upon binding to the Z1Z2 domains.

The cross-linking role of telethonin and the possible mechanical function of the complex raised the question of its mechanical stability. Molecular dynamics simulations performed by Lee et al. predicted an unusually large unfolding force for the complex, in contrast with the relatively low mechanical stability predicted for Z1Z2 alone [30]. The actual strength of the Z1Z2-telethonin bond has been recently measured by stretching the complex using an atomic force microscope (AFM) [31]. The observed dissociation forces were indeed unusually high (~700 pN), far exceeding unfolding forces observed for the Z1Z2 domains alone (~168 pN) or previously measured unfolding forces of other titin Ig-like domains [32]. In addition, Bertz et al., by using protein engineering techniques, demonstrated that the mechanical stability of the complex is sensitive to the pulling direction [30]. Although the forces necessary to unfold Z1Z2 and to disrupt its complex with telethonin have been measured, the stability of Z1Z2 under varying loading rates is not known. Here we explored the dynamic strength of Z1Z2 by exposing the chemical dimer of a recombinant Z1Z2 fragment to a range of mechanical loading rates in nanomechanical experiments.

2. Materials and Methods

2.1. Cloning, Expression and Protein Purification. The human skeletal muscle cDNA library was a generous gift of Siegfried Labeit [33]. The nucleotide sequence corresponding to the Z1Z2 titin domain pair was amplified by polymerase chain reaction (PCR). Nucleotide sequence boundaries of the Z1Z2 fragment, based on GenBank accession no. X90568 (version X90568.1, [33]) were 133–717 (aa: 1–195). The fragment was cloned into a pET28a vector (Novagen, Darmstadt, Germany), that carried a kanamycin resistance gene, between NheI and XhoI sites introduced independently with PCR by using specific oligonucleotides. The recombinant protein contained a hexahistidine (His₆) tag on the N-terminus and two vicinal cysteines on the C-terminus, added to aid subsequent single-molecule manipulation. *Escherichia coli* BL21(DE3) pLysS cells were transformed with the pET28a-Z1Z2 construct and grown in 2 × YT Microbial EZMix medium (Sigma-Aldrich) in the presence of 30 µg/mL kanamycin until the OD₆₀₀ of the culture reached 0.6–0.8. Expression was induced by addition of 1 mM isopropylthio-β-D-galactoside and performed for 3 hours at 37°C. Harvested cells were resuspended in lysis buffer (50 mM NaH₂PO₄, 300 mM NaCl pH 8.0) supplemented with 0.01 mg/mL DNaseI, and were lysed by pulsed sonication (5 minutes, 80% intensity, Bandelin Sonopuls HD3100). Cell debris was removed by centrifugation at 100,000 × g for one hour at 4°C. The supernatant was applied to Talon polyhistidine-Tag purification resin columns (Clontech) equilibrated with lysis buffer. The bound protein was eluted with increasing imidazole concentration series (from 10 mM to 240 mM in lysis buffer). The eluted protein was dialysed against PBS-buffer (pH 7.2). Protein concentration was determined spectrophotometrically, using the molar extinction coefficient determined with the ProtParam tool. The electrophoretogram of the purified Z1Z2 fragment is shown on Figure 2(a).

2.2. Single-Molecule Force Spectroscopy. To facilitate the specific binding of the N-terminal, His₆-tagged end of the protein to the substrate, in our single-molecule experiments we used glass slides coated with Ni-NTA. Preparation of the slides was described previously [34]. Briefly, cleaned microscope slides were first incubated for 12 hours in toluene vapor containing 2% Glymo (3-Glycidioxypropyl-trimethoxysilane) (Fluka), then washed with distilled water and dried. Subsequently, the glymo-covered slides were incubated in 0.01 M Na₂CO₃ (pH 10), containing 2% (wt/vol) N-(5-amino 1-carboxypentyl)-iminodiacetic acid (NTA) (Dojindo) for 16 hours at 60°C, then washed with distilled water and dried. Finally, the slides were activated with PBS buffer containing 10 mM NiCl₂ and 5 mM glycine (pH 8.0) for two hours at room temperature. Z1Z2 fragments were kept in PBS buffer (137 mM NaCl, 2.7 mM KCl, 7.8 mM Na₂HPO₄, 2.2 mM KH₂PO₄, pH = 7.3). We created an oxidative environment by omitting DDT from the buffer, to facilitate the formation of Z1Z2 chemical dimers through disulfide bonds between the C-terminal cysteine residues (Figure 2(b)).

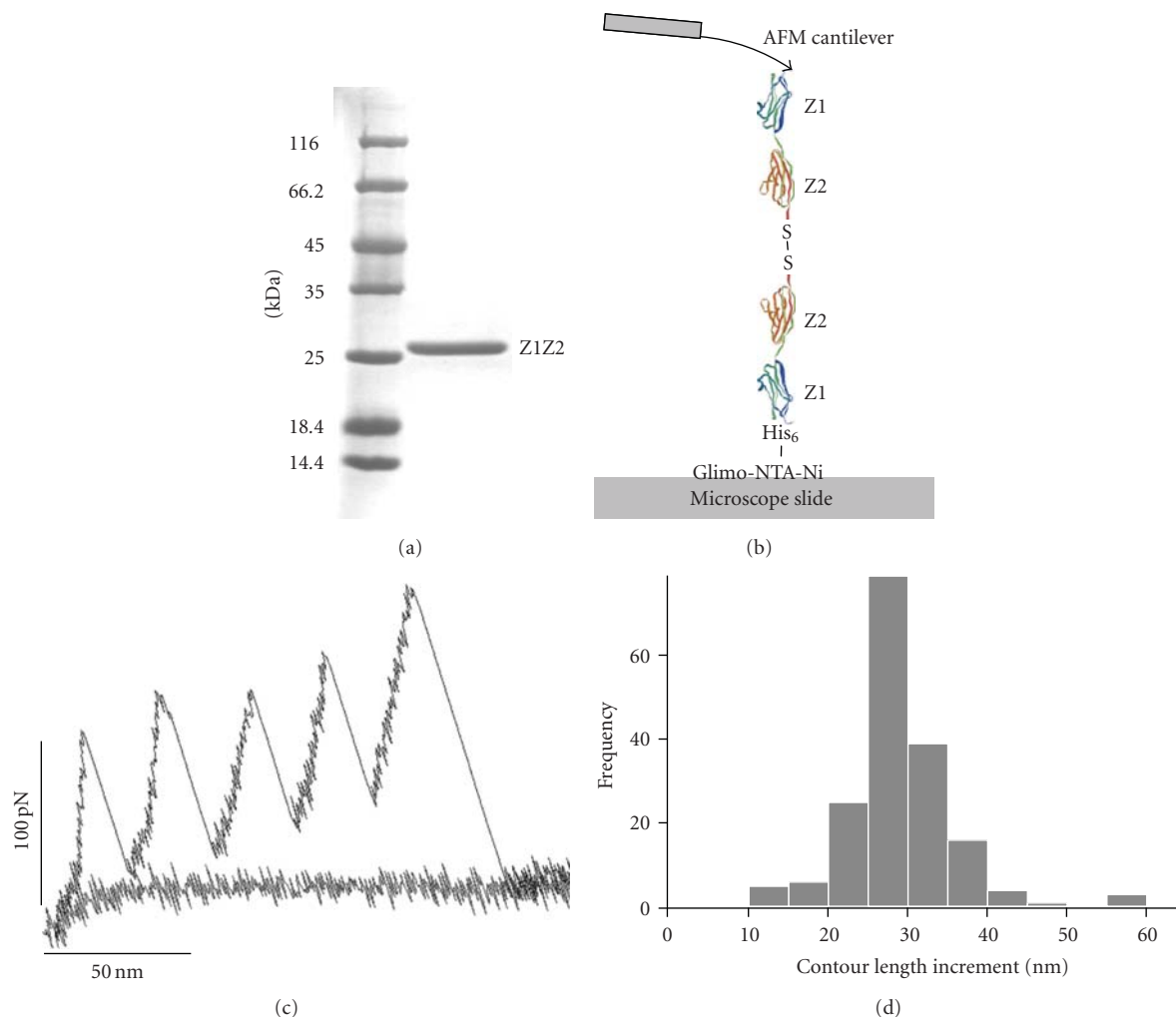


FIGURE 2: (a) SDS-polyacrylamide electrophoretogram of the recombinant Z1Z2 fragment. (b) Nanomechanical manipulation of the Z1Z2 chemical dimer. The molecular design of the Z1Z2 chemical dimer is indicated. Two recombinant Z1Z2 modules, each with a His₆-tag at its N-terminus and a cysteine at its C-terminus, respectively, are dimerized via a disulphide bond under oxidizing conditions. The dimer is manipulated by using single-molecule AFM. (c) Force versus end-to-end length curve of a Z1Z2 dimer. The first four sawtooth peaks correspond to the unfolding of each of the four domains (two Z1 and two Z2), and the fifth peak corresponds to the final dissociation of the complex from either the AFM tip or the substrate surface. (d) Distribution of contour-length gain during the sawtooth force transitions. Average contour-length gain per transition was 29.1 ± 0.6 nm (\pm SEM).

Molecules were mechanically stretched by using an atomic force microscope (AFM) dedicated for single-molecule manipulation (MFP1D, Asylum Research, Santa Barbara, CA), mounted on a custom-built, low-profile inverted light microscope. The experimental layout is shown in Figure 2(b). Z1Z2 dimers were allowed to bind to the surface of Ni-NTA-coated glass slides for 10 minutes. Unbound molecules were removed by washing the slide with PBS. The AFM cantilever (Bio-lever, type B; Olympus, Tokyo, Japan) was brought gently in contact with the Ni-NTA-coated substrate, then pulled away from the surface at a constant rate. Stretch rate (cantilever base velocity) was typically 500 nm/s, or 30, 100, 300, 1000, and 3000 nm/s in pulling-speed-dependent measurements. Compression forces used during the nanomechanical manipulation were between 300

and 700 pN. Dwell time on the surface, used to facilitate the binding of a molecule to the tip, was 1 s.

Force versus displacement curves were collected in repeated stretch and release cycles. Force was determined from the bending and stiffness of the cantilever. Cantilever stiffness (κ) was obtained by calibration with the thermal method [35]. Typical cantilever stiffness was ~ 6 pN/nm. The force-displacement curves were corrected for several factors to obtain force versus molecular end-to-end length functions. The zero-length, zero-force data point was obtained from the force response that corresponded to the cantilever tip reaching (or departing from) the substrate surface. Forces (F) were corrected for baseline slope obtained from the force response of the displaced but unloaded cantilever. The end-to-end length (z) of the tethered molecule was

calculated by correcting the cantilever base displacement (s) with cantilever bending as

$$z = s - \frac{F}{\kappa}. \quad (1)$$

2.3. Analysis of Force Data. Force versus molecular end-to-end length curves displaying repetitive force peak were further analyzed to obtain unfolding force values for the Z1Z2 construct. The peak force for individual unfolding events in each data set was measured. The last peak, presumably due to the detachment of the molecule either from the tip or from the glass surface, was omitted from analysis. Force peaks associated with a contour-length gain that was significantly different from the value expected based on the length of the unfolded Z1 or Z2 domains were also excluded from the analysis. The theoretically expected contour length gain for the Z1 and Z2 domains is 32–34 nm, calculated based on the number of residues (101 and 94 for Z1 and Z2, resp.) and the size of a folded Ig domain (~ 4 nm). The relative frequencies of curves (in measurements using 500 pN/nm pulling speed) with a different number of peaks were the following: 2 peaks: 13%, 3 peaks: 39%, 4 peaks: 30%, 5 peaks: 17%.

Kinetic parameters of Z1Z2 domain unfolding were investigated by two methods: (i) one based on the theory of Bell [36] and Evans and Ritchie [37], and (ii) one using a Monte-Carlo method (see below). The theory of Bell and Evans and Ritchie assumes a single barrier for protein unfolding/refolding. The mean unfolding force depends on x_u , the distance along the unfolding trajectory in configuration space between the native and transition states, and k_u^0 , the unfolding rate constant at zero applied force according to

$$F = \frac{k_B T}{x_u} \ln \left(\frac{r x_u}{k_B T k_u^0} \right), \quad (2)$$

where r is the force loading rate, k_B is Boltzmann's constant, and T is absolute temperature. At 300 K, $k_B T = 4.14$ pNnm. The loading rate was calculated by fitting a line to the rising phase of the force trace immediately preceding the unfolding event. Mean unfolding forces were plotted against the loading rate, and fitted with the above function, and k_u^0 and x_u were determined from the fit.

2.4. Monte-Carlo Simulation. Forced unfolding of the Z1Z2 titin Ig domains was simulated using a two-state model [38, 39]. Initially the domains were assumed to be in the folded state. The folding and unfolding rate constants at a given applied force (F) were calculated according to

$$k_{u/f} = k_{u/f}^0 \exp \left(\pm \frac{F x_{u/f}}{k_B T} \right), \quad (3)$$

where u and f correspond to unfolding and folding, respectively, and $k_{u/f}^0$ is the unfolding/folding rate constant at zero applied force. Negative sign is associated with folding, as force acts against this process. The protein was extended with

preset values for $k_{u/f}^0$, $x_{u/f}$ and pulling speed. Force as well as the unfolding/folding rate constants were calculated in small time increments. The force acting on the protein was calculated using the wormlike chain equation:

$$F = \frac{k_B T}{P} \left(\frac{1}{4(1-x/L)^2} - \frac{1}{4} + \frac{x}{L} \right), \quad (4)$$

where P is the persistence length, and L is the contour length of the protein, calculated as $mL_f + (n-m)L_u$, where L_f and L_u are the lengths of the folded and unfolded domains, respectively, while n and m are the numbers of total and folded protein regions, respectively. At each extension the probabilities of unfolding and folding were calculated and compared with a randomly generated number. If an unfolding/folding event took place, the contour length (L), the force (F) and the probabilities were recalculated. The parameters $k_{u/f}^0$ and x_u were varied until the simulated dependence of unfolding force on the pulling speed best fitted the experimental data. To mimic the experimental arrangement as closely as possible and to avoid the effect of chain length, the stretch and release of four-domain-long molecular segments were simulated.

3. Results and Discussion

The dynamic stability of the Z-disk region of the giant muscle protein titin was investigated by mechanically manipulating recombinant fragments consisting of titin's Z1 and Z2 domains. Under oxidative conditions, two Z1Z2 domain pairs were assembled via their C-terminal cysteine residues, yielding a 4-domain-long chemical dimer [40–42]. Force versus extension curves measured by stretching the above construct displayed sawtooth patterns, a characteristic of the unfolding of individual domains (Figure 2(c)). Up to four force peaks were observed for the Z1Z2 dimer excluding the last peak, which corresponds to the detachment of the molecule either from the tip or from the glass surface. Data analysis was performed by analyzing the unfolding force as well as the contour length gain. The obtained contour-length gain was 29.1 ± 0.6 nm (\pm SEM) (Figure 2(d)). This value is comparable to the theoretically expected contour-length gain (32–34 nm) calculated based on the number of residues (101 and 94 for Z1 and Z2, resp.) and the size of a folded Ig domain (≈ 4 nm). Force peaks with contour-length gains significantly different from the expected value were excluded from the analysis.

The distribution of unfolding forces was relatively wide (Figure 3(a)), with an average value of 101 ± 3 pN (\pm SEM) for a pulling speed of 1000 nm/s. The unfolding forces observed here are significantly lower than those found by Bertz et al. [31] for a construct in which a single Z1Z2 fragment was flanked by three ubiquitin domains on both the N- and C-terminal ends. Using this construct Bertz et al. observed an average contour-length gain of 29.4 ± 0.2 nm (\pm SEM) [31], which is essentially identical to our results. However, the unfolding forces were 168 ± 2 pN, which far exceed our findings. Even these greater values, however, fall below most of the unfolding forces measured so far

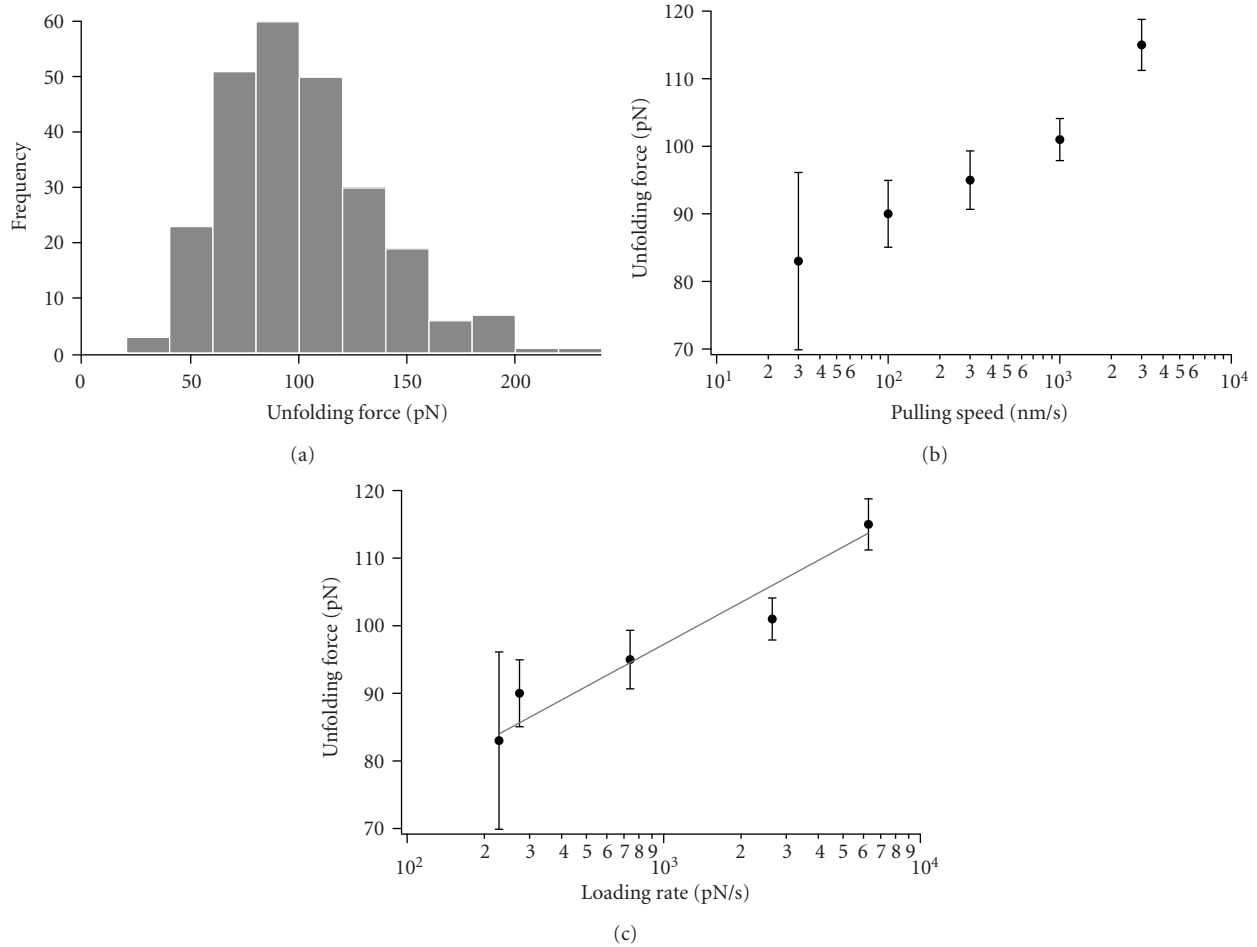


FIGURE 3: (a) Distribution of unfolding forces of Z1Z2 at 500 nm/s pulling speed. (b) Instantaneous unfolding force versus pulling speed. Error bars represent SEM; the average number of data points for the different pulling speeds was 25. (c) Unfolding force versus loading rate. The average number of data points for the different loading rates was 23. Data were fitted with (2).

for an array of titin's globular domains [32], suggesting that the Z1Z2 domains represent a mechanically weak part of titin. We can only speculate about the origin of the difference between our results and the findings of Bertz et al. [31]. It might be possible that the molecular environment imposed on the Z1 and Z2 domains by the recombinant constructs led to either structural stabilization [31] or destabilization (observed here). Although it is generally assumed that recombinant constructs represent well the in situ molecular structure and stability [43], sequence-specific and environmental factors may contribute to an alteration of the dynamic characteristics of the protein. Whatever might be the exact source of variation in structural stability, the Z1Z2 domains seem to be particularly unstable domains within titin.

To obtain an estimate on the kinetic parameters of the unfolding process, we performed the experiments at different pulling speeds ranging from 30 to 3000 nm/s. The pulling speed dependence of unfolding forces is shown in Figure 3(b). Pulling-speed data were converted to loading rate from the derivative of the force versus extension curves

(Figure 3(c)). By fitting the data with (2), we obtained $8.0 \times 10^{-4} \text{ s}^{-1}$ and 0.52 nm for the spontaneous unfolding rate (k_u^0) and the width of the unfolding potential (x_u), respectively. Using these parameters in a Monte-Carlo simulation, the nanomechanical data were successfully recovered (Figure 4). In contrast to the kinetic parameters found here for Z1Z2, spontaneous unfolding rates of $3.3 \times 10^{-4} \text{ s}^{-1}$ and $2.8 \times 10^{-5} \text{ s}^{-1}$ have been observed for titin's I27 and I28 immunoglobulin domains, respectively [44]. The unfolding potential width was calculated as 0.25 nm for both of these domains [44]. The spontaneous unfolding rate for the Z1Z2 domains is significantly greater than that of titin's I27 and I28 domains, indicating faster unfolding and hence lower stability under unloaded conditions. By estimating the shape of the unfolding potential with x_u , we may explore the dynamic stability of Z1Z2 as well. The x_u value for the Z1Z2 fragment is approximately two times larger than that for either I27 or I28. The smaller x_u value of I27/I28 indicates that during mechanical unfolding work is done over a very short distance, allowing high forces to be withstood while maintaining structure [45]. By contrast, the large x_u of

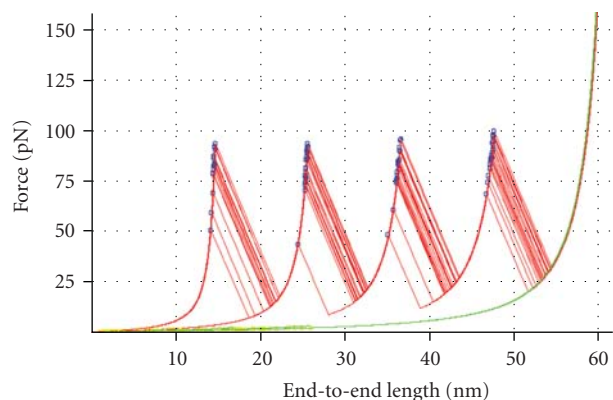


FIGURE 4: Monte-Carlo simulation of force versus extension data of Z1Z2 using (2) and (3). Data obtained in 15 consecutive stretch-release cycles at a pulling velocity of 100 nms^{-1} are displayed.

Z1Z2 indicates that work is done over a greater distance, resulting in larger structural changes at relatively low forces. Altogether, the dynamic stability of Z1Z2 is remarkably low.

Our findings indicate that both the thermodynamic stability and the dynamic stability of titin's Z1Z2 domains are very low. Thus, the Z1Z2 domains may not withstand high forces by themselves without severe structural consequences. In the muscle sarcomere, Z1Z2 is tightly associated with telethonin. The extensive network of hydrogen bonds formed between a telethonin molecule and two anti-parallel Z1Z2 domains is thought to result in a structural stabilization so large that the energetics of the Z1Z2-telethonin-Z1Z2 complex become comparable to that of a covalent bond [29, 31]. We speculate that the primary *in vivo* function of the strong Z1Z2-telethonin association is the formation of mechanical continuity along the titin-based scaffold of consecutive sarcomeres, and anchorage of titin within the Z-disk might be a secondary function. Mechanically weak domains in titin are also found among the fibronectin domains located in the A-band section of the molecule [46]. Titin's A-band section is thought to be inextensible and therefore structurally stable, conceivably because of tight association with constituents of the thick filament [47]. Tight association with binding partners is thus a common organizing principle in stabilizing mechanically weak regions in titin. Whether and how these nearly static interactions allow structural rearrangements during myofibrillogenesis and sarcomeric protein turnover await further investigation.

4. Conclusions

The dynamic stability of titin's Z1Z2 domains was explored here by mechanically manipulating a chemical dimer formed of recombinant protein fragments. Z1Z2 domains have a remarkably low dynamic stability, preventing them from withstanding high mechanical forces regardless of loading rates. It is the association of Z1Z2 domains with telethonin that provides sufficient structural stabilization so that titin becomes tightly anchored in the Z-disk.

Acknowledgments

This work was supported by Grants from the Hungarian Science Foundation (OTKA K73256) and the Hungarian National Office of Research and Technology (NANOAMI KFKT-1-2006-0021, OMFB-380/2006) to Miklós S. Z. Keller-mayer, and by a grant from the Hungarian Science Foundation (OTKA F49514) to László Grama.

References

- [1] C. C. Gregorio, H. Granzier, H. Sorimachi, and S. Labeit, "Muscle assembly: a titanic achievement?" *Current Opinion in Cell Biology*, vol. 11, no. 1, pp. 18–25, 1999.
- [2] K. Maruyama, "Connectin/titin, giant elastic protein of muscle," *FASEB Journal*, vol. 11, no. 5, pp. 341–345, 1997.
- [3] K. Wang, "Titin/connectin and nebulin: giant protein rulers of muscle structure and function," *Advances in Biophysics*, vol. 33, pp. 123–134, 1996.
- [4] T. Funatsu, H. Higuchi, and S. Ishiwata, "Elastic filaments in skeletal muscle revealed by selective removal of thin filaments with plasma gelsolin," *Journal of Cell Biology*, vol. 110, no. 1, pp. 53–62, 1990.
- [5] H. L. Granzier and T. C. Irving, "Passive tension in cardiac muscle: contribution of collagen, titin, microtubules, and intermediate filaments," *Biophysical Journal*, vol. 68, no. 3, pp. 1027–1044, 1995.
- [6] R. Horowitz, E. S. Kempner, M. E. Bisher, and R. J. Podolsky, "A physiological role for titin and nebulin in skeletal muscle," *Nature*, vol. 322, no. 6084, pp. 160–164, 1986.
- [7] W. A. Linke, M. Ivemeyer, N. Olivieri, B. Kolmerer, J. C. Rüegg, and S. Labeit, "Towards a molecular understanding of the elasticity of titin," *Journal of Molecular Biology*, vol. 261, no. 1, pp. 62–71, 1996.
- [8] H. Yajima, H. Ohtsuka, Y. Kawamura, et al., "A 11.5-kb 5'-terminal cDNA sequence of chicken breast muscle connectin/titin reveals its Z line binding region," *Biochemical and Biophysical Research Communications*, vol. 223, no. 1, pp. 160–164, 1996.
- [9] M. Gautel, D. Goulding, B. Bullard, K. Weber, and D. O. Fürst, "The central Z-disk region of titin is assembled from a novel repeat in variable copy numbers," *Journal of Cell Science*, vol. 109, no. 11, pp. 2747–2754, 1996.
- [10] M.-L. Bang, T. Centner, F. Fornoff, et al., "The complete gene sequence of titin, expression of an unusual ≈ 700 -kDa titin isoform, and its interaction with obscurin identify a novel Z-line to I-band linking system," *Circulation Research*, vol. 89, no. 11, pp. 1065–1072, 2001.
- [11] H. Sorimachi, A. Freiburg, B. Kolmerer, et al., "Tissue-specific expression and α -actinin binding properties of the Z-disk titin: implications for the nature of vertebrate Z-discs," *Journal of Molecular Biology*, vol. 270, no. 5, pp. 688–695, 1997.
- [12] R. A. Atkinson, C. Joseph, F. Dal Piaz, et al., "Binding of α -actinin to titin: implications for Z-disk assembly," *Biochemistry*, vol. 39, no. 18, pp. 5255–5264, 2000.
- [13] P. Young, C. Ferguson, S. Bañuelos, and M. Gautel, "Molecular structure of the sarcomeric Z-disk: two types of titin interactions lead to an asymmetrical sorting of α -actinin," *The EMBO Journal*, vol. 17, no. 6, pp. 1614–1624, 1998.
- [14] J. O. Vigoreaux, "The muscle Z band: lessons in stress management," *Journal of Muscle Research and Cell Motility*, vol. 15, no. 3, pp. 237–255, 1994.

- [15] D. Frank, C. Kuhn, H. A. Katus, and N. Frey, "Role of the sarcomeric Z-disc in the pathogenesis of cardiomyopathy," *Future Cardiology*, vol. 3, no. 6, pp. 611–622, 2007.
- [16] W. G. Pyle and R. J. Solaro, "At the crossroads of myocardial signaling: the role of Z-discs in intracellular signaling and cardiac function," *Circulation Research*, vol. 94, no. 3, pp. 296–305, 2004.
- [17] W. A. Linke, "Sense and stretchability: the role of titin and titin-associated proteins in myocardial stress-sensing and mechanical dysfunction," *Cardiovascular Research*, vol. 77, no. 4, pp. 637–648, 2008.
- [18] M. K. Miller, H. Granzier, E. Ehler, and C. C. Gregorio, "The sensitive giant: the role of titin-based stretch sensing complexes in the heart," *Trends in Cell Biology*, vol. 14, no. 3, pp. 119–126, 2004.
- [19] G. Valle, G. Faulkner, A. De Antoni, et al., "Telethonin, a novel sarcomeric protein of heart and skeletal muscle," *FEBS Letters*, vol. 415, no. 2, pp. 163–168, 1997.
- [20] C. C. Gregorio, K. Trombitás, T. Centner, et al., "The NH2 terminus of titin spans the Z-disc: its interaction with a novel 19-kD ligand (T-cap) is required for sarcomeric integrity," *Journal of Cell Biology*, vol. 143, no. 4, pp. 1013–1027, 1998.
- [21] E. S. Moreira, T. J. Wiltshire, G. Faulkner, et al., "Limb-girdle muscular dystrophy type 2G is caused by mutations in the gene encoding the sarcomeric protein telethonin," *Nature Genetics*, vol. 24, no. 2, pp. 163–166, 2000.
- [22] R. Knöll, M. Hoshijima, H. M. Hoffman, et al., "The cardiac mechanical stretch sensor machinery involves a Z disc complex that is defective in a subset of human dilated cardiomyopathy," *Cell*, vol. 111, no. 7, pp. 943–955, 2002.
- [23] J. M. Bos, R. N. Poley, M. Ny, et al., "Genotype-phenotype relationships involving hypertrophic cardiomyopathy-associated mutations in titin, muscle LIM protein, and telethonin," *Molecular Genetics and Metabolism*, vol. 88, no. 1, pp. 78–85, 2006.
- [24] C. Geier, A. Perrot, C. Özcelik, et al., "Mutations in the human muscle LIM protein gene in families with hypertrophic cardiomyopathy," *Circulation*, vol. 107, no. 10, pp. 1390–1395, 2003.
- [25] A. Mues, P. F. M. van der Ven, P. Young, D. O. Fürst, and M. Gautel, "Two immunoglobulin-like domains of the Z-disc portion of titin interact in a conformation-dependent way with telethonin," *FEBS Letters*, vol. 428, no. 1–2, pp. 111–114, 1998.
- [26] M. Marino, P. Zou, D. Svergun, et al., "The Ig doublet Z1Z2: a model system for the hybrid analysis of conformational dynamics in Ig tandems from titin," *Structure*, vol. 14, no. 9, pp. 1437–1447, 2006.
- [27] E. H. Lee, J. Hsin, O. Mayans, and K. Schulten, "Secondary and tertiary structure elasticity of titin Z1Z2 and a titin chain model," *Biophysical Journal*, vol. 93, no. 5, pp. 1719–1735, 2007.
- [28] P. Zou, M. Gautel, A. Geerlof, M. Wilmanns, M. H. J. Koch, and D. I. Svergun, "Solution scattering suggests cross-linking function of telethonin in the complex with titin," *Journal of Biological Chemistry*, vol. 278, no. 4, pp. 2636–2644, 2003.
- [29] P. Zou, N. Pinotsis, S. Lange, et al., "Palindromic assembly of the giant muscle protein titin in the sarcomeric Z-disk," *Nature*, vol. 439, no. 7073, pp. 229–233, 2006.
- [30] E. H. Lee, M. Gao, N. Pinotsis, M. Wilmanns, and K. Schulten, "Mechanical strength of the titin Z1Z2-telethonin complex," *Structure*, vol. 14, no. 3, pp. 497–509, 2006.
- [31] M. Bertz, M. Wilmanns, and M. Rief, "The titin-telethonin complex is a directed, superstable molecular bond in the muscle Z-disk," *Proceedings of the National Academy of Sciences of the United States of America*, vol. 106, no. 32, pp. 13307–13310, 2009.
- [32] L. Grama, A. Nagy, C. Scholl, T. Huber, and M. S. Z. Kellermayer, "Local variability in the mechanics of titin's tandem Ig segments," *Croatica Chemica Acta*, vol. 78, no. 3, pp. 405–411, 2005.
- [33] S. Labeit and B. Kolmerer, "Titins: giant proteins in charge of muscle ultrastructure and elasticity," *Science*, vol. 270, no. 5234, pp. 293–296, 1995.
- [34] A. Nagy, L. Grama, T. Huber, et al., "Hierarchical extensibility in the PEVK domain of skeletal-muscle titin," *Biophysical Journal*, vol. 89, no. 1, pp. 329–336, 2005.
- [35] J. L. Hutter and J. Bechhoefer, "Calibration of atomic-force microscope tips," *Review of Scientific Instruments*, vol. 64, no. 7, pp. 1868–1873, 1993.
- [36] G. I. Bell, "Models for the specific adhesion of cells to cells," *Science*, vol. 200, no. 4342, pp. 618–627, 1978.
- [37] E. Evans and K. Ritchie, "Dynamic strength of molecular adhesion bonds," *Biophysical Journal*, vol. 72, no. 4, pp. 1541–1555, 1997.
- [38] M. S. Z. Kellermayer, S. B. Smith, H. L. Granzier, and C. Bustamante, "Folding-unfolding transitions in single titin molecules characterized with laser tweezers," *Science*, vol. 276, no. 5315, pp. 1112–1116, 1997.
- [39] M. Rief, J. M. Fernandez, and H. E. Gaub, "Elastically coupled two-level systems as a model for biopolymer extensibility," *Physical Review Letters*, vol. 81, no. 21, pp. 4764–4767, 1998.
- [40] H. Dietz, M. Bertz, M. Schlierf, et al., "Cysteine engineering of polyproteins for single-molecule force spectroscopy," *Nature Protocols*, vol. 1, no. 1, pp. 80–84, 2006.
- [41] H. Dietz and M. Rief, "Exploring the energy landscape of GFP by single-molecule mechanical experiments," *Proceedings of the National Academy of Sciences of the United States of America*, vol. 101, no. 46, pp. 16192–16197, 2004.
- [42] L. Grama, A. Málnási-Csizmadia, and C. R. Bagshaw, "Mechanical characterization of single green fluorescent protein homopolymer molecules," *Biophysical Journal*, vol. 82, no. 193a, 2002.
- [43] H. Li, W. A. Linke, A. F. Oberhauser, et al., "Reverse engineering of the giant muscle protein titin," *Nature*, vol. 418, no. 6901, pp. 998–1002, 2002.
- [44] H. Li, A. F. Oberhauser, S. B. Fowler, J. Clarke, and J. M. Fernandez, "Atomic force microscopy reveals the mechanical design of a modular protein," *Proceedings of the National Academy of Sciences of the United States of America*, vol. 97, no. 12, pp. 6527–6531, 2000.
- [45] D. J. Brockwell, G. S. Beddard, J. Clarkson, et al., "The effect of core destabilization on the mechanical resistance of 127," *Biophysical Journal*, vol. 83, no. 1, pp. 458–472, 2002.
- [46] M. Rief, M. Gautel, H. E. Gaub, et al., "Unfolding forces of titin and fibronectin domains directly measured by AFM," *Advances in Experimental Medicine and Biology*, vol. 481, pp. 129–141, 2000.
- [47] J. Trinick, "Gytoskeleton titin as a scaffold and spring," *Current Biology*, vol. 6, no. 3, pp. 258–260, 1996.

Research Article

Titin-Isoform Dependence of Titin-Actin Interaction and Its Regulation by S100A1/Ca²⁺ in Skinned Myocardium

Hideto Fukushima,^{1,2} Charles S. Chung,¹ and Henk Granzier¹

¹Department of Physiology, Sarver Molecular Cardiovascular Research Program, University of Arizona, P.O. Box 245217, Tucson, AZ 85724, USA

²Department of Food Science and Technology, National Fisheries University, 2-7-1 Nagata-honmachi, Shimonoseki, Yamaguchi 759-6595, Japan

Correspondence should be addressed to Henk Granzier, granzier@email.arizona.edu

Received 6 December 2009; Accepted 15 January 2010

Academic Editor: Aikaterini Kontrogianni-Konstantopoulos

Copyright © 2010 Hideto Fukushima et al. This is an open access article distributed under the Creative Commons Attribution License, which permits unrestricted use, distribution, and reproduction in any medium, provided the original work is properly cited.

Titin, also known as connectin, is a large filamentous protein that greatly contributes to passive myocardial stiffness. In vitro evidence suggests that one of titin's spring elements, the PEVK, interacts with actin and that this adds a viscous component to passive stiffness. Differential splicing of titin gives rise to the stiff N2B and more compliant N2BA isoforms. Here we studied the titin-isoform dependence of titin-actin interaction and studied the bovine left atrium (BLA) that expresses mainly N2BA titin, and the bovine left ventricle (BLV) that expresses a mixture of both N2B and N2BA isoforms. For comparison we also studied mouse left ventricular (MLV) myocardium which expresses predominately N2B titin. Using the actin-severing protein gelsolin, we obtained evidence that titin-actin interaction contributes significantly to passive myocardial stiffness in all tissue types, but most in MLV, least in BLA, and an intermediate level in BLV. We also studied whether titin-actin interaction is regulated by S100A1/calcium and found that calcium alone or S100A1 alone did not alter passive stiffness, but that combined they significantly lowered stiffness. We propose that titin-actin interaction is a "viscous break" that is on during diastole and off during systole.

1. Introduction

Passive tension development in the sarcomere plays a critical role in diastolic function. The giant protein titin/connectin spans the half-sarcomere from Z-disk to M-line [1] and is responsible for the development of passive tension within the sarcomere [2]. Titin-based passive tension constitutes a large fraction of the myocardial passive tension; the other main contributor is the extracellular matrix [2, 3]. Titin contains an extensible *I*-band region that comprises three distinct regions: serially-linked immunoglobulin (Ig)-like domains, the N2B element, and the PEVK region (which primarily contains proline (P), glutamate (E), valine (V), and lysine (K) residues) [4]. These three spring-like elements develop force when extended and, along with collagen, determine myocardial passive stiffness [5].

Isoform splicing is a long-term mechanism that alters titin-based myocardial passive stiffness [6–8]. Cardiac titin is

present as two isoforms: the small (3.0 MDa) N2B titin and larger N2BA titin isoform (~3.3 MDa) [4, 6]. Differential expression of titin's *I*-band region results in N2BA titin containing a larger PEVK domain than in N2B titin, in addition to a variable number of additional Ig domains [4, 6, 9]. At a given extension, the cardiac N2BA isoform develops less force than the N2B isoform, which can be explained by its longer end-to-end length. This longer length results in a lower fractional extension of the elastic elements in the *I*-band, which leads to lower force development [10, 11]. Consistent with this, mouse knockout models, in which the spring region of titin has been shortened, develop higher passive force [12, 13].

Adding to the complexity of the sarcomeric response to external stretch is the viscous interaction between cardiac PEVK and actin [14–17]. In vitro motility assays [14–16, 18], single molecule studies [19], myocyte mechanics [14], electron microscopy [20], and single myofibril recoil

experiments [21] have provided evidence for a dynamic interaction between the PEVK and F-actin that retards filament sliding. As the sarcomeres change length during active contraction (systole) and passive stretch (diastole), titin's *I*-band region and actin are displaced with respect to one another. F-actin contains negatively-charged regions on its outer surface [22], and the ionic strength dependence of the PEVK-actin interaction suggests that electrostatic interactions play a role in determining the magnitude of the "viscous drag" force of this interaction [14]. In vitro evidence suggests that the PEVK-actin interaction might be regulated by S100A1 [14], a soluble calcium-binding protein present in the myocardium [23], with the interaction reduced in the presence of S100A1 and physiological calcium levels. Thus, isoform splicing represents a long-term response to changing demands on the cardiovascular system, and Ca^{2+} /S100A1 modulated PEVK-actin association might represent a short-term mechanism for changing passive stiffness.

The presence of titin-actin interaction has mainly been investigated in N2B expressing rodent myocardium [14, 15]. However, large mammals, including human, typically express higher levels of N2BA cardiac titin [8] and here we investigated titin-actin interaction in bovine left atrium (BLA) which expresses predominately N2BA titin, and bovine left ventricle (BLV) which coexpresses both N2B and N2BA titin [24, 25]. We compared results to those from the N2B dominant mouse left ventricle (MLV). We used skinned myocardium and studied passive stiffness before and after actin extraction using the actin severing protein gelsolin. We also focused on the possible regulation of actin-titin interaction by S100A1 and calcium, a mechanism of regulation for which support exists from in vitro binding and in vitro motility studies [14], but which has not been tested in a sarcomeric context. The sarcomere has many geometric constraints and contains countless proteins that are absent in the in vitro assays, and these might mask or accentuate properties measured in vitro. The findings of our studies support that titin-actin interaction is universally present in the different titin isoforms, and that the level scales with the stiffness of the isoform. We also found support for regulation of titin-actin interaction by S100A1 and calcium in skinned myocardium. The data indicate that during the cardiac cycle, titin-actin interaction fluctuates, and is strong during diastole when the calcium level is low but considerably weaker during systole when calcium is high.

2. Materials and Method

2.1. Muscles. Hearts were rapidly excised from ~3 mo old C57/BL6, male mice. The left ventricle (LV) was opened and immediately placed in a modified Krebs solution [composition in mM: NaCl 122, KCl 5, NaHCO_3 25, MgCl_2 1.08, NaH_2PO_4 1.3, CaCl_2 0.2, 2, 3–6 butanedione monoxime (BDM) 30, glucose 11.2, insulin 5 U/L, gassed with 95% O_2 , 5% CO_2 , pH 7.4]. Bovine hearts (animals >18 months old and weighing >1100 lbs) were obtained from local slaughterhouses. The hearts were excised within ~15 minutes following death. The left atrium (LA) and

left ventricle were cut into small pieces and placed into oxygenated Krebs solution. Small wall muscle strips (length: 1.5–3.0 mm; diameter ~0.3 mm) were dissected using a high-resolution binocular scope. Extreme care was taken to dissect the strips in the direction of the fibers and to avoid stretching during dissection. Visual inspection under the dissection microscope revealed that some areas of the BLA contained relatively high levels of collagen and these areas were avoided in this study. Muscle strips were skinned in relaxing solution (BES 40 mM, EGTA 10 mM, MgCl_2 6.56 mM, ATP 5.88 mM, DTT 1 mM, K-propionate 46.35 mM, creatine phosphate 15 mM, pH 7.0) (chemicals from Sigma-Aldrich, MO, USA) with 1% Triton-X-100, overnight at ~4°C. The muscle strips were then washed and used for mechanical experiments. To prevent degradation, all solutions contained protease inhibitors (PMSF: 0.5 mM; leupeptin: 0.04 mM, and E64: 0.01 mM). All animal experiments were approved by the University of Arizona Institutional Animal Care and Use Committee and followed the U.S. National Institutes of Health "Using Animals in Intramural Research" guidelines for animal use.

Passive tension was measured with a silicon semiconductor strain gauge (model AE-801, SensoNor, Horten, Norway). Muscle length was controlled by a high-speed motor (Model 308B, Aurora Scientific Inc., Richmond Hill, Ontario, Canada). Preparations were attached to the motor arm and the force transducer via aluminum clips. Using a small prism, the two perpendicular diameters of the muscle were measured and the cross-sectional area was calculated, assuming the cross-section is elliptical in shape. This area was used to calculate the force per unit area (in mN/mm^2), allowing us to compare results from different muscles. Experiments were performed at room temperature (20–22°C). We determined titin's contribution to total passive tension using its fractional contribution in MLV, BLV, and BLA as previously determined (this previous work used the exact same experimental conditions as the present work); see [3]. We also determined the passive stiffness from the local slope of the titin-based tension-SL relation.

Sarcomere length (SL) was measured with laser-diffraction [26, 27]. The diffraction pattern was collected with a bright-field objective, a telescope lens was focused on the back focal plane of the objective, and the diffraction pattern was projected, after compression with a cylindrical lens, onto a photodiode array. The first order diffraction peak position was obtained using a digital spot-position detector board installed in an IBM AT computer. This signal was converted to sarcomere length using a calibration curve that was established with diffraction peaks of a 25 μm grating that was present in the chamber. For further details see [26, 27].

Maximum active force was measured at an SL of 2.0 μm , using an activating solution with pCa 4.5 (pCa = $-\log[\text{Ca}^{2+}]$). Passive force was measured while the muscle was in relaxing solution and stretching the preparation with a constant velocity from its slack length to a predetermined amplitude followed by a release to the slack length at the same velocity. Most experiments were done utilizing a stretch/release velocity of 0.1 length/sec with the length referenced to the slack sarcomere length (~1.9 μm), except

for those in Figure 6 that were done at both 0.1 and 2.0 length/sec. Stretch–release cycles were followed by ~20-min rest periods at the slack length.

To eliminate titin-actin interaction in the *I*-band region of the sarcomere, we used a calcium-independent gelsolin fragment (amino acids 1–406; dissolved in 10 mM 3-(*N*-morpholino) propanesulfonic acid (MOPS), 1.0 mM EGTA, 1.0 mM Mg-acetate, 20 mM K-propionate, 1 mM DTT, and 20 $\mu\text{g}/\text{mL}$ leupeptin, pH 7.0 at 21–23°C), as described previously [28]. Skinned muscle strips were mechanically characterized and the chamber solution was then replaced by gelsolin (3 $\mu\text{g}/\mu\text{L}$) in relaxing solution, as described previously [29, 30], and incubated at room temperature for 4 hours, followed by extensive washing with relaxing solution and a mechanical characterization identical to the one carried out before actin extraction. To determine the degree of thin filament extraction, the maximal active tension (pCa 4.0) at a starting SL of 2.0 μm was measured before and after actin extraction.

To test the effect of low level of calcium or S100A1, a separate group of skinned muscles were incubated in a relaxing solution (pCa 9.0), a calcium (pCa 6.8) solution (solution composition calculated by the program of Fabiato and Fabiato [31]), and either a relaxing solution that contains S100A1 (1 $\mu\text{g}/\mu\text{L}$; S100A1 from Sigma) or a solution that contains both calcium (pCa 6.8) and S100A1. The skinned muscles were incubated in these solutions and were then stretch/released at 0.1 length/sec, allowed to rest 20 minutes, and then stretch/released at 2.0 length/sec.

2.2. Statistics. Data are presented as mean \pm SE. Significant differences were determined using a *t*-test or where appropriate ANOVA. Post hoc comparisons were made using Tukey HSD. Probability values $< .05$ were taken as significant.

3. Results

We focused on the contribution of titin-actin interaction to passive stiffness and its modulation via S100A1 and calcium. We utilized myocardial wall strips from MLV, as a representative of a myocardium that expresses predominately N2B titin, BLA, as a representative of an N2BA dominant sample, and BLV, as a representative of myocardium that coexpresses both N2BA and N2B titin isoforms [11]. The N2B:N2BA expression ratio in the BLV tissues was determined with agarose gels [32] to be 1.2 ± 0.2 ; the inset of Figure 1(b) shows an example of a gel with BLV and BLA samples. We measured passive tension during stretch of the skinned myocardium, before and after extracting actin with gelsolin, in order to deduce whether actin-titin interaction contributes to passive tension. To determine the degree of actin extraction, we measured maximal active tension before and after gelsolin treatment.

Gelsolin treatment resulted in a nearly 95% loss in active tension (Table 1), suggesting that the majority of the thin filaments was extracted in all tissues, consistent with previous work [28]. Although the remaining few percent of active tension could have been eliminated by extending the gelsolin

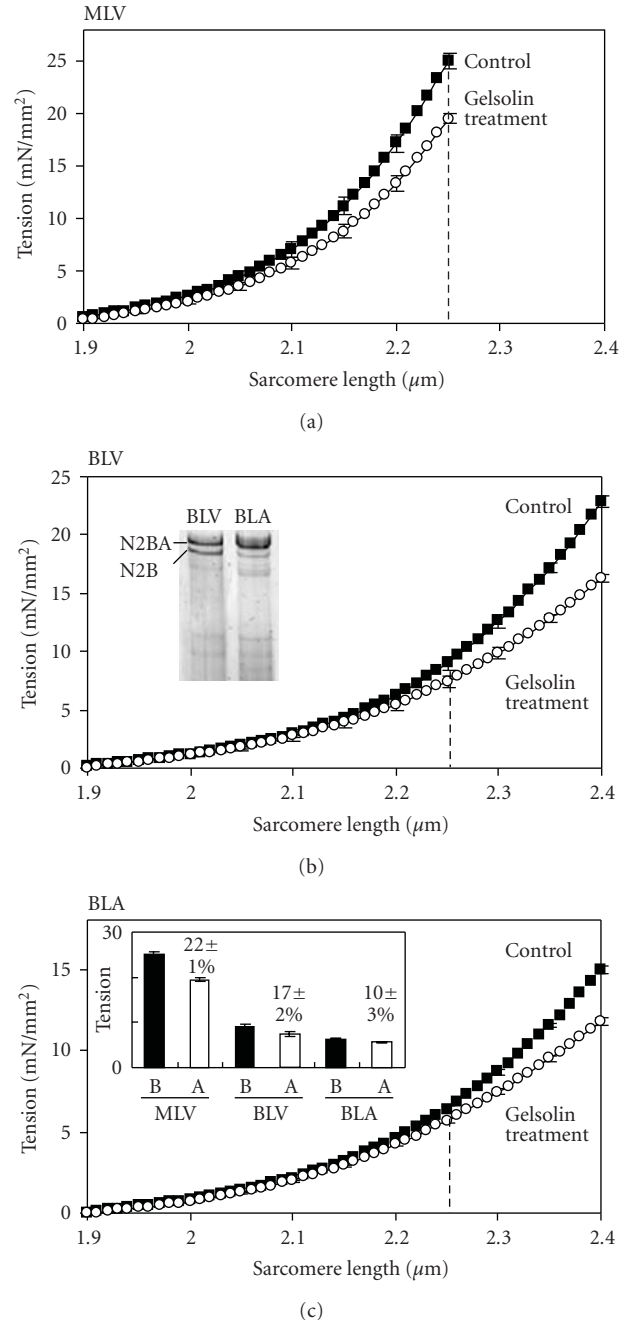


FIGURE 1: Measurements of total passive tension, before and after gelsolin treatment. (a) mouse left ventricle (MLV), (b) bovine left ventricle (BLV), (c) bovine left atrium (BLA) before gelsolin extraction (control, black) and after gelsolin treatment (white). Gelsolin treatment decreases passive tension. Inset of (b): example of titin gel (SDS agarose) with BLV and BLA samples. Inset of (c): tension at SL = 2.25 μm before and after gelsolin treatment with % tension reduction. MLV is more greatly affected by thin filament extraction than BLA, with BLV at an intermediate level. Error bars are SE (for clarity plotted only every 0.05 μm).

treatment duration, because this might recruit titin from near the Z-disc [30], which is normally inextensible, we limited the gelsolin treatment duration such that a very

TABLE 1: Measurement of maximal active tension (pCa 4.5) before and after gelsolin treatment. Percent reduction not different between groups. (SL $2.0\ \mu\text{m}$; $n = 6$ per group; data are mean \pm SE; *** $P < .001$).

Muscle	Dominant Isoform	Active tension before gelsolin treatment (mN/mm ²)	Active tension after gelsolin treatment (mN/mm ²)	Percent tension reduction (%)
MLV	N2B	36.7 \pm 0.9	2.25 \pm 0.26***	93.8 \pm 0.8
BLV	Coexpressing	41.8 \pm 1.5	2.24 \pm 0.16***	94.6 \pm 0.3
BLA	N2BA	33.2 \pm 0.5	2.31 \pm 0.24***	93.0 \pm 0.7

small amount of active tension remained. Thus by comparing passive stiffness of different tissue types and utilizing gelsolin as a tool to extract actin, we investigated the contribution of titin-actin interaction to passive tension in N2B expressing myocardium (MLV), N2BA expressing myocardium (BLA), and N2B and N2BA coexpressing myocardium (BLV).

3.1. Changes in Passive Tension by Thin Filament Extraction.

Because titin-actin interaction is thought to provide a viscous force, the passive tension measured during stretch is expected to be increased by this interaction. We examined passive tension during stretch to sarcomere length $2.25\ \mu\text{m}$ for MLV or $2.4\ \mu\text{m}$ for BLV and BLA. MLV tissues were only stretched to sarcomere lengths (SL) of $2.25\ \mu\text{m}$ so that the tissues would not encounter damage [3]. BLA and BLV tissues were stretched to SL of $2.4\ \mu\text{m}$, which for these tissues is in the reversible length regime [3]. Between tissue types, N2B expressing MLV was found to be stiffer than N2B/N2BA coexpressing BLV, which was stiffer than N2BA expressing BLA (Figure 1, control curves), reproducing earlier findings [3]. Following thin filament extraction, passive tension was reduced and the magnitude was small at short lengths and grew as SL increased (Figure 1). The effect was most pronounced in MLV, intermediate in BLV, and lowest in BLA. Comparing data at an SL of $2.25\ \mu\text{m}$, showed that the magnitude of the reduction was 22, 17, and 10%, respectively (Figure 1(c), inset).

Results in Figure 1 represent total passive tension. Previously, we determined titin's and collagen's fractional contribution to total passive tension of MLV, BLV, and BLA (using the exact same experimental conditions as in the present work) and we used those results [3] to calculate from the total measured tension (Figure 1), the titin-based passive tension. Results are shown in Figure 2, with findings at an SL of $2.25\ \mu\text{m}$ shown in the inset of Figure 2(c). The percent titin-based passive tension reduction at the full SL range is shown in Figure 3(a). In all tissue types, titin-based passive tension increases with SL, and at all SLs the reduction is largest in MLV, less in BLV, and lowest in BLA with values at $2.25\ \mu\text{m}$ of 44, 20, and 12%, respectively. We also determined the passive stiffness from the local slope of the tension-SL relation and calculated the stiffness reduction due to actin extraction. Results shown in Figure 3(b) reveal that in all three tissue types, actin extraction has a large effect on titin-based stiffness, and that the reduction is again largest in N2B expressing MLV and smallest in N2BA expressing BLA with BLV being intermediate.

3.2. Hysteresis in Thin Filament Extracted Tissue.

It is well known that passive tension displays hysteresis (i.e., passive tension is higher during stretch than during release) and because titin-actin interaction appears to contribute to passive tension during stretch we wished to examine whether titin-actin interaction contributes to hysteresis. In the three muscle types, we imposed stretch-releases cycles before and after thin filament extraction and determined hysteresis from the area of the force-length loop of stretches to different SLs (an example of the protocol is shown in Figure 4(a)). In all tissue types, hysteresis increased with SL and, interestingly, gelsolin treatment significantly decreased hysteresis at all lengths. At an SL of $2.25\ \mu\text{m}$ (Figure 4(b)), the decrease was the same in MLV and BLA (33 and 35%, resp.) and larger in BLV (52%). It is important to highlight that hysteresis is not abolished by actin extraction, showing that titin-actin interaction is only partially responsible for hysteresis and that there must be other sources of hysteresis as well.

3.3. Modulation of Titin-Actin Interaction via S100A1 and Ca^{2+} .

While titin-actin interactions might be useful in providing resistance to stretch during diastole, during systole, these interactions could hinder ejection when thin filaments rapidly slide past the extensible region of titin. Thus it is worth examining whether titin-actin interaction is regulated. Based on in vitro studies, we had previously proposed that the Ca^{2+} -binding protein S100A1 regulates actin-titin interaction [3]. Here we investigated the possibility of modulation of passive stiffness via S100A1 and Ca^{2+} . We used a pCa of 6.8 because this is just below the level that causes activation [33]. We focused on MLV because titin-actin interactions are most pronounced in this tissue type, making it easier to detect regulation, if indeed it exists. The example experiment of Figure 5 shows that Ca^{2+} alone or S100A1 alone did not change tension during stretch (Figure 5(a)) but that when combined (pCa 6.8 plus S100A1) passive tension was reduced (Figure 5(b)). We performed experiments at two stretch speeds (0.1 and 2.0 length/sec) and their summarized results are shown in Figure 6. In the presence of Ca^{2+} alone or S100A1 alone, passive tension at both speeds was slightly increased compared to that measured in Ca^{2+} free solution (Figure 6, upper curves). In the presence of both S100A1 and Ca^{2+} , a significant decrease in passive stiffness was observed, with up to 20% decrease at the fastest speed (Figure 6, bottom two curves).

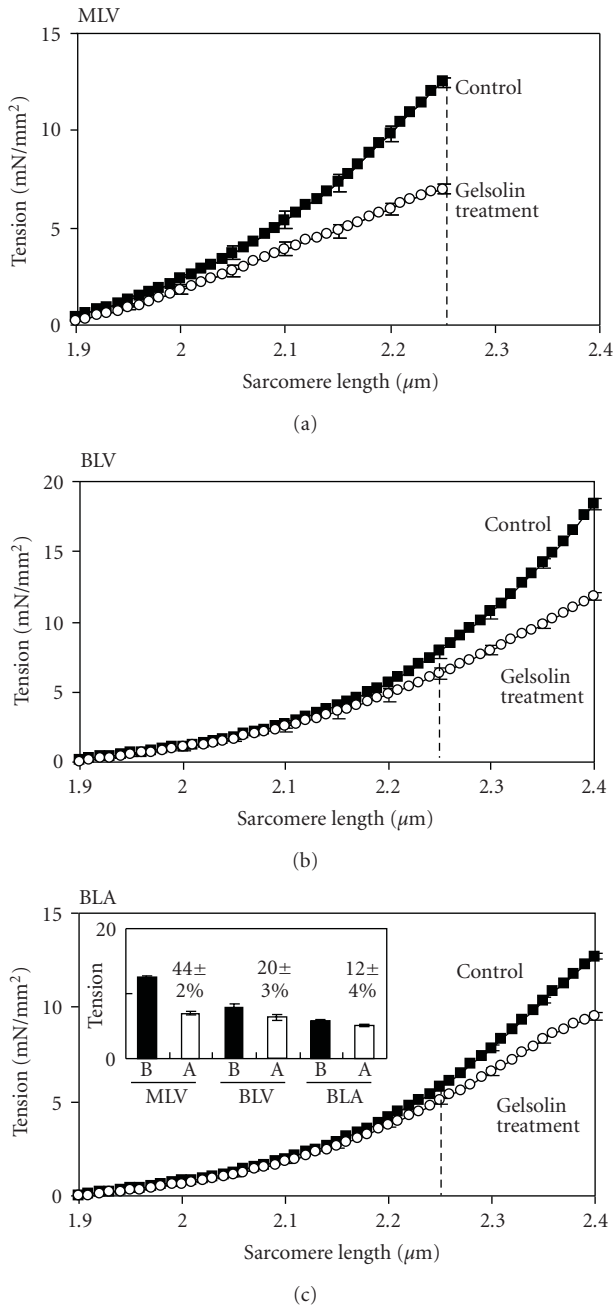


FIGURE 2: Measurements of titin-based passive tension, before and after gelsolin treatment. (a)–(c) In MLV, BLV, and BLA titin-based passive tension is reduced following gelsolin treatment. At a SL of $2.25 \mu\text{m}$. Decrease in titin-based passive tension is largest in MLV, smallest in BLA, with BLV being intermediate. Data are based on Figure 1; see text for details. Error bars are SE (for clarity plotted only every $0.05 \mu\text{m}$).

4. Discussion

We found in this work that thin filament extraction, with the actin-severing protein gelsolin, reduces passive tension during stretch of skinned myocardium. These findings support previous studies that suggest that passive tension

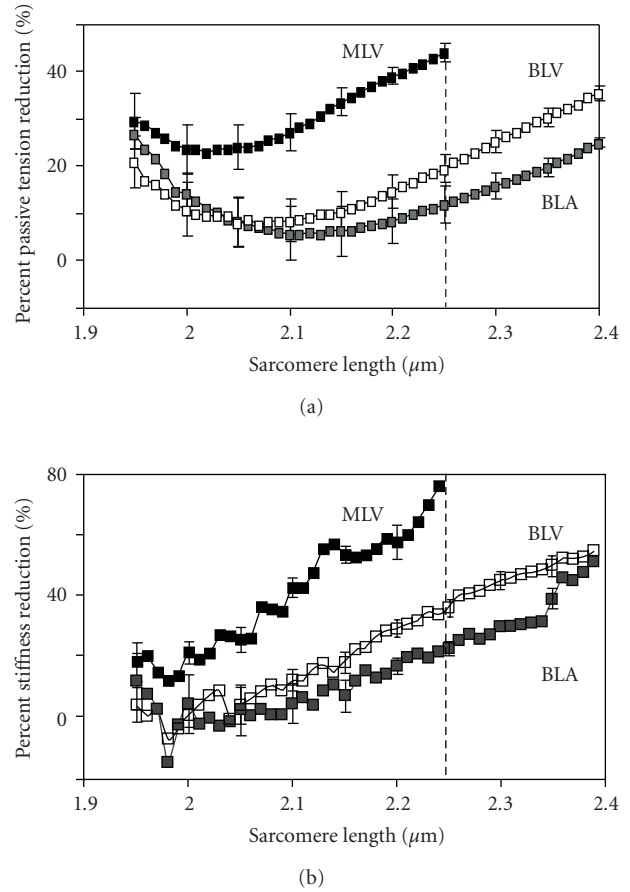


FIGURE 3: Reduction in titin-based tension (a) and titin-based stiffness (b). Data are based on measurements shown in Figure 2 (tension) and from the slope of the tension-SL curve shown in Figure 2 (stiffness). The reductions in tension and stiffness are SL dependent, in all tissue types, and are highest in MLV, lowest in BLA and intermediate in BLV. Error bars are SE (for clarity plotted only every $0.05 \mu\text{m}$).

measured during stretch in cardiac muscle is not solely determined by titin’s intrinsic elasticity, but also includes contributions from a transient (or viscous) force that is due to titin–actin interaction [14, 15]. In vitro binding and motility studies have shown that amongst the three spring elements of cardiac titin, the tandem Ig segments and N2B element do not bind actin, but that the PEVK region does interact with titin [14, 15, 18]. Important evidence for functional significance of titin-actin interaction was obtained in mechanical experiments with mouse cardiac myocytes in which a recombinant protein fragment consisting of the PEVK region of the N2B titin isoform was added to skinned myocytes, and passive tension during stretch was lowered due to a competition with endogenous titin molecules for binding sites on the thin filament [14]. Our present work on mouse skinned myocardium in which we found that thin filament extraction also lowers passive tension during stretch, similarly to what had been found earlier in myocytes with exogenous PEVK, further supports the notion that titin-actin interaction contributes to passive tension

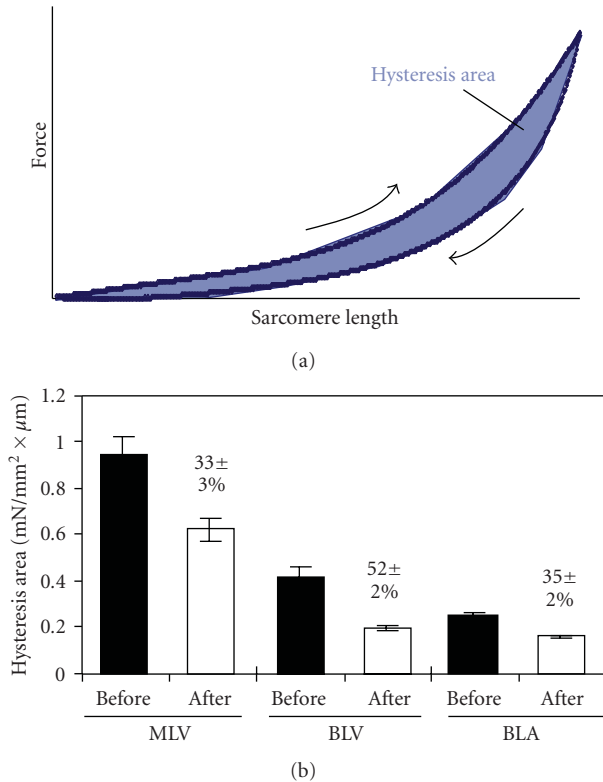


FIGURE 4: Hysteresis before and after gelsolin treatment. (a) Protocol. Skinned muscles were stretched to a given length followed by a release back to slack and hysteresis was calculated from the area of the resultant force-sarcomere length curve. Measurements were made before and after gelsolin treatment. (b) Comparison of hysteresis at SL 2.25 μm with % hysteresis reduction. All tissues showed an increase in hysteresis with SL and a reduction in hysteresis following actin extraction with gelsolin. Error bars are SE. * $P < .01$.

during stretch. Furthermore, our finding that thin filament extraction lowers passive tension in bovine myocardium as well as mouse myocardium (Figures 1–3) suggests that N2BA cardiac titin also interacts with actin and that PEVK-titin interaction is universally represented in different cardiac isoforms.

In vitro binding studies have shown that the binding between F-actin and the PEVK is ionic strength dependent [14, 18, 19], suggesting that the interaction is at least in part electrostatic. F-actin contains a large patch of negatively charged residues on its exposed surface [22], and several actin-binding proteins are known to bind to this region via basic charge clusters [34–36]. The PEVK region of N2B cardiac titin is comprised of basic (pI 9–10) ~28-residue PEVK repeats [6, 37]. At physiological pH, the cardiac PEVK therefore carries a net positive charge, which likely facilitates its interaction with the negatively charged actin filament. Proline-rich regions (PRRs) often assume extended conformations, such as the polyproline II (PPII)-helix that has been predicted for PEVK fragments [38]. Due to the conformational restrictions that proline residues impose on

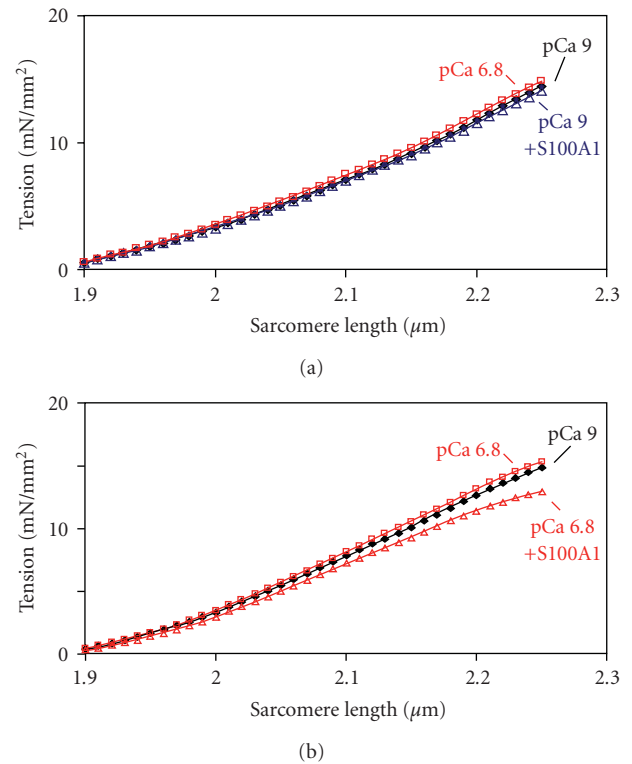


FIGURE 5: Example experiment addressing effect of calcium and S100A1 on tension in skinned muscle during stretch. (a) Skinned MLV muscle was stretched (0.1 length/sec) in pCa 9.0 (black), pCa 6.8 (red), and pCa 9.0 plus S100A1 solution (blue). Calcium (pCa 6.8) or S100A1 alone did not affect tension during stretch. (b) Skinned MLV muscle was stretched (0.1 length/sec) in pCa 9.0 (black), pCa 6.8 (red squares), and pCa 6.8 plus S100A1 solution (red triangles). Only when calcium (pCa 6.8) and S100A1 are both present is passive tension reduced.

the polypeptide backbone, PRRs experience a small reduction of entropy upon ligand binding [39]. This property makes them energetically favorable sites for protein-protein interactions, and there are numerous examples of PRRs that perform binding functions in vivo [39]. The binding of actin by the N2B PEVK may therefore be both electrostatically and thermodynamically favorable.

The in vitro studies discussed above were all carried out with a recombinant PEVK fragment that represents the PEVK sequence found in the human N2B cardiac isoform. The high sequence conservation of the N2B PEVK [28] makes it likely that the same binding properties exist in different species. Additionally, the PEVK sequence of the N2B titin isoform is constitutively expressed in different titin isoforms and thus PEVK-titin interaction is expected to occur in N2BA cardiac titin as well [4, 7, 28]. The N2BA isoform contains additional PEVK residues many of which belong to the above discussed PEVK repeat sequence motif. Others belong to a second PEVK motif (absent in the N2B isoform), the so-called E-rich motif which contains a preponderance of glutamate [4, 40]. Nagy et al. [18] studied

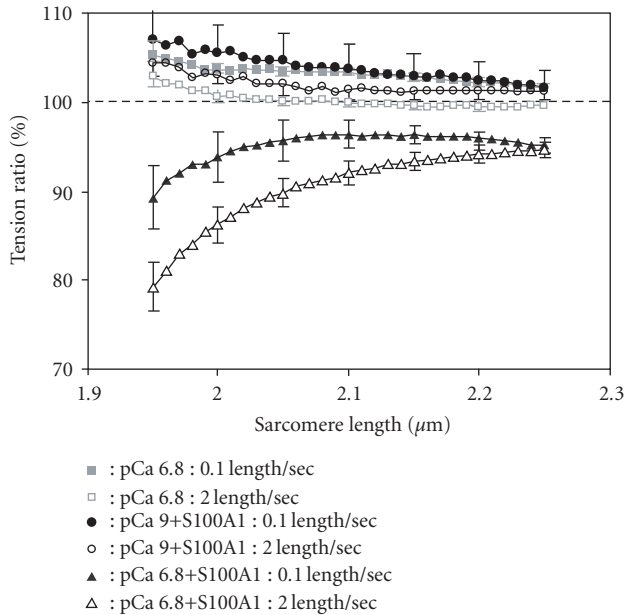


FIGURE 6: Effect of calcium, S100A1, and calcium plus S100A1 on tension. Skinned MLV was stretched at two velocities (0.1 and 2.0 length/sec; dark and open symbols, resp.) in calcium alone (pCa 6.8; grey), S100A1 alone (circles), or calcium plus S100A1 (triangles). Calcium alone or S100A1 alone slightly increases tension (3–8%). When S100A1 is added to pCa 6.8 solutions, tension is decreased, an effect that is largest at the fastest stretch speed. Tensions are expressed relative to tensions measure in the pCa 9.0 solution (See methods for details). Error bars are SE (for clarity plotted only every 0.05 μm).

recombinant PEVK proteins with different motif structures and found that the presence of E-rich motifs *enhances* the actin binding property of the PEVK. Thus, although the PEVK of the N2BA isoform has not been studied in vitro, it is expected that PEVK-actin interaction is present in this titin isoform, consistent with our present findings.

We found that the effect of thin filament extraction was highest in N2B expressing MLV and lowest in N2BA expressing BLA. Although this might suggest that the interaction between the PEVK and actin is less in N2BA titin, as discussed above, this is unlikely to be the case (the interaction might actually be enhanced in N2BA titin) and it is worthwhile therefore to explore alternative explanations. A likely explanation is as follows. The interaction between the PEVK region and the actin filament will during sarcomere stretch impede the extension of the PEVK element, and as a result the extension of the tandem Ig and N2B spring elements (which do not interact with actin) will be increased. The degree to which this increased extension affects force will depend on how much it will increase titin's fractional extension (end-to-end length divided by the contour length) [41–43]. Because N2BA titin has a much longer contour length than N2B titin (due to the extra PEVK residues and additional Ig domains), its increase in fractional extension will be less and hence its increase in force will be less as well (titin's force is a function of its fractional extension; see

[41, 44]). Thus, our findings are consistent with a model in which all titin isoforms interact with actin and in which the isoform's contour length is inversely related to the titin-actin interaction induced force increase. The contour length of N2BA titin is longer than that of N2B titin [11], explaining why the passive tension increase of BLA is much lower than that of MLV. It is also important to highlight that although the effect of titin-thin filament interaction at a given SL is lower in bovine tissues than in mouse, the effects are more similar in the two species when they are compared at their end diastolic SL, which in large mammals has been reported to be $\sim 2.4 \mu\text{m}$ [45], and in rodents $\sim 2.2 \mu\text{m}$ [46]. Thus, titin-actin interaction is likely to play important physiological roles in species as diverse as mouse and bovine.

We have previously shown a correlation between the level of N2B expression and heart beat frequency [8]. We proposed that the short times available for diastolic filling when the heart beats fast (in the mouse, the filling time is only ~ 40 msec) necessitates a stiff ventricle, to ensure that early diastolic filling is fast (titin contributes to the early diastolic suction force [47–49]) and that during late diastole, overfilling is prevented [8]. Because the increased stiffness due to titin-actin interaction is most pronounced at longer SLs (Figure 3(b)), titin-actin interaction might function primarily as a determinant of the maximal filling volume. It is also important to highlight that the contribution of titin-actin interaction to passive stiffness increases with stretch speed (due to its viscous nature, see e.g., [19]), and thus as the heart beats more forceful and faster (as occurs during beta-adrenergic stimulation) titin-actin interaction will further increase stiffness at the large volumes and enhance thereby control over the maximal filling volume. Titin also plays a structural role that includes centering of the A-band in the middle of the sarcomere [50]. Any unevenness in active force generation in the two halves of a sarcomere (which might be due to, for example, micro-variation in the timing of calcium release) is expected to result during systole in movement of the A-band away from its central location in the sarcomere. During diastole, passive tension will reset the A-band to its central location. However, if diastolic durations are extremely short, this is hard to accomplish and stiff titin will speed recentering, with a viscous component at longer length preventing overshoot and possible oscillations. Thus, we propose that titin-actin interaction is important for controlling both late diastolic filling and the structural integrity of the sarcomere.

Although titin-actin interaction is likely to be functionally important during diastole, during systole it is not beneficial because it impedes filament sliding. It has been shown in vitro that S100A1 regulates PEVK-actin interaction [14] and, thus, S100A1 might provide a mechanism for switching PEVK-actin interaction off during part of the heart cycle when it is not a desirable feature to have. S100 is a 25-member family of EF hand proteins, with S100A1 as the most abundant member found in the heart [23]. Physiological levels of calcium activate S100A1, by exposing a hydrophobic domain on S100A1 that is a primary site for protein interactions [23]. Immunoelectron microscopy has shown that in the presence of calcium, S100A1 binds

at several sites along titin's extensible region, including the PEVK domain [14]. Furthermore, gel overlay analysis has revealed that S100A1 binds the PEVK region in a calcium-dependent manner, and in vitro motility assays indicate that S100A1-PEVK interaction reduces the force that arises as F-actin slides relative to the PEVK domain [14]. Thus we had previously proposed that S100A1 provides a mechanism to free the thin filament from titin and reduce titin-based tension before active contraction and rapid filament sliding take place [14]. The present work is the first critical test of this proposal. We used a low level of calcium (pCa 6.8), just below the threshold for contraction, and showed that this alone has no clear effect on tension of skinned myocardium during stretch, and neither has S100A1 alone (5 and 6). However, when both are present, a significant reduction in passive tension during stretch is observed, that scales with stretch speed, as expected from being derived from a viscous source. Thus because S100A1 is constant during the cardiac cycle, and calcium fluctuates, titin-actin interaction will vary: it is strong during diastole when the calcium level is low but considerably weaker during systole when calcium is high.

In summary, our studies support that all cardiac titin isoforms interact with actin and that the degree to which this increases passive stiffness is inversely related to the isoform's contour length. Titin-actin interaction is expected to contribute to the structural integrity of the sarcomere (A-band centering) and the control of late diastolic filling. Furthermore, evidence was obtained for regulation of titin-actin interaction by S100A1/Ca²⁺. We propose that titin-actin interaction functions as "viscous break" that is on during diastole and off during systole.

Acknowledgments

The authors are grateful to Dr. Yiming Wu for training and assistance. This paper is supported by NIH Grant HL62881 (HG), NIH T32 HL07249 (CSC), and AHA Pacific Mountain Affiliate (0825748G) to CSC. Dr. H. Fukushima is currently with the Department of Food Science and Technology, National Fisheries University, Japan.

References

- [1] D. O. Furst, M. Osborn, R. Nave, and K. Weber, "The organization of titin filaments in the half-sarcomere revealed by monoclonal antibodies in immunoelectron microscopy: a map of ten nonrepetitive epitopes starting at the Z line extends close to the M line," *Journal of Cell Biology*, vol. 106, no. 5, pp. 1563–1572, 1988.
- [2] H. L. Granzier and T. C. Irving, "Passive tension in cardiac muscle: contribution of collagen, titin, microtubules, and intermediate filaments," *Biophysical Journal*, vol. 68, no. 3, pp. 1027–1044, 1995.
- [3] Y. Wu, O. Cazorla, D. Labeit, S. Labeit, and H. Granzier, "Changes in titin and collagen underlie diastolic stiffness diversity of cardiac muscle," *Journal of Molecular and Cellular Cardiology*, vol. 32, no. 12, pp. 2151–2161, 2000.
- [4] S. Labeit and B. Kolmerer, "Titins: giant proteins in charge of muscle ultrastructure and elasticity," *Science*, vol. 270, no. 5234, pp. 293–296, 1995.
- [5] M. Helmes, K. Trombitas, T. Centner, et al., "Mechanically driven contour-length adjustment in rat cardiac titin's unique N2B sequence. Titin is an adjustable spring," *Circulation Research*, vol. 84, no. 11, pp. 1339–1352, 1999.
- [6] A. Freiburg, K. Trombitas, W. Hell, et al., "Series of exon-skipping events in the elastic spring region of titin as the structural basis for myofibrillar elastic diversity," *Circulation Research*, vol. 86, no. 11, pp. 1114–1121, 2000.
- [7] H. Granzier, M. Radke, J. Royal, et al., "Functional genomics of chicken, mouse, and human titin supports splice diversity as an important mechanism for regulating biomechanics of striated muscle," *American Journal of Physiology*, vol. 293, no. 2, pp. R557–R567, 2007.
- [8] O. Cazorla, A. Freiburg, M. Helmes, et al., "Differential expression of cardiac titin isoforms and modulation of cellular stiffness," *Circulation Research*, vol. 86, no. 1, pp. 59–67, 2000.
- [9] M.-L. Bang, T. Centner, F. Fornoff, et al., "The complete gene sequence of titin, expression of an unusual approximately 700-kDa titin isoform, and its interaction with obscurin identify a novel Z-line to I-band linking system," *Circulation Research*, vol. 89, no. 11, pp. 1065–1072, 2001.
- [10] K. Trombitás, A. Freiburg, T. Centner, S. Labeit, and H. Granzier, "Molecular dissection of N2B cardiac titin's extensibility," *Biophysical Journal*, vol. 77, no. 6, pp. 3189–3196, 1999.
- [11] K. Trombitás, A. Redkar, T. Centner, Y. Wu, S. Labeit, and H. Granzier, "Extensibility of isoforms of cardiac titin: variation in contour length of molecular subsegments provides a basis for cellular passive stiffness diversity," *Biophysical Journal*, vol. 79, no. 6, pp. 3226–3234, 2000.
- [12] M. H. Radke, J. Peng, Y. Wu, et al., "Targeted deletion of titin N2B region leads to diastolic dysfunction and cardiac atrophy," *Proceedings of the National Academy of Sciences of the United States of America*, vol. 104, no. 9, pp. 3444–3449, 2007.
- [13] H. L. Granzier, M. H. Radke, J. Peng, et al., "Truncation of titin's elastic PEVK region leads to cardiomyopathy with diastolic dysfunction," *Circulation Research*, vol. 105, no. 6, pp. 557–564, 2009.
- [14] R. Yamasaki, M. Berri, Y. Wu, et al., "Titin-actin interaction in mouse myocardium: passive tension modulation and its regulation by calcium/S100A1," *Biophysical Journal*, vol. 81, no. 4, pp. 2297–2313, 2001.
- [15] M. Kulke, S. Fujita-Becker, E. Rostkova, et al., "Interaction between PEVK-titin and actin filaments origin of a viscous force component in cardiac myofibrils," *Circulation Research*, vol. 89, no. 10, pp. 874–881, 2001.
- [16] W. A. Linke, M. Kulke, H. Li, et al., "PEVK domain of titin: an entropic spring with actin-binding properties," *Journal of Structural Biology*, vol. 137, no. 1-2, pp. 194–205, 2002.
- [17] M. S. Z. Kellermayer and H. L. Granzier, "Calcium-dependent inhibition of in vitro thin-filament motility by native titin," *FEBS Letters*, vol. 380, no. 3, pp. 281–286, 1996.
- [18] A. Nagy, P. Cacciafesta, L. Grama, A. Kengyel, A. Málnási-Csizmadia, and M. S. Z. Kellermayer, "Differential actin binding along the PEVK domain of skeletal muscle titin," *Journal of Cell Science*, vol. 117, no. 24, pp. 5781–5789, 2004.
- [19] P. Bianco, A. Nagy, A. Kengyel, et al., "Interaction forces between F-actin and titin PEVK domain measured with optical tweezers," *Biophysical Journal*, vol. 93, no. 6, pp. 2102–2109, 2007.
- [20] T. Funatsu, E. Kono, H. Higuchi, et al., "Elastic filaments in situ in cardiac muscle: deep-etch replica analysis in combination with selective removal of actin and myosin filaments," *Journal of Cell Biology*, vol. 120, no. 3, pp. 711–724, 1993.

- [21] C. A. Opitz, M. Kulke, M. C. Leake, et al., "Damped elastic recoil of the titin spring in myofibrils of human myocardium," *Proceedings of the National Academy of Sciences of the United States of America*, vol. 100, no. 22, pp. 12688–12693, 2003.
- [22] W. Kabsch, H. G. Mannherz, D. Suck, E. F. Pai, and K. C. Holmes, "Atomic structure of the actin:DNase I complex," *Nature*, vol. 347, no. 6288, pp. 37–44, 1990.
- [23] R. Donato, "S100: a multigenic family of calcium-modulated proteins of the EF-hand type with intracellular and extracellular functional roles," *International Journal of Biochemistry and Cell Biology*, vol. 33, no. 7, pp. 637–668, 2001.
- [24] N. Fukuda, Y. Wu, G. Farman, T. C. Irving, and H. Granzier, "Titin isoform variance and length dependence of activation in skinned bovine cardiac muscle," *Journal of Physiology*, vol. 553, no. 1, pp. 147–154, 2003.
- [25] K. Trombitás, Y. Wu, D. Labeit, S. Labeit, and H. Granzier, "Cardiac titin isoforms are coexpressed in the half-sarcomere and extend independently," *American Journal of Physiology*, vol. 281, no. 4, pp. H1793–H1799, 2001.
- [26] H. L. M. Granzier and G. H. Pollack, "The descending of the force-sarcomere length relation of the frog revisited," *Journal of Physiology*, vol. 421, pp. 595–615, 1990.
- [27] H. L. M. Granzier and G. H. Pollack, "Effect of active pre-shortening on isometric and isotonic performance of single frog muscle fibres," *Journal of Physiology*, vol. 415, pp. 299–327, 1989.
- [28] C. Hidalgo, B. Hudson, J. Bogomolovas, et al., "PKC phosphorylation of titin's PEVK element: a novel and conserved pathway for modulating myocardial stiffness," *Circulation Research*, vol. 105, no. 7, pp. 631–638, 2009.
- [29] H. Granzier, M. Helmes, and K. Trombitás, "Nonuniform elasticity of titin in cardiac myocytes: a study using immunoelectron microscopy and cellular mechanics," *Biophysical Journal*, vol. 70, no. 1, pp. 430–442, 1996.
- [30] K. Trombitás and H. Granzier, "Actin removal from cardiac myocytes shows that near Z line titin attaches to actin while under tension," *American Journal of Physiology*, vol. 273, no. 2, part 1, pp. C662–C670, 1997.
- [31] A. Fabiato and F. Fabiato, "Calculator programs for computing the composition of the solutions containing multiple metals and ligands used for experiments in skinned muscle cells," *Journal de Physiologie*, vol. 75, no. 5, pp. 463–505, 1979.
- [32] S. Lahmers, Y. Wu, D. R. Call, S. Labeit, and H. Granzier, "Developmental control of titin isoform expression and passive stiffness in fetal and neonatal myocardium," *Circulation Research*, vol. 94, no. 4, pp. 505–513, 2004.
- [33] O. Cazorla, Y. Wu, T. C. Irving, and H. Granzier, "Titin-based modulation of calcium sensitivity of active tension in mouse skinned cardiac myocytes," *Circulation Research*, vol. 88, no. 10, pp. 1028–1035, 2001.
- [34] G. Fulgenzi, L. Graciotti, A. L. Granata, et al., "Location of the binding site of the mannose-specific lectin comitin on F-actin," *Journal of Molecular Biology*, vol. 284, no. 5, pp. 1255–1263, 1998.
- [35] E. Friederich, K. Vancompernelle, C. Huet, et al., "An actin-binding site containing a conserved motif of charged amino acid residues is essential for the morphogenic effect of villin," *Cell*, vol. 70, no. 1, pp. 81–92, 1992.
- [36] M. Pfuhl, S. J. Winder, and A. Pastore, "Nebulin, a helical actin binding protein," *EMBO Journal*, vol. 13, no. 8, pp. 1782–1789, 1994.
- [37] M. Greaser, "Identification of new repeating motifs in titin," *Proteins*, vol. 43, no. 2, pp. 145–149, 2001.
- [38] K. Ma, L.-S. Kan, and K. Wang, "Polyproline II helix is a key structural motif of the elastic PEVK segment of titin," *Biochemistry*, vol. 40, no. 12, pp. 3427–3438, 2001.
- [39] M. P. Williamson, "The structure and function of proline-rich regions in proteins," *Biochemical Journal*, vol. 297, no. 2, pp. 249–260, 1994.
- [40] D. Labeit, K. Watanabe, C. Witt, et al., "Calcium-dependent molecular spring elements in the giant protein titin," *Proceedings of the National Academy of Sciences of the United States of America*, vol. 100, no. 23, pp. 13716–13721, 2003.
- [41] M. S. Z. Kellermayer, S. B. Smith, C. Bustamante, and H. L. Granzier, "Complete unfolding of the titin molecule under external force," *Journal of Structural Biology*, vol. 122, no. 1–2, pp. 197–205, 1998.
- [42] K. Watanabe, C. Muhle-Goll, M. S. Z. Kellermayer, S. Labeit, and H. Granzier, "Different molecular mechanics displayed by titin's constitutively and differentially expressed tandem Ig segments," *Journal of Structural Biology*, vol. 137, no. 1–2, pp. 248–258, 2002.
- [43] K. Watanabe, P. Nair, D. Labeit, et al., "Molecular mechanics of cardiac titin's PEVK and N2B spring elements," *The Journal of Biological Chemistry*, vol. 277, no. 13, pp. 11549–11558, 2002.
- [44] H. Granzier, M. Kellermayer, M. Helmes, and K. Trombitás, "Titin elasticity and mechanism of passive force development in rat cardiac myocytes probed by thin-filament extraction," *Biophysical Journal*, vol. 73, no. 4, pp. 2043–2053, 1997.
- [45] E. K. Rodriguez, W. C. Hunter, M. J. Royce, M. K. Leppo, A. S. Douglas, and H. F. Weisman, "A method to reconstruct myocardial sarcomere lengths and orientations at transmural sites in beating canine hearts," *American Journal of Physiology*, vol. 263, no. 1, part 2, pp. H293–H306, 1992.
- [46] A. F. Grimm, H. L. Lin, and B. R. Grimm, "Left ventricular free wall and intraventricular pressure-sarcomere length distributions," *American Journal of Physiology*, vol. 239, no. 1, pp. H101–H107, 1980.
- [47] M. Helmes, K. Trombitás, and H. Granzier, "Titin develops restoring force in rat cardiac myocytes," *Circulation Research*, vol. 79, no. 3, pp. 619–626, 1996.
- [48] N. Preetha, W. Yiming, M. Helmes, F. Norio, L. Siegfried, and H. Granzier, "Restoring force development by titin/connectin and assessment of Ig domain unfolding," *Journal of Muscle Research and Cell Motility*, vol. 26, no. 6–8, pp. 307–317, 2005.
- [49] S. P. Bell, L. Nyland, M. D. Tischler, M. McNabb, H. Granzier, and M. M. LeWinter, "Alterations in the determinants of diastolic suction during pacing tachycardia," *Circulation Research*, vol. 87, no. 3, pp. 235–240, 2000.
- [50] R. Horowitz and R. J. Podolsky, "The positional stability of thick filaments in activated skeletal muscle depends on sarcomere length: evidence for the role of titin filaments," *Journal of Cell Biology*, vol. 105, no. 5, pp. 2217–2223, 1987.

Review Article

S100A1: A Regulator of Striated Muscle Sarcoplasmic Reticulum Ca^{2+} Handling, Sarcomeric, and Mitochondrial Function

Mirko Völkers,¹ David Rohde,¹ Chelain Goodman,² and Patrick Most²

¹Division of Cardiology, Department of Internal Medicine III, Laboratory for Molecular and Translational Cardiology, University of Heidelberg, INF 350, 69120 Heidelberg, Germany

²Department of Medicine, Center for Translational Medicine, Laboratory for Cardiac Stem Cell and Gene Therapy, Thomas Jefferson University, Philadelphia, PA 19107, USA

Correspondence should be addressed to

Mirko Völkers, mirko.voelkers@med.uni-heidelberg.de and Patrick Most, patrick.most@jefferson.edu

Received 11 November 2009; Accepted 12 January 2010

Academic Editor: Henk L. M. Granzier

Copyright © 2010 Mirko Völkers et al. This is an open access article distributed under the Creative Commons Attribution License, which permits unrestricted use, distribution, and reproduction in any medium, provided the original work is properly cited.

Calcium (Ca^{2+}) signaling plays a key role in a wide range of physiological functions including control of cardiac and skeletal muscle performance. To assure a precise coordination of both temporally and spatially transduction of intracellular Ca^{2+} oscillations to downstream signaling networks and target operations, Ca^{2+} cycling regulation in muscle tissue is conducted by a plethora of diverse molecules. Ca^{2+} S100A1 is a member of the Ca^{2+} -binding S100 protein family and represents the most abundant S100 isoform in cardiac and skeletal muscle. Early studies revealed distinct expression patterns of S100A1 in healthy and diseased cardiac tissue from animal models and humans. Further elaborate investigations uncovered S100A1 protein as a basic requirement for striated muscle Ca^{2+} handling integrity. S100A1 is a critical regulator of cardiomyocyte Ca^{2+} cycling and contractile performance. S100A1-mediated inotropy unfolds independent and on top of β AR-stimulated contractility with unchanged β AR downstream signaling. S100A1 has further been detected at different sites within the cardiac sarcomere indicating potential roles in myofilament function. More recently, a study reported a mitochondrial location of S100A1 in cardiomyocytes. Additionally, normalizing the level of S100A1 protein by means of viral cardiac gene transfer in animal heart failure models resulted in a disrupted progression towards cardiac failure and enhanced survival. This brief review is confined to the physiological and pathophysiological relevance of S100A1 in cardiac and skeletal muscle Ca^{2+} handling with a particular focus on its potential as a molecular target for future therapeutic interventions.

1. Introduction

Ca^{2+} is a highly versatile intracellular signal that controls many different cellular functions. Therefore, Ca^{2+} signals need to be flexible yet precisely regulated. Besides controlling gene transcription and growth, Ca^{2+} regulates the contraction and relaxation in muscles tissue. Skeletal and cardiac muscle belong to the striated tissue and share many functional aspects. The Ca^{2+} signals require downstream proteins to connect Ca^{2+} oscillations to different signaling domains. Ca^{2+} cycling in muscle tissue is regulated by a plethora of proteins, transmitting the Ca^{2+} messages with precision and in a temporally and spatially coordinated manner. One of these specific Ca^{2+} binding protein families within muscle cells is the S100 protein family.

The process of excitation-contraction coupling (ECC) in skeletal and cardiac muscle cells requires membrane depolarization. After membrane depolarization, Ca^{2+} influx is activated via voltage-gated L-type Ca^{2+} channels into the cytosol of both skeletal muscle cells and cardiac myocytes [1]. This rise in cytoplasmic Ca^{2+} concentration leads to Ca^{2+} release from the sarcoplasmic reticulum (SR) (Ca^{2+} induced Ca^{2+} release-CICR) by activation of Ryanodine receptors (RyR), whereas in skeletal muscle voltage dependent Ca^{2+} release occurs (VICR). After Ca^{2+} release of the RyR, Ca^{2+} molecules subsequently bind to the contractile proteins such as troponin c, which causes contraction of the myocytes. Thereafter, Ca^{2+} is cleared from the cytosol by reuptake of Ca^{2+} into the SR by the action of a sarcoplasmic reticulum Ca^{2+} ATPase (SERCA).

Much evidence has accumulated that abnormal regulation of intracellular Ca^{2+} by the SR plays a key role in the development of cardiac diseases. A decreased Ca^{2+} transient leads to a decreased contractility of the cardiomyocytes. The reduced Ca^{2+} transients are mainly related to a decreased SR Ca^{2+} load. Correction of the disorder of Ca^{2+} cycling has a potential as a new and intriguing therapeutic strategy against cardiac disease states.

Among others proteins, it has been proven that S100A1 regulates sarcoplasmic reticulum Ca^{2+} handling in skeletal and cardiac muscles [2, 3]. In this brief review, we discuss the physiological role of S100A1 in the regulation of ECC in skeletal and cardiac muscles. In addition, we focus on pathophysiological consequences of altered S100A1 expression in cardiovascular disease to provide a comprehensive understanding of the role of S100A1. Finally, we aim to highlight the potential of an S100A1-targeted therapy in cardiovascular diseases.

2. S100 Protein Family

S100 Ca^{2+} -binding proteins are the largest subfamily of EF-hand proteins (25 human genes), putatively targeting more than 90 proteins (previously reviewed in [4, 5]). S100 proteins are small acidic proteins (10–12 kDa) that are found exclusively in vertebrates. These proteins were first identified by Moore in 1965 and characterized as “S100” in consequence for their unique solubility in 100% saturated solution with ammonium sulphate and were designated by consecutive arabic numbers placed behind the stem symbol, for example, *s100a1*, *s100a2*, *s100a3*, and so forth [4] due to their clustered organization on human chromosome 1q21.

Each S100 monomer contains two EF-hand Ca^{2+} binding domains interconnected by an intermediate region (hinge region) (Figure 1) [6] exerting unique features when compared with other EF-hand proteins. First, the two EF hands in each monomer differ in sequence and affinity for Ca^{2+} binding. The c-terminal EF hand contains the classical canonical Ca^{2+} binding motif and ligates Ca^{2+} in a similar manner to calmodulin and troponin C, resulting in *Kd* 10–50 μM . The NH2-terminal pseudo-EF hand contains two additional amino acids and is a characteristic of S100 proteins. Consequently, Ca^{2+} affinities decreased to a *Kd* between 200–500 μM (reviewed in [6]). Importantly, Ca^{2+} affinity is regulated by posttranslational mechanism facilitating Ca^{2+} binding and activation of S100 proteins even at nanomolar free Ca^{2+} concentrations. Ca^{2+} binding eventually triggers exposure of a hydrophobic epitope which is believed to mediate represent a major interaction site enabling accommodation of target proteins through the exposure of a hydrophobic epitope that surface represents the interaction site of most S100 proteins for the binding of target proteins (Figure 2). The second unique characteristic compared to EF-hand proteins of S100 proteins is their dimeric nature, as it has been shown both in vivo and in vitro that S100 proteins form noncovalent homo- and heterodimers (Figure 2). Third, S100 proteins are expressed in a tissue- and cell- specific fashion, pointing to higher

degree of specification. The most abundant S100 protein isoform in cardiac and skeletal muscle is S100A1 among other S100 isoforms such as S100A4, S100A6, and S100B and in heart S100A1 is mainly found in ventricular cardiomyocytes.

3. S100A1—A Member of the S100 Protein Family

In a wide range of small (mouse, rat) and large (rabbit, dog, swine) animals, S100A1 is preferentially found in the heart and in lower concentrations in skeletal muscle [8–10]. Healthy human tissue exhibits a similar distribution [11], and most recently, large-scale analyses of the human transcriptome by Su et al. [12] and Shmueli et al. [13] comprehensively confirmed that the human heart is the predominant location of S100A1. S100A1 expression steadily increases during cardiac development in mice and reaches a plateau in ventricular myocardium in the postnatal state [14]. Estimations of total intracellular concentrations of S100A1 in isolated murine and rat left ventricular myocytes revealed a range between 40 to 200 nM ([12], Völkers M, unpublished observations).

In the adult heart, S100A1 protein is not uniformly expressed but exhibits its highest mRNA and protein levels in the left ventricle, with lower concentrations in the right ventricle and atria [6, 15]. Analysis of the S100A1 promoter in rodents identified a subset of transcription-factor consensus sequences (i.e., homeobox protein NK-2 homolog E, myocyte enhancer factor-2, GATA4) [14] that are well known to drive cardiac-specific gene expression of cardiac troponin C or calsequestrin and potentially to convey predominant cardiac expression of S100A1. First clinical interest in S100A1 has been sparked due to its altered expression in diseased myocardium.

3.1. Protein Structure. The S100A1 monomer with a molecular weight of 10.4 kDa consists of two EF-hand Ca^{2+} binding motifs connected by a hinge region. In each EF-hand, a Ca^{2+} binding loop is flanked by α -helices, resulting in a helix-EF-hand-helix arrangement. Helix I and II flank the n-terminal loop, whereas helices III and IV flank the c-terminal loop (Figure 1). Stabilization of the homodimer occurs independent of Ca^{2+} binding through hydrophobic bonds between helices I and I' of each monomer [6]. After Ca^{2+} binding each monomer undergoes a conformational change resulting in the exposure of a hydrophobic pocket in the C-terminus which is believed to be the major docking site for Ca^{2+} -dependent interactions between S100A1 and its target proteins. This pocket consists of residues of the hinge region, helix III and the C-terminus. Since residues within the hinge region and C-terminus display the greatest sequence variability among S100 isoforms, they are viewed to mediate isoform-specific target recognition [6]. Ca^{2+} binding to individual EF-hands in the S100A1 dimer has been estimated to occur with a *Kd* of 200–500 μM at the N-terminal and a *Kd* of 10–50 μM at the C-terminal. However, Ca^{2+} affinity of both sides is tightly regulated by

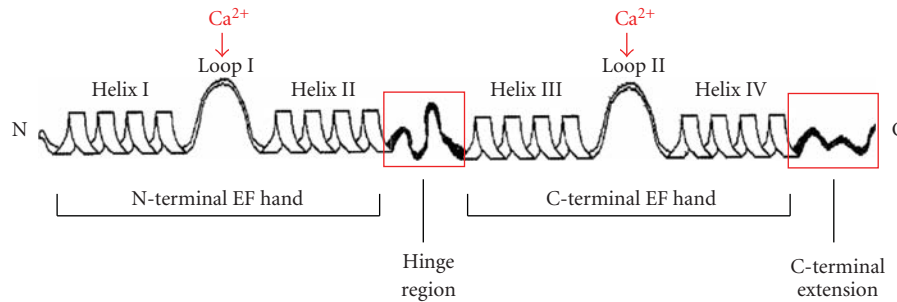


FIGURE 1: Schematic depiction of the secondary structure of an S100 protein. The monomeric structure consists of a repetitive EF-hand motif, whereas each Ca^{2+} -binding Loop (Loop I and II) is flanked by α -helices. The N-terminal and the C-terminal EF hands are connected by a linker region (hinge region). The hinge region and the C-terminal extension (boxed in red) display the least amount of sequence homology among S100 paralogs. Reproduced with modifications from Donato [5]. [http://www.ncbi.nlm.nih.gov/pubmed/11390274?itool=EntrezSystem2.PEntrez.Pubmed.Pubmed_ResultsPanel.Pubmed_RVDocSum&ordinalpos=9].

posttranslational mechanism, that is, redox dependent S-glutathionylation of cysteine residues which enables S100A1 to sense Ca^{2+} even at nanomolar concentration (see below).

3.2. Cardiac Subcellular S100A1 Location. Dependent on the Ca^{2+} binding in adult cardiomyocytes, S100A1 mainly resides on the SR, mitochondria and myofilaments. At the molecular level, S100A1 has been shown to interact with the cardiac ryanodine receptor (RyR2) [16–19], the SR Ca^{2+} -ATPase 2a (SERCA2a)-phospholamban (PLB) complex [16, 20, 21], the F1 portion of the mitochondrial ATP synthase [22] mostly in a Ca^{2+} -dependent manner and acts also as a binding partner for the giant myofilament protein titin [23, 24]. As mentioned, Ca^{2+} binding triggers exposure of hydrophobic epitope mainly dened by residues within the S100A1 hinge region and COOH-terminal extension (Figure 2) [7]. Because most actions of S100A1 apparently rely on transition to its Ca^{2+} -activated state, it is important to note that recent studies provided first evidence for redox-dependent posttranslational control of S100A1's Ca^{2+} sensitivity. NO-dependent S-glutathionylation of a single cysteine residue within the hydrophobic COOH terminus eventually facilitated binding of Ca^{2+} at nanomolar concentrations reflecting diastolic Ca^{2+} levels in cardiomyocytes [25, 26]. The only S-nitrosylation site of S100A1 is its unique Cys-85 residue. Recent studies indicate that under physiological conditions the ability of S100A1 protein to act as a calcium receptor can be turned on by glutathionylation (cysteinylation) of its Cys85 residue and off by reduction of the mixed disulfide S100A1–glutathione (S100A1–cysteine) species. To our knowledge no studies in cardiomyocytes exist which investigate the basal redox state of S100A1. However preliminary data indicate that the addition of reducing agents to the cardiomyocytes abolished the inotropic effects of S100A1 in vitro (M. Volkers, unpublished data).

Redox and NO-related posttranslational modification of single cysteine residue might therefore enable S100A1 to sense spatially defined short-term as well as long-term global Ca^{2+} oscillations in cardiac cells over a broad concentration range enabling its interaction with target proteins such as RyR and SERCA. However, the impact of altered redox

conditions and NO homeostasis on S100A1 actions in myocardium has not yet been tested.

4. Molecular Targets and Physiological Functions in Cardiac Myocytes

4.1. Lesson from Genetically Altered Miced. Gain- and loss-in-function studies comprehensively characterized S100A1 as a unique molecular inotrope in vivo and ex vivo. Increasing S100A1 protein levels in isolated adult and neonatal cardiomyocytes enhanced both their systolic and diastolic performance through modulation of cellular Ca^{2+} handling and myofilament function [17, 19, 20, 24, 27]. Cardiac-specific overexpression of S100A1 in mice displayed a phenotype of chronically heightened cardiac performance without detrimental effects on survival or development of cardiac hypertrophy [19]. The S100A1-mediated increase in cardiac performance is independent of beta-adrenergic stimulation and is even preserved under stimulation with catecholamines. Expression analysis yielded that S100A1-mediated inotropic effects are neither the result of altered abundance of SR and sarcolemmal Ca^{2+} regulators, respectively, nor that they depend on β -AR signalling [2, 15, 17–19, 21, 28–35]. To our knowledge, the apparent independence of S100A1 inotropic actions from the β -AR signalling pathway is a unique feature of the Ca^{2+} sensing protein and of particular importance in cardiovascular physiology and therapy.

In line with cardiac specific overexpression of S100A1 in transgenic mice, viral-based overexpression of S100A1 in rabbit and rat hearts and isolated cardiomyocytes recapitulated the hypercontractile phenotype based on enhanced Ca^{2+} cycling but independent, and additive to beta-AR signalling [15, 17, 18, 33, 34]. Therefore, it is interesting to note that acute or chronic elevated S100A1 proteins in cardiomyocytes induce sustained cardiac inotropy, without toxic effects to the cardiomyocytes. This is clinically important because chronic inotropic stimulation of the heart through activation of the beta-receptors or downstream effectors such as PKA eventually led to cardiac hypertrophy and failure.

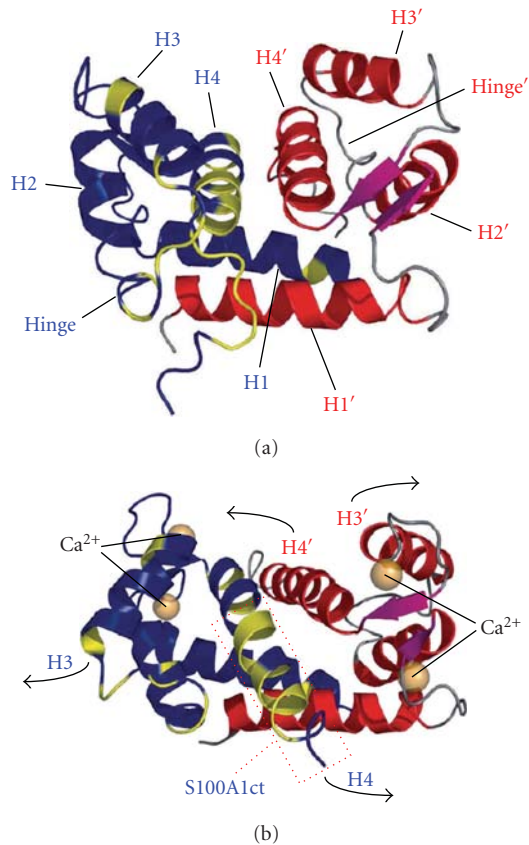


FIGURE 2: The three-dimensional structure of S100A1 as determined by NMR spectroscopy. (a) S100A1 in the apo state: S100A1 is composed of two identical subunits connected by a linker region (hinge region). Dimerization occurs in an antiparallel manner. (b) S100A1 in the Ca^{2+} bound state: Ca^{2+} binding to both the N- and C-terminal motif results in an altered orientation of H3/4 and the hinge region uncovering hydrophobic residues for the interaction with target molecules. S100A1 residues 75–94 are indicated by the red box. Reproduced with modifications from Wright et al. [7].

In contrast, heterozygous and homozygous S100A1 knockout (SKO) mice showed unaltered *in vivo* baseline cardiac function and heart rate, but displayed deficiencies in their contractile function in response to β -AR stimulation and enhanced transsarcolemmal Ca^{2+} influx [36].

This is interesting to note because heterozygous SKO hearts, with only 50% of S100A1 protein levels found in wild-type hearts, exhibit the same acute defects than homozygous SKO hearts with complete lack of S100A1 expression. Thus >50% of normal left-ventricular S100A1 protein levels are apparently required for cardiac adaptation to acute hemodynamic stress. Of note, loss of β -AR-dependent inotropy in SKO mice occurs despite regular β -AR signaling ranging from unaltered β -AR density to proper PKA-dependent target phosphorylation, thereby indicating that β -AR-mediated positive inotropy essentially relies on normal S100A1 protein levels in the heart.

Additional exploration of isolated S100A1 knock-out cardiomyocytes revealed blunted Ca^{2+} transients in response

to sympathetic stimulation and increased extracellular $[\text{Ca}^{2+}]$ [31]. This is mainly mediated by a decreased Ca^{2+} release (and reduced SR Ca^{2+} load). Similar results were obtained in neonatal ventricular cardiomyocytes, with a S100A1 protein knockdown to 20–30% of control protein levels [22].

Thus defective mobilization of Ca^{2+} from intracellular stores might provide a reasonable mechanism for the impaired inotropic reserve in S100A1-deficient and -depleted cardiomyocytes. In line with this, murine S100A1 knock out ventricular cardiomyocytes have enhanced l-type Ca^{2+} current $[I_{\text{Ca,L}}]$ (Most P, unpublished data), which indicates that desensitized Ca^{2+} induced Ca^{2+} release (CICR) under basal conditions might be compensated by increased $[I_{\text{Ca,L}}]$.

4.2. Molecular Targets: Sarcoplasmic Reticulum in Cardiac Myocytes. Studies focused on mechanisms underlying S100A1 inotropic actions provided evidence that S100A1 targets SR but not transsarcolemmal Ca^{2+} fluxes in ventricular cardiomyocytes. Several studies identified the impact of S100A1 on intracellular Ca^{2+} homeostasis and consistently found that S100A1 increases systolic and diastolic performance through an enhanced Ca^{2+} induced Ca^{2+} release and augmented SR Ca^{2+} reuptake [17–19, 21, 27, 31]. At the subcellular level, endogenous S100A1 displays a striated like pattern in ventricular cardiac myocytes and is found at the junctional and longitudinal sarcoplasmic reticulum. Accordingly, S100A1 was found to colocalize and interact with SERCA2 and RyR2 in a Ca^{2+} -dependent manner in human, mouse and rat myocardium.

In line with Ca^{2+} -dependent conformational changes, binding studies identified the S100A1 COOH terminus (S100A1ct) as the critical structure for the interaction with the SERCA-PLB complex [18]. Functional analysis in isolated SR vesicles and intact cardiomyocytes showed that S100A1 apparently stimulated SERCA2 activity resulting in increased SR Ca^{2+} reuptake and enhanced SR Ca^{2+} load. In isolated SR vesicles a similar increase in SERCA activity was obtained with S100A1ct consisting of the c-terminal amino acid residues 75–94, which indicates the crucial role of helix IV for the Ca^{2+} dependent functions of S100A1 [18].

The underlying molecular mechanism has not been explored yet, but it is important to note that neither S100A1 nor S100A1ct affects PLB phosphorylation at serine 16 or threonine 17 sites, suggesting that neither PKA nor CaMKII are involved in S100A1-mediated SERCA2 regulation. This might also indicate that S100A1 does not limit access of these kinases to their specific phosphorylation sites [17].

S100A1 binding to the RyR also seems to be Ca^{2+} -dependent since mapping studies also identified S100A1ct as the critical S100A1 epitope for its RyR2 interaction [27]. Recent studies found that S100A1 can bind to the calmodulin (CaM) binding domain in the cytoplasmic portion of skeletal ryanodine receptor isoform (RyR1), which is highly conserved between RyR1 and RyR2 [37, 38]. S100A1 modulates both diastolic and systolic RyR2 functions and thereby alters frequency and characteristics of elementary SR Ca^{2+} events

(Ca²⁺ sparks) and Ca²⁺ induced SR Ca²⁺ release, respectively. At nanomolar free Ca²⁺ concentrations, S100A1 decreased ³H-ryanodine binding to the SR Ca²⁺ release channel, suggesting an inhibitory effect on RyR2 opening under diastolic conditions [18, 20]. In line with this, S100A1 interaction with RyR2 even at diastolic Ca²⁺ concentration [150 nM] decreased Ca²⁺ spark frequency and diastolic SR Ca²⁺ leak in quiescent rabbit cardiac myocytes and cardiac SR vesicle preparations, which indicates that S100A1 can improve RyR2 closure during cardiomyocyte relaxation [27]. In contrast, at micromolar systolic Ca²⁺ concentrations S100A1 provoked increased ³H-ryanodine binding in isolated SR vesicles [18]. Accordingly, a recent study confirmed that S100A1 increased fractional Ca²⁺ release of the SR in voltage-clamped rabbit cardiomyocytes, suggesting that S100A1 can improve excitation-contraction coupling gain in cardiac myocytes under systolic conditions [20]. Taken together, these data support the hypothesis that S100A1 promotes RyR2 closure during diastole but can augment systolic RyR2. The differential effects predict more than only one binding site at the RyR2 and this notion is further supported by recent mapping studies. At least three different S100A1 binding domains have been identified with different binding affinities within the cytoplasmic portion of the RyR [39]. Further functional analyses confirmed that of S100A1 actions on diastolic RyR2 function neither changed FKBP12.6 nor sorcin stoichiometry with the RyR2 channel [27]. Therefore it is attractive to hypothesize that both inhibitory and stimulatory bindings sites for S100A1 might coexist at the RyR2, which eventually account for physiological normal diastolic and systolic performance of the SR Ca²⁺ release channel. Moreover, given the redox sensitivity of the RyR, NO-dependent posttranslational modifications of S100A1 might contribute to the actions on the SR release channel, that is, through transfers of NO moieties. In summary, the precise mechanism underlying S100A1-mediated regulation of RyR2 remains to be determined, but evidence points toward a biphasic modulation of RyR2 activity.

Interestingly, it has been shown that S100A1 neither altered L-type Ca²⁺ current nor sodium-calcium exchanger (NCX) reverse or forward mode in adult ventricular cardiomyocytes [27] and similar results were found for intracellular S100A1 in neonatal ventricular cardiac myocytes [21]. These results further support the notion that enhanced cardiomyocyte S100A1 proteins do not evoke cardiac hypertrophy, because the S100A1 Ca²⁺ sensor does not seem to enhance subsarcolemmal Ca²⁺ fluxes participating in Ca²⁺ dependent hypertrophic cardiac growth [19, 31].

4.2.1. Molecular Targets: Sarcomere. Inotropic actions of S100A1 are apparently not restricted to the SR, because S100A1 has been shown to regulate both myofilament Ca²⁺ sensitivity and diastolic compliance. S100A1 has been detected at different sites within the cardiac sarcomere, suggesting a possible role in myofilament function [23, 24, 40–42]. S100A1 has been detected at the Z-line, at the periphery of the M-lines as well as within I- and A-bands. In the I-band, Ca²⁺-dependent interaction with the PEVK

subdomain of titin has been shown to result in improved sarcomeric compliance [23, 24]. It remains to be established if the binding partner in the A-band is also titin or another thick-filament protein. Granzier and colleagues hypothesized if S100A1 does bind titin in the A-band, the location of the binding sites suggests interaction with titin's super-repeat domains.

Based on their results, Granzier and colleagues hypothesized that S100A1 inhibition of titin-actin interaction might result in reduced precontractile titin-based passive tension. In addition, it has been shown that S100A1 can reduce myofilament Ca²⁺ sensitivity without affecting maximal force development and PKA- and PKC-dependent troponin I phosphorylation. As a result, S100A1 might facilitate diastolic Ca²⁺ dissociation from myofilaments thereby improving cardiac relaxation by an additional, SR-independent mechanism. At present, it is unknown whether S100A1 has additional sarcomeric targets warranting further studies to determine the functional role of S100A1 location at Z-disc adjacent protein structures.

4.2.2. Molecular Targets: Additional Targets-Mitochondria. Bøerries et al. provided first evidence that S100A1 is found in cardiac mitochondria by immunofluorescence and immunoelectron microscopy. In the mitochondria S100A1 interacts with the F1-ATPase in a Ca dependent manner [22]. This resulted in enhanced activity of the ATP generation. The same study identified the adenine nucleotide translocator (ANT) as a mitochondrial S100A1 target. This suggests that interaction of S100A1 with ANT might influence the ADP and ATP exchange between the mitochondria and the cytoplasm. This might also be involved in the regulation of cardiac apoptosis, as another study yielded antiapoptotic effects of S100A1 in isolated neonatal rat ventricular myocytes [28]. In line with this, decreased S100A1 protein levels resulted in a reciprocal energetic phenotype with decreased ATP-levels and enhanced cardiomyocyte apoptosis. These findings support a crucial role for S100A1 in cardiac energy homeostasis [22]. Additional studies are underway to clarify the impact of S100A1 on the interplay between the SR and mitochondria.

4.3. Cardiomyocyte Ca²⁺ Handling and Contractile Performance. S100A1 plays an important role in cardiac myocytes Ca²⁺ cycling and contractile performance. Based on the molecular targets, numerous studies have shown that the overall effect of increased S100A1 protein levels can increase intracellular Ca²⁺ cycling, SR Ca²⁺ load, and contractile performance in field-stimulated mice, rat, and rabbit ventricular myocytes. These changes in cardiomyocyte performance most likely reflect altered function of S100A1 molecular targets as discussed above. Given the fact that S100A1 enhances both SERCA2 activity and diastolic RyR2 diastole, combined actions most likely contribute to enhanced SR Ca²⁺ load and accelerated cardiomyocyte relaxation. In addition, improved myofilament Ca²⁺ dissociation in concert with reduced presystolic passive tension might contribute to improved diastolic function. In systole, increased SR Ca²⁺

load, in concert with enhanced systolic RyR2 opening eventually represents a powerful mechanism by which S100A1 can augment systolic Ca^{2+} transients and cardiac contractile performance (Figure 3).

In summary, several important conclusions and hypotheses can be drawn from these results: first S100A1 is a molecular inotrope in cardiomyocytes exerting a PKA-independent enhancement of cardiac Ca^{2+} cycling thereby acting beyond and independently of cAMP-dependent signaling. Secondly, S100A1 specifically targets SR Ca^{2+} fluxes, improving both systolic SR Ca^{2+} release capability (enhances systolic RyR2 activity) and diastolic SR Ca^{2+} storage capability (decreases diastolic RyR2 open probability and enhances SERCA2a activity). The synchronous enhancement of SERCA2a activity and decreased RyR2 activity in diastole is a hitherto unique and potentially synergistic molecular mechanism which amplifies its inotropic actions but might help to prevent Ca^{2+} -triggered arrhythmias; finally, S100A1 modulation of cardiac titin function might adapt cardiac passive tension and sarcomeric Ca^{2+} sensitivity to improved Ca^{2+} cycling, thereby facilitating diastolic cardiac performance. Finally, S100A1 mitochondrial actions might reflect a mechanism to couple Ca^{2+} -dependent energetic demand with mitochondrial energy production. Figure 3 provides a scheme to illustrate the molecular mechanism of S100A1 in a normal cardiomyocyte.

4.4. Skeletal Muscle Ca^{2+} Handling. Skeletal muscle expresses S100A1 at lower levels than cardiac muscle [30]. However, numerous studies have demonstrated an important role of S100A1 in skeletal muscle EC-coupling [30, 37, 38, 43–45]. S100A1 binds to RyR1 and potentiates its open probability, which might be regulated by three identified S100A1 binding sites at the RyR1 [39]. Interestingly, one of the binding site overlaps with a Ca^{2+} -dependent CaM binding domain. In saponin skinned muscle fibers, addition of recombinant S100A1 protein enhanced SR Ca^{2+} release and isometric force development in a dose-dependent manner both in fast- and slow-twitch skeletal muscle fibers [30] and maximal effects were seen at nanomolar S100A1 protein concentrations. However, S100A1 neither activated RyR1 in its closed state nor initiated SR Ca^{2+} release at diastolic Ca^{2+} concentrations in the presence of physiologic Mg^{2+} concentrations. In contrast to cardiac myocytes, S100A1 neither enhanced SR Ca^{2+} load nor altered Ca^{2+} sensitivity of skeletal muscle myofilaments indicating that S100A1 action in skeletal muscle might be limited to SR Ca^{2+} release sites and eventually mitochondria [30].

In S100A1 deficient skeletal muscle fibers Wright et al. most recently found that voltage-induced SR Ca^{2+} release is decreased resulting in diminished global Ca^{2+} transients and contractile force development [37]. The same study revealed that viral-based S100A1 gene delivery can rescue the phenotype providing ultimate evidence for the hypothesis that S100A1 plays a significant physiological role in skeletal muscle EC-coupling. At a molecular level, the authors further showed that S100A1 and CaM can compete for the same binding site at the RyR1 in a Ca^{2+} -dependent manner

and identified RyR1 residues 3416–3427 as the putative common binding domain [38].

Interestingly, this interaction involves the hydrophobic pocket of S100A1, which is exposed in its Ca^{2+} activated state. At this point it is interesting to note that the S100A1/RyR1 binding domain is involved in the intersubunit interactions of the RyR1 as well as close in space to distal parts of the channel, so that the authors developed a model where S100A1 proteins might be involved in linking one or two subunits of the RyR tetramer. Recently another interesting study by the same group showed that decreased SR Ca^{2+} release in S100A1 KO fibres is responsible for the suppression of the temporally delayed component of intramembrane charge movement, Qgamma, which might operate as an indicator of optimized local Ca^{2+} release at the triad junction in skeletal muscle [44, 45]. In regard of the previously discussed importance of S100A1 in cardiac muscle, it is tempting to speculate that S100A1 plays a key role in skeletal muscle physiology.

Taken together, these data indicate that S100A1 plays a significant role in skeletal muscle EC coupling through modulation of RyR1 function, but not through modulation of SR Ca^{2+} load. Further studies are necessary to determine the impact of S100A1 in skeletal muscle disease to determine the pathophysiological role a therapeutic potential of S100A1 in skeletal muscle disorders like congenital myopathies.

5. S100A1 in Diseased Myocardium

The discovery of altered S100A1 protein abundance in failing human myocardium finally raised the question for a therapeutic potential of S100A1 since progressively diminished S100A1 mRNA and protein levels characterize failing human myocardium [46]. A recent proof of concept study employing both cardiac S100A1 transgenic and knock-out mouse models has provided evidence that diminished S100A1 protein levels critically contribute to progressive contractile dysfunction in postischemic heart failure (HF) and death [31]. The same study indicated that preserved cardiomyocyte S100A1 protein levels could actually prevent development of postischemic HF and cardiac death. In line with S100A1 molecular actions in isolated cardiomyocytes, remote myocardium from infarcted S100A1-overexpressing hearts showed preserved SR Ca^{2+} handling while S100A1 deficiency resulted in abnormal SR Ca^{2+} content and fluxes. In addition, S100A1 knock-out mice subjected to transaortic constriction showed accelerated deterioration of cardiac performance and transition to heart failure [36]. Therefore, normal S100A1 cardiac expression levels appear to be essential to cope with increased workload due to ischemic loss of myocardium or chronically elevated afterload.

Abnormal cardiomyocyte S100A1 protein levels have further been recapitulated *in vitro* by chronic stimulation with different hypertrophic stimuli like phenylephrine and endothelin-1 [31]. In light of the low abundance of S100A1 in neonatal and developing hearts, downregulation of S100A1 in the course of cardiac hypertrophy could therefore be considered as a part of fetal gene reprogramming.

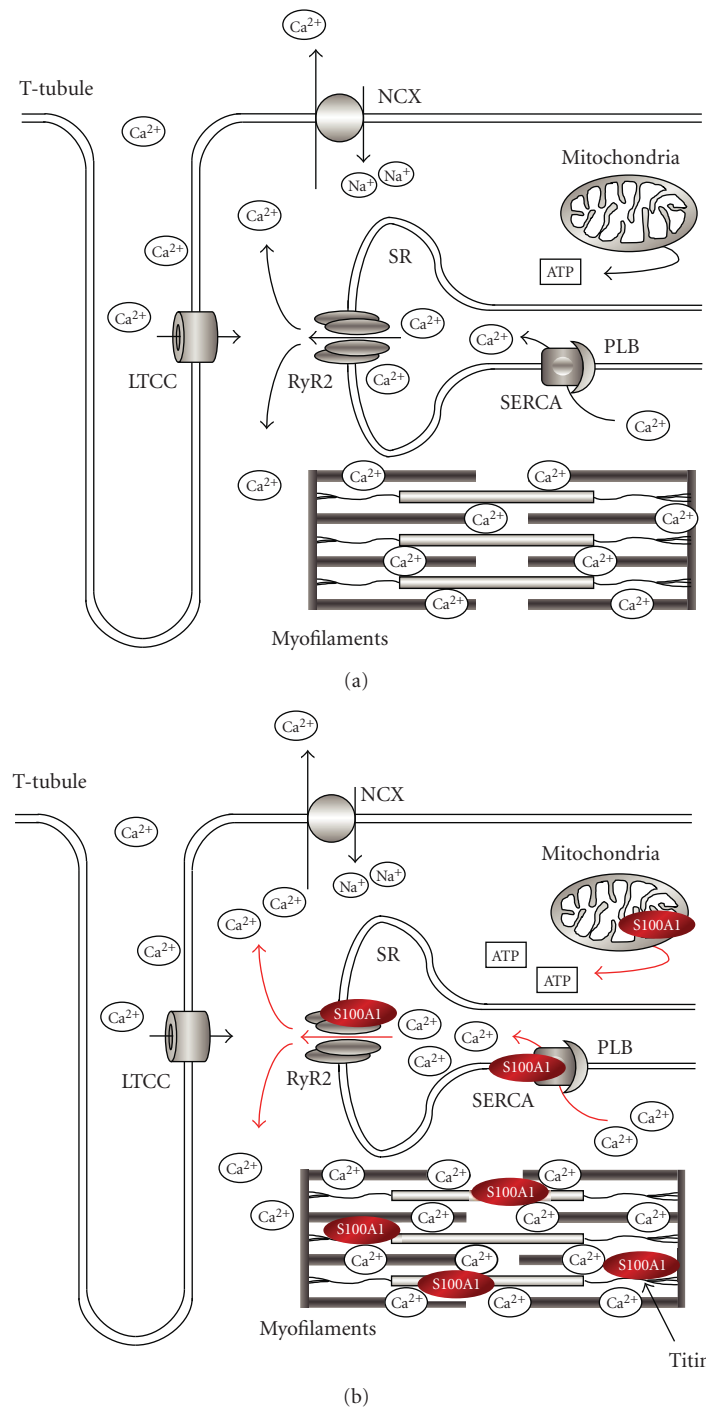


FIGURE 3: Proposed model for S100A1 inotropic actions in cardiomyocytes. (a) During excitation-contraction coupling, the action potential-dependent opening of the L-type Ca^{2+} channel (LTCC) results in a transsarcolemmal Ca^{2+} entry which triggers sarcoplasmic reticulum (SR) Ca^{2+} release via Ryanodine Receptor 2 (RyR2) that in turn activates myofilament cross-bridge cycling and mechanical contraction. During diastole, the SR Ca^{2+} reuptake is conducted by the SR Ca^{2+} ATPase (SERCA), whereas the sodium-calcium exchanger (NCX) extrudes Ca^{2+} from the cardiomyocyte to keep steady-state conditions. (b) S100A1 interacts with both RyR2 and the SERCA-Phospholamban (PLB)-complex and is present at myofilaments and mitochondria. Increased S100A1 protein levels result in an enhanced systolic SR Ca^{2+} release via RyR2 without influencing LTCC activity. Augmented SR Ca^{2+} release is balanced by an intensified SERCA activity leading to an improved Ca^{2+} cycling and a raised force generation. Additionally, the S100A1/F1-ATPase interference in mitochondria is associated with an enhanced generation of cytoplasmic ATP in cardiomyocytes. Moreover, S100A1 inhibits the actin-titin interactions in the sarcomere, resulting in a reduced precontractile passive tension [24].

The binding of S100A1 to the sarcomere could contribute to an altered diastolic function in diseased myocardium. Reduced binding of S100A1 to titin in this context could theoretically contribute to an increased precontractile titin-based passive tension. Interestingly, the myofilament relaxation seems to be dependent on the intracellular ATP-balance [47]. Because S100A1 deficiency reduced intracellular ATP-levels in cardiac myocytes (see above), it is tempting to speculate that lower ATP-levels due to S100A1 deficiency contribute to impaired diastolic function in cardiac disease. Moreover, it has been shown that S100A1 affects microtubules stability in the presence of Ca^{2+} [48]. Given the fact that recent work has shown that microtubules increase viscosity in cardiac hypertrophy and heart failure [49], further studies are needed to clarify the impact of altered S100A1 protein expression on diastolic function in cardiac diseases.

6. Therapeutic Implications and Clinical Perspectives

Owing to the pathophysiological relevance of altered S100A1 expression in cardiac disease and therapeutics effectiveness in clinically relevant experimental acute and chronic HF animal models, S100A1 might be considered as a future prototype of a novel class of Ca^{2+} -dependent inotropes. Intracoronary S100A1 adenoviral and adeno-associated viral gene delivery restored abnormal S100A1 expression in failing hearts thereby improving cardiac performance and reversing cardiac hypertrophy in vivo [15, 18, 32, 33]. So far, both RyR2 and SERCA have been considered as major therapeutic S100A1 targets in failing myocardium given normalization of dysfunctional Ca^{2+} cycling via restored SR Ca^{2+} content, improved systolic SR Ca^{2+} release, as well as decreased diastolic SR Ca^{2+} leakage. Because S100A1 augments both SR Ca^{2+} load and fractional SR Ca^{2+} release, it is tempting to speculate that S100A1 promotes inotropic SR Ca^{2+} handling but potentially limits Ca^{2+} triggered arrhythmias by stabilizing the RyR2 during diastole. This notion is based on the observation that S100A1 gene delivery to normal and failing cardiomyocytes can prevent β -AR triggered proarrhythmic SR Ca^{2+} leak and diastolic Ca^{2+} waves. Accordingly, S100A1 knock-out mice display enhanced proarrhythmic susceptibility in response to sympathetic stimulation [50] and prevention of this effect might actually contribute to improved postMI survival in S100A1 transgenic mice [51]. These findings might further substantiate the clinical relevance of S100A1-mediated regulation of SR Ca^{2+} handling through balanced modulation both of RyR2 and SERCA2. Moreover, S100A1 gene delivery in diseased myocardium exerts robust antihypertrophic effects in vivo and prevents progressive left ventricular chamber dilatation, potentially reflecting abrogated wall stress and interrupted sympathetic overdrive. Finally, S100A1 gene therapy also restored defective energy and sodium homeostasis which are closely linked to Ca^{2+} handling abnormalities [18] clearly warranting further investigation of the underlying molecular mechanisms.

From a clinical point of view, it is important to point out that viral-based S100A1 gene therapy has proven its therapeutic effectiveness both in an experimental postischemic large-animal HF model [52] and human failing ventricular cardiomyocytes (Most P, unpublished observation). Retroinfusion-facilitated delivery of AAV9-S100A1 gene via the anterior coronary vein 2 weeks postMI restored left ventricular performance and prevented transition to contractile failure as seen in control groups. In line with sustained improvement of cardiac performance, S100A1 gene therapy reversed cardiac remodeling and sympathetic overdrive [52]. Moreover, another proof of concept study provided evidence that S100A1 gene therapy normalized abnormal contractility and SR Ca^{2+} handling in failing human cardiomyocytes and restored a positive force-frequency response in these cells (Most P, unpublished observations). These translational studies might actually pave the way for novel S100A1-based clinical therapies including S100A1 gene therapy of human HF. However before S100A1 HF gene therapy can become a clinical reality, careful evaluation of its safety profile as well as effects on cardiac energetics, arrhythmias and compatibility with established pharmacological therapies needs to be conducted in large-animal models. Importantly, a recent study actually provided first evidence that S100A1 gene therapy neither interferes with sympathetic stimulation nor β -blocker treatment [32].

7. Summary

To improve human health, scientific discoveries must be translated into practical applications. Such discoveries typically begin with clinical observations further requiring basic research at “the bench” to uncover molecular mechanisms and proof of pathophysiological relevance before progressing to the clinical level, or the patient’s “bedside.” The clinical discovery of altered S100A1 protein abundance in failing human myocardium [46] ignited a challenging search for its pathophysiological relevance and potential therapeutic impact. Now, almost a decade later, ample evidence indicates that S100A1 functions as a Ca^{2+} -dependent molecular inotrope in cardiomyocytes with unique therapeutic properties. S100A1 targets several key regulators of SR, myofilament, and mitochondrial function thereby enhancing cardiomyocyte performance. In addition, several lines of evidence indicates that S100A1 plays a significant role in skeletal muscle function but its pathophysiological relevance and therapeutic potential in skeletal muscle disorders have not been fully explored yet. Dysregulation of cardiomyocyte S100A1 protein expression, however, accelerates development of cardiac hypertrophy, progression towards HF and cardiac death. Translational studies provided evidence for long-term rescue of cardiac performance and reversed remodeling in several small and large HF animal models. Importantly, S100A1 therapeutic actions extend to human failing myocardium showing restored contractile performance based on improved SR Ca^{2+} handling in S100A1-treated human failing cardiomyocytes [17]. Due to these findings, S100A1-based HF therapies further progress to

the clinical level moving forward towards first clinical safety trials. One could therefore speculate that S100A1 gene therapy might be applicable both to acute and chronic cardiac dysfunction potentially benefiting patients with acute cardiac decompensation as chronic HF. In theory, S100A1 gene therapy for HF may offer a promising and novel mode of action that will not only promote beneficial cardiomyocyte EC Ca^{2+} handling but also potentially limit arrhythmias through stabilization of RyR and decrease in diastolic Ca^{2+} leak. Moreover, the impact of S100A1 on the sarcomere and the mitochondria function completes the unique therapeutic potential of S100A1.

However, development of S100A1-based therapeutic will presumably not replace currently established drug regimens but rather complement and add on to these therapeutic strategies. Nevertheless, S100A1 might facilitate a clinical revival of inotropic therapeutic interventions by targeting defective Ca^{2+} cycling and providing future cardiologists with a novel weapon to combat heart failure.

Acknowledgments

The first and the second authors contributed equally to this article. This study was supported by grants from the National Institute of Health (R01 HL092130-01 and HL 092130-02S1 to P. Most), Deutsche Forschungsgemeinschaft (562/1-1 to P. Most and VO1659/1-1 to M. Voelkers) and Bundesministerium fuer Bildung und Forschung (01GUO572 to P. Most).

References

- [1] D. M. Bers, "Cardiac excitation-contraction coupling," *Nature*, vol. 415, no. 6868, pp. 198–205, 2002.
- [2] P. Most, A. Remppis, S. T. Pleger, H. A. Katus, and W. J. Koch, "S100A1: a novel inotropic regulator of cardiac performance. Transition from molecular physiology to pathophysiological relevance," *American Journal of Physiology*, vol. 293, no. 2, pp. R568–R577, 2007.
- [3] C. Kraus, D. Rohde, C. Weidenhammer, et al., "S100A1 in cardiovascular health and disease: closing the gap between basic science and clinical therapy," *Journal of Molecular and Cellular Cardiology*, vol. 47, no. 4, pp. 445–455, 2009.
- [4] I. Marenholz, C. W. Heizmann, and G. Fritz, "S100 proteins in mouse and man: from evolution to function and pathology (including an update of the nomenclature)," *Biochemical and Biophysical Research Communications*, vol. 322, no. 4, pp. 1111–1122, 2004.
- [5] R. Donato, "Intracellular and extracellular roles of S100 proteins," *Microscopy Research and Technique*, vol. 60, no. 6, pp. 540–551, 2003.
- [6] D. B. Zimmer, P. Wright Sadosky, and D. J. Weber, "Molecular mechanisms of S100-target protein interactions," *Microscopy Research and Technique*, vol. 60, no. 6, pp. 552–559, 2003.
- [7] N. T. Wright, K. M. Varney, K. C. Ellis, et al., "The three-dimensional solution structure of Ca^{2+} -bound S100A1 as determined by NMR spectroscopy," *Journal of Molecular Biology*, vol. 353, no. 2, pp. 410–426, 2005.
- [8] H. Haimoto and K. Kato, "S100a0 ($\alpha\alpha$) protein in cardiac muscle. Isolation from human cardiac muscle and ultrastructural localization," *European Journal of Biochemistry*, vol. 171, no. 1-2, pp. 409–415, 1988.
- [9] K. Kato, S. Kimura, H. Haimoto, and F. Suzuki, "S100a0 ($\alpha\alpha$) protein: distribution in muscle tissues of various animals and purification from human pectoral muscle," *Journal of Neurochemistry*, vol. 46, no. 5, pp. 1555–1560, 1986.
- [10] K. Kato and S. Kimura, "S100a0 ($\alpha\alpha$) protein is mainly located in the heart and striated muscles," *Biochimica et Biophysica Acta*, vol. 842, no. 2-3, pp. 146–150, 1985.
- [11] P. Ehlermann, A. Remppis, O. Guddat, et al., "Right ventricular upregulation of the Ca^{2+} binding protein S100A1 in chronic pulmonary hypertension," *Biochimica et Biophysica Acta*, vol. 1500, no. 2, pp. 249–255, 2000.
- [12] A. I. Su, T. Wiltshire, S. Batalov, et al., "A gene atlas of the mouse and human protein-encoding transcriptomes," *Proceedings of the National Academy of Sciences of the United States of America*, vol. 101, no. 16, pp. 6062–6067, 2004.
- [13] O. Shmueli, S. Horn-Saban, V. Chalifa-Caspi, et al., "GeneNote: whole genome expression profiles in normal human tissues," *Comptes Rendus Biologies*, vol. 326, no. 10-11, pp. 1067–1072, 2003.
- [14] R. Kiewitz, G. E. Lyons, B. W. Schäfer, and C. W. Heizmann, "Transcriptional regulation of S100A1 and expression during mouse heart development," *Biochimica et Biophysica Acta*, vol. 1498, no. 2-3, pp. 207–219, 2000.
- [15] S. T. Pleger, P. Most, M. Boucher, et al., "Stable myocardial-specific AAV6-S100A1 gene therapy results in chronic functional heart failure rescue," *Circulation*, vol. 115, no. 19, pp. 2506–2515, 2007.
- [16] R. Kiewitz, C. Acklin, B. W. Schäfer, et al., " Ca^{2+} -dependent interaction of S100A1 with the sarcoplasmic reticulum Ca^{2+} -ATPase2a and phospholamban in the human heart," *Biochemical and Biophysical Research Communications*, vol. 306, no. 2, pp. 550–557, 2003.
- [17] P. Most, J. Bernotat, P. Ehlermann, et al., "S100A1: a regulator of myocardial contractility," *Proceedings of the National Academy of Sciences of the United States of America*, vol. 98, no. 24, pp. 13889–13894, 2001.
- [18] P. Most, S. T. Pleger, M. Völkers, et al., "Cardiac adenoviral S100A1 gene delivery rescues failing myocardium," *Journal of Clinical Investigation*, vol. 114, no. 11, pp. 1550–1563, 2004.
- [19] P. Most, A. Remppis, S. T. Pleger, et al., "Transgenic overexpression of the Ca^{2+} -binding protein S100A1 in the heart leads to increased in vivo myocardial contractile performance," *Journal of Biological Chemistry*, vol. 278, no. 36, pp. 33809–33817, 2003.
- [20] S. Kettlewell, P. Most, S. Currie, W. J. Koch, and G. L. Smith, "S100A1 increases the gain of excitation-contraction coupling in isolated rabbit ventricular cardiomyocytes," *Journal of Molecular and Cellular Cardiology*, vol. 39, no. 6, pp. 900–910, 2005.
- [21] P. Most, M. Boerries, C. Eicher, et al., "Distinct subcellular location of the Ca^{2+} -binding protein S100A1 differentially modulates Ca^{2+} -cycling in ventricular rat cardiomyocytes," *Journal of Cell Science*, vol. 118, no. 2, pp. 421–431, 2005.
- [22] M. Boerries, P. Most, J. R. Gledhill, et al., " Ca^{2+} -dependent interaction of S100A1 with $\text{F}_1\text{-ATPase}$ leads to an increased ATP content in cardiomyocytes," *Molecular and Cellular Biology*, vol. 27, no. 12, pp. 4365–4373, 2007.
- [23] G. Gutierrez-Cruz, A. H. Van Heerden, and K. Wang, "Modular motif, structural folds and affinity profiles of the PEVK segment of human fetal skeletal muscle titin," *Journal of Biological Chemistry*, vol. 276, no. 10, pp. 7442–7449, 2001.
- [24] R. Yamasaki, M. Berri, Y. Wu, et al., "Titin-actin interaction in mouse myocardium: passive tension modulation and its

- regulation by calcium/S100A1," *Biophysical Journal*, vol. 81, no. 4, pp. 2297–2313, 2001.
- [25] G. Goch, S. Vdovenko, H. Kozłowska, and A. Bierzyński, "Affinity of S100A1 protein for calcium increases dramatically upon glutathionylation," *FEBS Journal*, vol. 272, no. 10, pp. 2557–2565, 2005.
- [26] L. Zhukova, I. Zhukov, W. Bal, and A. Wyslouch-Cieszynska, "Redox modifications of the C-terminal cysteine residue cause structural changes in S100A1 and S100B proteins," *Biochimica et Biophysica Acta*, vol. 1742, no. 1–3, pp. 191–201, 2004.
- [27] M. Völkers, C. M. Loughrey, N. MacQuaide, et al., "S100A1 decreases calcium spark frequency and alters their spatial characteristics in permeabilized adult ventricular cardiomyocytes," *Cell Calcium*, vol. 41, no. 2, pp. 135–143, 2007.
- [28] P. Most, M. Boerries, C. Eicher, et al., "Extracellular S100A1 protein inhibits apoptosis in ventricular cardiomyocytes via activation of the extracellular signal-regulated protein kinase 1/2 (ERK1/2)," *Journal of Biological Chemistry*, vol. 278, no. 48, pp. 48404–48412, 2003.
- [29] P. Most and W. J. Koch, "S100A1: a calcium-modulating inotropic prototype for future clinical heart failure therapy," *Future Cardiology*, vol. 3, no. 1, pp. 5–11, 2007.
- [30] P. Most, A. Remppis, C. Weber, et al., "The C terminus (amino acids 75-94) and the linker region (amino acids 42-54) of the Ca²⁺-binding protein S100A1 differentially enhance sarcoplasmic Ca²⁺ release in murine skinned skeletal muscle fibers," *Journal of Biological Chemistry*, vol. 278, no. 29, pp. 26356–26364, 2003.
- [31] P. Most, H. Seifert, E. Gao, et al., "Cardiac S100A1 protein levels determine contractile performance and propensity toward heart failure after myocardial infarction," *Circulation*, vol. 114, no. 12, pp. 1258–1268, 2006.
- [32] S. T. Pleger, P. Most, B. Heidt, et al., "S100A1 gene transfer in myocardium," *European Journal of Medical Research*, vol. 11, no. 10, pp. 418–422, 2006.
- [33] S. T. Pleger, A. Remppis, B. Heidt, et al., "S100A1 gene therapy preserves in vivo cardiac function after myocardial infarction," *Molecular Therapy*, vol. 12, no. 6, pp. 1120–1129, 2005.
- [34] A. Remppis, P. Most, E. Löffler, et al., "The small EF-hand Ca²⁺ binding protein S100A1 increases contractility and Ca²⁺ cycling in rat cardiac myocytes," *Basic Research in Cardiology*, vol. 97, supplement 1, pp. I56–I62, 2002.
- [35] A. Remppis, S. T. Pleger, P. Most, et al., "S100A1 gene transfer: a strategy to strengthen engineered cardiac grafts," *Journal of Gene Medicine*, vol. 6, no. 4, pp. 387–394, 2004.
- [36] X.-J. Du, T. J. Cole, N. Tennis, et al., "Impaired cardiac contractility response to hemodynamic stress in S100A1-deficient mice," *Molecular and Cellular Biology*, vol. 22, no. 8, pp. 2821–2829, 2002.
- [37] B. L. Prosser, N. T. Wright, E. O. Hernandez-Ochoa, et al., "S100A1 binds to the calmodulin-binding site of ryanodine receptor and modulates skeletal muscle excitation-contraction coupling," *Journal of Biological Chemistry*, vol. 283, no. 8, pp. 5046–5057, 2008.
- [38] N. T. Wright, B. L. Prosser, K. M. Varney, D. B. Zimmer, M. F. Schneider, and D. J. Weber, "S100A1 and calmodulin compete for the same binding site on ryanodine receptor," *Journal of Biological Chemistry*, vol. 283, no. 39, pp. 26676–26683, 2008.
- [39] S. Treves, E. Scutari, M. Robert, et al., "Interaction of S100A1 with the Ca²⁺ release channel (ryanodine receptor) of skeletal muscle," *Biochemistry*, vol. 36, no. 38, pp. 11496–11503, 1997.
- [40] J. Heierhorst, B. Kobe, S. C. Feil, et al., "Ca²⁺/S100 regulation of giant protein kinases," *Nature*, vol. 380, no. 6575, pp. 636–639, 1996.
- [41] J. Heierhorst, X. Tang, J. Lei, et al., "Substrate specificity and inhibitor sensitivity of Ca²⁺/S100-dependent twitchin kinases," *European Journal of Biochemistry*, vol. 242, no. 3, pp. 454–459, 1996.
- [42] N. T. Wright, B. R. Cannon, D. B. Zimmer, and D. J. Weber, "S100A1: structure, function, and therapeutic potential," *Current Chemical Biology*, vol. 3, no. 2, pp. 138–145, 2009.
- [43] E. O. Hernandez-Ochoa, B. L. Prosser, N. T. Wright, M. Contreras, D. J. Weber, and M. F. Schneider, "Augmentation of Cav1 channel current and action potential duration after uptake of S100A1 in sympathetic ganglion neurons," *American Journal of Physiology*, vol. 297, no. 4, pp. C955–C970, 2009.
- [44] B. L. Prosser, E. O. Hernandez-Ochoa, D. B. Zimmer, and M. F. Schneider, "The Q_y component of intra-membrane charge movement is present in mammalian muscle fibres, but suppressed in the absence of S100A1," *Journal of Physiology*, vol. 587, no. 18, pp. 4523–4541, 2009.
- [45] B. L. Prosser, E. O. Hernandez-Ochoa, D. B. Zimmer, and M. F. Schneider, "Simultaneous recording of intramembrane charge movement components and calcium release in wild-type and S100A1^{-/-} muscle fibres," *Journal of Physiology*, vol. 587, no. 18, pp. 4543–4559, 2009.
- [46] A. Remppis, T. Greten, B. W. Schäfer, et al., "Altered expression of the Ca²⁺-binding protein S100A1 in human cardiomyopathy," *Biochimica et Biophysica Acta*, vol. 1313, no. 3, pp. 253–257, 1996.
- [47] R. Stehle, M. Krüger, and G. Pfitzer, "Does cross-bridge activation determine the time course of myofibrillar relaxation?" *Advances in Experimental Medicine and Biology*, vol. 538, pp. 469–479, 2003.
- [48] G. Sorci, A. L. Agneletti, and R. Donato, "Effects of S100A1 and S100B on microtubule stability. An in vitro study using triton-cytoskeletons from astrocyte and myoblast cell lines," *Neuroscience*, vol. 99, no. 4, pp. 773–783, 2000.
- [49] S. Nishimura, S. Nagai, M. Katoh, et al., "Microtubules modulate the stiffness of cardiomyocytes against shear stress," *Circulation Research*, vol. 98, no. 1, pp. 81–87, 2006.
- [50] G. E. Ackermann, A. A. Domenighetti, A. Deten, et al., "S100A1 deficiency results in prolonged ventricular repolarization in response to sympathetic activation," *General Physiology and Biophysics*, vol. 27, no. 2, pp. 127–142, 2008.
- [51] M. Völkers, et al., "S100A1 prevents arrhythmogenic diastolic sarcoplasmic reticulum calcium leak in ventricular cardiomyocytes," *Circulation*, vol. 118, p. S.527, 2008.
- [52] S. Pleger, et al., "Retroinfusion-facilitated inotropic AAV-S100A9 gene therapy restores global cardiac function in a clinically relevant pig heart failure model," *Circulation*, vol. 118, p. S.792, 2008.

Review Article

Myosin Binding Protein-C Slow: An Intricate Subfamily of Proteins

Maegen A. Ackermann and Aikaterini Kontrogianni-Konstantopoulos

Department of Biochemistry and Molecular Biology, School of Medicine, University of Maryland, Baltimore, MD 21201, USA

Correspondence should be addressed to Aikaterini Kontrogianni-Konstantopoulos, akons001@umaryland.edu

Received 7 December 2009; Accepted 1 February 2010

Academic Editor: Henk L. M. Granzier

Copyright © 2010 M. A. Ackermann and A. Kontrogianni-Konstantopoulos. This is an open access article distributed under the Creative Commons Attribution License, which permits unrestricted use, distribution, and reproduction in any medium, provided the original work is properly cited.

Myosin binding protein C (MyBP-C) consists of a family of thick filament associated proteins. Three isoforms of MyBP-C exist in striated muscles: cardiac, slow skeletal, and fast skeletal. To date, most studies have focused on the cardiac form, due to its direct involvement in the development of hypertrophic cardiomyopathy. Here we focus on the slow skeletal form, discuss past and current literature, and present evidence to support that: (i) MyBP-C slow comprises a subfamily of four proteins, resulting from complex alternative shuffling of the single MyBP-C slow gene, (ii) the four MyBP-C slow isoforms are expressed in variable amounts in different skeletal muscles, (iii) at least one MyBP-C slow isoform is preferentially found at the periphery of *M*-bands and (iv) the MyBP-C slow subfamily may play important roles in the assembly and stabilization of sarcomeric *M*- and *A*-bands and regulate the contractile properties of the actomyosin filaments.

1. Introduction

Myofibrils, the workhorses of skeletal muscle, consist of interdigitating thick and thin filaments, and their associated membrane systems [1]. Muscle contraction and relaxation is mediated by the sliding of thick myosin filaments past thin actin filaments, under the strict regulation of Ca^{2+} release and reuptake via the sarcoplasmic reticulum (SR) [2]. In addition to housing the basic thick and thin filaments, the sarcomere also contains several accessory proteins that are involved in the assembly, maintenance, and regulation of contractile activity [1]. Myosin Binding Protein-C (MyBP-C) comprises a family of accessory proteins that contributes to the assembly and stabilization of thick filaments, and regulates the formation of cross-bridges between myosin and actin by interacting directly with both filamentous systems (as reviewed in [3]).

MyBP-C was originally identified from mammalian skeletal muscle as an impurity of isolated myosin. Using SDS-polyacrylamide gel electrophoresis (SDS-PAGE), Star and Offer were the first to separate a number of unidentified myosin-associated proteins that were consistently found in preparations of purified myosin [4]. MyBP-C, originally

termed C-protein for its location on SDS-PAGE as band C, was further characterized as a myosin binding protein of ~140 kDa using a combination of biochemical methods, ranging from gel filtration, to ammonium sulfate fractionation and single molecule electron microscopy [4–6]. The location of MyBP-C at striped intervals within the C-zone of the A-band of skeletal muscle was first observed with X-ray diffraction and immunoelectron microscopy [7], further supporting its association with the thick myosin filaments. Subsequent studies revealed that MyBP-C is arranged along the length of the A-band in 7–9 transverse stripes that are ~43 nm apart, with ~2–4 molecules of MyBP-C associating with each myosin cross-bridge [8–11].

The family of MyBP-C contains three isoforms: cardiac, slow skeletal, and fast skeletal, which are encoded by separate genes; in humans, these map to chromosomes 11, 12, and 19, respectively [12, 13]. The different isoforms have been cloned and sequenced from various species, including human, chicken, rabbit and mouse, allowing a thorough comparison of their molecular composition and primary sequence [13–16]. An ~65% identity is shared among the individual isoforms across species, while an ~50% homology is shared among the human cardiac, slow and fast forms.

The core structure of MyBP-C is composed of seven immunoglobulin (Ig) domains and three fibronectin type III (Fn-III) repeats, numbered from the NH₂-terminus as C1–C10 [17]. The C1 domain is flanked by two unique motifs, one enriched in proline and alanine residues, termed proline/alanine rich motif and a conserved linker, referred to as MyBP-C motif. Notably, the cardiac isoform possesses three additional features, which are absent from the skeletal forms of the protein. These include an Ig domain at the extreme NH₂-terminus of the molecule, termed C0, a unique 9-residues long insertion within the MyBP-C motif containing phosphorylation sites necessary for the protein's regulatory role in contraction, and a 28-amino acids long loop in the middle of the C5 domain [12, 16].

In mammals, cardiac MyBP-C is expressed early in development, along with titin and myosin [18, 19]. The skeletal isoforms of MyBP-C, however, are detected later in development, after the expression of titin and myosin, with the expression of slow MyBP-C preceding that of fast [18, 20]. By contrast, in chicken skeletal muscles the slow and fast isoforms appear concurrently at the end of late embryogenesis [21]. As development proceeds, though, the amounts of the slow form diminish, while the expression of the fast form persists through adulthood [21]. The fast and slow skeletal isoforms have been shown to coexpress in the same muscle type and can even coexist in the same sarcomere; expression of the cardiac isoform, however, is restricted to the developing and mature heart [15, 18, 22–24]. Interestingly, a recent study demonstrated that the expression of MyBP-C slow is not restricted to skeletal muscle but is also evidenced in the right atrium and interatrial septum of adult mammalian cardiac muscle [25].

To date, much of our knowledge on the molecular properties and functional activities of MyBP-C originates from the numerous studies that focus on the cardiac isoform. The reader is referred to excellent reviews discussing the structure of cardiac MyBP-C, its key roles in maintaining the normal structure of thick filaments and regulating cross-bridge cycling, and its involvement in the development of hypertrophic cardiomyopathy [3, 26, 27]. Here, we will focus on the slow form(s) of MyBP-C found in skeletal muscles. We will review past and current literature, discuss its role in the organization and stabilization of thick filaments, and provide evidence that MyBP-C slow comprises a subfamily of four alternatively spliced proteins that are expressed in variable amounts in slow and fast twitch skeletal muscles.

2. Materials and Methods

2.1. Reverse Transcription-Polymerase Chain Reaction. Total RNA was isolated with Trizol reagent (Invitrogen, Carlsbad, CA) from P1 rat skeletal myotubes cultured for seven days and from adult rat extensor digitorum longus (EDL), flexor digitorum brevis (FDB), tibialis anterior (TA), gastrocnemius (gastroc), quadriceps (quad), and soleus muscles. Aliquots containing ~5 µg of RNA were reverse transcribed using the Superscript First Strand Synthesis System for RT-PCR (Invitrogen, Carlsbad, CA) following the

manufacturer's instructions. PCR amplification of MyBP-C slow transcripts was performed with primer sets that flanked each of the three insertions; for the NH₂-terminal insert: Forward-1 (F1): 5' CCAGAACCCACTAAGAAAG 3' and Reverse-1 (R1): 5' GATCCTCGAGGTGCACTT CAA-GATCAA 3', for the insert within Ig7: Forward-2 (F2): 5' GATCGAATTCAGCCC TCCTACTCTT 3' and Reverse-2 (R2): 5' GATCCTCGAGGGGCTCGCTGGCACCA 3' and for the COOH-terminal insert: Forward-3 (F3): 5' CACC-CATGTTTACTCAACCCT 3' and Reverse-3 (R-3) 5' GTGACAAATATACATTGAA 3'. To amplify the COOH-terminal insert from EDL and TA muscles, it was necessary to reamplify 0.5 µL of the original PCR for an additional 30 cycles for a total of 80 cycles. All other PCRs were carried out for 50 cycles. PCR products were analyzed by electrophoresis in 1% agarose gels and their authenticity was verified by sequence analysis.

2.2. Generation of Protein Lysates from P1 Myotubes and Adult Rat Muscle. Homogenates of P1 myotubes cultured for seven days as well as of EDL, FDB, TA, gastrocnemius, quadriceps and soleus muscles of adult Sprague-Dawley rats (Zivic-Miller Laboratories, Zelienople, PA) were prepared at RT with a Brinkman Polytron homogenizer at setting 3 (VWR, West Chester, PA) in 10 mM NaPO₄, pH 7.2, 2 mM EDTA, 10 mM NaN₃, 120 mM NaCl, 0.5% deoxycholate, 0.5% NP-40, supplemented with Complete protease inhibitors (Roche, Indianapolis, IN). Each sample (~60 µg) was solubilized in 4xNuPAGE reducing sample buffer (Invitrogen, Carlsbad, CA) at 90°C for 5 minutes, fractionated by 4–12% SDS-PAGE BisTris gel using MES running buffer (Invitrogen, Carlsbad, CA), transferred to nitrocellulose and probed with an antibody that recognizes the slow forms of MyBP-C (300 ng/mL, Abnova) or with an antibody that specifically recognizes the COOH-terminal insert [28]. After incubation with the appropriate secondary antibodies, immunoreactive bands were visualized with a chemiluminescence detection kit (Tropix, Bedford, MA).

2.3. Immuno-Electron Microscopy. Immuno-electron microscopy was performed as previously described with minor modifications [29, 30]. Briefly, adult mouse FDB skeletal muscle was fixed both *in situ*, via whole animal perfusion-fixation and *ex vivo* with 2% paraformaldehyde in PBS. Samples were snap-frozen in a slush of liquid N₂, cryosectioned (~20 µm thick), and incubated overnight at 4°C with the antibody that specifically recognizes the COOH-terminal insert of MyBP-C slow. Samples were incubated with secondary goat antirabbit IgG adsorbed on 1 nm gold particles (Nanoprobes Incorporated; Yaphank, NY) and subsequently with fluorescein-conjugated anti-goat IgG (Jackson ImmunoResearch Laboratories Inc., West Grove, PA). Samples were enhanced with silver (HiQ Silver Kit, Nanoprobes) for 5 minutes, fixed overnight at 4°C in 2% glutaraldehyde and 5 mg/mL tannic acid in 0.2 M cacodylate buffer and postfixed with 50 mM acetate buffer 1% osmium tetroxide. They were further stained *en bloc* for 2 hours with 1% uranyl acetate in 65% ethanol,

dehydrated, and embedded in araldite (Electron Microscopy Sciences, Fort Washington, PA). Ultrathin (60–90 nm) sections were prepared with an MT5000 ultramicrotome (LKB instruments Inc., Gaithersburg, MD), mounted on grids, labeled with 1% uranyl acetate followed by Reynolds lead citrate, and examined with a Philips-201 electron microscope.

3. Results and Discussion

3.1. MyBP-C Slow: A Subfamily of Proteins. To date, four different MyBP-C slow transcripts have been identified in human skeletal muscle referred to as variants 1–4 (Figure 1; accession numbers NM_002465, NM_206819, NM_206820, and NM_206821, respectively). The four variants differ from one another at three regions, due to alternative splicing events that result in inclusion of exons 3 and 4 in the proline/alanine-rich motif, exon 23 in the Ig7 domain and exon 31 at the extreme COOH-terminus (Figure 1(a)); these encode novel sequences of 25 (Figure 1(b)), 18 (Figure 1(c)), and 26 (Figure 1(d)) amino acids, respectively. Analysis of the primary sequence of the four MyBP-C slow variants indicated that variants 1 and 2 contain the NH₂-terminal insertion located in the proline/alanine rich motif, variant 3 carries the insertion within domain Ig7, while variant 4 also contains the unique COOH-terminal region (Figure 1(a)). Notably, variant 3 is the prototypical human isoform of MyBP-C slow that was characterized by Furst and colleagues in 1992 [14].

To study the relative expression of the four MyBP-C slow transcripts in different rat skeletal muscles, we used RT-PCR analysis to amplify the unique regions described above. To this end, we prepared cDNAs from a panel of adult and developing rat skeletal muscles that contained distinct compositions of slow and fast twitch skeletal myofibers. These included extensor digitorum longus (EDL; ~90:10, fast:slow; [31, 32]), flexor digitorum brevis (FDB; ~80:20, fast:slow; [33]), tibialis anterior (TA; ~70:30, fast:slow; [34]), gastrocnemius (gastroc; ~40:60, fast:slow; [35]), quadriceps (quad; ~60:40, fast:slow; [36]), soleus (20:80, fast:slow; [35]), and hindlimb skeletal myotubes of postnatal day 1 (P1) rat pups (Figure 2). Primer sets were designed to flank each of the three novel insertions (Figures 2(a)–2(c), cartoons in the upper left corner). Amplification of two PCR products with distinct sizes within each reaction indicated the presence of a mixed population of transcripts that contained (larger size product) and lacked (smaller size product) the respective insertion. On the contrary, amplification of one PCR product indicated the presence of a homogeneous population of transcripts that either included or excluded the corresponding insertion, depending on its size. Accordingly, PCR products that carry the NH₂-terminal, Ig7 and COOH-terminal inserts would be ~600, ~310, and ~350 nucleotides long, respectively, whereas PCR products that lack them would be ~530, ~260, and ~290 nucleotides long, respectively.

All skeletal muscles examined, independent of their fiber type composition, contained sufficient amounts of MyBP-C

slow transcripts to be amplified by conventional RT-PCR. Figure 2(a) shows the results following amplification of the NH₂-terminal insertion located within the proline/alanine rich motif. All muscle samples express MyBP-C slow transcripts that include the NH₂-terminal insert, albeit to varying degrees, as seen by the presence of an ~600 nts amplicon (Figure 2(a), upper band). This finding suggested that all muscles tested express variants 1 and/or 2, with EDL, TA, and soleus containing the highest amounts. Notably, all seven muscles also contain different amounts of transcripts that lack the NH₂-terminal insert, as shown by the presence of an ~530 nts product, indicating that they also express variants 3 and/or 4, with FDB showing the highest levels (Figure 2(a), lower band). Contrary to EDL, TA, soleus, and FDB that appear to preferentially contain MyBP-C slow variants that either include (EDL, TA and soleus) or exclude (FDB) the NH₂-terminal insert, gastroc, quad, and P1 myotubes show similar amounts of both amplification products, suggesting that transcripts possessing and lacking the NH₂-terminal insert may exist in similar levels within these muscles (Figure 2(a) lanes 4–5 and 7).

Next, we extended our analysis to the second novel insertion located within Ig7. As before, our primers set was designed to amplify MyBP-C slow variants that contained or skipped the Ig7 insert. Only soleus and P1 myotubes possess transcripts that include the unique insertion within Ig7, as indicated by the presence of an ~310 nts band (Figure 2(b), lanes 6 and 7, upper band), corresponding to variant 3. As expected, all skeletal muscles tested contained transcripts that lack the Ig7 insertion, as shown by the amplification of an ~260 nts product, representing variants 1, 2 and/or 4. Thus, variant 3 is restricted to soleus muscle and developing myotubes.

Last, we generated the appropriate primers to amplify the region flanking the COOH-terminal insert of MyBP-C slow. With the exception of quadriceps muscle, all other muscles tested, contained an amplification product of ~350 nucleotides, that includes the novel COOH-terminal insert detected only in variant 1, with soleus and FDB showing the highest amounts (Figure 2(c), lanes 6 and 2, upper band). A second amplification product of ~290 nucleotides was also detected in all seven muscles, which lacks the unique COOH-terminal insertion, present in variant 1, but includes the common COOH-terminal region shared by variants 2, 3, and 4 (Figure 2(c), lower band).

The RT-PCR data is summarized in Table 1. Taken together, our results suggest that: (i) mRNA encoding MyBP-C slow is present in all skeletal muscles examined, regardless of fiber type composition or age, and (ii) complex alternative shuffling of the single MyBP-C slow gene in the various muscles results in the differential expression of the four MyBP-C slow isoforms.

To correlate the mRNA expression of the transcripts that contain or lack the three novel insertions, as seen by the RT-PCR, to the expression of the proteins that they encode, we used western blot analysis. Homogenates from EDL, FDB, TA, gastroc, quad, soleus, and P1 skeletal myotubes were separated on 4–12% gradient gel, which our laboratory has previously shown to provide optimal

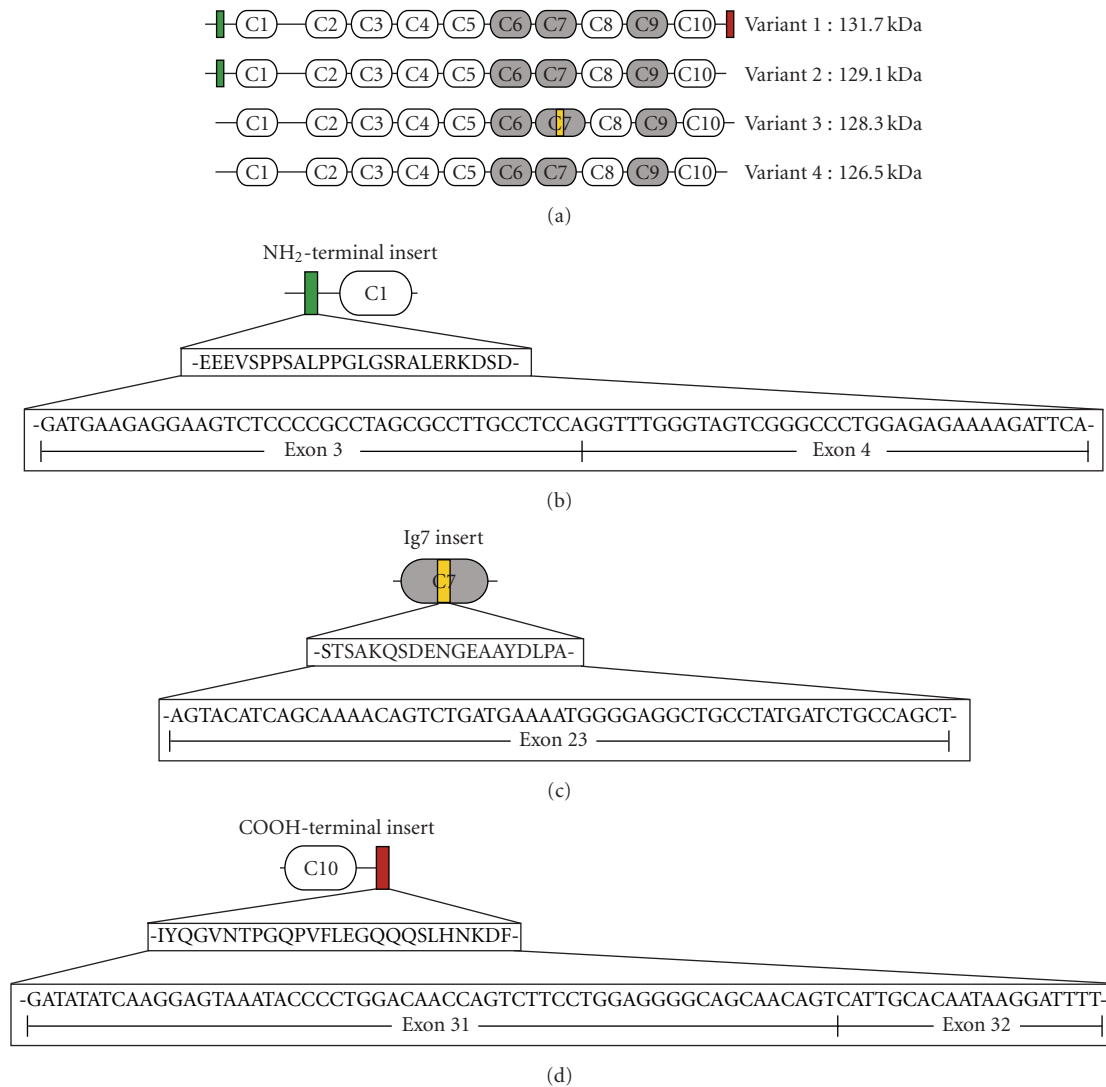


FIGURE 1: (a): Schematic representation of MyBP-C slow variants 1–4, showing their common structural motifs and novel insertions; white and grey ovals represent Ig and FN-III domains, respectively, while green, yellow, and red rectangles correspond to the NH₂-terminal, Ig7, and COOH-terminal inserts, respectively. The NH₂-terminal insert is present in variants 1 and 2, while the Ig7 and COOH-terminal inserts are present in variants 3 and 1, respectively. Variant 4 does not contain any of the three inserts. (b–d): Complex alternative splicing events result in the inclusion of exons 3 and 4, exon 23 and exon 31 that encode the NH₂-terminal (b), Ig7 (c), and COOH-terminal (d) novel insertions. The amino acid and nucleotide compositions of the three insertions are shown.

separation of the MyBP-C slow isoforms (see Section 2, and [28]). Homogenates were probed with a commercial antibody that recognizes a region within domain C5 common to all MyBP-C slow variants (Figure 3(a)). We were able to resolve at least 3 immunoreactive bands based on their distinct electrophoretic mobilities. The top band may represent variant 1 (~132 kDa, Figure 3(a), top panel, marked with a blue dot), the middle band may correspond to variants 2 and/or 3 (~129 and ~128 kDa, respectively, Figure 3(a), top panel, denoted with a red dot), and the bottom band may represent variant 4 (~126 kDa, Figure 3(a), top panel, marked with a green dot). The cartoon shown in the bottom panel of Figure 3(a) illustrates a representative image of several western blots, analyzed at

varying exposure times. The dotted lines indicate immunoreactive bands that only become evident after periods of long exposure.

Consistent with the RT-PCR data, our immunoblots also demonstrated the presence of at least one form of MyBP-C slow in each skeletal muscle tested. EDL and gastrocnemius possess three immunoreactive bands with the most prominent being the middle one (Figure 3(a), lanes 1 and 4). FDB also contains three distinct bands, however, the top and middle bands appear to be of similar intensities and occasionally appear as a broad, single band (Figure 3(a), lane 2). Similar to FDB, TA also shows two closely migrating bands, but lacks the bottom one (Figure 3(a) lane 3). Contrary to the rest of the muscles analyzed, quadriceps

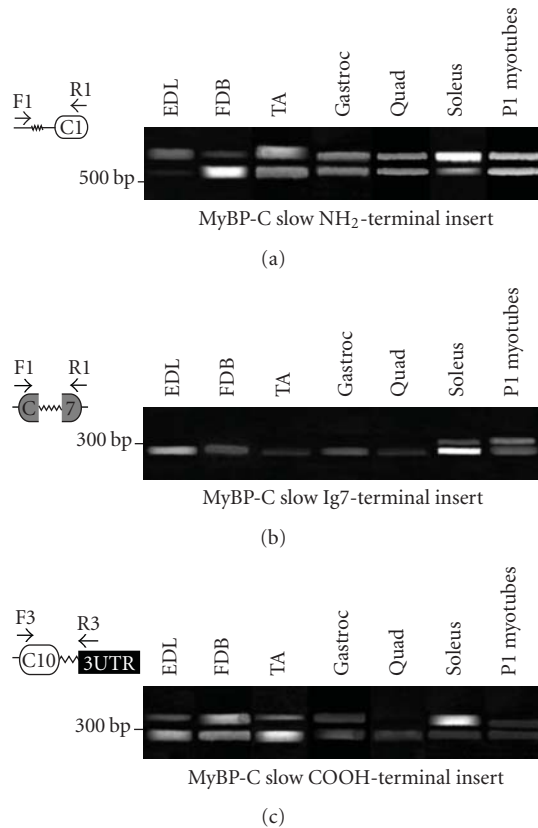


FIGURE 2: RT-PCR analysis using cDNA generated from developing and adult rat extensor digitorum longus (EDL), flexor digitorum brevis (FDB), tibialis anterior (TA), gastrocnemius (gastroc), quadriceps (quad) and soleus skeletal muscles and primer sets designed to flank the NH₂-terminal (a), Ig7 (b), and COOH-terminal (c) insertions. A schematic representation of the amplified region is shown in the upper left corner of each panel. White and grey ovals depict Ig and FN-III domains, respectively, while the 3' UTR is shown as a black line. The zig-zag lines denote the three novel insertions. In each amplification reaction, the top band corresponds to transcripts that include the insertion of interest, whereas the bottom band corresponds to transcripts that lack it. (a): All skeletal muscles tested contain a mixed population of MyBP-C slow variants that contain and lack the NH₂-terminal insertion, as indicated by the presence of two amplification products. (b): On the contrary, only soleus and developing myotubes express transcripts that include the Ig7 insertion. (c): With the exception of quadriceps muscle that only contains MyBP-C slow variants that lack the COOH-terminal insertion, all other muscles examined contain a mixed pool of transcripts that carry and lack the novel COOH-terminal insertion.

appears to contain only the middle band, although, the bottom one becomes evident after long exposure times (Figure 3(a) lane 5). Soleus expresses high amounts of the upper and lower bands, but moderate to low amounts of the middle one (Figure 3(a) lane 6). Finally, developing P1 skeletal myotubes show only one immunoreactive band with the same mobility as the top one, however, following longer exposure, the middle immunoreactive band is also apparent (Figure 3(a) lane 7).

TABLE 1: Tabulated summary of the RT-PCR data shown in Figure 2. The plus (+) and minus (–) signs denote the presence or absence of mRNAs encoding the three regions of interest, respectively; the relative abundance of the respective transcripts is illustrated by the number of plus signs.

Muscle Type	NH ₂ -insert	Ig7-insert	COOH-insert
Extensor Digitorum Longus	++	–	+
Flexor Digitorum Brevis	+	–	++
Tibialis Anterior	+++	–	+
Gastrocnemius	++	–	+
Quadriceps	++	–	–
Soleus	++++	+	+++
P1 Myotubes	+++	++	+

We also probed the same muscle homogenates with an antibody that is specific for the COOH-terminal insert and therefore only recognizes MyBP-C slow variant 1 (Figure 3(b)). With the exception of quadriceps, all of the other muscles were immunopositive for variant 1. This finding is in agreement with our immunoblot data shown in panel A, and the RT-PCR analysis shown in Figure 2(c), which revealed that quadriceps was the sole muscle to lack the top immunoreactive band (i.e., variant 1) and the COOH-terminal insert, respectively. Notably, MyBP-C slow variant 1 appears to be expressed more abundantly in soleus muscle and least prominently in developing myotubes, while the remaining muscles tested contained intermediate amounts. The slight differences in the sizes of the bands detected in the different muscles are likely due to posttranslational modifications, as it has previously been shown that MyBP-C slow is capable of phosphorylation [37, 38].

Taken together, our RT-PCR and immunoblotting data (summarized in Table 2) clearly indicate that all skeletal muscles tested, apart from quadriceps, express variant 1, albeit to different extents, with soleus and FDB containing the highest amounts. Variants 2 and 3 have complementary expression profiles, with variant 2 being preferentially expressed in muscles that have a higher composition of fast twitch fibers, such as EDL, FDB, TA, gastrocnemius and quadriceps, and variant 3 being selectively present in slow twitch muscles, like soleus, and developing myotubes. Finally, variant 4 is detected in all muscles examined, with the exception of TA and developing myotubes. It therefore appears that different forms of MyBP-C slow are present within the same muscle, independently of its fiber type composition, developmental stage, or age.

3.2. MyBP-C at the A-band. Early studies have confirmed the direct interaction between MyBP-C and myosin and identified the sites of binding on both proteins. The light meromyosin (LMM) region of the myosin rod, that forms the backbone of the thick filament, binds the COOH-terminal C10 region of all three MyBP-C isoforms [39–41]. Positively charged residues on the surface of the C10 domain mediate binding to LMM [42], however, the interaction is significantly strengthened by the presence of the C8

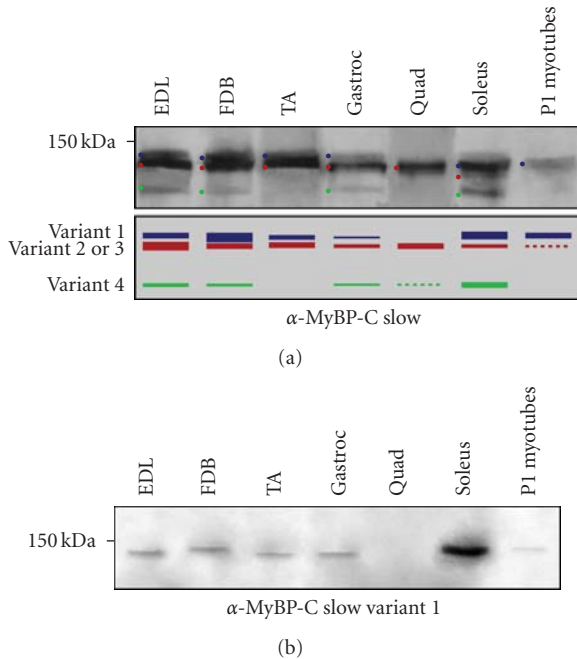


FIGURE 3: Western blot analysis of protein homogenates prepared from rat skeletal muscles and blotted with antibodies to the fifth Ig domain that recognize all MyBP-C slow variants (a) or to the novel COOH-terminal insertion that specifically recognizes variant 1 (b). (a) Top panel: With the exception of quadriceps, all other muscles express variant 1, represented by the upper most band, marked by a blue dot. All adult skeletal muscles tested, but not the developing myofibers, express variants 2 and/or 3, corresponding to the band with the intermediate mobility, and denoted with a red dot. As variants 2 and 3 have similar molecular weights (129 and 128 kDa, respectively), it is not feasible to separate them in the current gel system. Moreover, variant 4 is detected in homogenates prepared from EDL, FDB, gastrocnemius, and soleus, and is represented by the lower immunoreactive band, marked with a green dot. Bottom panel: A cartoon showing the presence of the different MyBP-C slow variants in developing and adult skeletal muscles. Dotted lines correspond to immunoreactive bands, which are evident only after long exposure times. (b) In agreement with the immunoblot shown in panel (a), antibodies specific for the novel COOH-terminal insert demonstrated that EDL, FDB, TA, gastrocnemius, soleus, and P1 skeletal myotubes express variant 1, with soleus containing the highest amounts.

and C9 regions. Another interaction between the MyBP-C motif, located at the NH₂-terminus of MyBP-C and subfragment 2 (S2) of myosin has been also identified, albeit of weaker affinity [43]. In addition to binding myosin, MyBP-C associates with actin, in a Ca²⁺ dependent manner, through its NH₂-terminal proline/alanine rich motif [44–46]. The ability of MyBP-C to directly interact with both myosin and actin facilitates its role as a regulator of cross-bridge formation during contraction. Interestingly, at low ionic strength MyBP-C inhibits actomyosin ATPase activity, while at higher ionic strength it acts as a mild activator [47, 48].

In addition to myosin, MyBP-C also associates with titin at the A-band [14, 49–51]. The COOH-terminal C8–C10

TABLE 2: MyBP-C slow variants 1–4 are present in varying amounts in different skeletal muscles. A plus (+) sign indicates the presence of the respective variant in a select muscle. The relative abundance of variants 1–4 in the skeletal muscles tested is illustrated by the number of plus signs.

Muscle Type	Variant 1	Variant 2	Variant 3	Variant 4
Extensor Digitorum Longus	++	+++	—	++
Flexor Digitorum Brevis	+++	++	—	++
Tibialis Anterior	++	++	—	—
Gastrocnemius	+	+	—	+
Quadriceps	—	++	—	—
Soleus	++++	—	+	+++
P1 Myotubes	++	—	+	—

domains of MyBP-C directly bind to the 11-domain super-repeat [Ig-(FN-III)₂-Ig-(FN-III)₃-Ig-(FN-III)₃] present in the C-zone portion of titin, and specifically the first Ig domain, although flanking motifs further strengthen the interaction [52, 53]. Notably, the arrangement of MyBP-C in 11 transverse stripes at regular intervals of ~43 nm corresponds to that of the 11-domain super-repeat of titin, to which MyBP-C binds. Consequently, It has been suggested that binding to titin's super-repeats specifies the subsarcomeric distribution of MyBP-C in the C-zone of the A-band [52].

Recent studies have proposed that MyBP-C forms a trimeric “collar” around each thick filament in which domains C5–C7 of one molecule overlap with domains C8–C10 of the neighboring molecule [54, 55]. In vitro binding studies using the respective peptides postulated that this arrangement might apply to the cardiac and fast skeletal isoforms, but not the slow isoform. Interestingly, for these studies Flashman and coworkers generated a recombinant protein that contained domains C8–C10, present in all four slow variants, followed by the novel COOH-terminal insertion, present only in variant 1. It is, therefore, possible that the presence of the COOH-terminal 26-amino acids may inhibit binding of the C8–C10 domains of variant 1 to the C5–C7 domains of the neighboring molecule of MyBP-slow. Indeed, this is consistent with our recent studies indicating that variant 1 is preferentially localized at the periphery of the M-band [28]. Conversely, an interaction between the respective motifs present in variants 2–4 is likely, as these contain a short COOH-terminus following domain C10 that, similar to the cardiac and fast isoforms, consists of four amino acids.

Through its interactions with myosin and titin, MyBP-C contributes to the stabilization and maintenance of the sarcomeric A-band. In vitro studies indicate that myosin filaments are capable of forming in the absence of MyBP-C, however, its addition results in increased filament length, and improved structure and uniformity across the filament [40, 56, 57]. Additionally, in vivo deletion of the myosin

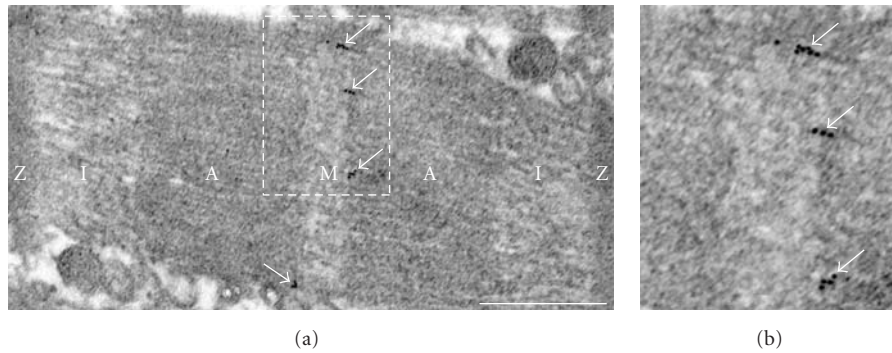


FIGURE 4: Ultrathin cryo-sections of adult mouse FDB skeletal muscle were labeled with antibodies specific for the COOH-terminal insertion present in MyBP-C slow variant 1. (a) Variant 1 was detected at the periphery of the *M*-band (arrows). The boxed area in (a) is blown up in (b) for ease of visualization of the immunolabeling. Scale bar corresponds to 0.5 μm .

and titin binding sites on MyBP-C results in disorganized *A*-bands [58, 59]. Consistent with this, the C8–C10 domains that harbor the binding sites for myosin and titin are deleted in patients suffering from familial hypertrophic cardiomyopathy [3, 60, 61]. Interestingly, though, normal *A*-bands are formed in animals deficient of cardiac MyBP-C [62, 63], suggesting the presence of a compensatory mechanism that maintains the myosin and titin filaments within the *A*-band of the sarcomere. Taken together, these studies suggest that MyBP-C, through its direct interaction with myosin and titin, and possibly its self-association, may stabilize the sarcomeric *A*-band.

In addition to maintaining the structure of thick filaments, MyBP-C may also play key roles in regulating contractile function by modulating the rate of cross-bridges formation. Consistent with this, in cardiomyocytes lacking MyBP-C, actomyosin filaments exhibited increased power output during contraction and faster rates of force development at half maximal Ca^{2+} activation [64]. Reintroduction of the NH_2 -terminal region of cardiac MyBP-C, containing the myosin S2 binding site (i.e., domains C1 and C2), enhanced Ca^{2+} sensitivity and restored the contractile properties of the null cardiomyocytes to normal levels [65], suggesting that cardiac MyBP-C contributes to the regulation of myofilament tension and their cycling rates.

Contrary to the cardiac isoform that has been directly implicated in the regulation of the contractile properties of cardiomyocytes (reviewed in [3]), studies focusing on the function of the skeletal forms of MyBP-C are limited. However, early studies have suggested that the role of MyBP-C in skeletal muscle likely parallels that of the cardiac isoform [66]. Consistent with this, the amounts of MyBP-C slow were recently found significantly increased in EDL muscles from a mouse model in which the kinase domain of titin was deleted [67]. Deficient EDL muscles exhibited reduced myofilament Ca^{2+} sensitivity and altered contractile properties, which were restored to normal levels upon extraction of MyBP-C slow. Contrary to the slow form of MyBP-C, the fast form was significantly downregulated in the same muscles, while the expression levels of other proteins of the *A*- and *M*-bands remained unaffected. It is, therefore, likely that the

kinase domain of titin affects the expression of genes involved in the regulation of myofilament Ca^{2+} sensitivity and force production. Experimental evidence has therefore started to emerge suggesting a key role for the skeletal forms of MyBP-C in modulating contractility, too.

3.3. Mybp-C Slow Variant 1 Selectively Concentrates at the *M*-Band. The presence of MyBP-C slow at the C-zones of the *A*-band has been studied extensively during the last three decades [3, 26, 68]. Recent studies from our laboratory, however, have provided evidence that at least one form of MyBP-C slow, specifically variant 1, has a unique topography in the muscle cell [28]. Detailed immunofluorescence studies combined with confocal microscopy demonstrated that MyBP-C slow variant 1 is selectively localized at the periphery of the *M*-band in adult rat soleus muscle [28]. The unique localization of MyBP-C slow variant 1 is further supported by our ultrastructural studies, shown in Figure 4. Immunolabeling of ultrathin cryosections prepared from adult mouse FDB muscle with antibodies to the unique COOH-terminus of variant 1 also demonstrated that it preferentially concentrates at the edges of the sarcomeric *M*-band (Figures 4(a)–4(b), arrowheads). Thus, it appears that the different MyBP-C slow isoforms have distinct distributions in skeletal myofibers, with variants 2–4 localizing at the *A*-band and variant 1 at the *M*-band.

At the *M*-band, MyBP-C slow variant 1 interacts with obscurin and four and a half lim protein 1 (FHL1) [28, 69]. The second Ig domain of obscurin and the last Ig domain of MyBP-C slow variant 1 are both necessary and sufficient to support their interaction, however, binding is enhanced significantly in the presence of the novel 26 amino acids at the COOH-terminus of variant 1. Overexpression of the second Ig domain of obscurin in primary cultures of skeletal myotubes inhibited the integration of MyBP-C slow variant 1 at the *M*-band and severely disrupted the formation of *M*- and *A*-bands. These findings suggested that variant 1 might contribute to the assembly and integrity of these structures via its interaction with obscurin and possibly other proteins. Similarly, McGrath et al. also demonstrated

that overexpression or downregulation of FHL1, which is localized at the A-I junction and the M-band, in adult mouse soleus muscle resulted in impaired thick filament assembly, which was accompanied by reduced sarcomeric incorporation of different forms of MyBP-C slow, including variant 1 [69].

3.4. MyBP-C Slow in Muscle Disease. Mutations within the cardiac isoform of MyBP-C cause familial hypertrophic cardiomyopathy (reviewed in [70, 71]). To date, there are no muscle diseases causally associated with mutations in the transcripts of the skeletal forms of MyBP-C. However, changes in the expression levels of the skeletal isoforms have been reported in hypertrophic and dystrophic skeletal muscles. The expression levels of MyBP-C slow were significantly increased in rat plantaris muscle induced to hypertrophy by surgical ablation of the neighboring soleus and gastrocnemius muscles, whereas the amounts of MyBP-C fast were dramatically decreased [72]. Likewise, the protein levels of MyBP-C slow were increased in both chicken and mouse dystrophic skeletal muscles [20, 24]. Further research is required in order to understand the molecular mechanisms that lead to the differential regulation of the skeletal forms of MyBP-C in these models, and their potentially unique roles in regulating the formation and activity of contractile structures.

4. Summary and Future Perspectives

MyBP-C slow comprises a subfamily of at least four isoforms that result from complex alternative splicing of the single MyBP-C slow gene. The presence of the four MyBP-C slow variants is not restricted to slow-twitch muscles, as select isoforms are abundantly expressed in fast-twitch muscles, too, where they may coexist with MyBP-C fast. More importantly, the four isoforms of MyBP-C slow may be coexpressed in the same muscle, fiber or sarcomere, where they may exhibit unique topographies concentrating either at A-bands (variants 2, 3, and 4) or M-bands (variant 1). Previous and current findings strongly favor a structural role for MyBP-C slow at the sarcomeric A- and M-bands, and point to a regulatory role on muscle contraction. Consequently, the detailed characterization of the biochemical and biophysical properties of the four MyBP-C slow variants, and the development of the appropriate molecular tools and animal models are imperative in order to study the cell biology and functional properties of this intricate subfamily of proteins.

Acknowledgments

The authors wish to thank S. Adediran and N. Perry for their technical assistance in the initial stages of this work. Our research has been supported by Grants to Aikaterini Kontrogianni-Konstantopoulos from the National Institutes of Health (R01 AR52768) and the Muscular Dystrophy Association (RG 4214) and to Maegen A. Ackermann from the National Institutes of Health (F32 AR058079).

References

- [1] K. A. Clark, A. S. McElhinny, M. C. Beckerle, and C. C. Gregorio, "Striated muscle cytoarchitecture: an intricate web of form and function," *Annual Review of Cell and Developmental Biology*, vol. 18, pp. 637–706, 2002.
- [2] C. Franzini-Armstrong, "Functional significance of membrane architecture in skeletal and cardiac muscle," *Society of General Physiologists series*, vol. 51, pp. 3–18, 1996.
- [3] C. E. Oakley, J. Chamoun, L. J. Brown, and B. D. Hambly, "Myosin binding protein-C: enigmatic regulator of cardiac contraction," *International Journal of Biochemistry and Cell Biology*, vol. 39, no. 12, pp. 2161–2166, 2007.
- [4] R. Starr and G. Offer, "Polypeptide chains of intermediate molecular weight in myosin preparations," *FEBS Letters*, vol. 15, no. 1, pp. 40–44, 1971.
- [5] H. C. Hartzell and W. S. Sale, "Structure of C protein purified from cardiac muscle," *Journal of Cell Biology*, vol. 100, no. 1, pp. 208–215, 1985.
- [6] G. Offer, C. Moos, and R. Starr, "A new protein of the thick filaments of vertebrate skeletal myofibrils. Extraction, purification and characterization," *Journal of Molecular Biology*, vol. 74, no. 4, pp. 653–662, 1973.
- [7] R. Craig and G. Offer, "The location of C protein in rabbit skeletal muscle," *Proceedings of the Royal Society of London. Series B*, vol. 192, no. 1109, pp. 451–461, 1976.
- [8] P. Bennett, R. Craig, R. Starr, and G. Offer, "The ultrastructural location of C-protein, X-protein and H-protein in rabbit muscle," *Journal of Muscle Research and Cell Motility*, vol. 7, no. 6, pp. 550–567, 1986.
- [9] F. A. Pepe, "Structure of muscle filaments from immunohistochemical and ultrastructural studies," *Journal of Histochemistry and Cytochemistry*, vol. 23, no. 7, pp. 543–562, 1975.
- [10] F. A. Pepe, F. T. Ashton, C. Street, and J. Weisel, "The myosin filament. X. Observation of nine subfilaments in transverse sections," *Tissue and Cell*, vol. 18, no. 4, pp. 499–508, 1986.
- [11] E. Rome, G. Offer, and F. A. Pepe, "X ray diffraction of muscle labelled with antibody to C protein," *Nature: New Biology*, vol. 244, no. 135, pp. 152–154, 1973.
- [12] M. Gautel, M. A. C. Morelli, M. Pfuhl, A. Motta, and A. Pastore, "A calmodulin-binding sequence in the C-terminus of human cardiac titin kinase," *European Journal of Biochemistry*, vol. 230, no. 2, pp. 752–759, 1995.
- [13] F. E. Weber, K. T. Vaughan, F. C. Reinach, and D. A. Fischman, "Complete sequence of human fast-type and slow-type muscle myosin-binding-protein C (MyBP-C). Differential expression, conserved domain structure and chromosome assignment," *European Journal of Biochemistry*, vol. 216, no. 2, pp. 661–669, 1993.
- [14] D. O. Fürst, U. Vinkemeier, and K. Weber, "Mammalian skeletal muscle C-protein: purification from bovine muscle, binding to titin and the characterization of a full-length human cDNA," *Journal of Cell Science*, vol. 102, no. 4, pp. 769–778, 1992.
- [15] F. C. Reinach, T. Masaki, and D. A. Fischman, "Characterization of the C-protein from posterior latissimus dorsi muscle of the adult chicken: heterogeneity within a single sarcomere," *Journal of Cell Biology*, vol. 96, no. 1, pp. 297–300, 1983.
- [16] M. Yasuda, S. Koshida, N. Sato, and T. Obinata, "Complete primary structure of chicken cardiac C-protein (MyBP-C) and its expression in developing striated muscles," *Journal of Molecular and Cellular Cardiology*, vol. 27, no. 10, pp. 2275–2286, 1995.

- [17] S. Einheber and D. A. Fischman, "Isolation and characterization of a cDNA clone encoding avian skeletal muscle C-protein: an intracellular member of the immunoglobulin superfamily," *Proceedings of the National Academy of Sciences of the United States of America*, vol. 87, no. 6, pp. 2157–2161, 1990.
- [18] M. Gautel, D. O. Fürst, A. Cocco, and S. Schiaffino, "Isoform transitions of the myosin binding protein C family in developing human and mouse muscles: lack of isoform transcomplementation in cardiac muscle," *Circulation Research*, vol. 82, no. 1, pp. 124–129, 1998.
- [19] M. Kawashima, S. Kitani, T. Tanaka, and T. Obinata, "The earliest form of C-protein expressed during striated muscle development is immunologically the same as cardiac-type C-protein," *Journal of Biochemistry*, vol. 99, no. 4, pp. 1037–1047, 1986.
- [20] M. Kurasawa, N. Sato, A. Matsuda, S. Koshida, T. Totsuka, and T. Obinata, "Differential expression of C-protein isoforms in developing and degenerating mouse striated muscles," *Muscle and Nerve*, vol. 22, no. 2, pp. 196–207, 1999.
- [21] T. Obinata, F. C. Reinach, D. M. Bader, T. Masaki, S. Kitani, and D. A. Fischman, "Immunohistochemical analysis of C-protein isoform transitions during the development of chicken skeletal muscle," *Developmental Biology*, vol. 101, no. 1, pp. 116–124, 1984.
- [22] F. Fougères, A.-L. Delezoide, M. Y. Fiszman, K. Schwartz, J. S. Beckmann, and L. Carrier, "Cardiac myosin binding protein C gene is specifically expressed in heart during murine and human development," *Circulation Research*, vol. 82, no. 1, pp. 130–133, 1998.
- [23] T. Obinata, S. Kitani, T. Masaki, and D. A. Fischman, "Coexistence of fast-type and slow-type C-proteins in neonatal chicken breast muscle," *Developmental Biology*, vol. 105, no. 1, pp. 253–256, 1984.
- [24] T. Obinata and K. Shinbo, "Slow-type C-protein in dystrophic chicken fast pectoralis muscle," *Muscle and Nerve*, vol. 10, no. 4, pp. 351–358, 1987.
- [25] G. K. Dhoot and S. V. Perry, "Expression of slow skeletal myosin binding C-protein in normal adult mammalian heart," *Journal of Muscle Research and Cell Motility*, vol. 26, no. 2, pp. 143–148, 2005.
- [26] L. Carrier, "Cardiac myosin-binding protein C in the heart," *Archives des Maladies du Coeur et des Vaisseaux*, vol. 100, no. 3, pp. 238–243, 2007.
- [27] P. P. de Tombe, "Myosin binding protein C in the heart," *Circulation Research*, vol. 98, no. 10, pp. 1234–1236, 2006.
- [28] M. A. Ackermann, L.-Y. R. Hu, A. L. Bowman, R. J. Bloch, and A. Kontogianni-Konstantopoulos, "Obscurin interacts with a novel isoform of MyBP-C slow at the periphery of the sarcomeric M-band and regulates thick filament assembly," *Molecular Biology of the Cell*, vol. 20, no. 12, pp. 2963–2978, 2009.
- [29] A. Kontogianni-Konstantopoulos and R. J. Bloch, "Obscurin: a multitasking muscle giant," *Journal of Muscle Research and Cell Motility*, vol. 26, no. 6-8, pp. 419–426, 2005.
- [30] S. V. Yap, E. Vafiadaki, J. Strong, and A. Kontogianni-Konstantopoulos, "HAX-1: a multifaceted antiapoptotic protein localizing in the mitochondria and the sarcoplasmic reticulum of striated muscle cells," *Journal of Molecular and Cellular Cardiology*. In press.
- [31] J. Lexell, J. C. Jarvis, J. Currie, D. Y. Downham, and S. Salmons, "Fibre type composition of rabbit tibialis anterior and extensor digitorum longus muscles," *Journal of Anatomy*, vol. 185, no. 1, pp. 95–101, 1994.
- [32] T. Soukup, G. Zacharova, and V. Smerdu, "Fibre type composition of soleus and extensor digitorum longus muscles in normal female inbred Lewis rats," *Acta Histochemica*, vol. 104, no. 4, pp. 399–405, 2002.
- [33] E. Gonzalez, M. L. Messi, Z. Zheng, and O. Delbono, "Insulin-like growth factor-1 prevents age-related decrease in specific force and intracellular Ca^{2+} in single intact muscle fibres from transgenic mice," *Journal of Physiology*, vol. 552, no. 3, pp. 833–844, 2003.
- [34] N. Hamalainen and D. Pette, "The histochemical profiles of fast fiber types IIB, IID, and IIA in skeletal muscles of mouse, rat, and rabbit," *Journal of Histochemistry and Cytochemistry*, vol. 41, no. 5, pp. 733–743, 1993.
- [35] P. D. Gollnick, B. Sjoedin, J. Karlsson, E. Jansson, and B. Saltin, "Human soleus muscle: a comparison of fiber composition and enzyme activities with other leg muscles," *Pflügers Archiv European Journal of Physiology*, vol. 348, no. 3, pp. 247–255, 1974.
- [36] A. R. Tupling, E. Bombardier, R. D. Stewart, C. Vigna, and A. E. Aquiri, "Muscle fiber type-specific response of Hsp70 expression in human quadriceps following acute isometric exercise," *Journal of Applied Physiology*, vol. 103, no. 6, pp. 2105–2111, 2007.
- [37] M. S. Lim and M. P. Walsh, "Phosphorylation of skeletal and cardiac muscle C-proteins by the catalytic subunit of cAMP-dependent protein kinase," *Biochemistry and Cell Biology*, vol. 64, no. 7, pp. 622–630, 1986.
- [38] I. M. Vikhliantsev and Z. A. Podlubnaia, "Phosphorylation of sarcomeric cytoskeletal proteins—an adaptive factor for inhibiting the contractile activity of muscle during hibernation," *Biofizika*, vol. 48, no. 3, pp. 499–504, 2003.
- [39] T. N. Alyonycheva, T. Mikawa, F. C. Reinach, and D. A. Fischman, "Isoform-specific interaction of the myosin-binding proteins (MyBPs) with skeletal and cardiac myosin is a property of the C-terminal immunoglobulin domain," *Journal of Biological Chemistry*, vol. 272, no. 33, pp. 20866–20872, 1997.
- [40] C. Moos, G. Offer, R. Starr, and P. Bennett, "Interaction of C protein with myosin, myosin rod and light meromyosin," *Journal of Molecular Biology*, vol. 97, no. 1, pp. 1–9, 1975.
- [41] T. Okagaki, F. E. Weber, D. A. Fischman, K. T. Vaughan, T. Mikawa, and F. C. Reinach, "The major myosin-binding domain of skeletal muscle MyBP-C (C protein) resides in the COOH-terminal, immunoglobulin C2 motif," *Journal of Cell Biology*, vol. 123, no. 3, pp. 619–626, 1993.
- [42] C. A. Miyamoto, D. A. Fischman, and F. C. Reinach, "The interface between MyBP-C and myosin: site-directed mutagenesis of the CX myosin-binding domain of MyBP-C," *Journal of Muscle Research and Cell Motility*, vol. 20, no. 7, pp. 703–715, 1999.
- [43] R. Starr and G. Offer, "The interaction of C-protein with heavy meromyosin and subfragment-2," *Biochemical Journal*, vol. 171, no. 3, pp. 813–816, 1978.
- [44] C. Moos, "Fluorescence microscope study of the binding of added C protein to skeletal muscle myofibrils," *Journal of Cell Biology*, vol. 90, no. 1, pp. 25–31, 1981.
- [45] C. Moos, C. M. Mason, and J. M. Besterman, "The binding of skeletal muscle C-protein to F-actin, and its relation to the interaction of actin with myosin subfragment-1," *Journal of Molecular Biology*, vol. 124, no. 5, pp. 571–586, 1978.
- [46] K. Yamamoto, "The binding of skeletal muscle C-protein to regulated actin," *FEBS Letters*, vol. 208, no. 1, pp. 123–127, 1986.

- [47] N. A. Freydina, Z. I. Vishnevskaya, S. N. Udaltsov, and Z. A. Podlubnaya, "Effect of C-protein and LC-light chains on actomyosin ATPase at various ionic strength and calcium levels," *Acta Biochimica et Biophysica Hungarica*, vol. 21, no. 3, pp. 247–256, 1986.
- [48] C. Moos and I. N. Feng, "Effect of C-protein on actomyosin ATPase," *Biochimica et Biophysica Acta*, vol. 632, no. 2, pp. 141–149, 1980.
- [49] J. F. Koretz, T. C. Irving, and K. Wang, "Filamentous aggregates of native titin and binding of C-protein and AMP-deaminase," *Archives of Biochemistry and Biophysics*, vol. 304, no. 2, pp. 305–309, 1993.
- [50] S. Labeit, M. Gautel, A. Lakey, and J. Trinick, "Towards a molecular understanding of titin," *The EMBO Journal*, vol. 11, no. 5, pp. 1711–1716, 1992.
- [51] A. Soteriou, M. Gamage, and J. Trinick, "A survey of interactions made by the giant protein titin," *Journal of Cell Science*, vol. 104, no. 1, pp. 119–123, 1993.
- [52] A. Freiburg and M. Gautel, "A molecular map of the interactions between titin and myosin-binding protein C: implications for sarcomeric assembly in familial hypertrophic cardiomyopathy," *European Journal of Biochemistry*, vol. 235, no. 1–2, pp. 317–323, 1996.
- [53] A. Kontrogianni-Konstantopoulos, M. A. Ackermann, A. L. Bowman, S. V. Yap, and R. J. Bloch, "Muscle giants: molecular scaffolds in sarcomerogenesis," *Physiological Reviews*, vol. 89, no. 4, pp. 1217–1267, 2009.
- [54] E. Flashman, L. Korkie, H. Watkins, C. Redwood, and J. C. Moolman-Smook, "Support for a trimeric collar of myosin binding protein C in cardiac and fast skeletal muscle, but not in slow skeletal muscle," *FEBS Letters*, vol. 582, no. 3, pp. 434–438, 2008.
- [55] B. Decker and M. S. Z. Kellermyer, "Periodically arranged interactions within the myosin filament backbone revealed by mechanical unzipping," *Journal of Molecular Biology*, vol. 377, no. 2, pp. 307–310, 2008.
- [56] J. S. Davis, "Interaction of C-protein with pH 8.0 synthetic thick filaments prepared from the myosin of vertebrate skeletal muscle," *Journal of Muscle Research and Cell Motility*, vol. 9, no. 2, pp. 174–183, 1988.
- [57] J. F. Koretz, "Effects of C-protein on synthetic myosin filament structure," *Biophysical Journal*, vol. 27, no. 3, pp. 433–446, 1979.
- [58] R. Gilbert, J. A. Cohen, S. Pardo, A. Basu, and D. A. Fischman, "Identification of the A-band localization domain of myosin binding proteins C and H (MyBP-C, MyBP-H) in skeletal muscle," *Journal of Cell Science*, vol. 112, no. 1, pp. 69–79, 1999.
- [59] R. Gilbert, M. G. Kelly, T. Mikawa, and D. A. Fischman, "The carboxyl terminus of myosin binding protein C (MyBP-C, C-protein) specifies incorporation into the A-band of striated muscle," *Journal of Cell Science*, vol. 109, no. 1, pp. 101–111, 1996.
- [60] G. Bonne, L. Carrier, J. Bercovici, et al., "Cardiac myosin binding protein-C gene splice acceptor site mutation is associated with familial hypertrophic cardiomyopathy," *Nature Genetics*, vol. 11, no. 4, pp. 438–440, 1995.
- [61] C. E. Oakley, B. D. Hambly, P. M. Curmi, and L. J. Brown, "Myosin binding protein C: structural abnormalities in familial hypertrophic cardiomyopathy," *Cell research*, vol. 14, no. 2, pp. 95–110, 2004.
- [62] L. Carrier, R. Knöll, N. Vignier, et al., "Asymmetric septal hypertrophy in heterozygous cMyBP-C null mice," *Cardiovascular Research*, vol. 63, no. 2, pp. 293–304, 2004.
- [63] S. P. Harris, C. R. Bartley, T. A. Hacker, et al., "Hypertrophic cardiomyopathy in cardiac myosin binding protein-C knockout mice," *Circulation Research*, vol. 90, no. 5, pp. 594–601, 2002.
- [64] F. S. Korte, K. S. McDonald, S. P. Harris, and R. L. Moss, "Loaded shortening, power output, and rate of force redevelopment are increased with knockout of cardiac myosin binding protein-C," *Circulation Research*, vol. 93, no. 8, pp. 752–758, 2003.
- [65] S. P. Harris, E. Rostkova, M. Gautel, and R. L. Moss, "Binding of myosin binding protein-C to myosin subfragment S2 affects contractility independent of a tether mechanism," *Circulation Research*, vol. 95, no. 9, pp. 930–936, 2004.
- [66] P. A. Hofmann, M. L. Greaser, and R. L. Moss, "C-protein limits shortening velocity of rabbit skeletal muscle fibres at low levels of Ca^{2+} activation," *Journal of Physiology*, vol. 439, pp. 701–715, 1991.
- [67] C. A. C. Ottenheijm, C. Hidalgo, K. Rost, M. Gotthardt, and H. Granzier, "Altered contractility of skeletal muscle in mice deficient in titin's M-band region," *Journal of Molecular Biology*, vol. 393, no. 1, pp. 10–26, 2009.
- [68] S. Winegrad, "Cardiac myosin binding protein C," *Circulation Research*, vol. 84, no. 10, pp. 1117–1126, 1999.
- [69] M. J. McGrath, D. L. Cottle, M.-A. Nguyen, et al., "Four and a half LIM protein 1 binds myosin-binding protein C and regulates myosin filament formation and sarcomere assembly," *Journal of Biological Chemistry*, vol. 281, no. 11, pp. 7666–7683, 2006.
- [70] E. Flashman, C. Redwood, J. Moolman-Smook, and H. Watkins, "Cardiac myosin binding protein C: its role in physiology and disease," *Circulation Research*, vol. 94, no. 10, pp. 1279–1289, 2004.
- [71] D. Sanoudou, E. Vafiadaki, D. A. Arvanitis, E. Kranias, and A. Kontrogianni-Konstantopoulos, "Array lessons from the heart: focus on the genome and transcriptome of cardiomyopathies," *Physiological Genomics*, vol. 21, pp. 131–143, 2005.
- [72] K. M. McCormick, K. M. Baldwin, and F. Schachat, "Coordinate changes in C protein and myosin expression during skeletal muscle hypertrophy," *American Journal of Physiology*, vol. 267, no. 2, pp. C443–C449, 1994.

Research Article

Functional Differences between the N-Terminal Domains of Mouse and Human Myosin Binding Protein-C

Justin F. Shaffer,^{1,2} Peony Wong,¹ Kristina L. Bezold,¹ and Samantha P. Harris¹

¹Department of Neurobiology, Physiology and Behavior, University of California-Davis, Davis, CA 95616-8519, USA

²Department of Bioengineering, University of Washington, Seattle, WA 98195-5061, USA

Correspondence should be addressed to Samantha P. Harris, samharris@ucdavis.edu

Received 16 December 2009; Accepted 31 January 2010

Academic Editor: Henk L. M. Granzier

Copyright © 2010 Justin F. Shaffer et al. This is an open access article distributed under the Creative Commons Attribution License, which permits unrestricted use, distribution, and reproduction in any medium, provided the original work is properly cited.

The N-terminus of cMyBP-C can activate actomyosin interactions in the absence of Ca^{2+} , but it is unclear which domains are necessary. Prior studies suggested that the Pro-Ala rich region of human cMyBP-C activated force in permeabilized human cardiomyocytes, whereas the C1 and M-domains of mouse cMyBP-C activated force in permeabilized rat cardiac trabeculae. Because the amino acid sequence of the P/A region differs between human and mouse cMyBP-C isoforms (46% identity), we investigated whether species-specific differences in the P/A region could account for differences in activating effects. Using chimeric fusion proteins containing combinations of human and mouse C0, Pro-Ala, and C1 domains, we demonstrate here that the human P/A and C1 domains activate actomyosin interactions, whereas the same regions of mouse cMyBP-C are less effective. These results suggest that species-specific differences between homologous cMyBP-C isoforms confer differential effects that could fine-tune cMyBP-C function in hearts of different species.

1. Introduction

Myosin binding protein-C (MyBP-C) is a regulatory and structural protein associated with the A-bands (thick filaments) of vertebrate striated muscle sarcomeres. Regulatory effects are mediated in part by the N-terminus of cardiac cMyBP-C, which is made up of modular immunoglobulin- (Ig-) like domains, termed C0 at the N-terminus, followed by domains C1 through C10 (Figure 1(a)). Between the C0 and C1 domains there is a sequence of ~50 amino acids that contains a high percentage of proline and alanine residues (referred to as the Pro-Ala rich region (P/A)). Between the C1 and C2 domains there is a stretch of ~100 highly conserved amino acids referred to as MyBP-C motif or M-domain. The M-domain is phosphorylated by β -adrenergic agonists and phosphorylation increases the rate of cross-bridge cycling [1], thereby contributing to increased inotropic responses of the heart [2]. Phosphorylation reduces binding of the M-domain to actin [3] and myosin S2 in vitro [4], but the precise mechanism(s) by which phosphorylation accelerates actomyosin interactions is not well understood.

In efforts to uncover mechanisms by which the N-terminus of cMyBP-C affects cross-bridge cycling several groups have investigated the effects of recombinant proteins containing N-terminal cMyBP-C domains on actomyosin interactions. For instance, Razumova et al. [5] investigated effects of N-terminal domains in in vitro motility assays and found that recombinant proteins containing the C1 through C2 domains of mouse cMyBP-C (referred to as C1C2, inclusive of the M-domain) could activate thin filament motility even in the absence of Ca^{2+} . Incubation of permeabilized rat trabeculae with C1C2 also increased Ca^{2+} sensitivity of force and increased the rate of tension redevelopment (k_{tr}) [6]. The activating effects of C1C2 were attributed to the combined effects of the C1 and M-domains because these domains together were necessary and sufficient to increase Ca^{2+} sensitivity of force, whereas other domains including the C0, P/A, and C1 domains had little, if any, effect on force activation. However, in apparent contrast to these results, Herron et al. [7] found that a recombinant protein comprised of the human C0, P/A, and C1 domains (i.e., C0C1) activated tension and increased

TABLE 1: Sequence identity between domains of human and mouse cMyBP-C.

Protein or Domain	Number of Amino Acids		Percent Identity
	<i>Mouse</i>	<i>Human</i>	
cMyBP-C	1270	1274	89
C0C2	447	451	84
C0	104	101	81
Pro-Ala	46	51	46
C1	111	111	90
M	105	107	91
C2	81	81	96

calculated from Swiss Institute for Bioinformatics software [9].

2.2. Engineered Chimeric C0C1 Proteins. The In-Fusion PCR Cloning System (Clontech, Mountain View, CA) was used according to manufacturer's instructions and the protocol by Zhu et al. [10] to create seamless chimeric C0C1 proteins consisting of various combinations of mouse and human C0, P/A, and C1 domains. Boundaries of the C0, P/A, and C1 domains are shown in Figure 1(b) and were as described by Gautel et al. [11] and as listed for human and mouse cMyBP-C on the Universal Protein Resources Databank (UniProt) [12]. PCR products encoding the mouse and human domains were amplified from mouse and human cMyBP-C cDNA with additional 15 bp flanking sequences at the 5' and 3' ends that overlap with the adjacent segment of the construct (Table 2, Figure 1(c)). The pQE-2 expression vector (Qiagen) was digested with NdeI and HindIII and gel-purified. PCR products and the digested pQE-2 vector were mixed at a 1 : 2 : 2 : 2 molar ratio with the In-Fusion enzyme according to manufacturer's instructions and transformed into Top10 cells (Invitrogen). Correctly ligated plasmids were chosen after selection with carbenicillin and sequences were verified by DNA sequencing at the UC Davis DNA Sequencing Facility. Selected clones were transformed into M15 cells for expression and purification as described previously [5]. Chimeric C0C1 proteins used in this study are shown schematically in Figure 1(c).

2.3. Native Protein Purification. Heavy meromyosin (HMM) and S1 were prepared from rabbit psoas skeletal myosin via α -chymotryptic digest as described [13]. Bovine cardiac F-actin, tropomyosin, and troponin were purified from ether powder as described [14–16]. Thin filaments, comprised of F-actin and regulatory proteins, were reconstituted in AB buffer (in mmol/L: 25 KCl, 25 imidazole (pH 7.4), 4 MgCl₂, 1 EGTA, and 1 DTT) by combining at an actin:tropomyosin:troponin ratio of 4:1:1 for in vitro motility assays and at 7:2:2 for ATPase assays. The thin filament mix was labeled with rhodamine-phalloidin according to Homsher et al. [17] and used in in vitro motility assays.

2.4. Mechanical Force Measurements. Treatment of all animals was in strict accordance with guidelines and protocols

established by the University of California Institutional Animal Care and Use Committee. Male Sprague-Dawley rats (200–250 g) were euthanized by intraperitoneal injection of sodium pentobarbital. Hearts were then rapidly excised and right ventricles were dissected in a Ringer's solution at pH 7.4 (in mmol/L: 100 NaCl, 24 NaHCO₃, 2.5 KCl, 1 MgSO₄, 1 Na₂HPO₄, and 1 CaCl₂). Trabeculae were permeabilized in situ by incubation of splayed ventricles overnight in a relaxing solution containing 50% glycerol and 1% Triton X-100 (Sigma, St. Louis, Missouri) at 4°C. Individual trabeculae were dissected free from ventricle walls, pinned to the bottom of a sylgar-coated Petri dish, and stored for up to one week in glycerinated relaxing solution at –20°C.

Steady state force and rate of tension redevelopment (k_{tr}) measurements were performed as previously described [6]. Briefly, permeabilized trabeculae were mounted between a force transducer (model 403A, Aurora Scientific Inc.) and a torque motor (Model 312-Cl, Aurora Scientific Inc). Sarcomere length was adjusted to $\sim 2.3 \mu\text{m}$ in relaxing solution and monitored throughout the course of the experiment using an inverted microscope (Olympus IX-71) fitted with a 12-Mega pixel digital camera (Olympus DP70). Relaxing, preactivating, and Ca²⁺-activating solutions were prepared as previously described using a custom software package [18, 19]. Solutions were maintained at 0.18 M ionic strength and pH 7.0 at 15°C (in mmol/L: 15 phosphocreatine, 15 EGTA, at least 40 MOPS, 1 free Mg²⁺, 135 Na⁺ + K⁺, 1 DTT, 250 units ml⁻¹ creatine kinase (CK), and 5 ATP). Ca²⁺ concentration (reported as pCa = $-\log[\text{Ca}^{2+}]$) was established by varying amounts of CaCl₂. Recombinant proteins were added to relaxing and preactivating solutions by buffer exchange using desalting spin columns (Pierce, Rockford, IL).

2.5. In Vitro Motility Assays. In vitro motility assays were performed as described previously [5]. Briefly, HMM was applied to a nitrocellulose-coated coverslip followed by incubation with bovine serum albumin (BSA) to prevent non-specific adsorption of thin filaments or recombinant proteins to the motility surface. Shredded actin filaments followed by ATP were then added to block nonfunctional myosin heads (dead-heads). Next, rhodamine-phalloidin labeled bovine cardiac thin filaments (4:1:1 actin:tropomyosin:troponin) were added, followed by a motility buffer containing AB buffer, 2 mM ATP, and an oxygen-scavenging system to limit photo-bleaching. Recombinant cMyBP-C proteins were dialyzed into AB buffer and added to the slide surface in the motility buffer. Motility was viewed using an Olympus IX-71 microscope with an Hg-arc lamp, TRITC filter, and a 100 \times /1.4 NA oil-immersion objective. Video files were recorded using a Q-Imaging Retiga Exi digital camera and ImageProPlus software. Filament motility was analyzed using custom software developed in LabView and NI Vision Development (National Instruments, Austin, TX) kindly provided by Dr. Michael Regnier (University of Washington).

2.6. ATPase Assay. ATPase assays were performed by mixing 0.2 μM myosin S1 and 3.5 μM reconstituted

TABLE 2: Primers used to create recombinant chimeric C0C1 proteins.

cMyBP-C domain	Primer pairs (upstream/downstream primer)
Mouse C0	5'-ATCACCATCACCATATGCCGGAGCCAGGGAAGAAACCA -3'/ 5'-AGGGGCCAGCATGGGTTCTGCCTTCTCTGGAGGGGC -3'
Mouse P/A	5'-TCTGAAGTTGCTCCAGGAGCC -3'/ 5'-GTCATCAGGGGCTCCCTGATG -3'
Mouse C1	5'-GGAGCCCCCGATGACCCATTGGCCTCTTTCTGATGCGA -3'/ 5'-TCAGCTAATTAAGCTTTCATCCAGAACCAATCGCCTCATGGAC -3'
Human C0	5'-ATCACCATCACCATATGCCTGAGCCGGGAAGAAGC -3'/ 5'-TGGAGCAACTTCAGACTCTGCCTTCTCTGCCTCATGAC -3'
Human P/A	5'-CCCATGCTGGCCCTGC -3'/ 5'-GTCATCGGGGCTCCAGG -3'
Human C1	5'-GGAGCCCCTGATGACCCATTGGCCTCTTCGTGATGC -3'/ 5'-TCAGCTAATTAAGCTTTCATCCGGTGCCCATGGCCT -3'

bovine cardiac thin filaments (mixed at a 7:2:2 actin:tropomyosin:troponin ratio) in ATPase buffer (in mmol/L: 10 imidazole (pH 7.4), 2 MgCl₂, 1 EGTA, and 1 DTT) with or without 1 μ M recombinant cMyBP-C proteins. The addition of 1 mM ATP started the reaction and reactions were quenched at three different time points with stop solution (3.3% SDS, 0.12 M Na-EDTA, pH 7.4). Phosphate production was determined via colorimetric assay as described [20].

2.7. *Statistical Tests.* Data were compared using ANOVA followed by Bonferroni post-hoc comparisons. Significance was considered at $P < .05$.

3. Results

3.1. *Human C0C1 Increases Ca²⁺ Sensitivity of Tension in Permeabilized Trabeculae.* Effects of recombinant mouse and human C0C1 proteins (inclusive of the C0, P/A, and C1 domains) were first assessed in permeabilized rat cardiac trabeculae. Figure 2(a) shows effects of human (h)C0C1 and mouse (m)C0C1 on force generation at pCa 9.0 and at maximal Ca²⁺ activation (pCa 4.5). Neither hC0C1 nor mC0C1 affected resting force in the absence of Ca²⁺ (pCa 9.0) or maximal force at pCa 4.5 even at concentrations up to 80 μ M, the highest concentration used by Herron et al. [7]. This result is consistent with observations by Razumova et al. [6] who found that preincubation of rat trabeculae with 30 μ M mC0C1 did not affect force, but it differs somewhat from Herron et al. [7] who found that 30 μ M hC0C1 activated force generation even in the absence of Ca²⁺ at pCa 9.0. Because measurements by Herron et al. [7] were conducted primarily using permeabilized myocytes from human myocardium, species-specific differences (rat versus human) could potentially contribute to the different effects observed here. However, as shown in Figures 2(b) and 2(c), hC0C1 was effective at increasing force and k_{tr} at submaximal Ca²⁺ (pCa 5.3) near the half-maximal [Ca²⁺] (pCa₅₀) required for maximal force generation [6]. Effects were significant after preincubation with 50 μ M hC0C1.

50 μ M mC0C1 also increased Ca²⁺ sensitivity of tension, albeit to a lesser extent than hC0C1, but had no effect on k_{tr} .

3.2. *The Human Pro-Ala Rich Region Activates Filament Motility in the Absence of Ca²⁺.* Because results from permeabilized rat trabeculae suggested that species-specific differences contribute to differences in effects of hC0C1 and mC0C1, we sought to compare effects of hC0C1 versus mC0C1 in a defined system that minimizes variability in cross-species isoform expression. We therefore compared effects of hC0C1 and mC0C1 using in vitro motility assays with reconstituted cardiac thin filaments and skeletal HMM. Control values for average filament velocities in the absence (pCa 9) and presence (pCa 5) of Ca²⁺ were $0.3 \pm 0.1 \mu\text{m/s}$ ($n = 12$) and $3.8 \pm 0.5 \mu\text{m/s}$ ($n = 9$), respectively, demonstrating that reconstituted thin filaments were well regulated by Ca²⁺ under control conditions in the absence of added recombinant proteins. Figure 3(a) compares filament sliding speeds at pCa 9.0 in the absence or presence of hC0C1 or mC0C1. Under control conditions at low Ca²⁺, filament sliding speed was low and the vast majority of filaments were stopped (fraction moving was 4%). Addition of 1 μ M mC0C1 to motility buffers did not activate motility, whereas addition of hC0C1 significantly increased motility. These results are similar to those obtained in rat trabeculae (Figure 2) where hC0C1 increased Ca²⁺ sensitivity of tension and k_{tr} to a greater extent than mC0C1. They are also consistent with Herron et al. [7] who found that hC0C1 could activate tension development in myocytes in the absence of Ca²⁺.

To determine whether the P/A region contributes to the activating properties of hC0C1, chimeric C0C1 proteins were created that substituted human and mouse P/A regions. Figure 3(b) shows effects on filament motility of exchanging the human and mouse P/A domains in chimeric proteins. Insertion of the human P/A region into mouse C0C1 to create the chimeric protein mhmC0C1 (mouse C0, human P/A, and mouse C1) increased filament motility at pCa 9. This result demonstrates that the human P/A region but not the mouse P/A region is sufficient to confer activating effects on C0C1 proteins. However, activation was not complete

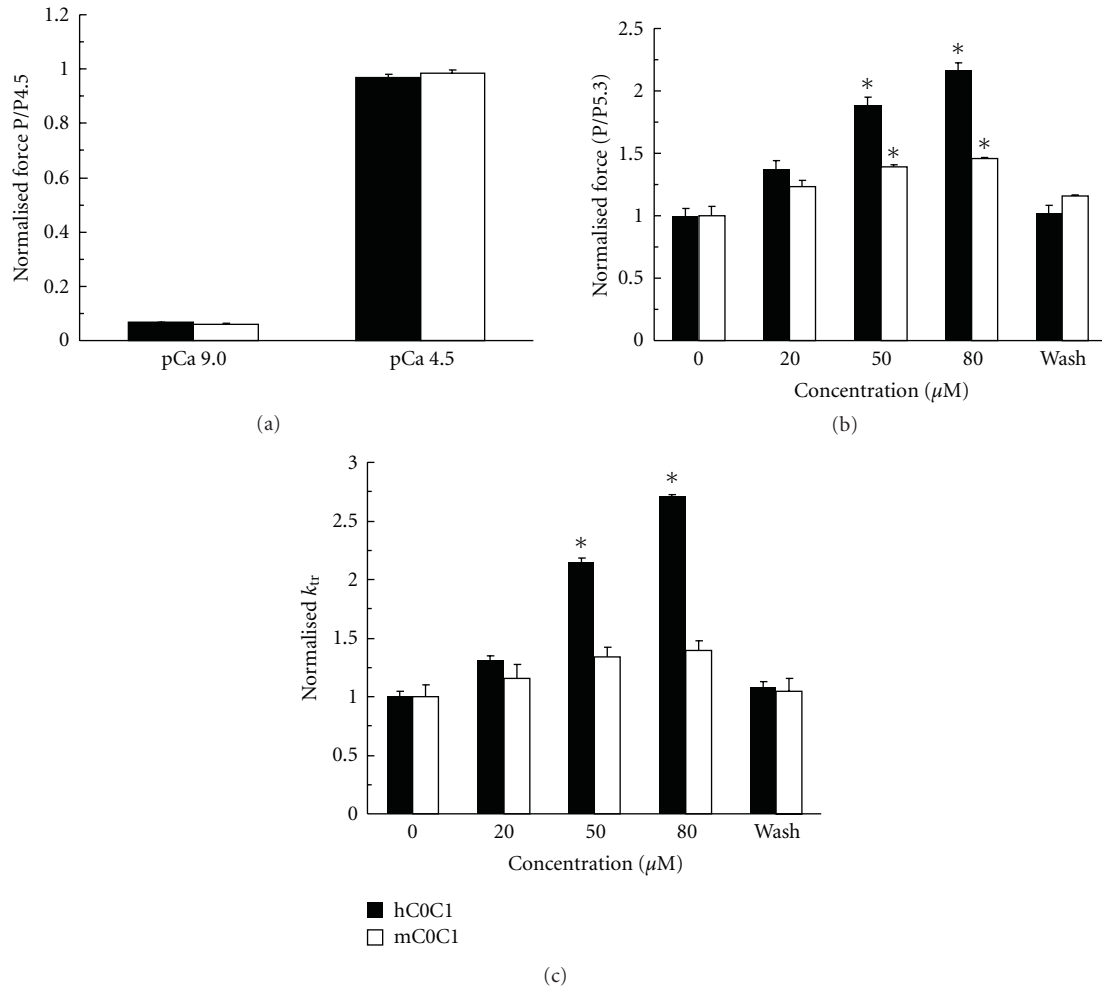


FIGURE 2: Effects of mC0C1 and hC0C1 on steady state force and rate of tension redevelopment (k_{tr}) in permeabilized rat trabeculae. (a) Preincubation of trabeculae with 80 μ M mC0C1 or hC0C1 did not affect resting force at pCa 9.0 or maximal Ca^{2+} activated force at pCa 4.5. However, hC0C1 increased force (b) and k_{tr} (c) at intermediate [Ca^{2+}] (pCa 5.3) with effects significant at 50 μ M. mC0C1 increased force at 50 μ M but did not significantly increase k_{tr} . Data are mean \pm SEM ($n = 4$ for hC0C1 and $n = 3$ for mC0C1). Asterisks denote significant differences in compared values obtained prior to protein addition ($P < .05$).

since sliding speeds were still somewhat less than in the presence of hC0C1 comprised of all human sequences. This suggests that domains outside of the P/A region must also contribute to the activating effects of hC0C1. Consistent with this idea, when the mouse P/A region was exchanged into hC0C1, that is, in hmhC0C1 (human C0, mouse P/A, and human C1), filament sliding speeds were increased relative to control but were less than in the presence of hC0C1. Collectively, these results demonstrate that the human P/A rich region is sufficient to activate motility in the absence of Ca^{2+} , but that the C0 or C1 domains must also contribute to the ability of hC0C1 to activate filament motility.

3.3. Human C1, but not C0, Activates Motility in the Absence of Ca^{2+} . To determine whether human C1 or C0 domains also contribute to the activating effects of hC0C1, we created additional chimeric proteins that substituted human and mouse C0 and C1 domains. To assess if the C1 domain is

required for activating effects, 1 μ M mmhC0C1 or hhmC0C1 proteins were added to in vitro motility assays. As shown in Figure 3(c), adding the human C1 to mouse C0 and P/A domains, (mmhC0C1) activated thin filament motility at pCa 9, demonstrating that the human C1 domain can also confer activating effects. However, filament velocity was reduced compared to hC0C1 (Figure 3(a)), indicating that other domains (e.g., P/A; Figure 3(b)) contribute to the activating effects of hC0C1. Conversely, when the mouse C1 domain was added to human C0 and P/A domains (hhmC0C1) activation occurred but to a lesser extent than hC0C1 (Figure 3(a)). These results show that mouse C1 cannot substitute for human C1 and cannot restore full activating effects when expressed with the human C0 and P/A domains.

To assess whether the human C0 domain also contributes to activating effects of hC0C1, hmmC0C1 and mhhC0C1 proteins were created and their effects in motility assays

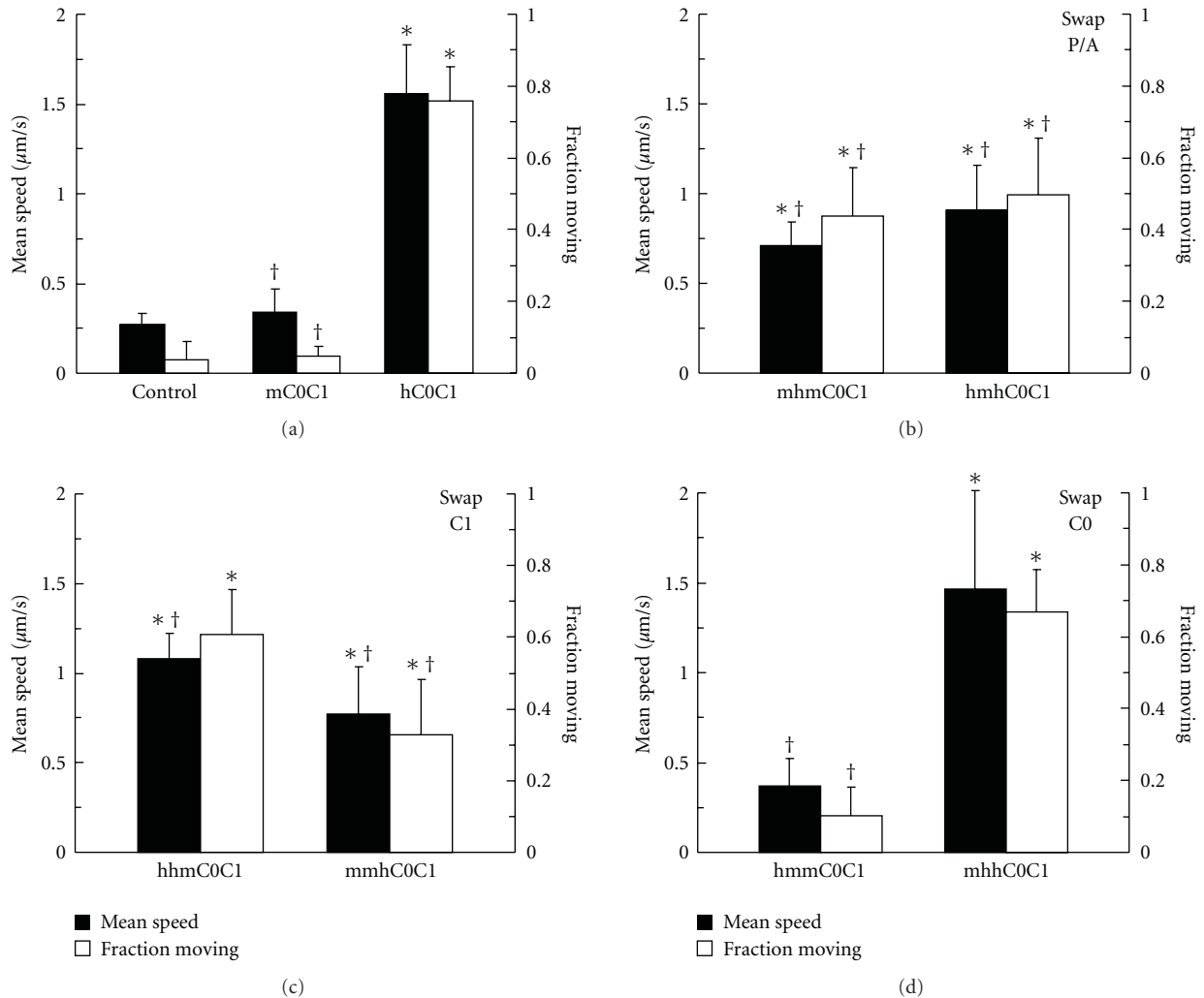


FIGURE 3: Effects of mouse and human C0, P/A, and C1 domains on motility of regulated thin filaments (F-actin + Tm + Tn) at pCa 9. (a) Compared to control experiments in the absence of added protein ($n = 12$), $1 \mu\text{M}$ hC0C1 significantly activated filament sliding speed motility and the fraction of filaments moving ($n = 8$), whereas $1 \mu\text{M}$ mC0C1 did not affect motility ($n = 9$). (b) Substitution of the human for mouse P/A domain in the mouse C0C1 backbone (mhmC0C1) activated motility ($n = 7$), whereas substitution of the mouse P/A domain into the human backbone (hmhC0C1) depressed motility relative to hC0C1 ($n = 5$). (c) Exchange of mouse and human C1 domains. The human C1 domain (mmhC0C1) activated motility (compared to mC0C1, $n = 5$), whereas the mouse C1 domain (hhmC0C1) depressed motility (compared to hC0C1, $n = 6$). (d) Exchange of mouse and human C0 domains. The human C0 (hmmC0C1, $n = 5$) and mouse C0 (mhhC0C1, $n = 10$) domains did not affect thin filament motility (compared to mC0C1 and hC0C1 controls, resp.). Data are mean \pm SD. Asterisks (*) and crosses (†) denote significant differences compared to mC0C1 and hC0C1, respectively, ($P < .05$).

were assessed at pCa 9. As shown in Figure 3(d), when the human C0 domain was added to mouse P/A and C1 domains (hmmC0C1), activation of filament motility did not occur and effects of hmmC0C1 were not different from the parent mC0C1. Similarly, when the mouse C0 domain was expressed with the human P/A and C1 domains (mhhC0C1), filament motility was the same as in the presence of hC0C1 (Figure 3(a)). These results show that C0 does not contribute to the activating effects of hC0C1 in motility assays, and that the human P/A and C1 domains together are sufficient to account for the full activating properties of hC0C1 on actomyosin interactions in the absence of Ca^{2+} .

3.4. Activating Effects Are Independent of Myosin S2. When expressed in rat neonatal cardiomyocytes, hC0C1 localized to sarcomere A-bands [7], suggesting that interactions of hC0C1 with myosin or other thick filament proteins are required for the observed activating effects. Consistent with this idea, the C0 domain was reported to bind to myosin S1 [21] and C1 can bind to myosin S2 [22]. Therefore to test whether interactions with myosin S2 are required for the activating effects of the human P/A and C1 domains, effects of chimeric C0C1 proteins were assessed in ATPase assays using myosin S1 (without S2) and regulated thin filaments. As shown in Figure 4, under control conditions in

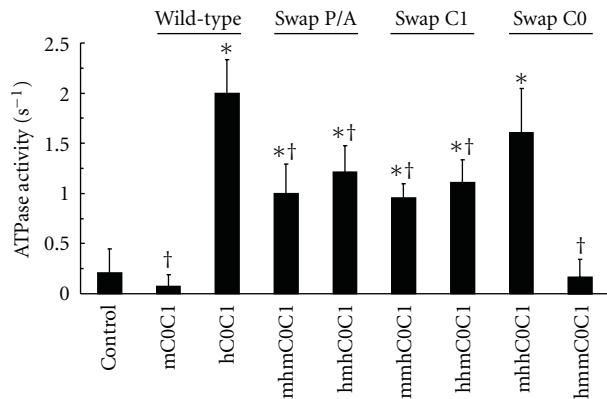


FIGURE 4: Effects of mouse and human C0, P/A, and C1 domains on thin filament activated myosin S1 ATPase assays at pCa 10 in the absence of myosin S2. 1 μ M mC0C1 had no effect on ATPase activity ($n = 9$), whereas 1 μ M hC0C1 increased ATPase activity ($n = 9$). The human P/A and C1 domains each activated ATPase activity (mhmC0C1 ($n = 7$) and mmhC0C1 ($n = 5$), resp.) to intermediate values. The mouse P/A and C1 domains (hmhC0C1, ($n = 5$) and hhmC0C1, ($n = 6$), resp.) depressed ATPase activity when compared to hC0C1. The human C0 domain (hmmC0C1, $n = 6$) had no activating effects on actin-activated S1 ATPase activity, while the mouse C0 domain (mhhC0C1, $n = 4$) did not affect activity when compared to hC0C1. Data are mean \pm SD. Asterisks (*) and crosses (†) denote significant differences when compared to mC0C1 and hC0C1, respectively, ($P < .05$).

the absence of recombinant proteins, ATPase rates were low ($0.2 \pm 0.2 \text{ sec}^{-1}$, $n = 17$) at low Ca^{2+} (pCa 10) and increased ($3.3 \pm 1.0 \text{ sec}^{-1}$, $n = 16$) in the presence of maximal Ca^{2+} (pCa 3). These results demonstrate that the thin filaments were well regulated by Ca^{2+} . Similar to the results obtained in the in vitro motility assays, addition of 1 μ M hC0C1 activated ATPase activity at pCa 10, whereas mC0C1 did not significantly affect ATPase rates. Addition of the human P/A domain or the C1 domains to the mouse C0C1 backbone (mhmC0C1 or mmhC0C1) also activated ATPase activity in the absence of Ca^{2+} , but not to the full extent of hC0C1. Substituting the mouse P/A and C1 domains in the human C0C1 backbone (hmhC0C1 and hhmC0C1) reduced ATPase activity when compared to hC0C1. Similar to motility assays (Figure 3(d)), exchanging the C0 domains (hmmC0C1 and mhhC0C1) had no effect on the ATPase rates when compared to mC0C1 and hC0C1 controls (Figure 4). Taken together, these results confirm conclusions from the in vitro motility assays that *either* the human P/A or C1 domains can confer activating properties to the hC0C1 protein, but that *both* domains are required for full effects. However, because all activating effects occurred in the absence of myosin S2, results from the ATPase assays demonstrate that activation does not require interactions of hC0C1 with myosin S2.

4. Discussion

The major result from this study is that species-specific differences between mouse and human cMyBP-C contribute to functional differences in the activities of recombinant

cMyBP-C proteins. In particular, we found significant sequence divergence (46% identity) in a proline-alanine (P/A) rich region near the N-terminus of the molecule. The human P/A rich region but not the mouse P/A region promoted actomyosin interactions as shown by the ability of proteins containing the human P/A region to increase thin filament motility and actomyosin ATPase activity even in the absence of Ca^{2+} (Figure 3). Interestingly, the human C1 domain but not mouse C1 also conferred activating effects even though the sequences of the C1 domains are much more similar (90% identity). Taken together, these results suggest that even modest sequence variations in conserved domains can lead to significant functional differences between homologous cMyBP-C proteins.

Results from this study partially reconcile disparate results from two previously published studies. Using human cMyBP-C recombinant proteins, Herron et al. [7] attributed activating effects to the P/A rich region, whereas Razumova et al. [6], using mouse recombinant proteins, found that the C1 and M domains together were required to activate force. In the present study we performed a side-by-side comparison of the effects of mouse and human C0C1 proteins and found in good agreement with Herron et al. [7] that the human P/A region can confer activating effects on actomyosin interactions, whereas also in good agreement with Razumova et al. [6] that the mouse P/A region does not. Thus, species-specific differences can account in part for the different conclusions reached in the two studies.

The precise mechanism(s) by which the P/A and C1 domains promote actomyosin interactions is not known, but interactions with either thick filaments [23] or actin [3] are possible. In support of the former, hC0C1 localizes to sarcomere A-bands when expressed in rat neonatal cardiomyocytes [7] and C1 can bind to myosin S2 [22]. However, the present results exclude interactions with thick filaments because myosin S2 was not required for hC0C1 to increase acto-S1 ATPase activity (Figure 4). Furthermore, while C0 was reported to bind to myosin S1 [21], C0 made little or no contribution to the activating effects of hC0C1 (Figures 3 and 4). Thus, interactions with myosin do not appear important for the activating effects of hC0C1, although interactions with other thick filament proteins (e.g., myosin light chains) cannot be excluded. Alternatively, the P/A region could interact with thin filaments to promote activation. In support of this idea Squire et al. [24] proposed that the P/A region of human cMyBP-C binds actin based on sequence similarity to a P/A rich segment found in essential myosin light chains (MLC). Although in a previous study we found little evidence that the mouse P/A region binds to actin because mC0C1 bound weakly if at all to F-actin in cosedimentation assays [3], Kulikovskaya et al. [25] reported that human C0C1 can bind actin. Side-by-side comparisons of binding affinity are needed, but these data are thus in the right direction for the Pro-Ala sequence to contribute to functional effects in human (e.g., because of greater actin binding affinity) but exert less effects in mouse because of reduced interactions with actin [6, 7].

The functional significance of the Pro-Ala rich sequence of cMyBP-C in vivo is not known. However, the Pro-Ala

rich sequences have been identified in other thick filament regulatory proteins including cardiac and skeletal isoforms of myosin essential light chains (MLC) [26]. In these proteins the Pro-Ala sequences modulate cross-bridge cycling rates and shortening velocity (V_{\max}) by binding to actin [27]. The proline-alanine rich regions of different MLC isoforms slow cross-bridge kinetics either by binding directly to actin [28] or by functioning as a rigid spacer arm that extends an actin binding site located near the N-terminus of the MLC out toward the thin filament [29]. In either case, interactions with actin are thought to create a drag that limits filament sliding and slows cross-bridge cycling and shortening velocity [30]. Consistent with this idea, atrial myocytes that express an atrial MLC isoform with reduced affinity for actin have nearly twice the V_{\max} and maximal power output than ventricular myocytes expressing an MLC that binds to actin with greater affinity [26].

By analogy with MLC, it is possible that the Pro-Ala rich region of cMyBP-C performs a similar role and contributes to the ability of cMyBP-C to limit myocyte shortening velocity, cross-bridge cycling, and power output [31]. If so, then the species-specific differences described here between the Pro-Ala regions of mouse and human cMyBP-C could serve to fine-tune shortening velocity to optimize power output (the product of force and velocity) such that contractile efficiency is maximized in hearts that contract under different hemodynamic loads and at different speeds. Consistent with this idea, we found that the percentage of proline and alanine residues in the Pro-Ala region varies inversely with heart rate in mammals such that larger mammals have a greater proportion of Pro-Ala residues, Shaffer and Harris [32]. Thus, decreased Pro-Ala content of cMyBP-C in small mammals could accelerate cross-bridge cycling kinetics, whereas increased Pro-Ala content in larger mammals could slow cycling rates. Species-specific changes in cMyBP-C could thereby fine-tune larger shifts in cross-bridge cycling kinetics that occur due to differences in isoform expression of other contractile proteins such as in myosin heavy chain that shifts from fast α -MHC (high ATPase activity and cross-bridge cycling) expressed in small mammals to slow β -MHC expressed in larger mammals [33–36]. Such systematic changes in cross-bridge cycling kinetics could also tune cardiac relaxation rates, for instance, to ensure adequate diastolic filling times even at high heart rates in small mammals.

In summary, results presented here demonstrate significant species-specific differences in the ability of the P/A rich region and C1 domains of mouse versus human cMyBP-C to activate actomyosin interactions. These differences suggest that the function of cMyBP-C varies in different species and raises the intriguing possibility that cMyBP-C fine-tunes cardiac contraction in different animals to better match contractile speed to hemodynamic load. Experiments to test these ideas are in progress.

Acknowledgments

The authors thank Elaine Hoye and David Dai for assistance in protein expression and purification, and Gordon Freeman

for helpful advice regarding use of the In-Fusion cloning system. They also thank Martha Mathiason and Mike Regnier for motion analysis software for filament motility assays. Support for this study was provided by NIH HL080367 to SPH and a NSF Graduate Research Fellowship to JFS.

References

- [1] J. E. Stelzer, J. R. Patel, J. W. Walker, and R. L. Moss, "Differential roles of cardiac myosin-binding protein C and cardiac troponin I in the myofibrillar force responses to protein kinase A phosphorylation," *Circulation Research*, vol. 101, no. 5, pp. 503–511, 2007.
- [2] C. W. Tong, J. E. Stelzer, M. L. Greaser, P. A. Powers, and R. L. Moss, "Acceleration of crossbridge kinetics by protein kinase A phosphorylation of cardiac myosin binding protein C modulates cardiac function," *Circulation Research*, vol. 103, no. 9, pp. 974–982, 2008.
- [3] J. F. Shaffer, R. W. Kensler, and S. P. Harris, "The myosin-binding protein C motif binds to F-actin in a phosphorylation-sensitive manner," *Journal of Biological Chemistry*, vol. 284, no. 18, pp. 12318–12327, 2009.
- [4] M. Gruen, H. Prinz, and M. Gautel, "cAPK-phosphorylation controls the interaction of the regulatory domain of cardiac myosin binding protein C with myosin-S2 in an on-off fashion," *FEBS Letters*, vol. 453, no. 3, pp. 254–259, 1999.
- [5] M. V. Razumova, J. F. Shaffer, A.-Y. Tu, G. V. Flint, M. Regnier, and S. P. Harris, "Effects of the N-terminal domains of myosin binding protein-C in an in vitro motility assay: evidence for long-lived cross-bridges," *Journal of Biological Chemistry*, vol. 281, no. 47, pp. 35846–35854, 2006.
- [6] M. V. Razumova, K. L. Bezold, A.-Y. Tu, M. Regnier, and S. P. Harris, "Contribution of the myosin binding protein C motif to functional effects in permeabilized rat trabeculae," *Journal of General Physiology*, vol. 132, no. 5, pp. 575–585, 2008.
- [7] T. J. Herron, E. Rostkova, G. Kunst, R. Chaturvedi, M. Gautel, and J. C. Kentish, "Activation of myocardial contraction by the N-terminal domains of myosin binding protein-C," *Circulation Research*, vol. 98, no. 10, pp. 1290–1298, 2006.
- [8] S. Bicer and P. J. Reiser, "Variations in apparent mass of mammalian fast-type myosin light chains correlate with species body size, from shrew to elephant," *American Journal of Physiology*, vol. 292, no. 1, pp. R527–R534, 2007.
- [9] E. Gasteiger, A. Gattiker, C. Hoogland, I. Ivanyi, R. D. Appel, and A. Bairoch, "ExpASY: the proteomics server for in-depth protein knowledge and analysis," *Nucleic Acids Research*, vol. 31, no. 13, pp. 3784–3788, 2003.
- [10] B. Zhu, G. Cai, E. O. Hall, and G. J. Freeman, "In-fusionTM assembly: seamless engineering of multidomain fusion proteins, modular vectors, and mutations," *BioTechniques*, vol. 43, no. 3, pp. 354–359, 2007.
- [11] M. Gautel, O. Zuffardi, P. Freiburg, and S. Labeit, "Phosphorylation switches specific for the cardiac isoform of myosin binding protein-C: a modulator of cardiac contraction?" *EMBO Journal*, vol. 14, no. 9, pp. 1952–1960, 1995.
- [12] E. Jain, A. Bairoch, S. Duvaud, et al., "Infrastructure for the life sciences: design and implementation of the UniProt website," *BMC Bioinformatics*, vol. 10, article 136, 2009.
- [13] S. S. Margossian and S. Lowey, "Preparation of myosin and its subfragments from rabbit skeletal muscle," *Methods in Enzymology*, vol. 85, part B, pp. 55–71, 1982.
- [14] J. D. Potter, "Preparation and properties of the components from troponin," *Methods in Enzymology*, vol. 85, part B, pp. 241–263, 1982.

- [15] J. D. Pardee and J. A. Spudich, "Purification of muscle actin," *Methods in Enzymology*, vol. 85, part B, pp. 164–181, 1982.
- [16] L. B. Smillie, "Preparation and identification of α - and β -tropomyosins," *Methods in Enzymology*, vol. 85, part B, pp. 234–241, 1982.
- [17] E. Homsher, B. Kim, A. Bobkova, and L. S. Tobacman, "Calcium regulation of thin filament movement in an in vitro motility assay," *Biophysical Journal*, vol. 70, no. 4, pp. 1881–1892, 1996.
- [18] D. A. Martyn, P. B. Chase, J. D. Hannon, L. L. Huntsman, M. J. Kushmerick, and A. M. Gordon, "Unloaded shortening of skinned muscle fibers from rabbit activated with and without Ca^{2+} ," *Biophysical Journal*, vol. 67, no. 5, pp. 1984–1993, 1994.
- [19] M. Regnier, A. J. Rivera, C.-K. Wang, M. A. Bates, P. B. Chase, and A. M. Gordon, "Thin filament near-neighbour regulatory unit interactions affect rabbit skeletal muscle steady-state force- Ca^{2+} relations," *Journal of Physiology*, vol. 540, pp. 485–497, 2002.
- [20] H. D. White, "Special instrumentation and techniques for kinetic studies of contractile systems," *Methods in Enzymology*, vol. 85, part B, pp. 698–708, 1982.
- [21] J. Flavigny, M. Souchet, P. Sébillon, et al., "COOH-terminal truncated cardiac myosin-binding protein C mutants resulting from familial hypertrophic cardiomyopathy mutations exhibit altered expression and/or incorporation in fetal rat cardiomyocytes," *Journal of Molecular Biology*, vol. 294, no. 2, pp. 443–456, 1999.
- [22] A. Ababou, E. Rostkova, S. Mistry, C. L. Masurier, M. Gautel, and M. Pfuhl, "Myosin binding protein C positioned to play a key role in regulation of muscle contraction: structure and interactions of domain C1," *Journal of Molecular Biology*, vol. 384, no. 3, pp. 615–630, 2008.
- [23] M. Gruen and M. Gautel, "Mutations in β -myosin S2 that cause familial hypertrophic cardiomyopathy (FHC) abolish the interaction with the regulatory domain of myosin-binding protein-C," *Journal of Molecular Biology*, vol. 286, no. 3, pp. 933–949, 1999.
- [24] J. M. Squire, P. K. Luther, and C. Knupp, "Structural evidence for the interaction of C-protein (MyBP-C) with actin and sequence identification of a possible actin-binding domain," *Journal of Molecular Biology*, vol. 331, no. 3, pp. 713–724, 2003.
- [25] I. Kulikovskaya, G. McClellan, J. Flavigny, L. Carrier, and S. Winegrad, "Effect of MyBP-C binding to actin on contractility in heart muscle," *Journal of General Physiology*, vol. 122, no. 6, pp. 761–774, 2003.
- [26] M. C. Schaub, et al., "Modulation of contractility in human cardiac hypertrophy by myosin essential light chain isoforms," *Cardiovascular Research*, vol. 37, no. 2, pp. 381–404, 1998.
- [27] O. A. Andreev, L. D. Saraswat, S. Lowey, C. Slaughter, and J. Borejdo, "Interaction of the N-terminus of chicken skeletal essential light chain 1 with F-actin," *Biochemistry*, vol. 38, no. 8, pp. 2480–2485, 1999.
- [28] I. P. Trayer, H. R. Trayer, and B. A. Levine, "Evidence that the N-terminal region of A1-light chain of myosin interacts directly with the C-terminal region of actin. A proton magnetic resonance study," *European Journal of Biochemistry*, vol. 164, no. 1, pp. 259–266, 1987.
- [29] D. J. Timson and I. P. Trayer, "The role of the proline-rich region in A1-type myosin essential light chains: implications for information transmission in the actomyosin complex," *FEBS Letters*, vol. 400, no. 1, pp. 31–36, 1997.
- [30] H. L. Sweeney, C. Reggiani, S. Lowey, et al., "Function of the N terminus of the myosin essential light chain of vertebrate striated muscle," *Biophysical Journal*, vol. 68, no. 4, supplement, pp. 112S–119S, 1995.
- [31] F. S. Korte, K. S. McDonald, S. P. Harris, and R. L. Moss, "Loaded shortening, power output, and rate of force redevelopment are increased with knockout of cardiac myosin binding protein-C," *Circulation Research*, vol. 93, no. 8, pp. 752–758, 2003.
- [32] J. F. Shaffer and S. P. Harris, "Species-specific differences in the Pro-Ala rich region of cardiac myosin binding protein-C," *Journal of Muscle Research and Cell Motility*, vol. 30, no. 7-8, pp. 303–306, 2009.
- [33] N. Hamilton and C. D. Ianuzzo, "Contractile and calcium regulating capacities of myocardia of different sized mammals scale with resting heart rate," *Molecular and Cellular Biochemistry*, vol. 106, no. 2, pp. 133–141, 1991.
- [34] B. Pope, J. F. Hoh, and A. Weeds, "The ATPase activities of rat cardiac myosin isoenzymes," *FEBS Letters*, vol. 118, no. 2, pp. 205–208, 1980.
- [35] I. Morano, H. Arndt, C. Gartner, and J. C. Ruegg, "Skinned fibers of human atrium and ventricle: myosin isoenzymes and contractility," *Circulation Research*, vol. 62, no. 3, pp. 632–639, 1988.
- [36] K. Schwartz, Y. Lecarpentier, and J. L. Martin, "Myosin isoenzymic distribution correlates with speed of myocardial contraction," *Journal of Molecular and Cellular Cardiology*, vol. 13, no. 12, pp. 1071–1075, 1981.

Review Article

New Insights into the Structural Roles of Nebulin in Skeletal Muscle

Coen A. C. Ottenheijm^{1,2} and Henk Granzier²

¹Laboratory for Physiology, Institute for Cardiovascular Research, VU University Medical Center, 1081 BT Amsterdam, The Netherlands

²Department of Physiology, University of Arizona, P.O. Box 245217, Tucson, AZ 85724, USA

Correspondence should be addressed to Henk Granzier, granzier@email.arizona.edu

Received 11 January 2010; Accepted 26 March 2010

Academic Editor: Guy M. Benian

Copyright © 2010 C. A. C. Ottenheijm and H. Granzier. This is an open access article distributed under the Creative Commons Attribution License, which permits unrestricted use, distribution, and reproduction in any medium, provided the original work is properly cited.

One important feature of muscle structure and function that has remained relatively obscure is the mechanism that regulates thin filament length. Filament length is an important aspect of muscle function as force production is proportional to the amount of overlap between thick and thin filaments. Recent advances, due in part to the generation of nebulin KO models, reveal that nebulin plays an important role in the regulation of thin filament length. Another structural feature of skeletal muscle that is not well understood is the mechanism involved in maintaining the regular lateral alignment of adjacent sarcomeres, that is, myofibrillar connectivity. Recent studies indicate that nebulin is part of a protein complex that mechanically links adjacent myofibrils. Thus, novel structural roles of nebulin in skeletal muscle involve the regulation of thin filament length and maintaining myofibrillar connectivity. When these functions of nebulin are absent, muscle weakness ensues, as is the case in patients with nemaline myopathy with mutations in nebulin. Here we review these new insights in the role of nebulin in skeletal muscle structure.

1. Nebulin Specifies Thin Filament Length

Skeletal muscles are organized into regular arrays of thin and thick filaments of well-defined length. Filament length is an important aspect of muscle function because a muscle generates force in proportion to thin and thick filament overlap. Whereas thick filament length is considered a constant 1.6 μm , thin filament lengths are fine-tuned at ~ 1.0 – $1.3 \mu\text{m}$, depending on species and muscle type [1] to overlap with thick filaments and to meet the muscle's physiological demands [1, 2]. Changes in thin filament length affect thin-thick filament overlap and impact a muscle's force-generating capacity at a given sarcomere length: thus, thin filament length is a key aspect of muscle function. Since length is not an intrinsic property of actin-filaments (actin monomers assemble in vitro to highly variable polymer lengths [3]), thin filament length is likely to be specified in vivo by an actin binding protein; for this, nebulin has been considered for a long time a prime candidate [4–6], but critical evidence has been lacking up until recently.

Nebulin is a giant protein (Mw 700–800 kDa) expressed in skeletal muscle, and makes up 2%–3% of the myofibrillar protein mass. Immuno-electronmicroscopy revealed that a single nebulin molecule spans the thin filament with its C-terminus anchored at the Z-disk and its N-terminal region directed towards the thin filament pointed end (for a schematic representation, see Figure 1(a)) [4]. The first evidence for nebulin's proposed role in specifying thin filament length came from the analysis of nebulin's cDNA sequence. This revealed that the bulk of the molecule is comprised of modules with the centrally located modules M9 to M162, each thought to represent individual actin-binding motifs and organized into seven-module superrepeats that match the repeat of the actin filament (Figure 1(b)). This precise arrangement is thought to allow each nebulin module to interact with a single monomer of the actin filament [5, 6], and each nebulin super-repeat to associate with a single tropomyosin (Tm)/troponin (Tn) complex [7–9]. Nebulin's extreme N-terminal modules M1–M3 (Figure 1(b)) contain a high-affinity binding site for the thin filament pointed-end capping protein tropomodulin [10]. Tropomodulin, in

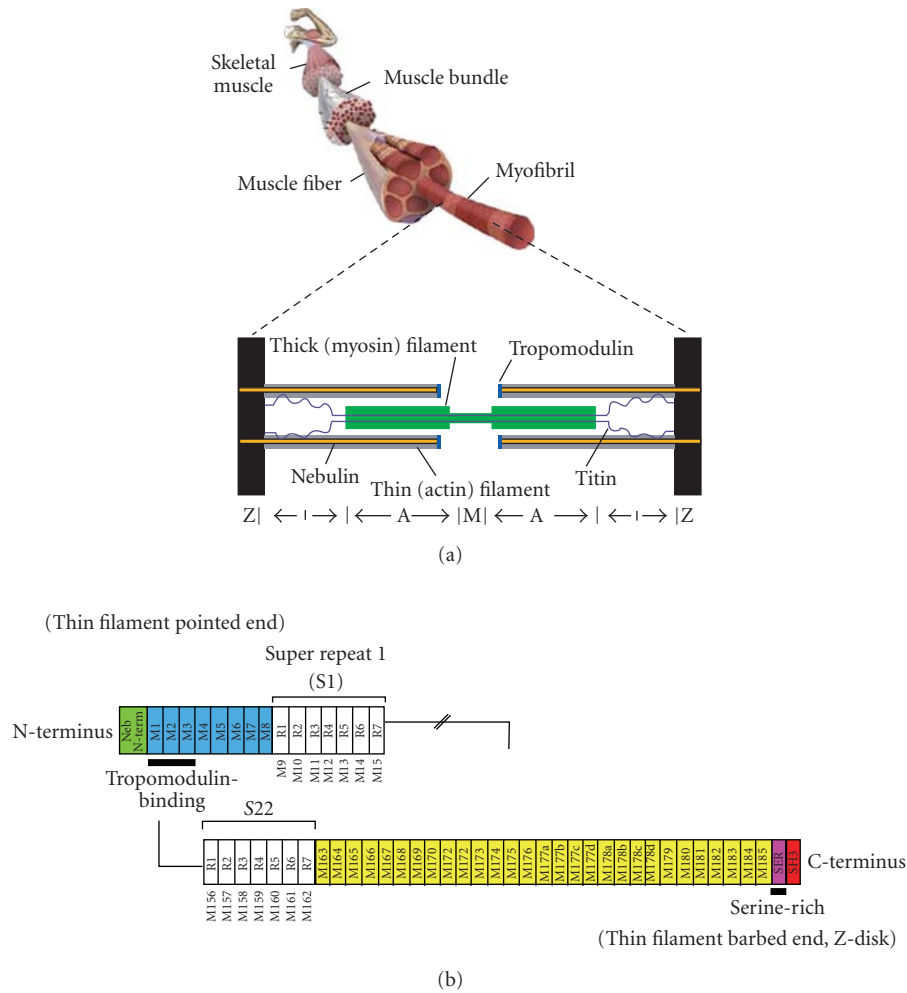


FIGURE 1: (a) Schematic of the structural organization of skeletal muscle (top) and sarcomere (bottom). (b) Schematic of the human nebulin sequence. Nebulin has a highly modular structure, with, in the central region, (M9–M162) seven modular repeats arranged into twenty-two superrepeats (only two of which are shown).

addition to binding nebulin's N-terminus, binds actin and tropomyosin with high affinity and prevents actin filaments from elongating or shortening at the pointed end [11]. Furthermore, earlier studies revealed that the electrophoretic mobility of nebulin from different muscle types correlates with thin filament length [5, 12].

Although the findings discussed above were consistent with the hypothesis that nebulin is involved in specifying thin filament length, direct evidence was lacking. More conclusive evidence for a role for nebulin in specifying thin filament length required studies of muscle that lack nebulin. Such studies were first performed by McElhinny and coworkers [13]. It was found that upon RNAi knockdown of nebulin transcripts in cultured cardiac myocytes, thin filaments elongated to unrestricted lengths, thus supporting a role for nebulin in regulating thin filament length. These experiments were carried out in cardiac myocytes where nebulin expression is less than 1% of the levels found in skeletal muscle [14]. Thus, to test the role of nebulin in skeletal muscle *in vivo*, nebulin KO mouse models were

generated [14, 15]. The first work on these models revealed that in nebulin-deficient skeletal muscle the thin filaments are on average shorter, thus supporting a role for nebulin in the *in vivo* regulation of thin filament length [14, 15]. Witt et al. [14] performed an immunoelectronmicroscopy study and reported that thin filament lengths in wildtype tibialis cranialis muscle are a constant $1.2 \mu\text{m}$, but in nebulin-deficient muscle are on average $\sim 0.8 \mu\text{m}$, and range from ~ 0.4 to $1.2 \mu\text{m}$ (for a schematic, see Figure 2(a)). That such reduction in thin filament length greatly affects force production was illustrated by Ottenheim et al. [16] by measuring force as a function of sarcomere length for both wildtype and nebulin-deficient muscle. In these experiments, skinned muscle fibers were activated by supramaximal levels of exogenous calcium at various sarcomere lengths and the force response was measured (note that in skinned fiber preparations, factors outside of the myofilaments, e.g., calcium handling by the sarcoplasmic reticulum, do not contribute to force production). As shown in Figure 2(b), the force-sarcomere length relation of wildtype muscle is

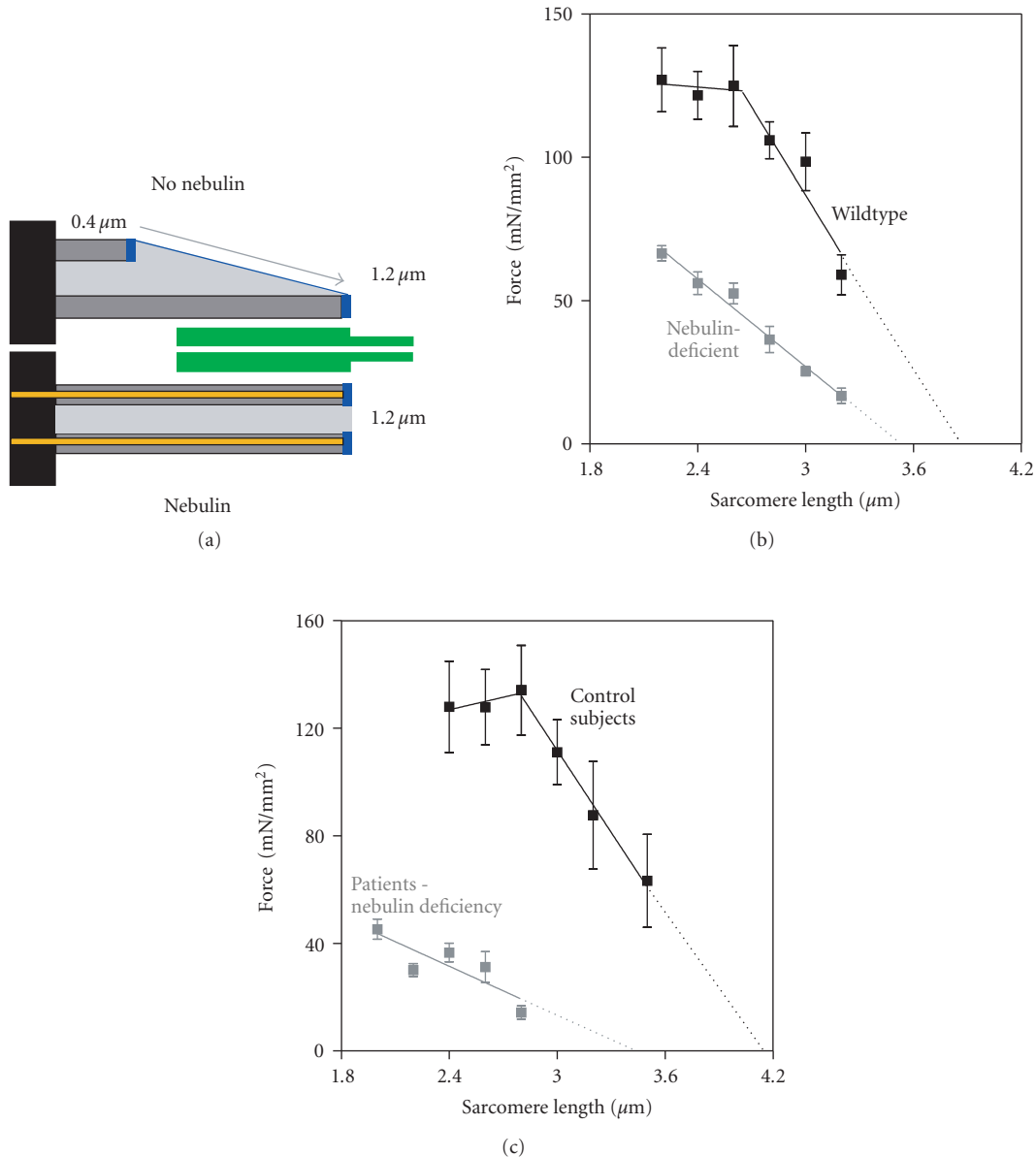


FIGURE 2: (a) Schematic illustrating the range of thin filament lengths found in nebulin-deficient muscle fibers. Immunoelectron microscopy [14] showed that thin filament lengths in wildtype tibialis cranialis muscle are a constant $1.2 \mu\text{m}$, but in nebulin-deficient muscle are on average $\sim 0.8 \mu\text{m}$ and range from ~ 0.4 to $1.2 \mu\text{m}$. (b) The force-sarcomere length relation of murine wt muscle fibers has a characteristic force plateau followed by a descending limb. The force-sarcomere length relation of nebulin-deficient fibers is shifted leftward compared to wt fibers, and the force plateau is absent. (c) Similarly, the force-sarcomere length relation of nebulin-deficient human muscle fibers (dissected from biopsies obtained from patients with nemaline myopathy) is shifted to the left, and the force plateau is absent as well [16].

characterized by a force plateau reflecting optimal thick-thin filament overlap, followed by a descending limb at higher sarcomere lengths reflecting the decreased filament overlap. That the descending limb in wildtype muscle starts at a sarcomere length of $\sim 2.6 \mu\text{m}$ and ends at $\sim 4.0 \mu\text{m}$ suggests a thin filament length of $\sim 1.2 \mu\text{m}$, which is in line with the previously mentioned electron-microscopy data. In nebulin-deficient muscle, the shortened thin filaments reduce thin-thick filament overlap at a given sarcomere length, impairing force production and resulting in a leftward shift of the

force-sarcomere length relation (see Figure 2(b)). Furthermore, when thin filaments are nonuniform in length, no optimal thick-thin filament overlap exists, and consistent with this the force-sarcomere length relation of nebulin-deficient muscle lacks the characteristic plateau. Supporting these findings on demembrated muscle, studies on *intact* nebulin-deficient muscle from another nebulin knockout model [17], in which muscles were activated at various lengths by electrical field stimulation, also revealed a leftward shift of the force-muscle length relation of nebulin-deficient

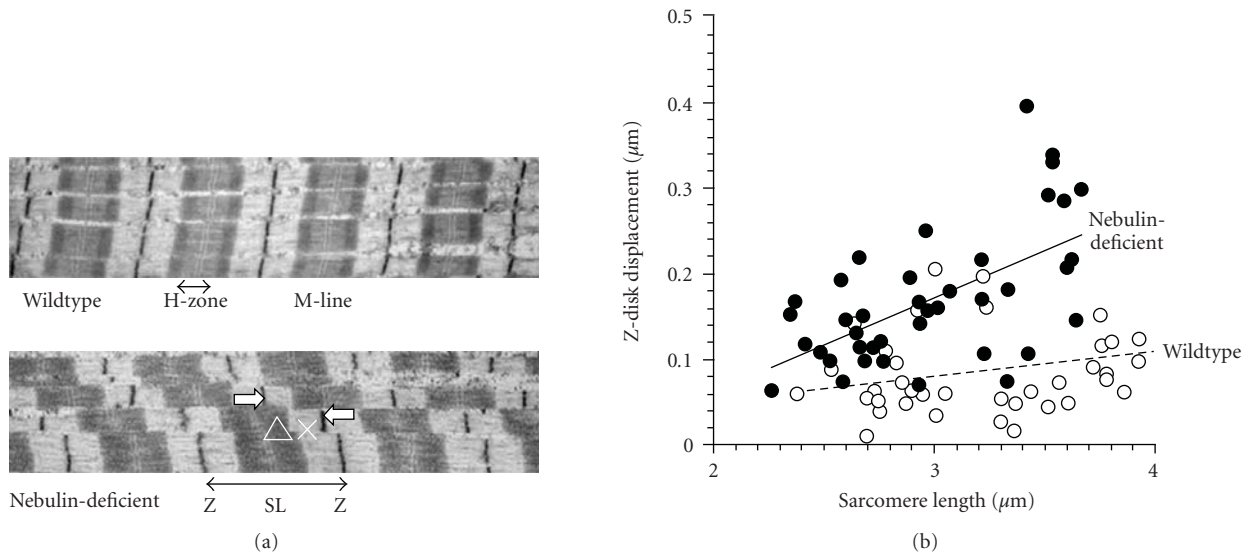


FIGURE 3: (a) Wildtype fibers have a regular structure with well-aligned sarcomeres. In nebulin-deficient fibers sarcomeres are misaligned and the Z-disk are out of register. Arrows indicate how Z-disk displacement (ΔX) was defined. (b) Z-disk displacement is significantly increased in nebulin-deficient fibers. (modified from Tonino et al. [27]).

muscle. Thus, the force-length relation of nebulin-deficient muscle is altered in a manner that is consistent with the presence of shorter thin filament lengths.

Work by Bang et al. [15] on their nebulin KO model, using confocal microscopy on 1-day-old mice, indicated that in the absence of nebulin thin filament lengths are reduced from $\sim 1.15\text{--}1.3\ \mu\text{m}$ (depending on muscle type) in wildtype muscle to a consistent $\sim 1.0\ \mu\text{m}$ in all muscles types. These findings led to the proposal [1] that a nebulin-independent mechanism specifies uniform thin filament lengths of $\sim 1.0\ \mu\text{m}$ in all muscle types whereas nebulin is responsible for specifying longer thin filament lengths in a muscle-specific manner. An opposite conclusion was drawn by Castillo et al. [18] who used immunofluorescence microscopy on rabbit muscle and concluded that nebulin specifies the minimum thin filament length ($\sim 1.0\ \mu\text{m}$) with a nebulin-independent mechanism regulating the final length according to the requirements of a particular muscle. It is unclear as to what causes this apparent discrepancy between these studies. Detecting differences in thin filament length, especially length gradients, with high precision is challenging and might be hard to accomplish with confocal microscopy, as was done in the two aforementioned studies. In contrast, Witt et al. [14] used electronmicroscopy and decorated thin filaments with gold beads (attached to actin monomers with the actin-binding peptide phalloidin). This made it possible to determine thin filament length gradients and showed that thin filaments varied in length and were on average shorter than in wildtype muscle. Thus, this study does not support the conclusion by Bang et al. [15] that there is a nebulin-independent mechanism that sets a constant thin filament length of $1.0\ \mu\text{m}$, but is consistent with the conclusion of Castillo et al. that there is a nebulin-dependent mechanism that sets a minimum thin filament length. To resolve these discrepancies additional studies on a range of mouse muscle

types are needed that measure by electronmicroscopy thin filament length and the location of nebulin's N-terminus. It is clear, however, from the above referenced studies that nebulin plays a critical role in regulating thin filament length: in its absence the average thin filament length is shorter and force is greatly reduced.

Nebulin's role in thin filament length regulation provides a mechanism for the first time to explain severe muscle weakness in patients with nemaline myopathy, a debilitating disease frequently caused by nebulin gene mutations and reduced nebulin protein levels [19, 20]. Indeed, muscle fibers from patients suffering from nebulin-based nemaline myopathy show remarkable phenotypic similarities to fibers from nebulin KO mice, that is, shorter and non-uniform thin filament lengths and significantly impaired force-generating capacity [16] (see Figure 2(c)). Thus, loss of thin filament length regulation appears to play a prominent role in the pathogenesis of muscle weakness in patients with nemaline myopathy.

2. Nebulin Maintains Intermyoibrillar Connectivity

Longitudinally, sarcomeres are connected by Z-disk lattices that anchor thin filaments and transmit force along the myofibril. In the transverse direction, linkage of myofibrils at the Z-disks allows for lateral force transmission and limits the degree to which adjacent myofibrils translocate relative to each other during active contraction or passive stretch, thereby preventing damage to intermyofibrillar membrane systems, such as T-tubules and the sarcoplasmic reticulum. An important protein involved in linking adjacent Z-disks is the intermediate filament protein desmin, which forms a network of filaments that surrounds myofibrils at the level of the Z-disk [21, 22]. The subunit proteins of desmin filaments

are elongated coiled-coils with extensive intermolecular ionic and hydrophobic interactions between individual subunits, giving rise to filaments with high tensile strength as well as plasticity [23]. That desmin tethers adjacent Z-disks is supported by work on a desmin KO mouse in which Z-disk misalignment was shown to occur in stretched muscle [24]. In vitro work, using a yeast two-hybrid approach, suggested that desmin binds to the C-terminal region of nebulin [25], which is anchored in the Z-disk, and recently it was shown that nebulin modules M160–164 are involved in this interaction [26]. These findings lead Bang et al. to speculate that this desmin-nebulin interaction links myofibrillar Z-disks to the intermediate filament system, thereby forming a lateral linkage system which maintains adjacent Z-disks in register. This role for nebulin in intermyofibrillar connectivity was tested recently by studies using a nebulin KO mouse model [27]. In these studies it was found that upon stretch, myofibrils devoid of nebulin translocate to a much higher degree than WT muscle, resulting in much larger Z-disk displacement (Figure 3). Although desmin is present in muscle devoid of nebulin, it is reduced in the intermyofibrillar spaces that surround the Z-disks, suggesting that nebulin is required for proper localization of desmin at the Z-disk. Consistent with this, both knockdown of nebulin with siRNA and overexpression of M160–M170 did not interfere with the formation of normal striation patterns but did prevent desmin localization at the mature Z-disk. Thus, nebulin is required to laterally link myofibrils at the Z-disk by desmin filaments; in the absence of nebulin myofibrillar connectivity is significantly reduced leading to Z-disk displacement.

In addition to linking adjacent myofibrils, evidence also suggests that nebulin's C-terminus regulates Z-disk width. Z-disks of different muscles can vary greatly in width, from less than 100 nm in fast skeletal muscle to more than 150 nm in slow skeletal muscle [27]. The importance of regulation of Z-disk width is illustrated by muscle from patients with nemaline myopathy, which displays greatly widened z-disks, including the characteristic nemaline rods [28]. Previously, titin has been suggested to play a role in Z-disk assembly [29]. The Z-disk region of titin contains a family of differentially expressed repeats, the titin Z-repeats [29]. These Z-repeats are a family of α -actinin-binding motifs, which are differentially expressed in a tissue- and developmental-stage-specific fashion [29]. As previously pointed out, it is unlikely that the differential expression of the titin Z-repeats alone can determine the Z-disk width, because too few isoforms exist to account for the wide range of different Z-disk widths [30]. Electronmicroscopy on nebulin KO fibers revealed that nebulin-deficient muscle contains electron-dense Z-disk-like bodies that are similar to the nemaline rod bodies that are a hallmark of nemaline myopathy in humans [14, 15, 27]. Furthermore, in nebulin-deficient myofibrils the average Z-disk width is increased by 40–80 nm depending on muscle type. These findings support a model in which titin, and nebulin together specify Z-disk width, with titin constructing the central region of the Z-disk, including the number and positions of α -actinin cross-links and nebulin determining the ending of the Z-disk structure and its transition to the I-band, that is, nebulin functions as a Z-disk terminator. The

mechanism by which nebulin terminates the Z-disk might involve interaction between nebulin and Z-disk-localized proteins, such as CapZ. CapZ is a barbed-end actin-capping protein that binds near the C-terminus of nebulin [31]. In muscle fibers devoid of nebulin [14, 31] CapZ does not localize properly, allowing the barbed ends of thin filaments to continue to grow beyond the Z-disk resulting in widened Z-disks. Thus, in addition to laterally linking myofibrils at the Z-disk, nebulin regulates Z-disk width. When this feature of nebulin is not present, Z-disks widen, ultimately culminating in the formation of nemaline rods.

In summary, recent studies provide evidence that nebulin's structural roles within the muscle's sarcomere involve (1) specifying thin filament length to optimize thin-thick filament overlap and force production, (2) maintaining intermyofibrillar connectivity, and (3) setting physiological Z-disk widths. These findings provide important novel insights into the role of nebulin in skeletal muscle structure and function and provide new avenues for understanding and combating the severe muscle weakness in nemaline myopathy, a debilitating disease which is frequently caused by nebulin deficiency.

Acknowledgments

This work was supported by National Institutes of Health, AR-053897 (HG), and by a VENI grant from the Dutch Organization for Scientific Research (CO).

References

- [1] R. S. Littlefield and V. M. Fowler, "Thin filament length regulation in striated muscle sarcomeres: pointed-end dynamics go beyond a nebulin ruler," *Seminars in Cell and Developmental Biology*, vol. 19, no. 6, pp. 511–519, 2008.
- [2] T. J. Burkholder, B. Figado, S. Baron, and R. L. Lieber, "Relationship between muscle fiber types and sizes and muscle architectural properties in the mouse hindlimb," *Journal of Morphology*, vol. 221, no. 2, pp. 177–190, 1994.
- [3] T. D. Pollard and G. G. Borisy, "Cellular motility driven by assembly and disassembly of actin filaments," *Cell*, vol. 112, no. 4, pp. 453–465, 2003.
- [4] K. Wang and J. Wright, "Architecture of the sarcomere matrix of skeletal muscle: immunoelectron microscopic evidence that suggests a set of parallel inextensible nebulin filaments anchored at the Z line," *Journal of Cell Biology*, vol. 107, no. 6, pp. 2199–2212, 1988.
- [5] S. Labeit, T. Gibson, A. Lakey, et al., "Evidence that nebulin is a protein-ruler in muscle thin filaments," *FEBS Letters*, vol. 282, no. 2, pp. 313–316, 1991.
- [6] S. Labeit and B. Kolmerer, "The complete primary structure of human nebulin and its correlation to muscle structure," *Journal of Molecular Biology*, vol. 248, no. 2, pp. 308–315, 1995.
- [7] A. S. McElhinny, S. T. Kazmierski, S. Labeit, and C. C. Gregorio, "Nebulin: the nebulous, multifunctional giant of striated muscle," *Trends in Cardiovascular Medicine*, vol. 13, no. 5, pp. 195–201, 2003.
- [8] O. Ogut, M. M. Hossain, and J.-P. Jin, "Interactions between nebulin-like motifs and thin filament regulatory proteins," *Journal of Biological Chemistry*, vol. 278, no. 5, pp. 3089–3097, 2003.

- [9] J.-P. Jin and K. Wang, "Cloning, expression, and protein interaction of human nebulin fragments composed of varying numbers of sequence modules," *Journal of Biological Chemistry*, vol. 266, no. 31, pp. 21215–21223, 1991.
- [10] A. S. McElhinny, B. Kolmerer, V. M. Fowler, S. Labeit, and C. C. Gregorio, "The N-terminal end of nebulin interacts with tropomodulin at the pointed ends of the thin filaments," *Journal of Biological Chemistry*, vol. 276, no. 1, pp. 583–592, 2001.
- [11] C. G. dos Remedios, D. Chhabra, M. Kekic, et al., "Actin binding proteins: regulation of cytoskeletal microfilaments," *Physiological Reviews*, vol. 83, no. 2, pp. 433–473, 2003.
- [12] M. Kruger, J. Wright, and K. Wang, "Nebulin as a length regulator of thin filaments of vertebrate skeletal muscles: correlation of thin filament length, nebulin size, and epitope profile," *Journal of Cell Biology*, vol. 115, no. 1, pp. 97–107, 1991.
- [13] A. S. McElhinny, C. Schwach, M. Valichnac, S. Mount-Patrick, and C. C. Gregorio, "Nebulin regulates the assembly and lengths of the thin filaments in striated muscle," *Journal of Cell Biology*, vol. 170, no. 6, pp. 947–957, 2005.
- [14] C. C. Witt, C. Burkart, D. Labeit, et al., "Nebulin regulates thin filament length, contractility, and Z-disk structure in vivo," *EMBO Journal*, vol. 25, no. 16, pp. 3843–3855, 2006.
- [15] M.-L. Bang, X. Li, R. Littlefield, et al., "Nebulin-deficient mice exhibit shorter thin filament lengths and reduced contractile function in skeletal muscle," *Journal of Cell Biology*, vol. 173, no. 6, pp. 905–916, 2006.
- [16] C. A. C. Ottenheijm, C. C. Witt, G. J. Stienen, S. Labeit, A. H. Beggs, and H. Granzier, "Thin filament length dysregulation contributes to muscle weakness in nemaline myopathy patients with nebulin deficiency," *Human Molecular Genetics*, vol. 18, no. 13, pp. 2359–2369, 2009.
- [17] D. S. Gokhin, M.-L. Bang, J. Zhang, J. Chen, and R. L. Lieber, "Reduced thin filament length in nebulin-knockout skeletal muscle alters isometric contractile properties," *American Journal of Physiology*, vol. 296, no. 5, pp. C1123–C1132, 2009.
- [18] A. Castillo, R. Nowak, K. P. Littlefield, V. M. Fowler, and R. S. Littlefield, "A nebulin ruler does not dictate thin filament lengths," *Biophysical Journal*, vol. 96, no. 5, pp. 1856–1865, 2009.
- [19] K. Pelin, P. Hilpelä, K. Donner, et al., "Mutations in the nebulin gene associated with autosomal recessive nemaline myopathy," *Proceedings of the National Academy of Sciences of the United States of America*, vol. 96, no. 5, pp. 2305–2310, 1999.
- [20] K. Pelin, K. Donner, M. Holmberg, H. Jungbluth, F. Muntoni, and C. Wallgren-Pettersson, "Nebulin mutations in autosomal recessive nemaline myopathy: an update," *Neuromuscular Disorders*, vol. 12, no. 7-8, pp. 680–686, 2002.
- [21] Y. Capetanaki, R. J. Bloch, A. Kouloumenta, M. Mavroidis, and S. Psarras, "Muscle intermediate filaments and their links to membranes and membranous organelles," *Experimental Cell Research*, vol. 313, no. 10, pp. 2063–2076, 2007.
- [22] K. Wang and R. Ramirez Mitchell, "A network of transverse and longitudinal intermediate filaments is associated with sarcomeres of adult vertebrate skeletal muscle," *Journal of Cell Biology*, vol. 96, no. 2, pp. 562–570, 1983.
- [23] M. L. Costa, R. Escalera, A. Cataldo, F. Oliveira, and C. S. Mermelstein, "Desmin: molecular interactions and putative functions of the muscle intermediate filament protein," *Brazilian Journal of Medical and Biological Research*, vol. 37, no. 12, pp. 1819–1830, 2004.
- [24] S. B. Shah, F.-C. Su, K. Jordan, et al., "Evidence for increased myofibrillar mobility in desmin-null mouse skeletal muscle," *Journal of Experimental Biology*, vol. 205, no. 3, pp. 321–325, 2002.
- [25] M.-L. Bang, C. Gregorio, and S. Labeit, "Molecular dissection of the interaction of desmin with the C-terminal region of nebulin," *Journal of Structural Biology*, vol. 137, no. 1-2, pp. 119–127, 2002.
- [26] G. M. Conover, S. N. Henderson, and C. C. Gregorio, "A myopathy-linked desmin mutation perturbs striated muscle actin filament architecture," *Molecular Biology of the Cell*, vol. 20, no. 3, pp. 834–845, 2009.
- [27] P. Tonino, C. T. Pappas, B. D. Hudson, S. Labeit, C. C. Gregorio, and H. Granzier, "Reduced myofibrillar connectivity and increased Z-disk width in nebulin-deficient skeletal muscle," *Journal of Cell Science*, vol. 123, no. 3, pp. 384–391, 2010.
- [28] C. Wallgren-Pettersson, K. Pelin, K. J. Nowak, et al., "Genotype-phenotype correlations in nemaline myopathy caused by mutations in the genes for nebulin and skeletal muscle alpha-actin," *Neuromuscular Disorders*, vol. 14, no. 8-9, pp. 461–470, 2004.
- [29] M. Gautel, D. Goulding, B. Bullard, K. Weber, and D. O. Furst, "The central Z-disk region of titin is assembled from a novel repeat in variable copy numbers," *Journal of Cell Science*, vol. 109, part 11, pp. 2747–2754, 1996.
- [30] S. Millevoi, K. Trombitas, B. Kolmerer, et al., "Characterization of nebulin and nebulin and emerging concepts of their roles for vertebrate Z-discs," *Journal of Molecular Biology*, vol. 282, no. 1, pp. 111–123, 1998.
- [31] C. T. Pappas, N. Bhattacharya, J. A. Cooper, and C. C. Gregorio, "Nebulin interacts with CapZ and regulates thin filament architecture within the Z-disc," *Molecular Biology of the Cell*, vol. 19, no. 5, pp. 1837–1847, 2008.

Research Article

Isolation of Nebulin from Rabbit Skeletal Muscle and Its Interaction with Actin

Ryo Chitose, Atsushi Watanabe, Masato Asano, Akira Hanashima, Kouhei Sasano, Yulong Bao, Koscak Maruyama, and Sumiko Kimura

Department of Biology, Graduate School of Science, Chiba University, Chiba 263-8522, Japan

Correspondence should be addressed to Sumiko Kimura, sumiko@faculty.chiba-u.jp

Received 1 December 2009; Accepted 15 February 2010

Academic Editor: Henk L. M. Granzier

Copyright © 2010 Ryo Chitose et al. This is an open access article distributed under the Creative Commons Attribution License, which permits unrestricted use, distribution, and reproduction in any medium, provided the original work is properly cited.

Nebulin is about 800 kDa filamentous protein that binds the entire thin filament of vertebrate skeletal muscle sarcomeres. Nebulin cannot be isolated from muscle except in a completely denatured form by direct solubilization of myofibrils with SDS because nebulin is hardly soluble under salt conditions. In the present study, nebulin was solubilized by a salt solution containing 1 M urea and purified by DEAE-Toyopearl column chromatography via 4 M urea elution. Rotary-shadowed images of nebulin showed entangled knit-like particles, about 20 nm in diameter. The purified nebulin bound to actin filaments to form loose bundles. Nebulin was confirmed to bind actin, α -actinin, β -actinin, and tropomodulin, but not troponin or tropomyosin. The data shows that full-length nebulin can be also obtained in a functional and presumably native form, verified by data from experiments using recombinant subfragments.

1. Introduction

Single molecules of nebulin (the precise molecular weight expressed in a certain tissue depends on the respective splice isoform; for a 773 kDa species, see [1]) associate along the entire length of the thin filament of vertebrate skeletal muscle. Therefore, nebulin is thought to be a molecular ruler for determining length of $\sim 1 \mu\text{m}$ [2–4]. To ascertain such potential of nebulin, its effect on the length of actin filaments should be examined *in vitro*. However, nebulin has not been successfully isolated from skeletal muscle due to difficulties in solubilization under salt conditions, although isolation of a completely denatured nebulin has been achieved by gel filtration of SDS-solubilized myofibrils [5].

Complete sequencing of human nebulin by Labeit and Kolmerer showed that a large portion (97%) of nebulin comprises 185 repeats of approximately 35 amino acids with a central consensus sequence of SDXXYK [1].

In the sarcomere, the N-terminal region of nebulin localizes at the pointed end of the thin filaments, central region along the thin filaments, and C-terminal region in the Z-line [2]. Each nebulin repeat (SDXXYK) can bind to

actin [6–8], while nebulin repeats 1–3 bind to tropomodulin [9], 163–170 bind to desmin [10], 185–SH3 domain bind to connectin (also called titin) [11], and the SH3 domain binds to myopalladin [12] and β -actinin (also called CapZ) [11].

In 2009, Yadavalli et al. reported that they extracted full-length nebulin from rabbit longissimus dorsi muscle using 0.45% sodium deoxycholate (DOC), and then purified it with an NaCl gradient in the presence of 0.45% DOC. However, the detailed preparation method has not been published yet [13].

In the present study, we describe the purification of nebulin from rabbit skeletal muscle. For solubilization, 1 M urea was required, and during purification, 4 M urea were employed. Using these conditions, a purification procedure for nebulin was developed. The purified nebulin was confirmed to bind actin filaments and to form loose bundles, and therefore was able to adopt a folded state.

2. Materials and Methods

2.1. Protein Preparations. Actin was prepared from an acetone powder of rabbit skeletal muscle by the method of

Spudich and Watt [14] and further purified by gel filtration through a Sephadex G-150 column equilibrated with 0.2 mM ATP, 0.1 mM CaCl_2 , 0.01% NaN_3 , and 2 mM Tris/HCl, pH 8.0. β -Actinin was purified from rabbit skeletal muscle as reported by Maruyama et al. [15], and α -actinin was prepared from rabbit skeletal muscle by the method of Goll et al. [16]. Tropomodulin was isolated from rabbit skeletal muscle as described previously [17]. Tropomyosin was extracted from actin-extracted acetone powder of rabbit skeletal muscle and purified according to Woods [18], and troponin was prepared from rabbit skeletal muscle using the method described by Ebashi et al. [19]. The purity of the binding partners (actin, tropomyosin, troponin, tropomodulin, and β -actinin) was described in Figure 1 of the tropomodulin paper in 1999 [17], and the purity of α -actinin was described at lane 2 in Figure 6 of the amphioxus nebulin paper in 2009 [20].

2.2. SDS-Polyacrylamide Gel Electrophoresis (PAGE) and Immunoblotting. Isolated protein samples were resolved by SDS-PAGE using 2–15% gradient polyacrylamide gels, and then transferred to nitrocellulose membranes. Membranes were treated with primary antibodies followed by secondary horseradish-labeled antibodies (Dako). Polyclonal antibodies to nebulin (PcNeb) [21], actin (A2066, Sigma-Aldrich), and connectin (Pc1200) [22] and the monoclonal antibody to connectin (Mc3B9) [23] were used.

2.3. Electron Microscopy. Negative staining was examined using 2% uranylacetate with the JEOL JEM-100S electron microscope.

2.3.1. Rotary-Shadowed Electron Microscopy. A purified nebulin solution in 50% glycerol was dropped onto a mica plate. In the case of centrifuging, the mica-taped rotor was centrifuged for 25 s at $12,000 \times g$ as previously reported [24–26]. The sample was rotary-shadowed at 7.5° with platinum-carbon, followed by carbon on the uncooled specimen stage of a JEOL JFD-9000 freeze fracture apparatus. The resulting specimen was observed under a JEOL 100S electron microscope.

2.4. Binding Tests by Cosedimentation. Nebulin from modified purification was dialyzed against 0.18 M KPO_4 (pH 7.0), 0.1 mM MgCl_2 , 0.1 mM EGTA, and 0.5 M urea overnight and then centrifuged for 30 minutes at $56,000 \times g$. The supernatant of nebulin was mixed with G-actin in 0.11 M KPO_4 , 0.27 mM ATP, 0.1 mM MgCl_2 , and 0.31 M urea, pH 7.0 at 4°C for 20 hours. The mixture was centrifuged ($6,000 \times g$, 4°C , 30 min), and the supernatant and pellet were diluted with SDS sample buffer and subjected to SDS-PAGE.

2.5. Binding Tests by Far Western Blotting. Proteins ($0.2 \mu\text{g}$) adsorbed onto a nitrocellulose membrane were first blocked with 0.2% gelatin in Tris-buffered saline and then incubated in nebulin solution (0.18 M KPO_4 (pH 7.0), 0.1 mM MgCl_2 , 0.1 mM EGTA, and 0.5 M urea) ($15 \mu\text{g}/\text{ml}$) for 20 hours at 4°C . After washing, the membrane was treated with

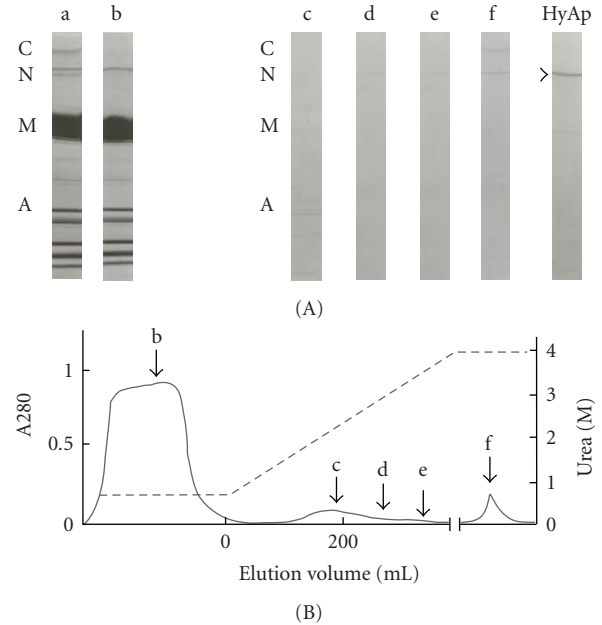


FIGURE 1: Purification of nebulin from rabbit skeletal muscle by DEAE-Toyopearl column chromatography. A muscle extract in 0.18 M KPO_4 (pH 7.0), 0.2 mM ATP, 0.1 mM MgCl_2 , 0.1 mM EGTA, and 1 M urea was loaded to DEAE-Toyopearl column and linear urea gradient up to 4 M was applied. (A) SDS-PAGE patterns of each fraction of (B), (B) Elution pattern. a, applied sample; b, flow-through fraction; c–e, eluted fraction; f, overnight fraction with 4 M urea; HyAp, purified nebulin using hydroxylapatite column chromatography.

antinebulin polyclonal antibody [21] followed by secondary horseradish-labeled antibodies (Dako).

3. Results

3.1. Isolation of Nebulin from Rabbit Skeletal Muscle. Preliminary trials to solubilize nebulin from rabbit skeletal myofibrils proved unsuccessful under conventional salt conditions. However, with the addition of 1 M urea, a solution containing 0.18 M KPO_4 (pH 7.0) and 0.1 mM EGTA could solubilize nebulin together with myosin, actin, and other muscle proteins. Purification by DEAE-Toyopearl column chromatography yielded a fraction containing nebulin and actin. However, it was very difficult to separate the two proteins. Thus, we modified the procedure to prevent actin from denaturation.

Rabbit skeletal muscle (approximately 120 g) was briefly homogenized in 1 L of 50 mM KCl solution containing 1 mM NaHCO_3 and 1 mM EGTA and then sedimented by centrifugation for 6 minutes at $5,000 \times g$, and all procedures were carried out at 4°C . The precipitate was suspended in the same solution and recentrifuged. This procedure was repeated four times. After washing with 5 mM NaHCO_3 , the pellet was extracted with 1 L of 0.2 M NaPO_4 (pH 7.0) to remove connectin and then with 0.3 M KCl-0.15 M KPO_4 (pH 7.0) to remove myosin. The pellet was washed three times with cold 0.1 mM MgCl_2 , and the swollen precipitate

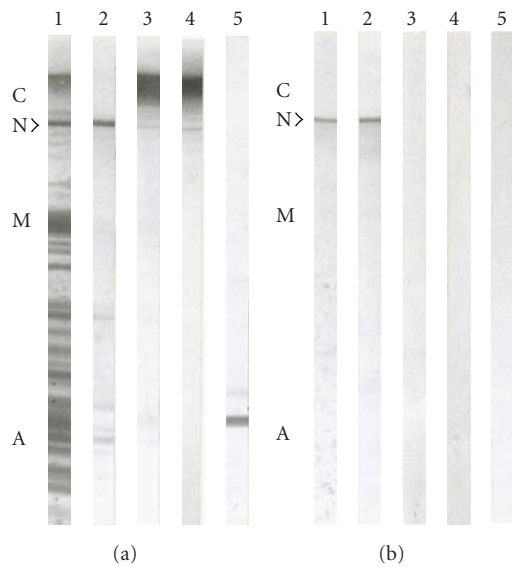


FIGURE 2: Immunoblot detection of purified nebulin. (a) SDS extract of whole rabbit back muscle, (b) nebulin fraction. (1) Amido black stained nitrocellulose sheets, (2) treated with PcNeb, (3) treated with Pc1200, (4) treated with Mc3B9, (5) treated with actin.

was extracted at 4°C for 15 minutes with an equal volume of the same precipitate in a solution with a final concentration of 0.18 M KPO₄ (pH 7.0), 0.2 mM ATP, 0.1 mM MgCl₂, and 0.1 mM EGTA, plus 1 M urea, which was required for nebulin extraction (Figure 1(A)-a). The sample was loaded onto the DEAE-Toyopearl 650 M column (1.9 × 18 cm) equilibrated with 0.18 M KPO₄ (pH 7.0), 0.1 M MgCl₂, 0.1 mM EGTA, and 1 M urea, where a large amount of solubilized myosin and other proteins were not absorbed on the DEAE-Toyopearl resin (Figure 1(A)-b). Bound proteins were eluted by a gradient of 1 to 4 M urea. Actin and nebulin were eluted at around 2 M (Figure 1(A)-c) and 3 M (Figures 1(A)-d and 1(A)-e) urea, respectively. Further elution with 4 M urea overnight (0.02–0.03 mg/ml) was more effective at eluting nebulin (Figure 1(A)-f); however, these fractions contained traces of connectin (also called titin) (Figures 1(A)-e and 1(A)-f). The eluates were dialyzed against 0.18 M KPO₄ (pH 7.0), 0.1 mM MgCl₂, 0.1 mM EGTA, and 2 M urea and then centrifuged for 30 minutes at 12,000 × g. The supernatant was loaded onto the hydroxylapatite column equilibrated with the dialysis solution. As connectin was adsorbed onto the column, nebulin alone was obtained as the flow through fraction (Figure 1(A)-HyAp), but in low yield: 0.03–0.06 mg nebulin (from 120 g rabbit skeletal muscle).

Immunoblotting clearly showed specific reaction to the purified nebulin fraction using anti-nebulin antibody (Figure 2(b)-2); no reaction was observed for anti-actin and anti-connectin antibodies (Figures 2(b)-3, 2(b)-4, and 2(b)-5).

3.2. Modified Purification Method for Nebulin. The protein yield was too low because our procedure was a pared preparation of nebulin. Therefore, we modified the procedure to improve the overall yield of nebulin. First, the well-washed myofibrils were extracted with 0.18 M KPO₄ (pH

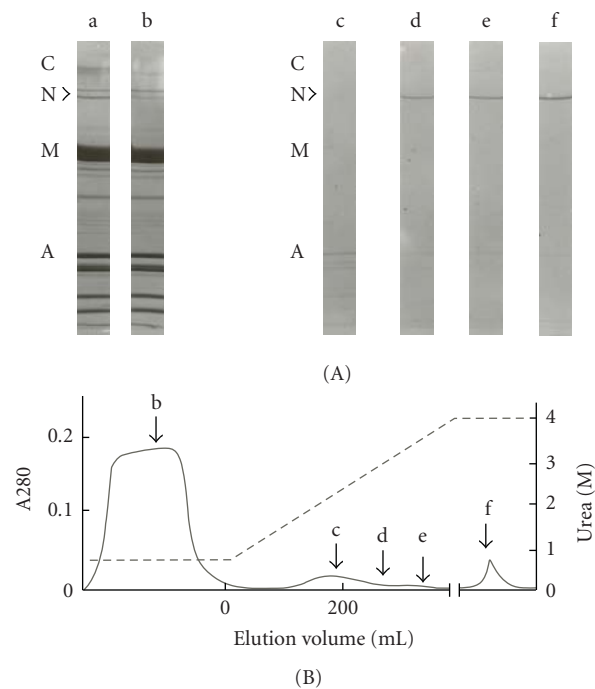


FIGURE 3: Modified purification of nebulin from rabbit skeletal muscle by DEAE-Toyopearl column chromatography. A muscle extract in 0.18 M KPO₄ (pH 7.0), 0.1 mM MgCl₂, 0.1 mM EGTA, and 1 M urea was loaded to DEAE-Toyopearl column and linear urea gradient up to 4 M was applied. (A) SDS-PAGE patterns of each fraction of (B), (B) Elution pattern. a, applied sample; b, flow-through fraction; c–e, eluted fraction; f, overnight fraction with 4 M urea.

7.0), 0.1 mM MgCl₂, 0.1 mM EGTA, and 1 M urea without the addition of ATP, which resulted in a smaller amount of extracted myosin (Figure 3(A)-b) than for extraction in the presence of ATP (Figure 1(A)-b). Consequently, nebulin was extracted to a larger extent under the same DEAE-Toyopearl column chromatography conditions described above. Overnight reelution with 4 M urea thus resulted in a nebulin solution of 1 ~ 1.5 mg/ml, although it was slightly contaminated with actin (Figure 3-f)).

3.3. Electron Microscopy of Isolated Nebulin. Rotary shadowing was applied to purified nebulin samples for visualization of its electron microscopic structure. The nebulin fraction contaminated with traces of connectin (prior to hydroxylapatite chromatography, Figures 1(A)-e and 1(A)-f) showed a number of particles and few entangled filaments (data not shown). Upon further purification of nebulin, the entangled filaments disappeared leaving only small particles (Figure 4), indicating that the filaments were contaminated with connectin molecules, as has been reported previously [25].

The remaining particles having approximately 20-nm in diameter were regarded to be nebulin molecules (Figure 4). The particles had an irregular shape and formed a compact bundle of actin filaments, suggesting a densely aggregated form of the long nebulin molecule. Further application of centrifugal forces to extend these filamentous molecules as

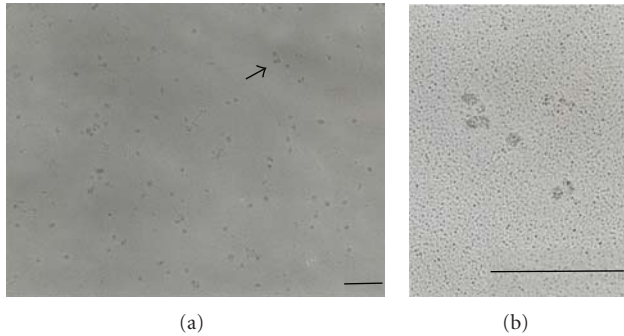


FIGURE 4: Rotary shadowed images of purified nebulin from rabbit back muscle. (a) typical images of nebulin molecules. (b), enlarged images of arrow at (a). Bar, 200 nm.

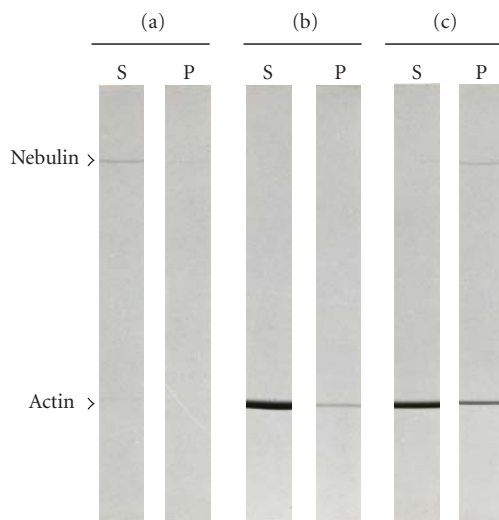


FIGURE 5: Binding of purified nebulin and F-actin examined by cosedimentation. (a) nebulin only, (b) actin only, (c) nebulin + actin. (S) supernatant after centrifugation, (P) pellet after centrifugation. Nebulin and actin were mixed in 0.11 M KPO_4 , 0.31 M urea, 0.27 mM ATP, and 0.1 mM MgCl_2 , pH 7.0. Electrophoresis was performed on a 2–15% polyacrylamide gel.

previously performed for connectin [24–26] failed to change the particle shape of nebulin.

3.4. Interaction of Actin with Purified Nebulin. Purified nebulin was clarified by ultracentrifugation (30 min, $56,000 \times g$) and then mixed with G-actin. To polymerize G-actin, the solution conditions were changed to 0.11 M KPO_4 (pH 7.0), 0.31 M urea, 0.27 mM ATP and 0.1 mM MgCl_2 . The concentration of G-actin and nebulin was 0.2 mg/ml and 19 $\mu\text{g}/\text{ml}$, respectively, giving a 1 : 188 molar ratio of nebulin to actin. After 20 hours incubation at 4°C , the samples were centrifuged for 30 minutes at $6,000 \times g$. As shown in Figure 5, nebulin coprecipitated with actin whereas nebulin alone did not precipitate; a small amount of actin alone was also precipitated. Thus, the large bundles of actin filaments were formed in the presence of nebulin, which was verified by negative-stained electron micrographs (Figure 6).

These bundles were 30 ~ 50 μm long and 0.05–0.13 μm wide, containing 10- to 20-nm-diameter patches thought to be the nebulin particles.

3.5. Binding of Thin Filament Proteins to Purified Nebulin. The interaction of nebulin with several actin-binding proteins was examined by far western blot analysis. As shown in Figure 7, α -actinin and F-actin strongly bound to nebulin. β -Actinin and tropomodulin weakly bound to nebulin, while troponin and tropomyosin showed no binding ability.

4. Discussion

Since nebulin is very insoluble in salt, until now it could only be extracted and purified in the presence of a detergent such as SDS [5]. In this study, however, we were able to extract nebulin from the skeletal muscle of a rabbit by adding 1 M urea to 0.18 M KPO_4 (pH 7.0). However, when we removed all of the urea from this nebulin crude extract solution by dialysis, the solubility of the nebulin deteriorated remarkably, and most of it precipitated. Therefore, in order to prevent nebulin from interacting with other proteins and decreasing its solubility, we purified it by column chromatography in the presence of urea.

We also tried eluting the nebulin from an ion-exchange column chromatography in a salt concentration gradient, but we were unable to remove the contaminants. We therefore, used a urea concentration gradient for elution. After the elution in the urea concentration gradient was complete, we let the nebulin stand for 12 hours and eluted it again. Consequently, we obtained a high-concentration fraction of nebulin. The reason we were able to obtain this high-concentration fraction of nebulin after the second elution, not after the first elution, might be that the nebulin needed time to dissociate from the resin in the column chromatography since the urea with which the nebulin was eluted was at a concentration of 4 M, the minimum concentration necessary for the elution. In this study, we were unable to perform a circular dichroism spectra measurement of the purified nebulin because its content was too low. However, the results of electron microscopic observation and the fact that nebulin could bind to actin suggested that the purified nebulin corresponded at least to a significant extent to a folded state.

Since nebulin is known to exist along thin filaments in skeletal muscle sarcomeres, it is thought to have a filamentous molecular shape. However, observation of isolated nebulin by the rotary shadowing method revealed that its molecular shape was not filamentous but a lump with about 20 nm in diameter (Figure 4). Both in the nebulin fraction obtained in the low urea concentration and the nebulin solution whose urea concentration was reduced by dialysis, the shape of nebulin was same as the nebulin eluted in 4 M urea. Even when the nebulin was dialyzed in pH 9.0 solution because the pI of nebulin is 9.3 [1], we did not see any change in this shape. Furthermore, even though we tried elongating the nebulin molecules by centrifuging them just like connectin, we were unable to see any change in molecular

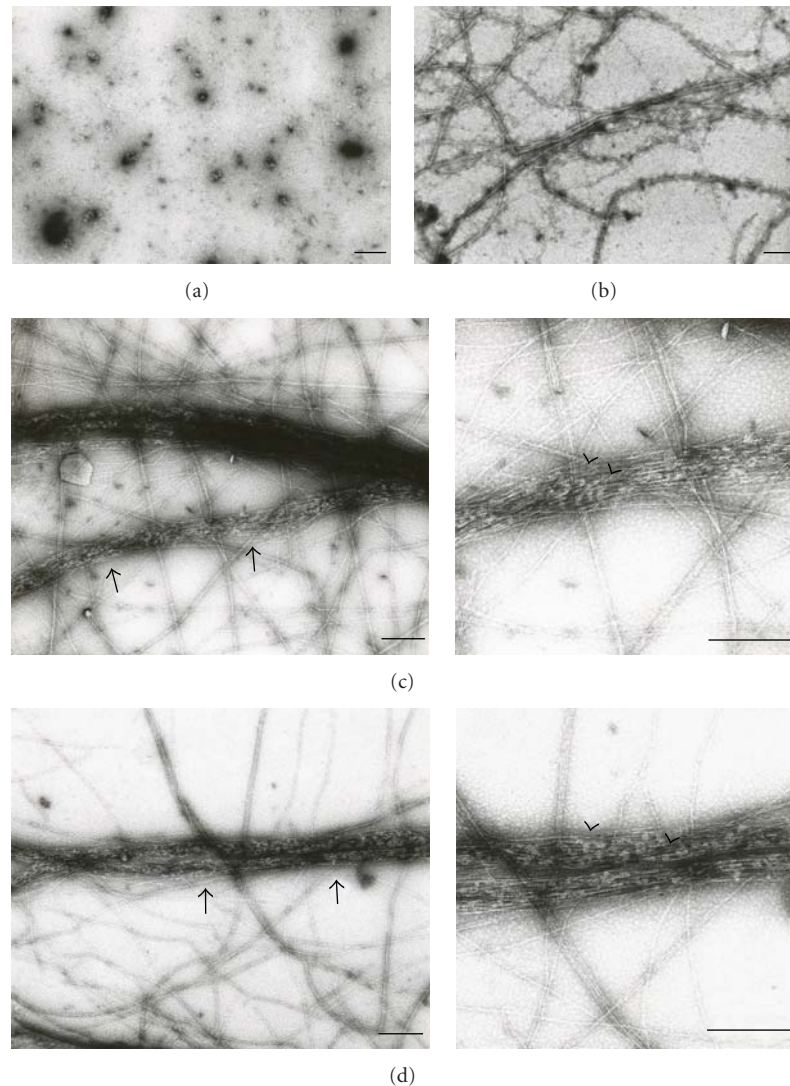


FIGURE 6: Negative-stained electron micrographs of actin filaments under the influence of purification nebulin. (a) nebulin only, 19 $\mu\text{g/ml}$; (b) actin only, 0.2 mg/ml; (c and d) actin (0.2 mg/ml) was mixed with nebulin (19 $\mu\text{g/ml}$) in 0.11 M KPO_4 , 0.31 M urea, 0.27 mM ATP and 0.1 mM MgCl_2 , pH 7.0. Bar, 200 nm.

shape. We were also unable to elongate the lump-shaped molecules even when we used nonionic or amphoteric detergent. However, when we used the anionic detergent SDS, the lumped-shape molecules mostly disappeared, and we observed amorphous images (data not shown). These results suggest that since nebulin molecules are insoluble in salt, they become entangled after they are isolated from skeletal muscle. In contrast, the filamentous form of nebulin in skeletal muscle sarcomeres is probably maintained by their interaction with actin.

In this study, a cosedimentation assay revealed that nebulin isolated from skeletal muscle bound to actin (Figure 5). Other studies have verified by the ELISA method and by cosedimentation assays that the protein which is a part of the nebulin expressed in *Escherichia coli* bound to actin [6, 27–32], and the binding results of our study are consistent with the results of these studies.

Based on the contents of total proteins in muscle *in vivo*, it has been calculated that there are 2 molecules of nebulin per thin filament [2, 4]. Furthermore, since it has been estimated from the primary structure that 1 molecule of actin corresponds to 1 module of nebulin in a thin filament [1, 3, 4], human nebulin is calculated to interact with 185 actin molecules. We performed a cosedimentation assay of nebulin with actin at a ratio based on this calculation, but not all of the actin precipitated, and only part of it bound to nebulin (Figure 5). This may have been because only part of the actin-binding site of nebulin acts on actin.

On the other hand, the assay also showed that actin filaments were bundled by nebulin (Figure 6(c)). In 1998, Gonsior et al. reported that actin filament bundles were formed by the mixing of F-actin and proteins of 6 nebulin modules expressed in *E. coli* [31]. In our study, the bundles of actin filaments formed by the purified nebulin were

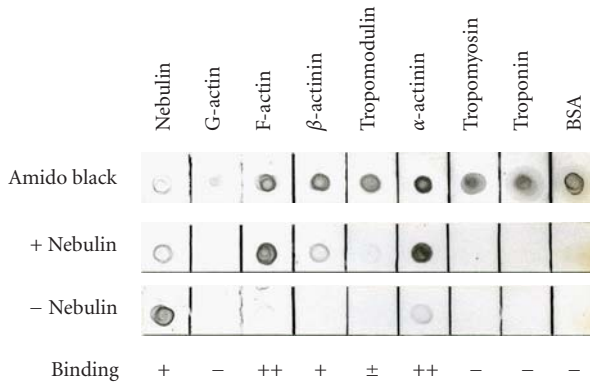


FIGURE 7: Binding of thin filament proteins to purified nebulin by far western blot analysis. Proteins ($0.2\ \mu\text{g}$) adsorbed onto a nitrocellulose membrane were incubated in nebulin reaction solution ($0.18\ \text{M}\ \text{KPO}_4$, $0.1\ \text{mM}\ \text{MgCl}_2$, $0.1\ \text{mM}\ \text{EGTA}$, and $0.5\ \text{M}$ urea, pH 7.0) for 20 hours at 4°C . Amido black: amido black staining; +nebulin: incubation in nebulin ($15\ \mu\text{g}/\text{ml}$), -nebulin: incubation in reaction solution alone.

morphologically similar to these bundles. The fact that the cosedimentation assay showed binding between nebulin and actin at a relatively weak centrifugal force also suggests that actin may be bundled by nebulin.

A widely accepted present day theory about the role of nebulin is the molecular ruler theory, which says that nebulin regulates the length of thin filaments. In skeletal muscle sarcomere, it has been shown that the barbed-end (fast-growing end) of thin filaments is capped by β -actinin at the Z line, while the pointed-end (slow-growing end) of the filaments is capped by tropomodulin (TMD)[33, 34]. Erythrocyte tropomodulin (E-TMD) and skeletal muscle tropomodulin (Sk-TMD) among four tropomodulin isoforms have a function of length regulation of actin filaments. However, McElhinny et al. have revealed that Sk-TMD binds to nebulin with higher affinity than E-TMD does, and suggested that TMD and nebulin may work together as a linked mechanism to control thin filament lengths in skeletal muscle [9]. In this experiment, even though actin was polymerized in the presence of purified nebulin, the lengths of the actin filaments were not uniform. This may have been because actin-capping proteins were not added. In the future, it will be necessary to add β -actinin and Sk-TMD and investigate the interactions between purified nebulin and actin.

α -Actinin is a major component of the Z-line and several different approaches have been used to dissect the set of interactions made by nebulin within the Z-disk lattice. In 1990, Nave et al. showed that chicken nebulin binds to α -actinin by far western blot analysis [35], while in 1999, Moncman and Wang used an ELISA method to show that the SH3 domain of human nebulin binds to α -actinin [36]. However, this was contradicted in 2000 by Ojima et al. who used the GST-pull down method to reveal that such binding does not occur [37]. In 2001, Bang et al. reported that the SH3 domain of human nebulin binds to the newly discovered protein myopalladin, and that the orientation of nebulin to the Z-line is maintained through the binding

of myopalladin to α -actinin [12]. Thus, regarding binding between α -actinin and nebulin, the contradict results have been reported. In our study, the results of far-western blot analysis showed that purified nebulin binds directly to α -actinin. Since the C-terminal region of nebulin localizes at the Z-line in sarcomere, nebulin and α -actinin may bind directly and the C-terminal region of nebulin is probably linked to the Z-line.

The N-terminal region of nebulin is known to bind to TMD which is a pointed end actin-capping protein [9], and the C-terminal region of nebulin is known to bind to β -actinin, which is a barbed end actin-capping protein. Our study showed that purified nebulin also bound to both TMD and β -actinin even though the reaction was weak (Figure 7). The reason that this binding is weak may be that the binding region of the nebulin molecule is at its terminus and is only a small portion of the entire molecule. Our study and others have shown that nebulin binds to actin capping proteins on both ends of the actin filaments. This result supports the idea that nebulin regulates the length of actin filaments.

Because nebulin is extremely insoluble in salt, biochemical analysis has not yet made progress. The novel purification method described here is likely to support future functional studies on nebulin since it provides a full-length source of nebulin peptide that allows to further study its role in thin filament assembly and its potential ruler functions.

5. Conclusion

In this study, nebulin was solubilized by $0.18\ \text{M}\ \text{KPO}_4$ (pH 7.0) solution containing $1\ \text{M}$ urea and purified by DEAE-Toyopearl column chromatography via $4\ \text{M}$ urea elution. The nebulin molecule took on a lump-like molecular shape, and we were unable to observe any molecular-ruler function. However, since the nebulin purified by the present method bound to actin and actin-capping proteins (β -actinin and tropomodulin), this nebulin may have retained some of its in vivo functions. In the future, it may become important to perform more detailed investigations of nebulin's biochemical characteristics, such as whether isolated nebulin retains its high-order structure. It may also become important to keep the concentration of urea low when purifying nebulin.

Acknowledgment

This work was supported by KAKENHI (Grants-in-Aid for Scientific Research) from the Ministry of Education, Culture, Sports, Science and Technology of Japan to Sumiko Kimura.

References

- [1] S. Labeit and B. Kolmerer, "The complete primary structure of human nebulin and its correlation to muscle structure," *Journal of Molecular Biology*, vol. 248, no. 2, pp. 308–315, 1995.
- [2] K. Wang and J. Wright, "Architecture of the sarcomere matrix of skeletal muscle: immunoelectron microscopic evidence that suggests a set of parallel inextensible nebulin filaments anchored at the Z line," *The Journal of Cell Biology*, vol. 107, no. 6, part 1, pp. 2199–2212, 1988.

- [3] M. Kruger, J. Wright, and K. Wang, "Nebulin as a length regulator of thin filaments of vertebrate skeletal muscles: correlation of thin filament length, nebulin size, and epitope profile," *The Journal of Cell Biology*, vol. 115, no. 1, pp. 97–107, 1991.
- [4] S. Labeit, T. Gibson, A. Lakey, et al., "Evidence that nebulin is a protein-ruler in muscle thin filaments," *FEBS Letters*, vol. 282, no. 2, pp. 313–316, 1991.
- [5] K. Wang, "Purification of titin and nebulin," *Methods in Enzymology B*, vol. 85, pp. 264–274, 1982.
- [6] M. J. Chen, C.-L. Shih, and K. Wang, "Nebulin as an actin zipper. A two-module nebulin fragment promotes actin nucleation and stabilizes actin filamen," *The Journal of Biological Chemistry*, vol. 268, no. 27, pp. 20327–20334, 1993.
- [7] N. Lukoyanova, M. S. VanLoock, A. Orlova, V. E. Galkin, K. Wang, and E. H. Egelman, "Each actin subunit has three nebulin binding sites: implications for steric blocking," *Current Biology*, vol. 12, no. 5, pp. 383–388, 2002.
- [8] J.-P. Jin and K. Wang, "Cloning, expression, and protein interaction of human nebulin fragments composed of varying numbers of sequence modules," *The Journal of Biological Chemistry*, vol. 266, no. 31, pp. 21215–21223, 1991.
- [9] A. S. McElhinny, B. Kolmerer, V. M. Fowler, S. Labeit, and C. C. Gregorio, "The N-terminal end of nebulin interacts with tropomodulin at the pointed ends of the thin filaments," *The Journal of Biological Chemistry*, vol. 276, no. 1, pp. 583–592, 2001.
- [10] M.-L. Bang, C. Gregorio, and S. Labeit, "Molecular dissection of the interaction of desmin with the C-terminal region of nebulin," *Journal of Structural Biology*, vol. 137, no. 1–2, pp. 119–127, 2002.
- [11] C. C. Witt, C. Burkart, D. Labeit, et al., "Nebulin regulates thin filament length, contractility, and Z-disk structure in vivo," *EMBO Journal*, vol. 25, no. 16, pp. 3843–3855, 2006.
- [12] M.-L. Bang, R. E. Mudry, A. S. McElhinny, et al., "Myopalladin, a novel 145-kilodalton sarcomeric protein with multiple roles in Z-disc and I-band protein assemblies," *The Journal of Cell Biology*, vol. 153, no. 2, pp. 413–427, 2001.
- [13] V. K. Yadavalli, J. G. Forbes, and K. Wang, "Nanomechanics of full-length nebulin: an elastic strain gauge in the skeletal muscle sarcomere," *Langmuir*, vol. 25, no. 13, pp. 7496–7505, 2009.
- [14] J. A. Spudich and S. Watt, "The regulation of rabbit skeletal muscle contraction. I. Biochemical studies of the interaction of the tropomyosin-troponin complex with actin and the proteolytic fragments of myosin," *The Journal of Biological Chemistry*, vol. 246, no. 15, pp. 4866–4871, 1971.
- [15] K. Maruyama, H. Kurokawa, M. Oosawa, et al., " β -Actinin is equivalent to Cap Z protein," *The Journal of Biological Chemistry*, vol. 265, no. 15, pp. 8712–8715, 1990.
- [16] D. E. Goll, A. Suzuki, J. Temple, and G. R. Holmes, "Studies on purified α -actinin. I. Effect of temperature and tropomyosin on the α -actinin/F-actin interaction," *Journal of Molecular Biology*, vol. 67, no. 3, pp. 469–472, 1972.
- [17] S. Kimura, A. Ichikawa, J. Ishizuka, S. Ohkouchi, T. Kake, and K. Maruyama, "Tropomodulin isolated from rabbit skeletal muscle inhibits filament formation of actin in the presence of tropomyosin and troponin," *European Journal of Biochemistry*, vol. 263, no. 2, pp. 396–401, 1999.
- [18] E. F. Woods, "Peptide chains of tropomyosin," *Nature*, vol. 207, no. 992, pp. 82–83, 1965.
- [19] S. Ebashi, T. Wakabayashi, and F. Ebashi, "Troponin and its components," *Journal of Biochemistry*, vol. 69, no. 2, pp. 441–445, 1971.
- [20] A. Hanashima, K. Kubokawa, and S. Kimura, "Characterization of amphioxus nebulin and its similarity to human nebulin," *Journal of Experimental Biology*, vol. 212, no. 5, pp. 668–672, 2009.
- [21] H. Sugita, I. Nonaka, Y. Itoh, et al., "Is nebulin the product of Duchenne muscular dystrophy gene?" *Proceedings of Japan Academy B*, vol. 63, no. 5, pp. 107–110, 1987.
- [22] S. Kimura, T. Matsuura, S. Ohtsuka, Y. Nakauchi, A. Matsuno, and K. Maruyama, "Characterization and localization of α -connectin (titin 1) an elastic protein isolated from rabbit skeletal muscle," *Journal of Muscle Research and Cell Motility*, vol. 13, no. 1, pp. 39–47, 1992.
- [23] Y. Itoh, T. Suzuki, S. Kimura, et al., "Extensible and less-extensible domains of connectin filaments in stretched vertebrate skeletal muscle sarcomeres as detected by immunofluorescence and immunoelectron microscopy using monoclonal antibodies," *Journal of Biochemistry*, vol. 104, no. 4, pp. 504–508, 1988.
- [24] R. Nave, D. O. Furst, and K. Weber, "Visualization of the polarity of isolated titin molecules: a single globular head on a long thin rod as the M band anchoring domain?" *The Journal of Cell Biology*, vol. 109, no. 5, pp. 2177–2187, 1989.
- [25] M. Sonoda, S. Kimura, H. Moriya, Y. Shimada, and K. Maruyama, "Molecular shape of α -connectin, an elastic filamentous protein of skeletal muscle," *Proceedings of Japan Academy B*, vol. 66, pp. 213–216, 1990.
- [26] J. Suzuki, S. Kimura, and K. Maruyama, "Electron microscopic filament lengths of connectin and its fragments," *Journal of Biochemistry*, vol. 116, no. 2, pp. 406–410, 1994.
- [27] J.-P. Jin and K. Wang, "Nebulin as a giant actin-binding template protein in skeletal muscle sarcomere. Interaction of actin and cloned human nebulin fragments," *FEBS Letters*, vol. 281, no. 1–2, pp. 93–96, 1991.
- [28] M. J. G. Chen and K. Wang, "Conformational studies of a two-module fragment of nebulin and implications for actin association," *Archives of Biochemistry and Biophysics*, vol. 310, no. 2, pp. 310–317, 1994.
- [29] M. Pfuhl, S. J. Winder, and A. Pastore, "Nebulin, a helical actin binding protein," *EMBO Journal*, vol. 13, no. 8, pp. 1782–1789, 1994.
- [30] M. Pfuhl, S. J. Winder, M. A. C. Morelli, S. Labeit, and A. Pastore, "Correlation between conformational and binding properties of nebulin repeats," *Journal of Molecular Biology*, vol. 257, no. 2, pp. 367–384, 1996.
- [31] S. M. Gonsior, M. Gautel, and H. Hinssen, "A six-module human nebulin fragment bundles actin filaments and induces actin polymerization," *Journal of Muscle Research and Cell Motility*, vol. 19, no. 3, pp. 225–235, 1998.
- [32] J. Q. Zhang, A. Weisberg, and R. Horowitz, "Expression and purification of large nebulin fragments and their interaction with actin," *Biophysical Journal*, vol. 74, no. 1, pp. 349–359, 1998.
- [33] D. A. Schafer and J. A. Cooper, "Control of actin assembly at filament ends," *Annual Review of Cell and Developmental Biology*, vol. 11, pp. 497–518, 1995.
- [34] R. S. Fischer and V. M. Fowler, "Tropomodulins: life at the slow end," *Trends in Cell Biology*, vol. 13, no. 11, pp. 593–601, 2003.
- [35] R. Nave, D. O. Furst, and K. Weber, "Interaction of alpha-actinin and nebulin in vitro. Support for the existence of a fourth filament system in skeletal muscle," *FEBS Letters*, vol. 269, no. 1, pp. 163–166, 1990.

- [36] C. L. Moncman and K. Wang, "Functional dissection of nebulin demonstrates actin binding of nebulin-like repeats and Z-line targeting of SH3 and linker domains," *Cell Motility and the Cytoskeleton*, vol. 44, no. 1, pp. 1–22, 1999.
- [37] K. Ojima, Z. X. Lin, M.-L. Bang, et al., "Distinct families of Z-line targeting modules in the COOH-terminal region of nebulin," *The Journal of Cell Biology*, vol. 150, no. 3, pp. 553–566, 2000.

Review Article

Cardiac Troponin Mutations and Restrictive Cardiomyopathy

Michelle S. Parvatiyar, Jose Renato Pinto, David Dweck, and James D. Potter

Department of Molecular and Cellular Pharmacology, Miller School of Medicine, University of Miami, Room 6085A, RMSB, 1600 NW 10th Avenue, Miami, FL 33136, USA

Correspondence should be addressed to James D. Potter, jdpotter@miami.edu

Received 13 November 2009; Accepted 22 February 2010

Academic Editor: Aikaterini Kontrogianni-Konstantopoulos

Copyright © 2010 Michelle S. Parvatiyar et al. This is an open access article distributed under the Creative Commons Attribution License, which permits unrestricted use, distribution, and reproduction in any medium, provided the original work is properly cited.

Mutations in sarcomeric proteins have recently been established as heritable causes of Restrictive Cardiomyopathy (RCM). RCM is clinically characterized as a defect in cardiac diastolic function, such as, impaired ventricular relaxation, reduced diastolic volume and increased end-diastolic pressure. To date, mutations have been identified in the cardiac genes for desmin, α -actin, troponin I and troponin T. Functional studies in skinned muscle fibers reconstituted with troponin mutants have established phenotypes consistent with the clinical findings which include an increase in myofilament Ca^{2+} sensitivity and basal force. Moreover, when RCM mutants are incorporated into reconstituted myofilaments, the ability to inhibit the ATPase activity is reduced. A majority of the mutations cluster in specific regions of cardiac troponin and appear to be mutational “hot spots”. This paper highlights the functional and clinical characteristics of RCM linked mutations within the troponin complex.

1. Introduction

Cardiac contractility is governed by the thin filament regulatory proteins, cardiac troponin (cTn) and tropomyosin (Tm), and available levels of intracellular free calcium ($[\text{Ca}^{2+}]_i$). Cardiac troponin is located at regular intervals along the thin filament and consists of three subunits: cardiac troponin C (cTnC), troponin I (cTnI), and troponin T (cTnT). The cTn complex plays an important role in the regulation of striated muscle contraction. Within the cTn complex, cTnC acts as a Ca^{2+} sensor which confers Ca^{2+} sensitivity to muscle contraction [1]. Cardiac TnI is the inhibitory subunit, primarily functioning to prevent actin and myosin from interacting in the absence of Ca^{2+} . The cTnT subunit binds to tropomyosin (Tm) and is responsible for transmitting the Ca^{2+} binding signal from cTn to Tm. During systole, the rise in $[\text{Ca}^{2+}]_i$ allows binding of Ca^{2+} to the regulatory site of cTnC which leads to the movement of Tm over the actin filament. This permits myosin to interact with actin, subsequently leading to the generation of muscle tension [2]. Alternatively in diastole, the $[\text{Ca}^{2+}]_i$ levels decline and Ca^{2+} dissociates from cTnC, allowing Mg^{2+} to bind to the C-terminal sites. This enables the muscle to relax and allows ventricular filling to occur. Currently, only cTnI

and cTnT have been linked to restrictive cardiomyopathy (RCM) since no mutations have been identified in cTnC yet. Notably, mutations in sarcomeric proteins have the potential to disrupt essential thin filament interactions which can lead to the enhanced Ca^{2+} sensitivity of contraction, arrhythmogenesis, cardiomyopathy and even sudden cardiac death (SCD) [3]. This paper will address the clinical aspects, as well as the functional studies reported to date for the known troponin mutations associated with RCM.

2. Troponin and Cardiac Muscle Regulation

The functional roles of the individual cTn subunits are distinct and involve complex short and long range protein-protein interactions. The binding of Ca^{2+} to the regulatory site of cTnC evokes the minimal exposure of a hydrophobic cleft within the N-domain of cTnC. This enables the regulatory region of cTnI (residues 148–163) to associate with cTnC [4, 5]. Structural analysis has determined that cTnI interacts with cTnC in an antiparallel manner [5, 6]. The association of cTnI with cTnC in the presence of Ca^{2+} facilitates the release of cTnI's inhibitory region (residues 128–147) from actin [7]. When cTnI dissociates from actin, Tm changes its conformation and allows for

the full interaction of myosin heads with actin [1]. Current models propose that thin filament activation is regulated by Ca^{2+} binding to cTnC which influences the number of accessible cross-bridges by shifting the equilibrium from weakly (nonforce-producing) to strongly (force-producing) bound cross-bridges [8, 9].

Cardiac TnI has a unique feature absent in the fast and slow skeletal muscle isoforms such that it possesses a 30-amino acid N-terminal extension which contains two Protein Kinase A (PKA) phosphorylation sites (Ser 22 and 23) [10, 11]. Activation of PKA by β -adrenergic stimulation enhances the rate of cross-bridge cycling and increases the rate of Ca^{2+} uptake by the sarcoplasmic reticulum [12–14]. Both of these phenomena contribute to the lusitropic effect associated with phosphorylation by PKA [15–17]. Occasionally, troponin mutations may interfere with the processes involved with thin filament phosphorylation and diminish the subsequent Ca^{2+} desensitizing effects.

The thin filament undergoes activation due to important associations coordinated by cTnT. The N-terminal region of cTnT anchors cTn to Tm and this interaction modulates ATPase activation when Ca^{2+} concentrations achieve threshold levels [18]. Cardiac TnT has two main interactions with Tm. The first is located in the N-terminus of cTnT and is Ca^{2+} dependent [19]; and the second is located in the C-terminal portion of cTnT which also interacts with cTnC and cTnI [19, 20]. In addition to anchoring cTn to the thin filament, cTnT has a critical role in the activation of actomyosin ATPase activity [21]. When cTnT is combined with cTnI-cTnC, the actomyosin ATPase is activated in a Ca^{2+} -dependent manner. Critical to this process is the region of overlap that exists between TnT1 (residues 1–158) at the head-to-tail junction of two adjacent Tm molecules [22, 23]. These interactions confer cooperativity to muscle activation when Ca^{2+} reaches threshold levels [24]. Inhibition of contraction is dependent on cTnI; however, in the absence of TnI, both TnT and TnT1 are able to inhibit the actin activated myosin subfragment-1 (S1) ATPase [22, 25].

3. Restrictive Cardiomyopathy in Humans

RCM is a rare cardiac disorder that manifests primarily as an abnormality of diastolic filling which is also reported as a reduced ventricular compliance or increased stiffness [26]. This results in a restriction of ventricular filling (reduced diastolic volume) and an increase in end-diastolic pressure while maintaining normal to near normal systolic function [27]. Clinically, RCM presents in patients as dyspnea and pulmonary edema [28]. Generally, both atria become dilated, which is likely due to the restriction of ventricular filling. The heart may not be enlarged and the septal and ventricular wall thickness dimensions are minimally affected [29]. Over time, the systolic function declines as the disease approaches end stages and ultimately results in heart failure [30]. The prognosis of RCM is poor, especially in pediatric cases where heart transplantation is often the only preferred treatment. SCD is prevalent in pediatric RCM with a two-year mean survival rate for pediatric cases reaching ~50% after diagnosis [30–33]. SCD is also prevalent in pediatric

RCM cases that display electrocardiographic evidence of ischemia [30].

Several studies confirmed that restrictive cardiomyopathy can be inherited in a familial manner (see Table 1). The first study in 1992 reported the familial inheritance of a disease that resembled RCM and Hypertrophic Cardiomyopathy (HCM) [34]. In 2003, Mogensen and colleagues firmly established that troponin I mutations were etiological causes of RCM [35]. In one case, after evaluating a child and his mother for RCM, examination of the extended family revealed that 12 individuals had died suddenly, with the surviving relatives presenting symptoms of heart disease [35]. Linkage analysis identified a novel missense mutation (D190H) in a conserved region of the cTnI gene (*TNNI3*) that cosegregated in family members presenting symptoms of cardiac disease. This study also included unrelated patients with idiopathic RCM (IRCM) to assess if a genetic basis could be determined. Genetic analysis of several pediatric IRCM patients identified two different de novo mutations (R192H and K178E) in the *TNNI3* gene. Additional patients with adult onset IRCM were also evaluated and the genetic analysis revealed three more mutations in the *TNNI3* gene (R145W, A171T, and L144Q) [35]. Notably, these mutations cluster in specific regions of cTnI that participate in important thin filament interactions.

Since 2005, numerous mutations linked to RCM have been identified in the *TNNI3* gene. A study utilizing a candidate gene approach identified the deletion of a nucleotide in the *TNNI3* gene that causes a frame shift in codon 168 from a 23-year-old patient diagnosed with RCM [36]. This deletion resulted in a premature stop codon at position 176 which leads to the expression of a C-terminal truncated mutant protein. During a six-year follow-up, the patient's heart had undergone progressive and concentric remodeling of the left ventricle. A strong family history was also present as the patient's father had experienced SCD at age 29 and two pregnant relatives experienced intrauterine fetal death in their third trimester. At least two family members under the age of 1 year had suddenly died. The authors established that the frame shift mutation caused a 50% decrease in the myocardium's total cTnI content while the truncated cTnI was undetectable. These results suggest that the frame shift exerted its deleterious effects through haploinsufficiency. This might be due to cTnI degradation or the failure of the mutant cTnI to associate with the thin filament. In any event, the reduced cTnI content may lead to altered interactions of cTn with the actin-tropomyosin complex that resulted in severe diastolic dysfunction within this family [36].

In 2008, Kaski et al. identified two other cTnI mutations from two pediatric RCM patients [37]. The first was a de novo substitution (K178E) identified in a 7-year-old girl who had biatrial enlargement, abnormal sinus rhythm and ST-T waves. Histological evaluation of her cardiac tissue revealed cardiomyocyte disarray. The second, identified in a 6-year-old girl, was a novel deletion of two nucleotides that resulted in a frame shift at residue 177 and the occurrence of a premature stop codon at residue 209. Her electrocardiogram also revealed abnormalities in sinus rhythm and

TABLE 1: Clinical data were collected from in vivo and/or ex vivo human and transgenic mice hearts containing the RCM-associated mutation. The diagnosis of RCM was given on the basis of echocardiographic, electrocardiographic, and/or cardiac catheterization examination. The maximal wall thickness (MWT) was measured from the septal or free wall (or both). In vitro data were collected from skinned cardiac muscle preparations reconstituted with the mutant or expressed as a transgene product. The maximal force and ATPase generating capabilities (max force/ATPase) were tested in high $[Ca^{2+}]_i$; whereas the ability of the muscle to relax or inhibit the ATPase activity (relax/inhibit) was measured in low $[Ca^{2+}]_i$. ΔpCa_{50} , $-\log[Ca^{2+}]_{free}$ at which 50% of the maximal response occurs ($-$ or $+$ denotes an increase or decrease in the Ca^{2+} sensitivity, resp.). BA: both atria; DP: diastolic pressure; E/A: ratio of early diastolic filling [E] to atrial filling [A]; EF: ejection fraction; IF: impaired filling; IRT: intraventricular or isovolumic relaxation time; LV: left ventricle; LVOTO: LV outflow tract obstruction; SCD: sudden cardiac death; ND: not determined.

Protein	Mutation	MWT range (mm)	ex and in vivo properties				In vitro effects				Ref.
			Diastolic	Systolic	Enlarged	SCD	ΔpCa_{50}	Max Force/ATPase	Relax/inhibition	In/ex vivo	
TnT	$\Delta E96$	normal	IF, \uparrow DR, \uparrow E/A	\downarrow EF	LV, BA	unclear	+0.43	no Δ or \uparrow	\downarrow	[33]	[38]
	E136K	normal	IF, \uparrow IRT, \uparrow DP, \uparrow E/A	Preserved	BA	unclear	ND	ND	ND	[37]	
TnI	L144Q, R145W	≤ 15	IE, \uparrow IRT, \uparrow DP, \uparrow E/A, LVOTO	Preserved	LV, BA	yes	+0-0.30	\uparrow or \uparrow	\downarrow	[35, 39]	[40-43]
	A171T	≤ 14	IE, \downarrow IRT, \uparrow E/A	Preserved	LV, BA	no	+0.14-0.30	\downarrow	\downarrow	[35]	[40-42]
	K178E	≤ 15	IE, \downarrow IRT, \uparrow E/A	Preserved	LV, BA	no	+0.15-0.47	\downarrow	\downarrow	[35, 37]	[40-42]
	D190H/G	15-17	IE, \downarrow IRT, \uparrow E/A	Preserved	LV, BA	yes	+0.17-0.30	no Δ	\downarrow	[35]	[40, 42, 44]
	R192H	10-17	IE, \downarrow IRT, \uparrow E/A	Preserved	LV, BA	yes	+0.28-0.36	\downarrow	\downarrow	[35, 45]	[40, 41, 44, 46]
	R204H	11-13	IE, \uparrow DP	Preserved	BA	yes	ND	ND	ND	[47]	
	E177 fs X209	normal	IF, \downarrow IRT, \uparrow DP, \uparrow E/A	Preserved	BA	unclear	ND	ND	ND	[37]	
	D168 fs X176	10-11	IF, \downarrow IRT, \uparrow DP, \uparrow E/A	Preserved	BA	yes	ND	ND	ND	[36]	

ST-T waves. Morphologically, her heart presented with bi-atrial enlargement and dysplastic coronaries. Histological evaluation showed cardiomyocyte disarray [37]. The authors suggested that de novo mutations that arise in sarcomeric proteins are generally associated with an earlier onset of the disease and a more deleterious prognosis. These mutations may result from germ line mosaicism [48] or somatic mutations that occur in heart progenitor cells [49].

Another HCM-associated *TNNI3* mutation (R204H) was recently identified in a young girl that developed bi-atrial enlargement during her early teenage years which developed into RCM. Her brother had died suddenly at age 18. Subsequently, she was under clinical observation and developed RCM between the ages of 14–18. The patient had frequent episodes of diastolic heart failure and underwent a heart transplant at age 23. The histopathology performed on her explanted heart showed an absence of hypertrophy, even though myocyte disarray was evident which further supported the RCM diagnosis [47].

Restrictive cardiomyopathy shares some similar clinical features with HCM. For example, both diseases result in the failure of the myocardium to relax fully during diastole. Therefore, the diagnosis of patients with sarcomeric mutations can be confounded when they present with IRCM and HCM. The R192H cTnI mutation identified by Mogensen in 2003 in an RCM patient [35] was also found in another family in 2009 which presented with features of HCM [45]. The proband had a maximal left ventricular wall thickness of 17 mm, a restrictive physiology and a parent and sibling diagnosed with RCM [45]. The R192H mutation is located within the actin binding region of cTnI and is expected to impair cardiac relaxation since it caused a decrease in the left ventricular end diastolic dimension and enlarged the atria in the patient [45]. Generally, RCM and HCM with restrictive physiology caused by mutations in the *TNNI3* gene have worse clinical outcomes and disease progression.

Initially, familial RCM occurred primarily in the genes encoding cTnI and cardiac desmin (*DES*) [26, 35, 36, 40, 47]. However, mutations in the α -cardiac actin (*ACTC*), β -myosin heavy chain (β -MHC), and cTnT (*TNNT2*) genes have recently emerged as etiological causes of RCM [33, 37, 50]. In 2006, the first mutation in the cTnT gene (*TNNT2*) linked to RCM was identified in a patient, a deletion of Glu at residue 96 [33]. This twelve-month-old girl was found cyanotic and limp. Upon evaluation, her electrocardiogram (ECG) revealed abnormal sinus rhythm, left axis deviation, and nonspecific changes in the ST-T wave. Echocardiography showed severe atrial dilation with no regurgitation of the mitral and tricuspid valves. In addition, the patient had mild-to-moderate left ventricular systolic dysfunction with a reduced fractional shortening and mild right-ventricular systolic dysfunction. While waiting for transplantation, she experienced recurrent episodes of sinus bradycardia and tachycardia associated with diffuse ischemic ECG changes and pronounced hypertension [33].

Recently, another mutation (E136K) was identified in the *TNNT2* gene from a patient diagnosed with RCM [37]. Interestingly, the mutation was also identified in the father and brother, who revealed nothing abnormal upon clinical

evaluation. Cardiac tissue from the explanted heart showed that vacuolation was present but was lacking cardiomyocyte disarray normally associated with cTnT-based cardiomyopathies. Since the two relatives were unaffected clinically, the true etiology of the disease remains undetermined. It is possible that another undetected mutation contributes to the phenotype seen in the RCM proband that was absent in the relatives.

As the number of genes associated with RCM has increased, it has become evident that mutations previously determined to cause HCM can also cause RCM or HCM with a restrictive phenotype. A study by Menon (2008) identified a large family displaying cardiac disease inherited in an autosomal dominant pattern. Characterization of the RCM proband showed the existence of massive bi-atrial enlargement and abnormal diastolic function [51]. However, the proband had mild mid-septal hypertrophy without left ventricular outflow obstruction. Interestingly, other relatives presented with clinical features of RCM, HCM, and/or dilated cardiomyopathy (DCM). It was suspected that a single mutation was responsible for the variable disease outcomes; therefore, a targeted linkage analysis was performed for nine sarcomeric genes which determined that the I79N mutation in the *TNNT2* gene cosegregated with the disease phenotype. Previously, this mutation was identified in other individuals diagnosed with HCM [52, 53]. Studies using transgenic mice containing the I79N TnT mutation have shown that their cardiac function is consistent with a restrictive physiology [54–56].

Other studies have also examined the prevalence and clinical significance of HCM with a restrictive phenotype. Three previously characterized *TNNI3* mutations (L144Q, R145W, and D190G) were identified in patients manifesting the restrictive phenotype. HCM is generally associated with mild to moderate disability and normal life expectancies as long as SCD is avoided; however, patients with the “restrictive phenotype” have a very poor prognosis [39]. The restrictive phenotype is characterized as an absence of or minimal hypertrophy with restrictive filling, elevated rates of atrial fibrillation/flutter, diastolic heart failure and stroke. The overall survival rate of these patients is 56% five years after diagnosis with the main cause of fatality being heart failure [39]. Until recently, it was believed that HCM, DCM and RCM were distinct and separate diseases. However, the R145G and R145W mutations located at the same locus in the cTnI gene can cause HCM or RCM, respectively. This indicates that RCM is included in the spectrum of hereditary cardiac contractile disorders [35, 57]. To date, the existence of simultaneous multiple mutations, modifier genes or the influence of genetic background has not been fully explored. These aspects will gain increasing interest as knowledge of cardiomyopathies expands in the coming years.

4. Reconstituted and Structural Assays

The functional effects of cTnT and cTnI RCM mutations have been explored in different types of reconstituted systems (see Table 1). The in vitro and in situ experimental models involve skinned fibers exchanged with RCM mutant

proteins, myosin-actin-Tm-cTn reconstituted ATPase assays, and spectroscopic measurements utilizing fluorescence and circular dichroism. Much of this data can be correlated to the clinical observations seen in patients. Furthermore, in addition to linkage analysis, these studies assist in establishing de novo mutations as causative agents of the disease.

4.1. Skinned Fiber Data. Skinned cardiac fiber experiments provide a method of exploring myofilament function with a level of complexity that approaches the intact muscle. These assays are considered one of the most relevant physiological techniques available. Importantly, the sarcomeric proteins at the M- and Z-band remain in the skinned fiber in contrast to other reconstituted methods. These experiments measure the Ca^{2+} buffering capacities of the myofilament while measuring the development of tension or maximal force [58, 59]. Several groups have also reported differences in the level of basal force (at low Ca^{2+} concentrations) after the incorporation of mutant cTnT or cTnI [38, 41].

Our group first investigated the functional effects of cTnI mutations linked to RCM [41]. All five RCM mutants that were investigated (L144Q, R145W, A171T, K178E, and R192H) increased the Ca^{2+} sensitivity of force development in skinned fibers. The maximal tension was diminished for all mutants, except R192H. The L144Q, R145W, and K178E mutants showed a significant increase in the basal force levels compared to WT [41]. Other studies using these mutants also produced a large leftward shift in the Ca^{2+} sensitivity of force development in exchanged cardiac skinned fibers [40]. The maximal force was reduced in the presence of the L144Q, R145W, A171T, and R192H mutants; however D190G had no effect on the maximal force when compared to the WT [40]. Using adenoviral gene transfer techniques, Davis et al. introduced RCM mutations into cardiomyocytes and studied their functional consequences at the cellular level [42]. In contrast to the previous study [41], skinned rat cardiomyocytes containing the rat cTnI mutations, L145Q and R146W (corresponding to L144Q and R145W), did not show changes in the Ca^{2+} sensitivity of force development [42]. It is possible that the cTnI mutants located in the inhibitory peptide were poorly incorporated into the thin filament which could mask the effects of the mutations on the Ca^{2+} sensitivity of contraction. However, the rat cTnI mutations, A172T, K179E and D191G (corresponding to human A171T, K178E, and D190G) increased the Ca^{2+} sensitivity of force development [42]. Moreover, the transfected cardiomyocytes bearing the mutant cTnIs could be desensitized to Ca^{2+} upon PKA treatment [42], however, these mutations did not influence the ability of cTnI to respond to adrenergic stimulation. In a separate study, Davis et al. investigated the functional effects of the cTnI R193H mutant incorporated into the thin filament which caused significant Ca^{2+} sensitization of the myofilaments and slowed the Ca^{2+} transient decay rate [46].

Previously, we studied the functional consequences of the first cTnT mutation related to RCM where glutamic acid was deleted at position 96 (cTnT- Δ E96) [38]. The skinned fiber measurements showed significant Ca^{2+} sensitization of

the myofilaments and the mutant cTn complex increased the basal force after troponin exchange. The mutation did not affect the maximal force recovery at saturating Ca^{2+} concentrations. In addition, the same mutation was also studied as the corresponding residue of the fetal isoform of cTnT (cTnT1). Interestingly, in the fetal environment, i.e., the cTn complex containing the cTnT isoform 1 (cTnT- Δ E106) and slow skeletal TnI, the mutation caused a less pronounced effect than when in the adult environment [38]. This suggests that fetal cTn isoforms have a protective role and may explain why the disease occurs early after birth. The mutation significantly reduced the cooperativity (i.e., n_{Hill}) of Ca^{2+} binding to the regulatory units. This information can be correlated with the previous findings and related to the time of onset and the severity of the disease [60].

4.2. Myosin-Actin-Tm-Tn ATPase Assays. The measurement of myofilament ATPase activity is very important since these experiments indicate the ability of the troponin complex to initiate activation and inhibition of the myosin-actin ATPase activity. The Ca^{2+} concentration can be adjusted to activate or inhibit the ATPase activity. In other words, this experiment evaluates the influence of Tn in modulating cross-bridge kinetics. Additionally, it is possible to measure the rate of ATP hydrolysis as a function of the free Ca^{2+} concentration.

In an elegant set of experiments, Gomes et al. showed the dependence of different ratios of WT and mutant cTnI related to RCM on the ability to inhibit the ATPase activity. For example, cTnI R145W in a 50%:50% mixture with WT was able to fully inhibit the ATPase; however L144Q in a 50%:50% ratio with WT had the greatest inability to inhibit ATPase activity and had a dominant regulatory effect over the WT. Regarding the acto-myosin ATPase activation, cTn containing the L144Q mutation partially lost its ability to activate [41]. Kobayashi and Solaro also investigated the functional consequences of the R145W, D190H, and R192H RCM mutations in cTnI. All of the RCM mutants markedly increased the Ca^{2+} sensitivity of ATPase activity. In addition, the R145W mutant which is located in the inhibitory portion of cTnI showed an increase in the basal ATPase activity at low Ca^{2+} concentrations [44]. These experimental results suggest that RCM mutations in the inhibitory peptide have a more drastic effect than mutations located in the cTnI C-terminal domain. In the absence of Ca^{2+} , the inhibitory region is very important for maintaining proper thin filament function in the off state.

Thin filaments reconstituted with the first described cTnT mutant (Δ E96) were used to measure actomyosin ATPase activity. In the presence of this mutant, the actomyosin ATPase activity was poorly inhibited at low Ca^{2+} levels. However, it appears that introducing the mutation into the fetal cTnT isoform in the presence of the fetal slow skeletal TnI diminished these deleterious effects [38].

These functional studies confirm that the RCM phenotype can be directly correlated with clinical data obtained from patients. For example, the increased Ca^{2+} sensitivity, impaired inhibition of ATPase activity by the Tn complex containing

RCM mutants, and increased basal force can be directly correlated with diastolic dysfunction.

4.3. Spectroscopy Measurements. Steady-state fluorescence measurements were used to show that the R145W, D190H and R192H cTnI RCM mutants only increased the apparent Ca^{2+} binding affinity of cTnC in the presence of the other thin filament components [44]. Structural studies with NMR using the $^{13}\text{C}/^{15}\text{N}$ -labeled cTnI_{129–210} peptide containing the K178E RCM mutation revealed local structural changes in the region immediately adjacent to the mutated residue. The cTnI K178E mutant was also evaluated by circular dichroism and no changes were observed in the cTnI K178E structure compared to WT [40]. Together, this data suggests that local yet minor changes in the structure of the isolated mutants may disrupt crucial interactions with other thin filament proteins. In general, the alteration of a few key residues in sites of interactions may be sufficient to alter cTn function.

5. Transgenic Models

A specific functional phenotype is emerging for RCM that includes large increases in the Ca^{2+} sensitivity of tension, impaired ability to inhibit the myosin ATPase activity and increased basal force in skinned fibers. All of these factors when manifested in vivo can contribute to severe diastolic dysfunction and may account for the RCM disease [61]. One of the advantages of using animal models is that the mutant protein is naturally incorporated into the thin filament. Therefore, characterizing the effects of RCM mutations in transgenic or knock-in animals is imperative in determining if cardiac function is affected. Unlike HCM and DCM, the diagnosis of RCM is not based on the morphological appearance of the heart but primarily on the properties of the working heart. Abnormal diastolic filling is the primary defect that leads to increased myocardial stiffness and higher ventricular pressures [27–29, 61].

Two transgenic mouse models for cTnI RCM mutations have been reported which investigated the physiological effects of the R192H and R145W mutations. Du et al. designed a transgenic mouse carrying the R193H mutation (which corresponds to human R192H) and evaluated its effects on gross cardiac morphology. The transgenic R193H mice demonstrated RCM characteristics, i.e., atrial dilation and decreased left ventricular end-diastolic dimension without significant changes in systolic function. Also, they observed a significant change in the ejection fraction in middle aged (11 months old) mice. Histological evaluation indicated that the cardiac tissue was structurally normal [62]. Functionally, the most significant changes that occurred were impaired relaxation manifested by prolonged IRT (isovolumic relaxation time) and DT (deceleration time). The restrictive physiology was evident by the reduced E peak velocity and reversed E/A on doppler tissue imaging [63]. These observations directly correlated with the clinical phenotype used to establish RCM in a patient.

In another study, Du et al. evaluated the progression of RCM in a cTnI R193H transgenic mouse over a period of 12 months. During this time, cardiac function was assessed to

monitor the development of diastolic dysfunction. Initially, the mutation caused abnormal relaxation which gradually manifested as diastolic dysfunction as age progressed. High-resolution echocardiography was used to characterize the mutation's effects on diastolic function by a reversed E to A ratio, increased DT and prolonged IRT. Some of the cTnI R193H middle-aged mice (1 year) had a significant reduction in cardiac output and a few died from congestive heart failure. Morphologically, the mutant mouse hearts had dilated atria and ventricular restriction similar to those of RCM patients carrying the cTnI R193H mutation. The mutation affected mouse cardiac function in the same manner as seen in the patients by recapitulating the diastolic dysfunction and diastolic heart failure. Altogether, this data suggests that the C-terminus of cTnI plays an important role in maintaining the diastolic parameters of the heart [63].

The cTnI R145W RCM mouse model was investigated to determine how a different substitution at the same locus which causes HCM (R145G) can lead to two different diseases [57]. In transgenic R145W cardiac myofibrils, an increase in the Ca^{2+} sensitivity of force and ATPase was observed. Interestingly, the intracellular Ca^{2+} and force transients measured in intact fibers were delayed which may contribute to the diastolic dysfunction. One possible explanation for the distinct phenotypic differences between RCM and HCM is the presence of an increase in the maximal force as observed only in the R145W mice. The contractility of the ventricular muscle containing the R145W mutant is increased 53% during systole, thus compensating for the diastolic dysfunction. In contrast, the R145G HCM mice showed a decrease in the maximal force which may explain why the development of cardiac hypertrophy occurs [43].

6. Isoform Switch, Disease Onset, and Lethality

During fetal heart development, the expression and presence of different isoforms of cTnI and cTnT varies. These changes in isoform expression may underlie the early onset and aggressive course of pediatric cardiomyopathies. The slow skeletal TnI isoform is a product of a distinct gene and is expressed and incorporated in the heart during fetal and neonatal development. The effects of mutations in the cardiac isoform of TnI appear later, as regulated by the activation of cTnI gene expression. It was determined in the rat that cTnI is expressed by the fourth day after birth and isoform switching continues up to the fourteenth day [64, 65]. Mutations in the cardiac TnI gene that change cTn function would consequently alter the Ca^{2+} homeostasis of the cell and manifest their deleterious effects shortly after birth. Cardiac TnT also undergoes an isoform switch. The fetal heart expresses a different isoform by alternative splicing of the *TNNT2* gene. The fetal isoform of cTnT (cTnT1) contains both exons 4 and 5, while the adult isoform (cTnT3) contains only exon 4 [66–68]. When the corresponding RCM mutation (ΔE96 adult isoform cTnT3) was introduced into cTnT1 (i.e., ΔE106) in the presence of slow skeletal TnI, the functional effects were less dramatic [38]. This observation suggests that the combination of fetal cTnT and ssTnI isoforms can rescue the effects of an RCM mutation in

the cTnT gene. In contrast, throughout cardiac development, cTnC is continually expressed; therefore, it is expected that RCM causing mutations in cTnC may lead to late term or spontaneous abortion. This may explain why mutations in cTnC linked to RCM have not been identified yet.

7. Structural Consideration and Perspectives

The two reported cTnT RCM mutations are located in a hot spot region of the TnT N-terminal domain which interfaces with Tm. We speculate that the mutations in cTnT may disrupt the communication between TnT-Tm and thus affect the actomyosin interaction and cooperative activation of the thin filament. Therefore, future investigations using cTnT RCM mutants may help to dissect the modulatory role and function of the cTnT N-terminal domain.

The RCM mutations found in TnI are located within the inhibitory peptide or within the C-terminal domain. The C-terminal domain of cTnI binds to actin and helps to maintain the thin filament in a blocked state. These cTnI mutations may be destabilizing, i.e., decreasing the interactions between the cTnI C-terminal domain and actin in the absence of Ca^{2+} , consequently relieving cTnI inhibition. The small region termed the inhibitory peptide is necessary for the regulatory role of cTnI on muscle contraction. It is also possible that mutations located within the cTnI C-terminal domain may alter the structure and function of the inhibitory peptide.

The discovery of new mutations in RCM patients is crucial for dissecting how they alter function and may lead to a better understanding of the disease. The functional and clinical data should be weighed equally in order to better link mutations as causes of cardiomyopathies. In addition, functional studies may help to further define the RCM and HCM phenotypes which share similar features, such as, an increase in the Ca^{2+} sensitivity of force development. Exploration of RCM causing mutations provides an excellent framework on which new therapeutic strategies can be developed to target the effects of this disease.

Acknowledgments

This work was supported by NIH Grants HL-67415 and HL-42325 (J. D. Potter) and postdoctoral fellowships from the American Heart Association, AHA 0825368E (for J. R. Pinto) and AHA 09POST2300030 (M. S. Parvatiyar). M. S. Parvatiyar and J. R. Pinto contributed equally to this manuscript; therefore, they are considered cofirst authors.

References

- [1] A. M. Gordon, E. Homsher, and M. Regnier, "Regulation of contraction in striated muscle," *Physiological Reviews*, vol. 80, no. 2, pp. 853–924, 2000.
- [2] A. M. Gordon, M. Regnier, and E. Homsher, "Skeletal and cardiac muscle contractile activation: tropomyosin "rocks and rolls"" *News in Physiological Sciences*, vol. 16, no. 2, pp. 49–55, 2001.
- [3] B. C. Knollmann, P. Kirchhof, S. G. Sirenko, et al., "Familial hypertrophic cardiomyopathy-linked mutant troponin T causes stress-induced ventricular tachycardia and Ca^{2+} -dependent action potential remodeling," *Circulation Research*, vol. 92, no. 4, pp. 428–436, 2003.
- [4] M. X. Li, L. Spyropoulos, and B. D. Sykes, "Binding of cardiac troponin-I 147-163 induces a structural opening in human cardiac troponin-C," *Biochemistry*, vol. 38, no. 26, pp. 8289–8298, 1999.
- [5] S. Takeda, A. Yamashita, K. Maeda, and Y. Maéda, "Structure of the core domain of human cardiac troponin in the Ca^{2+} -saturated form," *Nature*, vol. 424, no. 6944, pp. 35–41, 2003.
- [6] C. S. Farah, C. A. Miyamoto, C. H. I. Ramos, et al., "Structural and regulatory functions of the NH_2 - and COOH -terminal regions of skeletal muscle troponin I," *Journal of Biological Chemistry*, vol. 269, no. 7, pp. 5230–5240, 1994.
- [7] K. Murakami, F. Yumoto, S.-Y. Ohki, T. Yasunaga, M. Tanokura, and T. Wakabayashi, "Structural basis for Ca^{2+} -regulated muscle relaxation at interaction sites of troponin with actin and tropomyosin," *Journal of Molecular Biology*, vol. 352, no. 1, pp. 178–201, 2005.
- [8] C. A. Morris, L. S. Tobacman, and E. Homsher, "Modulation of contractile activation in skeletal muscle by a calcium-insensitive troponin C mutant," *Journal of Biological Chemistry*, vol. 276, no. 23, pp. 20245–20251, 2001.
- [9] D. F. A. McKillop and M. A. Geeves, "Regulation of the interaction between actin and myosin subfragment 1: evidence for three states of the thin filament," *Biophysical Journal*, vol. 65, no. 2, pp. 693–701, 1993.
- [10] A. J. G. Moir, R. J. Solaro, and S. V. Perry, "The site of phosphorylation of troponin I in the perfused rabbit heart. The effect of adrenaline," *Biochemical Journal*, vol. 185, no. 2, pp. 505–513, 1980.
- [11] T. A. Noland Jr., X. Guo, R. L. Raynor, et al., "Cardiac troponin I mutants. Phosphorylation by protein kinases C and A and regulation of Ca^{2+} -stimulated MgATPase of reconstituted actomyosin S-1," *Journal of Biological Chemistry*, vol. 270, no. 43, pp. 25445–25454, 1995.
- [12] J. C. Kentish, D. T. McCloskey, J. Layland, et al., "Phosphorylation of troponin I by protein kinase A accelerates relaxation and crossbridge cycle kinetics in mouse ventricular muscle," *Circulation Research*, vol. 88, no. 10, pp. 1059–1065, 2001.
- [13] K. P. Ray and P. J. England, "Phosphorylation of the inhibitory subunit of troponin and its effects on the calcium dependence of cardiac myofibril adenosine triphosphatase," *FEBS Letters*, vol. 70, no. 1, pp. 11–16, 1976.
- [14] R. J. Solaro, A. J. G. Moir, and S. V. Perry, "Phosphorylation of troponin I and the inotropic effect of adrenaline in the perfused rabbit heart," *Nature*, vol. 262, no. 5569, pp. 615–617, 1976.
- [15] R. Zhang, J. Zhao, A. Mandveno, and J. D. Potter, "Cardiac troponin I phosphorylation increases the rate of cardiac muscle relaxation," *Circulation Research*, vol. 76, no. 6, pp. 1028–1035, 1995.
- [16] D. E. Michele, M. L. Szatkowski, F. P. Albayya, and J. M. Metzger, "Parvalbumin gene delivery improves diastolic function in the aged myocardium in vivo," *Molecular Therapy*, vol. 10, no. 2, pp. 399–403, 2004.
- [17] R. Zhang, J. Zhao, and J. D. Potter, "Phosphorylation of both serine residues in cardiac troponin I is required to decrease the Ca^{2+} affinity of cardiac troponin C," *Journal of Biological Chemistry*, vol. 270, no. 51, pp. 30773–30780, 1995.
- [18] B. Malnic, C. S. Farah, and F. C. Reinach, "Regulatory properties of the NH_2 - and COOH -terminal domains of troponin T: ATPase activation and binding to troponin I and troponin C," *Journal of Biological Chemistry*, vol. 273, no. 17, pp. 10594–10601, 1998.

- [19] J. R. Pearlstone and L. B. Smillie, "Effects of troponin-I plus-C on the binding of troponin-T and its fragments to α -tropomyosin. Ca^{2+} sensitivity and cooperativity," *Journal of Biological Chemistry*, vol. 258, no. 4, pp. 2534–2542, 1983.
- [20] S. P. White, C. Cohen, and G. N. Phillips Jr., "Structure of co-crystals of tropomyosin and troponin," *Nature*, vol. 325, no. 6107, pp. 826–828, 1987.
- [21] A. S. Zot and J. D. Potter, "Structural aspects of troponin-tropomyosin regulation of skeletal muscle contraction," *Annual Review of Biophysics and Biophysical Chemistry*, vol. 16, pp. 535–559, 1987.
- [22] R. Maytum, M. A. Geeves, and S. S. Lehrer, "A modulatory role for the troponin T tail domain in thin filament regulation," *Journal of Biological Chemistry*, vol. 277, no. 33, pp. 29774–29780, 2002.
- [23] L. S. Tobacman, "Structure-function studies of the amino-terminal region of bovine cardiac troponin T," *Journal of Biological Chemistry*, vol. 263, no. 6, pp. 2668–2672, 1988.
- [24] A. Hinkle, A. Goranson, C. A. Butters, and L. S. Tobacman, "Roles for the troponin tail domain in thin filament assembly and regulation: a deletional study of cardiac troponin T," *Journal of Biological Chemistry*, vol. 274, no. 11, pp. 7157–7164, 1999.
- [25] L. S. Tobacman, M. Nihli, C. Butters, et al., "The troponin tail domain promotes a conformational state of the thin filament that suppresses myosin activity," *Journal of Biological Chemistry*, vol. 277, no. 31, pp. 27636–27642, 2002.
- [26] X.-P. Huang and J.-F. Du, "Troponin I, cardiac diastolic dysfunction and restrictive cardiomyopathy," *Acta Pharmacologica Sinica*, vol. 25, no. 12, pp. 1569–1575, 2004.
- [27] S. E. Hughes and W. J. McKenna, "New insights into the pathology of inherited cardiomyopathy," *Heart*, vol. 91, no. 2, pp. 257–264, 2005.
- [28] A. Angelini, V. Calzolari, G. Thiene, et al., "Morphologic spectrum of primary restrictive cardiomyopathy," *American Journal of Cardiology*, vol. 80, no. 8, pp. 1046–1050, 1997.
- [29] S. S. Kushwaha, J. T. Fallon, and V. Fuster, "Restrictive cardiomyopathy," *The New England Journal of Medicine*, vol. 336, no. 4, pp. 267–276, 1997.
- [30] S. M. Rivenes, D. L. Kearney, E. O. Smith, J. A. Towbin, and S. W. Denfield, "Sudden death and cardiovascular collapse in children with restrictive cardiomyopathy," *Circulation*, vol. 102, no. 8, pp. 876–882, 2000.
- [31] S.-C. Chen, I. C. Balfour, and S. Jureidini, "Clinical spectrum of restrictive cardiomyopathy in children," *Journal of Heart and Lung Transplantation*, vol. 20, no. 1, pp. 90–92, 2001.
- [32] M. T. Kimberling, D. T. Balzer, R. Hirsch, E. Mendeloff, C. B. Huddleston, and C. E. Canter, "Cardiac transplantation for pediatric restrictive cardiomyopathy: presentation, evaluation, and short-term outcome," *Journal of Heart and Lung Transplantation*, vol. 21, no. 4, pp. 455–459, 2002.
- [33] S. B. Peddy, L. A. Vricella, J. E. Crosson, et al., "Infantile restrictive cardiomyopathy resulting from a mutation in the cardiac troponin T gene," *Pediatrics*, vol. 117, no. 5, pp. 1830–1833, 2006.
- [34] S. Feld and A. Caspi, "Familial cardiomyopathy with variable hypertrophic and restrictive features and common HLA haplotype," *Israel Journal of Medical Sciences*, vol. 28, no. 5, pp. 277–280, 1992.
- [35] J. Mogensen, T. Kubo, M. Duque, et al., "Idiopathic restrictive cardiomyopathy is part of the clinical expression of cardiac troponin I mutations," *Journal of Clinical Investigation*, vol. 111, no. 2, pp. 209–216, 2003.
- [36] A. Kostareva, A. Gudkova, G. Sjöberg, et al., "Deletion in TNNI3 gene is associated with restrictive cardiomyopathy," *International Journal of Cardiology*, vol. 131, no. 3, pp. 410–412, 2009.
- [37] J. P. Kaski, P. Syrris, M. Burch, et al., "Idiopathic restrictive cardiomyopathy in children is caused by mutations in cardiac sarcomere protein genes," *Heart*, vol. 94, no. 11, pp. 1478–1484, 2008.
- [38] J. R. Pinto, M. S. Parvatiyar, M. A. Jones, J. Liang, and J. D. Potter, "A troponin T mutation that causes infantile restrictive cardiomyopathy increases Ca^{2+} sensitivity of force development and impairs the inhibitory properties of troponin," *Journal of Biological Chemistry*, vol. 283, no. 4, pp. 2156–2166, 2008.
- [39] T. Kubo, J. R. Gimeno, A. Bahl, et al., "Prevalence, clinical significance, and genetic basis of hypertrophic cardiomyopathy with restrictive phenotype," *Journal of the American College of Cardiology*, vol. 49, no. 25, pp. 2419–2426, 2007.
- [40] F. Yumoto, Q.-W. Lu, S. Morimoto, et al., "Drastic Ca^{2+} sensitization of myofilament associated with a small structural change in troponin I in inherited restrictive cardiomyopathy," *Biochemical and Biophysical Research Communications*, vol. 338, no. 3, pp. 1519–1526, 2005.
- [41] A. V. Gomes, J. Liang, and J. D. Potter, "Mutations in human cardiac troponin I that are associated with restrictive cardiomyopathy affect basal ATPase activity and the calcium sensitivity of force development," *Journal of Biological Chemistry*, vol. 280, no. 35, pp. 30909–30915, 2005.
- [42] J. Davis, H. Wen, T. Edwards, and J. M. Metzger, "Allele and species dependent contractile defects by restrictive and hypertrophic cardiomyopathy-linked troponin I mutants," *Journal of Molecular and Cellular Cardiology*, vol. 44, no. 5, pp. 891–904, 2008.
- [43] Y. Wen, Y. Xu, Y. Wang, J. R. Pinto, J. D. Potter, and W. G. L. Kerrick, "Functional effects of a restrictive-cardiomyopathy-linked cardiac troponin I mutation (R145W) in transgenic mice," *Journal of Molecular Biology*, vol. 392, no. 5, pp. 1158–1167, 2009.
- [44] T. Kobayashi and R. J. Solaro, "Increased Ca^{2+} affinity of cardiac thin filaments reconstituted with cardiomyopathy-related mutant cardiac troponin I," *Journal of Biological Chemistry*, vol. 281, no. 19, pp. 13471–13477, 2006.
- [45] T. S. Rai, S. Ahmad, T. S. Ahluwalia, et al., "Genetic and clinical profile of Indian patients of idiopathic restrictive cardiomyopathy with and without hypertrophy," *Molecular and Cellular Biochemistry*, vol. 331, no. 1-2, pp. 187–192, 2009.
- [46] J. Davis, H. Wen, T. Edwards, and J. M. Metzger, "Thin filament disinhibition by restrictive cardiomyopathy mutant R193H troponin I induces Ca^{2+} -independent mechanical tone and acute myocyte remodeling," *Circulation Research*, vol. 100, no. 10, pp. 1494–1502, 2007.
- [47] F. I. Gambarin, M. Tagliani, and E. Arbustini, "Pure restrictive cardiomyopathy associated with cardiac troponin I gene mutation: mismatch between the lack of hypertrophy and the presence of disarray," *Heart*, vol. 94, no. 10, p. 1257, 2008.
- [48] J.-F. Forissier, P. Richard, S. Briault, et al., "First description of germline mosaicism in familial hypertrophic cardiomyopathy," *Journal of Medical Genetics*, vol. 37, no. 2, pp. 132–134, 2000.
- [49] H. Watkins, L. Thierfelder, D.-S. Hwang, W. McKenna, J. G. Seidman, and C. E. Seidman, "Sporadic hypertrophic cardiomyopathy due to de novo myosin mutations," *Journal of Clinical Investigation*, vol. 90, no. 5, pp. 1666–1671, 1992.

- [50] S. Karam, M.-J. Raboisson, C. Ducreux, et al., "A de novo mutation of the beta cardiac myosin heavy chain gene in an infantile restrictive cardiomyopathy," *Congenital Heart Disease*, vol. 3, no. 2, pp. 138–143, 2008.
- [51] S. C. Menon, V. V. Michels, P. A. Pellikka, et al., "Cardiac troponin T mutation in familial cardiomyopathy with variable remodeling and restrictive physiology," *Clinical Genetics*, vol. 74, no. 5, pp. 445–454, 2008.
- [52] H. Watkins, W. J. McKenna, L. Thierfelder, et al., "Mutations in the genes for cardiac troponin T and α -tropomyosin in hypertrophic cardiomyopathy," *The New England Journal of Medicine*, vol. 332, no. 16, pp. 1058–1064, 1995.
- [53] A. M. Varnava, P. M. Elliott, C. Baboonian, F. Davison, M. J. Davies, and W. J. McKenna, "Hypertrophic cardiomyopathy: histopathological features of sudden death in cardiac troponin T disease," *Circulation*, vol. 104, no. 12, pp. 1380–1384, 2001.
- [54] E. M. Rust, F. P. Albayya, and J. M. Metzger, "Identification of a contractile deficit in adult cardiac myocytes expressing hypertrophic cardiomyopathy-associated mutant troponin T proteins," *Journal of Clinical Investigation*, vol. 103, no. 10, pp. 1459–1467, 1999.
- [55] T. Miller, D. Szczesna, P. R. Housmans, et al., "Abnormal contractile function in transgenic mice expressing a familial hypertrophic cardiomyopathy-linked troponin T (I79N) mutation," *Journal of Biological Chemistry*, vol. 276, no. 6, pp. 3743–3755, 2001.
- [56] D. Westermann, B. C. Knollmann, P. Steendijk, et al., "Diltiazem treatment prevents diastolic heart failure in mice with familial hypertrophic cardiomyopathy," *European Journal of Heart Failure*, vol. 8, no. 2, pp. 115–121, 2006.
- [57] Y. Wen, J. R. Pinto, A. V. Gomes, et al., "Functional consequences of the human cardiac troponin I hypertrophic cardiomyopathy mutation R145G in transgenic mice," *Journal of Biological Chemistry*, vol. 283, no. 29, pp. 20484–20494, 2008.
- [58] D. S. Wood, M. M. Sorenson, A. B. Eastwood, W. E. Charash, and J. P. Reuben, "Duchenne dystrophy: abnormal generation of tension and Ca^{++} regulation in single skinned fibers," *Neurology*, vol. 28, no. 5, pp. 447–457, 1978.
- [59] D. S. Wood, J. Zollman, J. P. Reuben, and P. W. Brandt, "Human skeletal muscle: properties of the 'chemically skinned' fiber," *Science*, vol. 187, no. 4181, pp. 1075–1076, 1975.
- [60] J. Mogensen and E. Arbustini, "Restrictive cardiomyopathy," *Current Opinion in Cardiology*, vol. 24, no. 3, pp. 214–220, 2009.
- [61] N. M. Ammash, J. B. Seward, K. R. Bailey, W. D. Edwards, and A. J. Tajik, "Clinical profile and outcome of idiopathic restrictive cardiomyopathy," *Circulation*, vol. 101, no. 21, pp. 2490–2496, 2000.
- [62] J. Du, C. Zhang, J. Liu, C. Sidky, and X. P. Huang, "A point mutation (R192H) in the C-terminus of human cardiac troponin I causes diastolic dysfunction in transgenic mice," *Archives of Biochemistry and Biophysics*, vol. 456, no. 2, pp. 143–150, 2006.
- [63] J. Du, J. Liu, H.-Z. Feng, et al., "Impaired relaxation is the main manifestation in transgenic mice expressing a restrictive cardiomyopathy mutation, R193H, in cardiac TnI," *American Journal of Physiology*, vol. 294, no. 6, pp. H2604–H2613, 2008.
- [64] A. M. Murphy, L. Jones II, H. F. Sims, and A. W. Strauss, "Molecular cloning of rat cardiac troponin I and analysis of troponin I isoform expression in developing rat heart," *Biochemistry*, vol. 30, no. 3, pp. 707–712, 1997.
- [65] J. M. Metzger, D. E. Michele, E. M. Rust, A. R. Borton, and M. V. Westfall, "Sarcomere thin filament regulatory isoforms: evidence of a dominant effect of slow skeletal troponin I on cardiac contraction," *Journal of Biological Chemistry*, vol. 278, no. 15, pp. 13118–13123, 2003.
- [66] S. V. Perry, "Troponin T: genetics, properties and function," *Journal of Muscle Research and Cell Motility*, vol. 19, no. 6, pp. 575–602, 1998.
- [67] L. S. Tobacman and R. Lee, "Isolation and functional comparison of bovine cardiac troponin T isoforms," *Journal of Biological Chemistry*, vol. 262, no. 9, pp. 4059–4064, 1987.
- [68] A. V. Gomes, G. Guzman, J. Zhao, and J. D. Potter, "Cardiac troponin T isoforms affect the Ca^{2+} sensitivity and inhibition of force development: insights into the role of troponin T isoforms in the heart," *Journal of Biological Chemistry*, vol. 277, no. 38, pp. 35341–35349, 2002.

Review Article

The Functional Role of Calcineurin in Hypertrophy, Regeneration, and Disorders of Skeletal Muscle

Kunihiro Sakuma¹ and Akihiko Yamaguchi²

¹ *Research Center for Physical Fitness, Sports and Health, Toyohashi University of Technology, 1-1 Hibarigaoka, Tenpaku-cho, Toyohashi 441-8580, Japan*

² *School of Dentistry, Health Sciences University of Hokkaido, Kanazawa, Ishikari-Tobetsu, Hokkaido 061-0293, Japan*

Correspondence should be addressed to Kunihiro Sakuma, ksakuma@las.tut.ac.jp

Received 30 October 2009; Accepted 9 February 2010

Academic Editor: Henk L. M. Granzier

Copyright © 2010 K. Sakuma and A. Yamaguchi. This is an open access article distributed under the Creative Commons Attribution License, which permits unrestricted use, distribution, and reproduction in any medium, provided the original work is properly cited.

Skeletal muscle uses calcium as a second messenger to respond and adapt to environmental stimuli. Elevations in intracellular calcium levels activate calcineurin, a serine/threonine phosphatase, resulting in the expression of a set of genes involved in the maintenance, growth, and remodeling of skeletal muscle. In this review, we discuss the effects of calcineurin activity on hypertrophy, regeneration, and disorders of skeletal muscle. Calcineurin is a potent regulator of muscle remodeling, enhancing the differentiation through upregulation of myogenin or MEF2A and downregulation of the Id1 family and myostatin. Foxo may also be a downstream candidate for a calcineurin signaling molecule during muscle regeneration. The strategy of controlling the amount of calcineurin may be effective for the treatment of muscular disorders such as DMD, UCMD, and LGMD. Activation of calcineurin produces muscular hypertrophy of the slow-twitch soleus muscle but not fast-twitch muscles.

1. Introduction

Calcium serves as a second messenger in signal transduction pathways, using spatiotemporal patterns of intracellular calcium to generate oscillatory changes in calcium concentrations. It is well established that the elevations in intracellular calcium levels in skeletal muscle that are essential for contractile activity also give rise to muscle-specific gene expression through downstream transcriptional pathways [1, 2]. Changes in intracellular Ca^{2+} concentrations regulate the physiological activities of calmodulin. Calmodulin is a multifunctional signal transducer that undergoes conformational changes before activating a wide range of binding substrates, mainly downstream phosphatases (calcineurin) and kinases (CaMKs) [3]. The serine/threonine phosphatase calcineurin plays a major role in a variety of physiological and pathological processes, including immune responses, neuronal plasticity, and cardiac development and hypertrophy [4]. For example, transgenic mice overexpressing calcineurinA developed a profound hypertrophic responses

and heart failure that mimicked human heart disease [5]. Bueno et al. [6] demonstrated that calcineurin $A\beta$ null mice showed a reduced basal heart size. In addition, the absence of NFATc2 (the nuclear factor of activated T cells c2) has been shown to inhibit pathological (biomechanical stress) but not physiological (voluntary exercise training) cardiac enlargement [7]. Although the downstream pathway of calcineurin is not completely clear [8], calcineurin signaling seems to play an important role in cardiac muscle. Many excellent reviews [8, 9] have indicated a central role for calcineurin signaling in determining fiber types and myosin heavy chain (MHC) (IIB \rightarrow IID \rightarrow IIA \rightarrow I). However, few systematic and descriptive reviews have dealt with the role of calcineurin in regulating the hypertrophy and regeneration of skeletal muscle in mature mammals. This review aims to outline the functional role of calcineurin in the hypertrophy and regeneration of skeletal muscle. In addition, it discusses the present situation and future therapeutic applications for modulating calcineurin levels to alleviate muscular disorders.

2. Structure of Calcineurin

Calcineurin enzymatic activity requires a catalytic subunit (CnA, 59 to 62 kDa) and a calcium-binding regulatory subunit (CnB, 19 kDa), which comprise several isoforms coded by different genes or generated by alternative splicing. The CnA subunit includes domains for catalytic activity, CnB interaction, and calmodulin-binding. A C-terminal autoinhibitory domain, which blocks the catalytic site, is removed in response to an increase in calcium. Three calcineurin genes have been described; *cN α* and *CnA β* expressed ubiquitously, and *CnA γ* restricted to brain and testis. Two *CnA β* isoforms, *CnA β 1* and *CnA β 2*, which differ in their C-terminal domain, are encoded by alternatively spliced transcripts [10]. The typical autoinhibitory domain present in *CnA β 2* and other calcineurin isoforms is absent from *CnA β 1*, in which an unrelated C-terminal domain is generated by the translation of intronic sequences [11]. This novel domain is preserved in *CnA β 1* orthologues from different species [11], especially in higher vertebrates, suggesting an evolutionarily conserved role for this calcineurin variant. When activated by Ca^{2+} -calmodulin binding, calcineurin affects gene expression by dephosphorylating specific substrates, including the four calcineurin-dependent members of NFAT gene family, NFATc1, NFATc2, NFATc3, and NFATc4. Following dephosphorylation, NFAT translocates from the cytoplasm to the nucleus and activates target genes in cooperation with other transcription factors [12]. Calcineurin activity and the ability to activate NFAT are directly antagonized by the immunosuppressive agents FK 506 and cyclosporine A (CsA) through complexes with cyclophilins and FK506-binding proteins, respectively [13, 14], or by endogenous protein inhibitors, such as cain (also known as cabin-1) and MCIP-1 (myocyte-enriched calcineurin interacting protein 1), the latter being particularly abundant in slow-twitch muscle but not detectable in fast-twitch glycolytic muscles [15, 16]. More recently, reporter assays using cultured myoblasts indicated that the transcriptional activation of NFAT by calcineurin was also inhibited by calsarcin-2 [17].

3. Muscle Regeneration

Skeletal muscle satellite cells are generally in a quiescent state in adult muscle, but when minor damage or injury occurs, signals are generated within the muscle that activate these satellite cells, stimulating them to migrate to the site of an injury where they proliferate, differentiate, and fuse with the damaged fibers or form new fibers [18, 19]. Studies in vitro have documented many factors, primarily protein growth factors, which can modulate satellite cell activity [18, 19]. In particular, insulin-like growth factor I (IGF-I), whose expression is known to be upregulated in regenerating muscle in vivo [20], positively regulated the proliferation and differentiation of satellite cells/myoblasts in vitro via different pathways. Calcineurin is a major candidate for a component in the pathway downstream of IGF-I as well as Akt. In fact, the inhibition of calcineurin completely blocked the growth of myotubes on treatment with IGF-I in vitro [21]. Local expression of IGF-I in muscle protected both motor

neurons and innervating muscle fibers in a mouse model of amyotrophic lateral sclerosis (the SOD1^{G93A} transgenic mouse) possibly due to the enhancement of CnA β 1 [22]. Since activated calcineurin promotes the transcription and activation of myocyte enhance factor 2 (MEF2), myogenin, and MyoD [23–25], calcineurin seems to control satellite cell differentiation and myofiber growth and maturation, all of which are involved in muscle regeneration. In fact, our previous Western blot analysis [26] showed a long-term (1–14 days post bupivacaine injection) increase in the amount of calcineurin protein in the regenerating muscle of adult rats. Immunofluorescence microscopy revealed marked immunolabeling of calcineurin in many myoblasts and myotubes that expressed MyoD and myogenin at an active differentiation phase (4–6 days post injection). In addition, our biochemical approach demonstrated that the amount of calcineurin coprecipitating with NFATc1 and GATA-2 and NFATc1 coprecipitating with GATA-2 gradually increased in the regenerating muscle. Furthermore, we showed that the inhibition of calcineurin by CsA induced extensive inflammation, marked fiber atrophy, the appearance of immature myotubes, and calcification in the regenerating muscle compared with placebo-treated mice [26]. Several other studies indicated such defects in skeletal muscle when calcineurin was inhibited [27, 28], whereas transgenic activation of calcineurin is known to markedly promote the remodeling of muscle fibers after damage [11, 29].

Myostatin is a member of the transforming growth factor- β (TGF- β) family that negatively regulates skeletal muscle growth, with its inhibition shown to enhance muscle size. Mice, which are null for (knock-out) or display inactivating mutations of myostatin, exhibit obvious skeletal muscle hyperplasia and hypertrophy [30, 31]. Recent evidence [32–34] has also identified myostatin as well as Id1 [22], Id3 [22], and Egr-1 [25] as a possible downstream negative hypertrophic effector target of the calcineurin-NFAT pathway. In addition, using a pharmacological approach (intraperitoneal CsA treatment), our recent study [35] demonstrated that the inhibition of calcineurin enhanced the expression of myostatin and Smad3 mRNA in regeneration-defective TA muscle after an injection of bupivacaine. An increase in myostatin levels is closely linked with muscle atrophy after unloading in mice and humans [36–38] and with severe muscle wasting in HIV patients [39]. Myostatin has been shown to interact with Smad2 and Smad3 [40, 41], and the activation of the myostatin pathway inhibits myogenic differentiation through a downregulation of MyoD expression [40, 41]. The possibility that myostatin is a downstream mediator of calcineurin signaling has been indicated by recent experiments with two different transgenic mice [42]. Muthuri et al. [42] found that myostatin mRNA levels in skeletal muscle were significantly lower in mice expressing high levels of calcineurin and significantly higher in mice displaying inhibited calcineurin signals. Moreover, levels of calcineurin mRNA were higher in null myostatin transgenic mice than wild-type mice [42]. On the other hand, using MCK-CnA α transgenic mice, Stupka et al. [29] demonstrated that calcineurin activates two differentiation-enhancing molecules, myogenin, and MEF2A, during muscle

regeneration. Indeed, calcineurins pharmacological inhibition caused a decline in the transcription and activation of MEF2, myogenin and MyoD during myogenic differentiation *in vitro* [23–25]. However, the notion that muscle regeneration is promoted by a myogenic transgene with CnA α is controversial [11, 29]. A more recent study using a similar mouse model found that transgenic expression of CnA α excessively stimulated the inflammatory response after muscle damage and prevented prompt muscle regeneration [11].

The induction of MAFbx/Atrogin-1 expression by Foxo has been shown to inhibit calcineurin activity [43, 44]. More recently, the calcineurin variant CnA β 1 was suggested to block the nuclear localization of Foxo protein and the expression of several Foxo-targeted genes (MuRF1, Gadd45a, Pmaip1, and atrogin) in C2C12 myoblasts [11]. In addition, transgenic upregulation of CnA β 1 expression promoted the remodeling of cardiotoxin-treated damaged muscle fibers [11]. Foxo factors play a crucial role in skeletal muscle atrophy through the induction of MAFbx/Atrogin-1 and MuRF1 [45, 46]. Interaction between CnA β 1 and Foxo in muscle regeneration is an attractive notion, although it has not been demonstrated in adult skeletal muscle *in vivo*.

4. Muscle Hypertrophy

The major extracellular mediator of skeletal muscle hypertrophy is thought to be IGF-I which binds to its receptor to initiate a cascade of signaling pathways via phosphoinositide 3-kinase (PI3-K/Akt/mammalian target of rapamycin (mTOR)) [47–49]. However, several lines of evidence suggest that IGF-I also mediates hypertrophy through calcineurin/NFAT signaling pathways. Overexpression of IGF-I in murine C2C12 myoblasts [21] and rat L6MLC cells [50] induced hypertrophy of myotubes, which was abolished by treating the cells with CsA. Dunn et al. [51] proposed that calcineurin signaling regulates the hypertrophy of muscle fiber in mature rats. They concluded that the enlargement of fibers in the plantaris muscle after mechanical overloading was completely blocked at both 2 and 4 weeks post surgery by subcutaneous treatment with CsA at 25 mg/Kg twice per day. However, several lines of evidence exclude a functional role for calcineurin in the hypertrophy of muscle fiber *in vivo* [52–55]. For example, different to the positive effect of rapamycin, the calcineurin inhibitors CsA and FK506 for up to 30 days did not block the hypertrophy of plantaris muscle that followed surgical removal of the soleus, medial, and lateral gastrocnemius muscles in the rat [53]. Consistent with these findings, others have demonstrated that even a tenfold increase in the expression of activated calcineurin in transgenic mice did not induce muscle hypertrophy [53] in spite of an increase in the proportion of slow muscle fibers due to the influence of CnA. In addition, Parsons et al. [54] indicated that neither CnA α nor CnA β null mice showed any growth-related alterations in skeletal muscle, and fiber size or number was not altered in glycolytic/fast muscle types (tibialis anterior, gastrocnemius, quadriceps, etc). Furthermore, no change in the size of several fast-type

muscles has been observed in mice with a transgenic upregulation of calcineurin [56], although a transgenic mouse with a constitutively active form of Akt exhibited rapid and significant hypertrophy of fast-type muscles [57]. However, Talmadge et al. [56] also demonstrated that overexpression of calcineurin induced marked hypertrophy of slow- and fast-twitch fibers of the slow-type soleus muscle. In addition, fiber size in the soleus muscle was markedly reduced by a null mutation of CnA β different to CnA α [54]. Muscle-specific overexpression of MCIP1, an inhibitor of calcineurin, using the Flox-On approach resulted in a marked reduction (about 30%) in cross-sectional area of the soleus muscle [58]. Moreover, our recent study [59] using ICR mice did not detect any apparent hypertrophy of fibers in the soleus muscle after mechanical overloading on treatment with CsA. Other researchers also suggest growth-retarded effects in the soleus muscle caused by calcineurins inhibition during recovery from hindlimb unloading [60–62]. These lines of evidence seem to indicate a selective influence of calcineurin or Akt on the size of antigravity/slow-type soleus and fast-type muscles, respectively. Table 1 shows an overview of the effect of calcineurin activation or inhibition on fiber growth (hypertrophy) of skeletal muscle *in vivo*.

Although calcineurin activity appears critical to mediating the hypertrophy of slow-type muscle, the downstream effector genes or targets in this process have yet to be clearly defined. Various downstream mediators of calcineurin-dependent signaling have been proposed [34], including NFAT and MEF2 proteins as well as GATA transcription factors. These factors are known to costimulate the transcriptional response of certain hypertrophic marker genes in the heart [63, 64] and affect IGF-I-related growth of skeletal myocytes *in vitro* [50]. GATA-2 expression is upregulated [65] and NFAT more extensively dephosphorylated [63] in hypertrophying fast-type plantaris muscle *in vivo*. In addition, mice with targeted inactivation of NFATc2 or NFATc3 exhibited reduced muscle size as well as fiber type abnormalities [66] or defects in muscle formation [67], respectively. Cultured C2C12 murine myoblasts expressing activated calcineurin showed increased enzymatic activity in association with NFATc3's nuclear translocation during the initiation of myogenic differentiation [23]. Given these findings, NFAT and GATA seem to play an important role in the normal growth and hypertrophy of skeletal muscle. Therefore, NFAT-GATA complexes may be mediators of calcineurin signaling during the hypertrophic process in soleus muscle. In contrast, a more recent study in our laboratory [58] suggested that MEF2C, not MEF2D or myogenin, regulates the hypertrophic process in slow-twitch soleus muscle subjected to mechanical overloading (MOV). Hypertrophy-defect soleus muscle after mechanical overloading by calcineurin inhibition contained less MEF2C protein than a placebo-treated control. In addition, this growth-failed soleus muscle showed less extensive immunoreactivity to MEF2C in the subsarcolemmal region in a group of myotubes and/or myofibers during an active-differentiation period (4 days postsurgery) [59]. Two recent findings [68, 69] clearly showed that MEF2C is required for thick filaments to form in nascent muscle fibers and for the integrity of

TABLE 1: Effect of calcineurin activation or inhibition on fiber growth (hypertrophy) of skeletal muscle in vivo.

References	Species	Experimental system	Modulating method of calcineurin activity	Outcomes
Dunn et al. 1999 [51]	Mouse	Mechanical overloading	Pharmacological inhibition for 4 weeks (CsA; 25 mg/Kg twice daily)	Inhibition of fiber hypertrophy of the plantaris muscle
Bodine et al. 2001 [53]	Mouse	Mechanical overloading	Pharmacological inhibition for 30 days (CsA; 15 mg/Kg once daily)	No inhibition of fiber hypertrophy of the plantaris muscle
Sakuma et al. 2008 [59]	Mouse	Mechanical overloading	Pharmacological inhibition for 2 weeks (CsA; 25 mg/Kg once daily)	Inhibition of fiber hypertrophy of the soleus muscle
Parsons et al. 2003 [54]	Mouse		Gene-knock out (complete inactivation of $cna \alpha$ or $cna \beta$)	Slow-twitch soleus muscle; hypertrophy ($cna \alpha$ KO), atrophy ($cna \beta$ KO), Several fast-twitch muscles (gastrocnemius, tibialis anterior, triceps brachii); no change (both $cna \alpha$ and $cna \beta$ KO)
Talmadge et al. 2004 [56]	Mouse		Transgenic manipulation (high-level expression of a constitutively active form of calcineurin)	Slow-twitch soleus muscle; marked hypertrophy Several fast-twitch muscles (extensor digitorum longus, tibialis anterior, plantaris); no change
Oh et al. 2006 [58]	Mouse		(Transgenic manipulation (FloX-On approach), upregulation of calcineurin inhibitor (MCIP1))	Atrophy of the soleus muscle
Mitchell et al. 2002 [60]	Mouse	Reloading after hindlimb suspension	Pharmacological inhibition for 2 weeks (CsA; 12.5, 25, and 50 mg/Kg once daily)	Inhibition of fiber growth (recovery) of both the soleus (25 and 50 mg/Kg) and plantaris (12.5, 25, and 50 mg/Kg) muscles
Miyazaki et al. 2006 [61]	Mouse	Reloading after hindlimb suspension	Pharmacological inhibition for 4 weeks (FK506; 3–5 mg/Kg once daily)	Inhibition of fiber growth (recovery) of the soleus muscle
Oishi et al. 2008 [62]	Rat	Reloading after hindlimb suspension	Pharmacological inhibition for 2 weeks (CsA; 25 mg/Kg twice daily)	Inhibition of fiber growth (recovery) of the soleus muscle

the sarcomere and M-line during postnatal muscle growth, by directly regulating several muscle structural genes such as the genes for myomesin, MHC, and myosin light chain. Further study will be required to identify downstream modulators of calcineurin signaling during hypertrophy of slow-twitch soleus muscle. Figure 1 provides an overview of molecular pathway of calcineurin to regulate hypertrophy and regeneration of skeletal muscle.

5. The Ameliorating Role of Calcineurin in Muscular Disorders

Calcineurin signaling is considered to regulate the degenerative symptoms of various muscular disorders [74–84]. In animal models, pharmacological inhibition of calcineurin in regenerating muscles of young mdx dystrophic mice,

a model of DMD, severely compromised muscle structure and function [76]. Moreover, transgenic mice overexpressing the activated form of CnA have been used to determine whether signaling through CnA improves the dystrophic pathology due to alterations in the expression of utrophin A, a therapeutically relevant protein that can compensate for the lack of dystrophin, and improved muscle membrane integrity [75]. Breeding CnA transgenic mice with mdx counterparts led to offspring (mdx-CnA) with both genes altered in their skeletal muscle, but displaying a marked improvement in the dystrophic phenotype. Muscles from transgenic mdx-CnA mice showed improvements in various markers of muscle damage, including a decrease in central nucleation (indicating denervation or fiber regeneration), a decrease of variation in fiber size, a decrease in the intracellular presence of immunoglobulin M (a marker of

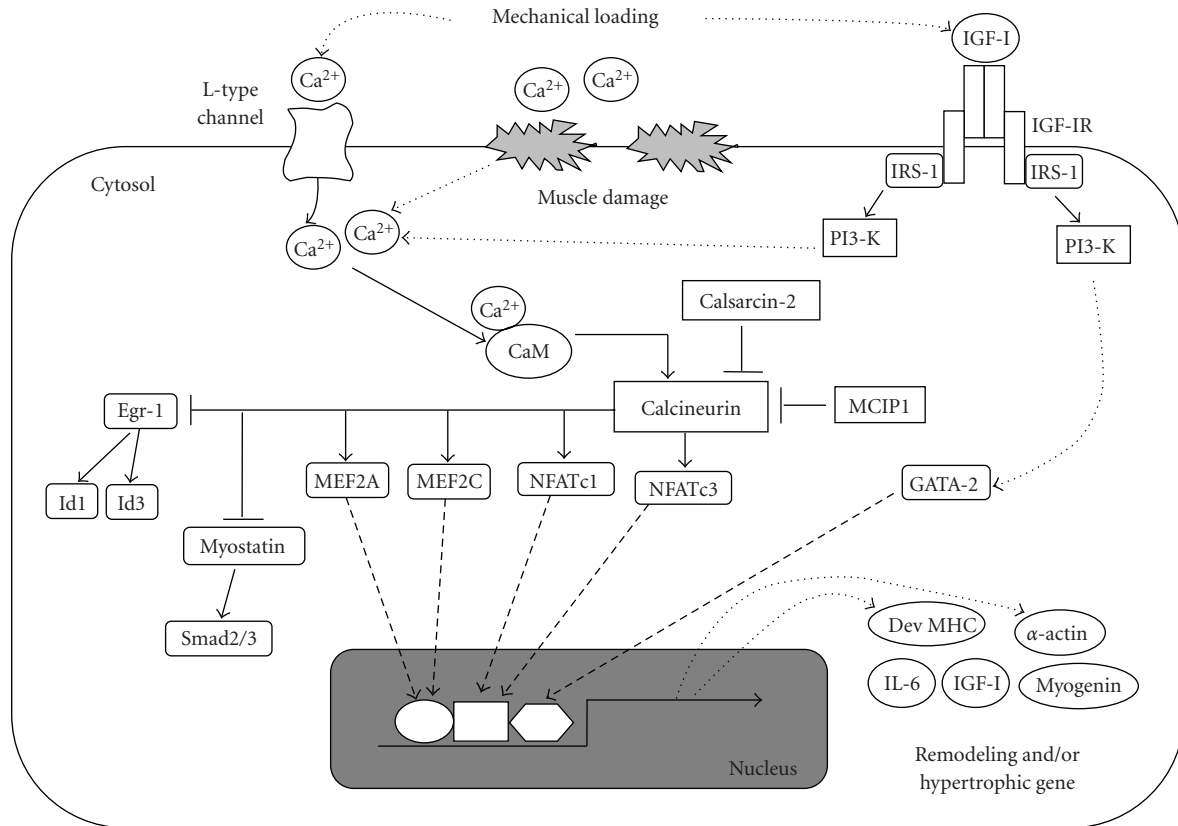


FIGURE 1: Schematic diagram of calcineurin signaling to regulate hypertrophy and regeneration of skeletal muscle. Mechanical loading of skeletal muscle increase intracellular Ca^{2+} levels via the influx (L-type Ca^{2+} channel) of Ca^{2+} from the extracellular space and its efflux from the sarcoplasmic reticulum. The damage of muscle fiber membrane after treatment with myotoxin also elicits an increase in intracellular Ca^{2+} levels via the influx of Ca^{2+} from the extracellular space. Binding of the Ca^{2+} /CaM complex to the calcineurin regulatory subunit led to its activation. Activated calcineurin dephosphorylates NFATc1 [26, 65, 70], NFATc3 [23], MEF2C [59], and MEF2A [29, 70] resulting in their translocation from the cytoplasm to the nucleus. These transcription factors induce the expression of hypertrophic and/or remodeling genes such as Dev MHC [29], α -actin, IGF-I [71], myogenin [25], and IL-6 [72]. In addition, activated calcineurin inhibits the functional role of Egr-1 [25] and myostatin [32–34]. Mechanical overloading upregulates gene expression of IGF-I. IGF-I modulates calcineurin signaling via increasing intracellular Ca^{2+} levels [25] and activating GATA-2 [50, 73]. MCIP1 [58] and calsarcin-2 [17] are potent inhibitors of calcineurin signaling. MEF2A: Myocyte enhancer factor 2A; NFATc1: nuclear factor of activated T cells c1; MCIP1: Modulatory calcineurin-interacting protein 1; IRS-1: Insulin receptor substrate-1; PI3-K: Phosphatidylinositol 3-kinase; CaM: Calmodulin; Dev MHC: Developmental myosin heavy chain; IL-6: Interleukin-6.

sarcolemmal integrity), a decrease in the uptake of Evans blue dye by muscle fibers *in vivo* (indicating sarcolemmal microdamage), and a decrease in numbers of infiltrating immune cells revealed by Mac-1 antibody staining (a marker of an inflammatory response) [75]. Thus, an attenuation of the muscle pathology-associated dystrophin deficiency is observed when utrophin A is upregulated via activation of CnA-NFAT signaling. In fact, Chakkalakal et al. [74] showed that calcineurin/NFATc1 signaling as well as peroxisome proliferator γ co-activator-1 α (PGC-1 α)/GA-binding protein (GABP α) [77] can stimulate the transcriptional activity of utrophin A. Subsequent similar crossbreeding experiments by others [81, 83], leading to mdx-CnA mice with potentiated CnA-NFAT activation, showed related improvements in the contractile function and attenuation of contractile-induced injury in muscles from these animals compared with mdx counterparts.

On the other hand, transgenic upregulation of the CaM-binding protein (CaMBP), a small peptide inhibitor for calmodulin, exacerbated the dystrophic phenotype in mdx mouse muscle. mdx/CaMBP mice revealed an impairment of both the Ca^{2+} /CaM-regulated enzyme calcineurin and a Ca^{2+} /calmodulin-dependent kinase [78]. These mice exhibited significant reductions in utrophin A attributable to the marked decrease in nuclear accumulated NFATc1 and MEF2C and in CABP α mRNA expression. In contrast, pharmacological and genetic inhibition of calcineurin signaling was suggested to be effective in a mouse model and in patients with several other muscular disorders such as limb-girdle muscular dystrophy (LGMD), Ullrich congenital muscular dystrophy (UCMD), and collagen VI myopathies [81, 82, 84]. For example, in an open pilot trial, oral CsA treatment for 1 month markedly ameliorated mitochondrial dysfunction and reduced the frequency of apoptotic nuclei

in muscle fibers in patients with collagen VI myopathies [84]. In addition, genetic deletion of the loxP-targeted calcineurin B1 or CnA β gene resulted in enlarged muscle fibers and decreases in the frequency of centrally nucleated fibers and of fibrosis, and in the amount of hydroxyproline in scgd $-/-$ mice [82]. These findings clearly showed that inhibition of calcineurin signaling reduced skeletal muscle degeneration and the histopathology of LGMD. Since the therapeutic effectiveness of the pharmacological attenuation or activation of calcineurin signaling differs entirely among muscular disorders, careful attention should be paid to this application.

6. Conclusions

This review summarised and highlighted current understanding of the role of calcineurin in the regulation of hypertrophy, regeneration, and disorders of skeletal muscle. Although several lines of evidence exclude a functional role for calcineurin in the hypertrophy of muscle fiber in vivo, recent findings have suggested that the hypertrophy of slow-twitch soleus muscle is regulated by calcineurin signaling. A possible downstream modulator of the calcineurin pathway during muscle regeneration may be MEF2A, myostatin, or Foxo. The strategy of controlling the amount of calcineurin may be effective in the future treatment of muscular disorders.

Acknowledgment

This work was supported by a research Grant-in-Aid for Scientific Research C (no. 20500575) from the Ministry of Education, Science, Culture, Sports, Science and Technology of Japan.

References

- [1] D. Pette and R. S. Staron, "Cellular and molecular diversities of mammalian skeletal muscle fibers," *Reviews of Physiology Biochemistry and Pharmacology*, vol. 116, pp. 1–76, 1990.
- [2] M. W. Berchtold, H. Brinkmeier, and M. Muntener, "Calcium ion in skeletal muscle: Its crucial role for muscle function, plasticity, and disease," *Physiological Reviews*, vol. 80, no. 3, pp. 1215–1265, 2000.
- [3] M. B. Swindells and M. Ikura, "Pre-formation of the semi-open conformation by the apo-calmodulin C-terminal domain and implications for binding IQ-motifs," *Nature Structural Biology*, vol. 3, no. 6, pp. 501–504, 1996.
- [4] R. A. Schulz and K. E. Yutzey, "Calcineurin signaling and NFAT activation in cardiovascular and skeletal muscle development," *Developmental Biology*, vol. 266, no. 1, pp. 1–16, 2004.
- [5] J. D. Molkentin, J.-R. Lu, C. L. Antos, et al., "A calcineurin-dependent transcriptional pathway for cardiac hypertrophy," *Cell*, vol. 93, no. 2, pp. 215–228, 1998.
- [6] O. F. Bueno, B. J. Wilkins, K. M. Tymitz, et al., "Impaired cardiac hypertrophic response in calcineurin A β -deficient mice," *Proceedings of the National Academy of Sciences of the United States of America*, vol. 99, no. 7, pp. 4586–4591, 2002.
- [7] M. Bourajjaj, A.-S. Armand, P. A. da Costa Martins, et al., "NFATc2 is a necessary mediator of calcineurin-dependent cardiac hypertrophy and heart failure," *Journal of Biological Chemistry*, vol. 283, no. 32, pp. 22295–22303, 2008.
- [8] J. Mallinson, J. Meissner, and K. C. Chang, "Chapter 2. Calcineurin signaling and the slow oxidative skeletal muscle fiber type," *International Review of Cell and Molecular Biology*, vol. 277, pp. 67–101, 2009.
- [9] S. Schiaffino, M. Sandri, and M. Murgia, "Activity-dependent signaling pathways controlling muscle diversity and plasticity," *Physiology*, vol. 22, no. 4, pp. 269–278, 2007.
- [10] D. Guerini and C. B. Klee, "Cloning of human calcineurin A: evidence for two isozymes and identification of a polyproline structural domain," *Proceedings of the National Academy of Sciences of the United States of America*, vol. 86, no. 23, pp. 9183–9187, 1989.
- [11] E. Lara-Pezzi, N. Winn, A. Paul, et al., "A naturally occurring calcineurin variant inhibits FoxO activity and enhances skeletal muscle regeneration," *Journal of Cell Biology*, vol. 179, no. 6, pp. 1205–1218, 2007.
- [12] G. R. Crabtree and E. N. Olson, "NFAT signaling: choreographing the social lives of cells," *Cell*, vol. 109, no. 2, supplement 1, pp. S67–S79, 2002.
- [13] G. R. Crabtree, "Generic signals and specific outcomes: signaling through Ca $^{2+}$, calcineurin, and NF-AT," *Cell*, vol. 96, no. 5, pp. 611–614, 1999.
- [14] F. Rusnak and P. Mertz, "Calcineurin: form and function," *Physiological Reviews*, vol. 80, no. 4, pp. 1483–1521, 2000.
- [15] R. B. Vega, B. A. Rothermel, C. J. Weinheimer, et al., "Dual roles of modulatory calcineurin-interacting protein 1 in cardiac hypertrophy," *Proceedings of the National Academy of Sciences of the United States of America*, vol. 100, no. 2, pp. 669–674, 2003.
- [16] J. Yang, B. Rothermel, R. B. Vega, et al., "Independent signals control expression of the calcineurin inhibitory proteins MCIP1 and MCIP2 in striated muscles," *Circulation Research*, vol. 87, no. 12, pp. E61–E68, 2000.
- [17] N. Frey, D. Frank, S. Lippl, et al., "Calsarcin-2 deficiency increases exercise capacity in mice through calcineurin/NFAT activation," *Journal of Clinical Investigation*, vol. 118, no. 11, pp. 3598–3608, 2008.
- [18] R. Bischoff, "The satellite cell and muscle regeneration," in *Myology*, A. G. Engel and F. Armstrong, Eds., pp. 97–118, McGraw-Hill, New York, NY, USA, 1994.
- [19] T. J. Hawke and D. J. Garry, "Myogenic satellite cells: physiology to molecular biology," *Journal of Applied Physiology*, vol. 91, no. 2, pp. 534–551, 2001.
- [20] E. Jennische and G. L. Matejka, "IGF-I binding and IGF-I expression in regenerating muscle of normal and hypophysectomized rats," *Acta Physiologica Scandinavica*, vol. 146, no. 1, pp. 79–86, 1992.
- [21] C. Semsarian, M.-J. Wu, Y.-K. Ju, et al., "Skeletal muscle hypertrophy is mediated by a Ca $^{2+}$ -dependent calcineurin signalling pathway," *Nature*, vol. 400, no. 6744, pp. 576–581, 1999.
- [22] G. Dobrowolny, C. Giacinti, L. Pelosi, et al., "Muscle expression of a local Igf-1 isoform protects motor neurons in an ALS mouse model," *Journal of Cell Biology*, vol. 168, no. 2, pp. 193–199, 2005.
- [23] U. Delling, J. Tureckova, H. W. Lim, L. J. De Windt, P. Rotwein, and J. D. Molkentin, "A calcineurin-NFATc3-dependent pathway regulates skeletal muscle differentiation and slow myosin heavy-chain expression," *Molecular and Cellular Biology*, vol. 20, no. 17, pp. 6600–6611, 2000.

- [24] B. B. Friday, V. Horsley, and G. K. Pavlath, "Calcineurin activity is required for the initiation of skeletal muscle differentiation," *Journal of Cell Biology*, vol. 149, no. 3, pp. 657–666, 2000.
- [25] B. B. Friday, P. O. Mitchell, K. M. Kegley, and G. K. Pavlath, "Calcineurin initiates skeletal muscle differentiation by activating MEF2 and MyoD," *Differentiation*, vol. 71, no. 3, pp. 217–227, 2003.
- [26] K. Sakuma, J. Nishikawa, R. Nakao, et al., "Calcineurin is a potent regulator for skeletal muscle regeneration by association with NFATc1 and GATA-2," *Acta Neuropathologica*, vol. 105, no. 3, pp. 271–280, 2003.
- [27] K. L. Abbott, B. B. Friday, D. Thaloor, T. J. Murphy, and G. K. Pavlath, "Activation and cellular localization of the cyclosporine A-sensitive transcription factor NF-AT in skeletal muscle cells," *Molecular Biology of the Cell*, vol. 9, no. 10, pp. 2905–2916, 1998.
- [28] N. Koulmann, H. Sanchez, B. N'Guessan, et al., "The responsiveness of regenerated soleus muscle to pharmacological calcineurin inhibition," *Journal of Cellular Physiology*, vol. 208, no. 1, pp. 116–122, 2006.
- [29] N. Stupka, J. D. Schertzer, R. Bassel-Duby, E. N. Olson, and G. S. Lynch, "Calcineurin- $\text{A}\alpha$ activation enhances the structure and function of regenerating muscles after myotoxic injury," *American Journal of Physiology*, vol. 293, no. 2, pp. R686–R694, 2007.
- [30] L. Grobet, D. Pirottin, F. Farnir, et al., "Modulating skeletal muscle mass by postnatal, muscle-specific inactivation of the myostatin gene," *Genesis*, vol. 35, no. 4, pp. 227–238, 2003.
- [31] A. C. McPherron, A. M. Lawler, and S.-J. Lee, "Regulation of skeletal muscle mass in mice by a new TGF- β superfamily member," *Nature*, vol. 387, no. 6628, pp. 83–90, 1997.
- [32] K. Sakuma, R. Nakao, W. Aoi, et al., "Cyclosporin A treatment upregulates Id1 and Smad3 expression and delays skeletal muscle regeneration," *Acta Neuropathologica*, vol. 110, no. 3, pp. 269–280, 2005.
- [33] N. Al-Shanti and C. E. Stewart, " Ca^{2+} /calmodulin-dependent transcriptional pathways: potential mediators of skeletal muscle growth and development," *Biological Reviews*, vol. 84, no. 4, pp. 637–652, 2009.
- [34] R. N. Michel, S. E. Dunn, and E. R. Chin, "Calcineurin and skeletal muscle growth," *Proceedings of the Nutrition Society*, vol. 63, no. 2, pp. 341–349, 2004.
- [35] R. N. Michel, E. R. Chin, J. V. Chakkalakal, J. K. Eibl, and B. J. Jasmin, " Ca^{2+} /calmodulin-based signalling in the regulation of the muscle fibre phenotype and its therapeutic potential via modulation of utrophin A and myostatin expression," *Applied Physiology, Nutrition and Metabolism*, vol. 32, no. 5, pp. 921–929, 2007.
- [36] K. Sakuma, K. Watanabe, M. Sano, I. Uramoto, and T. Tot-suka, "Differential adaptation of growth and differentiation factor 8/myostatin, fibroblast growth factor 6 and leukemia inhibitory factor in overloaded, regenerating and denervated rat muscles," *Biochimica et Biophysica Acta*, vol. 1497, no. 1, pp. 77–88, 2000.
- [37] K. Sakuma, K. Watanabe, N. Hotta, et al., "The adaptive responses in several mediators linked with hypertrophy and atrophy of skeletal muscle after lower limb unloading in humans," *Acta Physiologica*, vol. 197, no. 2, pp. 151–159, 2009.
- [38] M. Wehling, B. Cai, and J. G. Tidball, "Modulation of myostatin expression during modified muscle use," *FASEB Journal*, vol. 14, no. 1, pp. 103–110, 2000.
- [39] N. F. Gonzalez-Cadavid, W. E. Taylor, K. Yarasheski, et al., "Organization of the human myostatin gene and expression in healthy men and HIV-infected men with muscle wasting," *Proceedings of the National Academy of Sciences of the United States of America*, vol. 95, no. 25, pp. 14938–14943, 1998.
- [40] D. L. Allen and T. G. Unterman, "Regulation of myostatin expression and myoblast differentiation by FoxO and SMAD transcription factors," *American Journal of Physiology*, vol. 292, no. 1, pp. C188–C199, 2007.
- [41] B. Langley, M. Thomas, A. Bishop, M. Sharma, S. Gilmour, and R. Kambadur, "Myostatin inhibits myoblast differentiation by down-regulating MyoD expression," *Journal of Biological Chemistry*, vol. 277, no. 51, pp. 49831–49840, 2002.
- [42] S. K. Muthuri, E. R. Chin, and R. N. Michel, "Myostatin as a putative downstream gene target of calcineurin signaling associated with muscle growth remodeling," *FASEB Journal*, vol. 21, p. 895.14, 2007.
- [43] H.-H. Li, V. Kedar, C. Zhang, et al., "Atrogin-1/muscle atrophy F-box inhibits calcineurin-dependent cardiac hypertrophy by participating in an SCF ubiquitin ligase complex," *Journal of Clinical Investigation*, vol. 114, no. 8, pp. 1058–1071, 2004.
- [44] Y. G. Ni, K. Berenji, N. Wang, et al., "Foxo transcription factors blunt cardiac hypertrophy by inhibiting calcineurin signaling," *Circulation*, vol. 114, no. 11, pp. 1159–1168, 2006.
- [45] M. Sandri, C. Sandri, A. Gilbert, et al., "Foxo transcription factors induce the atrophy-related ubiquitin ligase atrogin-1 and cause skeletal muscle atrophy," *Cell*, vol. 117, no. 3, pp. 399–412, 2004.
- [46] T. N. Stitt, D. Drujan, B. A. Clarke, et al., "The IGF-1/PI3K/Akt pathway prevents expression of muscle atrophy-induced ubiquitin ligases by inhibiting FOXO transcription factors," *Molecular Cell*, vol. 14, no. 3, pp. 395–403, 2004.
- [47] R. A. Frost and C. H. Lang, "Protein kinase B/Akt: a nexus of growth factor and cytokine signaling in determining muscle mass," *Journal of Applied Physiology*, vol. 103, no. 1, pp. 378–387, 2007.
- [48] D. J. Glass, "Skeletal muscle hypertrophy and atrophy signaling pathways," *International Journal of Biochemistry and Cell Biology*, vol. 37, no. 10, pp. 1974–1984, 2005.
- [49] C. Rommel, S. C. Bodine, B. A. Clarke, et al., "Mediation of IGF-1-induced skeletal myotube hypertrophy by PI(3)K/Akt/mTOR and PI(3)K/Akt/GSK3 pathways," *Nature Cell Biology*, vol. 3, no. 11, pp. 1009–1013, 2001.
- [50] A. Musaró, K. J. A. McCullagh, F. J. Naya, E. N. Olson, and N. Rosenthal, "IGF-1 induces skeletal myocyte hypertrophy through calcineurin in association with GATA-2 and NF-ATc1," *Nature*, vol. 400, no. 6744, pp. 581–585, 1999.
- [51] S. E. Dunn, J. L. Burns, and R. N. Michel, "Calcineurin is required for skeletal muscle hypertrophy," *Journal of Biological Chemistry*, vol. 274, no. 31, pp. 21908–21912, 1999.
- [52] F. J. Naya, B. Mercer, J. Shelton, J. A. Richardson, R. S. Williams, and E. N. Olson, "Stimulation of slow skeletal muscle fiber gene expression by calcineurin in vivo," *Journal of Biological Chemistry*, vol. 275, no. 7, pp. 4545–4548, 2000.
- [53] S. C. Bodine, T. N. Stitt, M. Gonzalez, et al., "Akt/mTOR pathway is a crucial regulator of skeletal muscle hypertrophy and can prevent muscle atrophy in vivo," *Nature Cell Biology*, vol. 3, no. 11, pp. 1014–1019, 2001.
- [54] S. A. Parsons, B. J. Wilkins, O. F. Bueno, and J. D. Molkentin, "Altered skeletal muscle phenotypes in calcineurin $\text{A}\alpha$ and $\text{A}\beta$ gene-targeted mice," *Molecular and Cellular Biology*, vol. 23, no. 12, pp. 4331–4343, 2003.
- [55] S. A. Parsons, D. P. Millay, B. J. Wilkins, et al., "Genetic loss of calcineurin blocks mechanical overload-induced skeletal muscle fiber type switching but not hypertrophy," *Journal of Biological Chemistry*, vol. 279, no. 25, pp. 26192–26200, 2004.

- [56] R. J. Talmadge, J. S. Otis, M. R. Rittler, et al., "Calcineurin activation influences muscle phenotype in a muscle-specific fashion," *BMC Cell Biology*, vol. 5, article 28, 2004.
- [57] K.-M. V. Lai, M. Gonzalez, W. T. Poueymirou, et al., "Conditional activation of Akt in adult skeletal muscle induces rapid hypertrophy," *Molecular and Cellular Biology*, vol. 24, no. 21, pp. 9295–9304, 2004.
- [58] M. Oh, I. I. Rybkin, V. Copeland, et al., "Calcineurin is necessary for the maintenance but not embryonic development of slow muscle fibers," *Molecular and Cellular Biology*, vol. 25, no. 15, pp. 6629–6638, 2005.
- [59] K. Sakuma, M. Akiho, H. Nakashima, et al., "Cyclosporin A modulates cellular localization of MEF2C protein and blocks fiber hypertrophy in the overloaded soleus muscle of mice," *Acta Neuropathologica*, vol. 115, no. 6, pp. 663–674, 2008.
- [60] P. O. Mitchell, S. T. Mills, and G. K. Pavlath, "Calcineurin differentially regulates maintenance and growth of phenotypically distinct muscles," *American Journal of Physiology*, vol. 282, no. 5, pp. C984–C992, 2002.
- [61] M. Miyazaki, Y. Hitomi, T. Kizaki, et al., "Calcineurin-mediated slow-type fiber expression and growth in reloading condition," *Medicine and Science in Sports and Exercise*, vol. 38, no. 6, pp. 1065–1072, 2006.
- [62] Y. Oishi, T. Ogata, K.-I. Yamamoto, et al., "Cellular adaptations in soleus muscle during recovery after hindlimb unloading," *Acta Physiologica*, vol. 192, no. 3, pp. 381–395, 2008.
- [63] J. D. Molkentin, J.-R. Lu, C. L. Antos, et al., "A calcineurin-dependent transcriptional pathway for cardiac hypertrophy," *Cell*, vol. 93, no. 2, pp. 215–228, 1998.
- [64] B. J. Wilkins and J. D. Molkentin, "Calcineurin and cardiac hypertrophy: where have we been? Where are we going?" *The Journal of Physiology*, vol. 541, no. 1, pp. 1–8, 2002.
- [65] S. E. Dunn, E. R. Chin, and R. N. Michel, "Matching of calcineurin activity to upstream effectors is critical for skeletal muscle fiber growth," *Journal of Cell Biology*, vol. 151, no. 3, pp. 663–672, 2000.
- [66] V. Horsley, B. B. Friday, S. Matteson, K. M. Kegley, J. Gephart, and G. K. Pavlath, "Regulation of the growth of multinucleated muscle cells by an NFATC2-dependent pathway," *Journal of Cell Biology*, vol. 153, no. 2, pp. 329–338, 2001.
- [67] K. M. Kegley, J. Gephart, G. L. Warren, and G. K. Pavlath, "Altered primary myogenesis in NFATC3^{-/-} mice leads to decreased muscle size in the adult," *Developmental Biology*, vol. 232, no. 1, pp. 115–126, 2001.
- [68] Y. Hinitz and S. M. Hughes, "Mef2s are required for thick filament formation in nascent muscle fibres," *Development*, vol. 134, no. 13, pp. 2511–2519, 2007.
- [69] M. J. Potthoff, M. A. Arnold, J. McAnally, J. A. Richardson, R. Bassel-Duby, and E. N. Olson, "Regulation of skeletal muscle sarcomere integrity and postnatal muscle function by Mef2c," *Molecular and Cellular Biology*, vol. 27, no. 23, pp. 8143–8151, 2007.
- [70] S. E. Dunn, A. R. Simard, R. Bassel-Duby, R. S. Williams, and R. N. Michel, "Nerve activity-dependent modulation of calcineurin signaling in adult fast and slow skeletal muscle fibers," *Journal of Biological Chemistry*, vol. 276, no. 48, pp. 45243–45254, 2001.
- [71] C. M. Alfieri, H. J. Evans-Anderson, and K. E. Yutzey, "Developmental regulation of the mouse IGF-I exon 1 promoter region by calcineurin activation of NFAT in skeletal muscle," *American Journal of Physiology*, vol. 292, no. 5, pp. C1887–C1894, 2007.
- [72] D. L. Allen, J. J. Uyenishi, A. S. Cleary, R. S. Mehan, S. F. Lindsay, and J. M. Reed, "Calcineurin activates interleukin-6 transcription in mouse skeletal muscle in vivo and in C2C12 myotubes in vitro," *American Journal of Physiology*, vol. 298, no. 1, pp. R198–R210, 2010.
- [73] A. C. Paul and N. Rosenthal, "Different modes of hypertrophy in skeletal muscle fibers," *Journal of Cell Biology*, vol. 156, no. 4, pp. 751–760, 2002.
- [74] J. V. Chakkalakal, M. A. Stocksley, M.-A. Harrison, et al., "Expression of utrophin A mRNA correlates with the oxidative capacity of skeletal muscle fiber types and is regulated by calcineurin/NFAT signaling," *Proceedings of the National Academy of Sciences of the United States of America*, vol. 100, no. 13, pp. 7791–7796, 2003.
- [75] J. V. Chakkalakal, M.-A. Harrison, S. Carbonetto, E. Chin, R. N. Michel, and B. J. Jasmin, "Stimulation of calcineurin signaling attenuates the dystrophic pathology in mdx mice," *Human Molecular Genetics*, vol. 13, no. 4, pp. 379–388, 2004.
- [76] N. Stupka, P. Gregorevic, D. R. Plant, and G. S. Lynch, "The calcineurin signal transduction pathway is essential for successful muscle regeneration in mdx dystrophic mice," *Acta Neuropathologica*, vol. 107, no. 4, pp. 299–310, 2004.
- [77] L. M. Angus, J. V. Chakkalakal, A. Mejat, et al., "Calcineurin-NFAT signaling, together with GABP and PGC-1 α , drives utrophin gene expression at the neuromuscular junction," *American Journal of Physiology*, vol. 289, no. 4, pp. C908–C917, 2005.
- [78] J. V. Chakkalakal, S. A. Michel, E. R. Chin, R. N. Michel, and B. J. Jasmin, "Targeted inhibition of Ca²⁺/calmodulin signaling exacerbates the dystrophic phenotype in mdx mouse muscle," *Human Molecular Genetics*, vol. 15, no. 9, pp. 1423–1435, 2006.
- [79] N. Stupka, B. J. Michell, B. E. Kemp, and G. S. Lynch, "Differential calcineurin signalling activity and regeneration efficacy in diaphragm and limb muscles of dystrophic mdx mice," *Neuromuscular Disorders*, vol. 16, no. 5, pp. 337–346, 2006.
- [80] N. Stupka, D. R. Plant, J. D. Schertzer, et al., "Activated calcineurin ameliorates contraction-induced injury to skeletal muscles of mdx dystrophic mice," *Journal of Physiology*, vol. 575, no. 2, pp. 645–656, 2006.
- [81] A. Angelin, T. Tiepolo, P. Sabatelli, et al., "Mitochondrial dysfunction in the pathogenesis of Ullrich congenital muscular dystrophy and prospective therapy with cyclosporins," *Proceedings of the National Academy of Sciences of the United States of America*, vol. 104, no. 3, pp. 991–996, 2007.
- [82] S. A. Parsons, D. P. Millay, M. A. Sargent, et al., "Genetic disruption of calcineurin improves skeletal muscle pathology and cardiac disease in a mouse model of limb-girdle muscular dystrophy," *Journal of Biological Chemistry*, vol. 282, no. 13, pp. 10068–10078, 2007.
- [83] N. Stupka, J. D. Schertzer, R. Bassel-Duby, E. N. Olson, and G. S. Lynch, "Stimulation of calcineurin A α activity attenuates muscle pathophysiology in mdx dystrophic mice," *American Journal of Physiology*, vol. 294, no. 3, pp. R983–R992, 2008.
- [84] L. Merlini, A. Angelin, T. Tiepolo, et al., "Cyclosporin A corrects mitochondrial dysfunction and muscle apoptosis in patients with collagen VI myopathies," *Proceedings of the National Academy of Sciences of the United States of America*, vol. 105, no. 13, pp. 5225–5229, 2008.

Research Article

Modulation of Muscle Atrophy, Fatigue and MLC Phosphorylation by MuRF1 as Indicated by Hindlimb Suspension Studies on MuRF1-KO Mice

Siegfried Labeit,¹ Christine H. Kohl,¹ Christian C. Witt,¹ Dittmar Labeit,¹ Jeong Jung,² and Henk Granzier²

¹Department of Integrative Pathophysiology, Universitätsmedizin Mannheim, University of Heidelberg, Theodor-Kutzer-Ufer 1–3, 68167 Mannheim, Germany

²Department of Physiology, University of Arizona, Tucson, AZ 85724, USA

Correspondence should be addressed to Siegfried Labeit, labeit@embl.de

Received 20 February 2010; Accepted 13 April 2010

Academic Editor: Aikaterini Kontrogianni-Konstantopoulos

Copyright © 2010 Siegfried Labeit et al. This is an open access article distributed under the Creative Commons Attribution License, which permits unrestricted use, distribution, and reproduction in any medium, provided the original work is properly cited.

MuRF1 is a member of the TRIM/RBCC superfamily, a gene family that encompasses a large variety of proteins, all sharing the conserved TRIM (Tripartite Motive) sequential array of RING, B-box, and coiled-coil domains. Within this family, MuRF1 (also named TRIM63) is a specialized member that contributes to the development of muscle atrophy and sarcopenia. Here we studied MuRF1's role in muscle atrophy during muscle unloading induced by hindlimb suspension. Consistent with previous studies, we found that MuRF1 inactivation leads to an attenuated muscle atrophy response. The amount of protection was higher as compared to the denervation model, and within the 10 day-suspension period the soleus muscle was spared from atrophy in MuRF1-KO mice. Contractility studies on hindlimb suspended muscle tissues suggested that MuRF1's functions extend beyond muscle trophicity and implicate MuRF1 in muscle fatigue and MLC phosphorylation control: soleus muscle from MuRF1-KO mice fatigued significantly faster and in addition showed a reduced posttetanic twitch potentiation. Thus the present work further established the role of MuRF1 in muscle atrophy and for the first time shows that MuRF1 plays a role in muscle fatigue and twitch potentiation.

1. Introduction

Skeletal muscle tissues can be extensively remodeled, both structurally and functionally (for reviews see [1, 2]). Such remodeling takes places, for example, in response to exercise or passive muscle stretch and results in large changes in metabolic activity, fiber-type, and force generation (for reviews see [3, 4]). Increased force production is due to an increase in fiber diameter, an adaptation referred to as hypertrophy. In contrast, when muscle is unloaded, as occurs, for example, in space flight or in bedridden patients, fiber diameter is rapidly reduced, a state referred to as atrophy. Muscle atrophy also accompanies the natural process of aging, and is then referred to as sarcopenia,

and leads to a progressive and large reduction in muscle strength as ageing progresses [5]. Skeletal muscle atrophy is also a debilitating response to starvation and many systemic diseases including diabetes, cancer, and renal failure [6]. Thus understanding the mechanisms that underlie atrophy is clinically highly significant for space flight, patients that have a wide range of diseases or that are bedridden, and to understand and perhaps ameliorate sarcopenia.

Because of the clinical and health-economic importance of sarcopenia, the molecular pathways involved have attracted wide interest. Comparative studies on healthy and wasting muscle tissues identified numerous mechanisms involved in the regulation of muscle trophicity, including

the calcineurin-NFAT pathway (stimulated by the calcium influx into the sarcoplasm), the mTOR/p70S6K pathway (modulated by myofibrillar stretch), and stress signaling (modulated by p38/ERK/MEK kinase pathways, see for example [7, 8]). More recently, molecular insights into the mechanisms counteracting these trophic pathways could be obtained. Importantly, atrogin-1 and MuRF1 genes were found to be transcriptionally upregulated during diverse states of muscle wasting [9, 10]. Furthermore, studies using atrogin-1 and MuRF1-deficient mouse models further supported a potential causal role of these two genes in the development of muscle atrophy: Knock-out mouse models of atrogin-1 and MuRF1 develop about 50% less muscle atrophy in quadriceps muscle after lesion of its innervation [11]. Mechanistically, it was proposed that these two genes act as atrogins via the control of proteasome-dependent degradation of muscle proteins, a concept, that is supported in vitro by the enzymatic E3 ligase activity of expressed MuRF1 protein. Therefore, an upregulation of these E3 ubiquitin ligase activities during muscle wasting would enhance the UPS-dependent degradation of muscle proteins (for review see [12]).

Current studies on MuRF1 and atrogin-1 are therefore focused on the identification of their in vivo targets. In vitro studies demonstrated that MuRF1 efficiently catalyzes the addition of multiubiquitin groups to troponin-I (TnI), myosin, and actin [9, 10]. However, target recognition in vivo is likely to be more selective and to be regulated by yet unknown factors. For example, a recent study using a CreLox-recombinase induced conditional KO model where MuRF1 activity can be downregulated in adult mice suggested that myosin, actin, and TnI are not preferred in vivo targets of MuRF1 [13]. Rather, a partial protection of MLC-2 and myosin binding protein C turnover after denervation was observed in an MuRF1-deficient conditional background [13]. Consistent with the idea that MuRF1 target recognition in vivo is still poorly understood is the finding that overexpression of MuRF1 in skeletal muscles alone is not sufficient to cause muscle atrophy [14]. Instead of muscle wasting, overexpression of MuRF1 resulted in a perturbation of muscle metabolism and insulin signaling [14]. This raises the possibility that MuRF1 could also play a role in muscle trophicity via more complex pathways that include metabolic pathways, rather than the direct degradation of myofibrillar proteins.

Here we used hindlimb suspension as an alternative model to study MuRF1's role in muscle atrophy (in this model muscle maintains its innervation), and studied fiber type distribution, muscle force, and fatigue resistance during repetitive stimulation. Results indicate that muscles from suspended wildtype (wt) and MuRF1-KO (KO) mice have comparable contractile characteristics, suggesting that degradation of myofibrillar proteins by MuRF1 is unlikely. However, inactivation of MuRF1 resulted after hindlimb suspension in a reduced fatigue tolerance and reduced post-tetanic potentiation, linking MuRF1 to MLC phosphorylation. These findings implicate that MuRF1's functional roles in muscle extend beyond a pathophysiological role in causing muscle atrophy.

2. Methods

2.1. Animals and Hindlimb Suspension. All mice were bred in-house and genotyped by standard methods. MuRF1 null mice were on a C57/BL6 background and MuRF1 gene disruption by homologous recombination was as previously described [15]. Animals were housed in standard cages in an animal room with controlled environmental conditions and maintained on standard food and water *ad libitum*. To suspend the hindlimbs, the tail of each mouse was placed in a harness, which was used to elevate the pelvis so that the feet of the hindlimbs did not contact the cage floor. The harness consisted of SkinTrac (a commercially available adhesive tape) in which the entire length of the tail was trapped. The distal end of the SkinTrac was attached to a paperclip which was then attached to a swivel on a plexiglass cross-bar. The cross-bar was positioned ~15 cm above the cage floor. In this way, the hindlimb-suspended mice were able to freely move around the cage on their front limbs and had unlimited access to food and water. The hindlimb suspension lasted 10 days, afterwards one group of mice was sacrificed whereas another group was allowed to recover for 5 days (reload phase).

2.2. Characterization of Dissected Soleus Muscle. After 10 days of hindlimb suspension mice were anaesthetized with isoflurane and sacrificed via cervical dislocation. The soleus muscle was then rapidly dissected in an oxygenated bath on ice. After dissection, a suture was attached to the tendon at the proximal and distal ends of the muscle. The muscle was then attached, via sutures, to an Aurora 1200A Intact Muscle Test System and was placed in an oxygenated physiological solution at 30°C. Next, the optimal twitch length (L_0) was determined at 30°C by incrementally lengthening the muscle until gains in twitch force reached a plateau. After three minutes, the muscles were then passively stretched to four different lengths (5%, 10%, 15%, 20% of L_0) at a rate of 10%/sec, held at the respective length for 60 seconds and released then to L_0 . Muscle strips were allowed to recover by waiting for 7 minutes between each stretch protocol. Seven minutes after the last stretch, a single twitch and tetanus was imposed on the muscle from L_0 . A force-frequency protocol followed using the following frequencies in the following order 1, 5, 10, 20, 40, 60, 80, 100, and 150 Hz, and waiting 30, 30, 60, 90, 120, 120, 120, 120 seconds, respectively, in between each activation. The muscle was then fatigued by stimulation at 60 Hz every three seconds for a total of 100 stimuli. The data from each experiment were analyzed with Aurora's DMA software, Microsoft Excel, and Kaleidagraph 3.6. Twitch and tetanus force and kinetics were determined using Aurora's DMA software. When the experiment was completed muscles were dried with blotting paper and were then weighed. The average cross-sectional area was obtained by dividing the weight by the specific gravity of muscle (1.06) and by the muscle length.

2.3. Immunohistochemistry. The primary antibodies used for immunostaining are commercially available: (1) monoclonal

mouse anti-myosin heavy chain (MHC) II, clone MY-32 (1:1,000; cat# M4276, Sigma) and (2) monoclonal mouse anti-skeletal myosin MHC I, clone NOQ7.5.4D (1:4,000; cat# M8421, Sigma), and (3) MuRF1 was detected with specific antibodies as recently described [16]. The secondary antibodies used for immunostaining were (1) goat anti-mouse IgG-Cyanine Cy2 (1:100; cat# 115-225-174, Jackson Lab), (2) donkey anti-chicken IgY-Cyanine Cy3 (1:1000; cat# 703-165-155, Jackson Lab), (3) donkey anti-mouse Cyanine Cy3 (1:1000; cat# 715-165-150, Jackson Lab), and (4) donkey anti-rabbit Cyanine Cy3 (1:100; cat# 711-165-152, Jackson Lab). Frozen cross-sections of muscles for immunostaining were fixed with 4% paraformaldehyde in 0.2 M phosphate buffer (PB) for 10 minutes at room temperature, washed with PBS 3 times for 3 minutes each and then blocked/permeabilized with 0.1 M glycine/0.2% triton X-100 in phosphate-buffered saline (PBS) for 1 hour. Subsequently the slides were incubated with a solution containing the primary antibody, 3% normal goat serum and 0.3% triton X-100/0.1 M PB overnight in a moisture chamber (4°C). After washing with 0.1 M PBS (3 times for 10 minutes each), a solution containing the secondary antibody and 0.3% triton X-100/0.1 M PBS was added for 2 hours in a dark chamber. The slides were then washed in 0.1 M PB (3 times for 10 minutes each) and mounted with Vectashield mounting medium for fluorescence with 4', 6-diamidino-2-phenylindole (DAPI) (cat# H-1200, Vector Labs) and coverslipped.

2.4. Quantitative and Morphometric Analysis. The quantitative and morphometric analysis were evaluated on a microscope (Nikon Eclipse E600, Fukuoka, Japan) equipped with a digital video camera and image software (Metamorph, Universal Imaging Corporation, Downingtown, USA) digitizing unit connected to a computer (Image Pro-plus, Media Cybernetic). For the determination of muscle fiber type I and II and cross-sectional area (CSA), a total of approximately 500 fibers per muscle per each group were studied. Three to four cross-sections of the soleus and muscles from different animals were analyzed in all groups. For classification of type I and type II fibers, positive immunolabeling for MHC I and MHC II antibodies were used, respectively. Fibers which were lightly labeled were considered intermediary.

2.5. Gel Electrophoresis and Western Blots. Protein extracts were prepared from frozen samples of soleus and tibialis cranialis muscles of 6 unsuspended, suspended and reloaded wild type mice. A total of 50 µg of solubilized extracts were loaded on gel, and separated on 4–10% gradient SDS-acrylamide gels (Invitrogen) followed by transfer onto PVDF membranes. The protein levels of MuRF1 were determined with specific antibodies previously described [17, 18]. After incubation with primary antibodies, specific bands were visualized by enzymatic chemiluminescence using horseradish-peroxidase-conjugated secondary antibodies, (Super Signal West Pico; Pierce, Bonn, Germany), that were quantified by densitometry using a one-dimensional scan software package (Scanalytics, Rockville,

USA). Loading and blotting variability was monitored on duplicate Westernblots, reacted with antibodies specific for alpha-Tubulin (monoclonal rabbit anti-alpha-Tubulin antibody from CellSignalling (#2125); used at 1:1,000).

2.6. Statistics. Multiple comparisons of mean values were performed with analysis of variance (ANOVA), for comparisons of only two groups, the unpaired *t*-test was used. For all comparisons, a $P < .05$ was considered significant.

3. Results

3.1. MuRF1 Induction during Hindlimb Suspension and Its Effect on Muscle Atrophy. First, we used the hindlimb suspension model to monitor MuRF1 protein expression by Western blots. For this, we compared unsuspended, suspended and reloaded muscles and included in our study soleus muscle (SO; because it has mixed-fiber types), as well the M. tibialis cranialis (TC, because it is an almost pure fast-fiber type muscle). Our blots detected basal levels of MuRF1 expression also in all nonsuspended WT control samples (about 25% of suspended protein levels; see Figure 1). Hindlimb suspension resulted in a severalfold upregulation of MuRF1 protein expression (3.9 fold in tibialis cranialis, 3.6-fold in soleus). This process was fully reversible: 5 days of reloading resulted in a return of MuRF1 expression to basal levels (Figure 1). Finally, our blot results were similar for tibialis and soleus muscle types (Figure 1).

Functionally, ten days of hindlimb suspension resulted in a 25% weight reduction of the soleus muscle. This effect was absent in the MuRF1-KO mouse (Table 1). We also determined the cross-sectional area of the muscles and found that the area was significantly reduced during hindlimb suspension of the wt mice ($P < .01$) but that there was no change in the during hindlimb suspension of the KO mice ($P > .05$) (Figure 2). We next measured the cross-sectional area of muscle fibers in the soleus muscle (measurements at L_0 , see below), using immunohistochemistry to classify fibers as type I and II, because a recent study suggested that MuRF1 regulates type-II fiber trophicity in the denervation model [19]. We found that during hindlimb suspension of WT mice the cross-sectional area was significantly reduced in both type I and type II fibers (Figure 3, $P < .05$). A minor reduction of cross-sectional area in MuRF1-KO animals was detectable but not significant. Fiber type distribution was not altered in the wt or in the MuRF1-KO soleus after hindlimb suspension. This conclusion is consistent with an SDS-PAGE based analysis of MHC isotypes in the respective samples (see Table 2). In sum, during hindlimb suspension the soleus muscle atrophies in WT mice, due to a reduction in the cross-sectional area of both type I and type II fibers. Soleus from MuRF1-KO mice seems to be affected only marginally.

3.2. Soleus Muscles from MuRF1-KO Mice Have Normal Contractility. Next, we studied contractile parameters of soleus muscle. Muscles were twitch activated and gradually stretched to L_0 , the length at which twitch force is maximal.

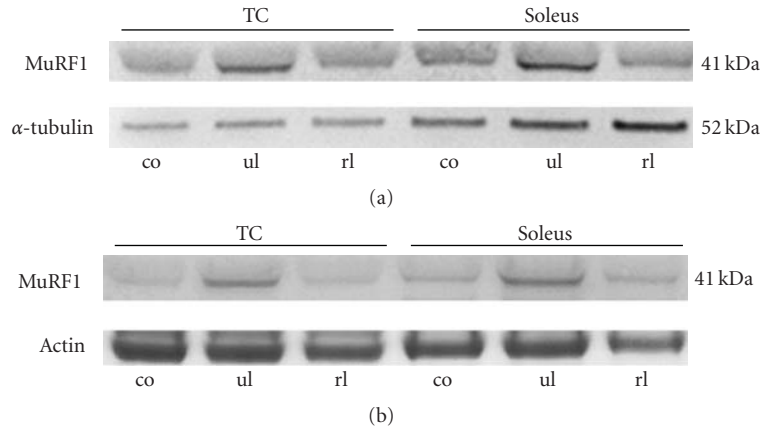


FIGURE 1: MuRF1 protein expression and hindlimb suspension. MuRF1 protein expression was monitored in tibialis cranialis (TC) and soleus (Sol.) muscles before (co; control), after unloading by hindlimb suspension (ul), and after reloading (rl). MuRF1 expression was compared relative to alpha-tubulin (a) or actin (b) as a control for loading and blotting. Low levels of MuRF1 protein were detected in control TC and Sol.; MuRF1 was severalfold elevated after unloading by hindlimb suspension in both muscle types and returned to nearly normal expression levels after 5 days of reloading (rl).

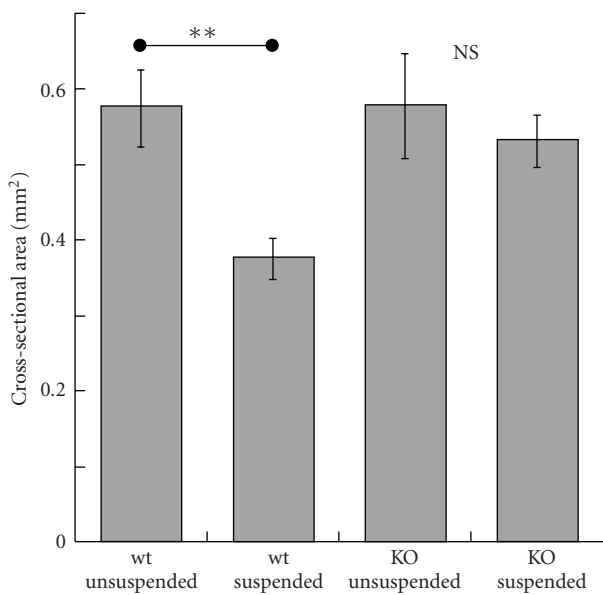


FIGURE 2: Cross-sectional analysis of soleus muscle. The cross-section of wt soleus muscle is significantly reduced during hindlimb suspension (wt sus), but not in the MuRF1-KO mice. “**” indicates statistical significance and “NS” its absence.

TABLE 1: Soleus weights (mg).

	WT	KO
Control	6.9 ± 0.5 (8)	6.2 ± 0.6(6)
Susp.	5.2 ± 0.5 (8)	6.5 ± 0.5 (8)
<i>P</i> -value	0.03	NS

We then determined the force-frequency relation by imposing a 1 second pulse train at progressively higher frequency (see Section 2). No differences were found in the force frequency relation of the four studied groups (WT and KO,

TABLE 2: Soleus fiber types based on MHC/SDS-PAGE typing.

		WT	KO
Control	Type I	32.2 ± 1.9 (8)	35.7 ± 2.1 (6)
	Type IIA+IIB	67.8 ± 3.9 (8)	64.3 ± 4.1 (8)
Susp.	Type I	34.1 ± 2.7 (8)	34.7 ± 2.0 (6)
	Type IIA+IIB	65.9 ± 4.9 (8)	65.3 ± 3.9 (8)
<i>P</i> -value		NS	NS

suspended and unsuspended). In all groups, muscle force reached a maximum at a stimulation frequency of ~100 Hz and the half-maximal force was reached at a stimulation frequency of ~35 Hz. The identical force-frequency relations suggest that hindlimb suspension and the absence of MuRF1 does not affect calcium cycling.

We next studied the effect of hindlimb suspension on the maximal tetanic force (stimulation frequency 150 Hz) in both wt and KO mice and found that this force was significantly reduced during hindlimb suspension of wt mice ($P < .01$), with no effect in MuRF1-KO mice (see Figures 4(a) and 4(b)). However, when the maximal force was normalized to the cross-sectional area of the muscle, the obtained specific forces were not different amongst the 4 groups (see Figure 4(c)). Thus, the atrophy that occurs in wt mice fully explains the reduction in tetanic force during hindlimb suspension of wt mice. The absence of an effect of hindlimb suspension on both total force and specific force in MuRF1-KO mice (Figures 4(b) and 4(c)) is consistent with the absence of atrophy. Additionally, the finding that the force of MuRF1-KO mice is the same as that of unsuspended wt mice suggests that under our experimental conditions the absence of MuRF1 does not affect the functionality of the contractile proteins. This is also suggested by the absence of differences between wt and KO groups in the time required to reach maximal tetanic force and the force relaxation time when stimulation was terminated (results not shown).

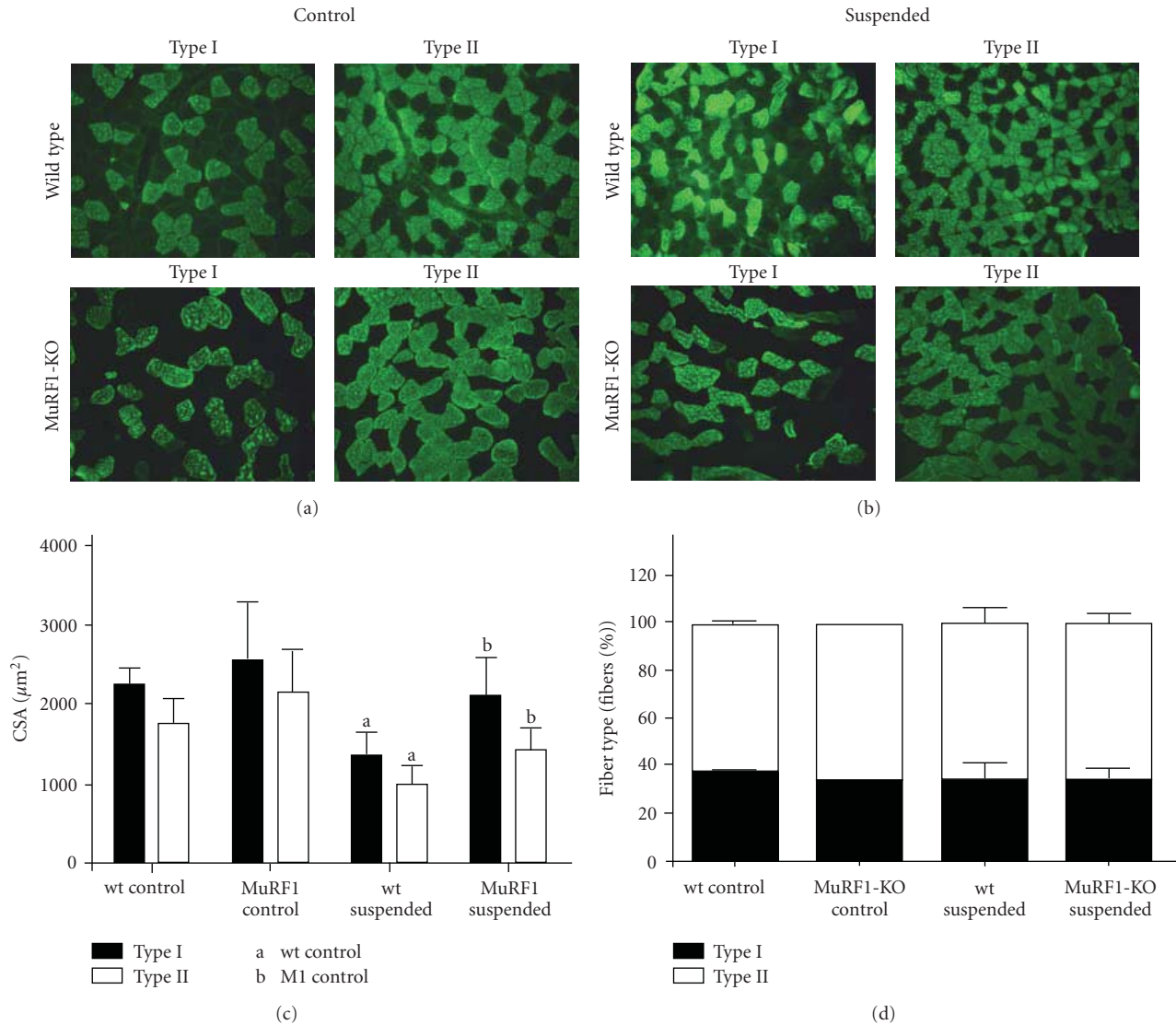
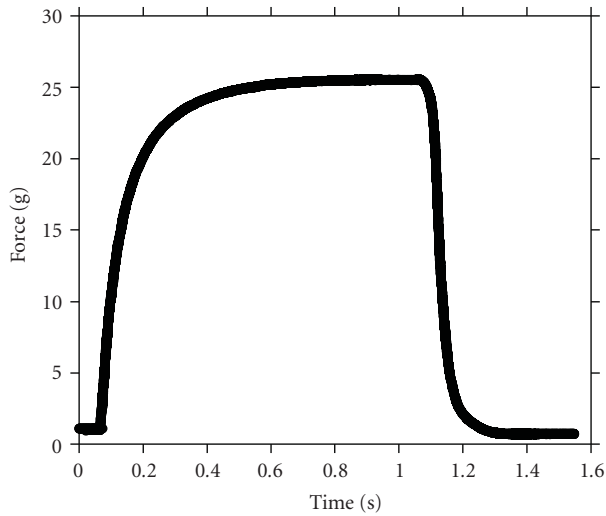


FIGURE 3: Fiber cross-sectional and fiber type analysis. (a) and (b): examples of cross-sections of soleus muscle stained for type I and type II fibers of wt (top row) and MuRF1-KO (bottom row) of control (left two columns) and suspended (right two columns) mice. (c): cross-sectional area analysis; (d): fiber type analysis.

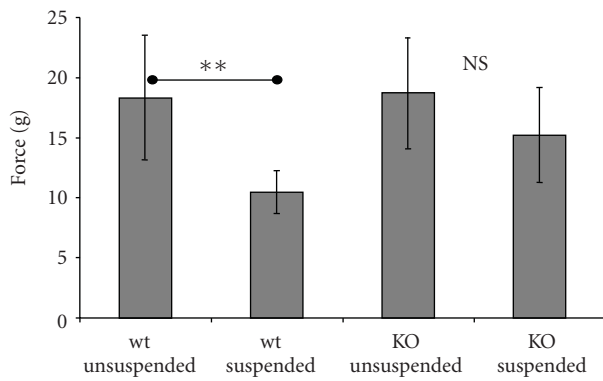
3.3. Altered Twitch Potentiation and Fatigability in MuRF1-Deficient Soleus Muscle. We also measured the well-known phenomenon of twitch potentiation, by measuring twitch force prior to a tetanic stimulation and immediately after tetanic stimulation. Figure 5(a) shows an example of the used protocol. The increase in twitch force after the tetanus (i.e., twitch potentiation) has been shown to be due to increased myosin light chain 2 (MLC2) phosphorylation during the tetanus [20] which in turn increases calcium sensitivity. Interestingly hindlimb suspension results in a significant reduction in the twitch potentiation of MuRF1-KO mice (Figure 5(b)). This finding suggests that MuRF1 is likely to play a role in MLC2 phosphorylation, by either having an effect on the activity of the myosin light kinase or on the ability of the MLC2 to become phosphorylated. Additional experiments with phospho-specific

antibodies will be required to further investigate this hypothesis.

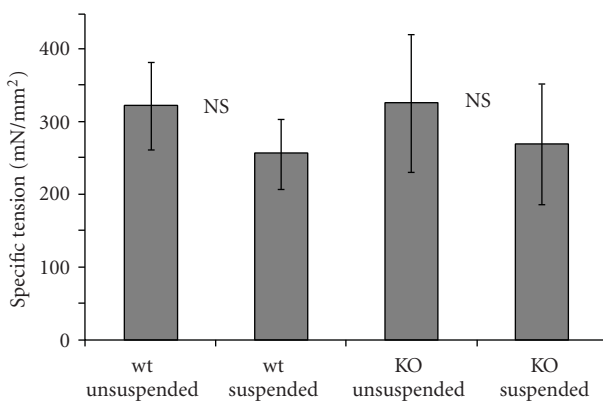
Next, we studied the development of fatigue of soleus muscle by stimulation at a submaximal frequency (60 Hz for 1 second) every three seconds for a total of 5 minutes. The mean data of all muscles are shown in Figure 6(a). The percent of maximum peak force for the first five stimuli and subsequent every fifth were plotted and fitted to a double sigmoidal curve. We found that the muscles from the hindlimb suspended mice had a significant difference between wt and MuRF1-KO mice in that the wt mice had significantly less fatigue than the KO mice. Figure 6(b) shows the force after 2 minutes of the fatigue protocol; the results clearly reveal that muscles from the KO suspended mice had fatigued significantly more than those from the wt suspended mice.



(a)

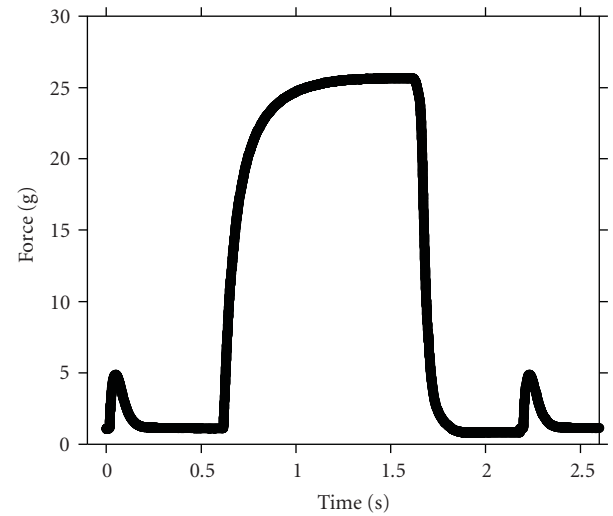


(b)

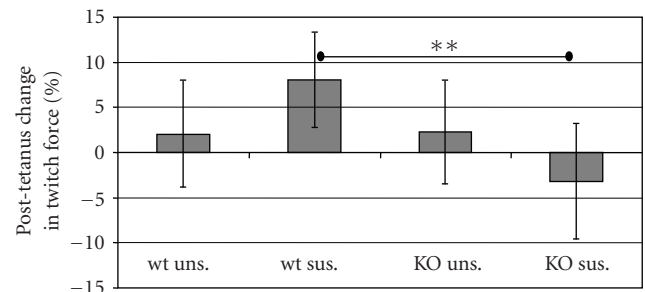


(c)

FIGURE 4: Tetanus Contraction. We stimulated the soleus muscle to a maximum tetanic contraction at a stimulus frequency of 150 Hz. (a) Example of a tetanus of a wt mouse. (b) Mean results of wt and MuRF1-KO mice who had been suspended or unsuspended. There is a significant difference when comparing the absolute peak tetanic force. The data from wt unsuspended mice are significantly different from those of wt suspended mice. However, there is no significant force reduction between the KO unsuspended and the KO suspended mice. (c) Specific tetanic force comparisons did not reveal a significant difference.



(a)



(b)

FIGURE 5: Twitch potentiation. (a) example of protocol. A twitch was elicited before and following a tetanus contraction and peak twitch force after contraction was compared to that before. (b) There is a significant difference between the wt suspended and KO suspended in twitch potentiation, indicating a difference in MLC phosphorylation between the wt and KO mice.

4. Discussion

4.1. MuRF1's Role in Atrophy. Previous studies on MuRF1's role in the development of muscle atrophy were carried out in a denervation (DEN) model in which the sciatic nerve was cut and the lower limb muscles were denervated in wt and MuRF1-KO mice [11]. Results showed that MuRF1-KO mice had a 36% reduction in atrophy after 14 days of denervation. Because denervation might activate catabolic pathways via inflammatory and stress-related pathways that in turn might overlap with MuRF1 signaling pathways (e.g., for shared TNF-alpha and MuRF1 signaling, see [21]) we used a hindlimb suspension model which induces atrophy but keeps innervation intact. Furthermore we limited our analysis to 10 days after suspension when atrophy is significant but not yet severe, and reaches ~25% atrophy in wt mice in the here analyzed two muscle types, tibialis cranialis and soleus. We intentionally focused our analysis on this shortened time period in an attempt to potentially gain insights into physiological rather than purely pathophysiological roles of MuRF1. Furthermore, we focused in our analysis on soleus

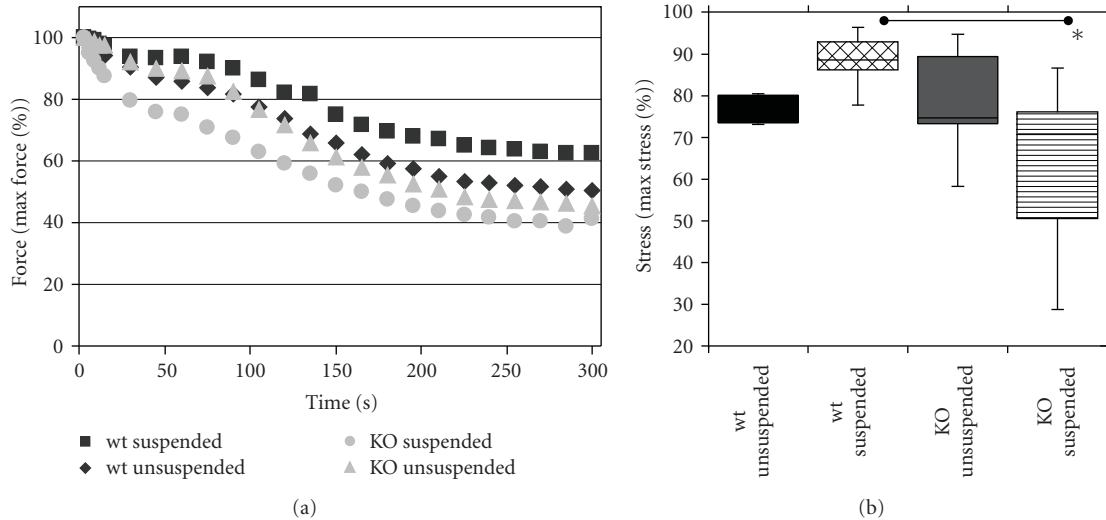


FIGURE 6: Muscle Fatigue. We fatigued the soleus muscle by stimulating the soleus muscle at a submaximal frequency (60 Hz, inset of Figure 5(a)) every three seconds for a total of 100 stimuli. (a) The mean force of all muscles. (b) Force at the 105 second time point. There is a significant difference between the wt suspended and the MuRF1-KO suspended mice.

muscle because it is one of the few muscles in the mouse with a high number of slow twitch fibers, making it possible to test for fiber-type differences in MuRF1-based muscle protection.

Future studies are required to address the effect of longer hindlimb suspension periods, extending for 2 weeks or longer. However, here, using this study design, we found a remarkable protection of the soleus muscle in the MuRF1-KO mice during the tested 10-day-suspension period, displaying virtually complete protection (Table 1 and Figure 2). This high degree of protection is remarkable because MuRF1-KO muscle tissues will express other atrogenes such as atrogin-1, thought to be capable of catalyzing multi-ubiquitination and UPS-dependent degradation of muscle proteins [6, 12]. Also interestingly, we could not detect a fiber-type dependence of MuRF1-based muscle protection here: both nonsuspended and suspended MuRF1-KO soleus tissues had comparable fiber type distributions, and both fiber type subpopulations were protected from atrophy in the absence of MuRF1 as shown by immunohistochemical typing as well as SDS-PAGE based MHC I/ MHC II quantification. This contrasts recent data that were obtained with the MuRF1-KO mice when using the denervation model: here, MuRF1 protein was preferentially induced in type-II fibers from the fast TA muscle. Consistent with an MuRF1 induction in type-II fibers by DEN, we found a preferential protection of type II fast fibers in the MuRF1-KO mice during DEN-induced atrophy [19]. Taken together, our data confirm an important role for MuRF1 during muscle atrophy development, but also stress the importance of using different atrophy induction models, and to analyze the effects that occur in fast and slow fiber type populations separately.

4.2. MuRF1 and Fatigue Control. Because we recently noted that MuRF1 overexpression causes metabolism effects we also compared wt and MuRF1-KO M soleus muscle with

regards to their fatigue resistance when stressed by repetitive stimulations. Consistent with the idea that the role of MuRF1 extends to energy metabolism control [22], we found that inactivation of MuRF1 increases sensitivity to fatigue. A degradation or modification of contractile or regulatory proteins within the myofibril by MuRF1 is an unlikely explanation, because specific tetanic force and the force-frequency relation of suspended soleus muscle from wt and from MuRF1-KO mice were comparable (we also obtained similar findings from MuRF1-overexpressing MuRF1-TG mice, data not shown). Therefore, possibly MuRF1 signalling affects the control of oxidative phosphorylation, either indirectly by affecting mitochondrial functions (for an effect of MuRF1 overexpression on the mitochondrial matrix protein PDC, see [14]), or indirectly by affecting the ATP regenerating MCK enzyme activity [23]. Such a model where MuRF1 exerts its effects on muscle indirectly via its control of energy metabolism would also explain why overexpression of MuRF1 alone is not sufficient to cause a muscle atrophy but instead affects energy metabolism [14], for a review see [24].

In our study we found significant differences in twitch potentiation between wt and MuRF1-KO muscle (Figure 5). Twitch potentiation can be explained as follows. The calcium that is released into the sarcoplasm when a muscle is tetanized not only activates the thin filament, allowing contraction to take place, but also activates the skeletal muscle Ca^{2+} /calmodulin-dependent myosin light chain kinase (skMLCK) to initiate phosphorylation of MLC2 (also known as regulatory light chain, RLC). MLC2 phosphorylation does not increase maximal tetanic force but increases force at submaximal calcium levels, such as occur during a twitch contraction. Thus after the tetanus has been terminated, the phosphorylation status of MLC2 is elevated for some time (ultimately phosphatases reduce the phosphorylation state back to baseline) and twitch force is potentiated [20]. We

previously noted that MuRF1 interacts in the Y2H system with MLC2 [16]. Possibly MuRF1 functions as an adapter protein to facilitate MLCK and MLC2 interactions. Because MuRF1 has been suggested to regulate the turnover of MLC-2 [13] it is also possible that the absence of MuRF1 negatively impacts the degree to which MLC2 is phosphorylated during tetanic stimulation. Alternatively MuRF1 might have an effect on skMLCK or on the phosphatase that dephosphorylates MLC2P. Future work is needed to establish the mechanisms by which MuRF1 deficiency reduced twitch potentiation in muscle from hindlimb suspended mice.

Taken together, our data indicate that the functions of MuRF1 extend beyond regulating myofibrillar protein breakdown, and include intricate fine-tunings of the phosphorylation status of MLC2 and metabolic properties of the skeletal muscle apparatus.

Author's Contributions

The first and the second authors contributed equally to this work.

Acknowledgments

The authors would like to thank Nick King for help with the hindlimb suspension experiments, Anselmo Moriscot for supervision of their fiber type studies, and Nicole Macha for excellent mouse breeding support. Supported by the DFG (La668/13-1), WI3278/2-1 (to C.C.W.) and the NAR University of Heidelberg (to S.L.), and by the NIH (HL062881 to H.G.).

References

- [1] M. J. Potthoff, E. N. Olson, and R. Bassel-Duby, "Skeletal muscle remodeling," *Current Opinion in Rheumatology*, vol. 19, no. 6, pp. 542–549, 2007.
- [2] R. S. Lee-Young, B. J. Canny, D. E. Myers, and G. K. McConell, "AMPK activation is fiber type specific in human skeletal muscle: Effects of exercise and short-term exercise training," *Journal of Applied Physiology*, vol. 107, no. 1, pp. 283–289, 2009.
- [3] D. A. Hood, "Mechanisms of exercise-induced mitochondrial biogenesis in skeletal muscle," *Applied Physiology, Nutrition, and Metabolism*, vol. 34, no. 3, pp. 465–472, 2009.
- [4] C. T. Putman, X. Xu, E. Gillies, I. M. MacLean, and G. J. Bell, "Effects of strength, endurance and combined training on myosin heavy chain content and fibre-type distribution in humans," *European Journal of Applied Physiology*, vol. 92, no. 4-5, pp. 376–384, 2004.
- [5] S. H. Lecker, R. T. Jagoe, A. Gilbert et al., "Multiple types of skeletal muscle atrophy involve a common program of changes in gene expression," *FASEB Journal*, vol. 18, no. 1, pp. 39–51, 2004.
- [6] D. J. Glass, "Signalling pathways that mediate skeletal muscle hypertrophy and atrophy," *Nature Cell Biology*, vol. 5, no. 2, pp. 87–90, 2003.
- [7] N. Frey, D. Frank, S. Lippl et al., "Calsarcin-2 deficiency increases exercise capacity in mice through calcineurin/NFAT activation," *Journal of Clinical Investigation*, vol. 118, no. 11, pp. 3598–3608, 2008.
- [8] T. Snijders, L. B. Verdijk, and L. J. C. van Loon, "The impact of sarcopenia and exercise training on skeletal muscle satellite cells," *Ageing Research Reviews*, vol. 8, no. 4, pp. 328–338, 2009.
- [9] S. H. Lecker, V. Solomon, W. E. Mitch, and A. L. Goldberg, "Muscle protein breakdown and the critical role of the ubiquitin-proteasome pathway in normal and disease states," *Journal of Nutrition*, vol. 129, no. 1, pp. 2275–2375, 1999.
- [10] S. C. Bodine, E. Latres, S. Baumhueter, et al., "Identification of ubiquitin ligases required for skeletal muscle atrophy," *Science*, vol. 294, no. 5547, pp. 1704–1708, 2001.
- [11] S. C. Bodine, E. Latres, S. Baumhueter, et al., "Identification of ubiquitin ligases required for skeletal Muscle Atrophy," *Science*, vol. 294, no. 5547, pp. 1704–1708, 2001.
- [12] G. Mearini, S. Schlossarek, M. S. Willis, and L. Carrier, "The ubiquitin-proteasome system in cardiac dysfunction," *Biochimica et Biophysica Acta*, vol. 1782, no. 12, pp. 749–763, 2008.
- [13] S. Cohen, J. J. Brault, S. P. Gygi et al., "During muscle atrophy, thick, but not thin, filament components are degraded by MuRF1-dependent ubiquitylation," *Journal of Cell Biology*, vol. 185, no. 6, pp. 1083–1095, 2009.
- [14] S. Hirner, C. Krohne, A. Schuster et al., "MuRF1-dependent regulation of systemic carbohydrate metabolism as revealed from transgenic mouse studies," *Journal of Molecular Biology*, vol. 379, no. 4, pp. 666–677, 2008.
- [15] C. C. Witt, S. H. Witt, S. Lerche, D. Labeit, W. Back, and S. Labeit, "Cooperative control of striated muscle mass and metabolism by MuRF1 and MuRF2," *EMBO Journal*, vol. 27, no. 2, pp. 350–360, 2008.
- [16] S. H. Witt, H. Granzier, C. C. Witt, and S. Labeit, "MURF-1 and MURF-2 target a specific subset of myofibrillar proteins redundantly: towards understanding MURF-dependent muscle ubiquitination," *Journal of Molecular Biology*, vol. 350, no. 4, pp. 713–722, 2005.
- [17] T. Centner, J. Yano, E. Kimura et al., "Identification of muscle specific ring finger proteins as potential regulators of the titin kinase domain," *Journal of Molecular Biology*, vol. 306, no. 4, pp. 717–726, 2001.
- [18] C. C. Witt, S. H. Witt, S. Lerche, D. Labeit, W. Back, and S. Labeit, "Cooperative control of striated muscle mass and metabolism by MuRF1 and MuRF2," *EMBO Journal*, vol. 27, no. 2, pp. 350–360, 2008.
- [19] A. S. Moriscot, I. L. Baptista, J. Bogomolovas et al., "MuRF1 is a muscle fiber-type II associated factor and together with MuRF2 regulates type-II fiber trophicity and maintenance," *Journal of Structural Biology*, vol. 170, no. 2, pp. 344–353, 2010.
- [20] G. Zhi, J. W. Ryder, J. Huang et al., "Myosin light chain kinase and myosin phosphorylation effect frequency-dependent potentiation of skeletal muscle contraction," *Proceedings of the National Academy of Sciences of the United States of America*, vol. 102, no. 48, pp. 17519–17524, 2005.
- [21] V. Adams, N. Mangner, A. Gasch et al., "Induction of MuRF1 is essential for TNF-alpha-induced loss of muscle function in mice," *Journal of Molecular Biology*, vol. 384, no. 1, pp. 48–59, 2008.
- [22] S. Koyama, S. Hata, C. C. Witt et al., "Muscle RING-finger protein-1 (MuRF1) as a connector of muscle energy metabolism and protein synthesis," *Journal of Molecular Biology*, vol. 376, no. 5, pp. 1224–1236, 2008.

- [23] M. S. Willis, M. Rojas, L. Li et al., “Muscle ring finger 1 mediates cardiac atrophy in vivo,” *American Journal of Physiology*, vol. 296, no. 4, pp. H997–H1006, 2009.
- [24] O. Mayans and S. Labeit, “MuRFs: specialized members of the TRIM/RBCC family with roles in the regulation of the trophic state of muscle and its metabolism,” in *TRIM/RBCC Proteins*, G. Meroni, Ed., Landes Biosciences, 2010.

Review Article

Aquaporin Expression in Normal and Pathological Skeletal Muscles: A Brief Review with Focus on AQP4

Yoshihiro Wakayama

Department of Neurology, Showa University Fujigaoka Hospital, 1-30 Fujigaoka, Aoba-ku, Yokohama, 227-8501, Japan

Correspondence should be addressed to Yoshihiro Wakayama, wakayama@showa-university-fujigaoka.gr.jp

Received 18 September 2009; Revised 12 January 2010; Accepted 17 January 2010

Academic Editor: Aikaterini Kontrogianni-Konstantopoulos

Copyright © 2010 Yoshihiro Wakayama. This is an open access article distributed under the Creative Commons Attribution License, which permits unrestricted use, distribution, and reproduction in any medium, provided the original work is properly cited.

Freeze-fracture electron microscopy enabled us to observe the molecular architecture of the biological membranes. We were studying the myofiber plasma membranes of health and disease by using this technique and were interested in the special assembly called orthogonal arrays (OAs). OAs were present in normal myofiber plasma membranes and were especially numerous in fast twitch type 2 myofibers; while OAs were lost from sarcolemmal plasma membranes of severely affected muscles with dystrophinopathy and dysferlinopathy but not with caveolinopathy. In the mid nineties of the last century, the OAs turned out to be a water channel named aquaporin 4 (AQP4). Since this discovery, several groups of investigators have been studying AQP4 expression in diseased muscles. This review summarizes the papers which describe the expression of OAs, AQP4, and other AQPs at the sarcolemma of healthy and diseased muscle and discusses the possible role of AQPs, especially that of AQP4, in normal and pathological skeletal muscles.

1. Introduction

Water is an essential substance for mammals, invertebrates, plants, and microorganisms. Water channel proteins named aquaporins (AQPs) have been found in the cell membranes of these organisms. In mammals, they have been identified in cell membranes such as in epithelial and endothelial cells. The first cloned water channel, AQP1, was purified from human erythrocytes by Agre and his associates [1] and its cDNA sequence was reported by Preston and Agre [2]. Then its water transporting capacity was demonstrated by cDNA expression studies in *Xenopus* oocytes [3]. So far 13 AQPs (AQP0~AQP12) have been cloned and sequenced in mammalian tissues. Each is a small intrinsic membrane protein of molecular weight ~30 kDa. These AQPs are classified into two groups: one is water selective channel (orthodox AQPs) and another is water, glycerol, and urea channel (aquaglyceroporins). Among 13 AQPs, AQP4 has a characteristic ultrastructural feature, since AQP4 can be identified by freeze-fracture (F-F) electron microscopy and can be seen as orthogonal arrays (OAs) in this method [4, 5]. We have so far been studying the pathophysiology

of dystrophic muscles at RNA and protein levels including F-F electron microscopy. We found that the densities of both OAs and their subunit particles were reduced in Duchenne muscular dystrophy (DMD) muscles [6, 7]. So I would like to begin this review from F-F aspect of biological membrane especially focusing on OAs.

2. Tissue Distribution of Orthogonal Arrays (OAs)

The cleavage line of F-F goes into hydrophobic interior of biological membrane and F-F technique yields two leaflets of biological membrane: one is protoplasmic (P) face and another is extracellular (E) face [8]. The presence of OAs in cytoplasmic half (P face) of frozen cleaved biological plasma membranes has been described in different cell types of different species and different organs and tissues. Those containing OAs in their membranes include epithelial cells of the small intestine [9], brain astrocytes [10, 11], skeletal muscle cells [12–14], cardiac muscle cells [15], light cells of the kidney collecting tubules [16], tracheal epithelial

cells [17], satellite cells of developing spinal ganglia [18], sympathetic ganglia [19], gastric parietal cells [20], olfactory receptor cells of the newt [21], and tanycytes of the organum vasculosum of the lamina terminalis in dog [22]. The functional significance of this specific assembly (OAs) was unknown until Verkman and his coworkers discovered its function as water channel [4, 23–25]. Possible functions thought before the discovery included (1) regulation of membrane permeability [10, 16], (2) membrane transport of ions and so on [10, 14, 19–22, 26], (3) regulation of osmotic pressure [21], (4) conduction of activities of epithelial cells [17], (5) cell-to-cell communication [27], (6) adhesive properties [19], and (7) cellular junction [9, 22]. Before the discovery of OAs function as water channel, it was unknown whether the OAs acted as a monofunctional apparatus or one with several functions that differed in different organs and/or tissues.

3. OAs in Skeletal Muscle

In skeletal muscle, P face of muscle plasma membrane contains OAs and E face contains pits of OAs. Sirken and Fischbeck [28] reported that, in normal rat muscle, OAs were virtually absent at birth, but increased steadily from day 1 to day 27. After day 27, the number of OAs declined somewhat, then plateaued. The OA density is the highest at two months after birth in mouse skeletal muscle and, then, decreases gradually after that time [29]. The OA density is reported to be high in fast twitch type 2 myofibers; while it is few in slow twitch type 1 myofibers [30]. In human skeletal muscle, distribution frequency of OAs per square micron in normal muscle plasma membrane showed that almost all myofibers contained the OAs [7]. The age-related changes of OA densities were not studied in human skeletal muscles.

4. Discovery of Dystrophin and Its Associated Glycoproteins

DMD is a devastating disorder characterized by severe progressive muscle wasting and cardiac involvement both of which lead to a loss of ambulation by about 11 years of age and death by the third decade, mostly due to cardiac and/or pulmonary insufficiency [31]. Novel studies by Kunkel and his associates cloned the entire cDNA responsible for DMD [32] and determined its complete sequence [33]. The protein product of the cDNA is a large 427-kDa muscle protein that has been named dystrophin [34]. The immunofluorescent studies performed by the several groups of investigators demonstrated the localization of dystrophin at the surface membranes of the normal skeletal myofibers [35–38]. The immunoelectron microscopic investigations revealed the localization of dystrophin along the inner surface of muscle plasma membrane [39, 40]. Dystrophin constitutes 5% of membrane cytoskeletons in skeletal muscle [41]. Dystrophin is a membrane cytoskeletal protein anchored to the inner surface of the sarcolemma of normal myofibers by dystrophin-associated glycoproteins (DAGs) [42, 43]. DAGs

contain extracellular α -dystroglycan, the transmembrane β -dystroglycan, α -, β -, γ -, δ -sarcoglycan and sarcospan, and cytoplasmic syntrophins and dystrobrevins [43]. The transmembrane β -dystroglycan and extracellular α -dystroglycan are encoded by a single messenger RNA and are translated in-frame from a single 97-kDa precursor protein [44, 45]. The α -dystroglycan binds to laminin of extracellular matrices in muscle and nonmuscle tissue [45]; whereas β -dystroglycan interacts directly with dystrophin [46]. α -, β -, γ -, and δ -Sarcoglycans contain one transmembranous domain; while sarcospan has four transmembranous domains [47–52]. Syntrophins and dystrobrevins are the cytoplasmic components of DAGs [43]. Syntrophins contain α , β 1, β 2, γ 1, and γ 2 isoforms which have been characterized so far [53, 54]; while dystrobrevins have α ($-1 \sim -5$) and β -isoforms [55–58]. Alternative splicing yields five forms of α -dystrobrevin, of which two predominate in skeletal muscle: full-length α -dystrobrevin-1 (84 kDa), and C-terminal truncated α -dystrobrevin-2 (65 kDa) [57]. α -Dystrobrevin-2, short isoform, binds dystrophin; whereas α -dystrobrevin-1 binds both dystrophin and utrophin [57]. Among five syntrophin isoforms, α 1-syntrophin is present at its highest levels in skeletal muscle [59, 60] where it is located close to the inner surface of muscle plasma membrane together with β 1-syntrophin. In contrast, β 2-syntrophin is mainly concentrated at the neuromuscular junction [61]. AQP4 molecule turned out to be associated with α 1-syntrophin as described below, although the association is not always the case.

5. Discovery of AQP4 and Its Relation to OAs

In 1995, Frigeri et al. [24] proposed that the OAs seen in F-F electron microscopy are AQP4. Then Yang et al. [25] first demonstrated that OAs are AQP4. Finally Verbavatz et al. [4] showed that OAs are absent in AQP4 knockout mouse. In central nervous tissues, astroglial endfeet membranes contain numerous OAs. Rash et al. [62] described that the direct immunogold labeling of AQP4 was observed in OAs of astrocyte and ependymocyte plasma membranes in rat brain and spinal cord. In skeletal muscle, Shibuya et al. [63] reported that anti-AQP4 antibody labeled OAs in the plasma membrane of normal rat skeletal myofiber by using fracture label electron microscopy.

6. AQP4 Binds to α -Syntrophin

α 1-Syntrophin knockout mice do not reveal any abnormal clinical phenotype and their skeletal muscles do not show pathological features in hematoxylin-eosin staining specimens. However, their muscle specimens with anti-AQP4 antibody immunostaining did not reveal any positive immunoreactivity [64, 65]. Adams et al. [66] thought that the C-terminal amino acid sequence of AQP4 is-VLSSV which is a potential class I PDZ domain interaction sequence. So they generated transgenic mice to determine whether the membrane localization of AQP4 depended on a syntrophin PDZ domain. Using their mice, they found that AQP4 was

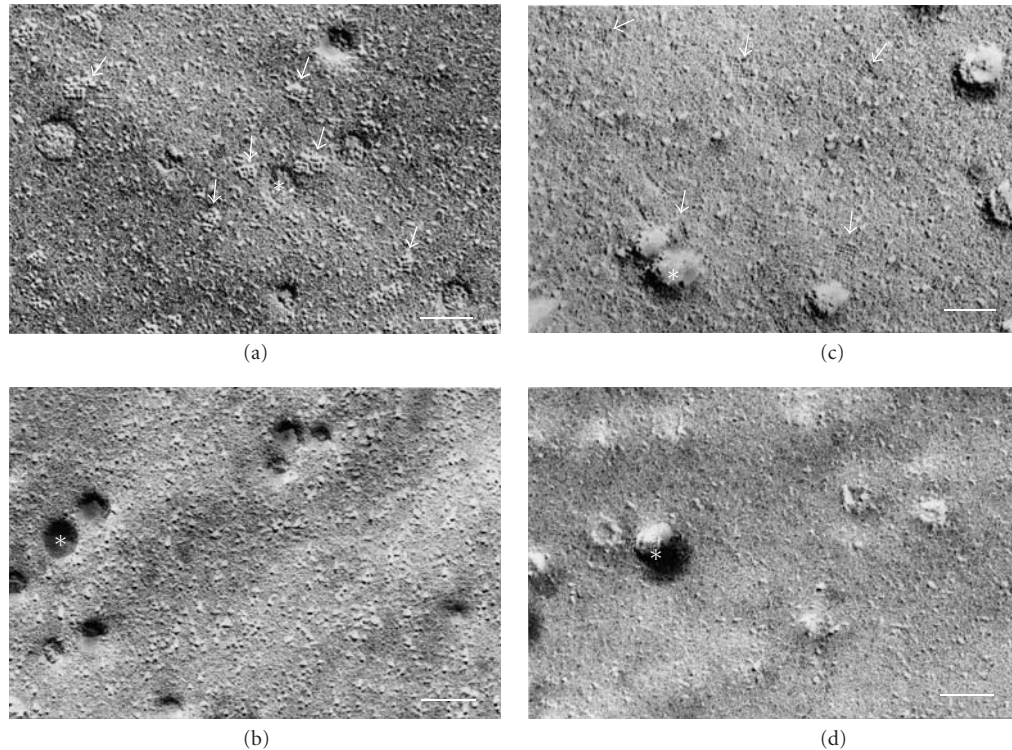


FIGURE 1: High magnification freeze-fracture view of muscle plasma membrane P faces (a) and (b) and E faces (c) and (d). Normal control muscle contains numerous orthogonal arrays (arrows in (a)) and their pits (arrows in (c)); while Duchenne muscular dystrophy muscle contains apparently no orthogonal arrays (b) and their pits (d). Asterisk in (a)–(d) is caveolae. Scale bar in (a)–(d) = 0.1 μm .

absent from the sarcolemma and thought that the syntrophin PDZ domain is likely involved in targeting or stabilizing AQP4 [66]. Amiry-Moghaddam et al. [67] studied mice homozygous for targeted disruption of the gene encoding α -syntrophin ($\alpha\text{-Syn}^{-/-}$) and also found that these mice showed a marked loss of AQP4 from perivascular and subplial membranes but no decrease in other membrane domains [67]. In addition, Au et al. [68] described that AQP4 loss did not always correlate with loss of α -syntrophin in muscle disease. Based on these reports, it is suggested that AQP4 is associated with α -syntrophin, although this association is not always the case.

7. OAs and AQP4 Expression in Diseased Muscles and Muscles of Animal Models

The myofiber plasma membrane of DMD was thought to be fragile [69] and, in fact, the plasma membrane defect of DMD myofiber was demonstrated by electron microscopic observations [70–72]. So expression and distribution frequency of OAs in the diseased muscles were the interesting research subject at that time. Those of DMD were well analyzed [6, 73, 74]. The F-F findings of DMD muscle plasma membrane were the decreased density of individual intramembranous particles as well as OAs, or the loss of OAs [6, 33, 34] (Figure 1). The subunit particles constituting OAs were also reduced in the muscle plasma membrane of

DMD [7]. Similar findings were recognized in the muscle plasma membrane of Fukuyama type congenital muscular dystrophy (FCMD) [75]. The muscle plasma membranes with Becker muscular dystrophy also showed the decrease of OA density. In the muscles of the mdx mouse, the mouse model of DMD, the muscle plasma membranes revealed the decrease of OA density but there was less conspicuous depletion of the individual intramembranous particles [76, 77]. The depletion of OAs was also seen in the muscle plasma membranes of dy/dy mice [78] and dystrophin exon 52 knockout mice [79]. In the denervated muscles, the muscle plasma membranes with early to moderate stage of amyotrophic lateral sclerosis (ALS) contained the substantial number of OAs [35]. Although the F-F study of muscle plasma membranes with advanced stage of ALS has not been reported, the muscle plasma membranes of advanced stage of ALS may have few OAs, since the rat muscles with early denervation contained no OAs [28]. DMD is a major type of human muscular dystrophy and AQP4 expression in DMD muscles has been intensively investigated. Three groups of investigators [68, 80, 81] reported the results of AQP4 expression of DMD muscles and those of mdx mouse muscles have also been described [82, 83]. All reports described that the AQP4 protein expression was reduced in the muscles of DMD boys (Figure 2) and mdx mice by immunohistochemistry. At RNA level, the results of the relative AQP4 mRNA contents of muscles with DMD boys [68, 81] and mdx mice [83] were somewhat different.

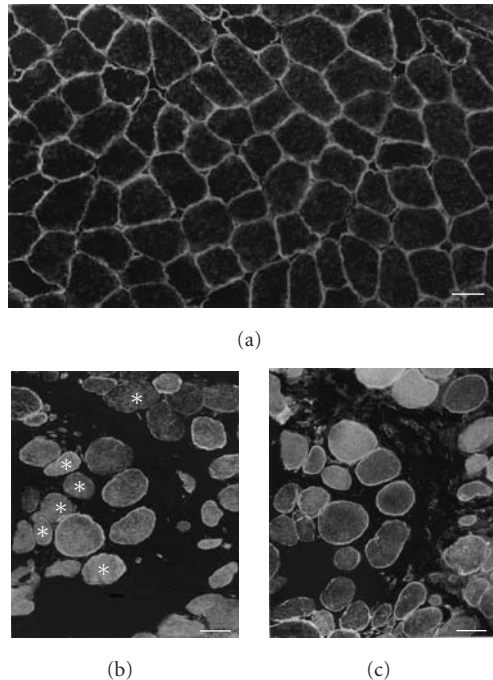


FIGURE 2: Immunofluorescence with anti-AQP4 antibody of normal control muscle (a) and Duchenne muscular dystrophy muscle (DMD) (b), and that with anti-spectrin antibody of serial muscle section of DMD (c). Positive immunoreactivity with anti-AQP4 antibody is seen in apparently all myofibers of normal control muscles (a); while it is noted in mosaic pattern in DMD muscle (b). DMD muscle contains less numerous myofibers with positive immunoreactivity of anti-AQP4 antibody (b) than myofibers with that of anti-spectrin antibody (c). Scattered anti-AQP4 immunonegative fibers (asterisks in (b)) are noted in DMD muscle. Scale bar in (a)–(c) = 50 μm .

We [81] and Au et al. [68] reported the decreased contents of AQP4 mRNA in DMD muscles; while Frigeri et al. [83] reported the normal level of AQP4 mRNA content of mdx mouse muscles and described that the decreased total content of AQP4 protein was not at transcriptional level. Au et al. [68] conducted the immunohistochemistry of AQP4 in the cultured DMD muscle cells and found the normal expression of AQP4. So they suggested that the reduced expression of AQP4 in DMD muscles was secondary to dystrophic process. Reduced AQP4 expression was also reported in severe muscular dystrophies such as FCMD [84], limb girdle muscular dystrophy (LGMD) type 2B [68, 85], sarcoglycanopathies [85], and animal models of sarcoglycanopathies [86]. However, in immunofluorescence analysis, AQP4 was reported to be expressed normally at the sarcolemma of biopsy samples from LGMD type 1C and facioscapulohumeral muscular dystrophy [80]. Many investigations revealed that the muscle contractile cycle appears to be associated with water entry into and exit out of the muscle cell [87, 88]. Muscle contraction needs energy supply which depends on anaerobic glycolysis in the fast twitch type 2 myofibers. The end product of anaerobic glycolysis is lactate and an increase of lactate by exercise prompts a rapid flux of

water from the vascular compartment. The fast twitch type 2 myofibers contain many OAs (AQP4) in their sarcolemmal plasma membranes. The water molecule passes the cell membrane very rapidly through AQP4 water channel [89]. This water displacement may affect the membrane potential and thus muscle membrane excitability. Thus AQP4 is suggested to play a role in determining a rapid osmotic transfer of water from blood to muscle cell during muscle contraction. The dystrophic muscle immunohistochemistry tends to show the slow twitch type 1 fiber predominance. Slow twitch type 1 fiber contains less numerous OAs (AQP4) in the sarcolemmal plasma membrane. The decreased expression of AQP4 in the diseased muscles may relate to the slow contraction of voluntary muscles and thus, in part, may have relation to the slow motion of the myopathic patients, although the patient's slowness mostly results from their muscle weakness. The defective expression of AQP4 in FCMD muscles may be based on the reduced expression of α 1-syntrophin, which binds to AQP4, in FCMD muscles [90]. The central part of FCMD pathophysiology is the defective glycosylation of α -dystroglycan [91], however, the decreased expression of α 1-syntrophin in FCMD muscles is reported to be due to the retarded maturation of FCMD muscles [91]. Reduced density of OAs was also reported in Becker muscular dystrophy (BMD) muscles and this reduction was correlated to the severity of BMD [92]. Furthermore, AQP4 expression of muscles with neurogenic muscular atrophy such as ALS was studied by Jimi et al. [93]. They reported that reduced expression of AQP4 was detected in ALS muscles. This phenomenon is confirmed by experimental studies [28, 94]. The implication of decreased AQP4 expression in the muscles of human muscular dystrophies and neurogenic atrophy is unknown. Animal models such as AQP4 knockout mice [95] and AQP4 overexpressing mice [96] showed no abnormal clinical phenotype. In *dy/dy* (laminin 2 deficient) mice, the reduction of OAs in the muscle plasma membrane was more marked than that of *mdx* mice [78].

8. Other AQPs Expressed in Sarcolemma

The presence of AQP1, 3, 4 mRNAs in skeletal muscle has been described [97–99]. Further Wang et al. [100] reported that they detected the mRNAs of AQP1, 3, 4, 7, 8, 9, and 10 in human masseter muscle and those of AQP1, 3, 4, and 10 in human infrahyoid muscle by RT-PCR. However, these AQPs mRNA expressions were considered to be the contamination of blood vessels (AQP1), adipocytes (AQP7), and leukocytes (AQP9) in skeletal muscle tissues [95]. To rule out this possibility, we and others conducted the immunocytochemical investigation of AQP1, 3, 5, 7, 9 of skeletal muscles, and confirmed the presence of these AQPs [101–105]. However, AQP1, 7 expression of normal skeletal myofiber is controversial. The negative immunostainings of AQP1 [106] and AQP7 [107] were described at the plasma membrane of skeletal myofiber, although the AQP1 and AQP7 immunoreactivities were recognized at the endothelial cells of endomysial blood vessels. We [104] and Au et al. [68] have performed the immunohistochemical study of AQP1

in the skeletal muscle and showed the presence of AQP1 at the muscle membrane as well as the endothelial cells of endomysial blood vessels. With regard to AQP1 expression in the DMD muscles, Au et al. [68] reported that AQP1 transcript and protein expression was significantly elevated in DMD biopsies and was localized to the sarcolemma of muscle fibers and endothelia of muscle capillaries. The functional significance of aquaglyceroporins in skeletal muscle is unknown, however, these aquaglyceroporins function as a glycerol channel and may relate to the lipid metabolism in skeletal myofibers [108, 109].

9. Triglyceride Utilization and Its Possible Aquaglyceroporin Participation in Skeletal Muscle

The intracellular triglyceride in liver and skeletal muscle has a metabolic importance [110, 111]. Fatty acids of muscle triglyceride are derived from both circulating lipoprotein-triglyceride and free fatty acid which comes at least partially from adipose tissue lipolysis [110]. Lipolysis of circulating lipoprotein-triglyceride occurs in the capillary lumen prior to cellular uptake of fatty acids [110]. This extracellular lipolysis is controlled by lipoprotein lipase which is associated with the luminal side of the capillary endothelium. Lipoprotein lipase is activated by circulating apolipoprotein CII and inhibited by apolipoprotein CIII [110]. Adipose tissue lipoprotein lipase activity is the greatest [112] and is reciprocally regulated by hormone-sensitive lipase [113]. Adipose tissue lipoprotein lipase activity has diurnal fluctuation and is most active postprandially for the aim of fatty acids uptake for storage; while its activity decreases when there is a flux of fatty acids from adipose tissue such as the case in fasting [114]. In lipogenic conditions, intracellular glucose is converted by glycerol kinase to glycerol-3-phosphate which is then esterified into triglycerides in adipocytes [115].

The discovery of AQPs has greatly influenced the medical sciences. AQP3, 7, 9, and 10 are subcategorized as aquaglyceroporins, which transport the glycerol in addition to water. Adipocytes are a major source of glycerol which is one of the substrates for hepatic gluconeogenesis [115]. AQP7 and 9 are the glycerol channels in adipocytes and hepatocytes, respectively, [115]. Recently AQP9 is reported to be expressed weakly at the surface membrane of skeletal myofibers [105]. Hepatocytes and myocytes are two major insulin-sensitizing cells [115]. Through AQP7, the hydrolyzed glycerol is efficiently released from adipocytes into the blood stream. AQP7 mRNA levels in adipose tissue are reduced by feeding and increased by fasting in opposite to the changes in plasma insulin levels. Insulin suppresses AQP7 mRNA levels through the insulin negative element located on the promoter region of the AQP7 gene [115]. Therefore, plasma glycerol levels are partly determined by the action of insulin in adipose tissue. Thus long-term regulation of AQP7 is controlled by insulin at the transcriptional level; while short-term regulation is under the control of catecholamines [115].

AQP9 is a glycerol channel in liver cells and is localized at the sinusoidal plasma membrane which faces the portal vein [115–118]. On the other hand, weakly expressed skeletal muscle AQP9 is localized at the myofiber surface membrane [105]. AQP9 mRNA levels are increased by fasting and decreased by feeding [115–117], and this pattern of changes is similar to that for glycerol kinase and for phosphoenolpyruvate carboxykinase, the latter of which is a key enzyme in gluconeogenesis [115]. In the feeding state, an elevation of plasma insulin suppresses lipolysis in adipocytes, reduces adipose AQP7 mRNA levels, and lowers the rate of glycerol release; while liver and possibly myocyte AQP9 mRNA levels are reduced, and glycerol-based gluconeogenesis seems to be suppressed [115]. The investigations of aquaglyceroporins' expression including that of AQP9 in the pathological muscles due to endocrine disorders such as muscles with type 2 diabetes mellitus will suggest some in the functional role(s) of muscle aquaglyceroporins in these pathological conditions.

10. Closing Remarks

The expression of AQPs in normal skeletal muscles and their altered expression in the diseased muscles so far reported were summarized in this review. The research of AQPs in skeletal muscles has not been done so extensively until now and has just begun in recent years. Further studies will throw light into the functional role(s) of AQP4 and other AQPs in the normal muscle physiology as well as in the pathophysiology of diseased muscles.

Acknowledgments

This study was partly supported by The Research Grant (20B-13) for Nervous and Mental Disorders from the Ministry of Health, Labour and Welfare. Thanks were extended to Mr. Hiroaki Oniki and Mrs. Tomoko Nagami for their kind help.

References

- [1] B. M. Denker, B. L. Smith, F. P. Kuhajda, and P. Agre, "Identification, purification, and partial characterization of a novel M_r 28,000 integral membrane protein from erythrocytes and renal tubules," *Journal of Biological Chemistry*, vol. 263, no. 30, pp. 15634–15642, 1988.
- [2] G. M. Preston and P. Agre, "Isolation of the cDNA for erythrocyte integral membrane protein of 28 kilodaltons: member of an ancient channel family," *Proceedings of the National Academy of Sciences of the United States of America*, vol. 88, no. 24, pp. 11110–11114, 1991.
- [3] G. M. Preston, T. P. Carroll, W. B. Guggino, and P. Agre, "Appearance of water channels in *Xenopus* oocytes expressing red cell CHIP28 protein," *Science*, vol. 256, no. 5055, pp. 385–387, 1992.
- [4] J.-M. Verbavatz, T. Ma, R. Gobin, and A. S. Verkman, "Absence of orthogonal arrays in kidney, brain and muscle from transgenic knockout mice lacking water channel aquaporin-4," *Journal of Cell Science*, vol. 110, no. 22, pp. 2855–2860, 1997.

- [5] C. S. Furman, D. A. Gorelick-Feldman, K. G. V. Davidson, et al., "Aquaporin-4 square array assembly: opposing actions of M1 and M23 isoforms," *Proceedings of the National Academy of Sciences of the United States of America*, vol. 100, no. 23, pp. 13609–13614, 2003.
- [6] D. L. Schotland, E. Bonilla, and Y. Wakayama, "Freeze fracture studies of muscle plasma membrane in human muscular dystrophy," *Acta Neuropathologica*, vol. 54, no. 3, pp. 189–197, 1981.
- [7] Y. Wakayama, H. Okayasu, S. Shibuya, and T. Kumagai, "Duchenne dystrophy: reduced density of orthogonal array subunit particles in muscle plasma membrane," *Neurology*, vol. 34, no. 10, pp. 1313–1317, 1984.
- [8] D. Branton, "Fracture faces of frozen membranes," *Proceedings of the National Academy of Sciences of the United States of America*, vol. 55, no. 5, pp. 1048–1056, 1966.
- [9] L. A. Staehelin, "Three types of gap junctions interconnecting intestinal epithelial cells visualized by freeze-etching," *Proceedings of the National Academy of Sciences of the United States of America*, vol. 69, no. 5, pp. 1318–1321, 1972.
- [10] D. M. D. Landis and T. S. Reese, "Arrays of particles in freeze fractured astrocytic membranes," *Journal of Cell Biology*, vol. 60, no. 1, pp. 316–320, 1974.
- [11] D. M. D. Landis and T. S. Reese, "Astrocyte membrane structure: changes after circulatory arrest," *Journal of Cell Biology*, vol. 88, no. 3, pp. 660–663, 1981.
- [12] J. E. Rash and M. H. Ellisman, "Studies of excitable membranes. I. Macromolecular specializations of the neuromuscular junction and the nonjunctional sarcolemma," *Journal of Cell Biology*, vol. 63, no. 2, part 1, pp. 567–586, 1974.
- [13] J. E. Rash, L. A. Staehelin, and M. H. Ellisman, "Rectangular arrays of particles on freeze cleaved plasma membranes are not gap junctions," *Experimental Cell Research*, vol. 86, no. 1, pp. 187–190, 1974.
- [14] H. Schmalbruch, "'Square arrays' in the sarcolemma of human skeletal muscle fibres," *Nature*, vol. 281, no. 5727, pp. 145–146, 1979.
- [15] N. S. McNutt, "Ultrastructure of the myocardial sarcolemma," *Circulation Research*, vol. 37, no. 1, pp. 1–13, 1975.
- [16] F. Humbert, C. Pricam, A. Perrelet, and L. Orci, "Specific plasma membrane differentiations in the cells of the kidney collecting tubule," *Journal of Ultrastructure Research*, vol. 52, no. 1, pp. 13–20, 1975.
- [17] S. Inoue and J. C. Hogg, "Freeze etch study of the tracheal epithelium of normal guinea pigs with particular reference to intercellular junctions," *Journal of Ultrastructure Research*, vol. 61, no. 1, pp. 89–99, 1977.
- [18] E. Pannese, L. Luciano, S. Iurato, and E. Reale, "Intercellular junctions and other membrane specializations in developing spinal ganglia: a freeze fracture study," *Journal of Ultrastructure Research*, vol. 60, no. 2, pp. 169–180, 1977.
- [19] L. G. Elfvin and C. Forsman, "The ultrastructure of junctions between satellite cells in mammalian sympathetic ganglia as revealed by freeze-etching," *Journal of Ultrastructure Research*, vol. 63, no. 3, pp. 261–274, 1978.
- [20] C. Bordi and A. Perrelet, "Orthogonal arrays of particles in plasma membranes of the gastric parietal cell," *Anatomical Record*, vol. 192, no. 2, pp. 297–303, 1978.
- [21] J. Usukura and E. Yamada, "Observations on the cytolemma of the olfactory receptor cell in the newt. I. Freeze replica analysis," *Cell and Tissue Research*, vol. 188, no. 1, pp. 83–98, 1978.
- [22] Y. Nakai, J. Kudo, and A. Hashimoto, "Specific cell membrane differentiation in the tanocytes and glial cells of the organum vasculosum of the lamina terminalis in dog," *Journal of Electron Microscopy*, vol. 29, no. 2, pp. 144–150, 1980.
- [23] A. S. Verkman, "Aquaporin water channels and endothelial cell function," *Journal of Anatomy*, vol. 200, no. 6, pp. 617–627, 2002.
- [24] A. Frigeri, M. A. Gropper, F. Umenishi, M. Kawashima, D. Brown, and A. S. Verkman, "Localization of MIWC and GLIP water channel homologs in neuromuscular, epithelial and glandular tissues," *Journal of Cell Science*, vol. 108, no. 9, pp. 2993–3002, 1995.
- [25] B. Yang, D. Brown, and A. S. Verkman, "The mercurial insensitive water channel (AQP-4) forms orthogonal arrays in stably transfected Chinese hamster ovary cells," *Journal of Biological Chemistry*, vol. 271, no. 9, pp. 4577–4580, 1996.
- [26] J. D. Hatton and M. H. Ellisman, "The distribution of orthogonal arrays and their relationship to intercellular junctions in neuroglia of the freeze-fractured hypothalamo-neurohypophysial system," *Cell and Tissue Research*, vol. 215, no. 2, pp. 309–323, 1981.
- [27] R. Dermietzel, "Visualization by freeze-fracturing of regular structures in glial cell membranes," *Naturwissenschaften*, vol. 60, no. 4, p. 208, 1973.
- [28] S. M. Sirken and K. H. Fischbeck, "Freeze-fracture studies of denervated and tenotomized rat muscle," *Journal of Neuropathology and Experimental Neurology*, vol. 44, no. 2, pp. 147–155, 1985.
- [29] S. Shibuya and Y. Wakayama, "Changes in muscle plasma membranes in young mice with X chromosome-linked muscular dystrophy: a freeze-fracture study," *Neuropathology and Applied Neurobiology*, vol. 17, no. 4, pp. 335–344, 1991.
- [30] A. Frigeri, G. P. Nicchia, J. M. Verbavatz, G. Valenti, and M. Svelto, "Expression of aquaporin-4 in fast-twitch fibers of mammalian skeletal muscle," *Journal of Clinical Investigation*, vol. 102, no. 4, pp. 695–703, 1998.
- [31] A. G. Engel and E. Ozawa, "Dystrophinopathies," in *Myology*, A. G. Engel and C. Franzini-Armstrong, Eds., pp. 961–1025, The McGraw-Hill, New York, NY, USA, 2003.
- [32] M. Koenig, E. P. Hoffman, C. J. Bertelson, A. P. Monaco, C. Feener, and L. M. Kunkel, "Complete cloning of the Duchenne muscular dystrophy (DMD) cDNA and preliminary genomic organization of the DMD gene in normal and affected individuals," *Cell*, vol. 50, no. 3, pp. 509–517, 1987.
- [33] M. Koenig, A. P. Monaco, and L. M. Kunkel, "The complete sequence of dystrophin predicts a rod-shaped cytoskeletal protein," *Cell*, vol. 53, no. 2, pp. 219–228, 1988.
- [34] E. P. Hoffman, R. H. Brown Jr., and L. M. Kunkel, "Dystrophin: the protein product of the Duchenne muscular dystrophy locus," *Cell*, vol. 51, no. 6, pp. 919–928, 1987.
- [35] Y. Wakayama, T. Jimi, N. Misugi, et al., "Dystrophin immunostaining and freeze-fracture studies of muscles of patients with early stage amyotrophic lateral sclerosis and Duchenne muscular dystrophy," *Journal of the Neurological Sciences*, vol. 91, no. 1-2, pp. 191–205, 1989.
- [36] K. Arahata, S. Ishiura, T. Ishiguro, et al., "Immunostaining of skeletal and cardiac muscle surface membrane with antibody against Duchenne muscular dystrophy peptide," *Nature*, vol. 333, no. 6176, pp. 861–863, 1988.
- [37] E. Bonilla, C. E. Samitt, A. F. Miranda, et al., "Duchenne muscular dystrophy: deficiency of dystrophin at the muscle cell surface," *Cell*, vol. 54, no. 4, pp. 447–452, 1988.

- [38] E. E. Zubrzycka-Gaarn, D. E. Bulman, G. Karpati, et al., "The Duchenne muscular dystrophy gene product is localized in sarcolemma of human skeletal muscle," *Nature*, vol. 333, no. 6172, pp. 466–469, 1988.
- [39] S. C. Watkins, E. P. Hoffman, H. S. Slayter, and L. M. Kunkel, "Immunoelectron microscopic localization of dystrophin in myofibres," *Nature*, vol. 333, no. 6176, pp. 863–866, 1988.
- [40] Y. Wakayama and S. Shibuya, "Observations on the muscle plasma membrane-associated cytoskeleton of mdx mice by quick-freeze, deep-etch, rotary-shadow replica method," *Acta Neuropathologica*, vol. 80, no. 6, pp. 618–623, 1990.
- [41] K. Ohlendieck and K. P. Campbell, "Dystrophin constitutes 5% of membrane cytoskeleton in skeletal muscle," *FEBS Letters*, vol. 283, no. 2, pp. 230–234, 1991.
- [42] J. M. Ervasti, K. Ohlendieck, S. D. Kahl, M. G. Gaver, and K. P. Campbell, "Deficiency of a glycoprotein component of the dystrophin complex in dystrophic muscle," *Nature*, vol. 345, no. 6273, pp. 315–319, 1990.
- [43] E. Ozawa, "The muscle fiber cytoskeleton: the dystrophin system," in *Myology*, A. G. Engel and C. Franzini-Armstrong, Eds., pp. 455–470, The McGraw-Hill, New York, NY, USA, 2003.
- [44] O. Ibraghimov-Beskrovnaya, J. M. Ervasti, C. J. Leveille, C. A. Slaughter, S. W. Sernett, and K. P. Campbell, "Primary structure of dystrophin-associated glycoproteins linking dystrophin to the extracellular matrix," *Nature*, vol. 355, no. 6362, pp. 696–702, 1992.
- [45] O. Ibraghimov-Beskrovnaya, A. Milatovich, T. Ozcelik, et al., "Human dystroglycan: skeletal muscle cDNA, genomic structure, origin of tissue specific isoforms and chromosomal localization," *Human Molecular Genetics*, vol. 2, no. 10, pp. 1651–1657, 1993.
- [46] A. Suzuki, M. Yoshida, K. Hayashi, Y. Mizuno, Y. Hagiwara, and E. Ozawa, "Molecular organization at the glycoprotein-complex-binding site of dystrophin—three dystrophin-associated proteins bind directly to the carboxy-terminal portion of dystrophin," *European Journal of Biochemistry*, vol. 220, no. 2, pp. 283–292, 1994.
- [47] S. L. Roberds, R. D. Anderson, O. Ibraghimov-Beskrovnaya, and K. P. Campbell, "Primary structure and muscle-specific expression of the 50-kDa dystrophin-associated glycoprotein (adhalin)," *Journal of Biological Chemistry*, vol. 268, no. 32, pp. 23739–23742, 1993.
- [48] C. G. Bönnemann, R. Modi, S. Noguchi, et al., " β -sarcoglycan (A3b) mutations cause autosomal recessive muscular dystrophy with loss of the sarcoglycan complex," *Nature Genetics*, vol. 11, no. 3, pp. 266–273, 1995.
- [49] L. E. Lim, F. Duclos, O. Broux, et al., " β -sarcoglycan: characterization and role in limb-girdle muscular dystrophy linked to 4q12," *Nature Genetics*, vol. 11, no. 3, pp. 257–265, 1995.
- [50] S. Noguchi, E. M. McNally, K. Ben Othmane, et al., "Mutations in the dystrophin-associated protein γ sarcoglycan in chromosome 13 muscular dystrophy," *Science*, vol. 270, no. 5237, pp. 819–822, 1995.
- [51] V. Nigro, G. Piluso, A. Belsito, et al., "Identification of a novel sarcoglycan gene at 5q33 encoding a sarcolemmal 35 kDa glycoprotein," *Human Molecular Genetics*, vol. 5, no. 8, pp. 1179–1186, 1996.
- [52] R. H. Crosbie, J. Heighway, D. P. Venzke, J. C. Lee, and K. P. Campbell, "Sarcospan, the 25-kDa transmembrane component of the dystrophin-glycoprotein complex," *Journal of Biological Chemistry*, vol. 272, no. 50, pp. 31221–31224, 1997.
- [53] A. H. Ahn, C. A. Freener, E. Gussoni, M. Yoshida, E. Ozawa, and L. M. Kunkel, "The three human syntrophin genes are expressed in diverse tissues, have distinct chromosomal locations, and each bind to dystrophin and its relatives," *Journal of Biological Chemistry*, vol. 271, no. 5, pp. 2724–2730, 1996.
- [54] G. Piluso, M. Mirabella, E. Ricci, et al., " γ 1- and γ 2-syntrophins, two novel dystrophin-binding proteins localized in neuronal cells," *Journal of Biological Chemistry*, vol. 275, no. 21, pp. 15851–15860, 2000.
- [55] D. J. Blake, R. Nawrotzki, M. F. Peters, S. C. Froehner, and K. E. Davies, "Isoform diversity of dystrobrevin, the murine 87-kDa postsynaptic protein," *Journal of Biological Chemistry*, vol. 271, no. 13, pp. 7802–7810, 1996.
- [56] M. F. Peters, K. F. O'Brien, H. M. Sadoulet-Puccio, L. M. Kunkel, M. E. Adams, and S. C. Froehner, " β -dystrobrevin, a new member of the dystrophin family: identification, cloning, and protein associations," *Journal of Biological Chemistry*, vol. 272, no. 50, pp. 31561–31569, 1997.
- [57] M. F. Peters, H. M. Sadoulet-Puccio, M. R. Grady, et al., "Differential membrane localization and intermolecular associations of α -dystrobrevin isoforms in skeletal muscle," *Journal of Cell Biology*, vol. 142, no. 5, pp. 1269–1278, 1998.
- [58] R. M. Grady, R. W. Grange, K. S. Lau, et al., "Role for α -dystrobrevin in the pathogenesis of dystrophin-dependent muscular dystrophies," *Nature Cell Biology*, vol. 1, no. 4, pp. 215–220, 1999.
- [59] M. E. Adams, M. H. Butler, T. M. Dwyer, M. F. Peters, A. A. Murnane, and S. C. Froehner, "Two forms of mouse syntrophin, a 58 kd dystrophin-associated protein, differ in primary structure and tissue distribution," *Neuron*, vol. 11, no. 3, pp. 531–540, 1993.
- [60] M. Durbeej and K. P. Campbell, "Muscular dystrophies involving the dystrophin-glycoprotein complex: an overview of current mouse models," *Current Opinion in Genetics & Development*, vol. 12, no. 3, pp. 349–361, 2002.
- [61] M. F. Peters, N. R. Kramarcy, R. Sealock, and S. C. Froehner, " β 2-syntrophin: localization at the neuromuscular junction in skeletal muscle," *NeuroReport*, vol. 5, no. 13, pp. 1577–1580, 1994.
- [62] J. E. Rash, T. Yasumura, C. S. Hudson, P. Agre, and S. Nielsen, "Direct immunogold labeling of aquaporin-4 in square arrays of astrocyte and ependymocyte plasma membranes in rat brain and spinal cord," *Proceedings of the National Academy of Sciences of the United States of America*, vol. 95, no. 20, pp. 11981–11986, 1998.
- [63] S. Shibuya, Y. Wakayama, and M. Inoue, "Identification of aquaporin 4 molecule in the replica of normal rat sarcolemma: fracture-label immunoelectron microscopic study," *Annals of Neurology*, vol. 46, p. 460, 1999.
- [64] S. Kameya, Y. Miyagoe, I. Nonaka, et al., " α 1-syntrophin gene disruption results in the absence of neuronal-type nitric oxide synthase at the sarcolemma but does not induce muscle degeneration," *Journal of Biological Chemistry*, vol. 274, no. 4, pp. 2193–2200, 1999.
- [65] T. Yokota, Y. Miyagoe, Y. Hosaka, et al., "Aquaporin-4 is absent at the sarcolemma and at perivascular astrocyte endfeet in α 1-syntrophin knockout mice," *Proceedings of the Japan Academy Series B*, vol. 76, no. 2, pp. 22–27, 2000.
- [66] M. E. Adams, H. A. Mueller, and S. C. Froehner, "In vivo requirement of the α -syntrophin PDZ domain for the sarcolemmal localization of nNOS and aquaporin-4," *Journal of Cell Biology*, vol. 155, no. 1, pp. 113–122, 2001.

- [67] M. Amiry-Moghaddam, T. Otsuka, P. D. Hurn, et al., "An α -syntrophin-dependent pool of AQP4 in astroglial end-feet confers bidirectional water flow between blood and brain," *Proceedings of the National Academy of Sciences of the United States of America*, vol. 100, no. 4, pp. 2106–2111, 2003.
- [68] C. G. Au, T. L. Butler, J. R. Egan, et al., "Changes in skeletal muscle expression of AQP1 and AQP4 in dystrophinopathy and dysferlinopathy patients," *Acta Neuropathologica*, vol. 116, no. 3, pp. 235–246, 2008.
- [69] L. P. Rowland, "Pathogenesis of muscular dystrophies," *Archives of Neurology*, vol. 33, no. 5, pp. 315–321, 1976.
- [70] B. Mokri and A. G. Engel, "Duchenne dystrophy: electron microscopic findings pointing to a basic or early abnormality in the plasma membrane of the muscle fiber," *Neurology*, vol. 25, no. 12, pp. 1111–1120, 1975.
- [71] H. Schmalbruch, "Segmental fibre breakdown and defects of the plasmalemma in diseased human muscles," *Acta Neuropathologica*, vol. 33, no. 2, pp. 129–141, 1975.
- [72] Y. Wakayama, E. Bonilla, and D. L. Schotland, "Muscle plasma membrane abnormalities in infants with Duchenne muscular dystrophy," *Neurology*, vol. 33, no. 10, pp. 1368–1370, 1983.
- [73] D. L. Schotland, E. Bonilla, and M. Van Meter, "Duchenne dystrophy: alteration in muscle plasma membrane structure," *Science*, vol. 196, no. 4293, pp. 1005–1007, 1977.
- [74] D. Peluchetti, M. Mora, A. Protti, and F. Cornelio, "Freeze-fracture analysis of the muscle fiber plasma membrane in Duchenne dystrophy," *Neurology*, vol. 35, no. 6, pp. 928–930, 1985.
- [75] Y. Wakayama, T. Kumagai, and S. Shibuya, "Freeze-fracture studies of muscle plasma membrane in Fukuyama-type congenital muscular dystrophy," *Neurology*, vol. 35, no. 11, pp. 1587–1593, 1985.
- [76] S. Shibuya and Y. Wakayama, "Freeze-fracture studies of myofiber plasma membrane in X chromosome-linked muscular dystrophy (mdx) mice," *Acta Neuropathologica*, vol. 76, no. 2, pp. 179–184, 1988.
- [77] H. Ito, T. Yoshimura, M. Tsujihata, and S. Nagataki, "Distribution of intramembranous particle size in the muscle plasma membrane of the mdx mouse," *Journal of the Neurological Sciences*, vol. 148, no. 2, pp. 147–151, 1997.
- [78] S. Shibuya, Y. Wakayama, H. Oniki, et al., "A comparative freeze-fracture study of plasma membrane of dystrophic skeletal muscles in dy/dy mice with merosin (laminin 2) deficiency and mdx mice with dystrophin deficiency," *Neuropathology and Applied Neurobiology*, vol. 23, no. 2, pp. 123–131, 1997.
- [79] S. Shibuya, Y. Wakayama, M. Murahashi, et al., "Muscle plasma membrane changes in dystrophin gene exon 52 knockout mouse," *Pathology Research and Practice*, vol. 197, no. 6, pp. 441–447, 2001.
- [80] A. Frigeri, G. P. Nicchia, S. Repetto, M. Bado, C. Minetti, and M. Svelto, "Altered aquaporin-4 expression in human muscular dystrophies: a common feature?" *The FASEB Journal*, vol. 16, no. 9, pp. 1120–1122, 2002.
- [81] Y. Wakayama, T. Jimi, M. Inoue, et al., "Reduced aquaporin 4 expression in the muscle plasma membrane of patients with Duchenne muscular dystrophy," *Archives of Neurology*, vol. 59, no. 3, pp. 431–437, 2002.
- [82] J. W. Liu, Y. Wakayama, M. Inoue, et al., "Immunocytochemical studies of aquaporin 4 in the skeletal muscle of mdx mouse," *Journal of the Neurological Sciences*, vol. 164, no. 1, pp. 24–28, 1999.
- [83] A. Frigeri, G. P. Nicchia, B. Nico, et al., "Aquaporin-4 deficiency in skeletal muscle and brain of dystrophic mdx mice," *The FASEB Journal*, vol. 15, no. 1, pp. 90–98, 2001.
- [84] Y. Wakayama, T. Jimi, M. Inoue, et al., "Altered aquaporin 4 expression in muscles of Fukuyama-type congenital muscular dystrophy," *Virchows Archiv*, vol. 443, no. 6, pp. 761–767, 2003.
- [85] S. Assereto, M. Mastrototaro, S. Stringara, et al., "Aquaporin-4 expression is severely reduced in human sarcoglycanopathies and dysferlinopathies," *Cell Cycle*, vol. 7, no. 14, pp. 2199–2207, 2008.
- [86] R. H. Crosbie, S. A. Dovico, J. D. Flanagan, J. S. Chamberlain, C. L. Ownby, and K. P. Campbell, "Characterization of aquaporin-4 in muscle and muscular dystrophy," *The FASEB Journal*, vol. 16, no. 9, pp. 943–949, 2002.
- [87] G. Sjøgaard, R. P. Adams, and B. Saltin, "Water and ion shifts in skeletal muscle of humans with intense dynamic knee extension," *American Journal of Physiology*, vol. 248, no. 2, part 2, pp. R190–R196, 1985.
- [88] J. M. Kowalchuk, G. J. F. Heigenhauser, M. I. Lindinger, J. R. Sutton, and N. L. Jones, "Factors influencing hydrogen ion concentration in muscle after intense exercise," *Journal of Applied Physiology*, vol. 65, no. 5, pp. 2080–2089, 1988.
- [89] Y. Hiroaki, K. Tani, A. Kamegawa, et al., "Implications of the aquaporin-4 structure on array formation and cell adhesion," *Journal of Molecular Biology*, vol. 355, no. 4, pp. 628–639, 2006.
- [90] Y. Wakayama, M. Inoue, H. Kojima, et al., "Altered α 1-syntrophin expression in myofibers with Duchenne and Fukuyama muscular dystrophies," *Histology and Histopathology*, vol. 21, no. 1, pp. 23–34, 2006.
- [91] Y. Wakayama, M. Inoue, H. Kojima, et al., "Reduced expression of sarcospan in muscles of Fukuyama congenital muscular dystrophy," *Histology and Histopathology*, vol. 23, no. 12, pp. 1425–1438, 2008.
- [92] S. Shibuya, Y. Wakayama, T. Jimi, et al., "Freeze-fracture analysis of muscle plasma membrane in Becker's muscular dystrophy," *Neuropathology and Applied Neurobiology*, vol. 20, no. 5, pp. 487–494, 1994.
- [93] T. Jimi, Y. Wakayama, Y. Matsuzaki, H. Hara, M. Inoue, and S. Shibuya, "Reduced expression of aquaporin 4 in human muscles with amyotrophic lateral sclerosis and other neurogenic atrophies," *Pathology Research and Practice*, vol. 200, no. 3, pp. 203–209, 2004.
- [94] T. Jimi and Y. Wakayama, "Effect of denervation on regenerating muscle plasma membrane integrity: freeze-fracture and dystrophin immunostaining analyses," *Acta Neuropathologica*, vol. 80, no. 4, pp. 401–405, 1990.
- [95] B. Yang, J.-M. Verbavatz, Y. Song, et al., "Skeletal muscle function and water permeability in aquaporin-4 deficient mice," *American Journal of Physiology. Cell Physiology*, vol. 278, no. 6, pp. C1108–C1115, 2000.
- [96] Y. Wakayama, J. Takahashi, S. Shibuya, et al., "Generation of muscle aquaporin 4 overexpressing transgenic mouse: its characterization at RNA and protein levels including freeze-fracture study," *Micron*, vol. 38, no. 3, pp. 257–267, 2007.
- [97] T. Ma, A. Frigeri, H. Hasegawa, and A. S. Verkman, "Cloning of a water channel homolog expressed in brain meningeal cells and kidney collecting duct that functions as a stilbene-sensitive glycerol transporter," *Journal of Biological Chemistry*, vol. 269, no. 34, pp. 21845–21849, 1994.

- [98] F. Umenishi, A. S. Verkman, and M. A. Gropper, "Quantitative analysis of aquaporin mRNA expression in rat tissues by RNase protection assay," *DNA and Cell Biology*, vol. 15, no. 6, pp. 475–480, 1996.
- [99] A. Mobasheri, S. Wray, and D. Marples, "Distribution of AQP2 and AQP3 water channels in human tissue microarrays," *Journal of Molecular Histology*, vol. 36, no. 1-2, pp. 1–14, 2005.
- [100] W. Wang, P. S. Hart, N. P. Piesco, X. Lu, M. C. Gorry, and T. C. Hart, "Aquaporin expression in developing human teeth and selected orofacial tissues," *Calcified Tissue International*, vol. 72, no. 3, pp. 222–227, 2003.
- [101] S. M. Hwang, R. H. Lee, J. M. Song, et al., "Expression of aquaporin-5 and its regulation in skeletal muscle cells," *Experimental & Molecular Medicine*, vol. 34, no. 1, pp. 69–74, 2002.
- [102] Y. Wakayama, T. Jimi, M. Inoue, et al., "Expression of aquaporin 3 and its localization in normal skeletal myofibres," *Histochemical Journal*, vol. 34, no. 6-7, pp. 331–337, 2002.
- [103] Y. Wakayama, M. Inoue, H. Kojima, et al., "Expression and localization of aquaporin 7 in normal skeletal myofiber," *Cell and Tissue Research*, vol. 316, no. 1, pp. 123–129, 2004.
- [104] T. Jimi, Y. Wakayama, M. Inoue, et al., "Aquaporin 1: examination of its expression and localization in normal human skeletal muscle tissue," *Cells Tissues Organs*, vol. 184, no. 3-4, pp. 181–187, 2006.
- [105] M. Inoue, Y. Wakayama, H. Kojima, et al., "Aquaporin 9 expression and its localization in normal skeletal myofiber," *Journal of Molecular Histology*, vol. 40, no. 3, pp. 165–170, 2009.
- [106] A. Frigeri, G. P. Nicchia, R. Balena, B. Nico, and M. Svelto, "Aquaporins in skeletal muscle: reassessment of the functional role of aquaporin-4," *The FASEB Journal*, vol. 18, no. 7, pp. 905–907, 2004.
- [107] M. T. Skowronski, J. Lebeck, A. Rojek, et al., "AQP7 is localized in capillaries of adipose tissue, cardiac and striated muscle: implications in glycerol metabolism," *American Journal of Physiology. Renal Physiology*, vol. 292, no. 3, pp. F956–F965, 2007.
- [108] E. A. Newsholme and K. Taylor, "Glycerol kinase activities in muscles from vertebrates and invertebrates," *Biochemical Journal*, vol. 112, no. 4, pp. 465–474, 1969.
- [109] N. Maeda, T. Hibuse, and T. Funahashi, "Role of aquaporin-7 and aquaporin-9 in glycerol metabolism; involvement in obesity," *Handbook of Experimental Pharmacology*, no. 190, pp. 233–249, 2009.
- [110] G. R. Dagenais, R. G. Tancredi, and K. L. Zierler, "Free fatty acid oxidation by forearm muscle at rest, and evidence for an intramuscular lipid pool in the human forearm," *Journal of Clinical Investigation*, vol. 58, no. 2, pp. 421–431, 1976.
- [111] S. W. Coppack, M. D. Jensen, and J. M. Miles, "In vivo regulation of lipolysis in humans," *Journal of Lipid Research*, vol. 35, no. 2, pp. 177–193, 1994.
- [112] R. H. Eckel, "Lipoprotein lipase: a multifunctional enzyme relevant to common metabolic diseases," *The New England Journal of Medicine*, vol. 320, no. 16, pp. 1060–1068, 1989.
- [113] D. Steinberg and J. C. Khoo, "Hormone-sensitive lipase of adipose tissue," *Federation Proceedings*, vol. 36, no. 7, pp. 1986–1990, 1977.
- [114] H. Lithell, J. Boberg, K. Hellsing, G. Lundqvist, and B. Vessby, "Lipoprotein lipase activity in human skeletal muscle and adipose tissue in the fasting and the fed states," *Atherosclerosis*, vol. 30, no. 1, pp. 89–94, 1978.
- [115] N. Maeda, T. Funahashi, and I. Shimomura, "Metabolic impact of adipose and hepatic glycerol channels aquaporin 7 and aquaporin 9," *Nature Clinical Practice Endocrinology & Metabolism*, vol. 4, no. 11, pp. 627–634, 2008.
- [116] H. Kuriyama, I. Shimomura, K. Kishida, et al., "Coordinated regulation of fat-specific and liver-specific glycerol channels, aquaporin adipose and aquaporin 9," *Diabetes*, vol. 51, no. 10, pp. 2915–2921, 2002.
- [117] J. M. Carbrey, D. A. Gorelick-Feldman, D. Kozono, J. Praetorius, S. Nielsen, and P. Agre, "Aqua-glyceroporin AQP9: solute permeation and metabolic control of expression in liver," *Proceedings of the National Academy of Sciences of the United States of America*, vol. 100, no. 5, pp. 2945–2950, 2003.
- [118] P. Portincasa, G. Palasciano, M. Svelto, and G. Calamita, "Aquaporins in the hepatobiliary tract. Which, where and what they do in health and disease," *European Journal of Clinical Investigation*, vol. 38, no. 1, pp. 1–10, 2008.

Research Article

Epo Is Relevant Neither for Microvascular Formation Nor for the New Formation and Maintenance of Mice Skeletal Muscle Fibres in Both Normoxia and Hypoxia

Luciana Hagström,¹ Onnik Agbulut,² Raja El-Hasnaoui-Saadani,¹ Dominique Marchant,¹ Fabrice Favret,¹ Jean-Paul Richalet,¹ Michèle Beaudry,¹ and Thierry Launay^{1,3}

¹Laboratoire "Réponses Cellulaires et Fonctionnelles à l'hypoxie", Université Paris 13, EA 2363, 97017 Bobigny, France

²Laboratoire Stress et Pathologies du Cytosquelette, Unité de Biologie Adaptative et Fonctionnelle, Université Paris Diderot-Paris 7 CNRS, 75013 Paris, France

³Université Paris-Descartes, 75015 Paris, France

Correspondence should be addressed to Thierry Launay, thy.launay@free.fr

Received 30 October 2009; Revised 28 January 2010; Accepted 9 February 2010

Academic Editor: Aikaterini Kontrogianni-Konstantopoulos

Copyright © 2010 Luciana Hagström et al. This is an open access article distributed under the Creative Commons Attribution License, which permits unrestricted use, distribution, and reproduction in any medium, provided the original work is properly cited.

Erythropoietin (Epo) and vascular growth factor (VEGF) are known to be involved in the regulation of cellular activity when oxygen transport is reduced as in anaemia or hypoxic conditions. Because it has been suggested that Epo could play a role in skeletal muscle development, regeneration, and angiogenesis, we aimed to assess Epo deficiency in both normoxia and hypoxia by using an Epo-deficient transgenic mouse model (Epo-TAg^h). Histoimmunology, ELISA and real time RT-PCR did not show any muscle fiber atrophy or accumulation of active HIF-1 α but an improvement of microvessel network and an upregulation of VEGFR2 mRNA in Epo-deficient gastrocnemius compared with Wild-Type one. In hypoxia, both models exhibit an upregulation of VEGF120 and VEGFR2 mRNA but no accumulation of Epo protein. EpoR mRNA is not up-regulated in both Epo-deficient and hypoxic gastrocnemius. These results suggest that muscle deconditioning observed in patients suffering from renal failure is not due to Epo deficiency.

1. Introduction

Erythropoietin (Epo) is known as a key-regulator of erythropoiesis stimulating proliferation, differentiation, and survival growth of erythroid precursor resulting in the increased production of red blood cells [1]. In both men and mice exposed to altitude, plasma Epo concentration reached a peak after a 24-hour period of exposure [2] and subsequently declining in a progressive manner within days or weeks [3, 4]. It has been demonstrated the relative importance of altitude Epo-induced polycythemia in the process of acclimatisation to altitude hypoxia performed between days 4 and 9 of exposure [2].

Through specific binding to its receptor (EpoR), Epo triggers a chain of intracellular signaling events that depends on activation of Jak2 tyrosine kinase [5]. Studies dealing

with the expression of EpoR revealed a role for Epo, in addition to erythropoiesis, on various tissues such as those of the central nervous system, pancreas, liver, lung, smooth, cardiac and skeletal muscles (for review see [6]). As a result, the effects of Epo as growth factor, antiapoptotic factor or angiogenic factor on these tissues are considered of a great interest.

Indeed, the EpoR has been identified in mouse C2C12 primary myoblast cultures [7] as well as in human skeletal muscle [8]. On both C2C12 cells and primary cultures of mouse myoblasts, Epo activates the proliferation of myogenic precursor cells [7]. More recently, the injection of recombinant human Epo (rHuEpo) has been shown to improve the regeneration process of rat soleus muscle [9]. Taken together, these results suggest a role for Epo on the development and regeneration of skeletal muscle.

Epo was shown to have the same angiogenic power as vascular endothelial growth factor (VEGF) [10]. Kertesz et al. [11] demonstrated the role of Epo and VEGF in the formation of new blood vessels during the early development of tissues. Using Epo knock-out mutant, these authors showed that angiogenesis was defective while the vasculogenesis was relatively normal. On the other hand, Suzuki et al. [12] observed that the nonhematopoietic role of Epo is dispensable to organism development and angiogenesis under normal conditions. From those data, we suggest a compensatory mechanism to Epo deficiency in tissues. Then we may hypothesise that the default of oxygen transport to tissues leads to local hypoxia which induces the accumulation of Hypoxia-Inducible Factor-1 α (HIF-1 α) and then the expression of the angiogenic factor VEGF as shown in anemic brain [13].

The VEGF-A (also referred as VEGF) protein comprises various isoforms of 121 to 206 amino acids in humans (120 to 205 in rodents), produced by alternative splicing during transcription [14, 15]. The 120, 164 and 188 isoforms are the most frequently expressed ones although each one has specific biological activities [16, 17]. VEGF121 is a freely diffusible protein whereas VEGF189 is almost completely sequestered in the extracellular matrix (ECM). VEGF165 has intermediate properties, as it is moderately diffusible but a significant fraction remains bound to the cell surface and ECM. Actually, the longer forms of VEGF are stably incorporated to the ECM but can be released in a diffusible form by several agents [18].

Epo deficiency is observed in patients suffering from severe renal failure inducing intense anaemia. Skeletal muscles of these patients present structural and functional abnormalities that contribute to explain, at least partly, their impaired exercise capacity, muscle deconditioning and decreased resistance to fatigue. There is a reduction in muscle mass associated with myofiber atrophy, mainly in type II fibers [19, 20]. Moreover, reductions in muscle capillarity, as well as abnormalities of mitochondria are contributing factors for muscle fatigability [19–21]. Although muscle deconditioning in those patients could also be due to physical inactivity [20], those results suggest that Epo deficiency could have consequences on muscle structure and capillarisation.

In order to understand whether Epo is an important factor for muscle and capillary development and maintenance in hypoxia, we propose to use a model of erythropoietin-SV40 T antigen (Epo-TAg^h) transgenic mice with a targeted disruption in the 5' untranslated region of the Epo gene that dramatically reduces its expression [22, 23] and then induces severe anaemia. We aim to assess whether Epo deficiency alters skeletal muscle structure in either normoxia or hypoxia.

For this purpose, Epo-TAg^h and wild-type (WT) mice were exposed to acute and chronic hypobaric hypoxia (equivalent to 4500 m). Results were compared to those obtained in age-matched WT normoxic mice. We measured plasma and muscle Epo concentrations, active HIF-1 α and VEGF protein by Enzyme-linked immunosorbent assay (ELISA). To analyse the expression profile of each VEGF

isoform, VEGFR1, VEGFR2 and EpoR mRNA, we used the real-time reverse transcriptase-polymerase chain reaction (RT-PCR). The expression of Epo mRNA was evaluated first by classical RT-PCR and second by real-time RT-PCR. Moreover, the microvessel network was analysed in gastrocnemius muscles as described by Charifi et al. using the specific platelet endothelial cell adhesion molecule (PECAM) antibody directed against CD31. The capillary-to-fiber ratio (C/F), the number of capillaries around a single fiber and the index of capillary tortuosity (LC/PF) were measured to evaluate the development of elongated vessels running parallel to the muscle fibers and the new sprouts from loops and cross connections [24].

2. Materials and Methods

2.1. Animal Model and Experimental Groups. For this study, male Wild-Type F1 BL6/CBA (Charles River, L'Arbresle, France) and male Epo deficient SV-40 T antigen (Epo-TAg^h) mice were divided randomly into six groups: (a) normoxic wild-type (Nx WT); (b) normoxic Epo-TAg^h (Nx Epo-TAg^h); (c) acute hypoxic wild-type (AHx WT); (d) acute hypoxic Epo-TAg^h (AHx Epo-TAg^h); (e) chronic hypoxic wild-type (CHx WT); and (f) chronic hypoxic Epo-TAg^h (CHx Epo-TAg^h). At the moment of dissection all mice were 8 weeks old. The experimental procedures were performed in agreement with the *Guide for the Care and Use of Laboratory Animals* published by the National Institutes of Health (NIH Publication No. 85–23, Revised 1996) and were approved by the French “Ministère de l'Agriculture” Guidelines (authorisation number A-93-008-01).

Mice undergoing AHx and CHx were housed for 24 hours and 14 days, respectively, in a hypoxic chamber connected to a gas pump where air circulated at a pressure of 420 mm Hg (~4500 m). Hypobaric hypoxia was maintained by a vacuum source at flow rates sufficient to prevent CO₂ build-up. Chamber pressure was interrupted 20–30 minutes three times a week for cleaning, and food and water replacement. Pressure changes were achieved slowly and the renewal of air in the chamber was sufficient to ensure the composition of atmospheric air. Normoxic groups were kept in a normobaric normoxic environment (760 mm Hg) outside the hypobaric chamber. All animals were housed in standard conditions (temperature 20–23°C with a 12 hours light: 12 hours dark cycle) and had free access to tap water and food.

At the end of time of each experiment, the mice were anaesthetized with pentobarbital, 60 mg/Kg intraperitoneally. Two intra cardiac blood samples were taken for hematocrit determination with a microcentrifuge (Microspin AMES, Germany) and hemoglobin measurement (OSM 3, Radiometer, Copenhagen, Denmark).

Under sterile conditions, gastrocnemius muscles were removed, rinsed in sterile phosphate buffered saline solution (PBS). The muscles were snap frozen in liquid nitrogen or mounted in tissue freezing embedding medium (Cryoblock, Labonord, France) for immunohistochemistry techniques and then immediately placed in liquid nitrogen cooled

isopentane. Samples were stored at -80°C until time of analysis. The mice were then killed with a lethal dose of pentobarbital.

2.2. Plasma and Muscle Epo Immunoassay. The quantitative determination of mouse Epo concentration in plasma and muscle extracts was assayed by Enzyme-Linked Immunosorbent assay (ELISA) by using the Quantikine Mouse Epo Immunoassay (R&D systems Europe, Abingdon, UK). Plasma collection and assay procedure were carried out following the manufacturer's instructions. For determination of Epo plasma concentration, Nx WT, Nx Epo-TAg^h, AHx WT and AHx Epo-TAg^h were used ($n = 4$ in each group). The plasma was collected using heparin as an anticoagulant, centrifuged at $13,000 \times g$, 15 minutes at 4°C and stored at -20°C . Because nothing is known about Epo concentration in skeletal muscle, the gastrocnemius, soleus, plantaris, extensor digitorum longus and tibialis anterior muscles (hindlimb muscles) were mixed to ensure an adequate extraction volume and a sufficient protein quantity to ensure the detection by the kit. For this experiment all conditions were tested ($n = 5$ in each group). These five muscles were homogenized together in a very small volume of PBS (1:4 weight/volume) to concentrate total proteins, centrifuged for 10 minutes, $5,000 \times g$ at 4°C and directly stored at -20°C . After 2 freeze-thaw cycles to break-up the cell membranes, muscle homogenates were assayed without prior dilution whereas plasma samples required a 2-fold dilution in a calibrator diluent provided in the kit. A standard curve was done in duplicate using a stock solution of Epo standard to produce a 2-fold dilution series ranging from 3000 to 0 pg/mL. In parallel, 50 μL of sample were added to 50 μL of assay diluent specific for mouse samples into each well of a microplate coated with a monoclonal antibody against mouse Epo and incubated for 2 hours on a microplate shaker at room temperature. A positive control consisting of a recombinant Epo solution, provided in the kit, was also loaded. After washing, 100 μL of a monoclonal antibody against mouse Epo conjugated to horse radish peroxidase (HRP) were added to each well and incubated for 2 hours on a microplate shaker at room temperature. Finally, 100 μL of substrate solution were added after 4 washes and incubated for 30 minutes at room temperature on the benchtop in the dark. After 30 minutes, the reaction was stopped using 100 μL of a stop solution in each well. The optical density was measured at 450 nm. The concentration of Epo (pg/mL) detected in each sample was compared to the Epo standard curve. Finally, data were expressed as the ratio of the quantity of Epo (in pg) to that of total protein (in mg) for muscles.

2.3. Determination of Active HIF-1 α . Nuclear extracts of gastrocnemius of Nx WT, Nx Epo-Tg^h, AHx WT, AHx Epo-TAg^h, CHx WT and CHx Epo-TAg^h mice ($n = 5$ per group) were obtained by using lysis buffer A: 10 mM HEPES (pH 7.9), 1.5 mM MgCl₂, 10 mM KCl, 0.5 mM DTT, 0.1% NP-40, 2 mM Na₃VO₄, 5 mM NaF, an antiproteinase cocktail and lysis buffer B: 20 mM HEPES (pH 7.9), 1.5 mM MgCl₂, 420 mM NaCl, 0.5 mM DTT, 25% glycerol, 2 mM

Na₃VO₄, 5 mM NaF and antiprotease cocktail as described in the protocol of DuoSet IC Mouse active HIF-1 α (R&D System, Europe, Abingdon, UK). The determination of active HIF1- α has been carried out as described by the manufacturer (R&D System, Europe, Abingdon, UK).

2.4. Total RNA Isolation and cDNA Synthesis. Total RNA was extracted from the gastrocnemius muscle of mice from different groups (Nx, AHx and CHx from WT and Epo-TAg^h mice; $n = 5$ in each group) by using the RNeasy Mini Kit and it was digested with RNase free DNase Set (Qiagen, Courtaboeuf, France) following the method provided by the manufacturer. RNA preparations were quantified by using an ultraviolet visible recording spectrophotometer (LKB Pharmacia Ultrospec) using absorbencies at 260 and 280 nm. To evaluate the purity of the extracted RNA, absorbance ratios at 260 nm/280 nm (RNA/protein) were determined. We controlled the 260/280 ratio which was between 1.8 and 1.9, indicative of pure RNA. Reverse transcription (RT) was carried out to synthesize the first strand cDNA from 1.9 μg of mRNA with the SuperScript III First-Strand Synthesis System (Invitrogen, Carlsbad, CA, USA).

2.5. Semiquantitative RT-PCR. Polymerase chain reaction (PCR) techniques were used to identify the expression of Epo mRNA in the experimental samples. The cDNA sequences for the genes of interest were obtained from GenBank. All the primers sequences and RT-PCR parameters used in this study are described in Table 1. The PCR reaction mix contained 10X reaction buffer, 50 mM MgCl₂, dNTP mix (10 mM each dATP, dGTP, dCTP and dTTP at neutral pH), 1 μM primers of Epo or β -actin, Taq polymerase (Invitrogen, France), cDNA and sterile water. PCR was carried out by using a DNA Thermal Cycler (R&D Sytem, England) as follows: 95°C for 5 minutes; then 35 cycles for β -actin and 38 for Epo of denaturation at 95°C for 1 minute, annealing at 60°C for 1 minute and extension at 72°C for 1 minute each. A 10 μL portion of the amplified PCR product was analysed by electrophoresis on a 2% agarose gel that was stained with ethidium bromide for visualization of DNA bands by ultraviolet illumination. A 50–base pair (bp) ladder DNA molecular weight marker was used (Fermentas, France) to provide a size reference for the test reactions.

2.6. Real-Time RT-PCR. Real-time RT-PCR technique was used to identify the distribution of VEGF isoforms, VEGFR1 VEGFR2 and EpoR in the RNA samples. The cDNA sequences were obtained as described above and presented in Table 1. The VEGF common forward primer is located on exon 4, the VEGF120 reverse primer is located on the boundary of exon 5 and exon 7, VEGF164 reverse primer is located on the boundary of exon 5 and exon 8, and VEGF188 reverse primer is located on the boundary of exon 5 and exon 6.

The Light Cycler FastStart DNA Master SYBR Green I (Roche Biochemicals, Stockholm, Sweden) was used for quantitative analyses of the generated cDNA. The RT-PCR amplifications were performed in a total volume of 20 μL ,

TABLE 1: Sequence and hybridization temperature (T_m) of specific primers.

Gene name	Forward 5' to 3'	Reverse 5' to 3'	T_m	Amplicon size bps	Genbank accession number
VEGF120	GCCAGCACATAGAGAGAATGAGC	GGCTTGTCACATTTTCTGG	63°C	94	NM.001025257
VEGF164	GCCAGCACATAGAGAGAATGAGC	CAAGGCTCACAGTGATTTTCTGG	63°C	97	M95200
VEGF188	GCCAGCACATAGAGAGAATGAGC	AACAAGGCTCACAGTGAACGCT	63°C	171	NM.001025250
VEGFR1	CGAACTCCACCTCCATGTTT	TATCTTCATGGAGGCCTTGG	60°C	116	NM.010228.3
VEGFR2	AGAGTTGGTGGAGCATTGG	TAGGCAGGGAGAGTCCAGAA	60°C	125	NM.010612.2
Epo	AATGGAGGTGGAAGAACAGG	ACCCGAAGCAGTGAAGTGA	60°C	155	NM.007942
EpoR	GCTCCGGGATGGACTTCA	GAGCCTGGTGCAGGCTACAT	60°C	86	NM.010149
β -actin	AGAGGGAAATCGTGCCTGAC	CAATAGTGATGACCTGGCCGT	62°C	138	NM.007393

containing 5 μ L cDNA sample, 4 μ L LightCycler-FastStart DNA Master SYBR Green I, 0.5 μ L of each primer, and 2.5 mM MgCl₂. For each reaction, the polymerase was activated by a preincubation at 95°C for 10 minutes. Amplification was then performed for 45 cycles of switching between 95°C for 10 s, gene dependant T_m for 5 to 8 s, and 72°C for 8 to 15 s depending on the length of the amplicon and followed by a melting point analysis from 65 to 95°C. The results were represented as threshold cycle numbers (C_t values). Control cDNA of normoxic mouse lung was diluted and amplified to create standard curves by plotting C_t values versus cDNA templates. Relative amounts of mRNA, normalised by β -actin were calculated from C_t values according to the manufacturer's description.

2.6.1. Calculation of Relative Quantification Values. The relative quantification values were calculated according to the manufacturer's protocol (Roche Biochemicals, Stockholm, Sweden). The C_p represents the PCR cycle at which an increase in fluorescence above a baseline signal can be detected. C_p value was used to calculate the amount of RT-PCR product compared with the internal control, β -actin. The C_p value of β -actin was subtracted from the gene C_p value to evaluate the mean change in C_p in each experimental group.

2.7. Analysis of VEGFA Protein Concentration by ELISA. Gastrocnemius muscles from different groups (Nx, AHx and CHx from WT and Epo-TAG^h mice; $n = 4$ in each group) were weighted and homogenized in 5-fold volume in ice cold buffer (10 mM tris, pH 8). The suspension was centrifuged at 13,000 g at 4°C for 15 minutes. The protein content of the supernatant was determined by the Bradford assay using bovine serum albumin (BSA) as standard. The quantity of total VEGFA in the gastrocnemius muscles from WT and Epo-TAG^h mice in normoxia and following acute and chronic hypoxic exposure was determined by a commercial high-sensitivity ELISA kit (DuoSet Kit) according to the manufacturer's instructions (R&D Systems Europe, Abingdon, UK). Measurements were done in duplicate.

2.8. Immunohistochemistry

2.8.1. Section Preparation. For visualization of vascular endothelial cells we used the monoclonal antibody CD31 which recognizes platelet endothelial cell adhesion molecule (PECAM-1), a glycoprotein strongly expressed in all endothelial cells. To that end, serial 10 μ m transverse sections from the midbelly region of frozen gastrocnemius muscles samples from Nx WT, Nx Epo-TAG^h, CHx WT and CHx Epo-TAG^h ($n = 5$ in each group) were cut in a cryostat (Leica, France) at -20°C and mounted in microscope slides (Superfrost Plus, Fisher Scientific, France). The slides were fixed in cold acetone and incubated in 3% hydrogen peroxidase (H₂O₂) to inhibit any endogenous peroxidase. Then, they were blocked with 3% BSA before incubating with rat antimouse CD31/PECAM-1 monoclonal antibody (BD Biosciences Pharmingen, France) diluted 1 : 100 in the protein blocking solution. Tissue sections were incubated with a biotinylated antirat secondary antibody (Dako, France) diluted 1 : 200 in blocking solution. Staining was carried out using streptavidin-HRP (Dako, France) and revelation was done by incubating slides in the dark in a 3, 3'-diaminobenzidine (DAB) solution (Sigma, France). Negative controls were obtained by omitting the primary or secondary antibody. The sections were counterstained with haematoxylin (Sigma, France) and mounted in aqueous mounting agent (Aquatex, Darmstadt, Germany).

Because the capillary tortuosity in muscles is a function of sarcomere length, the longitudinal 10 μ m cryo-sections were stained by using haematoxylin (Sigma, France) and eosin (Sigma, France) to make sure it was constant between the different conditions. The length occupied by 10 consecutive sarcomeres was measured per longitudinal section in 2 samples of Nx and CHx with the software described below.

This technique of immunostaining does not allow to identify the various types of blood vessels (arterioles, capillaries or venules) nor the diameter of them. Consequently we used "microvessel network" as a generic term.

2.8.2. Morphometry and Assessment of Microvessel Network. Stained sections were studied under a light microscope

TABLE 2: Body weight, hematocrit and haemoglobin concentration in wild-type (WT) and Epo-Tag^h mice in normoxia (Nx), acute hypoxia for 24 hours (AHx) and chronic hypoxia for 14 days (CHx) ($n = 14$ in each group).

	WT			Epo-TAG ^h		
	Nx	AHx	CHx	Nx	AHx	CHx
Body weight (g)	24.2 ± 1.3	23.1 ± 1.1	23.5 ± 0.9	23.0 ± 1.1	23.6 ± 1.3	23.1 ± 1.9
Muscle weight (g)	0.15 ± 0.03	0.12 ± 0.01	0.15 ± 0.03	0.15 ± 0.02	0.12 ± 0.02	0.13 ± 0.01
Hematocrit (%)	45.3 ± 1.6	51.7 ± 1.3*	60.3 ± 1.6*#	19.3 ± 1.1\$	21.6 ± 1.5*\$	27 ± 1.9*\$
[Haemoglobin] g/dL	17.3 ± 0.3	16.9 ± 0.4	19.2 ± 0.5*	6.7 ± 0.5\$	6.1 ± 0.2\$	7.1 ± 0.5\$

Values are means ± SD.

*Significantly different from corresponding Nx group, $P < .05$; #, significantly different from corresponding AHx group, $P < .01$; \$, significantly different from corresponding WT group, $P < .05$.

connected to a digital camera (Coolpix 990, Nikon). Photographs were taken at x40 magnification. Image calibration was done by taking a photo of a micrometric glass coverslip at X40 magnification. Explora Nova image analysing software (Explora Nova Morpho, La Rochelle, France) was used to analyse the images. To determine the microvessel network we analysed two different sections. On each section, we have chosen two different areas for the deep region and for the superficial region. Capillary density (CD) and capillary-to-fiber ratio (C/F) were quantified for each entire area. All transversely cut capillaries were counted and if a capillary was sectioned longitudinally, it was counted as one each time it crossed a junction between three or more muscle fibers. The individual fiber parameters were evaluated by counting an average of 70 fibers by area. For each individual fiber the following parameters were evaluated: (a) the number of capillaries around a single fiber (capillary contacts, CC); (b) the CC relative to the area of the fiber (CCFA); (c) the length of the contact between the microvessels and the fibers (LC); (d) the capillary-to-fiber ratio on an individual-fiber basis (C/F_i); (e) fiber cross-sectional area (FA); and (f) fiber perimeter (PF). Obliquity in fiber sectioning was assessed by using the form factor (FF) that represents: $(4\pi \times \text{fiber area})/(\text{fiber perimeter})^2$ (a perfect circle will have a FF of 1, whereas a line's FF will approach zero). The capillary-to-fiber perimeter exchange (CFPE) index was calculated to obtain an index of the size of the capillary-to-fiber interface and was determined from the equation: $\text{CFPE index} = (C/F_i)/P$ [25].

The index of capillary tortuosity can be indirectly determined by LC/PF . This index is expressed as a percentage of muscle fiber perimeters in contact with the capillary wall.

All quantitative analyses were blinded by the same observer.

2.9. Statistical Analysis. Two-way analysis of variance (ANOVA; hypoxia versus Epo deficiency) was carried out and Newman-Keuls test was used for post hoc test. A nonparametric Mann-Whitney test was exceptionally used for plasma Epo measurements since the Nx WT group was only three mice making impossible to perform a two-way ANOVA. The statistical analyses were performed using Stastitica software (StartSoft, Tulsa, OK). All values are expressed as mean ± SD. Differences were considered to be significant at $P \leq .05$.

3. Results

3.1. Animal Characteristics. Body and muscle weights, hematocrits and haemoglobin concentrations of Nx, AHx and CHx of WT and Epo-TAG^h mice are presented in Table 2. Body and muscle weights were similar in all groups whether submitted or not to hypoxia. Hematocrit and haemoglobin concentrations were significantly 57% and 61% lower in Nx Epo-TAG^h mice than in Nx WT group demonstrating severe anaemia (global effect, $P < .001$). Exposure to hypoxia for 14 days induced a polycythemia in WT ($P < .05$). Epo-TAG^h mice also responded to hypoxia exposure, and hematocrit values were 40% higher in CHx than in Nx mice ($P < .05$). However, haemoglobin concentration in Epo-TAG^h mice did not change when compared to normoxic values.

3.2. Epo Is Not Expressed in Skeletal Muscle in both Normoxia and Acute Hypoxia. In order to validate our model we first determined the amount of Epo. We chose to measure the plasma concentration in Nx and AHx conditions for 24 hours because the hypoxia-induced erythropoiesis activation occurred during the early phase of exposure (5–9 days) [2] with a peak of expression of Epo at 24 hours. The plasma and muscle Epo measurements showed a strong reduction in Epo-deficient mice (Epo-TAG^h mice) (Table 3). In Nx Epo-TAG^h mice, Epo plasma concentration was 56% lower than in Nx WT group ($P < .05$). Acute hypoxia exposure increased Epo plasma concentration in both groups, but remained 3-fold lower than in AHx WT animals ($P < .05$). Similar results were reported for Epo muscle concentration which was 2-fold lower in Nx Epo-TAG^h mice than in Nx WT group ($P < .05$). Acute and chronic hypoxia exposure did not change Epo concentration in the skeletal muscle in neither WT nor Epo-TAG^h mice. Those results raise the question of the secretion of Epo within the skeletal muscle. Our results of classical RT-PCR did not demonstrate any expression of mRNA encoding Epo whatever the experimental condition (Figure 1(a)). Those results were confirmed by real-time RT-PCR (data not shown).

3.3. mRNA Encoding EpoR is Not Upregulated in Epo-Deficient Skeletal Muscles. Using the same transgenic model [13] we demonstrated an upregulation of mRNA encoding the EpoR in the brain which suggests an optimization of Epo signalling

TABLE 3: Plasma and muscle Epo concentration in wild-type (WT) and Epo-TAg^h mice in normoxia (Nx), after acute hypoxia for 24 hours (AHx) and chronic hypoxia for 14 days (CHx) ($n = 4$ or 5 in each group).

	Plasma [Epo] pg/mL		Muscle [Epo] pg/mg of total protein		
	Nx	AHx	Nx	AHx	CHx
WT	122 ± 16	460 ± 39*	0.121 ± 0.03	0.097 ± 0.02	0.128 ± 0.06
Epo-TAg ^h	53 ± 18\$	162 ± 25*\$	0.060 ± 0.04\$	0.082 ± 0.02	0.101 ± 0.07

Values are means ± SD.

*significantly different from corresponding Nx group, $P < .05$; \$, significantly different from corresponding WT group, $P < .05$.

TABLE 4: Indices of the microvascular supply and morphological data of gastrocnemius muscle fibers in normoxia (Nx), and after exposure to chronic hypoxia for 14 days (CHx) ($n = 5$ in each group).

	Nx				CHx			
	Superficial region		Deep region		Superficial region		Deep region	
	WT	Epo-TAg ^h	WT	Epo-TAg ^h	WT	Epo-TAg ^h	WT	Epo-TAg ^h
Global microvessel indices								
CD (cap/mm ²)	546 ± 174	611 ± 95	1699 ± 350	1587 ± 180	601 ± 105	624 ± 81	1845 ± 393	1701 ± 211
C/F	1.33 ± 0.16	1.70 ± 0.17*	2.23 ± 0.29	2.69 ± 0.29*	1.27 ± 0.15	1.65 ± 0.26*	2.28 ± 0.20	2.62 ± 0.29*
Individual fiber microvessels indices								
CC	2.89 ± 0.63	3.57 ± 0.56*	5.20 ± 0.78	6.27 ± 0.54*	2.95 ± 0.16	3.54 ± 0.46*	5.22 ± 0.82	6.19 ± 0.41*
C/F _i	1.05 ± 0.11	1.37 ± 0.21*	2.16 ± 0.26	2.46 ± 0.35*	1.09 ± 0.13	1.34 ± 0.20*	2.15 ± 0.19	2.58 ± 0.21*
LC/PF (%)	8.96 ± 1.26	11.9 ± 0.93*	30.2 ± 7.3	35.4 ± 8.7	10.2 ± 1.84	12.56 ± 0.82*	32.5 ± 8.0	37.0 ± 3.90
Morphological data of muscle fibers								
FA (μm ²)	2521 ± 286	2411 ± 188	1259 ± 158	1494 ± 165	2189 ± 314	2499 ± 204	1232 ± 246	1361 ± 133
PF (μm)	215 ± 17	222 ± 21	160 ± 16	173 ± 14	198 ± 13	220 ± 7	153 ± 18	165 ± 11
Form factor	0.63 ± 0.02	0.63 ± 0.03	0.64 ± 0.06	0.64 ± 0.03	0.62 ± 0.02	0.63 ± 0.02	0.65 ± 0.04	0.65 ± 0.04

Values are means ± SD;

Main effect of Epo deficiency: significantly different from WT group: * $P < .05$.

CD: capillary density; C/F: capillary-to-fiber ratio; CC: number of capillaries around single fibers; C/F_i: individual capillary-to-fiber ratio; LC/PF: length of the contact between microvessels and the fiber/perimeter of the fibers; FA: fiber area; PF: perimeter.

to Epo deficiency. In the skeletal muscle we did not find any upregulation of EpoR mRNA (Figure 1(b)). Moreover, it can be noticed that the amount of EpoR is extremely weak when compared to β -actin (Figure 1(b)).

3.4. Epo Deficient Gastrocnemius Does Not Exhibit Fiber Atrophy and it Presents Developed Microvessel Network. We hypothesised that Epo deficiency could induce changes in the microvessel network of the skeletal muscle as well as muscle fiber atrophy. Immunostaining analysis of CD 31/PECAM-1 was designed to visualise the distribution of vessels in gastrocnemius muscles (superficial and deep region) of WT and Epo-TAg^h mice after exposure to chronic hypoxia (Figure 2). The morphometric parameters measured are reported in Table 4. The two-way ANOVA showed a main global effect of Epo deficiency in the microvessel network when expressed in C/F, C/F_i and CC. These three parameters were higher in Epo-TAg^h mice when compared to WT ($P < .05$; Table 4) in both superficial and deep regions of the gastrocnemius muscle (Figure 2).

The LC/PF ratio was higher in Epo-deficient mice compared with WT mice, but only in the superficial region of

gastrocnemius (+34% and +23% in Nx Epo-TAg^h and CHx Epo-TAg^h groups, resp.; main global effect of Epo deficiency, $P < .05$). No statistical difference was shown in the deep regions, but the values of Epo-TAg^h mice tended to be higher than WT mice in normoxia and after chronic hypoxia (Table 4). The absence of any change in FF showed that the cross-sectional morphology of muscle fibers remained unchanged (Table 4). Taken together, the results of FF and LC/PF suggest a change in microvessel tortuosity in the superficial region of the gastrocnemius muscle in Epo-TAg^h mice.

The CD, FA and PF were not significantly altered in any examined groups and experimental conditions (Table 4). Equality, the CC expressed in relation to fiber area (CCFA) and the C/F_i ratio expressed in relation to fiber perimeter (CFPE) were similar in all groups, whether submitted to hypoxia or not (data not shown).

3.4.1. Sarcomere Length. The sarcomere length of the gastrocnemius was homogeneous among myofibrils of each group (data not shown).

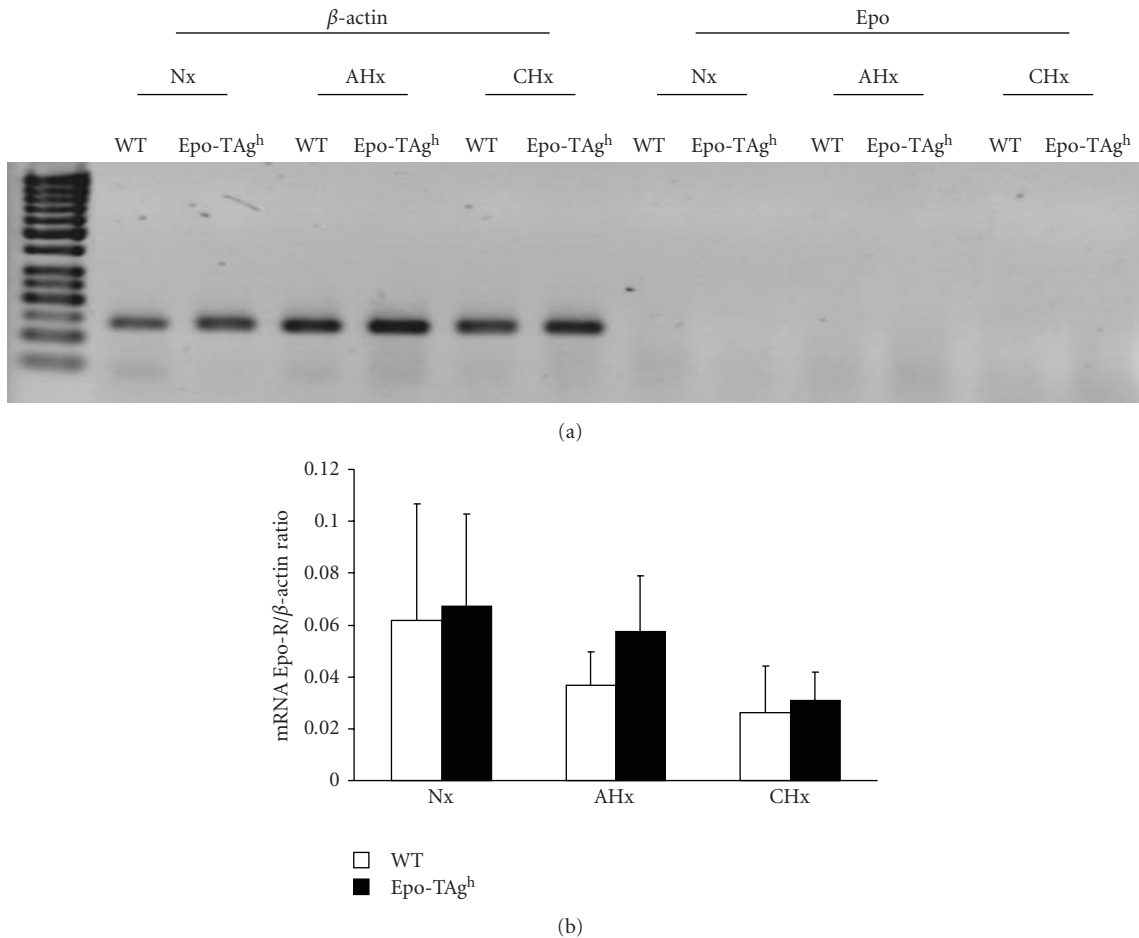


FIGURE 1: Expression of Epo and EpoR mRNA in gastrocnemius muscle of wild-type (WT) and Epo-TAg^h mice in normoxia (Nx) and following acute hypoxia for 24 hours (AHx) and chronic hypoxia for 14 days (CHx). (a) Semi-quantitative RT-PCR of Epo mRNA compare to β -actin. (b) Quantitative determination of EpoR mRNA in all experimental conditions. Values are means \pm SD.

3.5. Local Hypoxia Is Not Observed in Adult Epo-Deficient Gastrocnemius. Because Epo is required for oxygen delivery we suggested that Epo deficiency could induce local hypoxia. Then the amount of HIF-1 α was evaluated in normoxia as well as in hypoxia. The amount of active HIF-1 α was not changed between WT and Epo-TAg^h mice in both normoxia and hypoxia (Figure 3(a)). mRNA encoding HIF-1 α is unchanged in Nx Epo-TAg^h mice compared to Nx WT one (Figure 3(b)). When exposed to acute hypoxia both groups exhibit an upregulation of HIF-1 α mRNA ($P < .001$; Figure 3(b)) while no difference was observed in the CHx groups.

3.6. VEGF Protein Is Not Over-Expressed in Epo-Deficient Gastrocnemius Muscle. We analysed the amount of VEGF protein in gastrocnemius muscle of WT and Epo-TAg^h mice both in normoxia and submitted to acute and chronic hypoxia by ELISA. The VEGF protein concentrations are presented in Figure 3(c).

No significant difference was observed in VEGF protein level between WT and Epo-TAg^h normoxic groups. In WT mice, the level of VEGF protein increased by 29% ($P < .01$)

after acute exposure to hypoxia. In contrast, VEGF protein content was reduced by 21% after CHx, in comparison with normoxic values ($P < .05$). The VEGF protein content in Epo-TAg^h mice failed to change with hypoxia exposure.

In comparison with AHx WT, the amount of VEGF protein was 30% lower in AHx Epo-TAg^h ($P < .01$) whereas it was 28% higher in CHx Epo-TAg^h than in CHx WT ($P < .01$).

3.7. Differential Regulation of mRNA VEGF120, 164 and 188 Isoforms and VEGFR1 and 2 mRNA. Using real-time RT-PCR, we quantified the expression of mRNA spliced variant isoforms VEGF120, VEGF164 and VEGF188 as well as VEGFR1 and VEGFR2 of WT and Epo-TAg^h in the gastrocnemius muscle of Nx, AHx and CHx mice groups in order to examine the responses of VEGF isoforms to Epo deficiency and decreased oxygen transfer. Our results showed that the expression of VEGF120 and VEGFR2 were modulated in hypoxia and/or Epo deficiency only (Figures 4(a) and 4(e)). VEGF 120 mRNA was up regulated ($P < .001$) in acute hypoxia in WT mice compared to Nx groups. For Epo-deficient mice, significant upregulation of VEGF120

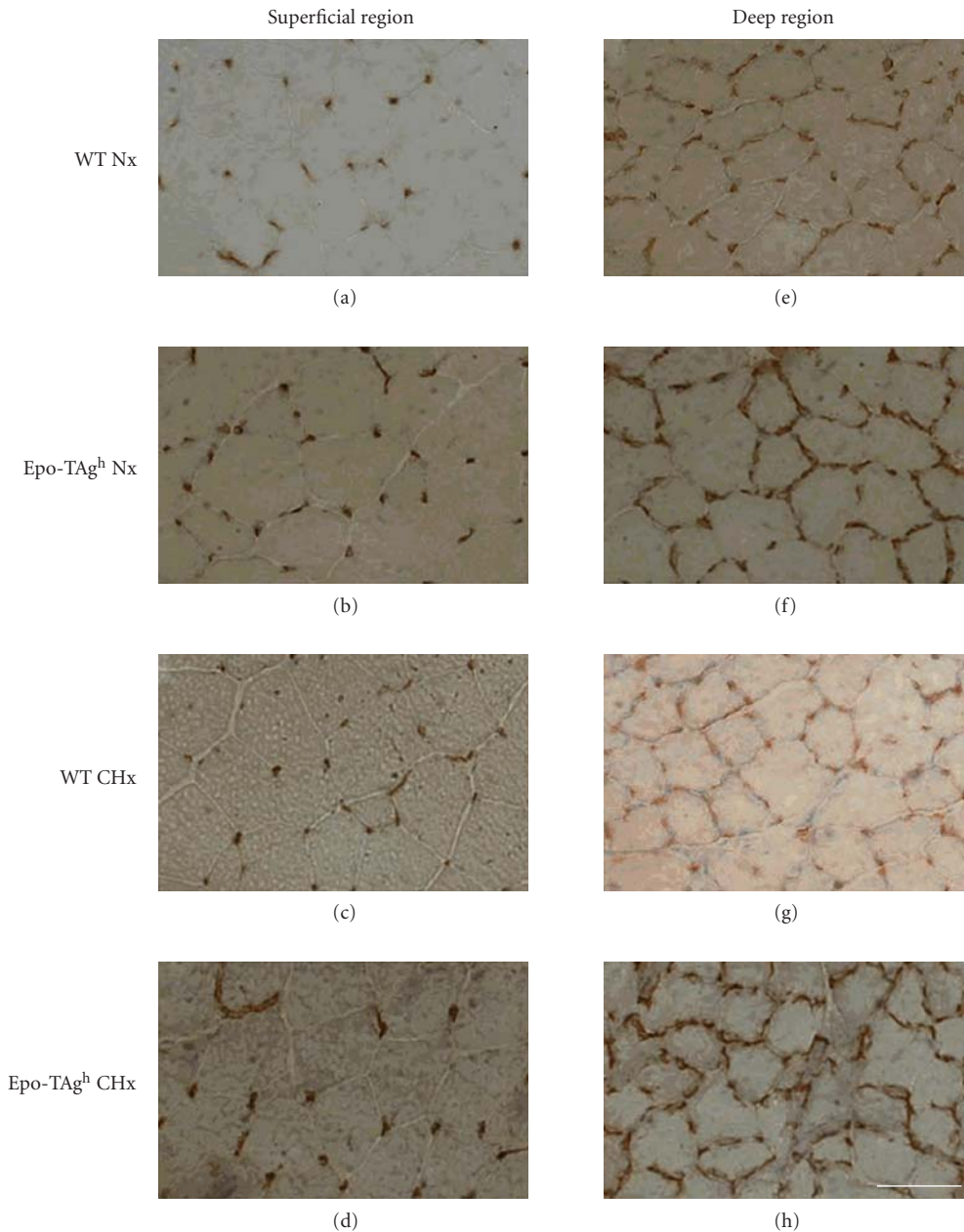


FIGURE 2: Muscle cross-section of the superficial ((a) to (d)) and deep region ((e) to (h)) of the gastrocnemius muscle of wild-type (WT) and Epo-TAg^h mice stained by using the monoclonal antibody antiCD31 for the detection of the microvessel network in normoxia (Nx) and following chronic hypoxia for 14 days (CHx). Epo deficiency develops the microvessel network in mice. Bars = 50 μ m.

mRNA was observed in CHx only ($P < .001$). VEGFR2 mRNA was upregulated in Nx Epo-TAg^h group compared to Nx WT ($P < .001$). In chronic hypoxia, VEGFR2 mRNA were upregulated in both Epo and WT groups compared to corresponding normoxic ones (Figure 4(e)).

The rate of expression of VEGF164 and VEGF188 mRNA remained unaffected by either hypoxia exposure or Epo deficiency (Figures 4(b) and 4(c)). VEGFR1 mRNA was upregulated by acute hypoxia in Epo-TAg^h mice compared to Nx Epo-TAg^h and AHx WT ($P < .01$; Figure 4(d)). No difference was observed in chronic hypoxia and/or in normoxic Epo-deficient mice compared to WT ones.

4. Discussion

In this work, we aimed to determine whether Epo deficiency could be involved in the skeletal muscle fibers atrophy and the alteration of microvessel network. In fact, it has been suggested that Epo could be an important growth factor for skeletal muscle development and repair. Our principal findings are: (1) Epo-deficient anemic muscles do not exhibit atrophy in both normoxia and hypoxia; (2) microvessel network of Epo-deficient mice is improved compared to WT mice; (3) when exposed to hypoxia Epo is not accumulated in hindlimb muscles and both mice linages exhibit an

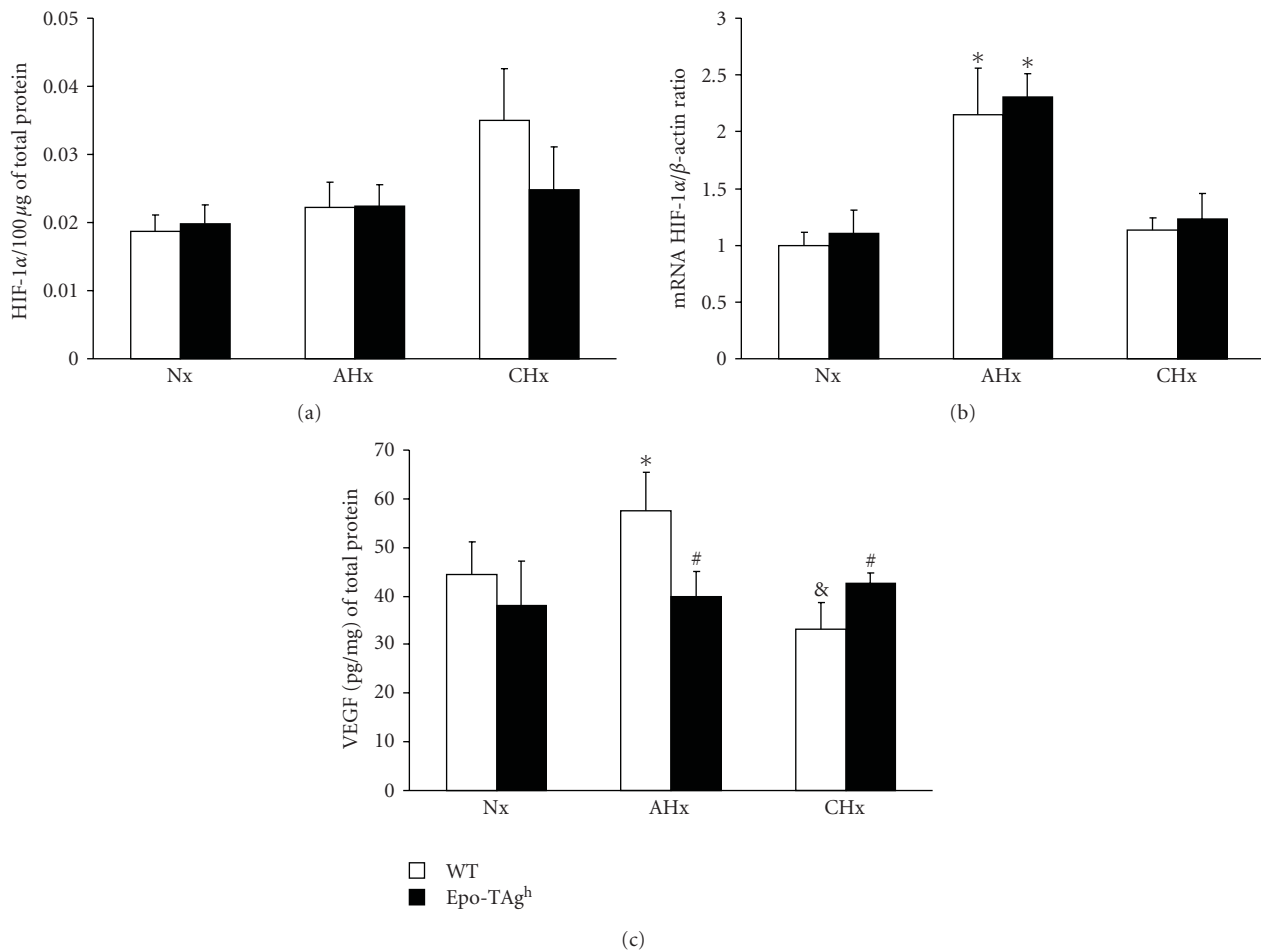


FIGURE 3: Quantitative determination of (a) activated HIF- α protein and (b) HIF- α mRNA and (c) VEGF protein in the gastrocnemius muscle of wild-type (WT) and Epo-TAG^h mice in normoxia (Nx) and following acute hypoxia for 24 hours (AHx) and chronic hypoxia for 14 days (CHx). Values are means \pm SD. *, significantly different from corresponding Nx group, $P < .01$. #, significantly different from corresponding WT group, $P < .05$. &, significantly different from corresponding AHx group, $P < .05$.

upregulation of VEGF120 and VEGFR2 in gastrocnemius muscle; (4) EpoR expression is not upregulated by either hypoxia or Epo deficiency.

Our transgenic model (Epo-TAG^h) is able to survive to 14 days in severe hypoxia (4500 m) despite the weak expression of Epo. In fact, in these mice, the expression of Epo gene is reduced, but the production of Epo still exists [23]. The amount of Epo is dramatically reduced in plasma resulting in a severe anaemia in these mice while a slight reduction is observed in hindlimb muscles. However, although Epo availability was lower in Epo-TAG^h than in WT mice after acute exposure to hypoxia (24 hours), the Epo protein expression remained responsive to the hypoxic stimulus as previously described [23]. Actually, in mice submitted to acute hypoxia, plasma Epo is increased in both WT and Epo-TAG^h compared to normoxic mice even if the Epo level is considerably lower in Epo-TAG^h than in WT mice. In hindlimb muscles, we did not find any difference between Epo levels in normoxic and acute hypoxic mice. In rodent, it has been demonstrated an upregulation of mRNA encoding Epo in kidney as early as the first hour of exposure to hypoxia

leading to a peak of plasma Epo between the 12th and the 24th h of exposure [26]. Similar results were obtained in the brain [13]. Since we did not detect the presence of RNA encoding Epo at any experimental point, the weak amount of Epo protein we measured in muscle probably corresponded to the Epo present in capillaries or in the interstitial environment of myofibers. Those results do not support the idea that Epo is secreted by the skeletal muscle when exposed to both normoxia or hypoxia at rest as it has been shown in rats submitted to exercise [27]. Furthermore, the low amount of EpoR encoding mRNA as well as the absence of regulation of its expression in Epo-deficient or hypoxic gastrocnemius consolidates the hypothesis by which Epo is not an important growth factor in the skeletal muscle in our experimental conditions. In order to explain the presence of mRNA encoding EpoR in the gastrocnemius muscle we suggest that few nonmuscle cells could express EpoR. Lately, LeBaron et al. [28] demonstrated that cells dispersed in the fascia of rat quadriceps were able to respond to Epo injections by STAT5 phosphorylation. Taken together these results suggest that circulating nonresident cells originating

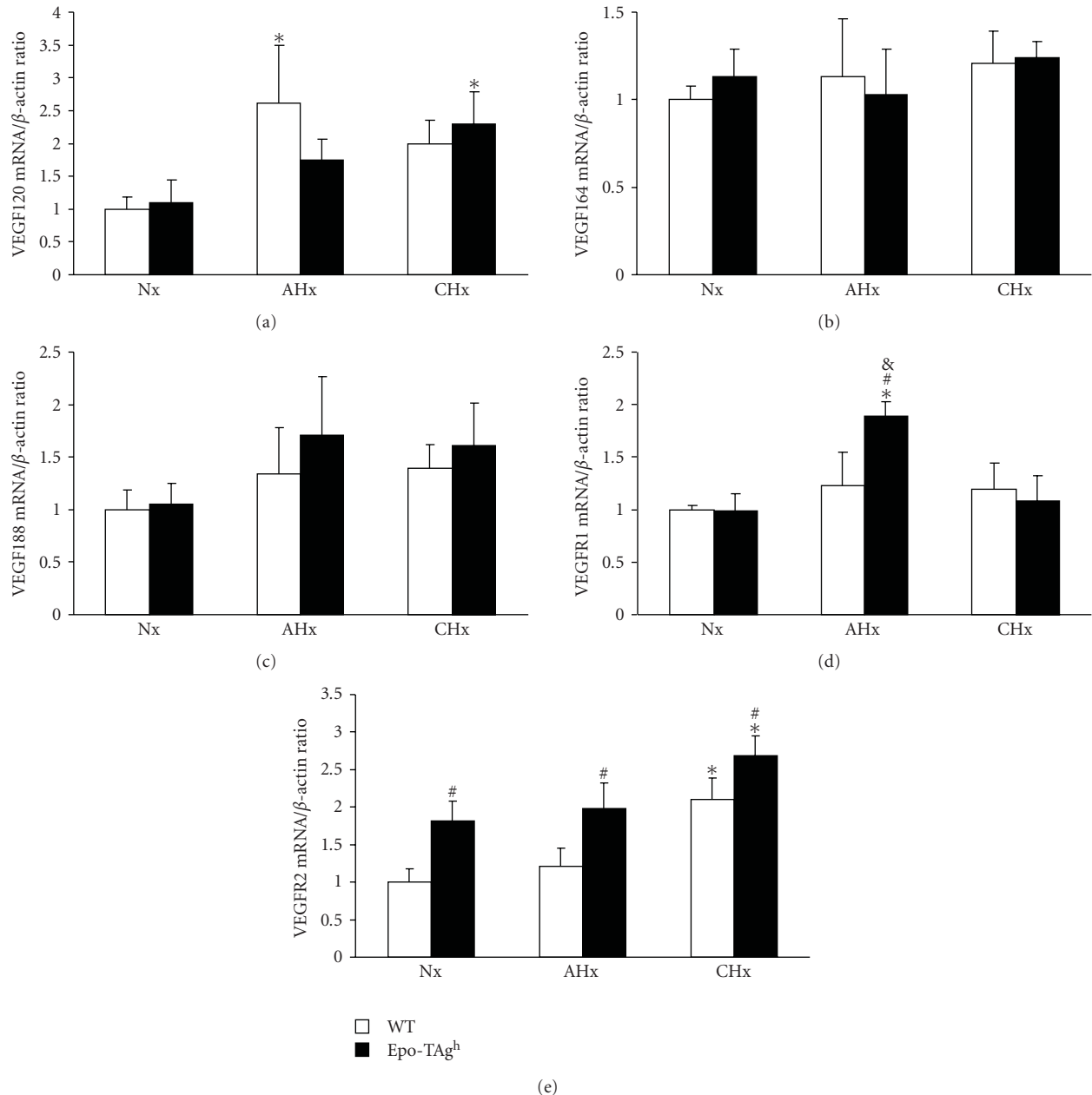


FIGURE 4: Quantitative determination of VEGF and VEGFR isoforms mRNA in the gastrocnemius muscle of wild-type (WT) and Epo-TAg^h mice in normoxia (Nx) and following acute hypoxia for 24 hours (AHx) and chronic hypoxia for 14 days (CHx). (a) VEGF120 mRNA. (b) VEGF164 mRNA. (c) VEGF188 mRNA. (d) VEGFR1 mRNA. (e) VEGFR2 mRNA. Values are means \pm SD. *, significantly different from corresponding Nx group, $P < .01$. #, significantly different from corresponding WT group, $P < .01$. &, significantly different from corresponding CHx group, $P < .05$.

from bone marrow could explain the expression of EpoR. Moreover, the injection of rHuEpo in musculocutaneous tissues induces the upregulation of endothelial nitric oxide synthase (eNOS) and prevents musculocutaneous tissues from ischemic damage [29]. These results suggest that Epo could have some indirect effects on the skeletal muscle such as increasing the perfusion of arteriolar or the mobilisation of nonresident stem cells in traumatizing conditions. In our work, we did not test these hypotheses.

In the present study, Epo deficiency does not induce skeletal muscle atrophy even when mice are exposed to hypoxia, but we observe the improvement of microvessel network when determined through parameters evaluating angiogenesis such as C/F , C/F_i , CC and LC/PF. The capillary number per area of muscle (CD) is an unreliable index of angiogenesis if the muscle fibers enlarge or atrophy [30, 31]. Indeed, some studies showed that body and muscle mass is reduced after exposure to hypoxia. These changes

induce a decrease in muscle fiber size and an increase in CD not necessarily by the formation of new capillaries [32]. In our work, we did not find a loss of body mass or muscle and the FA was not decreased in Epo-deficient mice. The great variations of surface area measures can explain the nonsignificant change in CD despite the increase of *C/F*. Therefore, we may conclude that the improvement of microvessel network can be attributed to angiogenesis in both studied regions. The improvement of both *C/F* and tortuosity (*LC/PF*) in the superficial region is probably due to the fact that glycolytic fibers, which are predominant in this region, are more sensitive to local hypoxia [33].

Epo and VEGF are important growth factors involved in angiogenesis [10]. Indeed, *in vitro*, these factors were shown to stimulate endothelial cell migration and proliferation, which are key steps in the formation of new vessels [10, 34]. Our data are consistent with conclusions of Suzuki et al. [12] suggesting that the lack of Epo induces a default of oxygen supply to tissues which in turn activates a locally HIF-VEGF dependent angiogenic pathway. Although we did not demonstrate any accumulation of either active HIF-1 α or VEGF protein, we suggest that the improvement of capillary network occurred during muscle development. These results show that Epo is dispensable first for microvessel formation and maintenance in the skeletal muscle.

In chronic altitude hypoxia, several biological responses occur to compensate for the negative effects of reduced oxygen availability [35]. Nevertheless, there has been a number of discrepancies in the literature about physiological adaptations to altitude and angiogenesis in the skeletal muscle (for review, see [36, 37]). Hansen-Smith et al. [38] found an increased capillary density in the white part of the gastrocnemius muscle but no change in the number of capillaries around a single fiber in the red and white parts of gastrocnemius of mice submitted to 7 and 21 days of hypoxia (~7200 m). Smith and Marshall [39] showed that an arteriolar remodelling within the skeletal muscle in rats during acclimatisation to chronic hypoxia occurs between the 7th and the 18th day of exposure to hypoxia (4500 m). Conversely, Snyder et al. [40] and Olfert et al. [41] did not find any hypoxia-induced angiogenesis in murin models. Deveci et al. [42] suggested that the angiogenic response might be divergent between oxidative and glycolytic rat muscles. For that reason we chose a regionalised muscle for our experiments: the gastrocnemius. The deep region of this muscle is characterized as predominantly fast-twitch red fibers and the superficial region as predominantly fast-twitch white fibers [43]. Our results confirm the idea that chronic hypoxia does not provide a sufficient stimulus to induce capillary growth in mice skeletal muscles at least in the early phase of acclimatisation of hypoxia. Actually, it has been described by some authors as a late acclimatisation (up to 5 weeks) to hypoxia which consists in skeletal muscle atrophy [44] inducing in some cases the increase of capillary density (for review [32]). The real cause of this atrophy is not yet well known and factors such as intestinal malabsorption or inactivity have been

suggested to be involved in this late acclimatisation to hypoxia. In this work we focused on the role of Epo on the Epo-dependent early phase of acclimatisation, so we may conclude that the lack of change in muscle capillary bed and the absence of skeletal muscle fiber atrophy in response to ambient hypoxia is not affected by Epo deficiency.

All studies dealing with hypoxia, VEGF and skeletal muscles have addressed the VEGF164, which is the major isoform of VEGF in the skeletal muscle [41]. We did not find any changes in VEGF164 and VEGF188 expression in both Epo-deficient or hypoxic gastrocnemius muscles. Interestingly, both Epo-deficient and WT mice exhibit a VEGF120 response to hypoxia. This response is combined with the upregulation of VEGFR2 in WT mice. Among all VEGF isoforms, VEGF120 has been shown to have the weakest angiogenic effect. VEGF120/120 mutants exhibit severe defects in vessel network [16, 45]. Moreover, it has been demonstrated that VEGF120 does not induce either the activation or the accumulation of endothelial cells in culture. Lately, it has been proposed that VEGF120, when binding to VEGFR2 receptor, may be involved in the control of dilatation and permeability of vessels [46] especially on endothelial cells of the human umbilical cord. Moreover, it has been demonstrated that VEGF120 in brain melanoma was able to diffuse away from the tumour in order to recruit vasculature from surrounding tissues [47]. Taken together, these results may suggest that acute hypoxia induces the upregulation of VEGF120 which acts through VEGFR2 signalling and improves the recruitment of existing capillaries in order to ameliorate oxygen supply to the muscle. Surprisingly, the upregulation of VEGF120 in Epo-deficient gastrocnemius is delayed when compared to WT. This phenomenon needs further investigation in order to understand if this delay is due to (1) Epo deficiency; (2) upregulation of VEGFR1, which is known to regulate the action of VEGFR2, or (3) the fact that VEGFR2 is already over-expressed in Epo-deficient mice. Furthermore, these results suggest a nonangiogenic adaptation of microvessels when both groups of mice were exposed to hypoxia but this hypothesis needs to be verified through further investigation, using new imaging techniques, for instance.

To conclude, this report showed that the gastrocnemius muscle possesses the remarkable feat to compensate Epo deficiency-induced anaemia by developing its microvessel network. Therefore Epo deficiency alone is not a sufficient factor to explain muscle deconditioning in patients suffering from severe renal failure. Moreover, we showed that the skeletal muscle exhibits an upregulation of VEGF120 and VEGFR2 when submitted to hypoxia, which suggests an improvement in the dilatation of pre-existing microvessel network in order to ameliorate oxygen supply.

Acknowledgment

The authors gratefully acknowledge Stephane Chambris for his technical support.

References

- [1] F. Li, Z. Z. Chong, and K. Maiese, "Erythropoietin on a tightrope: balancing neuronal and vascular protection between intrinsic and extrinsic pathways," *Neurosignals*, vol. 13, no. 6, pp. 265–289, 2004.
- [2] C. E. Bozzini, et al., "Enhanced erythropoietin production during hypobaric hypoxia in mice under treatments to keep the erythrocyte mass from rising: implications for the adaptive role of polycythemia," *High Altitude Medicine and Biology*, vol. 6, no. 3, pp. 238–246, 2005.
- [3] P. H. Abbrecht and J. K. Littell, "Erythrocyte life-span in mice acclimatized to different degrees of hypoxia," *Journal of Applied Physiology*, vol. 32, no. 4, pp. 443–445, 1972.
- [4] J. P. Richalet, J. C. Souberbielle, A. M. Antezana, et al., "Control of erythropoiesis in humans during prolonged exposure to the altitude of 6,542 m," *American Journal of Physiology*, vol. 266, no. 3, part 2, pp. R756–R764, 1994.
- [5] B. A. Witthuhn, F. W. Quelle, O. Silvennoinen, et al., "JAK2 associates with the erythropoietin receptor and is tyrosine phosphorylated and activated following stimulation with erythropoietin," *Cell*, vol. 74, no. 2, pp. 227–236, 1993.
- [6] W. Jelkmann, "Erythropoietin after a century of research: younger than ever," *European Journal of Haematology*, vol. 78, no. 3, pp. 183–205, 2007.
- [7] M. Ogilvie, X. Yu, V. Nicolas-Metral, et al., "Erythropoietin stimulates proliferation and interferes with differentiation of myoblasts," *Journal of Biological Chemistry*, vol. 275, no. 50, pp. 39754–39761, 2000.
- [8] C. Lundby, Y. Hellsten, M. B. F. Jensen, A. S. Munch, and H. Pilegaard, "Erythropoietin receptor in human skeletal muscle and the effects of acute and long-term injections with recombinant human erythropoietin on the skeletal muscle," *Journal of Applied Physiology*, vol. 104, no. 4, pp. 1154–1160, 2008.
- [9] R. Rotter, M. Menshykova, T. Winkler, et al., "Erythropoietin improves functional and histological recovery of traumatized skeletal muscle tissue," *Journal of Orthopaedic Research*, vol. 26, no. 12, pp. 1618–1626, 2008.
- [10] K. Jaquet, K. Krause, M. Tawakol-Khodai, S. Geidel, and K.-H. Kuck, "Erythropoietin and VEGF exhibit equal angiogenic potential," *Microvascular Research*, vol. 64, no. 2, pp. 326–333, 2002.
- [11] N. Kertesz, J. Wu, T. H.-P. Chen, H. M. Sucof, and H. Wu, "The role of erythropoietin in regulating angiogenesis," *Developmental Biology*, vol. 276, no. 1, pp. 101–110, 2004.
- [12] N. Suzuki, O. Ohneda, S. Takahashi, et al., "Erythroid-specific expression of the erythropoietin receptor rescued its null mutant mice from lethality," *Blood*, vol. 100, no. 7, pp. 2279–2288, 2002.
- [13] R. El Hasnaoui-Saadani, A. Pichon, D. Marchant, et al., "Cerebral adaptations to chronic anemia in a model of erythropoietin-deficient mice exposed to hypoxia," *American Journal of Physiology*, vol. 296, no. 3, pp. R801–R811, 2009.
- [14] Z. Poltorak, T. Cohen, R. Sivan, et al., "VEGF145, a secreted vascular endothelial growth factor isoform that binds to extracellular matrix," *Journal of Biological Chemistry*, vol. 272, no. 11, pp. 7151–7158, 1997.
- [15] E. Fischer, R. Mitchell, T. Hartman, et al., "The human gene for vascular endothelial growth factor: Multiple protein forms are encoded through alternative exon splicing," *Journal of Biological Chemistry*, vol. 266, no. 18, pp. 11947–11954, 1991.
- [16] Y.-S. Ng, R. Rohan, M. E. Sunday, D. E. Demello, and P. A. D'Amore, "Differential expression of VEGF isoforms in mouse during development and in the adult," *Developmental Dynamics*, vol. 220, no. 2, pp. 112–121, 2001.
- [17] C. J. Robinson and S. E. Stringer, "The splice variants of vascular endothelial growth factor (VEGF) and their receptors," *Journal of Cell Science*, vol. 114, no. 5, pp. 853–865, 2001.
- [18] J. E. Park, G.-A. Keller, and N. Ferrara, "The vascular endothelial growth factor (VEGF) isoforms: differential deposition into the subepithelial extracellular matrix and bioactivity of extracellular matrix-bound VEGF," *Molecular Biology of the Cell*, vol. 4, no. 12, pp. 1317–1326, 1993.
- [19] I. H. Fahal, G. M. Bell, J. M. Bone, and R. H. T. Edwards, "Physiological abnormalities of skeletal muscle in dialysis patients," *Nephrology Dialysis Transplantation*, vol. 12, no. 1, pp. 119–127, 1997.
- [20] J. D. Kopple, T. Storer, and R. Casburi, "Impaired exercise capacity and exercise training in maintenance hemodialysis patients," *Journal of Renal Nutrition*, vol. 15, no. 1, pp. 44–48, 2005.
- [21] E. Kouidi, M. Albani, K. Natsis, et al., "The effects of exercise training on muscle atrophy in haemodialysis patients," *Nephrology Dialysis Transplantation*, vol. 13, no. 3, pp. 685–699, 1998.
- [22] K. Binley, Z. Askham, S. Iqbal, et al., "Long-term reversal of chronic anemia using a hypoxia-regulated erythropoietin gene therapy," *Blood*, vol. 100, no. 7, pp. 2406–2413, 2002.
- [23] P. H. Maxwell, M. K. Osmond, C. W. Pugh, et al., "Identification of the renal erythropoietin-producing cells using transgenic mice," *Kidney International*, vol. 44, no. 5, pp. 1149–1162, 1993.
- [24] N. Charifi, F. Kadi, L. Féasson, F. Costes, A. Geysant, and C. Denis, "Enhancement of microvessel tortuosity in the vastus lateralis muscle of old men in response to endurance training," *Journal of Physiology*, vol. 554, no. 2, pp. 559–569, 2004.
- [25] R. T. Hepple, "A new measurement of tissue capillarity: the capillary-to-fibre perimeter exchange index," *Canadian Journal of Applied Physiology*, vol. 22, no. 1, pp. 11–22, 1997.
- [26] W. Jelkmann, "Erythropoietin," *Journal of Endocrinological Investigation*, vol. 26, no. 9, pp. 832–837, 2003.
- [27] H. Ameln, T. Gustafsson, C. J. Sundberg, et al., "Physiological activation of hypoxia inducible factor-1 in human skeletal muscle," *FASEB Journal*, vol. 19, no. 8, pp. 1009–1011, 2005.
- [28] M. J. LeBaron, T. J. Ahonen, M. T. Nevalainen, and H. Rui, "In vivo response-based identification of direct hormone target cell populations using high-density tissue arrays," *Endocrinology*, vol. 148, no. 3, pp. 989–1008, 2007.
- [29] F. Rezaeian, R. Wettstein, J.-F. Egger, et al., "Erythropoietin-induced upregulation of endothelial nitric oxide synthase but not vascular endothelial growth factor prevents musculocutaneous tissue from ischemic damage," *Laboratory Investigation*, vol. 90, no. 1, pp. 40–51, 2010.
- [30] O. Birot and A. X. Bigard, "Réponses du réseau capillaire du muscle squelettique à l'entraînement," *Science and Sports*, vol. 18, no. 1, pp. 1–10, 2003.
- [31] B. M. Prior, P. G. Lloyd, H. T. Yang, and R. L. Terjung, "Exercise-induced vascular remodeling," *Exercise and Sport Sciences Reviews*, vol. 31, no. 1, pp. 26–33, 2003.
- [32] H. Hoppeler and M. Vogt, "Muscle tissue adaptations to hypoxia," *The Journal of Experimental Biology*, vol. 204, part 18, pp. 3133–3139, 2001.

- [33] O. J. Birot, et al., "Exercise-induced expression of vascular endothelial growth factor mRNA in rat skeletal muscle is dependent on fibre type," *The Journal of Physiology*, vol. 552, part 1, pp. 213–221, 2003.
- [34] A. Anagnostou, E. S. Lee, N. Kessimian, R. Levinson, and M. Steiner, "Erythropoietin has a mitogenic and positive chemotactic effect on endothelial cells," *Proceedings of the National Academy of Sciences of the United States of America*, vol. 87, no. 15, pp. 5978–5982, 1990.
- [35] J. P. Richalet and J. P. Herry, *Médecine de L'alpinisme et des Sports de Montagne*, Masson, Paris, France, 4th edition, 2006.
- [36] E. Breen, K. Tang, M. Olfert, A. Knapp, and P. Wagner, "Skeletal muscle capillarity during hypoxia: VEGF and its activation," *High Altitude Medicine and Biology*, vol. 9, no. 2, pp. 158–166, 2008.
- [37] O. Mathieu-Costello, "Muscle adaptation to altitude: tissue capillarity and capacity for aerobic metabolism," *High Altitude Medicine and Biology*, vol. 2, no. 3, pp. 413–425, 2001.
- [38] F. M. Hansen-Smith, L. H. Blackwell, and G. R. Joswiak, "Expression of muscle capillary alkaline phosphatase is affected by hypoxia," *Journal of Applied Physiology*, vol. 73, no. 2, pp. 776–780, 1992.
- [39] K. Smith and J. M. Marshall, "Physiological adjustments and arteriolar remodelling within skeletal muscle during acclimation to chronic hypoxia in the rat," *Journal of Physiology*, vol. 521, no. 1, pp. 261–272, 1999.
- [40] G. K. Snyder, E. E. Wilcox, and E. W. Burnham, "Effects of hypoxia on muscle capillarity in rats," *Respiration Physiology*, vol. 62, no. 1, pp. 135–140, 1985.
- [41] I. M. Olfert, E. C. Breen, O. Mathieu-Costello, and P. D. Wagner, "Chronic hypoxia attenuates resting and exercise-induced VEGF, flt-1, and flk-1 mRNA levels in skeletal muscle," *Journal of Applied Physiology*, vol. 90, no. 4, pp. 1532–1538, 2001.
- [42] D. Deveci, J. M. Marshall, and S. Egginton, "Relationship between capillary angiogenesis, fiber type, and fiber size in chronic systemic hypoxia," *American Journal of Physiology*, vol. 281, no. 1, pp. H241–H252, 2001.
- [43] R. B. Armstrong and R. O. Phelps, "Muscle fiber type composition of the rat hindlimb," *American Journal of Anatomy*, vol. 171, no. 3, pp. 259–272, 1984.
- [44] J. D. Luedeke, R. D. McCall, R. M. Dillaman, and S. T. Kinsey, "Properties of slow- and fast-twitch skeletal muscle from mice with an inherited capacity for hypoxic exercise," *Comparative Biochemistry and Physiology—Part A*, vol. 138, no. 3, pp. 373–382, 2004.
- [45] V. Mattot, L. Moons, F. Lupu, et al., "Loss of the VEGF164 and VEGF188 isoforms impairs postnatal glomerular angiogenesis and renal arteriogenesis in mice," *Journal of the American Society of Nephrology*, vol. 13, no. 6, pp. 1548–1560, 2002.
- [46] Y. Zhang, M. Furumura, and E. Morita, "Distinct signaling pathways confer different vascular responses to VEGF 121 and VEGF 165," *Growth Factors*, vol. 26, no. 3, pp. 125–131, 2008.
- [47] B. Kusters, R. M. W. De Waal, P. Wesseling, et al., "Differential effects of vascular endothelial growth factor A isoforms in a mouse brain metastasis model of human melanoma," *Cancer Research*, vol. 63, no. 17, pp. 5408–5413, 2003.

Research Article

The Masticatory Contractile Load Induced Expression and Activation of Akt1/PKB α in Muscle Fibers at the Myotendinous Junction within Muscle-Tendon-Bone Unit

Yüksel Korkmaz,¹ Franz J. Klinz,² Mehrnoush Moghbeli,³ Klaus Addicks,² Wolfgang H.-M. Raab,¹ and Wilhelm Bloch³

¹ Department of Operative Dentistry, Periodontics and Endodontics, Heinrich-Heine-University, 40225 Düsseldorf, Germany

² Department I of Anatomy, University of Cologne, 50931 Cologne, Germany

³ Department of Molecular and Cellular Sports Medicine, German Sports University, 50933 Cologne, Germany

Correspondence should be addressed to Wilhelm Bloch, w.bloch@dshs-koeln.de

Received 2 November 2009; Accepted 4 March 2010

Academic Editor: Guy M. Benian

Copyright © 2010 Yüksel Korkmaz et al. This is an open access article distributed under the Creative Commons Attribution License, which permits unrestricted use, distribution, and reproduction in any medium, provided the original work is properly cited.

The cell specific detection of enzyme activation in response to the physiological contractile load within muscle-tendon-bone unit is essential for understanding of the mechanical forces transmission from muscle cells via tendon to the bone. The hypothesis that the physiological mechanical loading regulates activation of Akt1/PKB α at Thr308 and at Ser473 in muscle fibers within muscle-tendon-bone unit was tested using quantitative immunohistochemistry, confocal double fluorescence analysis, and immunoblot analysis. In comparison to the staining intensities in peripheral regions of the muscle fibers, Akt1/PKB α was detected with a higher staining intensity in muscle fibers at the myotendinous junction (MTJ) areas. In muscle fibers at the MTJ areas, Akt1/PKB α is dually phosphorylated at Thr308 and Ser473. The immunohistochemical results were confirmed by immunoblot analysis. We conclude that contractile load generated by masticatory muscles induces local domain-dependent expression of Akt1/PKB α as well as activation by dually phosphorylation at Thr308 and Ser473 in muscle fibers at the MTJ areas within muscle-tendon-bone unit.

1. Introduction

The muscle-tendon-bone unit contains myocytes, fibroblasts, nerve fibers, blood vessels, osteoblasts, osteoclasts, osteocytes, and extracellular matrix. The integrity of the muscle-tendon-bone unit is maintained through cell-cell and cell-extracellular matrix interactions. Tendons transmit forces generated from muscle cells at the muscle-tendon-junction (MTJ) to bone cells. During a signal transmission in cells of the muscle-tendon-bone unit, extracellular matrix, cell membrane, cytoskeleton, nuclear protein matrix, and gene expression are altered by mechanical loading in muscle cells and transmitted further to cells of the tendon-bone unit in autocrine as well as paracrine manner [1].

The serine/threonine protein kinase B (Akt/PKB) is a downstream effector of phosphatidylinositol 3-kinase (PI3K) and a regulator of a variety of cellular processes,

including transcription, survival, proliferation, growth, and metabolism [2, 3]. In mammals, Akt/PKB is expressed ubiquitously with three isoforms: Akt1/PKB α , Akt2/PKB β , and Akt3/PKB γ [4]. The activation of PI3K through binding of a growth factor to a receptor tyrosine kinase [5, 6] converts the membrane-bound plasma membrane lipid phosphatidylinositol 4,5-bisphosphate (PI(4,5)P₂) to phosphatidylinositol 3,4,5-trisphosphate (PI(3,4,5)P₃) [6, 7]. PI(3,4,5)P₃ anchors Akt/PKB to the plasma membrane and induces a conformational change, which results in the phosphorylation of Akt/PKB. Phosphorylated amino acid residues include the threonine residue Thr308 in the kinase catalytic domain and the serine residue Ser473 in the hydrophobic motif of Akt1/PKB α [3]. Full activation of Akt1/PKB α requires phosphorylation of the enzyme at Thr308 and at Ser473 [8]. It is well established that Thr308 is phosphorylated by 3-phosphoinositide-dependent kinase-1 (PDK1) [9]. The

phosphorylation of Akt1/PKB α at Ser473 is mediated by both mammalian target of rapamycin-ricor complex (mTORC2) [10] and DNA-dependent protein kinase (DNA-PK) [11] depending on type of stimulus.

The knowledge about bone remodelling by mechanical load generated from muscle cells to the bone cells requires understanding of the complete signal transmission between cells of the muscle-tendon-bone unit. However, in contrast to separate studies performed on muscle, tendon, or bone cells, there are no *in vivo* or *in vitro* studies about effects of the physiological forces generated by muscle cells and transmitted via tendon to the bone cells in model systems that contain muscle-tendon-bone unit cells.

The activation of Akt1/PKB α is involved in different functions of the muscle, tendon, and bone cells. Akt1/PKB α promotes muscle cell differentiation [12, 13] and induces muscle hypertrophy [14–16]. In tendon cells, IGF-I-dependent activation of Akt1/PKB α prevents apoptosis [17]. The cellular mechanism of the physiological mechanotransduction transmission that regulates Akt1/PKB α in different cell types of the muscle-tendon-bone unit is unknown. Therefore, the physiological stimuli including mastication contractile-dependent regulation of Akt1/PKB α in different types of cells within muscle-tendon-bone unit remain to be established. In sections of maxilla that contain cells of the muscle-tendon-bone unit, the expression, localization, and phosphorylation of Akt1/PKB α were investigated by quantitative immunohistochemistry using total and phospho-specific Akt1/PKB α Thr308 and Ser473 antibodies. To test the expression of Akt1/PKB α and p-Akt1/PKB α Ser473 in muscle cells at the periphery and at the myotendinous junction (MTJ) areas, immunoblot experiments were performed.

2. Materials and Methods

2.1. Reagents and Antibodies. Bovine serum albumin (BSA) was purchased from Sigma (Sigma, St. Louis, MO). Biotinylated goat antirabbit IgG, biotinylated antimouse IgG, normal goat serum (NGS), and Vectastain-ABC Kit were obtained from Vector Laboratories (Burlingame, CA, USA). Rabbit anti-Akt1/PKB α and rabbit antiphospho-Akt1/PKB α (Thr308) polyclonal antibodies were purchased from Upstate Biotechnology (Lake Placid, NY, USA). Mouse antiphospho-Akt1/PKB α (Ser473) monoclonal antibody was obtained from Cell Signaling Technology (Beverly, MA, USA). Cy3-conjugated goat antirabbit IgG was from Jackson ImmunoResearch Labs. (West Grove, PA). DyLight 488-conjugated NeutrAvidin (Pierce Biotechnology, Rockford, IL) was ligand for biotinylated antimouse IgG. DRAQ5 (Axorra, San Diego, CA) was used as a fluorescent DNA stain.

It is known that the antibody specificity is best determined by immunoblot techniques [18]. The specificities of Akt1/PKB α , p-Akt1/PKB α at Thr308 and at Ser473 were determined by immunoblot analysis [19].

2.2. Tissue Preparation. Male Wistar rats ($n = 12$; 3 months old, weighing 280–300 g) were fixed by transcardiac perfusion with 4% paraformaldehyde and 0.2% picric acid pH

7.4, under deep anesthesia with a mixture of Ketamine (100 mg/kg) and Xylazine (5 mg/kg). The jaws were dissected with masticatory muscle using forceps and the samples demineralized in 4 N formic acid at 4°C for 14 days.

For immunoblot experiments, after sacrifice of animals ($n = 3$) by exposure to a rising concentration of CO₂ inhalation, the masticatory muscle tissues were immediately cut into two areas as peripheral area and muscle near at the MTJ area by aid of an operating microscope.

Animal handling procedures were carried out in compliance with guidelines of the local animal ethics committee.

2.3. Immunohistochemistry. In the free floating sections, endogenous peroxidases were inhibited with 0.3% H₂O₂. To block nonspecific bindings, sections were treated with 1% BSA + 10% NGS. Thereafter, sections were incubated for 48 hours at 4°C with anti-Akt1/PKB α , anti-p-Akt1/PKB α Thr308, and anti-p-Akt1/PKB α Ser473 at 1 : 800 for each antibody. Then the sections were incubated with biotin-conjugated goat antirabbit IgG (1 : 500) and biotinylated antimouse IgG (1 : 500). The sections were incubated with avidin-biotin-peroxidase complex (1 : 100) for 1 hour and the immunohistochemical reaction was visualized with 0.05% 3,3'-diaminobenzidine tetrahydrochloride (Sigma, St. Louis, MO, USA) in 0.05 M Tris-HCl buffer, pH 7.6 containing 0.01% H₂O₂ and 0.01% nickel ammonium sulphate. Control experiments were performed by omission of the primary or secondary antibodies from incubations as well as by immunoblot analysis.

2.4. Double-Immunofluorescence Labelling and Confocal Microscopy. The free floating sections were incubated with mouse anti-p-Akt1/PKB α Ser473 (1 : 800) for 24 hours at 4°C. The sections were incubated with biotinylated goat antimouse IgG (1 : 1000) and with the DyLight 488-conjugated NeutrAvidin (1 : 200) for 1 hour at RT, respectively. Then, the sections were incubated with p-Akt/PKB Thr308 for 24 hours at 4°C. The sections were incubated with Cy3-conjugated goat antirabbit IgG (1 : 1000) for 1 hour at RT in the dark. Staining of nuclear DNA staining was done using DRAQ5 (1 : 2000) as described earlier [20]. Control experiments were performed in separate incubations by omission of the primary or secondary antibodies. Images of double immunofluorescence experiments were acquired on an LSM510 confocal microscope (Zeiss, Oberkochen, Germany).

2.5. Immunoblot. The tissues were homogenized in a buffer containing proteinase and phosphatase inhibitors. Protein concentrations were determined by the method of Bradford. Protein samples were separated on an SDS-PAGE gradient gel and transferred to PVDF filters. The blots were blocked with 5% dry milk for 1 hour and incubated with Akt1/PKB α (1 : 1000) and with p-Akt1/PKB α Ser473 (1 : 1000) antibodies overnight at 4°C. The blots were incubated with HRP-conjugated secondary antibody (1 : 5000) for 1 hour at RT and subsequently developed with enhanced chemiluminescence assay for 1 minute.

2.6. Densitometry of the Immunohistochemical and Immunoblot Results. The immunostained sections were captured with a CCD camera and the staining intensities of the antibodies in muscle cells were measured in a blinded fashion. In immunoblot, the films were scanned, and the density of the specific immunoreactive bands was measured and normalized with an internal loading β -actin control.

2.7. Statistical Analysis. Data are represented as mean \pm SD. Differences between groups were compared using Student's *t*-test or one-way ANOVA with Bonferroni post-hoc test used to compare multiple means. The criterion for statistical significance was considered at a *P* value $< .05$.

3. Results

3.1. Localization of Akt1/PKB α in Cells of the Muscle-Tendon-Bone Unit. Total (t) Akt1/PKB α (nonphosphorylated and phosphorylated) was detected in a moderate staining in the peripheral part of muscle fibers (Figures 1(a) and 1(b)). In comparison to the staining intensities in peripheral areas (Figures 1(a) and 1(g)), there was an increase in total Akt1/PKB α staining at the area near to the myotendinous junction (MTJ) in the muscle fibers (Figures 1(a), 1(b), and 1(g)). Immunohistochemical control incubations without primary or secondary antibodies resulted in the disappearance of the specific reaction product (data not shown).

3.2. Localization of p-Akt1/PKB α Thr308 and Ser473 in Muscle Fibers Near the Muscle-Tendon-Bone Unit. In comparison to the very weak staining intensities of p-Akt1/PKB α Thr308 in the periphery of muscle fibers (Figures 1(c), 1(d), and 1(g)) within muscle-tendon-bone unit, phosphorylation at Thr308 was detected with a higher staining intensity in muscle fibers near to the MTJ areas (Figures 1(c), 1(d), and 1(g)). In the periphery of muscle fibers, the staining intensity of the p-Akt1/PKB α Ser473 residue was very weakly (Figures 1(e), 1(f), and 1(g)). Phosphorylation at Ser473 was detected with a higher staining intensity nearby the MTJ (Figures 1(e), 1(f), and 1(g)). In all instances, the peripheral parts of the muscle fibers were very weakly positive or almost negative for p-Akt1/PKB α Thr308 (Figures 1(c) and 1(d)) as well Ser473 (Figures 1(e) and 1(f)). The immunohistochemical controls resulted in the disappearance of the signal product (data not shown). The specificity of antibodies against Akt1/PKB α , Akt1/PKB α phosphorylated at Thr308 and Ser473 was confirmed by immunoblot analysis [19].

3.3. Immunohistochemical Colocalization of p-Akt1/PKB α Thr308 and Ser473 in Muscle Cells Nearby the MTJ. To determine whether mastication forces could stimulate full activation of Akt1/PKB α in muscle fibers, double immunofluorescence analyses of Akt1/PKB α phosphorylated at Ser473 and at Thr308 were performed.

The nuclei in cells of the muscle and tendon were visualized by staining of DNA with DRAQ5 (blue color; Figure 2(a)). Immunohistochemical localization of green

reaction product for Akt phosphorylated at Ser473 was detected only in cross sectioned muscle cells at MTJ (Figure 2(b)). The cross sectioned muscle fibers revealed also a strong red staining for Akt1/PKB α phosphorylated at Thr308 (Figure 2(c)). In muscle fibers at the MTJ areas, the colocalization of p-Akt1/PKB α phosphorylated at Thr308 and at Ser473 was detected by yellow staining (Figure 2(d)). The immunohistochemical controls resulted in the disappearance of the specific immunofluorescence signal (data not shown).

3.4. Immunoblot Analysis. Results demonstrating higher immunohistochemical staining intensities of t-Akt1/PKB α (Figures 1(a), 1(b), and 1(g)) and p-Akt1/PKB α Ser473 in muscle fibers nearby the MTJ areas were confirmed by immunoblot analysis. Immunoblot results for Akt1/PKB α are presented in Figure 3 and for p-Akt1/PKB α Ser473 in Figure 4.

In comparison to the staining intensity in periphery of muscle fibers, t-Akt1/PKB α was detected as a band of approximately 60 kDa with higher staining intensity in muscle cells nearby MTJ areas (Figure 3). The staining intensity of the p-Akt1/PKB α Ser473 residue was very weak at the peripheral part of muscle, while a characteristic band of approximately at 60 kDa for p-Akt1/PKB α Ser473 was detected with a strong staining intensity at the area nearby MTJ (Figure 4). As a loading control muscle lysates were analyzed by immunoblot with an antibody against β -actin (data not shown).

4. Discussion

Under cell culture conditions, the importance of physical stresses on a variety of cellular activities has been examined only in a single cell type, including myocytes, fibroblasts, osteoblasts, and osteoclasts. Similarly, the mechanical loads on muscle fibers, tendon, and bone cells within the muscle-tendon unit were separately investigated. In comparison to studies only in muscle, tendon, or in bone cells, we performed a quantitative immunohistochemical analysis in sections, which allows localization of the functional Akt1/PKB α protein in all cells within the muscle-tendon-bone unit. In this model, muscle contractile activity should be generated by physiological mastication. Compared to the periphery of the muscle fibers within muscle-tendon-bone unit, the protein level of the Akt1/PKB α and the phosphorylation of Akt1/PKB α at Thr308 and Ser473 were significantly higher at the MTJ area.

Tendon cells connect muscle fibers to bones and transmit forces developed by muscle fibers to the bone cells. Thus, muscle fibers apply forces to the bone cells via tendon cells, which arise from a specialized region called the MTJ. In the MTJ, myofibrils and collagen fibers overlap, forming longitudinal infoldings [21, 22]. In comparison to end-to-end contact, these overlapping contacts between muscle cells and collagen fibers increase the strength of the junction because cell membranes support shear loads better than the tensile loads [21, 22]. In muscle fiber region nearby MTJ, the physiological mastication stimuli may induce expression

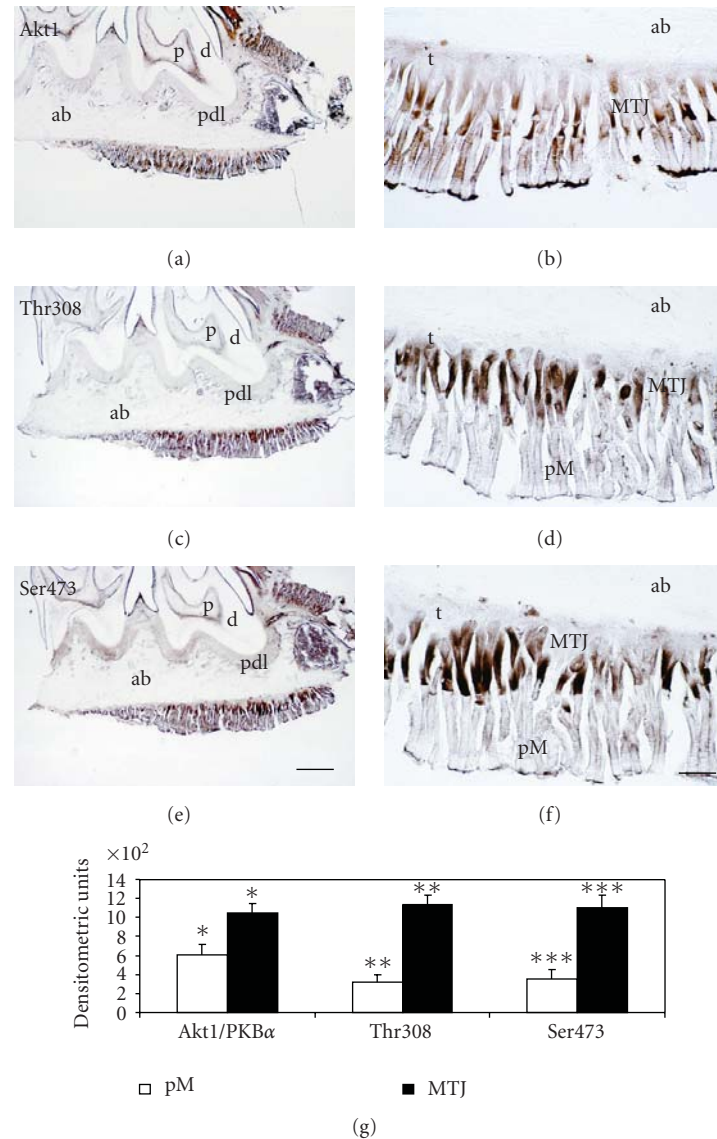


FIGURE 1: The constitutive localization of the t-Akt1/PKB α , phosphorylation of t-Akt1/PKB α at Thr308 and at Ser473 in muscle fibers within muscle-tendon-bone unit. In comparison to the staining of t-Akt1/PKB α (a, b), p-Akt1/PKB α Thr308 (c, d) and Ser473 (e, f) in the peripheral muscle fibers, t-Akt1/PKB α (b, MTJ), phosphorylation of Akt1/PKB α at Thr308 (d, MTJ) and at Ser473 (f, MTJ) were detected with higher staining intensities in muscle fibers at the myotendinous junction (MTJ) area. The staining intensity of Akt1/PKB α in peripheral muscle fibers (b, 602.70 ± 117.05) was weakly compared to those in the area near to the MTJ (b, 1050.63 ± 91.68). In comparison to the staining intensity of the p-Akt1/PKB α Thr308 in peripheral muscle fibers (d, 319.76 ± 74.57), the staining intensity of p-Akt1/PKB α Thr308 was higher in muscle fibers near to the MTJ areas (d, 1138.85 ± 98.99). The staining intensity of p-Akt1/PKB α Ser473 in muscle fibers at the MTJ areas (f, 351.65 ± 104.63) was greater than staining intensity of Ser473 in peripheral muscle areas (f, 1099.70 ± 135.93). Data are mean \pm SD; $n = 6$; significant differences were considered at a P value $< .05$. MTJ = myotendinous junction, pM = peripheral muscle fibers, ab = alveolar bone, pdl = periodontal ligament, p = pulpa, d = dentin. Bars: $640 \mu\text{m}$ for (a), (c), (e), $80 \mu\text{m}$ for (b), (d), and (f).

of Akt1/PKB α by nuclear domain regulation as well as by phosphorylation of the enzyme at Thr308 and at Ser473.

In response to physiological masticatory mechanical loading, Akt1/PKB α was detected in higher protein levels in muscle fibers nearby MTJ areas. The higher staining intensity of the t-Akt1/PKB α at MTJ may be explained by local regulation of Akt1/PKB α in different nuclear domains during transmission of forces generated by physiological mastication stimuli in muscle cells. In multinucleated muscle

fibres, it was reported that each nucleus is able to regulate protein biosynthesis in a local domain-dependent manner [23, 24]. It can be speculated that the higher number of nuclear domains present in muscle fibers nearby MTJ [25] responds to mechanical stimulation of mastication by higher production of Akt1/PKB α than nuclear domains in peripheral muscle areas.

In the consecutive muscle-tendon-bone unit sections, Thr308 and Ser473 phosphorylation sites of Akt1/PKB α were

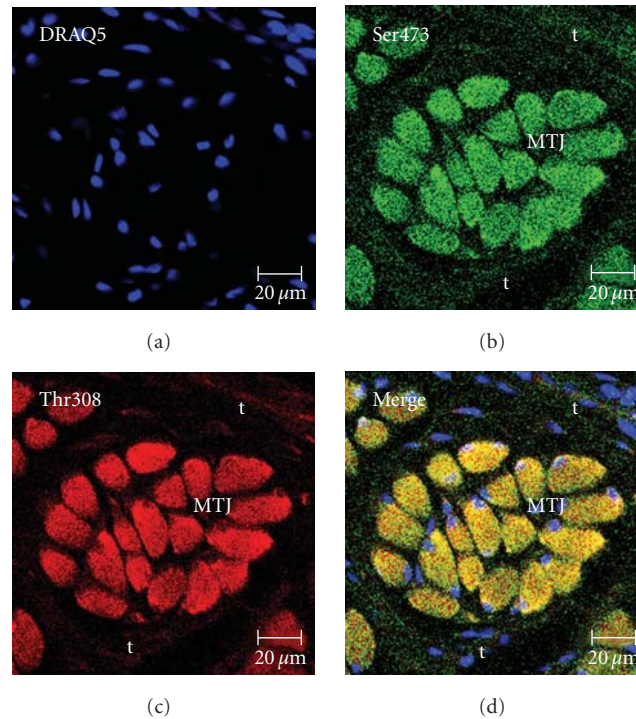


FIGURE 2: Immunofluorescence colocalization of Akt1/PKB α phosphorylated at Ser473 and at Thr308 in muscle fibers at the myotendinous areas. The nuclei in muscle fibers and tendocyte were visualized by staining of DNA with DRAQ5 (a, blue). The p-Akt1/PKB α Ser473 (b, green) was localized in across sectioned muscle fibers at the MTJ. In muscle fibers at the MTJ, p-Akt1/PKB α Thr308 (c, red) was identified. In same muscle fibers, p-Akt1/PKB α Ser473 and Thr308 were colocalized (d, yellow). The tendon cells were negative for localizations of Ser473 as well as of Thr308. MTJ = myotendinous junction, t = tendon. Bar: (a)–(d) = 20 μ m.

detected with a higher staining intensity in muscle fibers at MTJ area compared to the peripheral muscle fiber areas. Therefore, we have presumed that Akt1/PKB α may be dually phosphorylated in muscle fibers at MTJ areas. Full activation of Akt1/PKB α requires dually phosphorylation of the enzyme at Thr308 and at Ser473 [26, 27]. More recently, knockout experiments in murine embryonic fibroblast came to the conclusion that Akt/PKB monophosphorylated at Thr308 was able to activate several downstream targets [8]. In muscle cells at the MTJ areas, we have detected a colocalization of Thr308 and at Ser473. Our data indicate that full activation of Akt1/PKB α by phosphorylation at Thr308 and Ser473 is necessary for downstream signal transduction in muscle cells at the MTJ areas.

For skeletal muscle cells, it was shown by *in vitro* [28] and *in vivo* experiments [16, 29, 30] that constitutive activation of Akt1/PKB α induces hypertrophy. This effect of Akt1/PKB α in skeletal muscle is also supported by the finding that Akt1/PKB α inhibits atrophy *in vitro* as well as *in vivo* [31, 32]. In addition, mice lacking Akt1/PKB α show a decrease in muscle size compared with wild-type [15, 33]. Under consideration of these data, it is apparently that physiological constitutive phosphorylation of Akt1/PKB α in skeletal masticatory muscle cells at the MTJ areas may be involved in the muscle cell hypertrophy and muscle cell survival.

The skeletal muscle fibers are classified in type I (slow-twitch oxidative) and in type II (fast-twitch glycolytic) fibers [33]. Fast-twitch fibers are further subdivided into two general groups, the fast-twitch oxidative type IIA and fast-twitch glycolytic type IIB fibers [33]. Masticatory muscles are composed of a heterogeneous population of fiber types that vary according to their contractile properties [34, 35]. In the masseter, it was described that the type I fibers were absent [36]. The IIA and IIB fibers were distributed differently between the superior and inferior regions of the masseter [34–36]. In the deep masseter, the highest proportion of type IIB fibers is distributed [36]. The cross-sectional areas of type IIB fibers were the largest, followed by the type IIX and IIA fibers [36]. From our results, it may be suggested that physiological exercise represents a mechanism by which mastication *in vivo* induces simultaneous phosphorylation of Akt1/PKB at Ser473 and Thr308 in both fast-twitch muscle fiber types at the MTJ.

It was described that the muscle fiber type is regulated by calcineurin and the Ras-MAPK signaling, while fiber size is regulated by the PI3K-Akt/PKB-mTOR signaling [30, 37, 38]. The mTOR has been implicated in skeletal muscle hypertrophy during overload, and pharmacological inhibition of mTOR prevents overload-induced hypertrophy in both type I and type II of muscle fibers [29]. These results indicate that the hypertrophic effect on muscle

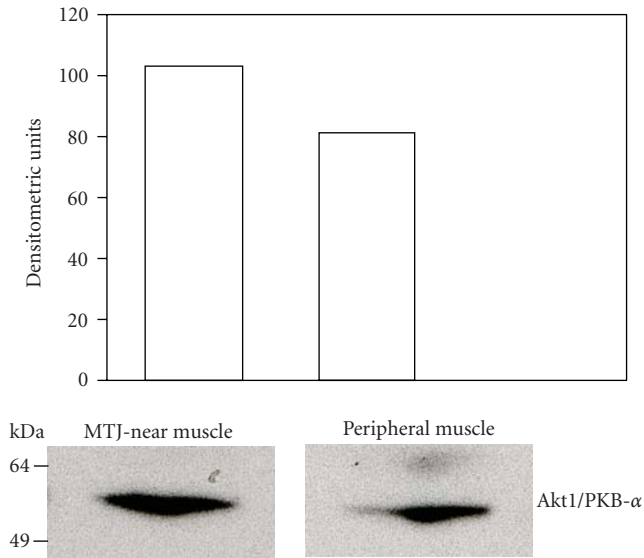


FIGURE 3: Immunoblot analysis of Akt/PKB in peripheral muscle fibers and in muscle cells near to the myotendinous areas. In peripheral masticatory muscle fibers and masticatory muscle fibers at MTJ, protein extracts were analyzed by immunoblot analysis using an antibody against Akt1/PKB α . The specific immunoblot bands of approximately 60 kDa identify Akt1/PKB α in peripheral muscle fibers and in muscle fibers near to the MTJ. The level of Akt1/PKB α in muscle fibers near to the MTJ was higher than that in peripheral muscle fibers.

fibers by Akt1/PKB α predominantly occurs through mTOR signaling [30]. Phosphorylation of Akt1/PKB α at Ser473 is mediated by mTORC2 [10]. Therefore, phosphorylation of Akt1/PKB α at Ser473 in muscle fibers at MTJ may be an important part of the mechanism by which contraction can activate Akt1/PKB α at Ser473 in fast-twitch muscles inducing masticatory muscle hypertrophy at the MTJ areas. However, it must be investigated in further studies if there is a different hypertrophy response in a single muscle fibers in masticatory muscle.

The present finding expands the current knowledge about load dependent muscle response. Beside the fact that contraction may regulate Akt1/PKB α in an intensity-, time-, and fiber type-specific manner [39, 40], it can be suggested that the response to a mechanical stimuli is inhomogeneous along a single muscle fiber at the activation and expression level. It is known that the loss of teeth and absent physiological masticatory contractile activities lead to a dramatic decrease in muscle cell masses and results especially in a strong atrophy of the alveolar bone [41]. Furthermore, it leads to an alteration of force transmission in the masticatory process [41]. Under consideration that mastication forces and mechanical loading of muscle cells are required for tissue integrity and extracellular matrix metabolism inducing phosphorylation of Akt1/PKB α in muscle cells located near to the MTJ within muscle-tendon-bone unit, it must be considered that the response is possibly not uniform along the fibres.

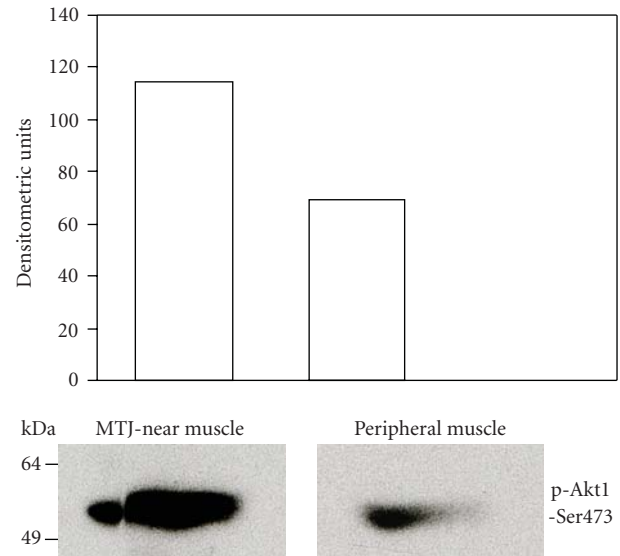


FIGURE 4: Immunoblot analysis of p-Akt1/PKB α Ser473 in peripheral muscle fibers and in muscle fibers near to the myotendinous areas. Protein extracts prepared from peripheral masticatory muscle fibers and masticatory muscle fibers at MTJ were analyzed by immunoblotting using an antibody against Akt1/PKB α phosphorylated at Ser473. The weakly phosphorylation of Akt1/PKB α at Ser473 in peripheral muscle fibers is significantly increased in muscle fibers near to the MTJ. A characteristic band almost at 60 kDa for p-Akt1/PKB α Ser473 was detectable with a higher staining intensity in muscle fibers near to the MTJ.

5. Conclusion

In the muscle-tendon-bone unit, tendons connect masticatory muscle cells to the alveolar bone and transmit masticatory forces generated by muscle cells to the alveolar bone cells. The transmission of this mechanical signal induces a full activation of Akt1/PKB α by simultaneous phosphorylation of the enzyme at Ser473 and at Thr308 in muscle fibers located near to the MTJ but not at the periphery of the muscle fibers. Therefore, we postulate that inhomogeneous physiological contractile load-dependent activation of the Akt1/PKB α phosphorylation at Thr308 and at Ser473 in masticatory muscle cells along the muscle fibers could play a role for the biological response, which can influence the development of muscle dystrophy.

Acknowledgment

This work contains part of the doctoral thesis of Mehrnoush Moghbeli.

References

- [1] M. Kjær, "Role of extracellular matrix in adaptation of tendon and skeletal muscle to mechanical loading," *Physiological Reviews*, vol. 84, no. 2, pp. 649–698, 2004.

- [2] D. P. Brazil and B. A. Hemmings, "Ten years of protein kinase B signalling: a hard Akt to follow," *Trends in Biochemical Sciences*, vol. 26, no. 11, pp. 657–664, 2001.
- [3] E. Fayard, L. A. Tintignac, A. Baudry, and B. A. Hemmings, "Protein kinase B/Akt at a glance," *Journal of Cell Science*, vol. 118, no. 24, pp. 5675–5678, 2005.
- [4] S. R. Datta, A. Brunet, and M. E. Greenberg, "Cellular survival: a play in three Akts," *Genes and Development*, vol. 13, no. 22, pp. 2905–2927, 1999.
- [5] M. P. Scheid and J. R. Woodgett, "Unravelling the activation mechanisms of protein kinase B/Akt," *FEBS Letters*, vol. 546, no. 1, pp. 108–112, 2003.
- [6] D. P. Brazil, Z.-Z. Yang, and B. A. Hemmings, "Advances in protein kinase B signalling: AKTion on multiple fronts," *Trends in Biochemical Sciences*, vol. 29, no. 5, pp. 233–242, 2004.
- [7] L. Stephens, K. Anderson, D. Stokoe, et al., "Protein kinase B kinases that mediate phosphatidylinositol 3,4,5-trisphosphate-dependent activation of protein kinase B," *Science*, vol. 279, no. 5351, pp. 710–714, 1998.
- [8] E. Jacinto, V. Facchinetti, D. Liu, et al., "SIN1/MIP1 maintains rictor-mTOR complex integrity and regulates Akt phosphorylation and substrate specificity," *Cell*, vol. 127, no. 1, pp. 125–137, 2006.
- [9] D. R. Alessi, M. Deak, A. Casamayor, et al., "3-Phosphoinositide-dependent protein kinase-1 (PDK1): structural and functional homology with the *Drosophila* DSTPK61 kinase," *Current Biology*, vol. 7, no. 10, pp. 776–789, 1997.
- [10] D. D. Sarbassov, D. A. Guertin, S. M. Ali, and D. M. Sabatini, "Phosphorylation and regulation of Akt/PKB by the rictor-mTOR complex," *Science*, vol. 307, no. 5712, pp. 1098–1101, 2005.
- [11] J. Feng, J. Park, P. Cron, D. Hess, and B. A. Hemmings, "Identification of a PKB/Akt hydrophobic motif Ser-473 kinase as DNA-dependent protein kinase," *Journal of Biological Chemistry*, vol. 279, no. 39, pp. 41189–41196, 2004.
- [12] E. M. Wilson and P. Rotwein, "Selective control of skeletal muscle differentiation by Akt1," *Journal of Biological Chemistry*, vol. 282, no. 8, pp. 5106–5110, 2007.
- [13] P. Rotwein and E. M. Wilson, "Distinct actions of Akt1 and Akt2 in skeletal muscle differentiation," *Journal of Cellular Physiology*, vol. 219, no. 2, pp. 503–511, 2009.
- [14] D. J. Glass, "Signalling pathways that mediate skeletal muscle hypertrophy and atrophy," *Nature Cell Biology*, vol. 5, no. 2, pp. 87–90, 2003.
- [15] X.-D. Peng, P.-Z. Xu, M.-L. Chen, et al., "Dwarfism, impaired skin development, skeletal muscle atrophy, delayed bone development, and impeded adipogenesis in mice lacking Akt1 and Akt2," *Genes and Development*, vol. 17, no. 11, pp. 1352–1365, 2003.
- [16] K.-M. V. Lai, M. Gonzalez, W. T. Poueymirou, et al., "Conditional activation of Akt in adult skeletal muscle induces rapid hypertrophy," *Molecular and Cellular Biology*, vol. 24, no. 21, pp. 9295–9304, 2004.
- [17] A. Scott, K. M. Khan, and V. Duronio, "IGF-I activates PKB and prevents anoxic apoptosis in Achilles tendon cells," *Journal of Orthopaedic Research*, vol. 23, no. 5, pp. 1219–1225, 2005.
- [18] R. W. Burry, "Specificity controls for immunocytochemical methods," *Journal of Histochemistry and Cytochemistry*, vol. 48, no. 2, pp. 163–165, 2000.
- [19] H.-V. Wang, L.-W. Chang, K. Brixius, et al., "Integrin-linked kinase stabilizes myotendinous junctions and protects muscle from stress-induced damage," *Journal of Cell Biology*, vol. 180, no. 5, pp. 1037–1049, 2008.
- [20] Y. Korkmaz, W. Bloch, F.-J. Klinz, et al., "The constitutive activation of extracellular signal-regulated kinase 1 and 2 in periodontal ligament nerve fibers," *Journal of Periodontology*, vol. 80, no. 5, pp. 850–859, 2009.
- [21] J. G. Tidball, "Force transmission across muscle cell membranes," *Journal of Biomechanics*, vol. 24, supplement 1, pp. 43–52, 1991.
- [22] B. M. Jockusch, P. Bubeck, K. Giehl, et al., "The molecular architecture of focal adhesions," *Annual Review of Cell and Developmental Biology*, vol. 11, pp. 379–416, 1995.
- [23] Z. W. Hall and E. Ralston, "Nuclear domains in muscle cells," *Cell*, vol. 59, no. 5, pp. 771–772, 1989.
- [24] K. Gundersen and J. C. Bruusgaard, "Nuclear domains during muscle atrophy: nuclei lost or paradigm lost?" *Journal of Physiology*, vol. 586, no. 11, pp. 2675–2681, 2008.
- [25] J. C. Bruusgaard, K. Liestol, M. Ekmark, K. Kollstad, and K. Gundersen, "Number and spatial distribution of nuclei in the muscle fibres of normal mice studied in vivo," *Journal of Physiology*, vol. 551, no. 2, pp. 467–478, 2003.
- [26] M. P. Scheid, P. A. Marignani, and J. R. Woodgett, "Multiple phosphoinositide 3-kinase-dependent steps in activation of protein kinase B," *Molecular and Cellular Biology*, vol. 22, no. 17, pp. 6247–6260, 2002.
- [27] A. Tokar and A. C. Newton, "Akt/protein kinase B is regulated by autophosphorylation at the hypothetical PDK-2 site," *Journal of Biological Chemistry*, vol. 275, no. 12, pp. 8271–8274, 2000.
- [28] A. Takahashi, Y. Kureishi, J. Yang, et al., "Myogenic Akt signaling regulates blood vessel recruitment during myofiber growth," *Molecular and Cellular Biology*, vol. 22, no. 13, pp. 4803–4814, 2002.
- [29] S. C. Bodine, T. N. Stitt, M. Gonzalez, et al., "Akt/mTOR pathway is a crucial regulator of skeletal muscle hypertrophy and can prevent muscle atrophy in vivo," *Nature Cell Biology*, vol. 3, no. 11, pp. 1014–1019, 2001.
- [30] G. Pallafacchina, E. Calabria, A. L. Serrano, J. M. Kalhovde, and S. Schiaffino, "A protein kinase B-dependent and rapamycin-sensitive pathway controls skeletal muscle growth but not fiber type specification," *Proceedings of the National Academy of Sciences of the United States of America*, vol. 99, no. 14, pp. 9213–9218, 2002.
- [31] M. Sandri, C. Sandri, A. Gilbert, et al., "Foxo transcription factors induce the atrophy-related ubiquitin ligase atrogin-1 and cause skeletal muscle atrophy," *Cell*, vol. 117, no. 3, pp. 399–412, 2004.
- [32] T. N. Stitt, D. Drujan, B. A. Clarke, et al., "The IGF-1/PI3K/Akt pathway prevents expression of muscle atrophy-induced ubiquitin ligases by inhibiting FOXO transcription factors," *Molecular Cell*, vol. 14, no. 3, pp. 395–403, 2004.
- [33] W. S. Chen, P.-Z. Xu, K. Gottlob, et al., "Growth retardation and increased apoptosis in mice with homozygous disruption of the Akt1 gene," *Genes and Development*, vol. 15, no. 17, pp. 2203–2208, 2001.
- [34] J. A. M. Korfage, J. H. Koolstra, G. E. J. Langenbach, and T. M. G. J. van Eijden, "Fiber-type composition of the human jaw muscles—(part 1) origin and functional significance of fiber-type diversity," *Journal of Dental Research*, vol. 84, no. 9, pp. 774–783, 2005.
- [35] J. A. M. Korfage, J. H. Koolstra, G. E. J. Langenbach, and T. M. G. J. van Eijden, "Fiber-type composition of the human jaw muscles—(part 2) role of hybrid fibers and factors responsible for inter-individual variation," *Journal of Dental Research*, vol. 84, no. 9, pp. 784–793, 2005.

- [36] R. Sano, E. Tanaka, J. A. M. Korfage, et al., "Heterogeneity of fiber characteristics in the rat masseter and digastric muscles," *Journal of Anatomy*, vol. 211, no. 4, pp. 464–470, 2007.
- [37] M. Murgia, A. L. Serrano, E. Calabria, G. Pallafacchina, T. Lomo, and S. Schiaffino, "Ras is involved in nerve-activity-dependent regulation of muscle genes," *Nature Cell Biology*, vol. 2, no. 3, pp. 142–147, 2000.
- [38] A. L. Serrano, M. Murgia, G. Pallafacchina, et al., "Calcineurin controls nerve activity-dependent specification of slow skeletal muscle fibers but not muscle growth," *Proceedings of the National Academy of Sciences of the United States of America*, vol. 98, no. 23, pp. 13108–13113, 2001.
- [39] K. Sakamoto, M. F. Hirshman, W. G. Aschenbach, and L. J. Goodyear, "Contraction regulation of Akt in rat skeletal muscle," *Journal of Biological Chemistry*, vol. 277, no. 14, pp. 11910–11917, 2002.
- [40] K. Sakamoto, W. G. Aschenbach, M. F. Hirshman, and L. J. Goodyear, "Akt signaling in skeletal muscle: regulation by exercise and passive stretch," *American Journal of Physiology*, vol. 285, no. 5, pp. E1081–E1088, 2003.
- [41] C. Field, Q. Li, W. Li, and M. Swain, "Influence of tooth removal on mandibular bone response to mastication," *Archives of Oral Biology*, vol. 53, no. 12, pp. 1129–1137, 2008.

Review Article

Skeletal Dysplasias Associated with Mild Myopathy—A Clinical and Molecular Review

Katarzyna A. Piróg and Michael D. Briggs

Wellcome Trust Centre for Cell Matrix Research, Faculty of Life Sciences, University of Manchester, Michael Smith Building, Oxford Road, Manchester M13 9PT, UK

Correspondence should be addressed to Katarzyna A. Piróg, katarzyna.pirog@manchester.ac.uk

Received 9 February 2010; Accepted 15 March 2010

Academic Editor: Henk L. M. Granzier

Copyright © 2010 K. A. Piróg and M. D. Briggs. This is an open access article distributed under the Creative Commons Attribution License, which permits unrestricted use, distribution, and reproduction in any medium, provided the original work is properly cited.

Musculoskeletal system is a complex assembly of tissues which acts as scaffold for the body and enables locomotion. It is often overlooked that different components of this system may biomechanically interact and affect each other. Skeletal dysplasias are diseases predominantly affecting the development of the osseous skeleton. However, in some cases skeletal dysplasia patients are referred to neuromuscular clinics prior to the correct skeletal diagnosis. The muscular complications seen in these cases are usually mild and may stem directly from the muscle defect and/or from the altered interactions between the individual components of the musculoskeletal system. A correct early diagnosis may enable better management of the patients and a better quality of life. This paper attempts to summarise the different components of the musculoskeletal system which are affected in skeletal dysplasias and lists several interesting examples of such diseases in order to enable better understanding of the complexity of human musculoskeletal system.

1. Introduction

Skeletal dysplasias are a diverse group of diseases primarily affecting the development of the osseous skeleton. They manifest with disproportionate short stature, malformations, and/or deformations and range from relatively mild to severe and lethal conditions. To date there are over 250 unique and well-characterised skeletal dysplasias, many of which can be grouped into different diagnostic groups and/or bone dysplasia families based on clinical similarities [1]. It is important to note that skeletal dysplasia mutations may also influence other nonskeletal organs, often mechanically by tightening the tracts in the body due to skeletal defects. For example, children with skeletal dysplasias often have respiratory problems and mental problems sometimes occur due to craniofacial defects [2]. Early diagnosis of skeletal dysplasias is therefore crucial for patient management and may enable relatively normal growing up and life span.

Skeletal dysplasias may sometimes be associated with muscular disorders. Skeletal muscle, tendon and ligament, and the bones themselves form a complicated biomechanical

system of levers and forces; therefore, abnormalities in one tissue may potentially affect the others. It is known that bones react and remodel according to the forces exerted by muscles. Tendons and ligaments also repair and remodel according to the biomechanical forces exerted upon them. Therefore, for the wellbeing of the patient, it is important to recognise all the tissues that the disease may be affecting. In this paper we summarise the relationships between different tissues in the musculoskeletal system and discuss several skeletal dysplasias in which muscle and/or tendon weakness has been recognised and described. This detailed paper will provide better understanding of the musculoskeletal biology and may enable better diagnosis and management of the patients in future.

2. Biomechanics of the Musculoskeletal System

2.1. Bones and Growth Plate Cartilage. Bone is a hard connective tissue consisting of osteocytes embedded in an abundant extracellular matrix (ECM). Bones act as a scaffold, attachment points, leverage, and protection for soft tissues.

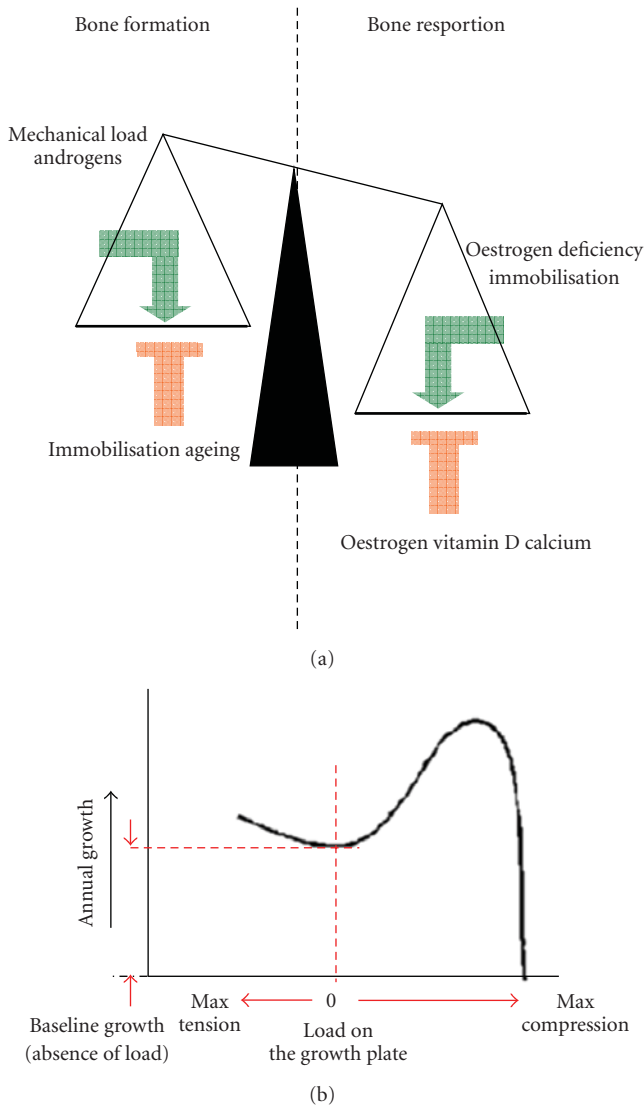


FIGURE 1: (a) A schematic representation of processes that may influence bone formation and resorption [3]. (b) A graph illustrating the Hueter-Volkman law [4].

During life, and to enable growth, repair and mineralisation, the bone is constantly being remodelled by osteoblasts and osteoclasts [5]. Furthermore, bone is a dynamic tissue which is able to remodel in response to the mechanical load. For example, an increase in loading bone formation increases and resorption decreases whilst unloading of the bone has an opposite effect (Figure 1(a)) [3].

The human skeleton consists of 206 bones of differing shapes and functions and distributed throughout the entire body [6]. Surprisingly, however, this complicated scaffolding is formed by only two distinct and very conserved processes [7]. Both processes begin with mesenchymal condensation. Bones of the craniofacial skeleton evolve from migrating neural crest cells in a process called intramembranous ossification. The rest of the skeleton is formed by mesenchymal cells forming a cartilage *anlagen*, which is later replaced by

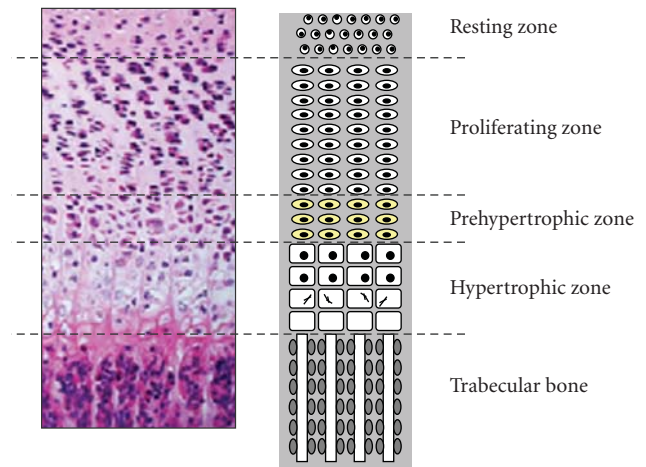


FIGURE 2: A histological H&E (haematoxylin and eosin) stained image of an adult mouse growth plate and a schematic representation of differentiation zones in the tissue. In the growth plate several distinct structural zones can be identified, reflecting the gradual transition of cells through different stages of differentiation [13]. Resting zone acts as a reserve of precursor cells for the proliferating chondrocytes in the columns [10]. Proliferating zone is where the cells flatten and divide, laying down a cartilage extracellular matrix that will later serve as a scaffold for bone formation [14]. In the prehypertrophic zone, the cells enter the maturation zone and begin to enlarge. In the hypertrophic zone, the chondrocytes and their lacunae become 5–12 times bigger [14]. These cells eventually die, triggering vascularisation and bone formation.

bone in endochondral (i.e., “in cartilage”) ossification [8]. Both ossification pathways are also implicated in bone repair at later stages of life, with intramembranous ossification being the method of repair for stabilised fractures, whilst unstable fractures heal via endochondral ossification [9]. These separate pathways share many common regulatory genes and proteins, local paracrine regulators, blood stream hormones, and transcription factors [10]. Mechanical forces are also extremely important for proper development of the skeleton, influencing the shape of the bones, their repair processes, and signalling pathways [11, 12].

Limb development begins with the condensation of mesenchyme after which the cells differentiate into chondrocytes, which form the cartilaginous template [7]. As the cartilage grows, the cells are forced apart by the extracellular matrix and become encapsulated in the thickening matrix. Meanwhile, within the cartilage *anlagen*, the encapsulated cells die due to their intensive growth and calcium salt deposition, and the ECM eventually erodes [15]. The blood vessels invade the cartilage, bringing bone-forming cells, which differentiate into osteoblasts and secrete additional extracellular matrix. This matrix is subsequently calcified forming *trabeculae*, some of which are later reabsorbed by the osteoclasts thus forming a bone marrow cavity [16]. As the bones continue to grow, a secondary ossification centre is established in the epiphyses [10] and between the shaft of the bone and the epiphysis a cartilage growth plate is formed (Figure 2), allowing longitudinal bone growth. The

thickening of bone is achieved by depositing further layers on the periosteum side by osteoblasts, and widening of the bone marrow cavity by osteoclasts. Eventually, the epiphysis and metaphysis in the bone fuse, usually around puberty, forming a diaphyseal mature bone [11].

Growth plate cartilage extracellular matrix is composed of type II collagen fibers and is abundant in proteoglycans, specifically aggrecan. This makes it a relatively compliant tissue and so it is able to respond to mechanical and gravity forces. To a certain extent, growing bones are able to align themselves according to the gravity forces exerted upon them, as can be seen in the correction of a mild *genu varum* in toddlers [17]. However, strong compression inhibits bone growth and tension has an opposite effect by increasing growth in bone length [4, 18]. This is known as the Hueter-Volkman law (Figure 1(b)), which was further defined by Frost in the twentieth century and is often used by clinicians in surgical correction of certain limb deformities [4, 17]. Lack of mechanical loading also results in decreased bone formation, as shown by weightlessness and suspension experiments (Figure 1(a)) [19–21].

Gravity induced mechanosensing in the growth plate cartilage is achieved by a microtubule-based organelle called the primary cilium [22–24]. Primary cilia are cytoplasmic protrusions that are associated with many proteins implicated in signal transduction, specifically integrins and extracellular matrix receptors, and enable the cells to respond to mechanical stimuli [22]. They exist on almost every cell in the human body and are very important for mechanosensing and biomechanics of many different tissues.

2.2. Articular Cartilage. Cartilage is a highly specialised connective tissue. Its mechanical properties allow it to withstand compressive forces and also to a smaller extent resist shearing and torsional forces [5]. Cartilage consists mostly of an extracellular matrix and its structure varies according to species, location, and age of the tissue [5]. Hyaline cartilage is the most abundant type of cartilage. It is a precursor to the growth plate (*physis*), and it is also found at the articular surface of bones, where it acts as a shock absorber and protection for the underlying subchondral bone [25]. Chondrocytes in the hyaline cartilage are ovoid, ranging in shape from round to flat [5]. Each chondrocyte occupies a space (lat. *lacuna*) encapsulated by the extracellular matrix, which is important for cartilage biomechanical properties. Chondrocyte together with its pericellular matrix is often termed “chondron” [26]. It has been shown that pericellular matrix of articular cartilage has a precise macromolecular architecture, with a high content of proteoglycans, such as aggrecan, embedded in the collagen matrix [27]. Aggrecan retains water, thus contributing to the cartilage tissue elasticity [28]. The shape of individual chondrons is also important and they respond to the gravitational forces by producing a compact matrix “cap” pointing towards the surface of the tissue and a looser “tail” extending into the ECM below [27]. Chondrons have often been referred to as fluid bladders and indeed they seem to function in a similar manner [29]. When cartilage is subjected to compression, the liquid is pushed out of the proteoglycan complex and the collagen

rich matrix deforms, thus increasing the pressure within the chondron. This change in osmotic pressure due to escaping water protects the chondrocyte and enables its full recovery at unloading [29]. Chondrocytes also have a primary cilium which helps them sense these changes in forces [22, 23, 26]. This seems to be especially important in the aetiology and management of osteoarthritis where even a ligamentous instability or a weakness of periarticular muscles, and therefore an abnormal biomechanical environment, may result in joint degeneration [30, 31].

2.3. Enteses (at the Bone to Tendon Junction). Fibrocartilage is an intermediate tissue between the hyaline cartilage and dense fibrous tissues [5, 32]. It only has a few chondrocytes in the *lacunae*, and its matrix contains many thick collagen fibres arranged in an ordered fashion. It can be found in intervertebral discs, symphysis pubis, articular disc of the sternoclavicular and temporomandibular joints, the menisci of the knee joints, and places where ligaments or tendons attach to bones and is formed as tendon’s reaction to compressive load [33]. Fibrocartilage is associated with epiphyseal tendons and ligaments and is important in force transduction as it dissipates the stress on the tendon fibers near the bone [32, 34, 35]. Its molecular composition is similar to that of tendon, but several cartilage specific molecules, such as type II and type IX collagen and aggrecan, are also present in the matrix [33].

2.4. Tendon and Ligament. Tendon (Figures 3(a) and 3(b)) and ligament are soft collagenous tissues, linking muscle to bone and bone to bone, respectively. They consist of densely packed bundles of fibrous collagen and are characterised by high tensile strength and elasticity [5]. Tendon and ligament both have similar hierarchical structure, consisting of fascicles, which are built of smaller basic fibrils and fibroblasts [36]. The main component of the basic fibril is type I collagen. Both ligaments and tendons are surrounded by a sheath of transparent material called the synovial membrane, a delicate connective tissue layer secreting synovium, a viscous lubricating fluid [5].

Tendons act as buffers and storage of elastic kinetic energy during walking [37]. They can remodel according to the forces exerted upon them [34, 38]. It has been shown that the immobilisation of limbs leads to a decrease in collagen turnover in the tendon and a decrease in tendon diameters [39], and conversely, exercise leads to an increase in tendon diameter and collagen turnover [40]. Increase in tendon diameters correlates with an increase in the stiffness of the tissue [38], which means thicker tendons can withstand higher tensile forces exerted upon them by stronger muscles. Tendons also become thicker and less compliant with age [37], which together with age-associated muscle wasting helps explain the weakness and difficulties in walking experienced by the elderly [41].

2.5. Myotendinous Junction and Perimysium. Another structure that is biomechanically important for conveying forces from muscle to tendon is the myotendinous junction (MTJ; Figure 4). This is the site where tendon meets, and merges,

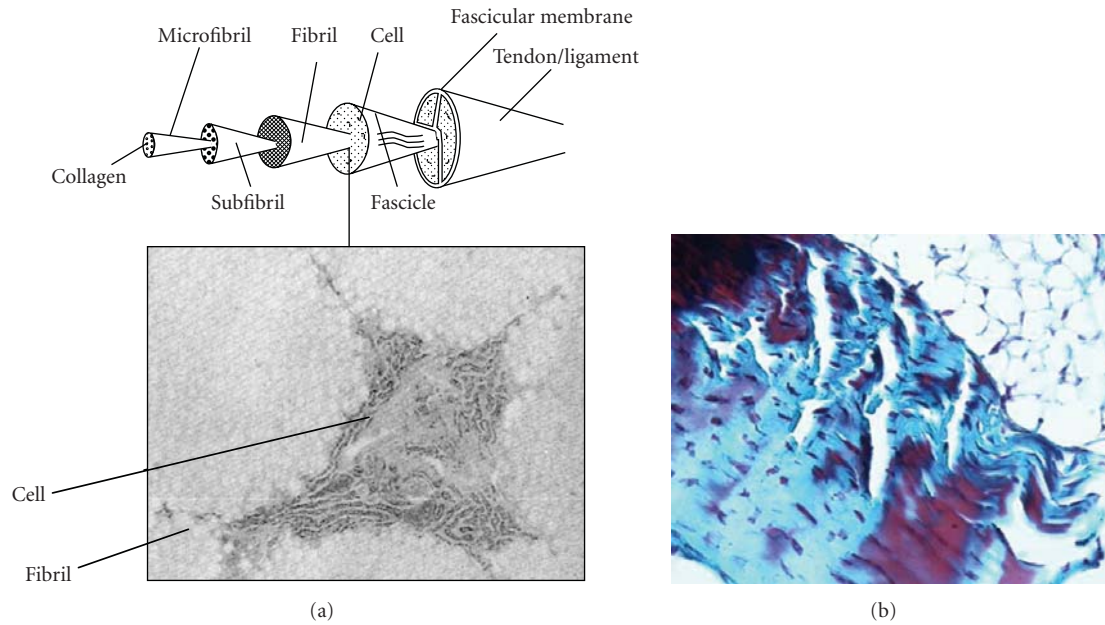


FIGURE 3: (a) A schematic representation of tendon hierarchical structure and a transmission electron microscopy image of a tenocyte embedded in the collagen matrix. (b) A histological (Gomori trichrome, staining collagenous tissues blue) image of a longitudinal section of patellar tendon showing parallel running collagen bundles in the tissue.

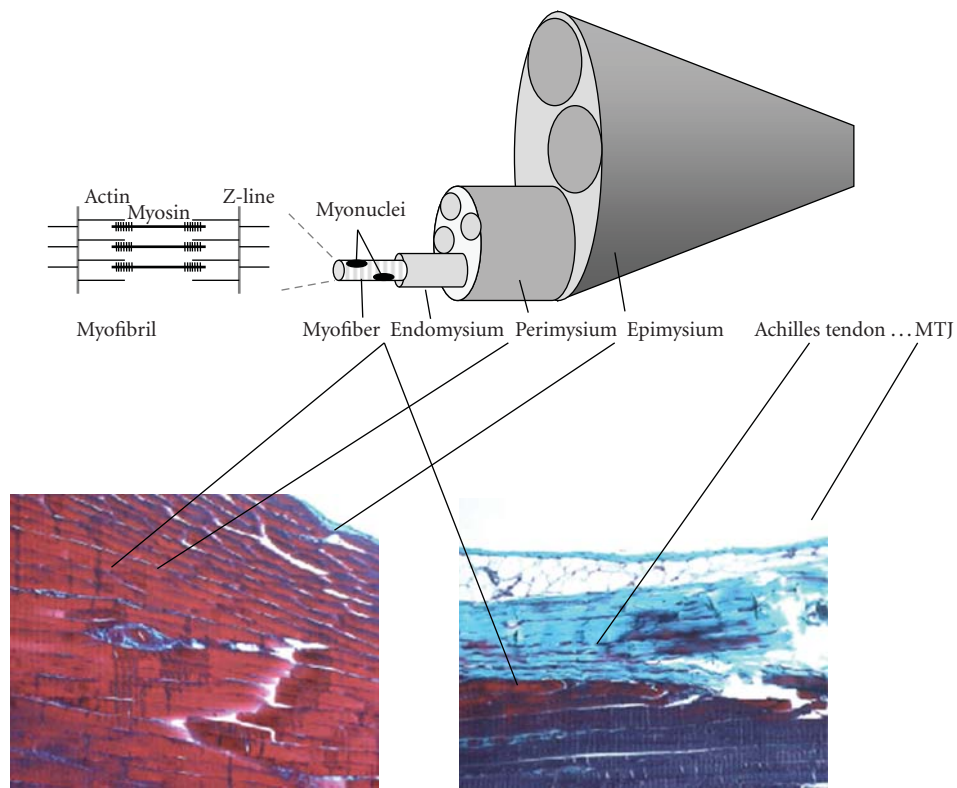


FIGURE 4: Schematic representation of the skeletal muscle structure and histological images of a longitudinal section of murine skeletal muscle and of murine Achilles tendon myotendinous junction (MTJ) stained with a trichrome Gomori stain to visualise collagenous tissues (staining muscle red, collagenous tissues blue, and nuclei black).

with the skeletal muscle and the point where muscle contractile forces are transmitted to the tendon [42]. The myotendinous junction membrane is extensively folded. This means that the tensile stress exerted by the contracting muscle fibers becomes shear stress instead, thus increasing the strength of the junction and protecting the tissues from injury [42]. The myotendinous junction is also connected to the collagenous perimysium surrounding the skeletal muscle fascicles [43]. The perimysium forms a lattice structure within the skeletal muscle and is involved in transmission of lateral forces in the muscle. MTJ and perimysium are together responsible for conveying the forces from muscle to tendon [43, 44].

2.6. Skeletal Muscle. Skeletal muscle acts as the motor of the body and is essential for locomotion. As such it has a very complex hierarchical structure (Figure 4). Each myofiber is a one multinuclear cell (with nuclei located to the periphery) that often spans the length of the entire muscle. Most of the myofiber is filled with contractile myofibrils consisting of actin and myosin and responsible for muscle contraction. The discovery of costameres by Pardo et al. in 1983 showed the first direct link between the surrounding extracellular matrix and the myofibers [45]. Costameres are regularly spaced around the Z-lines of the skeletal muscle and play a role in lateral force transmission, as shown by single myofiber studies performed by Street et al. [44, 46]. Every myofiber is covered by a connective tissue sheath called the endomysium [47]. Groups of muscle fibers are covered by another connective tissue sheath called the perimysium, which transmits the lateral forces between the muscle bundles [48]. Not every myofiber spans the entire muscle length and connects to the myotendinous junction; however, all the fibrous extracellular matrices are interconnected and eventually lead to the myotendinous junction and to the tendon itself [44]. Muscle can also remodel and adapt to the mechanical load [49], and muscle hypertrophy is often seen as a result of exercise [50].

3. Skeletal Dysplasias: Genetics Disorders Affecting the Osseous Skeleton

Skeletal dysplasias are a group of skeletal and musculoskeletal diseases that affect the development of the osseous skeleton. There are over 250 well-characterised phenotypes known to date, which affect the development of both flat and long bones [51]. The many different genes that are mutated in skeletal dysplasias span a wide range of cellular and metabolic processes and include those involved in the extracellular matrix, metabolic pathways, folding and degradation of macromolecules, hormones and signal transduction mechanisms, nuclear proteins and transcription factors, oncogenes and tumour suppressor genes and RNA, and DNA processing and metabolism [52].

Many skeletal dysplasia phenotypes are characterised by severe deformations and/or malformations of numerous skeletal elements and with such conditions it is sometimes easy to overlook other clinical aspects, such as the effect these

skeletal abnormalities may have on the soft tissues of the body [2]. Skeletal dysplasias may result in tightening of the tracts in the body thus affecting breathing and patient's well-being. Shorter limbs may result in a different distribution of biomechanical forces exerted by the muscles and thus may contribute to difficulties in walking. Furthermore, many of the extracellular matrix genes expressed in bone and cartilage and involved in skeletal dysplasias are also present in other musculoskeletal tissues, such as muscle and tendon, and may affect patients' well-being and quality of life.

4. Skeletal Dysplasias That Are Associated with Myopathies

There are several skeletal dysplasia phenotypes in which myopathy is a recognised neuromuscular complication of the disease. In some of the cases, the muscle pathology stems directly from the fact that the mutant protein is expressed in the muscle as well as in cartilage and bone, but in others the effect appears to be more indirect. A detailed analysis of the muscular symptoms in these phenotypes is very important since the neuromuscular complications often manifest prior to the skeletal deformations, which may arise during pre-pubertal growth, and therefore might allow quicker diagnosis and better management of the patient. We present a short summary of these conditions below and also in Table 1.

4.1. Multiple Epiphyseal Dysplasia: An Indirect ECM Defect?

Multiple epiphyseal dysplasia (MED) is a skeletal dysplasia in which an associated myopathy has only recently been recognised and reported in patients [53–55]. MED belongs to a “bone dysplasia family” that also includes the related and more severe disease known as pseudoachondroplasia (PSACH) [51, 56]. Together these phenotypes form a distinct spectrum of disease severity ranging from a mild MED through to severe PSACH at the other end of the spectrum. The PSACH-MED phenotype is characterised by disproportionate short stature, lower limb deformations (*genu varum* and *genu valgum*), joint laxity, and early onset degenerative joint disease [57]. Radiographic features of PSACH manifest in the epiphyses and the metaphyses of the long bones and in MED are restricted to the epiphyses [58]. PSACH and the more severe forms of MED result from mutations in the gene encoding cartilage oligomeric matrix protein (COMP), a pentameric ECM bridging molecule found in cartilage, tendon, ligament, and skeletal muscle [59]. PSACH-MED mutations in *COMP* cluster in the exons encoding the calcium-binding thrombospondin type 3 repeats (T3) and the C-terminal domain (CTD) of COMP. In chondrocytes the expression of these mutations results in various levels of endoplasmic reticulum (ER) stress and cell death [59, 60]. A role for COMP in collagen fibrillogenesis has been proposed and it is thought to be one of the catalysts of this process [61]. Furthermore, in the cartilage extracellular matrix COMP plays a bridging role and is able to interact with other ECM molecules such as matrilin-3, type IX collagen, aggrecan, fibronectin, and integrins [62–65]. It is therefore not surprising that other MED-causing

TABLE 1: Summary of the published skeletal dysplasias associated with a mild myopathy phenotype.

Disease name	Multiple epiphyseal dysplasia (MED)	Multiple epiphyseal dysplasia (MED)	Camurati-Englemann disease (CED)	Marfan syndrome (MFS1)	Schwartz-Jampel syndrome (SJS1)
Alternative name	EDM3	EDM1	Progressive diaphyseal dysplasia		Chondrodystrophic myotonia
Mode of inheritance	Autosomal dominant	Autosomal dominant	Autosomal dominant	Autosomal dominant	Autosomal recessive
Gene	COL9A3	COMP	TGF- β 1	Fibrilin-1	Perlecan
Skeletal symptoms	Epiphyseal dysplasia, early onset degenerative joint disease (knees), mild or no short limbed dwarfism	Epiphyseal dysplasia, early onset degenerative joint disease, mild short limbed dwarfism	Thicker bone diaphyses, thicker bones of the skull, tighter bone canals, bone pain, hyperlordosis, scoliosis	Increased height, scoliosis, thoracic lordosis, highly arched palate with tooth crowding	Short femurs, short stature, micrognathia, kyphoscoliosis, joint deformities, coxa valga, irregular capital femoral epiphyses
Skeletal onset	Childhood	~3 years	~3 years	Childhood	<3 years, muscle stiffness after birth
Muscular symptoms	Mild muscle weakness, difficulty rising from the floor	Muscle weakness, easy fatigue, difficulty rising from the floor	Easy fatigue, proximal muscle weakness and atrophy, waddling gait	Mild to moderate joint laxity, muscle weakness, muscle atrophy, hypoplasia, cannot increase muscle mass in response to exercise	Mild largely non-progressive muscle weakness, stiffness, myotonic myopathy, waddling gait, crouched stance, hypertrophy, reduced tendon reflexes, joint contractures
CK levels	Mildly elevated	Normal or mildly elevated	Elevated up to 40%	Normal or mildly elevated	Normal or mildly elevated
Muscle biopsy	Mild myopathy, a slight variability in fiber size	No variability in fiber size, scattered basophilic fibers and/or small atrophic fibers	Often normal, occasional variability in fiber size	Sometimes myopathic changes seen, abnormalities in fibrilin-1 immunoreactivity	Central nuclei, varied fiber size, changes of fiber type
Muscle electron microscopy	—	—	Thicker basement membrane around the blood vessels, few fibers with accumulated mitochondria	—	—
EMG	—	—	Short small action potentials in some muscles, myopathic	Myopathic and neurogenic	Myotonic abnormalities
Other affected tissues	—	—	Liver, spleen, gonads (hepatosplenomegaly and hypogonadism)	Eyes: myopia, ectopia lensis, corneal flatness	Eyes: myopia, blepharophimosis
Possible therapy	Not available	Not available	Corticosteroids	Lasartan (aortic aneurism, and muscle involvement)	Reducing muscle stiffness, anticonvulsants and antiarrhythmics

mutations were found in genes encoding proteins known to interact with COMP such as matrilin-3 and type IX collagen, although the precise rationale for this genetic heterogeneity of MED has yet to be determined.

Until recently, PSACH-MED has primarily been described as a disease affecting bone growth, joint stability, and ligamentous laxity. In 2000 however, a form of MED resulting from a mutation in one of the type IX

collagen genes (*COL9A3*) was as associated with a mild myopathy [54]. This initial observation was followed by the recognition that some forms of PSACH-MED resulting from CTD-COMP mutations may also present with mild myopathy [53, 55] (Tables 1 and 2).

4.1.1. MED Resulting from Mutations in COL9A3 (EDM3). In an MED family with a *COL9A3* mutation patients

presented with proximal muscle weakness (despite predominantly distal skeletal changes) and mildly elevated levels of creatine kinase (CK; an indicator of muscle degeneration and myopathy). These individuals tired easily and a muscle biopsy from one affected family member showed mild myopathic changes characterised by a mild variability in fiber size [54]. Interestingly, there is no evidence that type IX collagen is expressed in skeletal muscle as a fully functioning trimer [66, 67]. Therefore, it is tempting to speculate that the pathology in this case arises from an abnormal enthesis (the tendon to bone attachment site where type IX collagen is expressed). This may also explain why no gross myopathic changes were seen in the muscle biopsy from the patient, which would be the case if a muscle specific structural protein was mutated. Our recent analysis of a CTD-COMP mutant mouse model provided evidence in support of this hypothesis.

4.1.2. PSACH-MED Resulting from Mutations in COMP (EDM1). MED-COMP patients with a CTD-COMP mutation and an associated myopathy were described in 2003 by Jakkula et al. [53]. They suffered from muscle weakness from 3 years of age and had mildly elevated CK levels; however a muscle biopsy was not performed at the time. In 2005, a further two CTD-COMP mutations were reported by Kennedy et al. [55] (Table 2). The onset of the disease was early and included muscle weakness, fatigue, and difficulty rising from the floor, in comparison to the patient reported by Jakkula; the CK levels were also within normal limits. A biopsy of the patients' muscle showed no variability in fiber size, however, scattered basophilic and small atrophic fibers were noted, indicating a mild myopathy [55]. Inconclusive data exists with respect to the expression of COMP in skeletal muscle and tendon [69, 70]; therefore we analysed a knock-in mouse model carrying a CTD-COMP mutation to determine the pathomolecular mechanisms of PSACH-MED related myopathy.

4.1.3. Myopathy in Knock-In Transgenic Mouse Model of PSACH/MED. We have recently reported the clinical phenotype and investigated the pathology of PSACH-MED associated myopathy using a transgenic mouse model with a T585M COMP mutation in the C-terminal domain of COMP [71]. We detected COMP protein in skeletal muscle and in the tendons and ligaments of wild type and mutant mice, confirming that it is expressed in all of these tissues. Mice carrying the T585M CTD-COMP mutation experienced a progressive muscle weakness even though histological evidence of myopathy was found only at the myotendinous and perimysial junctions. The collagen fibril organisation was abnormal in mutant tendons and characterised by an overall increase in fiber diameter with a corresponding increase in the number of branching or bifurcating fibrils. These changes had the effect of producing thinner and more lax tendons.

COMP was expressed throughout skeletal muscle and tendon, yet the mutation resulted in a localised myopathy and a generalised tendinopathy. Therefore, we concluded

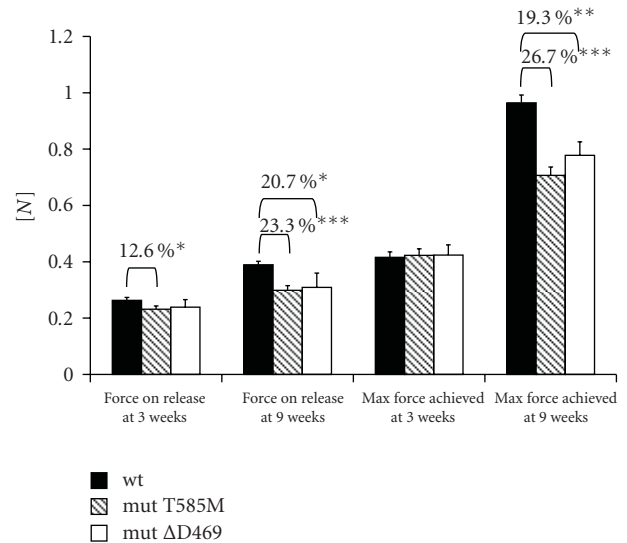


FIGURE 5: Grip strength measurement in COMP-CTD T585M knock-in mice and COMP-T3 Δ D469 knock-in mice at 3 weeks of age. COMP-CTD mice were getting tired and let go of the apparatus easier than their wild type controls, although they were not generally weaker at 3 weeks of age, as seen by the maximum strengths registered ($n = 15$) [71]. COMP Δ D469 mice were not getting tired and had the same maximum strength as the wild type controls at 3 weeks of age; however, by 9 weeks they were significantly weaker than their wild type littermates and tired easier, which is indicative of a mild myopathy ($n = 5$). Key: wt: wild type, mut: homozygous for the mutation, * $P < .05$, ** $P < .01$, *** $P < .001$ (independent samples t -test).

that the given myotendinous and perimysial junctions are responsible for transmitting the forces between the tendon and muscle fibers; the myopathy was perhaps the result of an underlying tendon problem. This finding is very important as it may help explain the myopathy seen in MED patients with type IX collagen gene mutations, and more recently, with matrilin-3 mutations (Table 2). Both of these molecules are not expressed in skeletal muscle; however, they are present in the fibrocartilage attachment point (enthesis) between the tendon and bone. A disruption to mechanical forces transmitted to the muscle and an altered ability of those tissues to remodel following stress may explain some of the musculoskeletal complications of the MED phenotype.

To test the hypothesis that myopathy is specifically associated with CTD-COMP mutations localised near the potential collagen and integrin binding sites, we have investigated a second mouse model, COMP Δ D469 knock-in mice (T3-COMP mutation), for muscle weakness using the experimental set-up as previously described in [71]. At 3 weeks of age we found no evidence of muscle weakness in Δ D469 mutant mice (Figure 5); however, by 9 weeks of age the mutant mice were weaker than their wild type littermates and tired easier, similar to the COMP-CTD mutant mice. This indicates that PSACH-MED COMP related myopathy may be a mutation specific phenomenon and be related directly to the proximity of the mutation to the potential

TABLE 2: Patient and mutation data were obtained from the European Skeletal Dysplasia Network (ESDN reference numbers) or recent publications, as referenced.

Reference	Features	Diagnosis	Gene	Mutation	Effect
ESDN 01071	<ul style="list-style-type: none"> – Fatigue during walking – Muscle disease suspected by paediatrician 	MED	MATN3	D176V	Potential misfolding
ESDN 01013	<ul style="list-style-type: none"> – Mild proximal muscle weakness at 7 years – Difficulty rising from squatting position 	MED	COL9A2	c186G > C	Exon skipping
ESDN 01003	<ul style="list-style-type: none"> – Mild muscle weakness – Muscle weakness – Suspected (unproven) muscular dystrophy – Problems with standing up from sitting position – Problems walking on stairs 	MED	COL9A2	c186 + 4a > c	Exon skipping
[68]	<ul style="list-style-type: none"> – Biopsy: <ul style="list-style-type: none"> – No morphological or histochemical changes – No fibers with central nuclei – Variation in fiber size – No degradation, regeneration, or necrosis – ATP + CrP production from pyruvate decreased – Neurological evaluation for abnormal walking pattern at 6 years 	MED	COL9A2	c186 + 2t > c	Exon skipping
[68]	<ul style="list-style-type: none"> – Proximal muscle weakness lower extremities – Family also affected (father, sister, sister's daughter) 	MED	COL9A2	c186G > A	Exon skipping
[54]	<ul style="list-style-type: none"> – Proximal muscle weakness (reported to the neuromuscular clinic at 10 years) – Mildly elevated serum creatine kinase (CK) levels – Difficulty walking and climbing stairs from 3 years on – Difficulty rising from the floor – Some signs of proximal muscle weakness in family members – Muscle biopsy: mild variability in fibre size 	MED	COL9A3	IVS2-1, G > A	Exon skipping
ESDN 00385	<ul style="list-style-type: none"> – Some signs of mild myopathy <ul style="list-style-type: none"> – Gower's sign (proximal muscle weakness) – Waddling gait – Difficulties climbing stairs – CPK normal 	PSACH	COMP	D326Y	Potential retention (T3 domain mutation)

TABLE 2: Continued.

Reference	Features	Diagnosis	Gene	Mutation	Effect
ESDN 00430	<ul style="list-style-type: none"> – Reported to neurologist at age 2 – Diminished muscle strength in: <ul style="list-style-type: none"> – Hips – Shoulders – Quadriceps muscle – Feet-lifting muscles – Diagnosed with a myopathy at 5 years – Biopsy inconclusive 	MED	COMP	E457del	Potential retention (T3 domain mutation)
[55]	<ul style="list-style-type: none"> – Difficulty walking at 2.5 years – Muscle weakness – Tired easily – Difficulty getting up from sitting – CK levels normal – EMG and nerve conduction velocities normal – Biopsy: <ul style="list-style-type: none"> – Mild myopathy, – No variability in fibre size – Scattered basophilic fibers – Some small atrophic fibers 	MED	COMP	D605N	Potential misfolding (CTD mutation)
[53, 55]	<ul style="list-style-type: none"> – Muscle weakness from 3 years on – Referred to neuromuscular clinic at 5 years – Mildly elevated CK levels 	MED	COMP	R718W	Potential misfolding (CTD mutation)

binding sites on COMP rather than the specific domain of the molecule.

4.1.4. PSACH and MED: New Findings. Recently, several PSACH and MED patients with COMP, type IX collagen, and also matrilin-3 mutations have been reported with muscular complications, and these patients were originally referred to neuromuscular clinics prior to the diagnosis of skeletal dysplasia. This seems to support our hypothesis that mutations in T3 domain of COMP and in other structural molecules of tendon and cartilaginous entheses may also result in a mild myopathy. Blood samples from the patients showed normal or mildly increased CK levels and their muscle biopsy showed increased number of basophilic fibers, fiber necrosis, and/or variability in fiber diameters. We now present an updated summary of novel PSACH-MED mutations associated with myopathic changes (Table 2). Interestingly, some of the newly found COMP mutations associated with a myopathy cluster in the T3 repeats of

the COMP protein. The T3 and CTD domains of COMP can form intramolecular interactions as demonstrated by the recent crystal structure model [72, 73]. Therefore, the mutations that associate specifically with a myopathy may do so due to their specific locations, possibly near a potential collagen or integrin binding sites and/or the intramolecular binding sites within COMP, and myopathic phenotype may not segregate directly with the domain, but rather with a specific location of the mutation. Type IX collagen and matrilin-3 mutations' association with a myopathic phenotype may potentially be explained by the expression of these molecules in the fibrocartilaginous entheses [33, 74]; however the pathomolecular mechanism of the muscle complications in these cases requires further investigation.

4.2. Schwartz-Jampel Syndrome: A Direct ECM Defect. An autosomal recessive disorder, Schwartz-Jampel syndrome (SJS1) [75], results from mutations in the extracellular matrix molecule perlecan [76]. Perlecan is a heparin sulphate

proteoglycan that is a major component of basement membranes. It is expressed in cartilage, the endomysium of skeletal muscle, the nervous system, and in basement membranes throughout the body. It can interact with both fibroblast growth factor 2 (FGF2) and transforming growth factor beta (TGF β) and is believed to play a role in tissue growth [77]. Schwartz-Jampel syndrome is characterised skeletally by short stature, irregular epiphyses, bowed diaphyses, general joint deformities, and *coxa valga*. In skeletal muscle SJS1 manifests with myotonic myopathy and joint contractures [78]. The onset of the disease is quite early, from around 3 years of age, and the muscular phenotype often precedes the skeletal abnormalities. Another affected tissue is the eye with patients often suffering from myopia and a dysplasia of the eyelids [75]. Interestingly, the skeletal symptoms of SJS1 are at least in part due to a defect in sodium and potassium gradients in the muscle and these may be pharmacologically corrected [79]. What is extremely interesting is that perlecan is not a part of a voltage channel per se, rather it is expressed in the endomysial extracellular matrix, thus suggesting a link (perhaps mechanical) exists between voltage channels and signalling and the surrounding ECM.

4.3. Marfan Syndrome: An Indirect Signalling Defect. Marfan syndrome is an autosomal dominant musculoskeletal and ocular syndrome resulting from mutations in the extracellular matrix protein, fibrillin-1. Fibrillin-1 is a component of extracellular microfibrils that are present in many connective tissues such as lung, skin, kidney, blood vessels, cartilage, muscle, cornea, and tendon [80]. Marfan syndrome patients are characterised by abnormally high stature, scoliosis, and highly arched palate with a crowding of the teeth [81]. The muscular component (skeletal muscle) of Marfan syndrome has been largely ignored until relatively recently [82]. Muscular abnormalities can include muscle hypoplasia, hypotonia, and weakness, and some patients also have problems with increasing the muscle mass upon exercise. The hypoplasia and hypotonia possibly result from the increased availability of TGF β 1, which is known to bind to fibrillin associated latent TGF β 1 binding protein (LTBP). This may in turn affect the satellite cell differentiation and proliferation [83]. Furthermore, the patients' biopsy shows abnormal distribution of fibrillin-1 in the endomysium [82]. Recently losartan, an antagonist of TGF β 1, has been shown to alleviate aortic aneurysm in a mouse model of Marfan syndrome, and it may also help to reverse the muscular symptoms of Marfan syndrome [84]. Since the onset of muscular symptoms can precede the bone pathology and the muscular symptoms may soon be treatable, an early diagnosis based on muscular phenomena may lead to better management and better quality of life for these patients.

4.4. Camurati-Engelmann Disease: A Direct Signalling Defect. Camurati-Engelmann disease (CED), also known as progressive diaphyseal dysplasia, is an early onset autosomal dominant skeletal dysplasia resulting in the thickening of the diaphyseal bones, sclerosis of the skull base, and bone pain [85]. The first symptoms usually manifest in early

childhood and always before 30 years of age [86]. CED is caused by mutations in transforming growth factor β 1 (TGF β 1), a molecule very important in proliferation and differentiation of many different cell types, including those of cartilage and bone [87]. Interestingly, CED patients are often initially referred to neuromuscular clinics with a suspicion of muscular dystrophy. They present with an increasing muscle weakness, easy fatigue, and a characteristic waddling gait [88]. However, their plasma creatine kinase (CK) level (an indicator of muscle degeneration) is usually normal or only mildly elevated [89]. Muscle biopsies are often normal or show nonspecific changes, with some atrophic fibers (but no group atrophy) and thickened basement membrane around the small vessels. Some degree of perimysial fibrosis (but no endomysial fibrosis) is also observed in a proportion of patients [89]. Electromyographs (EMG) show small action potentials indicative of a myopathy in some muscles, especially around the pelvic girdle whereas other muscles are normal [89]. These observations are extremely important as muscular complications often manifest themselves prior to the severe skeletal symptoms and some of the radiographic features of CED may be prevented or are treatable with corticosteroids [90]. Therefore, a muscle biopsy/assessment at the right site combined with radiological evidence could potentially enable better and earlier diagnosis and treatment of these patients.

5. Summary

The mammalian musculoskeletal system is a complex system of different tissues and biomechanical properties. Together these tissues enable locomotion, protect soft organs from damage, and act as a scaffold for our bodies. We sometimes forget however that all these tissues often develop together, are in fact interconnected, and can interact with each other, and that affecting one may have an effect on the others. Understanding these intertissue relationships may also dramatically improve the therapies and management of certain diseases, such as the ones described in this paper. Early detection of an asymptomatic or a mild myopathy may lead to an earlier diagnosis of an underlying skeletal dysplasia [88]. Identification of the tissues affected by the disease, and a better understanding of the disease aetiology may also lead to the alleviation of some of the disease symptoms, better corrective surgery, and better management of the patients. Understanding the biomechanics of the interconnected musculoskeletal system may lead to better physiotherapies for osteoarthritis and many other bone/muscle related diseases. Therefore, a thorough and interdisciplinary investigation of musculoskeletal diseases and tissues is required to further our understanding of these systems and to enable better management and a better quality of life for patients in the future.

Acknowledgments

The work included from the authors' laboratories was funded by the Wellcome Trust (the second author is a Wellcome

Trust Senior Research Fellow: Grant 084353/Z/07/Z), the EU (LSHM-CT-2007-037471), NIH (RO1 AR49547-01), and the ARC (grant 17221). Patient and mutation data were obtained from the European Skeletal Dysplasia Network (<http://www.ESDN.org/>). The research was undertaken in the Wellcome Trust Centre for Cell-Matrix Research and the Histology, Microscopy and Transgenic Core Facilities of the Faculty of Life Sciences at the University of Manchester.

References

- [1] C. A. Francomano, I. McIntosh, and D. J. Wilkin, "Bone dysplasias in man: molecular insights," *Current Opinion in Genetics and Development*, vol. 6, no. 3, pp. 301–308, 1996.
- [2] P. J. Mogayzel and C. L. Marcus, "Skeletal dysplasias and their effect on the respiratory system," *Paediatric Respiratory Reviews*, vol. 2, no. 4, pp. 365–371, 2001.
- [3] S.-I. Harada and G. A. Rodan, "Control of osteoblast function and regulation of bone mass," *Nature*, vol. 423, no. 6937, pp. 349–355, 2003.
- [4] H. M. Frost, "Biomechanical control of knee alignment: some insights from a new paradigm," *Clinical Orthopaedics and Related Research*, no. 335, pp. 335–342, 1997.
- [5] P. M. Royce and B. Heinmann, *Connective Tissue and Its Heritable Disorders*, John Wiley & Sons, Zurich, Switzerland, 2nd edition, 2002.
- [6] *Encyclopedia Britannica*.
- [7] G. Karsenty, "The complexities of skeletal biology," *Nature*, vol. 423, no. 6937, pp. 316–318, 2003.
- [8] B. R. Olsen, A. M. Reginato, and W. Wang, "Bone development," *Annual Review of Cell and Developmental Biology*, vol. 16, pp. 191–220, 2000.
- [9] E. Zelzer and B. R. Olsen, "Multiple roles of vascular endothelial growth factor (VEGF) in skeletal development, growth, and repair," *Current Topics in Developmental Biology*, vol. 65, pp. 169–187, 2004.
- [10] H. M. Kronenberg, "Developmental regulation of the growth plate," *Nature*, vol. 423, no. 6937, pp. 332–336, 2003.
- [11] F. Forriol and F. Shapiro, "Bone development: interaction of molecular components and biophysical forces," *Clinical Orthopaedics and Related Research*, no. 432, pp. 14–33, 2005.
- [12] A. Guadalupe-Grau, T. Fuentes, B. Guerra, and J. A. L. Calbet, "Exercise and bone mass in adults," *Sports Medicine*, vol. 39, no. 6, pp. 439–468, 2009.
- [13] W. A. Horton, "Skeletal development: insights from targeting the mouse genome," *The Lancet*, vol. 362, no. 9383, pp. 560–569, 2003.
- [14] J. A. Ogden and L. C. Rosenberg, "Defining the growth plate," in *Behaviour of the Growth Plate*, H. K. Uthoff and J. J. Wiley, Eds., Raven Press, New York, NY, USA, 1988.
- [15] N. Ortega, D. J. Behonick, and Z. Werb, "Matrix remodeling during endochondral ossification," *Trends in Cell Biology*, vol. 14, no. 2, pp. 86–93, 2004.
- [16] S. F. Gilbert, *Developmental Biology*, Sinauer Associates, Sunderland, Mass, USA, 6th edition, 2000.
- [17] F. Rauch, "Bone growth in length and width: the Yin and Yang of bone stability," *Journal of Musculoskeletal Neuronal Interactions*, vol. 5, no. 3, pp. 194–201, 2005.
- [18] P. H. L. de Freitas, T. Kojima, S. Ubaidus, et al., "Histological assessments on the abnormalities of mouse epiphyseal chondrocytes with short term centrifugal loading," *Biomedical Research*, vol. 28, no. 4, pp. 191–203, 2007.
- [19] A. C. Abram, T. S. Keller, and D. M. Spengler, "The effects of simulated weightlessness on bone biomechanical and biochemical properties in the maturing rat," *Journal of Biomechanics*, vol. 21, no. 9, pp. 755–767, 1988.
- [20] T. J. Wronski and E. R. Morey, "Recovery of the rat skeleton from the adverse effects of simulated weightlessness," *Metabolic Bone Disease and Related Research*, vol. 4, no. 6, pp. 347–352, 1983.
- [21] M. M. Shimano and J. B. Volpon, "Biomechanics and structural adaptations of the rat femur after hindlimb suspension and treadmill running," *Brazilian Journal of Medical and Biological Research*, vol. 42, no. 4, pp. 330–338, 2009.
- [22] S. R. McGlashan, C. G. Jensen, and C. A. Poole, "Localization of extracellular matrix receptors on the chondrocyte primary cilium," *Journal of Histochemistry & Cytochemistry*, vol. 54, no. 9, pp. 1005–1014, 2006.
- [23] J. F. Whitfield, "The solitary (primary) cilium-A mechanosensory toggle switch in bone and cartilage cells," *Cellular Signalling*, vol. 20, no. 6, pp. 1019–1024, 2008.
- [24] N. F. Berbari, A. K. O'Connor, C. J. Haycraft, and B. K. Yoder, "The primary cilium as a complex signaling center," *Current Biology*, vol. 19, no. 13, pp. R526–R535, 2009.
- [25] W. A. Beresford, *Lecture Notes on Histology*, Blackwell Scientific, Oxford, UK, 3rd edition, 1983.
- [26] C. A. Poole, A. Matsuoka, and J. R. Schofield, "Chondrons from articular cartilage: III. Morphologic changes in the cellular microenvironment of chondrons isolated from osteoarthritic cartilage," *Arthritis and Rheumatism*, vol. 34, no. 1, pp. 22–35, 1991.
- [27] C. A. Poole, "Articular cartilage chondrons: form, function and failure," *Journal of Anatomy*, vol. 191, no. 1, pp. 1–13, 1997.
- [28] L. Stryer, *Biochemistry*, W.H. Freeman, New York, NY, USA, 4th edition, 2000.
- [29] F. Guilak, A. Ratcliffe, and V. C. Mow, "Chondrocyte deformation and local tissue strain in articular cartilage: a confocal microscopy study," *Journal of Orthopaedic Research*, vol. 13, no. 3, pp. 410–421, 1995.
- [30] K. L. Bennell, M. A. Hunt, T. V. Wrigley, B.-W. Lim, and R. S. Hinman, "Role of muscle in the genesis and management of knee osteoarthritis," *Rheumatic Disease Clinics of North America*, vol. 34, no. 3, pp. 731–754, 2008.
- [31] K. D. Brandt, "Putting some muscle into osteoarthritis," *Annals of Internal Medicine*, vol. 127, no. 2, pp. 154–156, 1997.
- [32] M. Benjamin, H. Toumi, J. R. Ralphs, G. Bydder, T. M. Best, and S. Milz, "Where tendons and ligaments meet bone: attachment sites ('entheses') in relation to exercise and/or mechanical load," *Journal of Anatomy*, vol. 208, no. 4, pp. 471–490, 2006.
- [33] G. Riley, "Tendinopathy—from basic science to treatment," *Nature Clinical Practice Rheumatology*, vol. 4, no. 2, pp. 82–89, 2008.
- [34] M. Benjamin and J. R. Ralphs, "Tendons in health and disease," *Manual Therapy*, vol. 1, no. 4, pp. 186–191, 1996.
- [35] M. Benjamin and E. J. Evans, "Fibrocartilage," *Journal of Anatomy*, vol. 171, pp. 1–15, 1990.
- [36] S. L.-Y. Woo, J. A. Weiss, and D. A. M. Da, "Biomechanics and morphology of the medial collateral and anterior cruciate ligaments," in *Biomechanics of Diarthrodial Joints*, V. C. Mow and S. L.-Y. Woo, Eds., Springer, New York, NY, USA, 1990.
- [37] O. S. Mian, J. M. Thom, L. P. Ardigo, A. E. Minetti, and M. V. Narici, "Gastrocnemius muscle-tendon behaviour during walking in young and older adults," *Acta Physiologica*, vol. 189, no. 1, pp. 57–65, 2007.

- [38] M. Kjær, "Role of extracellular matrix in adaptation of tendon and skeletal muscle to mechanical loading," *Physiological Reviews*, vol. 84, no. 2, pp. 649–698, 2004.
- [39] J. Savolainen, K. Vaananen, J. Puranen, T. E. S. Takala, J. Komulainen, and V. Vihko, "Collagen synthesis and proteolytic activities in rat skeletal muscles: effect of cast-immobilization in the lengthened and shortened positions," *Archives of Physical Medicine and Rehabilitation*, vol. 69, no. 11, pp. 964–969, 1988.
- [40] A. Arampatzis, K. Karamanidis, and K. Albracht, "Adaptational responses of the human Achilles tendon by modulation of the applied cyclic strain magnitude," *The Journal of Experimental Biology*, vol. 210, no. 15, pp. 2743–2753, 2007.
- [41] M. V. Narici, C. N. Maganaris, and N. D. Reeves, "Myotendinous alterations and effects of resistive loading in old age," *Scandinavian Journal of Medicine and Science in Sports*, vol. 15, no. 6, pp. 392–401, 2005.
- [42] J. G. Tidball and T. L. Daniel, "Myotendinous junctions of tonic muscle cells: structure and loading," *Cell and Tissue Research*, vol. 245, no. 2, pp. 315–322, 1986.
- [43] E. Passerieux, R. Rossignol, T. Letellier, and J. P. Delage, "Physical continuity of the perimysium from myofibers to tendons: involvement in lateral force transmission in skeletal muscle," *Journal of Structural Biology*, vol. 159, no. 1, pp. 19–28, 2007.
- [44] P. A. Huijting, "Muscle as a collagen fiber reinforced composite: a review of force transmission in muscle and whole limb," *Journal of Biomechanics*, vol. 32, no. 4, pp. 329–345, 1999.
- [45] J. V. Pardo, J. D'Angelo Siliciano, and S. W. Craig, "A vinculin-containing cortical lattice in skeletal muscle: transverse lattice elements ("costameres") mark sites of attachment between myofibrils and sarcolemma," *Proceedings of the National Academy of Sciences of the United States of America*, vol. 80, no. 4, pp. 1008–1012, 1983.
- [46] S. F. Street, "Lateral transmission of tension in frog myofibers: a myofibrillar network and transverse cytoskeletal connections are possible transmitters," *Journal of Cellular Physiology*, vol. 114, no. 3, pp. 346–364, 1983.
- [47] S. R. Garfin, C. M. Tipton, S. J. Mubarak, et al., "Role of fascia in maintenance of muscle tension and pressure," *Journal of Applied Physiology Respiratory Environmental and Exercise Physiology*, vol. 51, no. 2, pp. 317–320, 1981.
- [48] J. G. Tidball, "Force transmission across muscle cell membranes," *Journal of Biomechanics*, vol. 24, supplement 1, pp. 43–52, 1991.
- [49] A. L. Mackey, K. M. Heinemeier, S. O. A. Koskinen, and M. Kjær, "Dynamic adaptation of tendon and muscle connective tissue to mechanical loading," *Connective Tissue Research*, vol. 49, no. 3-4, pp. 165–168, 2008.
- [50] S. M. Phillips, "Physiologic and molecular bases of muscle hypertrophy and atrophy: impact of resistance exercise on human skeletal muscle (protein and exercise dose effects)," *Applied Physiology, Nutrition and Metabolism*, vol. 34, no. 3, pp. 403–410, 2009.
- [51] D. L. Rimoin, G. A. Francomano, A. Giedion, et al., "International nomenclature and classification of the osteochondrodysplasias (1997) international working group on constitutional diseases of bone," *American Journal of Medical Genetics*, vol. 79, no. 5, pp. 376–382, 1998.
- [52] G. R. Mortier, "The diagnosis of skeletal dysplasias: a multidisciplinary approach," *European Journal of Radiology*, vol. 40, no. 3, pp. 161–167, 2001.
- [53] E. Jakkula, J. Lohiniva, A. Capone, et al., "A recurrent R718W mutation in COMP results in multiple epiphyseal dysplasia with mild myopathy: clinical and pathogenetic overlap with collagen IX mutations," *Journal of Medical Genetics*, vol. 40, no. 12, pp. 942–948, 2003.
- [54] C. G. Bönnemann, G. F. Cox, F. Shapiro, et al., "A mutation in the alpha 3 chain of type IX collagen causes autosomal dominant multiple epiphyseal dysplasia with mild myopathy," *Proceedings of the National Academy of Sciences of the United States of America*, vol. 97, no. 3, pp. 1212–1217, 2000.
- [55] J. Kennedy, G. C. Jackson, F. S. Barker, et al., "Novel and recurrent mutations in the C-terminal domain of COMP cluster in two distinct regions and result in a spectrum of phenotypes within the pseudoachondroplasia—multiple epiphyseal dysplasia disease group," *Human Mutation*, vol. 25, no. 6, pp. 593–594, 2005.
- [56] J. Spranger, "Pattern recognition in bone dysplasias," *Progress in Clinical and Biological Research*, vol. 200, pp. 315–342, 1985.
- [57] A. Mabuchi, N. Manabe, N. Haga, et al., "Novel types of COMP mutations and genotype-phenotype association in pseudoachondroplasia and multiple epiphyseal dysplasia," *Human Genetics*, vol. 112, no. 1, pp. 84–90, 2003.
- [58] J. McKeand, J. Rotta, and J. T. Hecht, "Natural history study of pseudoachondroplasia," *American Journal of Medical Genetics*, vol. 63, no. 2, pp. 406–410, 1996.
- [59] M. D. Briggs, S. M. G. Huffman, L. M. King, et al., "Pseudoachondroplasia and multiple epiphyseal dysplasia due to mutations in the cartilage oligomeric matrix protein gene," *Nature Genetics*, vol. 10, no. 3, pp. 330–336, 1995.
- [60] K. L. Chapman, M. D. Briggs, and G. R. Mortier, "Review: clinical variability and genetic heterogeneity in multiple epiphyseal dysplasia," *Pediatric Pathology and Molecular Medicine*, vol. 22, no. 1, pp. 53–75, 2003.
- [61] K. Halász, A. Kassner, M. Mörgelin, and D. Heinegård, "COMP acts as a catalyst in collagen fibrillogenesis," *Journal of Biological Chemistry*, vol. 282, no. 43, pp. 31166–31173, 2007.
- [62] P. E. Di Cesare, F. S. Chen, M. Moergelin, et al., "Matrix-matrix interaction of cartilage oligomeric matrix protein and fibronectin," *Matrix Biology*, vol. 21, no. 5, pp. 461–470, 2002.
- [63] H. H. Mann, S. Özbek, J. Engel, M. Paulsson, and R. Wagener, "Interactions between the cartilage oligomeric matrix protein and matrilins: implications for matrix assembly and the pathogenesis of chondrodysplasias," *Journal of Biological Chemistry*, vol. 279, no. 24, pp. 25294–25298, 2004.
- [64] P. Holden, R. S. Meadows, K. L. Chapman, M. E. Grant, K. E. Kadler, and M. D. Briggs, "Cartilage oligomeric matrix protein interacts with type IX collagen, and disruptions to these interactions identify a pathogenetic mechanism in a bone dysplasia family," *Journal of Biological Chemistry*, vol. 276, no. 8, pp. 6046–6055, 2001.
- [65] M. J. Rock, P. Holden, W. A. Horton, and D. H. Cohn, "Cartilage oligomeric matrix protein promotes cell attachment via two independent mechanisms involving CD47 and $\alpha V\beta 3$ integrin," *Molecular and Cellular Biochemistry*, vol. 338, no. 1-2, pp. 215–224, 2010.
- [66] W. Müller-Glauser, B. Humbel, M. Glatt, et al., "On the role of type IX collagen in the extracellular matrix of cartilage: type IX collagen is localized to intersections of collagen fibrils," *Journal of Cell Biology*, vol. 102, no. 5, pp. 1931–1939, 1986.
- [67] M. H. Irwin, S. H. Silvers, and R. Mayne, "Monoclonal antibody against chicken type IX collagen: preparation, characterization, and recognition of the intact form of type IX collagen secreted by chondrocytes," *Journal of Cell Biology*, vol. 101, no. 3, pp. 814–823, 1985.

- [68] G. C. Jackson, D. Marcus-Soekarman, I. Stolte-Dijkstra, A. Verrips, J. A. Taylor, and M. D. Briggs, "Type IX collagen gene mutations can result in multiple epiphyseal dysplasia that is associated with osteochondritis dissecans and a mild myopathy," *American Journal of Medical Genetics, Part A*, vol. 152, no. 4, pp. 863–869, 2010.
- [69] C. Fang, C. S. Carlson, M. P. Leslie, et al., "Molecular cloning, sequencing, and tissue and developmental expression of mouse cartilage oligomeric matrix protein (COMP)," *Journal of Orthopaedic Research*, vol. 18, no. 4, pp. 593–603, 2000.
- [70] L. Svensson, A. Aszódi, D. Heinegård, et al., "Cartilage oligomeric matrix protein-deficient mice have normal skeletal development," *Molecular and Cellular Biology*, vol. 22, no. 12, pp. 4366–4371, 2002.
- [71] K. A. Piróg, O. Jaka, Y. Katakura, et al., "A mouse model offers novel insights into the myopathy and tendinopathy often associated with pseudoachondroplasia and multiple epiphyseal dysplasia," *Human Molecular Genetics*, vol. 19, no. 1, pp. 52–64, 2009.
- [72] K. Tan, M. Duquette, A. Joachimiak, and J. Lawler, "The crystal structure of the signature domain of cartilage oligomeric matrix protein: implications for collagen, glycosaminoglycan and integrin binding," *FASEB Journal*, vol. 23, no. 8, pp. 2490–2501, 2009.
- [73] C. B. Carlson, D. A. Bernstein, D. S. Annis, et al., "Structure of the calcium-rich signature domain of human thrombospondin-2," *Nature Structural and Molecular Biology*, vol. 12, no. 10, pp. 910–914, 2005.
- [74] F. Deák, R. Wagener, I. Kiss, and M. Paulsson, "The matrilins: a novel family of oligomeric extracellular matrix proteins," *Matrix Biology*, vol. 18, no. 1, pp. 55–64, 1999.
- [75] O. Schwartz and R. S. Jampel, "Congenital blepharophimosis associated with a unique generalized myopathy," *Archives of Ophthalmology*, vol. 68, pp. 52–57, 1962.
- [76] S. Nicole, C.-S. Davoine, H. Topaloglu, et al., "Perlecan, the major proteoglycan of basement membranes, is altered in patients with Schwartz-Jampel syndrome (chondrodystrophic myotonia)," *Nature Genetics*, vol. 26, no. 4, pp. 480–483, 2000.
- [77] R. V. Iozzo, J. Pillarisetti, B. Sharma, et al., "Structural and functional characterization of the human perlecan gene promoter: transcriptional activation by transforming growth factor- β via a nuclear factor 1-binding element," *Journal of Biological Chemistry*, vol. 272, no. 8, pp. 5219–5228, 1997.
- [78] A. C. van Huffelen, F. J. M. Gabreels, J. S. van Luypen van der Horst, et al., "Chondrodystrophic myotonia. A report of two unrelated Dutch patients," *Neuropadiatrie*, vol. 5, no. 1, pp. 71–90, 1974.
- [79] P. R. Huttenlocher, J. Landwirth, V. Hanson, B. B. Gallagher, and K. Bensch, "Osteo-chondro-muscular dystrophy. A disorder manifested by multiple skeletal deformities, myotonia, and dystrophic changes in muscle," *Pediatrics*, vol. 44, no. 6, pp. 945–958, 1969.
- [80] L. Y. Sakai, D. R. Keene, and E. Engvall, "Fibrillin, a new 350-kD glycoprotein, is a component of extracellular microfibrils," *Journal of Cell Biology*, vol. 103, no. 6, pp. 2499–2509, 1986.
- [81] J. R. Gray and S. J. Davies, "Marfan syndrom," *Journal of Medical Genetics*, vol. 33, no. 5, pp. 403–408, 1996.
- [82] W. M. H. Behan, C. Longman, R. K. H. Petty, et al., "Muscle fibrillin deficiency in Marfan's syndrome myopathy," *Journal of Neurology Neurosurgery and Psychiatry*, vol. 74, no. 5, pp. 633–638, 2003.
- [83] N. C. Voermans, C. G. Bönnemann, P. A. Huijting, et al., "Clinical and molecular overlap between myopathies and inherited connective tissue diseases," *Neuromuscular Disorders*, vol. 18, no. 11, pp. 843–856, 2008.
- [84] J. P. Habashi, D. P. Judge, T. M. Holm, et al., "Losartan, an AT1 antagonist, prevents aortic aneurysm in a mouse model of Marfan syndrome," *Science*, vol. 312, no. 5770, pp. 117–121, 2006.
- [85] A. Campos-Xavier, J. M. Saraiva, R. Savarirayan, et al., "Phenotypic variability at the TGF- β 1 locus in Camurati-Engelmann disease," *Human Genetics*, vol. 109, no. 6, pp. 653–658, 2001.
- [86] M. Ghadami, Y. Makita, K. Yoshida, et al., "Genetic mapping of the Camurati-Engelmann disease locus to chromosome 19q13.1-q13.3," *American Journal of Human Genetics*, vol. 66, no. 1, pp. 143–147, 2000.
- [87] M. E. Dickinson, M. S. Kobrin, C. M. Silan, et al., "Chromosomal localization of seven members of the murine TGF- β superfamily suggests close linkage to several morphogenetic mutant loci," *Genomics*, vol. 6, no. 3, pp. 505–520, 1990.
- [88] J. Bondestam, H. Pihko, S.-L. Vanhanen, et al., "Skeletal dysplasia presenting as a neuromuscular disorder—report of three children," *Neuromuscular Disorders*, vol. 17, no. 3, pp. 231–234, 2007.
- [89] H. Yoshioka, M. Mino, N. Kiyosawa, et al., "Muscular changes in Engelmann's disease," *Archives of Disease in Childhood*, vol. 55, no. 9, pp. 716–719, 1980.
- [90] T. Inaoka, N. Shuke, J. Sato, et al., "Scintigraphic evaluation of pamidronate and corticosteroid therapy in a patient with progressive diaphyseal dysplasia (Camurati-Engelmann disease)," *Clinical Nuclear Medicine*, vol. 26, no. 8, pp. 680–682, 2001.

Research Article

Impaired Skeletal Muscle Repair after Ischemia-Reperfusion Injury in Mice

**A. Vignaud,^{1,2,3,4} C. Hourde,^{1,2,3,4} F. Medja,^{1,2,3,4} O. Agbulut,⁵
G. Butler-Browne,^{1,2,3,4} and A. Ferry^{1,2,3,4,6}**

¹INSERM, U974, Paris 75013, France

²Institut de Myologie, Paris 75013, France

³UMR S974, Université Pierre et Marie Curie-Paris6, Paris 75013, France

⁴CNRS UMR 7215, Paris 75013, France

⁵Unité de BFA/CNRS EAC 4413, Université Paris Diderot, Paris 75013, France

⁶Université Paris Descartes, Paris 75006, France

Correspondence should be addressed to A. Ferry, arnaud.ferry@upmc.fr

Received 18 December 2009; Accepted 2 March 2010

Academic Editor: Henk L. M. Granzier

Copyright © 2010 A. Vignaud et al. This is an open access article distributed under the Creative Commons Attribution License, which permits unrestricted use, distribution, and reproduction in any medium, provided the original work is properly cited.

Ischemia/reperfusion (IR) injury can induce skeletal muscle fibre death and subsequent regeneration. By 14 days, absolute and specific maximal forces and fatigue resistance in ischemic/reperfused soleus muscles were still reduced (−89%, −81%, and −75%, resp.) as compared to control muscles ($P < .05$). The decrease of these parameters in ischemic/reperfused muscle was much greater than that of myotoxic injured muscles (−12%, −11%, and −19%; $P < .05$). In addition, at 14 days ischemic/reperfused muscle structure was still abnormal, showing small muscle fibres expressing neonatal myosin heavy chain and large necrotic muscle fibres that were not observed in myotoxin treated muscles. By 56 days, in contrast to myotoxin treated muscles, specific maximal force and muscle weight of the ischemic/reperfused muscles did not fully recover ($P < .05$). This differential recovery between ischemic/reperfused and myotoxin treated muscles was not related to the differences in the initial cell death, loss of satellite cells after injury, expression of growth factors (IGF1, IGF2..), or capillary density in regenerating muscles. In conclusion, our results demonstrate that IR injury in mice induces long term detrimental effects in skeletal muscles and that the recovery following IR injury was delayed for yet unknown reasons as compared to myotoxic injury.

1. Introduction

Restoration of blood flow after a period of ischemia causes ischaemia-reperfusion injury (IR). IR injury is a serious clinical problem that occurs in many diseases (myocardial infarction, trauma, tourniquet application as well as in certain neuromuscular diseases). Animal models of IR have been widely used to study the pathophysiology and consequences of IR injury, as well as in cellular and gene therapies. IR injury causes acute vascular leakage, nerve and skeletal muscle damage with consecutive deficit in neuromuscular function [1–3]. Mast cells, neutrophils, inflammatory cytokines, nitric oxide, and reactive oxygen species most likely play a role in the final damage which is observed in the skeletal muscle [1, 3, 4].

IR injury lasting for more than 2 hours causes extensive skeletal muscle fibre death. Since skeletal muscle is capable of regenerating following injury, subsequent formation of regenerating muscle fibres will occur in the following days. However, it was recently reported that at day 14 following 4 hours of IR injury complete recovery of muscle function had not been achieved [5]. Previous studies have also demonstrated that full recovery of muscle after myotoxin injury can take several weeks [6]. Therefore, it is important to study long-term muscle recovery following IR injury leading to cell death. A few studies have been carried out on long-term muscle recovery following IR injury but most probably they did not induce massive cell death in the models that were used [7, 8]. In contrast to Carvalho et al. [7], Fish et al. [8] found that full muscle recovery was not reached 42 days

after 2 hours of ischemia since maximal force production was still reduced in ischemic-reperfused muscles as compared to control muscles in rats.

We report here the results of experiments in mice, aimed at assessing the long-term outcome of IR injury in mouse hind limb muscles. We wanted to determine whether there is a full recovery of muscle function following an IR injury leading to extensive cell death. In order to have a better understanding of the potential effects of IR injury, ischemic/reperfused muscles were compared to myotoxin-treated muscles. The administration of myotoxic agents results in extensive muscle fibre necrosis [6, 9, 10], without disrupting nerve branches and blood vessels that are elements known to play a major role in muscle repair [11, 12]. Our findings indicate that muscle repair was less efficient following IR injury as compared to that observed after myotoxin injury. These results could provide helpful knowledge in relation to both vascular and neuromuscular diseases.

2. Materials and Methods

2.1. Animals. All procedures were performed in accordance with national and European legislations, using young adult rodents (3–6 month old). IR or myotoxic injury was performed on the right legs of male C57BL6 or Myf5-nlacZ (a gift from F. Relaix, INSERM U787, Paris) mice and the tibialis anterior muscles were studied. Animals were anaesthetised with pentobarbital (60 mg/kg), with supplemental anesthesia as needed. A few hours after IR and myotoxic injury, the animals recuperated a normal mobility.

2.2. Ischemia/Reperfusion Injury. In order to generate unilateral hindlimb ischemia the mice were kept on a heating pad to maintain the body temperature at 37°C and the right hindlimbs were made ischemic by placing rubber bands high on the thigh. After 3 hours of ischaemia, the bands were removed. Contralateral (left) legs were left intact and were used as control (nonischemic/reperfused) muscles.

2.3. Myotoxic Injury. Extensive muscle necrosis was created by injecting cardiotoxin, a myotoxic agent, into the muscles [6, 9, 10]. Cardiotoxin (C-3987, Sigma-Aldrich, 10 µM) was injected into right tibialis anterior in 70 µl of normal saline. A needle connected to a microsyringe was inserted near to the distal tendon, pushed up to the proximal tendon, and the cardiotoxin solution was injected into the muscle, the needle being pulled up in order to deliver the solution all along the muscle. Contralateral (left) legs were left intact and were used to provide control (myotoxin untreated) muscles.

2.4. Contractile Measurements. Muscle function was evaluated by the measurement of in situ muscle contraction in response to nerve stimulation, as previously described [13]. At 14, 28, and 56 days after injury, animals were anesthetized (pentobarbital 60 mg/kg). During experiments, supplemental doses were given as required to maintain deep anesthesia. The knee and foot were fixed with clamps and pins. The distal tendon of the *tibialis anterior* (TA) muscles were attached to an isometric transducer (Harvard

Bioscience) using a silk ligature. All data provided by the isometric transducer were recorded and analyzed on a micro-computer, using the PowerLab system (4SP, ADInstruments) and software (Chart 4, ADInstruments). The sciatic nerves were proximally crushed and distally stimulated by a bipolar silver electrode using supramaximal square wave pulses of 0.1 ms duration. All isometric measurements were made at an initial muscle length of L0 (length at which maximal tension was obtained during the twitch). Responses to tetanic stimulation (pulse frequency 50–143 Hz, 500 ms duration) were successively recorded. At least 1 minute was allowed between contractions. Absolute maximal tetanic forces (P0) were determined. Muscle masses (m) were measured to calculate specific tensions (P0/m). Fatigue resistance (FR) was then determined after a 5 minutes rest period. The muscle was continuously stimulated at 50 Hz during 2 minutes (sub-maximal continuous tetanus). The duration corresponding to a force decreased by 20% was noted FR. Body temperature was maintained at 37°C using radiant heat. After contractile measurements, the animals were killed with an overdose of pentobarbital. Muscles were then weighed, frozen in liquid nitrogen, respectively, precooled in isopentane and stored at –80°C until histological and other analyses.

2.5. Histology. Transverse serial frozen sections of TA muscles (8 µm) were obtained using a cryostat. Some of the sections were stained with hematoxylin and eosin solution, or Sirius red stain and others were used for immunohistochemistry. For immunohistochemistry, frozen sections were fixed 10 minutes in 2% paraformaldehyde and incubated overnight in a blocking solution (BSA 1%, sheep serum 1%, triton X-100 0.3%). Sections were then incubated with either a mouse antibody directed against neonatal MHC, or a rat antibody directed against CD31 (PharMingen, 553370) in order to measure muscle capillary bed density. The antibody against neonatal MHC was prepared as previously described [14]. The neonatal antibody had previously been shown to react with mouse neonatal heavy chain but not with mouse adult fast MHC [15]. Sections were then washed four times in phosphate-buffered saline (PBS) and incubated with a Cy3 AffiniPure Goat Anti-Rabbit IgG (H+L) (111-165-144, Jackson ImmunoResearch), or Alexa Fluor 488 goat anti-rat IgG (H+L) (A11006, Invitrogen). After four washes in PBS slides were mounted in a mounting solution (mowiol/dabco/hoechst). Images were acquired using a digital camera mounted on a bright-field or a fluorescence microscope.

2.6. Satellite Cell Number. The number of satellite cells was determined using the Myf5-nlacZ heterozygous mice [16], which have a reporter gene encoding nuclear-localizing β-galactosidase (nlacZ), targeted to the Myf5 locus. nlacZ reporter gene-β-Gal activity was detected histochemically as previously described [17, 18]. The majority of quiescent and activated satellite cells expressed Myf5 [17, 18].

2.7. Cytokine Antibody Array. RayBio Mouse Cytokine Antibody C Series 1000 kit (RayBiotech) was used for estimating the differential amount of cytokines in pooled protein

extracts, accordingly to the manufacturer's instructions. Only a selection of cytokines is shown, on the basis of their role in muscle repair. The complete list of cytokines and their full names are available on the manufacturer's web site. Muscle proteins were extracted with Array Lysis Buffer (kit component) and incubated at final concentration of $1\ \mu\text{g}/\mu\text{l}$. Each membrane was blocked and incubated with protein extracts. Membranes were washed and then incubated with a biotin-conjugated antibody for 2 hours. Finally, the membranes were washed, incubated with HRP-conjugated streptavidin at room temperature for 1 hour and with detection buffer for 1 minute, and exposed to Fuji Film LAS-4000. The intensities of signals were quantified by densitometric analysis with Multi Gauge V 3.0 software and the positive control (biotin-conjugated IgG) was used to normalize the results from each membrane. We performed proteomic analyses using 3 different pooled samples from 4-5 animals/group (ischemic-reperfused muscles, myotoxin-treated and untreated muscles).

2.8. Statistical Analysis. Data were analysed using Statistica 5.5 software (StatSoft, Paris, France). Ischemic/reperfused muscles or myotoxin-treated muscles were statistically compared to control muscles using variance analysis. If necessary, subsequent contrast analysis was also performed. Values of IR muscles and myotoxin-treated muscles were also expressed as a percentage of control (normal) muscles, that is, contralateral muscles. Values are means \pm SEM.

3. Results

3.1. Effect of IR Injury. At 14 days after IR in contrast to control muscles (Figure 1(a)), ischemic/reperfused muscles exhibited centronucleated muscle fibres of small diameter (regenerating muscle fibres, Figure 1(c)) and "ghosts" that are most likely dead muscle fibres that have not yet disappeared (Figure 1(d)). These observations indicate that IR injury resulted in extensive muscle fibre death, with no apparent survival of muscle fibres and induced insufficient muscle regeneration by day 14. In order to have a wider insight on the potential effects of IR, ischemic/reperfused muscles were also compared to myotoxin-treated muscles. These muscles exhibited similar extensive muscle damage. However, regeneration was more advanced and more homogeneous since centronucleated muscle fibres filled >90% of the muscle cross-section of myotoxin-treated muscles (Figure 1(b)). Fibrosis, based on Sirius Red stainings, was also observed in ischemic/reperfused muscles (Figure 1(h)).

Muscle function also shows drastic changes after IR injury. By 14 days, absolute maximal force (P0, Figure 2), specific maximal force (P0/m, Figure 3), fatigue resistance (FR, Figure 4) and muscle weight (Figure 5) were still markedly reduced in ischemic/reperfused muscles as compared to control muscles ($P < .05$). The fact that absolute maximal force was reduced by 89% at day 14 confirmed that none of the muscle fibres had survived to IR injury. In contrast, we found no significant difference between myotoxin-treated muscles and control muscles at day 14 (Figures 2–5). Accordingly, the levels of recovery (% of control muscles) of absolute maximal force (Figure 2) and specific maximal force (Figure 3), fatigue resistance (Figure 4), and weight (Figure 5) in ischemic/reperfused muscles were reduced when compared to myotoxin-treated muscles, by day 14. By day 28, the level of recovery of absolute maximal force and weight in ischemic/reperfused muscles was still lower as compared to myotoxin-treated muscles (Figures 2 and 5, $P < .05$). By 56 days, ischemic/reperfused muscles fully recovered absolute maximal force (Figure 2) and fatigue resistance (Figure 4). However, specific maximal force (Figure 3) was still reduced in ischemic/reperfused muscles as compared to control muscles, by day 56 ($P < .05$). This last result was explained by the fact that ischemic/reperfused muscles were heavier by day 56 (Figure 5, $P < .05$) whereas absolute maximal force was normal (Figure 2).

3.2. Further Analysis of Injured Muscles. To determine whether the difference in muscle recovery between the ischemic/reperfused and myotoxin-treated muscles was related to delayed muscle regeneration, we analysed the expression of neonatal myosin heavy chain (MHC), that is an MHC isoform expressed at the earlier stage of muscle repair. We found that neonatal MHC was still strongly expressed in ischemic/reperfused muscles (Figure 1(e)) at day 14 but not in myotoxin-treated muscles (Figure 1(f)), confirming delayed muscle regeneration.

It has been previously documented that a reduced blood supply impairs muscle recovery following injury [19]. To test the hypothesis that a reduction in muscle blood supply could explain the difference between ischemic/reperfused and myotoxin-treated muscles, we also analysed muscle capillarity. At day 14, we observed that there was no difference in capillary density between ischemic/reperfused and myotoxin-treated muscles (Figure 6).

We next analysed some of the earlier events in muscle regeneration to try to explain the delayed muscle regeneration observed in the IR group. Since cytokines are known to be involved both in proliferation and differentiation we examined the expression of selected cytokines using a cytokine antibody array that was performed on muscle extracts obtained at day 7. We did not find any marked difference between these two types of muscle injury concerning the level of growth factors (IGF-1, IGF-2, FGF-2, ...) classically involved in muscle repair [20] (Table 1). However, some results did show differences in the 2 types of injured muscles. For example, proteins contributing to angiogenesis (VEGFR1), extracellular matrix remodeling (MMP-2 and MMP-3) were not upregulated in ischemic/reperfused muscles as compared to myotoxin injured muscles, whereas some factors regulating the activation and migration of leukocytes in injured tissues (MIP-1, MIP-2 and MIP-3) and inflammation (sTNF R1 and sTNF R2) were increased in ischemic/reperfused muscles (Table 1).

Muscle fibers are regenerated by the activation and proliferation of satellite cells that fuse together to form myotubes. To determine whether the deficient regeneration observed in ischemic/reperfused muscles was the result of a reduced satellite cell pool, the number of cells expressing

of control muscles) of absolute maximal force (Figure 2) and specific maximal force (Figure 3), fatigue resistance (Figure 4), and weight (Figure 5) in ischemic/reperfused muscles were reduced when compared to myotoxin-treated muscles, by day 14. By day 28, the level of recovery of absolute maximal force and weight in ischemic/reperfused muscles was still lower as compared to myotoxin-treated muscles (Figures 2 and 5, $P < .05$). By 56 days, ischemic/reperfused muscles fully recovered absolute maximal force (Figure 2) and fatigue resistance (Figure 4). However, specific maximal force (Figure 3) was still reduced in ischemic/reperfused muscles as compared to control muscles, by day 56 ($P < .05$). This last result was explained by the fact that ischemic/reperfused muscles were heavier by day 56 (Figure 5, $P < .05$) whereas absolute maximal force was normal (Figure 2).

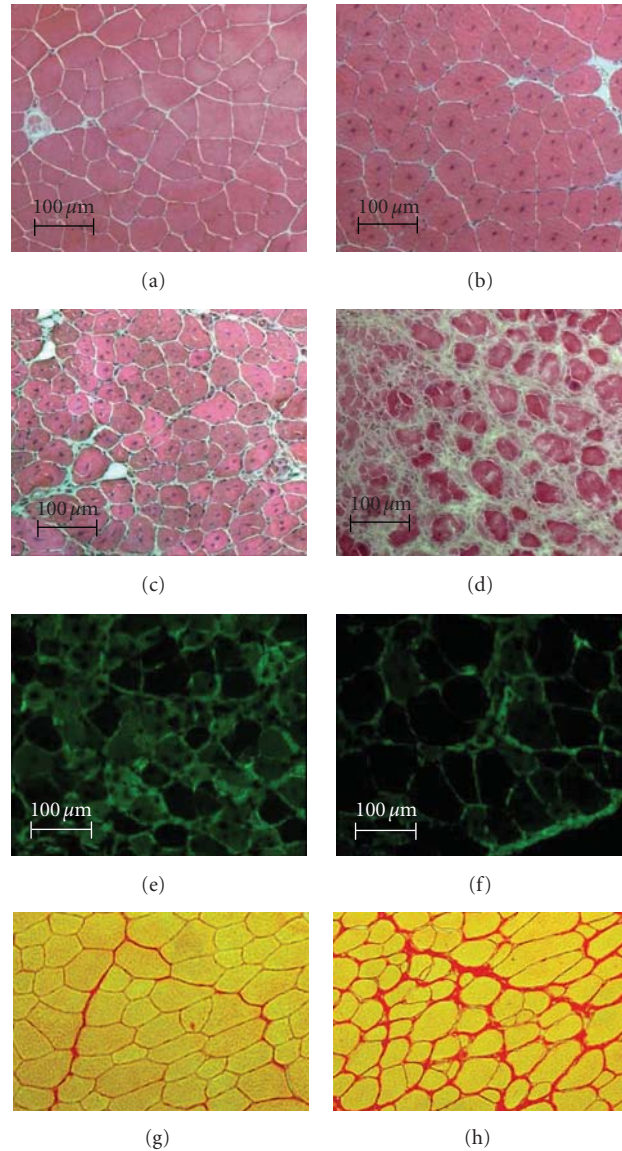


FIGURE 1: Cross-section of muscles after IR injury and myotoxic injury. Cross-sections 14 days after injury was stained with hematoxylin and eosin solution ((a), (b), (c), (d)) or revealed for neonatal MHC reactivity ((e), (f)). Cross-section 2 months after IR injury were stained with Sirius red stain ((g), (h)). ((a), (g)) control muscles (corresponding to myotoxin-treated muscles); ((c), (d), (e), (h)) Ischaemic/reperfused muscles (IR+); ((b), (f)) myotoxin-treated muscles (MI+).

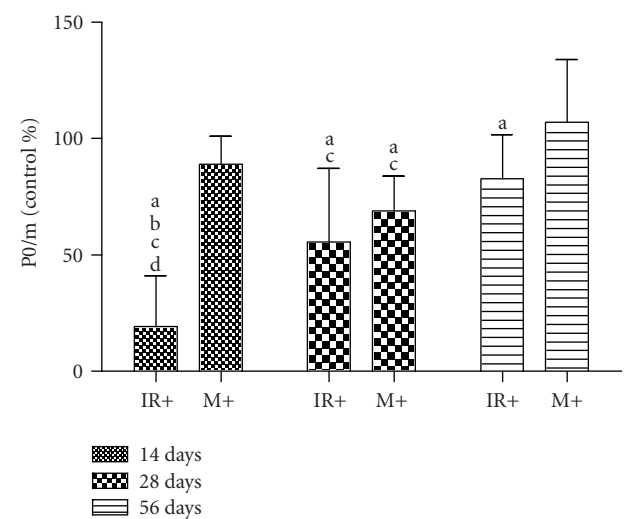
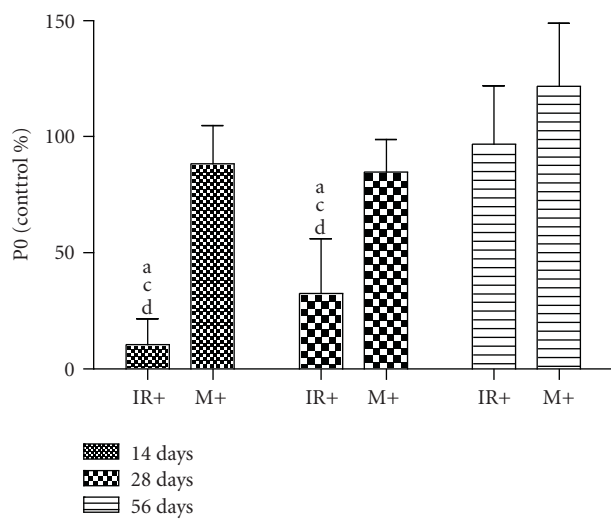
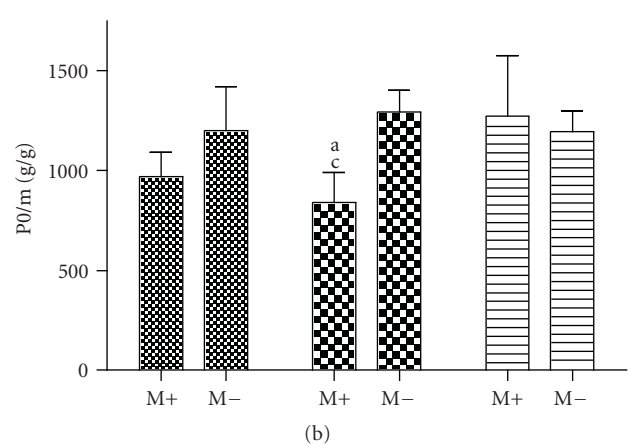
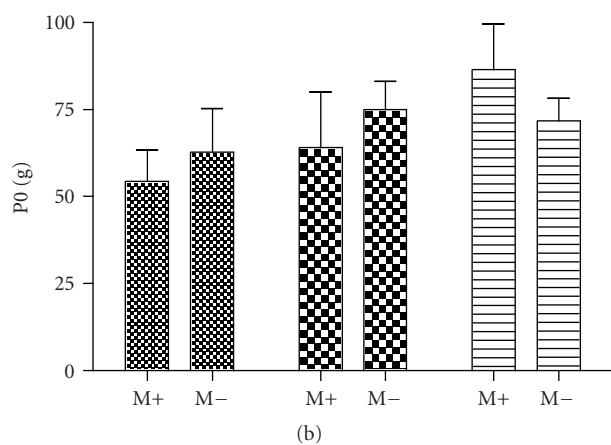
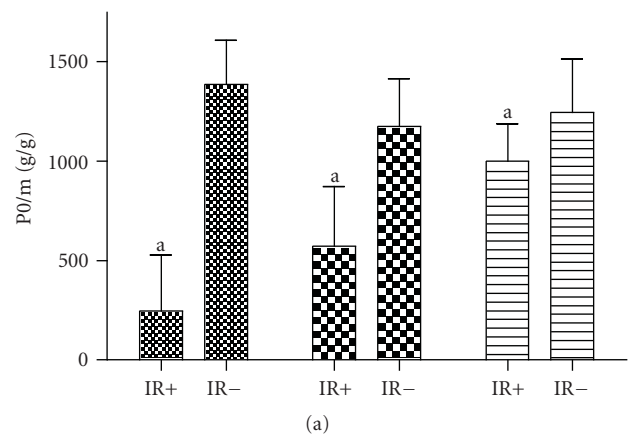
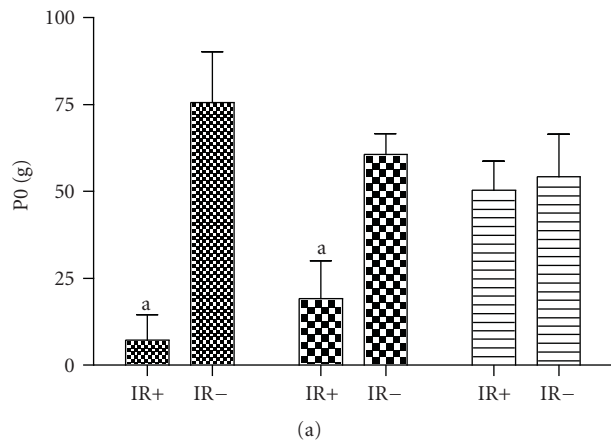
Myf5 was measured after 3 hours of reperfusion. We found that ischemic/reperfused muscles contained a lower number of Myf5 cells as compared to control muscles ($P < .05$, Figure 7). However the loss of Myf5 cells was similar in ischemic/reperfused and myotoxin-treated muscles (Figure 7).

4. Discussion

The aim of this study was to examine the long-term consequence of IR injury on murine hindlimb skeletal muscles. Very little information exists on the rate and on the ultimate extent of muscle recovery following IR injury in this

animal model. Our findings indicate that IR injury has a long lasting and detrimental effect on muscle recovery.

Reduced ATP production [7] and mitochondrial dysfunction [2] are the cause of the extensive cellular death after IR injury. Consequently there is a very marked reduction in muscle function observed just after IR [5, 7, 21]. Our results indicate that maximal force and fatigue resistance in ischemic-reperfused muscles were still markedly reduced 14 days after IR injury, in agreement with previous observations [5, 21]. At this time point, the deficit in absolute maximal force production (-89%) can be explained by the decrease in muscle mass and in specific maximal force. This was related to the poor muscle fibre regeneration, since there were regions of the muscle cross section with no regenerating



(a)

(a)

(b)

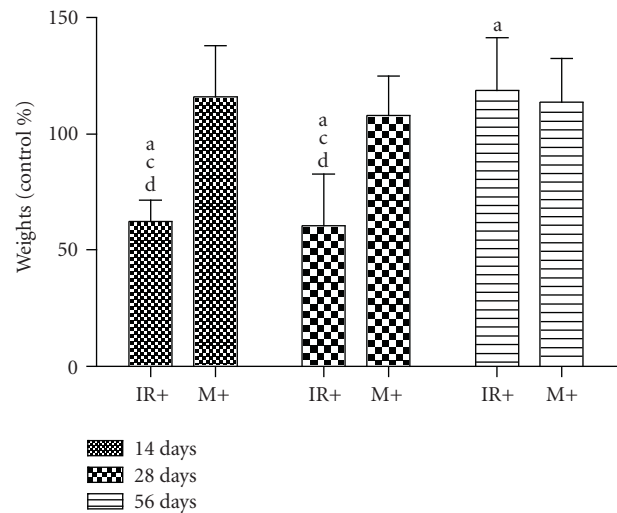
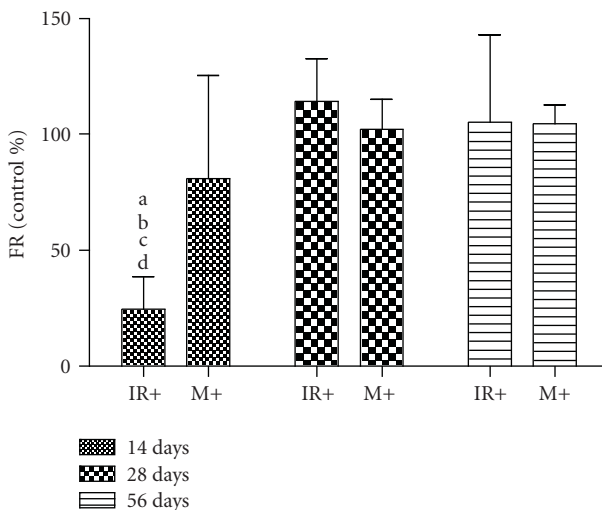
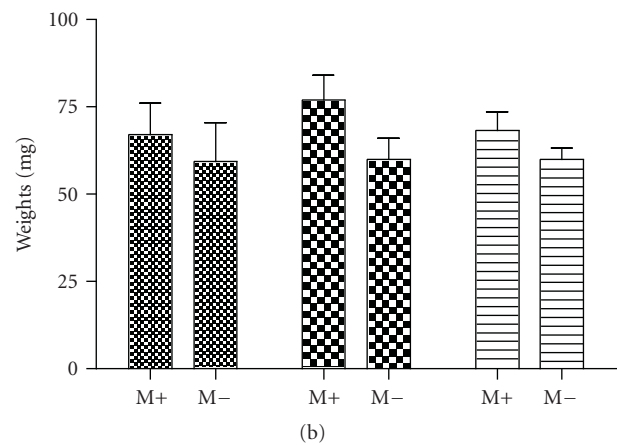
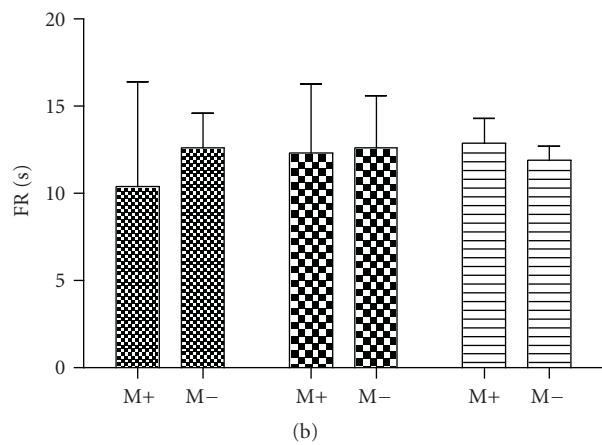
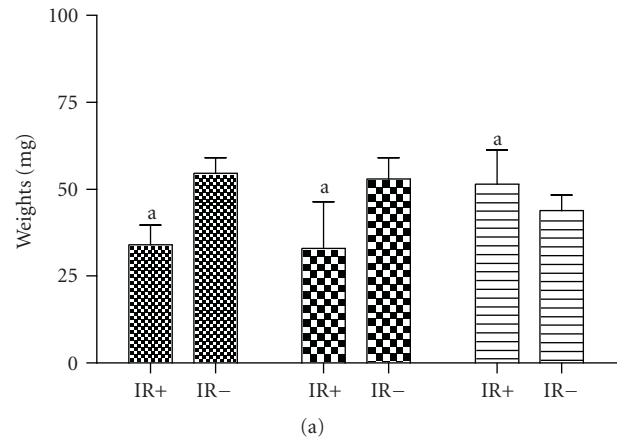
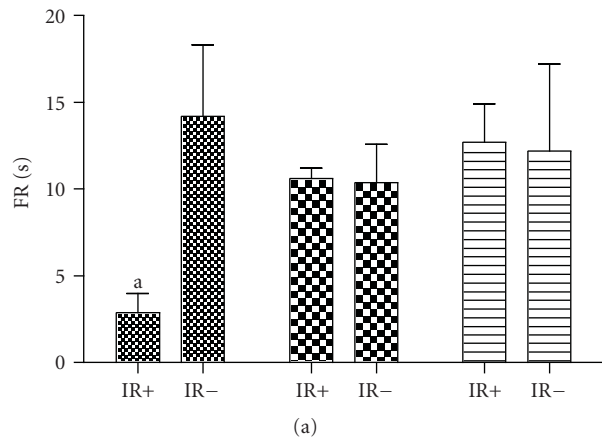
(b)

(c)

(c)

FIGURE 2: Maximal tetanic force (P_0) of muscles after ischemia-reperfusion injury and myotoxic injury. Values are means \pm SEM. Number of data per group is 4–6. IR+: ischaemic/reperfused muscles, IR–: control muscles of ischaemic/reperfused muscles, M+: myotxin-treated muscles, M–: control muscles of myotxin-treated muscles. (a) significantly different from control ($P < .05$), (b) significantly different from 28 days ($P < .05$), (c) significantly different from 56 days ($P < .05$), (d) significantly different from M+.

FIGURE 3: Specific maximal tetanic force (P_0/m) of muscles after ischemia-reperfusion injury and myotxin injury. Values are means \pm SEM. Number of data per group is 4–6. IR+: ischaemic/reperfused muscles, IR–: control muscles of ischaemic/reperfused muscles, M+: myotxin-treated muscles, M–: control muscles of myotxin-treated muscles. (a) significantly different from control ($P < .05$), (b) significantly different from 28 days ($P < .05$), (c) significantly different from 56 days ($P < .05$), (d) significantly different from M+.



(c)

(c)

FIGURE 4: Fatigue resistance of muscles after ischemia-reperfusion injury and myotoxin injury. Values are means \pm SEM. Number of data per group is 4–6. IR+: ischaemic/reperfused muscles, IR–: control muscles of ischaemic/reperfused muscles, M+: myotoxin-treated muscles, M–: control muscles of myotoxin-treated muscles. (a) significantly different from control ($P < .05$), (b) significantly different from 28 days ($P < .05$), (c) significantly different from 56 days ($P < .05$), (d) significantly different from M+.

FIGURE 5: Muscle weights after ischemia-reperfusion injury and myotoxic injury. Values are means \pm SEM. Number of data per group is 4–6. IR+: ischaemic/reperfused muscles, IR–: control muscles of ischaemic/reperfused muscles, M+: myotoxin-treated muscles, M–: control muscles of myotoxin-treated muscles-do not you-mean contralateral muscle of myotoxin-treated mice?. (a) significantly different from control ($P < .05$), (b) significantly different from 28 days ($P < .05$), (c) significantly different from 56 days ($P < .05$), (d) significantly different from M+.

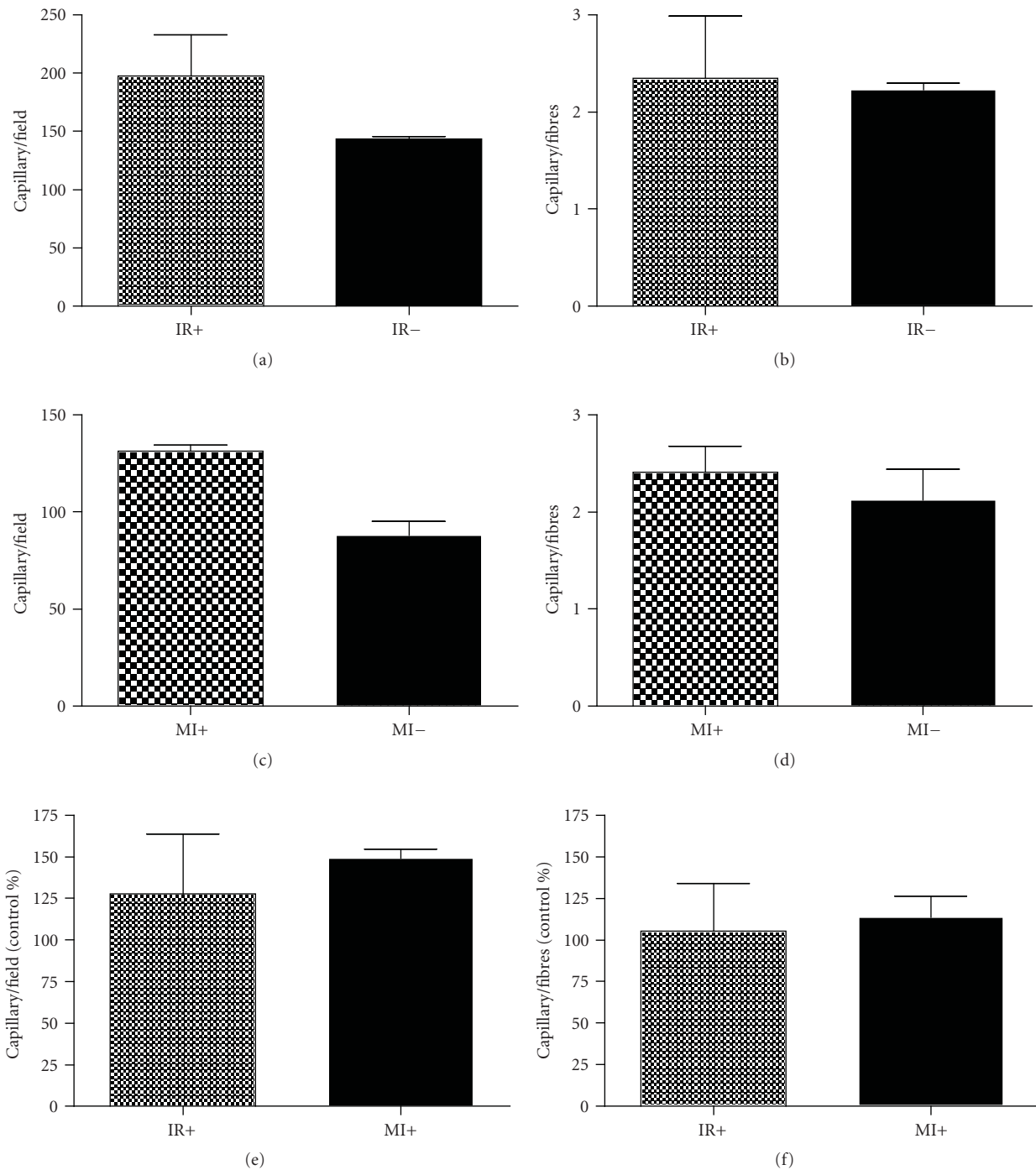


FIGURE 6: Capillary density 14 days after ischemia-reperfusion injury and myotoxic injury. Values are means \pm SEM. Number of data per group is 3. IR+: ischaemic/reperfused muscles, IR-: control muscles of ischaemic/reperfused muscles, M+: myotoxin-treated muscles, M-: control muscles of myotoxin-treated muscles.

muscle fibres, resulting in a reduced number of cross-bridges in parallel. Modified neuromuscular transmission cannot be excluded, although a recent study reports that nerve and muscle stimulation resulted in similar force production by day 14 [5].

Full recovery of absolute maximal force and fatigue resistance occurred by days 28 and 56. However, even at

56 days specific maximal force production was still lower in ischemic-reperfused muscles (-17.5%) as compared to control muscles. One reason leading to the long-term deficit in specific maximal force is that ischaemia-reperfused muscles exhibit a lower density of cross-bridges due to increased fibrosis (as shown at days 56). In contrast, myotoxin-treated muscles fully recovered. Therefore our

TABLE 1: Cytokine expressed in the ischemic-reperfused and myotoxin-treated muscles at day 7.

	IR+ (% uninjured)	MI+ (% uninjured)
<i>Myogenesis</i>		
IGF-I	71	63
IGF-II	43	64
IGFBP-2	65	65
IGFBP-3	107	122
IGFBP-5	109	126
IGFBP-6	109	110
bFGF	106	97
HGF R	0	19
<i>Angiogenesis</i>		
VEGF	132	113
VEGF R1	103	138
VEGF R2	0	0
VEGF R3	0	0
VEGF-D	0	0
<i>ECM remodelling</i>		
MMP-2	65	153
MMP-3	87	52
TIMP-1	93	85
TIMP-2	96	73
Pro-MMP-9	44	48
<i>Chemokines</i>		
Fractalkine	111	90
GCSF	95	91
GM-CSF	91	97
KC (IL8)	129	113
MCP1	75	85
MCP-5	72	79
MIP-1 _α	136	104
MIP-1 _β	196	135
MIP-2	146	119
MIP-3 _α	153	113
MIP-3 _β	132	118
RANTES	119	141
<i>Inflammation</i>		
IL-1 b	117	94
IL-6	89	69
TNF _α	107	92
sTNF RI	146	94
sTNF RII	135	102

results suggest that complete recovery of mouse hindlimb skeletal muscles might never be reached after IR injury, with IR injury reducing the final extent of muscle repair. Thus the long-term consequence of IR injury is that muscle might be heavier (+18.7%) to produce a normal level of maximal force, indicating that the functional “quality” of ischemia-reperfused muscle is lower. Interestingly, a deficit in specific maximal force is also observed in the murine model of Duchenne muscular dystrophy, the mdx mice

(−20–25% [22]). Thus our findings substantiate the concept that myopathy is an aspect of peripheral arterial occlusive disease [2, 3].

Another important finding of the present study is that the level of recovery of maximal force, fatigue resistance and muscle weight was delayed in ischaemia-reperfused muscles as compared to myotoxin-treated muscles at day 14. The differences between ischaemia-reperfused and myotoxic injury were not a result of greater initial injury in the ischaemia-reperfused muscles since all muscle fibers were destroyed by both types of injury. Interestingly, in contrast to myotoxic injury, at 14 days postinjury developmental MHC was not downregulated in ischaemia-reperfused muscles. Therefore our results indicate that muscle regeneration is not only unable to restore normal characteristics but is also delayed following IR injury.

Differential muscle repair between ischemic-reperfused and myotoxin-treated muscles could be explained by different reasons. Satellite cells, local environment, blood vessels and nerve branches are all elements known to play a major role in muscle regeneration. An explanation of our findings could be that part of the satellite cell reservoir, that is, the main source of regenerating muscle fibers was lethally affected by ischemia-reperfusion, resulting in fewer myoblasts, and consequently smaller or less numerous regenerating muscle fibres. In favour of this explanation are data suggesting that muscle recovery increases with the number of satellite cells that escape killing after cryodamage [23]. However we found that the number of Myf5lacZ cells (satellite cells) was similarly reduced by ischemia-reperfusion injury and myotoxic injury. The fact that myotoxic injury can result in satellite cell death was surprising but in agreement with a recent study [24]. Another possibility could be that satellite cell activation proliferation or cell fusion are inhibited by the fact that IR induced an unfavourable environment to muscle repair, such as diabetes [25]. The inflammatory response must be resolved to allow muscle repair [26]. So it is plausible that the reduced muscle repair was the result of a prolonged and combined effect of oxidative stress and inflammation induced by IR injury [1, 3]. Our cytokine antibody array supports this hypothesis. In contrast to myotoxin-treated muscles, some chemokines and markers of inflammation are still increased in ischemic/reperfused muscles at day 7. However, the reduced muscle repair that we observed was not caused by a decrease in growth factors that are key players of muscle regeneration (IGF-1, IGF-2, FGF-2,...), at least at day 7. Blood supply is also considered to play an important role in muscle repair [11, 12]. This was recently confirmed by a study reporting that arterial peripheral insufficiency decreased muscle recovery after injury [19]. We therefore hypothesised that the reduced blood supply due to microvascular leakage observed after IR [1] explains the reduced muscle recovery after IR injury. Our findings showed that by 14 days there was no reduction in capillarity density. However, our results did not rule out the possibility of a reduced blood supply at earlier stage of muscle regeneration. We noted at day 7 a reduced level of VEGFR1. Finally, it is plausible that terminal nerve damage could be induced by IR injury [27], resulting in

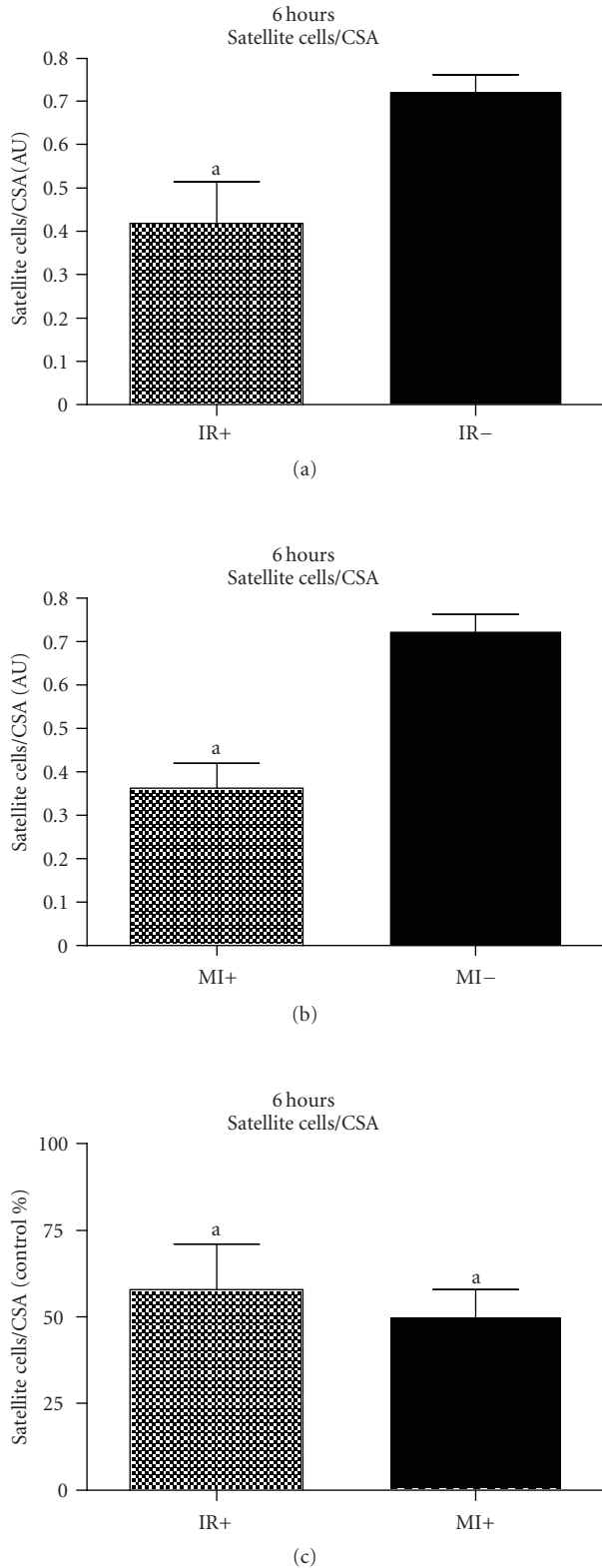


FIGURE 7: Number of Myf5 cells 3 hours after ischemia-reperfusion injury and myotoxin injury. Values are means \pm SEM. Number of data per group is 4–6. IR+: ischaemic/reperfused muscles, IR–: control muscles of ischaemic/reperfused muscles, MI+: myotoxin-treated muscles, MI–: control muscles of myotoxin-treated muscles. (a) significantly different from control ($P < .05$).

a lower level of neuromuscular activity during the early stage of muscle recovery. It has been reported that although nerves retract from the neuromuscular junction immediately after myotoxin injury there is a very rapid restoration of a functional innervation within 3–5 days [11]. Neural activity and mechanical loading are essential for correct muscle regeneration after myotoxin injury [28, 29].

5. Conclusion

In this study we have documented the muscle regeneration that occurs following a period of 3 hours of ischemia in mice. We show that IR injury results in a long-term deficit in muscle function. This was the result of a muscle repair process that was not only delayed but was unable to restore the normal functional characteristics to the regenerated muscle. The lower rate and extent of muscle regeneration after IR injury was not related to a specific loss of satellite cells, nor to a decreased capillary bed density or expression of major growth factors controlling myogenesis. It could however be related to the prolonged inflammation and oxidative stress that does occur after IR. These results confirm the necessity to develop ways to prevent muscle damage induced by IR injury. They should also encourage the research of successful therapies that accelerate muscle repair in the context of vascular deficiency or trauma.

Acknowledgments

This work has been supported by the Association Française contre les Myopathies, INSERM, University Pierre and Marie Curie, European Commission 6th Framework programme, the Myoeres Network of Excellence (contract 5111978) and Myoage EU network. The authors would like to thank Paul Ayesteran (UMR 787) for his help during experiments.

References

- [1] D. C. Gute, T. Ishida, K. Yarimizu, and R. J. Korthuis, "Inflammatory responses to ischemia and reperfusion in skeletal muscle," *Molecular and Cellular Biochemistry*, vol. 179, no. 1-2, pp. 169–187, 1998.
- [2] I. I. Pipinos, A. R. Judge, J. T. Selsby, et al., "The myopathy of peripheral arterial occlusive disease. Part 2. Oxidative stress, neuropathy, and shift in muscle fiber type," *Vascular and Endovascular Surgery*, vol. 42, no. 2, pp. 101–112, 2008.
- [3] I. I. Pipinos, S. A. Swanson, Z. Zhu, et al., "Chronically ischemic mouse skeletal muscle exhibits myopathy in association with mitochondrial dysfunction and oxidative damage," *American Journal of Physiology*, vol. 295, no. 1, pp. R290–R296, 2008.
- [4] T. V. Arumugam, I. A. Shiels, T. M. Woodruff, D. N. Granger, and S. M. Taylor, "The role of the complement system in ischemia-reperfusion injury," *Shock*, vol. 21, no. 5, pp. 401–409, 2004.
- [5] T. J. Walters, J. F. Kragh, D. S. Kauvar, and D. G. Baer, "The combined influence of hemorrhage and tourniquet application on the recovery of muscle function in rats," *Journal of Orthopaedic Trauma*, vol. 22, no. 1, pp. 47–51, 2008.

- [6] A. Vignaud, J. P. Caruelle, I. Martelly, and A. Ferry, "Differential effects of post-natal development, animal strain and long term recovery on the restoration of neuromuscular function after neuromyotoxic injury in rat," *Comparative Biochemistry and Physiology C*, vol. 143, no. 1, pp. 1–8, 2006.
- [7] A. J. Carvalho, P. Hollett, and N. H. McKee, "Recovery of synergistic skeletal muscle function following ischemia," *Journal of Surgical Research*, vol. 59, no. 5, pp. 527–533, 1995.
- [8] J. S. Fish, N. E. McKee, W. M. Kuzon, and M. J. Pyley, "The effect of hypothermia on changes in isometric contractile function in skeletal muscle after tourniquet ischemia," *Journal of Hand Surgery*, vol. 18, no. 2, pp. 210–217, 1993.
- [9] R. Couteaux, J.-C. Mira, and A. d'Albis, "Regeneration of muscles after cardiotoxin injury. I. Cytological aspects," *Biology of the Cell*, vol. 62, no. 2, pp. 171–182, 1988.
- [10] A. Vignaud, J. Cebrian, I. Martelly, J.-P. Caruelle, and A. Ferry, "Effect of anti-inflammatory and antioxidant drugs on the long-term repair of severely injured mouse skeletal muscle," *Experimental Physiology*, vol. 90, no. 4, pp. 487–495, 2005.
- [11] J. B. Harris, "Myotoxic phospholipases A2 and the regeneration of skeletal muscles," *Toxicon*, vol. 42, no. 8, pp. 933–945, 2003.
- [12] C. Pastoret and T. A. Partridge, "Muscle regeneration," in *Cellular and Molecular Basis of Regeneration*, P. A. G. Ferretti, Ed., pp. 309–334, John Wiley and Sons, New York, NY, USA, 1998.
- [13] A. Vignaud, C. Hourde, S. Torres, et al., "Functional, cellular and molecular aspects of skeletal muscle recovery after injury induced by snake venom from *Notechis scutatus scutatus*," *Toxicon*, vol. 45, no. 6, pp. 789–801, 2005.
- [14] G. S. Butler-Browne and R. G. Whalen, "Myosin isozyme transitions occurring during the postnatal development of the rat soleus muscle," *Developmental Biology*, vol. 102, no. 2, pp. 324–334, 1984.
- [15] R. G. Whalen, "Myosin isoenzymes as molecular markers for muscle physiology," *Journal of Experimental Biology*, vol. 115, pp. 43–53, 1985.
- [16] S. Tajbakhsh, E. Bober, C. Babinet, S. Pournin, H. Arnold, and M. Buckingham, "Gene targeting the *myf-5* locus with *n lacZ* reveals expression of this myogenic factor in mature skeletal muscle fibres as well as early embryonic muscle," *Developmental Dynamics*, vol. 206, no. 3, pp. 291–300, 1996.
- [17] J. R. Beauchamp, L. Heslop, D. S. W. Yu, et al., "Expression of CD34 and *Myf5* defines the majority of quiescent adult skeletal muscle satellite cells," *Journal of Cell Biology*, vol. 151, no. 6, pp. 1221–1234, 2000.
- [18] R. N. Cooper, S. Tajbakhsh, V. Mouly, G. Cossu, M. Buckingham, and G. S. Butler-Browne, "In vivo satellite cell activation via *Myf5* and *MyoD* in regenerating mouse skeletal muscle," *Journal of Cell Science*, vol. 112, part 17, pp. 2895–2901, 1999.
- [19] C. Hourde, A. Vignaud, I. Beurdy, I. Martelly, A. Keller, and A. Ferry, "Sustained peripheral arterial insufficiency durably impairs normal and regenerating skeletal muscle function," *Journal of Physiological Sciences*, vol. 56, no. 5, pp. 361–367, 2006.
- [20] S. Charge and M. A. Rudnicki, "Fusion with the fused: a new role for interleukin-4 in the building of muscle," *Cell*, vol. 113, no. 4, pp. 422–423, 2003.
- [21] M. D. Woitaske and R. J. M. McCarter, "Effects of fiber type on ischemia-reperfusion injury in mouse skeletal muscle," *Plastic and Reconstructive Surgery*, vol. 102, no. 6, pp. 2052–2063, 1998.
- [22] C. Dellorusso, R. W. Crawford, J. S. Chamberlain, and S. V. Brooks, "Tibialis anterior muscles in *mdx* mice are highly susceptible to contraction-induced injury," *Journal of Muscle Research and Cell Motility*, vol. 22, no. 5, pp. 467–475, 2001.
- [23] E. Ghins, M. Colson-van Schoor, and G. Marechal, "The origin of muscle stem cells in rat triceps surae regenerating after mincing," *Journal of Muscle Research and Cell Motility*, vol. 5, no. 6, pp. 711–722, 1984.
- [24] A. Poleskaya, P. Seale, and M. A. Rudnicki, "Wnt signaling induces the myogenic specification of resident CD45⁺ adult stem cells during muscle regeneration," *Cell*, vol. 113, no. 7, pp. 841–852, 2003.
- [25] A. Vignaud, F. Ramond, C. Hourde, A. Keller, G. Butler-Browne, and A. Ferry, "Diabetes provides an unfavorable environment for muscle mass and function after muscle injury in mice," *Pathobiology*, vol. 74, no. 5, pp. 291–300, 2007.
- [26] L. Pelosi, C. Giacinti, C. Nardis, et al., "Local expression of IGF-1 accelerates muscle regeneration by rapidly modulating inflammatory cytokines and chemokines," *FASEB Journal*, vol. 21, no. 7, pp. 1393–1402, 2007.
- [27] B. Baxter, T. H. Gillingwater, and S. H. Parson, "Rapid loss of motor nerve terminals following hypoxia-reperfusion injury occurs via mechanisms distinct from classic Wallerian degeneration," *Journal of Anatomy*, vol. 212, no. 6, pp. 827–835, 2008.
- [28] P. Noirez, O. Agbulut, and A. Ferry, "Differential modification of myosin heavy chain expression by tenotomy in regenerating fast and slow muscles of the rat," *Experimental Physiology*, vol. 85, no. 2, pp. 187–191, 2000.
- [29] R. G. Whalen, J. B. Harris, G. S. Butler-Browne, and S. Sesodia, "Expression of myosin isoforms during notexin-induced regeneration of rat soleus muscles," *Developmental Biology*, vol. 141, no. 1, pp. 24–40, 1990.

Research Article

Temporal Adaptive Changes in Contractility and Fatigability of Diaphragm Muscles from Streptozotocin-Diabetic Rats

Marco Brotto,¹ Leticia Brotto,¹ J.-P. Jin,² Thomas M. Nosek,³ and Andrea Romani³

¹ Muscle Biology Research Group (MUBIG), Schools of Nursing & Medicine, University of Missouri-Kansas City, Kansas City, MO 64108, USA

² Department of Physiology, School of Medicine, Wayne State University, Detroit, MI 48201, USA

³ Department of Physiology & Biophysics, School of Medicine, Case Western Reserve University, 10900 Euclid Avenue, Cleveland, OH 44106, USA

Correspondence should be addressed to Andrea Romani, amr5@po.cwru.edu

Received 21 December 2009; Accepted 18 February 2010

Academic Editor: Guy M. Benian

Copyright © 2010 Marco Brotto et al. This is an open access article distributed under the Creative Commons Attribution License, which permits unrestricted use, distribution, and reproduction in any medium, provided the original work is properly cited.

Diabetes is characterized by ventilatory depression due to decreased diaphragm (DPH) function. This study investigated the changes in contractile properties of rat DPH muscles over a time interval encompassing from 4 days to 14 weeks after the onset of streptozotocin-induced diabetes, with and without insulin treatment for 2 weeks. Maximum tetanic force in intact DPH muscle strips and recovery from fatiguing stimulation were measured. An early (4-day) depression in contractile function in diabetic DPH was followed by gradual improvement in muscle function and fatigue recovery (8 weeks). DPH contractile function deteriorated again at 14 weeks, a process that was completely reversed by insulin treatment. Maximal contractile force and calcium sensitivity assessed in Triton-skinned DPH fibers showed a similar bimodal pattern and the same beneficial effect of insulin treatment. While an extensive analysis of the isoforms of the contractile and regulatory proteins was not conducted, Western blot analysis of tropomyosin suggests that the changes in diabetic DPH response depended, at least in part, on a switch in fiber type.

1. Introduction

Increased fatigability of skeletal muscles, characterized by difficulty in squatting and in performing repetitive motions, is commonly observed in both type I and type II diabetes. Insulin-dependent diabetes mellitus (IDDM) can also lead to ventilatory depression and decreased sensitivity to hypercapnia [1]. Diaphragm function is a limiting factor for overall muscle performance, in as much as intense physical activity causes fatigue of diaphragm muscle even in healthy individuals of varying fitness levels [2]. As for the cause of the observed weakness in skeletal and respiratory muscles in diabetics, it has been generally attributed to the motor and sensory neuropathy [3] often present in diabetic patients. Yet, modifications in nerve function and conductance are not consistently observed in these patients, and when they do appear, they usually do so at a later stage of the disease, thus implying that diabetic neuropathy cannot be the only cause of muscular dysfunction [4].

An increased susceptibility to muscle fatigue not only affects the quality of life but also reinforces the tendency to physical inactivity typical of the diabetic patient. Decreased physical activity is very deleterious since even moderate exercise is beneficial in controlling glycemia in diabetic patients, limiting the dependence on insulin or oral antidiabetic drugs [5]. In recent years, the lack of or a decrease in physical activity has been considered one of the main causes, if not a direct trigger, of the increased incidence in chronic diseases such as diabetes, obesity, hypertension, and other cardiovascular disorders [6]. Therefore, understanding factors that in addition to inactivity limit exercise tolerance in diabetic patients is very important.

Whilst several studies have focused on understanding how muscle contractility exerts its regulatory role on glycemia under physiological and diabetic conditions [1–3], little is known about the cellular mechanisms responsible for the increased muscle fatigability under diabetic conditions. Moreover, the majority of the studies performed to date

have been carried out in hind-limb skeletal muscles or in cardiac tissue [7–11] whereas scarce attention has been paid to diaphragm muscle performance. In two previous studies in diaphragm muscles, Hida et al. [12] reported a worsening of diaphragm contractile function at 3 and 7 days after streptozotocin administration, while McGuire and MacDermott [13] reported a compromised contractile function in diabetic diaphragm muscles at ~3 months. To our knowledge, neither of these two studies, nor any other study to date, has investigated the effects of diabetes on diaphragm muscles within a sequential time frame that encompasses acute, steady-state, and chronic effects of diabetes.

Hence, the main aim of our study was to investigate changes induced by diabetes in diaphragm contractility and fatigability in a system in which alterations in nerve function and conductivity have no direct impact on muscle performance throughout a broad time span. To achieve our aim, we used streptozotocin- (STZ-) induced diabetic rats and age-matched controls over a period ranging from 4 days to 14 weeks after STZ administration. The effect of insulin supplementation at a later time point (12 weeks STZ-diabetic + 2 weeks of insulin treatment) was also investigated. We utilized intact diaphragm muscle to concomitantly study maximal tetanic force produced by the muscles as well as the contractile response to, and recovery from, fatiguing stimulation. Skinned fibers were used to assess changes in calcium sensitivity.

Our data demonstrate that there is an early acute, deleterious effect of diabetes on muscle function. This phase is followed first by a gradual improvement in muscle function reflecting a compensatory adaptation that peaks at ~8 weeks and then a marked deterioration in muscle function at 14 weeks after diabetes onset. Two weeks of insulin treatment at 12 weeks after STZ administration completely reversed the compromised muscle function observed at 14 weeks. A similar bimodal pattern of response was also observed in contractility studies conducted in skinned diaphragm muscle fibers.

These results are discussed in a context of clinical relevance as the time frame observed (days to weeks in rats) would be approximately equivalent to changes that would occur over months to several years of pathology in humans. Our results suggest that changes in diaphragm contractile machinery composition and function play a role in the pathophysiology of respiratory diseases secondary to diabetes in addition to limiting physical activity in diabetic patients.

2. Materials and Methods

2.1. Animals and Euthanasia. Male Sprague Dawley rats weighting 180–210 g (Harlan Laboratories, Indianapolis, IN) were sacrificed by CO₂ inhalation. All procedures were performed in accordance with the “Guiding Principles in the Care and Use of Animals” approved by the American Physiological Society and the Animal Protocol Review Committee of the School of Medicine at CWRU.

2.2. Materials. Insulin and glucose-reader strips were from Gemco (Hudson, OH). Urine glucose/ketones strips were from Fisher (Pittsburgh, PA). Streptozotocin and all other chemicals were of analytical grade (Sigma, St Louis, MO).

2.3. Induction of Diabetes. Rats were randomly divided into two groups. One group of animals was rendered diabetic by a single intraperitoneal (ip) injection of 65 mg/kg streptozotocin (STZ) in citrate buffer (pH 4.0), while control animals received an equivalent volume of vehicle. Diabetes onset occurred within 48 hours following STZ administration and it was determined by the appearance of glucose in the urine with glucose strips. The diabetic animals and the age-matched controls were sacrificed at 3–4 days (referred to as 4-day animals for simplicity), 2 weeks, 4 weeks, 8 weeks, and 14 weeks after STZ administration. After 12 weeks from diabetes onset, a subgroup of diabetic animals were placed on daily ip injection of Ultralente insulin (2 U/50 g body weight). These animals were sacrificed at 14 weeks from diabetes induction (i.e., after 2 weeks of insulin treatment).

2.4. Intact Muscle Preparation . These experiments were performed following the protocols established by de Paula Brotto et al. [14]. After the animals were sacrificed, the intact diaphragm (DPH) muscles were removed and placed in a dissecting dish containing a modified Ringer solution having the following composition (mM): 136.5 NaCl, 5.0 KCl, 1.8 CaCl₂, 0.4 NaH₂PO₄, 0.5 MgCl₂, 11.9 NaHCO₃, and 10 glucose, pH 7.4, continuously bubbled with 95% O₂, 5% CO₂, 25°C, to establish control, normoxic conditions. DPH muscles were carefully dissected into small muscle strips measuring 35–40 mm in length and less than 1 mm in thickness to favor optimal oxygen diffusion throughout the muscle strips [14]. For each experimental data point 2–3 strips per animals and 3–6 animals per group (diabetic or nondiabetic) were utilized, and the obtained data were averaged. DPH muscle strips were mounted vertically from the central tendon to the rib cage tissue on a Radnoti (Monrovia, CA) system. The muscle sutures were attached to an isometric force transducer and to a stationary post. The output of the force transducer was digitized and stored in a computer for later analysis. The resting tension and the stimulatory voltage (provided by a Grass digital stimulator) were adjusted to produce maximal isometric tetanic force (T_{max}). The stimulation pattern for these experiments was completely automated after the muscles were mounted. Powerlab/400 E series (ADInstruments, Mountain View, CA) was used to drive a digital Grass stimulator and Chart for Windows v4.0.1 (ADInstruments, Mountain View, CA) was used to collect, digitize, analyze, and store the data to a PC.

2.5. Intermittent Fatiguing Protocols. After T_{max} was determined, the intact DPH strips were allowed to equilibrate for 20 minutes in the Ringer’s solution described above (Equilibration Period, Equil in Figure 1). During equilibration, muscle strips were stimulated with 100 Hz, 330 mA, 500 msec electrical pulse-train administered with a periodicity of 1 minute to generate T_{max} . Stimulation during equilibration

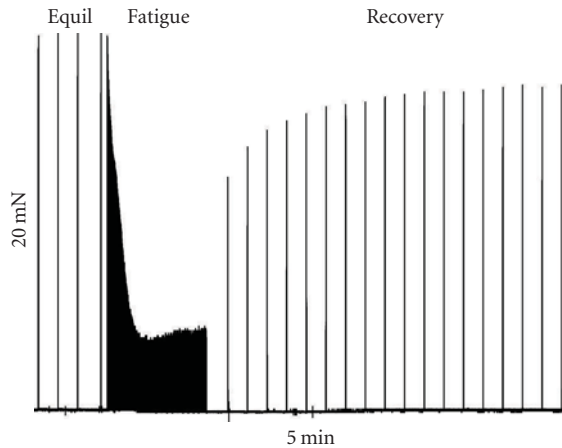


FIGURE 1: Original raw digital tracing of a control DPH muscle strip showing our intact contractility protocol. This intact contractility record shows the last 4 minutes of equilibration (Equil), followed by the fatiguing stimulation period (Fatigue, 5 minutes) and by the recovery period. During Equil and Recovery, the muscle strip was stimulated with tetanic contractions every minute, while during the fatigue period, the muscles were stimulated every second. Calibration bars for this specific experiment are shown. The horizontal bar denotes time in minutes and the vertical bar the relative force in mN produced by the preparation.

allowed us to monitor the condition of the muscle and did not cause measurable fatigue over the 20-minute equilibration period. Following equilibration, the muscles from the fatigue group were subjected to a 5-minute fatiguing protocol (Fatiguing Period, Fatigue, Figure 1) consisting of the same stimulatory pattern administered at a 1-second periodicity. Thereafter, the periodicity of the stimulus train was returned to 1-minute intervals and the muscles were allowed to recover for 30 minutes (Recovery Period, Figure 1). All force data were normalized to the last tetanic contraction at the end of the equilibration period and just prior to the start of the fatiguing protocol (this $T_{\max} = 100\%$). Absolute force, normalized per cross-sectional area (in N/cm^2), was determined at the end of the equilibration period as previously described [14].

2.6. Triton-Skinned Muscle Fibers. Force-versus-pCa relationships were measured using skinned muscle preparations dissected from the same DPH strips used for the intact muscle experiments described above. The technique has been described in detail elsewhere [15, 16]. In brief, single muscle fibers were dissected under a microscope and mounted between an isometric force transducer and a stationary post. All membranes were removed by exposure to Triton X-100. Fibers were activated by transferring them to troughs containing different amounts of free calcium. Calcium-activated force was recorded and normalized to the cross-sectional area of each fiber (in N/cm^2) and to the maximal force produced by each fiber (100%, F_{\max}). The force-versus-pCa curve for each fiber was fit to Boltzmann-Sigmoidal equation as previously described [15, 16]. Ca^{2+} sensitivity was

evaluated from Ca_{50} (the Ca^{2+} concentration producing half-maximal force). The steepness of the curve was evaluated from N , the Hill coefficient. After each parameter was obtained for individual fibers, an average force versus pCa was calculated. In Table 1, n represents the number of individual muscle preparations studied while the number in parenthesis indicates the number of animals from which the fibers were isolated.

2.7. Western Blot Analysis of Tropomyosin Isoforms. The rat skeletal muscle SDS-gel samples were resolved by SDS-PAGE using 14% Laemmli gels with an acrylamide: bisacrylamide ratio of 180:1 cast using a Bio-Rad mini-Protean II system. The resolved protein bands were electrically transferred to nitrocellulose membrane ($0.45\ \mu\text{m}$ pore size) using a Bio-Rad semidry transfer apparatus at $5\ \text{mA}/\text{cm}^2$ for 15 minutes. The membrane was blocked in Tris-buffered saline (TBS) composed of (in mM) 137 NaCl, 5 KCl, and 25 Tris-HCl (pH 7.4) containing 1% BSA at room temperature for 1 hour and incubated with monoclonal antibody (mAb) CH1 against α - and β -Tm mixed with mAb CG3 against γ -Tm (provided by Dr. Jim Lin, University of Iowa) [17] in TBS containing 0.1% BSA at 4°C overnight. After three washes with TBS containing 0.5% Triton X-100 and 0.05% SDS and two TBS rinses, the membrane was incubated with alkaline phosphatase-conjugated antimouse IgG second antibody (Sigma) in TBS containing 0.1% BSA at room temperature for 1.5 hours. After washes as above, 5-bromo-4-chloro-3-indolyl phosphate/nitro blue tetrazolium substrate reaction was carried out as described previously [17] to visualize the tropomyosin isoforms.

2.8. Statistical Analyses. Values are mean \pm SD. Significance was determined by ANOVA followed by either Tukey's or Bonferroni's tests. A value of $P < .05$ was used as criterion for statistical significance.

3. Results

At the time of sacrifice, the level of glycemia was measured by glucose-strip reader on $25\ \mu\text{l}$ of blood and found to be 425 ± 15 versus $88 \pm 5\ \text{mg}/100\ \text{mL}$ for 2-week diabetic and age-matched control animals, respectively ($n = 12$ for both experimental groups, $P < .05$), not increasing significantly with diabetes progression (e.g., 459 ± 17 versus $93 + 7\ \text{mg}/100\ \text{mL}$ in 4-week diabetic and age-matched control animals, respectively ($n = 10$ for both experimental groups, $P < .05$). Rats receiving insulin supplementation presented a glycemia of $98 \pm 10\ \text{mg}/100\ \text{mL}$ at the time of sacrifice as compared to 96 ± 6 and $461 \pm 11\ \text{mg}/100\ \text{mL}$ in age-matched control and 14-week diabetic animals, respectively ($n = 6$ for all experimental groups).

Maximal tetanic force (T_{\max} , normalized to cross-sectional area in N/cm^2 at the end of the equilibration period) was significantly reduced by $\sim 25\%$ for muscles isolated from 4-day diabetic animals compared with age-matched controls (see Table 1). Figure 2(a) illustrates the response of the 4-day diabetic and age-matched control

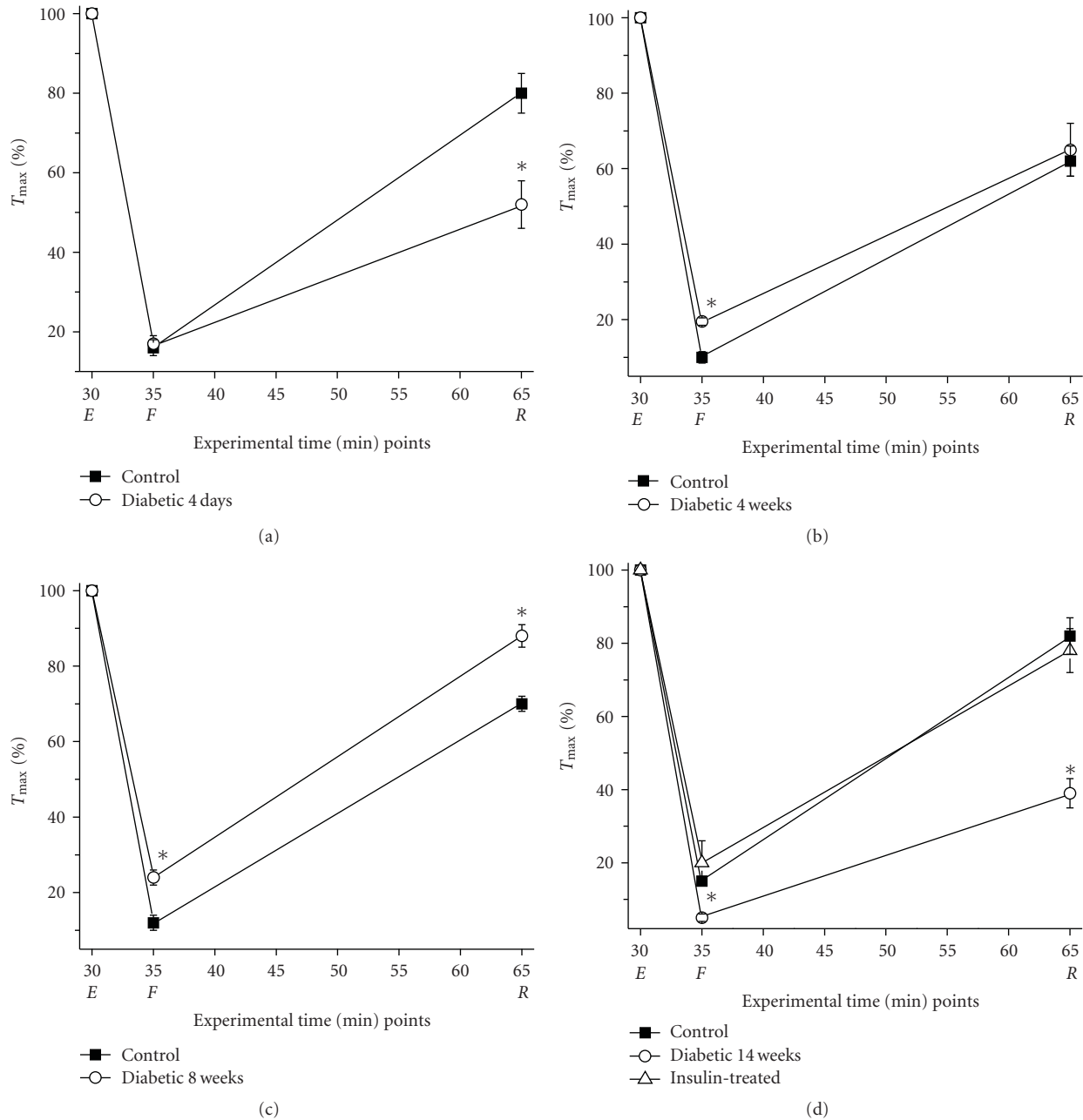


FIGURE 2: Temporal adaptation of intact diaphragm (DPH) muscle contractile function in diabetic muscles. All data are presented as the mean \pm SD. (a) Diabetes exerts an acute deleterious effect on DPH contractile function that is reverted with time (b and c) and profoundly deteriorates with the progression of diabetes (d). After 2 weeks of insulin treatment DPH contractile function significantly improves to levels comparable to control levels (d). In all panels, closed squares show data for control muscles, open circles for diabetic muscles, and the open triangle represents the diabetic + insulin treatment. * means $P < .05$. T_{max} , number of experiments and statistical details are presented in Table 1 and methods.

muscles to the fatiguing protocol, with all data normalized to T_{max} for each muscle. While there was an identical decrease in force in both muscle sets at the end of the fatigue period to approximately 15% of T_{max} , the diabetic muscles regained force to only 52% of T_{max} after 30 minutes of recovery compared to 80% for the age-matched controls. The acute effect of diabetes on the recovery of intact muscle strip function to fatiguing stimulation at 4 days

post streptozotocin administration suggests that acute loss of insulin signaling renders diaphragm muscle susceptible to fatigue-induced damage.

We found that the diaphragm muscle of 4-week diabetic animals may have adapted to the high glucose levels (Table 1, Figure 2(b)). T_{max} was significantly increased from the value in 4-day diabetic animals and was only slightly reduced (by approximately 10%) from the value in age-matched

TABLE 1: Contractile data from diaphragm of diabetic animals and age-matched controls.

	Intact muscles								
	4 days		4 weeks		8 weeks		14 weeks		Insulin
	Control	Diabetic	Control	Diabetic	Control	Diabetic	Control	Diabetic	
<i>n</i> = 7 (4)	<i>n</i> = 7 (4)	<i>n</i> = 9 (5)	<i>n</i> = 8 (4)	<i>n</i> = 10 (5)	<i>n</i> = 10 (5)	<i>n</i> = 7 (4)	<i>n</i> = 7 (4)	<i>n</i> = 8 (4)	
T_{\max} (N/cm ²)	25 ± 2.2	18 ± 1.2	25.5 ± 2.5	22.9 ± 1.5 ^b	24.8 ± 2.1	20 ± 2.2 ^c	25.3 ± 1.1	15.2 ± 1.2 ^d	24.7 ± 2.3 ^e
Fatigue (% T_{\max})	16 ± 2	17 ± 2	10 ± 1.5	19.5 ± 1 ^b	12 ± 2	24 ± 2 ^c	15 ± 1	5 ± 1 ^d	20 ± 6 ^e
Recovery (% T_{\max})	80 ± 5	52 ± 6 ^a	62 ± 4	65 ± 7	70 ± 2	88 ± 3 ^c	82 ± 5	39 ± 4 ^d	78 ± 6 ^e
	Skinned fibers								
	<i>n</i> = 12(3)	<i>n</i> = 9 (3)	<i>n</i> = 8 (3)		<i>n</i> = 9 (3)		<i>n</i> = 12 (4)	<i>n</i> = 12 (4)	
F_{\max} (N/cm ²)	23 ± 3.1	17.3 ± 2.2*	21 ± 1.1 [#]		19.5 ± 1.8 [#]		14.5 ± 2.8*	23.8 ± 3.8 [§]	
pCa50	5.62 ± 0.03	5.46 ± 0.05*	5.70 ± 0.12 [#]		5.87 ± 0.02 [#]		5.33 ± 0.04*	5.63 ± 0.07 [§]	
<i>N</i>	4.45 ± 0.22	3.55 ± 0.09*	3.25 ± 0.22 [#]		2.85 ± 0.12 [#]		3.35 ± 0.20*	4.23 ± 0.18 [§]	

n represents the number of individual muscle preparations studied while the number in parenthesis indicates the number of animals from which the fibers were isolated.

^a T_{\max} and recovery decreased in diabetic muscles ($P < .05$)

^b T_{\max} decreased and recovery enhanced in diabetic muscles ($P < .05$)

^c T_{\max} decreased, fatigue reduced and recovery enhanced in diabetic muscles ($P < .05$)

^d T_{\max} decreased, fatigue increased and recovery decreased in diabetic muscles ($P < .05$)

^e T_{\max} , fatigue and recovery returned to control levels in diabetic muscles treated with insulin ($P < .05$)

* F_{\max} reduced, pCa50 reduced (less sensitive) and *N* decreased (reduced cooperativity) in diabetic fibers ($P < .05$)

[#] F_{\max} reduced, pCa50 increased (more sensitive) and *N* decreased (reduced cooperativity) in diabetic fibers ($P < .05$)

[§] F_{\max} , pCa50 and *N* returned to control levels in diabetic fibers treated with insulin ($P < .05$).

control muscles. Unlike the 4-day diabetic muscles strips that recovered to a lesser degree than the control muscle strips, after 4 weeks of diabetes, the muscles from these animals recovered to the same extend as the age-matched controls. Interestingly, by 4 weeks, diabetic muscles fatigued significantly less than the age-matched controls. The adaptation to lack of insulin persisted through 8 weeks of diabetes (Table 1, Figure 2(c)); the diabetic muscles fatigued even less and recovery from fatiguing stimulation became nearly complete (88% of T_{\max} versus 70% in the age-matched controls). T_{\max} was further reduced in 8-week diabetic muscles to approximately 20% of control levels. However, this seemingly beneficial adaptive response pattern to fatiguing stimulation dramatically changed at 14 weeks of diabetes (Table 1, Figure 2(d)); all three contractile properties significantly decreased when compared to the age-matched controls. By 14 weeks, T_{\max} was drastically reduced by 40% in diabetic muscles. We found that these late-stage responses to diabetes were completely reversed by insulin. When insulin was administered for two weeks to a set of animals diabetic for 12 weeks, T_{\max} and force at the end of the fatiguing and recovery periods all returned to the levels observed in the age-matched controls.

While our intact muscle experiments were able to reveal clear temporally related phenotypic changes in DPH muscles from diabetic rats, it is difficult to infer from these types of experiments any cellular mechanisms that might account for the observed responses. Triton-skinned muscle fibers provide a suitable model system to identify specific modifications within the contractile machinery/proteins that are occurring at various times after streptozotocin treatment, particularly considering the temporal changes in T_{\max} we detected in our studies. Figure 3 shows the force-versus-pCa

relationships for single skinned muscle fibers from control (nondiabetic, 3 months of age), 4-day diabetic, 4-week, 8-week diabetic, 14-week diabetic, and insulin-treated animals. At 4 days, the maximum calcium-activated force (F_{\max}) significantly decreased (by 25%) in a manner that closely matched the observed reduction in T_{\max} of intact muscles (Table 1). In addition, the calcium concentration at which half-maximal activation was achieved (Ca_{50}) significantly increased, indicating that the fibers had become less sensitive to calcium (see Table 1, Figure 3). The slope of the curve (*N*) also significantly decreased in the 4-day diabetic fibers. Just as the intact diabetic muscle strips improved their performance after 4 and 8 weeks of diabetes, single skinned fibers from diabetic animals recovered to a significant extent from the loss in F_{\max} (reduced by ~9% at 4 weeks and 15% at 8 weeks) while their sensitivity to calcium progressively increased. It is interesting to note that a lower F_{\max} and an increased calcium sensitivity are observed in slow-twitch, oxidative muscles as compared to fast-twitch, glycolytic muscles [15, 18]. The slope of the force-versus-pCa curves continued to be reduced at these time points. As observed in intact muscles, this adaptive response was lost at 14 weeks after diabetes onset, with F_{\max} and calcium sensitivity decreasing significantly. Muscles from 12-week diabetic animals treated for 2 weeks with insulin showed a dramatic change in the characteristics of their skinned fibers; the deterioration of function observed in 14-week diabetic animals was completely reversed with F_{\max} , Ca_{50} , and *N* values returning to control levels.

We sought to determine potential molecular mechanisms that might explain the adaptive responses of the muscles to diabetes. The reduction in force (both T_{\max} and F_{\max}) and the increase in calcium sensitivity suggest a change in fiber type. Therefore, we performed Western blot analysis

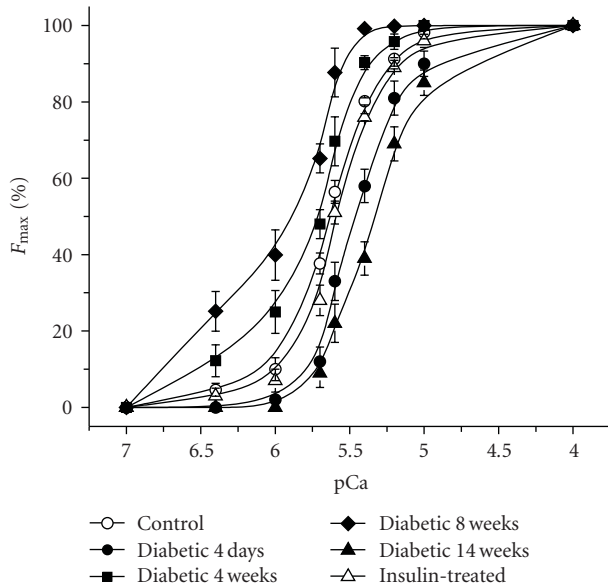


FIGURE 3: Diabetes alters the essential contractile properties in Triton-skinned muscle fibers. All data are presented as the mean \pm SD. Force-versus-pCa relationships for all conditions are shown. The open circle symbol shows the average control force-versus-pCa curve, closed circles show 3-4 days diabetic, closed squares 4 weeks diabetic, closed diamonds 8 weeks diabetic, closed triangles 14 weeks diabetic, and open triangles the insulin-treated muscle fibers. F_{\max} , number of experiments and statistical details are presented in Table 1 and methods.

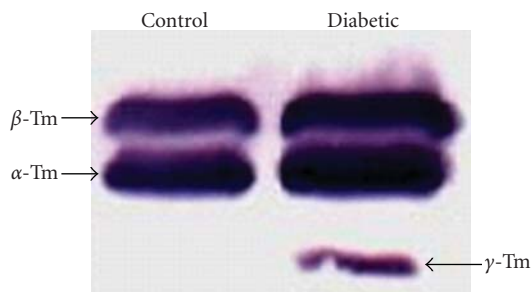


FIGURE 4: Expression of the slowest Tm isoform occurs in untreated DPH muscles after 8 weeks of diabetes. Western blot shows the control and diabetic expression patterns for all three Tm isoforms. The slowest Tm isoform is only detected in 8-week diabetic muscle homogenates. See experimental details in Section 2.

of tropomyosin (Tm) isoforms in muscle homogenates from control and 8-week diabetic rats (Figure 4). We discovered that while control muscle samples only contained the α - and β -Tm isoforms, 8-week diabetic samples contained the γ -Tm isoform, an isoform which uniquely appears in slow-twitch muscles [19].

4. Discussion

To our knowledge, this is the first study to investigate the effects of diabetes induced by STZ on DPH muscles

from mammals during a sequential time frame extending from 4 days to 14 weeks. Our results clearly demonstrate that diabetes causes a detrimental acute effect on the ability of intact DPH muscles to generate maximal tetanic force (T_{\max} was decreased by 28%), a condition where the contractile proteins are maximally stimulated with saturating intracellular calcium. Because the isolated muscle strips used in this study are directly stimulated, any effect of diabetes on force generation would be due to a decrease in the force-generating capability of the contractile apparatus and not to effects on either nerve activity or the neuromuscular junction. In fact, when single DPH fibers were isolated from the same muscles, maximum calcium-activated force (F_{\max}) was reduced by essentially the same amount (25%). By 4 weeks after streptozotocin treatment, both T_{\max} and F_{\max} significantly recovered but were still less than control values. It would appear that the contractile proteins are adapting to the diabetic state. However, by 14 weeks post streptozotocin, there was a major loss in the force-generating capabilities of the contractile proteins, both T_{\max} and F_{\max} decreased by approximately 40%. Therefore, the myofilament protein adaptation is incapable of chronically compensating muscle function in diabetic conditions. This loss in force is due to altered glucose metabolism and/or lack of circulating insulin since DPH muscles from 12-week diabetic animals supplemented with insulin for 2 weeks presented a complete reversal of this detrimental effect. A recent study in muscle-specific G protein α -subunit ($G_s\alpha$) knockout mice [20] showed that this disruption of insulin signaling in skeletal muscles resulted in an adaptive fiber-type switch toward increased slow fiber contents in the absence of hyperglycemia. The results in our present study are consistent with this observation and further demonstrate a beneficial effect of the increase in slow fibers on compensating fatigue tolerance in diabetes.

Diabetic patients exhibit increased muscle fatigability and difficulty in squatting and in performing repetitive motions. Therefore, we stimulated the isolated DPH muscle strips from control and diabetic animals with a pattern of fatiguing stimulation to determine how they respond to, and recover from, the stress of increased activity. Both slow- and fast-twitch muscle fibers typically respond to fatiguing stimulation with a decrease in tetanic force that will recover to a varying degree upon cessation of stimulation [21]. Loss of force during the fatigue period can be due to (1) loss of the maximum force-producing capability of the contractile apparatus, (2) a decrease in the calcium sensitivity of the contractile apparatus, (3) disruption of the excitation-contraction coupling process that provides calcium to the contractile proteins, and (4) depletion of energy substrates, including ATP, creatine phosphate, and glucose. We found that after 4 days of diabetes, T_{\max} decreases to the same extent after the fatiguing period when compared to age-matched control muscles. However, the fact that T_{\max} does not recover to the same extent in diabetic as in control muscles signifies that one or more of these effects of fatiguing stimulation is/are irreversible in the diabetic muscles, at least at this time point. Irreversible damage of fatiguing stimulation to

DPH muscle can account not only for possible respiratory complications but also for the increased muscle fatigue and propensity to inactivity experienced by many diabetic patients.

An adaptation to diabetes similar in time course to that observed for T_{\max} and F_{\max} was also observed in the response of the muscles to fatiguing stimulation. After 4 weeks of diabetes, the intact muscles fatigued less and recovered to the same extent as age-matched controls. After 8 weeks of diabetes, the fatigue response was significantly less than at 4 weeks of diabetes and the recovery was now significantly greater in the diabetic animals. The observation that the calcium sensitivity of the skinned fibers at both 4 and 8 weeks after diabetes was greater than control may at least partially account for this observation; even if the excitation-contraction coupling (ECC) process is permanently compromised by fatiguing stimulation, the increased calcium sensitivity of the fibers would limit the loss of tetanic force at the end of the recovery period. The potential beneficial effects of this adaptation are lost by 14 weeks post diabetes. At this time, corresponding to years of diabetes in humans, intact fibers fatigue to only 5% of the maximal T_{\max} and the recovery is only to approximately 40%. The corresponding loss of calcium sensitivity of the contractile proteins and the loss of cooperativity between the contractile proteins (as reflected in the decreased slope of the force-versus-calcium curve) can contribute to this response. Our functional data at the extreme periods studied here (4 days and 14 weeks) are in complete agreement with the findings of Hida et al. [12] and McGuire and MacDermott [13], respectively. Interestingly, all of these detrimental effects of diabetes on muscle function were completely reversed by 2 weeks of insulin treatment in our study, demonstrating the fundamental role of insulin signaling in maintaining skeletal muscle function. Whereas these benefits were concurrent with renormalized glycemia, which minimizes protein glycation and AGEs generation, the role of insulin-mediated cell signaling warrants further investigation.

Based on data available in the literature and on the progressive decrease in absolute force developed by DPH muscles from diabetic rats, it is conceivable that part of the process activated by diabetes involves alterations/adaptations in the contractile proteins. Contractile force is directly related to intracellular Ca^{2+} levels. The more calcium is released from the sarcoplasmic reticulum (SR), the higher the contractile force becomes due to the saturation of contractile proteins by Ca^{2+} (see Figure 3). It is evident from this relationship that the contractile force produced at higher frequencies of stimulation mirrors the events associated with the contractile proteins, while SR-related events are better reflected at the ascending part of the curve [22]. Because our studies were conducted under conditions where the frequency of stimulation used produced maximal tetanic force (T_{\max}), we can postulate that the adaptation observed in DPH muscles from diabetic rats is probably intrinsic to the contractile proteins although other steps of the ECC process cannot be completely ruled out by our present study. This is supported by our studies on skinned fibers. The adaptive response during weeks 4–8 of diabetes is similar

to what one would find if the fibers with the diaphragm were switching from primarily fast-twitch to primarily slow-twitch, F_{\max} would decrease and the fibers would become more sensitive to calcium [23]. We tested this hypothesis by measuring the isoforms of Tm that were present in control and diabetic muscles. α - and β -Tm isoforms are characteristic of fast-twitch muscles and we found only these isoforms in the control muscles. In contrast, 8-week diabetic muscle samples in addition to the α - and β -Tm isoforms contained the γ -Tm isoform, which is only found in slow-twitch muscle fibers [19]. While this is not a thorough analysis of isoforms changes in the contractile and regulatory proteins under these conditions, the studies of Zhi et al. [17] suggest that an increase in the γ -Tm isoform would be accompanied by an increase in the myosin heavy chain isoforms I and IIa, a decrease in the myosin heavy chain isoforms IIb and IIx, and a switch from fast to slow isoforms of Troponin I and Troponin T. Therefore, it would appear that at least part of the compensation observed at 4 and 8 weeks of diabetes is due to a certain degree of fiber-type switching. While this adaptation is potentially beneficial in that it can help the diaphragm by functional compensation, it is incapable of sustaining diaphragm function while diabetic lesion progresses, which will ultimately cause an uncompensated loss of function. The fiber-type switching, however, may represent only one aspect of the decreasing compensatory adaptation over time. Changes in energy metabolism, calcium cycling within the muscle fibers, diabetes progression, increased formation of reactive oxygen species, and AGEs products can all constitute causes or concourses of the observed phenomenon. It is very encouraging to note, however, that the loss of function can be fully reversed by insulin treatment. This finding is in agreement with the clinical observation that diabetic patients report fewer complaints about muscle fatigue when on insulin therapy and glucose levels are normalized [24].

5. Conclusions

In conclusion, our study is the first to indicate the occurrence of significant temporal adaptations in diaphragm contractility in type I diabetic animals. This change is triphasic, in that an initial deterioration is followed by a marked amelioration and by a tardy stage in which muscle function is again severely impaired. Our studies in skinned muscle fibers suggest that the cellular site of perturbation in diabetic muscle fibers is the contractile machinery/proteins. While our inaugural biochemical studies indicate the appearance of a slow tropomyosin isoform, additional biochemical approaches are required to more precisely determine the cellular basis of these changes in diabetic diaphragm as well as their pathophysiological significance. Protein modification might be an adaptive response to the diabetic milieu stress, while insulin therapy and glucose normalization might protect the contractile machinery against the deleterious effects of the oxidative and inflammatory milieu induced by diabetes.

References

- [1] V. Y. Polotsky, J. A. Wilson, A. S. Haines, et al., "The impact of insulin-dependent diabetes on ventilatory control in the mouse," *American Journal of Respiratory and Critical Care Medicine*, vol. 163, no. 3, part 1, pp. 624–632, 2001.
- [2] M. A. Babcock, D. F. Pegelow, C. A. Harms, and J. A. Dempsey, "Effects of respiratory muscle unloading on exercise-induced diaphragm fatigue," *Journal of Applied Physiology*, vol. 93, no. 1, pp. 201–206, 2002.
- [3] H. Andersen, "Motor function in diabetic neuropathy," *Acta Neurologica Scandinavica*, vol. 100, no. 4, pp. 211–220, 1999.
- [4] H. W. Sander and S. Chokroverty, "Diabetic amyotrophy: current concepts," *Seminars in Neurology*, vol. 16, no. 2, pp. 173–178, 1996.
- [5] R. R. Henry, "Glucose control and insulin resistance in non-insulin-dependent diabetes mellitus," *Annals of Internal Medicine*, vol. 124, no. 1, part 2, pp. 97–103, 1996.
- [6] F. W. Booth and D. R. Vyas, "Genes, environment, and exercise," *Advances in Experimental Medicine and Biology*, vol. 502, pp. 13–20, 2001.
- [7] N. Khandoudi, A. C. Guo, M. Chesnais, and D. Feuvray, "Skinned cardiac fibres of diabetic rats: contractile activation and effects of 2,3-butanedione monoxime (BDM) and caffeine," *Cardiovascular Research*, vol. 27, no. 3, pp. 447–452, 1993.
- [8] I. Murat, V. L. Veksler, and R. Ventura-Clapier, "Effects of halothane on contractile properties of skinned fibers from cardiomyopathic animals," *Journal of Molecular and Cellular Cardiology*, vol. 21, no. 12, pp. 1293–1304, 1989.
- [9] I. Murat and R. Ventura-Clapier, "Effects of halothane on skinned cardiac fibers from the myopathic hamster and the diabetic rat," *Annales Francaises d'Anesthesie et de Reanimation*, vol. 8, supplement, p. R137, 1989.
- [10] G. M. M. Stephenson, A. O'Callaghan, and D. G. Stephenson, "Single-fiber study of contractile and biochemical properties of skeletal muscles in streptozotocin-induced diabetic rats," *Diabetes*, vol. 43, no. 5, pp. 622–628, 1994.
- [11] V. I. Veksler, I. Murat, and R. Ventura-Clapier, "Creatine kinase and mechanical and mitochondrial functions in hereditary and diabetic cardiomyopathies," *Canadian Journal of Physiology and Pharmacology*, vol. 69, no. 6, pp. 852–858, 1991.
- [12] W. Hida, C. Shindoh, J. O. Satoh, et al., "N-acetylcysteine inhibits loss of diaphragm function in streptozotocin-treated rats," *American Journal of Respiratory and Critical Care Medicine*, vol. 153, no. 6, pp. 1875–1879, 1996.
- [13] M. McGuire and M. MacDermott, "The influence of streptozotocin-induced diabetes and the antihyperglycaemic agent metformin on the contractile characteristics and the membrane potential of the rat diaphragm," *Experimental Physiology*, vol. 83, no. 4, pp. 481–487, 1998.
- [14] M. de Paula Brotto, S. A. van Leyen, L. S. Brotto, J.-P. Jin, C. M. Nosek, and T. M. Nosek, "Hypoxia/fatigue-induced degradation of troponin I and troponin C: new insights into physiologic muscle fatigue," *Pflugers Archiv European Journal of Physiology*, vol. 442, no. 5, pp. 738–744, 2001.
- [15] M. A. P. Brotto, R. Y. Nagaraj, L. S. Brotto, H. Takeshima, J. Ma, and T. M. Nosek, "Defective maintenance of intracellular Ca^{2+} homeostasis is linked to increased muscle fatigability in the MG29 null mice," *Cell Research*, vol. 14, no. 5, pp. 373–378, 2004.
- [16] M. A. P. Brotto and T. M. Nosek, "Hydrogen peroxide disrupts Ca^{2+} release from the sarcoplasmic reticulum of rat skeletal muscle fibers," *Journal of Applied Physiology*, vol. 81, no. 2, pp. 731–737, 1996.
- [17] B. Y. Zhi, F. Gao, Z. F. Han, and J.-P. Jin, "Differential regulation of myofilament protein isoforms underlying the contractility changes in skeletal muscle unloading," *American Journal of Physiology*, vol. 292, no. 3, pp. C1192–C1203, 2007.
- [18] N. Weisleder, M. Brotto, S. Komazaki, et al., "Muscle aging is associated with compromised Ca^{2+} spark signaling and segregated intracellular Ca^{2+} release," *Journal of Cell Biology*, vol. 174, no. 5, pp. 639–645, 2006.
- [19] W. A. LaFramboise, R. C. Jayaraman, K. L. Bombach, et al., "Acute molecular response of mouse hindlimb muscles to chronic stimulation," *American Journal of Physiology*, vol. 297, no. 3, pp. C556–C570, 2009.
- [20] M. Chen, H.-Z. Feng, D. Gupta, et al., " $G_s\alpha$ deficiency in skeletal muscle leads to reduced muscle mass, fiber-type switching, and glucose intolerance without insulin resistance or deficiency," *American Journal of Physiology*, vol. 296, no. 4, pp. C930–C940, 2009.
- [21] M. A. P. Brotto, M. T. Marrelli, L. S. Brotto, M. Jacobs-Lorena, and T. M. Nosek, "Functional and biochemical modifications in skeletal muscles from malarial mice," *Experimental Physiology*, vol. 90, no. 3, pp. 417–425, 2005.
- [22] M. A. de Paula Brotto, T. M. Nosek, and R. C. Kolbeck, "Influence of ageing on the fatigability of isolated mouse skeletal muscles from mature and aged mice," *Experimental Physiology*, vol. 87, no. 1, pp. 77–82, 2002.
- [23] M. A. Brotto, B. J. Biesiadecki, L. S. Brotto, T. M. Nosek, and J.-P. Jin, "Coupled expression of troponin T and troponin I isoforms in single skeletal muscle fibers correlates with contractility," *American Journal of Physiology*, vol. 290, no. 2, pp. C567–C576, 2006.
- [24] A. I. Vinik and Q. Zhang, "Adding insulin glargine versus rosiglitazone: health-related quality-of-life impact in type 2 diabetes," *Diabetes Care*, vol. 30, no. 4, pp. 795–800, 2007.

Research Article

Proteomic Profiling of the Dystrophin-Deficient MDX Heart Reveals Drastically Altered Levels of Key Metabolic and Contractile Proteins

Caroline Lewis,¹ Harald Jockusch,² and Kay Ohlendieck¹

¹Department of Biology, National University of Ireland, Maynooth, Kildare, Ireland

²Developmental Biology and Molecular Pathology, University of Bielefeld, D33501 Bielefeld, Germany

Correspondence should be addressed to Kay Ohlendieck, kay.ohlendieck@nuim.ie

Received 7 October 2009; Accepted 25 February 2010

Academic Editor: Aikaterini Kontrogianni-Konstantopoulos

Copyright © 2010 Caroline Lewis et al. This is an open access article distributed under the Creative Commons Attribution License, which permits unrestricted use, distribution, and reproduction in any medium, provided the original work is properly cited.

Although Duchenne muscular dystrophy is primarily classified as a neuromuscular disease, cardiac complications play an important role in the course of this X-linked inherited disorder. The pathobiochemical steps causing a progressive decline in the dystrophic heart are not well understood. We therefore carried out a fluorescence difference in-gel electrophoretic analysis of 9-month-old dystrophin-deficient versus age-matched normal heart, using the established MDX mouse model of muscular dystrophy-related cardiomyopathy. Out of 2,509 detectable protein spots, 79 2D-spots showed a drastic differential expression pattern, with the concentration of 3 proteins being increased, including nucleoside diphosphate kinase and lamin-A/C, and of 26 protein species being decreased, including ATP synthase, fatty acid binding-protein, isocitrate dehydrogenase, NADH dehydrogenase, porin, peroxiredoxin, adenylate kinase, tropomyosin, actin, and myosin light chains. Hence, the lack of cardiac dystrophin appears to trigger a generally perturbed protein expression pattern in the MDX heart, affecting especially energy metabolism and contractile proteins.

1. Introduction

The identification of the gene responsible for the primary defect in X-linked muscular dystrophy [1] led to the discovery of its protein product, the large membrane cytoskeletal element dystrophin [2]. The full-length Dp427 isoform of dystrophin is almost completely missing from the dystrophic surface membrane [3], which triggers the characteristic dystrophic phenotype of progressive skeletal muscle weakness and fibre wasting [4]. Mutations in the dystrophin gene cause the most prevalent and lethal gender-specific genetic disease of childhood, Duchenne muscular dystrophy (DMD), and its more benign and less frequent counterpart Becker's muscular dystrophy, as well as X-linked dilated cardiomyopathy [5]. Dystrophin forms a supramolecular complex with various surface glycoproteins [6] that are involved in cellular signaling, receptor clustering and stabilization of the cellular periphery [7]. Tissue-specific variations in dystrophin isoforms delegate the composition

and subcellular localization of the dystrophin-glycoprotein complex, and hence the function of the specific membrane assembly may vary between the brain, heart, and skeletal muscles [8]. In muscular dystrophy, deficiency in dystrophin causes a significant reduction in the surface-associated glycoprotein complex, which severely impairs the integrity of the sarcolemma [9] and causes a broad spectrum of downstream alterations such as enhanced proteolytic destruction of muscle proteins and abnormal Ca^{2+} -handling [10]. This classifies DMD primarily as a genetic disorder of skeletal muscle, but pathological alterations are also present in cardiac muscle and diaphragm, as well as the peripheral and central nervous system [11].

The majority of DMD patients develop clinical cardiac symptoms during the second decade of life [12], including arrhythmias, cardiomyopathy, and regional wall abnormalities, leading to fatal cardiac complications in about 20% of cases [13]. On the cellular level, the gradual replacement of cardiac fibres by connective and fatty tissue is a hallmark

of the dystrophic heart [14]. While dystrophin-deficient skeletal muscles undergo cycles of fibre degeneration and regeneration, dystrophic heart fibres exhibit only a limited regenerative capacity causing a progressive decline in the cardiomyocyte population of the dystrophic heart [15]. Since cardiomyopathy is a frequent occurrence in inherited muscular dystrophies [16], a number of novel therapeutic approaches are tested to specifically address the cardiac symptoms [17, 18], especially membrane-stabilizing agents such as tri-block poloxamers [19]. In this study, we used the X-linked muscular dystrophy (MDX) mouse, a well-established animal model of DMD [20] that is missing dystrophin isoform Dp427 [21]. Although the dystrophic phenotype of young MDX hearts does not represent a perfect replica of DMD-related cardiomyopathic complications [22], in aged MDX hearts the pathological changes are of considerable clinical relevance [23–25] and cardiac MDX fibres are frequently used to evaluate new treatment strategies to counteract cardiomyopathic complications [26–29].

The absence of cardiac dystrophin is clearly associated with necrotic changes, extensive infiltration of inflammatory cells, increase in adipose tissue, interstitial fibrosis, tachycardia, and impaired contractile properties in the MDX heart [22, 30, 31]. In analogy to DMD hearts, the expression of dystrophin-associated glycoproteins is also greatly reduced in dystrophin-deficient MDX heart cells [32]. Secondary abnormalities in cardiac fibres from the MDX mouse include the drastic reduction in key luminal Ca^{2+} -binding proteins [33] and abnormal stress-induced Ca^{2+} -influx into the cytosol [34]. Interestingly, both physical exercise and aging seem to accelerate the dystrophic process in cardiac MDX tissue [35, 36], whereby a recent study by Spurney et al. [37] revealed that heart dysfunction was most prominent at 9 months of age. This makes this age group of MDX hearts a suitable DMD model for investigating global changes in the cardiac MDX protein complement and was therefore chosen in this study.

The development of mass spectrometry-based proteomics for the swift identification of proteins has decisively enhanced the analytical capability of comparative biomedical studies [38]. In addition, the introduction of fluorescent dyes has drastically increased the total number of identifiable two-dimensional spots, whereby fluorescence difference in-gel electrophoresis (DIGE) can be considered one of the most advanced biomedical tools for studying two different sets of soluble protein complements [39]. DIGE analysis generates highly reproducible findings due to greatly reduced gel-to-gel variations [40]. We have therefore used this technique here for the proteomic profiling of the dystrophic MDX heart. The usefulness of proteomics for determining the biomarker signature of animal disease models of muscular disorders has recently been reviewed [41]. An important aspect of genetic mouse models is that they show, due to their inbred status, genetically much less interindividual differences than human patients. Therefore, considerably fewer experimental repeats are capable of producing meaningful proteomic data. With respect to X-linked muscular dystrophy, proteomic studies have mostly focused on MDX skeletal muscles and have

identified numerous biomarker candidates, such as adenylate kinase [42], calsequestrin [43], regucalcin [44], and the small stress protein cvHsp [45]. In general, dystrophic skeletal muscles show an extremely perturbed protein expression pattern. Although the initial pathobiochemical consequence of a primary genetic abnormality in dystrophin is a severe reduction in dystrophin-associated proteins, this seems to result in a variety of downstream alterations in various classes of muscle proteins involved in fibre contraction, chaperone function, ion homeostasis, cytoskeleton formation and metabolism [41].

In contrast, relatively little is known about global alterations in the dystrophic heart. Building on the recent findings of a combined metabolomic and proteomic investigation into dystrophin deficiency in cardiac muscle [46], this report describes the detailed DIGE analysis of the expression levels of fluorescently-tagged dystrophic versus normal cardiac proteins using both pH 4–7 and pH 6–11 range gels. Following the densitometric determination of the expression pattern of 2,509 cardiac protein spots, mass spectrometry identified 26 proteins being decreased, including various myosin light chains, tropomyosin, actin, adenylate kinase, creatine kinase, vimentin, ATP synthase, fatty acid binding-protein, isocitrate dehydrogenase, NADH dehydrogenase, myozenin, porin, and peroxiredoxin, and 3 proteins being increased, including lamin-A/C and nucleoside diphosphate kinase. These findings suggest that the loss in dystrophin causes abnormalities in cardiac metabolism, the cellular stress response, the cytoskeleton, and the contractile machinery. In the future, these results will be useful for complementing studies into the molecular mechanisms of muscular dystrophy and for evaluating the effects of novel drugs, genetic modifications, or cell-based therapies on disease progression.

2. Materials and Methods

2.1. Materials. For gel electrophoretic analyses, analytical grade chemicals and materials were purchased from Amersham Biosciences/GE Healthcare, Little Chalfont, Buckinghamshire, UK (CyDye DIGE fluor minimal dyes Cy3 and Cy5; 24 cm pH 4–7 and 18 cm pH 6–11 immobilized pH gradient (IPG) strips; IPG buffer; iodoacetamide), Biorad Laboratories, Hemel-Hempstead, Hertfordshire, UK (Laemmli-type buffer system; protein molecular mass markers), National Diagnostics, Atlanta, GA, USA (ultrapure Protogel acrylamide stock solution), Cosmo Bio Company, Tokyo, Japan (2D silver stain II kit), and Perbio Science, Northumberland, UK (Coomassie Brilliant Blue G-250). Protease inhibitors and chemiluminescence substrate were obtained from Roche Diagnostics (Mannheim, Germany). Sequencing grade-modified trypsin was purchased from Promega (Madison, WI, USA). Nitrocellulose transfer stacks were from Invitrogen (Carlsbad, CA, USA). Primary antibodies were obtained from Abcam Ltd., Cambridge, UK (ab28172 to prohibitin; ab36329 to isocitrate dehydrogenase; ab14734 to porin isoform VDAC1; ab54824 to adenylate kinase isoform AK1; ab5432 to ATP synthase, ab16915 to cardiac fatty acid

binding protein), Sigma Chemical Company, Dorset, UK (mAb NOQ7.5.4D to slow/cardiac myosin heavy chain; pAb to laminin), Visionbiosystems Novocastra, Newcastle upon Tyne, UK (mAb NCL-DYS1 against the Dp427 isoform of dystrophin), Thermo Fisher Scientific Inc., Rockford, IL, USA (mAb Rd301 to desmin) and Santa Cruz Biotechnology, Santa Cruz, CA, USA (sc27992 to succinate dehydrogenase). All secondary antibodies were purchased from Chemicon International (Temecula, CA, USA). For confocal microscopy, Superfrost Plus positively-charged microscope slides were purchased from Menzel Glaesser (Braunschweig, Germany). Optimum cutting temperature (OCT) compound was from Sakura Finetek Europe B.V (Zoeterwoude, Netherlands) and p-phenylenediamine (PPD)-glycerol was purchased from Citifluor Ltd. (London, UK). MitoTracker Red CMXRos dye and Alexa Fluor-conjugated secondary antibodies were from Invitrogen Molecular Probes (Bio Sciences Ltd., Dun Laoghaire, Ireland). The DNA binding dye diamidino-phenylindole (DAPI) and all other chemicals used were of analytical grade and purchased from Sigma Chemical Company, Dorset, UK.

2.2. Dystrophic MDX Animal Model. Hearts from male 9-month old C57 control mice and age-matched dystrophic *mdx* mice were obtained through the Bioresource Unit of NUI Maynooth and the Animal House of the University of Bielefeld. Animals were kept under standard conditions and all procedures were performed in accordance with German and Irish guidelines on the use of animals for scientific experiments. Mice were killed by cervical dislocation and their hearts removed and snap-frozen [32]. As previously demonstrated by immunoblotting, the MDX mouse cohort used in this study lacks the 427 kDa isoform of cardiac dystrophin and shows a drastic reduction in dystrophin-associated glycoproteins, such as dystroglycans and sarcoglycans [32, 33].

2.3. Preparation of Total Heart Muscle. For the proteomic profiling of crude cardiac extracts, three normal and three age-matched dystrophic hearts were separately prepared by washing with distilled water to remove excess blood. Muscle tissue was pulverized by grinding in liquid nitrogen using a mortar and pestle. Ground hearts were solubilized in lysis buffer with the ratio 100 mg wet weight to 1 mL lysis buffer consisting of 9.5 M urea, 2% CHAPS, 0.8% IPG buffer pH 3–10, 1% (w/v) DTT and protease inhibitors [45]. Samples for DIGE analysis were placed in buffer containing only urea and CHAPS. Samples were gently rocked for 30 minutes and protein concentration was determined using the Bradford assay system [47]. For immunoblot analysis samples were placed into homogenization buffer (0.5 M HEPES pH 7.4, 200 mM EGTA, 10% (w/v) sucrose, 3 mM MgCl₂, and 0.1% (w/v) NaN₃). The buffer was supplemented with a protease inhibitor cocktail to prevent protein degradation [45]. Extracts were shaken at 4°C on a Thermomixer from Eppendorf (Hamburg, Germany) for 4 hours and then centrifuged at 4°C for 20 minutes at 20,000×g in an Eppendorf 5417R bench centrifuge.

2.4. Difference in-Gel Electrophoretic Analysis. Potential differences in the expression pattern of the soluble proteome from normal and MDX cardiac muscle were analysed using the fluorescence difference in-gel electrophoretic DIGE technique [39], as recommended by Karp and Lilley [48]. The fluorescent dyes Cy3 and Cy5 were reconstituted as a stock solution of 1 mM in fresh dimethylformamide, then diluted to a 0.2 mM solution prior to use. Labeling was performed with 200 pmols of Cy3 fluor dye per 25 µg protein. An internal pooled standard of every sample was prepared with the Cy5 fluor. Labelled samples were then vortexed and incubated for 30 minutes on ice in the dark. The reaction was quenched with 10 mM lysine on ice for 10 minutes [49]. For isoelectric focusing, pH 6–11 IPG strips were rehydrated for 12 hours in rehydration buffer (8 M Urea, 0.5% CHAPS, 0.2% DTT, and 0.2% ampholytes) with the addition of 1.2% (v/v) DeStreak rehydration solution (Amersham Biosciences/GE Healthcare, Little Chalfont, Buckinghamshire, UK). Sample and equal volumes of reducing lysis buffer (9.5 M Urea, 2% CHAPS, 2% DTT, and 1.6% ampholytes) were added by anodic cup loading. For pH 4–7 focusing, IPG strips were in-gel rehydrated with sample and equal volumes of reducing lysis buffer made up in rehydration buffer. The strips were run on an Amersham IPGphor IEF system with the following running conditions: 3500 V for 21.3 hours, a 3500 to 8000 V gradient over 10 minutes in, and 8000 V for 2 hours. For first dimension separation in the pH 6–11 range the following protocol was employed: 80 V for 4 hours, 100 V for 2 hours, 500 V for 1.5 hours, 1000 V for 1 hour, 2000 V for 1 hour, 4000 V for 1 hour, 6000 V for 2 hours, and finally 8000 V for 2.5 hours. Following isoelectric focusing, the IPG strips were equilibrated for 20 minutes firstly in buffer containing 6 M urea, 30% (w/v) glycerol, 2% (w/v) SDS, 100 mM Tris-HCl, pH 8.8 with the addition of 100 mM DTT and subsequently for 20 minutes in buffer supplemented with 0.25 M iodoacetamide [49]. Strips were briefly washed in sodium dodecyl sulfate-containing running buffer (125 mM Tris, 0.96 M glycine, 0.1% (w/v) SDS) and placed on top of 12.5% (w/v) resolving gels. To seal the strip gels, they were overlaid with the above-described running buffer containing 1% (w/v) agarose. The separation of the cardiac proteins was carried out in the second dimension by standard SDS polyacrylamide gel electrophoresis using the DodecaCell system from Bio-Rad Laboratories (Hemel Hempstead, Herts., UK). Slab gels contained 50 µg protein per gel. Electrophoresis was carried out overnight for approximately 18 hours in the dark at 1.5 V per 21 cm-gel until the Bromophenol Blue tracking dye just ran off the gel.

2.5. Protein Visualization and Data Analysis. Fluorescent CyDye-labelled cardiac proteins were visualized using a Typhoon Trio variable mode imager from Amersham Biosciences/GE Healthcare (Little Chalfont, Bucks., UK). For image acquisition, Cy5- and Cy3-labelled proteins were scanned at a wavelength of $\lambda = 650$ nm and $\lambda = 550$ nm, respectively. Photomultiplier tube (PMT) values were optimised so that the volume of the most abundant spot was between 80,000 and 99,000 when scanned at

a resolution of 100 μm . This guaranteed that no spot would be saturated on the gel, therefore interfering with accurate analysis. The Cy3 images were then analysed using Progenesis SameSpots software version 3.2.3 from NonLinear Dynamics (Newcastle upon Tyne, UK) and normalised against their corresponding Cy5 image. Gels were aligned to the reference image. Following detection of spots, the gels were placed into groups (MDX versus normal) and analysed to determine significant differences in 2D spot abundance. An ANOVA score of 0.5 was required for spots to be included in the subsequent analysis. Then principal component analysis (PCA) was verified with changes displaying power of <0.8 being removed from the analysis. All remaining changed spots that met the significance criteria were visually checked on the aligned gels to ensure feasibility and were subsequently identified by LC-MS/MS analysis.

2.6. Mass Spectrometric Identification of Cardiac Proteins. Preparative gels containing 400 μg of protein (1:1 MDX to normal) were stained with the dye Ruthenium II Bathophenanthroline Disulfonate Chelate (RuBPs) [50]. RuBPs-stained gels were scanned at a wavelength of $\lambda = 550\text{nm}$ using the criteria outlined above. Prior to identification via LC-MS/MS technology, 2D protein spots of interest were excised using the automated Ettan spot picker system from Amersham Biosciences (Little Chalfont, Bucks., UK). Spots were digested as outlined by Shevchenko et al. [51]. Briefly, gel pieces were destained before the addition of 400 ng trypsin per spot, incubated for 30 minutes at 4°C before being digested overnight at 37°C. 100 μL of extraction buffer (1:2 v/v of 5% formic acid/acetonitrile) was added to the peptides and incubated for 15 minutes at 37°C. All supernatant was then transferred into fresh tubes and extracts were dried down completely in a vacuum centrifuge. Peptides were reconstituted in 12 μL of 0.1% formic acid, vortexed, sonicated, and the mixture was centrifuged for 20 minutes in cellulose spin filter tubes to remove any gel particles. The remaining solution was placed into LC-MS vials. Samples were analysed on an Agilent 6340 Ion Trap LC mass spectrometer using electrospray ionization (Agilent Technologies, Santa Clara, CA, USA) on a 10-minute gradient of 5–100% acetonitrile/0.1% formic acid with a post run of 1 minute [52]. Separation of peptides was performed with a nanoflow Agilent 1200 series system, equipped with a Zorbax 300 SB C18 μm , 4 mm 40 nl pre-column. Mobile phases used were A: 0.1% formic acid, B: 90% acetonitrile and 0.1% formic acid. Samples (8 μL) were loaded onto the enrichment column with capillary flow rate set at 4 $\mu\text{L}/\text{min}$ with a mix of A : B at a ratio of 19 : 1. Elution was carried out with the nano pump flow rate set at 0.6 $\mu\text{L}/\text{minute}$. Database searches were carried out using Mascot MS/MS Ion search. Criterion for each search was set at (i) species *Mus musculus*, (ii) two missed cleavages by trypsin, (iii) variable modification: oxidation of methioine, (iv) fixed modification: carboxymethylation of cysteines, and (v) mass tolerance of precursor ions $\pm 2\text{Da}$ and product ions $\pm 1\text{Da}$.

2.7. Immunoblot Analysis. In order to verify changes in the expression of select cardiac proteins, 1-D gel electrophoresis, Coomassie staining and immunoblotting was performed as previously described in detail [32]. Gels were transferred to an “iblot” transfer unit from Invitrogen (Carlsbad, CA, USA) for semi-dry blotting. Electrophoretic transfer was carried out for 6 min. Blocking of nitrocellulose sheets was achieved with a milk protein solution (5% (w/v) fat-free milk powder in 0.9% (w/v) NaCl, 50 mM sodium phosphate, pH 7.4) for 1 hour. Incubation with sufficiently diluted primary antibody was carried out overnight with gentle agitation. Nitrocellulose sheets were washed and then incubated for 1 hour with secondary peroxidase-conjugated antibodies, diluted in blocking solution. Immuno-decorated bands were visualized by the enhanced chemiluminescence method using BM Chemiluminescence Blotting substrate from Roche Diagnostics (Mannheim, Germany). Densitometric scanning of immunoblots was performed on a Molecular Dynamics 300 S computing densitometer (Sunnyvale, CA, USA) with ImageJ (NIH, USA) and GraphPad Prism (San Diego, CA, USA) software.

2.8. Confocal Microscopy. For the localization of nuclei, mitochondria and select marker proteins, confocal microscopy was used as previously described in detail [45]. Normal and dystrophic MDX hearts were mounted on cryocassettes at -20°C and transverse cryosections of 10 μm thickness were cut on a Shandon Cryotome (Life Sciences International, Cheshire, UK). Unfixed tissue sections were transferred to Superfrost Plus positively-charged microscopy slides. For labeling of mitochondria, freshly cut tissue sections were incubated with a 1 : 100 diluted solution of MitoTracker Red Chloromethyl-X-Rosamine (CMXRos) dye for 30 minute, briefly washed in phosphate-buffered saline and then immediately examined by microscopy [53]. CMXRos is a well-established lipophilic cationic fluorescent dye that is highly specific for mitochondria [54] and is routinely used to measure mitochondrial function and morphology in cell culture and in whole tissues [55]. For immunofluorescence microscopy, cryosections were briefly fixed in ice-cold acetone for 5 minutes, followed by submersion in blocking solution (0.2% (w/v) bovine serum albumin, 0.2% (v/v) Triton X-100, and 2.5% (v/v) goat serum in phosphate-buffered saline) for 30 minute, and then incubated with primary antibodies diluted in 0.2% (w/v) bovine serum albumin and 0.2% (v/v) Triton X-100 in phosphate-buffered saline for 4 hours. Tissue sections were washed twice for 30 minute in above solution omitting antibodies and then labelled with secondary antibodies for 1 hour, followed by the above described washing procedure. In order to determine the number of nuclei in normal versus MDX hearts, cardiac tissue sections were labelled with 1 $\mu\text{g}/\text{ml}$ diamidino-phenylindole (DAPI) for 30 minute. One drop of p-phenylenediamine (PPD)-glycerol was applied to the immuno-decorated tissue sections and then coverslips carefully placed over the sections, avoiding the introduction of air bubbles. Fluorescent labelling patterns were visualised with an Olympus IX81 microscope (Olympus Life and Material Science Europe, Hamburg, Germany).

3. Results

3.1. Comparative Proteomic Profiling of MDX Versus Normal Heart Muscle. In contrast to non-fluorescent protein dye methodology, comparative studies using fluorescent CyDyes have an enhanced dynamic range of protein coverage [39]. DIGE analysis represents a highly accurate quantitative technique that enables multiple protein samples to be separated on the same two-dimensional gel. This reduces the introduction of potential artifacts due to gel-to-gel variations, making comparative DIGE approaches one of the most powerful analytical tools for conducting comparative biomedical investigations [40]. In order to determine global changes in the heart due to deficiency in the dystrophin isoform Dp427, we have carried out a DIGE analysis of crude tissue extracts from 9-month old normal versus age-matched dystrophic MDX mice. Due to the high cost of breeding and maintaining mice to old age, as well as the considerable cost of fluorescent tagging of large protein populations, the number of biological repeats and analytical DIGE gels was kept to a minimum. In order to satisfy the statistical requirements for the generation of proper proteomic data sets and perform an optimized DIGE analysis of normal versus affected proteomes, we have followed the recommendations by Urfer et al. [56] and Karp and Lilley [48], respectively. In the first dimensional separation step via isoelectric focusing, both a pH 4–7 and a pH 6–11 range were employed to cover as many cardiac proteins with differing charges as possible. Figure 1 illustrates the neutral and the more acidic range of protein species and Figure 2 shows the separation of neutral and more basic heart proteins. Shown are representative two-dimensional gels of Cy3-labelled normal muscle (Figure 1(a); Figure 2(a), Cy3-labelled dystrophic muscle (Figure 1(c); Figure 2(c) and corresponding Cy5-labelled pooled standards (Figures 1(b),1(d); Figures 2(b), 2(d), which were analysed with the help of a Typhoon Trio variable imager and Progenesis 2D analysis software. Overall, 2509 distinct protein species were recognized on the lower and higher pH-range gels. Recently Raddatz et al. [57] have catalogued the soluble murine heart protein complement. The protein spot pattern presented here agrees in large parts with their comprehensive 2D proteomic map of cardiac tissue. Out of 2048 detectable protein spots on the pH 4–7 gels and 487 detectable protein spots on pH 6–11 gels, 79 protein spots showed a drastic differential expression pattern, with 3 proteins being increased and 26 distinct protein species being decreased. Electrospray ionization MS/MS analysis was carried out to unequivocally identify the cardiac proteins with a changed abundance in dystrophic heart fibres.

3.2. DIGE Analysis of the Dystrophin-Deficient Heart. A list of the cardiac protein species with a drastically altered expression level in dystrophic MDX tissue is shown in Table 1. The information on the 79 DIGE-identified protein spots combine data from both pH 4–7 and pH 6–11 gels and contain the spot number, protein name, protein ID, number of matched peptides, percentage sequence coverage, the relative molecular mass, pI-value, Mascot score and

fold-change of individual proteins affected by deficiency in dystrophin. Since the MS-based analysis identified a large number of matched peptide sequences, these data are not shown. The majority of identified cardiac proteins belonged to the main classes of metabolic or contractile proteins. Components of the actomyosin apparatus, enzymatic and regulatory elements of mitochondria, glycolytic enzymes, metabolic transporters, cellular stress proteins and cytoskeletal components were clearly identified by MS analysis. Cardiac proteins with a dystrophy-related change in abundance ranged in molecular mass from apparent 14 kDa to 90 kDa and covered a pI-range from approximately 5 to 9. DIGE Cy5 master gels of both the pH 4–7 and the pH 6–11 range are shown in Figure 3(a), 3(b), so that it is possible to correlate MS-identified protein species, listed in Table 1, with distinct two-dimensional spots of altered density in the dystrophic heart. An increased expression level was shown for 3 cardiac proteins, that is, nucleoside diphosphate kinase B (spot 1), the nuclear lamina matrix protein lamin A/C (spot 2), and a component of the electron-transferring flavoprotein dehydrogenase (spot 3). All other identified protein species exhibited a decreased abundance in dystrophin-deficient myocardial tissue. These cardiac proteins are marked and numbered 4 to 79 in the Cy5-labelled master gels of Figure 3. The protein species with the highest decrease in concentration was identified as the anti-oxidant enzyme peroxiredoxin-6 (spot 79). In addition, mitochondrial ATP synthase (spots 50, 55, 69, 72, 73, 74, 77), isocitrate dehydrogenase (spot 38, 42), NADH dehydrogenase (spot 40), pyruvate dehydrogenase (spots 11, 14, 15, 20, 25, 34), isovaleryl-CoA dehydrogenase (spots 8, 19), dienoil-CoA isomerase (spot 17), oxoglutarate dehydrogenase (spot 7), prohibitin (spot 6), electron-transferring flavoprotein (spots 5, 17), myozenin-2 (spot 4), voltage-dependent anion-selective channel protein VDAC1 (spot 41), the slow/cardiac isoform of myosin light chain MLC2 (spots 26, 48, 62, 65, 70, 78), myosin light chain MLC3 (spots 53, 61, 76), cardiac alpha-actin (spots 21, 39, 45, 46, 56, 60, 64, 66, 67, 71, 75), alpha-1 tropomyosin (spots 35, 59), adenylate kinase AK1 (spot 68), creatine kinase (spot 16), cytochrome c oxidase (spots 22, 51), cytochrome b-c complex (spots 10, 30, 57, 63), desmin (spot 43, 47, 52, 54, 58), vimentin (spots 12, 23), cardiac fatty acid binding-protein FABP-3 (spots 27, 33, 49), heat shock protein Hsp27 (spot 18), heat shock protein Hsp60 (spots 31, 37, 44), enolase (spots 13, 28, 32), DJ-1 protein (spot 29), valsolin-containing protein VCP (spot 24), and albumin (spot 9) were identified. The results for 2 decreased protein spots have not been included in Table 1, since only 1 matched peptide per cardiac protein could be determined by MS analysis. It is international standard that proteomic studies only list proteins with sequence coverage of less than 10% when at least 2 separate matched peptide sequences are available for an independent identification. The peptide sequences LGANSLDLVVFGR (2% sequence coverage) and LTFDSSFSPNTGK (4% sequence coverage) identified the nonlisted cardiac proteins as succinate dehydrogenase (73.6 kDa; pI 7.1) and porin isoform VDAC1 (32.5 kDa; pI 8.6), respectively.

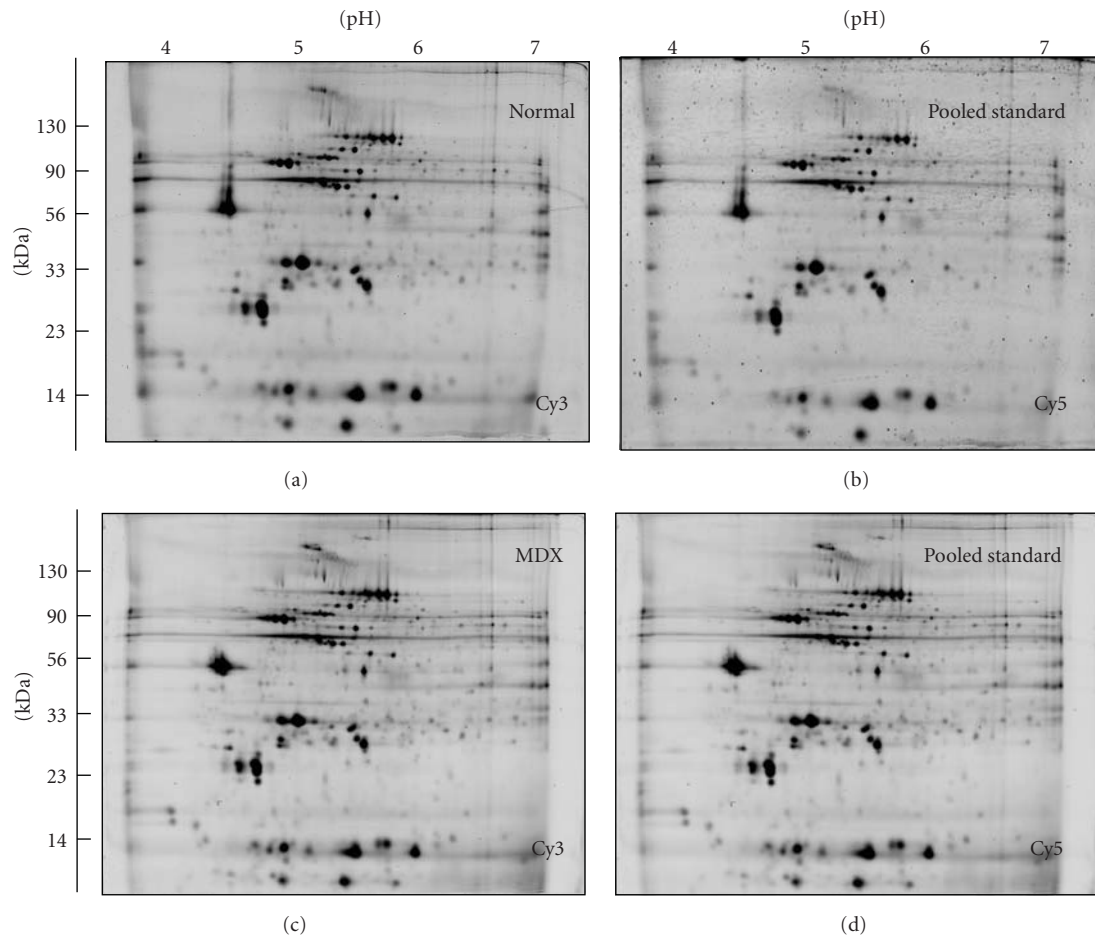


FIGURE 1: 2D gel electrophoretic analysis of the dystrophic heart using the pH 4–7 range. Shown are Cy3-labelled gels of the soluble fraction from normal (a) and dystrophic MDX (c) cardiac muscle, as well as Cy5-labelled gels containing pooled standards ((b), (d)). Representative fluorescent DIGE gels with electrophoretically separated proteins are shown for the pH 4–7 range. The pH-values of the first dimension gel system and molecular mass standards (in kDa) of the second dimension are indicated on the top and on the left of the panels, respectively.

3.3. Decreased Proteins in Dystrophic Heart Muscle. To illustrate representative examples of key cardiac proteins with a drastically decreased expression in dystrophin-deficient fibres, enlarged images of DIGE-identified protein spots are shown in Figure 4. The direct comparison of fluorescently labeled 2-D protein spots, which have been unequivocally identified by mass spectrometric analysis (Table 1), shows the cytosolic AK1 isoform of adenylate kinase, the mitochondrial proteins ATPase synthase, porin isoform VDAC1, isocitrate dehydrogenase, succinate dehydrogenase, and prohibitin, as well as DJ1-protein, the stress protein Hsp60 and myosin light chain isoform MLC2. A large proportion of the cardiac proteins identified in this study by DIGE analysis belong to the contractile apparatus, the cellular stress response and the cytoskeletal network, as well as mitochondrial metabolism including oxidative phosphorylation, the citric acid cycle and fatty acid transportation.

3.4. Immunoblot Analysis of Dystrophic Heart Muscle. Previous studies have clearly shown that the deficiency in dystrophin triggers a drastically reduced concentration of

the dystrophin-associated α/β -dystroglycan complex in the MDX heart [32]. Immunoblotting has established distinct alterations down-stream of the cardiac dystrophin-glycoprotein complex, such as the reduction in the luminal Ca^{2+} -binding proteins calsequestrin and sarcalumenin [33]. In analogy, we employed Western blotting here to verify the results of our DIGE analysis by immuno-decoration analysis of a select group of cardiac proteins. In this respect, it is important to stress that the mass spectrometry-based proteomic analysis of individual 2D spots identifies changes in distinct subspecies of proteins and not alterations in the total population of a protein isoform. The recent large-scale cataloguing of the heart proteome has shown that cardiac tissues contain thousands of different protein species, whereby many proteins are represented by a large number of distinct 2D-spots in analytical gels [57–59]. It is one of the great advantages of modern proteomics that this analytical approach can differentiate between differently charged or sized subspecies of individual proteins. Since 1D immunoblotting or immunofluorescence microscopy often do not recognize all forms of a specific protein due to

TABLE 1: List of DIGE-identified proteins with a changed abundance in 9-month old dystrophic MDX heart muscle.

Spot No.	Protein name	Protein ID	Peptides matched	Coverage (%)	Molecular mass (kDa)	Isoelectric point (pI)	Mascot score	Fold change
1	Nucleoside diphosphate kinase B	NDKB_MOUSE	4	34	17.5	6.9	69	4.4
2	Lamin-A/C	LMNA_MOUSE	4	6	74.5	6.5	111	1.9
3	Electron transfer flavoprotein-ubiquinone oxidoreductase, mitochondrial	ETFD_MOUSE	8	15	68.9	7.3	45	1.8
4	Myozenin-2	MYOZ2_MOUSE	4	20	29.8	8.5	145	0.67
5	Electron transfer flavoprotein subunit alpha, mitochondrial	ETFA_MOUSE	2	12	35.3	8.6	89	0.67
6	Prohibitin	PHB_MOUSE	8	41	29.9	5.6	290	0.67
7	Dihydrolipoyllysine-residue succinyltransferase component of 2-oxoglutarate dehydrogenase complex, mitochondrial	ODO2_MOUSE	3	6	49.3	9.1	86	0.63
8	Isovaleryl-CoA dehydrogenase, mitochondrial	IVD_MOUSE	7	23	46.7	8.5	89	0.59
9	Serum albumin	ALBU_MOUSE	3	5	70.7	5.8	82	0.59
10	Cytochrome b-c1 complex subunit Rieske, mitochondrial	UCRI_MOUSE	4	13	29.6	8.9	84	0.56
11	Dihydrolipoyllysine-residue acetyltransferase component of pyruvate dehydrogenase complex, mitochondrial	ODP2_MOUSE	10	20	68.5	8.8	117	0.53
12	Vimentin	VIME_MOUSE	11	20	53.7	5.1	118	0.53
13	Beta-enolase	ENOB_MOUSE	8	19	47.3	6.7	111	0.50
14	Pyruvate dehydrogenase E1 component subunit beta, mitochondrial	ODPB_MOUSE	8	31	39.3	6.4	279	0.50
15	Pyruvate dehydrogenase E1 component subunit beta, mitochondrial	ODPB_MOUSE	3	19	39.3	6.4	134	0.50
16	Creatine kinase M-type	KCRM_MOUSE	2	4	43.3	6.6	47	0.50
17	Delta(3,5)-Delta(2,4)-dienoyl-CoA isomerase, mitochondrial	ECH1_MOUSE	4	24	36.4	7.6	201	0.50

TABLE 1: Continued.

Spot No.	Protein name	Protein ID	Peptides matched	Coverage (%)	Molecular mass (kDa)	Isoelectric point (pI)	Mascot score	Fold change
18	Heat shock protein beta-1 Hsp27	HSPB1_MOUSE	2	8	23.1	6.1	50	0.50
19	Isovaleryl-CoA dehydrogenase, mitochondrial	IVD_MOUSE	7	17	46.7	8.5	98	0.50
20	Pyruvate dehydrogenase protein X component, mitochondrial	ODPX_MOUSE	5	11	54.3	7.6	63	0.48
21	Actin, alpha cardiac muscle 1	ACTC_MOUSE	6	19	42.3	5.2	104	0.48
22	Cytochrome c oxidase subunit 5B, mitochondrial	COX5A_MOUSE	2	14	14.1	8.7	52	0.48
23	Vimentin	VIME_MOUSE	13	27	53.7	5.1	122	0.48
24	Transitional endoplasmic reticulum ATPase (valosin-containing protein VCP)	TERA_MOUSE	5	10	89.9	5.1	171	0.46
25	Pyruvate dehydrogenase E1 component subunit beta, mitochondrial	ODPB_MOUSE	4	14	39.3	6.4	100	0.44
26	Myosin regulatory light chain 2, ventricular/cardiac muscle isoform	MLRV_MOUSE	9	52	18.9	4.9	209	0.44
27	Fatty acid-binding protein FABP-3, heart	FABPH_MOUSE	5	37	14.8	6.1	149	0.44
28	Enolase 1, alpha	ENOA_MOUSE	2	3	47.5	6.4	43	0.44
29	DJ-1 protein	PARK7_MOUSE	4	26	20.2	6.3	90	0.44
30	Cytochrome b-c1 complex	QCRI_MOUSE	6	17	53.4	5.8	83	0.44
31	60 kDa heat shock protein, Hsp60, mitochondrial	CH60_MOUSE	2	6	61.1	5.9	63	0.42
32	Beta-enolase	ENOB_MOUSE	3	7	47.3	6.7	92	0.42
33	Fatty acid binding protein, FABP-3, heart	FABPH_MOUSE	7	52	14.8	6.1	162	0.42
34	Pyruvate dehydrogenase protein X component, mitochondrial	ODPX_MOUSE	2	4	54.3	7.6	66	0.42
35	Tropomyosin alpha-1 chain	TPM1_MOUSE	15	43	32.7	4.7	302	0.40
36	Electron transfer flavoprotein subunit alpha, mitochondrial	ETFA_MOUSE	8	33	35.3	8.6	235	0.40

TABLE 1: Continued.

Spot No.	Protein name	Protein ID	Peptides matched	Coverage (%)	Molecular mass (kDa)	Isoelectric point (pI)	Mascot score	Fold change
37	60 kDa heat shock protein, Hsp60, mitochondrial	CH60_MOUSE	12	32	61.1	5.9	346	0.40
38	Isocitrate dehydrogenase [NAD] subunit alpha, mitochondrial	IDH3A_MOUSE	9	29	40.1	6.3	164	0.40
39	Actin, alpha cardiac muscle 1	ACTC_MOUSE	12	31	42.3	5.2	317	0.39
40	NADH dehydrogenase [ubiquinone] flavoprotein 2, mitochondrial	NDUV2_MOUSE	6	29	27.6	7.0	370	0.39
41	Voltage-dependent anion-selective channel protein VDAC1	VDAC1_MOUSE	10	29	32.5	8.6	292	0.39
42	Isocitrate dehydrogenase [NAD] subunit alpha, mitochondrial	IDH3A_MOUSE	13	39	40.1	6.3	376	0.39
43	Desmin	DESM_MOUSE	30	50	53.5	5.2	1184	0.39
44	60 kDa heat shock protein, Hsp60, mitochondrial	CH60_MOUSE	25	38	61.1	5.9	842	0.37
45	Actin, alpha cardiac muscle 1	ACTC_MOUSE	10	26	42.3	5.2	276	0.36
46	Actin, alpha cardiac muscle 1	ACTC_MOUSE	4	14	42.3	5.2	88	0.36
47	Desmin	DESM_MOUSE	15	37	53.5	5.2	349	0.36
48	Myosin regulatory light chain 2, atrial isoform	MLRA_MOUSE	9	57	19.6	4.8	299	0.36
49	Fatty acid-binding protein, FABP-3, heart	FABPH_MOUSE	12	61	14.8	6.1	425	0.35
50	ATP synthase subunit beta, mitochondrial	ATPB_MOUSE	18	40	56.3	5.2	1093	0.35
51	Cytochrome c oxidase subunit 5A	COX5A_MOUSE	7	28	16.3	6.1	286	0.35
52	Desmin	DESM_MOUSE	26	62	53.5	5.2	1657	0.35
53	Myosin light chain 3	MYL3_MOUSE	6	41	22.5	5.0	90	0.35
54	Desmin	DESM_MOUSE	12	30	53.5	5.2	431	0.33
55	ATP synthase subunit d, mitochondrial	ATP5H_MOUSE	3	21	18.8	5.5	48	0.33
56	Actin, alpha cardiac muscle 1	ACTC_MOUSE	16	40	42.3	5.2	598	0.32
57	Cytochrome b-c1 complex	QCRI_MOUSE	12	27	53.4	5.8	330	0.32

TABLE 1: Continued.

Spot No.	Protein name	Protein ID	Peptides matched	Coverage (%)	Molecular mass (kDa)	Isoelectric point (pI)	Mascot score	Fold change
58	Desmin	DESM_MOUSE	36	68	53.5	5.2	1289	0.32
59	Tropomyosin alpha-1 chain	TPM1_MOUSE	21	46	32.7	4.7	605	0.32
60	Actin, alpha cardiac muscle 1	ACTC_MOUSE	18	59	42.3	5.2	450	0.31
61	Myosin light chain 3	MYL3_MOUSE	11	63	22.5	5.0	231	0.30
62	Myosin regulatory light chain 2, ventricular/cardiac muscle isoform	MLRV_MOUSE	13	73	18.9	4.9	118	0.29
63	Cytochrome b-c1 complex	QCR1_MOUSE	12	31	53.4	5.8	342	0.29
64	Actin, alpha cardiac muscle 1	ACTC_MOUSE	7	36	42.3	5.2	160	0.29
65	Myosin regulatory light chain 2, ventricular/cardiac muscle isoform	MLRV_MOUSE	7	46	18.9	4.9	354	0.29
66	Actin, alpha cardiac muscle 1	ACTC_MOUSE	4	24	42.3	5.2	91	0.28
67	Actin, alpha cardiac muscle 1	ACTC_MOUSE	17	62	42.3	5.2	294	0.27
68	Adenylate kinase isoenzyme 1	KAD1_MOUSE	5	31	21.6	5.7	174	0.26
69	ATP synthase subunit beta, mitochondrial	ATPB_MOUSE	4	21	56.3	5.2	92	0.26
70	Myosin regulatory light chain 2	MLRA_MOUSE	6	47	19.6	4.8	168	0.25
71	Actin, alpha cardiac muscle 1	ACTC_MOUSE	18	61	42.3	5.2	302	0.25
72	ATP synthase subunit d, mitochondrial	ATP5H_MOUSE	5	36	18.8	5.5	69	0.25
73	ATP synthase subunit beta, mitochondrial	ATPB_MOUSE	18	51	56.3	5.2	640	0.25
74	ATP synthase subunit beta, mitochondrial	ATPB_MOUSE	25	71	56.3	5.2	1102	0.25
75	Actin, alpha cardiac muscle 1	ACTC_MOUSE	6	16	42.3	5.2	119	0.25
76	Myosin light chain 3	MYL3_MOUSE	6	30	22.5	5.0	99	0.25
77	ATP synthase subunit beta, mitochondrial	ATPB_MOUSE	24	70	56.3	5.2	871	0.24
78	Myosin light chain 2, ventricular/cardiac	MLRV_MOUSE	11	77	18.9	4.9	206	0.24
79	Peroxiredoxin-6	PRDX6_MOUSE	3	19	24.9	5.7	102	0.19

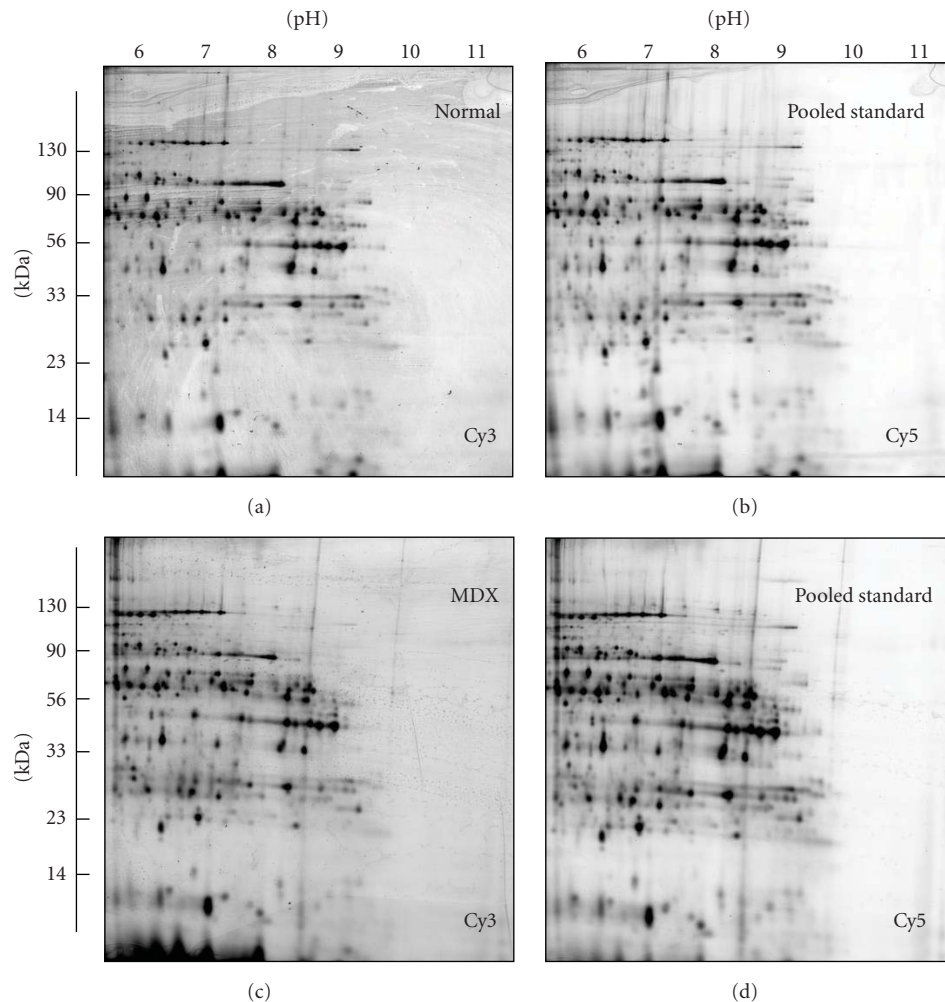


FIGURE 2: 2D gel electrophoretic analysis of the dystrophic heart using the pH 6–11 range. Shown are Cy3-labelled gels of the soluble fraction from normal (a) and dystrophic MDX (c) cardiac muscle, as well as Cy5-labelled gels containing pooled standards ((b), (d)). Representative fluorescent DIGE gels with electrophoretically separated proteins are shown for the pH 6–11 range. The pH-values of the first dimension gel system and molecular mass standards (in kDa) of the second dimension are indicated on the top and on the left of the panels, respectively.

a lack of antibody specificity, proteomic findings on an individual 2D protein spot sometimes do not correlate fully with the findings from biochemical or cell biological analyses of total protein cohorts. These apparent differences in the fate of individual subspecies of a protein versus the total protein population probably reflect the complexity of disease-related changes in the cardiac proteome. Figure 5(a) shows a Coomassie-stained gel of crude preparations from normal and dystrophic hearts and illustrates that no major differences exist in the overall protein expression levels between the two different phenotypes. The immunoblot analysis of laminin, desmin, the slow/cardiac myosin heavy chain and succinate dehydrogenase revealed no major differences in the concentration of these abundant cardiac proteins in normal versus MDX specimens (Figures 5(b)–5(d) and 5(g)). In contrast, immunoblotting of the enzyme adenylate kinase AK1, the fatty acid transporter FABP3, isocitrate dehydrogenase, ATP synthase and porin isoform VDAC1 showed a reduced abundance in MDX preparations (Figures 5(e), 5(f), 5(h)–5(j)). Figure 6 summarizes the

statistical evaluation of the immunoblot survey in a graphical presentation. The reduced expression of adenylate kinase isoform AK1, fatty acid binding protein FABP3, isocitrate dehydrogenase ICDH, porin isoform VDAC1, and ATP synthase was found to be statistically significant, while the concentration of desmin, myosin heavy chain and succinate dehydrogenase was shown not to be significantly different between normal and dystrophic preparations. Thus the overall isoform population of succinate dehydrogenase and desmin does not appear to be reduced in dystrophinopathy, although the above-described DIGE analysis showed a lower level of distinct subspecies of these cardiac elements. In general, the immunoblotting results support the main findings from our DIGE analysis of normal versus dystrophic heart tissue and demonstrate independently that the deficiency in dystrophin has a profound effect on the expression pattern of the cardiac protein complement.

3.5. Immunofluorescence Analysis of Dystrophic Heart Muscle. Since the DIGE analysis of the normal versus the dystrophic

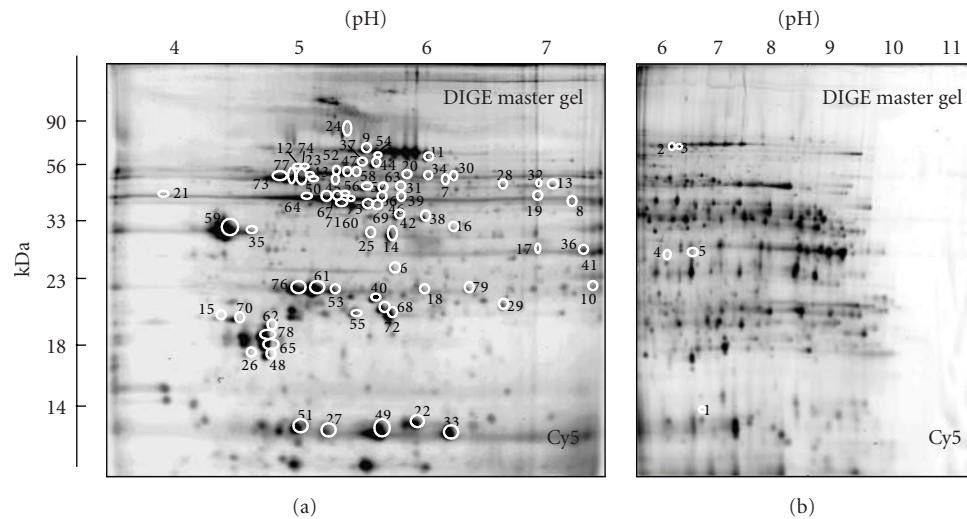


FIGURE 3: DIGE analysis of normal versus dystrophic MDX cardiac muscle. Shown are Cy5-labelled master gels of the soluble fraction from mouse heart muscle, covering both the pH 4–7 (a) and pH 6–11 (b) range. Protein spots with a drastically different expression level are marked by circles and are numbered 1 to 79. See Table 1 for a detailed listing of cardiac muscle proteins with a changed abundance in dystrophin-deficient tissue. The pH-values of the first dimension gel system and molecular mass standards (in kDa) of the second dimension are indicated on the top and on the left of the panels, respectively.

MDX heart has revealed changes in a variety of mitochondrial components, it was important to determine whether this alteration was due to a reduced number of mitochondria in the dystrophic heart or internal abundance changes in the mitochondrial protein complement. Figure 7 shows representative results from an immunofluorescence survey of mitochondrial content, nuclei and cardiac marker proteins in dystrophic tissue. Cryosections of MDX tissue showed a complete absence of the dystrophin isoform Dp427 (Figures 7(c), 7(d)), confirming the mutant status of the dystrophic hearts used in this study. DAPI staining revealed 229 ± 6 and 270 ± 18 nuclei per examined tissue section in normal versus dystrophic tissue sections, respectively (Figures 7(a), 7(b)). The slight increase of nuclei in MDX preparations was not statistically significant ($n = 4$). Thus the proteomic finding of a dystrophy-dependent increase in lamin-A/C is therefore not directly related to a drastic change in the number of nuclei per cardiac tissue unit. Fluorescent labeling of mitochondria with the MitoTracker dye CMXRos showed a characteristic internal staining pattern in cardiac fibres (Figures 7(e)–7(h)). Fluorescent intensity values of 1470 ± 36 and 1384 ± 40 for normal versus MDX preparations were found not to be significantly different ($n = 4$). Hence, lower levels of mitochondrial enzymes do not seem to be a consequence of a drastic decrease in mitochondrial density in the dystrophic MDX heart. In addition, confocal microscopy was employed for the localization of cardiac marker proteins. The immunofluorescence labeling of desmin (Figures 7(i)–7(l)), prohibitin (Figures 7(m)–7(p)) and succinate dehydrogenase (Figures 7(q)–7(t)) was shown to be comparable between control and pathological samples. The microscopical localization of desmin and succinate dehydrogenase revealed unexpectedly not a decrease of these proteins in dystrophic tissue sections, as found by DIGE analysis. Hence,

although distinct subspecies of certain cardiac proteins are affected in X-linked muscular dystrophy as determined by mass spectrometry-based proteomics, the overall isoform complement of these elements is not drastically altered. This indicates that no major differences exist in the expression levels of desmin-containing intermediate filament structures and the population of cardiac mitochondria in normal versus dystrophin-deficient cells.

4. Discussion

In order to enhance our knowledge of the molecular pathogenesis of cardiomyopathy linked to X-linked muscular dystrophy, a detailed proteomic profiling of the dystrophic heart was carried out. The biochemical establishment of a comprehensive disease-specific biomarker signature for X-linked muscular dystrophy is crucial for (i) the development of superior diagnostic methods, (ii) the identification of new therapeutic targets to address cellular alterations downstream of the primary abnormality in dystrophin, and (iii) the evaluation of new treatment approaches to counteract the various pathological aspects of dystrophinopathy [41]. The proteomic profiling of MDX skeletal muscle has recently established altered expression levels of soluble proteins involved in nucleotide metabolism, Ca^{2+} -handling and the cellular stress response [42–45]. The mass spectrometric analysis of experimental exon skipping therapy revealed a partial reversal of dystrophic changes in these new signature molecules [60], illustrating the potential of proteomic technology to decisively enhance the capabilities of biomedical research into the molecular mechanisms that underlie neuromuscular disorders. In contrast to skeletal muscle, very little is known about the global pathobiochemical mechanisms that lead to cardiac complications in the

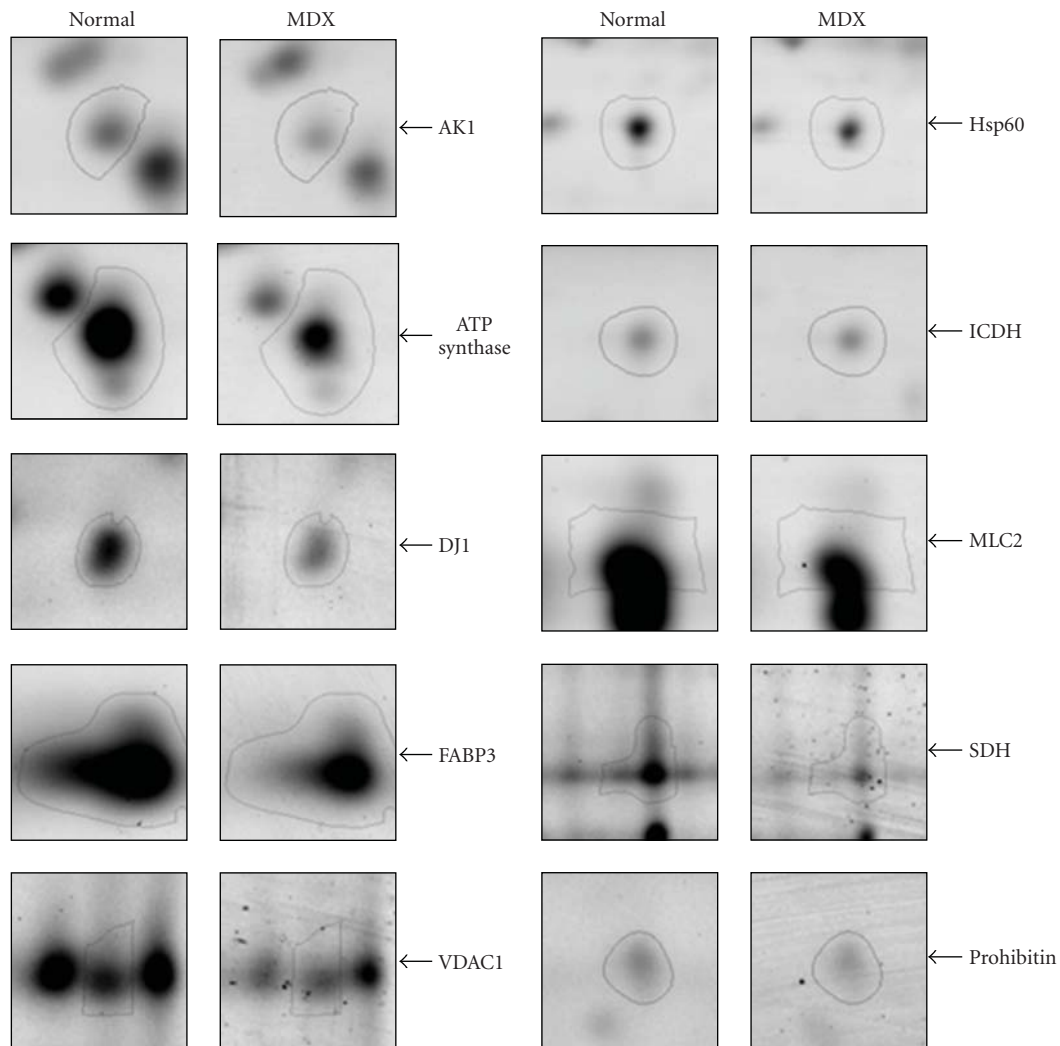


FIGURE 4: Decreased expression of key proteins in the dystrophin-deficient MDX heart. Shown are expanded views of 2-D gels of normal versus dystrophic MDX heart tissue. Shown are the AK1 isoform of adenylate kinase, ATP synthase, DJ1-protein, fatty acid binding protein FABP3, porin isoform VDAC1, stress protein Hsp60, isocitrate dehydrogenase (ICDH), myosin light chain MLC2, succinate dehydrogenase (SDH) and prohibitin. The position of 2-D spots representing distinct mitochondrial proteins is indicated by arrowheads on the right.

dystrophin-deficient organism. Here, we have successfully applied the fluorescent DIGE method to the large-scale analysis of the dystrophic heart. MS-based proteomics clearly revealed a drastic decrease in key metabolic, regulatory and contractile proteins, as well as components of the cytoskeleton and the cellular stress response. The pie chart of Figure 8 summarizes the apparent functions of DIGE-identified proteins with a differential expression in normal versus dystrophin-deficient heart muscle.

The DIGE analysis presented here showed a moderate increase in lamin-A/C, which might improve nuclear stability, chromatin structure and gene expression in the dystrophic heart. Since comparative DAPI staining indicates comparable numbers of nuclei in normal versus dystrophic fibres, tissue scarring is probably not responsible for an increase in the number of nuclei per tissue unit. Therefore, the elevated lamin concentration does not appear to be associated with increased numbers of nuclei. Cardiac lamins

make up the matrix that is located close to the inner nuclear membrane. Interestingly their deficiency causes familial dilated cardiomyopathy [61]. The only drastic increase in a cardiac protein was the 4-fold change in the expression of nucleoside diphosphate kinase B. Nucleoside diphosphate kinases are key regulatory enzymes involved in intracellular di- and tri-phosphonucleoside homeostasis. Their cellular functions are critical for signaling, proliferation, differentiation and bioenergetics [62], which suggests that the up-regulation of one of their isoforms could be considered a counter measure of the dystrophin-deficient heart to stabilize essential cellular functions in severely stressed muscle cells. In contrast to the 4-fold increase in nucleoside diphosphate kinase, our proteomic screening demonstrated a massive decrease in a variety of cardiac proteins in the MDX heart. The dystrophinopathy-associated loss in numerous key proteins, which belong to different cellular pathways and functions in the heart, agrees with the severity of the

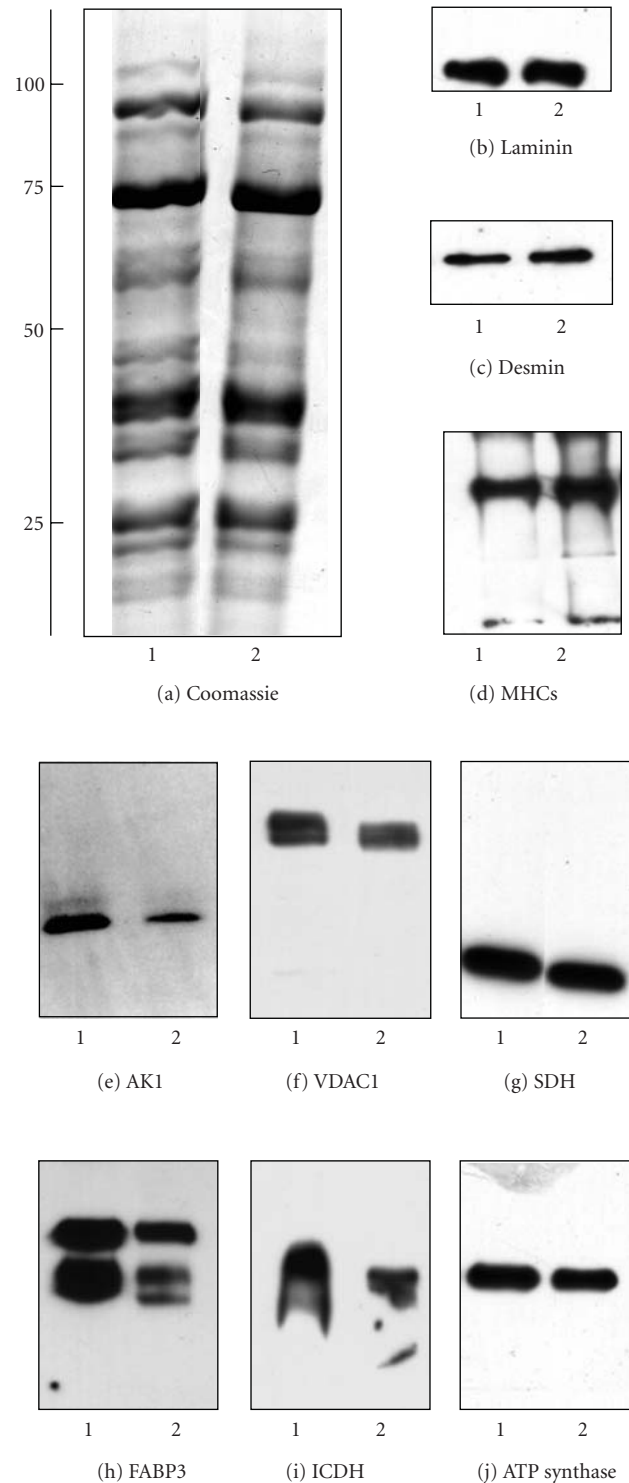


FIGURE 5: Immunoblotting survey of cardiac proteins in dystrophic tissue. Shown is a Coomassie-stained gel (a) and corresponding immunoblots with expanded views of immuno-decorated bands ((b)–(j)). Immunoblotting was performed with antibodies to laminin (b), desmin (c), slow/cardiac myosin heavy chain ((d); MHCs), adenylate kinase isoform AK1 (e), porin isoform VDAC1 (f), succinate dehydrogenase ((g); SDH), fatty acid binding protein FABP3 (h), isocitrate dehydrogenase ((i); ICDH), and ATP synthase (j). See Figure 6 for the statistical evaluation of this immunoblotting survey of cardiac proteins. Molecular mass standards (in kDa) are indicated on the left of panel (a). Lanes 1 and 2 represent normal and dystrophic muscle extracts from control and MDX mice, respectively.

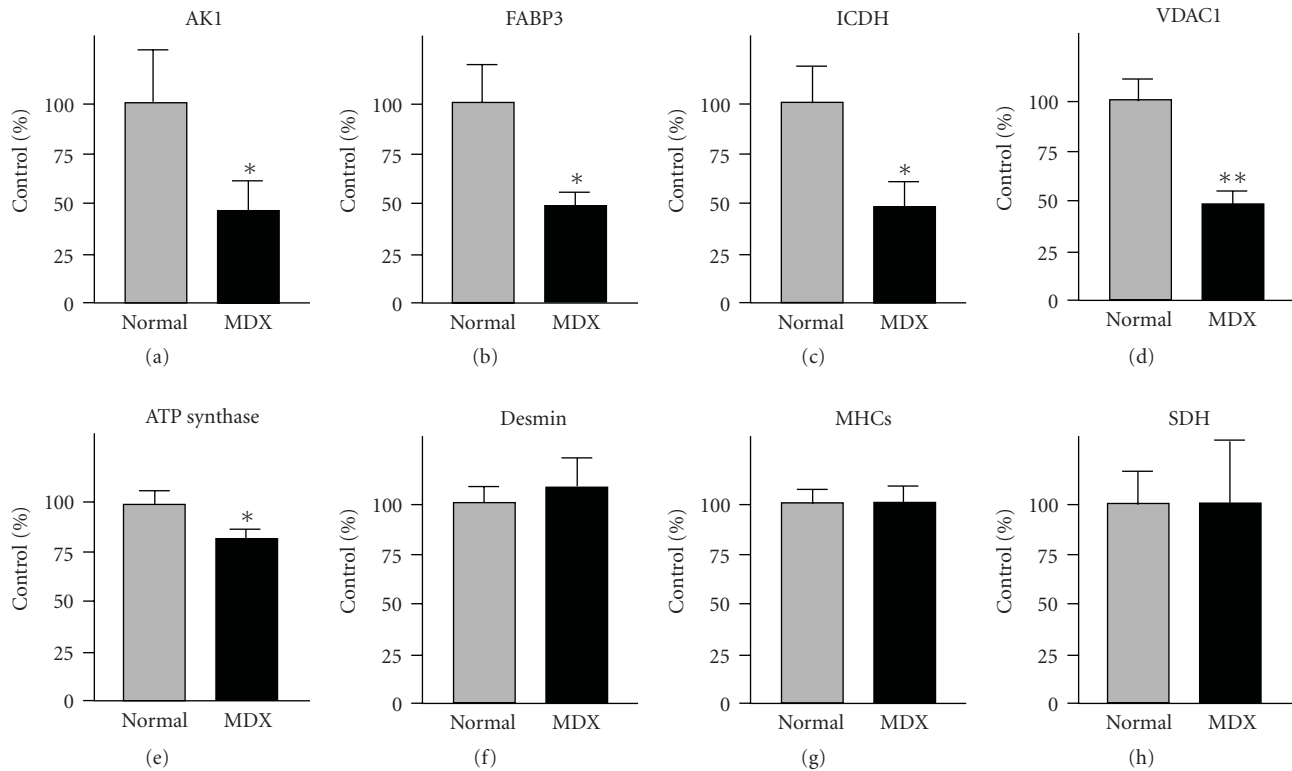


FIGURE 6: Graphical presentation of the immunoblot analysis of cardiac marker proteins in dystrophic tissue. Shown is the graphical presentation of the statistical evaluation of immuno-decoration using antibodies to adenylate kinase isoform AK1 (a), fatty acid binding protein FABP3 (b), isocitrate dehydrogenase ICDH (c), porin isoform VDAC1 (d), ATP synthase (e), desmin (f), slow/cardiac myosin heavy chain MHCs (G) and succinate dehydrogenase SDH (H). The comparative blotting was statistically evaluated using an unpaired Student's *t*-test ($n = 5$; * $P < .05$; ** $P < .01$). The concentration of desmin, myosin heavy chain and succinate dehydrogenase was found not to be significantly different between normal and dystrophic preparations. Lanes 1 and 2 represent normal and dystrophic muscle extracts from control and MDX mice, respectively.

cardiomyopathic complications observed in aged MDX mice and DMD patients [13–15].

Key proteins involved in cardiac contraction, cytoskeletal integrity, nucleotide metabolism, cellular stress response, mitochondrial metabolism, and fatty acid transportation were shown to be affected by a deficiency in cardiac dystrophin. Interestingly, Braun et al. [63] could show an altered integration of mitochondria and ATPases in slow-twitching MDX muscles. The coupling between mitochondrial creatine kinase and the adenine nucleotide translocase system appears to be weakened in dystrophin-deficient fibres. This seems to result in a rearrangement of intracellular energy transfer in dystrophic muscle [63]. The 6-fold decrease in peroxiredoxin-6 may have drastic consequences for the capability of the dystrophic heart to counter-act the detrimental effects of stressors. Peroxiredoxin-6 is a crucial enzyme that protects cells from oxidative stress [64]. In analogy to the reduced concentration of this antioxidant enzyme in cardiac MDX tissue, the decrease in the small heat shock protein Hsp27, as well as Hsp60 and DJ-1 protein, also agrees with an impaired cellular stress response in muscular dystrophy-associated cardiomyopathy. Small heat shock proteins provide crucial chaperone function in striated muscles and are upregulated in the heart following

exercise training [65]. An impaired stress response could result in the detrimental aggregation of misfolded proteins causing cellular dysfunction in the dystrophic heart. The dystrophinopathy-associated decrease in valsoin-containing protein VCP might also impair cardiac function. VCP belongs to the AAA-ATPase superfamily and is involved in various cellular functions such as membrane fusion and cell-cycle control, as well as protein degradation through the ubiquitin-proteasome pathway [66].

The DIGE analysis of the MDX heart presented here has clearly shown a severely altered concentration of numerous key players involved in cardiac contraction and cytoskeletal organization. In contrast to comparable levels of myosin heavy chain, other critical contractile proteins are affected by the lack of dystrophin. The biomolecules that form the thick and thin filaments of the basic contractile units exist in a complex arrangement of myosin heavy chains, myosin light chains, and actins. Muscle myosin consists of a hexameric arrangement that is formed by two heavy chains and two pairs of myosin light chains. Changes in myosin light chains have been implicated in severe cardiac impairments, such as familial hypertrophic cardiomyopathy [67]. Hence, the reduction in the cardiac isoform of myosin light chain MLC2, myosin light chain MLC3, and cardiac

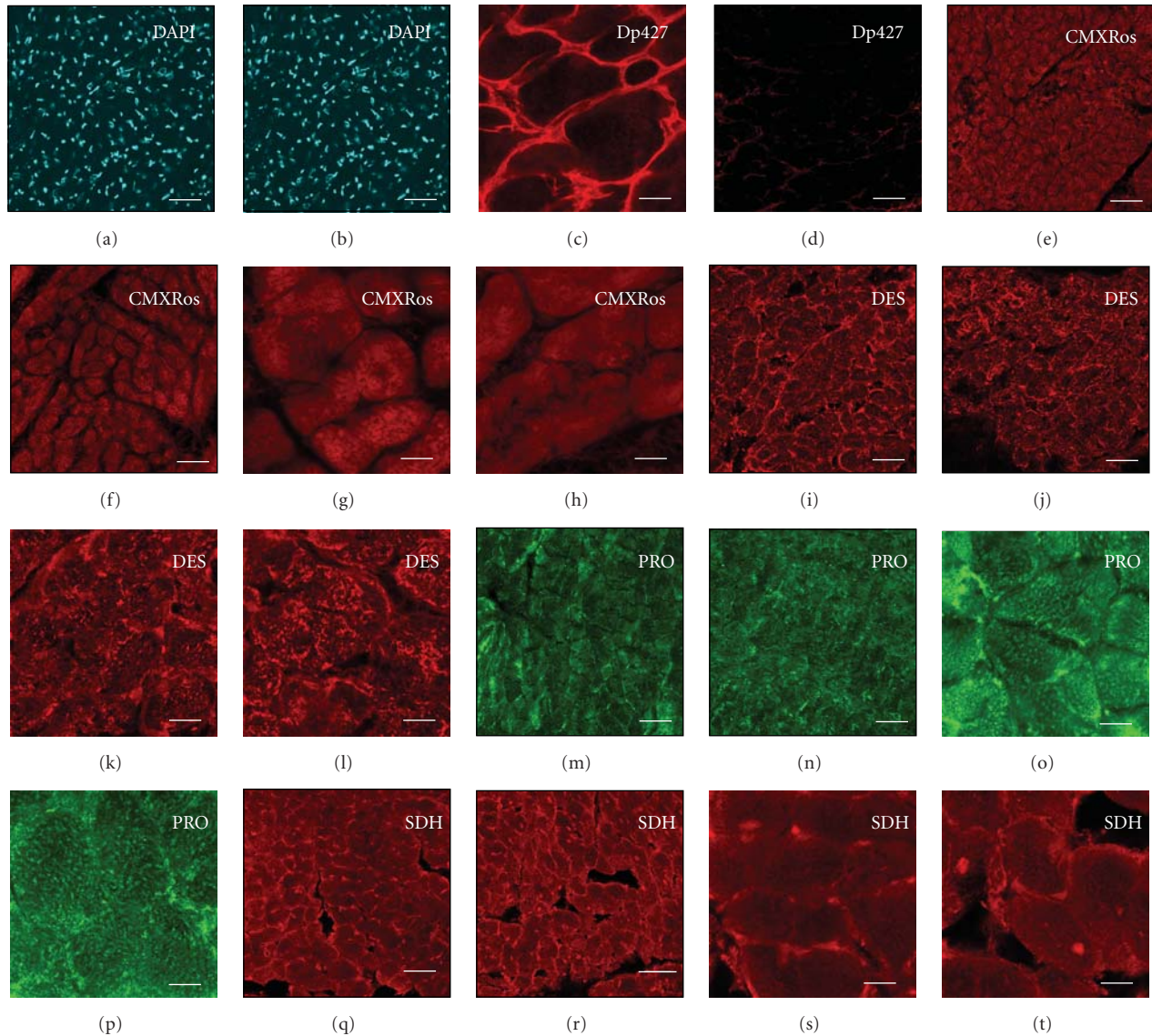


FIGURE 7: Immunofluorescence survey of mitochondrial content, nuclei and cardiac marker proteins in dystrophic tissue. Confocal microscopy was used for the localization of nuclei, mitochondria and cellular markers in normal ((a), (c), (e), (g), (i), (k), (m), (o), (q), (s)) versus dystrophic MDX ((b), (d), (f), (h), (j), (l), (n), (p), (r), (t)) heart cryosections. Shown is labeling of nuclei with the DNA binding dye DAPI ((a), (b)), visualization of mitochondria with the red-fluorescent MitoTracker dye CMXRos ((e)-(h)), and antibody labeling of full-length dystrophin isoform Dp427 ((c), (d)), desmin DES ((i)-(l)), prohibitin PRO ((m)-(p)) and succinate dehydrogenase SDH ((q)-(t)). The number of nuclei and the labeling of mitochondria with the MitoTracker dye CMXRos were found not to be significantly different between normal and dystrophic preparations. The bars in panels (a) to (t) equal $30\ \mu\text{m}$.

alpha-actin might have a severe impact on the contractile apparatus in the dystrophic heart. Contractile weakness observed in dystrophinopathy could be directly related to the altered concentration of myosin light chains and actin. Cardiac muscle cells are activated by Ca^{2+} -binding to TnC-subunit of troponin and is regulated by the interactions of tropomyosin and troponin in the thin filament. Thus, the observed reduction of alpha-1 tropomyosin in the MDX heart might also be of pathophysiological significance. Since the molecular coupling between the myosin head structure and actin filaments, in the presence of ATP, represents

the major step that underlies the sliding of thin filaments past thick filaments, abnormal concentrations of regulatory proteins may result in impaired patterns of sarcomeric shortening.

In addition, a close connection exists between the contractile apparatus, the membrane-associated actin network and the cytoskeleton. Intermediate filaments are of crucial importance for the mechanical integrity and elasticity of contractile fibres. Although proteomics showed that the expression levels of distinct subspecies of desmin were reduced in dystrophic preparations, confocal microscopy

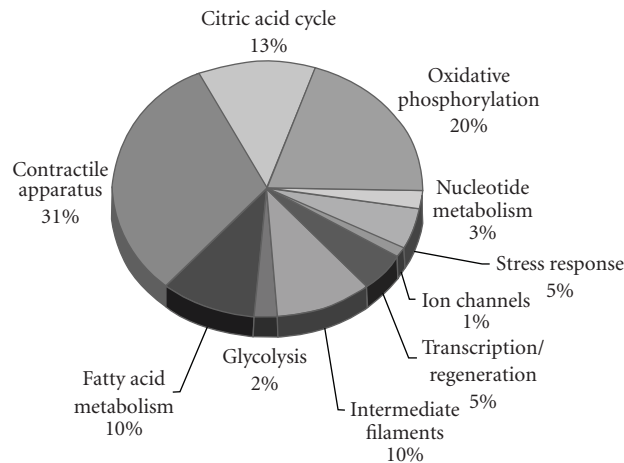


FIGURE 8: Overview of biological functions of DIGE-identified proteins with an altered expression in dystrophic heart muscle. The pie chart summarizes the apparent functions of DIGE-identified proteins with a differential expression in normal versus dystrophin-deficient MDX heart muscle. A large proportion of these affected proteins belong to cardiac mitochondria including metabolic elements of oxidative phosphorylation, the citric acid cycle and fatty acid transportation, as well as proteins associated with the contractile apparatus, the cellular stress response, and the cytoskeletal network.

and immunoblotting revealed that the overall population of desmin isoforms is comparable between normal and MDX heart. However, the deficiency in cardiac dystrophin appears to trigger a concomitant reduction in the density of myozenin-2 and vimentin. Myozenin-2 belongs to the caldesmon family of proteins, a new type of sarcomeric calcineurin-binding protein [68]. Vimentin is a crucial intermediary filament protein and plays a key role in cytoskeletal network formation. The abnormal expression levels of these proteins might therefore cause disturbed interfilament interactions and impaired cytoskeletal arrays, thereby causing cellular instability in the dystrophic heart.

One of the most important findings of this mass spectrometry-based proteomic study is the drastically reduced concentration of numerous mitochondrial proteins and metabolic transporters. Since mitochondria represent the primary site for energy generation via oxidative phosphorylation [69], a reduction in elements belonging to the oxidative phosphorylation complexes, the citric acid cycle and ion homeostasis will have a profound influence on the bioenergetic status of the dystrophic heart. Cardiac mitochondria are involved in intermediary metabolism, cell cycle progression, calcium signaling and the regulation of apoptosis, as well as the production of heme and iron-sulfur clusters. Proteomic investigations suggest that approximately 1,500 different mitochondrial proteins exist [70]. Previous studies have shown that altered expression levels within the mitochondrial proteome influence many aspects of normal development, diseases and the aging process. With respect to the heart, mitochondrial dysfunction appears to be associated with numerous pathologies such as congestive heart failure, ischaemia reperfusion injury and cardiomyopathy [71]. Therefore, the reduced expression of many mitochondrial proteins associated with the matrix, outer membrane and inner membrane system suggests an impaired metabolism in the dystrophic heart. Reduced expression levels within

the mitochondrial proteome appear to affect the functioning of the mitochondrial ATP synthase, isocitrate dehydrogenase, NADH dehydrogenase, oxoglutarate dehydrogenase, isovaleryl-CoA dehydrogenase, cytochrome c oxidase and the cytochrome b-c complex, all critical elements involved in mitochondrial function in the heart [69]. This agrees with a previous study by Zhang et al. [72], who reported a decreased citrate synthase activity in the MDX heart. Although a certain degree of cellular scarring and the infiltration of fatty and connective tissue may reduce the number of contractile fibres in the dystrophic heart, as previously shown by histochemical analysis [72], this does not appear to drastically alter the density of muscle-associated mitochondria. The confocal microscopy analysis shown in this report suggests no major changes in the number of mitochondria between normal and dystrophic heart muscle tissue, as judged by labeling with the established chloromethyl-X-rosamine MitoTracker dye which is concentrated inside mitochondria by their negative membrane potential [53–55].

Our DIGE analysis revealed that individual protein spots representing electron-transferring flavoprotein showed both increased and decreased abundance. Electron transfer flavoprotein ubiquinone oxidoreductase provides a crucial link between electrons derived from fatty acid oxidation and certain amino acids to the main respiratory chain system of mitochondria [73]. The differential effect on different isoforms of this protein is difficult to interpret, but dystrophin deficiency must affect distinct subspecies of this metabolic element with differing post-translational modifications in a dissimilar way. The observed reduction in the rate-limiting enzyme pyruvate dehydrogenase could have severe impact on the utilization of energy carriers and thereby impair the overall bioenergetics of the MDX heart. Isoforms of cardiac prohibitin are present in the inner mitochondrial membrane and are responsible for the efficient assembly of mitochondrial respiratory chain enzymes and perform chaperone

activity. Interestingly, a proteomic survey of mitochondrial proteins in cardiomyocytes from chronic stressed rats has shown a drastic increase in prohibitin [74]. Although the overall complement of prohibitin isoforms is not drastically affected in muscular dystrophy, a reduced expression of distinct subspecies of prohibitin in the dystrophic heart might be associated with an impaired cellular stress response. The only affected glycolytic enzyme appears to be enolase, indicating that mitochondrial metabolism is more severely affected than glycolysis in dystrophy-related cardiomyopathy. Interestingly, the abundance of the extracellular and intracellular fatty acid transporters albumin and FABP-3, which are considered limiting factors of oxidative metabolism in striated muscles, is decreased in the dystrophin-deficient heart. Thus, dystrophic heart cells would be starved of essential fuel supplies, which might trigger a decline in contractile strength. A mitochondrial receptor present in the outer mitochondrial membrane was identified as a porin isoform that forms voltage-dependent anion channels. These ion channels belong to a family of pore-forming proteins that provide large membrane-spanning aqueous channels [75]. The decreased concentration in the porin transport protein would indicate a dystrophy-associated decrease in mitochondrial function and abnormal ion homeostasis.

In contrast to a recent combined metabolomic and proteomic study of the MDX heart [46], and in agreement with two comprehensive proteomic studies on MDX skeletal muscle [42, 45], we could show here a decreased abundance of the AK1 isoform of adenylate kinase. The proteomic finding was clearly verified by immunoblot analysis. Nucleotide metabolism, involving adenylate kinase and creatine kinase appears to be disturbed in the dystrophic MDX heart, and this finding might be useful for the future development of a comprehensive biomarker signature of cardiomyopathy associated with muscular dystrophy. Overall, our DIGE-based screening of the soluble proteome from dystrophic MDX hearts has revealed a severely perturbed protein expression pattern due to deficiency in dystrophin. The observed changes in essential proteins involved in cardiac contraction, mitochondrial metabolism, the cellular stress response and nucleotide metabolism might be useful for the future improvement of differential diagnostic procedures, the assessment of cardiac disease progression in X-linked muscular dystrophies, the identification of novel therapeutic targets to treat cardiomyopathic complications in Duchenne muscular dystrophy, and the evaluation of novel treatment strategies to counter-act the loss in cardiac dystrophin.

Abbreviations

DIGE: Difference in-gel electrophoresis
 DMD: Duchenne muscular dystrophy
 Dp: Dystrophin protein
 MDX: X-linked muscular dystrophy.

Acknowledgments

Research was supported by a project Grant from Muscular Dystrophy Ireland (MDI-125437), a postgraduate stipend

from the Irish Research Council for Science, Engineering and Technology, Fonds der Chemischen Industrie and a Hume scholarship from NUI Maynooth, as well as equipment Grants from the Irish Health Research Board and the Higher Education Authority (HRB-EQ/2003/3, HEA-RERGS-07-NUIM, HRB-EQ/2004/2). The authors thank Dr. Peter Heimann (University of Bielefeld) for his professional help obtaining MDX muscle, Ms. Caroline Batchlor (NUI Maynooth) for assistance with mass spectrometry, and Dr. Ica Dix (NUI Maynooth) for her help with confocal microscopy. The Irish Higher Education Authority and the Deutscher Akademischer Austauschdienst supported laboratory visits of the Maynooth team in Bielefeld.

References

- [1] M. Koenig, E. P. Hoffman, C. J. Bertelson, A. P. Monaco, C. Feener, and L. M. Kunkel, "Complete cloning of the Duchenne muscular dystrophy (DMD) cDNA and preliminary genomic organization of the DMD gene in normal and affected individuals," *Cell*, vol. 50, no. 3, pp. 509–517, 1987.
- [2] E. P. Hoffman, R. H. Brown Jr., and L. M. Kunkel, "Dystrophin: the protein product of the Duchenne muscular dystrophy locus," *Cell*, vol. 51, no. 6, pp. 919–928, 1987.
- [3] E. Bonilla, C. E. Samitt, A. F. Miranda, et al., "Duchenne muscular dystrophy: deficiency of dystrophin at the muscle cell surface," *Cell*, vol. 54, no. 4, pp. 447–452, 1988.
- [4] N. Deconinck and B. Dan, "Pathophysiology of Duchenne muscular dystrophy: current hypotheses," *Pediatric Neurology*, vol. 36, no. 1, pp. 1–7, 2007.
- [5] I. Dalkilic and L. M. Kunkel, "Muscular dystrophies: genes to pathogenesis," *Current Opinion in Genetics and Development*, vol. 13, no. 3, pp. 231–238, 2003.
- [6] K. Ohlendieck, "Towards an understanding of the dystrophin-glycoprotein complex: linkage between the extracellular matrix and the membrane cytoskeleton in muscle fibers," *European Journal of Cell Biology*, vol. 69, no. 1, pp. 1–10, 1996.
- [7] J. M. Ervasti, "Dystrophin, its interactions with other proteins, and implications for muscular dystrophy," *Biochimica et Biophysica Acta*, vol. 1772, no. 2, pp. 108–117, 2007.
- [8] A. H. Ahn and L. M. Kunkel, "The structural and functional diversity of dystrophin," *Nature Genetics*, vol. 3, no. 4, pp. 283–291, 1993.
- [9] R. D. Cohn and K. P. Campbell, "Molecular basis of muscular dystrophies," *Muscle & Nerve*, vol. 23, no. 10, pp. 1456–1471, 2000.
- [10] C. L. Batchelor and S. J. Winder, "Sparks, signals and shock absorbers: how dystrophin loss causes muscular dystrophy," *Trends in Cell Biology*, vol. 16, no. 4, pp. 198–205, 2006.
- [11] J. L. Anderson, S. I. Head, C. Rae, and J. W. Morley, "Brain function in Duchenne muscular dystrophy," *Brain*, vol. 125, no. 1, pp. 4–13, 2002.
- [12] D. M. Connuck, L. A. Sleeper, S. D. Colan, et al., "Characteristics and outcomes of cardiomyopathy in children with Duchenne or Becker muscular dystrophy: a comparative study from the Pediatric Cardiomyopathy Registry," *American Heart Journal*, vol. 155, no. 6, pp. 998–1005, 2008.
- [13] J. Finsterer and C. Stollberger, "The heart in human dystrophinopathies," *Cardiology*, vol. 99, no. 1, pp. 1–19, 2003.
- [14] G. F. Cox and L. M. Kunkel, "Dystrophies and heart disease," *Current Opinion in Cardiology*, vol. 12, no. 3, pp. 329–343, 1997.

- [15] F. Muntoni, "Cardiomyopathy in muscular dystrophies," *Current Opinion in Neurology*, vol. 16, no. 5, pp. 577–583, 2003.
- [16] A. Sultan and M. Fayaz, "Prevalence of cardiomyopathy in Duchenne and Becker's muscular dystrophy," *Journal of Ayub Medical College, Abbottabad*, vol. 20, no. 2, pp. 7–13, 2008.
- [17] E. M. McNally, "New approaches in the therapy of cardiomyopathy in muscular dystrophy," *Annual Review of Medicine*, vol. 58, no. 1, pp. 75–88, 2007.
- [18] D. Duan, "Challenges and opportunities in dystrophin-deficient cardiomyopathy gene therapy," *Human Molecular Genetics*, vol. 15, no. 2, pp. R253–R261, 2006.
- [19] D. W. Townsend, S. Yasuda, and J. Metzger, "Cardiomyopathy of Duchenne muscular dystrophy: pathogenesis and prospect of membrane sealants as a new therapeutic approach," *Expert Review of Cardiovascular Therapy*, vol. 5, no. 1, pp. 99–109, 2007.
- [20] M. D. Grounds, H. G. Radley, G. S. Lynch, K. Nagaraju, and A. De Luca, "Towards developing standard operating procedures for pre-clinical testing in the MDX mouse model of Duchenne muscular dystrophy," *Neurobiology of Disease*, vol. 31, no. 1, pp. 1–19, 2008.
- [21] P. Scinski, Y. Geng, A. S. Ryder-Cook, E. A. Barnard, M. G. Darlison, and P. J. Barnard, "The molecular basis of muscular dystrophy in the MDX mouse: a point mutation," *Science*, vol. 244, no. 4912, pp. 1578–1580, 1989.
- [22] L. R. Bridges, "The association of cardiac muscle necrosis and inflammation with the degenerative and persistent myopathy of MDX mice," *Journal of the Neurological Sciences*, vol. 72, no. 2-3, pp. 147–157, 1986.
- [23] V. Chu, J. M. Otero, O. Lopez, et al., "Electrocardiographic findings in MDX mice: a cardiac phenotype of Duchenne muscular dystrophy," *Muscle and Nerve*, vol. 26, no. 4, pp. 513–519, 2002.
- [24] J. G. Quinlan, H. S. Hahn, B. L. Wong, J. N. Lorenz, A. S. Wenisch, and L. S. Levin, "Evolution of the MDX mouse cardiomyopathy: physiological and morphological findings," *Neuromuscular Disorders*, vol. 14, no. 8-9, pp. 491–496, 2004.
- [25] M. Khairallah, R. Khairallah, M. E. Young, J. R. B. Dyck, B. J. Petrof, and C. Des Rosiers, "Metabolic and signaling alterations in dystrophin-deficient hearts precede overt cardiomyopathy," *Journal of Molecular and Cellular Cardiology*, vol. 43, no. 2, pp. 119–129, 2007.
- [26] Y. Yue, Z. Li, S. Q. Harper, R. L. Davisson, J. S. Chamberlain, and D. Duan, "Microdystrophin gene therapy of cardiomyopathy restores dystrophin-glycoprotein complex and improves sarcolemma integrity in the MDX mouse heart," *Circulation*, vol. 108, no. 13, pp. 1626–1632, 2003.
- [27] M. Wehling-Henricks, M. C. Jordan, K. P. Roos, B. Deng, and J. G. Tidball, "Cardiomyopathy in dystrophin-deficient hearts is prevented by expression of a neuronal nitric oxide synthase transgene in the myocardium," *Human Molecular Genetics*, vol. 14, no. 14, pp. 1921–1933, 2005.
- [28] B. Wu, H. M. Moulton, P. L. Iversen, et al., "Effective rescue of dystrophin improves cardiac function in dystrophin-deficient mice by a modified morpholino oligomer," *Proceedings of the National Academy of Sciences of the United States of America*, vol. 105, no. 39, pp. 14814–14819, 2008.
- [29] G. M. Buyse, G. Van der Mieren, M. Erb, et al., "Long-term blinded placebo-controlled study of SNT-MC17/idebenone in the dystrophin deficient MDX mouse: cardiac protection and improved exercise performance," *European Heart Journal*, vol. 30, no. 1, pp. 116–124, 2009.
- [30] J. L. Sapp, J. Bobet, and S. E. Howlett, "Contractile properties of myocardium are altered in dystrophin-deficient MDX mice," *Journal of the Neurological Sciences*, vol. 142, no. 1-2, pp. 17–24, 1996.
- [31] B. L. Bia, P. J. Cassidy, M. E. Young, et al., "Decreased myocardial nNOS, increased iNOS and abnormal ECGs in mouse models of duchenne muscular dystrophy," *Journal of Molecular and Cellular Cardiology*, vol. 31, no. 10, pp. 1857–1862, 1999.
- [32] J. Lohan, K. Culligan, and K. Ohlendieck, "Deficiency in cardiac dystrophin affects the abundance of the α - β -dystroglycan complex," *Journal of Biomedicine and Biotechnology*, vol. 2005, no. 1, pp. 28–36, 2005.
- [33] J. Lohan and K. Ohlendieck, "Drastic reduction in the luminal Ca^{2+} -binding proteins calsequestrin and sarcoplumemin in dystrophin-deficient cardiac muscle," *Biochimica et Biophysica Acta*, vol. 1689, no. 3, pp. 252–258, 2004.
- [34] M. Fanchaouy, E. Polakova, C. Jung, J. Ogrodnik, N. Shirokova, and E. Niggli, "Pathways of abnormal stress-induced Ca^{2+} influx into dystrophic MDX cardiomyocytes," *Cell Calcium*, vol. 46, no. 2, pp. 114–121, 2009.
- [35] J. P. Lefaucheur, C. Pastoret, and A. Sebillé, "Phenotype of dystrophinopathy in old MDX mice," *Anatomical Record*, vol. 242, no. 1, pp. 70–76, 1995.
- [36] A. Nakamura, K. Yoshida, S. Takeda, N. Dohi, and S.-I. Ikeda, "Progression of dystrophic features and activation of mitogen-activated protein kinases and calcineurin by physical exercise, in hearts of MDX mice," *FEBS Letters*, vol. 520, no. 1–3, pp. 18–24, 2002.
- [37] C. F. Spurney, S. Knobloch, E. E. Pistilli, K. Nagaraju, G. R. Martin, and E. P. Hoffman, "Dystrophin-deficient cardiomyopathy in mouse: expression of Nox4 and Lox are associated with fibrosis and altered functional parameters in the heart," *Neuromuscular Disorders*, vol. 18, no. 5, pp. 371–381, 2008.
- [38] C. L. de Hoog and M. Mann, "Proteomics," *Annual Review of Genomics and Human Genetics*, vol. 5, no. 1, pp. 267–293, 2004.
- [39] S. Viswanathan, M. Unlu, and J. S. Minden, "Two-dimensional difference gel electrophoresis," *Nature Protocols*, vol. 1, no. 3, pp. 1351–1358, 2006.
- [40] R. Marouga, S. David, and E. Hawkins, "The development of the DIGE system: 2D fluorescence difference gel analysis technology," *Analytical and Bioanalytical Chemistry*, vol. 382, no. 3, pp. 669–678, 2005.
- [41] P. Doran, J. Gannon, K. O'Connell, and K. Ohlendieck, "Proteomic profiling of animal models mimicking skeletal muscle disorders," *Proteomics*, vol. 1, no. 9, pp. 1169–1184, 2007.
- [42] Y. Ge, M. P. Molloy, J. S. Chamberlain, and P. C. Andrews, "Proteomic analysis of MDX skeletal muscle: great reduction of adenylate kinase 1 expression and enzymatic activity," *Proteomics*, vol. 3, no. 10, pp. 1895–1903, 2003.
- [43] P. Doran, P. Dowling, J. Lohan, K. McDonnell, S. Poetsch, and K. Ohlendieck, "Subproteomics analysis of Ca^{2+} -binding proteins demonstrates decreased calsequestrin expression in dystrophic mouse skeletal muscle," *European Journal of Biochemistry*, vol. 271, no. 19, pp. 3943–3952, 2004.
- [44] P. Doran, P. Dowling, P. Donoghue, M. Buffini, and K. Ohlendieck, "Reduced expression of regucalcin in young and aged MDX diaphragm indicates abnormal cytosolic calcium handling in dystrophin-deficient muscle," *Biochimica et Biophysica Acta*, vol. 1764, no. 4, pp. 773–785, 2006.
- [45] P. Doran, G. Martin, P. Dowling, H. Jockusch, and K. Ohlendieck, "Proteome analysis of the dystrophin-deficient MDX diaphragm reveals a drastic increase in the heat shock

- protein cvHSP," *Proteomics*, vol. 6, no. 16, pp. 4610–4621, 2006.
- [46] M. K. Gulston, D. V. Rubtsov, H. J. Atherton, et al., "A combined metabolomic and proteomic investigation of the effects of a failure to express dystrophin in the mouse heart," *Journal of Proteome Research*, vol. 7, no. 5, pp. 2069–2077, 2008.
- [47] M. M. Bradford, "A rapid and sensitive method for the quantitation of microgram quantities of protein utilizing the principle of protein dye binding," *Analytical Biochemistry*, vol. 72, no. 1-2, pp. 248–254, 1976.
- [48] N. A. Karp and K. S. Lilley, "Maximising sensitivity for detecting changes in protein expression: experimental design using minimal CyDyes," *Proteomics*, vol. 5, no. 12, pp. 3105–3115, 2005.
- [49] P. Doran, K. O'Connell, J. Gannon, M. Kavanagh, and K. Ohlendieck, "Opposite pathobiochemical fate of pyruvate kinase and adenylate kinase in aged rat skeletal muscle as revealed by proteomic DIGE analysis," *Proteomics*, vol. 8, no. 2, pp. 364–377, 2008.
- [50] T. Rabilloud, J.-M. Strub, S. Luche, A. van Dorsselaer, and J. Lunardi, "A comparison between Sypro Ruby and ruthenium II tris (bathophenanthroline disulfonate) as fluorescent stains for protein detection in gels," *Proteomics*, vol. 1, no. 5, pp. 699–704, 2001.
- [51] A. Shevchenko, H. Tomas, J. Havlis, J. V. Olsen, and M. Mann, "In-gel digestion for mass spectrometric characterization of proteins and proteomes," *Nature Protocols*, vol. 1, no. 6, pp. 2856–2860, 2006.
- [52] J. Gannon, P. Doran, A. Kirwan, and K. Ohlendieck, "Drastic increase of myosin light chain MLC-2 in senescent skeletal muscle indicates fast-to-slow fibre transition in sarcopenia of old age," *European Journal of Cell Biology*, vol. 88, no. 11, pp. 685–700, 2009.
- [53] M. Poot, Y.-Z. Zhang, J. A. Kraemer, et al., "Analysis of mitochondrial morphology and function with novel fixable fluorescent stains," *Journal of Histochemistry and Cytochemistry*, vol. 44, no. 12, pp. 1363–1372, 1996.
- [54] W. Pendergrass, N. Wolf, and M. Pool, "Efficacy of Mito-Tracker Green and CMXrosamine to measure changes in mitochondrial membrane potentials in living cells and tissues," *Cytometry A*, vol. 61, no. 2, pp. 162–169, 2004.
- [55] B. Chazotte, "Labeling mitochondria with fluorescent dyes for imaging," *Cold Spring Harbor Protocols*, vol. 4, no. 6, 2009.
- [56] W. Urfer, M. Grzegorzcyk, and K. Jung, "Statistics for proteomics: a review of tools for analyzing experimental data," *Proteomics*, vol. 6, no. 2, supplement, pp. 48–55, 2006.
- [57] K. Raddatz, D. Albrecht, F. Hochgraefe, M. Hecker, and M. Gotthardt, "A proteome map of murine heart and skeletal muscle," *Proteomics*, vol. 8, no. 9, pp. 1885–1897, 2008.
- [58] J. A. Westbrook, J. X. Wheeler, R. Wait, S. Y. Welson, and M. J. Dunn, "The human heart proteome: two-dimensional maps using narrow-range immobilised pH gradients," *Electrophoresis*, vol. 27, no. 8, pp. 1547–1555, 2006.
- [59] E. McGregor and M. J. Dunn, "Proteomics of the heart: unraveling disease," *Circulation Research*, vol. 98, no. 3, pp. 309–321, 2006.
- [60] P. Doran, S. D. Wilton, S. Fletcher, and K. Ohlendieck, "Proteomic profiling of antisense-induced exon skipping reveals reversal of pathobiochemical abnormalities in dystrophic MDX diaphragm," *Proteomics*, vol. 9, no. 3, pp. 671–685, 2009.
- [61] R. Malhotra and P. K. Mason, "Lamin A/C deficiency as a cause of familial dilated cardiomyopathy," *Current Opinion in Cardiology*, vol. 24, no. 3, pp. 203–208, 2009.
- [62] N. Kimura, N. Shimada, M. Fukuda, et al., "Regulation of cellular functions by nucleoside diphosphate kinases in mammals," *Journal of Bioenergetics and Biomembranes*, vol. 32, no. 3, pp. 309–315, 2000.
- [63] U. Braun, K. Paju, M. Eimre, et al., "Lack of dystrophin is associated with altered integration of the mitochondria and ATPases in slow-twitch muscle cells of MDX mice," *Biochimica et Biophysica Acta*, vol. 1505, no. 2-3, pp. 258–270, 2001.
- [64] N. Nagy, G. Malik, A. B. Fisher, and D. K. Das, "Targeted disruption of peroxiredoxin 6 gene renders the heart vulnerable to ischemia-reperfusion injury," *American Journal of Physiology*, vol. 291, no. 6, pp. H2636–H2640, 2006.
- [65] M. O. Boluyt, J. L. Brevick, D. S. Rogers, M. J. Randall, A. F. Scalia, and Z. B. Li, "Changes in the rat heart proteome induced by exercise training: increased abundance of heat shock protein hsp20," *Proteomics*, vol. 6, no. 10, pp. 3154–3169, 2006.
- [66] E. A. Fisher, L. R. Lapierre, R. D. Junkins, and R. S. McLeod, "The AAA-ATPase p97 facilitates degradation of apolipoprotein B by the ubiquitin-proteasome pathway," *Journal of Lipid Research*, vol. 49, no. 10, pp. 2149–2160, 2008.
- [67] D. Szczesna, "Regulatory light chains of striated muscle myosin. Structure, function and malfunction," *Current Drug Targets—Cardiovascular & Haematological Disorders*, vol. 3, no. 2, pp. 187–197, 2003.
- [68] N. Frey, J. A. Richardson, and E. N. Olson, "Calsarcins, a novel family of sarcomeric calcineurin-binding proteins," *Proceedings of the National Academy of Sciences of the United States of America*, vol. 97, no. 26, pp. 14632–14637, 2000.
- [69] H. Lemieux and C. L. Hoppel, "Mitochondria in the human heart," *Journal of Bioenergetics and Biomembranes*, vol. 41, no. 2, pp. 99–106, 2009.
- [70] A. M. Distler, J. Kerner, and C. L. Hoppel, "Proteomics of mitochondrial inner and outer membranes," *Proteomics*, vol. 8, no. 19, pp. 4066–4082, 2008.
- [71] M. Y. White, A. V. G. Edwards, S. J. Cordwell, and J. E. Van Eyk, "Mitochondria: a mirror into cellular dysfunction in heart disease," *Proteomics*, vol. 2, no. 6, pp. 845–861, 2008.
- [72] W. Zhang, M. ten Hove, J. E. Schneider, et al., "Abnormal cardiac morphology, function and energy metabolism in the dystrophic MDX mouse: an MRI and MRS study," *Journal of Molecular and Cellular Cardiology*, vol. 45, no. 6, pp. 754–760, 2008.
- [73] M. A. Swanson, R. J. Usselman, F. E. Frerman, G. R. Eaton, and S. S. Eaton, "The iron-sulfur cluster of electron transfer flavoprotein-ubiquinone oxidoreductase is the electron acceptor for electron transfer flavoprotein," *Biochemistry*, vol. 47, no. 34, pp. 8894–8901, 2008.
- [74] X. H. Liu, L. J. Qian, J. B. Gong, J. Shen, X. M. Zhang, and X. H. Qian, "Proteomic analysis of mitochondrial proteins in cardiomyocytes from chronic stressed rat," *Proteomics*, vol. 4, no. 10, pp. 3167–3176, 2004.
- [75] V. De Pinto, S. Reina, F. Guarino, and A. Messina, "Structure of the voltage dependent anion channel: state of the art," *Journal of Bioenergetics and Biomembranes*, vol. 40, no. 3, pp. 139–147, 2008.

Research Article

Mechanical and Electrophysiological Properties of the Sarcolemma of Muscle Fibers in Two Murine Models of Muscle Dystrophy: Col6a1^{-/-} and Mdx

M. Canato,¹ M. Dal Maschio,^{1,2} F. Sbrana,^{3,4} R. Raiteri,⁴ C. Reggiani,¹ S. Vassanelli,¹ and A. Megighian¹

¹ Department of Human Anatomy and Physiology, University of Padova, 35131 Padova, Italy

² Department of Neuroscience and Brain Technology, IIT, 16163 Genova, Italy

³ CSDC-Department of Physics, University of Firenze, 50019 Sesto Fiorentino, Italy

⁴ Department of Biophysical and Electronic Engineering, University of Genova, 16145 Genova, Italy

Correspondence should be addressed to C. Reggiani, carlo.reggiani@unipd.it

Received 31 October 2009; Accepted 31 January 2010

Academic Editor: Henk L. M. Granzier

Copyright © 2010 M. Canato et al. This is an open access article distributed under the Creative Commons Attribution License, which permits unrestricted use, distribution, and reproduction in any medium, provided the original work is properly cited.

This study aimed to analyse the sarcolemma of Col6a1^{-/-} fibers in comparison with wild type and mdx fibers, taken as positive control in view of the known structural and functional alterations of their membranes. Structural and mechanical properties were studied in single muscle fibers prepared from FDB muscle using atomic force microscopy (AFM) and conventional electrophysiological techniques to measure ionic conductance and capacitance. While the sarcolemma topography was preserved in both types of dystrophic fibers, membrane elasticity was significantly reduced in Col6a1^{-/-} and increased in mdx fibers. In the membrane of Col6a1^{-/-} fibers ionic conductance was increased likely due to an increased leakage, whereas capacitance was reduced, and the action potential (ap) depolarization rate was reduced. The picture emerging from experiments on fibers in culture was consistent with that obtained on intact freshly dissected muscle. Mdx fibers in culture showed a reduction of both membrane conductance and capacitance. In contrast, in mdx intact FDB muscle resting conductance was increased while resting potential and ap depolarization rate were reduced, likely indicating the presence of a consistent population of severely altered fibers which disappear during the culture preparation.

1. Introduction

Bethlem myopathy and Ulrich congenital dystrophy are inherited diseases which share a common origin in mutations of collagen VI (COL VI) encoding gene leading to a defective extracellular matrix composition [1, 2]. The clinical symptoms are very different as Bethlem myopathy is a relatively mild and slowly progressive disorder characterized by early onset, weakness, and wasting of skeletal muscles, and multiple joint contractures, whereas Ulrich congenital muscle dystrophy (UCMD) is a severe disorder characterized by generalized and progressive muscle wasting and weakness, and by the coexistence of proximal joint contractures and striking distal hyper-extensibility. The link between altered extracellular matrix composition and

muscle fiber degeneration is not yet completely understood and the study of Col6a1^{-/-} mice, is expected to give an important contribution. Col6a1^{-/-} mice [3] carry a null mutation of the $\alpha 1$ chain of COL VI and exhibit a phenotype which is reminiscent of some features present in human Bethlem myopathy and UCMD. In particular, muscles of Col6a1^{-/-} mice share with muscles of humans affected by COL VI mutations the high rate of apoptosis with apoptotic nuclei being 5-6 fold more abundant than in muscles of wild type (wt) mice [3]. A mitochondrial mechanism based on increased opening probability of the permeability transition pore (PTP) within the mitochondrial inner membrane has been proposed and confirmed by the finding that treatment of Col6a1^{-/-} mice with Cyclosporin A, a PTP inhibitor, rescued the mutant dystrophic muscle

fibers [4]. More recently similar results have been obtained also in UCMD patients [5]. In spite of such important advancements, the signalling pathway connecting lack of COL VI and mitochondrial dysfunction remains unknown. Ultrastructural alterations of sarcoplasmic reticulum and mitochondria and abnormal variations in cytosolic calcium in the presence of the mitochondrial inhibitor oligomycin might suggest a possible involvement of calcium [4]. Integrin-mediated effects on mitochondrial function [6] have been considered. A possible role of NG2 which is significantly decreased in patients with COL VI mutation as well as in Col6a1^{-/-} mice, has been also proposed [7].

In view of the uncertainty on the pathogenic mechanisms of the myopathy induced by the lack of COLVI, we sought to investigate the structural and functional properties of the sarcolemma. Actually, the sarcolemma represents the barrier and, at the same time, the link between extracellular matrix and intracellular environment. It is, therefore, possible that the first effects of the lack of a structural component of the ECM, such as COL VI, can be detected at the sarcolemma. ECM molecules are linked to the cell cytoskeleton through large multimeric complexes where proteins like integrins [8] and dystroglycans [9] play a pivotal role. These protein complexes provide the connection with the intracellular cytoskeleton but are also involved in controlling intracellular signalling pathways and in the recruitment and clustering ion channels, thereby regulating the electrophysiological response of the cell membrane [10].

The present study was designed to assess whether biophysical properties of the sarcolemma are altered in muscle fibers of mice lacking COL VI. To this end we combined a structural and mechanical exploration based on Atomic Force Microscopy (AFM) with the analysis of the basic electrophysiological features of skeletal muscle fibers both in freshly dissected muscles and in culture. Wild type and mdx muscle fibers were utilized as controls. Actually, mdx muscle fibers can be considered a positive control as alterations in sarcolemmal electrophysiological and mechanical properties have been reported in previous studies [11, 12].

2. Materials and Methods

2.1. Animals. Experiments were carried out on young adult (1-2 month old) Col6a1^{-/-} mice, mdx mice and the related wild type mice C57 BL/6. Wild type and mdx mice were purchased at Charles River Italia (Calco, Italy). Col6a1^{-/-} mice (kind gift from Professor Paolo Bonaldo, University of Padova) were obtained as previously described using a targeting vector containing a neomycin resistance cassette in the second exon to inactivate the *col6a1* gene in embryonic stem cells [3]. The use of the animals and the experimental protocol was approved by the Department Ethical Committee and the University Ethical Commission (CEASA, Comitato Etico di Ateneo per la Sperimentazione sugli Animali). All efforts were made to minimize animal suffering and to keep low the number of animals necessary to obtain reliable data.

Mice were killed by cervical dislocation and FDB (Flexor Digitorum Brevis) muscles were quickly dissected out and pinned on the sylgard (Sylgard 184, Down Corning, Milano, Italy) coated bottom of a Petri dish. Muscles were continuously perfused with Tyrode solution bubbled with a 95% O₂ 5% CO₂ gas mixture.

2.2. Preparation and Culture of Muscle Fibers. Single muscle fibers were enzymatically isolated from FDB following a protocol derived from that described by Head [13]. After dissection FDB muscles were placed in a Petri dish filled with tyrode solution (mM: NaCl 140, KCl 2, CaCl₂ 2, Hepes 10, and glucose 5) containing 0,2% tipe I collagenase (C0130, Sigma-Aldrich, Milano, Italy) and 10% foetal bovine serum (FBS) for 1 hour at 4°C and then for another hour at 37°C in a water-saturated incubator with 5% CO₂. After three washes in Tyrode containing 10% FBS to block the collagenase effect and stabilize the fibers, the muscles were gently and repeatedly sucked in and out a fire-polished Pasteur pipettes of different diameters (30–300 μm) inside a glass Falcon until muscle fibers were dissociated. Dissociated fibers were plated on coverslips covered with mouse laminin which induced fiber attachment within 1 hour. Coverslips were kept in small Petri dishes filled with Tyrode supplemented with 10% FBS and 1% penicillin-streptomycin-anphotericin. Culture dishes were kept in incubator at 37°C, 5% CO₂.

2.3. Atomic Force Microscopy (AFM). An integrated AFM/inverted optical microscope system (5500ILM AFM, Agilent Technologies equipped with an Olympus IX70 inverted microscope) was used for imaging and elasticity measurements. This allowed to perform simultaneous optical (phase contrast) and AFM imaging on living or fixed (paraphormaldeyde 4% for 20 min) fibers. Fibers were examined 6 days after dissociation. The AFM was equipped with a 100-μm XY scanner. Triangular silicon nitride cantilevers with a spring constant $K = 0.012 \text{ N/m}$ and sharp pyramidal tips (Veeco, Santa Barbara, CA) were employed. The spring constant of each cantilever was determined by the thermal noise method which ensures a level of accuracy of 10%–15% [14].

Topography and elasticity images were acquired by recording force versus distance curves on a regular grid of 64×64 points over an $5 \times 5 \mu\text{m}^2$ area. Each force curve was taken at a rate of 2 Hz, applying a max load of 1 nN corresponding to a max indentation of 100 nm. The time to obtain a full force map was therefore approximately 50 minutes. For each point of the grid (i.e., for each curve) the values of the sample height at 500 pN load and of the elasticity were calculated. To exclude any possible contribution from plastic (i.e., permanent) deformation, only data from the unloading (retracting) part of each curve were considered and converted into a load versus indentation curve. The elasticity value (i.e. Young's modulus) E , was calculated at the indentation of 100 nm using the Oliver's and Pharr model for conical tips: [15]: $E = \pi^{0.5}/2(1-\nu^2)S/A^{0.5}$, where ν is the Poisson's ratio, S the slope or contact stiffness,

and A is the effective projected area of the indenter tip on the sample. We assumed a value for the Poisson's ratio $\nu = 0.5$ and approximated the tip geometry corresponding to a square-based pyramid with a 35° aperture angle, with a conical shape with the same angle of aperture.

The calculation of the average value E over the map of $64 \times 64 = 4096$ curves was performed using a custom analysis software developed in LabView (National Instruments, Austin, Texas): for each force curve in a map, the slope S of the unloading curve at the maximum load is automatically calculated. The histogram of the calculated S values for each single map showed one peak, and it was fitted with a Gaussian curve. 30% of the curves around the fit mean (typically 1000 curves) are then averaged. The averaged curve was used to calculate the E value.

2.4. Electrophysiology. Electrophysiological properties were investigated using intracellular electrodes on single enzymatically-dissociated fibers after 6 days of culture and on intact muscles dissected and pinned on the bottom of a sylgard-coated Petri dish. In both cases, experiments were carried out at room temperature (20° – 22° C). Whole FDB muscles or single dissociated fibers were bathed in normal physiological (Tyrode) saline with the following composition in mM: NaCl 140, KCl 2, CaCl_2 2, HEPES 10, glucose 5, and pH 7.4. In case of whole muscles, solution was continuously bubbled with 95% O_2 .

Fiber action potential was intracellularly recorded using a bridge amplifier (SEC 10L, NPI, Germany) and current-clamp approach. Amplified data were then digitized at 25 kHz with an ADC board (National Instruments PCI6071E or Axon Digidata 1200) and stored in a PC for offline analysis using appropriate software (WinWCP, Strathclyde University; pClamp6, Axon Instruments). After the insertion of the micropipette ($0.5 \mu\text{m}$ tip diameter; filled with 3 M KCl; 10 Mohm resistance), membrane potential was clamped to -100 mV by injecting a negative current.

In order to determine fiber excitability, once membrane potential was set at -100 mV, fibers were stimulated using positive square-wave current pulses (500 ms duration) of increasing intensity until an action potential was elicited. For the first action potential the amplitude in mV, the threshold current, in nA, and the latency of action potential, that is, the delay from the beginning of the current pulse to the onset of an action potential at threshold, in ms, were measured (see [14]). The amplitude and the rates of depolarization and repolarization were then measured in subsequent action potentials.

In order to investigate passive membrane properties, the cell membrane charging process in response to a negative current pulse (200ms duration; 1nA amplitude) from a holding potential of -100 mV, was analysed. A direct measurement of membrane conductance was made from the change in potential at the end of the hyperpolarizing pulse when membrane potential was stable. In a set of experiments anthracene 9-carboxylate (9-AC) (Sigma-Aldrich, Milano, Italy) was added to bath ($100 \mu\text{M}$) to block chloride currents.

Images of the fibers studied in electrophysiological experiments were taken at 20 and $300\times$ magnification and used to measure diameters and length and to calculate surface area, assuming a cylindrical shape.

To identify membrane capacitance and conductance, the membrane potential transients were described in terms of a time-independent component (R_i) which follows the current step within 5 ms and a time dependent component which was analysed in terms of a two parameters model describing the slow charging process of the cell membrane with the equation

$$\begin{aligned} \frac{V_M}{I_{\text{COM}}} &= R_M \cdot \left(1 - \exp\left(-\frac{t}{C_M} \cdot R_M\right) \right) \\ &= R_M \cdot \left(1 - \exp\left(-\frac{t}{\tau_M}\right) \right), \end{aligned} \quad (1)$$

derived from a simple membrane analogue with membrane capacitance C_M in parallel with membrane resistance R_M . From the parameters R_M and τ_M obtained with minimization of the squared mean error, the value for the membrane capacity C_M was calculated and normalized to the apparent cell surface. The time independent component was identified as the leakage branch of the model.

2.5. Statistical Analysis and Curve Fitting. Data were expressed as mean and standard error. Comparisons between Col6a1 $-/-$, mdx, and wild type muscle fibers were done using one way variance analysis followed by Newman-Keuls test. Differences were considered significant at $P < .05$.

The fitting of the membrane potential charging process was performed by a Labview (National Instruments, Austin, Texas) module of Levenberg-Marquardt algorithm of minimization applied to the root mean error calculated from the experimental dataset.

3. Results

3.1. Viability of Col6a1 $-/-$ Fibers in Culture. Single FDB fibers, dissociated and cultured as described in the Materials and Methods, were monitored up to 12 days. From the enzymatic dissociation of each FDB muscle approximately 300–400 fibers were obtained. As can be seen in Figure 1, both Col6a1 $-/-$ mutant and wild-type fibers showed a progressive loss of viability with the time, while the cultures of dystrophin lacking mdx fibers showed an initial drop during the first day. This suggests that all Col6a1 $-/-$ fibers damaged or apoptotic were removed during the preparation and only the fibers in good conditions could survive the collagenase treatment. Apparently, such fibers from Col6a1 $-/-$ mice did not show any significant alteration of viability or shorter survival time in culture conditions, at least within the 12 days time window considered. By contrast, for mdx fibers a severe selection occurred in the first day after dissociation and only a fraction of fibers were sufficiently viable to survive for many days in culture. Experiments were performed at day 6, when cells had recovered from dissociation and were capable to generate action potentials upon stimulation. At day 6, the measurements on enlarged

video images of randomly chosen groups of cells showed only minor and not significant differences in length and in diameter (Figure 1). Staining with Hoechst nuclear dye did not provide evidence of centrally located nuclei, thus suggesting that no regenerating fibers were present in the cultures (not shown).

3.2. Sarcolemma Topography and Elasticity Studied with Atomic Force Microscopy (AFM). Sarcolemma topography images of wt, Col6a1^{-/-} and mdx fibers were obtained with AFM on living fibers and after fixation with *paraformaldehyde*. In *paraformaldehyde*-fixed fibers (Figure 2) a periodic pattern of foldings perpendicular to the fiber long axis was clearly detectable and showed a periodicity of approximately $2\ \mu\text{m}$ ($1.98 \pm 0.08\ \mu\text{m}$ in wt and $1.88 \pm 0.15\ \mu\text{m}$ in Col6a1^{-/-} and $1.78 \pm 0.12\ \mu\text{m}$ mdx fibers resp., not significantly different). As demonstrated in our previous study [15], the periodicity of the major sarcolemmal folds corresponds to the periodicity of the sarcomeres, as determined by phase contrast microscopy, and the major folds correspond to the Z-lines. Interestingly, in all three fiber groups a less evident but consistent folding was detectable between the major folds. Such intermediate periodic feature might correspond to the M-line [15]. The depth of the major foldings range between 50 and 150 nm, without consistent differences between the three groups of fibers. Thus, no clear difference in the general sarcolemmal architecture was detectable with AFM topography.

Nine Col6a1^{-/-} fibers, 14 mdx fibers, and 18 wt fibers were considered for elasticity analysis with AFM (see Figure 3). The fibers were cultured in Petri dishes and examined without fixation, as described in the Methods. For each fiber, two or three topography and elasticity maps were recorded for a total of 18 maps for Col6a1^{-/-}, 21 maps for mdx, and 29 maps for wild type. In the same fibers, sarcomere periodicity was optically measured with phase contrast and average (\pm s.e.) sarcomere length was found to be $1.83 \pm 0.02\ \mu\text{m}$ in Col6a1^{-/-}, 1.78 ± 0.01 in mdx and 1.90 ± 0.01 in wild type fibers, values in good agreement with the results obtained for folding periodicity in fixed fibers. The differences, although very small, were statistically significant ($P < .05$). An example of phase contrast image of a Col6a1^{-/-} fiber cultured for 6 days in contact with the AFM cantilever is shown in Figure 3(g).

Topography and elasticity maps were obtained as described in the Methods. Examples of such maps for three fibers: wild type, Col6a1^{-/-} and mdx, respectively, are shown in Figures 3(a)–3(f). Periodic features are detectable both in the topography maps (Figures 3(a), 3(c), 3(e)), and elasticity maps (Figures 3(b), 3(d), 3(f)), in agreement with our previous observations [15]. The topography and the elasticity map in each row (a and b, c and d, e and f) refer to the same region of a given fiber (wild type a, b; Col6a1^{-/-} c, d; mdx e, f). Interestingly, as can be appreciated by the grey scale where white corresponds either to stiffer (higher elasticity or Young Modulus value) regions or to more elevated regions, the tops of the foldings roughly correspond to the stiffer parts of the sarcolemma. The average elasticity

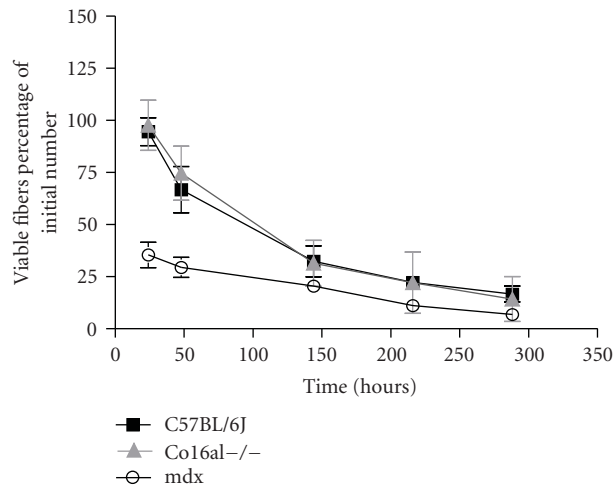
values are shown in the histogram in Figure 3(g) and, as can be seen, the surface of Col6a1^{-/-} fibers was significantly less stiff than the surface of wild type fibers, while the average stiffness of the surface of mdx fibers was significantly greater than that of wild type fibers.

3.3. Resting Potential and Action Potential Measured in FDB Fibers in Culture. Intracellular electrode recordings showed that resting membrane potential was similar in the mutant and wild type fibers (Figure 4(a)). Depolarizing current steps of increasing amplitude were applied until an action potential was elicited. Although some fibers from mutant mice were unexcitable (less than 20%), no significant difference of voltage threshold for action potentials between wild type and dystrophic fibers (with preserved excitability) was observed. The action potential rising rate and amplitude were also measured. Whereas the amplitude was identical in wild type, mdx, and Col6a1^{-/-} fibers, the depolarization rate was significantly lower in Col6a1^{-/-} fibers (Figures 4(b) and 4(c)).

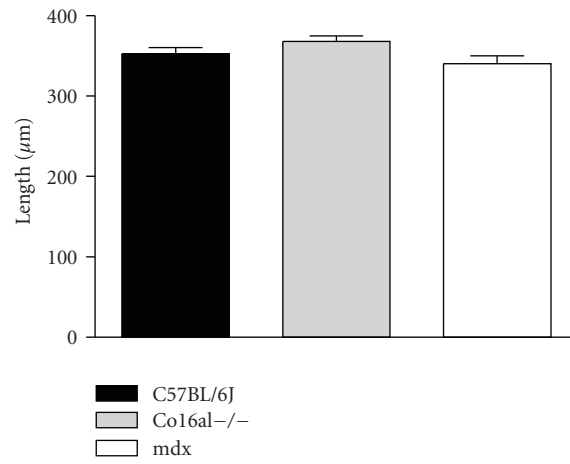
3.4. Membrane Conductance and Capacitance of FDB Fibers in Resting Potential Conditions. The membrane conductance at resting potential was measured by applying to the fibers a hyperpolarizing current step, as described in the Methods. Average conductance normalized to fiber surface was higher in Col6a1^{-/-} than in wild type fibers, while in mdx fibers was lower than in wild type fibers, as shown in Figure 4(d).

Since in mammalian skeletal muscle fibers the main determinant of resting sarcolemma conductance is chloride conductance [16], we repeated the measurement after blocking chloride channels with 9-anthracene carboxylic acid (9-AC) [17] to check whether the difference between wild type and Col6a1^{-/-} could be removed. As shown in Figure 4(e), 9-AC caused a significant reduction of membrane conductance both in wild type and Col6a1^{-/-} fibers. The reduction was, however, greater in wild type fibers (–40%) than in Col6a1^{-/-} fibers (–20%), thus suggesting that the higher conductance found in Col6a1^{-/-} was likely not due to chloride channels.

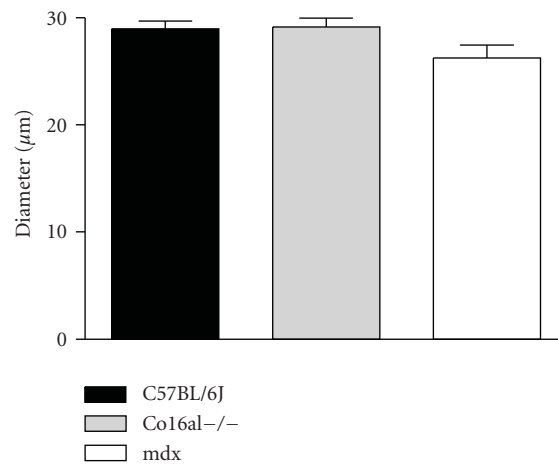
To further investigate the source of the different values of membrane conductance of Col6a1^{-/-} and mdx fibers, shown in Figure 4(d), the kinetics of intracellular voltage changes in response to a hyperpolarizing step was interpolated by (1) corresponding to the model described in the Methods (Figure 5). The parameters calculated by the best fitting provided an estimate of: (i) the resting conductance (R_M), (ii) the capacitance (C_M), and (iii) the instantaneous or time independent conductance (R_i), identified as the membrane leakage. The average values of the three parameters, obtained in wild-type and mutant fibers after 6 days in culture are reported in Figure 5, together with the values of the time constant τ_M of the membrane charging process. As can be seen in Figure 5(c), the time constants were significantly different and the lower value observed in Col6a1^{-/-} fibers was attributed by the model to a lower capacitance of the membrane associated with similar conductance values (Figures 5(e) and 5(f)). By contrast, mdx



(a)



(b)



(c)

FIGURE 1: Survival curve of muscle fibers in culture. Time 0 corresponds to muscle dissection and the fraction of the surviving fibers is expressed in % of the fibers attached on the bottom of the Petri dishes 24 hours after dissection. No difference is detectable in the survival between wild type and *Col6a1*^{-/-} fibers, while the survival of *mdx* fibers is significantly lower.

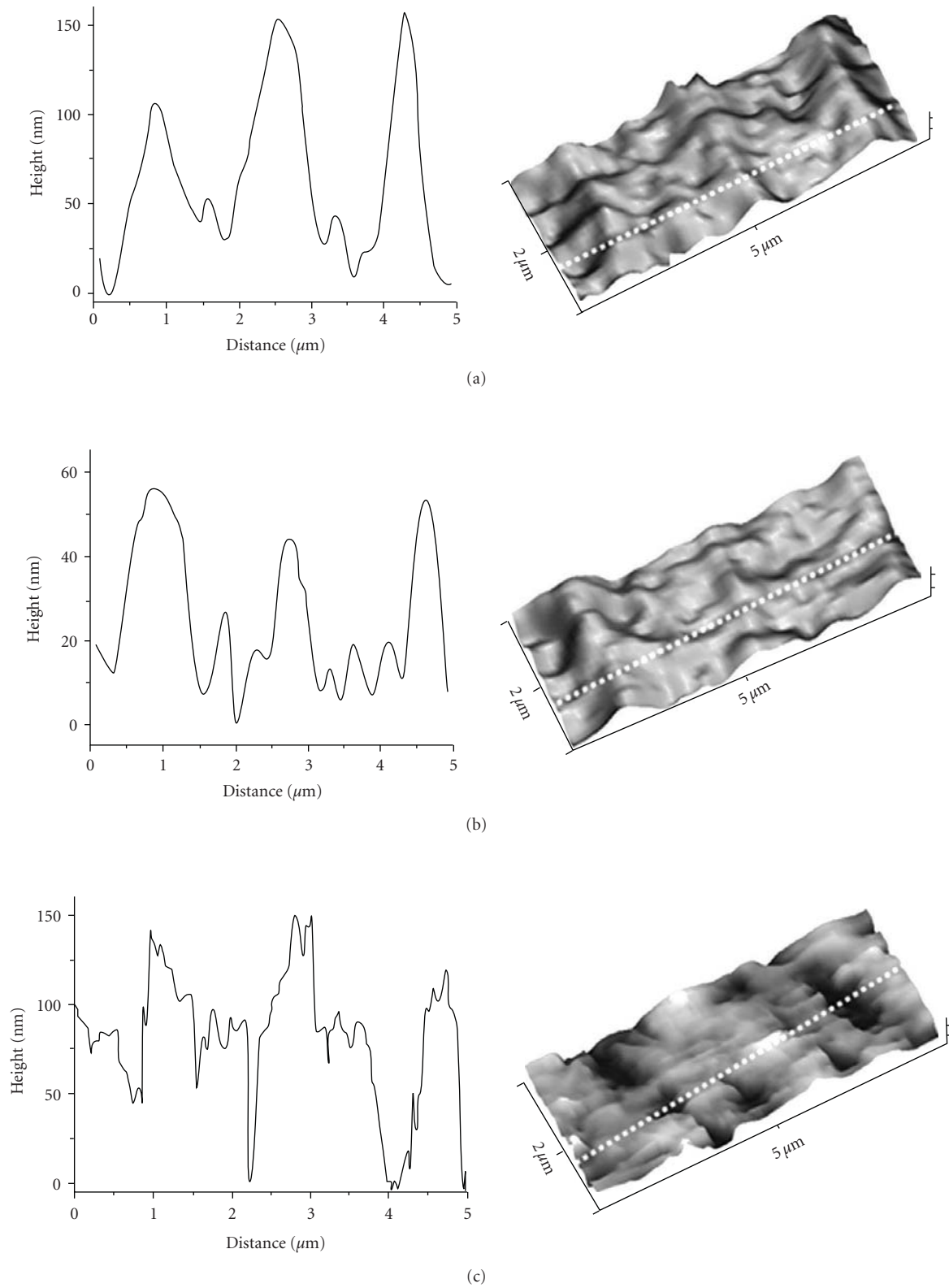


FIGURE 2: AFM topography (contact mode) of fixed fibers: wild type (a), *Col6a1*^{-/-} (b) and *mdx* (c) fibers. Two sets of foldings with a periodic pattern can be easily recognized in all three fiber types. The periodicity of the greater foldings, likely in phase with Z-line is about $2\ \mu\text{m}$, and the distance between the greater and the smaller foldings is about $1\ \mu\text{m}$. The profiles reported in the diagrams on the left are obtained along the dashed lines in the 3D images on the right side.

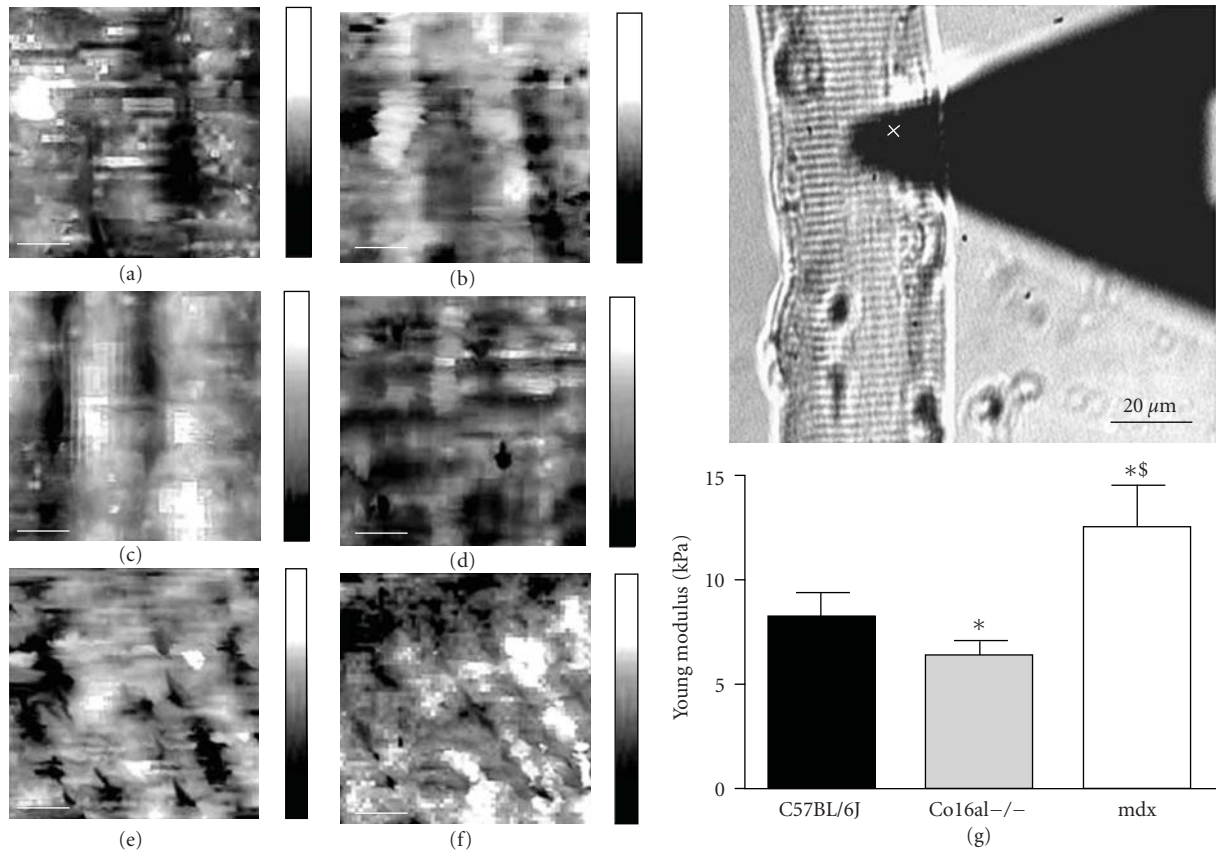


FIGURE 3: Topography (a, c, and e) and elasticity (b, d, and f) images obtained from a force map (64×64 force curves, max applied force = 1 nN) taken on a wild type (a,b), Col6a1^{-/-} (c, d) and mdx (e, f) fibers. The rectangles in the middle indicate in a grey scale (increasing from black to white) the depth with a range of 210 nm in the topography images and the elasticity with a range of 1 kPa in the elasticity images. The white segments in the left lower corner corresponds to $1 \mu\text{m}$. g: Phase contrast image of a Col6a1^{-/-} fiber in culture with the triangular AFM cantilever on top of it. The white cross indicates the position of the tip. The histogram in the right lower corner shows the average values of elasticity modulus Col6a1^{-/-}, mdx, and wild type fibers. *significant difference compared to wild type, \$ significant difference compared to Col6a1^{-/-}.

fibers showed a time constant similar to wild type fibers, but the model analysis indicated that such time constant value was the result of reduced values of both capacitance and conductance (Figures 5(e) and 5(f)). Importantly, the instantaneous, time-independent resistance measured in the first ms after current injection was significantly lower in mutant than in wild type fibers. Thus, according to the model analysis, the higher membrane conductance of Col6a1^{-/-} fibers was due to a higher leakage and was associated with a lower membrane capacitance.

3.5. Resting Potential and Action Potential Measured in Intact FDB Muscle Preparations. In intact muscles the lack of Collagen VI creates a clear difference between mutant and wild type fibers which grow in the absence or, respectively, in the presence of Collagen VI. Such difference is lost in the culture dishes, where both mutant and wild type fibers are maintained in culture for 6 days after dissociation in the same environmental conditions (culture medium, adhesion

substrate). In mdx muscles, a substantial subpopulation of fibers is severely damaged and necrotic and such fibers likely disappear during the dissociation procedure or in the first day in culture. To account for this and characterize the membrane properties of the fibers still embedded in the extracellular matrix, membrane conductance and excitability were measured also in fibers from FDB muscles dissected but kept intact “in vitro”, without enzymatic dissociation. In full agreement with the measurements performed on cultured fibers, the membrane resting resistance was significantly reduced in Col6a1^{-/-} and was also reduced in mdx muscle fibers compared to wild type muscle fibers (see Figure 6(b)), while the membrane resting potential was unaffected in Col6a1^{-/-} and significantly reduced in mdx (Figure 6(a)). Moreover, the action potential amplitude (Figure 6(c)) was not significantly different in Col6a1^{-/-} with respect to wild type, while it was slightly but significantly increased in mdx. The rate of depolarization showed a reduction in both mutant strains compared to wild type fibers (Figure 6(d)).

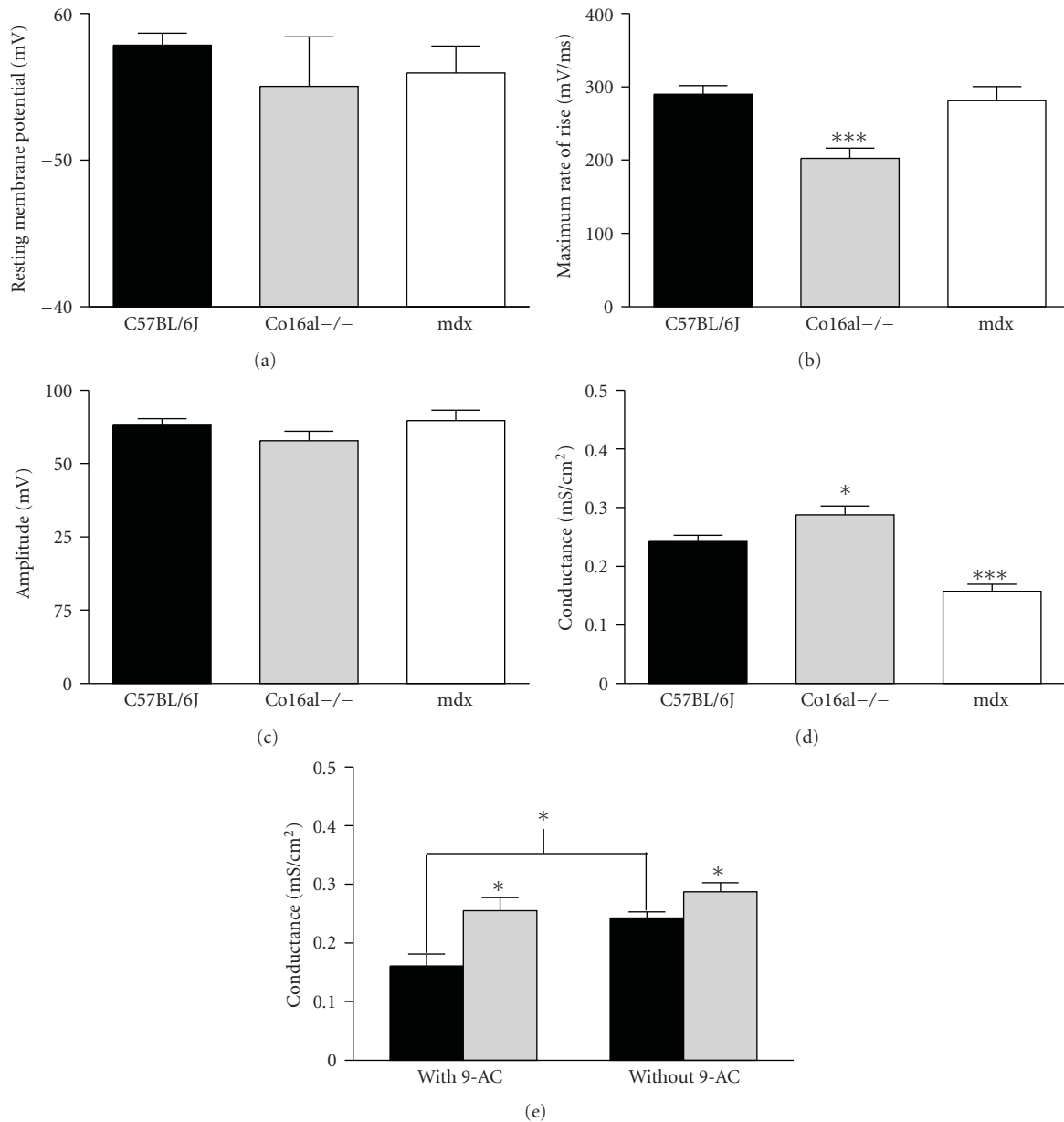


FIGURE 4: Passive and active membrane electrical properties of single muscle fibers kept in culture. Resting membrane potential (a), maximum rate of depolarization (b), action potential amplitude (c), and resting conductance determined with a hyperpolarizing step and normalized to sarcolemma surface of the wild type (black column), Col6a1^{-/-} (grey column), mdx (white column). Mean and standard errors of measurements obtained in 66 wild type, 52 Col6a1^{-/-} and 32 mdx fibers. * $P < .05$ and *** $P < .001$ compared to wild type. (e) shows the determination of membrane conductance in a separate set of wild type (black column) and Col6a1^{-/-} fibers (grey column) in the absence and in the presence of 9-anthracene carboxylic acid (9-AC). *denotes $P < .05$ both in comparison between the two fiber types and in comparison between absence and presence of 9-AC.

4. Discussion

The results obtained in the present study provide the first complete description of the biophysical properties of the sarcolemma of Col6a1^{-/-} muscle fibers in comparison with wild type and mdx muscle fibers. The mutant fibers not only displayed alterations in membrane conductance and capacitance as well as in sarcolemma elasticity when compared to wild type muscle fibers but were also different

from mdx muscle fibers. Importantly, such alterations were demonstrated in fibers in good conditions, able to survive for a long time in culture, and for this reason should not be considered expression of final degenerative processes, but more related to causal mechanisms of the muscle pathology. All experiments were carried out on FDB muscles which allow an easy dissociation of single fibers. FDB muscles are mainly composed of fast fibers [18] and, according to available data [4, 13], are clearly affected by

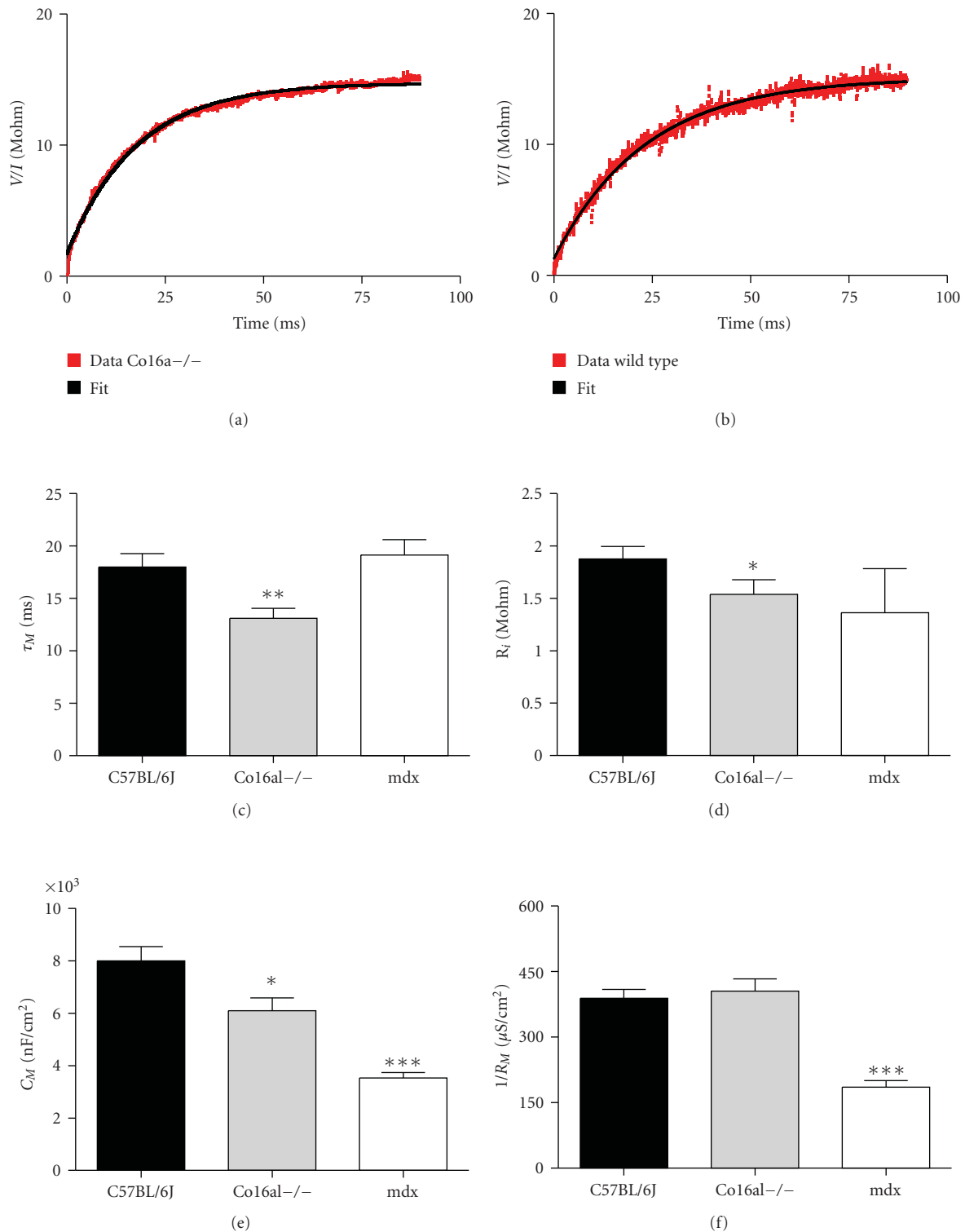


FIGURE 5: Analysis of resistance and capacity of the sarcolemma based on the kinetics of the membrane potential change during a hyperpolarizing step. Panels (a) and (b) show examples of fitting to the curves of membrane charging (expressed as the ratio V/I , membrane potential divided by injected current) with a step of hyperpolarizing current of 1 nA from a holding potential of -100 mV. Only the first 90 ms, corresponding to 5000 data points are shown. Note the initial instantaneous jump in potential. The values of the parameters calculated with the analysis are shown in the histograms (c)–(f) as means and standard errors. R_m and C_m are the resistance and the capacity calculated by the model, their product being equal to the time constant τ . R_i denotes the instantaneous, time-independent resistance. Wild type (black column), *Co16a1*^{-/-} (gray columns), mdx (white columns) are reported in each histogram with * $P < .05$, ** $P < .01$, *** $P < .001$ compared to wild type. The numbers of fibers studied is the same as in Figure 4.

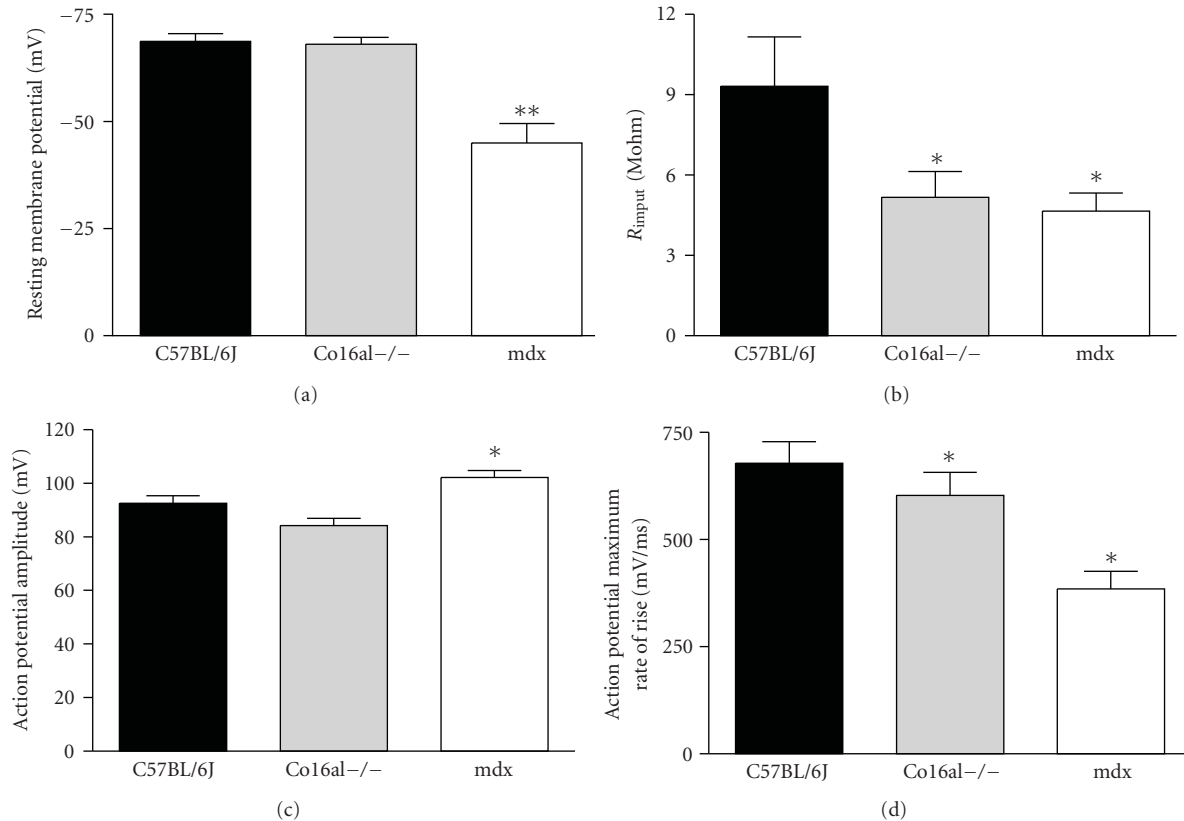


FIGURE 6: Passive and active membrane electrical properties of muscle fibers analysed in intact freshly dissected FDB muscle. Electrophysiological parameters determined in FDB fibers are shown as means with standard errors for wild type (black columns), Col6a1^{-/-} (gray columns) and mdx (white columns) muscles. Histogram (a) shows resting membrane potential (rpm), histogram (b) shows input resistance, histogram (c) shows action potential amplitude, and histogram (d) shows rate of depolarization during action potential. * $P < .05$ and ** $P < .01$ compared to wild type.

the dystrophic process both in mdx and in Col6a1^{-/-} mice.

Our previous studies have shown that the lack of Collagen VI (COL VI) causes a mild dystrophy in mice [3, 4], characterized by an increased rate of apoptosis which leads slowly but progressively to fiber death. Random sampling of fibers from muscles of mice lacking COL VI yield three main populations of fibers: a majority of fibers apparently healthy, many fibers with some structural alterations but still able to contract, and a few fibers positive to Evans Blue Dye (EBD), completely altered in their structure and unable of contractile response [4]. Enzymatic dissociation of FDB produced only fibers apparently healthy, likely because all damaged fibers were destroyed during dissociation. Such apparently healthy fibers, however, when put in culture and challenged with oligomycin, revealed a latent mitochondrial weakness likely causally related to apoptosis triggering mechanism [4]. Cyclosporin A, an inhibitor of the opening of the mitochondrial permeability transition pore, was effective in reducing apoptosis rate in murine and human myopathies due to lack of COLVI and this gives support to the causal role of the mitochondria [4, 5]. Muscle dystrophy in mdx mice shows a very different picture characterized by a high proportion of necrotic EBD positive fibers [19, 20] and a high

proportion of newly formed regenerating fibers. Such fibers likely disappear during the dissociation procedure and the first day in culture, but the surviving fibers still bear clear alterations of the sarcolemma which could be detected in this study. The choice of performing experiments on the sixth day after dissociation was aimed to restrict the comparison to fibers in good conditions. Thus, the alterations observed in the sarcolemma could not be attributed to the final degenerative process, but could be safely considered expression of the initial pathogenetic process. The diversity between the severe selection occurring in the culture of mdx muscle fibers and the greater stability of Col6a1^{-/-} muscle fiber culture suggested to repeat the electrophysiological measurements also in intact freshly dissected FDB muscles, where a complete, unselected fiber population could be sampled.

Compared to wild type, Col6a1^{-/-} muscle fibers displayed an increased resting conductance, detectable in fibers dissociated from FDB and kept in culture for 6 days as well as in fibers imbedded in freshly dissected FDB muscles. The first explanation considered was a change in chloride conductance, since chloride conductance is predominant in resting muscle membrane [16] and variations have been reported in relation to fiber type and pathological conditions [21].

Experiments with 9-Anthracene, a known blocker of chloride channels [17], lead to discard this hypothesis. Moreover, the analysis of the time course of the membrane charging after the step injection of a hyperpolarizing current showed that the difference in membrane conductance was mainly attributable to the initial time-independent component of membrane conductance. Such component was identified with a membrane leakage, possibly related to membrane fragility. Another finding plays in favour of an aspecific ionic leakage which might allow entrance of positive ions. Actually, the rate of rise of action potential was significantly decreased in Col6a1^{-/-} muscle fibers. The rate of depolarization during action potential is determined by the opening of sodium channels and the related inward current. Thus, a likely explanation is that a conserved channel density is accompanied by a reduced sodium concentration gradient which fits very well with the increased membrane leakage. Resting membrane potential however was not changed and this would require an increased potassium current at rest which might also fit with the reduced weight of chloride currents in mutant fibers.

Mdx fibers in culture showed a decreased membrane conductance compared to wild type and Col6a1^{-/-} muscle fibers. The finding was confirmed by the model analysis and is in agreement with previous observations [11] which linked such decrease to a reduced chloride conductance. Interestingly, the electrophysiological analysis of the intact freshly dissected FDB muscle gave an opposite indication, that is, a decreased membrane resistance. The likely explanation is given by the presence of a high number of pathological and deeply altered fibers in the population impaled with the microelectrodes in the intact muscle. The diversity between the features of the mdx fibers in culture compared to those in the intact muscle is also confirmed by the reduction of the resting membrane potential and of the rate of depolarization during action potential, two features present in intact muscle and not present in cultured fibers.

The aspecific leakage observed in Col6a1^{-/-} muscle fibers is suggestive of structural alterations of the sarcolemma. ECM proteins may play the role of organizer of the sarcolemma structure, as recently shown for biglycan [22] and their absence might induce structural alterations. The sarcolemma topography analysed with AFM (Atomic Force Microscopy), with a resolution comparable to the transmission electron microscopy (TEM) [15], did not provide, however, any clue in favour of such structural alterations in general agreement with previous studies with TEM, showing mitochondria and SR swelling but not sarcolemma disorganization [4]. AFM experiments, however, revealed a reduced membrane stiffness (Young modulus reduced by 30%) and the electrical capacitance, which is related to the membrane surface, was also found reduced (by 20%). Both Young modulus and capacitance were “normalized” to sarcolemma surface, calculated from optical microscopy imaging with the resolution of μm . However, the “true” membrane surface should also account for T tubules, caveolae, and foldings. It is thus possible that the “true” sarcolemma surface is changed in a way which is not quantified even with the high resolution achieved by AFM. As far as Young modulus reduction must

be taken into account that the indentation reached 100 nm and, therefore, some subsarcolemmal mitochondria might contribute to the calculated elasticity. Mitochondrial swelling was reported in our previous study [4].

The increased Young modulus in mdx fibers in culture was an unexpected result. Early attempts to determine the stiffness of the sarcolemma in mdx muscle dystrophy were carried out mainly in myotubes with various techniques (aspiration in micropipette [23], osmotic swelling [24], indentation with glass probes [25]) and with uncertain results. Few months ago, the results of measurements of sarcolemma stiffness on adult mdx fibers with AFM were published [12] and showed that stiffness was about 1/3 in mdx compared to wild type fibers. The disagreement between the results obtained in this study and those reported by [12] can find more than one explanation: (i) FDB fibers surviving in culture were examined in this study, while an unselected population of Tibialis anterior fibers was tested by Puttini and coworkers [12], (ii) the indentation amplitude was 500 nm in the experiments of Puttini and coworkers [12], while in this study the amplitude was only 100 nm and only the unloading curve was considered. It is important to recall that there are recent indications of changes in subsarcolemmal viscosity of mdx muscle fibers likely due to actin cytoskeleton reorganization [26] and that the distance between sarcolemma and superficial mitochondria or myofibrils is generally in the order of tenths of μm , and (iii) the sarcomere length of the fibers in culture was low (see below), while it was controlled in the experiments of Puttini and coworkers [12], it is likely that the sarcolemmal stiffness increases with sarcomere length in relation with the reduction of the “membrane reservoir” given by minor foldings and caveolae as suggested by Dulhunty and Franzini-Armstrong [27]. The topography of the sarcolemma as detected by AFM was not substantially altered in mdx as well as Col6a1^{-/-} muscle fibers when compared to wild type. The same folding periodicity could be observed and, if the greater foldings correspond to Z lines and to costameres as demonstrated by our previous study [15], the costamere structure is clearly preserved also in mdx muscle fibers, in spite of the lack of dystrophin. The lower folding likely corresponding to the M line was also detectable in mutant muscle fibers.

Differences in sarcomere length were also observed between mutant and wild type fibers and might represent an indication of subtle structural differences. Dissociated fibers attach to the laminin substrate without any constraint at their slack length, which is set in the first place by myofibrillar proteins such as titin [28–30]. There are, however, no reasons to believe that the shorter sarcomere length observed in Col6a1^{-/-} and mdx fibers is an indication of a difference in myofibrillar proteins. A contribution of the sarcolemma cannot be excluded either in terms of the mechanical alterations (see above Young Modulus) or in connection to a fiber swelling related to the changes in sarcolemma permeability.

In conclusion, the results obtained show that muscle fibers prepared from mice bearing two distinct types of muscle dystrophy, kept in culture and apparently in good

functional and structural conditions, exhibit clear sarcolemmal alterations which are likely related with the molecular defects responsible for the dystrophy. For mdx fibers, the present data allow the description of a set of fibers lacking dystrophin but apparently in good health, not affected by a progressive necrosis process and not regenerating. Such fibers show some previously demonstrated features, such as the reduced membrane conductance, but also reveal other interesting aspects such as the increased stiffness and the reduced membrane capacity. For Col6a1^{-/-} the reduced membrane stiffness and the increased leakage are suggestive of an initial sarcolemmal disorganization which might represent the still missing link between the lack of an important extracellular protein, such COL VI, and the well investigated mitochondrial dysfunction. The control of the opening of the mitochondrial permeability transition pore (PTP) has been the target of the attempts to treat the human muscle disease caused by mutations of COL VI, Bethlem myopathy, and Ulrich congenital dystrophy [4, 5]. The understanding of the pathway connecting COL VI in the extracellular matrix and mitochondria can open a new perspective to develop more effective treatments of the disease. The indications, emerging from the present study, of sarcolemma alterations may represent a step in this direction.

Acknowledgment

The study was supported by Telethon Grant GGP04113.

References

- [1] G. J. Jöbsis, J. M. Boers, P. G. Barth, and M. de Visser, "Bethlem myopathy: a slowly progressive congenital muscular dystrophy with contractures," *Brain*, vol. 122, no. 4, pp. 649–655, 1999.
- [2] O. Camacho Vanegas, E. Bertini, R.-Z. Zhang, et al., "Ullrich scleroatonic muscular dystrophy is caused by recessive mutations in collagen type VI," *Proceedings of the National Academy of Sciences of the United States of America*, vol. 98, no. 13, pp. 7516–7521, 2001.
- [3] P. Bonaldo, P. Braghetta, M. Zanetti, S. Piccolo, D. Volpin, and G. M. Bressan, "Collagen VI deficiency induces early onset myopathy in the mouse: an animal model for Bethlem myopathy," *Human Molecular Genetics*, vol. 7, no. 13, pp. 2135–2140, 1998.
- [4] W. A. Irwin, N. Bergamin, P. Sabatelli, et al., "Mitochondrial dysfunction and apoptosis in myopathic mice with collagen VI deficiency," *Nature Genetics*, vol. 35, no. 4, pp. 367–371, 2003.
- [5] A. Angelin, T. Tiepolo, P. Sabatelli, et al., "Mitochondrial dysfunction in the pathogenesis of Ullrich congenital muscular dystrophy and prospective therapy with cyclosporins," *Proceedings of the National Academy of Sciences of the United States of America*, vol. 104, no. 3, pp. 991–996, 2007.
- [6] E. Werner and Z. Werb, "Integrins engage mitochondrial function for signal transduction by a mechanism dependent on Rho GTPases," *Journal of Cell Biology*, vol. 158, no. 2, pp. 357–368, 2002.
- [7] S. Petrini, A. Tessa, W. B. Stallcup, et al., "Altered expression of the MCSP/NG2 chondroitin sulfate proteoglycan in collagen VI deficiency," *Molecular and Cellular Neuroscience*, vol. 30, no. 3, pp. 408–417, 2005.
- [8] U. Mayer, "Integrins: redundant or important players in skeletal muscle?" *Journal of Biological Chemistry*, vol. 278, no. 17, pp. 14587–14590, 2003.
- [9] R. Barresi and K. P. Campbell, "Dystrglycan: from biosynthesis to pathogenesis of human disease," *Journal of Cell Science*, vol. 119, no. 2, pp. 199–207, 2006.
- [10] S. H. Gee, R. Madhavan, S. R. Levinson, J. H. Caldwell, R. Sealock, and S. C. Froehner, "Interaction of muscle and brain sodium channels with multiple members of the syntrophin family of dystrophin-associated proteins," *Journal of Neuroscience*, vol. 18, no. 1, pp. 128–137, 1998.
- [11] A. De Luca, S. Pierno, and D. Conte Camerino, "Electrical properties of diaphragm and EDL muscles during the life of dystrophic mice," *American Journal of Physiology*, vol. 272, no. 1, pp. C333–C340, 1997.
- [12] S. Puttini, M. Lekka, O. M. Dorchie, et al., "Gene-mediated restoration of normal myofiber elasticity in dystrophic muscles," *Molecular Therapy*, vol. 17, no. 1, pp. 19–25, 2009.
- [13] S. I. Head, "Membrane potential, resting calcium and calcium transients in isolated muscle fibres from normal and dystrophic mice," *Journal of Physiology*, vol. 469, pp. 11–19, 1993.
- [14] S. Pierno, M. P. Didonna, V. Cippone, et al., "Effects of chronic treatment with statins and fenofibrate on rat skeletal muscle: a biochemical, histological and electrophysiological study," *British Journal of Pharmacology*, vol. 149, no. 7, pp. 909–919, 2006.
- [15] E. Defranchi, E. Bonaccorso, M. Tedesco, et al., "Imaging and elasticity measurements of the sarcolemma of fully differentiated skeletal muscle fibres," *Microscopy Research and Technique*, vol. 67, no. 1, pp. 27–35, 2005.
- [16] T. J. Jentsch, V. Stein, F. Weinreich, and A. A. Zdebik, "Molecular structure and physiological function of chloride channels," *Physiological Reviews*, vol. 82, no. 2, pp. 503–568, 2002.
- [17] P. T. Palade and R. L. Barchi, "Characterization of the chloride conductance in muscle fibers of the rat diaphragm," *The Journal of General Physiology*, vol. 69, pp. 325–342, 1977.
- [18] E. González, M. L. Messi, Z. Zheng, and O. Delbono, "Insulin-like growth factor-1 prevents age-related decrease in specific force and intracellular Ca²⁺ in single intact muscle fibres from transgenic mice," *Journal of Physiology*, vol. 552, no. 3, pp. 833–844, 2003.
- [19] P. Moens, P. H. W. W. Baatsen, and G. Maréchal, "Increased susceptibility of EDL muscles from mdx mice to damage induced by contractions with stretch," *Journal of Muscle Research and Cell Motility*, vol. 14, no. 4, pp. 446–451, 1993.
- [20] B. J. Petrof, J. B. Shrager, H. H. Stedman, A. M. Kelly, and H. L. Sweeney, "Dystrophin protects the sarcolemma from stresses developed during muscle contraction," *Proceedings of the National Academy of Sciences of the United States of America*, vol. 90, no. 8, pp. 3710–3714, 1993.
- [21] S. Pierno, J.-F. Desaphy, A. Liantonio, et al., "Change of chloride ion channel conductance is an early event of slow-to-fast fibre type transition during unloading-induced muscle disuse," *Brain*, vol. 125, no. 7, pp. 1510–1521, 2002.
- [22] M. L. Mercado, A. R. Amenta, H. Hagiwara, et al., "Biglycan regulates the expression and sarcolemmal localization of dystrobrevin, syntrophin, and nNOS," *The FASEB Journal*, vol. 20, no. 10, pp. 1724–1726, 2006.
- [23] O. F. Hutter, F. L. Burton, and D. L. Bovell, "Mechanical properties of normal and mdx mouse sarcolemma: bearing on function of dystrophin," *Journal of Muscle Research and Cell Motility*, vol. 12, no. 6, pp. 585–589, 1991.

- [24] A. Menke and H. Jockusch, "Decreased osmotic stability of dystrophin-less muscle cells from the mdx mouse," *Nature*, vol. 349, no. 6304, pp. 69–71, 1991.
- [25] C. Pasternak, S. Wong, and E. L. Elson, "Mechanical function of dystrophin in muscle cells," *Journal of Cell Biology*, vol. 128, no. 3, pp. 355–361, 1995.
- [26] T. M. Suchyna and F. Sachs, "Mechanosensitive channel properties and membrane mechanics in mouse dystrophic myotubes," *Journal of Physiology*, vol. 581, no. 1, pp. 369–387, 2007.
- [27] A. F. Dulhunty and C. Franzini-Armstrong, "The passive electrical properties of frog skeletal muscle fibres at different sarcomere lengths," *Journal of Physiology*, vol. 266, no. 3, pp. 687–711, 1977.
- [28] K. Wang, R. McCarter, J. Wright, J. Beverly, and R. Ramirez-Mitchell, "Regulation of skeletal muscle stiffness and elasticity by titin isoforms: a test of the segmental extension model of resting tension," *Proceedings of the National Academy of Sciences of the United States of America*, vol. 88, no. 16, pp. 7101–7105, 1991.
- [29] S. Labeit and B. Kolmerer, "Titins: giant proteins in charge of muscle ultrastructure and elasticity," *Science*, vol. 270, no. 5234, pp. 293–296, 1995.
- [30] N. Preetha, W. Yiming, M. Helmes, F. Norio, L. Siegfried, and H. Granzier, "Restoring force development by titin/connectin and assessment of Ig domain unfolding," *Journal of Muscle Research and Cell Motility*, vol. 26, no. 6–8, pp. 307–317, 2005.

Review Article

There Goes the Neighborhood: Pathological Alterations in T-Tubule Morphology and Consequences for Cardiomyocyte Ca^{2+} Handling

William E. Louch,^{1,2} Ole M. Sejersted,^{1,2} and Fredrik Swift^{1,2}

¹ Institute for Experimental Medical Research, Oslo University Hospital Ullevaal, 0407 Oslo, Norway

² Centre for Heart Failure Research, Faculty of Medicine, University of Oslo, 0316 Oslo, Norway

Correspondence should be addressed to William E. Louch, w.e.louch@medisin.uio.no

Received 17 November 2009; Accepted 15 January 2010

Academic Editor: Aikaterini Kontrogianni-Konstantopoulos

Copyright © 2010 William E. Louch et al. This is an open access article distributed under the Creative Commons Attribution License, which permits unrestricted use, distribution, and reproduction in any medium, provided the original work is properly cited.

T-tubules are invaginations of the cardiomyocyte membrane into the cell interior which form a tortuous network. T-tubules provide proximity between the electrically excitable cell membrane and the sarcoplasmic reticulum, the main intracellular Ca^{2+} store. Tight coupling between the rapidly spreading action potential and Ca^{2+} release units in the SR membrane ensures synchronous Ca^{2+} release throughout the cardiomyocyte. This is a requirement for rapid and powerful contraction. In recent years, it has become clear that T-tubule structure and composition are altered in several pathological states which may importantly contribute to contractile defects in these conditions. In this review, we describe the “neighborhood” of proteins in the dyadic cleft which locally controls cardiomyocyte Ca^{2+} homeostasis and how alterations in T-tubule structure and composition may alter this neighborhood during heart failure, atrial fibrillation, and diabetic cardiomyopathy. Based on this evidence, we propose that T-tubules have the potential to serve as novel therapeutic targets.

1. Structure and Role of T-Tubules

1.1. Morphology. The plasma membrane of ventricular cardiomyocytes is comprised of both the surface sarcolemma and a branching network of T-tubules which project into the cell interior. These invaginations were so named since they were initially observed as *transverse* elements, which occur near the Z lines at regular intervals along the cell [1]. However, detailed imaging has shown that the T-tubule network is actually quite complex, and contains numerous longitudinal components which run from one Z line to the next [2, 3]. While T-tubule diameter varies between 20 and 450 nm throughout the cardiomyocyte, more than 50% of tubules have a diameter between 180 and 280 nm [3]. Their total volume has been estimated to be 0.8–3.6% of the cardiomyocytes volume [4, 5]. Estimates of the fraction of the total sarcolemma in the T-tubules (versus surface membrane) range from 21–64% [4], although in a recent review employing computer modeling, it was suggested that

the true fraction is close to 50% [6]. The large variability in these estimates likely reflects the different methodologies used for calculation and differences between species, but might also be due to the considerable plasticity of the T-tubules. Indeed, T-tubules are absent in the neonatal heart [7, 8] and develop progressively after birth [9, 10]. Also, as we will discuss in this review, there is an important remodeling of the T-tubules during pathological conditions.

1.2. The Dyadic “Neighborhood”. During the cardiac action potential, contraction is triggered in myocytes by a process known as excitation-contraction (EC) coupling [4]. During this process, electrical excitation of the cell membrane triggers a transient rise in intracellular Ca^{2+} concentration ($[\text{Ca}^{2+}]$), which results in myocyte contraction as Ca^{2+} binds to the myofilaments. T-tubules play a pivotal role in EC coupling by allowing the action potential to propagate into the cell interior, and by providing proximity between the

excitable cell membrane and the sarcoplasmic reticulum (SR), the main intracellular Ca^{2+} store. The SR membrane is apposed to the T-tubule membrane in highly specialized junctional microdomains (Figure 1). Here L-type Ca^{2+} channels face SR Ca^{2+} release channels, known as ryanodine receptors (RyRs), with a stoichiometry of 4–10 RyRs per L-type Ca^{2+} channel [11]. The two adjacent membranes are separated by a gap of 10–15 nm called the dyadic cleft. Clusters of RyRs and L-type Ca^{2+} channels and the dyadic cleft which separates them together constitute a functional unit called a couplon, or dyad [12] (Figure 1). The number of RyRs in a single dyad is still a matter of debate; analysis from electron micrographs reports numbers from 30 to 270, depending on species [13]. A recent study using a combination of confocal imaging and image processing suggested that the true number is in the upper range (120 to 260 RyRs) in rat [14]. However, a new electron microscopy tomography study in mouse demonstrated that there is a large variability in the size of the dyad [5]. The authors also showed that most dyads are significantly smaller than previously estimated; more than one-third of dyads are equal or smaller than the size necessary to hold ~ 15 RyRs, and the average dyad holds only 7.7 RyR tetramers.

When one or several L-type Ca^{2+} channels are open, Ca^{2+} release is triggered from RyRs in that couplon by an amplification system known as Ca^{2+} -induced Ca^{2+} release (CICR) [15]. This can be observed as evoked Ca^{2+} sparks in unstimulated myocytes [16, 17], although Ca^{2+} sparks can also result from spontaneous RyR openings in the absence of L-type Ca^{2+} current [18]. When an action potential travels through the cardiomyocyte, thousands of individual Ca^{2+} sparks are triggered, and their spatiotemporal summation constitutes the Ca^{2+} transient [4]. The extent of CICR and magnitude of the Ca^{2+} transient are critically dependent on the SR Ca^{2+} content [19], which in turn is determined by the balance between SR refilling and release. However, efficient coupling between Ca^{2+} influx and SR Ca^{2+} release also requires the precise positioning of Ca^{2+} channels, RyRs, and other proteins within the dyadic “neighborhood”, as will be discussed below.

Following release, Ca^{2+} is recycled into the SR by the SR/ER Ca^{2+} ATPase (SERCA) and extruded from the cell by the $\text{Na}^+/\text{Ca}^{2+}$ -exchanger (NCX) and the plasma membrane Ca^{2+} ATPase (PMCA). The PMCA is believed to be a quite minor contributor to overall Ca^{2+} removal due to its relatively slow kinetics [20]. In addition, it has not been demonstrated that the PMCA is present in the T-tubules, which is a requirement for an efficient Ca^{2+} extrusion pathway. On the other hand, NCX plays an important role in Ca^{2+} extrusion. It is localized both in the surface membrane and in the T-tubular membrane, but with a three times higher density in the T-tubules [21] (Figure 1). The contribution of NCX to total Ca^{2+} removal from the cytosol varies across species from $\sim 30\%$ in the rabbit to $\sim 7\%$ in the rat [22, 23]. The NCX is electrogenic since it exchanges 3 Na^+ for 1 Ca^{2+} , which means that its transport rate is dependent on both the membrane potential and transmembrane concentration gradients for Na^+ and Ca^{2+} . Since ionic concentrations may vary considerably in

different submembrane spaces or ion pockets, NCX activity will very much depend on its localization as well as the localization of other nearby Na^+ and Ca^{2+} handling proteins. For example, we have observed that the Na^+/K^+ -ATPase α_2 isoform is preferentially localized in the T-tubules where it regulates an Na^+ pool which is shared by NCX [24]. Data from several other studies also support a close relationship between Na^+/K^+ -ATPase and NCX function [25–28]. Since NCX and SERCA compete for Ca^{2+} , this local control of Na^+ homeostasis can importantly regulate SR Ca^{2+} load and the magnitude of the Ca^{2+} transient [29]. Thus, alterations in T-tubule structure or more subtle alterations in the dyadic neighborhood would be expected to have important functional consequences.

Although the NCX functions predominantly to extrude Ca^{2+} from the cell (forward mode), it can also function in reverse mode to facilitate Ca^{2+} entry. We have recently shown that NCX-mediated Ca^{2+} influx contributes to an early phase of Ca^{2+} entry which actually precedes that from Ca^{2+} channels [30]. Ca^{2+} influx via reverse-mode NCX can even trigger SR Ca^{2+} release, albeit with low efficiency [31]. We have calculated that such a role requires the presence of an Na^+ channel in the dyad to locally elevate intracellular $[\text{Na}^+]$ [30] (Figure 1). However, the localization of both NCX and the Na^+ channel in the dyad has been disputed [32]. Further study of the localization of these proteins is therefore required, both in normal cardiomyocytes and in disease states where the efficiency of NCX-mediated CICR may be altered.

1.3. T-tubule Density/Organization: Control of Ca^{2+} Release Synchrony. The vast majority of studies of T-tubular structure and function have been conducted on ventricular myocytes. Interestingly, other cardiac cell types are often stated to lack T-tubules. In reality, however, T-tubules have been observed in Purkinje cells [33] and their presence has been clearly documented in atrial myocytes from a number of species [34–42], albeit at a lower density than that observed in ventricular cells. To our knowledge, T-tubules have not yet been examined in human atrial cells, but are very likely to be present since large mammals such as sheep ([40, 41] see Figure 2(b), left panel) and dog [42] exhibit a surprisingly high T-tubule density.

The extent and organization of the T-tubule network is an important determinant of the spatial homogeneity of SR Ca^{2+} release throughout the cardiomyocyte. A dense, well-organized T-tubule network, such as that observed in mouse and rat ventricle myocytes, (Figures 2(c) and 2(d), left panels) allows for very synchronized CICR in these cells (Figure 3(a)) [43, 44, 47]. Heinzel et al. [48] demonstrated that a somewhat lower T-tubule density in pig ventricular myocytes was associated with less synchronous Ca^{2+} release (Figure 3(a)). In cat atrial cells, which have a very low T-tubule density, there is a wave-like propagation of the Ca^{2+} transient from the sarcolemma to the cell interior [49] (Figure 3(a)). Thus, in all of these cell types, Ca^{2+} release is initially triggered following influx of Ca^{2+} at the surface sarcolemma and at locations where T-tubules (and Ca^{2+}

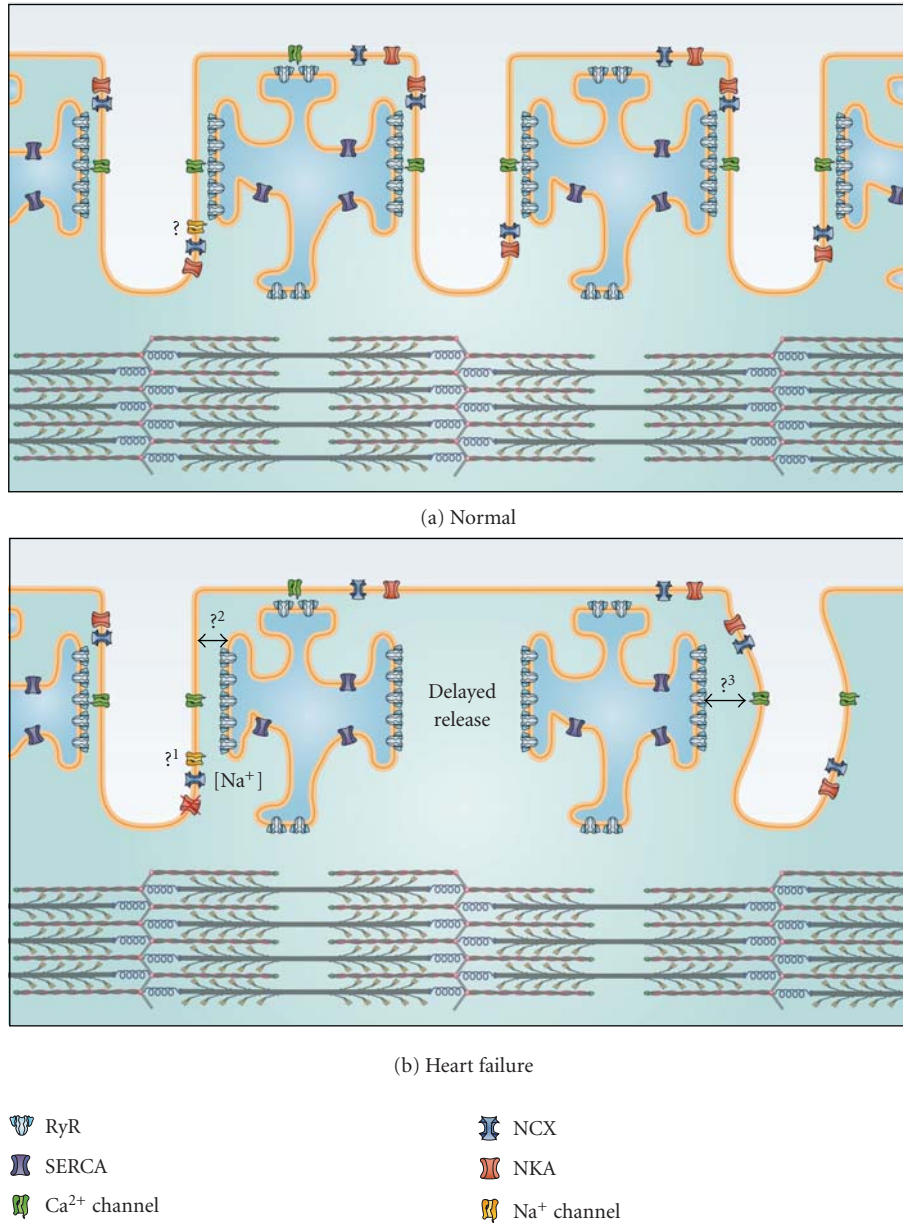
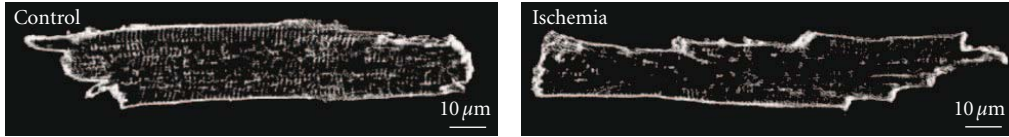


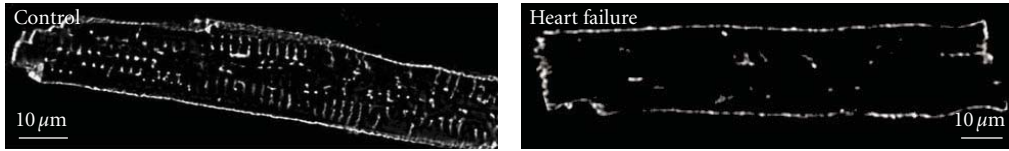
FIGURE 1: Schematic representation of the dyadic neighborhood in normal and failing cells. (a) Excitation-contraction coupling occurs at functional junctions between Ca²⁺ channels in the T-tubules and ryanodine receptors in the SR. Depending on their localization, other proteins in the dyadic neighborhood such as SR Ca²⁺ ATPase (SERCA), NCX, NKA, and Na⁺ channels can also regulate Ca²⁺ homeostasis. Question mark: The positioning of the Na⁺ channel at the dyad is still controversial. (b) During heart failure, T-tubule loss and/or disorganization occurs leading to the formation of orphaned ryanodine receptors, which do not have apposing Ca²⁺ channels. Ca²⁺ release in these regions is delayed leading to slower and weaker contractions. Other putative alterations in the dyadic neighborhood are indicated by the question marks: (1) it is unclear whether the Na⁺ channel is present in the dyad of failing cardiomyocytes. Some experimental evidence suggests that the distance between the SR and T-tubule is increased in heart failure (2), while T-tubule disorganization may lead to dyadic clefts with variable width (3).

channels) are present, followed by propagation of released Ca²⁺ into regions where T-tubules are absent. Since there is a uniform distribution of RyRs across myocytes [47, 48, 50], this diffusing Ca²⁺ may then trigger SR Ca²⁺ release. Meethal et al. [51] observed spontaneous Ca²⁺ sparks at sites of

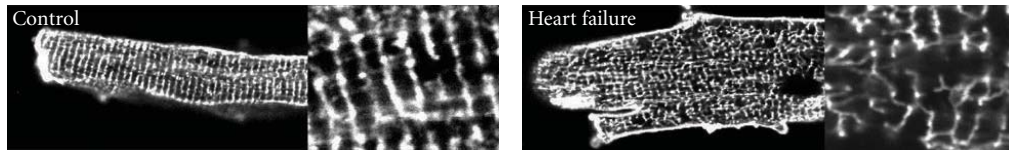
irregular gaps occurring between adjacent T-tubules in dog cardiomyocytes. This shows the presence of functional RyRs and suggests that a propagating Ca²⁺ wave could trigger CICR at these locations. In atrial myocytes, the extent of CICR propagation into the interior of the cell has been



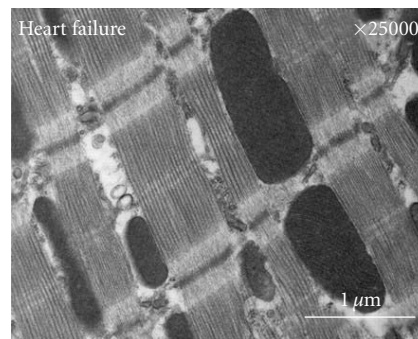
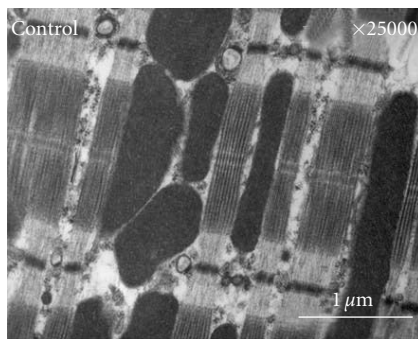
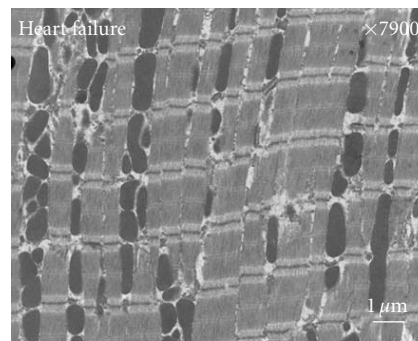
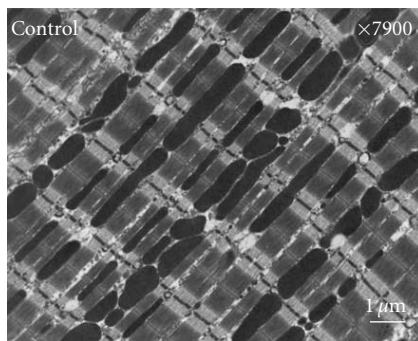
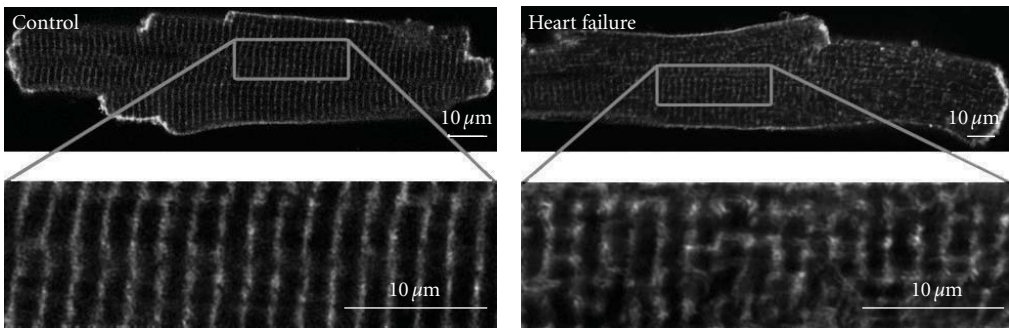
(a) Chronically ischemic myocardium (pig)



(b) Failing atrial cardiomyocytes (sheep)



(c) Postinfarction heart failure (mouse)



(d) Postinfarction heart failure (rat)

FIGURE 2: Continued.

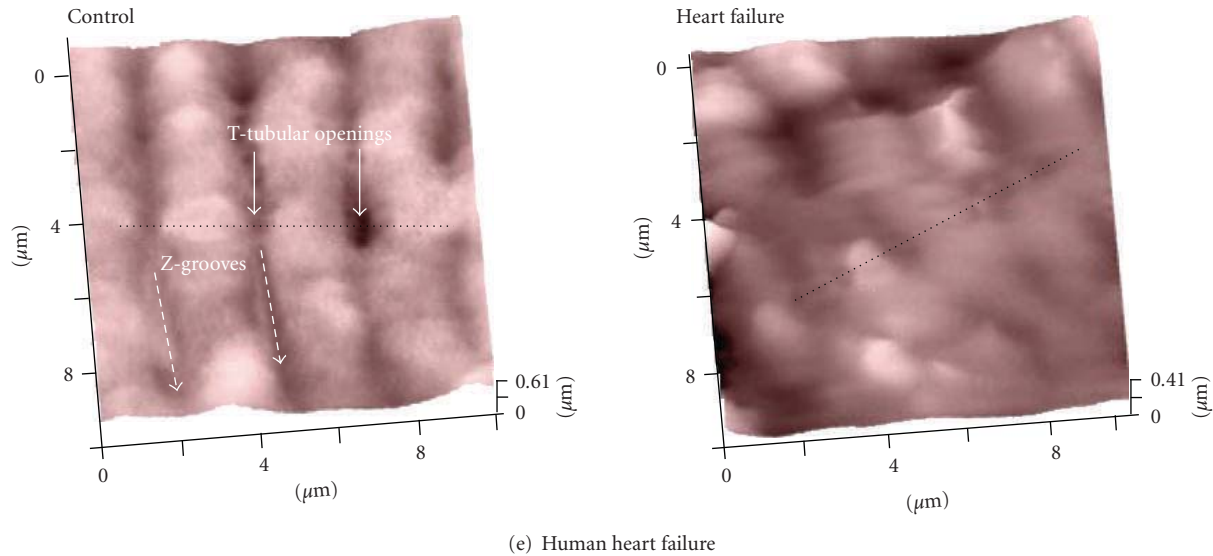


FIGURE 2: Examples of T-tubule alterations in various pathological states. Left panels show images from controls; right panels show images from (a) chronically ischemic pig myocardium (from [43]), (b) failing atrial ovine cardiomyocytes (from [40]), and post-infarction heart failure models in (c) mouse (from [44]) and (d) rat (from [45]). Panel (d) shows representative electron micrographs from control and failing rat hearts showing T-tubule disruption. (e) Scanning ion conductance microscope images from the surface of human nonfailing (control) and failing cardiomyocytes showing loss of T-tubular openings (from [46]). All figures are reproduced with permission.

shown to depend on both SR content and β -adrenergic tone [50]. Thus, control of Ca^{2+} release synchrony does not solely rely on T-tubular structure, but also on cardiomyocyte status. These considerations may have particular significance in pathological conditions, as will be described in the following chapters. This discussion will initially and most thoroughly address T-tubule alterations in heart failure, where there are now considerable data available, followed by a briefer discussion of more preliminary data from atrial fibrillation and diabetes.

2. Heart Failure

Heart failure is a progressive and chronic disease, characterized by an impaired ability of the heart to pump blood. This condition is on the rise in the western world, and diagnosis carries an alarmingly high mortality rate of more than 60% after 5 years [54]. Depressed contractility in heart failure is widely believed to result, at least in part, from reduced magnitude of the cardiomyocyte Ca^{2+} transient [29]. A number of studies have indicated that decreased SR Ca^{2+} release in this condition results from lowered SR Ca^{2+} content [55, 56], due to reduced SERCA function and/or greater Ca^{2+} leak from the SR [29]. In addition, the ability of the Ca^{2+} current to trigger CICR, the so-called “gain of Ca^{2+} release”, is reduced in failing cells [43, 57–60]. Slowing of SR Ca^{2+} release also occurs in heart failure, which slows contraction and additionally reduces the power of the heartbeat [46, 61–69].

2.1. T-tubule Loss/Disorganization. A growing body of evidence indicates that impaired Ca^{2+} homeostasis in failing

myocytes may involve alterations in T-tubular structure. Kamp and colleagues [70, 71] observed loss of T-tubules in ventricular cardiomyocytes in a dog model of tachycardia-induced heart failure. This finding has since been confirmed in other animal models of heart failure including post-infarction rabbit [72] and rat [46], and pigs with chronic ischemia [43] (Figure 2). Similar observations have also been reported in failing human ventricular myocytes [46, 73]. A recent investigation of atrial T-tubules in heart failure also showed dramatic T-tubule loss in sheep following atrial pacing [40] (Figure 2).

Others have not observed decreased T-tubule density in failing myocytes, but rather a structural disorganization. We reported that heart failure progression in mice and rats following myocardial infarction was associated with loss of the uniform, transverse T-tubule pattern, with a greater proportion of tubules present in the longitudinal direction ([44, 45], Figure 2). We additionally observed the appearance of irregular gaps between adjacent T-tubules in failing cells. Similar T-tubular disorganization has been observed in myocytes from failing spontaneously hypertensive rats [47] and in failing human left ventricle [74]. Dilated T-tubules have also been reported in human heart failure [53, 73, 75]. Thus, there is now compelling evidence supporting altered T-tubular structure in heart failure, although it is unclear under what conditions this may be manifested as T-tubule loss or reorganization.

2.2. Slowed, Dyssynchronous Ca^{2+} Release. The consequences of T-tubule alterations for EC-coupling were initially investigated by experimentally promoting T-tubule loss by either cell culture [53, 76] or detubulation [52, 77]. In both cases,

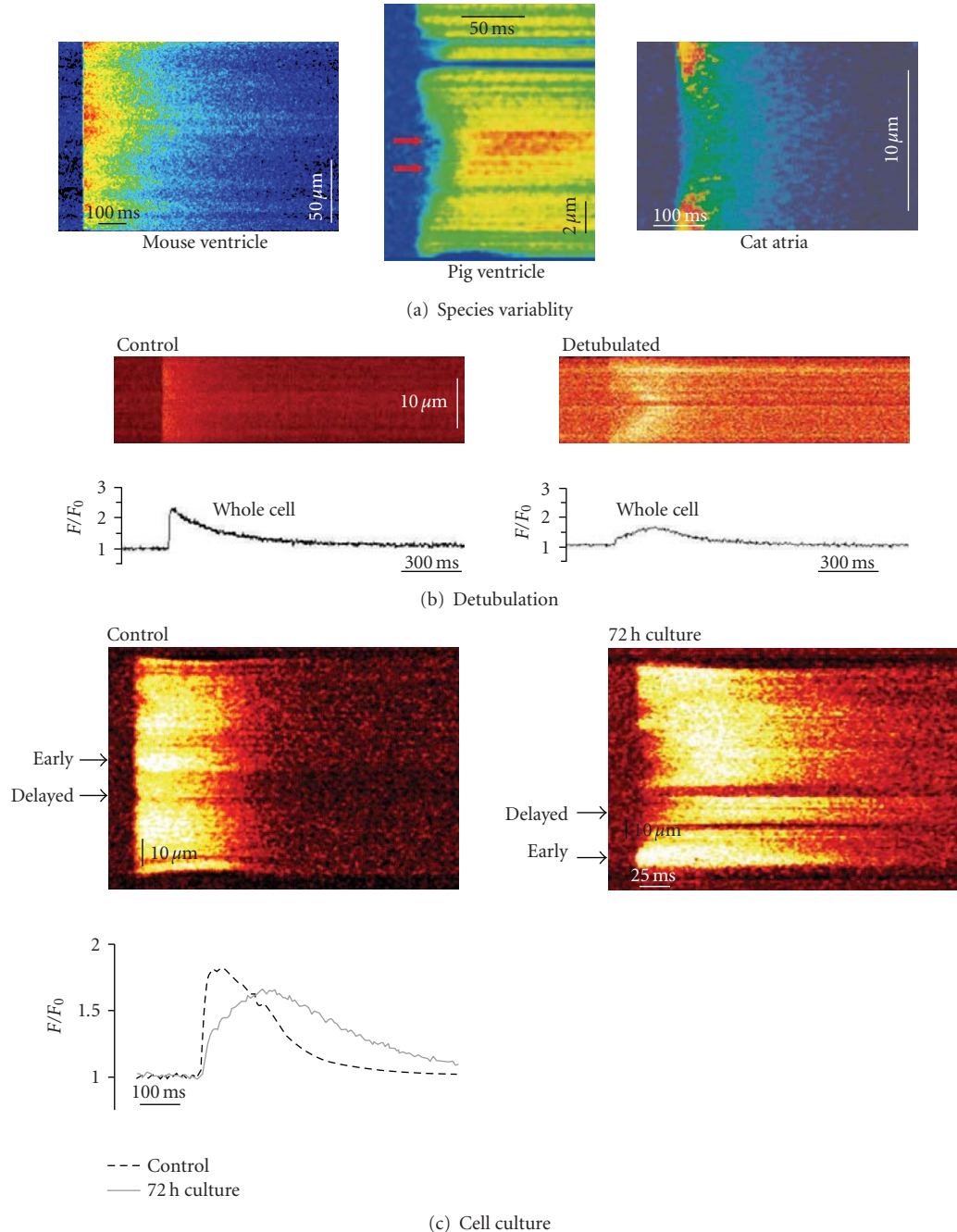


FIGURE 3: T-tubule density affects Ca^{2+} release synchrony. (a) Variable amount of T-tubules in different cell types affects the homogeneity of the Ca^{2+} transient, as illustrated in confocal line scans of myocytes from mouse ventricle ((a), unpublished data), pig ventricle ((b), from [43]), and cat atria ((c), from [49]). (b) Experimental loss of T-tubules using the detubulation technique causes delayed Ca^{2+} release in the centre of the cardiomyocyte (from [52]). (c) T-tubules are lost when cardiomyocytes are kept in culture resulting in dyssynchronous slowing of the Ca^{2+} transient (from [53]). All figures are reproduced with permission.

T-tubule loss was associated with desynchronization of Ca^{2+} release across the cell. When cells were detubulated, wave-like propagation of the Ca^{2+} transient from the sarcolemma to the cell interior was observed [52, 77, 78] (Figure 3(b)), which resembled the pattern of Ca^{2+} release reported in other cells with very low T-tubule density [8, 49, 79, 80]

(Figure 3(a)). With less dramatic T-tubule reduction during cell culture, a fragmented Ca^{2+} release pattern was observed [53] (Figure 3(c)). This indicated that SR Ca^{2+} release was initially triggered at sites where T-tubules were present, followed by propagation into regions devoid of T-tubules [53]. This situation is similar then to that observed in normal

myocytes which have a moderate T-tubular density, such as pig ventricular myocytes ([43], Figure 3(a)), and sheep atrial myocytes [40]. Spatially summing Ca^{2+} release in cells which had lost T-tubules showed that the overall Ca^{2+} transient became slowed and reduced in magnitude [52, 53] (Figures 3(b) and 3(c)). Therefore, such experiments served as proof of principle that large reductions in T-tubule density could reproduce reported alterations in the failing Ca^{2+} transient.

Although dyssynchronous Ca^{2+} release was first observed in failing myocytes by Litwin et al. [81], it was not until later studies by Louch et al. [44] and Song et al. [47] that such alterations were directly linked to alterations in T-tubular structure. In both studies, small regions of delayed Ca^{2+} release were observed to occur at irregular gaps between adjacent T-tubules following T-tubule disorganization (Figure 4). We demonstrated this phenomenon by simultaneously visualizing the T-tubule network and intracellular $[\text{Ca}^{2+}]$ (Figure 4(a)). Song et al. [47] employed an alternative approach, and demonstrated that when intracellular Ca^{2+} was highly buffered, regions of delayed Ca^{2+} release did not occur, as Ca^{2+} diffusion into the gaps between T-tubules was prevented. They observed, however, that the ryanodine receptor distribution remained intact in failing myocytes, suggesting that T-tubule disorganization resulted in some ryanodine receptors becoming “orphaned”, without opposing Ca^{2+} channels. More recent work has similarly linked T-tubule loss in failing ventricular [43, 46] and atrial myocytes [40] to reduced Ca^{2+} release synchrony. Importantly, as in studies with experimental loss of T-tubules [52, 53, 76, 78], reduced Ca^{2+} release synchrony in failing cells has been shown by a number of investigators to promote slowing and broadening of the overall Ca^{2+} transient [43, 44, 46, 47], a hallmark of the failing condition. Results from studies with experimental reduction in T-tubules (discussed above) suggest that reduced T-tubular organization and/or density also likely contributes to the reduction in Ca^{2+} transient amplitude in heart failure.

2.3. Ca^{2+} Current and Gain of Ca^{2+} Release. The concept of orphaned ryanodine receptors, a spatial mismatching of Ca^{2+} channels and ryanodine receptors (Figure 1(b)), was initially proposed by Gómez et al. [82] to account for reduced gain of Ca^{2+} release in failing myocytes. Recent direct observation of divergent T-tubule and ryanodine receptor localization supports this hypothesis [43, 47]. However, reduced efficiency of the Ca^{2+} release trigger may also have other underlying mechanisms. There is a general consensus that L-type Ca^{2+} current density is unchanged in heart failure when measured during voltage-clamp steps (for review, see [29]). However, prolongation of the action potential and loss of an early repolarization notch in failing cells reduce the driving force for Ca^{2+} entry, resulting in decreased peak Ca^{2+} current [65, 83, 84]. In addition, the time course of Ca^{2+} entry is prolonged during the failing action potential, which reduces efficiency for triggering Ca^{2+} release [65, 84]. Such alterations in Ca^{2+} current desynchronize Ca^{2+} release, as has been demonstrated by switching a voltage-clamped action

potential stimulus from a normal human action potential to a failing human action potential [83, 84]. Importantly, this dyssynchronous Ca^{2+} release pattern is variable from beat to beat [83], which distinguishes it from the consistent pattern maintained across beats caused by alterations in T-tubule structure [44, 47]. We believe that slowed, dyssynchronous Ca^{2+} release in failing cells likely results from a combination of alterations in T-tubules and action potentials.

An alternative proposal put forward to explain reduced gain of Ca^{2+} release in failing myocytes is an expansion of the dyadic cleft, resulting in a greater distance between Ca^{2+} channels and ryanodine receptors [60, 82]. To our knowledge, there is not yet direct evidence based on imaging to support this hypothesis. However, we have observed that failing myocytes exhibit a longer delay between the upstroke of the action potential and the upstroke of the Ca^{2+} transient [44], which is consistent with this notion. Importantly, this delay was observed at all locations across the cell, not simply at those locations where large gaps between neighboring T-tubules had led to the formation of orphaned ryanodine receptors. We have proposed that a more subtle drift of T-tubules may occur throughout the cell, which less dramatically increases the T-tubule to SR distance (Figure 1(b)), yet is sufficient to delay CICR and reduce gain [44]. This hypothesis is supported by the findings of Xu et al. [60], who also observed that failing cells exhibited a slowed response of RyRs to the opening of a single Ca^{2+} channel. This was associated with reduced CICR efficiency, since there was a greater chance that RyRs would not open, and Ca^{2+} release which was desynchronized across the cell. Further work employing high resolution imaging and detailed examination of local control of EC coupling is required to confirm the hypothesis that expansion of the dyadic cleft impairs cross-talk between L-type Ca^{2+} channels and RyRs.

While L-type Ca^{2+} current density is generally observed to be unchanged in heart failure [29], the number of Ca^{2+} channels is reportedly reduced [70, 85]. However, increased single channel activity appears to maintain normal Ca^{2+} current density [85, 86], and this may result from increased phosphorylation of the Ca^{2+} channel by protein kinase A and/or CaMKII [86, 87]. Since Ca^{2+} channels are concentrated in the T-tubules, a decrease in Ca^{2+} channel number would, in fact, be expected in failing myocytes if T-tubules are lost. Indeed, experimentally promoting loss of T-tubules results in decreased Ca^{2+} current density [53, 88]. The consequence of reduced Ca^{2+} channel number for EC-coupling in failing cells is unknown. Litwin et al. [81] observed that reduced Ca^{2+} current density in cardiomyocytes isolated from the border zone of post-infarction rabbit promoted dyssynchronous Ca^{2+} transients. It is unclear whether loss of Ca^{2+} channels in failing cardiomyocytes from non-infarcted myocardium might also promote dyssynchrony, but this almost certainly depends on the localization of remaining channels. Are they redistributed between T-tubules and the surface sarcolemma? Some dyads are clearly disrupted by T-tubule reorganization (Figure 1(b)), but do those which remain intact have a normal composition of Ca^{2+} channels and ryanodine receptors? This issue could be addressed by

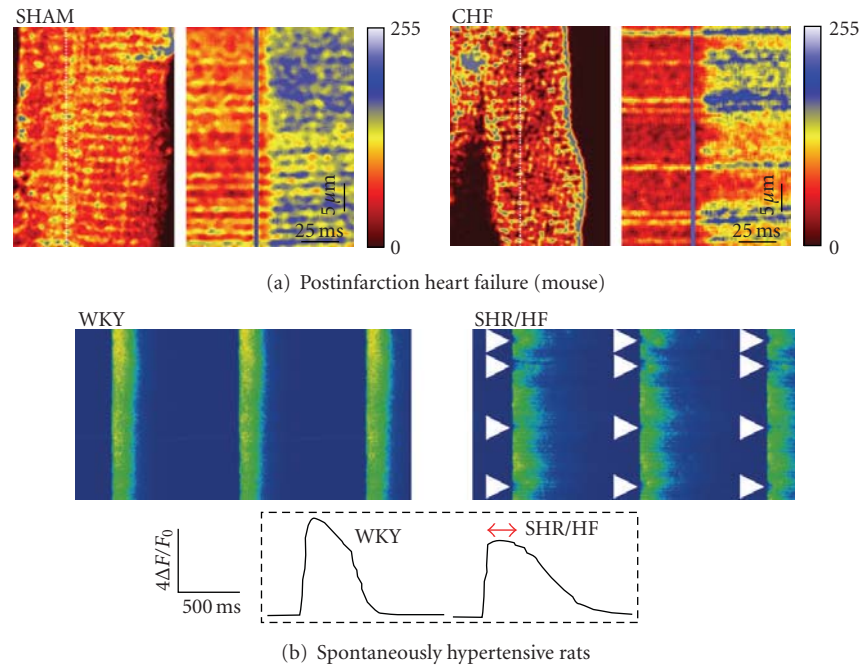


FIGURE 4: Dyssynchronous Ca²⁺ transients in failing cardiomyocytes. (a) Simultaneous imaging of T-tubules stained with di-8-ANEPPS and Ca²⁺ transients in fluo-4-AM loaded myocytes using confocal line scans. The position of the line scan is indicated as a vertical dotted line in T-tubule images, and T-tubules appear as horizontal lines in line-scan images. In myocytes from mice with congestive heart failure (CHF) following myocardial infarction, Ca²⁺ release was delayed in regions lacking T-tubules (right panel), but was synchronous in sham-operated controls (left panel), from [44]. (b) Regions of delayed Ca²⁺ release were also observed in cardiomyocytes from spontaneously hypertensive rats with heart failure (SHR/HF), but not in controls (Wistar-Kyoto (WKY) rats). From [47] Copyright (2006) National Academy of Sciences, USA. All figures are reproduced with permission.

the technique of Hayashi et al. [5], who recently employed electron tomography to estimate the number of RyRs in each dyad based on the calculated dyadic volume. In addition, the number of Ca²⁺ channels present in a couplon could be calculated by detailed analysis of Ca²⁺ sparks [89, 90]. To date, more rudimentary analyses of Ca²⁺ sparks have indicated that sparks in failing myocytes have similar characteristics to those from normal cells [57, 60].

Even without alterations in T-tubular structure, L-type Ca²⁺ current characteristics would be expected to be altered in heart failure. The reduced amplitude and slowed time course of Ca²⁺ release would be predicted to reduce Ca²⁺-dependent inactivation. However, alterations in Ca²⁺ current kinetics have often not been observed in failing myocytes [87, 91]. Bito et al. [87] have suggested that this apparent discrepancy may result from superimposition of NCX current over Ca²⁺ currents, which impairs detection of altered Ca²⁺ current kinetics. On the other hand, at least at high stimulation frequencies, greater Ca²⁺ current inactivation might be expected in failing myocytes, as lowered SERCA function promotes cytosolic Ca²⁺ accumulation [87, 92–94]. Such alterations may contribute to the negative force-frequency response which is a characteristic of human heart failure [56]. Finally, facilitation of Ca²⁺ current might be altered since this phenomenon is tightly regulated by SR-derived Ca²⁺ release [95], which is reduced in heart failure, and CaMKII [96] which is upregulated [97]. Importantly,

loss of T-tubules may reduce facilitation, since Ca²⁺ current is preferentially modulated by SR Ca²⁺ release at the T-tubules rather than at the surface sarcolemma [88]. Indeed, studies conducted to date have shown decreased facilitation in failing human atrial and ventricular myocytes [88, 98, 99].

2.4. Ryanodine Receptor Function. There is growing evidence that ryanodine receptor function is importantly altered in heart failure. In isolated bilayer experiments, Marx et al. observed greater RyR activity [69] and suggested that greater SR Ca²⁺ leak via RyRs contributes to reduced SR Ca²⁺ content. This finding has since been confirmed in intact myocytes [100, 101]. The Marks group proposed that increased leak results from “hyper-phosphorylation” of RyR by PKA, which causes dissociation of FKBP12.6 from RyR [69]. This destabilizes the RyR complex, and causes functional uncoupling of neighboring RyRs [102]. Thus, while arrays of RyRs normally tend to open and close together, RyR uncoupling in failing myocytes is proposed to result in a greater open probability during diastole. However, these findings remain controversial as other groups have not been able to document dissociation of FKBP12.6 from RyR in either healthy or diseased myocytes [103–105]. Instead, recent work has suggested that greater RyR activity in heart failure may result from phosphorylation by Ca²⁺/calmodulin-dependent protein kinase II [106] or

increased relative expression of RyR regulatory proteins triadin and junctin [100]. Regardless of the underlying mechanism, increased SR Ca^{2+} leak is believed to be detrimental in heart failure since reduced SR content impairs contractility. In addition, increased Ca^{2+} leak is thought to be proarrhythmic since spontaneously released Ca^{2+} is extruded from the cell by NCX, resulting in afterdepolarizations which may trigger an extra action potential [29].

It is unclear if and how alterations in RyR function in heart failure are related to T-tubular changes. However, Meethal et al. recently reported that in failing cells, spontaneous Ca^{2+} sparks occur more frequently at the irregular gaps between T-tubules created by T-tubule loss [51]. Resting Ca^{2+} levels were also higher at these locations. These observations suggest that orphaned ryanodine receptors exhibit greater activity than those in intact dyads, and that this overactivity may importantly contribute to increased SR leak and arrhythmic potential in failing cells. Are groups of orphaned RyRs also functionally uncoupled? Perhaps, and if so, such alterations might theoretically exacerbate Ca^{2+} release dyssynchrony by slowing propagation of CICR into regions where T-tubules are absent. Similarly, altered SR content and β -adrenergic tone might also influence synchrony by affecting wave propagation speed [77].

2.5. Other Alterations in the Dyadic “Neighborhood”. The neighborhood of proteins controlling local Ca^{2+} concentration in the dyad is complex, and includes many more proteins besides L-type Ca^{2+} channels and ryanodine receptors. As described in the introduction, Ca^{2+} regulation is closely linked to the activity of Na^+ -handling proteins. NCX expression and activity are increased in heart failure, and reverse-mode function is enhanced due to action potential prolongation, a reduced Ca^{2+} transient, and elevation of intracellular $[\text{Na}^+]$ (for review see [107]). Depending on the precise arrangement of the dyadic neighborhood, greater NCX-mediated Ca^{2+} entry might play an increased role in triggering Ca^{2+} release in heart failure. However, such a role depends on the relative proximity of NCX, ryanodine receptors, and the Na^+ channel [30], and these measurements have not yet been reported in failing myocytes. Regardless, increased NCX-mediated Ca^{2+} entry is believed to support the Ca^{2+} transient in heart failure, partially counteracting reductions in SR content resulting from SERCA downregulation [107]. However, Fowler et al. [108] showed that Na^+ accumulation was not translated into SR loading when cells were detubulated, and that this resulted in the development of a negative force-frequency relationship. Therefore, loss of NCX molecules along with T-tubules in failing myocytes may have significant consequences, especially at physiological frequencies. Confirmation of this hypothesis awaits a detailed examination of NCX distribution in failing cells.

Increased Na^+ levels in heart failure [109–111] appear to result, at least in part, from reduced expression and activity of the Na^+ - K^+ ATPase [28, 45]. We have observed that the Na^+ - K^+ ATPase α_2 isoform is preferentially localized in the T-tubules, where it regulates local $[\text{Na}^+]$ near NCX [24]. Therefore, down-regulation of α_2 isoform in heart failure

impairs crosstalk between the Na^+ - K^+ ATPase and NCX, which may locally elevate $[\text{Na}^+]$ and impair NCX-mediated Ca^{2+} extrusion [28, 45]. There is also growing evidence that increased late Na^+ current [112–114] and increased Na^+ - H^+ exchanger activity [111, 115] additionally contribute to Na^+ accumulation in failing cells.

Interestingly, although T-type Ca^{2+} channels are normally expressed at very low density in ventricular cells, a number of studies have reported that their expression is up-regulated in hypertrophy and heart failure (for review see [116]). In myocytes from rats with pressure overload, Martínez et al. [117] observed that T-type Ca^{2+} channel entry was one-third that carried by L-type channels, and thus a significant contributor to overall Ca^{2+} influx. It is unknown if T-type channels are expressed in the dyad or T-tubules of failing cells, but if so it is possible that they may importantly modulate local $[\text{Ca}^{2+}]$, or even serve as triggers for Ca^{2+} release. However, in possible contradiction to this notion, a recent study employing T-type channel overexpression showed preferential targeting of these channels to the surface sarcolemma [118]. Nevertheless, increased T-type Ca^{2+} channel expression is not without consequence, as it has been shown to play an important role in triggering of pathological cellular hypertrophy [119], and may be proarrhythmic [120].

Although the PMCA is believed to be only a minor contributor to Ca^{2+} removal during the decline of the Ca^{2+} transient [20], data from the NCX knockout mouse suggest that this Ca^{2+} pump can have a surprisingly large capacity to extrude Ca^{2+} when challenged [121]. Similarly, we have suggested that PMCA up-regulation might help maintain diastolic function following SERCA knockout [28, 122]. Therefore, with reduced SERCA function and impaired NCX-mediated Ca^{2+} extrusion (due to $[\text{Na}^+]_i$ accumulation) in failing cells, the PMCA may theoretically become a more important Ca^{2+} extrusion pathway. However, a recent study by Mackiewicz et al. [123] showed that PMCA function is, in fact, progressively reduced during heart failure progression in rats following myocardial infarction. To our knowledge, no other data on PMCA function in heart failure are currently available, and protein localization is unknown. Based on available information, it appears that PMCA function in heart failure is most importantly involved with signaling pathways underlying cellular hypertrophy [124, 125] and not maintenance of the Ca^{2+} transient.

Another Ca^{2+} transporting protein which has recently come into focus in ventricular cardiomyocytes is the inositol 1,4,5-triphosphate receptor (IP_3R). Initially thought to play only a minor role in ventricular cells since it is markedly outnumbered by the RyRs (50:1) [126], recent evidence shows that there is an important upregulation of IP_3Rs in the junctional SR during hypertrophy and heart failure [127]. The authors showed that although Ca^{2+} fluxes through IP_3Rs are smaller than through RyRs [128], enhanced Ca^{2+} release through IP_3Rs in hypertrophic cardiomyocytes increases Ca^{2+} transient magnitude. Although such an effect might be thought beneficial, increased IP_3R -mediated Ca^{2+} release is arrhythmogenic since the close proximity of IP_3Rs and RyRs leads to RyR sensitization [127]. The presence of NCX

nearby IP₃Rs would promote early afterdepolarizations and thus extra-systolic Ca²⁺ transients. However, it remains to be determined how loss/disorganization of the T-tubules affects the distance between NCX and IP₃Rs during heart failure. Ankyrin-B may be importantly involved, since this protein coordinates NCX, NKA and IP₃R in a cardiac T-tubule/SR microdomain [129].

The above discussion illustrates that there are complex modifications in the dyadic neighborhood in heart failure, involving RyR, the L-type Ca²⁺ channel, and Na⁺ handling proteins such as the Na⁺-K⁺ ATPase and NCX. To fully understand the heart failure phenotype, it is critical that alterations in the distribution and function of these proteins are elucidated. This investigation will require a detailed analysis of T-tubule composition, and not simply overt changes in T-tubular structure as has largely been conducted to date.

3. Atrial Fibrillation

Atrial fibrillation is a common type of arrhythmia which is caused by local reentry circuits. This prevents coordinated atrial contraction, which compromises the heart's blood pumping capacity [130]. There is also an increased risk of stroke in this condition since blood pools and clots in the dysfunctional atria [131]. Recent evidence suggests that decreased contractile force of the atrial muscle [132] may, at least partly, result from pathological alteration of T-tubular structure. Lenaerts et al. [41] observed a 45% reduction in T-tubule density in right atrial cardiomyocytes following persistent atrial fibrillation. As in reports from failing myocytes described above, T-tubule loss during atrial fibrillation was associated with spatially dyssynchronous Ca²⁺ release but an intact ryanodine receptor distribution [41]. Therefore, the authors suggested that a reduced efficiency of EC coupling in this condition results from fewer Ca²⁺ channel-RyR couplings (more orphaned ryanodine receptors), and that this effect contributes to reduced Ca²⁺ transient and contraction magnitude.

While some myocyte alterations following atrial fibrillation may resemble those that occur in failing myocytes, there are also important differences. Unlike in heart failure, atrial myocytes following persistent fibrillation are widely reported to exhibit reduced L-type current density [41, 133–136]. Interestingly, L-type Ca²⁺ channel expression is reported to be reduced in both conditions [41, 70, 85, 133], while single channel function is increased [85, 86, 137]. It is unclear why this increase in function is sufficient to maintain normal current density in heart failure but not atrial fibrillation. Another important difference between the two conditions is that SR content is widely reported to be reduced in heart failure [55, 56] but may be normal in atrial fibrillation [41]. This might suggest that loss of T-tubules and associated Ca²⁺ channels is a primary defect in Ca²⁺ homeostasis in atrial fibrillation, but only one component of more complex alterations in heart failure. In both conditions, impaired function of the contractile machinery has also been proposed [138, 139].

Lenaerts et al. [41] were the first to examine T-tubule alterations in atrial fibrillation, but more investigation is required. For example, the importance of slowing of Ca²⁺ release has not yet been demonstrated in this condition, but would be expected to reduce contractile power. As discussed above, important pathological alterations in the dyadic neighborhood may include modified targeting and regulation of Ca²⁺- and Na⁺-handling proteins, and this issue also remains largely unexplored in atrial fibrillation.

4. Diabetic Cardiomyopathy

Many diabetic patients exhibit cardiac dysfunction [140]. In type-2 diabetes, reduced *in vivo* and cardiomyocyte contractile functions are modeled in the db/db insulin-resistant “diabetic” mouse [141–144]. Decreased contractility in these mice is associated with greater SR Ca²⁺ leak, which reduces SR Ca²⁺ content and the magnitude of the Ca²⁺ transient [142, 144]. In addition, the magnitude of the L-type Ca²⁺ current is reduced while single channel activity is increased [141]. This suggests that there are a decreased number of Ca²⁺ channels, similar to that reported in heart failure and atrial fibrillation. In a recent study, Stølen et al. [144] showed that cardiomyocytes from sedentary db/db mice exhibit reduced T-tubule density, which may account for Ca²⁺ channel loss. As expected, T-tubule loss was associated with dyssynchronous SR Ca²⁺ release and reduced Ca²⁺ transient amplitude. Although Ca²⁺ release kinetics were not reported in this study, an expected reduced rate of rise of the Ca²⁺ transient could contribute to the slowed contraction observed *in vivo* [142]. Another interesting observation in myocytes from db/db mice is a longer delay between the stimulus and the upstroke of the Ca²⁺ transient [144]. This is in agreement with our finding in failing post-infarction cardiomyocytes [44], which we have hypothesized reflects an expansion of the dyadic cleft (Figure 1(b)). Although such alterations together with T-tubule loss would be expected to reduce CICR efficiency, Pereira et al. [141] reported unaltered gain of EC coupling in db/db cardiomyocytes. The reason for this apparent discrepancy is unclear, but it may result from other unknown alterations in the dyadic neighborhood.

T-tubule alterations have also been reported in GK/Jcl and SDT/Jcl rat models of type II diabetes [145]. Although T-tubule loss was not observed in these models, the authors showed a disorganization of T-tubules and a decrease in the number of complete SR/T-tubule junctions. Ca²⁺ homeostasis was not investigated in this study, but dyssynchronous Ca²⁺ release would be expected. However, dyssynchronous Ca²⁺ transients have been reported in cardiomyocytes isolated from rats with streptozotocin-induced type-1 diabetes [146]. However, in this study dyssynchrony was attributed to a subpopulation of RyRs (37% of total RyR number) which were unresponsive to Ca²⁺. They proposed that some of these inactive RyRs may be localized in the dyad, preventing Ca²⁺ influx through L-type Ca²⁺ channels from triggering SR Ca²⁺ release. We suggest that Ca²⁺ channels in these inactive dyads could be described as “functionally orphaned”, a reversal

of the situation that arises when ryanodine receptors are orphaned by removal of dyadic Ca^{2+} channels following T-tubule disruption. Interestingly, Shao et al. [146] observed that functional RyRs remaining in diabetic myocytes were hyperphosphorylated, which resulted in greater activity, increased SR Ca^{2+} leak, and reduced SR content [146]. Both Ca^{2+} transients and contractions were reduced in magnitude and exhibited a slowed rate of rise, as expected when SR content is reduced and SR Ca^{2+} release desynchronized. If and how modifications in T-tubular structure contribute to altered Ca^{2+} homeostasis in type-1 diabetes remains to be determined.

5. Mechanisms Controlling T-tubular Structure and Growth

Our discussion thus far has described T-tubules and the dyadic neighborhood in health and disease, but not the mechanisms controlling their formation and maintenance. T-tubules are absent at birth, and develop thereafter by progressive invagination from the surface sarcolemma [2, 10]. Caveolae, which are small bulbous pockets at the cell surface, and the associated protein caveolin are believed to play an essential role in this process [147]. However, RyRs are present in the SR and aligned at the Z-disc very early in development [148]. The formation of dyads is therefore dependent on the later development of T-tubules. Ziman et al. [9] recently showed that dyad formation occurs as junctophilin-2 arrives with the maturing T-tubules. This protein spans the dyadic cleft, and anchors the T-tubular and SR membranes [149]. This role is believed critical for dyad formation, as junctophilin arrival at this location establishes efficient and spatially synchronous EC coupling [9].

Junctophilin alterations may promote loss of dyadic integrity in pathophysiological conditions. The interaction between junctophilin and caveolin-3 is down-regulated in cardiomyopathy [150]. In addition, junctophilin mutations are reported in cardiomyopathy patients [151, 152]. We hypothesize that abnormal junctophilin expression or function may promote drift of L-type Ca^{2+} channels from RyRs as the dyad becomes unanchored, resulting in reduced CICR gain. Indeed, decreased junctophilin expression in the triadin knockout mouse was recently reported to be associated with decreased colocalization of Ca^{2+} channels and RyRs [153].

A tubule-forming protein called amphiphysin-2 may also be involved in T-tubule maintenance. In skeletal muscle, this protein has been shown to be highly concentrated at the T-tubules [154], and Lee et al. [155] reported that expressing amphiphysin 2 in nonmuscle cells induces T-tubule-like invaginations in the plasma membrane. In addition, amphiphysin 2 mutation results in disorganized T-tubular structure in skeletal muscle [156]. Since this protein links the plasma membrane with submembranous cytosolic scaffolds [157], this finding suggests that unanchoring of the T-tubules from the cytoskeleton may lead to T-tubule drift. Although a role of amphiphysin 2 in T-tubule formation and maintenance is not yet established in cardiomyocytes, connections between the sarcolemma and cytoskeleton are

well known [158]. Interestingly, failing cardiomyocytes show disorganization of cytoskeleton structure [158], and loss of T-tubules during cell culture has been linked to changes in actin [159]. Therefore, while T-tubule drift may occur if cytoskeletal anchors are disrupted, alterations in the structure of the cytoskeleton itself might also contribute to T-tubule changes in disease states.

During normal myocyte maintenance, lysosomes are known to degrade cellular organelles by autophagy [160, 161]. Interestingly, Meethal et al. [51] recently reported that in both normal and failing cardiomyocytes, lysosomes were present at gaps between T-tubules, suggesting that T-tubule degradation was occurring at these locations. They also observed that T-tubule loss in failing myocytes was associated with increased density of lysosomes. It is as yet unclear whether greater lysosome activity is the initiating event responsible for abnormal T-tubule degradation. Insight into this issue might be provided by an investigation of T-tubules in lysosomal storage diseases, although we are unaware of any such study to date.

The finding that heart failure, atrial fibrillation, and type-2 diabetes are all associated with T-tubule disruption, suggests that this may be a common outcome triggered by hypertrophy. Interestingly, physiological hypertrophy resulting from training is not associated with T-tubule disruption [144]. This suggests that T-tubule disruption may result from activation of signaling pathways which are specifically involved in pathological hypertrophy.

6. Treatment/Future Perspectives

Based on what is now extensive evidence that altered T-tubular structure may contribute to the pathophysiology of several disease states, it is clear that T-tubules have the potential to serve as therapeutic targets. Preventing T-tubule loss and/or disorganization would be expected to improve Ca^{2+} release synchrony, leading to a more rapid rise of the Ca^{2+} transient and greater contractile power. To our knowledge, the only such intervention reported to date is exercise training. Stølen et al. [144] observed that db/db diabetic mice which underwent aerobic interval training avoided the T-tubule loss and Ca^{2+} release dyssynchrony present in sedentary mice. It is unknown which pathways activated by exercise training afforded this protection.

Development of more targeted treatment strategies will almost certainly rely on an improved understanding of the mechanisms underlying T-tubular maintenance as discussed above. Molecular targets may include components of the cytoskeleton and signaling molecules involved in triggering hypertrophy. Theoretically, promoting growth of new T-tubules could also be beneficial. For example, proliferation of longitudinal tubules, as has been observed in pathological conditions might provide greater opportunity for Ca^{2+} cycling across the sarcolemma, and also SR Ca^{2+} release if dyads form at these new tubules. Synchrony of Ca^{2+} release also might be increased by reducing the occurrence and size of delayed release regions by increasing the velocity at which Ca^{2+} propagates. Although the precise mechanisms

controlling Ca^{2+} wave speed are only beginning to be elucidated, it appears that increasing SR Ca^{2+} content and β -adrenergic tone may promote greater Ca^{2+} release synchrony [77]. Altering T-tubule composition also has therapeutic potential. Strategies aimed at increasing expression of the L-type Ca^{2+} channel and NCX may be beneficial, as we have recently observed that enhanced transsarcolemmal Ca^{2+} cycling can remarkably compensate for impaired SR function [28, 122]. Finally, it may be possible to optimize the role of NCX as a Ca^{2+} release trigger in failing cardiomyocytes by precisely localizing other Na^+ handling proteins in the dyad, or by direct molecular enhancement of NCX activity.

7. Summary

In this review, we have described the dyadic neighborhood established by the close proximity and functional coupling of the T-tubular and SR membranes. This neighborhood allows for tight local control of $[\text{Ca}^{2+}]_i$. It includes Ca^{2+} channels and RyRs, as well as proteins involved with Na^+ homeostasis and maintenance of dyadic integrity. We have summarized data indicating that T-tubule loss and/or disorganization occurs in heart failure, atrial fibrillation, and diabetic cardiomyopathy. Resulting alterations in the dyadic neighborhood are associated with reduced Ca^{2+} release synchrony and impaired efficiency of CICR. Other modifications in EC coupling proteins which may be shared between these disease states include greater RyR leak, decreased Ca^{2+} channel number, and increased single Ca^{2+} channel activity. While the mechanisms responsible for disruption of the dyadic neighborhood remain largely unknown, recent evidence indicates that anchoring of the dyad may be importantly compromised. We suggest that further investigation of these mechanisms will reveal novel therapeutic targets for improving EC coupling in pathophysiological conditions.

References

- [1] F. Brette and C. Orchard, "Resurgence of cardiac T-tubule research," *Physiology*, vol. 22, no. 3, pp. 167–173, 2007.
- [2] M. S. Forbes and N. Sperelakis, "The presence of transverse and axial tubules in the ventricular myocardium of embryonic and neonatal guinea pigs," *Cell and Tissue Research*, vol. 166, no. 1, pp. 83–90, 1976.
- [3] C. Soeller and M. B. Cannell, "Examination of the transverse tubular system in living cardiac rat myocytes by 2-photon microscopy and digital image-processing techniques," *Circulation Research*, vol. 84, no. 3, pp. 266–275, 1999.
- [4] D. M. Bers, *Excitation-Contraction Coupling and Cardiac Contractile Force*, Kluwer Academic Publishers, Dordrecht, The Netherlands, 2001.
- [5] T. Hayashi, M. E. Martone, Z. Yu, et al., "Three-dimensional electron microscopy reveals new details of membrane systems for Ca^{2+} signaling in the heart," *Journal of Cell Science*, vol. 122, no. 7, pp. 1005–1013, 2009.
- [6] M. Pásek, F. Brette, A. Nelson, et al., "Quantification of t-tubule area and protein distribution in rat cardiac ventricular myocytes," *Progress in Biophysics and Molecular Biology*, vol. 96, no. 1–3, pp. 244–257, 2008.
- [7] F. Chen, G. Mottino, T. S. Klitzner, K. D. Philipson, and J. S. Frank, "Distribution of the $\text{Na}^+/\text{Ca}^{2+}$ exchange protein in developing rabbit myocytes," *American Journal of Physiology*, vol. 268, no. 5, pp. C1126–C1132, 1995.
- [8] P. S. Haddock, W. A. Coetzee, E. Cho, et al., "Subcellular $[\text{Ca}^{2+}]_i$ gradients during excitation-contraction coupling in newborn rabbit ventricular myocytes," *Circulation Research*, vol. 85, no. 5, pp. 415–427, 1999.
- [9] A. P. Ziman, N. L. Gómez-Viquez, R. J. Bloch, and W. J. Lederer, "Excitation-contraction coupling changes during postnatal cardiac development," *Journal of Molecular and Cellular Cardiology*, vol. 48, no. 2, pp. 379–386, 2010.
- [10] A. Di Maio, K. Karko, R. M. Snopko, R. Mejía-Alvarez, and C. Franzini-Armstrong, "T-tubule formation in cardiomyocytes: two possible mechanisms?" *Journal of Muscle Research and Cell Motility*, vol. 28, no. 4–5, pp. 231–241, 2007.
- [11] D. M. Bers and V. M. Stiffel, "Ratio of ryanodine to dihydropyridine receptors in cardiac and skeletal muscle and implications for E-C coupling," *American Journal of Physiology*, vol. 264, no. 6, pp. C1587–C1593, 1993.
- [12] D. M. Bers and T. Guo, "Calcium signaling in cardiac ventricular myocytes," *Annals of the New York Academy of Sciences*, vol. 1047, pp. 86–98, 2005.
- [13] C. Franzini-Armstrong, F. Protasi, and V. Ramesh, "Shape, size, and distribution of Ca^{2+} release units and couplons in skeletal and cardiac muscles," *Biophysical Journal*, vol. 77, no. 3, pp. 1528–1539, 1999.
- [14] C. Soeller, D. Crossman, R. Gilbert, and M. B. Cannell, "Analysis of ryanodine receptor clusters in rat and human cardiac myocytes," *Proceedings of the National Academy of Sciences of the United States of America*, vol. 104, no. 38, pp. 14958–14963, 2007.
- [15] A. Fabiato, "Calcium induced release of calcium from the sarcoplasmic-reticulum of skinned fibers from the frog semitendinosus," *Biophysical Journal*, vol. 47, no. 2, p. A195, 1985.
- [16] H. Cheng, W. J. Lederer, and M. B. Cannell, "Calcium sparks: elementary events underlying excitation-contraction coupling in heart muscle," *Science*, vol. 262, no. 5134, pp. 740–744, 1993.
- [17] E. Niggli and N. Shirokova, "A guide to sparkology: the taxonomy of elementary cellular Ca^{2+} signaling events," *Cell Calcium*, vol. 42, no. 4–5, pp. 379–387, 2007.
- [18] H. Cheng and W. J. Lederer, "Calcium sparks," *Physiological Reviews*, vol. 88, no. 4, pp. 1491–1545, 2008.
- [19] T. R. Shannon, K. S. Ginsburg, and D. M. Bers, "Potentiation of fractional sarcoplasmic reticulum calcium release by total and free intra-sarcoplasmic reticulum calcium concentration," *Biophysical Journal*, vol. 78, no. 1, pp. 334–343, 2000.
- [20] R. A. Bassani, J. W. M. Bassani, and D. M. Bers, "Mitochondrial and sarcolemmal Ca^{2+} transport reduce $[\text{Ca}^{2+}]_i$ during caffeine contractures in rabbit cardiac myocytes," *Journal of Physiology*, vol. 453, pp. 591–608, 1992.
- [21] S. Despa, F. Brette, C. H. Orchard, and D. M. Bers, "Na/Ca exchange and Na/K-ATPase function are equally concentrated in transverse tubules of rat ventricular myocytes," *Biophysical Journal*, vol. 85, no. 5, pp. 3388–3396, 2003.
- [22] N. Negretti, S. C. O'Neill, and D. A. Eisner, "The relative contributions of different intracellular and sarcolemmal systems to relaxations in rat ventricular myocytes," *Cardiovascular Research*, vol. 27, no. 10, pp. 1826–1830, 1993.
- [23] J. W. M. Bassani, R. A. Bassani, and D. M. Bers, "Relaxation in rabbit and rat cardiac cells: species-dependent differences

- in cellular mechanisms," *Journal of Physiology*, vol. 476, no. 2, pp. 279–293, 1994.
- [24] F. Swift, N. Tovsrud, U. H. Enger, I. Sjaastad, and O. M. Sejersted, "The Na^+/K^+ -ATPase α_2 -isoform regulates cardiac contractility in rat cardiomyocytes," *Cardiovascular Research*, vol. 75, no. 1, pp. 109–117, 2007.
- [25] R. G. Berry, S. Despa, W. Fuller, D. M. Bers, and M. J. Shattock, "Differential distribution and regulation of mouse cardiac Na^+/K^+ -ATPase α_1 and α_2 subunits in T-tubule and surface sarcolemmal membranes," *Cardiovascular Research*, vol. 73, no. 1, pp. 92–100, 2007.
- [26] S. Despa and D. M. Bers, "Functional analysis of Na^+/K^+ -ATPase isoform distribution in rat ventricular myocytes," *American Journal of Physiology*, vol. 293, no. 1, pp. C321–C327, 2007.
- [27] P. F. James, I. L. Grupp, G. Grupp, et al., "Identification of a specific role for the Na,K -ATPase α_2 isoform as a regulator of calcium in the heart," *Molecular Cell*, vol. 3, no. 5, pp. 555–563, 1999.
- [28] W. E. Louch, K. Hougen, H. K. Mørk, et al., "Sodium accumulation promotes diastolic dysfunction in end-stage heart failure following *Serca2* knockout," *Journal of Physiology*, vol. 588, no. 3, pp. 465–478, 2010.
- [29] D. M. Bers, "Altered cardiac myocyte Ca regulation in heart failure," *Physiology*, vol. 21, no. 6, pp. 380–387, 2006.
- [30] G. T. Lines, J. B. Sande, W. E. Louch, H. K. Mørk, P. Grøttum, and O. M. Sejersted, "Contribution of the $\text{Na}^+/\text{Ca}^{2+}$ exchanger to rapid Ca^{2+} release in cardiomyocytes," *Biophysical Journal*, vol. 91, no. 3, pp. 779–792, 2006.
- [31] K. R. Sipido, M. Maes, and F. Van de Werf, "Low efficiency of Ca^{2+} entry through the $\text{Na}^+-\text{Ca}^{2+}$ exchanger as trigger for Ca^{2+} release from the sarcoplasmic reticulum: a comparison between L-type Ca^{2+} current and reverse-mode $\text{Na}^+-\text{Ca}^{2+}$ exchange," *Circulation Research*, vol. 81, no. 6, pp. 1034–1044, 1997.
- [32] D. R. L. Scriven, P. Dan, and E. D. W. Moore, "Distribution of proteins implicated in excitation-contraction coupling in rat ventricular myocytes," *Biophysical Journal*, vol. 79, no. 5, pp. 2682–2691, 2000.
- [33] A. Di Maio, H. E. Ter Keurs, and C. Franzini-Armstrong, "T-tubule profiles in Purkinje fibres of mammalian myocardium," *Journal of Muscle Research and Cell Motility*, vol. 28, no. 2-3, pp. 115–121, 2007.
- [34] S.-H. Woo, L. Cleemann, and M. Morad, "Diversity of atrial local Ca^{2+} signalling: evidence from 2-D confocal imaging in Ca^{2+} -buffered rat atrial myocytes," *Journal of Physiology*, vol. 567, no. 3, pp. 905–921, 2005.
- [35] W. G. Forssmann and L. Girardier, "A study of the T system in rat heart," *Journal of Cell Biology*, vol. 44, no. 1, pp. 1–19, 1970.
- [36] A. S. Ayettey and V. Navaratnam, "The T-tubule system in the specialized and general myocardium of the rat," *Journal of Anatomy*, vol. 127, part 1, pp. 125–140, 1978.
- [37] M. M. Kirk, L. T. Izu, Y. Chen-Izu, et al., "Role of the transverse-axial tubule system in generating calcium sparks and calcium transients in rat atrial myocytes," *Journal of Physiology*, vol. 547, no. 2, pp. 441–451, 2003.
- [38] T. Gotoh, "Quantitative studies on the ultrastructural differentiation and growth of mammalian cardiac muscle cells. The atria and ventricles of the cat," *Acta Anatomica*, vol. 115, no. 2, pp. 168–177, 1983.
- [39] J. G. Tidball, J. E. Cederdahl, and D. M. Bers, "Quantitative analysis of regional variability in the distribution of transverse tubules in rabbit myocardium," *Cell and Tissue Research*, vol. 264, no. 2, pp. 293–298, 1991.
- [40] K. M. Dibb, J. D. Clarke, M. A. Horn, et al., "Characterization of an extensive transverse tubular network in sheep atrial myocytes and its depletion in heart failure," *Circulation: Heart Failure*, vol. 2, no. 5, pp. 482–489, 2009.
- [41] I. Lenaerts, V. Bito, F. R. Heinzel, et al., "Ultrastructural and functional remodeling of the coupling between Ca^{2+} influx and sarcoplasmic reticulum Ca^{2+} release in right atrial myocytes from experimental persistent atrial fibrillation," *Circulation Research*, vol. 105, no. 9, pp. 876–885, 2009.
- [42] P. C. Dolber, R. P. Bauman, J. C. Rembert, and J. C. Greenfield Jr., "Regional changes in myocyte structure in model of canine right atrial hypertrophy," *American Journal of Physiology*, vol. 267, no. 4, pp. H1279–H1287, 1994.
- [43] F. R. Heinzel, V. Bito, L. Biesmans, et al., "Remodeling of T-tubules and reduced synchrony of Ca^{2+} release in myocytes from chronically ischemic myocardium," *Circulation Research*, vol. 102, no. 3, pp. 338–346, 2008.
- [44] W. E. Louch, H. K. Mørk, J. Sexton, et al., "T-tubule disorganization and reduced synchrony of Ca^{2+} release in murine cardiomyocytes following myocardial infarction," *Journal of Physiology*, vol. 574, no. 2, pp. 519–533, 2006.
- [45] F. Swift, J. A. K. Birkeland, N. Tovsrud, et al., "Altered $\text{Na}^+/\text{Ca}^{2+}$ -exchanger activity due to downregulation of Na^+/K^+ -ATPase α_2 -isoform in heart failure," *Cardiovascular Research*, vol. 78, no. 1, pp. 71–78, 2008.
- [46] A. R. Lyon, K. T. MacLeod, Y. Zhang, et al., "Loss of T-tubules and other changes to surface topography in ventricular myocytes from failing human and rat heart," *Proceedings of the National Academy of Sciences of the United States of America*, vol. 106, no. 16, pp. 6854–6859, 2009.
- [47] L.-S. Song, E. A. Sobie, S. McCulle, W. J. Lederer, C. W. Balke, and H. Cheng, "Orphaned ryanodine receptors in the failing heart," *Proceedings of the National Academy of Sciences of the United States of America*, vol. 103, no. 11, pp. 4305–4310, 2006.
- [48] F. R. Heinzel, V. Bito, P. G. A. Volders, G. Antoons, K. Mubagwa, and K. R. Sipido, "Spatial and temporal inhomogeneities during Ca^{2+} release from the sarcoplasmic reticulum in pig ventricular myocytes," *Circulation Research*, vol. 91, no. 11, pp. 1023–1030, 2002.
- [49] K. A. Sheehan and L. A. Blatter, "Regulation of junctional and non-junctional sarcoplasmic reticulum calcium release in excitation-contraction coupling in cat atrial myocytes," *Journal of Physiology*, vol. 546, no. 1, pp. 119–136, 2003.
- [50] M. D. Bootman, D. R. Higazi, S. Coombes, and H. L. Roderick, "Calcium signalling during excitation-contraction coupling in mammalian atrial myocytes," *Journal of Cell Science*, vol. 119, no. 19, pp. 3915–3925, 2006.
- [51] S. V. Meethal, K. T. Potter, D. Redon, et al., "Structure-function relationships of Ca spark activity in normal and failing cardiac myocytes as revealed by flash photography," *Cell Calcium*, vol. 41, no. 2, pp. 123–134, 2007.
- [52] F. Brette, P. Rodriguez, K. Komukai, J. Colyer, and C. H. Orchard, " β -adrenergic stimulation restores the Ca transient of ventricular myocytes lacking t-tubules," *Journal of Molecular and Cellular Cardiology*, vol. 36, no. 2, pp. 265–275, 2004.
- [53] W. E. Louch, V. Bito, F. R. Heinzel, et al., "Reduced synchrony of Ca^{2+} release with loss of T-tubules—a comparison to Ca^{2+} release in human failing cardiomyocytes," *Cardiovascular Research*, vol. 62, no. 1, pp. 63–73, 2004.

- [54] L. H. Curtis, D. J. Whellan, B. G. Hammill, et al., "Incidence and prevalence of heart failure in elderly persons, 1994–2003," *Archives of Internal Medicine*, vol. 168, no. 4, pp. 418–424, 2008.
- [55] V. Piacentino III, C. R. Weber, X. Chen, et al., "Cellular basis of abnormal calcium transients of failing human ventricular myocytes," *Circulation Research*, vol. 92, no. 6, pp. 651–658, 2003.
- [56] B. Pieske, L. S. Maier, D. M. Bers, and G. Hasenfuss, "Ca²⁺ handling and sarcoplasmic reticulum Ca²⁺ content in isolated failing and nonfailing human myocardium," *Circulation Research*, vol. 85, no. 1, pp. 38–46, 1999.
- [57] A. M. Gómez, H. H. Valdivia, H. Cheng, et al., "Defective excitation-contraction coupling in experimental cardiac hypertrophy and heart failure," *Science*, vol. 276, no. 5313, pp. 800–806, 1997.
- [58] I. Sjaastad, J. Bøkenes, F. Swift, J. A. Wasserstrom, and O. M. Sejersted, "Normal contractions triggered by I_{Ca,L} in ventricular myocytes from rats with postinfarction CHF," *American Journal of Physiology*, vol. 283, no. 3, pp. H1225–H1236, 2002.
- [59] I. Sjaastad, J. A. Birkeland, G. Ferrier, et al., "Defective excitation-contraction coupling in hearts of rats with congestive heart failure," *Acta Physiologica Scandinavica*, vol. 184, no. 1, pp. 45–58, 2005.
- [60] M. Xu, P. Zhou, S. M. Xu, et al., "Intermolecular failure of L-type Ca²⁺ channel and ryanodine receptor signaling in hypertrophy," *PLoS Biology*, vol. 5, no. 2, article e21, 2007.
- [61] D. Vinereanu, P. O. Lim, M. P. Frenneaux, and A. G. Fraser, "Reduced myocardial velocities of left ventricular long-axis contraction identify both systolic and diastolic heart failure—a comparison with brain natriuretic peptide," *European Journal of Heart Failure*, vol. 7, no. 4, pp. 512–519, 2005.
- [62] J. Bøkenes, J. M. Aronsen, J. A. Birkeland, et al., "Slow contractions characterize failing rat hearts," *Basic Research in Cardiology*, vol. 103, no. 4, pp. 328–344, 2008.
- [63] A. Yoneyama, J. Koyama, T. Tomita, et al., "Relationship of plasma brain-type natriuretic peptide levels to left ventricular longitudinal function in patients with congestive heart failure assessed by strain Doppler imaging," *International Journal of Cardiology*, vol. 130, no. 1, pp. 56–63, 2008.
- [64] C. H. Davies, K. Davia, J. G. Bennett, J. R. Pepper, P. A. Poole-Wilson, and S. E. Harding, "Reduced contraction and altered frequency response of isolated ventricular myocytes from patients with heart failure," *Circulation*, vol. 92, no. 9, pp. 2540–2549, 1995.
- [65] H. K. Mørk, I. Sjaastad, O. M. Sejersted, and W. E. Louch, "Slowing of cardiomyocyte Ca²⁺ release and contraction during heart failure progression in postinfarction mice," *American Journal of Physiology*, vol. 296, no. 4, pp. H1069–H1079, 2009.
- [66] F. del Monte, P. O'Gara, P. A. Poole-Wilson, M. Yacoub, and S. E. Harding, "Cell geometry and contractile abnormalities of myocytes from failing human left ventricle," *Cardiovascular Research*, vol. 30, no. 2, pp. 281–290, 1995.
- [67] S. E. Harding, C. H. Davies, D. G. Wynne, and P. A. Poole-Wilson, "Contractile function and response to agonists in myocytes from failing human heart," *European Heart Journal*, vol. 15, pp. 35–36, 1994.
- [68] L. Sen, G. Cui, G. C. Fonarow, and H. Laks, "Differences in mechanisms of SR dysfunction in ischemic vs. idiopathic dilated cardiomyopathy," *American Journal of Physiology*, vol. 279, no. 2, pp. H709–H718, 2000.
- [69] S. O. Marx, S. Reiken, Y. Hisamatsu, et al., "PKA phosphorylation dissociates FKBP12.6 from the calcium release channel (ryanodine receptor): defective regulation in failing hearts," *Cell*, vol. 101, no. 4, pp. 365–376, 2000.
- [70] J.-Q. He, M. W. Conklin, J. D. Foell, et al., "Reduction in density of transverse tubules and L-type Ca²⁺ channels in canine tachycardia-induced heart failure," *Cardiovascular Research*, vol. 49, no. 2, pp. 298–307, 2001.
- [71] R. C. Balijepalli, A. J. Lokuta, N. A. Maertz, et al., "Depletion of T-tubules and specific subcellular changes in sarcolemmal proteins in tachycardia-induced heart failure," *Cardiovascular Research*, vol. 59, no. 1, pp. 67–77, 2003.
- [72] F. R. Quinn, S. Currie, A. M. Duncan, et al., "Myocardial infarction causes increased expression but decreased activity of the myocardial Na⁺-Ca²⁺ exchanger in the rabbit," *Journal of Physiology*, vol. 553, no. 1, pp. 229–242, 2003.
- [73] S. Kostin, D. Scholz, T. Shimada, et al., "The internal and external protein scaffold of the T-tubular system in cardiomyocytes," *Cell and Tissue Research*, vol. 294, no. 3, pp. 449–460, 1998.
- [74] M. B. Cannell, D. J. Crossman, and C. Soeller, "Effect of changes in action potential spike configuration, junctional sarcoplasmic reticulum micro-architecture and altered t-tubule structure in human heart failure," *Journal of Muscle Research and Cell Motility*, vol. 27, no. 5–7, pp. 297–306, 2006.
- [75] R. R. Kaprielian, S. Stevenson, S. M. Rothery, M. J. Cullen, and N. J. Severs, "Distinct patterns of dystrophin organization in myocyte sarcolemma and transverse tubules of normal and diseased human myocardium," *Circulation*, vol. 101, no. 22, pp. 2586–2594, 2000.
- [76] P. Lipp, J. Hüser, L. Pott, and E. Niggli, "Spatially non-uniform Ca²⁺ signals induced by the reduction of transverse tubules in citrate-loaded guinea-pig ventricular myocytes in culture," *Journal of Physiology*, vol. 497, no. 3, pp. 589–597, 1996.
- [77] F. Brette, S. Despa, D. M. Bers, and C. H. Orchard, "Spatiotemporal characteristics of SR Ca²⁺ uptake and release in detubulated rat ventricular myocytes," *Journal of Molecular and Cellular Cardiology*, vol. 39, no. 5, pp. 804–812, 2005.
- [78] Z. Yang, C. Pascarel, D. S. Steele, K. Komukai, F. Brette, and C. H. Orchard, "Na⁺-Ca²⁺ exchange activity is localized in the t-tubules of rat ventricular myocytes," *Circulation Research*, vol. 91, no. 4, pp. 315–322, 2002.
- [79] J. Hüser, S. L. Lipsius, and L. A. Blatter, "Calcium gradients during excitation-contraction coupling in cat atrial myocytes," *Journal of Physiology*, vol. 494, no. 3, pp. 641–651, 1996.
- [80] J. M. Cordeiro, K. W. Spitzer, W. R. Giles, P. E. Ershler, M. B. Cannell, and J. H. B. Bridge, "Location of the initiation site of calcium transients and sparks in rabbit heart Purkinje cells," *Journal of Physiology*, vol. 531, no. 2, pp. 301–314, 2001.
- [81] S. E. Litwin, D. Zhang, and J. H. B. Bridge, "Dyssynchronous Ca²⁺ sparks in myocytes from infarcted hearts," *Circulation Research*, vol. 87, no. 11, pp. 1040–1047, 2000.
- [82] A. M. Gómez, S. Guatimosim, K. W. Dilly, G. Vassort, and W. J. Lederer, "Heart failure after myocardial infarction altered excitation-contraction coupling," *Circulation*, vol. 104, no. 6, pp. 688–693, 2001.
- [83] D. M. Harris, G. D. Mills, X. Chen, et al., "Alterations in early action potential repolarization causes localized failure

- of sarcoplasmic reticulum Ca^{2+} release," *Circulation Research*, vol. 96, no. 5, pp. 543–550, 2005.
- [84] R. Sah, R. J. Ramirez, G. Y. Oudit, et al., "Regulation of cardiac excitation-contraction coupling by action potential repolarization: role of the transient outward potassium current (I_{to})," *Journal of Physiology*, vol. 546, no. 1, pp. 5–18, 2003.
- [85] F. Schröder, R. Handrock, D. J. Beuckelmann, et al., "Increased availability and open probability of single L-type calcium channels from failing compared with nonfailing human ventricle," *Circulation*, vol. 98, no. 10, pp. 969–976, 1998.
- [86] X. Chen, V. Piacentino III, S. Furukawa, B. Goldman, K. B. Margulies, and S. R. Houser, "L-type Ca^{2+} channel density and regulation are altered in failing human ventricular myocytes and recover after support with mechanical assist devices," *Circulation Research*, vol. 91, no. 6, pp. 517–524, 2002.
- [87] V. Bito, F. R. Heinzel, L. Biesmans, G. Antoons, and K. R. Sipido, "Crosstalk between L-type Ca^{2+} channels and the sarcoplasmic reticulum: alterations during cardiac remodeling," *Cardiovascular Research*, vol. 77, no. 2, pp. 315–324, 2008.
- [88] F. Brette, L. Sallé, and C. H. Orchard, "Differential modulation of L-type Ca^{2+} current by SR Ca^{2+} release at the T-tubules and surface membrane of rat ventricular myocytes," *Circulation Research*, vol. 95, no. 1, pp. e1–e7, 2004.
- [89] M. Inoue and J. H. B. Bridge, " Ca^{2+} sparks in rabbit ventricular myocytes evoked by action potentials: involvement of clusters of L-type Ca^{2+} channels," *Circulation Research*, vol. 92, no. 5, pp. 532–538, 2003.
- [90] M. Inoue and J. H. B. Bridge, "Variability in couplon size in rabbit ventricular myocytes," *Biophysical Journal*, vol. 89, no. 5, pp. 3102–3110, 2005.
- [91] I. A. Hobai and B. O'Rourke, "Decreased sarcoplasmic reticulum calcium content is responsible for defective excitation-contraction coupling in canine heart failure," *Circulation*, vol. 103, no. 11, pp. 1577–1584, 2001.
- [92] J. Altamirano and D. M. Bers, "Effect of intracellular Ca^{2+} and action potential duration on L-type Ca^{2+} channel inactivation and recovery from inactivation in rabbit cardiac myocytes," *American Journal of Physiology*, vol. 293, no. 1, pp. H563–H573, 2007.
- [93] K. R. Sipido, T. Stankovicova, W. Flameng, J. Vanhaecke, and F. Verdonck, "Frequency dependence of Ca^{2+} release from the sarcoplasmic reticulum in human ventricular myocytes from end-stage heart failure," *Cardiovascular Research*, vol. 37, no. 2, pp. 478–488, 1998.
- [94] G.-R. Li, B. Yang, J. Feng, R. F. Bosch, M. Carrier, and S. Nattel, "Transmembrane I_{Ca} contributes to rate-dependent changes of action potentials in human ventricular myocytes," *American Journal of Physiology*, vol. 276, no. 1, pp. H98–H106, 1999.
- [95] S. Richard, E. Perrier, J. Fauconnier, et al., "' Ca^{2+} -induced Ca^{2+} entry' or how the L-type Ca^{2+} channel remodels its own signalling pathway in cardiac cells," *Progress in Biophysics and Molecular Biology*, vol. 90, no. 1–3, pp. 118–135, 2006.
- [96] I. Dzura, Y. Wu, R. J. Colbran, J. R. Balsler, and M. E. Anderson, "Calmodulin kinase determines calcium-dependent facilitation of L-type calcium channels," *Nature Cell Biology*, vol. 2, no. 3, pp. 173–177, 2000.
- [97] R. Zhang, M. S. C. Khoo, Y. Wu, et al., "Calmodulin kinase II inhibition protects against structural heart disease," *Nature Medicine*, vol. 11, no. 4, pp. 409–417, 2005.
- [98] C. Piot, S. Lemaire, B. Albat, J. Seguin, J. Nargeot, and S. Richard, "High frequency-induced upregulation of human cardiac calcium currents," *Circulation*, vol. 93, no. 1, pp. 120–128, 1996.
- [99] S. Barrère-Lemaire, C. Piot, F. Leclercq, J. Nargeot, and S. Richard, "Facilitation of L-type calcium currents by diastolic depolarization in cardiac cells: impairment in heart failure," *Cardiovascular Research*, vol. 47, no. 2, pp. 336–349, 2000.
- [100] Z. Kubalova, D. Terentyev, S. Viatchenko-Karpinski, et al., "Abnormal intrastore calcium signaling in chronic heart failure," *Proceedings of the National Academy of Sciences of the United States of America*, vol. 102, no. 39, pp. 14104–14109, 2005.
- [101] T. R. Shannon, S. M. Pogwizd, and D. M. Bers, "Elevated sarcoplasmic reticulum Ca^{2+} leak in intact ventricular myocytes from rabbits in heart failure," *Circulation Research*, vol. 93, no. 7, pp. 592–594, 2003.
- [102] S. O. Marx, J. Gaburjakova, M. Gaburjakova, C. Henrikson, K. Ondrias, and A. R. Marks, "Coupled gating between cardiac calcium release channels (ryanodine receptors)," *Circulation Research*, vol. 88, no. 11, pp. 1151–1158, 2001.
- [103] M. T. Jiang, A. J. Lokuta, E. F. Farrell, M. R. Wolff, R. A. Haworth, and H. H. Valdivia, "Abnormal Ca^{2+} release, but normal ryanodine receptors, in canine and human heart failure," *Circulation Research*, vol. 91, no. 11, pp. 1015–1022, 2002.
- [104] M. Stange, L. Xu, D. Balshaw, N. Yamaguchi, and G. Meissner, "Characterization of recombinant skeletal muscle (Ser-2843) and cardiac muscle (Ser-2809) ryanodine receptor phosphorylation mutants," *Journal of Biological Chemistry*, vol. 278, no. 51, pp. 51693–51702, 2003.
- [105] B. Xiao, M. T. Jiang, M. Zhao, et al., "Characterization of a novel PKA phosphorylation site, serine-2030, reveals no PKA hyperphosphorylation of the cardiac ryanodine receptor in canine heart failure," *Circulation Research*, vol. 96, no. 8, pp. 847–855, 2005.
- [106] X. Ai, J. W. Curran, T. R. Shannon, D. M. Bers, and S. M. Pogwizd, " Ca^{2+} /calmodulin-dependent protein kinase modulates cardiac ryanodine receptor phosphorylation and sarcoplasmic reticulum Ca^{2+} leak in heart failure," *Circulation Research*, vol. 97, no. 12, pp. 1314–1322, 2005.
- [107] D. M. Bers, S. Despa, and J. Bossuyt, "Regulation of Ca^{2+} and Na^{+} in normal and failing cardiac myocytes," *Annals of the New York Academy of Sciences*, vol. 1080, pp. 165–177, 2006.
- [108] M. R. Fowler, R. S. Dobson, C. H. Orchard, and S. M. Harrison, "Functional consequences of detubulation of isolated rat ventricular myocytes," *Cardiovascular Research*, vol. 62, no. 3, pp. 529–537, 2004.
- [109] B. Pieske, L. S. Maier, V. Piacentino III, J. Weisser, G. Hasenfuss, and S. Houser, "Rate dependence of $[\text{Na}^{+}]_{\text{i}}$ and contractility in nonfailing and failing human myocardium," *Circulation*, vol. 106, no. 4, pp. 447–453, 2002.
- [110] S. Despa, M. A. Islam, C. R. Weber, S. M. Pogwizd, and D. M. Bers, "Intracellular Na^{+} concentration is elevated in heart failure but Na/K pump function is unchanged," *Circulation*, vol. 105, no. 21, pp. 2543–2548, 2002.
- [111] A. Baartscheer, C. A. Schumacher, M. M. G. J. van Borren, C. N. W. Belterman, R. Coronel, and J. W. T. Fiolet, "Increased $\text{Na}^{+}/\text{H}^{+}$ -exchange activity is the cause of increased $[\text{Na}^{+}]_{\text{i}}$ and underlies disturbed calcium handling in the rabbit pressure and volume overload heart failure model," *Cardiovascular Research*, vol. 57, no. 4, pp. 1015–1024, 2003.
- [112] C. R. Valdivia, W. W. Chu, J. Pu, et al., "Increased late sodium current in myocytes from a canine heart failure model and

- from failing human heart,” *Journal of Molecular and Cellular Cardiology*, vol. 38, no. 3, pp. 475–483, 2005.
- [113] S. Sossalla, S. Wagner, E. C. L. Rasenack, et al., “Ranolazine improves diastolic dysfunction in isolated myocardium from failing human hearts—role of late sodium current and intracellular ion accumulation,” *Journal of Molecular and Cellular Cardiology*, vol. 45, no. 1, pp. 32–43, 2008.
- [114] V. A. Maltsev, N. Silverman, H. N. Sabbah, and A. I. Undrovinas, “Chronic heart failure slows late sodium current in human and canine ventricular myocytes: implications for repolarization variability,” *European Journal of Heart Failure*, vol. 9, no. 3, pp. 219–227, 2007.
- [115] A. Baartscheer, C. A. Schumacher, M. M. G. J. van Borren, et al., “Chronic inhibition of Na^+/H^+ -exchanger attenuates cardiac hypertrophy and prevents cellular remodeling in heart failure,” *Cardiovascular Research*, vol. 65, no. 1, pp. 83–92, 2005.
- [116] K. Ono and T. Iijima, “Cardiac T-type Ca^{2+} channels in the heart,” *Journal of Molecular and Cellular Cardiology*, vol. 48, no. 1, pp. 65–70, 2010.
- [117] M. L. Martínez, M. P. Heredia, and C. Delgado, “Expression of T-type Ca^{2+} channels in ventricular cells from hypertrophied rat hearts,” *Journal of Molecular and Cellular Cardiology*, vol. 31, no. 9, pp. 1617–1625, 1999.
- [118] N. Jaleel, H. Nakayama, X. Chen, et al., “ Ca^{2+} influx through T- and L-type Ca^{2+} channels have different effects on myocyte contractility and induce unique cardiac phenotypes,” *Circulation Research*, vol. 103, no. 10, pp. 1109–1119, 2008.
- [119] C.-S. Chiang, C.-H. Huang, H. Chieng, et al., “The $\text{Ca}_v3.2$ T-type Ca^{2+} channel is required for pressure overload-induced cardiac hypertrophy in mice,” *Circulation Research*, vol. 104, no. 4, pp. 522–530, 2009.
- [120] K. Kuwahara, Y. Saito, M. Takano, et al., “NRSF regulates the fetal cardiac gene program and maintains normal cardiac structure and function,” *The EMBO Journal*, vol. 22, no. 23, pp. 6310–6321, 2003.
- [121] H. Reuter, S. A. Henderson, T. Han, et al., “Cardiac excitation-contraction coupling in the absence of $\text{Na}^+/\text{Ca}^{2+}$ exchange,” *Cell Calcium*, vol. 34, no. 1, pp. 19–26, 2003.
- [122] K. B. Andersson, J. A. K. Birkeland, A. V. Finsen, et al., “Moderate heart dysfunction in mice with inducible cardiomyocyte-specific excision of the *Serca2* gene,” *Journal of Molecular and Cellular Cardiology*, vol. 47, no. 2, pp. 180–187, 2009.
- [123] U. Mackiewicz, M. Maczewski, A. Konior, et al., “Sarcolemmal Ca^{2+} -ATPase ability to transport Ca^{2+} gradually diminishes after myocardial infarction in the rat,” *Cardiovascular Research*, vol. 81, no. 3, pp. 546–554, 2009.
- [124] A. Hammes, S. Oberdorf-Maass, T. Rother, et al., “Overexpression of the sarcolemmal calcium pump in the myocardium of transgenic rats,” *Circulation Research*, vol. 83, no. 9, pp. 877–888, 1998.
- [125] X. Wu, B. Chang, N. S. Blair, et al., “Plasma membrane Ca^{2+} -ATPase isoform 4 antagonizes cardiac hypertrophy in association with calcineurin inhibition in rodents,” *Journal of Clinical Investigation*, vol. 119, no. 4, pp. 976–985, 2009.
- [126] M. C. Moschella and A. R. Marks, “Inositol 1,4,5-trisphosphate receptor expression in cardiac myocytes,” *Journal of Cell Biology*, vol. 120, no. 5, pp. 1137–1146, 1993.
- [127] D. Harzheim, M. Movassagh, R. S.-Y. Foo, et al., “Increased InsP_3 Rs in the junctional sarcoplasmic reticulum augment Ca^{2+} transients and arrhythmias associated with cardiac hypertrophy,” *Proceedings of the National Academy of Sciences of the United States of America*, vol. 106, no. 27, pp. 11406–11411, 2009.
- [128] A. V. Zima and L. A. Blatter, “Inositol-1,4,5-trisphosphate-dependent Ca^{2+} signalling in cat atrial excitation-contraction coupling and arrhythmias,” *Journal of Physiology*, vol. 555, no. 3, pp. 607–615, 2004.
- [129] P. J. Mohler, J. Q. Davis, and V. Bennett, “Ankyrin-B coordinates the Na/K ATPase, Na/Ca exchanger, and InsP_3 receptor in a cardiac T-tubule/SR microdomain,” *PLoS Biology*, vol. 3, no. 12, article e423, 2005.
- [130] J. S. Alpert, P. Petersen, and J. Godtfredsen, “Atrial fibrillation: natural history, complications, and management,” *Annual Review of Medicine*, vol. 39, pp. 41–52, 1988.
- [131] P. A. Wolf, R. D. Abbott, and W. B. Kannel, “Atrial fibrillation as an independent risk factor for stroke: the Framingham Study,” *Stroke*, vol. 22, no. 8, pp. 983–988, 1991.
- [132] U. Schotten, J. Ausma, C. Stellbrink, et al., “Cellular mechanisms of depressed atrial contractility in patients with chronic atrial fibrillation,” *Circulation*, vol. 103, no. 5, pp. 691–698, 2001.
- [133] L. Yue, P. Melnyk, R. Gaspo, Z. Wang, and S. Nattel, “Molecular mechanisms underlying ionic remodeling in a dog model of atrial fibrillation,” *Circulation Research*, vol. 84, no. 7, pp. 776–784, 1999.
- [134] T. Christ, P. Boknik, S. Wöhr, et al., “L-type Ca^{2+} current downregulation in chronic human atrial fibrillation is associated with increased activity of protein phosphatases,” *Circulation*, vol. 110, no. 17, pp. 2651–2657, 2004.
- [135] C. A. Carnes, P. M. L. Janssen, M. L. Ruehr, et al., “Atrial glutathione content, calcium current, and contractility,” *Journal of Biological Chemistry*, vol. 282, no. 38, pp. 28063–28073, 2007.
- [136] M. Greiser, C. R. Halaszovich, D. Frechen, et al., “Pharmacological evidence for altered src kinase regulation of $\text{I}_{\text{Ca,L}}$ in patients with chronic atrial fibrillation,” *Naunyn-Schmiedeberg’s Archives of Pharmacology*, vol. 375, no. 6, pp. 383–392, 2007.
- [137] G. Klein, F. Schröder, D. Vogler, et al., “Increased open probability of single cardiac L-type calcium channels in patients with chronic atrial fibrillation: role of phosphatase 2A,” *Cardiovascular Research*, vol. 59, no. 1, pp. 37–45, 2003.
- [138] H. Sun, R. Gaspo, N. Leblanc, and S. Nattel, “Cellular mechanisms of atrial contractile dysfunction caused by sustained atrial tachycardia,” *Circulation*, vol. 98, no. 7, pp. 719–727, 1998.
- [139] P. P. de Tombe, “Altered contractile function in heart failure,” *Cardiovascular Research*, vol. 37, no. 2, pp. 367–380, 1998.
- [140] A. Cohen-Solal, F. Beauvais, and D. Logeart, “Heart failure and diabetes mellitus: epidemiology and management of an alarming association,” *Journal of Cardiac Failure*, vol. 14, no. 7, pp. 615–625, 2008.
- [141] L. Pereira, J. Matthes, I. Schuster, et al., “Mechanisms of $[\text{Ca}^{2+}]_i$ transient decrease in cardiomyopathy of db/db type 2 diabetic mice,” *Diabetes*, vol. 55, no. 3, pp. 608–615, 2006.
- [142] D. D. Belke, E. A. Swanson, and W. H. Dillmann, “Decreased sarcoplasmic reticulum activity and contractility in diabetic db/db mouse heart,” *Diabetes*, vol. 53, no. 12, pp. 3201–3208, 2004.
- [143] P. M. Kralik, G. Ye, N. S. Metreveli, X. Shem, and P. N. Epstein, “Cardiomyocyte dysfunction in models of type 1 and type 2 diabetes,” *Cardiovascular Toxicology*, vol. 5, no. 3, pp. 285–292, 2005.

- [144] T. O. Stølen, M. A. Høydal, O. J. Kemi, et al., "Interval training normalizes cardiomyocyte function, diastolic Ca^{2+} control, and SR Ca^{2+} release synchronicity in a mouse model of diabetic cardiomyopathy," *Circulation Research*, vol. 105, no. 6, pp. 527–536, 2009.
- [145] K. F. McGrath, A. Yuki, Y. Manaka, H. Tamaki, K. Saito, and H. Takekura, "Morphological characteristics of cardiac calcium release units in animals with metabolic and circulatory disorders," *Journal of Muscle Research and Cell Motility*, vol. 30, no. 5-6, pp. 225–231, 2009.
- [146] C.-H. Shao, G. J. Rozanski, K. P. Patel, and K. R. Bidasee, "Dyssynchronous (non-uniform) Ca^{2+} release in myocytes from streptozotocin-induced diabetic rats," *Journal of Molecular and Cellular Cardiology*, vol. 42, no. 1, pp. 234–246, 2007.
- [147] R. G. Parton, M. Way, N. Zorzi, and E. Stang, "Caveolin-3 associates with developing T-tubules during muscle differentiation," *Journal of Cell Biology*, vol. 136, no. 1, pp. 137–154, 1997.
- [148] F. Sedarat, L. Xu, E. D. W. Moore, and G. F. Tibbits, "Colocalization of dihydropyridine and ryanodine receptors in neonate rabbit heart using confocal microscopy," *American Journal of Physiology*, vol. 279, no. 1, pp. H202–H209, 2000.
- [149] H. Takeshima, S. Komazaki, M. Nishi, M. Iino, and K. Kangawa, "Junctophilins: a novel family of junctional membrane complex proteins," *Molecular Cell*, vol. 6, no. 1, pp. 11–22, 2000.
- [150] S. Minamisawa, J. Oshikawa, H. Takeshima, et al., "Junctophilin type 2 is associated with caveolin-3 and is down-regulated in the hypertrophic and dilated cardiomyopathies," *Biochemical and Biophysical Research Communications*, vol. 325, no. 3, pp. 852–856, 2004.
- [151] A. P. Landstrom, N. Weisleder, K. B. Batalden, et al., "Mutations in JPH2-encoded junctophilin-2 associated with hypertrophic cardiomyopathy in humans," *Journal of Molecular and Cellular Cardiology*, vol. 42, no. 6, pp. 1026–1035, 2007.
- [152] Y. Matsushita, T. Furukawa, H. Kasanuki, et al., "Mutation of junctophilin type 2 associated with hypertrophic cardiomyopathy," *Journal of Human Genetics*, vol. 52, no. 6, pp. 543–548, 2007.
- [153] N. Chopra, T. Yang, P. Asghari, et al., "Ablation of triadin causes loss of cardiac Ca^{2+} release units, impaired excitation-contraction coupling, and cardiac arrhythmias," *Proceedings of the National Academy of Sciences of the United States of America*, vol. 106, no. 18, pp. 7636–7641, 2009.
- [154] M. H. Butler, C. David, G.-C. Ochoa, et al., "Amphiphysin II (SH3p9; BIN1), a member of the amphiphysin/Rvs family, is concentrated in the cortical cytomatrix of axon initial segments and nodes of ranvier in brain and around T tubules in skeletal muscle," *Journal of Cell Biology*, vol. 137, no. 6, pp. 1355–1367, 1997.
- [155] E. Lee, M. Marcucci, L. Daniell, et al., "Amphiphysin 2 (Bin1) and T-tubule biogenesis in muscle," *Science*, vol. 297, no. 5584, pp. 1193–1196, 2002.
- [156] A. Razzaq, I. M. Robinson, H. T. McMahon, et al., "Amphiphysin is necessary for organization of the excitation-contraction coupling machinery of muscles, but not for synaptic vesicle endocytosis in *Drosophila*," *Genes and Development*, vol. 15, no. 22, pp. 2967–2979, 2001.
- [157] V. I. Slepnev and P. De Camilli, "Accessory factors in clathrin-dependent synaptic vesicle endocytosis," *Nature Reviews Neuroscience*, vol. 1, no. 3, pp. 161–172, 2000.
- [158] V. G. Sharov, S. Kostin, A. Todor, J. Schaper, and H. N. Sabbah, "Expression of cytoskeletal, linkage and extracellular proteins in failing dog myocardium," *Heart Failure Reviews*, vol. 10, no. 4, pp. 297–303, 2005.
- [159] R. N. Leach, J. C. Desai, and C. H. Orchard, "Effect of cytoskeleton disruptors on L-type Ca channel distribution in rat ventricular myocytes," *Cell Calcium*, vol. 38, no. 5, pp. 515–526, 2005.
- [160] D. Gozuacik and A. Kimchi, "Autophagy as a cell death and tumor suppressor mechanism," *Oncogene*, vol. 23, no. 16, pp. 2891–2906, 2004.
- [161] B. Levine and D. J. Klionsky, "Development by self-digestion: molecular mechanisms and biological functions of autophagy," *Developmental Cell*, vol. 6, no. 4, pp. 463–477, 2004.

Review Article

Mitochondrial Translation and Beyond: Processes Implicated in Combined Oxidative Phosphorylation Deficiencies

Paulien Smits, Jan Smeitink, and Lambert van den Heuvel

Department of Pediatrics, Nijmegen Center for Mitochondrial Disorders, Radboud University Nijmegen Medical Center, Geert Grooteplein 10, P.O. Box 9101, 6500 HB Nijmegen, The Netherlands

Correspondence should be addressed to Lambert van den Heuvel, b.vandenheuvel@cukz.umcn.nl

Received 31 October 2009; Accepted 29 January 2010

Academic Editor: Aikaterini Kontrogianni-Konstantopoulos

Copyright © 2010 Paulien Smits et al. This is an open access article distributed under the Creative Commons Attribution License, which permits unrestricted use, distribution, and reproduction in any medium, provided the original work is properly cited.

Mitochondrial disorders are a heterogeneous group of often multisystemic and early fatal diseases, which are amongst the most common inherited human diseases. These disorders are caused by defects in the oxidative phosphorylation (OXPHOS) system, which comprises five multisubunit enzyme complexes encoded by both the nuclear and the mitochondrial genomes. Due to the multitude of proteins and intricacy of the processes required for a properly functioning OXPHOS system, identifying the genetic defect that underlies an OXPHOS deficiency is not an easy task, especially in the case of combined OXPHOS defects. In the present communication we give an extensive overview of the proteins and processes (in)directly involved in mitochondrial translation and the biogenesis of the OXPHOS system and their roles in combined OXPHOS deficiencies. This knowledge is important for further research into the genetic causes, with the ultimate goal to effectively prevent and cure these complex and often devastating disorders.

1. Introduction

Mitochondria are essential organelles that are present in virtually all eukaryotic cells. They originated from an ancestral alpha-proteobacterial endosymbiont [1]. The primary function of the mitochondrion is ATP production via the oxidative phosphorylation (OXPHOS) pathway. Additionally, mitochondria have been found to perform crucial roles in many other metabolic, regulatory and developmental processes. Mitochondrial dysfunction can therefore result in a variety of diseases, including common multifactorial disorders such as diabetes [2, 3] and Parkinson's disease [4]. Furthermore, mitochondria are implicated in the normal aging process [5, 6]. The term mitochondrial disorder usually refers to diseases that are caused by disturbances in the OXPHOS system. This is a heterogeneous group of often multi-systemic and early fatal diseases, which are amongst the most common inherited human diseases [7].

The OXPHOS system is embedded in the mitochondrial inner membrane and consists of five multiprotein enzyme complexes (I–V) and two electron carriers [8]. The main function of the system is the coordinated transport

of electrons and protons, resulting in the production of ATP. The great complexity of the OXPHOS system, which comprises almost 90 proteins encoded by both the nuclear and the mitochondrial genomes, explains the heterogeneity in clinical phenotypes that are associated with genetic defects in oxidative phosphorylation. Approximately 67% of the OXPHOS disorders diagnosed at our centre consist of isolated enzyme deficiencies, whereas in 33% of the cases multiple enzyme complexes show lowered activities [9]. Due to the dual genetic control, the defect can be located on the nuclear (n) as well as the mitochondrial (mt) DNA. Isolated OXPHOS deficiencies are generally caused by mutations in structural genes (encoding subunits of the OXPHOS system) or in genes encoding proteins involved in the assembly of a specific OXPHOS enzyme complex [10, 11]. For combined deficiencies the situation is more complicated. Most mutations associated with combined OXPHOS defects have been reported in mtDNA-encoded transfer (t) and ribosomal (r) RNAs [12]. Additionally, nDNA-encoded proteins required for the replication and integrity of mtDNA, such as polymerase γ and thymidine kinase, are implicated in combined deficiencies [13].

Recently, mutations in nine different nuclear gene products involved in mitochondrial protein synthesis were reported: elongation factors mtEFG1, mtEFTs and mtEFTu, small ribosomal subunit proteins MRPS16 and MRPS22, aspartyl- and arginyl-tRNA synthetases, and tRNA-modifying enzymes PUS1 and TRMU [14–25]. These findings defined a new class of gene defects underlying combined OXPHOS disorders. In general, when multiple OXPHOS enzymes are affected, the genetic defect is presumed not to be located in genes encoding OXPHOS subunits, but rather in genes needed for mtDNA maintenance, mitochondrial transcription or translation including posttranscriptional or -translational processes, import of nDNA-encoded proteins into the mitochondrion or mitochondrial membrane biogenesis. Given the number of proteins involved in these processes, a comprehensive overview of the processes and proteins that could be implicated in combined OXPHOS deficiencies is important for further research into the cause of these complex diseases.

This review will focus on the mammalian mitochondrial translation and its role in mitochondrial disorders. However, other processes implicated in combined OXPHOS deficiencies, in particular combined OXPHOS deficiencies with normal complex II activities, and indirectly related to mitochondrial translation will also be outlined. We will first describe which processes are required before protein synthesis can take place in the mammalian mitochondrion and which components are needed for these processes. Second, the current state of knowledge of the mitochondrial translation machinery and the mechanism of translation, including regulation and functions of translation factors beyond protein synthesis, will be discussed. Third, we will cover post-translational processes with a functional OXPHOS system as end result. Fourth, we will give a non-exhaustive overview of the mutations that have been reported to impair mitochondrial protein synthesis and result in OXPHOS deficiencies. And finally, prospects of research into the pathogenesis of mitochondrial disorders will be mentioned.

2. Requirements before Mitochondrial Translation Can Take Place

For translation in the mitochondrion to be able to take place, a number of conditions have to be fulfilled. First of all, mtDNA has to be present, maintained, replicated and transcribed. Additionally, nuclear-encoded proteins required for the proper functioning of the mitochondrion have to be imported from the cell cytoplasm. These processes will now be discussed successively. Figure 1 gives an overview of the major processes (in)directly involved in the biogenesis of the OXPHOS system and covered in this review.

2.1. Human mtDNA. The mitochondrial genome is a double-stranded, circular molecule of 16 659 base pairs. It is a highly compact genome that lacks introns and contains only one major non-coding region (the displacement or D-loop) and 37 genes, which code for 22 tRNAs, 2 rRNAs and 13 polypeptide subunits of the OXPHOS complexes I, III,

IV and V [26]. These genes are located on both strands of the mtDNA molecule, the heavy (H) and light (L) strand. MtDNA has a mutation rate 10–20 times that of nDNA [27–29], which is thought to be caused by the lack of protective histones, slightly limited DNA repair and proximity to damaging reactive oxygen species (ROS) generated at the inner membrane. The unique features of mitochondrial genetics are essential for understanding the etiology and pathogenesis of mitochondrial disorders [30]: (a) mtDNA is maternally inherited; (b) cells typically contain hundreds of mitochondria and thousands of mtDNA molecules (polyplasm); (c) mutations can affect all mtDNA copies in an individual (homoplasm) or only some copies resulting in the coexistence of two or more mtDNA genotypes within a single cell, organ or individual (heteroplasm); (d) in case of heteroplasm, a minimum percentage of mutated mtDNAs has to be present in a cell for the OXPHOS system to malfunction (threshold effect) and this threshold level varies widely between different tissues; (e) during mitosis both normal and mutant mtDNA are randomly distributed to the daughter cells, which can result in changing mutational loads during the life of the patient and different mutational loads in different cells and tissues (mitotic segregation).

2.2. Maintenance and Replication of mtDNA. Unlike nDNA, which replicates only once during cell division, mtDNA is continuously replicated, independent of the cell cycle and also in non-dividing cells such as skeletal muscle fibers and central neurons [31]. Replication is generally thought to take place via a strand-asynchronous mechanism involving two unidirectional, independent origins [32, 33]. Synthesis starts at the origin of H-strand replication (O_H) in the D-loop and proceeds along the parental L-strand to produce a full daughter H-strand. When the second origin (O_L) at two thirds of the way around the genome is reached, DNA synthesis of the L-strand initiates in the opposite direction. Recently, however, a bidirectional mode of mtDNA replication has been proposed [34, 35]. This second mechanism involves a coupled leading- and lagging-strand synthesis and is reported to exist along with the strand-asynchronous mechanism.

MtDNA replication is achieved by a number of nuclear-encoded proteins. First of all, the only DNA polymerase present in mammalian mitochondria: polymerase γ . Polymerase γ is a heterotrimer consisting of a catalytic subunit with proof-reading ability (POLG) and two identical accessory subunits (POLG2) that bind DNA and increase the processivity of POLG. Second, Twinkle is a 5' to 3' DNA helicase that unwinds double-stranded mtDNA and thereby plays a role in mtDNA maintenance and regulation of mtDNA copy number. Third, the mitochondrial single-stranded binding protein (mtSSB) is thought to maintain the integrity of single-stranded regions of DNA at replication forks and to stimulate the activity of Twinkle and polymerase γ . Additionally, several topoisomerases regulate supercoiling of mtDNA. Furthermore, mtDNA ligase III is involved in replication as well as repair of the mitochondrial genome. For replication initiation, RNA primers are needed. An as yet unidentified mtDNA primase likely provides the

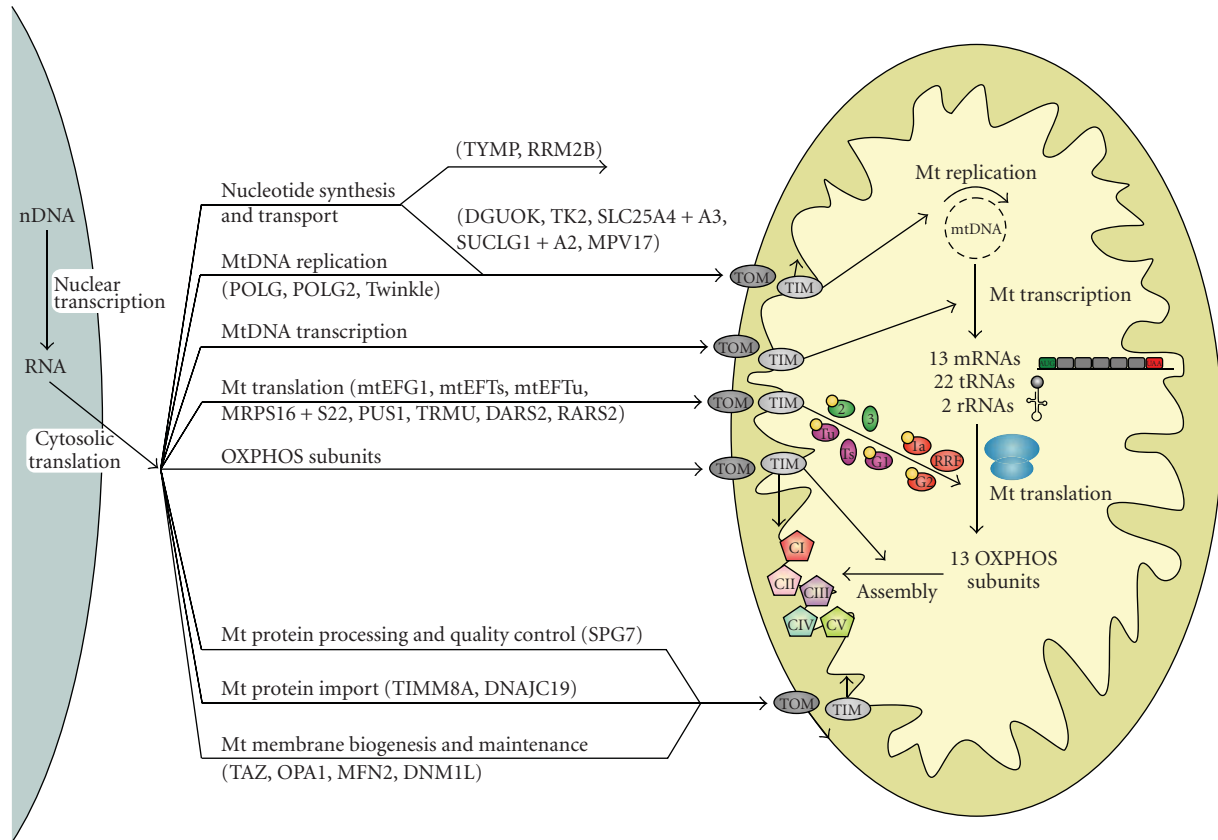


FIGURE 1: Schematic overview of the processes involved in mitochondrial translation and the biogenesis of the OXPHOS system. Before translation can take place in the mitochondrion, the mtDNA needs to be maintained, replicated and transcribed and numerous nDNA-encoded proteins have to be imported into the mitochondrion for these processes and for mitochondrial translation itself (see Figure 2 for more details on mitochondrial translation and its components depicted here). For the formation of the OXPHOS system, the nDNA- and mtDNA-encoded subunits need to be synthesized, imported, inserted into the inner membrane and assembled into enzyme complexes. The 13 mRNAs depicted refer to 9 monocistronic and 2 dicistronic transcripts. Proteins implicated in mitochondrial disorders are mentioned in brackets (also see Table 1). CI–CV = complex I–V of the OXPHOS system; TIM and TOM = translocase of the inner and outer mitochondrial membranes.

RNA primer for L-strand synthesis, whereas the mitochondrial transcription machinery is involved in RNA primer formation for H-strand synthesis (see Section 2.3). RNase mitochondrial RNA processing endonuclease (RNase MRP) and endonuclease G are implicated in processing of the precursor RNA primers for H-strand replication. Last, RNase H1 has been proposed to be involved in replication of the mitochondrial genome by removal of the RNA primers. Ligase III, RNase MRP and RNase H1 are not specific mitochondrial proteins; they are also located in the cell nucleus. For a more detailed description of mitochondrial replication see a review by Graziewicz et al. [36].

Furthermore, various other proteins are indirectly involved in the maintenance of mtDNA either through protecting the mitochondrial genome, repairing mtDNA damage, or supplying nucleotide pools. Firstly, the protection of the mitochondrial genome. MtDNA is packaged into protein-DNA complexes called nucleoids, which are believed to be the units of mtDNA transmission and inheritance [37, 38]. Among the nucleoid components

are proteins involved in the maintenance, replication and/or transcription of mtDNA, such as mtSSB, Twinkle, POLG and TFAM (mitochondrial transcription factor A). Secondly, mtDNA repair is crucial to avoid accumulation of damage to the rapidly replicating mitochondrial genome. Mitochondria possess multiple repair mechanisms, but these are beyond the scope of this review (detailed descriptions of mtDNA repair have been published previously [39, 40]). Thirdly, a proper balance of the mitochondrial (deoxy)nucleoside triphosphate ((d)NTP) pools, accomplished by mitochondrial transport proteins and salvage pathway enzymes, is also essential for mtDNA maintenance and replication (for an overview of mitochondrial dNTP metabolism and all proteins involved, see [41]). Shortage and/or imbalance of the dNTP pool could affect the efficiency and accuracy of mitochondrial replication. Additionally, disturbances of the NTP pool may interfere with replication by affecting the synthesis of the RNA primers necessary for replication initiation. This could subsequently lead to deletions in the mtDNA or depletion (i.e., reduced copy number) of

the mitochondrial genome. A number of mitochondrial disorders are caused by defects in the mitochondrial dNTP metabolism due to mutations in the following nine nuclear genes: *DGUOK*, *TK2*, *TYMP*, *SLC25A4*, *SLC25A3*, *SUCLG1*, *SUCLA2*, *RRM2B*, and *MPV17* (for reviews see [13, 42, 43]). Mitochondrial deoxyguanosine kinase (DGUOK) and thymidine kinase (TK2) catalyze the first step in the salvage pathways of pyrimidine and purine deoxynucleosides, respectively. In the salvage pathway, deoxynucleosides are activated by stepwise phosphorylation leading to formation of the dNTPs. The cytoplasmic enzyme thymidine phosphorylase (TYMP) catalyzes the reversible phosphorylation of thymidine and thereby regulates the availability of thymidine for DNA synthesis. Additionally, adenine nucleotide translocators (ANT) are needed to regulate the concentration of adenine nucleotides by exchanging ATP for ADP in and out of the mitochondrial matrix; SLC25A4 (ANT1) is the heart and skeletal muscle specific isoform. The mitochondrial phosphate carrier SLC25A3 transports inorganic phosphate into the mitochondrial matrix. *SUCLG1* and *SUCLA2* encode the α - and β -subunits of the Krebs cycle enzyme succinate-CoA ligase (SUCL). Defects in these genes could lead to mtDNA depletion through decreased activity of the mitochondrial nucleotide diphosphate kinase (NDPK), which functions in the last step of the mitochondrial dNTP salvage pathway and associates with SUCL. The p53R2 subunit (encoded by *RRM2B*) of the cytosolic enzyme ribonucleotide reductase is required for de novo deoxyribonucleotide synthesis in nonproliferating cells, thereby supplying dNTPs for nDNA repair and mtDNA synthesis. Finally, the mitochondrial inner membrane protein MPV17 is also involved in dNTP metabolism, with defects causing mtDNA depletion; the exact function of MPV17 remains to be elucidated, however. In addition to disturbed homeostasis of mitochondrial dNTP pools, mtDNA instability can naturally be caused by mutations in genes affecting mtDNA replication directly. Mutations have been reported in *POLG*, *POLG2*, and *C10orf2* (Twinkle), with *POLG* being the most important contributor [13].

2.3. Transcription of mtDNA. Transcription originates from three promoters: two H strand promoters (HSP1 and HSP2) and one L strand promoter (LSP). The HSP1 and LSP are located in the D-loop, whereas HSP2 is located downstream of HSP1 close to the 5' end of the 12S rRNA gene. Transcription from both the HSP2 and LSP generates polycistronic molecules covering nearly the entire H or L strand, corresponding to 12 protein-coding genes, 14 tRNA genes and 2 rRNA genes (HSP2) or 1 protein-coding gene and 8 tRNA genes (LSP). Additionally, transcription from the LSP produces the RNA primers necessary for initiating mtDNA replication of the H-strand. Transcripts derived from HSP1, on the other hand, contain mainly the 12S and 16S rRNAs. The basic human mitochondrial transcription machinery consists of three components: mtRNA polymerase (POLRMT), TFAM and either mitochondrial transcription factor B1 (TFB1M) or B2 (TFB2M). Promoter recognition and transcription initiation require

the simultaneous presence of these three factors, however, the precise contribution of each has not yet been fully determined [44, 45]. Termination of transcription appears to be regulated by multiple termination factors, but the exact mechanism and all factors involved still need to be elucidated [45, 46]. Termination sites have been identified for transcription from HSP1 and HSP2; the two proteins binding to the HSP2 termination site await identification. Even though the mitochondrial transcription termination factor MTERF1 (or MTERF) has been shown to bind the HSP1 termination site (at the 3' end of the 16S rRNA gene) and be required for HSP1 transcription termination in vitro, it seems to block L strand transcription more effectively than transcription from the H strand; the precise function of the protein in vivo is unclear. Recently, MTERF1 was found to be essential for transcription initiation in vitro, which led to the hypothesis that MTERF1 regulates and promotes transcription at HSP1 by forming a loop between the MTERF1 initiation and termination binding sites. This way it helps favor a higher synthesis rate of rRNAs compared to mRNAs from the H strand. Furthermore, MTERF1 appears to modulate mtDNA replication pausing; its dual role could be important for coordination of replication and transcription [47]. Three homologs of MTERF1 and thus potential mitochondrial transcription termination factors have been identified: MTERF2 (or MTERFD3 or MTERFL), MTERF3 (or MTERFD1) and MTERF4 (or MTERFD2) [48]. MTERF2 is proposed to regulate cell growth through modulation of mitochondrial transcription [49]. MTERF2 shows the opposite expression pattern in response to serum compared to MTERF1, suggesting that they have divergent roles. Additionally, MTERF2 was found to be present in nucleoids, displaying non sequence-specific DNA-binding activity [50]. Contrastingly, Wenz et al. demonstrated specific binding of MTERF2 to the HSP promoter region [51]. Furthermore, MTERF2 knock-out resulted in decreased mitochondrial transcription and mRNA levels. MTERF3, on the other hand, has been shown in mouse in vivo and in human in vitro to function as a negative regulator of transcription initiation through interaction with the mtDNA promoter region [52]. Moreover, MTERF3 knock-down in *Drosophila* led to a decreased rate of mitochondrial protein synthesis, possibly through downregulation of TFB1M (see Section 3.3 for more information on TFB1M's function in translation) [46, 53]. In summary, the current view is as follows: MTERF1 through 3 share a common binding site in the D-loop; both MTERF1 and 2 promote transcription initiation, whereas MTERF3 inhibits it; all three factors are needed to maintain optimal transcript levels and thereby ensure proper functioning of the OXPHOS system. The role of MTERF4 has not been investigated in detail, however, it appears to bind mtDNA in the D-loop region and form a stable homodimer with a putative RNA methyltransferase [54].

Processing of the polycistronic primary transcripts is thought to require four enzymes. The tRNA genes mark most of the junctions between mitochondrial protein-coding and rRNA genes. According to the tRNA punctuation model, the secondary structures of the tRNA sequences provide the signals for endonucleolytic excision of the tRNAs, yielding

most of the tRNAs, mRNAs and rRNAs [55]. This initial processing step is performed by the mitochondrial RNase P (5'-end endonucleolytic cleavage) and tRNase Z (3'-end cleavage) enzymes. Maturation of the excised tRNAs is completed by addition of a CCA triplet to their 3'-end, which is catalyzed by an ATP(CTP):tRNA nucleotidyltransferase. After post-transcriptional modification and correct folding of the tRNAs, the amino acid can be attached to the CCA triplet by the corresponding aminoacyl-tRNA synthetase. The tRNA acceptor stem and the anticodon play important roles for the recognition of the tRNA by the appropriate synthetase. During or immediately after cleavage of the tRNAs, the rRNAs and mRNAs are polyadenylated by a mitochondrial poly(A) polymerase. This post-transcriptional modification creates the stop codons for some mRNAs and may also be necessary for stabilization of some RNAs (for a review see Montoya et al. [56]). In this way, 9 monocistronic and 2 dicistronic mRNA transcripts are formed. Another important post-transcriptional process is RNA degradation, which is required to control RNA levels and eliminate processing by-products and aberrant transcripts [57]. Nevertheless, the players involved and the exact mechanism have yet to be revealed. SUV3 and polynucleotide phosphorylase are possible candidates [58, 59].

Until now, no mutations causing mitochondrial disease have been reported in genes coding for proteins involved in mitochondrial transcription. Nonetheless, a mutation in the MTERF1 binding site (in the tRNA^{Leu(UUR)} gene) is associated with the mitochondrial disorder MELAS (mitochondrial myopathy, encephalopathy, lactic acidosis and stroke-like episodes). This mutation reduces the binding affinity for MTERF1 and results in a drastic impairment of transcription termination *in vitro*, however, *in vivo* the transcription termination defect could not be confirmed [60, 61]. Furthermore, TFB1M modifies the phenotypic expression of the deafness-associated 1555A>G mtDNA mutation (see Section 3.3). Additionally, post-transcriptional modification of tRNAs is disturbed in patients with mitochondrial myopathy and sideroblastic anemia (MLASA) due to a mutation in pseudouridylate synthase *PUS1* [14, 17]. *PUS1* converts uridine into pseudouridine in cytosolic as well as mitochondrial tRNAs. Recently, mutations in *TRMU*, a mitochondria-specific enzyme that is required for the 2-thiolation on the wobble position of the tRNA anticodon, were detected in patients with acute liver failure in infancy [24]. Previously, *TRMU* was identified as another nuclear modifier gene for the mitochondrial 12S rRNA mutation 1555A>G [62]; see Section 5.2 for more details on defects in the latter two genes.

2.4. Import of nDNA Encoded Proteins. Most mitochondrial proteins, including all proteins involved in mitochondrial translation, are encoded in the nucleus and therefore have to be transported to and imported into the mitochondrion. Cytosolic chaperones, such as heat shock proteins Hsp70 and Hsp90, guide the precursor proteins to translocation channel receptors on the mitochondrial surface, keep the proteins unfolded to prevent aggregation and enable entrance into the translocation channels. Alternatively, preproteins seem

also to be imported into mitochondria in a co-translational manner [63–67]. These proteins, produced on ribosomes bound to the outer mitochondrial membrane, are almost exclusively of prokaryotic origin [68, 69]. The cytoplasmic and mitochondrial translation machineries are suggested to be localized in close proximity on either side of the mitochondrial membranes, thereby allowing efficient assembly of the OXPHOS system [70]. Import and sorting of nDNA-encoded proteins into mitochondria is achieved by translocases in the outer and inner mitochondrial membrane [71, 72]. The translocase of the outer mitochondrial membrane (TOM complex) forms the entrance for basically all nuclear-encoded mitochondrial proteins. After passing through the TOM complex, the preproteins can follow various routes depending on their targeting signals: (1) outer membrane proteins are integrated into the membrane by the sorting and assembly machinery (SAM complex); (2) translocation to the intermembrane space is mediated by the TIM23 complex (translocase of the inner mitochondrial membrane) or by components in the intermembrane space; (3) matrix proteins reach their destination through the TIM23 channel; (4) for inner membrane proteins there are three pathways, (a) insertion by the TIM22 complex, (b) lateral integration after arrest at the TIM23 complex, and (c) import into the matrix via TIM23 followed by export to the inner membrane (see Section 4.2 for more information on the export to the inner membrane). After translocation, mitochondrial targeting sequences are removed proteolytically and the proteins fold into their functional structures.

Two syndromes have been related to defects in mitochondrial import. Mutations in the gene for the translocase subunit TIMM8A (or DDP1) have been reported to result in the deafness dystonia syndrome or Mohr-Tranebjaerg syndrome (MTS) [73, 74]. TIMM8A is part of a small alternative TIM complex that is involved in the import of TIMM23, an essential constituent of the TIM23 complex, and a few other proteins [71]. Remarkably, no impairment of the OXPHOS system has been observed [73, 75]. The exact mechanism by which *TIMM8A* mutations affect mitochondrial function remains to be clarified. Dilated cardiomyopathy with ataxia (DCMA) is caused by a mutation in *DNAJC19*, which is thought to be a homolog of yeast Tim14 [76]. Tim14 is an essential component of the TIM23 complex [77], suggesting that the underlying disease mechanism is defective import of nDNA-encoded proteins into the mitochondrion. However, this has not been verified yet.

3. Mitochondrial Translation

Although most of the proteins present in mitochondria are encoded by the nDNA, a few are encoded by the mtDNA and are synthesized by the separate mitochondrial translation system. The human mitochondrial genome codes for 22 tRNAs, 2 rRNAs and 13 polypeptide subunits of the enzyme complexes I, III, IV, and V [26]. Whereas the components and mechanisms of translation are well characterized for bacterial and eukaryotic cytoplasmic systems, far less is known about mitochondrial protein synthesis due to the lack of a proper *in vitro* mitochondrial translation system. For

a review on mammalian mitochondrial protein synthesis, insertion and disorders associated with these processes see Pérez-Martínez et al. [78].

The mitochondrial translation more closely resembles its prokaryotic than its eukaryotic cytoplasmic counterpart. However, the protein-synthesizing system of mitochondria has a number of interesting characteristics not observed in prokaryotes or the eukaryotic cell cytoplasm. First of all, mitochondria use a genetic code that has several distinct differences from the universal code [79]. For example, human mitochondria use the universal arginine codons AGG and AGA, in addition to UAA and UAG, for termination. Furthermore, UGA serves as a codon for tryptophan rather than as a stop codon. Additionally, AUA has been reassigned to Met rather than serving as an Ile codon. Secondly, also the mitochondrial mRNAs have unusual features: they contain no or very few 5' untranslated nucleotides [80], are uncapped [81], and contain a poly(A) tail that immediately follows or even forms part of the stop codon [55]. The small subunit of mitochondrial ribosomes (mitoribosomes) appears to bind these mRNAs tightly in a sequence-independent manner and in the absence of initiation factors or initiation tRNA [82], unlike the prokaryotic [83] and eukaryotic cytoplasmic [84] systems. Thirdly, mitochondria use a simplified decoding mechanism that allows translation of all codons with only 22 tRNAs instead of the 31 predicted by Crick's wobble hypothesis [26, 85]. Fourthly, mammalian mitochondria use a single tRNA^{Met} for both the initiation and elongation phases (depending on the presence or absence of a formyl group, resp.), whereas not only in the prokaryotic and eukaryotic cytoplasmic translation systems but also in the mitochondria of most lower eukaryotes two specialized tRNA^{Met} species exist [86].

In this section, we will cover in subsequent paragraphs the components of the protein synthesis machinery, the translation process steps, its regulation, and additional roles of mitochondrial translation proteins outside the translation process.

3.1. The Mitochondrial Translation Machinery. The basic mitochondrial translation machinery comprises mtDNA-encoded rRNAs and tRNAs as well as many proteins coded for by the nuclear genome: (1) initiation, elongation and termination translation factors; (2) mitochondrial ribosomal proteins (MRPs); (3) mitochondrial aminoacyl-tRNA synthetases and methionyl-tRNA transformylase. These components will be described in more detail successively.

First of all, the translation factors. The exact functions of the mitochondrial translation factors will be discussed in Section 3.2. Bacterial translation initiation involves three factors: IF1, IF2, and IF3. Whereas IF1 and IF2 are considered to be universal and essential initiation factors, IF3 orthologs have not been found in archaea or the cytoplasm of eukaryotes [87, 88]. Surprisingly, the mitochondrial translation machinery consists of two initiation factors orthologous to prokaryotic IF2 [89] and IF3 [90] and despite extensive searches, no IF1 ortholog has been detected [91]. Recently, mitochondrial IF2 (mtIF2) was demonstrated to perform functions of both bacterial IF1 and IF2; a conserved 37 amino

acid insertion in mtIF2 seems to have assumed the role of IF1, facilitating the bond between mtIF2 and the mitoribosome and the formation of the initiation complex [92]. All three prokaryotic elongation factors have also been found in human mitochondria: mtEFTu, mtEFTs, and mtEFG [93–95]. In contrast to most bacteria, which have merely one EFG protein that acts during both the elongation and termination phases of the translation process, mitochondria contain two EFG homologs, mtEFG1 and mtEFG2 [93], that are 35% identical [91]. The importance of mtEFG1 for mitochondrial protein synthesis has been demonstrated by mtEFG1 defects in patients with a mitochondrial disorder [15, 22, 25] and its translocation activity was shown in vitro [96]. Even though expression levels of mtEFG2 are greatest in skeletal muscle, heart and liver [93], three tissues with high metabolic energy rates, the functional significance of mtEFG2 for mitochondrial translation is not entirely clear. Notably, deletion of the mtEFG2 ortholog in yeast (*MEF2*) does not lead to impaired mitochondrial protein synthesis and respiratory defects, as is the case for *MEF1*, the mtEFG1 yeast ortholog [97]. Moreover, complementation of mtEFG1 defects through overexpression of mtEFG2 could not be attained [15, 25], indicating that mtEFG2 might not play a role in the translocation step of mitochondrial translation. This was recently confirmed by Tsuboi et al., who demonstrated that mtEFG1 specifically catalyzes translocation, whereas mtEFG2 has an essential function in ribosome recycling and lacks translocation activity [98]. Thus the dual role of prokaryotic EFG is distributed between mtEFG1 and mtEFG2. Bacteria contain four factors responsible for translation termination: the three release factors RF1–3 and the ribosome recycling factor RRF [99]. The release factors are divided into two classes, with class I factors (RF1 and RF2) promoting codon-specific hydrolysis of peptidyl-tRNA and class II factors (RF3) lacking specificity but stimulating the activity of class I factors and their dissociation from the ribosome. Bacteria utilize three stop codons; both class I release factors recognize UAA, whereas UAG and UGA are decoded only by RF1 or RF2, respectively. In the eukaryotic cytosol, two release factors, RF1 and RF3 orthologs, are required for the termination step with just one class I factor recognizing all three stop codons [100]. A factor equivalent to bacterial RRF appears to be absent. The termination process in mitochondria, on the other hand, has not yet been fully elucidated. Two release factors, mtRF1 and mtRF1a (or HMRF1L), and a recycling factor (mtRRF) have been identified and partly characterized [101–104]. Being involved in ribosome recycling instead of the elongation phase, mtEFG2 should be added to this list and be renamed mtRRF2 [96]. MtRF1 was proposed to be a member of the class I release factors based on bioinformatic analyses [103], but recently this factor failed to exhibit release factor activity in vitro and in vivo [101, 102]. Nonetheless, the newly identified release factor mtRF1a was shown to terminate translation at UAA and UAG codons, analogous to bacterial RF1. Thus the question whether a mitochondrial release factor exists that recognizes the other two mitochondrial stop codons, AGG and AGA, which are found in just two of the mitochondrial transcripts, remains

unresolved. The fact that release activity was not observed for mtRF1 could be attributed to the use of bacterial and yeast systems that naturally do not terminate with these codons [102]. Therefore, the possibility remains that mtRF1 is indeed a mitochondrial release factor. Alternatively, AGA and AGG might not be used as stop codons since there is no experimental data supporting this and remarkably, in rat and mouse mitochondria the codons AGA and AGG are unassigned and UAA appears to be the single stop codon utilized [105, 106]. The terminal AGA and AGG codons could be edited posttranscriptionally, creating UAG stop codons, which could then be decoded by mtRF1a [101]. Whether mitochondria contain a class II factor equivalent to bacterial RF3 is unclear.

Secondly, the mitoribosomes that are made up of rRNAs and MRPs and comprise two subunits, the small (SSU or 28S) and the large (LSU or 39S) subunit. The human mitoribosome consists of 2 rRNAs (12S and 16S) and around 81 MRPs [107]. Mammalian mitoribosomes differ markedly from bacterial, cytosolic and even from other mitochondrial ribosomes [108]. They lack nearly half the rRNA present in bacterial ribosomes, resulting in a sedimentation coefficient of 55S compared with 70S in bacteria. Nevertheless, mitoribosomes contain a correspondingly higher protein content due to enlargement of proteins and recruitment of numerous extra proteins, causing a greater molecular mass and size than bacterial ribosomes. Most of these enlarged and supernumerary proteins do not seem to compensate for the missing rRNA segments since they occupy new positions in the mitoribosome [109], suggesting that they perform mitochondria-specific functions.

Third, the mitochondrial tRNAs. In general, human mitochondrial tRNAs deviate from the canonical tRNAs, but still fold into mostly classical cloverleaf secondary structures and presumably also into L-shaped tertiary structures [110]. Mitochondrial tRNAs are shorter than bacterial or eukaryotic cytoplasmic tRNAs, have large variations in the size of the D- and T-loops, and lack multiple conserved nucleotides that are involved in classical tertiary interactions creating the L-shape, which possibly results in a weaker tertiary structure. Post-transcriptional base modification appears to be more important for the proper tertiary structure and functioning of mitochondrial tRNAs compared with cytosolic tRNAs [111]. Certain mitochondrial tRNAs will consequently be completely non-functional when they lack the post-transcriptional modification resulting in an aberrant structure [112]. Furthermore, modifications can improve tRNA specificity and its recognition by mRNA codons and to a lesser extent by aminoacyl-tRNA synthetases [113, 114]. In total, 19 mitochondrial aminoacyl-tRNA synthetases have been identified, of which two are encoded by the same gene as the cytosolic enzyme [115]. Only the gene for mitochondrial glutamyl-tRNA synthetase has not been found yet. After aminoacylation, the tRNA^{Met} needs to be formylated by methionyl-tRNA transformylase to initiate mitochondrial translation.

Although the core components of the mitochondrial translation machinery have been identified, many more factors are likely to be involved, directly or indirectly, and

have yet to be discovered. Recently, Davies et al. showed that pentatricopeptide repeat domain protein 3 (PTCD3) associates with the mitoribosomal SSU and is necessary for mitochondrial protein synthesis [116]. The precise function of PTCD3 remains to be clarified, however.

3.2. The Mitochondrial Translation Process. The basic model of protein synthesis is derived from studies in bacteria (see [87, 99, 117] for reviews on the processes involved in protein synthesis). Our understanding of the mechanisms of mitochondrial translation is based on this model and additional studies in mitochondria.

Protein synthesis is divided into three phases: initiation, elongation and termination. The exact starting mechanism of the translation process in mitochondria is poorly understood. Due to the unusual characteristics of mitochondrial mRNAs, neither the Shine-Dalgarno sequence observed in prokaryotes nor the 7-methylguanylate cap structure found in the eukaryotic cell cytoplasm can facilitate ribosome binding and direct the ribosome to the start codon. It is thought that the mRNA entry gate on the SSU of the mitoribosome has evolved in such way that it recognizes the unique mitochondrial mRNAs with their unstructured 5' sequences [109, 118]. Many questions remain concerning the precise sequence of events during the initiation phase in mammalian mitochondria. In the current model, mitochondrial translation factor mtIF3 catalyzes the dissociation of the mitoribosome into its two component subunits (Figure 2, step 1), which may be an active rather than a passive process, thereby permitting the assembly of the initiation complex while preventing premature binding of the LSU [90, 119]. Possibly, complete subunit dissociation is not essential for initiation of translation, however, the subunit interface must become accessible for fMet-tRNA^{Met} and mRNA binding. It has been postulated that the first step in initiation complex formation is sequence-independent binding of mRNA to the SSU (Figure 2, step 2) [82, 120]. MtIF3 is thought to assist the mRNA to bind the SSU so that the start codon (AUG) is correctly positioned at the peptidyl (P) site of the mitoribosome. Both fMet-tRNA and mtIF2 can bind weakly to the SSU in the absence of mRNA and mtIF3 is hypothesized to prevent or correct the premature binding of these components [119]. The binding of fMet-tRNA^{Met} to the SSU requires mtIF2, which is markedly enhanced by GTP (Figure 2, step 3) [121, 122]. Recombining of the LSU with the SSU (Figure 2, step 4) probably stimulates the dissociation of mtIF3 (Figure 2, step 5) [123]. Additionally, GTP hydrolysis on mtIF2 is triggered by the LSU, leading to its release from the complex (Figure 2, step 6). The initiation phase is now complete and translation can proceed with the elongation phase.

The basic steps in the elongation phase are the same in bacteria and mitochondria, however, the equilibrium dissociation constants for interactions between mtEFTu and its ligands differ considerably between the prokaryotic and mitochondrial systems [124, 125]. The relative ratios of the elongation factors are important for efficient translation [21, 25, 126]. These ratios differ between tissues and can be adapted in response to dysfunction of one of the elongation

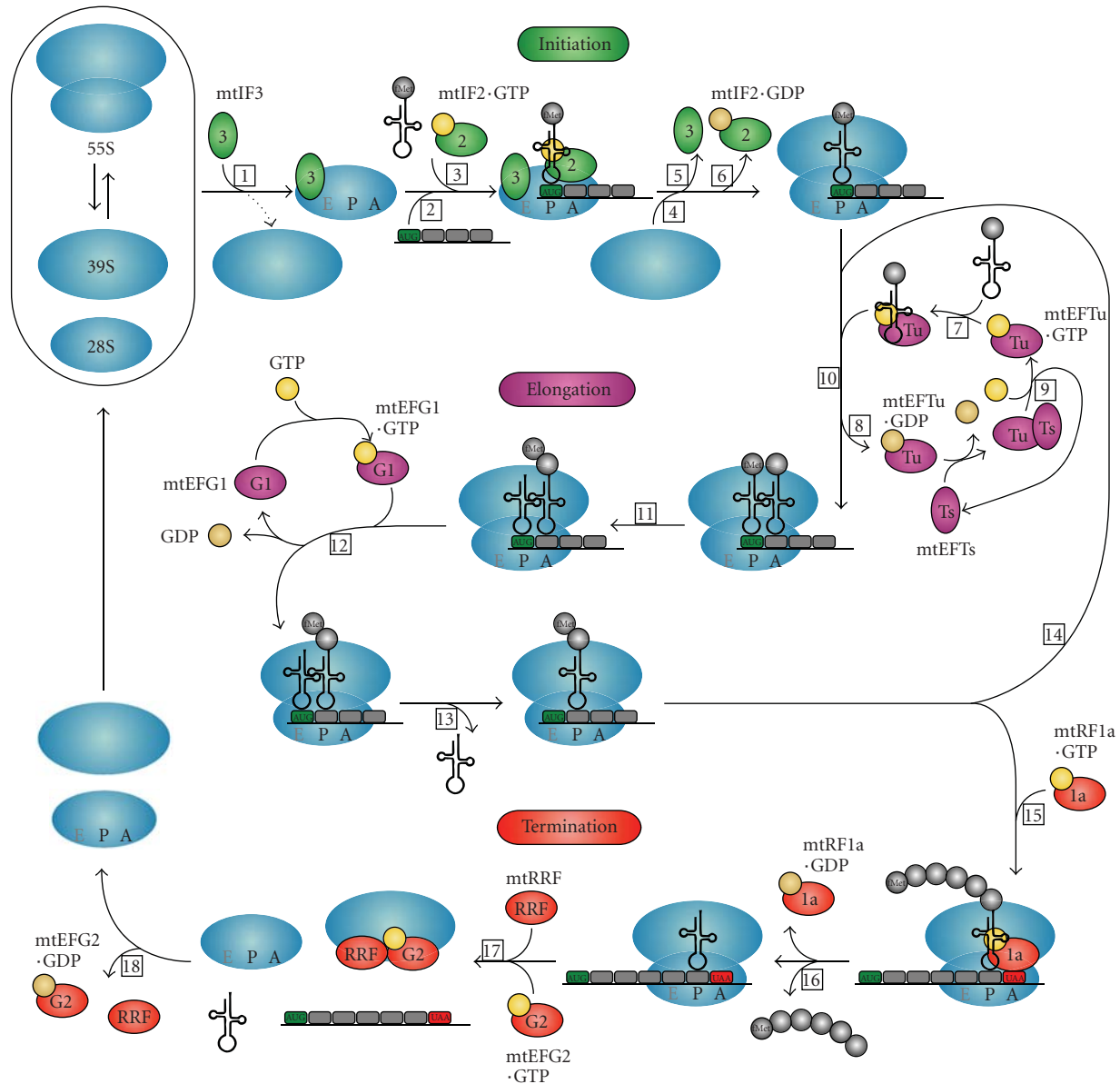


FIGURE 2: Diagram of human mitochondrial protein synthesis. The three phases of mitochondrial translation—initiation, elongation and termination—and all translation factors involved are represented in this figure. See Section 3.2 in the text for a detailed description of all steps (numbered in boxes) of the mitochondrial translation process. Initiation, elongation and termination factors are represented by green, purple and red ovals, respectively. GTP and GDP are shown in yellow and beige circles, respectively.

factors [25]. Elongation factor mtEFTu forms a ternary complex with GTP and an aminoacylated tRNA (Figure 2, step 7). It is proposed to be critical for translational accuracy through surveillance of aminoacyl-tRNAs for misacylation [127]. MtEFTu protects the tRNA from hydrolysis and, after a proofreading step, carries it to the mitoribosomal aminoacyl or acceptor (A) site for the decoding of mRNA by codon-anticodon interactions on the SSU (Figure 2, step 10). When the codon-anticodon recognition occurs, GTP hydrolysis on mtEFTu is stimulated by the mitoribosome, resulting in the release of mtEFTu-GDP (Figure 2, step 8). The nucleotide exchange protein mtEFTs converts mtEFTu-GDP in active mtEFTu-GTP (Figure 2, step 9). Following the release from

mtEFTu, the 3' end of the aminoacyl-tRNA moves into the peptidyl transferase center of the LSU where peptide bond formation is catalyzed, adding one amino acid to the growing peptide (Figure 2, step 11). The elongation factor mtEFG1 with bound GTP catalyzes the translocation step by conformational changes in both mtEFG1 and the mitoribosome, during which the A and P site tRNAs move to the P and exit (E) sites of the mitoribosome and mRNA is advanced by one codon (Figure 2, step 12). Subsequently, the tRNA leaves the mitoribosome via the E site (Figure 2, step 13) and a new elongation cycle can start (Figure 2, step 14). Whether the mitoribosome contains an actual E site is uncertain. The bovine mitoribosomal structure and a

comparative analysis of ribosome sequences revealed that the mitoribosomal E site deviates substantially from the prokaryotic and eukaryotic cytosolic situations [109, 128, 129]. Based on these findings, the E site has been suggested to be very weak or even absent in the mitoribosome. Moreover, the mitoribosomal polypeptide exit tunnel is markedly different, allowing premature exposure of the nascent polypeptide to the mitochondrial matrix or membrane before reaching the conventional exit site [109]. Whether all or some nascent polypeptide chains emerge prematurely from the peculiar mitoribosomal exit tunnel is currently unknown.

The third and last step in protein synthesis, termination, begins when a stop codon (UAA, UAG, AGA or AGG) is encountered in the A site. A mitochondrial release factor, mtRF1a or possibly also mtRF1 or an as yet unidentified protein, recognizes the stop codon (Figure 2, step 15) and causes the protein that is attached to the last tRNA molecule in the P site to be released (Figure 2, step 16). The ester bond between the tRNA and the nascent polypeptide is hydrolyzed, presumably by the peptidyl transferase center on the LSU triggered by the release factor, and this process is catalyzed by GTP. After release of the newly synthesized protein, mtRRF and mtEFG2·GTP together enable the mitoribosomal subunits, tRNA and mRNA to dissociate from each other (Figure 2, step 17), making the components available for a new round of protein synthesis. GTP hydrolysis is required for the release of mtRRF and mtEFG2·GDP from the LSU (Figure 2, step 18) [96].

3.3. Regulation of Mitochondrial Translation. In yeast, nuclear-encoded, gene-specific activation factors are required for mitochondrial translation initiation [130, 131]. Currently, translational activation factors have been found for (nearly) all eight yeast mtDNA-encoded proteins and synthesis of some proteins, for example, Cox3, depends on multiple activation factors [130–132]. These activators bind to the 5′ untranslated leader (5′-UTL) sequences of the mRNA, probably to assist in positioning the mitoribosomes over the initiation codon. All translational activator proteins studied so far are integral membrane proteins or bound to the mitochondrial inner membrane, suggesting that they are also involved in tethering mitochondrial translation to the inner membrane. This way they can promote co-translational insertion of newly synthesized proteins and subsequent assembly into the OXPHOS complexes. Thus the yeast mitochondrial translational activators regulate not only the levels of mitochondrially synthesized gene products, but also the location of mitochondrial translation.

The mechanisms of human mitochondrial translation regulation are poorly understood. Human mitochondrial mRNAs lack 5′-UTL sequences and until recently no clear evidence was found for the existence of mRNA-specific translation activators, which suggests that modulation of mitochondrial protein synthesis in humans involves other strategies than in yeast [133]. Genome-wide linkage analysis and chromosome transfer in a patient presenting with Leigh syndrome due to an isolated complex IV deficiency resulted in the identification of a human translational activator of the complex IV subunit COXI: CCDC44 or TACO1

[134]. A homozygous base insertion, creating a premature stop codon, led to severely decreased levels of TACO1 in patient fibroblasts. Consequently, only a small amount of COXI was synthesized despite normal concentrations of the COXI transcript, compromising complex IV assembly and activity. Remarkably, deletion of the TACO1 ortholog in yeast produced no respiration or mitochondrial translation defect. In contrast to the human situation, TACO1 is apparently not essential for respiration in yeast.

Furthermore, another potential translational activator for COXI has been identified in humans: a member of the pentatricopeptide (PPR) family, leucine-rich PPR-motif containing protein (LRPPRC, also known as LRP130). The PPR motif has been found in proteins that interact with RNA, such as POLRMT, which contains two PPR motifs in the amino-terminal domain (ATD) [135]. LRPPRC has been postulated to be a homolog of Pet309 [136], the yeast mitochondrial translational activator for COXI [137]. Mutations in *LRPPRC* lead to the neurodegenerative disorder Leigh Syndrome French-Canadian type (LSFC), with a deficiency of complex IV of the OXPHOS system [136]. LRPPRC appears to play a role in the translation and/or stability of COXI and COXIII mRNAs, similar to yeast Pet309 [138]. In addition to its role as translational activator, Pet309 might be involved in coupling mitochondrial transcription to translation through interaction with Nam1 [139], a protein that is postulated to stabilize and direct mRNAs to the mitochondrial inner membrane for translation [140] and that binds to the ATD of yeast mtRNA polymerase [135]. LRPPRC has been suggested to function together with heterogeneous nuclear ribonucleoprotein K (hnRNP K) and POLRMT in coupling the mitochondrial transcription and translation machineries in a manner analogous to the yeast system [141]. However, the situation is more complex than depicted here, encompassing additional proteins for which homology between yeast and human has not been identified yet. Moreover, LRPPRC binds not only mitochondrial but also nuclear mRNAs, indicating that it could be involved in coordinating nuclear and mitochondrial gene expression [142].

Nolden et al. proposed a negative-feedback loop mechanism for regulation of mitochondrial translation [143]. The ATP-dependent m-AAA protease plays an important role in quality control of mitochondrial inner membrane proteins. One of the substrates of this enzyme is the ribosomal protein MRPL32. Processing of MRPL32 by the m-AAA protease results in a tight association of MRPL32 with the inner membrane and allows completion of mitoribosome assembly in close proximity to the inner membrane. Maturation of MRPL32 seems to be required for mitochondrial translation since synthesis of mtDNA-encoded proteins was substantially impaired in cells lacking the m-AAA protease. Regulation of translation via the m-AAA protease could for instance take place when nuclear and mitochondrial gene expression are unbalanced. Excess respiratory subunits and other nonnative substrates of the m-AAA protease may then accumulate and compete with MRPL32 for binding to the protease. This will hamper MRPL32 processing, ribosome assembly, and finally mitochondrial translation. Accordingly,

the amount of respiratory subunits available to the m-AAA protease decreases and MRPL32 processing increases again. The importance of this regulation process has been demonstrated by loss-of-function mutations in paraplegin, a subunit of the human m-AAA protease, which result in the neurodegenerative disorder hereditary spastic paraplegia [144].

Possibly, TFB1M and TFB2M are involved in a retrograde pathway regulating mitochondrial biogenesis and function [145, 146]. Overexpression of *TFB2M* resulted in increased TFB1M levels and consequently an increase in mitochondrial biogenesis. In addition to their transcriptional stimulatory activity, TFB1M and TFB2M have rRNA methyltransferase activity. Thus these factors are indirectly involved in mitochondrial protein synthesis via their ability to methylate the mitochondrial 12S rRNA, which is important for mitoribosome activity. TFB1M has been identified as a nuclear modifier of the 1555A>G mutation in the 12S rRNA gene that causes nonsyndromic or aminoglycoside antibiotic-induced deafness [147]. Presumably, altered or lack of methylation due to malfunctioning TFB1M can diminish the effect of the 1555A>G mutation on mitoribosome conformation. In vivo studies in mice revealed that TFB1M is an essential rRNA methyltransferase, needed for stability of the mitoribosomal SSU, that does not directly modulate transcription, whereas TFB2M is suggested to have transcriptional activation as its primary function [148]. Therefore, differential expression of these two factors could modulate not only transcription, but also replication (via the transcription factor activity) and translation (via the rRNA methyltransferase activity), and in this manner ensure a balance between the amounts of mitochondrial transcripts and fully assembled mitoribosomes [145, 148].

Mitochondria are under general nuclear control through transcription factors, such as nuclear respiratory factors 1 and 2 (NRF-1 and -2) [149]. These factors coordinate the expression of the nuclear and mitochondrial gene products required for oxidative phosphorylation and other essential mitochondrial functions. They act directly on nuclear genes coding for OXPHOS subunits as well as various nuclear genes encoding proteins involved in mtDNA replication, mitochondrial transcription or translation, by which they exert indirect control over expression of mitochondrial genes. Transcription factor CREB (cAMP response element-binding protein) promotes transcription of mitochondrial (in addition to nuclear) genes after its import into the mitochondrion directly [150].

3.4. Functions of the Mitochondrial Translation Machinery beyond Translation. Initiation factor mtIF2 might be involved in mitochondrial mRNA degradation and apoptosis. The endoribonuclease RNase L is an important player in apoptosis induced by interferons (IFNs) [151]. After binding its IFN-induced activator, RNase L degrades single-stranded RNAs, leading to inhibition of protein synthesis. RNase L was shown to interact with mtIF2 and thereby modulate the stability of mitochondrial mRNAs, which appears to be essential for IFN α -induced apoptosis [152]. RNase L is brought into association with the mitochondrial mRNA

during their translation through interaction with mtIF2. In the presence of IFN α , RNase L becomes activated and degrades mRNA, which can eventually result in apoptosis. An excess level of mtIF2 could hold RNase L away from the mRNAs, preventing their degradation and thus also inhibiting IFN α -induced apoptosis.

In addition to its function in the elongation phase of the mitochondrial translation, mtEFTu has been reported to act as a chaperone [153]. It plays a role in protein quality control in mitochondria, as has been found for its cytosolic and prokaryotic counterparts. MtEFTu interacts with unfolded proteins, especially with misfolded, newly synthesized polypeptides, and is hypothesized to recruit these proteins to a mitochondrial protease complex for their degradation. This protease complex presumably consists of the homologs of the bacterial GroEL/ES (Hsp60 class) chaperone and ClpA/ClpP protease systems, with which EFTu can interact via the heat shock protein Hsp31 [154].

Recently, human mitochondrial ribosomal protein MRPL12 was demonstrated to bind to POLRMT, which enhances transcription [155]. Free MRPL12, that is, MRPL12 not incorporated in the mitoribosome, appears to interact with POLRMT and consequently might coordinate the rate of mitochondrial transcription with the rate of mitoribosomal biogenesis. When the import rate of MRPs is exceeding the rate of mtDNA-encoded rRNA expression, free MRPL12 will accumulate and associate with POLRMT. Subsequently, the rate of mtDNA transcription increases, which rebalances the system.

Furthermore mitochondrial ribosomal proteins MRPS29 and MRPS30 seem to be bifunctional proteins [156]. These two proteins are the proapoptotic proteins death-associated protein 3 (DAP3) and programmed cell death protein 9 (PDCD9 or p52), respectively. Whether MRPS29 and/or MRPS30 are released from the mitoribosome and exported to the cytosol during apoptosis or whether they carry out their proapoptotic role while still associated with the mitoribosome is unknown. Possibly, inner membrane-associated mitoribosomes affect the mitochondrial permeability transition pores via MRPS29 and MRPS30 and thereby induce apoptosis.

4. Posttranslational Processes Required for Functional OXPHOS Complexes

After translation has taken place, the mtDNA-encoded and imported nDNA-encoded proteins need to be incorporated into the inner membrane to form a functional OXPHOS system. Mitochondria contain chaperones, proteases and assembly factors for particular OXPHOS complexes to aid in this process.

4.1. Quality Control by Chaperones and Proteases. The entire chaperone system represents a mechanism for quality control that determines the fate of all mitochondrial proteins: proteolytic degradation or folding and assembly. Chaperones from the Hsp60 and Hsp70 class bind to and stabilize (partially) unfolded or newly synthesized or imported proteins, thereby preventing their aggregation and facilitating their proper

folding [157]. Hsp100/Clp family chaperones are involved in the re-solubilization of protein aggregates and unfolding of misfolded proteins, resulting in either refolding by other chaperones or degradation by proteases. Excess or non-native proteins are degraded into peptides by ATP-dependent proteases and subsequently into amino acids by oligopeptidases [158]. Mammalian mitochondria have three major ATP-dependent proteases: Lon, Clp-like, and other AAA proteases. Both Lon protease and proteins from the Clp family are located in the matrix and contain proteolytic as well as chaperone activities. Two membrane-bound ATP-dependent AAA-proteases, active on the intermembrane space side (i-AAA) or on the matrix side (m-AAA), are responsible for quality control of inner membrane proteins. Additionally, as mentioned in Section 3.3, they regulate mitochondrial biogenesis through selective processing of mitochondrial proteins, for example, MRPL32. The significance of these AAA proteases is demonstrated by the severe defects due to dysfunction of one of the AAA proteases found in several species. The prohibitin complex, consisting of Phb1 and Phb2 and also located in the inner membrane, is thought to act as a chaperone that stabilizes mitochondrially synthesized OXPHOS subunits against degradation by AAA proteases [159, 160]. While the exact functions of the prohibitin complex remain poorly understood, its role in mitochondrial biogenesis and metabolism has been corroborated by numerous findings, such as different prohibitin expression levels depending on metabolic demand and lack of prohibitin leading to reduced mitochondrial membrane potential and instability of mtDNA-encoded OXPHOS subunits [160].

4.2. Protein Insertion into the Inner Membrane. A subset of mitochondrial inner membrane proteins that are synthesized in the cytosol are imported into the mitochondrial matrix prior to their export to the inner membrane; all other nuclear-encoded proteins are integrated directly into the inner membrane during import into the mitochondrion (also see Section 2.4). All proteins synthesized by the human mitochondrial translation system are destined for the inner membrane and become inserted through the same export machinery as used by nDNA-encoded proteins. At least half of the mitoribosomes are associated with the inner membrane [161] and it has been proposed that only membrane-bound mitoribosomes are translationally active [143]. It appears that mitochondrial gene products become inserted into the inner membrane as they are undergoing synthesis on mitoribosomes, that is, in a co-translational fashion [162–166]. However, the relative contributions of co- and post-translational insertion and the exact mechanisms are unknown. The inner membrane protein Oxa1 plays an important role in insertion of both mitochondrial- and nuclear-encoded proteins from the mitochondrial matrix into the inner membrane [167, 168]. Recently, the interaction of Oxa1 with the mitoribosome was concluded to involve at least the two yeast LSU proteins Mrp20 and Mrpl40, orthologs of bacterial ribosomal proteins L23 and L24 respectively, which are located close to the polypeptide exit tunnel [169, 170]. Furthermore, mitoribosomal protein MRPL45 was postulated to function in the

co-translational insertion of mtDNA-encoded proteins into the inner membrane [107]. The yeast ortholog of MRPL45, Mba1, associates with the inner membrane and is involved in protein insertion into the membrane in a concerted action with Oxa1, possibly by positioning the mitoribosomal exit tunnel at the right location for insertion [164, 171]. Nonetheless, mitoribosomes remain partially anchored to the mitochondrial inner membrane in absence of MRPL45 and Oxa1, indicating that additional factors are involved in the membrane association [164]. One of these factors could be LETM1, leucine zipper EF-hand-containing transmembrane protein 1, located in the chromosomal region that is deleted in patients suffering from Wolf-Hirschhorn syndrome [172]. It is the homolog of yeast inner membrane protein Mdm38, which has been proposed to function in an Oxa1-independent transport pathway across the inner membrane [173]. LETM1 was found to associate with MRPL36 and could thereby anchor the mitoribosome to the inner membrane [174]. Overexpression of *LETM1* resulted in inhibition of mitochondrial biogenesis and ATP production. Conversely, *LETM1* knockdown caused mitochondrial swelling, loss of tubular networks and disassembly of OXPHOS complexes I, III, and IV [175]. Much of the exact functions of LETM1 remain to be clarified, however, such as its role in cell viability and tumorigenesis, in addition to its potential interaction with the mitoribosome [174–176].

Coupling mitochondrial protein synthesis to insertion of the protein into the inner membrane will be advantageous for the efficient formation of OXPHOS complexes. As mentioned previously, transcription seems to be coupled to the translation system as well. A similar process called transertion, the coupled transcription-translation-insertion of proteins into and through membranes, is found in bacteria [177, 178]. Linking of these processes generates hyperstructures, which are assemblies of different types of (macro)molecules that form an organizational level intermediate between genes/proteins and whole cells [179]. Thus the mtDNA, transcription and translation machineries may be dynamically connected to the inner membrane into hyperstructures at assembly sites for the OXPHOS system.

4.3. Assembly of OXPHOS Complexes. Each OXPHOS complex has a specific assembly pathway, which involves chaperones that are not part of the functional complex but are implicated in its formation: the assembly factors. Up till now, 22 assembly factors have been identified and the list is still growing (see [180] for an overview, including defects in assembly): eleven for complex I (NDUFA12L or B17.2L [181], NDUFAF1 or CIA30 [182], NDUFAF2 [181, 183], NDUFAF3 or C3ORF60 [184], NDUFAF4 or C6ORF66 [185], Ecsit [186], C8ORF38 [187], C20ORF7 [188, 189], and possibly the CIA84 ortholog PTCD1 [190], AIF [191] and IND1 [192]), one for complex II (SDHAF1 [193]), one for complex III (BCS1L [194]), six for complex IV (SURF1, COX10, COX15, SCO1, SCO2, and supposedly LRPPRC [138, 195]), and four for complex V (ATP11, ATP12 [196], and possibly ATP23 [197] and OXA1L [198]). Naturally, structural proteins can have additional functions in the assembly of the particular OXPHOS complex.

The organization of the OXPHOS system is more intricate than separately assembled complexes that are arranged in sequence in the inner mitochondrial membrane. Two models for the organization of the mitochondrial respiratory chain have been proposed: (1) the “fluid-state” or “random collision” model, which has been the preferred description, where all OXPHOS complexes diffuse individually in the membrane and electron transfer depends on the random collision of the complexes and electron carriers; (2) the “solid-state” model, which was proposed over 50 years ago and has recently received more attention, where the complexes together form large supramolecular structures termed supercomplexes or respirasomes [199, 200]. The most plausible scenario, however, is a combination of these two models: the “plasticity” model [201]. In this model, single complexes (“fluid-state” model) and different types of supercomplexes (“solid-state” model) coexist in the inner membrane. Complex I, for instance, is mainly found in association with complex III in various supercomplexes that additionally contain the electron carriers coenzyme Q and cytochrome *c*, complex IV, and sometimes complex II or V, and are able to respire. On the other hand, most of the complexes II and IV are present as individual entities. How the supercomplexes are assembled is currently not known, but the significance of this arrangement for the stability of the different complexes is certain. This is emphasized by the finding that primary defects in, for example, complex III can lead to secondary instability of another complex, such as complex I, through improper supercomplex formation [202]. More often, though, a mutation results merely in an isolated deficiency of the particular complex. Recently, defects in Tafazzin, a protein required for the metabolism of the inner membrane phospholipid cardiolipin, was shown to affect complex I/III₂/IV supercomplex stability [203]. The cardiolipin deficiency resulted in weakened interactions between complexes I, III, and IV, unstable supercomplexes, and decreased levels and activities of the complexes themselves, ultimately causing Barth syndrome. Thus combined OXPHOS deficiencies can also be caused by defects in the assembly of supercomplexes.

For proper assembly of the OXPHOS system, mitochondrial fusion and fission events are crucial since they control mitochondrial morphology and thereby also mitochondrial function. Disruption of fusion or fission primarily affects two key functions of mitochondria: respiration and regulation of apoptosis [204, 205]. Defects in fusion proteins MFN2 (mitofusin 2) and OPA1 (optic atrophy 1), for instance, cause a reduction in membrane potential and OXPHOS enzyme activities and are associated with the neurodegenerative diseases Charcot-Marie-Tooth type 2A and dominant optic atrophy, respectively. Additionally, down-regulating the expression of DNML1 (dynamin 1-like, also called DRP1 or DLP1), a protein involved in mitochondrial and peroxisomal fission, led to loss of mtDNA and a decrease in mitochondrial respiration [206]. In a patient with a DNML1 deficiency, however, no mitochondrial morphology abnormalities or impairment in respiratory function could be detected, despite elevated lactate levels [206, 207].

5. Mutations That Impair Mitochondrial Translation and Result in Mitochondrial Disorders

Given the multitude of proteins and complexity of the processes that are required for a properly functioning OXPHOS system, it is not surprising that in many patients with a mitochondrial disorder the underlying molecular genetic defect has not yet been identified. Nonetheless, since the discovery of the first mtDNA mutations associated with mitochondrial disorders in 1988 [208, 209], numerous mutations in mtDNA and nDNA have been reported and the list is still expanding (for an overview see e.g., [43]). In each of the previous sections we have briefly mentioned the relevant genes implicated in mitochondrial disorders, with the exception of genes of the mitochondrial translation process. Here we will discuss in more detail the mutations found in this class of genes. Table 1 gives an overview of the genes implicated in combined OXPHOS deficiencies. These genes are also depicted in Figure 1.

5.1. MtDNA Mutations. As already stated in the introduction, the majority of mutations associated with combined OXPHOS deficiencies and a mitochondrial translation defect are located in the mitochondrial genome. Approximately 150 mutations, of which a large percentage awaits proper determination of their pathological significance (see [210] for a scoring system), have been reported in mitochondrial tRNA genes and a few in rRNA genes [12]. It is beyond the scope of this review to discuss these mutations in detail; overviews of mitochondrial tRNA mutations and their molecular and clinical consequences have been published before [210–212].

The tRNA^{Leu(UUR)} gene forms a hotspot for pathogenic mutations with nearly 30 different mutations, but in all tRNA genes, mutations have been detected now. A pathogenic tRNA gene mutation is expected to lead to a combined OXPHOS defect through a decreased rate of mitochondrial protein synthesis. The exact complexes that show a deficiency differ for each mutation, partly depending on which tRNA is affected and the percentages of the corresponding amino acid in the different OXPHOS subunits. The pathogenic mechanisms involved in the translation defect due to a tRNA mutation are numerous and frequently multiple events are involved; potential effects are: impaired transcription termination, impaired tRNA maturation, defective post-transcriptional modification of the tRNA, effect on tRNA structure (e.g., global structural weakness or conformational alteration), decreased tRNA stability (found for all mutations investigated), reduced aminoacylation, decreased binding to translation factor mtEFTu or the mitoribosome, and disturbed codon reading [211]. However, cases are known where mitochondrial translation was not or only slightly affected despite clear impairment of the OXPHOS system (e.g., [220, 221]). Possibly, this is due to toxic effects of premature translation products generated by the absence of the correctly functioning tRNA [222]. These peptides could interfere with the assembly of the OXPHOS complexes

TABLE 1: Genes involved in the biogenesis or maintenance of multiple OXPHOS complexes and implicated in mitochondrial disorders.

Affected process	Gene	Protein (function)	References
<i>Combined OXPHOS deficiencies with normal complex II activities^a</i>			
MtDNA replication	POLG	Polymerase γ catalytic subunit	[13, 213]
	POLG2	Polymerase γ accessory subunit	[13, 214]
	C10orf2	Twinkle (mtDNA helicase)	[13]
Nucleotide synthesis and transport	DGUOK	Deoxyguanosine kinase	[13]
	TK2	Thymidine kinase 2	[13]
	TYMP	Endothelial cell growth factor 1 (thymidine phosphorylase)	[13]
	SLC25A4	Adenine nucleotide translocator 1	[13]
	SLC25A3	Solute carrier family 25 member 3 (phosphate transporter)	[43, 215] ^c
	SUCLG1	Succinate-CoA ligase α -subunit	[43, 216]
	SUCLA2	Succinate-CoA ligase β -subunit	[13, 216]
	RRM2B	Ribonucleotide reductase M2 B	[13, 217]
	MPV17	Mt inner membrane protein	[13]
	22 mitochondrial tRNA genes		[12]
	2 mitochondrial rRNA genes		[12]
Mt translation	GFM1	Mt translation elongation factor G1	[15]
	TSMF	Mt translation elongation factor Ts	[21]
	TUFM	Mt translation elongation factor Tu	[22]
	MRPS16	Mt ribosomal protein S16	[18]
	MRPS22	Mt ribosomal protein S22	[19]
	PUS1	Pseudouridine synthase 1	[14]
	TRMU	tRNA 5-methylaminomethyl-2-thiouridylate methyltransferase	[24]
	DARS2	Mt aspartyl-tRNA synthetase 2	[20] ^c
	RARS2	Mt arginyl-tRNA synthetase 2	[16]
<i>Other combined OXPHOS deficiencies^b</i>			
Mt protein import	TIMM8A	Translocase of inner mt membrane 8 homolog A (small TIM complex subunit)	[74] ^c
	DNAJC19	DnaJ homolog, subfamily C, member 19 (TIM23 complex subunit)	[76]
Mt membrane biogenesis and maintenance	TAZ	Tafazzin (cardiolipin metabolism)	[203, 218]
	OPA1	Optic atrophy 1 (mt fusion)	[205]
	MFN2	Mitofusin 2 (mt fusion)	[205]
	DNM1L	Dynamin 1-like (mt and peroxisomal fission)	[207] ^c
Mt protein processing and quality control	SPG7	Spastic paraplegia 7 or paraplegin (m-AAA protease subunit)	[144, 219]

^aBased on the function of the affected proteins, a combined complex I, III, IV and V deficiency would be expected, however, not always do all these enzyme complexes display decreased activities.

^bAll OXPHOS complexes are expected to malfunction based on the function of the affected proteins; nonetheless, large variations have been found in the exact OXPHOS complexes involved.

^cThe OXPHOS complexes showed normal activities.

or exert their toxic effect through interactions with other (non)mitochondrial components, while a quantitative deficit in mitochondrial protein synthesis cannot be detected.

The best-studied mitochondrial tRNA mutations are 3243A>G in tRNA^{Leu(UUR)} (*MT-TL1*) and 8344A>G in

tRNA^{Lys} (*MT-TK*). The 3243A>G mutation is one of the most common mutations and causes a range of clinical phenotypes, of which MELAS is the most prevalent [223]. There is controversy over the pathogenic mechanism of the 3243A>G mutation: both loss-of-function (due to poor

aminoacylation, reduced stability or lack of wobble-base U hypermodification) and gain-of-function (due to lack of the hypermodification) of the mutant tRNA have been proposed [224]. The post-transcriptional taurine modification at the anticodon wobble position is needed to restrict decoding to leucine UUR codons. Loss of this modification leads to varying degrees of mitochondrial translation malfunctioning in different cellular backgrounds through a combination of a decoding defect of UUG (and UUA) codons (loss-of-function) and amino acid misincorporation (gain-of-function) [126, 225]. Additionally, the 3243A>G mutation was shown to diminish 16S rRNA transcription termination and alter processing of the primary transcript [61, 226], but these effects are likely to contribute less to the disease etiology than the previously mentioned mechanisms. The 8344A>G mutation is associated with MERRF (myoclonic epilepsy with ragged-red fibers). It has also been reported to affect aminoacylation and taurine modification of the wobble-base U, the latter which abolishes codon-anticodon pairing on the mitoribosomes for both tRNA^{Lys} codons [225, 227]. This generates a marked decrease in mitochondrial protein synthesis that is most pronounced in proteins with a high lysine content and is believed to result from premature translation termination.

Most rRNA mutations have been reported in the 12S rRNA gene (*MT-RNR1*) and all of these are associated with nonsyndromic sensorineural hearing loss or aminoglycoside-induced deafness, with the 1555A>G mutation forming one of the most common causes [12, 228]. This mutation is located in the decoding site of the mitoribosomal SSU and results in a secondary rRNA structure that more closely resembles the corresponding region of the bacterial 16S rRNA, impairing mitochondrial protein synthesis and facilitating interaction with aminoglycoside antibiotics, which again exacerbates the translation defect. The mutation alone does not lead to disease, only in combination with modulators such as the aminoglycosides, mitochondrial haplotypes and nuclear modifier genes (e.g., *TFB1M*, as already mentioned in Section 3.3). In the 16S rRNA gene (*MT-RNR2*) merely 3 mutations have been found: 2835C>T, 3093C>G, and 3196G>A [12]. These mutations are thought to be associated with Rett syndrome, MELAS, and Alzheimer and Parkinson disease, respectively, [229–231]. Nevertheless, further investigations are necessary to determine their pathogenicity.

5.2. nDNA Mutations. Up till now, mutations in nine nuclear genes implicated in mitochondrial protein synthesis have been associated with mitochondrial disorders. The first report was a homozygous missense mutation in the tRNA modifying gene *PUS1* [14], and shortly thereafter homozygous mutations were detected in the genes for elongation factor mtEFG1 [15] and mitoribosomal protein MRPS16 [18]. Subsequently, four compound heterozygous mutations in *GFM1* (coding for mtEFG1) [22, 25] and homozygous mutations in *TUFM* (encoding mtEFTu) [22], *TFSM* (coding for mtEFTs) [21], *MRPS22* [19], *PUS1* again [17], and in the arginine tRNA synthetase gene (*RARS2*) [16] were found, bringing the total number of mutations on

12. Additionally, several compound heterozygous mutations have been reported in the gene for mitochondrial aspartyl-tRNA synthetase (*DARS2*) [20, 23]. Recently, 9 mutations were identified in the gene for another tRNA modifying gene, *TRMU* [24]. All patients harboring these mutations show combined OXPHOS deficiencies, with (near) normal complex II activities, and a clear defect in mitochondrial translation (the latter was not tested for the *MRPS22*, *RARS2*, and *DARS2* mutations). The one exception is *DARS2*: surprisingly, Blue-native PAGE as well as spectrophotometric measurements revealed normal OXPHOS enzyme activities [20]. The clinical features differ substantially between all patients and even between patients that carry the same mutation, but generally the mutations result in severe and early-fatal diseases.

As already mentioned in Section 2.3, defects in the tRNA-modifying enzymes *PUS1* and *TRMU* can result in mitochondrial disease. *PUS1* converts uridine into pseudouridine at several cytoplasmic and mitochondrial tRNA positions and thereby improves translation efficiency in the cytosol as well as the mitochondrion [17]. Thus it is not part of the translation machinery, but it is required for protein synthesis due to its function in post-transcriptional modification of tRNAs. Pseudouridylation is the most frequently found modification in tRNAs [232], however, the exact function is not entirely clear. The marked variability in the severity of the MLASA syndrome, despite the presence of an identical *PUS1* mutation, could partly be explained by the dual localization of *PUS1* [17]. A defect in *PUS1* therefore impairs both cytosolic and mitochondrial translation, resulting in corresponding clinical symptoms that can vary due to individual differences in compensation mechanisms in both cell compartments. Bykhovskaya et al. suggested that compensatory changes in transcript levels of ribosomal proteins can overcome the lack of pseudouridylation of tRNAs and that pleiotropic effects of *PUS1* on non-tRNA substrates involved in transcription and iron metabolism are a major cause of the disease phenotype [233]. Notably, complex II can be affected slightly in addition to the other OXPHOS complexes that all contain mtDNA-encoded subunits [17]. This could be a primary effect of the decrease in cytosolic translation or it could be a secondary effect of the mitochondrial translation deficit, leading to disruption of the mtDNA-dependent complexes, which can subsequently cause destabilization of the entire OXPHOS system. *TRMU* (tRNA 5-methylaminomethyl-2-thiouridylate methyltransferase) is responsible for the 2-thio modification of the wobble-base of the mitochondrial tRNA^{Lys}, tRNA^{Gln} and tRNA^{Glu}. Defects in this enzyme result in reduced steady-state levels of these three tRNAs and consequently impaired mitochondrial protein synthesis [24, 62]. The 2-thiouridylation is reported to be critical for effective codon-anticodon interaction and ribosome binding [234, 235].

Concerning the mitochondrial translation factors, defects have only been found in proteins involved in the elongation phase, in all elongation factors except for mtEFG2, which appears to function in termination instead elongation. In *GFM1*, mutations have been reported in nearly all protein domains, leading to severe hepato(encephalo)pathy

[15, 22, 25]. All mutations result in a marked global translation defect, with the strongest deficit in the three complex IV subunits and the two complex I subunits ND5 and ND6. Both subunits of complex V (ATP6 and ATP8) show normal or even increased synthesis rates, possibly caused by more efficient protein synthesis of bicistronic compared to monocistronic mRNAs, which would then also explain the near normal mitochondrial translation levels of ND4 and ND4L. This variable pattern in translation impairment was also found for a mutation in *TSMF* [21], which will be described below. Surprisingly, tissues are selectively affected by *GFM1* mutations, in spite of its ubiquitous expression, with liver being most severely affected and heart hardly showing a defect [25]. This tissue specificity appears to result from differences among tissues in the relative ratios of the elongation factors and in adaptive changes herein in response to dysfunction. For example, transcription of *TUFM* was upregulated in cardiac tissue in patients with a *GFM1* mutation and overexpression of either *TUFM* or *TSMF* in control and patient fibroblasts impaired mitochondrial translation. Overexpression of *GFM2*, on the contrary, did not have a clear effect on protein synthesis in either control or patient cells [15, 25]. Remarkably, mtEFTu or mtEFG2, but not mtEFTs or mtEFG1, can partially suppress the combined OXPHOS system defect caused by the 3243A>G mutation in tRNA^{Leu(UUR)} [126]. These observations evidence that efficient mitochondrial translation partly depends on appropriate ratios of the elongation factors. A homozygous mutation in *TUFM* was shown to be responsible for rapidly progressive encephalopathy [22]. The mutation, located in the tRNA-binding region of mtEFTu, hampers the formation of the ternary complex with GTP and an aminoacylated tRNA, resulting in a severe decrease in mitochondrial protein synthesis [22, 236]. Notably, a homozygous mutation in *TSMF* led to encephalomyopathy in one patient and hypertrophic cardiomyopathy in another [21]. This could be due to individual differences in relative abundance of the translation factors and compensatory mechanisms in the various tissues. Alternatively, as yet unknown genetic modifiers of the mitochondrial translation machinery could be involved. Steady-state levels of not only mtEFTs but also mtEFTu were reduced, and overexpression of either factor rescued the OXPHOS deficiency and translation defect. The most likely explanation for these findings is that the mutation, situated in a subdomain of mtEFTs that interacts with mtEFTu, destabilizes the mtEFTu·mtEFTs complex and promotes turnover of its components. Additional mtEFTu or mtEFTs would then stabilize the complex.

Of all 81 human MRPs, mutations have been found in merely two of them: MRPS16 and MRPS22 [18, 19]. Both defects resulted in a marked decrease in the 12S rRNA transcript level, probably caused by impaired assembly of the mitoribosomal small subunit, generating unincorporated and instable 12S rRNA. MRPS16 is evolutionary highly conserved, however, MRPS22 is only present in metazoa [107]. Recently, both proteins were shown to be important for assembly of the SSU [123]. In fibroblasts from patients

with a *MRPS16* or *MRPS22* mutation, the level of MRPS11 was significantly reduced, whereas considerable amounts of MRPS2 were present. Furthermore, MRPS16 was barely detectable in the *MRPS22*-mutated patient. The presence of MRPS22 was not determined in these patients. On the other hand, near normal levels of MRPL13, MRPL15 [123] as well as 16S rRNA [18, 19] were found. These observations indicate that both MRPS16 and MRPS22 are essential for assembly and stability of the SSU. A lack of these MRPs results in the failure to assemble part of the mitoribosome, containing at least MRPS11, MRPS16, MRPS22, and 12S rRNA, and subsequent degradation of its components. Both a macromolecular complex containing MRPS2 and the mitoribosomal large subunit can still be formed in the absence of a functional SSU, suggesting that the assembly of the mitoribosome is a process consisting of relatively independent subassembly steps.

Mutations in the mitochondrial arginyl- and aspartyl-tRNA synthetases (*RARS2* and *DARS2*) are associated with severe encephalopathy with pontocerebellar hypoplasia and LBSL (leukoencephalopathy with brain stem and spinal cord involvement and lactate elevation), respectively [16, 20, 23]. In both genes, intronic mutations that affect splicing were detected. The absence of extracerebral symptoms might be explained by a potential difference in abundance of splicing factors between brain and the unaffected tissues, enabling synthesis of small amounts of wild-type transcript of the synthetases in most tissues. Alternatively, the vulnerability of the brain for aminoacyl-tRNA synthetase defects could be due to the high expression of mitochondrial tRNAs in this tissue [237]. The tRNA^{Arg} transcript is scarcely present, but almost fully acylated, in patient fibroblasts harboring a *RARS2* mutation. Presumably, the little available wild-type *RARS2* can aminoacylate a small portion of the tRNA^{Arg} molecules and the uncharged transcripts then become unstable. This will impair mitochondrial protein synthesis, which has only been confirmed in yeast [238]. In contrast, *DARS2* mutations do not seem to affect mitochondrial translation and likewise do not result in defects of the OXPHOS complexes, notwithstanding a clear reduction in aminoacylation activity [20]. The reason for this is currently not understood.

Besides these nine gene products, numerous proteins are indirectly involved in mitochondrial translation, as should be evident from the current review, and defects in these proteins could undoubtedly also interfere with the translation process. For example, lack of the protease paraplegin (see Section 3.3 for information on its function) results in impaired mitochondrial translation in yeast and in a hereditary spastic paraplegia (HSP) mouse model [143]. Nonetheless, HSP patients with mutations in paraplegin (*HSP7*) do not show consistent OXPHOS enzyme deficiencies [239–241]; often only or mainly complex I is affected, while a combined defect would be expected. The selective involvement of certain neurons could in this case be rationalized by tissue-specific differences in the expression of m-AAA protease subunits and their assembly into proteolytic complexes, which vary in their subunit composition depending on subunit availability [242]. This

is analogous to the importance of elongation factor ratios for efficient mitochondrial translation and tissue-specific variability herein.

6. Future Prospects

We have provided an extensive overview of the proteins and processes (in)directly involved in mitochondrial translation and the biogenesis of the OXPHOS system. Even though our understanding of the mechanisms implicated in mitochondrial disease has increased rapidly over the last two decades, it is far from complete. Due to the multitude of proteins and intricacy of the processes needed for a properly functioning OXPHOS system, identifying the genetic defect that underlies an OXPHOS deficiency is not an easy task. The shortage of large or consanguineous families as well as the substantial clinical and genetic heterogeneity of mitochondrial disorders complicate the search by limiting the available strategies. For instance, techniques such as linkage analysis and homozygosity mapping that form powerful tools in combination with whole-genome experimental data sets [136, 243] often cannot be applied and mutation chips are currently only available for the mtDNA. Consequently, the molecular basis of many OXPHOS disorders remains unresolved. In the future, molecular genetic diagnosis of patients suspected to suffer from a mitochondrial disorder might no longer require extensive investigations that integrate information from clinical phenotype, family history, brain imaging and laboratory findings to direct the laborious tasks of screening known candidate genes and, when this is unsuccessful, searching for new genetic causes [43]. Instead, recent progress in the development of next-generation DNA sequencing technologies, which are much cheaper and faster than the conventional approach of polymerase chain reaction followed by capillary sequencing, indicates that within the next few decades high-throughput sequencing could become a feasible option for mutation detection [244, 245]. These methods are anticipated to eventually enable sequencing of the entire human genome for under \$1000 within a day, allowing their routine clinical use and accelerating the discovery of novel disease genes. Exome sequencing, that is, the targeted sequencing of all protein-coding regions, offers an alternative to whole-genome sequencing by facilitating direct identification of the causative gene at a fraction of the costs [246, 247]. However, much remains to be achieved, for example proper bioinformatic tools to deal with the tremendous amounts of data, before such technologies can be readily applied to elucidate the genetic etiology of OXPHOS deficiencies and other disorders. Systems biology techniques will keep increasing our knowledge of the mechanisms underlying complex diseases and in combination with high-throughput sequencing these approaches will advance disease-gene discovery even more. Integrative analysis of functional data is useful especially for gaining insight into the scarcely understood field of modifier genes, which are thought to account for part of the clinical variability seen in mitochondrial diseases. Systematic mapping of genetic interactions revealed a class of modifier or “hub” genes that are proposed to enhance the phenotypic consequences of

mutations in many different genes, the “specifier” genes that define the specific disorders, and thus serve as global modifier genes in multiple mechanistically unrelated disorders [248]. Hopefully, these and other important findings will lead to the discovery of additional modifier genes implicated in mitochondrial disorders. Progress in mutation detection, both in specifier and modifier genes, is crucial for extending the possibilities for genetic counseling, prenatal diagnosis, and interventions to prevent transmission now and to cure these serious disorders in the future. Currently, no effective therapy is available; the various existing treatment strategies are mainly supportive [249, 250]. Gene therapy might offer a solution since it allows for curative treatment without the need for a clear genotype-phenotype correlation, which is often lacking in mitochondrial disorders. Although the development is still in its infancy for both mtDNA and nDNA gene therapy and many challenges are to be overcome, promising results have been obtained in cell cultures and animal models, providing hope for a cure in the not-too-distant future. Thus rapid advances in technologies and consequently in our understanding of the pathogenesis of OXPHOS defects should lead to the ultimate goal of effectively preventing and curing these often devastating disorders.

Acknowledgment

This work was supported by the European Union’s Sixth Framework Program, contract number LSHMCT-2004-005260 (MITOCIRCLE).

References

- [1] M. W. Gray, G. Burger, and B. F. Lang, “Mitochondrial evolution,” *Science*, vol. 283, no. 5407, pp. 1476–1481, 1999.
- [2] K.-D. Gerbitz, K. Gempel, and D. Brdiczka, “Mitochondria and diabetes: genetic, biochemical, and clinical implications of the cellular energy circuit,” *Diabetes*, vol. 45, no. 2, pp. 113–126, 1996.
- [3] K. Hojlund, M. Mogensen, K. Sahlin, and H. Beck-Nielsen, “Mitochondrial dysfunction in type 2 diabetes and obesity,” *Endocrinology and Metabolism Clinics of North America*, vol. 37, no. 3, pp. 713–731, 2008.
- [4] W. Mandemakers, V. A. Morais, and B. De Strooper, “A cell biological perspective on mitochondrial dysfunction in Parkinson disease and other neurodegenerative diseases,” *Journal of Cell Science*, vol. 120, no. 10, pp. 1707–1716, 2007.
- [5] D. C. Chan, “Mitochondria: dynamic organelles in disease, aging, and development,” *Cell*, vol. 125, no. 7, pp. 1241–1252, 2006.
- [6] L. Guarente, “Mitochondria—a nexus for aging, calorie restriction, and sirtuins?” *Cell*, vol. 132, no. 2, pp. 171–176, 2008.
- [7] A. M. Schaefer, R. W. Taylor, D. M. Turnbull, and P. F. Chinnery, “The epidemiology of mitochondrial disorders—past, present and future,” *Biochimica et Biophysica Acta*, vol. 1659, no. 2-3, pp. 115–120, 2004.
- [8] M. Saraste, “Oxidative phosphorylation at the fin de siècle,” *Science*, vol. 283, no. 5407, pp. 1488–1493, 1999.
- [9] J. L. C. M. Loeffen, J. A. M. Smeitink, J. M. F. Trijbels, et al., “Isolated complex I deficiency in children: clinical,

- biochemical and genetic aspects," *Human Mutation*, vol. 15, no. 2, pp. 123–134, 2000.
- [10] F.-G. Debray, M. Lambert, and G. A. Mitchell, "Disorders of mitochondrial function," *Current Opinion in Pediatrics*, vol. 20, no. 4, pp. 471–482, 2008.
- [11] M. Zeviani and S. Di Donato, "Mitochondrial disorders," *Brain*, vol. 127, no. 10, pp. 2153–2172, 2004.
- [12] "MITOMAP: A Human Mitochondrial Genome Database," 2009, <http://www.mitomap.org/MITOMAP>.
- [13] W. C. Copeland, "Inherited mitochondrial diseases of DNA replication," *Annual Review of Medicine*, vol. 59, pp. 131–146, 2008.
- [14] Y. Bykhovskaya, K. Casas, E. Mengesha, A. Inbal, and N. Fischel-Ghodsian, "Missense mutation in pseudouridine synthase 1 (PUS1) causes mitochondrial myopathy and sideroblastic anemia (MLASA)," *American Journal of Human Genetics*, vol. 74, no. 6, pp. 1303–1308, 2004.
- [15] M. J. H. Coenen, H. Antonicka, C. Ugalde, et al., "Mutant mitochondrial elongation factor G1 and combined oxidative phosphorylation deficiency," *New England Journal of Medicine*, vol. 351, no. 20, pp. 2080–2086, 2004.
- [16] S. Edvardson, A. Shaag, O. Kolesnikova, et al., "Deleterious mutation in the mitochondrial arginyl-transfer RNA synthetase gene is associated with pontocerebellar hypoplasia," *American Journal of Human Genetics*, vol. 81, no. 4, pp. 857–862, 2007.
- [17] E. Fernandez-Vizarrá, A. Berardinelli, L. Valente, V. Tiranti, and M. Zeviani, "Nonsense mutation in pseudouridylate synthase 1 (PUS1) in two brothers affected by myopathy, lactic acidosis and sideroblastic anaemia (MLASA)," *Journal of Medical Genetics*, vol. 44, no. 3, pp. 173–180, 2007.
- [18] C. Miller, A. Saada, N. Shaul, et al., "Defective mitochondrial translation caused by a ribosomal protein (MRPS16) mutation," *Annals of Neurology*, vol. 56, no. 5, pp. 734–738, 2004.
- [19] A. Saada, A. Shaag, S. Arnon, et al., "Antenatal mitochondrial disease caused by mitochondrial ribosomal protein (MRPS22) mutation," *Journal of Medical Genetics*, vol. 44, no. 12, pp. 784–786, 2007.
- [20] G. C. Scheper, T. van der Kloek, R. J. van Andel, et al., "Mitochondrial aspartyl-tRNA synthetase deficiency causes leukoencephalopathy with brain stem and spinal cord involvement and lactate elevation," *Nature Genetics*, vol. 39, no. 4, pp. 534–539, 2007.
- [21] J. A. M. Smeitink, O. Elpeleg, H. Antonicka, et al., "Distinct clinical phenotypes associated with a mutation in the mitochondrial translation elongation factor EFTs," *American Journal of Human Genetics*, vol. 79, no. 5, pp. 869–877, 2006.
- [22] L. Valente, V. Tiranti, R. M. Marsano, et al., "Infantile encephalopathy and defective mitochondrial DNA translation in patients with mutations of mitochondrial elongation factors EFG1 and EFTu," *American Journal of Human Genetics*, vol. 80, no. 1, pp. 44–58, 2007.
- [23] P. Isohanni, T. Linnankivi, J. Buzkova, et al., "DARS2 mutations in mitochondrial leukoencephalopathy and multiple sclerosis," *Journal of Medical Genetics*, vol. 47, no. 1, pp. 66–70, 2010.
- [24] A. Zeharia, A. Shaag, O. Pappo, et al., "Acute infantile liver failure due to mutations in the TRMU gene," *American Journal of Human Genetics*, vol. 85, no. 3, pp. 401–407, 2009.
- [25] H. Antonicka, F. Sasarman, N. G. Kennaway, and E. A. Shoubridge, "The molecular basis for tissue specificity of the oxidative phosphorylation deficiencies in patients with mutations in the mitochondrial translation factor EFG1," *Human Molecular Genetics*, vol. 15, no. 11, pp. 1835–1846, 2006.
- [26] S. Anderson, A. T. Bankier, and B. G. Barrell, "Sequence and organization of the human mitochondrial genome," *Nature*, vol. 290, no. 5806, pp. 457–465, 1981.
- [27] W. M. Brown, M. George Jr., and A. C. Wilson, "Rapid evolution of animal mitochondrial DNA," *Proceedings of the National Academy of Sciences of the United States of America*, vol. 76, no. 4, pp. 1967–1971, 1979.
- [28] M. Lynch, B. Koskella, and S. Schaack, "Mutation pressure and the evolution of organelle genomic architecture," *Science*, vol. 311, no. 5768, pp. 1727–1730, 2006.
- [29] C. Richter, J.-W. Park, and B. N. Ames, "Normal oxidative damage to mitochondrial and nuclear DNA is extensive," *Proceedings of the National Academy of Sciences of the United States of America*, vol. 85, no. 17, pp. 6465–6467, 1988.
- [30] R. W. Taylor and D. M. Turnbull, "Mitochondrial DNA mutations in human disease," *Nature Reviews Genetics*, vol. 6, no. 5, pp. 389–402, 2005.
- [31] D. Bogenhagen and D. A. Clayton, "Mouse l cell mitochondrial DNA molecules are selected randomly for replication throughout the cell cycle," *Cell*, vol. 11, no. 4, pp. 719–727, 1977.
- [32] D. A. Clayton, "Replication of animal mitochondrial DNA," *Cell*, vol. 28, no. 4, pp. 693–705, 1982.
- [33] G. S. Shadel and D. A. Clayton, "Mitochondrial DNA maintenance in vertebrates," *Annual Review of Biochemistry*, vol. 66, pp. 409–436, 1997.
- [34] I. J. Holt, H. E. Lorimer, and H. T. Jacobs, "Coupled leading- and lagging-strand synthesis of mammalian mitochondrial DNA," *Cell*, vol. 100, no. 5, pp. 515–524, 2000.
- [35] T. Yasukawa, M.-Y. Yang, H. T. Jacobs, and I. J. Holt, "A bidirectional origin of replication maps to the major noncoding region of human mitochondrial DNA," *Molecular Cell*, vol. 18, no. 6, pp. 651–662, 2005.
- [36] M. A. Graziewicz, M. J. Longley, and W. C. Copeland, "DNA polymerase γ in mitochondrial DNA replication and repair," *Chemical Reviews*, vol. 106, no. 2, pp. 383–405, 2006.
- [37] I. J. Holt, J. He, C.-C. Mao, et al., "Mammalian mitochondrial nucleoids: organizing an independently minded genome," *Mitochondrion*, vol. 7, no. 5, pp. 311–321, 2007.
- [38] F. Malka, A. Lombès, and M. Rojo, "Organization, dynamics and transmission of mitochondrial DNA: focus on vertebrate nucleoids," *Biochimica et Biophysica Acta*, vol. 1763, no. 5–6, pp. 463–472, 2006.
- [39] N. B. Larsen, M. Rasmussen, and L. J. Rasmussen, "Nuclear and mitochondrial DNA repair: similar pathways?" *Mitochondrion*, vol. 5, no. 2, pp. 89–108, 2005.
- [40] J. A. Stuart and M. F. Brown, "Mitochondrial DNA maintenance and bioenergetics," *Biochimica et Biophysica Acta*, vol. 1757, no. 2, pp. 79–89, 2006.
- [41] A. Saada, "Deoxyribonucleotides and disorders of mitochondrial DNA integrity," *DNA and Cell Biology*, vol. 23, no. 12, pp. 797–806, 2004.
- [42] A. Spinazzola and M. Zeviani, "Disorders of nuclear-mitochondrial intergenomic signaling," *Gene*, vol. 354, no. 1–2, pp. 162–168, 2005.
- [43] D. M. Kirby and D. R. Thorburn, "Approaches to finding the molecular basis of mitochondrial oxidative phosphorylation disorders," *Twin Research and Human Genetics*, vol. 11, no. 4, pp. 395–411, 2008.
- [44] N. D. Bonawitz, D. A. Clayton, and G. S. Shadel, "Initiation and beyond: multiple functions of the human mitochondrial

- transcription machinery,” *Molecular Cell*, vol. 24, no. 6, pp. 813–825, 2006.
- [45] M. Falkenberg, N.-G. Larsson, and C. M. Gustafsson, “DNA replication and transcription in mammalian mitochondria,” *Annual Review of Biochemistry*, vol. 76, pp. 679–699, 2007.
- [46] M. Roberti, P. L. Polosa, F. Bruni, et al., “The MTERF family proteins: mitochondrial transcription regulators and beyond,” *Biochimica et Biophysica Acta*, vol. 1787, no. 5, pp. 303–311, 2009.
- [47] A. K. Hyvärinen, J. L. O. Pohjoismäki, A. Reyes, et al., “The mitochondrial transcription termination factor mTERF modulates replication pausing in human mitochondrial DNA,” *Nucleic Acids Research*, vol. 35, no. 19, pp. 6458–6474, 2007.
- [48] T. Linder, C. B. Park, J. Asin-Cayuela, et al., “A family of putative transcription termination factors shared amongst metazoans and plants,” *Current Genetics*, vol. 48, no. 4, pp. 265–269, 2005.
- [49] Y. Chen, G. Zhou, M. Yu, et al., “Cloning and functional analysis of human mTERFL encoding a novel mitochondrial transcription termination factor-like protein,” *Biochemical and Biophysical Research Communications*, vol. 337, no. 4, pp. 1112–1118, 2005.
- [50] M. Pellegrini, J. Asin-Cayuela, H. Erdjument-Bromage, P. Tempst, N.-G. Larsson, and C. M. Gustafsson, “MTERF2 is a nucleoid component in mammalian mitochondria,” *Biochimica et Biophysica Acta*, vol. 1787, no. 5, pp. 296–302, 2009.
- [51] T. Wenz, C. Luca, A. Torraco, and C. T. Moraes, “mTERF2 regulates oxidative phosphorylation by modulating mtDNA transcription,” *Cell Metabolism*, vol. 9, no. 6, pp. 499–511, 2009.
- [52] C. B. Park, J. Asin-Cayuela, Y. Cámara, et al., “MTERF3 is a negative regulator of mammalian mtDNA transcription,” *Cell*, vol. 130, no. 2, pp. 273–285, 2007.
- [53] M. Roberti, F. Bruni, P. Loguercio Polosa, C. Manzari, M. N. Gadaleta, and P. Cantatore, “MTERF3, the most conserved member of the mTERF-family, is a modular factor involved in mitochondrial protein synthesis,” *Biochimica et Biophysica Acta*, vol. 1757, no. 9–10, pp. 1199–1206, 2006.
- [54] A. Cayuela, Y. Shi, and C. M. Gustafsson, “Initial characterization of MTERF4, a paralogue of MTERF1 (mTERF),” in *Proceedings of the 7th European Meeting on Mitochondrial Pathology (EUROMIT '08)*, p. 20, Stockholm, Sweden, June 2008, abstract no. 14.
- [55] D. Ojala, J. Montoya, and G. Attardi, “tRNA punctuation model of RNA processing in human mitochondria,” *Nature*, vol. 290, no. 5806, pp. 470–474, 1981.
- [56] J. Montoya, M. J. López-Pérez, and E. Ruiz-Pesini, “Mitochondrial DNA transcription and diseases: past, present and future,” *Biochimica et Biophysica Acta*, vol. 1757, no. 9–10, pp. 1179–1189, 2006.
- [57] D. Gagliardi, P. P. Stepien, R. J. Temperley, R. N. Lightowlers, and Z. M. A. Chrzanowska-Lightowlers, “Messenger RNA stability in mitochondria: different means to an end,” *Trends in Genetics*, vol. 20, no. 6, pp. 260–267, 2004.
- [58] H.-W. Chen, C. M. Koehler, and M. A. Teitell, “Human polynucleotide phosphorylase: location matters,” *Trends in Cell Biology*, vol. 17, no. 12, pp. 600–608, 2007.
- [59] L. Khidr, G. Wu, A. Davila, V. Procaccio, D. Wallace, and W.-H. Lee, “Role of SUV3 helicase in maintaining mitochondrial homeostasis in human cells,” *Journal of Biological Chemistry*, vol. 283, no. 40, pp. 27064–27073, 2008.
- [60] A. Chomyn, A. Martinuzzi, M. Yoneda, et al., “MELAS mutation in mtDNA binding site for transcription termination factor causes defects in protein synthesis and in respiration but no change in levels of upstream and downstream mature transcripts,” *Proceedings of the National Academy of Sciences of the United States of America*, vol. 89, no. 10, pp. 4221–4225, 1992.
- [61] J. F. Hess, M. A. Parisi, J. L. Bennett, and D. A. Clayton, “Impairment of mitochondrial transcription termination by a point mutation associated with the MELAS subgroup of mitochondrial encephalomyopathies,” *Nature*, vol. 351, no. 6323, pp. 236–239, 1991.
- [62] M.-X. Guan, Q. Yan, X. Li, et al., “Mutation in TRMU related to transfer RNA modification modulates the phenotypic expression of the deafness-associated mitochondrial 12S ribosomal RNA mutations,” *American Journal of Human Genetics*, vol. 79, no. 2, pp. 291–302, 2006.
- [63] C. Knox, E. Sass, W. Neupert, and O. Pines, “Import into mitochondria, folding and retrograde movement of fumarase in yeast,” *Journal of Biological Chemistry*, vol. 273, no. 40, pp. 25587–25593, 1998.
- [64] J. A. MacKenzie and R. M. Payne, “Ribosomes specifically bind to mammalian mitochondria via protease-sensitive proteins on the outer membrane,” *Journal of Biological Chemistry*, vol. 279, no. 11, pp. 9803–9810, 2004.
- [65] K. Verner, “Co-translational protein import into mitochondria: an alternative view,” *Trends in Biochemical Sciences*, vol. 18, no. 10, pp. 366–371, 1993.
- [66] P. Marc, A. Margeot, F. Devaux, C. Blugeon, M. Corral-Debrinski, and C. Jacq, “Genome-wide analysis of mRNAs targeted to yeast mitochondria,” *EMBO Reports*, vol. 3, no. 2, pp. 159–164, 2002.
- [67] A. Mukhopadhyay, L. Ni, and H. Weiner, “A co-translational model to explain the in vivo import of proteins into HeLa cell mitochondria,” *Biochemical Journal*, vol. 382, no. 1, pp. 385–392, 2004.
- [68] M. Garcia, X. Darzacq, T. Delaveau, L. Jourdain, R. H. Singer, and C. Jacq, “Mitochondria-associated yeast mRNAs and the biogenesis of molecular complexes,” *Molecular Biology of the Cell*, vol. 18, no. 2, pp. 362–368, 2007.
- [69] A. Margeot, M. Garcia, W. Wang, E. Tetaud, J. P. di Rago, and C. Jacq, “Why are many mRNAs translated to the vicinity of mitochondria: a role in protein complex assembly?” *Gene*, vol. 354, no. 1–2, pp. 64–71, 2005.
- [70] F. J. Iborra, H. Kimura, and P. R. Cook, “The functional organization of mitochondrial genomes in human cells,” *BMC Biology*, vol. 2, article 9, 2004.
- [71] W. Neupert and J. M. Herrmann, “Translocation of proteins into mitochondria,” *Annual Review of Biochemistry*, vol. 76, pp. 723–749, 2007.
- [72] N. Wiedemann, A. E. Frazier, and N. Pfanner, “The protein import machinery of mitochondria,” *Journal of Biological Chemistry*, vol. 279, no. 15, pp. 14473–14476, 2004.
- [73] J. R. Blesa, A. Solano, P. Briones, J. A. Prieto-Ruiz, J. Hernández-Yago, and F. Coria, “Molecular genetics of a patient with Mohr-Tranebjaerg syndrome due to a new mutation in the DDP1 gene,” *NeuroMolecular Medicine*, vol. 9, no. 4, pp. 285–291, 2007.
- [74] K. Roesch, S. P. Curran, L. Tranebjaerg, and C. M. Koehler, “Human deafness dystonia syndrome is caused by a defect in assembly of the DDP1/TIMM8a-TIMM13 complex,” *Human Molecular Genetics*, vol. 11, no. 5, pp. 477–486, 2002.
- [75] J. Binder, S. Hofmann, S. Kreisel, et al., “Clinical and molecular findings in a patient with a novel mutation in the

- deafness-dystonia peptide (DDP1) gene," *Brain*, vol. 126, no. 8, pp. 1814–1820, 2003.
- [76] K. M. Davey, J. S. Parboosingh, D. R. McLeod, et al., "Mutation of DNAJC19, a human homologue of yeast inner mitochondrial membrane co-chaperones, causes DCMA syndrome, a novel autosomal recessive Barth syndrome-like condition," *Journal of Medical Genetics*, vol. 43, no. 5, pp. 385–393, 2006.
- [77] D. Mokranjac, M. Sighting, W. Neupert, and K. Hell, "Tim14, a novel key component of the import motor of the TIM23 protein translocase of mitochondria," *EMBO Journal*, vol. 22, no. 19, pp. 4945–4956, 2003.
- [78] X. Pérez-Martínez, S. Funes, Y. Camacho-Villasana, S. Marjavaara, F. Tavares-Carreón, and M. Shingú-Vázquez, "Protein synthesis and assembly in mitochondrial disorders," *Current Topics in Medicinal Chemistry*, vol. 8, no. 15, pp. 1335–1350, 2008.
- [79] S. Osawa, T. H. Jukes, K. Watanabe, and A. Muto, "Recent evidence for evolution of the genetic code," *Microbiological Reviews*, vol. 56, no. 1, pp. 229–264, 1992.
- [80] J. Montoya, D. Ojala, and G. Attardi, "Distinctive features of the 5'-terminal sequences of the human mitochondrial mRNAs," *Nature*, vol. 290, no. 5806, pp. 465–470, 1981.
- [81] K. Grohmann, F. Amalric, S. Crews, and G. Attardi, "Failure to detect "cap" structures in mitochondrial DNA-coded poly(A)-containing RNA from HeLa cells," *Nucleic Acids Research*, vol. 5, no. 3, pp. 637–651, 1978.
- [82] H.-X. Liao and L. L. Spemulli, "Interaction of bovine mitochondrial ribosomes with messenger RNA," *Journal of Biological Chemistry*, vol. 264, no. 13, pp. 7518–7522, 1989.
- [83] B. S. Laursen, H. P. Sørensen, K. K. Mortensen, and H. U. Sperling-Petersen, "Initiation of protein synthesis in bacteria," *Microbiology and Molecular Biology Reviews*, vol. 69, no. 1, pp. 101–123, 2005.
- [84] M. López-Lastra, A. Rivas, and M. I. Barría, "Protein synthesis in eukaryotes: the growing biological relevance of cap-independent translation initiation," *Biological Research*, vol. 38, no. 2-3, pp. 121–146, 2005.
- [85] B. G. Barrell, S. Anderson, and A. T. Bankier, "Different pattern of codon recognition by mammalian mitochondrial tRNAs," *Proceedings of the National Academy of Sciences of the United States of America*, vol. 77, no. 6, pp. 3164–3166, 1980.
- [86] R. Mikelsaar, "Human mitochondrial genome and the evolution of methionine transfer ribonucleic acids," *Journal of Theoretical Biology*, vol. 105, no. 2, pp. 221–232, 1983.
- [87] A. Marintchev and G. Wagner, "Translation initiation: structures, mechanisms and evolution," *Quarterly Reviews of Biophysics*, vol. 37, no. 3-4, pp. 197–284, 2004.
- [88] A. Roll-Mecak, B.-S. Shin, T. E. Dever, and S. K. Burley, "Engaging the ribosome: universal IFs of translation," *Trends in Biochemical Sciences*, vol. 26, no. 12, pp. 705–709, 2001.
- [89] L. Ma and L. L. Spemulli, "Cloning and sequence analysis of the human mitochondrial translational initiation factor 2 cDNA," *Journal of Biological Chemistry*, vol. 270, no. 4, pp. 1859–1865, 1995.
- [90] E. C. Koc and L. L. Spemulli, "Identification of mammalian mitochondrial translational initiation factor 3 and examination of its role in initiation complex formation with natural mRNAs," *Journal of Biological Chemistry*, vol. 277, no. 38, pp. 35541–35549, 2002.
- [91] L. L. Spemulli, A. Coursey, T. Navratil, and S. E. Hunter, "Initiation and elongation factors in mammalian mitochondrial protein biosynthesis," *Progress in Nucleic Acid Research and Molecular Biology*, vol. 77, pp. 211–261, 2004.
- [92] R. Gaur, D. Grasso, P. P. Datta, et al., "A single mammalian mitochondrial translation initiation factor functionally replaces two bacterial factors," *Molecular Cell*, vol. 29, no. 2, pp. 180–190, 2008.
- [93] M. Hammarsund, W. Wilson, M. Corcoran, et al., "Identification and characterization of two novel human mitochondrial elongation factor genes, hEFG2 and hEFG1, phylogenetically conserved through evolution," *Human Genetics*, vol. 109, no. 5, pp. 542–550, 2001.
- [94] M. Ling, F. Merante, H.-S. Chen, C. Duff, A. M. V. Duncan, and B. H. Robinson, "The human mitochondrial elongation factor tu (EF-Tu) gene: CDNA sequence, genomic localization, genomic structure, and identification of a pseudogene," *Gene*, vol. 197, no. 1-2, pp. 325–336, 1997.
- [95] H. Xin, V. Worriax, W. Burkhart, and L. L. Spemulli, "Cloning and expression of mitochondrial translational elongation factor Ts from bovine and human liver," *Journal of Biological Chemistry*, vol. 270, no. 29, pp. 17243–17249, 1995.
- [96] K. Bhargava, P. Templeton, and L. L. Spemulli, "Expression and characterization of isoform 1 of human mitochondrial elongation factor G," *Protein Expression and Purification*, vol. 37, no. 2, pp. 368–376, 2004.
- [97] E. A. Winzeler, D. D. Shoemaker, A. Astromoff, et al., "Functional characterization of the *S. cerevisiae* genome by gene deletion and parallel analysis," *Science*, vol. 285, no. 5429, pp. 901–906, 1999.
- [98] M. Tsuboi, H. Morita, Y. Nozaki, et al., "EF-G2mt is an exclusive recycling factor in mammalian mitochondrial protein synthesis," *Molecular Cell*, vol. 35, no. 4, pp. 502–510, 2009.
- [99] G. Bertram, S. Innes, O. Minella, J. P. Richardson, and I. Stansfield, "Endless possibilities: translation termination and stop codon recognition," *Microbiology*, vol. 147, no. 2, pp. 255–269, 2001.
- [100] L. D. Kapp and J. R. Lorsch, "The molecular mechanics of eukaryotic translation," *Annual Review of Biochemistry*, vol. 73, pp. 657–704, 2004.
- [101] Y. Nozaki, N. Matsunaga, T. Ishizawa, T. Ueda, and N. Takeuchi, "HMRFL is a human mitochondrial translation release factor involved in the decoding of the termination codons UAA and UAG," *Genes to Cells*, vol. 13, no. 5, pp. 429–438, 2008.
- [102] H. R. Soleimanpour-Lichaei, I. Kühn, M. Gaisne, et al., "mtRF1a is a human mitochondrial translation release factor decoding the major termination codons UAA and UAG," *Molecular Cell*, vol. 27, no. 5, pp. 745–757, 2007.
- [103] Y. Zhang and L. L. Spemulli, "Identification and cloning of human mitochondrial translational release factor 1 and the ribosome recycling factor," *Biochimica et Biophysica Acta*, vol. 1443, no. 1-2, pp. 245–250, 1998.
- [104] J. Rorbach, R. Richter, H. J. Wessels, et al., "The human mitochondrial ribosome recycling factor is essential for cell viability," *Nucleic Acids Research*, vol. 36, no. 18, pp. 5787–5799, 2008.
- [105] M. J. Bibb, R. A. Van Etten, C. T. Wright, M. W. Walberg, and D. A. Clayton, "Sequence and gene organization of mouse mitochondrial DNA," *Cell*, vol. 26, no. 2, pp. 167–180, 1981.
- [106] G. Gadaleta, G. Pepe, G. De Candia, C. Quagliariello, E. Sbisà, and C. Saccone, "The complete nucleotide sequence of the *Rattus norvegicus* mitochondrial genome: cryptic signals revealed by comparative analysis between vertebrates," *Journal of Molecular Evolution*, vol. 28, no. 6, pp. 497–516, 1989.
- [107] P. Smits, J. A. M. Smeitink, L. P. van den Heuvel, M. A. Huynen, and T. J. G. Ettema, "Reconstructing the evolution

- of the mitochondrial ribosomal proteome," *Nucleic Acids Research*, vol. 35, no. 14, pp. 4686–4703, 2007.
- [108] T. W. O'Brien, "Properties of human mitochondrial ribosomes," *IUBMB Life*, vol. 55, no. 9, pp. 505–513, 2003.
- [109] M. R. Sharma, E. C. Koc, P. P. Datta, T. M. Booth, L. L. Spremulli, and R. K. Agrawal, "Structure of the mammalian mitochondrial ribosome reveals an expanded functional role for its component proteins," *Cell*, vol. 115, no. 1, pp. 97–108, 2003.
- [110] M. Helm, H. Brulé, D. Friede, R. Giegé, D. Pütz, and C. Florentz, "Search for characteristic structural features of mammalian mitochondrial tRNAs," *RNA*, vol. 6, no. 10, pp. 1356–1379, 2000.
- [111] M. Helm, "Post-transcriptional nucleotide modification and alternative folding of RNA," *Nucleic Acids Research*, vol. 34, no. 2, pp. 721–733, 2006.
- [112] M. Helm, R. Giegé, and C. Florentz, "A Watson-Crick base-pair-disrupting methyl group (m1A9) is sufficient for cloverleaf folding of human mitochondrial tRNA(Lys)," *Biochemistry*, vol. 38, no. 40, pp. 13338–13346, 1999.
- [113] Y. Kirino and T. Suzuki, "Human mitochondrial diseases associated with tRNA wobble modification deficiency," *RNA Biology*, vol. 2, no. 2, pp. 41–44, 2005.
- [114] R. Giegé, M. Sissler, and C. Florentz, "Universal rules and idiosyncratic features in tRNA identity," *Nucleic Acids Research*, vol. 26, no. 22, pp. 5017–5035, 1998.
- [115] L. Bonnefond, A. Fender, J. Rudinger-Thirion, R. Giegé, C. Florentz, and M. Sissler, "Toward the full set of human mitochondrial aminoacyl-tRNA synthetases: characterization of AspRS and TyrRS," *Biochemistry*, vol. 44, no. 12, pp. 4805–4816, 2005.
- [116] S. M. K. Davies, O. Rackham, A.-M. J. Shearwood, et al., "Pentatricopeptide repeat domain protein 3 associates with the mitochondrial small ribosomal subunit and regulates translation," *FEBS Letters*, vol. 583, no. 12, pp. 1853–1858, 2009.
- [117] V. Ramakrishnan, "Ribosome structure and the mechanism of translation," *Cell*, vol. 108, no. 4, pp. 557–572, 2002.
- [118] C. N. Jones, K. A. Wilkinson, K. T. Hung, K. M. Weeks, and L. L. Spremulli, "Lack of secondary structure characterizes the 5' ends of mammalian mitochondrial mRNAs," *RNA*, vol. 14, no. 5, pp. 862–871, 2008.
- [119] B. E. Christian and L. L. Spremulli, "Evidence for an active role of IF3mt in the initiation of translation in mammalian mitochondria," *Biochemistry*, vol. 48, no. 15, pp. 3269–3278, 2009.
- [120] K. Bhargava and L. L. Spremulli, "Role of the N- and C-terminal extensions on the activity of mammalian mitochondrial translational initiation factor 3," *Nucleic Acids Research*, vol. 33, no. 22, pp. 7011–7018, 2005.
- [121] H.-X. Liao and L. L. Spremulli, "Identification and initial characterization of translational initiation factor 2 from bovine mitochondria," *Journal of Biological Chemistry*, vol. 265, no. 23, pp. 13618–13622, 1990.
- [122] J. Ma and L. L. Spremulli, "Expression, purification, and mechanistic studies of bovine mitochondrial translational initiation factor 2," *Journal of Biological Chemistry*, vol. 271, no. 10, pp. 5805–5811, 1996.
- [123] Md. E. Haque, D. Grasso, and L. L. Spremulli, "The interaction of mammalian mitochondrial translational initiation factor 3 with ribosomes: evolution of terminal extensions in IF3mt," *Nucleic Acids Research*, vol. 36, no. 2, pp. 589–597, 2008.
- [124] Y.-C. Cai, J. M. Bullard, N. L. Thompson, and L. L. Spremulli, "Interaction of mitochondrial elongation factor Tu with aminoacyl-tRNA and elongation factor Ts," *Journal of Biological Chemistry*, vol. 275, no. 27, pp. 20308–20314, 2000.
- [125] V. L. Woriach, J. M. Bullard, L. Ma, T. Yokogawa, and L. L. Spremulli, "Mechanistic studies of the translational elongation cycle in mammalian mitochondria," *Biochimica et Biophysica Acta*, vol. 1352, no. 1, pp. 91–101, 1997.
- [126] F. Sasarman, H. Antonicka, and E. A. Shoubridge, "The A3243G tRNA^{Leu}(UUR) MELAS mutation causes amino acid misincorporation and a combined respiratory chain assembly defect partially suppressed by overexpression of EFTu and EFG2," *Human Molecular Genetics*, vol. 17, no. 23, pp. 3697–3707, 2008.
- [127] A. Nagao, T. Suzuki, and T. Suzuki, "Aminoacyl-tRNA surveillance by EF-Tu in mammalian mitochondria," *Nucleic Acids Symposium Series*, no. 51, pp. 41–42, 2007.
- [128] J. A. Mears, J. J. Cannone, S. M. Stagg, R. R. Gutell, R. K. Agrawal, and S. C. Harvey, "Modeling a minimal ribosome based on comparative sequence analysis," *Journal of Molecular Biology*, vol. 321, no. 2, pp. 215–234, 2002.
- [129] J. A. Mears, M. R. Sharma, R. R. Gutell, et al., "A structural model for the large subunit of the mammalian mitochondrial ribosome," *Journal of Molecular Biology*, vol. 358, no. 1, pp. 193–212, 2006.
- [130] J. Towpik, "Regulation of mitochondrial translation in yeast," *Cellular and Molecular Biology Letters*, vol. 10, no. 4, pp. 571–594, 2005.
- [131] A. Chacinska and M. Boguta, "Coupling of mitochondrial translation with the formation of respiratory complexes in yeast mitochondria," *Acta Biochimica Polonica*, vol. 47, no. 4, pp. 973–991, 2000.
- [132] X. Zeng, A. Hourset, and A. Tzagoloff, "The *Saccharomyces cerevisiae* ATP22 gene codes for the mitochondrial ATPase subunit 6-specific translation factor," *Genetics*, vol. 175, no. 1, pp. 55–63, 2007.
- [133] E. C. Koc and L. L. Spremulli, "RNA-binding proteins of mammalian mitochondria," *Mitochondrion*, vol. 2, no. 4, pp. 277–291, 2003.
- [134] W. Weraarpachai, H. Antonicka, F. Sasarman, et al., "Mutation in TACO1, encoding a translational activator of COX I, results in cytochrome c oxidase deficiency and late-onset Leigh syndrome," *Nature Genetics*, vol. 41, no. 7, pp. 833–837, 2009.
- [135] M. S. Rodeheffer, B. E. Boone, A. C. Bryan, and G. S. Shadel, "Nam1p, a protein involved in RNA processing and translation, is coupled to transcription through an interaction with yeast mitochondrial RNA polymerase," *Journal of Biological Chemistry*, vol. 276, no. 11, pp. 8616–8622, 2001.
- [136] V. K. Mootha, P. Lepage, K. Miller, et al., "Identification of a gene causing human cytochrome c oxidase deficiency by integrative genomics," *Proceedings of the National Academy of Sciences of the United States of America*, vol. 100, no. 2, pp. 605–610, 2003.
- [137] G. M. Manthey and J. E. McEwen, "The product of the nuclear gene PET309 is required for translation of mature mRNA and stability or production of intron-containing RNAs derived from the mitochondrial COX1 locus of *Saccharomyces cerevisiae*," *EMBO Journal*, vol. 14, no. 16, pp. 4031–4043, 1995.
- [138] F. Xu, C. Morin, G. Mitchell, C. Ackerley, and B. H. Robinson, "The role of the LRPPRC (leucine-rich pentatricopeptide

- repeat cassette) gene in cytochrome oxidase assembly: mutation causes lowered levels of COX (cytochrome c oxidase) I and COX III mRNA," *Biochemical Journal*, vol. 382, no. 1, pp. 331–336, 2004.
- [139] S. Naithani, S. A. Saracco, C. A. Butler, and T. D. Fox, "Interactions among COX1, COX2, and COX3 mRNA-specific translational activator proteins on the inner surface of the mitochondrial inner membrane of *Saccharomyces cerevisiae*," *Molecular Biology of the Cell*, vol. 14, no. 1, pp. 324–333, 2003.
- [140] M. G. Wallis, O. Groudinsky, P. P. Slonimski, and G. Dujardin, "The NAM1 protein (NAM1p), which is selectively required for *cox1*, *cytb* and *atp6* transcript processing/stabilisation, is located in the yeast mitochondrial matrix," *European Journal of Biochemistry*, vol. 222, no. 1, pp. 27–32, 1994.
- [141] G. S. Shadel, "Coupling the mitochondrial transcription machinery to human disease," *Trends in Genetics*, vol. 20, no. 10, pp. 513–519, 2004.
- [142] S. Mili and S. Piñol-Roma, "LRP130, a pentatricopeptide motif protein with a noncanonical RNA-binding domain, is bound in vivo to mitochondrial and nuclear RNAs," *Molecular and Cellular Biology*, vol. 23, no. 14, pp. 4972–4982, 2003.
- [143] M. Nolden, S. Ehses, M. Koppen, A. Bernacchia, E. I. Rugarli, and T. Langer, "The m-AAA protease defective in hereditary spastic paraplegia controls ribosome assembly in mitochondria," *Cell*, vol. 123, no. 2, pp. 277–289, 2005.
- [144] G. Casari, M. De Fusco, S. Ciarmatori, et al., "Spastic paraplegia and OXPHOS impairment caused by mutations in paraplegin, a nuclear-encoded mitochondrial metalloprotease," *Cell*, vol. 93, no. 6, pp. 973–983, 1998.
- [145] G. S. Shadel, "Expression and maintenance of mitochondrial DNA: new insights into human disease pathology," *American Journal of Pathology*, vol. 172, no. 6, pp. 1445–1456, 2008.
- [146] J. Cotney, Z. Wang, and G. S. Shadel, "Relative abundance of the human mitochondrial transcription system and distinct roles for h-mtTFB1 and h-mtTFB2 in mitochondrial biogenesis and gene expression," *Nucleic Acids Research*, vol. 35, no. 12, pp. 4042–4054, 2007.
- [147] Y. Bykhovskaya, E. Mengesha, D. Wang, et al., "Human mitochondrial transcription factor B1 as a modifier gene for hearing loss associated with the mitochondrial A1555G mutation," *Molecular Genetics and Metabolism*, vol. 82, no. 1, pp. 27–32, 2004.
- [148] M. D. Metodiev, N. Lesko, C. B. Park, et al., "Methylation of 12S rRNA is necessary for in vivo stability of the small subunit of the mammalian mitochondrial ribosome," *Cell Metabolism*, vol. 9, no. 4, pp. 386–397, 2009.
- [149] R. C. Scarpulla, "Transcriptional paradigms in mammalian mitochondrial biogenesis and function," *Physiological Reviews*, vol. 88, no. 2, pp. 611–638, 2008.
- [150] D. De Rasmio, A. Signorile, E. Roca, and S. Papa, "cAMP response element-binding protein (CREB) is imported into mitochondria and promotes protein synthesis," *FEBS Journal*, vol. 276, no. 16, pp. 4325–4333, 2009.
- [151] S.-L. Liang, D. Quirk, and A. Zhou, "RNase L: its biological roles and regulation," *IUBMB Life*, vol. 58, no. 9, pp. 508–514, 2006.
- [152] F. Le Roy, M. Silhol, T. Salehzada, and C. Bisbal, "Regulation of mitochondrial mRNA stability by RNase L is translation-dependent and controls IFN α -induced apoptosis," *Cell Death and Differentiation*, vol. 14, no. 8, pp. 1406–1413, 2007.
- [153] H. Suzuki, T. Ueda, H. Taguchi, and N. Takeuchi, "Chaperone properties of mammalian mitochondrial translation elongation factor Tu," *Journal of Biological Chemistry*, vol. 282, no. 6, pp. 4076–4084, 2007.
- [154] A. Malki, T. Caldas, J. Abdallah, et al., "Peptidase activity of the *Escherichia coli* Hsp31 chaperone," *Journal of Biological Chemistry*, vol. 280, no. 15, pp. 14420–14426, 2005.
- [155] Z. Wang, J. Cotney, and G. S. Shadel, "Human mitochondrial ribosomal protein MRPL12 interacts directly with mitochondrial RNA polymerase to modulate mitochondrial gene expression," *Journal of Biological Chemistry*, vol. 282, no. 17, pp. 12610–12618, 2007.
- [156] E. C. Koc, A. Ranasinghe, W. Burkhart, et al., "A new face on apoptosis: death-associated protein 3 and PDCD9 are mitochondrial ribosomal proteins," *FEBS Letters*, vol. 492, no. 1–2, pp. 166–170, 2001.
- [157] W. Voos and K. Röttgers, "Molecular chaperones as essential mediators of mitochondrial biogenesis," *Biochimica et Biophysica Acta*, vol. 1592, no. 1, pp. 51–62, 2002.
- [158] M. Koppen and T. Langer, "Protein degradation within mitochondria: versatile activities of AAA proteases and other peptidases," *Critical Reviews in Biochemistry and Molecular Biology*, vol. 42, no. 3, pp. 221–242, 2007.
- [159] L. G. J. Nijtmans, S. M. Artal, L. A. Grivell, and P. J. Coates, "The mitochondrial PHB complex: roles in mitochondrial respiratory complex assembly, ageing and degenerative disease," *Cellular and Molecular Life Sciences*, vol. 59, no. 1, pp. 143–155, 2002.
- [160] M. Artal-Sanz and N. Tavernarakis, "Prohibitin and mitochondrial biology," *Trends in Endocrinology and Metabolism*, vol. 20, no. 8, pp. 394–401, 2009.
- [161] M. Liu and L. Spremulli, "Interaction of mammalian mitochondrial ribosomes with the inner membrane," *Journal of Biological Chemistry*, vol. 275, no. 38, pp. 29400–29406, 2000.
- [162] K. Hell, J. M. Herrmann, E. Pratje, W. Neupert, and R. A. Stuart, "Oxa1p, an essential component of the N-tail protein export machinery in mitochondria," *Proceedings of the National Academy of Sciences of the United States of America*, vol. 95, no. 5, pp. 2250–2255, 1998.
- [163] K. Hell, W. Neupert, and R. A. Stuart, "Oxa1p acts as a general membrane insertion machinery for proteins encoded by mitochondrial DNA," *EMBO Journal*, vol. 20, no. 6, pp. 1281–1288, 2001.
- [164] M. Ott, M. Prestele, H. Bauerschmitt, S. Funes, N. Bonnefoy, and J. M. Herrmann, "Mba1, a membrane-associated ribosome receptor in mitochondria," *EMBO Journal*, vol. 25, no. 8, pp. 1603–1610, 2006.
- [165] M. E. Sanchirico, T. D. Fox, and T. L. Mason, "Accumulation of mitochondrially synthesized *Saccharomyces cerevisiae* Cox2p and Cox3p depends on targeting information in untranslated portions of their mRNAs," *EMBO Journal*, vol. 17, no. 19, pp. 5796–5804, 1998.
- [166] K. Watson, "The organization of ribosomal granules within mitochondrial structures of aerobic and anaerobic cells of *Saccharomyces cerevisiae*," *Journal of Cell Biology*, vol. 55, no. 3, pp. 721–726, 1972.
- [167] R. A. Stuart, "Insertion of proteins into the inner membrane of mitochondria: the role of the Oxa1 complex," *Biochimica et Biophysica Acta*, vol. 1592, no. 1, pp. 79–87, 2002.
- [168] N. Bonnefoy, H. L. Fiumera, G. Dujardin, and T. D. Fox, "Roles of Oxa1-related inner-membrane translocases in assembly of respiratory chain complexes," *Biochimica et Biophysica Acta*, vol. 1793, no. 1, pp. 60–70, 2009.

- [169] L. Jia, M. Dienhart, M. Schramp, M. McCauley, K. Hell, and R. A. Stuart, "Yeast Oxa1 interacts with mitochondrial ribosomes: the importance of the C-terminal region of Oxa1," *EMBO Journal*, vol. 22, no. 24, pp. 6438–6447, 2003.
- [170] L. Jia, J. Kaur, and R. A. Stuart, "Mapping of the *Saccharomyces cerevisiae* oxa1-mitochondrial ribosome interface and identification of MrpL40, a ribosomal protein in close proximity to oxal and critical for oxidative phosphorylation complex assembly," *Eukaryotic Cell*, vol. 8, no. 11, pp. 1792–1802, 2009.
- [171] M. Preuss, K. Leonhard, K. Hell, R. A. Stuart, W. Neupert, and J. M. Herrmann, "Mba1, a novel component of the mitochondrial protein export machinery of the yeast *Saccharomyces cerevisiae*," *Journal of Cell Biology*, vol. 153, no. 5, pp. 1085–1096, 2001.
- [172] S. Schlickum, A. Moghekar, J. C. Simpson, et al., "LETM1, a gene deleted in Wolf-Hirschhorn syndrome, encodes an evolutionarily conserved mitochondrial protein," *Genomics*, vol. 83, no. 2, pp. 254–261, 2004.
- [173] A. E. Frazier, R. D. Taylor, D. U. Mick, et al., "Mdm38 interacts with ribosomes and is a component of the mitochondrial protein export machinery," *Journal of Cell Biology*, vol. 172, no. 4, pp. 553–564, 2006.
- [174] L. Piao, Y. Li, S. J. Kim, et al., "Association of LETM1 and mrpl36 contributes to the regulation of mitochondrial ATP production and necrotic cell death," *Cancer Research*, vol. 69, no. 8, pp. 3397–3404, 2009.
- [175] S. Tamai, H. Iida, S. Yokota, et al., "Characterization of the mitochondrial protein LETM1, which maintains the mitochondrial tubular shapes and interacts with the AAA-ATPase BCS1L," *Journal of Cell Science*, vol. 121, no. 15, pp. 2588–2600, 2008.
- [176] K. S. Dimmer, F. Navoni, A. Casarin, et al., "LETM1, deleted in Wolf-Hirschhorn syndrome is required for normal mitochondrial morphology and cellular viability," *Human Molecular Genetics*, vol. 17, no. 2, pp. 201–214, 2008.
- [177] A. S. Lynch and J. C. Wang, "Anchoring of DNA to the bacterial cytoplasmic membrane through cotranscriptional synthesis of polypeptides encoding membrane proteins or proteins for export: a mechanism of plasmid hypernegative supercoiling in mutants deficient in DNA topoisomerase I," *Journal of Bacteriology*, vol. 175, no. 6, pp. 1645–1655, 1993.
- [178] G. H. Vos-Scheperkeuter and B. Witholt, "Co-translational insertion of envelope proteins: theoretical considerations and implications," *Annales de Microbiologie*, vol. 133A, no. 1, pp. 129–138, 1982.
- [179] M. Trinei, J.-P. Vannier, M. Beurton-Aimar, and V. Norris, "A hyperstructure approach to mitochondria," *Molecular Microbiology*, vol. 53, no. 1, pp. 41–53, 2004.
- [180] E. Fernández-Vizarra, V. Tiranti, and M. Zeviani, "Assembly of the oxidative phosphorylation system in humans: what we have learned by studying its defects," *Biochimica et Biophysica Acta*, vol. 1793, no. 1, pp. 200–211, 2009.
- [181] I. Ogilvie, N. G. Kennaway, and E. A. Shoubridge, "A molecular chaperone for mitochondrial complex I assembly is mutated in a progressive encephalopathy," *Journal of Clinical Investigation*, vol. 115, no. 10, pp. 2784–2792, 2005.
- [182] R. O. Vogel, R. J. R. J. Janssen, C. Ugalde, et al., "Human mitochondrial complex I assembly is mediated by NDUFAF1," *FEBS Journal*, vol. 272, no. 20, pp. 5317–5326, 2005.
- [183] S. J. G. Hoefs, C. E. J. Dieteren, R. J. Rodenburg, et al., "Baculovirus complementation restores a novel NDUFAF2 mutation causing complex I deficiency," *Human Mutation*, vol. 30, no. 7, pp. E728–E736, 2009.
- [184] A. Saada, R. O. Vogel, S. J. Hoefs, et al., "Mutations in NDUFAF3 (C3ORF60), encoding an NDUFAF4 (C6ORF66)-interacting complex I assembly protein, cause fatal neonatal mitochondrial disease," *American Journal of Human Genetics*, vol. 84, no. 6, pp. 718–727, 2009.
- [185] A. Saada, S. Edvardson, M. Rapoport, et al., "C6ORF66 is an assembly factor of mitochondrial complex I," *American Journal of Human Genetics*, vol. 82, no. 1, pp. 32–38, 2008.
- [186] R. O. Vogel, R. J. R. J. Janssen, M. A. M. van den Brand, et al., "Cytosolic signaling protein Ecsit also localizes to mitochondria where it interacts with chaperone NDUFAF1 and functions in complex I assembly," *Genes and Development*, vol. 21, no. 5, pp. 615–624, 2007.
- [187] D. J. Pagliarini, S. E. Calvo, B. Chang, et al., "A mitochondrial protein compendium elucidates complex I disease biology," *Cell*, vol. 134, no. 1, pp. 112–123, 2008.
- [188] M. Gerards, W. Sluiter, B. J. van den Bosch, et al., "Defective complex I assembly due to C20orf7 mutations as a new cause of Leigh syndrome," *Journal of Medical Genetics*. In press.
- [189] C. Sugiana, D. J. Pagliarini, M. McKenzie, et al., "Mutation of C20orf7 disrupts complex I assembly and causes lethal neonatal mitochondrial disease," *American Journal of Human Genetics*, vol. 83, no. 4, pp. 468–478, 2008.
- [190] R. O. Vogel, J. A. M. Smeitink, and L. G. J. Nijtmans, "Human mitochondrial complex I assembly: a dynamic and versatile process," *Biochimica et Biophysica Acta*, vol. 1767, no. 10, pp. 1215–1227, 2007.
- [191] N. Vahsen, C. Candé, J.-J. Brière, et al., "AIF deficiency compromises oxidative phosphorylation," *EMBO Journal*, vol. 23, no. 23, pp. 4679–4689, 2004.
- [192] K. Bych, S. Kerscher, D. J. A. Netz, et al., "The iron-sulphur protein Ind1 is required for effective complex I assembly," *EMBO Journal*, vol. 27, no. 12, pp. 1736–1746, 2008.
- [193] D. Ghezzi, P. Goffrini, G. Uziel, et al., "SDHAF1, encoding a LYR complex-II specific assembly factor, is mutated in SDH-defective infantile leukoencephalopathy," *Nature Genetics*, vol. 41, no. 6, pp. 654–656, 2009.
- [194] P. de Lonlay, I. Valnot, A. Barrientos, et al., "A mutant mitochondrial respiratory chain assembly protein causes complex III deficiency in patients with tubulopathy, encephalopathy and liver failure," *Nature Genetics*, vol. 29, no. 1, pp. 57–60, 2001.
- [195] P. Pecina, H. Houšková, H. Hansíková, J. Zeman, and J. Houšťek, "Genetic defects of cytochrome c oxidase assembly," *Physiological Research*, vol. 53, supplement 1, pp. S213–S223, 2004.
- [196] Z.-G. Wang, P. S. White, and S. H. Ackerman, "Atp11p and Atp12p are assembly factors for the F1-ATPase in human mitochondria," *Journal of Biological Chemistry*, vol. 276, no. 33, pp. 30773–30778, 2001.
- [197] X. Zeng, W. Neupert, and A. Tzagoloff, "The metalloprotease encoded by ATP23 has a dual function in processing and assembly of subunit 6 of mitochondrial ATPase," *Molecular Biology of the Cell*, vol. 18, no. 2, pp. 617–626, 2007.
- [198] L. Stiburek, D. Fornuskova, L. Wenchich, M. Pejznochova, H. Hansikova, and J. Zeman, "Knockdown of human Oxa1 impairs the biogenesis of F1Fo-ATP synthase and NADH:ubiquinone oxidoreductase," *Journal of Molecular Biology*, vol. 374, no. 2, pp. 506–516, 2007.
- [199] N. V. Dudkina, S. Sunderhaus, E. J. Boekema, and H.-P. Braun, "The higher level of organization of the oxidative phosphorylation system: mitochondrial supercomplexes," *Journal of Bioenergetics and Biomembranes*, vol. 40, no. 5, pp. 419–424, 2008.

- [200] E. A. Schon and N. A. Dencher, "Heavy breathing: energy conversion by mitochondrial respiratory supercomplexes," *Cell Metabolism*, vol. 9, no. 1, pp. 1–3, 2009.
- [201] R. Acín-Pérez, P. Fernández-Silva, M. L. Peleato, A. Pérez-Martos, and J. A. Enriquez, "Respiratory active mitochondrial supercomplexes," *Molecular Cell*, vol. 32, no. 4, pp. 529–539, 2008.
- [202] H. Schägger, R. De Coo, M. F. Bauer, S. Hofmann, C. Godino, and U. Brandt, "Significance of respirasomes for the assembly/stability of human respiratory chain complex I," *Journal of Biological Chemistry*, vol. 279, no. 35, pp. 36349–36353, 2004.
- [203] M. McKenzie, M. Lazarou, D. R. Thorburn, and M. T. Ryan, "Mitochondrial respiratory chain supercomplexes are destabilized in Barth Syndrome patients," *Journal of Molecular Biology*, vol. 361, no. 3, pp. 462–469, 2006.
- [204] H. Chen and D. C. Chan, "Emerging functions of mammalian mitochondrial fusion and fission," *Human Molecular Genetics*, vol. 14, no. 2, pp. R283–R289, 2005.
- [205] M. Liesa, M. Palacin, and A. Zorzano, "Mitochondrial dynamics in mammalian health and disease," *Physiological Reviews*, vol. 89, no. 3, pp. 799–845, 2009.
- [206] P. A. Parone, S. Da Cruz, D. Tondera, et al., "Preventing mitochondrial fission impairs mitochondrial function and leads to loss of mitochondrial DNA," *PLoS One*, vol. 3, no. 9, article e3257, 2008.
- [207] H. R. Waterham, J. Koster, C. W. T. van Roermund, P. A. W. Mooyer, R. J. A. Wanders, and J. V. Leonard, "A lethal defect of mitochondrial and peroxisomal fission," *New England Journal of Medicine*, vol. 356, no. 17, pp. 1736–1741, 2007.
- [208] I. J. Holt, A. E. Harding, and J. A. Morgan-Hughes, "Deletions of muscle mitochondrial DNA in patients with mitochondrial myopathies," *Nature*, vol. 331, no. 6158, pp. 717–719, 1988.
- [209] D. C. Wallace, G. Singh, M. T. Lott, et al., "Mitochondrial DNA mutation associated with Leber's hereditary optic neuropathy," *Science*, vol. 242, no. 4884, pp. 1427–1430, 1988.
- [210] F. Scaglia and L.-J. C. Wong, "Human mitochondrial transfer RNAs: role of pathogenic mutation in disease," *Muscle and Nerve*, vol. 37, no. 2, pp. 150–171, 2008.
- [211] C. Florentz, B. Sohm, P. Tryoen-Tóth, J. Pütz, and M. Sissler, "Human mitochondrial tRNAs in health and disease," *Cellular and Molecular Life Sciences*, vol. 60, no. 7, pp. 1356–1375, 2003.
- [212] E. Zifa, S. Giannouli, P. Theotokis, C. Stamatis, Z. Mamuris, and C. Stathopoulos, "Mitochondrial tRNA mutations: clinical and functional perturbations," *RNA Biology*, vol. 4, no. 1, pp. 38–66, 2007.
- [213] S. S. L. Chan and W. C. Copeland, "DNA polymerase gamma and mitochondrial disease: understanding the consequence of POLG mutations," *Biochimica et Biophysica Acta*, vol. 1787, no. 5, pp. 312–319, 2009.
- [214] M. J. Longley, S. Clark, C. Y. W. Man, et al., "Mutant POLG2 disrupts DNA polymerase γ subunits and causes progressive external ophthalmoplegia," *American Journal of Human Genetics*, vol. 78, no. 6, pp. 1026–1034, 2006.
- [215] J. A. Mayr, O. Merkel, S. D. Kohlwein, et al., "Mitochondrial phosphate-carrier deficiency: a novel disorder of oxidative phosphorylation," *American Journal of Human Genetics*, vol. 80, no. 3, pp. 478–484, 2007.
- [216] E. Ostergaard, E. Christensen, E. Kristensen, et al., "Deficiency of the α subunit of succinate-coenzyme A ligase causes fatal infantile lactic acidosis with mitochondrial DNA depletion," *American Journal of Human Genetics*, vol. 81, no. 2, pp. 383–387, 2007.
- [217] A. Bourdon, L. Minai, V. Serre, et al., "Mutation of RRM2B, encoding p53-controlled ribonucleotide reductase (p53R2), causes severe mitochondrial DNA depletion," *Nature Genetics*, vol. 39, no. 6, pp. 776–780, 2007.
- [218] K. D. Hauff and G. M. Hatch, "Cardiolipin metabolism and Barth Syndrome," *Progress in Lipid Research*, vol. 45, no. 2, pp. 91–101, 2006.
- [219] E. I. Rugarli and T. Langer, "Translating m-AAA protease function in mitochondria to hereditary spastic paraplegia," *Trends in Molecular Medicine*, vol. 12, no. 6, pp. 262–269, 2006.
- [220] G. M. C. Janssen, J. A. Maassen, and J. M. W. van Den Ouweland, "The diabetes-associated 3243 mutation in the mitochondrial tRNA(Leu(UUR)) gene causes severe mitochondrial dysfunction without a strong decrease in protein synthesis rate," *Journal of Biological Chemistry*, vol. 274, no. 42, pp. 29744–29748, 1999.
- [221] M. Toompuu, V. Tiranti, M. Zeviani, and H. T. Jacobs, "Molecular phenotype of the np 7472 deafness-associated mitochondrial mutation in osteosarcoma cell hybrids," *Human Molecular Genetics*, vol. 8, no. 12, pp. 2275–2283, 1999.
- [222] H. T. Jacobs, "Disorders of mitochondrial protein synthesis," *Human Molecular Genetics*, vol. 12, no. 2, pp. R293–R301, 2003.
- [223] J. Finsterer, "Genetic, pathogenetic, and phenotypic implications of the mitochondrial A3243G tRNA_{Leu}(UUR) mutation," *Acta Neurologica Scandinavica*, vol. 116, no. 1, pp. 1–14, 2007.
- [224] H. T. Jacobs and I. J. Holt, "The np 3243 MELAS mutation: damned if you aminoacylate, damned if you don't," *Human Molecular Genetics*, vol. 9, no. 4, pp. 463–465, 2000.
- [225] Y. Kirino, T. Yasukawa, S. Ohta, et al., "Codon-specific translational defect caused by a wobble modification deficiency in mutant tRNA from a human mitochondrial disease," *Proceedings of the National Academy of Sciences of the United States of America*, vol. 101, no. 42, pp. 15070–15075, 2004.
- [226] M. P. King, Y. Koga, M. Davidson, and E. A. Schon, "Defects in mitochondrial protein synthesis and respiratory chain activity segregate with the tRNA(Leu(UUR)) mutation associated with mitochondrial myopathy, encephalopathy, lactic acidosis, and stroke-like episodes," *Molecular and Cellular Biology*, vol. 12, no. 2, pp. 480–490, 1992.
- [227] J. A. Enriquez, A. Chomyn, and G. Attardi, "MtDNA mutation in MERRF syndrome causes defective aminoacylation of tRNA(Lys) and premature translation termination," *Nature Genetics*, vol. 10, no. 1, pp. 47–55, 1995.
- [228] G. Xing, Z. Chen, and X. Cao, "Mitochondrial rRNA and tRNA and hearing function," *Cell Research*, vol. 17, no. 3, pp. 227–239, 2007.
- [229] E. Cardaioli, M. T. Dotti, G. Hayek, M. Zappella, and A. Federico, "Studies on mitochondrial pathogenesis of Rett syndrome: ultrastructural data from skin and muscle biopsies and mutational analysis at mtDNA nucleotides 10463 and 2835," *Journal of Submicroscopic Cytology and Pathology*, vol. 31, no. 2, pp. 301–304, 1999.
- [230] R.-H. Hsieh, J.-Y. Li, C.-Y. Pang, and Y.-H. Wei, "A novel mutation in the mitochondrial 16S rRNA gene in a patient with MELAS syndrome, diabetes mellitus, hyperthyroidism and cardiomyopathy," *Journal of Biomedical Science*, vol. 8, no. 4, pp. 328–335, 2001.

- [231] J. M. Shoffner, M. D. Brown, A. Torroni, et al., "Mitochondrial DNA variants observed in Alzheimer disease and Parkinson disease patients," *Genomics*, vol. 17, no. 1, pp. 171–184, 1993.
- [232] J. Rozenski, P. F. Crain, and J. A. McCloskey, "The RNA modification database: 1999 update," *Nucleic Acids Research*, vol. 27, no. 1, pp. 196–197, 1999.
- [233] Y. Bykhovskaya, E. Mengesha, and N. Fischel-Ghodsian, "Pleiotropic effects and compensation mechanisms determine tissue specificity in mitochondrial myopathy and sideroblastic anemia (MLASA)," *Molecular Genetics and Metabolism*, vol. 91, no. 2, pp. 148–156, 2007.
- [234] S. S. Ashraf, E. Sochacka, R. Cain, R. Guenther, A. Malkiewicz, and P. F. Agris, "Single atom modification (O → S) of tRNA confers ribosome binding," *RNA*, vol. 5, no. 2, pp. 188–194, 1999.
- [235] C. Yarian, M. Marszalek, E. Sochacka, et al., "Modified nucleoside dependent Watson-Crick and wobble codon binding by tRNA(Lys)(UUU) species," *Biochemistry*, vol. 39, no. 44, pp. 13390–13395, 2000.
- [236] L. Valente, N. Shigi, T. Suzuki, and M. Zeviani, "The R336Q mutation in human mitochondrial EFTu prevents the formation of an active mt-EFTu · GTP · aa-tRNA ternary complex," *Biochimica et Biophysica Acta*, vol. 1792, no. 8, pp. 791–795, 2009.
- [237] K. A. Dittmar, J. M. Goodenbour, and T. Pan, "Tissue-specific differences in human transfer RNA expression," *PLoS Genetics*, vol. 2, no. 12, article e221, 2006.
- [238] A. Tzagoloff and A. Shtanko, "Mitochondrial and cytoplasmic isoleucyl-, glutamyl- and arginyl-tRNA synthetases of yeast are encoded by separate genes," *European Journal of Biochemistry*, vol. 230, no. 2, pp. 582–586, 1995.
- [239] A. Arnoldi, A. Tonelli, F. Crippa, et al., "A clinical, genetic, and biochemical characterization of SPG7 mutations in a large cohort of patients with hereditary spastic paraplegia," *Human Mutation*, vol. 29, no. 4, pp. 522–531, 2008.
- [240] L. Atorino, L. Silvestri, M. Koppen, et al., "Loss of m-AAA protease in mitochondria causes complex I deficiency and increased sensitivity to oxidative stress in hereditary spastic paraplegia," *Journal of Cell Biology*, vol. 163, no. 4, pp. 777–787, 2003.
- [241] P. A. Wilkinson, A. H. Crosby, C. Turner, et al., "A clinical, genetic and biochemical study of SPG7 mutations in hereditary spastic paraplegia," *Brain*, vol. 127, no. 5, pp. 973–980, 2004.
- [242] M. Koppen, M. D. Metodiev, G. Casari, E. I. Rugarli, and T. Langer, "Variable and tissue-specific subunit composition of mitochondrial m-AAA protease complexes linked to hereditary spastic paraplegia," *Molecular and Cellular Biology*, vol. 27, no. 2, pp. 758–767, 2007.
- [243] V. Tiranti, P. D'Adamo, E. Briem, et al., "Ethylmalonic encephalopathy is caused by mutations in ETHE1, a gene encoding a mitochondrial matrix protein," *American Journal of Human Genetics*, vol. 74, no. 2, pp. 239–252, 2004.
- [244] W. J. Ansorge, "Next-generation DNA sequencing techniques," *New Biotechnology*, vol. 25, no. 4, pp. 195–203, 2009.
- [245] T. Tucker, M. Marra, and J. M. Friedman, "Massively parallel sequencing: the next big thing in genetic medicine," *American Journal of Human Genetics*, vol. 85, no. 2, pp. 142–154, 2009.
- [246] S. B. Ng, E. H. Turner, P. D. Robertson, et al., "Targeted capture and massively parallel sequencing of 12 human exomes," *Nature*, vol. 461, no. 7261, pp. 272–276, 2009.
- [247] G. J. Porreca, K. Zhang, J. B. Li, et al., "Multiplex amplification of large sets of human exons," *Nature Methods*, vol. 4, no. 11, pp. 931–936, 2007.
- [248] B. Lehner, C. Crombie, J. Tischler, A. Fortunato, and A. G. Fraser, "Systematic mapping of genetic interactions in *Caenorhabditis elegans* identifies common modifiers of diverse signaling pathways," *Nature Genetics*, vol. 38, no. 8, pp. 896–903, 2006.
- [249] S. DiMauro and M. Mancuso, "Mitochondrial diseases: therapeutic approaches," *Bioscience Reports*, vol. 27, no. 1–3, pp. 125–137, 2007.
- [250] S. Koene and J. Smeitink, "Mitochondrial medicine: entering the era of treatment," *Journal of Internal Medicine*, vol. 265, no. 2, pp. 193–209, 2009.

Review Article

The Role of Exercise-Induced Myokines in Muscle Homeostasis and the Defense against Chronic Diseases

Claus Brandt and Bente K. Pedersen

The Centre of Inflammation and Metabolism, The Department of Infectious Diseases, Copenhagen Muscle Research Centre, Rigshospitalet, The Faculty of Health Sciences, University of Copenhagen, 2100 Copenhagen, Denmark

Correspondence should be addressed to Bente K. Pedersen, bkp@rh.dk

Received 17 November 2009; Accepted 26 January 2010

Academic Editor: Henk L. M. Granzier

Copyright © 2010 C. Brandt and B. K. Pedersen. This is an open access article distributed under the Creative Commons Attribution License, which permits unrestricted use, distribution, and reproduction in any medium, provided the original work is properly cited.

Chronic inflammation is involved in the pathogenesis of insulin resistance, atherosclerosis, neurodegeneration, and tumour growth. Regular exercise offers protection against type 2 diabetes, cardiovascular diseases, colon cancer, breast cancer, and dementia. Evidence suggests that the protective effect of exercise may to some extent be ascribed to the anti-inflammatory effect of regular exercise. Here we suggest that exercise may exert its anti-inflammatory effect via a reduction in visceral fat mass and/or by induction of an anti-inflammatory environment with each bout of exercise. According to our theory, such effects may in part be mediated via muscle-derived peptides, so-called “myokines”. Contracting skeletal muscles release myokines with endocrine effects, mediating direct anti-inflammatory effects, and/or specific effects on visceral fat. Other myokines work locally within the muscle and exert their effects on signalling pathways involved in fat oxidation and glucose uptake. By mediating anti-inflammatory effects in the muscle itself, myokines may also counteract TNF-driven insulin resistance. In conclusion, exercise-induced myokines appear to be involved in mediating both systemic as well as local anti-inflammatory effects.

1. Introduction

Over the past several decades, numerous large cohort studies have attempted to quantify the protective effect of physical activity on cardiovascular and all-cause mortality. A recent meta-analysis included a total of 33 studies with 883,372 participants with a followup time of up to more than 20 years [1]. Concerning cardiovascular mortality, physical activity was associated with a risk reduction of 35%, whereas all-cause mortality was reduced by 33%. Taken together, there is no doubt that physical activity is independently associated with a marked decrease in risk of cardiovascular disease (CVD) as well as CVD mortality in both men and women.

Randomised controlled trials including people with impaired glucose tolerance have found that lifestyle modification (diet and moderate physical activity) protects against the development of type 2 diabetes. A Finnish trial randomised 522 overweight middle-aged people with impaired glucose tolerance to physical training combined with diet or to control and followed them for 3.2 years

[2]. The risk of type 2 diabetes was reduced by 58% in the intervention group. The effect was largest in the patients who made the greatest lifestyle modification. An American trial randomised 3,234 people with impaired glucose tolerance to treatment with metformin, lifestyle modification entailing dietary change and at least 150 minutes of physical exercise weekly, or placebo and followed them for 2.8 years [3]. The lifestyle modification reduced the risk of type 2 diabetes by 58%. The reduction was, thus, the same as in the Finnish trial [2], whereas treatment with metformin only reduced the risk of diabetes by 31%. After a median of 4 years of active intervention period, participants in the Finnish study who were still free of diabetes were further followed up for a median of 3 years. During the total followup, the incidence of type 2 diabetes was 4.3 and 7.4 per 100 person-years in the intervention and control groups, respectively, indicating 43% reduction in relative risk. The risk reduction was related to the success in achieving the intervention goals of weight loss, reduced intake of total and saturated fat and increased intake of dietary fibre, and increased physical activity [4].

In humans, type 2 diabetes are associated with impaired cognitive function, including learning, memory, and processing speed [5]. Large longitudinal population-based studies show that the rate of cognitive decline is accelerated in elderly people with type 2 diabetes [6]. A recent review [7] showed that the incidence of ‘any dementia’ was higher in individuals with type 2 diabetes than in those without. This high risk included both Alzheimer’s disease and vascular dementia. Interestingly, a couple of studies suggest that regular exercise also protects against dementia [8–10].

Type 2 diabetes, cardiovascular diseases, colon cancer, breast cancer, and dementia constitute a cluster of diseases that defines “a diseasome of physical inactivity” [11]. Both physical inactivity and abdominal adiposity, reflecting accumulation of visceral fat mass, are associated with the occurrence of the diseases within the diseasome. We recently suggested that physical inactivity leads to accumulation of visceral fat and consequently the activation of a network of inflammatory pathways, which promote the development of insulin resistance, atherosclerosis, neurodegeneration, tumour growth, and thereby the development of the diseases belonging to the “diseasome of physical inactivity” [11].

Chronic inflammation accompanies the diseases within the “diseasome of physical inactivity”, potentially explaining the clustering of these chronic disorders in epidemiological studies. The aim of the present review is to summarize the evidence suggesting that regular exercise creates an anti-inflammatory environment, and thereby offers protection against a vast number of chronic diseases.

2. Inflammation as a Cause of Chronic Diseases

Systemic low-grade inflammation is defined as two- to four-fold elevations in circulating levels of proinflammatory and anti-inflammatory cytokines, naturally occurring cytokine antagonists, and acute-phase proteins, as well as minor increases in counts of neutrophils and natural killer cells [12–14]. Chronic inflammation contributes to the development of atherosclerosis, insulin resistance, tumour growth, and neurodegeneration [15], and thus directly influences pathogenesis of key importance for the development of the chronic diseases within the “diseasome of physical inactivity” [11].

It appears that TNF- α may play a direct role in the metabolic syndrome, recently reviewed in [16]. In vitro studies demonstrate that TNF- α has direct inhibitory effects on insulin signalling. Moreover, TNF- α infusion in healthy humans induces insulin resistance in skeletal muscle, without an effect on endogenous glucose production [17].

It has also been proposed that TNF- α causes insulin resistance indirectly in vivo by increasing the release of free fatty acids (FFAs) from adipose tissue. TNF- α increases lipolysis in human and 3T3-L1 adipocytes. However, TNF- α has no effect on muscle protein turnover or fatty acid oxidation but increases fatty acid incorporation into diacylglycerol, which may be involved in the development of the TNF- α -induced insulin resistance in skeletal muscle [18, 19]. Moreover, evidence suggests that TNF- α plays a direct role in

linking insulin resistance to vascular disease [20, 21]. Several downstream mediators and signalling pathways seem to provide the crosstalk between inflammatory and metabolic signalling. These include the discovery of c-Jun N-terminal kinase (JNK) and I kappa beta kinase (IKK) as critical regulators of insulin action activated by TNF- α [22]. In human TNF- α infusion studies, TNF- α increases phosphorylation of p70 S6 kinase, extracellular signal-regulated kinase-1/2, and c-Jun NH(2)-terminal kinase, concomitantly with increased serine and reduced tyrosine phosphorylation of insulin receptor substrate-1 [21]. These signalling effects are associated with impaired phosphorylation of Akt substrate 160, the most proximal step identified in the insulin signalling cascade regulating GLUT4 translocation and glucose uptake [21].

The role of IL-6 in insulin resistance is highly controversial, as reviewed in [16]. Infusion of recombinant human (rh)IL-6 into resting healthy humans does not impair whole body, lower limb, or subcutaneous adipose tissue glucose uptake or endogenous glucose production (EGP), although IL-6 contributes to the contraction-induced increase in endogenous glucose production [16]. A number of studies indicate that IL-6 enhances lipolysis, as well as fat oxidation, via an activation of AMP-activated protein kinase (AMPK), reviewed in [16]. Consistent with this idea, Wallenius et al. [23] demonstrated that IL-6 deficient mice developed mature-onset obesity and insulin resistance. In addition, when the mice were treated with IL-6, there was a significant decrease in body fat mass in the IL-6 knockout, but not in the wild-type mice. To determine whether physiological concentrations of IL-6 affected lipid metabolism, our group administered physiological concentrations of rhIL-6 to healthy young and elderly humans as well as to patients with type 2 diabetes [24, 25]. The latter studies identified IL-6 as a potent modulator of fat metabolism in humans, increasing lipolysis as well as fat oxidation without causing hypertriglycerolaemia.

Of note, whereas it is known that both TNF- α and IL-6 induce lipolysis, only IL-6 appears to induce fat oxidation [18, 25]. Although circulating levels of TNF- α and IL-6 coexist in epidemiological studies [26], the biological profiles of these cytokines are very different. TNF- α stimulates the release of IL-6 and one theory holds that it is TNF- α derived from adipose tissue that is actually the major “driver” behind inflammation-induced insulin resistance and atherosclerosis.

Importantly, also tumour progression is stimulated by systemic elevation of proinflammatory cytokines [15, 27]. In addition, a number of neurodegenerative diseases are linked to a local inflammatory response in the brain (neuroinflammation) and systemic inflammation may further exacerbate the progression of neurodegeneration [28].

In summary, inflammation is *directly* involved in the pathogenesis of insulin resistance, atherosclerosis, neurodegeneration, and tumour growth. Therefore, the finding that type 2 diabetes, cardiovascular diseases, Alzheimer’s disease and cancer is associated with chronic inflammation suggests that inflammatory mechanisms contribute as causative factors in the development of these disorders.

3. The Myokine Concept

The protective effect of exercise against diseases associated with chronic inflammation may to some extent be ascribed to an anti-inflammatory effect of regular exercise.

In line with the acceptance of adipose tissue as an endocrine organ, we came up with the innovative idea that also skeletal muscle should be viewed as an endocrine organ. We have suggested that cytokines and other peptides that are produced, expressed, and released by muscle fibres and exert paracrine or endocrine effects should be classified as “myokines”. This paradigm provides a conceptual basis explaining the multiple consequences of a physically inactive lifestyle. If the endocrine and paracrine functions of the muscle are not stimulated through contractions, this will cause dysfunction of several organs and tissues of the body as well as an increased risk of cardiovascular disease, cancer, and dementia.

Today, it appears that skeletal muscle has the capacity to express several myokines. The list includes IL-6, IL-8, IL-15 [29], BDNF [30], and LIF [31]. In addition, Kenneth Walsh, Boston, has recently identified the myokines FGF21 and Follistatin-like-1 [32, 33].

The prototype myokine, IL-6, appears to be able to mediate metabolic effects as well as anti-inflammatory effects. IL-6 was the first identified and to date most studied myokine. The gp130 receptor cytokine IL-6 was discovered as a myokine because of the observation that it increases up to 100-fold in the circulation during physical exercise. Identification of IL-6 production by skeletal muscle during physical activity generated renewed interest in the metabolic role of IL-6 because it created a paradox. On one hand, IL-6 is markedly produced and released in the post-exercise period when insulin action is enhanced but, on the other hand, IL-6 has also been associated with obesity and reduced insulin action. However, a number of studies during the past decade have revealed that in response to muscle contractions both type I and type II muscle fibres express the myokine IL-6, which subsequently exerts its effects both locally within the muscle (e.g., through activation of AMPK) and—when released into the circulation—peripherally in several organs in a hormone-like fashion. Within skeletal muscle, IL-6 acts locally to signal through gp130R β /IL-6R α , resulting in activation of AMPK and/or PI3-kinase to increase glucose uptake and fat oxidation. IL-6 may also work in an endocrine fashion to increase hepatic glucose production during exercise or lipolysis in adipose tissue, reviewed in [16].

IL-15 is expressed in human skeletal muscle, and has been identified as an anabolic factor in muscle growth, and appears also to play a role in lipid metabolism [34]. Recently, we demonstrated that IL-15 mRNA levels were upregulated in human skeletal muscle following a bout of strength training [35], suggesting that IL-15 may accumulate within the muscle as a consequence of regular training. Interestingly, a negative association exists between plasma IL-15 concentration and trunk fat mass. In support of the human data, we found a decrease in visceral fat mass, but not subcutaneous fat mass, when IL-15 was overexpressed

in murine muscle [36]. Quinn et al. found that elevated circulating levels of IL-15 resulted in significant reductions in body fat and increased bone mineral content, without appreciably affecting lean body mass or levels of other cytokines [37]. These findings lend support to the idea that muscle-expressed IL-15 may be involved in the regulation of visceral fat mass.

BDNF is recognized as playing a key role in regulating survival, growth, and maintenance of neurons [38], and BDNF plays a role in learning and memory [39]. Hippocampal samples from Alzheimer’s disease donors show decreased BDNF expression [40] and individuals with Alzheimer’s disease have low plasma levels of BDNF [41]. Also, patients with major depression have lower levels of serum BDNF than normal control subjects [42]. Other studies suggest that plasma BDNF is a biomarker of impaired memory and general cognitive function in ageing women [43] and a low circulating BDNF level was recently shown to be an independent and robust biomarker of mortality risk in old women [44]. Interestingly, we found low levels of circulating BDNF also in individuals with both obesity and type 2 diabetes [45]. Thus, BDNF is low in people with Alzheimer’s disease, major depression, impaired cognitive function, CVD, type 2 diabetes, and obesity.

We studied whether skeletal muscle would produce BDNF in response to exercise [46]. It was found that BDNF mRNA and protein expression was increased in human skeletal muscle after exercise; however, muscle-derived BDNF appeared not to be released into the circulation. In addition, BDNF mRNA and protein expression was increased in muscle cells that were electrically stimulated. Interestingly, BDNF increased phosphorylation of AMPK and Acetyl Co-carboxylase (ACC) and enhanced fat oxidation both in vitro and ex vivo. Thus, we have been able to identify BDNF as a novel contraction-induced muscle cell-derived protein that may increase fat oxidation in skeletal muscle in an AMPK-dependent fashion. BDNF appears to be a myokine that works in an autocrine or paracrine fashion with strong effects on peripheral metabolism, including fat oxidation with a subsequent effect on the size of adipose tissue [30].

In summary, contracting skeletal muscles release myokines, which create a systemic anti-inflammatory environment and exert specific endocrine effects on visceral fat. Such myokines may also work locally within the muscle and exert their effects on signalling pathways involved in fat oxidation and glucose uptake. Taken together, myokines may be involved in mediating the anti-inflammatory effects of exercise.

4. The Anti-inflammatory Effects of an Acute Bout of Exercise

Regular exercise appears to induce anti-inflammatory effects, suggesting that physical activity per se may suppress systemic low-grade inflammation [47]. Several studies show that markers of inflammation are reduced following longer-term behavioural changes involving both reduced energy intake and increased physical activity, reviewed in [48]. However,

the mediators of this effect are unresolved. A number of mechanisms have been identified. Exercise increases the release of epinephrine, cortisol, growth hormone, prolactin, and other factors that have immunomodulatory effects [15, 49].

IL-6 is the first cytokine present in the circulation during exercise and the appearance of IL-6 in the circulation is by far the most marked and its appearance precedes that of the other cytokines. The fact that the classical pro-inflammatory cytokines, TNF- α and IL-1 β , in general do not increase with exercise, whereas exercise provokes an increase in circulating levels of IL-1ra, IL-10, and sTNF-R [50, 51], suggests that exercise provokes an environment of anti-inflammatory cytokines. Importantly, we showed that rhIL-6 infusion as well as exercise inhibited the endotoxin-induced increase in circulating levels of TNF- α in healthy humans [52]. The anti-inflammatory effects of IL-6 have also been demonstrated by IL-6 stimulating the production of the classical anti-inflammatory cytokines IL-1ra and IL-10 [53].

Recent work has shown that both upstream and downstream signalling pathways for IL-6 differ markedly between myocytes and macrophages. It appears that unlike IL-6 signalling in macrophages, which is dependent upon activation of the NF κ B signalling pathway, intramuscular IL-6 expression is regulated by a network of signalling cascades, including the Ca²⁺/NFAT and glycogen/p38 MAPK pathways. Thus, when IL-6 is signalling in monocytes or macrophages, it creates a pro-inflammatory response, whereas IL-6 activation and signalling in muscle is totally independent of a preceding TNF-response or NF κ B activation.

In summary, the possibility exists that with regular exercise the anti-inflammatory effects of an acute bout of exercise will protect against chronic systemic low-grade inflammation, but such a direct link between the acute effects of exercise and the long-term benefits has yet to be established.

5. Conclusion

The authors suggest that the beneficial effects of regular exercise may be due to the anti-inflammatory effects of muscle contractions. Such exercise effects may be mediated via long-term effects on abdominal adiposity and/or by the anti-inflammatory environment that is created by each acute bout of exercise.

Acknowledgments

The Centre of Inflammation and Metabolism is supported by a grant from the Danish National Research Foundation (no. 02-512-55). The study was further supported by the Danish Medical Research Council (no. 22-01-009) and by the Commission of the European Communities (contract no. LSHM-CT-2004-005272 EXGENESIS). The Copenhagen Muscle Research Centre is supported by the Capital Region of Denmark and the University of Copenhagen.

References

- [1] M. Nocon, T. Hiemann, F. Muller-Riemenschneider, F. Thalau, S. Roll, and S. N. Willich, "Association of physical activity with all-cause and cardiovascular mortality: a systematic review and meta-analysis," *European Journal of Cardiovascular Prevention and Rehabilitation*, vol. 15, no. 3, pp. 239–246, 2008.
- [2] J. Tuomilehto, J. Lindstrom, J. G. Eriksson, et al., "Prevention of type 2 diabetes mellitus by changes in lifestyle among subjects with impaired glucose tolerance," *New England Journal of Medicine*, vol. 344, no. 18, pp. 1343–1350, 2001.
- [3] W. C. Knowler, E. Barrett-Connor, S. E. Fowler, et al., "Reduction in the incidence of type 2 diabetes with lifestyle intervention or metformin," *New England Journal of Medicine*, vol. 346, no. 6, pp. 393–403, 2002.
- [4] J. Lindstrom, P. Ilanne-Parikka, M. Peltonen, et al., "Sustained reduction in the incidence of type 2 diabetes by lifestyle intervention: follow-up of the Finnish Diabetes Prevention Study," *The Lancet*, vol. 368, no. 9548, pp. 1673–1679, 2006.
- [5] H. Bruunsgaard, *Ageing and immune function*, M.S. thesis/dissertation, University of Copenhagen, Copenhagen, Denmark, 2000.
- [6] K. V. Allen, B. M. Frier, and M. W. J. Strachan, "The relationship between type 2 diabetes and cognitive dysfunction: longitudinal studies and their methodological limitations," *European Journal of Pharmacology*, vol. 490, no. 1–3, pp. 169–175, 2004.
- [7] G. J. Biessels, S. Staekenborg, E. Brunner, C. Brayne, and P. Scheltens, "Risk of dementia in diabetes mellitus: a systematic review," *Lancet Neurology*, vol. 5, no. 1, pp. 64–74, 2006.
- [8] S. Rovio, I. Kareholt, E.-L. Helkala, et al., "Leisure-time physical activity at midlife and the risk of dementia and Alzheimer's disease," *Lancet Neurology*, vol. 4, no. 11, pp. 705–711, 2005.
- [9] R. Andel, M. Crowe, N. L. Pedersen, L. Fratiglioni, B. Johansson, and M. Gatz, "Physical exercise at midlife and risk of dementia three decades later: a population-based study of Swedish twins," *Journals of Gerontology*, vol. 63, no. 1, pp. 62–66, 2008.
- [10] N. T. Lautenschlager, K. L. Cox, L. Flicker, et al., "Effect of physical activity on cognitive function in older adults at risk for Alzheimer disease: a randomized trial," *Journal of the American Medical Association*, vol. 300, no. 9, pp. 1027–1037, 2008.
- [11] B. K. Pedersen, "The diseasome of physical inactivity—and the role of myokines in muscle-fat cross talk," *Journal of Physiology*, vol. 587, no. 23, pp. 5559–5568, 2009.
- [12] H. Bruunsgaard and B. K. Pedersen, "Age-related inflammatory cytokines and disease," *Immunology and Allergy Clinics of North America*, vol. 23, no. 1, pp. 15–39, 2003.
- [13] H. Bruunsgaard, S. Ladelund, A. N. Pedersen, M. Schroll, T. Jorgensen, and B. K. Pedersen, "Predicting death from tumour necrosis factor-alpha and interleukin-6 in 80-year-old people," *Clinical and Experimental Immunology*, vol. 132, no. 1, pp. 24–31, 2003.
- [14] H. Bruunsgaard, A. N. Pedersen, M. Schroll, P. Skinhoj, and B. K. Pedersen, "Impaired production of proinflammatory cytokines in response to lipopolysaccharide (LPS) stimulation in elderly humans," *Clinical and Experimental Immunology*, vol. 118, no. 2, pp. 235–241, 1999.
- [15] C. Handschin and B. M. Spiegelman, "The role of exercise and PGC1 α in inflammation and chronic disease," *Nature*, vol. 454, no. 7203, pp. 463–469, 2008.

- [16] B. K. Pedersen and M. A. Febbraio, "Muscle as an endocrine organ: focus on muscle-derived interleukin-6," *Physiological Reviews*, vol. 88, no. 4, pp. 1379–1406, 2008.
- [17] P. Plomgaard, K. Bouzakri, R. Krogh-Madsen, B. Mittendorfer, J. R. Zierath, and B. K. Pedersen, "Tumor necrosis factor- α induces skeletal muscle insulin resistance in healthy human subjects via inhibition of Akt substrate 160 phosphorylation," *Diabetes*, vol. 54, no. 10, pp. 2939–2945, 2005.
- [18] P. Plomgaard, C. P. Fischer, T. Ibfelt, B. K. Pedersen, and G. Van Hall, "Tumor necrosis factor- α modulates human in vivo lipolysis," *Journal of Clinical Endocrinology and Metabolism*, vol. 93, no. 2, pp. 543–549, 2008.
- [19] A. M. Petersen, P. Plomgaard, C. P. Fischer, T. Ibfelt, B. K. Pedersen, and G. Van Hall, "Acute moderate elevation of TNF- α does not affect systemic and skeletal muscle protein turnover in healthy humans," *Journal of Clinical Endocrinology and Metabolism*, vol. 94, no. 1, pp. 294–299, 2009.
- [20] J. S. Yudkin, E. Eringa, and C. D. A. Stehouwer, "Vasocrine" signalling from perivascular fat: a mechanism linking insulin resistance to vascular disease," *The Lancet*, vol. 365, no. 9473, pp. 1817–1820, 2005.
- [21] P. Plomgaard, P. Keller, C. Keller, and B. K. Pedersen, "TNF- α , but not IL-6, stimulates plasminogen activator inhibitor-1 expression in human subcutaneous adipose tissue," *Journal of Applied Physiology*, vol. 98, no. 6, pp. 2019–2023, 2005.
- [22] G. S. Hotamisligil, "Inflammatory pathways and insulin action," *International Journal of Obesity*, vol. 27, supplement 3, pp. S53–S55, 2003.
- [23] V. Wallenius, K. Wallenius, B. Ahren, et al., "Interleukin-6-deficient mice develop mature-onset obesity," *Nature Medicine*, vol. 8, no. 1, pp. 75–79, 2002.
- [24] E. W. Petersen, A. L. Carey, M. Sacchetti, et al., "Acute IL-6 treatment increases fatty acid turnover in elderly humans in vivo and in tissue culture in vitro," *American Journal of Physiology*, vol. 288, no. 1, pp. E155–E162, 2005.
- [25] G. Van Hall, A. Steensberg, M. Sacchetti, et al., "Interleukin-6 stimulates lipolysis and fat oxidation in humans," *Journal of Clinical Endocrinology and Metabolism*, vol. 88, no. 7, pp. 3005–3010, 2003.
- [26] P. Plomgaard, A. R. Nielsen, C. P. Fischer, et al., "Associations between insulin resistance and TNF- α in plasma, skeletal muscle and adipose tissue in humans with and without type 2 diabetes," *Diabetologia*, vol. 50, no. 12, pp. 2562–2571, 2007.
- [27] W.-W. Lin and M. Karin, "A cytokine-mediated link between innate immunity, inflammation, and cancer," *Journal of Clinical Investigation*, vol. 117, no. 5, pp. 1175–1183, 2007.
- [28] V. H. Perry, C. Cunningham, and C. Holmes, "Systemic infections and inflammation affect chronic neurodegeneration," *Nature Reviews Immunology*, vol. 7, no. 2, pp. 161–167, 2007.
- [29] B. K. Pedersen, "Edward F. Adolph distinguished lecture: muscle as an endocrine organ: IL-6 and other myokines," *Journal of Applied Physiology*, vol. 107, no. 4, pp. 1006–1014, 2009.
- [30] B. K. Pedersen, M. Pedersen, K. S. Krabbe, H. Bruunsgaard, V. B. Matthews, and M. A. Febbraio, "Role of exercise-induced brain-derived neurotrophic factor production in the regulation of energy homeostasis in mammals: experimental physiology-hot topic review," *Experimental Physiology*, vol. 94, no. 12, pp. 1153–1160, 2009.
- [31] C. Broholm, O. H. Mortensen, S. Nielsen, et al., "Exercise induces expression of leukaemia inhibitory factor in human skeletal muscle," *Journal of Physiology*, vol. 586, no. 8, pp. 2195–2201, 2008.
- [32] Y. Izumiya, H. A. Bina, N. Ouchi, Y. Akasaki, A. Kharitonkov, and K. Walsh, "FGF21 is an Akt-regulated myokine," *FEBS Letters*, vol. 582, no. 27, pp. 3805–3810, 2008.
- [33] N. Ouchi, Y. Oshima, K. Ohashi, et al., "Follistatin-like 1, a secreted muscle protein, promotes endothelial cell function and revascularization in ischemic tissue through a nitric-oxide synthase-dependent mechanism," *Journal of Biological Chemistry*, vol. 283, no. 47, pp. 32802–32811, 2008.
- [34] A. R. Nielsen and B. K. Pedersen, "The biological roles of exercise-induced cytokines: IL-6, IL-8, and IL-15," *Applied Physiology, Nutrition and Metabolism*, vol. 32, no. 5, pp. 833–839, 2007.
- [35] A. R. Nielsen, R. Mounier, P. Plomgaard, et al., "Expression of interleukin-15 in human skeletal muscle—effect of exercise and muscle fibre type composition," *Journal of Physiology*, vol. 584, no. 1, pp. 305–312, 2007.
- [36] A. R. Nielsen, P. Hojman, C. Erikstrup, et al., "Association between interleukin-15 and obesity: interleukin-15 as a potential regulator of fat mass," *Journal of Clinical Endocrinology and Metabolism*, vol. 93, no. 11, pp. 4486–4493, 2008.
- [37] L. S. Quinn, B. G. Anderson, L. Strait-Bodey, A. M. Stroud, and J. M. Argiles, "Oversecretion of interleukin-15 from skeletal muscle reduces adiposity," *American Journal of Physiology*, vol. 296, no. 1, pp. E191–E202, 2009.
- [38] M. P. Mattson, S. Maudsley, and B. Martin, "BDNF and 5-HT: a dynamic duo in age-related neuronal plasticity and neurodegenerative disorders," *Trends in Neurosciences*, vol. 27, no. 10, pp. 589–594, 2004.
- [39] W. J. Tyler, M. Alonso, C. R. Bramham, and L. D. Pozzo-Miller, "From acquisition to consolidation: on the role of brain-derived neurotrophic factor signaling in hippocampal-dependent learning," *Learning and Memory*, vol. 9, no. 5, pp. 224–237, 2002.
- [40] B. Connor, D. Young, Q. Yan, R. L. M. Faull, B. Synek, and M. Dragunow, "Brain-derived neurotrophic factor is reduced in Alzheimer's disease," *Molecular Brain Research*, vol. 49, no. 1–2, pp. 71–81, 1997.
- [41] C. Laske, E. Stransky, T. Leyhe, et al., "Stage-dependent BDNF serum concentrations in Alzheimer's disease," *Journal of Neural Transmission*, vol. 113, no. 9, pp. 1217–1224, 2006.
- [42] F. Karege, G. Perret, G. Bondolfi, M. Schwald, G. Bertschy, and J.-M. Aubry, "Decreased serum brain-derived neurotrophic factor levels in major depressed patients," *Psychiatry Research*, vol. 109, no. 2, pp. 143–148, 2002.
- [43] P. Komulainen, M. Pedersen, T. Hanninen, et al., "BDNF is a novel marker of cognitive function in ageing women: the DR's EXTRA Study," *Neurobiology of Learning and Memory*, vol. 90, no. 4, pp. 596–603, 2008.
- [44] K. S. Krabbe, E. L. Mortensen, K. Avlund, et al., "Brain-derived neurotrophic factor predicts mortality risk in older women," *Journal of the American Geriatrics Society*, vol. 57, no. 8, pp. 1447–1452, 2009.
- [45] K. S. Krabbe, A. R. Nielsen, R. Krogh-Madsen, et al., "Brain-derived neurotrophic factor (BDNF) and type 2 diabetes," *Diabetologia*, vol. 50, no. 2, pp. 431–438, 2007.
- [46] V. B. Matthews, M.-B. Åström, M. H. S. Chan, et al., "Brain-derived neurotrophic factor is produced by skeletal muscle cells in response to contraction and enhances fat oxidation via activation of AMP-activated protein kinase," *Diabetologia*, vol. 52, no. 7, pp. 1409–1418, 2009.
- [47] N. Mathur and B. K. Pedersen, "Exercise as a mean to control low-grade systemic inflammation," *Mediators of Inflammation*, vol. 2008, Article ID 109502, 6 pages, 2008.

- [48] A. M. W. Petersen and B. K. Pedersen, "The anti-inflammatory effect of exercise," *Journal of Applied Physiology*, vol. 98, no. 4, pp. 1154–1162, 2005.
- [49] D. C. Nieman, "Current perspective on exercise immunology," *Current Sports Medicine Reports*, vol. 2, no. 5, pp. 239–242, 2003.
- [50] K. Ostrowski, P. Schjerling, and B. K. Pedersen, "Physical activity and plasma interleukin-6 in humans—effect of intensity of exercise," *European Journal of Applied Physiology*, vol. 83, no. 6, pp. 512–515, 2000.
- [51] K. Ostrowski, T. Rohde, S. Asp, P. Schjerling, and B. K. Pedersen, "Pro- and anti-inflammatory cytokine balance in strenuous exercise in humans," *Journal of Physiology*, vol. 515, part 1, pp. 287–291, 1999.
- [52] R. Starkie, S. R. Ostrowski, S. Jauffred, M. Febbraio, and B. K. Pedersen, "Exercise and IL-6 infusion inhibit endotoxin-induced TNF-alpha production in humans," *The FASEB Journal*, vol. 17, no. 8, pp. 884–886, 2003.
- [53] A. Steensberg, C. P. Fischer, C. Keller, K. Moller, and B. K. Pedersen, "IL-6 enhances plasma IL-1ra, IL-10, and cortisol in humans," *American Journal of Physiology*, vol. 285, no. 2, pp. E433–E437, 2003.

Review Article

Skeletal Muscle Insulin Resistance in Endocrine Disease

Melpomeni Peppas,¹ Chrysi Koliaki,¹ Panagiotis Nikolopoulos,¹ and Sotirios A. Raptis^{1,2}

¹Endocrine Unit, Second Department of Internal Medicine-Propaedeutic, Research Institute and Diabetes Center, Athens University Medical School, Attikon University Hospital, 1 Rimini Street, Haidari, 12 462, Athens, Greece

²Hellenic National Center for the Research, Prevention and Treatment of Diabetes and Its Complications (H.N.D.C), 3 Ploutarchou Street, 10675 Athens, Greece

Correspondence should be addressed to Melpomeni Peppas, molypepa@otenet.gr

Received 10 November 2009; Accepted 3 February 2010

Academic Editor: Guy M. Benian

Copyright © 2010 Melpomeni Peppas et al. This is an open access article distributed under the Creative Commons Attribution License, which permits unrestricted use, distribution, and reproduction in any medium, provided the original work is properly cited.

We summarize the existing literature data concerning the involvement of skeletal muscle (SM) in whole body glucose homeostasis and the contribution of SM insulin resistance (IR) to the metabolic derangements observed in several endocrine disorders, including polycystic ovary syndrome (PCOS), adrenal disorders and thyroid function abnormalities. IR in PCOS is associated with a unique postbinding defect in insulin receptor signaling in general and in SM in particular, due to a complex interaction between genetic and environmental factors. Adrenal hormone excess is also associated with disrupted insulin action in peripheral tissues, such as SM. Furthermore, both hyper- and hypothyroidism are thought to be insulin resistant states, due to insulin receptor and postreceptor defects. Further studies are definitely needed in order to unravel the underlying pathogenetic mechanisms. In summary, the principal mechanisms involved in muscle IR in the endocrine diseases reviewed herein include abnormal phosphorylation of insulin signaling proteins, altered muscle fiber composition, reduced transcapillary insulin delivery, decreased glycogen synthesis, and impaired mitochondrial oxidative metabolism.

1. Introduction

Insulin resistance (IR) constitutes a common and broadly prevalent metabolic disorder, which seems to govern the pathophysiology of diabetes mellitus, metabolic syndrome, and obesity [1]. Furthermore, IR appears to be a clinically important manifestation of various endocrine diseases, including polycystic ovary syndrome (PCOS), thyroid and adrenal diseases, as well as their complications [2–5]. From a pathophysiological point of view, IR appears to be the end result of a complex interaction between genetic predisposition and environmental factors.

In general, IR indicates the presence of an impaired peripheral tissue response to endogenously secreted insulin. It is typically manifested as both decreased insulin-mediated glucose uptake (IMGU) at the level of adipose and skeletal muscle (SM) tissue, and as an impaired suppression of hepatic glucose output. A significant body of evidence supports the critical role of SM for the development of IR, most commonly through an interactive cross-talk with adipose and liver tissue [6–8].

2. Skeletal Muscle and Glucose Homeostasis

SM plays a crucial role in maintaining systemic glucose metabolism, accounting for 85% of whole body insulin-stimulated glucose uptake [7]. In SM, insulin stimulates glucose uptake by increasing the translocation of glucose transport molecules, mainly GLUT4, from intracellular vesicles to the cell surface [9]. This process is initiated upon binding of insulin to the transmembrane receptor and is mediated through an intracellular molecular signaling cascade, including the consecutive phosphorylation of several cytosolic proteins, such as insulin receptor substrate molecules (IRS), phosphatidylinositol 3-kinase (PI3K), and protein kinase B (PKB/Akt) [9]. To date, among the four different IRS molecules that have been cloned, IRS-1 and IRS-2 appear to be the predominant isoforms expressed in SM. IRS molecules serve as docking sites for specific signaling proteins, such as PI3K, and play a key role for downstream insulin signaling [9]. Recent studies have proposed four different PI3K isoforms in human SM, involved in the insulin-dependent PI3K signaling pathways [9]. These isoforms

elicit different, rather specific, insulin-induced responses. Although the exact molecular link between PI3K and glucose transport has not been fully elucidated yet, protein kinase B (PKB) or Akt (Akt/PKB) and members of the protein kinase C (PKC) family have been suggested as important molecules in the metabolic pathway of insulin-signaling, leading ultimately to increased intracellular glucose transport [9].

The activated insulin-signaling cascade results in the release of GLUT4 from an intracellular reservoir compartment and its translocation and final fusion with the plasma membrane. This is the rate-limiting step for the uptake of glucose, which is transported across the plasma membrane and further processed by either oxidative (glycolysis) or nonoxidative pathways (glycogen synthesis) [9].

However, glucose disposal in SM is not entirely independent from the metabolic effects of insulin on other peripheral tissues, such as adipose tissue (AT). It seems that IR at the level of SM might be also secondarily induced to adipose tissue IR. More specifically, it has been shown that mice with AT-specific knockout of GLUT4 had an impaired IMGU in SM as well, despite preserved GLUT4 expression in this tissue [6]. Moreover, AT overexpression of GLUT4 reversed the impaired IMGU observed in SM-specific GLUT4 knockout mice, without concomitantly restoring glucose transport in SM [8]. These experimental findings have highlighted the importance of interactive communication (cross-talk) between AT and SM in terms of regulating glucometabolic balance.

3. Skeletal Muscle and Insulin Resistance

SM is a principal tissue responsible for IMGU which has recently gained a lot of interest, as a major site involved in peripheral IR. Most of the available data have derived from studies in type 2 diabetes mellitus (T2DM), where SM has emerged as an important insulin-resistant peripheral tissue, via molecular mechanisms that are currently being extensively investigated.

In vitro and in vivo data from humans and laboratory animals support a selective insulin-signaling defect at the level of glucose transport in SM. In type 2 diabetic patients, IMGU in SM has been found to be significantly reduced by about 50%, without clarifying whether this is a permanent defect or rather a short-term downregulation secondary to the diabetic state. Furthermore, an additional possible explanation for the development of IR in SM is related to specific alterations in the insulin-signal transduction pathway, including decreased IRS-1 protein content, impaired IRS-1 phosphorylation, reduced PI3K activity, or altered protein expression of the regulatory subunit of PI3K [9, 10]. Alterations in the expression or translocation of GLUT4 to the plasma membrane have been also implicated as potential pathogenetic mechanisms. However, whether these defects are actually a primary cause of IR or rather a secondary effect to an altered metabolic milieu remains still unresolved [11].

Despite the considerable body of evidence supporting the critical role of SM for the development of IR in many clinical entities, the exact underlying mechanisms have not been

fully delineated and most commonly represent a complex interaction between multiple extrinsic and intrinsic factors.

3.1. The Role of Adipokines in Skeletal Muscle IR. Most commonly, IR in SM is considered to be the end result of a complex interaction involving several different tissues. AT can induce IR at the level of SM via secretion of adipokines, inflammatory mediators, and growth factors. Tumor necrosis factor α (TNF- α), adiponectin, and leptin are the main adipokines that appear to be implicated in the development of cross-communication between AT and SM.

TNF- α is the main autocrine/paracrine AT-derived factor, triggering the release of free fatty acids (FFAs) from AT into bloodstream circulation. This is mainly dependent on nuclear factor κ B (NF κ B) activation and is mediated by the suppression of many genes responsible for glucose and FFA uptake and utilization [12, 13]. TNF- α -mediated FFA release impairs insulin-signaling in insulin responsive peripheral tissues such as SM [10]. According to the lipid supply hypothesis, the increased FFA availability provides the predominant substrate for intermediate metabolism, resulting in increased NADH/NAD⁺ and acetyl-CoA/CoA ratios. Elevated FFA concentrations promote beta-oxidation, which diminishes glucose uptake and oxidation. In parallel, FFA clearance is decreased and their storage as triglyceride droplets in SM is significantly enhanced [14].

In addition, adiponectin, a protective adipokine secreted by adipocytes, plays a pivotal role for SM insulin sensitivity. Adiponectin stimulates FFA catabolism, either directly or indirectly through stimulation of PPAR- γ nuclear receptors, and promotes a marked decrease of circulating FFA and glucose levels [15]. Last but not least, leptin, a hormone secreted predominantly by AT, acts both on hypothalamus and on target tissues including SM and is significantly involved in the regulatory mechanisms determining peripheral insulin action and sensitivity [16].

3.2. Defects in Skeletal Muscle Glycogen Synthesis. The primary site of postabsorptive glucose disposal is SM and the primary mechanism of glucose storage is through its conversion to glycogen. In states of IR, a deficiency in the nonoxidative glucose disposal has been primarily related to a defect in glycogen synthesis. Freymond et al. studied biopsies of vastus lateralis muscle, both before and during a hyperinsulinemic-euglycemic clamp, and demonstrated that human subjects with IR display decreased insulin-stimulated glycogen synthase activity [17]. This defect at the level of glycogen synthase activity and thus glycogen synthesis in SM, provides a further pathogenetic mechanism, underlying systemic and muscle IR.

3.3. Glucocorticoids and Muscle IR. Chronic glucocorticoid excess, a typical biochemical feature of Cushing's syndrome, has been traditionally associated with IR in general. However, recent experimental observations suggest that glucocorticoids, as well as glucocorticoid receptor (GR) activity, can have adverse effects on peripheral insulin sensitivity. Reynolds et al., found increased GR mRNA levels and increased expression of glucocorticoid receptors in SM of

men with IR and hypertension, implicating the dysregulation of glucocorticoid receptor expression and/or function as a possible underlying pathogenetic mechanism for IR in SM [18].

3.4. Skeletal Muscle Vascular Bed, Blood Flow, and Insulin Action. Insulin-mediated increased blood flow seems to be an important step for insulin delivery and glucose metabolism in peripheral tissues, including SM [19]. This theory was first introduced by Baron, et al. who showed a remarkable correlation between insulin-mediated whole body glucose uptake and leg blood flow over a broad spectrum of insulin sensitivities in normal and IR states [20]. These correlations were typically observed several hours after the initiation of an insulin clamp, namely, under steady state conditions [21, 22]. In addition, metacholine infusion increased leg blood flow and glucose uptake, while these were diminished after L-N-monomethyl arginine infusion [23]. The above observations support the important role of insulin-mediated blood flow for glucose uptake and insulin action.

Insulin regulates blood flow in peripheral tissues through a variety of mechanisms. Insulin induces dilatation of terminal arterioles and provides a constant rate of vasodilatation or vasoconstriction, in order to maximally extend the period of peripheral tissue perfusion. In this way, insulin enhances nutrient delivery and expands the surface area available for exchange of insulin, glucose, and other nutrients in peripheral tissues, including SM. Furthermore, after its binding to the receptor, insulin seems to promote its own translocation across the endothelial cell barrier [24]. Most of the research work in this field has been conducted on skin microvasculature [25], without, however, ensuring that the insulin-mediated vascular responses observed in skin reflect also those in SM. Although far more data need to be obtained, it is currently proposed that various factors impair the insulin-mediated vascular response and tissue delivery of nutrients such as glucose and insulin, mediating the process of IR in SM.

4. Muscle Insulin Resistance and Endocrine Disease

Although generalized and muscle IR remains a hot topic for the investigation of metabolic disease, it would be quite interesting to expand this research to a number of common and clinically relevant endocrine diseases, including PCOS, adrenal dysfunction, and thyroid disorders.

4.1. PCOS and Muscle IR. PCOS is a common endocrine disorder with a worldwide prevalence of 6%-7% among premenopausal women [26]. However, despite its steadily increasing prevalence, the fundamental underlying defect remains still speculative and seems to be multifactorial in origin. Beyond the reproductive abnormalities (chronic anovulatory dysfunction, infertility), women with PCOS display several metabolic abnormalities as well, including disorders of glucose metabolism and insulin action, which

underlie the increased risk of developing impaired glucose tolerance and type 2 diabetes [27].

Women with PCOS exhibit basal hyperinsulinemia, decreased glucose-stimulated insulin release and IMGU, due to reduced hepatic insulin clearance and pancreatic β -cell dysfunction. In addition, they exhibit a generalized IR, which mainly involves an impaired insulin responsiveness of adipose tissue and SM [2, 28].

IR in PCOS is associated with a unique postbinding defect in insulin receptor signaling due to a complex interaction between intrinsic (genetically determined) and environmental factors [29]. It is supported that the disrupted insulin receptor tyrosine kinase activity in adipocytes and IRS-1-associated PI3K activity in SM are the key elements in the IR pathogenetic process [30]. In addition, extrinsic factors including inflammatory mediators, adipokines, androgens, free fatty acids (FFAs), amino acids, and increased glucose levels have been all implicated in the pathogenesis of IR in PCOS.

4.1.1. Adipokines, Inflammatory Mediators, FFAs, and Muscle IR in PCOS. In vitro studies have shown that cultured SM cells from women with PCOS display normal insulin sensitivity, while SM cells from in vivo studies in PCOS exhibit resistance to insulin, suggesting the important role of extrinsic factors in producing muscle IR in PCOS [28]. Among them, adipokines, TNF- α , FFAs, amino acids, androgens, and increased glucose levels have been all postulated to be involved in the pathogenesis of IR in PCOS [31]. Increased TNF- α levels and elevated plasma interleukin-6 (IL-6) concentrations have been consistently reported in both obese and normal weight women with PCOS, indicating the significant contribution of chronic low-grade inflammation to IR [32, 33]. As far as leptin is concerned, Pehlivanov and Mitkov reported higher serum leptin in PCOS demonstrating a positive correlation with IR, independently of markers of adiposity [34]. Data regarding adiponectin and resistin levels are rather conflicting in women with PCOS. These adipokines have been found either increased or conversely decreased, depending on the obesity status of the studied population [35, 36].

The existing data indicate that adipose tissue, which is also an insulin resistant site in PCOS, and especially when it is centrally accumulated, secretes increased levels of adipokines, FFA, and inflammatory mediators (TNF- α , IL-6), which in turn promote IR at the level of SM via a vicious cycle. In particular, elevated FFA levels have been consistently suggested in PCOS, especially when increased visceral fat is also present. This was well described by Ek et al. who reported an increased rate of visceral fat lipolysis in PCOS, suggesting a genetically determined upregulation in visceral fat lipolysis, associated with a selective increase in the function of both protein kinase A (PKA) and hormone-sensitive lipase (HSL) [37]. It is obvious that the increased FFA influx has detrimental effects for insulin metabolic signaling in SM [28, 37].

4.1.2. Androgens and Muscle IR. Multiple studies suggest the association between androgen excess and IR in women with

PCOS, but their cross-sectional nature does not allow safe conclusions about causality [31].

On one hand, hyperandrogenemia in women with PCOS appears to be an effect of the augmented steroidogenesis by hyperinsulinemia secondary to IR [38, 39]. On the other hand, hyperandrogenemia induces generalized and muscle IR, through either a direct effect of androgens on insulin action in AT and SM, or indirectly by affecting lipid metabolism and body fat distribution [31]. Hyperandrogenemia-induced IR is selective, affecting mainly the metabolic but not the mitogenic actions of insulin, since insulin-stimulated ovarian steroidogenesis is perfectly maintained [40]. Androgen excess has been associated with some of the typical insulin-signaling defects in PCOS [41]. Most of these effects have been mostly studied in female rats, while there is a relative paucity of similar clinical studies. Testosterone administration to female adult rats for 8–12 weeks caused hyperinsulinemia in both intact and ovariectomized animals [42], while in the latter it induced a 50% reduction in IMGU into SM. Impaired SM insulin action was combined with fewer type 1 muscle fibers (slow twitch, oxidative) and increased type 2 fibers (fast twitch, insulin resistant). In the same study, a decreased SM capillary density and an impaired muscle glycogen synthase activity were also reported, contributing to the observed IR of SM [43]. It seems that postinsulin receptor signaling events are involved in testosterone-induced IR in SM in this rat model. In support of this, experimental data in primary differentiated rat myotubes have demonstrated a synergistic interaction between testosterone and insulin in phosphorylation of intracellular signaling proteins (phosphorylation of IRS-1 at serine residues), resulting in a dissociation of insulin receptor from the PI3K signaling cascade and an impaired insulin metabolic signaling [44].

Summarizing the existing data, androgens promote IR at the tissue level of SM by reducing capillary network formation for adequate delivery of insulin to SM, switching muscle fiber isoforms, reducing glycogen synthase activity and impairing insulin-mediated GLUT4 plasma membrane translocation [44].

However, the finding of hyperinsulinemia in PCOS patients raises the questions what the cause is and what the effect is. Most of the existing clinical data suggest, without providing definitive confirmation, that hyperinsulinemia causes hyperandrogenism, more than the other way around [45].

4.1.3. Molecular Defects and Muscle IR in PCOS

(a) *In Vitro and In Vivo Studies.* Current evidence suggests that excessive serine phosphorylation of the insulin receptor or downstream signaling molecules plays a pivotal role for the pathogenesis of muscle IR in PCOS [46]. In vitro studies in cultured SM cells from obese and nonobese patients with PCOS reported an abnormal phosphorylation pattern, consisting in decreased tyrosine autophosphorylation of the insulin receptor and increased serine phosphorylation, similarly to the phosphorylation abnormalities observed in PCOS cultured skin fibroblasts [46].

Corbould et al. who studied cultured SM cells of obese nondiabetic women with PCOS and of age- and BMI-matched control women, did not observe a decrease in IMGU and basal autophosphorylation in vitro, while insulin-stimulated tyrosine phosphorylation of the insulin receptor was found to be normal [29]. Moreover, the protein expression of insulin receptor β -subunit, IRS-2, PI3K, and GLUT4 was similar to that of controls. However, a number of molecular signaling abnormalities were documented including a 35% increased expression and a two-fold increased constitutive phosphorylation of IRS-1 at serine 312, decreased IRS-1-associated PI3K activity after adjusting for the increased expression of IRS-1, decreased baseline IRS-2-associated PI3K activity, a tendency for decreased insulin-stimulated IRS-2-associated PI3K activity, and higher GLUT1 expression, being positively correlated with increased basal glucose uptake in PCOS SM [29]. The apparently normal insulin response of PCOS SM in terms of glucose uptake is possibly attributed to the increased IRS-1 and GLUT1 expression. Furthermore, the fact that IMGU is maintained in vitro but significantly impaired in vivo indicates that IR is not an intrinsic feature in PCOS SM but is greatly influenced by adverse in vivo environmental conditions.

A putative serine kinase, extrinsic to the insulin receptor, has been implicated in the abnormal pattern of phosphorylation in PCOS but has not been identified yet. Although there are at least 50 known potential serine/threonine phosphorylation sites on IRS-1, phosphorylation at both serine 312 and serine 636/639 has been frequently reported in several studies associating IRS-1 serine phosphorylation with IR [47].

The defective activation of aPKC (atypical protein kinase C), a downstream effector of PI3K, in SM of PCOS obese patients has been also involved in the pathogenesis of muscle IR in this syndrome. In humans, marked defects in aPKC activation in SM have been reported in T2DM, obesity, obesity-associated PCOS, and impaired glucose tolerance [48]. These defects in aPKC activation in SM are due to both impaired activation of IRS-1-dependent PI3K and diminished responsiveness of aPKCs to a lipid product of PI3K, called PI-3,4,5-(PO₄)₃ or PIP₃. Although it is still uncertain which underlying defect comes first, the resultant defect in aPKC activation in SM contributes significantly to the development of muscle IR [48].

Despite the well established identification of several molecular abnormalities in PCOS, it remained initially unclear whether the observed defects in insulin-signaling are actually intrinsic, genetically determined to SM, or rather acquired secondary to exposure to in vivo environmental factors such as hyperinsulinemia, hyperandrogenemia, increased circulating FFAs, or sustained hyperglycemia. According to Corbould et al. muscle IR is not an intrinsic feature in PCOS but appears rather to be significantly influenced by endogenous environmental factors [29].

Indeed, exposure to a number of molecules, including FFA, TNF- α , glucose, amino acids, diacylglycerol (DAG), and fatty acyl-CoA, increases serine phosphorylation of IRS-1 and results in impaired insulin-signaling. These molecules

are thought to act on IRS-1 through a variety of serine/threonine kinases including mTOR (mammalian target of rapamycin) and S6K. More specifically, FFA reduce IRS-1-associated PI3K activity, impair Akt/PKB phosphorylation, and activate PKC θ (protein kinase C theta), a serine kinase that increases serine phosphorylation of IRS-1 [28]. Concerning diacylglycerol, a potent activator of PKC, it is thought to be an additional important lipid mediator of muscle IR [49]. High insulin levels can also stimulate IRS-1 serine phosphorylation in human myoblasts, indicating that insulin can modulate its own signaling pathway [44]. Androgen excess induces muscle IR in PCOS by affecting, most possibly, postinsulin receptor signaling events. Recent *in vitro* data, in primary differentiated rat myotubes, have demonstrated a synergistic interaction between testosterone and insulin in phosphorylation of intracellular signaling proteins (phosphorylation of IRS-1 at serine residues) and a consequent dissociation of the insulin receptor from the PI3K signaling cascade, resulting in impaired insulin metabolic signaling [44].

(b) Human Studies. *In vivo* studies of PCOS patients, where serial SM biopsies were performed during hyperinsulinemic-euglycemic clamps, have revealed a significant impairment in IMGU, an increased expression of IRS-2, and normal expression of insulin receptor, IRS-1, and PI3K. These data suggest that the increased expression of IRS-2 might represent a compensatory adaptation for the decreased insulin-mediated IRS-1-associated PI3K activity, which is not, however, completely effective, since IMGU was not restored to normal [50]. Most recently, Hojlund et al. reported small reductions in insulin-stimulated phosphorylation of Akt (PKB) and AS160 (Akt substrate of 160 kDa) in intact muscle of women with PCOS, which was partially reversed by treatment with insulin-sensitizing agents such as pioglitazone [51].

Recently, another candidate pathogenetic mechanism for muscle IR in women with PCOS has been proposed, consisting in a defective insulin regulation of ERK 1/2 (extracellular signal-regulated kinases 1/2). Rajkhowa et al. compared the relative contribution of two distinct insulin-signaling pathways to muscle IR in nine women, diagnosed with PCOS. The study involved the Ras-ERK and the IRS-PKB pathways, mediating the mitogenic and metabolic effects of insulin, respectively, and found no significant difference in the expression, basal activity, or insulin activation of IRS-1 and PKB between PCOS subjects and controls [52]. However, there was a severe attenuation of insulin stimulation of the ERK pathway and an accompanying trend for higher basal phosphorylation of ERK 1/2 in SM biopsies obtained from nearly all women with PCOS [52]. Interestingly, the investigators observed a reduced ERK activity after acute *in vivo* exposure of SM to insulin, in almost all PCOS subjects of the study, contrasting with the physiologically expected increase in mitogenic ERK activity, in response to insulin stimulation. These results suggest that ERK activation might influence regulation of glucose uptake in SM and might be involved in muscle IR in women with PCOS [52].

Based on the few existing human *in vivo* studies, it seems that in PCOS there is a severe functional defect in

the insulin-signaling cascade within SM, consisting in an abnormal phosphorylation pattern of the insulin receptor or downstream key signaling proteins.

4.1.4. Transcriptional Defects Involved in Muscle IR in PCOS. It has been recently demonstrated that PCOS is associated with impaired mitochondrial structural integrity and oxidative metabolism. Skov et al. studying insulin resistant women with PCOS, demonstrated a significant downregulation of the expression of nuclear-encoded genes representing mitochondrial oxidative phosphorylation, ribosomal proteins, mRNA processing reactome, translation factors, and proteasome degradation (OXPHOS), compared to control women. This effect was mainly mediated by a decrease in PGC-1 α expression (PPAR- γ coactivator-1 α) and was partially restored after treatment with pioglitazone [53]. Thus, the insulin-sensitizing effects of pioglitazone may include reversal of preexisting abnormalities in ribosomal protein biosynthesis and mitochondrial biogenesis in women with PCOS [54].

Calcium transporter activity was also significantly downregulated in PCOS patients. Increasing evidence supports a modulating role for calcium influx, calmodulin and Ca⁺²/calmodulin-dependent protein kinase (CaMK) in IMGU in SM [55]. An increase in cytosolic calcium and activation of CaMK induce mitochondrial biogenesis and GLUT4 expression via activation of different transcription factors, including NRF-1 and -2 (nuclear respiratory factor) and the coactivator PGC-1 α [56]. Any potential dysregulation of calcium homeostasis could, therefore, have a pronounced disturbing effect on IMGU and mitochondrial functional capacity [57].

Future studies, unraveling the exact molecular mechanisms of IR in general or in SM in particular in PCOS, may help develop effective gene-based strategies in order to prevent the increased risk of early onset type 2 diabetes in women suffering from this condition.

4.2. Adrenal Disorders and Muscle IR. Adrenal disorders characterized by increased secretion of adrenocortical or adrenomedullary hormones such as hyperaldosteronism, Cushing's syndrome, hyperandrogenism, and pheochromocytoma have been associated with various metabolic disorders, including impaired glucose tolerance, IR, and overt diabetes [58]. These abnormalities constitute the end result of the adverse effects of adrenal hormones on various components of insulin action and glucose metabolism.

Adrenal hormone excess is associated with decreased insulin secretion by the pancreatic β cell or disrupted insulin action in peripheral tissues. SM has been recently recognized as an important insulin-target site with a major role in the pathogenesis of the glucometabolic abnormalities associated with hypersecreting adrenal disorders [59].

4.2.1. Aldosterone Excess and Muscle IR. Aldosterone is the final mediator of the renin-angiotensin-aldosterone system (RAS), which mediates blood pressure control and electrolytic balance in the kidney. However, a significant body of evidence indicates that aldosterone—in concert

with other independently acting mediators of RAS axis (renin and angiotensin)—impairs insulin secretion and metabolic signaling, resulting in impaired glucose tolerance and overt diabetes. Focusing on aldosterone, which can be significantly elevated in some patients with hypersecreting adrenal lesions, it promotes IR, inflammation, fibrosis, oxidative stress, and sodium retention, with detrimental cardiometabolic effects [60]. Recent literature data support that most of the adverse metabolic changes observed in primary hyperaldosteronism can be totally reversed after the surgical removal of the adrenal tumors or treatment with mineralocorticoid receptor blocking agents [61].

Mounting evidence supports that aldosterone exerts its diabetogenic actions by a direct effect on insulin receptor function and metabolic signaling cascade in several peripheral tissues, including cardiovascular and renal tissue, fat, liver and SM [60]. In addition, hypokalemia, as a result of aldosterone excess, can also impair both pancreatic insulin secretion and peripheral insulin action, providing an alternative explanation for the observed abnormalities in primary hyperaldosteronism [62].

However, the underlying molecular and cellular mechanisms linking aldosterone excess with changes in the glucose and insulin metabolism remain still elusive, especially regarding the contribution of SM.

In addition to its classic effects, aldosterone induces rapid (nongenomic) adverse responses in both vascular smooth muscle cells and SM. This effect is mediated by NADPH oxidase (nicotinamide adenine dinucleotide phosphate), which generates excess reactive oxygen species (ROS), redox imbalance, and oxidative stress [63]. Oxidative stress activates redox-sensitive serine kinases in these tissues, including PKC (protein kinase C), MAPKs (mitogen-activated protein kinases), c-Jun NH₂-terminal kinase, extracellular signal-regulated kinases 1 and 2 (ERK 1/2), and p-kinase. The activation of these kinases leads to increased serine phosphorylation of IRS-1, which impairs normal binding with PI3K and results in decreased activation of PKB (Akt) and adverse downstream metabolic effects such as impaired glucose transport in many tissues, including SM [64]. This effect is further substantiated by the significant improvement in systemic insulin sensitivity, insulin-signalling, and glucose uptake by SM, after treatment with mineralocorticoid receptor blocking agents in experimental animal models of RAS hyperactivation and IR [65]. The improvement in insulin sensitivity was closely associated with decreased NADPH oxidase activity in SM, suppressed levels of ROS, and improved mitochondrial structure and function. In addition, in rat vascular smooth muscle cells, aldosterone downregulated IRS-1 expression via stimulating the production of ROS, an effect which was markedly attenuated by treatment with the selective mineralocorticoid receptor antagonist eplerenone [66].

4.2.2. Glucocorticoid Excess and Muscle IR. Chronic exposure to glucocorticoid excess, a typical feature of Cushing's syndrome, is associated with various metabolic disorders, including glucose intolerance, IR, or overt diabetes [67].

Glucocorticoids (GCs) interfere with several steps of glucose metabolism and insulin-signaling cascade, resulting in reduced IMGU and IR in most peripheral tissues, including SM. GCs may induce IR, either directly by interfering with the insulin receptor cascade in SM, or indirectly through GC-induced changes in protein and lipid metabolism [67].

Since studies into the effects of GCs on the expression of insulin receptor in SM have yielded contradictory results, the markedly reduced IMGU under conditions of GC excess has been proposed as a postreceptor defect. In vitro studies using isolated SM cells treated with dexamethasone showed a decreased expression and phosphorylation of IRS-1, PI3K, and PKB/Akt as well as reduced GLUT4 migration to the cell surface [68, 69]. In addition to reducing glucose uptake, GCs have also been shown to decrease glycogen synthesis rate in Wistar rats by reducing PKB/Akt and GSK-3 (glycogen synthase kinase-3) phosphorylation [70]. Beyond experimental results, there are limited available data concerning the exact molecular effects of GCs on insulin-signaling in humans. As early as in 1988, Rebuffé-Scrive, was the first investigator who studied in detail the morphology and metabolism of SM in female patients with Cushing's syndrome [71]. In his study, leg muscle tissue of women with Cushing's syndrome was found to contain a relatively low proportion of type I fibers (insulin sensitive) and a high proportion of type IIb fibers (insulin resistant), a similar pattern of muscle fiber composition to that observed in android obesity. He also found a significantly low glycogen synthase activity in the lateral vastus muscle of the same women. This is the first study suggesting an abnormal muscle fiber composition (relative shift from type I to type IIb fibers) in a common clinical condition of chronic endogenous corticosteroid excess. In addition, healthy volunteers treated with dexamethasone for 5 days and patients exposed to long-term high-dose GCs after renal transplantation, displayed reduced glycogen synthesis rates with concomitant decreased concentration and activity of glycogen synthase in SM biopsies [72].

Some data support an indirect effect of GS on SM insulin-signaling, which is mediated through enhanced proteolysis, and thus increased circulating amino acid levels. Elevated circulating amino acids seem to inhibit insulin-stimulated IRS tyrosine phosphorylation and activation of PI3K in vitro [73]. In addition, they reduce IMGU and glycogen synthesis in humans [74].

Another indirect negative effect of GCs on SM insulin sensitivity appears to be mediated through the GC-induced dyslipidemia. GCs promote whole body lipolysis, resulting in increased plasma levels of FFAs, which enhance in turn the accumulation of intramyocellular lipids (IMCLs), such as fatty acyl CoA, diacylglycerol, and ceramide, affecting negatively glucose uptake and disposal [75]. It was originally proposed by Randle in 1963 that intracellular lipids decrease insulin-mediated glucose uptake by competing with glucose for oxidation [76]. However, more recent studies have demonstrated that IMCLs reduce IMGU by interfering directly with insulin-signaling. Intracellular lipids may activate various serine kinases, such as c-Jun aminoterminal

kinase (JNK) and IKB kinase- β (IKK- β), which phosphorylate serine sites on IRS-1, resulting in suppressed insulin-signaling [75].

In summary, GCs reduce insulin sensitivity and consequently IMGU in SM, not only by directly perturbing insulin-signaling and glycogen synthesis, but also secondarily to unfavorable changes in protein and lipid metabolism, which further affect negatively the insulin-signaling cascade, in peripheral tissues, including SM.

4.2.3. Adrenal Androgens and Muscle IR. The exact relationship between increased adrenal androgens and IR remains to be elucidated. It has been shown that experimentally induced hyperinsulinemia elicited an acute decline in dehydroepiandrosterone (DHEA) and dehydroepiandrosterone sulfate (DHEA-S). However, the regulatory role of insulin on adrenal androgen production and metabolism in normal physiology or disease remains still speculative [58]. In several animal models, DHEA appears to exert potent antiobesity and antidiabetogenic actions, but such effects have not been persuasively demonstrated in humans [58]. Human studies on DHEA are limited, and more research needs to be conducted in order to determine whether the experimental observations made in animal models can be also extrapolated to man. Recent experimental evidence indicates that DHEA may act at multiple steps in the regulation of glucose metabolism in the liver, suppressing the activity of hepatic gluconeogenic enzymes [77]. However, there are no data concerning the relationship of increased adrenal androgen production and peripheral insulin action, especially at the level of SM.

4.2.4. Catecholamine Excess and Muscle IR. Pheochromocytoma, typically characterized by endogenous catecholamine excess, is associated with several glucometabolic abnormalities, ranging from impaired glucose tolerance (25%–75%) to overt diabetes [78]. The main underlying pathogenetic mechanism for pheochromocytoma-associated glucose dysmetabolism is the catecholamine-induced decreased insulin secretion through α_2 adrenoreceptors, while the effects of catecholamines on peripheral glucose uptake seem to be less important [79]. However, in animal studies, epinephrine has been shown to induce IR in rat muscle [80]. Furthermore, Raz et al. [81] studied the effect of epinephrine in eight healthy patients and detected an inhibition of insulin-mediated glycogenesis because of an inactivation of glycogen synthase, suggesting that epinephrine inhibits insulin-mediated glucose utilization at the major site of IR namely, skeletal muscle. An additional study by Laakso et al. showed that epinephrine impairs the ability of insulin to increase SM glucose extraction in humans [82].

In summary, excessive catecholamines in patients with pheochromocytoma can induce or aggravate IR in peripheral tissues including SM, while the surgical treatment of pheochromocytoma can reverse the hyperinsulinemia and cardiometabolic abnormalities observed in these patients [79].

4.2.5. Adrenal Incidentalomas and IR. Adrenal incidentalomas (AIs) are defined as randomly discovered adrenal masses, which are diagnosed by abdominal ultrasound or computed tomography scan, performed for unrelated causes. Recent literature suggests that 10%–20% of solid AIs demonstrate a subclinical hormonal dysfunction, which may place patients at a higher risk for metabolic derangements such as IR [83]. Subclinical hypercortisolism is the most common abnormality detected in patients with AIs, with an average incidence of 9% [84]. Patients with AIs have a higher prevalence of diabetes or glucose intolerance (20%–75%), compared with the general population [85]. AIs are considered to be both a cause and an effect of hyperinsulinemia. The alternative hypothesis that AIs are actually caused by hyperinsulinemia has been formulated by Reincke et al. [86], who studied 13 patients with AIs and found that they were all insulin resistant. He also observed a proliferative effect of insulin on adrenal cell lines in vitro, indicating that insulin can stimulate adrenocortical tumor formation. The proposed theory was that AIs can be perceived as the clinical result of sustained hyperinsulinemia, just as PCOS is regarded as the result of insulin-mediated stimulation of ovary growth [86].

In a study from Japan, all 12 patients with AIs exhibited IR, based on the steady state of plasma glucose [87]. After surgical removal of the tumors, steady state of plasma glucose was significantly decreased, compared to pre-adrenalectomy values. A further study by Iovic et al. assessed insulin sensitivity in 22 patients with AIs and concluded that patients with AIs manifested lower insulin sensitivity than healthy controls [88].

Trying to provide an explanation for the increased risk of developing IR in patients with nonfunctioning AIs (NFAIs), Ermetici et al. have recently formulated the hypothesis of adipokine involvement [89]. Plasma IL-6, adiponectin, resistin, TNF- α , and monocyte chemoattractant protein 1 (MCP-1) levels were all found to be significantly higher in patients with NFAIs compared to controls. The pathogenetic role of proinflammatory cytokines in patients with AIs merits definitely further investigation.

In a recent study by our research team [90], in 29 patients with NFAIs, we demonstrated significant hepatic and peripheral IR, documented by both higher fasting glucose and insulin levels and abnormal glucose tolerance data, as well as an increased prevalence of several components of metabolic syndrome, such as hypertension, dyslipidemia, fatty liver disease, and central obesity. It is, therefore, useful to evaluate routinely IR in patients with AIs, since results can be quite helpful in clinical decision making [87].

4.3. Thyroid Disorders and Muscle IR. Thyroid hormones (THs) constitute important mediators of body metabolism and affect various metabolic aspects involving glucose and insulin metabolism, through a variety of mechanisms. Data from animal studies have shown that THs play a key role in the regulation and activation of insulin receptor and glucose transporter proteins, in signaling pathways and in the expression of different isoforms of SM myosin heavy chains [91]. In addition, THs regulate the differentiation,

growth, and metabolism of virtually every cell in the human body. In SM, triiodothyronine (T₃) regulates muscle fiber type and mitochondrial content through a genomic action, consisting in a direct modulation of gene transcription by ligand-dependent activation of TH receptors (TRs) and specific TH response elements (TREs). Other TH effects, such as modulation of ion channel activity, intracellular Ca²⁺ mobilization, phospholipase, and kinase activation, have been attributed to nongenomic actions of TH. This mode of action explained the TH-induced activation of a signaling cascade involving phospholipase C activation, inositol triphosphate (IP₃) accumulation, intracellular Ca²⁺ mobilization and phosphorylation of PKC and ERK 1/2, resulting ultimately in activation of plasma membrane Na⁺/H⁺ exchangers and increased intracellular pH in rat SM cells [92]. Furthermore, with the same mode of action, T₃ induces a rapid phosphorylation of both p38 and AMPK (AMP-dependent kinase) in SM fibers and stimulates mitochondrial biogenesis [93].

4.3.1. Hypothyroidism and Muscle IR. Hypothyroidism (HP) has been associated with disorders of glucose and insulin metabolism, involving defective insulin secretion in response to glucose, hyperinsulinemia, altered peripheral glucose disposal, and IR.

According to *in vivo* data, HP is associated with a decreased glucose-induced insulin secretion by the β cells due to changes in the physicochemical properties of the islet membranes and decreased amount of islets [94].

In addition, it is suggested that HP is an insulin resistant state. Interestingly, even subtle decreases in the levels of TH within the normal range have been shown to correlate inversely with markers of IR [95]. *In vivo* data, emerging from studies in propylthiouracil-induced hypothyroid animals during euglycemic-hyperinsulinemic clamps, showed an association of HP with an adipokine-mediated IR [96]. Mitrou et al. showed that euglycemic patients with clinical and subclinical HP were insulin resistant. In a recent study, the same authors supported the important role of adipokines in IR, showing a meal-induced IL-6 increase, primarily involved in the observed IR, and a concomitant increase of TNF- α , which seems to be the result rather the cause in this process [4].

The mechanisms linking HP with IR in general and in SM in particular are still under investigation. IR in HP is associated with a negative regulation of one or more intracellular enzymes involved in glucose catabolism [97]. An impaired translocation of GLUT4 transporters on the plasma membrane has been also observed in the monocytes of subjects with clinical and subclinical HP, in relation to a decreased IMGU [98]. Dimitriadis et al. documented a decreased glycogen synthesis rate at supraphysiological insulin concentrations in SM of hypothyroid rats, as well as a decreased rate of glucose oxidation at all insulin concentrations [99, 100]. An effect of TH on insulin receptors has been suggested, but the existing data are rather conflicting, supporting either no relationship between thyroid status and the affinity of insulin receptors or diminished high affinity insulin receptors (HAIRs) in HP [101]. The effect

of TH on insulin action in peripheral tissues such as SM has not been studied systematically *in vivo*. Dimitriadis et al. demonstrated a meal-induced increase in plasma insulin levels in subjects with HP and an unchanged rate of glucose uptake in the forearm muscles and AT, indicating that IR is possibly the result of diminished blood flow in AT and SM [96]. In support of this, Rochon et al. showed decreased forearm and AT blood flow and glucose disposal rates in patients with HP, during euglycemic-hyperinsulinemic clamps [102].

It is obvious that, although HP constitutes an insulin resistant state, more studies need to be done in order to clarify the underlying pathogenetic mechanisms. However, it has to be mentioned that IR appears to be similar in patients with overt clinical and subclinical HP [103, 104], while treatment with thyroxine does not restore IMGU in the forearm of patients with HP, suggesting that TH per se may not be entirely responsible for this manifestation, which seems to be a more complex interaction between tissues and molecules.

4.3.2. Hyperthyroidism and Muscle IR. Hyperthyroidism (HPR) is also associated with metabolic abnormalities, including disorders of the glucose and insulin metabolism [105].

Insulin secretory capacity seems to be disrupted in HPR, but the existing data are rather heterogeneous, suggesting increased, normal, or decreased insulin secretion. This estimation has been based on the measurement of circulating C-peptide levels. However, when individually derived C-peptide kinetic parameters were measured, the insulin secretory rate was significantly increased, possibly reflecting an increased response of β cell to glucose, under increased TH levels. The limitation of these studies is the use of C-peptide as a marker of insulin secretion, which is biased, given its rapid clearance from the circulation in HPR [106]. However, an increase in the β -cell mass in HPR has been also reported [107]. In addition, Liggett et al. [108] showed an increased insulin secretory response to epinephrine (increased plasma C-peptide) after T₃ administration, indicating an increased insulin secretory rate in HPR [108].

HPR has been also associated with hyperinsulinemia, which is considered to be compensatory for the increased insulin clearance [103, 104]. Insulin action and IMGU in HPR are ill defined, either in general, or in SM in particular. *In vitro* and *in vivo* studies of IMGU using euglycemic hyperinsulinemic clamps showed either normal or increased IMGU [109–111]. However, IR has been documented in HPR, especially in the liver, since there is still uncertainty concerning the involvement of other peripheral tissues, including SM. Dimitriadis et al. documented IR at the fasting state in AT in HPR, which was suppressed postprandially, stimulating the glucose uptake in SM [112]. The same authors documented a postmeal induced hyperinsulinemia in subjects with HPR, as well as IR at the level of SM [113].

However, there are only few data regarding the underlying pathogenetic mechanisms of IR in HPR. The existing data regarding the number of high and low affinity insulin receptors are conflicting, suggesting either an increased or

unaltered expression in HPR [114]. A decreased insulin stimulated glycogen synthesis has been also reported in SM from hyperthyroid subjects, indicating IR at the level of SM [103, 104]. Dimitriadis et al. documented a markedly decreased rate of IMGU in SM, which was compensated by an increase in blood flow, due to changes either in cardiac or in vascular function [113]. The same authors have demonstrated an IGF-1-induced increase in GLUT3 and GLUT4 translocation on the monocyte surface in HPR subjects [99].

A decreased insulin-mediated stimulation of major intracellular pathways of glucose metabolism has been also reported [99, 103, 109]. HPR has been associated with an increased activity and density of β -adrenergic receptor in SM [108, 115], as well as a decreased muscle oxidative capacity [116].

HPR is generally thought to be an insulin-resistant state, but further studies are definitely needed in order to prove this association and reveal the underlying pathogenetic mechanisms. It has been generally suggested that THs are not the only factors involved in the initiation of the IR cascade, but they most commonly interact with various tissues and molecules, in order to regulate glucose metabolism and insulin action.

5. Summary and Conclusions

SM constitutes an insulin-responsive peripheral tissue with a major role in maintaining systemic glucose metabolism. In a general overview of insulin-resistant states, including PCOS as well as adrenal and thyroid disorders, IR in SM appears to be a clinically important manifestation. Specific alterations at the insulin receptor level or the signal transduction pathway have been suggested as the main underlying pathogenetic mechanisms which lead to impaired IMGU and defective glycogen synthesis.

In PCOS, muscle IR has been associated with abnormal phosphorylation of insulin-signaling proteins, altered muscle fiber composition, reduced transcapillary insulin delivery, decreased glycogen synthesis, and impaired mitochondrial oxidative metabolism.

The metabolic abnormalities associated with hyper-secreting adrenal disorders constitute the end result of the adverse effects of adrenal hormones on various components of insulin action and glucose metabolism. Aldosterone is associated with IR in SM either directly through its effects on the insulin receptor function and metabolic signaling cascade, or indirectly through oxidative stress induction. GCs reduce IMGU in SM, either directly by perturbing insulin-signaling and glycogen synthesis, or indirectly through unfavorable changes in protein and lipid metabolism. Catecholamine excess can induce or aggravate IR in SM. Furthermore, AIs—including NFAs—are characterized by an increased prevalence of generalized and muscle IR, possibly due to the subclinical proinflammatory milieu and the biochemically silent endocrine abnormalities.

Thyroid disorders, including both hypo- and hyperthyroidism, have been associated with IR in SM and altered peripheral glucose disposal, due to impaired GLUT4

translocation, decreased glycogen synthesis, downregulated intracellular glucose catabolism, altered blood flow, and decreased muscle oxidative capacity.

Based on the data presented herein, it is strongly emphasized that all patients with common endocrine disorders such as PCOS as well as adrenal and thyroid disorders, should undergo a thorough metabolic evaluation, since IR—particularly at the level of SM—appears to be a prominent feature in these states. Far more clinical and experimental studies are required in order to fully clarify the underlying pathophysiology of the clinically meaningful relationship between endocrine disease and impaired SM insulin sensitivity.

List of Important Abbreviations

PCOS:	Polycystic Ovary Syndrome
IR:	Insulin Resistance
HP:	Hypothyroidism
HPR:	Hyperthyroidism
AIs:	Adrenal Incidentalomas
NFAIs:	Nonfunctioning Adrenal Incidentalomas
SM:	Skeletal Muscle
AT:	Adipose Tissue
IMGU:	Insulin-mediated glucose uptake
GLUT4:	Glucose Transporter 4
IRS-1:	Insulin receptor substrate-1
PI3K:	Phosphatidylinositol 3-kinase
Akt/PKB:	Akt/Protein kinase B
aPKC:	Atypical protein kinase C
GSK-3:	Glycogen synthase kinase-3
ERK 1/2:	Extracellular signal-regulated kinases 1/2
AS160:	Akt substrate of 160 kDa
mTOR:	mammalian Target Of Rapamycin
MAPKs:	Mitogen-activated Protein Kinases
IP3:	Inositol Triphosphate
AMPK:	AMP-dependent kinase
PKA:	Protein kinase A
HSL:	Hormone-Sensitive Lipase
TNF- α :	Tumor necrosis factor- α
FFA:	Free Fatty Acid
Il-6:	Interleukin-6
NF κ B:	Nuclear Factor κ B
PPAR- γ :	Peroxisome-Proliferator Activated Receptor- γ
PGC-1 α :	PPAR- γ coactivator 1 α
eNOS:	Endothelial Nitric Oxide Synthase
NADPH:	Nicotinamide Adenine Dinucleotide Phosphate
ROS:	Reactive Oxygen Species
RAS:	Renin-angiotensin-aldosterone system
OXPPOS:	Oxidative Phosphorylation
GCs:	Glucocorticoids
GRs:	Glucocorticoid Receptors
THs:	Thyroid Hormones
TRs:	Thyroid hormone Receptors
TREs:	Thyroid hormone response elements
DHEA:	Dehydroepiandrosterone
IMCLs:	Intramyocellular Lipids
HAIRs:	High-Affinity Insulin Receptors.

References

- [1] D. B. Savage, K. F. Petersen, and G. I. Shulman, "Mechanisms of insulin resistance in humans and possible links with inflammation," *Hypertension*, vol. 45, no. 5, pp. 828–833, 2005.
- [2] A. Dunaif, "Insulin resistance and the polycystic ovary syndrome: mechanism and implications for pathogenesis," *Endocrine Reviews*, vol. 18, no. 6, pp. 774–800, 1997.
- [3] E. Maratou, D. J. Hadjidakis, A. Kollias, et al., "Studies of insulin resistance in patients with clinical and subclinical hypothyroidism," *European Journal of Endocrinology*, vol. 160, no. 5, pp. 785–790, 2009.
- [4] P. Mitrou, E. Boutati, V. Lambadiari, et al., "Insulin resistance in hyperthyroidism: the role of IL-6 and TNF α ," *European Journal of Endocrinology*, vol. 162, p. 121, 2010.
- [5] C. Catena, R. Lapenna, S. Baroselli, et al., "Insulin sensitivity in patients with primary aldosteronism: a follow-up study," *Journal of Clinical Endocrinology and Metabolism*, vol. 91, no. 9, pp. 3457–3463, 2006.
- [6] E. D. Abel, O. Peroni, J. K. Kim, et al., "Adipose-selective targeting of the GLUT4 gene impairs insulin action in muscle and liver," *Nature*, vol. 409, no. 6821, pp. 729–733, 2001.
- [7] R. A. DeFronzo, E. Jacot, E. Jequier, E. Maeder, J. Wahren, and J. P. Felber, "The effect of insulin on the disposal of intravenous glucose. Results from indirect calorimetry and hepatic and femoral venous catheterization," *Diabetes*, vol. 30, no. 12, pp. 1000–1007, 1981.
- [8] E. Carvalho, K. Kotani, O. D. Peroni, and B. B. Kahn, "Adipose-specific overexpression of GLUT4 reverses insulin resistance and diabetes in mice lacking GLUT4 selectively in muscle," *American Journal of Physiology*, vol. 289, no. 4, pp. E551–E561, 2005.
- [9] A. R. Saltiel and C. R. Kahn, "Insulin signalling and the regulation of glucose and lipid metabolism," *Nature*, vol. 414, no. 6865, pp. 799–806, 2001.
- [10] L. Pirola, A. M. Johnston, and E. Van Obberghen, "Modulation of insulin action," *Diabetologia*, vol. 47, no. 2, pp. 170–184, 2004.
- [11] J. R. Zierath, A. Krook, and H. Wallberg-Henriksson, "Insulin action and insulin resistance in human skeletal muscle," *Diabetologia*, vol. 43, no. 7, pp. 821–835, 2000.
- [12] H. Ruan, N. Hacoheh, T. R. Golub, L. Van Parijs, and H. F. Lodish, "Tumor necrosis factor- α suppresses adipocyte-specific genes and activates expression of preadipocyte genes in 3T3-L1 adipocytes: nuclear factor- κ B activation by TNF- α is obligatory," *Diabetes*, vol. 51, no. 5, pp. 1319–1336, 2002.
- [13] H. Ruan, P. D. G. Miles, C. M. Ladd, et al., "Profiling gene transcription in vivo reveals adipose tissue as an immediate target of tumor necrosis factor- α : implications for insulin resistance," *Diabetes*, vol. 51, no. 11, pp. 3176–3188, 2002.
- [14] R. A. DeFronzo, R. Gunnarsson, O. Bjorkman, M. Olsson, and J. Wahren, "Effects of insulin on peripheral and splanchnic glucose metabolism in noninsulin-dependent (type II) diabetes mellitus," *Journal of Clinical Investigation*, vol. 76, no. 1, pp. 149–155, 1985.
- [15] W.-S. Yang, W.-J. Lee, T. Funahashi, et al., "Weight reduction increases plasma levels of an adipose-derived anti-inflammatory protein, adiponectin," *Journal of Clinical Endocrinology and Metabolism*, vol. 86, no. 8, pp. 3815–3819, 2001.
- [16] J. Tank, J. Jordan, A. Diedrich, et al., "Bound leptin and sympathetic outflow in nonobese men," *Journal of Clinical Endocrinology and Metabolism*, vol. 88, no. 10, pp. 4955–4959, 2003.
- [17] D. Freymond, C. Bogardus, M. Okubo, K. Stone, and D. Mott, "Impaired insulin-stimulated muscle glycogen synthase activation in vivo in man is related to low fasting glycogen synthase phosphatase activity," *Journal of Clinical Investigation*, vol. 82, no. 5, pp. 1503–1509, 1988.
- [18] R. M. Reynolds, K. E. Chapman, J. R. Seckl, B. R. Walker, P. M. McKeigue, and H. O. Lithell, "Skeletal muscle glucocorticoid receptor density and insulin resistance," *Journal of the American Medical Association*, vol. 287, no. 19, pp. 2505–2506, 2002.
- [19] E. J. Barrett, E. M. Eggleston, A. C. Inyard, et al., "The vascular actions of insulin control its delivery to muscle and regulate the rate-limiting step in skeletal muscle insulin action," *Diabetologia*, vol. 52, no. 5, pp. 752–764, 2009.
- [20] A. D. Baron, "Hemodynamic actions of insulin," *American Journal of Physiology*, vol. 267, no. 2, pp. E187–E202, 1994.
- [21] A. D. Baron, M. Laakso, G. Brechtel, and S. V. Edelman, "Mechanism of insulin resistance in insulin-dependent diabetes mellitus: a major role for reduced skeletal muscle blood flow," *Journal of Clinical Endocrinology and Metabolism*, vol. 73, no. 3, pp. 637–643, 1991.
- [22] M. Raitakari, P. Nuutila, J. Knuuti, et al., "Effects of insulin on blood flow and volume in skeletal muscle of patients with IDDM: studies using [15O]H₂O, [15O]CO, and positron emission tomography," *Diabetes*, vol. 46, no. 12, pp. 2017–2021, 1997.
- [23] A. D. Baron, G. Brechtel-Hook, A. Johnson, J. Cronin, R. Leaming, and H. O. Steinberg, "Effect of perfusion rate on the time course of insulin-mediated skeletal muscle glucose uptake," *American Journal of Physiology*, vol. 271, no. 6, pp. E1067–E1072, 1996.
- [24] H. Wang, A. X. Wang, Z. Liu, and E. J. Barrett, "Insulin signaling stimulates insulin transport by bovine aortic endothelial cells," *Diabetes*, vol. 57, no. 3, pp. 540–547, 2008.
- [25] E. H. Serné, R. G. Ijzerman, R. O. B. Gans, et al., "Direct evidence for insulin-induced capillary recruitment in skin of healthy subjects during physiological hyperinsulinemia," *Diabetes*, vol. 51, no. 5, pp. 1515–1522, 2002.
- [26] D. A. Ehrmann, "Polycystic ovary syndrome," *New England Journal of Medicine*, vol. 352, no. 12, pp. 1223–1236, 2005.
- [27] R. S. Legro, A. R. Kunesman, W. C. Dodson, and A. Dunaif, "Prevalence and predictors of risk for type 2 diabetes mellitus and impaired glucose tolerance in polycystic ovary syndrome: a prospective, controlled study in 254 affected women," *Journal of Clinical Endocrinology and Metabolism*, vol. 84, no. 1, pp. 165–169, 1999.
- [28] A. M. Venkatesan, A. Dunaif, and A. Corbould, "Insulin resistance in polycystic ovary syndrome: progress and paradoxes," *Recent Progress in Hormone Research*, vol. 56, pp. 295–308, 2001.
- [29] A. Corbould, Y.-B. Kim, J. F. Youngren, et al., "Insulin resistance in the skeletal muscle of women with PCOS involves intrinsic and acquired defects in insulin signaling," *American Journal of Physiology*, vol. 288, no. 5, pp. E1047–E1054, 2005.
- [30] T. P. Ciaraldi, A. El-Roeiy, Z. Madar, D. Reichart, J. M. Olefsky, and S. S. C. Yen, "Cellular mechanisms of insulin resistance in polycystic ovarian syndrome," *Journal of Clinical Endocrinology and Metabolism*, vol. 75, no. 2, pp. 577–583, 1992.
- [31] A. Corbould, "Effects of androgens on insulin action in women: is androgen excess a component of female metabolic syndrome?" *Diabetes/Metabolism Research and Reviews*, vol. 24, no. 7, pp. 520–532, 2008.

- [32] F. Gonzalez, K. Thusu, E. Abdel-Rahman, A. Prabhala, M. Tomani, and P. Dandona, "Elevated serum levels of tumor necrosis factor alpha in normal-weight women with polycystic ovary syndrome," *Metabolism*, vol. 48, no. 4, pp. 437–441, 1999.
- [33] I. Tarkun, B. Çetinarslan, E. Türemen, Z. Cantürk, and M. Biyikli, "Association between circulating tumor necrosis factor-alpha, interleukin-6, and insulin resistance in normal-weight women with polycystic ovary syndrome," *Metabolic Syndrome and Related Disorders*, vol. 4, no. 2, pp. 122–128, 2006.
- [34] B. Pehlivanov and M. Mitkov, "Serum leptin levels correlate with clinical and biochemical indices of insulin resistance in women with polycystic ovary syndrome," *European Journal of Contraception and Reproductive Health Care*, vol. 14, no. 2, pp. 153–159, 2009.
- [35] M. Yilmaz, N. Bukan, H. Demirc, et al., "Serum resistin and adiponectin levels in women with polycystic ovary syndrome," *Gynecological Endocrinology*, vol. 25, no. 4, pp. 246–252, 2009.
- [36] A. Senay, B. Mithat, T. Alpaslan, K. Ebru, and G. Deniz, "Serum resistin and adiponectin levels in women with polycystic ovary syndrome," *Gynecological Endocrinology*, vol. 26, no. 3, pp. 161–166, 2010.
- [37] I. Ek, P. Arner, M. Rydén, et al., "A unique defect in the regulation of visceral fat cell lipolysis in the polycystic ovary syndrome as an early link to insulin resistance," *Diabetes*, vol. 51, no. 2, pp. 484–492, 2002.
- [38] J. E. Nestler, D. J. Jakubowicz, A. F. de Vargas, C. Brik, N. Quintero, and F. Medina, "Insulin stimulates testosterone biosynthesis by human thecal cells from women with polycystic ovary syndrome by activating its own receptor and using inositolglycan mediators as the signal transduction system," *Journal of Clinical Endocrinology and Metabolism*, vol. 83, no. 6, pp. 2001–2005, 1998.
- [39] J. E. Nestler, L. P. Powers, D. W. Matt, et al., "A direct effect of hyperinsulinemia on serum sex hormone-binding globulin levels in obese women with the polycystic ovary syndrome," *Journal of Clinical Endocrinology and Metabolism*, vol. 72, no. 1, pp. 83–89, 1991.
- [40] E. Diamanti-Kandarakis, G. Argyrakopoulou, F. Economou, E. Kandaraki, and M. Koutsilieris, "Defects in insulin signaling pathways in ovarian steroidogenesis and other tissues in polycystic ovary syndrome (PCOS)," *Journal of Steroid Biochemistry and Molecular Biology*, vol. 109, no. 3–5, pp. 242–246, 2008.
- [41] A. Corbould, H. Zhao, S. Mirzoeva, F. Aird, and A. Dunaif, "Enhanced mitogenic signaling in skeletal muscle of women with polycystic ovary syndrome," *Diabetes*, vol. 55, no. 3, pp. 751–759, 2006.
- [42] A. Holmang, J. Svedberg, E. Jennische, and P. Bjorntorp, "Effects of testosterone on muscle insulin sensitivity and morphology in female rats," *American Journal of Physiology*, vol. 259, no. 4, pp. E555–E560, 1990.
- [43] A. Holmäng, M. Niklasson, B. Rippe, and P. Lönnroth, "Insulin insensitivity and delayed transcapillary delivery of insulin in oophorectomized rats treated with testosterone," *Acta Physiologica Scandinavica*, vol. 171, no. 4, pp. 427–438, 2001.
- [44] M. C. Allemand, B. A. Irving, Y. W. Asmann, et al., "Effect of testosterone on insulin stimulated IRS1 Ser phosphorylation in primary rat myotubes—a potential model for PCOS-related insulin resistance," *PLoS ONE*, vol. 4, no. 1, article e4274, 2009.
- [45] F. Giallauria, S. Palomba, C. Vigorito, et al., "Androgens in polycystic ovary syndrome: the role of exercise and diet," *Seminars in Reproductive Medicine*, vol. 27, no. 4, pp. 306–315, 2009.
- [46] A. Dunaif, J. Xia, C.-B. Book, E. Schenker, and Z. Tang, "Excessive insulin receptor serine phosphorylation in cultured fibroblasts and in skeletal muscle. A potential mechanism for insulin resistance in the polycystic ovary syndrome," *Journal of Clinical Investigation*, vol. 96, no. 2, pp. 801–810, 1995.
- [47] K. Bouzakri, M. Roques, P. Gual, et al., "Reduced activation of phosphatidylinositol-3 kinase and increased serine 636 phosphorylation of insulin receptor substrate-1 in primary culture of skeletal muscle cells from patients with type 2 diabetes," *Diabetes*, vol. 52, no. 6, pp. 1319–1325, 2003.
- [48] R. V. Farese, M. P. Sajan, and M. L. Standaert, "Atypical protein kinase C in insulin action and insulin resistance," *Biochemical Society Transactions*, vol. 33, no. 2, pp. 350–353, 2005.
- [49] M. Strackowski and I. Kowalska, "The role of skeletal muscle sphingolipids in the development of insulin resistance," *Review of Diabetic Studies*, vol. 5, no. 1, pp. 13–24, 2008.
- [50] A. Dunaif, X. Wu, A. Lee, and E. Diamanti-Kandarakis, "Defects in insulin receptor signaling in vivo in the polycystic ovary syndrome (PCOS)," *American Journal of Physiology*, vol. 281, no. 2, pp. E392–E399, 2001.
- [51] K. Hojlund, D. Glintborg, N. R. Andersen, et al., "Impaired insulin-stimulated phosphorylation of akt and AS160 in skeletal muscle of women with polycystic ovary syndrome is reversed by pioglitazone treatment," *Diabetes*, vol. 57, no. 2, pp. 357–366, 2008.
- [52] M. Rajkhowa, S. Brett, D. J. Cuthbertson, et al., "Insulin resistance in polycystic ovary syndrome is associated with defective regulation of ERK1/2 by insulin in skeletal muscle in vivo," *Biochemical Journal*, vol. 418, no. 3, pp. 665–671, 2009.
- [53] V. Skov, D. Glintborg, S. Knudsen, et al., "Reduced expression of nuclear-encoded genes involved in mitochondrial oxidative metabolism in skeletal muscle of insulin-resistant women with polycystic ovary syndrome," *Diabetes*, vol. 56, no. 9, pp. 2349–2355, 2007.
- [54] V. Skov, D. Glintborg, S. Knudsen, et al., "Pioglitazone enhances mitochondrial biogenesis and ribosomal protein biosynthesis in skeletal muscle in polycystic ovary syndrome," *PLoS ONE*, vol. 3, no. 6, article e2466, 2008.
- [55] J. T. Lanner, A. Katz, P. Tavi, et al., "The role of Ca²⁺ influx for insulin-mediated glucose uptake in skeletal muscle," *Diabetes*, vol. 55, no. 7, pp. 2077–2083, 2006.
- [56] E. O. Ojuka, "Role of calcium and AMP kinase in the regulation of mitochondrial biogenesis and GLUT4 levels in muscle," *Proceedings of the Nutrition Society*, vol. 63, no. 2, pp. 275–278, 2004.
- [57] J. Levy, "Abnormal cell calcium homeostasis in type 2 diabetes mellitus: a new look on old disease," *Endocrine*, vol. 10, no. 1, pp. 1–6, 1999.
- [58] J. E. Nestler and M. A. McClanahan, "Diabetes and adrenal disease," *Bailliere's Clinical Endocrinology and Metabolism*, vol. 6, no. 4, pp. 829–847, 1992.
- [59] S. P. Thomson, C. S. Stump, L. R. Kurukulasuriya, and J. R. Sowers, "Adrenal steroids and the metabolic syndrome," *Current Hypertension Reports*, vol. 9, no. 6, pp. 512–519, 2007.

- [60] J. R. Sowers, A. Whaley-Connell, and M. Epstein, "Narrative review: the emerging clinical implications of the role of aldosterone in the metabolic syndrome and resistant hypertension," *Annals of Internal Medicine*, vol. 150, no. 11, pp. 776–783, 2009.
- [61] G. Giacchetti, V. Ronconi, F. Turchi, et al., "Aldosterone as a key mediator of the cardiometabolic syndrome in primary aldosteronism: an observational study," *Journal of Hypertension*, vol. 25, no. 1, pp. 177–186, 2007.
- [62] L. M. Mosso, C. A. Carvajal, A. Maiz, et al., "A possible association between primary aldosteronism and a lower β -cell function," *Journal of Hypertension*, vol. 25, no. 10, pp. 2125–2130, 2007.
- [63] S. L. Liu, S. Schmuck, J. Z. Chorzyczewski, R. Gros, and R. D. Feldman, "Aldosterone regulates vascular reactivity: short-term effects mediated by phosphatidylinositol 3-kinase-dependent nitric oxide synthase activation," *Circulation*, vol. 108, no. 19, pp. 2400–2406, 2003.
- [64] G. E. Callera, R. M. Touyz, R. C. Tostes, et al., "Aldosterone activates vascular p38MAP kinase and NADPH oxidase via c-Src," *Hypertension*, vol. 45, no. 4, pp. 773–779, 2005.
- [65] G. Lastra, A. Whaley-Connell, C. Manrique, et al., "Low-dose spironolactone reduces reactive oxygen species generation and improves insulin-stimulated glucose transport in skeletal muscle in the TG(mRen2)27 rat," *American Journal of Physiology*, vol. 295, no. 1, pp. E110–E116, 2008.
- [66] H. Hitomi, H. Kiyomoto, A. Nishiyama, et al., "Aldosterone suppresses insulin signaling via the downregulation of insulin receptor substrate-1 in vascular smooth muscle cells," *Hypertension*, vol. 50, no. 4, pp. 750–755, 2007.
- [67] D. H. van Raalte, D. M. Ouwens, and M. Diamant, "Novel insights into glucocorticoid-mediated diabetogenic effects: towards expansion of therapeutic options?" *European Journal of Clinical Investigation*, vol. 39, no. 2, pp. 81–93, 2009.
- [68] M. J. A. Saad, F. Folli, J. A. Kahn, and C. R. Kahn, "Modulation of insulin receptor, insulin receptor substrate-1, and phosphatidylinositol 3-kinase in liver and muscle of dexamethasone-treated rats," *Journal of Clinical Investigation*, vol. 92, no. 4, pp. 2065–2072, 1993.
- [69] S. P. Weinstein, C. M. Wilson, A. Pritsker, and S. W. Cushman, "Dexamethasone inhibits insulin-stimulated recruitment of GLUT4 to the cell surface in rat skeletal muscle," *Metabolism*, vol. 47, no. 1, pp. 3–6, 1998.
- [70] J. Ruzzin, A. S. Wagman, and J. Jensen, "Glucocorticoid-induced insulin resistance in skeletal muscles: defects in insulin signalling and the effects of a selective glycogen synthase kinase-3 inhibitor," *Diabetologia*, vol. 48, no. 10, pp. 2119–2130, 2005.
- [71] M. Rebuffé-Scrive, M. Krotkiewski, J. Elfverson, and P. Björntorp, "Muscle and adipose tissue morphology and metabolism in Cushing's syndrome," *Journal of Clinical Endocrinology and Metabolism*, vol. 67, no. 6, pp. 1122–1128, 1988.
- [72] J. E. Henriksen, F. Alford, A. Vaag, A. Handberg, and H. Beck-Nielsen, "Intracellular skeletal muscle glucose metabolism is differentially altered by dexamethasone treatment of normoglycemic relatives of type 2 diabetic patients," *Metabolism*, vol. 48, no. 9, pp. 1128–1135, 1999.
- [73] M. E. Patti, E. Brambilla, L. Luzi, E. J. Landaker, and C. R. Kahn, "Bidirectional modulation of insulin action by amino acids," *Journal of Clinical Investigation*, vol. 101, pp. 1519–1529, 1998.
- [74] M. Krebs, M. Krssak, E. Bernroider, et al., "Mechanism of amino acid-induced skeletal muscle insulin resistance in humans," *Diabetes*, vol. 51, no. 3, pp. 599–605, 2002.
- [75] G. Perseghin, K. Petersen, and G. I. Shulman, "Cellular mechanism of insulin resistance: potential links with inflammation," *International Journal of Obesity*, vol. 27, supplement 3, pp. S6–S11, 2003.
- [76] P. J. Randle, P. B. Garland, C. N. Hales, and E. A. Newsholme, "The glucose fatty-acid cycle. Its role in insulin sensitivity and the metabolic disturbances of diabetes mellitus," *The Lancet*, vol. 281, no. 7285, pp. 785–789, 1963.
- [77] R. Yamashita, T. Saito, S. Satoh, K. Aoki, Y. Kaburagi, and H. Sekihara, "Effects of dehydroepiandrosterone on gluconeogenic enzymes and glucose uptake in human hepatoma cell line, HepG2," *Endocrine Journal*, vol. 52, no. 6, pp. 727–733, 2005.
- [78] G. Stenström, L. Sjöström, and U. Smith, "Diabetes mellitus in pheochromocytoma. Fasting blood glucose levels before and after surgery in 60 patients with pheochromocytoma," *Acta Endocrinologica*, vol. 106, no. 4, pp. 511–515, 1984.
- [79] T. D. Wiesner, M. Blüher, M. Windgassen, and R. Paschke, "Improvement of insulin sensitivity after adrenalectomy in patients with pheochromocytoma," *Journal of Clinical Endocrinology and Metabolism*, vol. 88, no. 8, pp. 3632–3636, 2003.
- [80] M. Niklasson, A. Holmäng, and P. Lönnroth, "Induction of rat muscle insulin resistance by epinephrine is accompanied by increased interstitial glucose and lactate concentrations," *Diabetologia*, vol. 41, no. 12, pp. 1467–1473, 1998.
- [81] I. Raz, A. Katz, and M. K. Spencer, "Epinephrine inhibits insulin-mediated glycogenesis but enhances glycolysis in human skeletal muscle," *American Journal of Physiology*, vol. 260, no. 3, part 1, pp. E430–E435, 1991.
- [82] M. Laakso, S. V. Edelman, G. Brechtel, and A. D. Baron, "Effects of epinephrine on insulin-mediated glucose uptake in whole body and leg muscle in humans: role of blood flow," *American Journal of Physiology*, vol. 263, no. 2, part 1, pp. E199–E204, 1992.
- [83] M. D. Stifelman and D. M. Fenig, "Work-up of the functional adrenal mass," *Current Urology Reports*, vol. 6, no. 1, pp. 63–71, 2005.
- [84] N. S. Ross and D. C. Aron, "Hormonal evaluation of the patient with an incidentally discovered adrenal mass," *New England Journal of Medicine*, vol. 323, no. 20, pp. 1401–1405, 1990.
- [85] L. Barzon, N. Sonino, F. Fallo, G. Palu, and M. Boscaro, "Prevalence and natural history of adrenal incidentalomas," *European Journal of Endocrinology*, vol. 149, no. 4, pp. 273–285, 2003.
- [86] M. Reincke, M. Faßnacht, S. Vöth, P. Mora, and B. Allolio, "Adrenal incidentalomas: a manifestation of the metabolic syndrome?" *Endocrine Research*, vol. 22, no. 4, pp. 757–761, 1996.
- [87] S. Midorikawa, H. Sanada, S. Hashimoto, T. Suzuki, and T. Watanabe, "The improvement of insulin resistance in patients with adrenal incidentaloma by surgical resection," *Clinical Endocrinology*, vol. 54, no. 6, pp. 797–804, 2001.
- [88] M. Ivovic, S. Vujović, Z. Penezić, M. Zarković, and M. Drezgic, "Insulin sensitivity in patients with adrenal incidentaloma," *Srpski Arhiv za Celokupno Lekarstvo*, vol. 134, no. 7–8, pp. 315–319, 2006.
- [89] F. Ermetici, A. E. Malavazos, S. Corbetta, et al., "Adipokine levels and cardiovascular risk in patients with adrenal incidentaloma," *Metabolism*, vol. 56, no. 5, pp. 686–692, 2007.

- [90] M. Peppas, E. Boutati, C. Koliaki, et al., "Insulin resistance and metabolic syndrome in patients with nonfunctioning adrenal incidentalomas: a cause-effect relationship?" *Metabolism*. (2010) In press.
- [91] F. Amati, J. J. Dubé, M. Stefanovic-Racic, F. G. Toledo, and B. H. Goodpaster, "Improvements in insulin sensitivity are blunted by subclinical hypothyroidism," *Medicine and Science in Sports and Exercise*, vol. 41, no. 2, pp. 265–269, 2009.
- [92] S. D'Arezzo, S. Incerpi, F. B. Davis, et al., "Rapid nongenomic effects of 3,5,3'-triiodo-L-thyronine on the intracellular pH of L-6 myoblasts are mediated by intracellular calcium mobilization and kinase pathways," *Endocrinology*, vol. 145, no. 12, pp. 5694–5703, 2004.
- [93] I. Irrcher, D. R. Walkinshaw, T. E. Sheehan, and D. A. Hood, "Thyroid hormone (T₃) rapidly activates p38 and AMPK in skeletal muscle in vivo," *Journal of Applied Physiology*, vol. 104, no. 1, pp. 178–185, 2008.
- [94] G. B. Diaz, A. A. Paladini, M. E. Garcia, and J. J. Gagliardino, "Changes induced by hypothyroidism in insulin secretion and in the properties of islet plasma membranes," *Archives Internationales de Physiologie, de Biochimie et de Biophysique*, vol. 101, no. 5, pp. 263–269, 1993.
- [95] A. Roos, S. J. L. Bakker, T. P. Links, R. O. B. Gans, and B. H. R. Wolffenbuttel, "Thyroid function is associated with components of the metabolic syndrome in euthyroid subjects," *Journal of Clinical Endocrinology and Metabolism*, vol. 92, no. 2, pp. 491–496, 2007.
- [96] G. Dimitriadis, P. Mitrou, V. Lambadiari, et al., "Insulin action in adipose tissue and muscle in hypothyroidism," *Journal of Clinical Endocrinology and Metabolism*, vol. 91, no. 12, pp. 4930–4937, 2006.
- [97] M. P. Czech, C. C. Malbon, K. Kerman, W. Gitomer, and P. F. Pilch, "Effect of thyroid status on insulin action in rat adipocytes and skeletal muscle," *Journal of Clinical Investigation*, vol. 66, no. 3, pp. 574–582, 1980.
- [98] E. Maratou, D. J. Hadjidakis, A. Kollias, et al., "Studies of insulin resistance in patients with clinical and subclinical hypothyroidism," *European Journal of Endocrinology*, vol. 160, no. 5, pp. 785–790, 2009.
- [99] G. D. Dimitriadis, B. Leighton, M. Parry-Billings, D. West, and E. A. Newsholme, "Effect of hypothyroidism on the sensitivity of glycolysis and glycogen synthesis to insulin in the soleus muscle of the rat," *Biochemical Journal*, vol. 257, no. 2, pp. 369–373, 1989.
- [100] G. Dimitriadis, M. Parry-Billings, S. Bevan, et al., "The effects of insulin on transport and metabolism of glucose in skeletal muscle from hyperthyroid and hypothyroid rats," *European Journal of Clinical Investigation*, vol. 27, no. 6, pp. 475–483, 1997.
- [101] P. Mackowiak, E. Ginalska, E. Nowak-Strojec, and T. Szkudelski, "The influence of hypo- and hyperthyreosis on insulin receptors and metabolism," *Archives of Physiology and Biochemistry*, vol. 107, no. 4, pp. 273–279, 1999.
- [102] C. Rochon, I. Tauveron, C. Dejoux, et al., "Response of glucose disposal to hyperinsulinaemia in human hypothyroidism and hyperthyroidism," *Clinical Science*, vol. 104, no. 1, pp. 7–15, 2003.
- [103] G. Dimitriadis, B. Baker, H. Marsh, et al., "Effect of thyroid hormone excess on action, secretion, and metabolism of insulin in humans," *The American Journal of Physiology*, vol. 248, no. 5, pp. E593–E601, 1985.
- [104] G. Dimitriadis, E. Maratou, E. Boutati, et al., "IGF-I increases the recruitment of GLUT4 and GLUT3 glucose transporters on cell surface in hyperthyroidism," *European Journal of Endocrinology*, vol. 158, no. 3, pp. 361–366, 2008.
- [105] E. Resmini, F. Minuto, A. Colao, and D. Ferone, "Secondary diabetes associated with principal endocrinopathies: the impact of new treatment modalities," *Acta Diabetologica*, vol. 46, no. 2, pp. 85–95, 2009.
- [106] P. E. Harris, M. Walker, F. Clark, P. D. Home, and K. G. M. M. Alberti, "Forearm muscle metabolism in primary hypothyroidism," *European Journal of Clinical Investigation*, vol. 23, no. 9, pp. 585–588, 1993.
- [107] N. M. O'Meara, J. D. Blackman, J. Sturis, and K. S. Polonsky, "Alterations in the kinetics of C-peptide and insulin secretion in hyperthyroidism," *Journal of Clinical Endocrinology and Metabolism*, vol. 76, no. 1, pp. 79–84, 1993.
- [108] S. B. Liggett, S. D. Shah, and P. E. Cryer, "Increased fat and skeletal muscle β -adrenergic receptors but unaltered metabolic and hemodynamic sensitivity to epinephrine in vivo in experimental human thyrotoxicosis," *Journal of Clinical Investigation*, vol. 83, no. 3, pp. 803–809, 1989.
- [109] J.-P. Randin, L. Tappy, and B. Scazziga, "Insulin sensitivity and exogenous insulin clearance in Graves' disease. Measurement by the glucose clamp technique and continuous indirect calorimetry," *Diabetes*, vol. 35, no. 2, pp. 178–181, 1986.
- [110] M. Laville, J. P. Riou, and P. F. Bougneres, "Glucose metabolism in experimental hyperthyroidism: intact in vivo sensitivity to insulin with abnormal binding and increased glucose turnover," *Journal of Clinical Endocrinology and Metabolism*, vol. 58, no. 6, pp. 960–965, 1984.
- [111] S. P. Weinstein, E. O'Boyle, and R. S. Haber, "Thyroid hormone increases basal and insulin-stimulated glucose transport in skeletal muscle: the role of GLUT4 glucose transporter expression," *Diabetes*, vol. 43, no. 10, pp. 1185–1189, 1994.
- [112] G. Dimitriadis, P. Mitrou, V. Lambadiari, et al., "Glucose and lipid fluxes in the adipose tissue after meal ingestion in hyperthyroidism," *Journal of Clinical Endocrinology and Metabolism*, vol. 91, no. 3, pp. 1112–1118, 2006.
- [113] G. Dimitriadis, P. Mitrou, V. Lambadiari, et al., "Insulin-stimulated rates of glucose uptake in muscle in hyperthyroidism: the importance of blood flow," *Journal of Clinical Endocrinology and Metabolism*, vol. 93, no. 6, pp. 2413–2415, 2008.
- [114] J. P. Randin, B. Scazziga, E. Jequier, and J. P. Felber, "Study of glucose and lipid metabolism by continuous indirect calorimetry in Graves' disease: effect of an oral glucose load," *Journal of Clinical Endocrinology and Metabolism*, vol. 61, no. 6, pp. 1165–1171, 1985.
- [115] W. H. Martin III, E. Korte, T. K. Tolley, and J. E. Saffitz, "Skeletal muscle β -adrenoceptor distribution and responses to isoproterenol in hyperthyroidism," *American Journal of Physiology*, vol. 262, no. 4, pp. E504–E510, 1992.
- [116] W. H. Martin III, R. J. Spina, E. Korte, et al., "Mechanisms of impaired exercise capacity in short duration experimental hyperthyroidism," *Journal of Clinical Investigation*, vol. 88, no. 6, pp. 2047–2053, 1991.

Review Article

Pathogenesis of Insulin Resistance in Skeletal Muscle

Muhammad A. Abdul-Ghani and Ralph A. DeFronzo

Division of Diabetes, University of Texas Health Science Center at San Antonio, 7703 Floyd Curl Dr, San Antonio, TX 78229, USA

Correspondence should be addressed to Muhammad A. Abdul-Ghani, abdulghani@uthscsa.edu

Received 7 December 2009; Accepted 20 January 2010

Academic Editor: Guy M. Benian

Copyright © 2010 M. A. Abdul-Ghani and R. A. DeFronzo. This is an open access article distributed under the Creative Commons Attribution License, which permits unrestricted use, distribution, and reproduction in any medium, provided the original work is properly cited.

Insulin resistance in skeletal muscle is manifested by decreased insulin-stimulated glucose uptake and results from impaired insulin signaling and multiple post-receptor intracellular defects including impaired glucose transport, glucose phosphorylation, and reduced glucose oxidation and glycogen synthesis. Insulin resistance is a core defect in type 2 diabetes, it is also associated with obesity and the metabolic syndrome. Dysregulation of fatty acid metabolism plays a pivotal role in the pathogenesis of insulin resistance in skeletal muscle. Recent studies have reported a mitochondrial defect in oxidative phosphorylation in skeletal muscle in variety of insulin resistant states. In this review, we summarize the cellular and molecular defects that contribute to the development of insulin resistance in skeletal muscle.

1. Introduction

Skeletal muscle is the major site for disposal of ingested glucose in lean healthy normal glucose tolerance (NGT) individuals [1–4]. Following a meal, approximately one third of ingested glucose is taken up by the liver and the rest by peripheral tissues, primarily skeletal muscle via an insulin dependent mechanism [1–4]. The postprandial hyperglycemia stimulates insulin secretion from the pancreas and the rise in plasma insulin concentration stimulates glucose uptake in skeletal muscle leading to the disposal of ingested glucose [1–4].

In insulin resistance states, such as T2DM and obesity, insulin-stimulated glucose disposal in skeletal muscle is markedly impaired [1–6]. The decreased insulin-stimulated glucose uptake is due to impaired insulin signaling and multiple postreceptor intracellular defects including impaired glucose transport and glucose phosphorylation, and reduced glucose oxidation and glycogen synthesis [7–10] (Table 1). Although the exact mechanism that leads to the development of insulin resistance in skeletal muscle is not yet fully understood, an increased intramyocellular fat content and fatty acid metabolites have been shown to play a pivotal role in the development of insulin resistance in skeletal muscle [11–15]. The recent studies have reported the existence of a defect in mitochondrial oxidative phosphorylation in skeletal

muscle in insulin resistance states [16–20] and suggest that this mitochondrial defect contributes to the increased intramyocellular fat content. In this paper we will summarize the evidence that supports the existence of insulin resistance in skeletal muscle, the cellular mechanism(s) that lead to the development of insulin resistance, and the clinical consequences of insulin resistance in skeletal muscle.

2. Normal Skeletal Muscle Metabolism

Skeletal muscle utilizes both glucose and free fatty acid (FFA) as fuel sources for energy production. During the postabsorptive state, the plasma insulin concentration is low. Since the plasma insulin concentration is the principal factor that restrains lipolysis in adipocytes [21] and stimulates glucose uptake in skeletal muscle [21], during the fasting state, muscle glucose uptake is low and the plasma FFA concentration is elevated. Thus, under fasting conditions, FFA serves as the principal fuel source for energy production in skeletal muscle, while the brain exclusively utilizes glucose.

Following glucose ingestion, the increase in plasma glucose concentration stimulates insulin secretion from the beta cell and the resultant hyperinsulinemia suppresses lipolysis, leading to decline in plasma FFA concentration and subsequent decrease in the rate of lipid oxidation. Simultaneously,

TABLE 1: Defects in Glucose Metabolism in Insulin Resistant Conditions.

Insulin signaling	(1) Reduced insulin receptor tyrosine phosphorylation (2) Decreased IRS-1 tyrosine phosphorylation (3) Decreased PI3-kinase activation
Glucose transport	(1) Impaired GLUT4 translocation (2) Impaired GLUT 12 translocation
Glucose metabolism	(1) Decreased glucose phosphorylation (2) Decreased glucose oxidation and glycolytic FLUX (3) Impaired glycogen synthase

insulin stimulates glucose uptake in skeletal muscle, and the increased glucose flux into skeletal muscle, together with the activation of key enzymes in glucose metabolism by insulin, leads a marked increase in muscle glucose oxidation [1]. Thus, under postprandial conditions, for example, mixed meal, muscle energy metabolism switches from predominant oxidization of fat during the fasting state, to predominant oxidization of glucose [22]. The ability of skeletal muscle to switch from fat oxidation during the fasting state to glucose oxidation during the postprandial state has been referred to as metabolic flexibility [23].

After glucose is transported into the myocyte via the GLUT4 transporter, it is immediately phosphorylated by hexokinase, and the phosphorylated glucose either is converted to, and stored as glycogen, or enters the glycolytic pathway for oxidation. Approximately 90% of glucose entering the glycolysis is oxidized and the remaining 10% is released as lactate. At low plasma insulin concentration, for example, fasting state, glycogen synthase, and glucose oxidation contribute equally to glucose disposal. However, with increasing plasma insulin concentration, glycogen synthase is activated by insulin and glycogen synthesis predominate (~70% of glucose disposal) [24].

3. Insulin Resistance in Skeletal Muscle

The term insulin resistance refers to an impairment in insulin action in insulin-target tissues, such as skeletal muscle, adipocytes, and liver. With respect to skeletal muscle, the primary action of insulin is to stimulate glucose uptake and metabolism [1–4]. In lean healthy individuals insulin stimulates glucose uptake into skeletal muscle in a dose-dependent manner, with a half-maximal effect (EC50) at a plasma insulin concentration ~60 $\mu\text{U}/\text{mL}$ [21]. In insulin resistant states, insulin-stimulated glucose uptake is markedly reduced in skeletal muscle (Figure 1).

Himsworth and Kerr [25], using a combined oral glucose and intravenous tolerance test, were the first to demonstrate

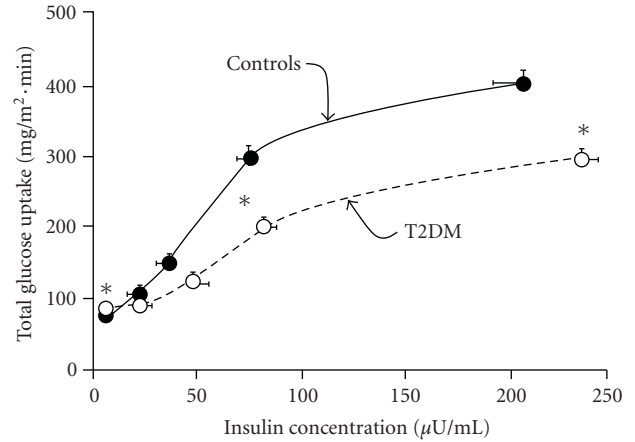


FIGURE 1: Dose-response curve relating the plasma insulin concentration to the rate of insulin mediated whole body glucose uptake in controls and type 2 diabetic subjects. * $P < .01$ (from [21]).

that tissue sensitivity to insulin is diminished in T2DM patients. In 1975, Ginsberg et al. [26], using the insulin suppression test, provided further evidence that the ability of insulin to promote tissue glucose uptake in T2DM was severely reduced. The most conclusive documentation for increased insulin resistance in skeletal muscle in lean, as well as obese T2DM subjects, has been provided by DeFronzo and colleagues [1–5, 21, 27, 28] and Butterfield and Whichelow [29]. Using the gold standard euglycemic hyperinsulinemic clamp technique to quantify insulin-stimulated glucose uptake, they demonstrated that both lean and obese T2DM subjects have marked decrease (>50%) in whole body glucose disposal during the insulin clamp.

Although glucose disposal during the insulin clamp represents insulin-stimulated glucose uptake by all peripheral tissues, the great majority of this glucose uptake take place in skeletal muscle. Under euglycemic conditions studies, using the insulin clamp in combination with femoral artery and vein catheterization [5] has shown that approximately 80% of total body glucose uptake occurs in skeletal muscle. In response to a physiologic increase in plasma insulin concentration (80–100 $\mu\text{U}/\text{mL}$), leg muscle glucose uptake increases progressively in healthy subjects and reaches a plateau value of approximately 10 mg/kg leg wt · min. In contrast, during the last hour of the insulin clamp study, the rate of glucose uptake is reduced by ~50% in lean T2DM subjects (Figure 2). Thus, the dose response curve relating insulin-stimulated glucose uptake and the plasma insulin concentration shifts to the right with an increase in EC50 (to ~120–140 $\mu\text{U}/\text{mL}$) in subjects with T2DM (Figure 1). In addition, the onset of insulin action in skeletal muscle in T2DM subjects is markedly delayed (Figure 2). Even though the insulin infusion is continued for an additional 60 minutes in subjects with T2DM to allow insulin to more fully express its biologic action, glucose uptake remains blunted. These studies indicate that insulin resistance in skeletal muscle in subjects with T2DM is manifested, not only by a reduction in the magnitude of insulin action, but also by a delayed onset of insulin action to stimulate glucose uptake.

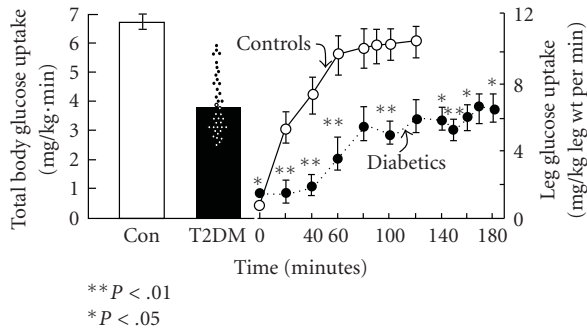


FIGURE 2: Insulin-stimulated whole body glucose uptake measured with the euglycemic clamp in lean healthy and type 2 diabetic subjects (left) and time course of change in leg glucose uptake in type 2 diabetic and control subjects (right) (from [5]).

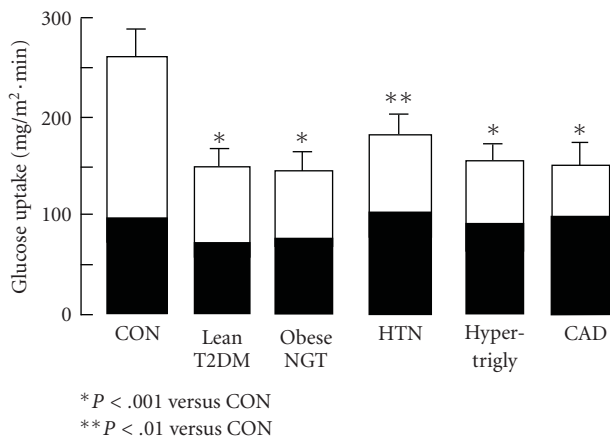


FIGURE 3: Insulin-stimulated glucose disposal (40 mU/m²·min euglycemic insulin clamp) in lean healthy control (CON) subjects, lean drug naïve type 2 diabetic subjects (T2DM), lean normal-glucose-tolerant (NGT) hypertensive subjects (HTN), NGT hypertriglyceridemic subjects, and nondiabetic subjects with coronary artery disease (CAD). The open portion of the bar represents nonoxidative glucose disposal (glycogen synthesis) and the solid portion represents glucose oxidation. See DeFronzo and Ferrannini [80], DeFronzo [81].

Insulin resistance in skeletal muscle is manifested long before the hyperglycemia becomes evident [2]. Thus, lean healthy offspring of diabetic parents have a significant decrease in insulin-stimulated total body and muscle glucose disposal which is of a similar magnitude to that observed in their diabetic parents [30–32]. Insulin resistance in skeletal muscle also can develop independent of family history of T2DM. Thus, obese NGT subjects without a family history for T2DM [33, 34] and individuals with essential hypertension [35] and ischemic heart disease [36] also have a 35–50% decrease in whole body insulin-mediated glucose disposal (Figure 3). Insulin resistance in skeletal muscle also has been reported in association with the normal ageing process [37], dyslipidemia (increased plasma triglyceride/decreased HDL cholesterol) [4, 26], and in association with many disease states including

polycystic ovary syndrome (PCOs) [38], chronic kidney failure [39], heart failure [40], myotonic dystrophy [41], and lipodystrophy [42]. In addition, insulin resistance develops in acute severe illnesses such as injury and sepsis, perhaps secondary to the acute inflammatory state that prevails [43]. Insulin resistance in skeletal muscle also can develop secondary to pharmacological therapy, for example, glucocorticoids [44], anti-HIV therapy [45], and beta blockers [46]. These studies indicate that although insulin resistance in skeletal muscle is a hallmark of T2DM, muscle insulin resistance and the accompanying insulin resistance syndrome are more widely prevalent and the metabolic and clinical consequences of insulin resistance (e.g., increased cardiovascular risk) affect nondiabetic individuals as well. Because the molecular mechanisms that lead to the development of insulin resistance in skeletal muscle have been extensively studied in obese and T2DM subjects, we will focus the discussion on the molecular/biochemical pathways that cause muscle insulin resistance in these two common metabolic disorders. However, similar molecular defects have been reported in other insulin resistant states [39].

Under basal conditions, for example, fasting state, the plasma insulin concentration is low (5–10 μ U/mL). Thus, glucose uptake that takes place in skeletal muscle during the postabsorptive state is insulin independent. The noninsulin dependent glucose uptake in skeletal muscle also is decreased in insulin resistant individuals [47]. The mechanism(s) responsible for the decrease in noninsulin dependent glucose uptake has (have) yet to be defined.

3.1. Relationship between Obesity and Insulin Resistance in Skeletal Muscle. Obese NGT subjects display marked skeletal muscle insulin resistance compared to lean age and sex matched individuals [33, 34], and the severity of muscle insulin resistance is related to the increase in BMI [34]. Studies in experimental animals and in man have demonstrated that the increase in body weight is accompanied with an increase in skeletal muscle insulin resistance [48–52]. Conversely, weight loss in obese NGT individuals improves/reverses insulin resistance in skeletal muscle [43]. Collectively, these studies demonstrate a causal role of obesity per se in the development of skeletal muscle insulin resistance.

The mechanism via which obesity causes insulin resistance in skeletal muscle is related to the accumulation of fat in the myocytes. Muscle biopsy studies [53, 54] have demonstrated increased triglyceride content in skeletal muscle of obese NGT subjects compared to lean individuals and an inverse relationship between muscle insulin sensitivity and the intramuscular triglyceride content. Although these initial studies documented the importance of increased muscle fat content in the etiology of insulin resistance in obesity, they did not distinguish between the contribution of fat accumulation inside the muscle fiber (intramyocellular, IMCL) versus fat accumulation in the muscle outside the muscle cell (extramyocellular, EMCL). More recent studies [55, 56] using magnetic resonance spectroscopy have demonstrated that although IMCL fat content contributes only a small fraction (~1%) to the total muscle fat content, it plays a key role

in the development of insulin resistance in skeletal muscle compared to EMCL. Muscle insulin resistance strongly correlates with IMCL, independent of total body fat mass and diabetes status [56], while the correlation between EMCL and insulin resistance is not significant.

Obese NGT individuals are characterized by an increase in plasma free fatty acid (FFA) concentration. The important role of elevated plasma FFA in the pathogenesis of insulin resistance is now well established [12, 14, 57]. Considerable data implicate a causative role for elevated plasma FFA level in insulin resistance in skeletal muscle. The majority of insulin resistant individuals, both diabetic and nondiabetics, are overweight or obese [58], and both lean and obese insulin resistant individuals manifest multiple disturbances in FFA metabolism [59]. Nondiabetic obese and type 2 diabetic individuals are characterized by day-long elevation in the plasma FFA concentration, which fails to suppress normally after ingestion of a mixed meal or an oral glucose load [60]. Elevated plasma FFA levels correlate strongly with reduced insulin-stimulated glucose disposal in skeletal muscle [61]. FFAs are stored within adipocytes in the form of triglycerides and serve as an important source of energy during fasting. Insulin is a potent inhibitor of lipolysis and restrains the release of FFAs from adipocytes. In insulin resistant individuals, for example, nondiabetic obese and lean type 2 diabetic subjects, the ability of insulin to inhibit lipolysis and reduce plasma FFA concentration is markedly impaired [21, 59], leading to an increased rate of lipolysis and chronic elevation in the plasma FFA concentration. It is well established that chronically elevated plasma FFA levels cause insulin resistance in skeletal muscle [1, 12, 14, 62–65]. Both acute (4 hours) and chronic (4 days) physiologic elevation of plasma FFA concentration in insulin sensitive individuals impairs insulin signaling and causes insulin resistance in skeletal muscle [28, 62–68]. The inhibition of insulin signaling and induction of skeletal muscle insulin resistance caused by elevation in the plasma FFA concentration is dose dependent [65]. Conversely, reduction of plasma FFA concentration in insulin resistant individuals, for example, type 2 diabetic subjects, augments insulin-stimulated glucose disposal in skeletal muscle [69–72], and the improvement in insulin sensitivity is closely associated with a reduction in intramyocellular FFA concentration [69]. Collectively, these results support a causative role of elevated plasma FFA levels in the pathogenesis of insulin resistance in skeletal muscle and have been referred to as “lipotoxicity” [73].

Much evidence supports the hypothesis that the lipotoxic action of FFA on skeletal muscle insulin sensitivity is due to an increase in intramyocellular fat content: (i) in insulin resistant individuals, insulin-stimulated glucose disposal correlates more strongly with intramyocellular fat content than with the extramitochondrial fat [55, 56]; (ii) the decrease in insulin resistance brought about by reducing the plasma FFA concentration with acipimox in insulin resistant individuals is associated with a reduction in intracellular FFA content, and the magnitude of decrease in insulin resistance strongly correlates with the decrease in FFA content [69]; (iii) the increase in insulin resistance caused by elevating the plasma FFA concentration in insulin sensitive individuals

is associated with an increase in the intramyocellular fat content [74]; (iv) in animals, a high fat diet causes an increase in intramuscular fat content, which correlates closely both with the severity and temporal development of insulin resistance [75, 76]; (v) in rodents, injection of recombinant adiponectin increases fat oxidation, reduces intramyocellular lipid, and improves insulin sensitivity [77]; (vi) muscle-specific over expression of lipoprotein lipase leads to the accumulation of fat/FFA in muscle and severe muscle insulin resistance, while the fat content and insulin sensitivity in other tissues, that is, liver, remain unchanged [78]; (vii) weight loss, induced by bariatric surgery, results in a complete normalization of insulin sensitivity despite the presence of continued obesity (BMI reduced from 49 to 39 kg/m²) [79]. The normalization of muscle insulin sensitivity is associated with a reduction of muscle fat content to normal despite a persistent increase in total body fat content [79]. These observations collectively indicate that muscle triglyceride (which is metabolic inert) is not directly involved in determining insulin sensitivity but rather represents a marker of imbalance between lipid supply and lipid oxidation in skeletal muscle, while increases in intramyocellular FFA and other lipotoxic metabolites (DAG, ceramide) have a more direct role in the development of skeletal muscle insulin resistance.

3.2. Increased Fat Supply or Impaired Mitochondrial Function in Insulin Resistance? Fat is an important fuel source in skeletal muscle. The accumulation of fat inside the muscle fiber could originate from excess supply of FFA to the muscle, a decreased rate of muscle fat oxidation, or some combination of the two.

3.2.1. Long-Chain Fatty Acid (LCFA) Transport into the Muscle. Considerable debate exists regarding the mechanism by which LCFAs are transported into skeletal muscle [82–84]. Because LCFAs are highly hydrophobic molecules and easily can cross the plasma membrane of muscle via passive diffusion, the rate of LCFA influx into muscle fiber is, in part, driven by the concentration gradient of LCFA across the plasma membrane. Thus, an increase in plasma FFA concentration is an important regulator of FFA supply to skeletal muscle [82]. Indeed, early studies demonstrated the rate of lipolysis was a key determinant of FFA uptake and oxidation in skeletal muscle and documented a linear relationship between the plasma LCFA concentration and their rate of uptake and oxidation in the muscle [85–87]. More recent studies have reported that under conditions of marked increase in energy demand in the muscle, for example, during exercise, LCFAs uptake initially increases linearly then plateaus [88], suggesting the existence of a facilitated transport mechanism for LCFA into skeletal muscle. Three putative fatty acid binding proteins located at the plasma membrane have been identified: (i) the plasma membrane-bound fatty acid binding protein (FABP); (ii) fatty acid translocase (CD36); (iii) fatty acid transport protein (FATP). There is abundant evidence which indicates that CD36 plays an important role in LCFA uptake into skeletal muscle in rodents and human and its concentration and activity are

increased following exercise [89–96]. However, the transport of LCFA by CD36 into skeletal muscle does not seem to regulate the rate of LCFA oxidation. During conditions of decreased fat oxidation and increased CD36 levels, muscle uptake of LCFA increased, resulting in increased muscle triglyceride synthesis and increased IMCL content [97, 98]. The CD36 content and LCFA transport capacity have been reported to be increased in obese and T2DM individuals and correlate with increased muscle triglyceride content, while fat oxidation is decreased. Further, insulin has been reported to increase CD36 content in skeletal muscle [99].

3.2.2. Fat Oxidation in Insulin Resistance. Several studies have reported decreased fat oxidation in skeletal muscle, independent of the plasma FFA concentration [100–102]. In one study that compared muscle fat oxidation across the leg in obese (BMI = 34 kg/m²) compared to lean (BMI = 23 kg/m²) individuals, the rate of fatty acid oxidation was reduced in the obese group despite similar arterial FFA concentrations [100]. These results suggest the presence of impaired muscle fat oxidation independent of fat supply to skeletal muscle. Similar results have been reported in rectus abdominus muscle in morbidly obese individuals [101] and in obese nondiabetic women [102]. Studies in experimental animals also have reported a decreased rate of lipid oxidation in skeletal muscle in obese Zucker rat [103]. Collectively, these studies indicate the existence of an intrinsic defect in mitochondrial capacity to oxidize fat in obesity and T2DM.

3.2.3. Mitochondrial Function in Insulin Resistant Conditions. Since the majority of fat oxidation take place in the mitochondria, impaired fat oxidation in insulin resistant individuals suggests the presence of a mitochondrial defect that contributes to the impaired muscle fat oxidation and increased IMCL fat content. Studies in humans, using molecular, biochemical, and MR spectroscopic techniques, have documented a defect in mitochondrial oxidative phosphorylation in a variety of insulin resistance states. Because of its accessibility, most of these studies have been performed in skeletal muscle. In vivo measurement of oxidative phosphorylation with ³¹P-NMR has demonstrated impaired ATP synthesis in a variety of insulin resistant states. Lean normal-glucose-tolerant (NGT), insulin-resistant offspring of T2DM parents have a 30–40% decrease in metabolic flux through the tricarboxylic acid cycle [104] and oxidative phosphorylation [31] in skeletal muscle under basal conditions. A similar impairment in resting flux through oxidative phosphorylation also has been reported in subjects with type 2 diabetes [105]. Furthermore, unlike lean insulin-sensitive individuals, both diabetic subjects and NGT insulin-resistant offspring of two diabetic parents fail to increase mitochondrial oxidative phosphorylation flux following insulin stimulation despite a significant increase in glucose disposal in skeletal muscle [105, 106]. Subjects with T2DM also have decreased exercise tolerance and impaired recovery of intracellular phosphocreatinine concentration following exercise [107, 108], indicating that the mitochondrial defect in oxidative phosphorylation may

contribute to the impairment in exercise capacity in insulin-resistant individuals. Insulin resistance also is a characteristic feature of the normal aging process and is associated with a decrease in mitochondrial ATP synthesis rate and an increase in intramyocellular fat content [109]. Lastly, experimental induction of insulin resistance in skeletal muscle, by a physiological increase in plasma FFA concentration in lean healthy insulin-sensitive individuals, is associated with a decrease in oxidative phosphorylation flux in skeletal muscle [110]. Collectively, these results indicate that, regardless of its etiology, insulin resistance in skeletal muscle is associated with decreased mitochondrial oxidative phosphorylation.

3.3. Qualitative or Quantitative Mitochondrial Defect. The mitochondrial defect in ATP synthesis rate documented in vivo with MRS could be due to a reduction in the number of mitochondria in skeletal muscle with normal function of individual mitochondria, an intrinsic defect in a quantitatively normal number of mitochondria, or some combination of the two. All three of these scenarios would result in a reduced in ATP synthesis rate measured in vivo with MRS. Other important unanswered questions are whether the mitochondrial defect is inherited or acquired and whether this defect is the cause or the effect of the insulin resistance. An acquired defect potentially could be reversed or prevented, while an inherited defect would be permanent.

Although several lines of evidence support a reduction in mitochondrial number in skeletal muscle in insulin resistant individuals, not all studies have yielded consistent results. Electron microscopic studies have revealed a significant reduction (~40%) in mitochondrial density in skeletal muscle in lean NGT offspring of type 2 diabetic parents, in obese nondiabetic individuals and in T2DM subjects compared to lean insulin-sensitive, age-matched controls [111, 112]. The decrease in mitochondrial density in skeletal muscle in insulin-resistant individuals is consistent with decreased expression of PGC-1 gene [113], the master regulator for mitochondrial biogenesis. Diabetic subjects have been reported to have a decrease in muscle fiber oxygen consumption measured ex vivo. However, when oxygen consumption was related to mitochondrial copy number, both diabetic and nondiabetic subjects had similar rates of muscle oxygen consumption, implying a decrease in mitochondrial density without an intrinsic mitochondrial defect in T2DM subjects. However, other studies have reported contradictory results. Thus, studies which have assessed mitochondrial copy number in skeletal muscle in insulin-resistant individuals have reported conflicting results [114–116]. Furthermore, insulin resistance, caused by physiological elevation in plasma FFA concentration in lean healthy individuals, was not associated with a significant change in mitochondrial density in skeletal muscle [117].

Several morphological and functional studies support the concept of an intrinsic mitochondrial defect in insulin resistant individuals. EM studies have demonstrated a variety of morphological abnormalities in mitochondria in insulin-resistant individuals [118] and these changes were reversible with weight loss and increased physical activity [119]. Ex vivo measurement of electron transport chain activity (ETC)

[112] and mitochondrial ATP synthesis in isolated mitochondria [120, 121] have demonstrated a decrease in ETC activity and ATP synthesis in obese insulin-resistant individuals compared to lean insulin-sensitive subjects. Since, in these studies [112, 120], ETC activity and mitochondrial ATP synthesis rate were related to the amount of mitochondrial protein and/or citrate synthase activity, these observations indicate the existence of a basic functional defect in mitochondrial activity in skeletal muscle of obese insulin-resistant individuals [115]. Biochemical studies have reported a decrease in the activity of a variety of mitochondrial enzymes [122], also supporting an intrinsic functional mitochondrial defect in type 2 diabetic subjects. An intrinsic mitochondrial defect, with or without a decrease in mitochondrial density, would be expected to result in impaired lipid oxidation, an increase in intramyocellular lipid content, and the development/exacerbation of insulin resistance. Additional studies are needed to resolve some of the inconsistencies reviewed above and to explore the biochemical/molecular basis of the mitochondrial defect measured in vivo in skeletal muscle in insulin resistant individuals.

3.4. Inherited or Acquired Mitochondrial Defect. An inherited mitochondrial oxidative defect in the absence (but especially in the presence) of enhanced FFA influx to skeletal muscle would be expected to lead to intramyocellular fat accumulation. An inherited defect in mitochondrial oxidative capacity should be present at or shortly after birth and, most importantly, not be reversible. With regard to this, several lines of evidence indicate that the mitochondrial defect associated with insulin resistant is reversible, at least in part: (i) modest weight reduction (~10% of body weight), produced by dieting and increased physical activity, reduces insulin resistance and intramyocellular lipid content and these changes are associated with increased fat oxidation in skeletal muscle [123]. Furthermore, the magnitude of increase in fat oxidation following weight loss correlated strongly with the decrease in insulin resistance [123]; (ii) marked weight reduction following bariatric surgery in morbidly obese, severely insulin-resistant subjects completely normalized insulin sensitivity, and correction of the insulin resistance was accompanied by depletion of intramyocellular fat content [124]. Although mitochondrial function was not assessed following weight loss in this latter study, the depletion of intramyocellular fat and normalization of insulin sensitivity suggests a reversible mitochondrial defect in these morbidly obese, insulin-resistant individuals; (iii) the morphological changes which characterize mitochondria in obese insulin-resistant individuals [118] can be reversed following weight loss and increased physical activity [119]; (iv) the improvement in insulin sensitivity following exercise is associated with improved muscle oxidative capacity [125, 126] and increases in both mitochondrial density [127] and activity [128–130]. These observations indicate that the mitochondrial defect which accompanies insulin resistance is, at least in part, reversible. The ability to reverse the defect in mitochondrial oxidative function argues against an inherited defect. Importantly, a mitochondrial defect similar to that observed in insulin-resistant individuals can

be produced in young lean healthy subjects by physiologic elevation of the plasma FFA concentration [110, 131]. In addition, the insulin resistance associated with aging in lean subjects with negative family history of diabetes is associated with a decrease in mitochondrial function [109]. Thus, normal mitochondrial function in young, insulin-sensitive subjects suggests that the mitochondrial defect and insulin-resistance are acquired as part of the normal ageing process.

The evidence reviewed above supports the hypothesis that the mitochondrial defect which accompanies insulin resistance is reversible, at least in part, and is likely to be acquired. Regarding the etiology of the acquired defect in mitochondrial function, in vivo mitochondrial ATP synthesis rate, measured with ³¹P-NMR strongly and inversely correlates with the fasting plasma FFA concentration [105], suggesting a possible role for elevated plasma FFA/toxic intramyocellular FFA metabolite concentrations in the mitochondrial dysfunction in insulin resistant individuals. With respect to this, we recently have demonstrated that a physiologic increase in FACoA concentration inhibits mitochondrial ATP synthesis in vitro in mitochondria isolated from skeletal muscle of NGT healthy lean subjects [132]. This observation is consistent with the decrease in oxidative phosphorylation observed following elevation in the plasma FFA concentration in lean healthy individuals [110], and it indicates that elevated plasma FFA/intramyocellular metabolite concentration can cause an acquired mitochondrial defect in oxidative phosphorylation.

3.5. Mitochondrial Defect in Insulin Resistance: Cause or Effect? The mitochondrial defect in oxidative phosphorylation described in vivo with MRS and ex vivo in muscle fibers and isolated mitochondria could contribute to the increase in intramyocellular FFA metabolite levels observed in obesity and T2DM and contribute to the insulin resistance. However, one also can imagine another scenario in which the mitochondrial defect results from insulin resistance. If the increase in intramyocellular fat content in insulin resistant individuals was associated with an increase in fat oxidation and excessive production of reactive oxygen species or other toxic metabolites, then the decrease in mitochondrial oxidative phosphorylation could result from the downregulation of mitochondrial function to ameliorate the production of these toxic molecules. Reproduction of the mitochondrial defect in oxidative phosphorylation in normal healthy individuals by elevation of the plasma FFA concentration would argue for a causative role of the mitochondrial defect in insulin resistance. However, since muscle insulin resistance also develops following lipid infusion and since the time course of the development of the mitochondrial defect and insulin resistance were not monitored during lipid infusion [110], one cannot completely exclude the possibility that the mitochondrial defect results secondary to insulin resistance.

Studies in experimental animals and cultured muscle cells have attempted to address the relationship between mitochondrial function and skeletal muscle insulin resistance. Over expression of the PGC-1 alpha gene in skeletal muscle in mice in vivo enhanced mitochondrial activity, augmented the expression of multiple proteins involved in

fat oxidation and glucose transport, and increased by ~35% insulin-stimulated glucose uptake [133]. Similarly, activation of SIRT1 with resveratrol in mice resulted in increased mitochondrial activity and protected the animals from diet-induced obesity and insulin resistance [134]. Studies in cultured skeletal muscle cells have been inconsistent. Down regulation of mitochondrial function in myotubes with oligomycin, which inhibits mitochondrial ATP synthesis, and with ethidium bromide, which impairs mitochondrial DNA replication, caused an increase in intracellular fat content, impaired insulin signaling, and decreased insulin-stimulated glucose uptake [135]. However, treatment of the muscle cells with azide, an inhibitor of mitochondrial complex IV, increased basal glucose uptake without affecting insulin-stimulated glucose uptake in myotubes [136]. Down regulation of electron transport chain activity in mice by knocking down apoptosis initiating factor (AIF) resulted in enhanced insulin sensitivity and protection the animal from fat-induced insulin resistance [137].

In summary it can be concluded that both decreased mitochondrial fat oxidation and increased FFA influx into skeletal muscle take place during insulin resistance state. If the rate of fat supply exceeds the demand for fat oxidation, the muscle redirects the fat entering the cell toward triglyceride synthesis leading to increased IMCL content. In contrast if fat oxidation exceeds the rate of fat supply, all fat entering the muscle will be directed to fat oxidation and no fat will accumulate in the muscle. Thus, the IMCL content in skeletal muscle reflects the dynamic balance between the demand for fat oxidation and fat supply to the muscle.

4. Cellular Mechanism of Insulin Resistance

The cellular events via which insulin initiates its stimulatory effect on glucose metabolism start with binding of the hormone to specific receptors that are present on the muscle cell surface [2, 138–140]. The binding of insulin activates the insulin receptor and the activated insulin receptor generates second messengers that activate a cascade of phosphorylation-dephosphorylation reactions that eventually result in the stimulation of intracellular glucose metabolism. The first step in glucose metabolism involves activation of the glucose transport system (GLUT4), leading to glucose influx into muscle cells. The free glucose, which has entered the cell, subsequently is metabolized by a series of enzymatic steps that are under the control of insulin. Of these, the most important are glucose phosphorylation (catalyzed by hexokinase II), glycogen synthase (which controls glycogen synthesis), and phosphofructokinase (PFK) and pyruvate dehydrogenase (PDH) (which regulate glycolysis and glucose oxidation, resp.).

4.1. Insulin Receptor/Insulin Receptor Tyrosine Kinase. The insulin receptor is a glycoprotein comprised of two α -subunits and two β -subunits linked by disulfide bonds [2, 138–140]. The two α -subunits of the insulin receptor are located at the extracellular surface of the muscle plasma membrane and contain the insulin-binding domain. The

β -subunits have an extracellular domain, a transmembrane domain, and an intracellular domain that expresses insulin-stimulated kinase activity directed toward its own tyrosine residues. The binding of insulin to the α -subunit causes phosphorylation of the β -subunit on multiple tyrosine residues. The activation of insulin receptor tyrosine kinase activity is essential for the action of insulin on glucose metabolism. Mutagenesis of any of the three major phosphorylation sites (at residues 1158, 1163, and 1162) impairs insulin receptor tyrosine kinase activity, leading to a decrease in the metabolic and growth-promoting effects of insulin [141, 142].

4.2. Insulin Receptor Signal Transduction. Following the activation of insulin receptor tyrosine kinase, specific intracellular proteins, of which at least nine have been identified [138, 143], become phosphorylated. In skeletal muscle insulin-receptor substrate (IRS)-1 serves as the major docking protein and undergoes tyrosine phosphorylation by the activated insulin receptor in regions containing specific amino acid sequence motifs (Figure 4). The phosphorylated motifs serve as recognition sites for proteins containing *src*-homology 2 (SH2) domains. Mutation of these specific tyrosine residues in IRS-1 severely impairs the ability of insulin to stimulate muscle glycogen synthesis, glucose uptake and oxidation, and other acute metabolic- and growth-promoting effects of insulin [142].

The phosphorylated tyrosine residues of IRS-1 mediate an association with the 85-kDa regulatory subunit of phosphatidylinositol 3-kinase (PI3K), leading to activation of the enzyme [138–140, 143, 144]. PI3K is composed of an 85-kDa regulatory subunit and a 110-kDa catalytic subunit. The latter catalyzes the 3' phosphorylation of PI 4-phosphate and PI 4,5-diphosphate. Activation of PI3K by phosphorylated IRS-1 leads to activation of protein kinase B/Akt which is a central intermediate for many of the metabolic and growth actions of insulin. It has been identified as one of the kinases responsible for the inactivation of glycogen synthase kinase through its phosphorylation, a process that leads to the activation of glycogen synthase. Akt also phosphorylates the newly identified Akt substrate AS160, leading to its redistribution in the cell and activation of Rab proteins required for the translocation of the vesicles containing GLUT4 to the plasma membrane.

Inhibitors of PI3K impair glucose transport and block the activation of glycogen synthase and hexokinase- (HK-) II expression [138–146]. The action of insulin to increase protein synthesis and inhibit protein degradation also is mediated by PI3K.

Other proteins with SH2 domains, including the adapter protein Grb2 and *Shc*, also interact with IRS-1 and become phosphorylated following exposure to insulin [138–140, 143]. Grb2 and *Shc* link IRS-1/IRS-2 to the mitogen-activated protein kinase- (MAPK-) signaling pathway, which plays an important role in the generation of transcription factors and promotes cell growth, proliferation, and differentiation [138, 143]. Inhibition of the MAPK kinase pathway prevents the stimulation of cell growth by insulin but has no effect on the metabolic actions of the hormone [147].

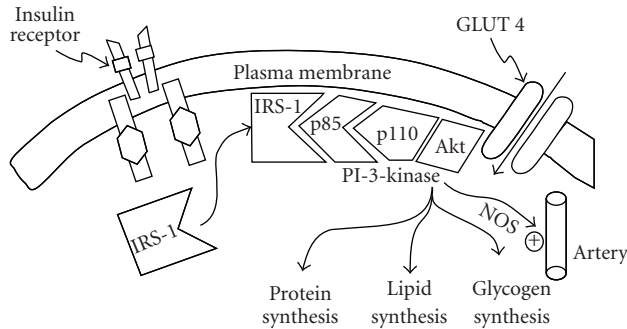


FIGURE 4: Insulin signal transduction system in normal glucose tolerant subjects (see text for a detailed discussion).

Under anabolic conditions, insulin augments glycogen synthesis by simultaneously activating glycogen synthase and inhibiting glycogen phosphorylase [148, 149]. The effect of insulin is mediated through the PI3K pathway, which inactivates kinases such as glycogen synthase kinase-3 and activates phosphatases, particularly PP1. PP1 is believed to be the primary regulator of glycogen metabolism. In skeletal muscle, PP1 associates with a specific glycogen-binding regulatory subunit, causing dephosphorylation (activation) of glycogen synthase. PP1 also phosphorylates (inactivates) glycogen phosphorylase. The precise steps that link insulin receptor tyrosine kinase/PI3K activation to stimulation of PP1 have yet to be defined. Studies [138, 150] have demonstrated convincingly that inhibitors of PI3K inhibit glycogen synthase activity and abolish glycogen synthesis.

4.3. Insulin Receptor Signal Transduction Defects in Insulin Resistance. Early studies have demonstrated a modest 20–30% reduction in insulin binding to monocytes and adipocytes from type 2 diabetic patients, but this has not been a consistent finding [1, 151–154]. The decrease in insulin binding is caused by a reduction in the number of insulin receptors without change in insulin receptor affinity. Some caution, however, should be used in interpreting these studies because muscle and liver, not adipocytes, are the major tissues responsible for the regulation of glucose homeostasis in vivo, and insulin binding to solubilized receptors obtained from skeletal muscle and liver has been shown to be normal in obese and lean diabetic individuals [152, 153, 155]. Moreover, a decrease in insulin receptor number cannot be demonstrated in over half of type 2 diabetic subjects, and it has been difficult to demonstrate a correlation between reduced insulin binding and the severity of insulin resistance [156–158]. A variety of defects in insulin receptor internalization and processing have been described in syndromes of severe insulin resistance and diabetes. The insulin receptor gene, however, has been sequenced in a large number of type 2 diabetic patients from diverse ethnic populations and, with very rare exceptions, physiologically significant mutations in the insulin receptor gene have not been observed [159, 160]. This excludes a structural gene abnormality in the insulin receptor as a common cause of insulin resistance in skeletal muscle.

4.4. Insulin Receptor Tyrosine Kinase Activity. Insulin receptor tyrosine kinase activity has been examined in skeletal muscle from normal-weight and obese diabetic subjects. Most [1, 7, 152, 153, 156, 161] but not all [155] investigators have found a reduction in tyrosine kinase activity that cannot be explained by alterations in insulin receptor number or insulin receptor binding affinity. Restoration of normoglycemia by weight loss, however, has been shown to correct the defect in insulin receptor tyrosine kinase activity [162], suggesting that the defect in tyrosine kinase activity, at least in part, is acquired secondary to some combination of hyperglycemia, distributed intracellular glucose metabolism, hyperinsulinemia, and insulin resistance, all of which improved after weight loss. Exposure of cultured fibroblasts to high glucose concentration also has been shown to inhibit insulin receptor tyrosine kinase activity [163]. Because insulin receptor tyrosine kinase activity assays are performed in vitro, the results of these assays could provide misleading information with regard to insulin receptor function in vivo. To circumvent this problem, investigators have used the euglycemic hyperinsulinemic clamp with muscle biopsies and antiphosphotyrosine immunoblot analysis to provide a “snap shot” of the insulin-stimulated tyrosine phosphorylation state of the receptor in vivo [7]. In insulin-resistant obese nondiabetic subjects, in the NGT insulin resistant offspring of two diabetic parents, and in type 2 diabetic subjects, a substantial decrease in insulin receptor tyrosine phosphorylation has been demonstrated. However, when insulin-stimulated insulin receptor tyrosine phosphorylation was examined in normal-glucose-tolerant insulin-resistant individuals (offspring of two diabetic parents) at high risk for developing type 2 diabetes, a normal increase in tyrosine phosphorylation of the insulin receptor was observed [164]. These findings are consistent with the concept that impaired insulin receptor tyrosine kinase activity in type 2 diabetic patients is acquired secondary to hyperglycemia or some other metabolic disturbance.

4.5. Insulin-Signaling (IRS-1 and PI3K) Defects (Figure 5). The ability of insulin to activate insulin receptor and IRS-1 tyrosine phosphorylation in muscle in obese nondiabetic subjects is modestly reduced; whereas in type 2 diabetics insulin-stimulated insulin receptor and IRS-1 tyrosine phosphorylation are severely impaired [7]. Association of the p85 subunit of PI3K with IRS-1 and activation of PI3K also are greatly attenuated in obese nondiabetic and type 2 diabetic subjects compared with lean healthy controls [7, 165, 166]. The decrease in insulin-stimulated association of the p85 regulatory subunit of PI3K with IRS-1 is closely correlated with the reduction in insulin-stimulated muscle glycogen synthase activity and in vivo insulin-stimulated glucose disposal [7]. Impaired regulation of PI3K gene expression by insulin also is impaired in skeletal muscle, and similar impairment has been demonstrated in adipose tissue of type 2 diabetic subjects [167]. In animal models of diabetes, an 80%–90% decrease in insulin-stimulated IRS-1 phosphorylation and PI3K activity has been reported [168, 169].

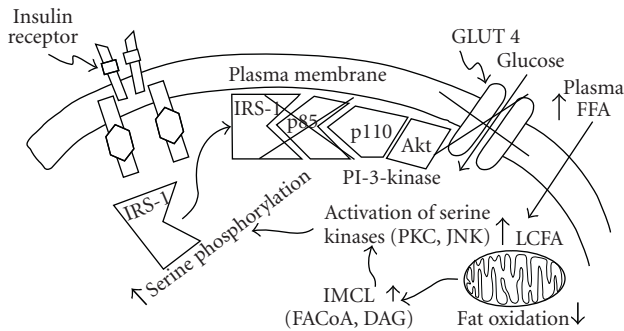


FIGURE 5: In insulin resistant individuals insulin signaling is impaired at the level of IRS-1 leading to decreased glucose transport/phosphorylation/metabolism and impaired nitric oxide synthase activation/endothelial function. Increased intramyocellular fat and fatty acid metabolism content and mitochondrial dysfunction also exist in skeletal muscle in insulin resistant individuals (see text for a detailed discussion).

In the insulin-resistant, normal glucose tolerant offspring of two type 2 diabetic parents, IRS-1 tyrosine phosphorylation and the association of p85 protein/PI3K activity with IRS-1 are markedly decreased despite normal tyrosine phosphorylation of the insulin receptor; these insulin signaling defects are correlated closely with the severity of insulin resistance measured with the euglycemic insulin clamp technique [164]. In summary, impaired association of PI3K with IRS-1 and its subsequent activation are characteristic abnormalities in type 2 diabetics, and these defects are correlated closely with in vivo muscle insulin resistance.

The nature of the defect in IRS-1 that impairs its ability to activate PI3-Kinase does not seem to include a structural defect in IRS-1. A common mutation in the IRS-1 gene (Gly-972-Arg) has been associated with type 2 diabetes, insulin resistance, and obesity, but the physiologic significance of this mutation remains to be established [170]. Rodent and human studies have suggested increased serine phosphorylation of IRS-1 in insulin resistant states [111, 171–173]. In general, serine phosphorylation of IRS-1 negates its ability to undergo tyrosine phosphorylation. Thus, conditions that increase serine phosphorylation of IRS-1 impair tyrosine phosphorylation by the insulin receptor and its activation, thus, leading to an impairment in the insulin signaling cascade. An important, yet an answered, question is the identity of the factor(s) responsible for the activation of serine kinases that phosphorylate IRS-1. Increased activity of protein kinase C (PKC- β and δ) has been reported in insulin resistant states and can be induced during lipid infusion [174, 175]. Furthermore, increased intramyocellular levels of fat metabolites, for example, FFA and DAG, which are strong activators of protein kinase C, have been demonstrated following lipid infusion [176]. Moreover, prevention of the IRS-1 serine phosphorylation by mutating key serine residues in the IRS-1 prevents the development of insulin resistance in skeletal muscle caused by high-fat feeding [169]. Increased stress kinase activity also has been

implicated in contribute to the serine phosphorylation of IRS-1 and subsequent impairment tyrosine phosphorylation [177, 178]. In summary, increased serine phosphorylation of IRS-1 is believed to impair its tyrosine phosphorylation by the insulin receptor and interrupt the insulin signaling cascade, leading to the development of insulin resistance in skeletal muscle.

Because nitric oxide synthase also is activated by the IRS-1/PI3-K pathway, impaired insulin signaling leads to reduced nitric oxide generation and endothelial dysfunction, which have implicated in the development of accelerated atherosclerosis in T2DM individuals.

Insulin resistance in the PI3K signaling pathway contrasts with an intact stimulation of the MAPK pathway by insulin in insulin-resistant type 2 diabetic and obese nondiabetic individuals [7, 165]. Physiologic hyperinsulinemia increases mitogen-activated protein kinase/extracellular signal-regulated kinase 1 activity (MEK-1) and extracellular signal-regulated kinase1/2 phosphorylation activity (ERK) similarly in lean healthy subjects, insulin-resistant obese nondiabetic, and type 2 diabetic patients. Intact stimulation of the MAPK pathway by insulin in the presence of insulin resistance in the PI3K pathway may play an important role in the development of atherosclerosis [7]. If the metabolic (PI3K) pathway is impaired, plasma glucose levels rise, resulting in increased insulin secretion and hyperinsulinemia. Because insulin receptor function is normal or only modestly impaired, especially early in the natural history of type 2 diabetes, this leads to excessive stimulation of the MAPK (mitogenic) pathway in vascular tissues, with resultant proliferation of vascular smooth muscle cells, increased collagen formation, and increased production of growth factors and inflammatory cytokines [179, 180].

4.6. Glucose Transport. Activation of the insulin signal transduction system in skeletal muscle stimulates glucose transport through a mechanism that involves translocation of a large intracellular pool of glucose transporters (associated with low-density microsomes) to the plasma membrane and their subsequent activation after insertion into the cell membrane [181, 182]. There are five major, different facilitative glucose transporters (GLUTs) with distinctive tissue distributions [183, 184]. GLUT4, the insulin regulatable transporter, is found in skeletal muscle, has a K_m of approximately 5 mmol/L, which is close to that of the plasma glucose concentration, and is associated with HK-II [173, 174]. GLUT4 concentration in the plasma membrane increases markedly after exposure to insulin, and this increase is associated with a reciprocal decline in the intracellular GLUT4 pool. A recent study has reported a parallel translocation of GLUT12 from the cytosol to the plasma membrane following insulin stimulation in human skeletal muscle [185].

GLUT1 is the predominant glucose transporter in the insulin-independent tissues (brain and erythrocytes) but also is found in muscle and probably contributes to muscle glucose uptake during the basal state. GLUT1 is located primarily in the plasma membrane where its concentration is

unchanged following exposure to insulin. Thus, it is likely to contribute to muscle glucose uptake during the basal state. It has a low K_m (~ 1 mmol/L) and is well suited for its function, which is to mediate basal glucose uptake. It is found in association with HK-I [186].

In insulin resistant individuals with T2DM, glucose transport activity is severely impaired [156, 181, 182, 187–189]. Muscle tissue from lean and obese type 2 diabetic subjects exhibits normal or increased levels of GLUT4 mRNA expression and normal levels of GLUT4 protein, thus demonstrating that transcriptional and translational regulation of GLUT4 is not impaired [190, 191]. Using a novel triple-tracer technique, the in vivo dose-response curve for the action of insulin on glucose transport in forearm skeletal muscle has been examined in type 2 diabetic subjects, and insulin-stimulated inward muscle glucose transport has been shown to be severely impaired [192, 193]. Impaired in vivo muscle glucose transport in type 2 diabetics also has been demonstrated using magnetic resonance imaging [194] and positron emission tomography [195]. Because the number of GLUT4 transporters in the muscle of diabetic subjects is normal, impaired GLUT4 translocation and decreased intrinsic activity of the glucose transporter must be responsible for the defect in muscle glucose transport. Large populations of type 2 diabetics have been screened for mutations in the GLUT4 gene [196]. Such mutations are very uncommon and, when detected, have been of questionable physiologic significance.

4.7. Glucose Phosphorylation. Glucose phosphorylation and glucose transport are tightly coupled processes [197]. Hexokinase isoenzymes (HK-I–IV) catalyze the first committed step of glucose metabolism, the intracellular conversion of free glucose to glucose-6-phosphate (Glu-6-P) [183, 184, 186, 198]. HK-I, HK-II, and HK-III are single-chain peptides that have a very high affinity for glucose and demonstrate product inhibition by Glu-6-P. HK-IV, also called glucokinase, has a lower affinity for glucose and is not inhibited by Glu-6-P.

In human skeletal muscle, HK-II transcription is regulated by insulin, whereas HK-I mRNA and protein levels are not affected by insulin [199, 200]. In response to physiologic euglycemic hyperinsulinemia of 2 to 4 hours' duration, HK-II cytosolic activity, protein content, and mRNA levels increase by 50% to 200% in healthy nondiabetic subjects, and this is associated with the translocation of hexokinase II from the cytosol to the mitochondria. In forearm muscle, insulin-stimulated glucose transport (measured with the triple-tracer technique) is markedly impaired in lean type 2 diabetics [192, 193], but the rate of intracellular glucose phosphorylation is impaired to an even greater extent, resulting in an increase in the free glucose concentration within the intracellular space that is accessible to glucose. These observations indicate that in type 2 diabetic individuals, although both glucose transport and glucose phosphorylation are severely resistant to the action of insulin, impaired glucose phosphorylation (HK-II) appears to be the rate-limiting step for insulin action. Studies using ^{31}P nuclear magnetic resonance in combination with

[1- ^{14}C] glucose also have demonstrated that both insulin-stimulated muscle glucose transport and glucose phosphorylation are impaired in type 2 diabetic subjects, but the defect in transport exceeds the defect in phosphorylation [194]. Because of methodologic differences, the results of the triple-tracer technique [192, 193] and magnetic resonance imaging [194] studies cannot be reconciled at present. Nonetheless, these studies are consistent in demonstrating that abnormalities in both muscle glucose phosphorylation and glucose transport are well established early in the natural history of type 2 diabetes and cannot be explained by glucose toxicity.

In healthy nondiabetic subjects, a physiologic increase in the plasma insulin concentration for as little as 2 to 4 hours increases muscle HK-II activity, gene transcription, and translation [201]. In lean type 2 diabetics, the ability of insulin to augment HK-II activity and mRNA levels are markedly reduced compared with controls [199]. Decreased basal muscle HK-II activity and mRNA levels and impaired insulin-stimulated HK-II activity in type 2 diabetic subjects have been reported by other investigators [200, 202]. A decrease in insulin-stimulated muscle HK-II activity also has been described in subjects with IGT [203]. Several groups have looked for point mutations in the HK-II gene in individuals with type 2 diabetes, and, although several nucleotide substitutions have been found, none are close to the glucose and ATP binding sites and none have been associated with insulin resistance [203–205]. Thus, an abnormality in the HK-II gene is unlikely to explain the inherited insulin resistance in common variety type 2 diabetes mellitus.

4.8. Glycogen Synthesis. Impaired insulin-stimulated glycogen synthesis is a characteristic finding in all insulin-resistant states. Obese, IGT, and diabetic subjects have severe impairment in insulin-stimulated glycogen synthase that accounts for the majority of the defect in insulin-mediated whole-body glucose disposal [1, 2, 21, 195, 206–218]. Impaired glycogen synthesis also has been documented in the normal-glucose tolerant offspring of two diabetic parents, in the first-degree relatives of type 2 diabetic individuals, and in the normoglycemic twin of a monozygotic twin pair in which the other twin has type 2 diabetes [206, 210, 211].

Glycogen synthase is the key insulin-regulated enzyme that controls the rate of muscle glycogen synthesis [148, 150, 200, 212–214]. Insulin activates glycogen synthase by stimulating a cascade of phosphorylation-dephosphorylation reactions which ultimately lead to the inhibition of glycogen synthase kinase and activation of PP1 (also called glycogen synthase phosphatase). The regulatory subunit of PP1 has two serine phosphorylation sites, called site 1 and site 2. Phosphorylation of site 2 by cAMP-dependent protein kinase inactivates PP1; whereas phosphorylation of site 1 by insulin activates PP1, leading to the stimulation of glycogen synthase. Phosphorylation of site 1 of PP1 by insulin in muscle is catalyzed by insulin-stimulated protein kinase (ISPK)-1. Because of their central role in muscle glycogen formation, the three enzymes, glycogen synthase, PP1, and

ISPK-1, have been extensively studied in individuals with type 2 diabetes.

Glycogen synthase exists in an active (dephosphorylated) and an inactive (phosphorylated) form [148–150]. Under basal conditions, total glycogen synthase activity in type 2 diabetic subjects is reduced, and the ability of insulin to activate glycogen synthase is severely impaired [7, 215–217]. The ability of insulin to stimulate glycogen synthase also is diminished in the normal glucose-tolerant, insulin-resistant relatives of type 2 diabetic individuals [218]. In insulin-resistant nondiabetic and diabetic Pima Indians, activation of muscle PP1 (glycogen synthase phosphatase) by insulin is severely reduced [219]. Because PP1 dephosphorylates glycogen synthase, leading to its activation, a defect in PP1 appears to play an important role in the muscle insulin resistance of type 2 diabetes mellitus.

The effect of insulin on glycogen synthase gene transcription and translation *in vivo* has been studied extensively. Most studies have demonstrated that insulin does not increase glycogen synthase mRNA or protein expression in human muscle [201, 220, 221]. Glycogen synthase mRNA and protein levels, however, are decreased in muscle of type 2 diabetic patients, partly explaining the decreased glycogen synthase activity [221, 222]. The major abnormality in glycogen synthase regulation in type 2 diabetes is its lack of dephosphorylation and activation by insulin, as a result of insulin receptor signaling abnormalities.

The glycogen synthase gene has been the subject of intensive investigation, and DNA sequencing has revealed either no mutations or rare nucleotide substitutions that cannot explain the defect in insulin-stimulated glycogen synthase activity [223–225]. The genes encoding the catalytic subunits of PP1 and ISPK-1 have been examined in Pima Indians and Danes with type 2 diabetes [226, 227]. Several silent nucleotide substitutions were found in the PP1 and ISPK-1 genes in the Danish population, but the mRNA levels of both genes were normal in skeletal muscle. No structural gene abnormalities in the catalytic subunit of PP1 were detected in Pima Indians. Thus, neither mutations in the PP1 and ISPK-1 genes nor abnormalities in their translation can explain the impaired enzymatic activities of glycogen synthase and PP1 that have been observed *in vivo*. Similarly, there is no evidence that an alteration in glycogen phosphorylase plays any role in the abnormality in glycogen formation in type 2 diabetes [228].

In summary, glycogen synthase activity is severely impaired in type 2 diabetic individuals, and the molecular cause of the defect most likely is related to impaired insulin signal transduction.

4.9. Glycolysis. Glucose oxidation accounts for approximately 90% of total glycolytic flux; whereas anaerobic glycolysis accounts for the other 10%. Phosphofructokinase and pyruvate dehydrogenase play pivotal roles in the regulation of glycolysis and glucose oxidation, respectively. In type 2 diabetic individuals, the glycolytic/glucose oxidative pathway has been shown to be impaired [229]. Although one study [230] has suggested that PFK activity is modestly reduced in muscle biopsies from type 2 diabetic subjects, most evidence

indicates that the activity of PFK is normal [216, 221]. Insulin has no effect on muscle PFK activity, mRNA levels, or protein content in either nondiabetic or diabetic individuals [221]. PDH is a key insulin-regulated enzyme with activity in muscle that is acutely stimulated by insulin [231]. In type 2 diabetic patients, insulin-stimulated PDH activity has been shown to be decreased in human skeletal muscle [231, 232].

Obesity and type 2 diabetes mellitus are associated with accelerated FFA turnover and oxidation [1, 2, 21, 233], which would be expected, according to the Randle cycle [234], to inhibit PDH activity and consequently glucose oxidation. Therefore, it is likely that the observed defects in glucose oxidation and PDH activity are acquired secondary to increased FFA oxidation and feedback inhibition of PDH by elevated intracellular levels of acetyl-CoA and reduced availability of NAD. Consistent with this scenario, the rates of basal and insulin-stimulated glucose oxidation are not reduced in the normal glucose-tolerant offspring of two diabetic parents and in the first-degree relatives of type 2 diabetic subjects; whereas they are decreased in overtly diabetic subjects.

5. Summary

In summary, a defect in the insulin signaling cascade at the level of IRS-1 is likely the primary defect that leads to insulin resistance in skeletal muscle. Other defects in the insulin signaling pathway, for example, diminished insulin binding, when present, are modest and secondary to downregulation of the insulin receptor by chronic hyperinsulinemia. In insulin resistant individuals with overt hyperglycemia, for example, T2DM, a number of postbinding defects have been demonstrated, including reduced insulin receptor tyrosine kinase activity and altered insulin signal transduction, decreased glucose transport, diminished glucose phosphorylation, and impaired glycogen synthase activity. From the quantitative standpoint, impaired glycogen synthesis represents the major pathway responsible for the insulin resistance and this defect is present long before the onset of overt diabetes, that is, in normal glucose-tolerant, insulin-resistant prediabetic subjects, and in individuals with IGT. The impairment in glycogen synthase activation is likely due to a defect in the ability of insulin to phosphorylate IRS-1, causing a reduced association of the p85 subunit of PI 3-kinase with IRS-1 and decreased activation of the enzyme PI3K.

Increased intramyocellular fat content and fatty acid metabolites, for example, FACoA and DAG, are likely to play a pivotal role in the development of insulin resistance in skeletal muscle. Through activation of serine/threonine kinases and serine phosphorylate the IRS-1, fatty acid metabolites impair IRS-1 phosphorylation by the insulin receptor and lead to the defect in insulin signaling in insulin resistant individuals. The cause for the intramyocellular accumulation of fat and fat metabolites has yet to be defined. A mitochondrial defect in oxidative phosphorylation has been reported in insulin resistant individuals. However, the contribution of this mitochondrial defect to the intramyocellular fat accumulation is not yet clear.

References

- [1] R. A. DeFronzo, "Pathogenesis of type 2 diabetes: metabolic and molecular implications for identifying diabetes genes," *Diabetes Reviews*, vol. 5, no. 3, pp. 177–269, 1997.
- [2] R. A. DeFronzo, "The triumvirate: β -cell, muscle, liver. A collusion responsible for NIDDM," *Diabetes*, vol. 37, no. 6, pp. 667–687, 1988.
- [3] R. A. DeFronzo, "Pathogenesis of type 2 diabetes mellitus," *Medical Clinics of North America*, vol. 88, no. 4, pp. 787–835, 2004.
- [4] R. A. DeFronzo, "From the triumvirate to the ominous octet: a new paradigm for the treatment of type 2 diabetes mellitus," *Diabetes*, vol. 58, no. 4, pp. 773–795, 2009.
- [5] R. A. DeFronzo, R. Gunnarsson, O. Bjorkman, M. Olsson, and J. Wahren, "Effects of insulin on peripheral and splanchnic glucose metabolism in noninsulin-dependent (type II) diabetes mellitus," *The Journal of Clinical Investigation*, vol. 76, no. 1, pp. 149–155, 1985.
- [6] A. Mitrakou, D. Kelley, T. Veneman, et al., "Contribution of abnormal muscle and liver glucose metabolism to postprandial hyperglycemia in NIDDM," *Diabetes*, vol. 39, no. 11, pp. 1381–1390, 1990.
- [7] K. Cusi, K. Maezono, A. Osman, et al., "Insulin resistance differentially affects the PI 3-kinase- and MAP kinase-mediated signaling in human muscle," *The Journal of Clinical Investigation*, vol. 105, no. 3, pp. 311–320, 2000.
- [8] M. Bajaj and R. A. DeFronzo, "Metabolic and molecular basis of insulin resistance," *Journal of Nuclear Cardiology*, vol. 10, no. 3, pp. 311–323, 2003.
- [9] K. Bouzakri, H. A. Koistinen, and J. R. Zierath, "Molecular mechanisms of skeletal muscle insulin resistance in type 2 diabetes," *Current Diabetes Reviews*, vol. 1, no. 2, pp. 167–174, 2005.
- [10] H. K. R. Karlsson and J. R. Zierath, "Insulin signaling and glucose transport in insulin resistant human skeletal muscle," *Cell Biochemistry and Biophysics*, vol. 48, no. 2–3, pp. 103–113, 2007.
- [11] A. Lettner and M. Roden, "Ectopic fat and insulin resistance," *Current Diabetes Reports*, vol. 8, no. 3, pp. 185–191, 2008.
- [12] J. D. McGarry, "Banting lecture 2001: dysregulation of fatty acid metabolism in the etiology of type 2 diabetes," *Diabetes*, vol. 51, no. 1, pp. 7–18, 2002.
- [13] K. F. Petersen and G. I. Shulman, "Etiology of insulin resistance," *American Journal of Medicine*, vol. 119, no. 5, supplement 1, pp. 10S–16S, 2006.
- [14] H. Bays, L. Mandarino, and R. A. DeFronzo, "Role of the adipocyte, free fatty acids, and ectopic fat in pathogenesis of type 2 diabetes mellitus: peroxisomal proliferator-activated receptor agonists provide a rational therapeutic approach," *Journal of Clinical Endocrinology and Metabolism*, vol. 89, no. 2, pp. 463–478, 2004.
- [15] M. Krssak and M. Roden, "The role of lipid accumulation in liver and muscle for insulin resistance and type 2 diabetes mellitus in humans," *Reviews in Endocrine and Metabolic Disorders*, vol. 5, no. 2, pp. 127–134, 2004.
- [16] M. Roden, "Muscle triglycerides and mitochondrial function: possible mechanisms for the development of type 2 diabetes," *International Journal of Obesity*, vol. 29, supplement 2, pp. S111–S115, 2005.
- [17] K. Morino, K. F. Petersen, and G. I. Shulman, "Molecular mechanisms of insulin resistance in humans and their potential links with mitochondrial dysfunction," *Diabetes*, vol. 55, supplement 2, pp. S9–S15, 2006.
- [18] M. A. Abdul-Ghani and R. A. DeFronzo, "Mitochondrial dysfunction, insulin resistance, and type 2 diabetes mellitus," *Current Diabetes Reports*, vol. 8, no. 3, pp. 173–178, 2008.
- [19] K. Højlund, M. Mogensen, K. Sahlin, and H. Beck-Nielsen, "Mitochondrial dysfunction in type 2 diabetes and obesity," *Endocrinology and Metabolism Clinics of North America*, vol. 37, no. 3, pp. 713–731, 2008.
- [20] B. B. Lowell and G. I. Shulman, "Mitochondrial dysfunction and type 2 diabetes," *Science*, vol. 307, no. 5708, pp. 384–387, 2005.
- [21] L. C. Groop, R. C. Bonadonna, S. DelPrato, et al., "Glucose and free fatty acid metabolism in non-insulin-dependent diabetes mellitus. Evidence for multiple sites of insulin resistance," *The Journal of Clinical Investigation*, vol. 84, no. 1, pp. 205–213, 1989.
- [22] E. E. Blaak, "Metabolic fluxes in skeletal muscle in relation to obesity and insulin resistance," *Best Practice and Research: Clinical Endocrinology and Metabolism*, vol. 19, no. 3, pp. 391–403, 2005.
- [23] B. Kiens, "Skeletal muscle lipid metabolism in exercise and insulin resistance," *Physiological Reviews*, vol. 86, no. 1, pp. 205–243, 2006.
- [24] D. Thiebaut, E. Jacot, R. A. DeFronzo, E. Maeder, E. Jequier, and J. P. Felber, "The effect of graded doses of insulin on total glucose uptake, glucose oxidation, and glucose storage in man," *Diabetes*, vol. 31, no. 11, pp. 957–963, 1982.
- [25] H. P. Himsworth and R. B. Kerr, "Insulin-sensitive and insulin-insensitive types of diabetes mellitus," *Clinical Science*, vol. 4, pp. 120–152, 1939.
- [26] H. Ginsberg, G. Kimmerling, J. M. Olefsky, and G. M. Reaven, "Demonstration of insulin resistance in untreated adult onset diabetic subjects with fasting hyperglycemia," *The Journal of Clinical Investigation*, vol. 55, no. 3, pp. 454–461, 1975.
- [27] R. A. DeFronzo, D. Deibert, R. Hendler, P. Felig, and V. Soman, "Insulin sensitivity and insulin binding to monocytes in maturity-onset diabetes," *The Journal of Clinical Investigation*, vol. 63, no. 5, pp. 939–946, 1979.
- [28] R. A. DeFronzo, V. Soman, R. S. Sherwin, R. Hendler, and P. Felig, "Insulin binding to monocytes and insulin action in human obesity, starvation, and refeeding," *The Journal of Clinical Investigation*, vol. 62, no. 1, pp. 204–213, 1978.
- [29] W. J. H. Butterfield and M. J. Whichelow, "Peripheral glucose metabolism in control subjects and diabetic patients during glucose, glucose-insulin and insulin sensitivity tests," *Diabetologia*, vol. 1, no. 1, pp. 43–53, 1965.
- [30] S. R. Kashyap, R. Belfort, R. Berria, et al., "Discordant effects of a chronic physiological increase in plasma FFA on insulin signaling in healthy subjects with or without a family history of type 2 diabetes," *American Journal of Physiology*, vol. 287, no. 3, pp. E537–E546, 2004.
- [31] K. Danadian, G. Balasekaran, V. Lewy, M. P. Meza, R. Robertson, and S. A. Arslanian, "Insulin sensitivity in African-American children with and without family history of type 2 diabetes," *Diabetes Care*, vol. 22, no. 8, pp. 1325–1329, 1999.
- [32] K. F. Petersen, S. Dufour, D. Befroy, R. Garcia, and G. I. Shulman, "Impaired mitochondrial activity in the insulin-resistant offspring of patients with type 2 diabetes," *The New England Journal of Medicine*, vol. 350, no. 7, pp. 664–671, 2004.
- [33] S. E. Kahn, R. L. Hull, and K. M. Utzschneider, "Mechanisms linking obesity to insulin resistance and type 2 diabetes," *Nature*, vol. 444, no. 7121, pp. 840–846, 2006.

- [34] C. Bogardus, S. Lillioja, D. Mott, G. R. Reaven, A. Kashiwagi, and J. E. Foley, "Relationship between obesity and maximal insulin-stimulated glucose uptake in vivo and in vitro in Pima Indians," *The Journal of Clinical Investigation*, vol. 73, no. 3, pp. 800–805, 1984.
- [35] E. Ferrannini, G. Buzzigoli, R. Bonadonna, et al., "Insulin resistance in essential hypertension," *The New England Journal of Medicine*, vol. 317, no. 6, pp. 350–357, 1987.
- [36] P. Bressler, S. R. Bailey, M. Matsuda, and R. A. DeFronzo, "Insulin resistance and coronary artery disease," *Diabetologia*, vol. 39, no. 11, pp. 1345–1350, 1996.
- [37] R. A. DeFronzo, "Glucose intolerance and aging. Evidence for tissue insensitivity to insulin," *Diabetes*, vol. 28, no. 12, pp. 1095–1101, 1979.
- [38] M. Lankarani, N. Valizadeh, R. Heshmat, M. Peimani, and F. Sohrabvand, "Evaluation of insulin resistance and metabolic syndrome in patients with polycystic ovary syndrome," *Gynecological Endocrinology*, vol. 25, no. 8, pp. 504–507, 2009.
- [39] J. L. Bailey, B. Zheng, Z. Hu, S. R. Price, and W. E. Mitch, "Chronic kidney disease causes defects in signaling through the insulin receptor substrate/phosphatidylinositol 3-kinase/Akt pathway: implications for muscle atrophy," *Journal of the American Society of Nephrology*, vol. 17, no. 5, pp. 1388–1394, 2006.
- [40] J. W. Swan, S. D. Anker, C. Walton, et al., "Insulin resistance in chronic heart failure: relation to severity and etiology of heart failure," *Journal of the American College of Cardiology*, vol. 30, no. 2, pp. 527–532, 1997.
- [41] J. N. Livingston and R. T. Moxley III, "Myotonic dystrophy—phenotype-genotype and insulin resistance," *Diabetes Reviews*, vol. 2, no. 1, pp. 29–42, 1994.
- [42] V. Simha and A. Garg, "Lipodystrophy: lessons in lipid and energy metabolism," *Current Opinion in Lipidology*, vol. 17, no. 2, pp. 162–169, 2006.
- [43] S. J. Van Cromphaut, I. Vanhorebeek, and G. Van den Berghe, "Glucose metabolism and insulin resistance in sepsis," *Current Pharmaceutical Design*, vol. 14, no. 19, pp. 1887–1899, 2008.
- [44] G. Pagano, P. Cavallo-Perin, M. Cassader, et al., "An in vivo and in vitro study of the mechanism of prednisone-induced insulin resistance in healthy subjects," *The Journal of Clinical Investigation*, vol. 72, no. 5, pp. 1814–1820, 1983.
- [45] P. W. Hruz, "HIV protease inhibitors and insulin resistance: lessons from in-vitro, rodent and healthy human volunteer models," *Current Opinion in HIV and AIDS*, vol. 3, no. 6, pp. 660–665, 2008.
- [46] S. Jacob, K. Rett, M. Wicklmayr, B. Agrawal, H. J. Augustin, and G.-J. Dietze, "Differential effect of chronic treatment with two beta-blocking agents on insulin sensitivity: the carvedilol-metoprolol study," *Journal of Hypertension*, vol. 14, no. 4, pp. 489–494, 1996.
- [47] R. Jani, M. Molina, M. Matsuda, et al., "Decreased non-insulin-dependent glucose clearance contributes to the rise in fasting plasma glucose in the nondiabetic range," *Diabetes Care*, vol. 31, no. 2, pp. 311–315, 2008.
- [48] R. A. DeFronzo, "Insulin secretion, insulin resistance, and obesity," *International Journal of Obesity*, vol. 6, supplement 1, pp. 73–82, 1982.
- [49] A. Lemay, L. Turcot, F. Déchêne, S. Dodin, and J. C. Forest, "Hyperinsulinemia in nonobese women reporting a moderate weight gain at the beginning of menopause: a useful early measure of susceptibility to insulin resistance," *Menopause*, vol. 17, no. 2, pp. 321–325, 2010.
- [50] N. M. Wedick, M. B. Snijder, J. M. Dekker, et al., "Prospective investigation of metabolic characteristics in relation to weight gain in older adults: the hoorn study," *Obesity*, vol. 17, no. 8, pp. 1609–1614, 2009.
- [51] J. Erdmann, B. Kallabis, U. Oppel, O. Sypchenko, S. Wagenpfeil, and V. Schusdziarra, "Development of hyperinsulinemia and insulin resistance during the early stage of weight gain," *American Journal of Physiology*, vol. 294, no. 3, pp. E568–E575, 2008.
- [52] P. Schrauwen, "High-fat diet, muscular lipotoxicity and insulin resistance," *Proceedings of the Nutrition Society*, vol. 66, no. 1, pp. 33–41, 2007.
- [53] D. A. Pan, S. Lillioja, A. D. Kriketos, et al., "Skeletal muscle triglyceride levels are inversely related to insulin action," *Diabetes*, vol. 46, no. 6, pp. 983–988, 1997.
- [54] D. I. W. Phillips, S. Caddy, V. Ilic, et al., "Intramuscular triglyceride and muscle insulin sensitivity: evidence for a relationship in nondiabetic subjects," *Metabolism*, vol. 45, no. 8, pp. 947–950, 1996.
- [55] G. Perseghin, P. Scifo, F. De Cobelli, et al., "Intramyocellular triglyceride content is a determinant of in vivo insulin resistance in humans: a 1H-13C nuclear magnetic resonance spectroscopy assessment in offspring of type 2 diabetic parents," *Diabetes*, vol. 48, no. 8, pp. 1600–1606, 1999.
- [56] M. Krssak, K. Falk Petersen, A. Dresner, et al., "Intramyocellular lipid concentrations are correlated with insulin sensitivity in humans: a 1H NMR spectroscopy study," *Diabetologia*, vol. 42, no. 1, pp. 113–116, 1999.
- [57] G. M. Reaven, "Role of insulin resistance in human disease," *Diabetes*, vol. 37, no. 12, pp. 1595–1607, 1988.
- [58] A. H. Mokdad, E. S. Ford, B. A. Bowman, et al., "Diabetes trends in the U.S.: 1990–1998," *Diabetes Care*, vol. 23, no. 9, pp. 1278–1283, 2000.
- [59] L. C. Groop, C. Saloranta, M. Shank, R. C. Bonadonna, E. Ferrannini, and R. A. DeFronzo, "The role of free fatty acid metabolism in the pathogenesis of insulin resistance in obesity and noninsulin-dependent diabetes mellitus," *Journal of Clinical Endocrinology and Metabolism*, vol. 72, no. 1, pp. 96–107, 1991.
- [60] G. M. Reaven, C. Hollenbeck, C.-Y. Jeng, M. S. Wu, and Y.-D. I. Chen, "Measurement of plasma glucose, free fatty acid, lactate, and insulin for 24 h in patients with NIDDM," *Diabetes*, vol. 37, no. 8, pp. 1020–1024, 1988.
- [61] G. Perseghin, S. Ghosh, K. Gerow, and G. I. Shulman, "Metabolic defects in lean nondiabetic offspring of NIDDM parents: a cross-sectional study," *Diabetes*, vol. 46, no. 6, pp. 1001–1009, 1997.
- [62] M. E. Griffin, M. J. Marcucci, G. W. Cline, et al., "Free fatty acid-induced insulin resistance is associated with activation of protein kinase C θ and alterations in the insulin signaling cascade," *Diabetes*, vol. 48, no. 6, pp. 1270–1274, 2000.
- [63] A. Dresner, D. Laurent, M. Marcucci, et al., "Effects of free fatty acids on glucose transport and IRS-1-associated phosphatidylinositol 3-kinase activity," *The Journal of Clinical Investigation*, vol. 103, no. 2, pp. 253–259, 1999.
- [64] C. Yu, Y. Chen, G. W. Cline, et al., "Mechanism by which fatty acids inhibit insulin activation of insulin receptor substrate-1 (IRS-1)-associated phosphatidylinositol 3-kinase activity in muscle," *The Journal of Biological Chemistry*, vol. 277, no. 52, pp. 50230–50236, 2002.
- [65] R. Belfort, L. Mandarino, S. Kashyap, et al., "Dose-response effect of elevated plasma free fatty acid on insulin signaling," *Diabetes*, vol. 54, no. 6, pp. 1640–1648, 2005.

- [66] S. I. Itani, N. B. Ruderman, F. Schmieder, and G. Boden, "Lipid-induced insulin resistance in human muscle is associated with changes in diacylglycerol, protein kinase C, and $\text{I}\kappa\text{B-}\alpha$," *Diabetes*, vol. 51, no. 7, pp. 2005–2011, 2002.
- [67] D. K. Richardson, S. Kashyap, M. Bajaj, et al., "Lipid infusion decreases the expression of nuclear encoded mitochondrial genes and increases the expression of extracellular matrix genes in human skeletal muscle," *The Journal of Biological Chemistry*, vol. 280, no. 11, pp. 10290–10297, 2005.
- [68] G. Boden and X. Chen, "Effects of fat on glucose uptake and utilization in patients with non-insulin-dependent diabetes," *The Journal of Clinical Investigation*, vol. 96, no. 3, pp. 1261–1268, 1995.
- [69] M. Bajaj, S. Suraamornkul, A. Romanelli, et al., "Effect of a sustained reduction in plasma free fatty acid concentration on intramuscular long-chain fatty acyl-CoAs and insulin action in type 2 diabetic patients," *Diabetes*, vol. 54, no. 11, pp. 3148–3153, 2005.
- [70] M. Bajaj, S. Suraamornkul, S. Kashyap, K. Cusi, L. Mandarino, and R. A. DeFronzo, "Sustained reduction in plasma free fatty acid concentration improves insulin action without altering plasma adipocytokine levels in subjects with strong family history of type 2 diabetes," *Journal of Clinical Endocrinology and Metabolism*, vol. 89, no. 9, pp. 4649–4655, 2004.
- [71] A. Vaag, P. Skott, P. Damsbo, M.-A. Gall, E. A. Richter, and H. Beck-Nielsen, "Effect of the antilipolytic nicotinic acid analogue acipimox on whole-body and skeletal muscle glucose metabolism in patients with non-insulin-dependent diabetes mellitus," *The Journal of Clinical Investigation*, vol. 88, no. 4, pp. 1282–1290, 1991.
- [72] A. T. M. G. Santomauro, G. Boden, M. E. R. Silva, et al., "Overnight lowering of free fatty acids with acipimox improves insulin resistance and glucose tolerance in obese diabetic and nondiabetic subjects," *Diabetes*, vol. 48, no. 9, pp. 1836–1841, 1999.
- [73] R. H. Unger, "Lipotoxicity in the pathogenesis of obesity-dependent NIDDM: genetic and clinical implications," *Diabetes*, vol. 44, no. 8, pp. 863–870, 1995.
- [74] G. Boden, B. Lebed, M. Schatz, C. Homko, and S. Lemieux, "Effects of acute changes of plasma free fatty acids on intramyocellular fat content and insulin resistance in healthy subjects," *Diabetes*, vol. 50, no. 7, pp. 1612–1617, 2001.
- [75] L. H. Storlien, A. B. Jenkins, D. J. Chisholm, W. S. Pascoe, S. Khouri, and E. W. Kraegen, "Influence of dietary fat composition on development of insulin resistance in rats. Relationship to muscle triglyceride and ω -3 fatty acids in muscle phospholipid," *Diabetes*, vol. 40, no. 2, pp. 280–289, 1991.
- [76] M. J. Pagliassotti, D. Pan, P. Prach, T. Koppenhafer, L. Storlien, and J. O. Hill, "Tissue oxidative capacity, fuel stores and skeletal muscle fatty acid composition in obesity-prone and obesity-resistant rats," *Obesity Research*, vol. 3, no. 5, pp. 459–464, 1995.
- [77] T. Yamauchi, J. Kamon, H. Waki, et al., "The fat-derived hormone adiponectin reverses insulin resistance associated with both lipoatrophy and obesity," *Nature Medicine*, vol. 7, no. 8, pp. 941–946, 2001.
- [78] J. K. Kim, J. J. Fillmore, Y. Chen, et al., "Tissue-specific overexpression of lipoprotein lipase causes tissue-specific insulin resistance," *Proceedings of the National Academy of Sciences of the United States of America*, vol. 98, no. 13, pp. 7522–7527, 2001.
- [79] A. V. Greco, G. Mingrone, A. Giancaterini, et al., "Insulin resistance in morbid obesity: reversal with intramyocellular fat depletion," *Diabetes*, vol. 51, no. 1, pp. 144–151, 2002.
- [80] R. A. DeFronzo and E. Ferrannini, "Insulin resistance: a multifaceted syndrome responsible for NIDDM, obesity, hypertension, dyslipidemia, and atherosclerotic cardiovascular disease," *Diabetes Care*, vol. 14, no. 3, pp. 173–194, 1991.
- [81] R. A. DeFronzo, "Insulin resistance: the metabolic link between non-insulin-dependent diabetes mellitus, obesity, hypertension, dyslipidemia, and atherosclerotic cardiovascular disease," *Current Opinion in Cardiology*, vol. 5, no. 5, pp. 586–593, 1990.
- [82] N. Abumrad, C. Coburn, and A. Ibrahim, "Membrane proteins implicated in long-chain fatty acid uptake by mammalian cells: CD36, FATP and FABPm," *Biochimica et Biophysica Acta*, vol. 1441, no. 1, pp. 4–13, 1999.
- [83] A. Bonen, C. R. Benton, S. E. Campbell, et al., "Plasmalemmal fatty acid transport is regulated in heart and skeletal muscle by contraction, insulin and leptin, and in obesity and diabetes," *Acta Physiologica Scandinavica*, vol. 178, no. 4, pp. 347–356, 2003.
- [84] H. J. Pownall and J. A. Hamilton, "Energy translocation across cell membranes and membrane models," *Acta Physiologica Scandinavica*, vol. 178, no. 4, pp. 357–365, 2003.
- [85] L. Hagenfeldt, "Metabolism of free fatty acids and ketone bodies during exercise in normal and diabetic man," *Diabetes*, vol. 28, supplement 1, pp. 66–70, 1979.
- [86] L. Hagenfeldt and J. Wahren, "Human forearm muscle metabolism during exercise. II. Uptake, release and oxidation of individual FFA and glycerol," *Scandinavian Journal of Clinical and Laboratory Investigation*, vol. 21, no. 3, pp. 263–276, 1968.
- [87] R. J. Havel, L. G. Ekelund, and A. Holmgren, "Kinetic analysis of the oxidation of palmitate-1- ^{14}C in man during prolonged heavy muscular exercise," *Journal of Lipid Research*, vol. 8, no. 4, pp. 366–373, 1967.
- [88] B. Kiens, B. Essen-Gustavsson, N. J. Christensen, and B. Saltin, "Skeletal muscle substrate utilization during submaximal exercise in man: effect of endurance training," *Journal of Physiology*, vol. 469, pp. 459–478, 1993.
- [89] C. E. Gargiulo, S. M. Stunlsatz-Krouper, and J. E. Schaffer, "Localization of adipocyte long-chain fatty acyl-CoA synthetase at the plasma membrane," *Journal of Lipid Research*, vol. 40, no. 5, pp. 881–892, 1999.
- [90] A. Ibrahim, A. Bonen, W. D. Blinn, et al., "Muscle-specific overexpression of FAT/CD36 enhances fatty acid oxidation by contracting muscle, reduces plasma triglycerides and fatty acids, and increases plasma glucose and insulin," *The Journal of Biological Chemistry*, vol. 274, no. 38, pp. 26761–26766, 1999.
- [91] M. Febbraio, N. A. Abumrad, D. P. Hajjar, et al., "A null mutation in murine CD36 reveals an important role in fatty acid and lipoprotein metabolism," *The Journal of Biological Chemistry*, vol. 274, no. 27, pp. 19055–19062, 1999.
- [92] J. J. F. P. Luiken, Y. Arumugam, D. J. Dyck, et al., "Increased rates of fatty acid uptake and plasmalemmal fatty acid transporters in obese Zucker rats," *The Journal of Biological Chemistry*, vol. 276, no. 44, pp. 40567–40573, 2001.
- [93] G. R. Steinberg, D. J. Dyck, J. Calles-Escandon, et al., "Chronic leptin administration decreases fatty acid uptake and fatty acid transporters in rat skeletal muscle," *The Journal of Biological Chemistry*, vol. 277, no. 11, pp. 8854–8860, 2002.

- [94] D. Cameron-Smith, L. M. Burke, D. J. Angus, et al., "A short-term, high-fat diet up-regulates lipid metabolism and gene expression in human skeletal muscle," *American Journal of Clinical Nutrition*, vol. 77, no. 2, pp. 313–318, 2003.
- [95] C. Roepstorff, J. W. Helge, B. Vistisen, and B. Kiens, "Studies of plasma membrane fatty acid-binding protein and other lipid-binding proteins in human skeletal muscle," *Proceedings of the Nutrition Society*, vol. 63, no. 2, pp. 239–244, 2004.
- [96] A. Bonen, M. L. Parolin, G. R. Steinberg, et al., "Triacylglycerol accumulation in human obesity and type 2 diabetes is associated with increased rates of skeletal muscle fatty acid transport increased sarcolemmal FAT/CD36," *FASEB Journal*, vol. 18, no. 10, pp. 1144–1146, 2004.
- [97] B. Kiens, T. H. M. Roemen, and G. J. Van der Vusse, "Muscular long-chain fatty acid content during graded exercise in humans," *American Journal of Physiology*, vol. 276, no. 2, pp. E352–E357, 1999.
- [98] C. Roepstorff, B. Vistisen, K. Roepstorff, and B. Kiens, "Regulation of plasma long-chain fatty acid oxidation in relation to uptake in human skeletal muscle during exercise," *American Journal of Physiology*, vol. 287, no. 4, pp. E696–E705, 2004.
- [99] S. S. Jain, A. Chabowski, L. A. Snook, et al., "Additive effects of insulin and muscle contraction on fatty acid transport and fatty acid transporters, FAT/CD36, FABPpm, FATP1, 4 and 6," *FEBS Letters*, vol. 583, no. 13, pp. 2294–2300, 2009.
- [100] D. E. Kelley, B. Goodpaster, R. R. Wing, and J.-A. Simoneau, "Skeletal muscle fatty acid metabolism in association with insulin resistance, obesity, and weight loss," *American Journal of Physiology*, vol. 277, no. 6, pp. E1130–E1141, 1999.
- [101] M. W. Hulver, J. R. Berggren, R. N. Cortright, et al., "Skeletal muscle lipid metabolism with obesity," *American Journal of Physiology*, vol. 284, no. 4, pp. E741–E747, 2003.
- [102] G. R. Steinberg, M. L. Parolin, G. J. F. Heigenhauser, and D. J. Dyck, "Leptin increases FA oxidation in lean but not obese human skeletal muscle: evidence of peripheral leptin resistance," *American Journal of Physiology*, vol. 283, no. 1, pp. E187–E192, 2002.
- [103] L. P. Turcotte, J. R. Swenberger, M. Z. Tucker, and A. J. Yee, "Increased fatty acid uptake and altered fatty acid metabolism in insulin-resistant muscle of obese Zucker rats," *Diabetes*, vol. 50, no. 6, pp. 1389–1396, 2001.
- [104] D. E. Befroy, K. F. Petersen, S. Dufour, et al., "Impaired mitochondrial substrate oxidation in muscle of insulin-resistant offspring of type 2 diabetic patients," *Diabetes*, vol. 56, no. 5, pp. 1376–1381, 2007.
- [105] J. Szendroedi, A. I. Schmid, M. Chmelik, et al., "Muscle mitochondrial ATP synthesis and glucose transport/phosphorylation in type 2 diabetes," *PLoS Medicine*, vol. 4, no. 5, article e154, 2007.
- [106] K. F. Petersen, S. Dufour, and G. I. Shulman, "Decreased insulin-stimulated ATP synthesis and phosphate transport in muscle of insulin-resistant offspring of type 2 diabetic parents," *PLoS Medicine*, vol. 2, no. 9, article e233, 2005.
- [107] M. Scheuermann-Freestone, P. L. Madsen, D. Manners, et al., "Abnormal cardiac and skeletal muscle energy metabolism in patients with type 2 diabetes," *Circulation*, vol. 107, no. 24, pp. 3040–3046, 2003.
- [108] V. B. Schrauwen-Hinderling, M. E. Kooi, M. K. C. Hesselink, et al., "Impaired in vivo mitochondrial function but similar intramyocellular lipid content in patients with type 2 diabetes mellitus and BMI-matched control subjects," *Diabetologia*, vol. 50, no. 1, pp. 113–120, 2007.
- [109] K. F. Petersen, D. Befroy, S. Dufour, et al., "Mitochondrial dysfunction in the elderly: possible role in insulin resistance," *Science*, vol. 300, no. 5622, pp. 1140–1142, 2003.
- [110] A. Brehm, M. Krssak, A. I. Schmid, P. Nowotny, W. Waldhäusl, and M. Roden, "Increased lipid availability impairs insulin-stimulated ATP synthesis in human skeletal muscle," *Diabetes*, vol. 55, no. 1, pp. 136–140, 2006.
- [111] K. Morino, K. F. Petersen, S. Dufour, et al., "Reduced mitochondrial density and increased IRS-1 serine phosphorylation in muscle of insulin-resistant offspring of type 2 diabetic parents," *The Journal of Clinical Investigation*, vol. 115, no. 12, pp. 3587–3593, 2005.
- [112] V. B. Ritov, E. V. Menshikova, J. He, R. E. Ferrell, B. H. Goodpaster, and D. E. Kelley, "Deficiency of subsarcolemmal mitochondria in obesity and type 2 diabetes," *Diabetes*, vol. 54, no. 1, pp. 8–14, 2005.
- [113] M. E. Patti, A. J. Butte, S. Crunkhorn, et al., "Coordinated reduction of genes of oxidative metabolism in humans with insulin resistance and diabetes: potential role of PGC1 and NRF1," *Proceedings of the National Academy of Sciences of the United States of America*, vol. 100, no. 14, pp. 8466–8471, 2003.
- [114] A. P. Rolo and C. M. Palmeira, "Diabetes and mitochondrial function: role of hyperglycemia and oxidative stress," *Toxicology and Applied Pharmacology*, vol. 212, no. 2, pp. 167–178, 2006.
- [115] R. Boushel, E. Gnaiger, P. Schjerling, M. Skovbro, R. Kraunsøe, and F. Dela, "Patients with type 2 diabetes have normal mitochondrial function in skeletal muscle," *Diabetologia*, vol. 50, no. 4, pp. 790–796, 2007.
- [116] Y. W. Asmann, C. S. Stump, K. R. Short, et al., "Skeletal muscle mitochondrial functions, mitochondrial DNA copy numbers, and gene transcript profiles in type 2 diabetic and nondiabetic subjects at equal levels of low or high insulin and euglycemia," *Diabetes*, vol. 55, no. 12, pp. 3309–3319, 2006.
- [117] A. Chavez-Velazquez, R. Jani, M. A. Abdul-Ghani, et al., "Short-Term Elevation of plasma free fatty acids (FFA) decreases skeletal muscle mitochondrial membrane potential in healthy glucose tolerant subjects," *Diabetes*, vol. 56, supplement 1, 2007.
- [118] D. E. Kelley, J. He, E. V. Menshikova, and V. B. Ritov, "Dysfunction of mitochondria in human skeletal muscle in type 2 diabetes," *Diabetes*, vol. 51, no. 10, pp. 2944–2950, 2002.
- [119] F. G. S. Toledo, S. Watkins, and D. E. Kelley, "Changes induced by physical activity and weight loss in the morphology of intermyofibrillar mitochondria in obese men and women," *Journal of Clinical Endocrinology and Metabolism*, vol. 91, no. 8, pp. 3224–3227, 2006.
- [120] M. A. Abdul-Ghani, R. Jani, M. Molina, A. Chavez, D. Tripathy, and R. A. DeFronzo, "Decreased mitochondrial ATP synthesis in obese non-diabetic subjects," *Diabetes*, vol. 56, supplement 1, 2008.
- [121] E. Phielix, V. B. Schrauwen-Hinderling, M. Mensink, et al., "Lower intrinsic ADP-stimulated mitochondrial respiration underlies in vivo mitochondrial dysfunction in muscle of male type 2 diabetic patients," *Diabetes*, vol. 57, no. 11, pp. 2943–2949, 2008.
- [122] M. Mogensen, K. Sahlin, M. Fernström, et al., "Mitochondrial respiration is decreased in skeletal muscle of patients with type 2 diabetes," *Diabetes*, vol. 56, no. 6, pp. 1592–1599, 2007.

- [123] B. H. Goodpaster, A. Katsiaras, and D. E. Kelley, "Enhanced fat oxidation through physical activity is associated with improvements in insulin sensitivity in obesity," *Diabetes*, vol. 52, no. 9, pp. 2191–2197, 2003.
- [124] A. V. Greco, G. Mingrone, A. Giancaterini, et al., "Insulin resistance in morbid obesity: reversal with intramyocellular fat depletion," *Diabetes*, vol. 51, no. 1, pp. 144–151, 2002.
- [125] S. A. Jubrias, P. C. Esselman, L. B. Price, M. E. Cress, and K. E. Conley, "Large energetic adaptations of elderly muscle to resistance and endurance training," *Journal of Applied Physiology*, vol. 90, no. 5, pp. 1663–1670, 2001.
- [126] J. O. Holloszy and E. F. Coyle, "Adaptations of skeletal muscle to endurance exercise and their metabolic consequences," *Journal of Applied Physiology Respiratory Environmental and Exercise Physiology*, vol. 56, no. 4, pp. 831–838, 1984.
- [127] P. D. Chilibeck, D. G. Syrotuik, and G. J. Bell, "The effect of concurrent endurance and strength training on quantitative estimates of subsarcolemmal and intermyofibrillar mitochondria," *International Journal of Sports Medicine*, vol. 23, no. 1, pp. 33–39, 2002.
- [128] T. Østergård, J. L. Andersen, B. Nyholm, et al., "Impact of exercise training on insulin sensitivity, physical fitness, and muscle oxidative capacity in first-degree relatives of type 2 diabetic patients," *American Journal of Physiology*, vol. 290, no. 5, pp. E998–E1005, 2006.
- [129] E. V. Menshikova, V. B. Ritov, F. G. S. Toledo, R. E. Ferrell, B. H. Goodpaster, and D. E. Kelley, "Effects of weight loss and physical activity on skeletal muscle mitochondrial function in obesity," *American Journal of Physiology*, vol. 288, no. 4, pp. E818–E825, 2005.
- [130] K. R. Short, J. L. Vittone, M. L. Bigelow, et al., "Impact of aerobic exercise training on age-related changes in insulin sensitivity and muscle oxidative capacity," *Diabetes*, vol. 52, no. 8, pp. 1888–1896, 2003.
- [131] A. O. Chavez, S. Kamath, R. Jani, et al., "Effect of short-term free fatty acids elevation on mitochondrial function in skeletal muscle of healthy individuals," *The Journal of Clinical Endocrinology & Metabolism*, vol. 95, no. 1, pp. 422–429, 2010.
- [132] M. A. Abdul-Ghani, F. Muller, Y. Liu, et al., "Deleterious effect of elevated fatty acid metabolites concentration on skeletal muscle mitochondrial ATP synthesis," *Diabetes*, vol. 56, supplement 1, 2007.
- [133] C. R. Benton, J. G. Nickerson, J. Lally, et al., "Modest PGC-1 α overexpression in muscle in vivo is sufficient to increase insulin sensitivity and palmitate oxidation in subsarcolemmal, not intermyofibrillar, mitochondria," *The Journal of Biological Chemistry*, vol. 283, no. 7, pp. 4228–4240, 2008.
- [134] M. Lagouge, C. Argmann, Z. Gerhart-Hines, et al., "Resveratrol improves mitochondrial function and protects against metabolic disease by activating SIRT1 and PGC-1 α ," *Cell*, vol. 127, no. 6, pp. 1109–1122, 2006.
- [135] J. H. Lim, J. I. Lee, Y. H. Suh, W. Kim, J. H. Song, and M. H. Jung, "Mitochondrial dysfunction induces aberrant insulin signalling and glucose utilisation in murine C2C12 myotube cells," *Diabetologia*, vol. 49, no. 8, pp. 1924–1936, 2006.
- [136] A. E. Brown, M. Elstner, S. J. Yeaman, D. M. Turnbull, and M. Walker, "Does impaired mitochondrial function affect insulin signaling and action in cultured human skeletal muscle cells?" *American Journal of Physiology*, vol. 294, no. 1, pp. E97–E102, 2008.
- [137] J. A. Pospisilik, C. Knauf, N. Joza, et al., "Targeted deletion of AIF decreases mitochondrial oxidative phosphorylation and protects from obesity and diabetes," *Cell*, vol. 131, no. 3, pp. 476–491, 2007.
- [138] A. R. Saltiel and C. R. Kahn, "Insulin signalling and the regulation of glucose and lipid metabolism," *Nature*, vol. 414, no. 6865, pp. 799–806, 2001.
- [139] J. E. Pessin and A. R. Saltiel, "Signaling pathways in insulin action: molecular targets of insulin resistance," *The Journal of Clinical Investigation*, vol. 106, no. 2, pp. 165–169, 2000.
- [140] J. P. Whitehead, S. F. Clark, B. Ursø, and D. E. James, "Signalling through the insulin receptor," *Current Opinion in Cell Biology*, vol. 12, no. 2, pp. 222–228, 2000.
- [141] L. Ellis, E. Clauser, D. O. Morgan, M. Edery, R. A. Roth, and W. J. Rutter, "Replacement of insulin receptor tyrosine residues 1162 and 1163 compromises insulin-stimulated kinase activity and uptake of 2-deoxyglucose," *Cell*, vol. 45, no. 5, pp. 721–732, 1986.
- [142] C. K. Chou, T. J. Dull, and D. S. Russell, "Human insulin receptors mutated at the ATP-binding site lack protein tyrosine kinase activity and fail to mediate postreceptor effects of insulin," *The Journal of Biological Chemistry*, vol. 262, no. 4, pp. 1842–1847, 1987.
- [143] A. Virkamäki, K. Ueki, and C. R. Kahn, "Protein-protein interaction in insulin signaling and the molecular mechanisms of insulin resistance," *The Journal of Clinical Investigation*, vol. 103, no. 7, pp. 931–943, 1999.
- [144] X. J. Sun, M. Miralpeix, M. G. Myers Jr., et al., "Expression and function of IRS-1 in insulin signal transmission," *Journal of Biological Chemistry*, vol. 267, no. 31, pp. 22662–22672, 1992.
- [145] D. Cross, D. Alessi, J. Vandenheede, H. McDowell, H. Hundal, and P. Cohen, "The inhibition of glycogen synthase kinase-3 by insulin or insulin-like growth factor 1 in the rat skeletal muscle cell line L6 is blocked by wortmannin but not rapamycin," *Biochemical Journal*, vol. 267, pp. 303–321, 1994.
- [146] H. Osawa, C. Sutherland, R. B. Robey, R. L. Printz, and D. K. Granner, "Analysis of the signaling pathway involved in the regulation of hexokinase II gene transcription by insulin," *The Journal of Biological Chemistry*, vol. 271, no. 28, pp. 16690–16694, 1996.
- [147] D. F. Lazar, R. J. Wiese, M. J. Brady, et al., "Mitogen-activated protein kinase kinase inhibition does not block the stimulation of glucose utilization by insulin," *The Journal of Biological Chemistry*, vol. 270, no. 35, pp. 20801–20807, 1995.
- [148] P. Dent, A. Lavoinne, S. Nakielny, F. B. Caudwell, P. Watt, and P. Cohen, "The molecular mechanism by which insulin stimulates glycogen synthesis in mammalian skeletal muscle," *Nature*, vol. 348, no. 6299, pp. 302–308, 1990.
- [149] C. B. Newgard, M. J. Brady, R. M. O'Doherty, and A. R. Saltiel, "Organizing glucose disposal: emerging roles of the glycogen targeting subunits of protein phosphatase-1," *Diabetes*, vol. 49, no. 12, pp. 1967–1977, 2000.
- [150] P. R. Shepherd, B. T. Nave, and K. Siddle, "Insulin stimulation of glycogen synthesis and glycogen synthase activity is blocked by wortmannin and rapamycin in 3T3-L1 adipocytes: evidence for the involvement of phosphoinositide 3-kinase and p70 ribosomal protein-56 kinase," *Biochemical Journal*, vol. 305, no. 1, pp. 25–28, 1995.
- [151] G. R. Freidenberg, R. R. Henry, H. H. Klein, D. R. Reichart, and J. M. Olefsky, "Decreased kinase activity of insulin receptors from adipocytes of non-insulin-dependent diabetic subjects," *Journal of Clinical Investigation*, vol. 79, no. 1, pp. 240–250, 1987.

- [152] J. F. Caro, M. K. Sinha, S. M. Raju, et al., "Insulin receptor kinase in human skeletal muscle from obese subjects with and without noninsulin dependent diabetes," *The Journal of Clinical Investigation*, vol. 79, no. 5, pp. 1330–1337, 1987.
- [153] J. F. Caro, O. Ittoop, W. J. Pories, et al., "Studies on the mechanism of insulin resistance in the liver from humans with noninsulin-dependent diabetes. Insulin action and binding in isolated hepatocytes, insulin receptor structure, and kinase activity," *The Journal of Clinical Investigation*, vol. 78, no. 1, pp. 249–258, 1986.
- [154] V. Trischitta, A. Brunetti, A. Chiavetta, L. Benzi, V. Papa, and R. Vigneri, "Defects in insulin-receptor internalization and processing in monocytes of obese subjects and obese NIDDM patients," *Diabetes*, vol. 38, no. 12, pp. 1579–1584, 1989.
- [155] H. H. Klein, H. Vestergaard, G. Kotzke, and O. Pedersen, "Elevation of serum insulin concentration during euglycemic hyperinsulinemic clamp studies leads to similar activation of insulin receptor kinase in skeletal muscle of subjects with and without NIDDM," *Diabetes*, vol. 44, no. 11, pp. 1310–1317, 1995.
- [156] A. Kashiwagi, M. A. Verso, and J. Andrews, "In vitro insulin resistance of human adipocytes isolated from subjects with noninsulin-dependent diabetes mellitus," *The Journal of Clinical Investigation*, vol. 72, no. 4, pp. 1246–1254, 1983.
- [157] P. Lonroth, M. Digirolamo, M. Krotkiewski, and U. Smith, "Insulin binding and responsiveness in fat cells from patients with reduced glucose tolerance and type II diabetes," *Diabetes*, vol. 32, no. 8, pp. 748–754, 1983.
- [158] J. M. Olefsky and G. M. Reaven, "Insulin binding in diabetes. Relationships with plasma insulin levels and insulin sensitivity," *Diabetes*, vol. 26, no. 7, pp. 680–688, 1977.
- [159] D. E. Moller, A. Yokota, and J. S. Flier, "Normal insulin-receptor cDNA sequence in Pima Indians with NIDDM," *Diabetes*, vol. 38, no. 11, pp. 1496–1500, 1989.
- [160] J. Kusari, U. S. Verma, J. B. Buse, R. R. Henry, and J. M. Olefsky, "Analysis of the gene sequences of the insulin receptor and the insulin-sensitive glucose transporter (GLUT-4) in patients with common-type non-insulin-dependent diabetes mellitus," *The Journal of Clinical Investigation*, vol. 88, no. 4, pp. 1323–1330, 1991.
- [161] J. J. Nolan, G. Freidenberg, R. Henry, D. Reichart, and J. M. Olefsky, "Role of human skeletal muscle insulin receptor kinase in the in vivo insulin resistance of noninsulin-dependent diabetes mellitus and obesity," *Journal of Clinical Endocrinology and Metabolism*, vol. 78, no. 2, pp. 471–477, 1994.
- [162] G. R. Freidenberg, D. Reichart, J. M. Olefsky, and R. R. Henry, "Reversibility of defective adipocyte insulin receptor kinase activity in non-insulin-dependent diabetes mellitus. Effect of weight loss," *The Journal of Clinical Investigation*, vol. 82, no. 4, pp. 1398–1406, 1988.
- [163] M. Kellerer, G. Kroder, S. Tippmer, et al., "Troglitazone prevents glucose-induced insulin resistance of insulin receptor in rat-1 fibroblasts," *Diabetes*, vol. 43, no. 3, pp. 447–453, 1994.
- [164] W. Pratipanawatr, T. Pratipanawatr, K. Cusi, et al., "Skeletal muscle insulin resistance in normoglycemic subjects with a strong family history of type 2 diabetes is associated with decreased insulin-stimulated insulin receptor substrate-1 tyrosine phosphorylation," *Diabetes*, vol. 50, no. 7–12, pp. 2572–2578, 2001.
- [165] A. Krook, M. Björnholm, D. Galuska, et al., "Characterization of signal transduction and glucose transport in skeletal muscle from type 2 diabetic patients," *Diabetes*, vol. 49, no. 2, pp. 284–292, 2000.
- [166] Y.-B. Kim, S. E. Nikoulina, T. P. Ciaraldi, R. R. Henry, and B. B. Kahn, "Normal insulin-dependent activation of Akt/protein kinase B, with diminished activation of phosphoinositide 3-kinase, in muscle in type 2 diabetes," *The Journal of Clinical Investigation*, vol. 104, no. 6, pp. 733–741, 1999.
- [167] F. Andreelli, M. Laville, P.-H. Ducluzeau, et al., "Defective regulation of phosphatidylinositol-3-kinase gene expression in skeletal muscle and adipose tissue of non-insulin-dependent diabetes mellitus patients," *Diabetologia*, vol. 42, no. 3, pp. 358–364, 1999.
- [168] F. Folli, M. J. A. Saad, J. M. Backer, and C. R. Kahn, "Regulation of phosphatidylinositol 3-kinase activity in liver and muscle of animal models of insulin-resistant and insulin-deficient diabetes mellitus," *The Journal of Clinical Investigation*, vol. 92, no. 4, pp. 1787–1794, 1993.
- [169] K. Morino, S. Neschen, S. Bilz, et al., "Muscle-specific IRS-1 ser → ala transgenic mice are protected from fat-induced insulin resistance in skeletal muscle," *Diabetes*, vol. 57, no. 10, pp. 2644–2651, 2008.
- [170] G. A. Hitman, K. Hawrami, M. I. McCarthy, et al., "Insulin receptor substrate-1 gene mutations in NIDDM; implications for the study of polygenic disease," *Diabetologia*, vol. 38, no. 4, pp. 481–486, 1995.
- [171] A. Dresner, D. Laurent, M. Marcucci, et al., "Effects of free fatty acids on glucose transport and IRS-1-associated phosphatidylinositol 3-kinase activity," *The Journal of Clinical Investigation*, vol. 103, no. 2, pp. 253–259, 1999.
- [172] W. A. Khan, G. C. Blobel, and Y. A. Hannun, "Arachidonic acid and free fatty acids as second messengers and the role of protein kinase C," *Cellular Signalling*, vol. 7, no. 3, pp. 171–184, 1995.
- [173] C. Yu, Y. Chen, G. W. Cline, et al., "Mechanism by which fatty acids inhibit insulin activation of insulin receptor substrate-1 (IRS-1)-associated phosphatidylinositol 3-kinase activity in muscle," *The Journal of Biological Chemistry*, vol. 277, no. 52, pp. 50230–50236, 2002.
- [174] C. Schmitz-Peiffer, C. L. Browne, N. D. Oakes, et al., "Alterations in the expression and cellular localization of protein kinase C isozymes ϵ and θ are associated with insulin resistance in skeletal muscle of the high-fat-fed rat," *Diabetes*, vol. 46, no. 2, pp. 169–178, 1997.
- [175] C. Schmitz-Peiffer, N. D. Oakes, C. L. Browne, E. W. Kraegen, and T. J. Biden, "Reversal of chronic alterations of skeletal muscle protein kinase C from fat-fed rats by BRL-49653," *American Journal of Physiology*, vol. 273, no. 5, pp. E915–E921, 1997.
- [176] T. K. Lam, H. Yoshii, C. A. Haber, et al., "Free fatty acid-induced hepatic insulin resistance: a potential role for protein kinase C-delta," *Am J Physiol Endocrinol Metab*, vol. 283, no. 4, pp. E682–91, 2002.
- [177] J.-F. Tanti and J. Jager, "Cellular mechanisms of insulin resistance: role of stress-regulated serine kinases and insulin receptor substrates (IRS) serine phosphorylation," *Current Opinion in Pharmacology*, vol. 9, no. 6, pp. 753–762, 2009.
- [178] H. Sell, J. Eckel, and D. Dietze-Schroeder, "Pathways leading to muscle insulin resistance—the muscle-fat connection," *Archives of Physiology and Biochemistry*, vol. 112, no. 2, pp. 105–113, 2006.

- [179] W. A. Hsueh and R. E. Law, "Insulin signaling in the arterial wall," *American Journal of Cardiology*, vol. 84, no. 1 A, pp. 21J–24J, 1999.
- [180] Z. Y. Jiang, Y.-W. Lin, A. Clemont, et al., "Characterization of selective resistance to insulin signaling in the vasculature of obese Zucker (fa/fa) rats," *The Journal of Clinical Investigation*, vol. 104, no. 4, pp. 447–457, 1999.
- [181] P. R. Shepherd and B. B. Kahn, "Glucose transporters and insulin action: implications for insulin resistance and diabetes mellitus," *The New England Journal of Medicine*, vol. 341, no. 4, pp. 248–257, 1999.
- [182] S. J. Hunter and W. T. Garvey, "Insulin action and insulin resistance: diseases involving defects in insulin receptors, signal transduction, and the glucose transport effector system," *American Journal of Medicine*, vol. 105, no. 4, pp. 331–345, 1998.
- [183] G. I. Bell, T. Kayano, J. B. Buse, et al., "Molecular biology of mammalian glucose transporters," *Diabetes Care*, vol. 13, no. 3, pp. 198–208, 1990.
- [184] H.-G. Joost, G. I. Bell, J. D. Best, et al., "Nomenclature of the GLUT/SLC2A family of sugar/polyol transport facilitators," *American Journal of Physiology*, vol. 282, no. 4, pp. E974–E976, 2002.
- [185] C. A. Stuart, M. E. A. Howell, Y. Zhang, and D. Yin, "Insulin-stimulated translocation of glucose transporter (GLUT) 12 parallels that of GLUT4 in normal muscle," *Journal of Clinical Endocrinology and Metabolism*, vol. 94, no. 9, pp. 3535–3542, 2009.
- [186] P. A. Rogers, R. A. Fisher, and H. Harris, "An electrophoretic study of the distribution and properties of human hexokinases," *Biochemical Genetics*, vol. 13, no. 11-12, pp. 857–866, 1975.
- [187] W. T. Garvey, T. P. Huecksteadt, S. Matthaei, and J. M. Olefsky, "Role of glucose transporters in the cellular insulin resistance of type II non-insulin-dependent diabetes mellitus," *The Journal of Clinical Investigation*, vol. 81, no. 5, pp. 1528–1536, 1988.
- [188] J. R. Zierath, L. He, A. Gumà, E. Odegaard Wahlström, A. Klip, and H. Wallberg-Henriksson, "Insulin action on glucose transport and plasma membrane GLUT4 content in skeletal muscle from patients with NIDDM," *Diabetologia*, vol. 39, no. 10, pp. 1180–1189, 1996.
- [189] A. Krook, M. Björnholm, D. Galuska, et al., "Characterization of signal transduction and glucose transport in skeletal muscle from type 2 diabetic patients," *Diabetes*, vol. 49, no. 2, pp. 284–292, 2000.
- [190] O. Pedersen, J. F. Bak, P. H. Andersen, et al., "Evidence against altered expression of GLUT1 or GLUT4 in skeletal muscle of patients with obesity for NIDDM," *Diabetes*, vol. 39, no. 7, pp. 865–870, 1990.
- [191] J. Eriksson, L. Koranyi, R. Bourey, et al., "Insulin resistance in type 2 (non-insulin-dependent) diabetic patients and their relatives is not associated with a defect in the expression of the insulin-responsive glucose transporter (GLUT-4) gene in human skeletal muscle," *Diabetologia*, vol. 35, no. 2, pp. 143–147, 1992.
- [192] R. C. Bonadonna, S. Del Prato, M. P. Saccomani, et al., "Transmembrane glucose transport in skeletal muscle of patients with non-insulin-dependent diabetes," *The Journal of Clinical Investigation*, vol. 92, no. 1, pp. 486–494, 1993.
- [193] R. C. Bonadonna, S. Del Prato, E. Bonora, et al., "Roles of glucose transport and glucose phosphorylation in muscle insulin resistance of NIDDM," *Diabetes*, vol. 45, supplement 3, pp. 915–925, 1996.
- [194] G. W. Cline, K. F. Petersen, M. Krssak, et al., "Impaired glucose transport as a cause of decreased insulin-stimulated muscle glycogen synthesis in type 2 diabetes," *The New England Journal of Medicine*, vol. 341, no. 4, pp. 240–246, 1999.
- [195] K. V. Williams, J. C. Price, and D. E. Kelley, "Interactions of impaired glucose transport and phosphorylation in skeletal muscle insulin resistance. A dose-response assessment using positron emission tomography," *Diabetes*, vol. 50, no. 9, pp. 2069–2079, 2001.
- [196] W.-H. Choi, S. O'Rahilly, J. B. Buse, et al., "Molecular scanning of insulin-responsive glucose transporter (GLUT4) gene in NIDDM subjects," *Diabetes*, vol. 40, no. 12, pp. 1712–1718, 1991.
- [197] L. M. Perriott, T. Kono, R. R. Whitesell, et al., "Glucose uptake and metabolism by cultured human skeletal muscle cells: rate-limiting steps," *American Journal of Physiology*, vol. 281, no. 1, pp. E72–E80, 2001.
- [198] R. L. Printz, H. Ardehali, S. Koch, and D. K. Granner, "Human hexokinase II mRNA and gene structure," *Diabetes*, vol. 44, no. 3, pp. 290–294, 1995.
- [199] C. Vogt, H. Ardehali, P. Iozzo, et al., "Regulation of hexokinase II expression in human skeletal muscle in vivo," *Metabolism*, vol. 49, no. 6, pp. 814–818, 2000.
- [200] M. Pendergrass, J. Koval, C. Vogt, et al., "Insulin-induced hexokinase II expression is reduced in obesity and NIDDM," *Diabetes*, vol. 47, no. 3, pp. 387–394, 1998.
- [201] L. J. Mandarino, R. L. Printz, K. A. Cusi, et al., "Regulation of hexokinase II and glycogen synthase mRNA, protein, and activity in human muscle," *American Journal of Physiology*, vol. 269, no. 4, pp. E701–E708, 1995.
- [202] P.-H. Ducluzeau, N. Perretti, M. Laville, et al., "Regulation by insulin of gene expression in human skeletal muscle and adipose tissue: evidence for specific defects in type 2 diabetes," *Diabetes*, vol. 50, no. 5, pp. 1134–1142, 2001.
- [203] M. Lehto, X. Huang, E. M. Davis, et al., "Human hexokinase II gene: exon-intron organization, mutation screening in NIDDM, and its relationship to muscle hexokinase activity," *Diabetologia*, vol. 38, no. 12, pp. 1466–1474, 1995.
- [204] M. Laakso, M. Malkki, P. Kekalainen, J. Kuusisto, and S. S. Deeb, "Polymorphisms of the human hexokinase II gene: lack of association with NIDDM and insulin resistance," *Diabetologia*, vol. 38, no. 5, pp. 617–622, 1995.
- [205] S. M. Echwald, C. Bjorbaek, T. Hansen, et al., "Identification of four amino acid substitutions in hexokinase II and studies of relationships to NIDDM, glucose effectiveness, and insulin sensitivity," *Diabetes*, vol. 44, no. 3, pp. 347–353, 1995.
- [206] G. Gulli, E. Ferrannini, M. Stern, S. Haffner, and R. A. DeFronzo, "The metabolic profile of NIDDM is fully established in glucose-tolerant offspring of two Mexican-American NIDDM parents," *Diabetes*, vol. 41, no. 12, pp. 1575–1586, 1992.
- [207] A. Golay, R. A. DeFronzo, E. Ferrannini, et al., "Oxidative and non-oxidative glucose metabolism in non-obese type 2 (non-insulin-dependent) diabetic patients," *Diabetologia*, vol. 31, no. 8, pp. 585–591, 1988.
- [208] S. Lillioja, D. M. Mott, J. K. Zawadzki, A. A. Young, W. G. Abbott, and C. Bogardus, "Glucose storage is a major determinant of in vivo 'insulin resistance' in subjects with normal glucose tolerance," *Journal of Clinical Endocrinology and Metabolism*, vol. 62, no. 5, pp. 922–927, 1986.

- [209] G. I. Shulman, D. L. Rothman, T. Jue, P. Stein, R. A. DeFronzo, and R. G. Shulman, "Quantitation of muscle glycogen synthesis in normal subjects and subjects with non-insulin-dependent diabetes by ^{13}C nuclear magnetic resonance spectroscopy," *The New England Journal of Medicine*, vol. 322, no. 4, pp. 223–228, 1990.
- [210] D. L. Rothman, I. Magnusson, G. Cline, et al., "Decreased muscle glucose transport/phosphorylation is an early defect in the pathogenesis of non-insulin-dependent diabetes mellitus," *Proceedings of the National Academy of Sciences of the United States of America*, vol. 92, no. 4, pp. 983–987, 1995.
- [211] A. Vaag, J. E. Henriksen, S. Madsbad, N. Holm, and H. Beck-Nielsen, "Insulin secretion, insulin action, and hepatic glucose production in identical twins discordant for non-insulin-dependent diabetes mellitus," *The Journal of Clinical Investigation*, vol. 95, no. 2, pp. 690–698, 1995.
- [212] H. Yki-Jarvinen, D. Mott, A. A. Young, K. Stone, and C. Bogardus, "Regulation of glycogen synthase and phosphorylase activities by glucose and insulin in human skeletal muscle," *The Journal of Clinical Investigation*, vol. 80, no. 1, pp. 95–100, 1987.
- [213] S. Frame and P. Cohen, "GSK3 takes centre stage more than 20 years after its discovery," *Biochemical Journal*, vol. 359, part 1, pp. 1–16, 2001.
- [214] P. Cohen, "The Croonian Lecture 1998. Identification of a protein kinase cascade of major importance in insulin signal transduction," *Philosophical Transactions of the Royal Society B*, vol. 354, no. 1382, pp. 485–495, 1999.
- [215] P. Damsbo, A. Vaag, O. Hother-Nielsen, and H. Beck-Nielsen, "Reduced glycogen synthase activity in skeletal muscle from obese patients with and without type 2 (non-insulin-dependent) diabetes mellitus," *Diabetologia*, vol. 34, no. 4, pp. 239–245, 1991.
- [216] L. J. Mandarino, K. S. Wright, L. S. Verity, et al., "Effects of insulin infusion on human skeletal muscle pyruvate dehydrogenase, phosphofructokinase, and glycogen synthase: evidence for their role in oxidative and nonoxidative glucose metabolism," *The Journal of Clinical Investigation*, vol. 80, no. 3, pp. 655–663, 1987.
- [217] A. W. Thorburn, B. Gumbiner, F. Bulacan, P. Wallace, and R. R. Henry, "Intracellular glucose oxidation and glycogen synthase activity are reduced in non-insulin-dependent (type II) diabetes independent of impaired glucose uptake," *The Journal of Clinical Investigation*, vol. 85, no. 2, pp. 522–529, 1990.
- [218] A. Vaag, J. E. Henriksen, and H. Beck-Nielsen, "Decreased insulin activation of glycogen synthase in skeletal muscles in young nonobese Caucasian first-degree relatives of patients with non-insulin-dependent diabetes mellitus," *The Journal of Clinical Investigation*, vol. 89, no. 3, pp. 782–788, 1992.
- [219] B. L. Nyomba, D. Freymond, I. Raz, K. Stone, D. M. Mott, and C. Bogardus, "Skeletal muscle glycogen synthase activity in subjects with non-insulin-dependent diabetes mellitus after glyburide therapy," *Metabolism*, vol. 39, no. 11, pp. 1204–1210, 1990.
- [220] T. Pratipanawatr, K. Cusi, P. Ngo, W. Pratipanawatr, L. J. Mandarino, and R. A. DeFronzo, "Normalization of plasma glucose concentration by insulin therapy improves insulin-stimulated glycogen synthesis in type 2 diabetes," *Diabetes*, vol. 51, no. 2, pp. 462–468, 2002.
- [221] H. Vestergaard, S. Lund, F. S. Larsen, O. J. Bjerrum, and O. Pedersen, "Glycogen synthase and phosphofructokinase protein and mRNA levels in skeletal muscle from insulin-resistant patients with non-insulin-dependent diabetes mellitus," *The Journal of Clinical Investigation*, vol. 91, no. 6, pp. 2342–2350, 1993.
- [222] H. Vestergaard, C. Bjorbaek, P. H. Andersen, J. F. Bak, and O. Pedersen, "Impaired expression of glycogen synthase mRNA in skeletal muscle of NIDDM patients," *Diabetes*, vol. 40, no. 12, pp. 1740–1745, 1991.
- [223] M. Majer, D. M. Mott, H. Mochizuki, et al., "Association of the glycogen synthase locus on 19q13 with NIDDM in Pima Indians," *Diabetologia*, vol. 39, no. 3, pp. 314–321, 1996.
- [224] M. Orho, P. Nikula-Ijas, C. Schalin-Jantti, M. A. Permutt, and L. C. Groop, "Isolation and characterization of the human muscle glycogen synthase gene," *Diabetes*, vol. 44, no. 9, pp. 1099–1105, 1995.
- [225] C. Bjørbaek, S. M. Echwald, P. Hubricht, et al., "Genetic variants in promoters and coding regions of the muscle glycogen synthase and the insulin-responsive GLUT4 genes in NIDDM," *Diabetes*, vol. 43, no. 8, pp. 976–983, 1994.
- [226] C. Bjørbaek, T. A. Vik, S. M. Echwald, et al., "Cloning of a human insulin-stimulated protein kinase (ISPK-1) gene and analysis of coding regions and mRNA levels of the ISPK-1 and the protein phosphatase-1 genes in muscle from NIDDM patients," *Diabetes*, vol. 44, no. 1, pp. 90–97, 1995.
- [227] M. Prochazka, H. Mochizuki, L. J. Baier, P. T. W. Cohen, and C. Bogardus, "Molecular and linkage analysis of type-1 protein phosphatase catalytic beta-subunit gene: lack of evidence for its major role in insulin resistance in Pima Indians," *Diabetologia*, vol. 38, no. 4, pp. 461–466, 1995.
- [228] C. Schalin-Jantti, M. Harkonen, and L. C. Groop, "Impaired activation of glycogen synthase in people at increased risk for developing NIDDM," *Diabetes*, vol. 41, no. 5, pp. 598–604, 1992.
- [229] S. Del Prato, R. C. Bonadonna, E. Bonora, et al., "Characterization of cellular defects of insulin action in type 2 (non-insulin-dependent) diabetes mellitus," *The Journal of Clinical Investigation*, vol. 91, no. 2, pp. 484–494, 1993.
- [230] K. Falholt, I. Jensen, S. Lindkaer Jensen, et al., "Carbohydrate and lipid metabolism of skeletal muscle in type 2 diabetic patients," *Diabetic Medicine*, vol. 5, no. 1, pp. 27–31, 1988.
- [231] L. J. Mandarino, Z. Madar, O. G. Kolterman, J. M. Bell, and J. M. Olefsky, "Adipocyte glycogen synthase and pyruvate dehydrogenase in obese and type II diabetic subjects," *American Journal of Physiology*, vol. 251, no. 4, pp. E489–E496, 1986.
- [232] D. E. Kelley, M. Mokan, and L. J. Mandarino, "Intracellular defects in glucose metabolism in obese patients with NIDDM," *Diabetes*, vol. 41, no. 6, pp. 698–706, 1992.
- [233] L. C. Groop, R. C. Bonadonna, D. C. Simonson, A. S. Petrides, M. Shank, and R. A. DeFronzo, "Effect of insulin on oxidative and nonoxidative pathways of free fatty acid metabolism in human obesity," *American Journal of Physiology*, vol. 263, no. 1, pp. E79–E84, 1992.
- [234] P. J. Randle, P. B. Garland, C. N. Hales, and E. A. Newsholme, "The glucose fatty-acid cycle its role in insulin sensitivity and the metabolic disturbances of diabetes mellitus," *The Lancet*, vol. 281, no. 7285, pp. 785–789, 1963.

Review Article

Inborn Errors of Energy Metabolism Associated with Myopathies

Anibh M. Das,¹ Ulrike Steuerwald,² and Sabine Illsinger¹

¹ Department of Paediatric Kidney-, Liver- and Metabolic Diseases, Hannover Medical School, Carl Neuberg Street 1, 30625 Hannover, Germany

² Screening Laboratory Hannover, Steinweg 13b, 30952 Ronnenberg, Germany

Correspondence should be addressed to Anibh M. Das, das.anibh@mh-hannover.de

Received 29 October 2009; Revised 19 January 2010; Accepted 22 February 2010

Academic Editor: Henk L. M. Granzier

Copyright © 2010 Anibh M. Das et al. This is an open access article distributed under the Creative Commons Attribution License, which permits unrestricted use, distribution, and reproduction in any medium, provided the original work is properly cited.

Inherited neuromuscular disorders affect approximately one in 3,500 children. Structural muscular defects are most common; however functional impairment of skeletal and cardiac muscle in both children and adults may be caused by inborn errors of energy metabolism as well. Patients suffering from metabolic myopathies due to compromised energy metabolism may present with exercise intolerance, muscle pain, reversible or progressive muscle weakness, and myoglobinuria. In this review, the physiology of energy metabolism in muscle is described, followed by the presentation of distinct disorders affecting skeletal and cardiac muscle: glycogen storage diseases types III, V, VII, fatty acid oxidation defects, and respiratory chain defects (i.e., mitochondriopathies). The diagnostic work-up and therapeutic options in these disorders are discussed.

1. Introduction

Both skeletal and heart muscle are highly dependent on energy supply. As energy demand of these muscle tissues varies by several orders of magnitude, energy metabolism has to be tightly regulated in order to meet varying energy requirement.

In this review, we shall first describe the physiology of energy metabolism in muscle, and then deal with different myopathies caused by inborn errors of energy metabolism.

2. Physiology of Energy Metabolism in Muscle

Glucose, fatty acids, and, to a lesser extent, amino acids serve as energy substrates for skeletal muscle cells. During quiescence, fatty acids are the main fuel. However, glucose and 6 amino acids (leucine, isoleucine, valine, asparagine, aspartate, glutamate) may also be used by the resting muscle [1, 2]. Only leucine and isoleucine can be oxidised in muscle after being converted to acetyl CoA. The other amino acids are used solely for de novo synthesis of citric acid cycle-intermediates.

Glycogen is stored in skeletal and heart muscle. In contrast to liver glycogen, muscle glycogen does not serve glucose homeostasis in the body but is almost exclusively

used for energy metabolism in muscle itself. In the initial phase of exercise, blood supply to skeletal muscle is not yet adequate; hence oxygen and blood-born energy substrates (i.e., fatty acids) are lacking. In this early phase, muscle relies on its own energy reserves, that is, muscle glycogen, and generates energy via anaerobic pathways. After a few minutes, blood vessels dilate, blood flow rises, and muscle cells are provided with oxygen and blood-born substrates. During this phase of exercise, muscle relies on aerobic energy generation via oxidative phosphorylation, mainly from fatty acids, but also (to a lesser extent) glucose and amino acids.

Fatty acids are metabolized in the mitochondrial matrix to acetyl-CoA via beta-oxidation (Figures 1 and 2). Fatty acids are the major source of energy in man, especially during fasting. Most tissues are able to oxidize fatty acids to CO₂ and water. In addition, liver has the capacity to synthesize ketone bodies (acetoacetate and 3-hydroxybutyrate from acetyl-CoA), which serve as an important fuel for extrahepatic organs, especially the brain, during catabolism. A rate-limiting step in mitochondrial fatty acid oxidation is the carnitine-palmitoyltransferase 1 (CPT1) reaction [3]. Adequate glucose supply, conversion of acetyl-CoA to malonyl-CoA by acetyl-CoA carboxylase, and the concomitant inhibition of CPT1 reduce long-chain fatty

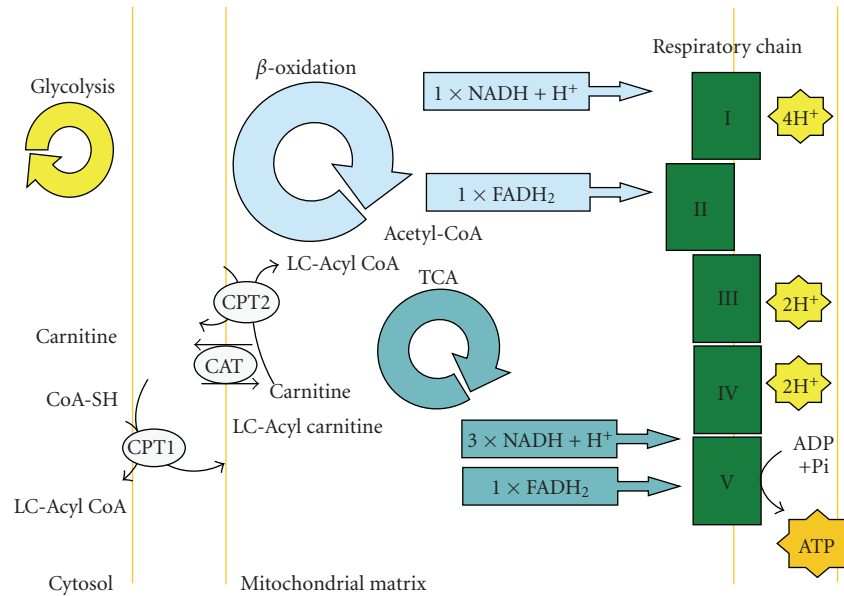


FIGURE 1: Mitochondrial biochemical pathways involved in energy production: including fatty acid oxidation, the respiratory chain, and TCA-cycle (Krebs-cycle) CPT1: Carnitine-Palmitoyltransferase 1; CPT2: Carnitine-Palmitoyltransferase 2; CAT: Carnitine-/Acylcarnitine-Transferase; LC: Long-chain; TCA: Tricarboxylic acid cycle.

acid uptake and oxidation (Figure 2). Although these effects have primarily been shown in liver and heart, there is also evidence for a regulatory function of malonyl-CoA in skeletal muscle [4]. Malonyl-CoA levels decrease when the muscle is fuel-deprived or energy consumption is increased during contraction. Long-chain fatty acids cannot freely cross the inner mitochondrial membrane and are shuttled via the carnitine system; acyl-CoA molecules are first coupled to carnitine, catalysed by carnitine-palmitoyltransferase I (CPT 1), and the acylcarnitine complex then crosses the highly impermeable inner mitochondrial membrane. In the mitochondrial matrix space, acylcarnitines are reconverted to acyl-CoA via carnitine-palmitoyltransferase 2 (CPT2) (Figure 1) and subsequently enter beta-oxidation [5]. Acetyl-CoA derived from beta-oxidation, amino acid-, or glucose-metabolism is channelled into the citric acid cycle. In the citric acid cycle, redox equivalents (FADH_2 , NADH) are produced which are substrates of the mitochondrial respiratory chain (Figures 1 and 2). Electrons released from these redox equivalents enter the respiratory chain and are finally transferred to oxygen. Electron transport is linked to the build-up of an electrochemical proton gradient across the inner mitochondrial membrane [6]. The electrochemical gradient can be used to synthesize ATP via the mitochondrial ATPsynthase (complex V) or drive transmembrane transport processes directly.

Creatine is phosphorylated by creatinekinase to creatinephosphate (CP) which can be used as an “energy buffer” and is split to ATP via reversal of the creatinekinase-reaction. CP-stores in muscle are only a short-term “energy buffer” and are used-up within the first 30 seconds of exercise.

As mentioned above, energy demand is highly variable in muscle. Energy supply has to be commensurated with energy demand; therefore energy demand is highly regulated.

Calcium (which mediates mechanical muscle contraction) serves as an important regulatory element of metabolism. Regulation of energy metabolism can occur at several levels.

- (1) The key enzyme in aerobic mitochondrial energy production via oxidative phosphorylation is *ATPsynthase (complex V)*. Classically, it was believed that ATPsynthase is regulated passively by its substrate ADP; mechanical activation of muscle results in breakdown of ATP to ADP, hence higher substrate saturation of the ATPsynthase and increased flux. We and others have shown in various tissues that the ATPsynthase is actively regulated [7–11], probably via the calcium binding inhibitor protein (CaBI) [12]. This regulatory protein dissociates from the ATPsynthase in response to elevated intramitochondrial calcium concentration during contraction, thus leading to desinhibition of the ATPsynthase, hence higher flux. In animal models, we have previously shown that this regulation breaks down under different pathophysiological conditions [7, 8, 13–16].
- (2) Similarly to ATPsynthase, enzymes of the *citric acid cycle* have been shown to be upregulated in response to increased intramitochondrial calcium levels [17, 18]. Thus, intramitochondrial concentrations of redox equivalents (NADH , FADH_2) as substrates of the mitochondrial respiratory chain rise in concert with the activity of mitochondrial ATPsynthase (cf. 1).
- (3) *Pyruvatedehydrogenase* occurs in a nonphosphorylated (active) and a phosphorylated (inactive) form. It is regulated by calcium [19]: muscle contraction is accompanied by increased muscle calcium

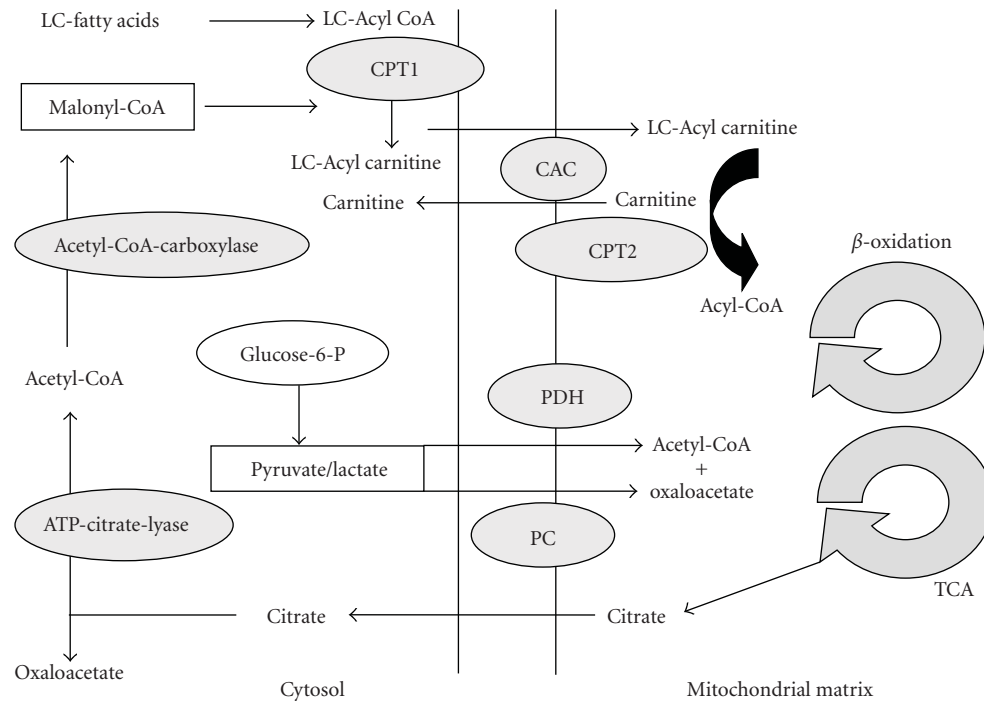


FIGURE 2: Illustration of biochemical interactions: the carnitine shuttle, fatty acid oxidation, and glycolysis. The mitochondrial membrane is not permeable to long-chain fatty acids. The carnitine shuttle has to be used to transfer long-chain fatty acids to the mitochondrial matrix space. Once in the mitochondrial matrix space, long-chain acylcarnitines are converted back to long-chain acyl-coenzyme A derivatives and free carnitine via CPT2. Free carnitine is released and the acyl-coenzyme A derivatives will enter the beta-oxidation pathway. CPT1: Carnitine-Palmitoyltransferase 1; CPT2: Carnitine-Palmitoyltransferase 2; CAT: Carnitine-/Acylcarnitine-Transferase; LC: Long-chain; TCA: Tricarboxylic acid cycle; PC: Pyruvate Carboxylase; PDH: Pyruvate Dehydrogenase.

concentrations which favours the nonphosphorylated form of pyruvate dehydrogenase by activating pyruvate dehydrogenase-phosphorylase and inhibiting kinase [20]. During exercise, muscle glycogenolysis leads to increased production of pyruvate. Pyruvate as the substrate of pyruvate dehydrogenase may subsequently lead to higher substrate saturation, hence higher flux. However, this mechanism is only of minor importance in human skeletal muscle in vivo [20].

Nitric oxide (NO) and its derivatives inhibit mitochondrial respiration by a variety of means. NO can inhibit mitochondrial cytochrome c-oxidase (complex IV) of the respiratory chain by reversibly competing with oxygen for the binding site. Higher concentrations of NO have been shown to uncouple mitochondria, inhibit complex I, and lead to permeability transition [21, 22]. Mitochondrial NO synthase may be of particular importance in this context as it is regulated by the mitochondrial membrane potential with reduced membrane potential leading to NO synthase inhibition [23, 24].

Specialized skeletal muscle fibres exist: red muscle fibres are rich in mitochondria and are used for slow and long-lasting contractions (endurance) while white muscle fibres predominantly rely on anaerobic glycolysis and can be found in 'fast and short twitch' muscle.

In contrast to skeletal muscle, energy metabolism in heart muscle is almost exclusively aerobic under physiological circumstances. Fatty acids are the main source of energy in the heart: under normal conditions up to 70% of the energy requirement of the heart is provided by fatty acid oxidation, which may be even higher under certain conditions. The regulatory elements described above for skeletal muscle are operative in cardiac muscle as well.

3. General Diagnostic Tools in Metabolic Myopathies

Here we give a general overview of diagnostic procedures which may be useful in the workup of metabolic myopathies. For more specific methods the reader is referred to the special disease section.

At the metabolite level, elevated lactate concentrations in blood and/or urine may be a clue to impaired aerobic energy metabolism (oxidative phosphorylation) and (compensatorily) increased rates of anaerobic glycolysis with lactate as the end product (Pasteur-effect). The lactate/pyruvate ratio in blood reflects the cytosolic NADH/NAD-ratio and may therefore be elevated when aerobic energy metabolism is compromised (e.g., defects of respiratory chain enzymes). The ketone-body ratio (β -hydroxybutyrate/acetoacetate, β HOB/AcAc) reflects the intramitochondrial NADH/NAD-ratio and may be elevated under certain conditions of

compromised aerobic energy production (e.g., respiratory chain defects) as well. Impaired oxidative phosphorylation may also be accompanied by elevated excretion of citric acid cycle intermediates (e.g., aconitate, succinate) which can be determined by analysing organic acids in spot-urine. Dicarboxylic acid excretion in urine is a metabolic hallmark both of defects in mitochondrial fatty acid oxidation and respiratory chain enzymes (leading to secondary inhibition of fatty acid oxidation). This finding might also be the result of a diet rich in medium chain triglycerides (MCT enriched diet as used in preterm infants and cholestatic hepatopathy).

Acylcarnitine profiles measured from dried blood spots using the tandem-mass spectrometry technique (tandem-MS) may be indicative of fatty acid oxidation disorders. They are now integrative part of the routine newborn screening programme in many countries as a strategy of primary prevention.

A lactate-ischaemia test may be indicated when glycogen storage diseases of muscle are suspected. In healthy individuals, forearm exercise leads to a rapid increase in lactate levels, paralleled by an increase in blood ammonia concentrations. In glycogen storage disease type V there is no or only attenuated lactate elevation in response to testing, while ammonia production is increased [25]. The nonischaemic forearm exercise test has been found to be less specific and sensitive and is therefore not recommended [26].

For morphological studies of muscle, ultrasound scans, MRI, and biopsy with subsequent histological work-up (including staining) as well as electron microscopy can be used. Traditionally, freeze clamping of percutaneous needle biopsy material has been used to biochemically study muscle energy metabolism. This method has limitations as far as stability of biochemical compounds and repetitive sampling in order to calculate kinetics are concerned.

^{31}P -magnetic resonance spectroscopy (MRS) is an elegant, noninvasive method to judge energy metabolism in vivo [27]. Several peaks corresponding to creatinephosphate (CP), inorganic phosphate, the 3 phosphate groups of ATP, and phosphomonesters can be observed. Kinetic studies using this technique may reveal delayed recovery of phosphocreatine [28, 29]. Recently, the use of ^{13}C -labeled substrates has been advocated to assess mitochondrial metabolism [30].

Another noninvasive technique to assess metabolic function in muscle is positron emission tomography (PET) with glucose as substrate [31]. ^{18}F -Deoxyglucose is commonly used as a marker of glucose metabolism. By comparing glucose metabolism after exercise with reference values, abnormalities may be detected in patients with defects in energy metabolism.

4. Inborn Errors of Energy Metabolism in Muscle

4.1. Disturbance of Glycogen Metabolism (Glycogen Storage Diseases)

4.1.1. General Aspects. In this section, we deal with defects of glycogen metabolism. Glycogen storage disease type II—also

known as Pompe disease—can lead to dysfunction of skeletal and cardiac muscle. As this disease involves lysosomal storage of glycogen but no abnormality in the biochemical pathways leading to energy generation, we shall not deal with this disease in detail. On the other hand, glycogen storage disease type VII is caused by a defect in the glycolytic pathway, with secondary storage of glycogen. As energy metabolism is compromised in this disease we shall describe this entity in detail below.

4.1.2. Glycogen Storage Disease Type III

(*M. Cori-Forbes; Deficiency of Amylo-1,6-Glucosidase; Debranching Enzyme*)

Pathogenesis. Glycogen storage disease type III (GSD III; OMIM 232400) is also known as Cori disease, Forbes disease, and limit dextrinosis. The symptoms associated with GSD III were first described in 1952 by Illingworth and Cori and were studied clinically by Forbes, hence the eponyms for this disorder. It is an autosomal recessive disease affecting glycogen metabolism. The overall incidence of this disease is approximately 1 : 100,000 live births in the USA. However, in other populations GSD III may occur with a higher frequency; for example, in the Faroe Islands a prevalence of 1 : 3,600 has been estimated [32].

GSD III is caused by deficiency of the glycogen debranching enzyme amylo-1,6-glucosidase, 4- α -glucanotransferase (AGL). It degrades glycogen branches releasing glucose in a two-step reaction. Debranching enzyme has two independent catalytic activities: oligo-1,4-1,4-glucantransferase and amylo-1,6-glucosidase, localised in two distinct protein regions. Patients with debrancher deficiency are classified into four types: IIIa: lack of both glucosidase and transferase activity in liver and muscle; IIIb: lack of both activities in liver only; IIIc: selective loss of glucosidase activity; and IIId: selective loss of transferase activity [33–35].

Most GSD III patients (about 85%) have AGL deficiency, expressed in both liver and muscle (type IIIa), but some only in liver but not muscle (type IIIb). Differences in tissue expression of the deficient enzyme have been described (immunoreactive material and enzyme activity) [34].

Debranching enzyme is encoded by the 85-kb AGL gene on chromosome 1p21. Genetic screening led to the observation that GSD IIIb patients had mutations in exon 3, whereas GSD IIIa patients had downstream mutations. To date, no common mutation has been described among GSD III patients, except for three alleles, two linked specifically with GSD IIIb, and the third found only in North African Jews with GSD IIIa.

Clinical Features. Clinically, patients with GSD III present in infancy or early childhood with hepatomegaly, hypoglycaemia, and growth retardation. Initially, the clinical picture may be quite similar to GSD I, however biochemically lactate and uric acid concentrations are usually normal in GSD III, and ketone bodies can be found in hypoglycaemia. During puberty and early adulthood, symptoms seem to regress and most patients have only minimal signs of hepatopathy

[36, 37]. There is, however, a risk for cirrhosis and in rare cases even hepatocellular carcinoma may develop in the long run [38]. Muscle weakness in those with GSD IIIa is usually minimal in childhood but can become more severe in adulthood; however the clinical course of myopathy is highly variable [39, 40]. The cause of muscle damage is not clear. Lactate—which could be used as an alternative fuel during exercise—does not increase in GSD IIIa patients (David Weinstein, personal communication) which may explain muscle damage.

The predominant myopathic symptoms in adults are distal weakness (affecting mostly calves and peroneal muscles) and proximal weakness of variable degree with a slow disease progression [40]. Back pain and fatigue may be present. Exercise-induced myoglobinuria is common beyond childhood. Many patients show elevated serum creatine kinase levels. Neuropathy may occur due to glycogen storage in Schwann cells and axons which clinically manifests as polyneuropathy [41].

Osteoporosis is another common symptom in GSD IIIa affecting nearly all patients. Its etiology is multifactorial [42].

Some patients have severe cardiac hypertrophy leading to compromised heart function and even death. Also dilatative cardiomyopathy of the left ventricle was described in anecdotal cases [43]. Heart disease may manifest as ventricular tachycardia as well [44]. Most patients with GSD IIIa do not develop symptoms of cardiomyopathy [45].

Diagnosis. For an accurate diagnosis, biochemical tests with glycogen quantitation and determination of amylo-1,6-glucosidase activity in a liver biopsy specimen or erythrocytes are required. Mutation analysis of the AGL gene may be helpful in some cases [46, 47] and has been advocated as a screening test using a commercially available test kit [48]. In our opinion, primary screening by mutation analysis is inappropriate. A molecular diagnostic scheme has been proposed to diagnose GSD III noninvasively.

Most of the mutations (more than 30 are known) are nonsense mutations caused by a nucleotide substitution or small insertion or deletion. Some important genotype-phenotype correlations have emerged. In particular a specific correlation of exon 3 mutations (17delAG and Q6X) with GSD IIIb has been observed. Three other mutations seem to have some phenotype correlation. Prenatal diagnosis is possible at enzymatic and genetic level [46].

Therapy. Curative therapy is not available for debranching enzyme deficiency. In order to avoid fasting hypoglycaemia in infancy, dietary measures have been proposed. Frequent daytime high protein feedings (45% carbohydrate, 25% protein, 30% fat) and supplementation of uncooked corn starch before sleep proved to be effective in young patients with regard to metabolic control (hypoglycaemia) and growth retardation.

Effects of dietary measures on myopathic symptoms in adults are less well established even though there are reports of improvement in patients following a high-protein diet. In GSD III, gluconeogenesis is intact and protein may be used as a precursor for glucose. Over-treatment with cornstarch can

cause deposition of glycogen, which cannot be broken down, leading to accumulation.

In patients with cardiomyopathy, symptomatic pharmacological treatment is mostly used. A diet providing 30% of energy from protein and avoidance of over-treatment with carbohydrate could be found to stabilize and even reverse cardiomyopathy [49].

4.1.3. Glycogen Storage Disease Type V (McArdle Disease; Deficiency of Muscle Phosphorylase)

Pathophysiology. Myophosphorylase activity is deficient in McArdle disease (OMIM 232600); the disorder is inherited as an autosomal recessive trait. The myophosphorylase gene is located on chromosome 11q13 and spans 20 exons [50]. The most common mutation in Northern Europe and North America is the nonsense mutation at R50X, previously referred to as R49X [51, 52]. Genotype-phenotype correlation is poor, modifying genes as angiotensin converting enzyme or actin 3 genes may play a role [53–55].

As a consequence of myophosphorylase deficiency, the contracting muscle is not able to mobilize adequate amounts of muscle glycogen during the initial anaerobic phase of exercise. This leads to an energy deficit which cannot be covered by creatinephosphate stores. During the aerobic phase of exercise, blood-borne substrates like fatty acids and amino acids as well as glucose can be used as energy substrates. However, the capacity of the tricarboxylic acid cycle (TCA- or Krebs-cycle) is compromised as well. This is due to the lack of pyruvate which is normally generated from glucose via glycolysis and has an anaplerotic effect on the TCA-cycle via oxaloacetate. We could show adaptive processes at the level of mitochondrial ATPsynthase in a patient with McArdle disease (poster presentation at the 4th World Muscle society Congress 1999: Das AM, Kohlschütter A; Upregulation of mitochondrial respiratory chain enzymes in GSD V).

Clinical Features. Symptoms typically begin in the second to third decade of life. As first reported by McArdle in 1951, patients typically suffer from exercise-induced muscle pain, cramps, and fatigue [56]. These symptoms are most pronounced during the first few minutes of exercise (anaerobic phase) and may be accompanied by rhabdomyolysis leading to myoglobinuria with burgundy discoloration of urine. Acute renal failure secondary to myoglobinuria has been reported in a few patients. After blood supply to the exercising muscle has increased, symptoms disappear as energy supply is reinstored; this phenomenon is known as “second wind”. Most patients with McArdle disease learn to cope with their problems by resting until muscle pain subsides and resuming activity as soon as the aerobic phase sets in (oxidizing fatty acids and other blood-borne substrates).

A less common manifestation of McArdle disease is permanent muscle weakness. This kind of symptom usually occurs later in life. Some patients may have proximal and symmetric weakness while others have asymmetric weakness mimicking facio-scapulohumeral dystrophy (FSHD) [57].

Diagnosis. Plasma creatinekinase activity is usually elevated at rest and rises in response to muscular activity. Patients fail to produce lactate during the ischaemic forearm test while ammonia concentration increases. Inosine, hypoxanthine, and uric acid also increase reflecting accelerated recycling of purine nucleotides in the face of insufficient ATP-production.

Muscle biopsy specimen usually shows subsarcolemmal and intermyofibrillar vacuoles filled with glycogen. Ultrastructurally, there are deposits of normal-looking free glycogen particles and occasional alterations of sarcoplasmic reticulum and mitochondria. Staining for phosphorylase is negative in muscle fibres whereas smooth muscle of blood vessels stains normally.

Biochemically, reduced activity of phosphorylase may be found by enzymatic assays. Diagnosis may be further corroborated by mutation analysis (see above). This allows definitive prenatal testing where appropriate.

Lack of lactate formation may lead to absent acidification of myoplasm as judged by ^{31}P -MRS [58]. The phosphocreatine/ATP-ratio is usually elevated at rest, phosphocreatine depletion during exercise is larger than normal, and recovery rate of phosphocreatine after exercise is slower [58, 59]. Changes in T2-relaxation are often absent in exercising muscle from McArdle patients [60]. EMG is usually unrevealing between acute attacks.

Treatment. Both pharmacological and dietary interventions have been tried in order to improve exercise intolerance. Therapy of McArdle disease was subject of a recent Cochrane review [61]. 24 studies were reviewed; 12 of these fulfilled the criteria for inclusion. High protein, high carbohydrate, and high fat diets as well as ketogenic diet have been tried without significant effects. Furthermore, glucagon administration, verapamil, ACE-inhibitors, sodium dantrolene, gentamicin, vitamin B6, and creatine have been tested. Low-dose creatine may have a modest benefit in some patients [62] while higher-doses may lead to deterioration [63]. All other interventions did not have any benefit. The Cochrane review concludes that none of the tested pharmacological or dietary interventions can be recommended.

4.1.4. Glycogen Storage Disease Type VII (Tarui Disease; Deficiency of Muscle Phosphofructokinase)

Pathophysiology. Tarui disease (GSD VII; OMIM 232800) is caused by deficiency of muscle phosphofructokinase. It is inherited as an autosomal-recessive trait (gene map locus of muscle phosphofructokinase PFKM 12q13.3).

Phosphofructokinase is a tetrameric enzyme derived from 3 distinct genetic loci that code for muscle, liver, and platelet isoforms. Mammalian PFK is a tetramer made up of various combinations of 3 subunits: muscle (PFKM), liver (PFKL), and platelet (PFKP), the genes for which are located on chromosomes 12q13, 21q22, and 10p, respectively. The composition of the tetramers differs according to the tissue type. Muscle and liver PFK are homotetramers of 4 M and 4 L subunits, respectively. Erythrocytes contain both L and M subunits.

The muscle phosphofructokinase gene is located on chromosome 12 and about 20 mutations have been described [64, 65]. Phosphofructokinase is not involved in glycogen metabolism but is a glycolytic enzyme. The PFKM gene encodes the muscle isoform of phosphofructokinase (PFK) (ATP:D-fructose-6-phosphate-1-phosphotransferase). PFK catalyzes the irreversible conversion of fructose-6-phosphate to fructose-1,6-bisphosphate and is a key regulatory enzyme in glycolysis.

Tarui disease has a relatively high prevalence in Japanese people; in the western hemisphere it is prevalent in patients of Jewish-Russian extraction.

If the muscle isoenzyme of phosphofructokinase (PFKM) is deficient, not only is glycolysis in muscle affected but also glycolysis in erythrocytes is reduced to about 50% (as the liver isoenzyme is fully active). As erythrocytes have no mitochondria, this relatively mild reduction of glycolytic flux can critically reduce energy supply resulting in haemolysis.

Clinical Features. Clinical symptoms are very similar to McArdle disease with exercise-induced pain, muscle cramps, and fatigue. As in McArdle disease the initial anaerobic phase of exercise is affected when the muscle has to rely on anaerobic glycolysis which is defective in Tarui disease. The resulting energy shortage leads to the clinical symptoms as first described by Tarui et al. in 1965 [66]. There are some features which may differentiate McArdle disease from Tarui disease: in Tarui disease, symptoms are more severe and often already present during childhood, often accompanied by nausea and vomiting as well as compensated haemolytic anaemia, hyperuricaemia, and an abnormal polysaccharide which is periodic acid-Schiff positive. This polysaccharide has a fine fibrillar appearance resembling amylopectine.

After carbohydrate-rich meals, exercise intolerance is often exacerbated. The pathophysiological basis for this observation is probably the inability of muscle to use glucose (anaerobically and aerobically) on one hand and hyperinsulinism caused by hyperglycaemia with subsequent lowering of fatty acids as energy substrates for muscle on the other hand.

As in McArdle disease, there are variant forms of the disease. One variant leads to muscle weakness in later adult life while the other leads to hypotonia during infancy with subsequent progressive myopathy leading to early death in younger children.

Diagnosis. As in glycogen storage disease type V the ischaemic forearm test has a pathologic result with insufficient lactate production accompanied by a rise in ammonia levels.

Histochemical and biochemical demonstration of the enzyme defect proves the suspected diagnosis. Mutation analysis may be added for further confirmation.

^{31}P -MRS shows increased phosphocreatine/ATP ratio in resting muscle, ATP depletion, larger than normal phosphocreatine depletion during exercise with slow recovery rate and absence of myoplasmic acidification [67, 68].

Therapy. There is no specific therapy for this condition. Most patients try to avoid strenuous exercise, by slowing down speed or pausing after onset of symptoms. Pain and fatigue can be reduced, after adequate blood (and fatty acid) supply sets in. Physical activity may be resumed without problems after a short break.

4.2. Disturbance of Fatty Acid Oxidation

4.2.1. General Aspects

General Aspects of Pathophysiology in FAO Disorders (FAODs). Mitochondrial fatty acid oxidation represents an important pathway for energy supply in skeletal muscle during both quiescence and periods of physical exercise. Cardiac muscle preferentially oxidizes fatty acids for energy generation and may have a limited ability to rely completely on glucose during periods of stress [4, 69].

Among metabolic myopathies, long-chain mitochondrial fatty acid oxidation defects (FAODs) are probably the most difficult to identify due to the episodic character of clinical and biochemical abnormalities which may completely disappear during anabolism. The pathway of fatty acid beta-oxidation includes at least 25 enzymes and specific transport proteins. Deficiencies in more than 50 percent of these enzymes are known to cause disease in humans. Apart from overall energy deficit in the muscle toxic (lipophilic) compounds resulting from compromised fatty acid oxidation, such as long-chain-acylcarnitines, CoA-esters, or their free long-chain fatty acids may play a role in the pathogenesis of clinical manifestations.

In this section we will focus on the following more common disorders: Carnitinepalmitoyltransferase 2 (CPT2), mitochondrial trifunctional protein (MTP), very-long-chain-acyl-CoA dehydrogenase (VLCAD), multiple acyl-CoA (MAD), as well as primary carnitine/carnitine transporter-deficiency (CTD).

General Clinical Aspects of Long-Chain FAOD. In disorders of long-chain fatty acid oxidation, clinical symptoms are usually triggered by common infections, prolonged exercise, and exposure to cold and prolonged fasting (catabolism). In long-chain FAOD, the phenotype ranges from benign forms with isolated skeletal muscle involvement to severe phenotypes leading to early death as has been initially described in patients with carnitine palmitoyltransferase 2 (CPT2) deficiency [70–72].

Newborns and infants commonly present with a multisystemic manifestation (including liver, muscle, and brain involvement) often triggered by physiological catabolism soon after birth, whereas onset later in life usually presents with exercise intolerance, muscle weakness, and sometimes myoglobinuria during metabolic decompensation. Myoglobinuria may result in acute renal failure if fluid intake is restricted. Long-chain FAOD-associated myopathies of the more chronic type manifest predominately during aerobic endurance-type activity or under metabolically stressful conditions. In contrast to patients with glycogen storage

diseases of muscle, patients suffering from FAOD do not experience a “second-wind” phenomenon.

General Diagnostic Procedures in FAOD. The diagnosis is based on detecting the accumulation of specific biochemical markers such as acylcarnitine metabolites in blood, dicarboxylic acids, and acylglycines in urine by routine newborn- or selective screening.

Medium- and long-chain fatty acid oxidation defects have been included in the routine neonatal screening program, for example, by the German screening commission. Newborn screening for FAOD promises to identify many affected patients before the onset of symptoms or in the early phase of metabolic decompensation. Physiological catabolism in the first days of life is helpful in demasking biochemical abnormalities at metabolite level. Confirmation of suspected mitochondrial fatty acid oxidation defects based on an initial abnormal newborn- or selective metabolic-screening by tandem mass spectrometry should include enzyme and whenever possible molecular analyses. Biochemical testing of urine (organic acids) may be unrevealing. Patients who are not aware of their defect could be easily at risk of decompensation when exposed to different triggers, that is, prolonged fasting, fever, or strenuous physical exercise. Therefore, neonates (and older patients) suspected to suffer from an FAOD should receive special monitoring and follow an emergency regime until the metabolic defect is excluded.

Pathologic findings in muscle biopsies are most often nonspecific. Moderate lipid storage is present in only some cases.

Of particular importance is the possibility of secondary respiratory chain dysfunction in patients with FAO defects or vice versa [73].

Diagnostic procedures in long-chain FAO disorders have recently been summarized based on the results of a consensus workshop [74].

Specific diagnostic options are mentioned in more detail below, where appropriate.

General Treatment Principles of FAOD. Evidence-based treatment recommendations for long-chain FAO defects are not available [75]. However, at national/multinational levels consensus protocols exist [76]. Current management of patients with long chain fatty acid oxidation defects includes long-term dietary therapy including avoidance of fasting, low fat diet with the restriction of long-chain fatty acid intake, and substitution with medium chain fatty acids. The long-term outcome of patients treated by dietary modification remains unknown [74, 76]. Dietary long-chain fat restriction depends on the severity of the underlying enzyme defect.

Episodic muscular symptoms such as rhabdomyolysis are pathogenetically attributed to energy deficiency, and symptoms are reversed or may be prevented by sufficient energy supply in the form of carbohydrates or MCT [77]. The incidence of overweight and obesity is increasing among children with long-chain FAOD. A diet higher in protein and lower in carbohydrate may help to lower total energy intake while maintaining good metabolic control [78].

In the past, supplementation with carnitine was proposed in fatty acid oxidation defects for detoxification of accumulating long-chain acyl-CoA esters. Actually, carnitine supplementation in long-chain FAOD is not recommended [74].

Further therapeutic options have anecdotally been described in single cases: Triheptanoin (seven-carbon medium chain fatty acid) supplementation could show an improvement of cardiac and muscular symptoms in patients suffering from long-chain fatty acid oxidation disorders [79]. PPAR-alpha agonists (like fibrates) stimulated mitochondrial fatty acid oxidation *in vivo* in both liver and muscle and might be a therapeutic option in inborn errors of FAO [80–82].

D,L-3-hydroxybutyrate could be a therapeutic option for cerebral and cardiac complications in severe FAO [83].

Disease-specific therapeutic options are discussed below.

4.2.2. Carnitine Palmitoyltransferase 2 (CPT2) Deficiency

Pathophysiology. CPT2 is located at the inner aspect of the inner mitochondrial membrane catalyzing the conversion of long-chain acyl-carnitines to acyl-CoA esters. CPT2 deficiency (OMIM 600650) is inherited as an autosomal recessive trait resulting in the accumulation of long-chain acylcarnitines. The gene is located on chromosome 1p32 [84]. There are three phenotypes of CPT2 deficiency: the “*classic muscular form*” (OMIM 255110) is most frequent and shows onset in childhood or adulthood with exercise-induced muscle weakness and rhabdomyolysis. CK levels are found to be elevated during symptomatic periods, and carnitine levels are usually normal [70]. The prevalent c.338C>T (p.Ser113Leu) mutation is found in about 60%–75% of mutant alleles [85]. This CPT2 mutation is thermolabile resulting in the degradation of the protein during fever or muscular exercise accompanied by elevated body temperature [86].

Clinical Features. A “*severe neonatal form*” (OMIM 608836) presents in the newborn period with nonketotic hypoglycemia, cardiomyopathy, muscle weakness, and renal dysgenesis in some patients [87]. Most of these patients die within days after birth [88]. The “*infantile multisystemic phenotype*” (OMIM 600649) is often fatal in the period from 3 to 18 months of age. It presents with seizures, hepatomegaly, nonketotic hypoglycemia, cardiomyopathy, and muscle weakness. Plasma free carnitine levels are low and long-chain acylcarnitines high [89]. These different clinical presentations appear to be correlated with different residual CPT2- and overall long-chain FAO-capacity [90].

Muscle CPT2 deficiency clinically manifests in patients harboring only a single heterozygous mutation [91]. Compound heterozygosity for a mild and a severe mutation can be associated with either the mild muscle or the severe multisystemic infantile form [92]. Several homozygous mutations have been reported, associated with either a prominent skeletal muscle involvement or with a severe generalized phenotype [93, 94]. Severe and intermediate phenotypes were found to correlate with biochemical indices and

genetic analysis. Milder phenotypes suggest little evidence for genotype-phenotype correlation [86].

The presence of only one severe mutation (the other being a milder one) in a CPT2 deficient patient might be sufficient to lead to life-threatening events [92]. Severely compromised long-chain fatty acid oxidation may point to a more severe course [90, 95].

4.2.3. The Mitochondrial Trifunctional Protein (MTP) Deficiency

Pathophysiology. MTP is an enzyme complex involved in the beta-oxidation of fatty acids with chain lengths of C12 to C18. It catalyzes three reactions in the oxidation of long chain fatty acids and consists of the following enzymes: 3-hydroxyacyl-CoA dehydrogenase (LCHAD), 2-enoyl-CoA hydratase, and 3-ketoacyl-CoA thiolase.

MTP is a hetero-octamer of 4 alpha- (OMIM 600890; with LCHAD and 2-enoyl-CoA hydratase activities) and 4 beta-subunits (OMIM 143450; with 3-ketoacyl-CoA thiolase activity). The alpha- and beta-subunits are encoded by different nuclear genes, consisting of 20 and 16 exons, respectively. Both are located on chromosome 2p23 [96].

A deficiency in this heteromeric complex (OMIM 609015) was first described in 1992 [97]. In contrast to the large number of isolated LCHAD-deficient patients (OMIM 609016), only few MTP alpha- and beta-subunit-deficient patients were published [98]. Molecular studies in MTP-deficient patients show a wide range of “private” mutations in both the alpha- and beta-subunit, in contrast to the common 1528 G>C mutation (E474Q) in LCHAD deficiency. Thiolase expression levels and the different rates of thiolase degradation as a result of either alpha- or beta-subunit mutations were found to correlate well with the severity of clinical manifestations [96].

The biochemical hallmarks of this disorder are the accumulation of long-chain 3-hydroxyacylcarnitines and free fatty acids in blood as well as dicarboxylic acids in urine.

Clinical Features. These long-chain FAO defects have variable presentations. They may present in the neonate or infant with sudden death, hepatopathy (Reye-like disease), hypoketotic hypoglycaemia, rhabdomyolysis, myopathy, cardiomyopathy, and capillary leak syndrome often associated with lung oedema. Late complications such as peripheral neuropathy, pigmentary retinopathy, retinal degeneration, and progressive visual loss occur [97–100]. The clinical spectrum in MTP-deficiency seems to be broader than in isolated LCHAD-deficiency, usually with a first manifestation earlier in life with a lethal outcome.

Three phenotypes have been reported in patients with alpha- or beta-subunit mutations: a “*lethal form*” with predominating cardiac involvement, an “*infancy-onset*” hepatic presentation, and a milder “*late-onset*” neuromyopathic form [96]. The main features of the neuromyopathic form with late-onset are progressive peripheral neuropathy and episodic, often exercise-induced myoglobinuria.

4.2.4. Very Long-Chain Acyl-CoA Dehydrogenase (VLCAD) Deficiency

Pathophysiology. VLCAD is bound to the inner mitochondrial membrane and catalyses the first step of the long-chain fatty acid beta oxidation spiral [101]. VLCAD deficiency (OMIM 201475) is inherited as an autosomal recessive trait (gene map locus 17p13).

Clinical Features. According to the age of onset, three phenotypes have been described [102–105]: a severe “*infantile form*” presenting in the neonatal period with hypertrophic cardiomyopathy and liver failure, a “*childhood-onset*” type with hypoketotic hypoglycaemia, and a “*juvenile or adult-onset*” muscular form characterized by recurrent episodes of rhabdomyolysis triggered by prolonged exercise or fasting (similar to CPT2 deficiency).

A clear genotype-phenotype correlation could be found [102]: patients with the severe childhood phenotype have mutations that result in absence of enzyme activity, whereas patients with the milder childhood and adult (myopathic) phenotypes have mutations that result in residual enzyme activity. However, a recent report of life-threatening disease with cardiomyopathy and hypoketotic hypoglycaemia in a previously healthy 32-year-old woman underscores the potential risk of severe complications, even in adults [106].

The milder form of VLCAD deficiency is increasingly recognised due to the more wide-spread use of tandem mass spectrometry, allowing the (presymptomatic) detection of abnormal long-chain acylcarnitines in blood samples during neonatal screening [107]. Some neonates show biochemical abnormalities in routine screening but do not suffer from clinical disease. For this, the term “Non-disease” (which is poorly defined as a condition where late-onset disease is possible) has been coined. Clinical observation of patients with late-onset presentation of VLCAD deficiency is scarce [106, 108–117].

4.2.5. Multiple Acyl-CoA Dehydrogenase Deficiency (MADD; Also Glutaric Aciduria Type II, GA II)

Pathophysiology. This is an autosomal recessively inherited disorder of fatty acid, amino acid, and choline metabolism. In multiple acyl-CoA dehydrogenase deficiency (MADD, OMIM 231680) large excretion not only of glutaric acid but also of lactic, ethylmalonic, butyric, isobutyric, 2-methylbutyric, and isovaleric acids in urine occurs. MADD results from deficiency of one of three molecules: the alpha (ETFA) and beta (ETFB) subunits of electron transfer flavoprotein (ETF), and electron transfer flavoprotein dehydrogenase (ETFHD), gene map locus 15q23-q25, 19q13.3, and 4q32-qter.

Clinical Features. The clinical picture of MADD due to the different defects appears to be similar. The most severely affected patients have congenital anomalies and die in the newborn period; other patients have hypoglycaemia, encephalopathy, muscle weakness, or cardiomyopathy. Mildly affected patients present with muscle weakness

only [118]. Some patients present with respiratory dysfunction [119]. Each of the single enzyme defects can lead to a mild or severe course, depending presumably on the location and nature of the intragenic lesion. Therefore, mutations can result in dysfunction of electron transfer flavoprotein (ETF) or ETF-ubiquinone oxidoreductase (ETF-QO). It results in secondary deficiencies of a variety of FAD-dependent enzymes, including glutaryl-CoA dehydrogenase, as well as acyl-CoA dehydrogenases from FAO and branched-chain amino acid metabolism [120].

Mutations in ETFDH, encoding ETF-QO, have been associated with both riboflavin-responsive and nonresponsive MADD as well as a myopathic form of CoQ 10 deficiency [121]. Pathomechanisms responsible for these different phenotypes are not well defined [122, 123]. As with VLCAD deficiency, there is a relationship between ETF/ETFHD genotype and phenotype in patients with MADD.

In MADD early diagnosis is essential as some patients respond to pharmacological doses of riboflavin. It has recently been shown that rapid diagnosis of MADD via newborn screening using tandem-MS is possible. Only in some of these children, disease causing mutations could be found; some were responsive to riboflavin even without a mutation (presented as an abstract at 11th ICIEM-congress in San Diego, 2009: Olsen et al. Multiple AcylCoA Dehydrogenation Deficiency). Furthermore, coenzyme Q10 concentrations should be determined in patients suffering from riboflavin responsive MADD.

Therapeutic Options in MADD. The effect of riboflavin and coenzyme Q10 should be tested [121]. Ketone bodies like D, L-3-hydroxybutyrate are discussed as a therapeutic option [83].

4.2.6. Systemic Primary Carnitine Deficiency/Carnitine Transporter Deficiency (CTD)

Pathophysiology of CTD. Carnitine is ubiquitous in nature, especially high in muscle tissue of higher organisms, but low in vegetables. In humans, biosynthesis takes place in liver and kidney. To fulfil its function, intracellular carnitine concentrations have to be rather high, especially in skeletal muscle cells. Therefore, active carnitine transport mechanisms from blood into the cell have to exist. Translocation is mediated by the carnitine transporter, a special protein, which is located in cell membranes. The active transport of carnitine into tissue takes place against a concentration gradient, permitting tissue carnitine concentrations to be 20- to 50-fold higher than plasma levels [124]. Furthermore, this carnitine transporter reabsorbs all carnitine from primary urine into blood. The sequence of the 557 amino acids of the carnitine transporter is encoded on chromosome 5q31.2-32.

In case of carnitine transporter deficiency (OMIM 212120)—inherited as an autosomal recessive trait—carnitine is lost in considerable amounts via urine; the body becomes depleted of carnitine. As a consequence, impaired oxidation of long chain fatty acids leads to deficient energy generation as well as reduced ketogenesis during fasting, and accumulation of lipids in liver and muscle [125].

Clinical Features of CTD. Different courses of CTD are known. The most severe presentation can lead to sudden infant death syndrome (SIDS) already in the neonatal period [126]. Mean age of presentation with “Reye-like” manifestations as hypoketotic hypoglycemic encephalopathy is between one month and a maximum of 5 years with an estimated median of 1.5 years [127].

The metabolic deterioration is usually triggered by prolonged fasting, reduced oral intake, or vomiting during viral illness. Those who survive critical illness suffer from recurrent episodes of encephalopathy if the defect is not diagnosed and no carnitine supplementation is given [128]. Later in life, the disorder can present with skeletal muscle disease causing muscular hypotonia with mild motor delay.

Progressive cardiomyopathy in late infancy or early childhood (usually between 1 and 7 years of age, median 3 years) leads to dilatative cardiomyopathy with greatly reduced left ventricular ejection fraction, abnormal T-waves, and signs of ventricular hypertrophy [128, 129]. Bradycardia and atrial arrhythmias are possible [130]. Sometimes no overt cardiomyopathy, but only mild interventricular septum hypertrophy, does occur [130]. If no carnitine replacement is given, progressive congestive heart failure may lead to death. Another form of cardiac deterioration was first described in 2004. A 15-year-old girl was diagnosed with cardiac arrest due to ventricular fibrillation without overt cardiomyopathy. ECG showed nonsustained ventricular tachycardia with periods of sinus rhythm and ventricular premature beats, while echocardiography revealed normal left ventricular dimensions and a borderline left ventricular hypertrophy with good contractility [131].

Nicola Longo (personal communication) stated that many of the patients who die suddenly with primary carnitine deficiency do not have cardiomyopathy (beyond childhood), but “only” sudden arrhythmias. The mechanism causing the arrhythmias is subject to ongoing studies. Adult-onset lipid storage myopathy presenting with myalgia and muscular fatigue during prolonged exercise could be shown to be caused by primary carnitine deficiency. Symptoms and abnormalities in muscle biopsy improved tremendously after four months of oral therapy with carnitine supplementation [132].

Asymptomatic courses are known as well: Spiekerkoetter et al. reported a 28-year-old man diagnosed with CTD, based on a positive family history with disease manifestation in one of his sons [133]. Four asymptomatic mothers were discovered to have CTD when being examined for low carnitine found by neonatal screening in blood spots of their offspring [134].

Patients with identical mutations can have different age of onset and different type of clinical presentation [135]. Frequency of the different courses is unknown. Many of the adults dying from ventricular fibrillation may have suffered from undiagnosed CTD. We are aware of at least 4 young adults from the Faroe Islands who showed this course (unpublished data).

Diagnostic Options in CTD. Laboratory hallmarks of CTD are very low free plasma carnitine concentrations (lower than

10 $\mu\text{mol/L}$) and increased fractional excretion of carnitine in urine. During decompensation, glucose and ketone bodies are inappropriately low. Transaminases and ammonia may be moderately elevated, and metabolic acidosis, prolonged prothrombin time, and elevated CK do occur.

Final confirmation of the diagnosis can be done by showing low activity of the transporter with decreased carnitine uptake in fibroblasts. Mutation analysis can be performed.

Therapeutic Options in CTD. The treatment of CTD is easy and without severe adverse reaction apart from a strange “fish-like” body odour. Carnitine is supplemented in a dose of 50–200 mg per kg body weight and day given in at least three portions.

4.3. Disturbance of Respiratory Chain Function

Pathophysiology. The respiratory chain is responsible for the aerobic energy generation from different substrates like fatty acids, glucose, and amino acids. It is integrated in the inner mitochondrial membrane which is almost impermeable. Electrons from the reduction equivalents NADH and FADH_2 enter the respiratory chain via complex I and complex II, respectively. Electrons then follow a potential gradient and are finally transferred to oxygen. Flow of electrons leads to the generation of an electrochemical proton gradient across the inner mitochondrial membrane as protons are pumped out of the mitochondrial matrix [6]. This gradient can be directly used, for example, for the transport of charged substances (e.g., ATP-ADP exchange). On the other hand it can be used to drive the ATPsynthase (complex V) reaction which dissipates the proton gradient across the inner mitochondrial membrane. The mitochondrial ATPsynthase has been shown to be actively regulated both in heart [136] and in skeletal muscle [137].

The mitochondrial genome consists of 16,569 base pairs (<http://www.mitomap.org/MITOMAP>). Mitochondria have their own mitochondrial DNA. Some 80 mitochondrial proteins are present in the mitochondrion, 13 of these are encoded on the mitochondrial DNA. Some subunits from complexes I, III, IV, and V are encoded on the mitochondrial DNA while other subunits from complexes I–V are nuclear-encoded. As mitochondrial DNA is inherited from the mother, respiratory chain defects due to mutations in the mitochondrial DNA follow a maternal pattern of inheritance. Mitochondrial DNA encodes both tRNA involved in protein synthesis and genes responsible for the generation of subunits of respiratory chain complexes. Nuclear-encoded mutations are inherited as an autosomal-recessive trait.

Most of the cells contain several mitochondria; each mitochondrion harbours up to 10 copies of mitochondrial DNA. Mutations in mitochondrial DNA normally do not affect all DNA of one cell and not all cells of one organ but there is a mixture of healthy and diseased cells (heteroplasmy). The relative distribution between both subsets can vary during life; the course of changes is unpredictable. Deleted DNA may replicate faster due to shortened DNA, leading to a shift towards mutated DNA.

Once a threshold is reached, clinical symptoms develop (depending on the organ involved). This also explains the high variability of clinical symptoms and lack of genotype-phenotype correlation. Highly specialized cells, like mature erythrocytes, do not contain mitochondria and are therefore spared from mitochondrial dysfunction; however immature forms of these cells may be affected.

Mitochondrial dysfunction leads to a lack of energy in aerobic tissues and production of possibly toxic free radicals which finally may induce apoptosis [138, 139]. Mitochondria are not only responsible for energy generation, but are able to take up and release calcium, thus regulating calcium homeostasis. This mitochondrial function is partly lost in respiratory chain defects.

Clinical Features. Based on the central role of energy generation within cells, almost all organs may be affected by respiratory chain disorders. Cellular heteroplasmy leads to a highly variable clinical picture of a single mutation. Organs showing a high rate of aerobic energy metabolism are often compromised first by respiratory chain disorders. Skeletal and heart muscle are frequently affected.

The first description of a mitochondrial myopathy was by Luft et al. [140], in a patient with increased thermogenesis in response to muscle exercise and ultrastructural abnormalities of mitochondria. This patient presumably had “loose coupling” between mitochondrial ATP production on one hand and flux of electrons across the respiratory chain on the other hand [141]. In the late 1980s and early 1990s, more and more patients with mitochondrialopathies due to mitochondrial dysfunction were reported.

Skeletal muscle dysfunction mostly presents as exercise intolerance; rarely pain is reported. There may be either isolated myopathy or a more complex disease with multisystemic manifestations.

Cardiac manifestations are limited exercise capacity, overt heart failure in later stages accompanied by lung oedema and hypertrophic cardiomyopathy; sometimes arrhythmias are the dominating feature. Echocardiography shows heart hypertrophy, sometimes dilatative cardiomyopathy, decreased shortening fraction, and often diastolic dysfunction. The latter is caused by incomplete (energy-dependent) uptake of calcium from the cytosol to the sarcoplasmic reticulum and mitochondria. The ECG may occasionally resemble infarction as this is also accompanied by energy depletion (in the case of infarction due to lack of oxygen).

Frequently, other organs are compromised by mitochondrialopathy and nonmuscular features like epilepsy, stroke, and so forth, may predominate. Certain combinations of clinical symptoms have been summarized as syndromes. The terms Kearns-Sayre syndrome, mitochondrial encephalopathy, lactic acidosis, and stroke-like episodes (MELASs), as well as Leber’s hereditary optic neuropathy (LHON) were coined and shown to be due to mutations in the mitochondrial DNA. However, this is rarely helpful in the diagnosis or treatment due to the large variability of clinical symptoms in one single mutation.

Diagnosis. Creatinekinase (CK) activity may often be elevated in plasma as an unspecific finding. Lactate concentration in blood—reflecting a compensatory increase in flux of anaerobic glycolysis—may be elevated (normal: <2.6 mmol/L). Lactate/pyruvate ratio reflects cytoplasmic NADH/NAD ratio and may be increased (normal: less than 20) in defects of respiratory chain complexes I–V. However, if only single organs are affected, lactate levels as well as lactate/pyruvate ratio in blood may be normal. Diagnostic accuracy of the lactate/pyruvate ratio in blood has been shown to increase with higher lactate concentrations [142]. In response to oral carbohydrates, lactate concentration in blood may rise inappropriately in respiratory chain disorders. If cytosolic NADH/NAD levels remain normal as in pyruvate dehydrogenase deficiency, lactate/pyruvate ratio in blood is normal. As many metabolic pathways have an effect on lactate and pyruvate metabolism, lactate/pyruvate ratios may easily fluctuate and may be unreliable. If determined in tissue cultures the reliability of the lactate/pyruvate ratio increases [143, 144]). The ketone body ratio (β -hydroxybutyrate/acetoacetate) reflects the intramitochondrial NADH/NAD ratio and may be increased in respiratory chain defects. Alanine may be elevated in blood.

In urine, increased amounts of lactate, pyruvate, and ketone bodies may be found. Dicarboxylic aciduria reflecting secondary inhibition of fatty acid oxidation (by accumulating NADH and FADH) may be observed. Ethylmalonic acid and 3-methylglutaconic acid excretion provide indirect evidence for mitochondrial dysfunction.

Muscle biopsy is an important diagnostic tool. The number of type I muscle fibres (red) may be compensatorily elevated. “Ragged red” fibres—seen on a modified Gomori trichrome stain—are the hallmark of mitochondrial disease, however these are not obligatory. Mitochondrial proliferation may also become evident using the succinate dehydrogenase and cytochrome oxidase stains. The classic electron microscopic findings are paracrystalline inclusions, crystals consisting of mitochondrial creatinekinase.

Muscle enzymology is the next biochemical step in the diagnostic work-up. Activities of respiratory chain complexes can be assayed either in a group of 2 enzymes or as single enzyme activities. Citrate synthase activity is usually determined as a mitochondrial marker enzyme. We have shown that the mitochondrial ATP synthase (complex V) is regulated both in rat heart [136] and in human skeletal muscle [137] in response to energy demand. Active regulation of mitochondrial ATP synthase requires an intact inner mitochondrial membrane. We therefore advocate measurement of respiratory chain enzymes in fresh muscle preparations, as freezing leads to the disruption of the inner mitochondrial membrane. Using this technique, we have shown that secondary downregulation of ATP synthase (complex V) occurs in response to reduced electron flow across complexes I–IV [145]. Respiratory chain activity can be influenced by a number of endogenous and exogenous factors. For example, limb immobilisation has been shown to lead to downregulation of mitochondrial pathways [146].

The heteroplasmic nature of most pathogenic mitochondrial DNA mutations makes genetic diagnosis difficult [147].

Genotype-phenotype correlation has been reported to be poor [148]. By mutation analysis, mitochondrial depletion syndromes may be identified which are characterized by a reduction in mitochondrial DNA copy number [149]. Some of these show myopathy, together with other organ manifestations.

In fresh, permeabilized muscle, respirometry can be performed using a Clark-type electrode. By using different inhibitors of the respiratory chain-enzymes and uncouplers, the rate-limiting step of respiration can be pinpointed [150, 151].

Using ^{31}P MRS, reduction of the ratio of phosphocreatine/inorganic phosphate can be detected, while ATP-levels are normal, phosphocreatine depletion during exercise is larger than normal, and the recovery rate of phosphocreatine after exercise is typically reduced [27].

Mutation analysis may be performed. Both mutations of the nuclear gene and the mitochondrial gene have been reported (see above).

Treatment. Management and support in a multidisciplinary team should be offered to patients and their families. Symptomatic treatment is important in order to prevent or improve morbidity. Seizure-control by antiepileptic drugs (valproic acid should be generally avoided, phenobarbital should be avoided in complex I deficiency) and control of diabetes by insulin are only few examples. A positive energetic balance is desirable; “fast” carbohydrates should be avoided as this may lead to excessive lactic acidosis.

Many single substances have been tried with the rationale of bypassing defective pathways, increasing residual enzyme activities, or having an antioxidant function. For example, succinate has been used to bypass deficient complex I activity, vitamin C and vitamin K may bypass deficient complex III, while vitamin E, alphasialic acid, and coenzyme Q10 have been advocated as antioxidants. However, a recent Cochrane review has stated that none of these as well as other forms of cofactor therapy have been shown to be of any benefit. Only coenzyme Q10 had a positive effect in patients presumably suffering from a disorder in coenzyme Q10 metabolism. Relatively high doses of 2.3 mg/kg per day are required.

Ketogenic diet has a remarkable effect on CNS-symptoms in PDH-deficiency but has also been tried in complex I deficiency.

Certain drugs inhibiting mitochondrial protein synthesis, like tetracyclines and chloramphenicol, should be avoided.

5. Miscellaneous

Some disorders in muscle energy metabolism are very rare and/or have mild symptoms. These are dealt with in this section.

Recently, sudden cardiac death has been reported in a child with muscle-specific glycogen synthase deficiency [152]. In horses, but so far not in humans gain of function mutations of glycogen synthase leading to myopathy has been found [153].

Reduced activity of the phosphorylase kinase, which is needed for glycogen breakdown, has been reported to lead to mild myopathy [154, 155].

Inhibition of the glycolytic pathway at the level of triosephosphate isomerase [156], phosphoglycerate kinase [157], phosphoglycerate mutase [158], and enolase [159] has been described to lead to myopathy with exercise-induced muscle cramps and myoglobinuria.

6. Special Problems

Malignant hyperthermia is due to mutations in the ryanodine receptor leading to defects in calcium homeostasis triggered by certain anaesthetic compounds [160–162]. Some neuromuscular diseases are known to be associated with an increased risk of malignant hyperthermia if triggering substances are used for anaesthesia.

Testing for malignant hyperthermia may be performed by the caffeine halothane contracture test or by looking for mutations of the ryanodine receptor gene. As the gene is large and many different mutations are found, it is often safer, faster, and less expensive to perform the caffeine halothane contracture test. However, this involves doing a muscle biopsy. It is often more practical to simply avoid anaesthetic compounds that trigger malignant hyperthermia, rather than doing the contracture test.

An increased risk for malignant hyperthermia has been discussed in several disorders of energy metabolism like CPT2 deficiency [163], respiratory chain defects [164, 165], and McArdle disease [166]. Depolarizing drugs like succinylcholine for muscle relaxation may trigger malignant hyperthermia. Though no firm correlation between inborn errors of energy metabolism and malignant hyperthermia has been established, it is probably wise to avoid triggering substances in these patients.

Furthermore, inhalative anaesthetic agents have been reported to interfere with NADH-linked respiratory chain function [167]. Therefore, these compounds should be avoided in patients with respiratory chain defects. Inhibition of the respiratory chain could lead to free radical generation which may mediate lipid peroxidation in cellular membranes, thus inducing calcium efflux from cell organelles which results in malignant hyperthermia [168].

Psychosocial problems may be another feature in myopathies due to defects in energy metabolism, as more and more patients with inborn errors of metabolism reach adulthood. Inherited neuromuscular disorders affect about one in 3,500 children, with Duchenne muscular dystrophy being the most common disease. To our knowledge, there are no studies on quality of life, and psychosocial problems in patients with myopathies based on compromised energy metabolism. However, studies on the special needs, quality of life and psychosocial problems in boys/men with Duchenne muscular dystrophy have been published [169, 170]. Obviously, inborn errors of energy metabolism are different from Duchenne muscular dystrophy where the physical handicap is enormous. However, it has been shown that quality of life is not correlated with physical handicap in Duchenne muscular dystrophy. Therefore, problems may also be expected in

TABLE 1

Disease	Enzyme/Transporter Defect	Main clinical features
GSD III (Cori-Forbes)	Amylo-1,6 glucosidase (debranching enzyme)	(distal) muscle weakness, cardiomyopathy, hepatomegaly, hypoglycaemia, growth retardation; osteoporosis, liver cirrhosis, hepatocellular carcinoma (later phase)
GSD V (Mc Ardle)	Muscle phosphorylase	Muscle pain (exercise-induced), myoglobinuria
GSD VII (Tarui)	Muscle phosphofructokinase	Muscle pain (+ vomiting, nausea), anaemia
CPT2-deficiency	Carnitine palmitoyl transferase 2	Muscle weakness, cardiomyopathy, hepatomegaly, hypoglycaemia, seizures
MTP (Mitochondrial trifunctional protein)	LCHAD, thiolase, enoyl-CoA hydratase	Sudden death, "Reye-like" syndrome, respiratory dysfunction, capillary leak syndrome, myopathy, myoglobinuria, cardiomyopathy, peripheral neuropathy, retinopathy
VLCAD-deficiency	VLCAD	Cardiomyopathy, muscle weakness, myoglobinuria, hypoglycaemia, liver failure
MAD-deficiency (Glutaric aciduria type II)	Electron transfer flavoprotein, electron transfer flavoprotein dehydrogenase	Muscle weakness, cardiomyopathy, hypoglycaemia, respiratory dysfunction, encephalopathy
CT-deficiency	Carnitine transporter	SIDS, "Reye-like" syndrome, encephalopathy, muscle hypotonia, myalgia (later), psychomotor delay, dilatative cardiomyopathy, arrhythmias, ventricular fibrillations
Respiratory chain defects	Respiratory chain complexes I–V (single or combined)	Multisystem-disease (e.g., myopathy, cardiomyopathy, hepatopathy, epilepsy, developmental delay, mental retardation, etc.)

metabolic myopathies. Further studies are required but may be difficult due to the rarity and high clinical variability of metabolic myopathies.

7. Summary

Fatty acids are the main fuel for energy metabolism in heart and skeletal muscle. In the initial anaerobic phase of skeletal muscle contraction, muscular glycogen is used as a substrate.

There are many inborn errors of energy metabolism leading to myopathies which have to be taken into account in the diagnostic work-up. These concern fatty acid oxidation, glycogen metabolism, as well as the "final common pathway", the mitochondrial respiratory chain. For most of the different metabolic disorders, specific therapeutic options exist. Therefore, a metabolic work-up is mandatory in myopathies (skeletal myopathy as well as cardiomyopathy) of unknown origin. An overview, including the most common disorders, is given in Table 1.

References

- [1] A. J. Wagenmakers, "Muscle amino acid metabolism at rest and during exercise: role in human physiology and metabolism," *Exercise and Sport Sciences Reviews*, vol. 26, pp. 287–314, 1998.
- [2] E. Blomstrand and B. Essén-Gustavsson, "Changes in amino acid concentration in plasma and type I and type II fibres during resistance exercise and recovery in human subjects," *Amino Acids*, vol. 37, no. 4, pp. 629–636, 2008.
- [3] J. D. McGarry and N. F. Brown, "The mitochondrial carnitine palmitoyltransferase system. From concept to molecular analysis," *European Journal of Biochemistry*, vol. 244, no. 1, pp. 1–14, 1997.
- [4] A. E. Jeukendrup, W. H. Saris, and A. J. Wagenmakers, "Fat metabolism during exercise: a review—part II: regulation of metabolism and the effects of training," *International Journal of Sports Medicine*, vol. 19, no. 5, pp. 293–302, 1998.
- [5] R. J. A. Wanders, P. Vreken, M. E. J. Den Boer, F. A. Wijburg, A. H. Van Gennip, and L. IJlst, "Disorders of mitochondrial fatty acyl-CoA β -oxidation," *Journal of Inherited Metabolic Disease*, vol. 22, no. 4, pp. 442–487, 1999.
- [6] P. Mitchell, "Chemiosmotic coupling in energy transduction: a logical development of biochemical knowledge," *Journal of Bioenergetics*, vol. 3, no. 1-2, pp. 5–24, 1972.
- [7] A. M. Das and D. A. Harris, "Intracellular calcium as a regulator of the mitochondrial ATP synthase in cultured cardiomyocytes," *Biochemical Society Transactions*, vol. 18, no. 4, pp. 554–555, 1990.
- [8] A. M. Das and D. A. Harris, "Regulation of the mitochondrial ATP synthase in intact rat cardiomyocytes," *Biochemical Journal*, vol. 266, no. 2, pp. 355–361, 1990.
- [9] A. M. Das, "Regulation of the mitochondrial ATP-synthase in health and disease," *Molecular Genetics and Metabolism*, vol. 79, no. 2, pp. 71–82, 2003.
- [10] D. A. Harris and A. M. Das, "Control of mitochondrial ATP synthesis in the heart," *Biochemical Journal*, vol. 280, part 3, pp. 561–573, 1991.
- [11] A. M. Das, "Regulation of mitochondrial ATP synthase activity in human myocardium," *Clinical Science*, vol. 94, no. 5, pp. 499–504, 1998.

- [12] E. W. Yamada and N. J. Huzel, "The calcium-binding ATPase inhibitor protein from bovine heart mitochondria. Purification and properties," *Journal of Biological Chemistry*, vol. 263, no. 23, pp. 11498–11503, 1988.
- [13] A. M. Das and D. A. Harris, "Control of mitochondrial ATP synthase in rat cardiomyocytes: effects of thyroid hormone," *Biochimica et Biophysica Acta*, vol. 1096, no. 4, pp. 284–290, 1991.
- [14] A. M. Das and D. A. Harris, "Mitochondrial ATP synthase regulation in heart: defects in hypertension are restored after treatment with captopril," *Cardioscience*, vol. 3, no. 4, pp. 227–232, 1992.
- [15] A. M. Das and D. A. Harris, "Regulation of the mitochondrial ATP synthase is defective in rat heart during alcohol-induced cardiomyopathy," *Biochimica et Biophysica Acta*, vol. 1181, no. 3, pp. 295–299, 1993.
- [16] A. M. Das and D. A. Harris, "Defects in regulation of mitochondrial ATP synthase in cardiomyocytes from spontaneously hypertensive rats," *American Journal of Physiology*, vol. 259, no. 4, part 2, pp. H1264–H1269, 1990.
- [17] R. M. Denton, G. A. Rutter, P. J. Midgley, and J. G. McCormack, "Effects of Ca^{2+} on the activities of the calcium-sensitive dehydrogenases within the mitochondria of mammalian tissues," *Journal of Cardiovascular Pharmacology*, vol. 12, no. 5, pp. S69–S72, 1988.
- [18] J. G. McCormack and R. M. Denton, "The effects of calcium ions and adenine nucleotides on the activity of pig heart 2-oxoglutarate dehydrogenase complex," *Biochemical Journal*, vol. 180, no. 3, pp. 533–544, 1979.
- [19] R. M. Denton, "Regulation of mitochondrial dehydrogenases by calcium ions," *Biochimica et Biophysica Acta*, vol. 1787, no. 11, pp. 1309–1316, 2009.
- [20] D. Constantin-Teodosiu, N. S. Peirce, J. Fox, and P. L. Greenhaff, "Muscle pyruvate availability can limit the flux, but not activation, of the pyruvate dehydrogenase complex during submaximal exercise in humans," *The Journal of Physiology*, vol. 561, no. 2, pp. 647–655, 2004.
- [21] G. C. Brown, "Regulation of mitochondrial respiration by nitric oxide inhibition of cytochrome *c* oxidase," *Biochimica et Biophysica Acta*, vol. 1504, no. 1, pp. 46–57, 2001.
- [22] G. C. Brown, "Nitric oxide and mitochondria," *Frontiers in Bioscience*, vol. 12, no. 3, pp. 1024–1033, 2007.
- [23] L. B. Valdez and A. Boveris, "Mitochondrial nitric oxide synthase, a voltage-dependent enzyme, is responsible for nitric oxide diffusion to cytosol," *Frontiers in Bioscience*, vol. 12, no. 4, pp. 1210–1219, 2007.
- [24] L. B. Valdez, T. Zaobornyj, and A. Boveris, "Mitochondrial metabolic states and membrane potential modulate mtNOS activity," *Biochimica et Biophysica Acta*, vol. 1757, no. 3, pp. 166–172, 2006.
- [25] N. Gordon, "Glycogenosis type V or McArdle's disease," *Developmental Medicine and Child Neurology*, vol. 45, no. 9, pp. 640–644, 2003.
- [26] F. Hanisch, K. Eger, S. Bork, H. Lehnich, M. Deschauer, and S. T. Zierz, "Lactate production upon short-term non-ischemic forearm exercise in mitochondrial disorders and other myopathies," *Journal of Neurology*, vol. 253, no. 6, pp. 735–740, 2006.
- [27] D. Bendahan, J. P. Mattéi, G. Kozak-Ribbens, and P. J. Cozzone, "Non invasive investigation of muscle diseases using ^{31}P magnetic resonance spectroscopy: potential in clinical applications," *Revue Neurologique*, vol. 158, no. 5, part 1, pp. 527–540, 2002.
- [28] B. Barbiroli, R. Medori, H. J. Tritschler, et al., "Lipoic (thioctic) acid increases brain energy availability and skeletal muscle performance as shown by in vivo ^{31}P -MRS in a patient with mitochondrial cytopathy," *Journal of Neurology*, vol. 242, no. 7, pp. 472–477, 1995.
- [29] G. M. Fabrizi, R. Lodi, M. D'Ettoire, et al., "Autosomal dominant limb girdle myopathy with ragged-red fibers and cardiomyopathy: a pedigree study by in vivo ^{31}P -MR spectroscopy indicating a multisystem mitochondrial defect," *Journal of the Neurological Sciences*, vol. 137, no. 1, pp. 20–27, 1996.
- [30] D. E. Befroy, K. Falk Petersen, D. L. Rothman, and G. I. Shulman, "Chapter 21 assessment of in vivo mitochondrial metabolism by magnetic resonance spectroscopy," *Methods in Enzymology*, vol. 457, pp. 373–393, 2009.
- [31] M. Tashiro, T. Fujimoto, M. Itoh, et al., " ^{18}F -FDG PET imaging of muscle activity in runners," *Journal of Nuclear Medicine*, vol. 40, no. 1, pp. 70–76, 1999.
- [32] R. Santer, M. Kinner, U. Steuerwald, et al., "Molecular genetic basis and prevalence of glycogen storage disease type IIIA in the Faroe Islands," *European Journal of Human Genetics*, vol. 9, no. 5, pp. 388–391, 2001.
- [33] J. H. Ding, T. De Barsy, B. I. Brown, R. A. Coleman, and Y. T. Chen, "Immunoblot analyses of glycogen debranching enzyme in different subtypes of glycogen storage disease type III," *The Journal of Pediatrics*, vol. 116, no. 1, pp. 95–100, 1990.
- [34] R. A. Coleman, H. S. Winter, B. Wolf, J. M. Gilchrist, and Y. T. Chen, "Glycogen storage disease type III (glycogen debranching enzyme deficiency): correlation of biochemical defects with myopathy and cardiomyopathy," *Annals of Internal Medicine*, vol. 116, no. 11, pp. 896–900, 1992.
- [35] Y. Endo, A. Horinishi, M. Vorgerd, et al., "Molecular analysis of the AGL gene: heterogeneity of mutations in patients with glycogen storage disease type III from Germany, Canada, Afghanistan, Iran, and Turkey," *Journal of Human Genetics*, vol. 51, no. 11, pp. 958–963, 2006.
- [36] S. Lucchiari, D. Santoro, S. Pagliarini, and G. P. Comi, "Clinical, biochemical and genetic features of glycogen debranching enzyme deficiency," *Acta Myologica*, vol. 26, no. 1, pp. 72–74, 2007.
- [37] B. Schoser, D. Gläser, and J. Müller-Höcker, "Clinicopathological analysis of the homozygous p.W1327X AGL mutation in glycogen storage disease type 3," *American Journal of Medical Genetics, Part A*, vol. 146, no. 22, pp. 2911–2915, 2008.
- [38] E. Demo, D. Frush, M. Gottfried, et al., "Glycogen storage disease type III-hepatocellular carcinoma a long-term complication?" *Journal of Hepatology*, vol. 46, no. 3, pp. 492–498, 2007.
- [39] S. Kiechl, J. Willeit, W. Vogel, U. Kohlendorfer, and W. Poewe, "Reversible severe myopathy of respiratory muscles due to adult-onset type III glycogenosis," *Neuromuscular Disorders*, vol. 9, no. 6-7, pp. 408–410, 1999.
- [40] S. Kiechl, U. Kohlendorfer, C. Thaler, et al., "Different clinical aspects of debrancher deficiency myopathy," *Journal of Neurology Neurosurgery and Psychiatry*, vol. 67, no. 3, pp. 364–368, 1999.
- [41] M. A. Kotb, H. K. Abdullah, and A. Kotb, "Liver glycogenoses: are they a possible cause of polyneuropathy? A cross-sectional study," *Journal of Tropical Pediatrics*, vol. 50, no. 4, pp. 196–202, 2004.

- [42] H. R. Mundy, J. E. Williams, P. J. Lee, and M. S. Fewtrell, "Reduction in bone mineral density in glycogenosis type III may be due to a mixed muscle and bone deficit," *Journal of Inherited Metabolic Disease*, vol. 31, no. 3, pp. 418–423, 2008.
- [43] H. Akazawa, T. Kuroda, S. Kim, H. Mito, T. Kojo, and K. Shimada, "Specific heart muscle disease associated with glycogen storage disease type III: clinical similarity to the dilated phase of hypertrophic cardiomyopathy," *European Heart Journal*, vol. 18, no. 3, pp. 532–533, 1997.
- [44] H. Tada, T. Kurita, T. Ohe, et al., "Glycogen storage disease type III associated with ventricular tachycardia," *American Heart Journal*, vol. 130, no. 4, pp. 911–912, 1995.
- [45] P. J. Lee, J. E. Deanfield, M. Burch, K. Baig, W. J. McKenna, and J. V. Leonard, "Comparison of the functional significance of left ventricular hypertrophy in hypertrophic cardiomyopathy and glycogenosis type III," *The American Journal of Cardiology*, vol. 79, no. 6, pp. 834–838, 1997.
- [46] J. J. Shen and Y. T. Chen, "Molecular characterization of glycogen storage disease type III," *Current Molecular Medicine*, vol. 2, no. 2, pp. 167–175, 2002.
- [47] Y. Aoyama, I. Ozer, M. Demirkol, et al., "Molecular features of 23 patients with glycogen storage disease type III in Turkey: a novel mutation p.R1147G associated with isolated glucosidase deficiency, along with 9 AGL mutations," *Journal of Human Genetics*, vol. 54, no. 11, pp. 681–686, 2009.
- [48] J. Seigel, D. A. Weinstein, R. Hillman, B. Colbert, B. Matthews, and B. Bachrach, "Glycogen storage disease type IIIa presenting as non-ketotic hypoglycemia: use of a newly approved commercially available mutation analysis to non-invasively confirm the diagnosis," *Journal of Pediatric Endocrinology and Metabolism*, vol. 21, no. 6, pp. 587–590, 2008.
- [49] A. I. Dagli, R. T. Zori, H. McCune, T. Ivsic, M. K. Maisenbacher, and D. A. Weinstein, "Reversal of glycogen storage disease type IIIa-related cardiomyopathy with modification of diet," *Journal of Inherited Metabolic Disease*, pp. 1–4, 2009.
- [50] C. Bartram, R. H. T. Edwards, J. Clague, and R. J. Beynon, "McArdle's disease: a nonsense mutation in exon 1 of the muscle glycogen phosphorylase gene explains some but not all cases," *Human Molecular Genetics*, vol. 2, no. 8, pp. 1291–1293, 1993.
- [51] C. Kubisch, E. M. Wicklein, and T. J. Jentsch, "Molecular diagnosis of McArdle disease: revised genomic structure of the myophosphorylase gene and identification of a novel mutation," *Human Mutation*, vol. 12, no. 1, pp. 27–32, 1998.
- [52] A. L. Andreu, G. Nogales-Gadea, D. Cassandrini, J. Arenas, and C. Bruno, "McArdle disease: molecular genetic update," *Acta Myologica*, vol. 26, no. 1, pp. 53–57, 2007.
- [53] F. Gómez-Gallego, C. Santiago, M. Morán, et al., "The *I* allele of the ACE gene is associated with improved exercise capacity in women with McArdle disease," *British Journal of Sports Medicine*, vol. 42, no. 2, pp. 134–140, 2008.
- [54] A. Lucia, F. Gómez-Gallego, C. Santiago, et al., "The 577X allele of the ACTN3 gene is associated with improved exercise capacity in women with McArdle's disease," *Neuromuscular Disorders*, vol. 17, no. 8, pp. 603–610, 2007.
- [55] A. Martinuzzi, A. Liava, E. Trevisi, L. Antoniazzi, and M. Frare, "Chronic therapy for McArdle disease: the randomized trial with ACE inhibitor," *Acta Myologica*, vol. 26, no. 1, pp. 64–66, 2007.
- [56] B. McArdle, "Myopathy due to a defect in muscle glycogen breakdown," *Clinical Science*, vol. 10, pp. 13–33, 1951.
- [57] A. A. Nadaj-Pakleza, C. M. Vincitorio, P. Laforêt, et al., "Permanent muscle weakness in McArdle disease," *Muscle and Nerve*, vol. 40, no. 3, pp. 350–357, 2009.
- [58] D. Bendahan, S. Confort-Gouny, G. Kozak-Ribbens, and P. J. Cozzone, "31-P NMR characterization of the metabolic anomalies associated with the lack of glycogen phosphorylase activity in human forearm muscle," *Biochemical and Biophysical Research Communications*, vol. 185, no. 1, pp. 16–21, 1992.
- [59] B. D. Ross, G. K. Radda, D. G. Gadian, G. Rocker, M. Esiri, and J. Falconer-Smith, "Examination of a case of suspected McArdle's syndrome by ³¹P nuclear magnetic resonance," *New England Journal of Medicine*, vol. 304, no. 22, pp. 1338–1342, 1981.
- [60] J. L. Fleckenstein, R. G. Haller, S. F. Lewis, et al., "Absence of exercise-induced MRI enhancement of skeletal muscle in McArdle's disease," *Journal of Applied Physiology*, vol. 71, no. 3, pp. 961–969, 1991.
- [61] R. Quinlivan, R. J. Beynon, and A. Martinuzzi, "Pharmacological and nutritional treatment for McArdle disease (Glycogen Storage Disease type V)," *Cochrane Database of Systematic Reviews (Online)*, no. 2, Article ID CD003458, 2008.
- [62] M. Vorgerd, T. Grehl, M. Jäger, et al., "Creatine therapy in myophosphorylase deficiency (McArdle disease): a placebo-controlled crossover trial," *Archives of Neurology*, vol. 57, no. 7, pp. 956–963, 2000.
- [63] M. Vorgerd, J. Zange, R. Kley, et al., "Effect of high-dose creatine therapy on symptoms of exercise intolerance in McArdle disease: double-blind, placebo-controlled crossover study," *Archives of Neurology*, vol. 59, no. 1, pp. 97–101, 2002.
- [64] A. Toscano and O. Musumeci, "Tarui disease and distal glycogenoses: clinical and genetic update," *Acta Myologica*, vol. 26, no. 2, pp. 105–107, 2007.
- [65] S. Vora, "Isozymes of phosphofructokinase," *Isozymes*, vol. 6, pp. 119–167, 1982.
- [66] S. Tarui, G. Okuno, Y. Ikura, T. Tanaka, M. Suda, and M. Nishikawa, "Phosphofructokinase deficiency in skeletal muscle. A new type of glycogenosis," *Biochemical and Biophysical Research Communications*, vol. 19, no. 4, pp. 517–523, 1965.
- [67] D. Duboc, P. Jehenson, and S. T. Dinh, "Phosphorus NMR spectroscopy study of muscular enzyme deficiencies involving glycogenolysis and glycolysis," *Neurology*, vol. 37, no. 4, pp. 663–671, 1987.
- [68] Z. Argov, N. De Stefano, and D. L. Arnold, "Muscle high-energy phosphates in central nervous system disorders. The phosphorus MRS experience," *The Italian Journal of Neurological Sciences*, vol. 18, no. 6, pp. 353–357, 1997.
- [69] P. Rinaldo, D. Matern, and M. J. Bennett, "Fatty acid oxidation disorders," *Annual Review of Physiology*, vol. 64, pp. 477–502, 2002.
- [70] S. DiMauro and P. M. M. DiMauro, "Muscle carnitine palmityltransferase deficiency and myoglobinuria," *Science*, vol. 182, no. 4115, pp. 929–931, 1973.
- [71] S. Illsinger, T. Lücke, M. Peter, et al., "Carnitine-palmitoyltransferase 2 deficiency: novel mutations and relevance of newborn screening," *American Journal of Medical Genetics, Part A*, vol. 146, no. 22, pp. 2925–2928, 2008.
- [72] S. Corti, A. Bordini, D. Ronchi, et al., "Clinical features and new molecular findings in Carnitine Palmitoyltransferase II (CPT II) deficiency," *Journal of the Neurological Sciences*, vol. 266, no. 1-2, pp. 97–103, 2008.

- [73] A. M. Das, R. Fingerhut, R. J. A. Wanders, and K. Ullrich, "Secondary respiratory chain defect in a boy with long-chain 3-hydroxyacyl-CoA dehydrogenase deficiency: possible diagnostic pitfalls," *European Journal of Pediatrics*, vol. 159, no. 4, pp. 243–246, 2000.
- [74] U. Spiekerkoetter, M. Lindner, R. Santer, et al., "Treatment recommendations in long-chain fatty acid oxidation defects: consensus from a workshop," *Journal of Inherited Metabolic Disease*, vol. 32, no. 4, pp. 498–505, 2009.
- [75] J. O. Solis and R. H. Singh, "Management of fatty acid oxidation disorders: a survey of current treatment strategies," *Journal of the American Dietetic Association*, vol. 102, no. 12, pp. 1800–1803, 2002.
- [76] U. Spiekerkoetter, M. Lindner, R. Santer, et al., "Management and outcome in 75 individuals with long-chain fatty acid oxidation defects: results from a workshop," *Journal of Inherited Metabolic Disease*, vol. 32, no. 4, pp. 488–497, 2009.
- [77] M. B. Gillingham, B. Scott, D. Elliott, and C. O. Harding, "Metabolic control during exercise with and without medium-chain triglycerides (MCT) in children with long-chain 3-hydroxy acyl-CoA dehydrogenase (LCHAD) or trifunctional protein (TFP) deficiency," *Molecular Genetics and Metabolism*, vol. 89, no. 1-2, pp. 58–63, 2006.
- [78] M. B. Gillingham, J. Q. Purnell, J. Jordan, D. Stadler, A. M. Haqq, and C. O. Harding, "Effects of higher dietary protein intake on energy balance and metabolic control in children with long-chain 3-hydroxy acyl-CoA dehydrogenase (LCHAD) or trifunctional protein (TFP) deficiency," *Molecular Genetics and Metabolism*, vol. 90, no. 1, pp. 64–69, 2007.
- [79] C. R. Roe, L. Sweetman, D. S. Roe, F. David, and H. Brunen-graber, "Treatment of cardiomyopathy and rhabdomyolysis in long-chain fat oxidation disorders using an anaplerotic odd-chain triglyceride," *Journal of Clinical Investigation*, vol. 110, no. 2, pp. 259–269, 2002.
- [80] S. Gobin-Limballe, F. Djouadi, F. Aubey, et al., "Genetic basis for correction of very-long-chain acyl-coenzyme A dehydrogenase deficiency by bezafibrate in patient fibroblasts: toward a genotype-based therapy," *American Journal of Human Genetics*, vol. 81, no. 6, pp. 1133–1143, 2007.
- [81] A. Minnich, N. Tian, L. Byan, and G. Bilder, "A potent PPAR α agonist stimulates mitochondrial fatty acid β -oxidation in liver and skeletal muscle," *American Journal of Physiology*, vol. 280, no. 2, pp. E270–E279, 2001.
- [82] F. Djouadi, F. Aubey, D. Schlemmer, et al., "Potential of fibrates in the treatment of fatty acid oxidation disorders: revival of classical drugs?" *Journal of Inherited Metabolic Disease*, vol. 29, no. 2-3, pp. 341–342, 2006.
- [83] J. L. K. Van Hove, S. Grunewald, J. Jaeken, et al., "D,L-3-hydroxybutyrate treatment of multiple acyl-CoA dehydrogenase deficiency (MADD)," *Lancet*, vol. 361, no. 9367, pp. 1433–1435, 2003.
- [84] C. Gellera, E. Verderio, G. Floridia, et al., "Assignment of the human carnitine palmitoyltransferase II gene (CPT1) to chromosome 1p32," *Genomics*, vol. 24, no. 1, pp. 195–197, 1994.
- [85] M. Deschauer, T. Wieser, and S. Zierz, "Muscle carnitine palmitoyltransferase II deficiency: clinical and molecular genetic features and diagnostic aspects," *Archives of Neurology*, vol. 62, no. 1, pp. 37–41, 2005.
- [86] S. E. Olpin, A. Affi, S. Clark, et al., "Mutation and biochemical analysis in carnitine palmitoyltransferase type II (CPT II) deficiency," *Journal of Inherited Metabolic Disease*, vol. 26, no. 6, pp. 543–557, 2003.
- [87] G. Hug, K. E. Bove, and S. Soukup, "Lethal neonatal multiorgan deficiency of carnitine palmitoyltransferase II," *New England Journal of Medicine*, vol. 325, no. 26, pp. 1862–1864, 1991.
- [88] F. Taroni and G. Uziel, "Fatty acid mitochondrial β -oxidation and hypoglycaemia in children," *Current Opinion in Neurology*, vol. 9, no. 6, pp. 477–485, 1996.
- [89] F. Demaugre, J. P. Bonnefont, M. Colonna, C. Cepanec, J. P. Leroux, and J. M. Saudubray, "Infantile form of carnitine palmitoyltransferase II deficiency with hepatomuscular symptoms and sudden death. Physiopathological approach to carnitine palmitoyltransferase II deficiencies," *Journal of Clinical Investigation*, vol. 87, no. 3, pp. 859–864, 1991.
- [90] L. Thuillier, H. Rostane, V. Droin, et al., "Correlation between genotype, metabolic data, and clinical presentation in carnitine palmitoyltransferase 2 (CPT2) deficiency," *Human Mutation*, vol. 21, no. 5, pp. 493–501, 2003.
- [91] G. D. Vladutiu, M. J. Bennett, D. Smail, L. J. Wong, R. T. Taggart, and H. B. Lindsley, "A variable myopathy associated with heterozygosity for the R503C mutation in the carnitine palmitoyltransferase II gene," *Molecular Genetics and Metabolism*, vol. 70, no. 2, pp. 134–141, 2000.
- [92] L. Thuillier, C. Sevin, F. Demaugre, et al., "Genotype/phenotype correlation in carnitine palmitoyl transferase II deficiency: lessons from a compound heterozygous patient," *Neuromuscular Disorders*, vol. 10, no. 3, pp. 200–205, 2000.
- [93] P. J. Isackson, M. J. Bennett, and G. D. Vladutiu, "Identification of 16 new disease-causing mutations in the CPT2 gene resulting in carnitine palmitoyltransferase II deficiency," *Molecular Genetics and Metabolism*, vol. 89, no. 4, pp. 323–331, 2006.
- [94] P. J. Isackson, M. J. Bennett, U. Lichter-Konecki, et al., "CPT2 gene mutations resulting in lethal neonatal or severe infantile carnitine palmitoyltransferase II deficiency," *Molecular Genetics and Metabolism*, vol. 94, no. 4, pp. 422–427, 2008.
- [95] J. P. Bonnefont, F. Taroni, P. Cavadini, et al., "Molecular analysis of carnitine palmitoyltransferase II deficiency with hepatocardiomyopathy expression," *American Journal of Human Genetics*, vol. 58, no. 5, pp. 971–978, 1996.
- [96] U. Spiekerkoetter, Z. Khuchua, Z. Yue, M. J. Bennett, and A. W. Strauss, "General mitochondrial trifunctional protein (TFP) deficiency as a result of either α - or β -subunit mutations exhibits similar phenotypes because mutations in either subunit alter TFP complex expression and subunit turnover," *Pediatric Research*, vol. 55, no. 2, pp. 190–196, 2004.
- [97] R. J. A. Wanders, L. Ijlst, F. Poggi, et al., "Human trifunctional protein deficiency: a new disorder of mitochondrial fatty acid β -oxidation," *Biochemical and Biophysical Research Communications*, vol. 188, no. 3, pp. 1139–1145, 1992.
- [98] A. M. Das, S. Illsinger, T. Lücke, et al., "Isolated mitochondrial long-chain ketoacyl-CoA thiolase deficiency resulting from mutations in the HADHB gene," *Clinical Chemistry*, vol. 52, no. 3, pp. 530–534, 2006.
- [99] O. Scheuerman, R. J. A. Wanders, H. R. Waterham, G. Dubnov-Raz, and B.-Z. Garty, "Mitochondrial trifunctional protein deficiency with recurrent rhabdomyolysis," *Pediatric Neurology*, vol. 40, no. 6, pp. 465–467, 2009.
- [100] M. E. J. Den Boer, C. Dionisi-Vici, A. Chakrapani, A. O. J. Van Thuijl, R. J. A. Wanders, and F. A. Wijburg, "Mitochondrial trifunctional protein deficiency: a severe fatty acid oxidation disorder with cardiac and neurologic involvement," *The Journal of Pediatrics*, vol. 142, no. 6, pp. 684–689, 2003.

- [101] K. Izai, Y. Uchida, T. Orii, S. Yamamoto, and T. Hashimoto, "Novel fatty acid beta-oxidation enzymes in rat liver mitochondria. I. Purification and properties of very-long-chain acyl-coenzyme A dehydrogenase," *The Journal of Biological Chemistry*, vol. 267, no. 2, pp. 1027–1033, 1992.
- [102] B. S. Andresen, S. Olpin, B. J. H. M. Poorthuis, et al., "Clear correlation of genotype with disease phenotype in very-long-chain acyl-CoA dehydrogenase deficiency," *American Journal of Human Genetics*, vol. 64, no. 2, pp. 479–494, 1999.
- [103] B. S. Andresen, C. Vianey-Saban, P. Bross, et al., "The mutational spectrum in very long-chain acyl-CoA dehydrogenase deficiency," *Journal of Inherited Metabolic Disease*, vol. 19, no. 2, pp. 169–172, 1996.
- [104] C. Bertrand, C. Largilliere, M. T. Zobot, M. Mathieu, and C. Vianey-Saban, "Very long chain acyl-CoA dehydrogenase deficiency: identification of a new inborn error of mitochondrial fatty acid oxidation in fibroblasts," *Biochimica et Biophysica Acta*, vol. 1180, no. 3, pp. 327–329, 1993.
- [105] C. Vianey-Saban, P. Divry, M. Brivet, et al., "Mitochondrial very-long-chain acyl-coenzyme A dehydrogenase deficiency: clinical characteristics and diagnostic considerations in 30 patients," *Clinica Chimica Acta*, vol. 269, no. 1, pp. 43–62, 1998.
- [106] S. Kluge, P. Kühnelt, A. Block, et al., "A young woman with persistent hypoglycemia, rhabdomyolysis, and coma: recognizing fatty acid oxidation defects in adults," *Critical Care Medicine*, vol. 31, no. 4, pp. 1273–1276, 2003.
- [107] A. Boneh, B. S. Andresen, N. Gregersen, et al., "VLCAD deficiency: pitfalls in newborn screening and confirmation of diagnosis by mutation analysis," *Molecular Genetics and Metabolism*, vol. 88, no. 2, pp. 166–170, 2006.
- [108] J. D. Hoffman, R. D. Steiner, L. Paradise, et al., "Rhabdomyolysis in the military: recognizing late-onset very long-chain acyl Co-A dehydrogenase deficiency," *Military Medicine*, vol. 171, no. 7, pp. 657–658, 2006.
- [109] B. Merinero, S. I. Pascual Pascual, C. Pérez-Cerdá, et al., "Adolescent myopathic presentation in two sisters with very long-chain acyl-CoA dehydrogenase deficiency," *Journal of Inherited Metabolic Disease*, vol. 22, no. 7, pp. 802–810, 1999.
- [110] C. Minetti, B. Garavaglia, M. Bado, et al., "Very-long-chain acyl-coenzyme A dehydrogenase deficiency in a child with recurrent myoglobinuria," *Neuromuscular Disorders*, vol. 8, no. 1, pp. 3–6, 1998.
- [111] I. Ogilvie, M. Pourfarzam, S. Jackson, C. Stockdale, K. Bartlett, and D. M. Turnbull, "Very long-chain acyl coenzyme A dehydrogenase deficiency presenting with exercise-induced myoglobinuria," *Neurology*, vol. 44, no. 3, part 1, pp. 467–473, 1994.
- [112] R. Pons, P. Cavadini, S. Baratta, et al., "Clinical and molecular heterogeneity in very-long-chain acyl-coenzyme A dehydrogenase deficiency," *Pediatric Neurology*, vol. 22, no. 2, pp. 98–105, 2000.
- [113] H. R. Scholte, R. N. A. Van Coster, P. C. De Jonge, et al., "Myopathy in very-long-chain acyl-CoA dehydrogenase deficiency: clinical and biochemical differences with the fatal cardiac phenotype," *Neuromuscular Disorders*, vol. 9, no. 5, pp. 313–319, 1999.
- [114] A. H. M. Smelt, B. J. H. M. Poorthuis, W. Onkenhout, et al., "Very long chain acyl-coenzyme A dehydrogenase deficiency with adult onset," *Annals of Neurology*, vol. 43, no. 4, pp. 540–544, 1998.
- [115] N. C. Voermans, B. G. van Engelen, L. A. Kluijtmans, N. M. Stikkelbroeck, and A. R. Hermus, "Rhabdomyolysis caused by an inherited metabolic disease: very long-chain Acyl-CoA dehydrogenase deficiency," *American Journal of Medicine*, vol. 119, no. 2, pp. 176–179, 2006.
- [116] A. Zia, E. H. Kolodny, and G. M. Pastores, "Very long chain acyl-CoA dehydrogenase deficiency in a pair of mildly affected monozygotic twin sister in their late fifties," *Journal of Inherited Metabolic Disease*, vol. 30, no. 5, p. 817, 2007.
- [117] P. Laforêt, C. Acquaviva-Bourdain, O. Rigal, et al., "Diagnostic assessment and long-term follow-up of 13 patients with Very Long-Chain Acyl-Coenzyme A dehydrogenase (VLCAD) deficiency," *Neuromuscular Disorders*, vol. 19, no. 5, pp. 324–329, 2009.
- [118] F. E. Frerman and S. I. Goodman, "Defects of electron transfer flavoprotein and electron transfer flavoprotein-ubiquinone oxidoreductase: glutaric acidemia type II," in *The Metabolic and Molecular Bases of Inherited Disease*, C. R. Scriver, A. L. Beaudet, W. S. Sly, and D. Valle, Eds., pp. 2357–2365, McGraw-Hill, New York, NY, USA, 8th edition, 2001.
- [119] R. K. J. Olsen, M. Pourfarzam, A. A. M. Morris, et al., "Lipid-storage myopathy and respiratory insufficiency due to ETFQO mutations in a patient with late-onset multiple acyl-CoA dehydrogenation deficiency," *Journal of Inherited Metabolic Disease*, vol. 27, no. 5, pp. 671–678, 2004.
- [120] E. Christensen, S. Kolvraa, and N. Gregersen, "Glutaric aciduria type II: evidence for a defect related to the electron transfer flavoprotein or its dehydrogenase," *Pediatric Research*, vol. 18, no. 7, pp. 663–667, 1984.
- [121] N. Gregersen, B. S. Andresen, C. B. Pedersen, R. K. J. Olsen, T. J. Corydon, and P. Bross, "Mitochondrial fatty acid oxidation defects—remaining challenges," *Journal of Inherited Metabolic Disease*, vol. 31, no. 5, pp. 643–657, 2008.
- [122] R. K. J. Olsen, S. E. Olpin, B. S. Andresen, et al., "ETFDH mutations as a major cause of riboflavin-responsive multiple acyl-CoA dehydrogenation deficiency," *Brain*, vol. 130, no. 8, pp. 2045–2054, 2007.
- [123] B. Wen, T. Dai, W. Li, et al., "Riboflavin-responsive lipid-storage myopathy caused by ETFDH gene mutations," *Journal of Neurology, Neurosurgery and Psychiatry*, vol. 81, no. 2, pp. 231–236, 2010.
- [124] J. Bremer, "Carnitine—metabolism and functions," *Physiological Reviews*, vol. 63, no. 4, pp. 1420–1480, 1983.
- [125] I. Tein, "Carnitine transport: pathophysiology and metabolism of known molecular defects," *Journal of Inherited Metabolic Disease*, vol. 26, no. 2-3, pp. 147–169, 2003.
- [126] P. Rinaldo, C. A. Stanley, B. Y. L. Hsu, L. A. Sanchez, and H. J. Stern, "Sudden neonatal death in carnitine transporter deficiency," *The Journal of Pediatrics*, vol. 131, no. 2, pp. 304–305, 1997.
- [127] C. A. Stanley, S. DeLeeuw, P. M. Coates, et al., "Chronic cardiomyopathy and weakness or acute coma in children with a defect in carnitine uptake," *Annals of Neurology*, vol. 30, no. 5, pp. 709–716, 1991.
- [128] R. Pons and D. C. De Vivo, "Primary and secondary carnitine deficiency syndromes," *Journal of Child Neurology*, vol. 10, supplement 2, pp. S8–S24, 1995.
- [129] I. Tein, D. C. De Vivo, F. Bierman, et al., "Impaired skin fibroblast carnitine uptake in primary systemic carnitine deficiency manifested by childhood carnitine-responsive cardiomyopathy," *Pediatric Research*, vol. 28, no. 3, pp. 247–255, 1990.
- [130] A. M. Lamhonwah, S. E. Olpin, R. J. Pollitt, et al., "Novel OCTN2 mutations: No genotype-phenotype correlations: early carnitine therapy prevents cardiomyopathy," *American Journal of Medical Genetics*, vol. 111, no. 3, pp. 271–284, 2002.

- [131] R. S. Rijlaarsdam, F. J. van Spronsen, M. T. H. E. Bink-Boelkens, et al., "Ventricular fibrillation without overt cardiomyopathy as first presentation of organic cation transporter 2-deficiency in adolescence," *Pacing and Clinical Electrophysiology*, vol. 27, no. 5, pp. 675–676, 2004.
- [132] S. Vielhaber, H. Feistner, J. Weis, et al., "Primary carnitine deficiency: adult onset lipid storage myopathy with a mild clinical course," *Journal of Clinical Neuroscience*, vol. 11, no. 8, pp. 919–924, 2004.
- [133] U. Spiekerkoetter, G. Huener, T. Baykal, et al., "Silent and symptomatic primary carnitine deficiency within the same family due to identical mutations in the organic cation/carnitine transporter OCTN2," *Journal of Inherited Metabolic Disease*, vol. 26, no. 6, pp. 613–615, 2003.
- [134] S. Vijay, A. Patterson, S. Olpin, et al., "Carnitine transporter defect: diagnosis in asymptomatic adult women following analysis of acylcarnitines in their newborn infants," *Journal of Inherited Metabolic Disease*, vol. 29, no. 5, pp. 627–630, 2006.
- [135] Y. Wang, S. H. Korman, J. Ye, et al., "Phenotype and genotype variation in primary carnitine deficiency," *Genetics in Medicine*, vol. 3, no. 6, pp. 387–392, 2001.
- [136] A. M. Das and D. A. Harris, "Control of mitochondrial ATP synthase in heart cells: inactive to active transitions caused by beating or positive inotropic agents," *Cardiovascular Research*, vol. 24, no. 5, pp. 411–417, 1990.
- [137] A. M. Das and D. J. Byrd, "Regulation of the mitochondrial ATP-synthase in skeletal muscle from children—a new diagnostic tool," *Journal of Inherited Metabolic Disease*, vol. 19, no. 2, pp. 137–139, 1996.
- [138] D. G. Nicholls and S. L. Budd, "Mitochondria and neuronal survival," *Physiological Reviews*, vol. 80, no. 1, pp. 315–360, 2000.
- [139] S. Raha and B. H. Robinson, "Mitochondria, oxygen free radicals, and apoptosis," *American Journal of Medical Genetics*, vol. 106, no. 1, pp. 62–70, 2001.
- [140] R. Luft, D. Ikkos, G. Palmieri, L. Ernster, and B. Afzelius, "A case of severe hypermetabolism of nonthyroid origin with a defect in the maintenance of mitochondrial respiratory control: a correlated clinical, biochemical, and morphological study," *The Journal of Clinical Investigation*, vol. 41, no. 9, pp. 1776–1804, 1962.
- [141] L. Ernster and R. Luft, "Further studies on a population of human skeletal muscle mitochondria lacking respiratory control," *Experimental Cell Research*, vol. 32, no. 1, pp. 26–35, 1963.
- [142] F. G. Debray, G. A. Mitchell, P. Allard, B. H. Robinson, J. A. Hanley, and M. Lambert, "Diagnostic accuracy of blood lactate-to-pyruvate molar ratio in the differential diagnosis of congenital lactic acidosis," *Clinical Chemistry*, vol. 53, no. 5, pp. 916–921, 2007.
- [143] B. H. Robinson, D. M. Glerum, W. Chow, R. Petrova-Benedict, R. Lightowers, and R. Capaldi, "The use of skin fibroblast cultures in the detection of respiratory chain defects in patients with lacticacidemia," *Pediatric Research*, vol. 28, no. 5, pp. 549–555, 1990.
- [144] N. Mackay and B. H. Robinson, "Measurement of the ratio of lactate to pyruvate in skin fibroblast cultures," *Methods in Cell Biology*, vol. 80, pp. 173–178, 2007.
- [145] A. M. Das and K. Ullrich, "Dysregulation of the mitochondrial ATP-synthase in respiratory chain defects: first experience," *Journal of Inherited Metabolic Disease*, vol. 21, no. 3, pp. 220–223, 1998.
- [146] A. Abadi, E. I. Glover, R. J. Isfort, et al., "Limb immobilization induces a coordinate down-regulation of mitochondrial and other metabolic pathways in men and women," *PLoS One*, vol. 4, no. 8, Article ID e6518, 2009.
- [147] L.-J. C. Wong, "Comprehensive molecular diagnosis of mitochondrial disorders: qualitative and quantitative approach," *Annals of the New York Academy of Sciences*, vol. 1011, pp. 246–258, 2004.
- [148] L.-J. C. Wong, "Diagnostic challenges of mitochondrial DNA disorders," *Mitochondrion*, vol. 7, no. 1-2, pp. 45–52, 2007.
- [149] C. T. Moraes, S. Shanske, H. J. Tritschler, et al., "mtDNA depletion with variable tissue expression: a novel genetic abnormality in mitochondrial diseases," *American Journal of Human Genetics*, vol. 48, no. 3, pp. 492–501, 1991.
- [150] W. Sperl, D. Skladal, E. Gnaiger, et al., "High resolution respirometry of permeabilized skeletal muscle fibers in the diagnosis of neuromuscular disorders," *Molecular and Cellular Biochemistry*, vol. 174, no. 1-2, pp. 71–78, 1997.
- [151] S. Vielhaber, A. Kudin, R. Schröder, C. E. Elger, and W. S. Kunz, "Muscle fibres: applications for the study of the metabolic consequences of enzyme deficiencies in skeletal muscle," *Biochemical Society Transactions*, vol. 28, no. 2, pp. 159–164, 2000.
- [152] J. M. Cameron, V. Levandovskiy, N. MacKay, et al., "Identification of a novel mutation in GYS1 (muscle-specific glycogen synthase) resulting in sudden cardiac death, that is diagnosable from skin fibroblasts," *Molecular Genetics and Metabolism*, vol. 98, no. 4, pp. 378–382, 2009.
- [153] M. E. McCue, S. J. Valberg, M. B. Miller, et al., "Glycogen synthase (GYS1) mutation causes a novel skeletal muscle glycogenosis," *Genomics*, vol. 91, no. 5, pp. 458–466, 2008.
- [154] W. I. M. Wuyts, E. Reyniers, C. Ceuterick, K. Storm, T. De Barys, and J. J. Martin, "Myopathy and phosphorylase kinase deficiency caused by a mutation in the PHKA1 gene," *American Journal of Medical Genetics*, vol. 133, no. 1, pp. 82–84, 2005.
- [155] M. C. Ørngreen, H. J. Schelhaas, T. D. Jeppesen, et al., "Is muscle glycogenolysis impaired in X-linked phosphorylase b kinase deficiency?" *Neurology*, vol. 70, no. 20, pp. 1876–1882, 2008.
- [156] B. T. Poll-The, J. Aicardi, R. Girot, and R. Rosa, "Neurological findings in triosephosphate isomerase deficiency," *Annals of Neurology*, vol. 17, no. 5, pp. 439–443, 1985.
- [157] R. Spiegel, E. A. Gomez, H. O. Akman, S. Krishna, Y. Horovitz, and S. DiMauro, "Myopathic form of phosphoglycerate kinase (PGK) deficiency: a new case and pathogenic considerations," *Neuromuscular Disorders*, vol. 19, no. 3, pp. 207–211, 2009.
- [158] S. J. Oh, K. S. Park, H. F. Ryan, et al., "Exercise-induced cramp, myoglobinuria, and tubular aggregates in phosphoglycerate mutase deficiency," *Muscle and Nerve*, vol. 34, no. 5, pp. 572–576, 2006.
- [159] G. P. Comi, F. Fortunato, S. Lucchiari, et al., "β-enolase deficiency, a new metabolic myopathy of distal glycolysis," *Annals of Neurology*, vol. 50, no. 2, pp. 202–207, 2001.
- [160] T. E. Nelson, "Malignant hyperthermia: a pharmacogenetic disease of Ca regulating proteins," *Current Molecular Medicine*, vol. 2, no. 4, pp. 347–369, 2002.
- [161] M. Steinfath, F. Wappler, and J. Scholz, "Malignant hyperthermia. General, clinical and experimental aspects," *Der Anaesthetist*, vol. 51, no. 4, pp. 328–345, 2002.
- [162] H. Rosenberg, M. Davis, D. James, N. Pollock, and K. Stowell, "Malignant hyperthermia," *Orphanet Journal of Rare Diseases*, vol. 2, article 21, 2007.
- [163] G. D. Vladutiu, K. Hogan, I. Saponara, L. Tassini, and J. Conroy, "Carnitine palmitoyl transferase deficiency in

- malignant hyperthermia," *Muscle and Nerve*, vol. 16, no. 5, pp. 485–491, 1993.
- [164] A. K. W. Brownell, "Malignant hyperthermia: relationship to other diseases," *British Journal of Anaesthesia*, vol. 60, no. 3, pp. 303–308, 1988.
- [165] E. W. S. Cheam and L. A. H. Critchley, "Anesthesia for a child with complex I respiratory chain enzyme deficiency," *Journal of Clinical Anesthesia*, vol. 10, no. 6, pp. 524–527, 1998.
- [166] J. Benca and K. Hogan, "Malignant hyperthermia, coexisting disorders, and enzymopathies: risks and management options," *Anesthesia and Analgesia*, vol. 109, no. 4, pp. 1049–1053, 2009.
- [167] G. M. Hall, S. J. Kirtland, and H. Baum, "The inhibition of mitochondrial respiration by inhalational anaesthetic agents," *British Journal of Anaesthesia*, vol. 45, no. 10, pp. 1005–1009, 1973.
- [168] G. G. Duthie and J. R. Arthur, "Free radicals and calcium homeostasis: relevance to malignant hyperthermia?" *Free Radical Biology and Medicine*, vol. 14, no. 4, pp. 435–442, 1993.
- [169] J. Rahbek, B. Werge, A. Madsen, J. Marquardt, B. F. Steffensen, and J. Jeppesen, "Adult life with Duchenne muscular dystrophy: observations among an emerging and unforeseen patient population," *Pediatric Rehabilitation*, vol. 8, no. 1, pp. 17–28, 2005.
- [170] E.-M. Strehle, "Long-term management of children with neuromuscular disorders," *Jornal de Pediatria*, vol. 85, no. 5, pp. 379–384, 2009.

Research Article

Extracorporeal Immunoglobulin Elimination for the Treatment of Severe Myasthenia Gravis

M. Blaha,¹ J. Pit'ha,² V. Blaha,³ M. Lanska,¹ J. Maly,¹ S. Filip,⁴ and H. Langrova⁵

¹2nd Department of Internal Medicine, Hematology, Faculty of Medicine and Teaching Hospital, Charles University, 500 05 Hradec Králové, Czech Republic

²Department of Neurology, 1st Faculty of Medicine and General Teaching Hospital, Charles University, 120 00 Prague, Czech Republic

³Department of Metabolic Care and Gerontology, Faculty of Medicine and Teaching Hospital, Charles University, 500 05 Hradec Králové, Czech Republic

⁴Department of Radiotherapy and Oncology, Faculty of Medicine and Teaching Hospital, Charles University, 500 05 Hradec Králové, Czech Republic

⁵Department of Ophthalmology, Faculty of Medicine and Teaching Hospital, Charles University, 500 05 Hradec Králové, Czech Republic

Correspondence should be addressed to M. Blaha, blaham@email.cz

Received 1 December 2009; Accepted 17 January 2010

Academic Editor: Guy M. Benian

Copyright © 2010 M. Blaha et al. This is an open access article distributed under the Creative Commons Attribution License, which permits unrestricted use, distribution, and reproduction in any medium, provided the original work is properly cited.

Myasthenia gravis (MG) is a neuromuscular disorder leading to fluctuating muscle weakness and fatigue. Rarely, long-term stabilization is not possible through the use of thymectomy or any known drug therapy. We present our experience with extracorporeal immunoglobulin (Ig) elimination by immunoadsorption (adsorbers with human Ig antibodies). Acetylcholine receptor antibodies (AChRAs) were measured during long-term monitoring (4.7 ± 2.9 years; range 1.1–8.0). A total of 474 samples (232 pairs) were analyzed, and a drop in AChRA levels was observed ($P = .025$). The clinical status of patients improved and stabilized. Roughly 6.8% of patients experienced clinically irrelevant side effects. The method of Ig elimination by extracorporeal immunoadsorption (IA) is a clinical application of the recent biotechnological advances. It offers an effective and safe therapy for severe MG even when the disease is resistant to standard therapy.

1. Introduction

Myasthenia gravis (MG) is an autoimmune disorder in which weakness is caused by circulating acetylcholine receptor antibodies (AChRAs) or muscle-specific kinase antibodies that block acetylcholine receptors at the postsynaptic neuromuscular junction [1]. MG is treated with cholinesterase inhibitors or immunosuppressive drugs. Surgical removal of the thymus (thymectomy) may result in permanent remission or a reduced need for drug therapy. When myasthenia is serious (myasthenic crisis), plasmapheresis can be used to remove putative antibodies from the circulation. Intravenous immunoglobulins (IVIg) can also be used to bind the circulating antibodies [2–5]. Both of these treatments have relatively short-lived benefits, which are typically measured in weeks [6]. When some patients are unresponsive to

such therapy while on the maximum-tolerated drug doses and sufficient stabilization is not achieved, they may be threatened by repeated myasthenic crises. Removal of the pathogenic agents from the blood may improve the patient's condition in these cases. Due to advances in biomedical technology, adsorbers with specific affinity for immunoglobulin G (IgG) and the pathogenic antiacetylcholine receptor antibody of MG [7] have been developed. In severe MG resistant to other treatments, extracorporeal elimination (EE) of immunoglobulins by immunoadsorption (IA) has been used as either a periodic cure [8] or long-term regular therapy.

In this paper, we review our use of EE of IgGs via adsorbers containing sheep antibodies against human IgG as a long-term therapy for severe MG refractory to standard drug therapy and thymectomy.

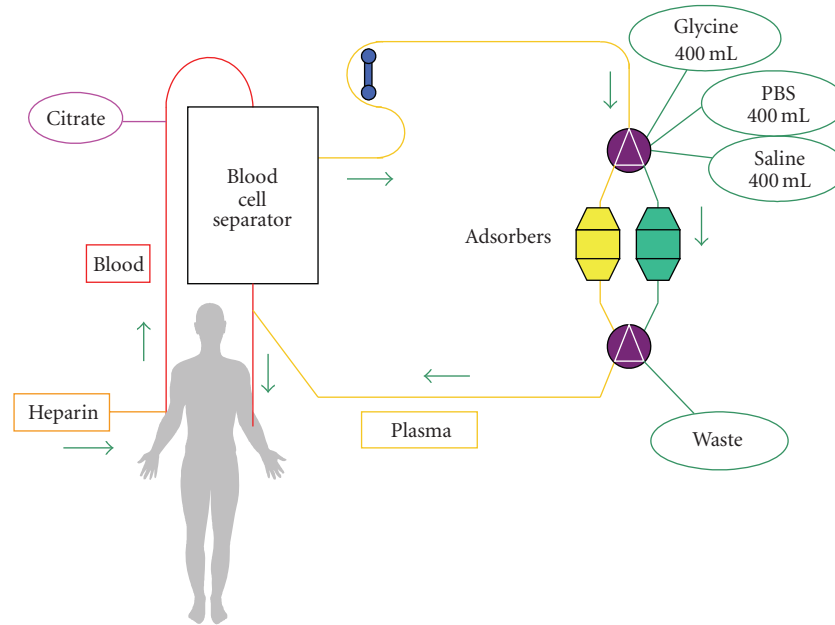


FIGURE 1: Our modification of immunoadsorption (modified by Borberg et al. [9, 10]). Vascular access for the extracorporeal circuit is established via two peripheral veins. Plasma without cellular elements obtained after high-speed centrifugation with a quality separator (Cobe-Spectra, Denver, USA) is drawn through an adsorbent Adasopak capsule. Plasma flow is continuous. After filling the adsorbent capsule, the Adasorb device (Medicap, Ulrichsteinn, Germany) switches automatically to the second adsorbent capsule; the first capsule is washed with glycine, PBS buffer, and saline to prepare it for reuse so the procedure can be repeated as necessary. Regeneration solutions are drained into a waste bag. Clean, washed plasma flows from the column back to the separator where it is mixed with blood elements and returns to the patient's peripheral veins. Anticoagulation is maintained by a continuous supply of citrate solution (ACD-A Baxter, Germany), and it is secured by an initial application of 2500 U heparin i.v., subsequent continuous infusion of 50 U of heparin/min and gradual dose lowering such that heparin application ceases in the middle of immunoadsorption.

2. Patients and Methods

2.1. Extracorporeal Elimination by Immunoadsorption. Here, we describe our own modification of an immunoadsorption method presented by Borberg et al. [9, 10]. The procedure consists of two main steps: (1) separation of plasma by continuous centrifugation in a Cobe-Spectra separator (Cobe, Denver, USA) and (2) subsequent passage of plasma through a pair of Adasopak 200 adsorbents (Pocard, Moscow, Russia) placed in an automatic adsorption-desorption device (Adasorb, Medicap, Ulrichstein, SRN). The device switches between two adsorbent capsules and finally returns plasma back to the patient. As soon as one of the adsorbent capsules is full, the automatic device switches to the second capsule; the first capsule is washed and prepared to be used again. The adsorption cycles are repeated according to the clinical condition of the patient up to ten times.

The Adasopak 200 adsorption column contains 200 mL of antihuman IgG Sepharose 4FF gel (binding capacity of 10–12 mg Ig protein/1 mL of adsorbent) and approximately 85 mL of phosphate buffer (pH 7.4). Polyclonal antibodies against human Ig bound to Sepharose 4FF are prepared from sheep serum immunized by human IgG. Adasopak 200 Ig columns are intended for use in therapeutic Ig apheresis procedures for patients requiring rapid reductions of immunoglobulin concentrations in the plasma. For the therapeutic scheme, see Figure 1.

2.2. Patients. This prospective observational study was conducted at the 2nd Department of Medicine, Hemapheretic Center of Charles University, Faculty of Medicine, Hradec Kralove, Czech Republic. In the Czech Republic, there are two main centers for the treatment of myasthenia gravis. Smaller centers are in other teaching hospitals. Presently, 1916 patients are treated at the Myasthenic Center in Prague. Only six of these patients were in severe condition despite thymectomy and drug therapy (including corticosteroids, immunosuppressive drugs and repeated doses of immunoglobulins) and could not be stabilized for a longer period of time. Therefore, these patients were included in the program of long-term therapy with extracorporeal elimination of immunoglobulins. Basic clinical data are given in Table 1.

All patients were women with a mean age of 46 years (range: 28–65 years). Patients 1 and 2 were successfully weaned off of EE therapy after 13 months and are on long-term immunosuppressive therapy and permanent care at the Myasthenic Center. Patients 3–6 are on long-term EE treatment (mean: 6.5 years, range: 5–8 years). Attempts to reduce therapeutic intensity by weaning off of EE were not successful in these patients. Patients 3 and 5 suffer from other diseases (hypertension, ischemic heart disease, and arthritic symptoms) compensated for by conventional therapy. Patients 5 and 6 experienced attacks of secondary depressive syndrome, and patient 4 attempted to commit

TABLE 1: Basic clinical data. Number of myasthenic crises experienced requiring artificial ventilation: + = 1-2, ++ = 2-5, +++ = more than 5. IA = immunotherapy, Mes: Mestinson, M: Medrol, P: Prednison, CC: CellCept, Pr: Prograf.

Patient no.	Classification (MGFA)	Age	Sex	Myasthen. crises	Therapy duration	Current condition	Current therapy
1	III b	35	F	++	13	Excellent, IA therapy stopped	Mes
2	IV b	33	F	+	13	Stabilization, IA therapy stopped	Mes
3	IV b	65	F	+++	96	Stabilization	Mes, M, CC, IVIG
4	IV b	28	F	+++	76	Stabilization	Mes, P, Pr
5	III b	53	F	+	79	Stabilization	Mes, P, CC, IVIG
6	IV b	60	F	++	62	Stabilization	Mes, P, CC

TABLE 2: AChRA levels. *N* = number of patients. Normal AChRA values in our laboratory: 0.00–0.40 nmol/L.

Patient no.	AChRA before the procedures (ng/L)				AChRA after the procedures (ng/L)			
	<i>N</i>	Mean ± SD	Range	Median	<i>N</i>	Mean ± SD	Range	Median
All	232	12.8 ± 11.4	2.6–99.7	11.2	231	5.46	1.3–57.3	5.5
1	13	51.4 ± 20.9	23.7–99.7	49.6	13	28.0 ± 12.8	13.2–57.3	23.3
2	12	4.8 ± 0.6	4.0–6.0	5.0	12	2.4 ± 0.7	1.6–4.0	2.3
3	43	5.5 ± 1.2	3.5–9.0	5.4	43	2.3 ± 0.5	1.3–3.5	2.4
4	71	11.9 ± 2.2	7.9–19.0	11.4	70	4.4 ± 0.8	2.8–7.1	4.3
5	58	15.3 ± 3.0	11.2–26.0	15.1	58	6.3 ± 1.0	4.8–9.0	6.3
6	35	7.8 ± 2.0	2.6–14.4	7.6	35	2.7 ± 0.4	2.2–4.4	2.6

suicide when in personal crisis. All patients are AChRA-positive. All underwent thymectomy at the beginning of therapy with subsequent irradiation. A thymoma was found in patient 6.

2.3. Ig and AChRA Examination. The levels of IgG, IgA, and IgM were determined using the immunonephelometric method (IMMAGE 800 System, Beckman Coulter, USA). Determination of autoantibodies against the acetylcholine receptor was carried out by radio receptor assay for the in vitro diagnostic quantitative determination of autoantibodies against the acetylcholine receptor in human serum and plasma (IBL International, Hamburg, Germany).

2.4. Statistics. Statistical calculations were performed with SYSTAT 8 software. A standard paired *t*-test (Paired Comparison *t*-Test) was used to evaluate changes before and after the procedures. The dependence of AChRA values on the number of procedures was calculated by linear regression (Simple Linear Regression). Differences were considered statistically significant when $P \leq .05$.

3. Results

3.1. AChRA Levels. To investigate AChRA levels, a total of 464 samples were collected (232 paired examinations). Because one measurement was defective, levels in 463 samples were measured. The results are presented in Table 2. The first line summarizes the results for all patients, and the remaining six lines present evaluations of individual patients. After the procedures, the drop in AChRA levels was 57% on

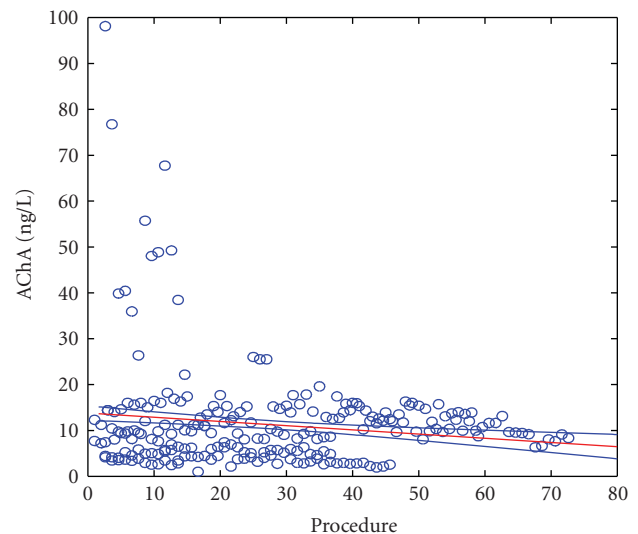


FIGURE 2: AChRA levels—all examinations. Y axis = AChRA level in ng/L; X axis: Procedure = numeral order of procedures from the start of therapy.

an average; a paired *t*-test revealed a significance value of $P < .0001$.

Linear correlation analysis showed that a gradual decrease in AChRA levels occurred after repeated procedures ($P = .025$) (Figure 2).

However, an evaluation of individual patients by linear regression showed that an important drop of AChRA levels ($P \leq .05$) was found only in patients 1, 2, and 3. In other

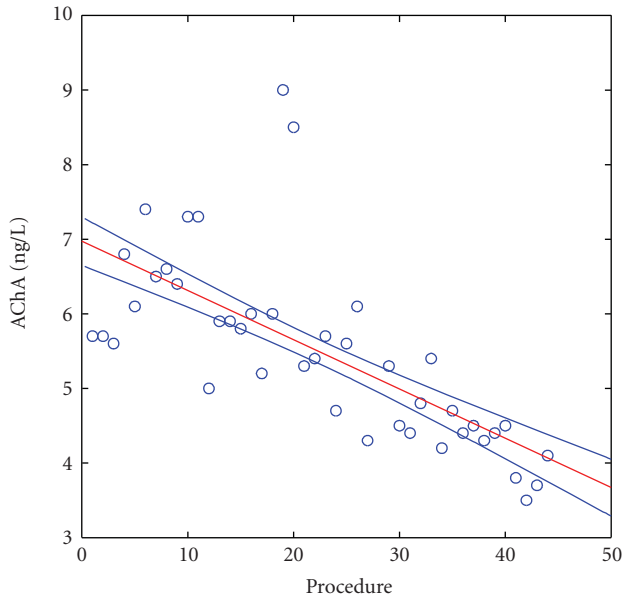


FIGURE 3: AChRA levels in patient no. 3. X axis: Procedure = numeral order of procedures from the start of therapy; Y axis = AChRA levels in ng/L. Normal value in our laboratory = 0.00–0.40 nmol/L.

patients, AChRA levels did not significantly change. As a positive example ($P \leq .0001$), we present patient 3 (see Figure 3). In this patient, a gradual decrease in AChRA levels occurred during long-term therapy (i.e., a level of 7.1 ng/L was measured before the first IA, and the last measurement three years later (September 5, 2009) was 4.1 ng/L). During these three years, the patient's condition was relatively stable without myasthenic crisis requiring artificial ventilation. (Figures 2 and 3, X axis: Procedures = numerical order of procedures from the start of therapy.)

In the rest of the patients, no gradual drop in AChRA levels was observed. Levels at the start of the therapy did not differ in a statistically significant manner from either those further in the course of illness or the last three values.

3.2. Immunoglobulins. Ig levels were examined in all patients regularly at the same time as AChRA levels. Table 3 shows that the levels of all three Ig classes significantly decreased after the procedures. This was most obvious for IgG (53.9% decrease) but was also true for IgM (42.5% decrease) and IgA (44.7% decrease). Correlation analysis did not find any dependence between the drop in Ig levels and AChRA levels.

3.3. Adverse Effects. IA is a kind of extracorporeal circulation that brings certain risks. However, the modifications presented here allowed it to be a safe and technically feasible method. Only 6.8% of patients in the 232 procedures experienced side effects, and none of these were life-threatening. Patient 3 once experienced aspiration of excreta during a cough attack and was treated with a short observation and bed rest. Vasovagal events (symptoms of

neurovegetative lability) were the most common adverse effects manifested as malaise, weakness, slight and short-term drop of blood pressure, or other general signs. All were well controlled by symptomatic therapy (Trendelenburg's position, cessation of the procedure and eventual quick dropping of saline). These reactions were under control in some tens of seconds or a few minutes at maximum. An ECG showed sinus bradycardia under a level of 50/min (46 and 48/min) in two cases. This event occurred in patient 6, but observation and short bed rest provided sufficient treatment.

4. Discussion

Myasthenia gravis is a rather rare neuromuscular disease of autoimmune origin. However, its course can be severe or even life-threatening. The annual incidence is from 2 to 4 million cases [11]. Most MG patients can be stabilized for a long time with either thymectomy or the application of symptomatic drugs, corticoids, immunosuppressives, immunoglobulins, or monoclonal agents. Myasthenic crises are mostly resolved by plasma exchange. This therapy is used in the few patients that are difficult to stabilize by any kind of drug therapy. Advances in biotechnology bring new knowledge and new methods that can be used in many branches of medicine [12–16]. One such advance is extracorporeal therapy, which can be either nonspecific (such as plasma exchange) or specific (such as IA). This type of procedure can constitute an important and sometimes decisive component of MG therapy. IA with regard to medical, technical, and economic demands is indicated in cases when classical methods fail. We attempted to manage this situation by extracorporeal elimination of AChRAs present in the IgG fraction. This was possible by the development of adsorbers that retain the clinically significant Ig component from extracorporeal plasma circulation. Adsopak adsorbers were used. These adsorbers contain antihuman IgG antibodies with a binding capacity of about 10 mg Ig protein per 1 mL of adsorbent. This capacity was sufficient to reduce AChRA levels by an average of 58% after the procedures.

The patients had different initial AChRA levels that did not correlate with the clinical activity of the disease [17] (Table 2). In all patients, AChRA levels significantly decreased (by about 57.7% on average) after the procedures ($P < .0001$). With regard to the clinical effect of therapy, the best result was observed in patient 1. This patient is now maintained on a small dose of pyridostigmin. She has born a healthy child and enjoys a happy family life without physical limitations. Presently, she does not experience any muscular weakness. Similarly, patient 2 was weaned off the IA program after 13 months after stabilization and clinical improvement. This patient is now on symptomatic medication but experiences residual weakness of the oropharyngeal muscles of small functional significance. Patients 3–6 are still under a periodic EE regime. Attempts to wean them off of treatment were not successful. In patient 4, procedures are repeated at 4-week intervals. In patients 4 and 5, the procedures are performed

TABLE 3: Immunoglobulins. N: number of patients, SD: standard deviation.

Level (g/L)	Before immunoapheresis					After immunoapheresis					P
	N	Average	SD	Range	Median	N	Average	SD	Range	Median	
IgG	240	7.93788	2.41842	1.59–14.2	7.25	239	3.65904	1.80996	1.51–12.3	3.21	.000000
IgM	240	0.94921	0.32584	0.18–2.01	0.955	239	0.54782	0.2622	0.15–1.51	0.54	.000000
IgA	240	2.32754	1.02688	0.24–4.51	2.44	239	1.28661	0.70743	0.23–4.07	1.22	.000000

at 3-week intervals. Patient 4 attempted to change to 4-week intervals after 23 months of EE but shortly thereafter had to return to 3-week intervals again. In patient 5, the IA program was initiated at 3-week intervals; after six months, 4-week intervals became sufficient. Patients 3 and 5 are on a periodic regime of EE followed by an IVIG dose performed during their last year of therapy. This therapy is sufficient for long-term stabilization. However, the clinical condition of patient 5 worsened during an attempt to wean off IVIG that led to a significant increase of AChAR levels; therefore, the IA regime has been continued.

It is well known that MG is more frequent in younger women and older men [18, 19]. Our group comprised only women. Due to the small number of patients in our group, this bias was due to mere chance.

We monitored the basic parameters of clinical status (blood pressure, pulse and breath frequency) in all of our patients. As IA is one method of extracorporeal circulation, all basic hematologic and biochemical parameters (blood count, minerals, creatinin, glycemia and total protein, albumin, bilirubin, aminotransferase, and lipoprotein levels; data not shown) were regularly monitored. The results showed that clinically significant changes did not occur.

The drop in Ig after immunoaphereses was significant, but Ig levels returned to their initial values in the time before the next procedure. The drop in Ig levels might lead to increased susceptibility to infections, but we did not observe such susceptibility. Furthermore, we did not find in the literature data or reports describing higher infection rates after immunoapheresis for MG [18] or immunoaphereses performed for other indications (e.g., LDL-apheresis in familial hypercholesterolemia) [9].

5. Conclusion

The IA method presented here utilizes current results and recent advances in biotechnology and is indicated in severe cases of MG when longer-term stabilization cannot be achieved by another means. The levels of AChRA are significantly lower after the procedures. Reduction of AChRA levels can also be observed when patients are evaluated chronologically (i.e., the levels were higher at the beginning of follow-up than at the end of monitoring). This method is medically, technically, and economically demanding. However, it offers a clinically effective method by which to improve or stabilize patients with severe MG, even when the disease is resistant to all standard therapies. In the long run, this method protects patients against myasthenic crises, and it is safe with a low occurrence of side-effects.

Acknowledgment

The work was supported by a grant from the Internal Grant Agency, Ministry of Health, Czech Republic, no. NS/9743-4.

References

- [1] B. M. Conti-Fine, M. Milani, and H. J. Kaminski, "Myasthenia gravis: past, present, and future," *Journal of Clinical Investigation*, vol. 116, no. 11, pp. 2843–2854, 2006.
- [2] J. Díaz-Manera, R. Rojas-García, and I. Illa, "Treatment strategies for myasthenia gravis," *Expert Opinion on Pharmacotherapy*, vol. 10, no. 8, pp. 1329–1342, 2009.
- [3] R. Gold and C. Schneider-Gold, "Current and future standards in treatment of myasthenia gravis," *Neurotherapeutics*, vol. 5, no. 4, pp. 535–541, 2008.
- [4] R. Manfredi, G. Fasulo, C. Fulgaro, and S. Sabbatani, "Associated thyroiditis, myasthenia gravis, thymectomy, Chron's disease, and erythema nodosum: pathogenetic and clinical correlations, immune system involvement, and systemic infectious complications," *Rheumatology International*, vol. 28, no. 11, pp. 1173–1175, 2008.
- [5] H. Borberg, C. Jimenez, M. Belák, W. F. Haupt, and P. Späth, "Treatment of autoimmune disease by immunomodulation through extracorporeal elimination and intravenous immunoglobulin," *Transfusion Science*, vol. 15, no. 4, pp. 409–418, 1994.
- [6] C. J. Symonette, B. V. Watson, W. J. Koopman, M. W. Nicolle, and T. J. Doherty, "Muscle strength and fatigue in patients with generalized myasthenia gravis," *Muscle & Nerve*, vol. 41, no. 3, pp. 362–9, 2010.
- [7] S. Nakaji and N. Hayashi, "Adsorption column for myasthenia gravis treatment: medisorba MG-50," *Therapeutic Apheresis and Dialysis*, vol. 7, no. 1, pp. 78–84, 2003.
- [8] N. I. Triantafyllou, E. I. Grapsa, E. Kararizou, E. Psimenou, A. Lagouranis, and A. Dimopoulos, "Periodic therapeutic plasma exchange in patients with moderate to severe chronic myasthenia gravis non-responsive to immunosuppressive agents: an eight year follow-up," *Therapeutic Apheresis and Dialysis*, vol. 13, no. 3, pp. 174–178, 2009.
- [9] H. Borberg, "28 years of LDL-apheresis: a review of experience," *Transfusion and Apheresis Science*, vol. 41, no. 1, pp. 49–59, 2009.
- [10] H. Borberg, R. Brunner, M. Tauchert, and R. Widder, "The current state of extracorporeal haemorrhotherapy: from haemodilution via cascadefiltration to rheohaemapheresis," *Transfusion and Apheresis Science*, vol. 24, no. 1, pp. 57–64, 2001.
- [11] F. Romi, N. E. Gilhus, and J. A. Aarli, "Myasthenia gravis: clinical, immunological, and therapeutic advances," *Acta Neurologica Scandinavica*, vol. 111, no. 2, pp. 134–141, 2005.

- [12] R. D. Sleator and C. Hill, "Rational design of improved pharmabiotics," *Journal of Biomedicine and Biotechnology*, vol. 2009, Article ID 275287, 7 pages, 2009.
- [13] L.-H. Zhang, L. Y. Wu, S. Zhang, et al., "Anti-hepatitis B virus X protein in sera is one of the markers of development of liver cirrhosis and liver cancer mediated by HBV," *Journal of Biomedicine and Biotechnology*, vol. 2009, Article ID 289068, 6 pages, 2009.
- [14] S. Karray-Chouayekh, F. Trifa, and A. Khabir, "Clinical significance of epigenetic inactivation of hMLH1 and BRCA1 in tunisian patients with invasive breast carcinoma," *Journal of Biomedicine and Biotechnology*, vol. 2009, Article ID 369129, 7 pages, 2009.
- [15] M. Iga, J. H. P. Robertson, M. C. Winslet, and A. M. Seifalian, "Clinical potential of quantum dots," *Journal of Biomedicine and Biotechnology*, vol. 2007, Article ID 76087, 10 pages, 2007.
- [16] A. El Andaloussi and C. Bilhou-Nabera, "New complex chromosomal translocation in chronic myeloid leukaemia: T(9;18;22)(q34;p11;q11)," *Journal of Biomedicine and Biotechnology*, vol. 2007, Article ID 92385, 3 pages, 2007.
- [17] M. N. Meriglioli and D. B. Sanders, "Autoimmune myasthenia gravis: emerging clinical and biological heterogeneity," *The Lancet Neurology*, vol. 8, no. 5, pp. 475–490, 2009.
- [18] J. F. Howard Jr., *Myasthenia Gravis: A Manual for the Health Care Provider*, Myasthenia Gravis Foundation of America, St. Paul, Minn, USA, 2008.
- [19] L. M. Chiang, B. T. Darras, and P. B. Kang, "Juvenile myasthenia gravis," *Muscle & Nerve*, vol. 39, no. 4, pp. 423–431, 2009.

Research Article

Combining Microdialysis and Near-Infrared Spectroscopy for Studying Effects of Low-Load Repetitive Work on the Intramuscular Chemistry in Trapezius Myalgia

Gerd M. Flodgren,^{1,2,3} Albert G. Crenshaw,¹ Fredrik Hellström,¹ and Martin Fahlström⁴

¹ Centre for Musculoskeletal Research, University of Gävle, P.O. Box 7629, S-907 12 Umeå, Sweden

² Department of Surgical and Perioperative Sciences, Sports Medicine Unit, Umeå University, S-901 87 Umeå, Sweden

³ Institute of Health and Society, Medical Faculty Baddiley-Clark building, Newcastle University, Richardson Road, Newcastle Upon Tyne, NE2 4AX, UK

⁴ Department of Community Medicine and Rehabilitation, Rehabilitation Medicine, Umeå University, S-901 87 Umeå, Sweden

Correspondence should be addressed to Gerd M. Flodgren, gerd.flodgren@ncl.ac.uk

Received 1 February 2010; Revised 31 March 2010; Accepted 31 March 2010

Academic Editor: Guy M. Benian

Copyright © 2010 Gerd M. Flodgren et al. This is an open access article distributed under the Creative Commons Attribution License, which permits unrestricted use, distribution, and reproduction in any medium, provided the original work is properly cited.

Epidemiological research provides strong evidence for a link between repetitive work (RW) and the development of chronic trapezius myalgia (TM). The aims were to further elucidate if an accumulation of sensitising substances or impaired oxygenation is evident in painful muscles during RW. Females with TM ($n = 14$) were studied during rest, 30 minutes RW and 60 minutes recovery. Microdialysate samples were obtained to determine changes in intramuscular microdialysate (IMMD) [glutamate], [PGE₂], [lactate], and [pyruvate] (i.e., [concentration]) relative to work. Muscle oxygenation (%StO₂) was assessed using near-infrared spectroscopy. During work, all investigated substances, except PGE₂, increased significantly: [glutamate] (54%, $P < .0001$), [lactate] (26%, $P < .005$), [pyruvate] (19%, $P < .0001$), while the %StO₂ decreased ($P < .05$). During recovery [PGE₂] decreased ($P < .005$), [lactate] remained increased ($P < .001$), [pyruvate] increased progressively ($P < .0001$), and %StO₂ had returned to baseline. Changes in substance concentrations and oxygenation in response to work indicate normal increase in metabolism but no ongoing inflammation in subjects with TM.

1. Introduction

Epidemiological research provides strong evidence for a link between repetitive work and the development of chronic muscle pain [1–3], but to fully understand this relationship, the pathophysiological mechanisms behind it needs further elucidating. Several hypotheses that focus on hypoxia or other metabolic effects in the muscle have been suggested [4–6].

While the muscle biopsy technique have only been able to provide a “snap-shot” of the muscle chemistry [7, 8], the possibilities for real-time in vivo investigations have been greatly improved by combining microdialysis and near-infrared spectroscopy [9, 10].

Microdialysis (MD) permits in vivo measurements of changes in substance concentrations in different tissues

in response to work, with minimal trauma [11]. MD is performed by implanting a probe with a semipermeable membrane in the tissue and slowly perfuses it with a physiological solution. Sample collection is based on passive diffusion of substances over the membrane, preferable during steady-state conditions.

We have previously reported significantly increased [lactate] and [glutamate] and unchanged [prostaglandin E₂, PGE₂] in the trapezius muscle of healthy females, in response to low-load repetitive work (RW) which we interpreted as normal responses to increased physical demands [9]. We have also reported similar absolute [glutamate] and [PGE₂] in females with trapezius myalgia (TM) and asymptomatic controls during rest [12]. Few other studies have used MD to further elucidate the pathophysiology behind work-related trapezius myalgia, and to some extent the findings

are conflicting. In a laboratory study Rosendal et al. [13] reported increased intramuscular [lactate] and [glutamate] in response to RW in TM, but not in healthy controls, findings which they were unable to verify in an occupational field study [14]. However, the pain subjects differed in severity of symptoms between studies. Ashina et al. [15] reported similar [glutamate] and [PGE₂] in trapezius muscle tender points in response to low-load static work in subjects with chronic tension type headache (CTTH).

Near-infrared spectroscopy (NIRS) is a noninvasive method for measuring muscle oxygenation (% StO₂), that is, the dynamic balance between oxygen delivery to and consumption within a tissue [16, 17]. The technique is based on the principle of differential absorption properties of oxygenated and deoxygenated forms of haemoglobin (and to a lesser extent, myoglobin) in the near infrared range (760–850 nm). NIRS is well suited to study the muscle microcirculation due to the minimal absorption of light in small vessels (i.e., arterioles, capillaries, and venules) compared to in veins and feed arteries [16, 17]. We have previously combined MD and NIRS to study the effects of RW of different duration [9] and RW with superimposed mental load [10] on % StO₂ in the pain-free trapezius muscle. We found small changes in % StO₂ and intramuscular lactate, indicative of a normal response to increased physical demands [9]. In one recent study no statistically significant differences for oxygenated haemoglobin during RW were reported between TM and healthy controls [18].

The aims of this study, which was purposely designed as a comparison to our previous study on asymptomatic females [9], were to investigate whether an interstitial accumulation of sensitising substances (glutamate, PGE₂), or local metabolic changes indicative of an insufficient oxygen supply (e.g., greatly increased [lactate] and decreased % StO₂) is evident during RW in subjects with TM ($n = 14$). We also wanted to investigate how % StO₂, blood lactate, and intramuscular [lactate] relate during RW in TM.

2. Materials and Methods

2.1. Participants. Fourteen females with trapezius myalgia (TM) participated in the study. The group had a mean age of 40 (± 8) years, height 167 (± 4) cm, weight 66 (± 9.5) kg, and BMI 23.0 (± 2.3). The pain subjects were matched in age to a group of healthy asymptomatic females, who had participated in a previous study at our laboratory, and in which the same experimental protocol was used [9], to admit comparisons to be made.

Participants were required to be right-handed, nonsmokers, and not allergic to local anaesthesia. Further inclusion criteria were as follows: during the clinical examination subjects were required to (i) report pain of a duration of at least 3 months from the neck-shoulder region, (ii) verify pain in the upper part of the trapezius muscle with a pain drawing, (iii) have the most pronounced complaints on the side subjected to the greatest workload, and (iv) have reason to believe that the pain was caused by their work, that is, that they reported that the onset of their pain problems coincided with performance of static and/or repetitive work tasks. Also,

that they reported less pain when being off work, and/or increased pain when coming back to work after a holiday.

All participants were examined by the same physiotherapist. Exclusion criteria were (a) previous trauma to the neck or shoulder, (b) signs of shoulder tendonitis or shoulder joint affection, (c) signs of nerve affection, (d) pronounced pain from more than three body regions, and (e) neurological or metabolic diseases, or (f) other diseases that demanded continuous medication.

The Nordic Ministry Council Questionnaire (NMCQ) [19] and the visual analogue scale (VAS) were used to survey pain during the last 12 months and at the time of participation. All participants reported pain from the neck-shoulder area during the last 7 days. The median (range) for the VAS-ratings of perceived pain in the right shoulder were 47 (12–79) for the last 12 months, 34 (14–63) for the last 7 days, and 27 (4–78) when arriving at the laboratory. The mean (\pm SD) duration of complaints from the neck-shoulder was 70.5 (± 74.7) months. None of the subjects were on sick-leave at the time of the study.

The participants were recruited through contacts with local industries and through advertisement on the university hospital's intranet. The participants either worked at an assembly line (in a car factory) or at a VDU-station, thus performing work tasks of a repetitive and static character. All participants gave their informed and signed consent prior to inclusion in the study. The study conformed to the ethical standards laid down in the 1964 Declaration of Helsinki and was approved by the Ethical Committee of the Medical Faculty of the University of Umeå (*Dnr 2004:M-150*).

2.2. Methods

2.2.1. Experimental Protocol. The experimental design is shown in Figure 1. The experimental conditions were exactly the same as in the previous study on asymptomatic control subjects [9] (same experimental protocol, same laboratory room and equipment, same controlled room temperature, all probe insertions were performed by the same medical doctor, and all analyses were performed by the same laboratory technicians). In addition to the previous protocol, the participants perceived pain intensity were also assessed. All experiments started at 7 a.m. The subjects were instructed not to perform any kind of heavy physical exercise 48 hours prior to the experiment, and to arrive fasting to the laboratory where they were given a standardised breakfast. They were also asked to refrain from using pain medication (NSAIDs) three days before the experiment to avoid interference with the pain substances under study, but also due to the increased risk of bleeding during the procedure (paracetamol was allowed). In the preparation period, before the MD-probe was inserted and the optical probe for oxygen saturation measurements was attached to the skin, measurements of skin-fat layer (SFL) and trapezius muscle thickness over the approximate site of the O₂-probe were performed using ultrasonography [9, 10]. Subjects then rested comfortably seated for a total of 120 minutes (90 minutes stabilisation + 30 minutes baseline) before the 30 minutes work-period began.

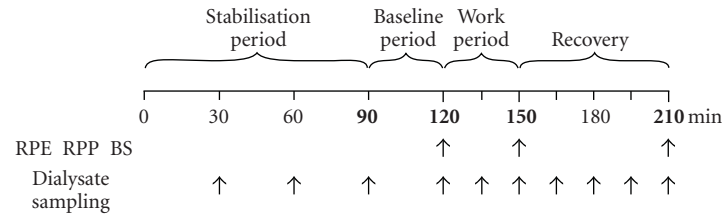


FIGURE 1: Experimental design. Schematic of the experimental design with 90 minutes stabilisation period, 30 minutes baseline, 30 minutes work, and a 60 minutes recovery period. Arrows indicate time points for sampling of dialysate, assessment of perceived exertion with the Borg CR-scale (RPE), assessment of perceived pain intensity with VAS (RPP), and capillary blood sampling (BS).

The repetitive low-load work, also used by Flodgren et al. [9, 10], was designed to simulate an occupational work task. It consisted in alternatively pushing in a piston and pressing down a button with the use of a handheld manipulandum (130 grams), while seated at a table. The subjects maintained a pace of 30 work cycles per minute, with the aid of a metronome; a single piston push followed by a button press constituting one work cycle. The workstation was adjusted to each subject to provide optimal ergonomic conditions (Figure 2). In a pilot study (unpublished data) we used electromyography to assess the trapezius muscle activity during the same type of work. We then found the mean electrical activity to be 9.3% of maximal voluntary contraction, which is similar to muscle activity measured during low-load RW at a real work place [20].

After the performance of the repetitive work subjects rested, comfortably seated, for yet another 60 minutes (see Figure 1). All subjects completed the work task. Throughout the experiment local % StO₂ was recorded, microdialysate samples and capillary blood for lactate analyses were obtained, subjectively perceived exertion (Borg CR-10) and perceived pain intensity (VAS) were assessed, as shown in Figure 1. The room temperature was between 22 and 24 degrees Celsius during experiments.

2.2.2. Microdialysis. After local anaesthesia of the skin and subcutaneous tissue by injection of 1.5 mL Xylocain (10 mg mL⁻¹), a microdialysis probe (CMA 60, CMA/Microdialysis AB, Sweden, 20 kDa molecular cut-off, membrane length 30 mm, 0.5 mm outer diameter) was implanted in the middle third of the upper part of the trapezius muscle in the direction lateral to medial. The same investigator performed all probe insertions, and ultrasonography was used to confirm the placement of the probe (Aloka SSD-2000, Aloka Co., Ltd., Japan). The catheter was secured to the skin with adhesives, connected to a portable syringe pump (CMA 107, CMA/Microdialysis, AB, Sweden), and perfused with solution containing 147 mM L⁻¹ Na⁺, 4 mM L⁻¹ K⁺, 2.3 mM L⁻¹ Ca²⁺, and 156 mM L⁻¹ Cl⁻ (perfusion fluid T1, CMA/Microdialysis AB, Stockholm, Sweden), at a flow rate of 2 μL min⁻¹. The pump was secured in level with the probe. After insertion of the probe in the muscle, the subjects rested for 90 minutes to allow the tissue to stabilise after the initial trauma of probe insertion [11, 12, 21]. Samples were obtained every 30th minute during the initial two hours of

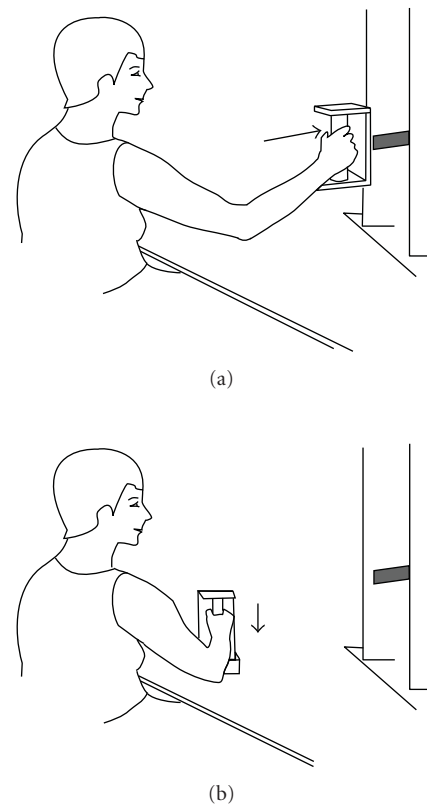


FIGURE 2: Repetitive work model. The low-load repetitive work consisted of (a) pushing in a piston and (b) pressing down a button on the table with a handheld manipulandum, at a pace of 30 work cycles per minute.

rest, and every 15th minute during work and recovery. The last sample obtained during rest will be referred to as baseline. All probes kept functioning throughout the experiment. The samples were immediately frozen to -70° until analyses were performed. All samples were coded by the authors and analysed blindly by an independent laboratory technician. Lactate, glutamate and pyruvate were analysed with the CMA 600 Microdialysis Analyser (CMA Microdialysis, Solna, Sweden), and PGE₂ with a radioimmunoassay kit (NEN, Du Pont, Boston, Mass, USA). The detection limits are 0.1 mmol × L⁻¹ for lactate, 10 μmol × L⁻¹ for pyruvate and 1 μmol × L⁻¹ for glutamate. The detection limit for the PGE₂ assay is 0.5 pg mL⁻¹.

2.2.3. Oxygen Saturation (% StO₂). Measurements of trapezius muscle % StO₂ were performed during the experiment using a near infrared spectrometer, NIRS (INSPECTRA Tissue Spectrometer—model 325, Hutchinson Technology Inc, Netherlands).

A self-adhesive O₂-shield was placed on the skin overlying the upper part of the trapezius muscle, medial of the MD-probe insertion site. Before connecting the optical cable to the shield, the system was calibrated according to instructions from the manufacturers, that is, inserted in a light scattering calibrator for capturing reference light intensities of all wavelengths. All tissue measurements were related to the reference measurement, thereby converting light intensity measurements to optical absorbance. Optical absorbance values were further processed into a scaled second derivative absorbance spectrum, whereby a measure of percent oxygen saturation was obtained. The software supplied with the In Spectra device allows for absolute values of % StO₂. The distance between the light transmitter and the detector was 12 mm, and the sampling frequency 0.3 Hz.

2.2.4. Blood Sampling. In order to assess possible systemic effects in response to work, that is, changes in blood lactate concentration, capillary blood samples were obtained from a right hand finger at baseline, directly after work and after the recovery period (Figure 1). The coded samples were immediately put on ice, and were later the same day analysed with a lactate analysis device YSI 2300 STAT plus (Clandon Scientific, Farnborough, UK) by an independent laboratory technician.

2.2.5. Rating of Perceived Exertion (RPE) and Perceived Pain Intensity (RPP). At baseline, and at the end of both the work and the recovery period (see Figure 1), subjects were required to rate their (i) perceived exertion of the right shoulder in accordance to the Borg CR-10 scale [22], with 0 = no fatigue and 10 = severe fatigue, and (ii) their perceived pain intensity in the right shoulder, using the nonhatched VAS, marked at one end as “no pain at all” and at the other “worst pain imaginable” [23].

2.2.6. Estimation of Skin-Fat Layer and Trapezius Muscle Thickness. Measurements of skin-fat layer (SFL) and trapezius muscle thickness were performed using ultrasonography, with a 75 mm probe (Aloka SSD-2000, Aloka Co., Ltd., Japan). Measurements were performed at three measuring-points over the upper trapezius muscle medially of the MD-probe insertion point. (1, 3.75 and 7.5 cm)

2.2.7. Data Analyses and Statistics. SPSS statistical software, version 13.0 (Chicago, III, USA) was used for all analyses. The level of significance was set to $P < .05$. The Kolmogorov-Smirnov test was used to test for normal distribution, and data for all variables was normally distributed.

The change in substance concentration relative to work was calculated as the baseline values subtracted from the values obtained after work (work-baseline = change).

Pearson test was used to investigate possible correlations between (i) pain substances (glutamate and PGE₂) and pain

intensity, (ii) IMMD lactate and local muscle oxygenation, (iii) local (IMMD lactate) and systemic (blood lactate) changes, and (iv) key metabolites (IMMD lactate and glutamate).

Repeated measures ANOVA (RM ANOVA) were used for the within group comparisons of data for the different variables in response to work and recovery (except for the RPE- and RPP-data). If the assumption of sphericity of variance was violated in the RM ANOVA, the Huyn-Feldt correction was used. The sequential Bonferroni [24] was used to compare specific pairs of means when the RM ANOVA revealed a significant difference.

To relate the oxygenation and the MD-data in time, a mean value of the oxygenation data recorded during a 5-min period just before each sampling of dialysate was calculated. Data are presented as means \pm SD in both text and graphs, except for the RPE and RPP which are presented as median and range. Wilcoxon nonparametric test was used for the within group comparisons of the subjective ratings.

3. Results

3.1. Biochemical Alterations during Work. During work [glutamate] increased (54%) ($P < .0001$, $F = 16.957$), and decreased to 26% below baseline during the recovery period ($P < .0001$, $F = 14.293$) (see Figure 3(a)).

The mean IMMD [PGE₂] remained unchanged during work ($P = .300$), but showed a significant overall decrease (40% lower than baseline) during recovery ($P = .004$, $F = 5.224$) (see Figure 3(b)).

An overall significant increase (28%) in mean IMMD [lactate] was found in response to work ($P = .003$, $F = 10.813$), and recovery ($P > .001$, $F = 7.392$) as compared to baseline (see Figure 3(c)).

Also, [pyruvate] increased significantly during work ($P < .0001$, $F = 36.4$), and continued to increase progressively (up to 60% > baseline) during the recovery period ($P < .0001$, $F = 25.3$) (see Figure 3(d)).

3.2. Oxygen Saturation (% StO₂). A small, but significant, decrease in % StO₂ in response to work was found ($P = .016$, $F = 7.816$), and directly after the cessation of work baseline was re-established (see Figure 4).

3.3. Blood Lactate. Plasma [lactate] decreased significantly in response to work ($P = .005$; $F = 8.109$), from 1.1 mmol \times L⁻¹ (SD \pm 0.3) at baseline to 0.9 mmol \times L⁻¹ (SD \pm 0.2) after work and baseline was re-established at the end of the recovery period (1.3 \pm 0.6).

3.4. Rating of Perceived Exertion (RPE) and Pain Intensity (RPP). The median (range) RPE in the right shoulder (Borg CR-10), increased significantly from 1.5 (0–3.5) at baseline to 7.0 (3.0–7.0) after work, and remained increased also after recovery 2.25 (0–4.5). The median (range) RPP in the right shoulder (VAS) increased ($P < .001$) from 17.5 (2–52) at baseline, to 69 (28–82) after work and tended to be significantly increased also at the end of recovery 26.5 (3–69) ($P = .054$).

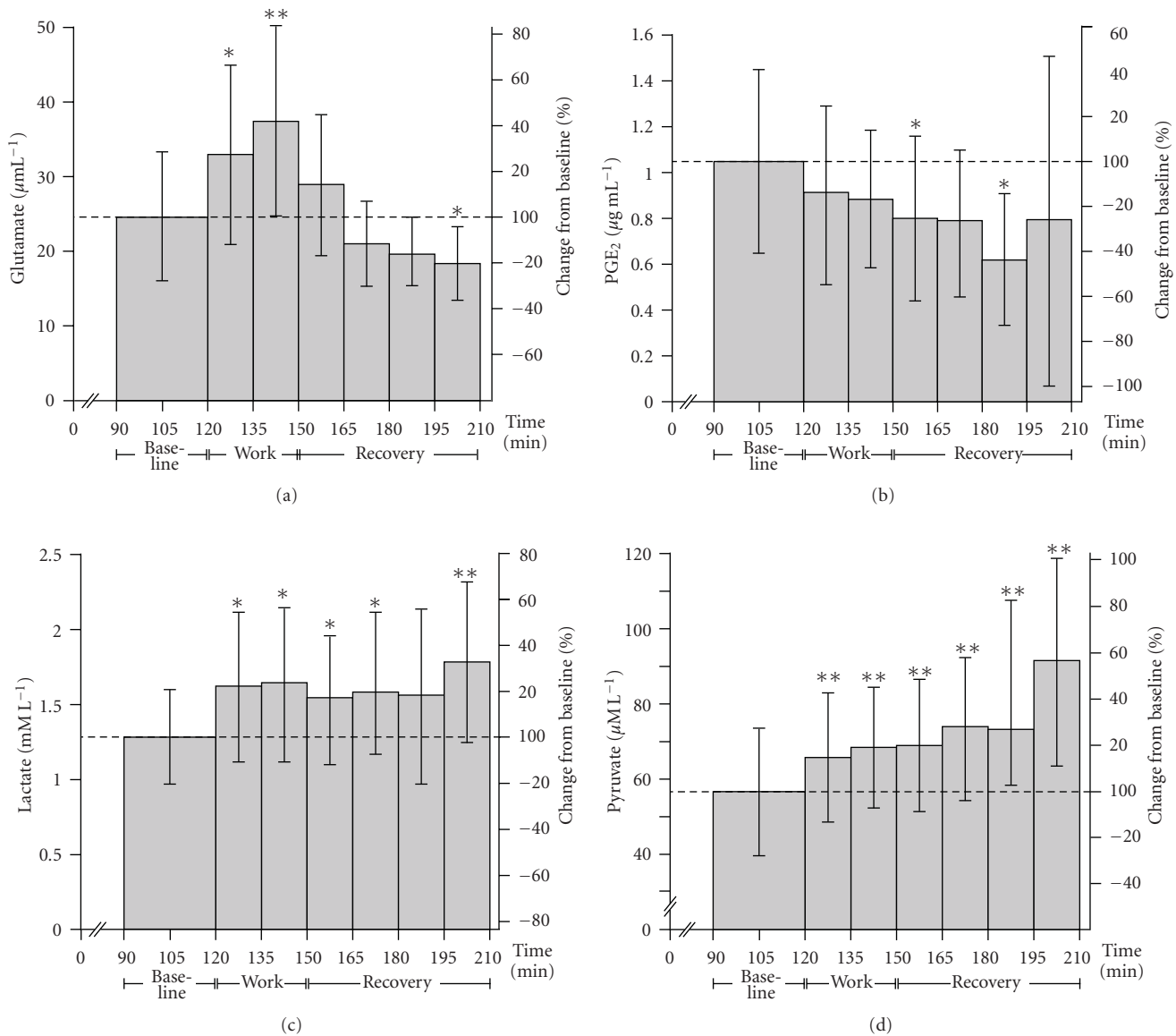


FIGURE 3: (a) IMMD glutamate concentrations. Mean (\pm SD) intramuscular microdialysate [glutamate] ($\mu\text{M L}^{-1}$) at baseline, in response to work and recovery. Percent difference in comparison to baseline is depicted on the right hand y -axis. Significant differences with respect to baseline concentrations are indicated with * for a P -value $< .05$ and ** for a P -value $< .001$. (b) IMMD PGE₂ concentrations. Mean (\pm SD) intramuscular microdialysate [PGE₂] ($\mu\text{g mL}^{-1}$) at baseline, in response to work and recovery. Percent difference in comparison to baseline is depicted on the right hand y -axis. Significant differences with respect to baseline concentrations are indicated with * for a P -value $< .05$ and ** for a P -value $< .001$. (c) IMMD lactate concentrations. Mean (\pm SD) intramuscular microdialysate [lactate] (mM L^{-1}) at baseline, in response to work and recovery. Percent difference in comparison to baseline is depicted on the right hand y -axis. Significant differences with respect to baseline concentrations are indicated with * for a P -value $< .05$ and ** for a P -value $< .001$. (d) IMMD pyruvate concentrations. Mean (\pm SD) interstitial microdialysate [pyruvate] (mM L^{-1}) at baseline, during work and recovery. Percent difference in comparison to baseline is depicted on the right hand y -axis. Significant differences with respect to baseline concentrations are indicated with * for a P -value $< .05$ and ** for a P -value $< .001$.

3.5. Skin-Fat Layer and Trapezius Muscle Thickness. The mean SFL (fascia included) and the mean trapezius muscle thickness for the three measuring-points medial to the MD-probe insertion point (1, 3.5 and 7 cm) were 4.6 ± 0.5 , 4.7 ± 0.3 and 4.5 ± 0.3 mm and 12.3 ± 0.4 mm, and 12.2 ± 0.5 and 10.0 ± 0.6 mm, respectively. Mean values for the SFL (4.6 ± 0.4 mm) and the trapezius muscle thickness (11.5 ± 0.5 mm) were calculated.

3.6. Correlations. A significant negative correlation was found between changes in IMMD [lactate] and plasma [lactate] during work ($P < .05$), and a tendency to a correlation between IMMD lactate and % StO₂ ($P = .073$). The pain intensity was uncorrelated to IMMD [glutamate] ($P = .276$) and [PGE₂] ($P = .492$), but significantly correlated to the perceived exertion in the shoulder ($P < .0001$). A significant correlation was also found between

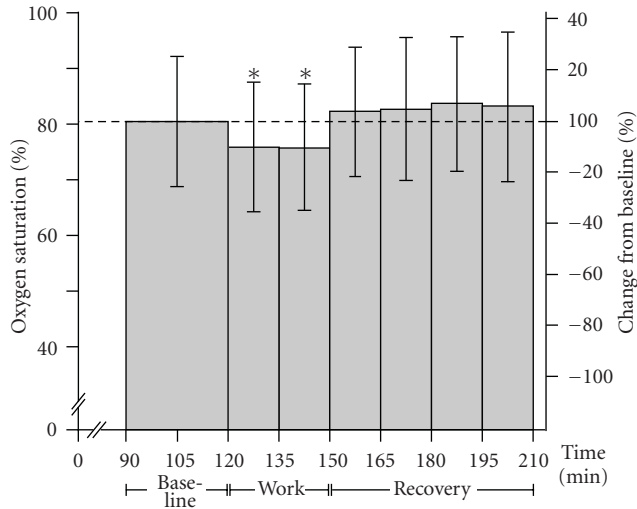


FIGURE 4: Muscle oxygen saturation. Mean (\pm SD) local trapezius muscle oxygen saturation (% StO₂) at baseline, during work and recovery. Significant differences with respect to baseline concentrations are indicated with * for a P -value $< .05$.

changes in IMMD [glutamate] and IMMD [lactate] during work ($P < .05$).

4. Discussion

The main results of the present study were: significantly increased IMMD [glutamate] and [lactate], unchanged [PGE₂], and decreased % StO₂ in the trapezius muscle during work in females with TM. Furthermore, that glutamate and PGE₂ were uncorrelated to pain intensity.

4.1. Glutamate and PGE₂. Glutamate is a well-known pain-mediator in the CNS [25, 26], and suggested to contribute to localised pain and peripheral sensitisation in certain pain conditions [13, 27, 28]. It is also a key metabolite in cellular metabolism [29]. In our study we found a significant increase in IMMD [glutamate] in response to work (54%), which was in accordance with our previous results for healthy controls [9]. However, at all time points [glutamate] was lower in TM, and uncorrelated to pain intensity [9]. While we found a moderate increase in [glutamate], the suggested concentration needed to excite and sensitize nociceptors is 2-3-fold greater than physiological concentrations [30]. These findings taken together do not support an involvement of glutamate in peripheral pain conditions. They are best interpreted as signs of normally increased metabolism in response to work.

The increase in [glutamate] in TM in response to work was also in accordance with results reported by others [13]. In contrast, Rosendal et al. found overall higher [glutamate] in TM, and a correlation between pain ratings and [glutamate] [13]. A recent study reported higher [glutamate] in TM, but no definite baseline was used as comparison [14]. It should be noted that the increased [glutamate] reported [13, 14] was similar to absolute resting concentrations reported in the trapezius of pain subjects and controls [12].

PGE₂ is known to act directly on nociceptors, and for its ability to sensitise nociceptors to other substances [31]. PGE₂ is also an important regulator of blood flow [16, 32], but its effect is highly dependent on intensity and mode of exercise, that is, during high intensity dynamic contractions, [PGE₂] is reported to increase significantly, but to remain unchanged during low intensity static contractions [33].

In our study IMMD [PGE₂] did not increase in response to work, which is in agreement with our previous results on healthy subjects [9]. Furthermore, [PGE₂] was uncorrelated to pain intensity. These findings suggest that there is no ongoing inflammation in the chronic phase of TM. Our findings and conclusions are in general agreement with the results for [PGE₂] reported by Ashina et al. [15].

However, tissue damage and inflammation may still be initiating factors for the development of muscle pain [34], and a shift from pain mechanisms in the periphery to the CNS may occur at a later stage in the disease process [35].

4.2. Lactate, Pyruvate, and % StO₂. Lactate is an important fuel source and a glukoneogenetic precursor [36, 37]. Muscles produce lactate to yield energy during anaerobic conditions, but there is also a significant lactate production in the fully oxygenated contracting muscle [38]. In our study, we found significantly increased [lactate] in response to work TM, which was in accordance with our previous results for healthy females [9]. Ashina et al. [39] also found similar [lactate] in pain subjects and controls in response to static work. However, higher [lactate] in TM in response to RW has been reported [13, 18], findings which the same authors were unable to verify in an occupational study [14]. However, many of the subjects in [13] were on sick-leave, while in the latter participants were occupationally active [18].

During prolonged low-intensity work oxidation of lactate into pyruvate is enhanced, and muscles revert from net lactate release to net uptake [40]. We found a significant increase in [pyruvate] during work, and a progressive increase during recovery, which differed from our results on healthy controls [9]. Larsson et al., reported unchanged [pyruvate] during work in both myalgic and healthy workers, but this study had no real baseline for comparison [14]. It may be speculated that the higher [pyruvate] may be due to a greater activation of fatigable type II fibres in subjects with TM, in comparison to asymptomatic subjects, which would be in accordance with muscle activation patterns reported for chronic pain cases [41].

As far as we know, we are first to combine MD and NIRS to investigate biochemical alterations in the trapezius muscle in response to RW [9, 10]. In the present study, we found a significant decrease in local muscle % StO₂ during work, and a tendency to a significant correlation between % StO₂ and IMMD [lactate]. Our findings are in general agreement with the results reported by Sjøgaard et al. [18]. The decrease in % StO₂ and the increase in IMMD [lactate] did not differ from our previous results on healthy controls, that is why these findings must be interpreted as a normal response to increased metabolic demands.

Blood [lactate] decreased during work and was negatively correlated with IMMD [lactate], which may be explained by

an enhanced uptake and use of lactate as a fuel by active muscles during prolonged low-load work [40]. During high-intensity work, [lactate] in muscle and blood is correlated [42, 43], while low-intensity work is suggested not to cause systemic effects [16, 44].

4.3. Methodological Considerations

4.3.1. Microdialysis. After the trauma of probe insertion, interstitial substance concentrations are abnormal and the influx of substances random. To avoid biased results sufficient time for the establishment of a new steady-state must be allowed [11]. We applied a 90 minutes stabilisation time, which is ample time for stabilisation of lactate, pyruvate [21], glutamate [12], but maybe not for PGE₂, which decreased below baseline during recovery.

Refraining from calibrating the probe *in vivo* is suggested to introduce bias since the relative recovery of substances (RR) is reported to increase with high intensity exercise in the absence of true interstitial changes [11, 44]. However, most studies of low-load work have reported no change [13, 14, 39, 45] or a small change [13] in RR of lactate in the trapezius muscle during work. This lack of change in RR may be explained by that intramuscular pressure does not increase in the trapezius during low-load work [46], and that the changes in blood flow are small [39], which are suggested not to affect RR of substances *in vivo* [47, 48]. We did not assess RR, and cannot therefore exclude the presence of a bias, although we find it unlikely that this bias is significant.

4.3.2. Near-Infrared Spectroscopy (NIRS). Ideally, we also should have measured blood-flow (BF), since metabolic insufficiencies may be the result of impaired BF [49]. Existing results are conflicting and provide no convincing evidence for impaired BF in TM as compared to healthy controls [14, 18, 39, 45].

NIRS may provide information about a possible mismatch between metabolic requirements and blood flow locally in muscle [16] and is considered a valid [50], and reliable tool [51] for measuring local muscle oxygenation during work.

Heterogeneity of blood flow and oxygen consumption distributions within a muscle [43, 52, 53], work intensity and level of training [16] and mode of exercise [54] may influence NIRS-measurements. In this, and in previous studies [9, 10], the work and the position of the probe were standardised, to enable appropriate comparison between studies [55].

The probe was chosen to ensure that data was obtained from the trapezius, and not from underlying muscle. It may be argued that the measuring depth of the probe may not have been sufficient to accurately assess changes in %StO₂. However, the muscle volume measured with NIRS is controversial, and while the signal is presumed to be obtained mostly from a tissue depth of approximately 60% of the transmitter-detector distance, a banana-shaped region of sensitivity extends both above and below this depth [17]. Since the skin overlying muscle in lean subjects contributes <5% of the signal [16], our measurement should mainly originate from muscle.

The discrepancies between the few studies that have studied the effect of low-load work on metabolism and sensitising substances, both in methodology, and subjects studied, emphasise that more independent studies are needed.

5. Conclusions

The changes in substance concentrations and oxygenation found in this study indicate normal increase in metabolism in response to work but no ongoing inflammation in subjects with TM. Our results do not support the role of glutamate as a pain mediator in the periphery.

Conflict of Interest

The authors have no conflicts of interest.

Acknowledgments

The financial support of the Swedish Agency for Innovation Systems, VINNOVA (project no. 510240) is gratefully acknowledged. Special thanks are due to laboratory technician Margaretha Marklund for qualified technical and graphical work, and to physiotherapist Åsa Svedmark for professional help with the clinical examinations. Thanks also to Dr. Lars Öhberg for help with interpreting the ultrasonographic images.

References

- [1] B. P. Bernard, *Musculoskeletal Disorders and Workplace Factors*, Department of Health and Human Services National Institute for Occupational Safety and Health, Cincinnati, Ohio, USA, 1997.
- [2] P. W. Buckle and J. J. Devereux, "The nature of work-related neck and upper limb musculoskeletal disorders," *Applied Ergonomics*, vol. 33, no. 3, pp. 207–217, 2002.
- [3] P. M. Bongers, S. Ijmker, S. van den Heuvel, and B. M. Blatter, "Epidemiology of work related neck and upper limb problems: psychosocial and personal risk factors (Part I) and effective interventions from a bio behavioural perspective (Part II)," *Journal of Occupational Rehabilitation*, vol. 16, no. 3, pp. 279–302, 2006.
- [4] G. Hägg, "Static work loads and occupational myalgia- a new explanation model," in *Electromyographical Kinesiology*, P. A. Anderson, D. J. Hobart, and J. V. Danoff, Eds., pp. 141–144, Elsevier, Amsterdam, The Netherlands, 1991.
- [5] H. Johansson and P. Sojka, "Pathophysiological mechanisms involved in genesis and spread of muscular tension in occupational muscle pain and in chronic musculoskeletal pain syndromes: a hypothesis," *Medical Hypotheses*, vol. 35, no. 3, pp. 196–203, 1991.
- [6] S. Knardahl, "Psychophysiological mechanisms of pain in computer work: the blood vessel-nociceptor interaction hypothesis," *Work and Stress*, vol. 16, no. 2, pp. 179–189, 2002.
- [7] B. Larsson, J. Björk, J. Elert, R. Lindman, and B. Gerdle, "Fibre type proportion and fibre size in trapezius muscle biopsies from cleaners with and without myalgia and its correlation with ragged red fibres, cytochrome-c-oxidase-negative fibres,

- biomechanical output, perception of fatigue, and surface electromyography during repetitive forward flexions," *European Journal of Applied Physiology*, vol. 84, no. 6, pp. 492–502, 2001.
- [8] B. Larsson, J. Björk, F. Kadi, R. Lindman, and B. Gerdle, "Blood supply and oxidative metabolism in muscle biopsies of female cleaners with and without myalgia," *Clinical Journal of Pain*, vol. 20, no. 6, pp. 440–446, 2004.
- [9] G. M. Flodgren, F. B. Hellström, M. Fahlström, and A. G. Crenshaw, "Effects of 30 versus 60 min of low-load work on intramuscular lactate, pyruvate, glutamate, prostaglandin E₂ and oxygenation in the trapezius muscle of healthy females," *European Journal of Applied Physiology*, vol. 97, no. 5, pp. 557–565, 2006.
- [10] G. M. Flodgren, A. G. Crenshaw, M. Gref, and M. Fahlström, "Changes in interstitial noradrenaline, trapezius muscle activity and oxygen saturation during low-load work and recovery," *European Journal of Applied Physiology*, vol. 107, no. 1, pp. 31–42, 2009.
- [11] U. Ungerstedt, "Microdialysis—principles and applications for studies in animals and man," *Journal of Internal Medicine*, vol. 230, no. 4, pp. 365–373, 1991.
- [12] G. M. Flodgren, A. G. Crenshaw, H. Alfredson, et al., "Glutamate and prostaglandin E₂ in the trapezius muscle of female subjects with chronic muscle pain and controls determined by microdialysis," *European Journal of Pain*, vol. 9, no. 5, pp. 511–515, 2005.
- [13] L. Rosendal, B. Larsson, J. Kristiansen, et al., "Increase in muscle nociceptive substances and anaerobic metabolism in patients with trapezius myalgia: microdialysis in rest and during exercise," *Pain*, vol. 112, no. 3, pp. 324–334, 2004.
- [14] B. Larsson, L. Rosendal, J. Kristiansen, et al., "Responses of algescic and metabolic substances to 8 h of repetitive manual work in myalgic human trapezius muscle," *Pain*, vol. 140, no. 3, pp. 479–490, 2008.
- [15] M. Ashina, B. Stallknecht, L. Bendtsen, et al., "Tender points are not sites of ongoing inflammation—in vivo evidence in patients with chronic tension-type headache," *Cephalalgia*, vol. 23, no. 2, pp. 109–116, 2003.
- [16] R. Boushel and C. A. Piantadosi, "Near-infrared spectroscopy for monitoring muscle oxygenation," *Acta Physiologica Scandinavica*, vol. 168, no. 4, pp. 615–622, 2000.
- [17] M. Ferrari, L. Mottola, and V. Quaresima, "Principles, techniques, and limitations of near infrared spectroscopy," *Canadian Journal of Applied Physiology*, vol. 29, no. 4, pp. 463–487, 2004.
- [18] G. Sjøgaard, L. Rosendal, J. Kristiansen, et al., "Muscle oxygenation and glycolysis in females with trapezius myalgia during stress and repetitive work using microdialysis and NIRS," *European Journal of Applied Physiology*, vol. 108, no. 4, pp. 657–669, 2010.
- [19] I. Kuorinka, B. Jonsson, A. Kilbom, et al., "Standardised Nordic questionnaires for the analysis of musculoskeletal symptoms," *Applied Ergonomics*, vol. 18, no. 3, pp. 233–237, 1987.
- [20] B. R. Jensen, B. Schibye, K. Sogaard, E. B. Simonsen, and G. Sjøgaard, "Shoulder muscle load and muscle fatigue among industrial sewing-machine operators," *European Journal of Applied Physiology and Occupational Physiology*, vol. 67, no. 5, pp. 467–475, 1993.
- [21] H. Rosdahl, K. Hamrin, U. Ungerstedt, and J. Henriksson, "Metabolite levels in human skeletal muscle and adipose tissue studied with microdialysis at low perfusion flow," *American Journal of Physiology*, vol. 274, no. 5, pp. E936–E945, 1998.
- [22] G. Borg, "A category scale with ratio properties for intermodal and interindividual comparisons," in *Psychophysical Judgement and the Process of Perception*, H.-G. Geissler, et al., Ed., pp. 25–34, VEB, Berlin, Germany, 1982.
- [23] R. Melzack and J. Katz, "Pain measurement in persons in pain," in *Textbook of Pain*, P. D. Wall and R. Melzack, Eds., pp. 409–411, Harcourt, London, UK, 4th edition, 1999.
- [24] S. Holm, "A simple sequentially rejective multiple test procedure," *Scandinavian Journal of Statistics*, pp. 65–70, 1979.
- [25] S. M. Carlton, "Peripheral excitatory amino acids," *Current Opinion in Pharmacology*, vol. 1, no. 1, pp. 52–56, 2001.
- [26] K. M. Hargreaves, J. Q. Swift, M. T. Roszkowski, W. Bowles, M. G. Garry, and D. L. Jackson, "Pharmacology of peripheral neuropeptide and inflammatory mediator release," *Oral Surgery, Oral Medicine, Oral Pathology*, vol. 78, no. 4, pp. 503–510, 1994.
- [27] H. Alfredson, K. Thorsen, and R. Lorentzon, "In situ microdialysis in tendon tissue: high levels of glutamate, but not prostaglandin E₂ in chronic Achilles tendon pain," *Knee Surgery, Sports Traumatology, Arthroscopy*, vol. 7, no. 6, pp. 378–381, 1999.
- [28] B. E. Cairns, P. Svensson, K. Wang, et al., "Activation of peripheral NMDA receptors contributes to human pain and rat afferent discharges evoked by injection of glutamate into the masseter muscle," *Journal of Neurophysiology*, vol. 90, no. 4, pp. 2098–2105, 2003.
- [29] E. P. A. Rutten, M. P. K. J. Engelen, A. M. W. J. Schols, and N. E. P. Deutz, "Skeletal muscle glutamate metabolism in health and disease: state of the art," *Current Opinion in Clinical Nutrition and Metabolic Care*, vol. 8, no. 1, pp. 41–51, 2005.
- [30] B. E. Cairns and X. Dong, "The role of peripheral glutamate and glutamate receptors in muscle pain," *Journal of Musculoskeletal Pain*, vol. 16, no. 1-2, pp. 85–91, 2008.
- [31] S. Mense, "Nociception from skeletal muscle in relation to clinical muscle pain," *Pain*, vol. 54, no. 3, pp. 241–289, 1993.
- [32] W. G. Schrage, M. J. Joyner, and F. A. Dinunno, "Local inhibition of nitric oxide and prostaglandins independently reduces forearm exercise hyperaemia in humans," *Journal of Physiology*, vol. 557, no. 2, pp. 599–611, 2004.
- [33] M. Karamouzis, H. Langberg, D. Skovgaard, J. Bulow, M. Kjaer, and B. Saltin, "In situ microdialysis of intramuscular prostaglandin and thromboxane in contracting skeletal muscle in humans," *Acta Physiologica Scandinavica*, vol. 171, no. 1, pp. 71–76, 2001.
- [34] M. F. Barbe and A. E. Barr, "Inflammation and the pathophysiology of work-related musculoskeletal disorders," *Brain, Behavior, and Immunity*, vol. 20, no. 5, pp. 423–429, 2006.
- [35] U. Windhorst, "Neuroplasticity and modulation of chronic pain," in *Chronic Work-Related Myalgia. Neuromuscular Mechanisms behind Work-Related Chronic Muscle Pain Syndromes*, H. Johansson, U. Windhorst, M. Djupsjöbacka, and M. Passatore, Eds., pp. 207–224, Gävle University Press, Gävle, Sweden, 2003.
- [36] G. A. Brooks, "Lactate shuttles in nature," *Biochemical Society Transactions*, vol. 30, no. 2, pp. 258–264, 2002.
- [37] R. A. Kreisberg, "Lactate homeostasis and lactic acidosis," *Annals of Internal Medicine*, vol. 92, no. 2, pp. 227–237, 1980.
- [38] W. C. Stanley, E. W. Gertz, and J. A. Wisneski, "Lactate extraction during net lactate release in legs of humans during exercise," *Journal of Applied Physiology*, vol. 60, no. 4, pp. 1116–1120, 1986.
- [39] M. Ashina, B. Stallknecht, L. Bendtsen, et al., "In vivo evidence of altered skeletal muscle blood flow in chronic tension-type headache," *Brain*, vol. 125, no. 2, pp. 320–326, 2002.

- [40] L. B. Gladden, "Lactate metabolism: a new paradigm for the third millennium," *Journal of Physiology*, vol. 558, no. 1, pp. 5–30, 2004.
- [41] L. A. C. Kallenberg and H. J. Hermens, "Motor unit action potential rate and motor unit action potential shape properties in subjects with work-related chronic pain," *European Journal of Applied Physiology*, vol. 96, no. 2, pp. 203–208, 2006.
- [42] B. Grassi, V. Quaresima, C. Marconi, M. Ferrari, and P. Cerretelli, "Blood lactate accumulation and muscle deoxygenation during incremental exercise," *Journal of Applied Physiology*, vol. 87, no. 1, pp. 348–355, 1999.
- [43] H. Miura, K. McCully, S. Nioka, and B. Chance, "Relationship between muscle architectural features and oxygenation status determined by near infrared device," *European Journal of Applied Physiology*, vol. 91, no. 2-3, pp. 273–278, 2004.
- [44] D. A. MacLean, J. Bangsbo, and B. Saltin, "Muscle interstitial glucose and lactate levels during dynamic exercise in humans determined by microdialysis," *Journal of Applied Physiology*, vol. 87, no. 4, pp. 1483–1490, 1999.
- [45] B. Gerdle, U. Hilgenfeldt, B. Larsson, J. Kristiansen, K. Sogaard, and L. Rosendal, "Bradykinin and kallidin levels in the trapezius muscle in patients with work-related trapezius myalgia, in patients with whiplash associated pain, and in healthy controls—a microdialysis study of women," *Pain*, vol. 139, no. 3, pp. 578–587, 2008.
- [46] U. Järvholm, G. Palmerud, D. Karlsson, P. Herberts, and R. Kadefors, "Intramuscular pressure and electromyography in four shoulder muscles," *Journal of Orthopaedic Research*, vol. 9, no. 4, pp. 609–619, 1991.
- [47] D. Scheller and J. Kolb, "The internal reference technique in microdialysis: a practical approach to monitoring dialysis efficiency and to calculating tissue concentration from dialysate samples," *Journal of Neuroscience Methods*, vol. 40, no. 1, pp. 31–38, 1991.
- [48] H. Rosdahl, U. Ungerstedt, L. Jorfeldt, and J. Henriksson, "Interstitial glucose and lactate balance in human skeletal muscle and adipose tissue studied by microdialysis," *Journal of Physiology*, vol. 471, pp. 637–657, 1993.
- [49] B. Visser and J. H. Van Dieën, "Pathophysiology of upper extremity muscle disorders," *Journal of Electromyography and Kinesiology*, vol. 16, no. 1, pp. 1–16, 2006.
- [50] D. M. Mancini, L. Bolinger, H. Li, K. Kendrick, B. Chance, and J. R. Wilson, "Validation of near-infrared spectroscopy in humans," *Journal of Applied Physiology*, vol. 77, no. 6, pp. 2740–2747, 1994.
- [51] M. C. P. Van Beekvelt, W. N. J. M. Colier, R. A. Wevers, and B. G. M. Van Engelen, "Performance of near-infrared spectroscopy in measuring local O₂ consumption and blood flow in skeletal muscle," *Journal of Applied Physiology*, vol. 90, no. 2, pp. 511–519, 2001.
- [52] V. Quaresima, W. N. J. M. Colier, M. van der Sluijs, and M. Ferrari, "Nonuniform quadriceps O₂ consumption revealed by near infrared multipoint measurements," *Biochemical and Biophysical Research Communications*, vol. 285, no. 4, pp. 1034–1039, 2001.
- [53] U. Wolf, M. Wolf, J. H. Choi, et al., "Localized irregularities in hemoglobin flow and oxygenation in calf muscle in patients with peripheral vascular disease detected with near-infrared spectrophotometry," *Journal of Vascular Surgery*, vol. 37, no. 5, pp. 1017–1026, 2003.
- [54] M. D. Kennedy, M. J. Haykowsky, C. A. Boliek, B. T. A. Esch, J. M. Scott, and D. E. R. Warburton, "Regional muscle oxygenation differences in vastus lateralis during different modes of incremental exercise," *Dynamic Medicine*, vol. 5, 8 pages, 2006.
- [55] Y. N. Bhamhani, "Muscle oxygenation trends during dynamic exercise measured by near infrared spectroscopy," *Canadian Journal of Applied Physiology*, vol. 29, no. 4, pp. 504–523, 2004.